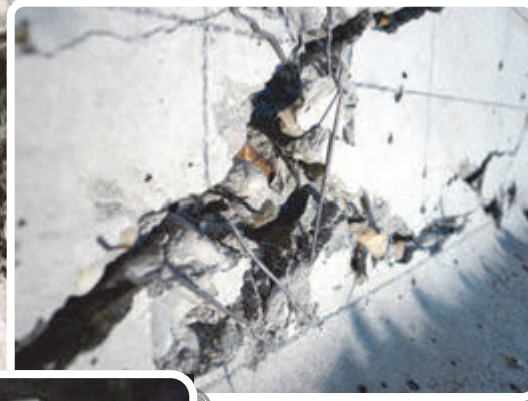
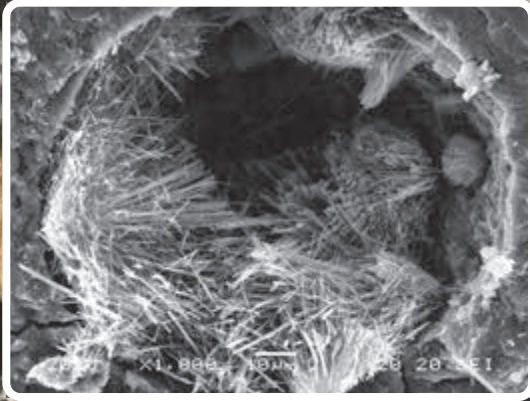




Tokaj 2017

The 12th Central European Congress on Concrete Engineering

Co-organizers:



Innovative materials and technologies for concrete structures

INNOVATIVE MATERIALS AND TECHNOLOGIES FOR CONCRETE STRUCTURES

Proceedings of the *fib* Congress

**Tokaj, Hungary
31 August to 1 September 2017**

Edited by

**György L. Balázs, Professor, Honorary President of *fib*
Dept. of Construction Materials and Technologies**

**Kálmán Koris, Assistant Professor
Dept. of Structural Engineering**

**Katalin Kopecskó, Assoc. Professor
Dept. of Engineering Geology and Geotechnics**

**Faculty of Civil Engineering
Budapest University of Technology and Economics, Budapest, Hungary**



This Volume was edited by György L. Balázs, Kálmán Koris and Katalin Kopecskó

© The Authors

Both the abstracts and the papers were reviewed by two members of the Scientific Committee.

Although the authors, the editors and the publisher did their best to provide accurate and current information, none of them, nor anyone else associated with this publication, shall be liable for any loss, damage or liability directly or indirectly caused or alleged to be caused by this Proceedings.

Published by the Hungarian Group of *fib*

ISBN 978-963-12-9651-8

PREFACE

A new tradition started in 2005 that is called **CENTRAL EUROPEAN CONGRESS ON CONCRETE ENGINEERING**. This is a series of yearly congresses to provide a forum for engineers of our neighbouring countries to meet and exchange experiences regularly. Engineers from all fields are addressed working in design, execution, prefabrication, material production, research or quality control.

In our Congresses new achievements are presented to a specific field of concrete engineering: The 1st CCC Congress in Graz (Austria) 2005 was devoted to *Fibre Reinforced Concrete in Practice*; 2006 Hradec Kralove (Czech Republic) *Concrete Structures for Traffic Network*, 2007 Visegrád (Hungary) *Innovative Materials and Technologies for Concrete Structures*; 2008 Opatija (Croatia) *Concrete Engineering in Urban Development*; 2009 Baden (Austria) *Innovative Concrete Technology in Practice*; 2009 Mariánské Lázně (Czech Republic) *Concrete Structures for Challenging Time*, 2011 Balatonfüred (Hungary) *Innovative Materials and Technologies for Concrete Structures*, 2012 Plitvice Lakes (Croatia) *Durability of Concrete Structures*, 2013 Wrocław (Poland) *Concrete Structures in Urban Areas*, 2014 Liberec (Czech Republic), 2015 Hainburg (Austria) *Innovative Concrete Technology in Practice*. In Hainburg in 2015 we decided to have the Congresses biannual in order to be able to give enough time for preparing contributions on important new constructions as well as on important new scientific results.

The 12th Central European Congress on Concrete Engineering will take place in the beautiful ambient of Tokaj region (Hungary) that is listed as a *UNESCO World Heritage site*.

The CCC2017 Congress in Tokaj focuses on *Innovative Materials and Technologies for Concrete Structures*. Concrete is an ever developing construction material. There is a continuous development on material properties, constructability, economy as well as aesthetics.

The Congress in Tokaj intends to overview properties of new types of concretes (including all constituent materials) and reinforcements as well as their possible applications. Therefore, we selected the following 5 topics for CCC2017 Tokaj:

- Topic 1: Tailored properties of concrete
- Topic 2: Advanced reinforcing and prestressing materials and technologies
- Topic 3: Advanced production and construction technologies.
- Topic 4: Advanced concrete structures
- Topic 5: Modelling, design and codification.

The host organisation of the CCC2017 Congress is the Hungarian Group of *fib*. The Congress is jointly organized by the Faculty of Civil Engineering of Budapest University of Technology and Economics. We have the pleasure to invite representatives of clients, designers, contractors, academics and students to take part at this regional event, which will give excellent social and technical conditions for exchange of experience in the field of concrete engineering.

As the Chairman of the CCC2017 Congress I am happy to welcome 83 papers in this Proceedings from 16 countries of Europe, America and Africa.



György L. Balázs, Chairman of CCC2017 Congress
Honorary President of *fib* (International Federation for Structural Concrete)
Professor at Faculty of Civil Engineering, Budapest University of Techn. and Economics

Scientific Committee

12th European Congress on Concrete Engineering
31 August - 1 September 2017 Tokaj, Hungary

BALÁZS, György L. (Hungary) Chairman	KOLLEGGER Johann (Austria)
BERGMEISTER, Konrad (Austria)	KOPECSKÓ, Katalin (Hungary)
BILISZCZUK, Jan (Poland)	KORIS, Kálmán (Hungary)
BLEIZIFFER, Jelena (Croatia)	KOTYNIA, Renata (Poland)
BÓDI, István (Hungary)	KREMNITZER, Peter (Austria)
COUFAL, Robert (Czech Rep.)	MANDIC IVANKOVIC, Ana (Croatia)
DEJA, Jan (Poland)	NAGRODZKA - GODYCKA, Krystyna (Poland)
DERKOWSKI, Wit (Poland)	NEHME, Salem G. (Hungary)
FARKAS, György (Hungary)	NGUYEN, Viet Tue (Austria)
KALNY, Milan (Czech Rep.)	PAUSER, Michael (Austria)
KINDIJ, Alex (Croatia)	PUZ, Goran, (Croatia)
KLEMCZAK, Barbara (Poland)	SALAMAK, Marek (Poland)
KOLISKO, Jiri (Czech Rep.)	STRASKY, Jiri (Czech Rep.)
KOHOUTKOVA, Alena (Czech Rep.)	STIPANOVIC OSLAKOVIC, Irina (Croatia)
KOLLÁR, László (Hungary)	VÍTEK, Jan L. (Czech Rep.)

Sponsoring Organizations

A-Híd Co.
Dun-DravaCement Ltd. Heidelberg Group
Moratus Ltd.
Sika Hungary Ltd.
MAPEI
Hydrastat Ltd.
Sauska Winery

Organizing Committee

12th European Congress on Concrete Engineering
31 August - 1 September 2017 Tokaj, Hungary

MAGYAR, János (Hungary)	NEMES, Rita (Hungary)
CZOBOLY, Olivér (Hungary)	ONYSYK, Jerzy (Poland)
HAWRYSZKÓW, Paweł (Poland)	SÓLYOM, Sándor (Hungary)
FENYVESI, Olivér (Hungary)	SCHNEIDER-IRSIGLER, Anke (Austria)
JOHOVA, Petra (Czech Rep.)	SRBIC, Mladen (Croatia)
KRONFUSS, Bernd (Austria)	SKOKANDIC, Dominik (Croatia)
KUSTER MARIC, Marija (Croatia)	STEVULA, Michal (Czech Rep.)
LUBLÓY, Éva (Hungary)	TEICHGRAEBER, Marco (Poland)
	VICH, Jiri (Czech Rep.)

Exhibitors

Cervenka Consulting Ltd. Concrete Engineering and Software Solutions
Swietelsky Hungary Ltd.
Meselia NewChem Group
Aigner Albrecht Ltd.

12th European Congress on Concrete Engineering
31 August - 1 September 2017 Tokaj, HUNGARY

CONTENT

Preface	4
Content	7
SELECTED PAPERS FOR THE OPENING	14
<i>Béla Csíki, Károly Kőszeghy, Zoltán Perczel</i> New type prefabricated water towers with prestressed mast	15
<i>Robert Schedler, Michael Fritsch, Iztok Arnuga</i> The longest integral bridge in Austria – A5.24 Bridge over the Satzengraben	23
<i>Jan L. Vitek, Robert Coufal, Jiří Kolísko, Radek Vašátko</i> Modulus of elasticity – specification, acceptance criteria and influence on structural performance	31
<i>Marek Salamak, Artur Salachna, Piotr Łaziński</i> Construction and load test of cable-stayed concrete tram bridge in Krakow	40
<i>Josip Galic, Ivan Klepo</i> Examples of advanced concrete structures in Croatia	48
TOPIC 1 TAILORED PROPERTIES OF CONCRETE	61
<i>Tamás Mészöly, Norbert Randl</i> An advanced approach to derive the constitutive law of UHPFRC	62
<i>Miquel Joseph, Zeger Sierens, Jeroen Massaer, Dylan Noppe, Jiabin Li, Luc Boehme</i> Influence of the purity of recycled concrete aggregates on the mechanical properties of dry and self-compacting precast concrete	70
<i>Olivér Czoboly, György L. Balázs</i> Effect of mixing time to the properties of steel fibres and SFRC	78
<i>Egon Milost, Tadeja Kosec, Aljoša Šajna, Irina Stipanović Oslaković, Andraž Legat, Violeta Bokan Bosiljkov</i> Effect of supplementary cementitious materials on mortar properties and corrosion of steel in different environments	86
<i>Jiří Kolísko, David Čítek, Petr Tej, Milan Rydval</i> Experimental pedestrian thin walled double curvature arch footbridge made of UHPFRC	94

<i>Tibor Kausay, Tamás K. Simon</i> Evaluation of the compressive strength of concrete	102
<i>Wojciech Kubissa, Roman Jaskulski, Tamás Simon</i> Surface blast-cleaning waste as a replacement of fine aggregate in concrete	111
<i>Szweda Zofia, Śliwka Andrzej</i> Predicting risk of corrosion of bridges made of concrete with portland cement and low alkali portland cement	118
<i>Faustyn Recha, Tomasz Jaśniok, Tomasz Krykowski</i> The simulation of corrosion degradation of concrete specimen in stationary heat and moisture condition	127
<i>Ahmed J. Al-Basha, Craig M. Newton, Brad D. Weldon</i> Compressive and flexural strengths of heat cured ultra-high performance concrete produced with local materials	135
<i>Peter Paulik, Michal Bačuvčík, Katarína Gajdošová, Jaroslav Halvoník</i> Material properties study of seven 100-years old concrete bridges in Slovakia	143
<i>Vlastimil Bílek, David Pytlík, Markéta Bambuchová, Sabina Bonczková</i> Comparison of modules of elasticity and mechanical properties of different concrete types	150
<i>Yupeng Yang</i> Value-added recycling and reuse of waste concrete on a construction site	155
<i>Daguang Han, Yongwang Geng, Jianfeng Bai, Yupeng Yang, Chunli Ying, Hongyuan Li, Jiabin Li</i> Feasibility of on-site recycling and reuse of waste concrete in China – a case study	163
<i>Čechmánek René, Drdlová Martina, Boháč Martin</i> Fresh and hardened state of fibre concrete	171
<i>Zoltán Gyurkó, Anna Szijártó, Mohammed Abed, Rita Nemes</i> Effect of cellular concrete powder on durability of normal strength concrete	179
<i>Zeger Sierens, Miquel Joseph, Luc Boehme, Jiabin Li</i> Early-age mechanical properties of recycled aggregate concrete	187
<i>Vanessa V. Rocha, Péter Ludvig</i> Characterization of portland cement composites prepared by a dispersion of carbon nanotubes on cement particles	195
<i>P. Łaziński, J. Krzakała</i> Estimation of modulus of elasticity of concrete on granite aggregate with the consideration of mechanical parameters of aggregate	202

<i>Katarzyna Domagała, Andrzej Śliwka</i> Application of potentiostatic measurements according to PN-EN 480-14 in assessment of the efficiency of reinforcement protection against corrosion by concrete with addition of fly ashes	211
<i>Andreas Haus</i> The effect of steel fibres for crack width limitation	219
<i>Barbara Słomka-Słupik, Adam Zybura</i> Thaumasite formation in cement paste exposed for 4 days to ammonium chloride saturated water solution at ambient temperature and pressure	225
<i>Abdulkader El Mir, Ágnes Péity, Salem G. Nehme</i> Effect of maximum aggregate size on mechanical properties of high-strength concrete	233
<i>Abdelmelek Nabil, Éva Lubláy</i> Improved fire resistance by using different dosages of metakaolin	240
<i>Viktor Hlavička, Éva Lubláy</i> Bonded anchors in thermally-damaged concrete	246
TOPIC 2 ADVANCED REINFORCING AND PRESTRESSING MATERIALS AND TECHNOLOGIES	254
<i>Vazul Boros, Balthasar Novák</i> Adjustment of internal prestressing in existing structures – a case study	255
<i>Michael Huss, Viet Tue Nguyen</i> Innovative steel fibers and their effect on fiber distribution in beams – experimental investigations	263
<i>Agnieszka Wiater</i> Research on the lightweight concrete bridge deck slabs reinforced with GFRP composite bars	270
<i>Viorel Constantin Todea, Valeriu Stoian, Daniel Dan, Tamás Nagy-György, Sorin Codruț Floruț, Emanuela Boita</i> Hybrid steel-concrete shear walls strengthened using high performance steel fibre reinforced composites	277
<i>E. Apostolidi, K. Bergmeister, A. Strauss, P. Winkler, P. Kremnitzer, C. Rauch, B. Schembera</i> Innovative perforated steel sheet reinforcement: Corbel approach	284
<i>Cronje Bruwer</i> Behaviour of multi-directional CFRP and unidirectional CFRP plate bonded to concrete by means of epoxy and a combination of epoxy and mechanical anchors	292

<i>Mária Erdélyiné Tóth, Anikó Pluzsik, Tamás Pluzsik, Bálint Morlin</i> Experimental investigations of pull-out behaviour of synthetic fibres	298
<i>Cronje Bruwer</i> Influence of unidirectional CFRP plate pull-off strength bonded to concrete by means of epoxy and a combination of epoxy and mechanical anchors	306
<i>Katarína Gajdošová, Róbert Sonnenschein, Peter Paulík, Jaroslav Halvoník</i> Long-term properties of FRP reinforcement	313
<i>Bartosz Piątek, Tomasz Siwowski</i> Research on the new CFRP prestressing system for strengthening of RC structures	319
<i>Sándor Sólyom, Anna Szijártó, György L. Balázs</i> Non-metallic reinforcements with different moduli of elasticity and surfaces for concrete structures	327
TOPIC 3 ADVANCED PRODUCTION AND CONSTRUCTION TECHNOLOGIES	336
<i>Michael Olipitz</i> Small bridges up to 32.5 m span in UHPC-construction – bridge systems with aesthetic requirements	337
<i>Michael Kleiser, Wolfgang Lindlbauer, Helmut Huber</i> An ASFINAG pilot project for a watertight structure without reinforcement for crack width control	346
<i>Vítězslav Vacek, Miroslav Sýkora, Jiří Kolísko, Vladimír Vančík</i> Effect of design and execution on quality and durability of multi-storey reinforced concrete parking garages	354
<i>Herbert Weier</i> The Sanna-bridge – “temporarily suspended” super-structure safely landed	362
<i>Árpád Orosz, János Nagy, Ernő Zábrádi, Aliz Horváth, Imre Répáczki</i> Foundation slabs supported by spot footing	368
<i>Vedad Terzić, Reuf Kadrić</i> Application of macro-synthetic-fiber-reinforced sprayed concrete for primary lining support on Highway Tunnel Project in Bosnia And Herzegovina	379
<i>Kálmán Koris, István Bódi</i> Shear capacity of prestressed FRC beams with sparse stirrup spacing	388

<i>Piotr Klikowicz, Marek Salamak, Mateusz Smolana</i> Various aspects of bridge health monitoring systems in Poland	396
<i>Łukasz Krawczyk, Michał Gołdyn, Tadeusz Urban</i> Digital image correlation systems in the experimental investigations: capabilities and limitations	404
<i>Czesław Machelski, Bartosz Pisarek</i> Change of the grade line of bridges constructed with cantilever concreting technology	410
TOPIC 4 ADVANCED CONCRETE STRUCTURES	418
<i>Johannes Oppeneder, Lutz Sparowitz, Bernhard Freytag, Nguyen Viet Tue</i> Material development for the QUICKWAY system	410
<i>Jan Biliszczuk, Paweł Hawryszków, Marco Teichgraeber</i> Structural Health Monitoring system of a concrete cable-stayed bridge	427
<i>Benjamin Kromoser, Johann Kollegger</i> Construction of a thin walled concrete shell event canopy	435
<i>Krzyszyna Nagrodzka-Godycka, Marta Wiśniowska</i> Design and construction of tilted walls in accordance with codes' provisions on the example of the construction of the museum of the second world war in Gdańsk	443
<i>Gábor Durovszky, Eörs Henrik Thék</i> Precast bridge girders to span 44 m	449
<i>Dragoș Alupoae, Elena Meteș, Sergiu Enache, Gavril Köllö, Edward Petzek</i> VTR [®] – Modular bridge concept for skew intersections	459
<i>Martin Schneider, Norbert Randl, Bernhard K. Hofer</i> Quantifying the effect of mixture properties of high performance concrete overlays on adhesive bond to NSC substrates on the basis of axial tensile tests	467
<i>Jan Tichý, Bohuslav Slánský, Stanislav Ševčík</i> Optimizing of UHPC railing panels and their practical application	475
<i>Hana Šimonová, Petr Daněk, Petr Frantík, Martin Sedlmajer, Zbyněk Keršner</i> Characterization of old/repairing structural concrete through mechanical fracture parameters	481
<i>Waldemar Bober</i> Experimental prestressed shell by Waclaw Zalewski	487
<i>Zoltán Teiter</i> Spectacular structure in an economical way	493

<i>Dalibor Sekulić, Mario Ille, Igor Džajić</i> Monitoring of RC structures with integrated sensors	501
TOPIC 5	
MODELLING, DESIGN AND CODIFICATION	508
<i>Jelena Bleiziffer, Ivana Milić</i> Advances in bridge management systems	509
<i>Andor Windisch</i> New concept for design of concrete structures	517
<i>Radomír Pukl, Vladimír Červenka, Tereza Sajdlová, Jan Červenka, Drahomír Novák</i> Probabilistic study about uncertainties in predicting shear beam cracking and failure	525
<i>Michaela Kopp, Markus Vill</i> Shear load assessment of existing concrete bridges by nonlinear FE-modelling	533
<i>Peter Joachim Heinrich, Dirk Schlicke, Nguyen Viet Tue</i> Adoption of a rheological body for the simulation of viscoelastic effects in hardening concrete	542
<i>Károly Péter Juhász, Péter Schaul, Lóránt Nagy</i> Optimisation of TBM Tunnel in the Shanghai Metro Extension using Macro Synthetic Fibre	549
<i>Péter Schaul, György L. Balázs</i> Shear design opportunities for synthetic reinforced concrete beams	557
<i>George C. Fanourakis</i> Validation of the <i>fib</i> 2010 and Rilem B4 models for predicting creep in concrete	566
<i>Marek Jasiński, Tomasz Płaszczuk, Marek Salamak</i> Visual programming and BIM technology in parametric concrete bridge superstructure design	575
<i>George C. Fanourakis</i> Evaluation of the creep coefficients of the <i>fib</i> 2010 and Rilem B4 concrete creep prediction models	583
<i>Andrzej Śliwka</i> Deformation of the ground caused by mining exploitation and internal forces in freely supported bridge	590
<i>Damian Szczech, Monika Kaszubska Renata Kotynia</i> Comparison of shear strength assessment according to Eurocode 2 and Model Code 2010 design procedures	598
<i>Miklós Gálos, Ákos Orosz, János P. Rádics, Kornél Tamás</i> Modelling the behaviour of concrete additives via discrete element numerical simulation	607

<i>Slaven Katalinić, Anđelko Vlašić</i> Comparison of different calculation methods and models for mixed core-frame structural system	615
<i>Mateusz Źarski, Tomasz Płaszczuk, Marek Salamak</i> Integrated lifecycle analysis of a concrete bridge	623
<i>Tereza Sajdlová, Radomír Pukl, Károly Péter Juhász, Lóránt Nagy, Péter Schaul</i> Fibre reinforced concrete constitutive laws for numerical simulation	632
<i>Károly Péter Juhász, Péter Schaul, John Hammond</i> Numerical modelling of a precast fibre reinforced concrete track slab	640
<i>Zsolt Roszevák, István Haris</i> Comparison of different models on different cast-in-situ RC joints	648
<i>Tomislav Brozović, Tomislav Kišiček, Ana Mandić Ivanković</i> Static and dynamic response of damaged prestressed RC beams flexural strengthened with CFRP	659
<i>Naser Alimrani, György L. Balázs</i> Structural consequences of fire on concrete structures - Review article	665

SELECTED PAPERS FOR THE OPENING

NEW TYPE PREFABRICATED WATER TOWERS WITH PRESTRESSED MAST

*Béla Csíki, Károly Kőszeghy, Zoltán Perczel
DCB Engineering Consulting Ltd.
H-1112 Budapest, Rózsabarack s. 8., Hungary*

SUMMARY

Two types of water towers almost fully made of prefabricated elements have been developed for lower and middle ranges of water storage capacities, recently. The first can be used for 50 m³ to 100 m³, while the second type from 150 m³ up to 750 m³ storage capacities. The paper summarizes the design aspects and also the experiences obtained during the construction of the 5 new type water towers having been realized, so far.

The new type water towers have proved to be economic even in the lower storage capacity ranges due to the short time of in-situ building works and also to the (for long time) existing prefabrication capacity.

1. INTRODUCTION

Due to the recent water supply developments in Hungary three of 100 m³, one of 200 m³ and one of 500 m³ capacity new type water towers have been realized in the country in the past few years. All of them are almost fully made of prefabricated reinforced concrete elements. Although in lower storage capacity ranges steel towers have been regarded more typical so far, developing and applying prefabricated reinforced concrete water towers have also appeared recently, based on the following capabilities:

- Exists, for long time, a prefabrication capacity for circular pipe elements widely used to underground conduits, and
- Exists also a prefabrication capacity for wall- and roof elements for prefab under surface basins often built for drinking water storage in the past few decades.

The idea of putting together the prefab pipe-, wall- and roof elements in order to shape the superstructure (the mast and the tank) of a water tower was coming from the manufacturer of such elements itself, AGM Beton Zrt. (H-2200 Monor, Külterület, Hrsz.: 0100/8). The company playing an increasing role in the civil engineering execution market in Hungary and abroad, acted as main contractor in the execution of the five new water towers.

There are many examples for reinforced concrete water towers built by using prefabricated elements. In most cases the mast is erected monolithically using sliding shutter, while the tank is assembled on the land surface from prefab elements before lifting it up to its final position (Koperniczky, 1969). An alternative method is also widely used: cast in situ concreting of the tank on mounted shutter elements at the bottom surface before moving it up the tower (Kiss, 1973).

There are much fewer instances for prefabrication spreading also to the mast of the water tower. An interesting example is a set of uniform 200 m³ water towers of such a kind in Italy, near Verona (Márkus, 1984). In addition to the tank also the mast of the towers was made of prefabricated elements connected by prestressing (post-tensioning). Mainly the mast prefabrication resulted in a very short (3 weeks/tower) building time of these towers often commemorated about.

2. TOWER TYPES

Two types of water towers almost fully made of prefabricated elements have been developed in connection with the arising demand for high water storage. The first one is for lower (from 50 to 100 m³) and the second one is for middle (from 150 to 750 m³) storage capacities, Fig. 1.

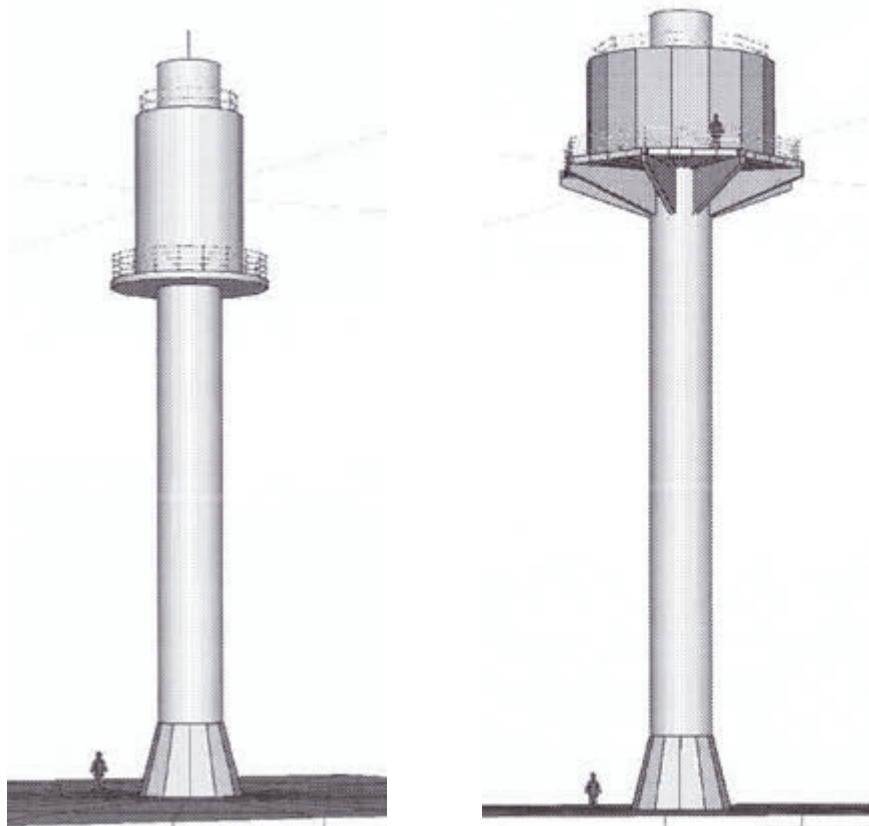


Fig. 1: Design views of the two water tower types (Type 1 left, Type 2 right)

Three of the first type with 100 m³ storage capacity were built and put in operation in Árpádhalom, Eperjes and Újiráz in 2015. Two of the second types have been built so far: one of 200 m³ capacity in Gádoros in 2015, and one of 500 m³ capacity in Dömsöd in 2014.

2. STRUCTURAL ARRANGEMENT

2.1 In general

The mast of both water tower types is made of vertically post-tensioned prefabricated reinforced concrete pipe elements. The storage tanks above the mast are also fully prefabricated with watertight connections, but the arrangements are slightly different. The vertical sections of both types, first for 100 m³ and the second for 200 m³ storage capacity are presented in Fig. 2.

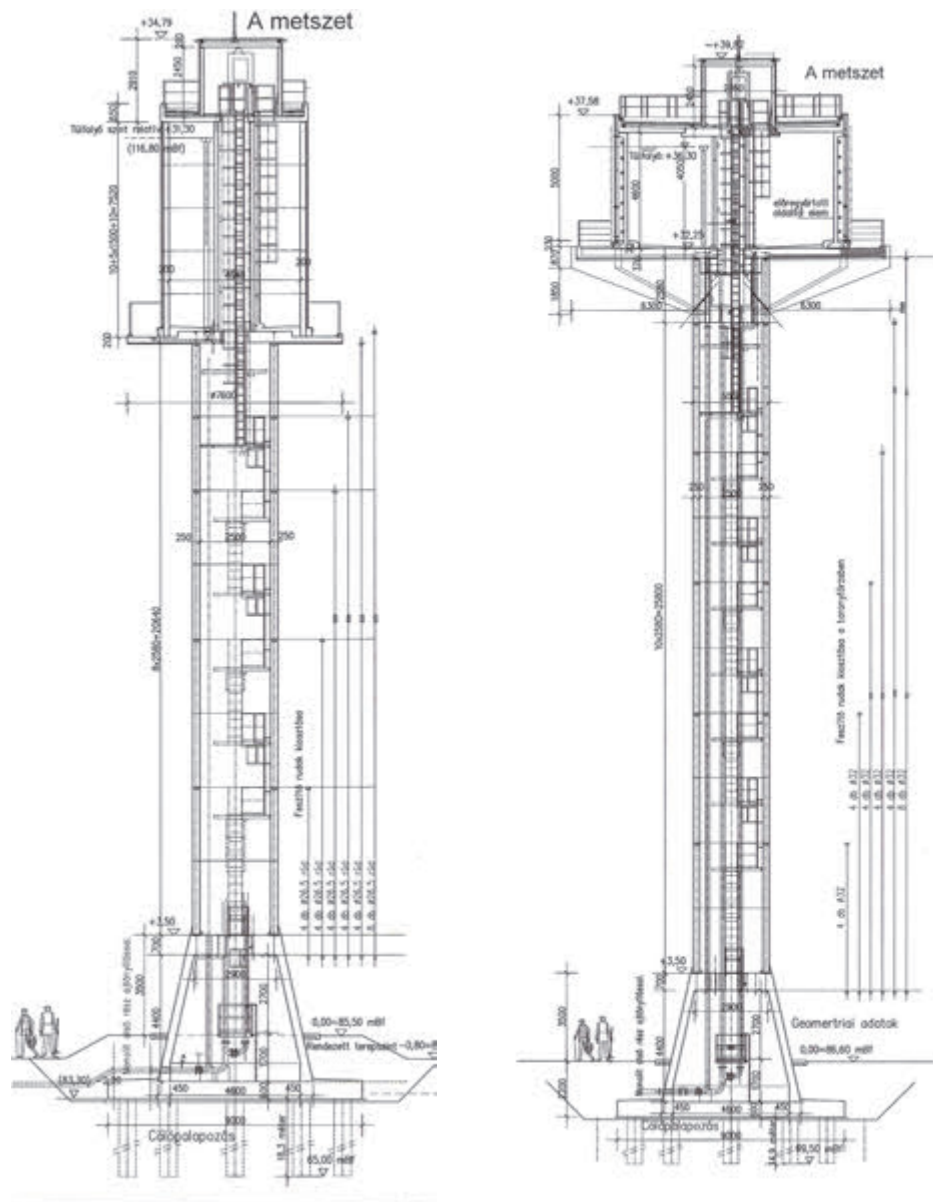


Fig. 2: Vertical sections of the two water tower types (Type 1 left, Type 2 right)

The circular tank-wall of the first type for smaller capacities consists of cylindrical segment elements. The tank-wall of the second type for the bigger capacity is polygonal in layout, and consists of vertical plain panels. The only main structural part of both types made of in-situ reinforced concrete is the founding of the water-towers.

2.2 Substructure and foundation

The substructure consisting of a foundation slab and of a founding cone at both water tower types is made of in-situ (monolithic) reinforced concrete.

Depending on the soil conditions of the site plane- or piled foundation is applied. The foundation method determines the necessary layout measure of the applied (circular or polygonal) foundation slab. (A piled foundation may need smaller sizes in layout.)

The founding cone stiffening the substructure on the one hand secures the entrance of the tower, on the other hand serves as anchoring space for the prestressing bars of the mast. The height of the cone is about 5 m, the diameter is changing from 3 m to 5 m. The thickness of the roof slab of the cone where the mast prestressing bars are fixed to is 0.7 m.

The applied grade of structural concrete for the substructure is C35/45-XC4-XF1-XA1, with a reinforcing steel category of B500B.

2.3 Prestressed mast

The mast of both tower types consists of prefabricated reinforced concrete pipe elements of 3.0 m outer diameter and of 250 mm wall thickness. The height of the pipe elements is 2.58 m. The number of the mast elements can be about 9 to 11 pieces depending on the required tower height. At tower Type 2 the last element is special to allow for anchoring radial cantilever beams directly supporting the tank.

The mast elements are gradually post-tensioned through the pipe-walls in vertical direction by prestressing bars anchored at the bottom of the thick roof of the founding cone. In the realized cases Dywidag prestressing bars (DSI 950/1050) of 26.5 and 32 mm diameter were used.

The applied grade of structural concrete for the mast elements is C50/60-XC4-XF1-16-F3, with reinforcing bars of B500B.

2.4 Tank supporting

The direct supporting of the tank at the top of the mast is different for the two tower types.

At Type 1 (tank for lower storage capacities) an in-situ prefabricated reinforced concrete circular plate is lifted and fixed directly to the final mast element. Then, the prefab segment elements of the tank are placed directly to the circular plate functioning as bottom plate of the tank.

At Type 2 (tank for higher storage capacities) radially located, reinforced concrete cantilever beams are used for supporting the tank. The bottom plate is made of in-situ reinforced concrete casting on prefabricated shallow shutter slabs after they have been lifted up to the cantilevers. Fixing and anchoring of the radial prefabricated cantilevers to the specially arranged, final mast element was one of the most challenging questions to be solved during the design, Fig. 3.



Fig. 3: Anchoring of cantilevers to the final mast element (Type 2)

2.5 Tank structures

The storage tanks above the mast are also fully prefabricated with watertight connections, but the arrangements of the sidewalls are slightly different, Fig.4. The effective layout of tanks for water storage is circular ring-shaped (not circle) because of a central circular pipe-element with a steel ladder inside connecting the mast area with the tank-roof to secure free access. This central pipe acts as an inner support of the tank-roof, as well.

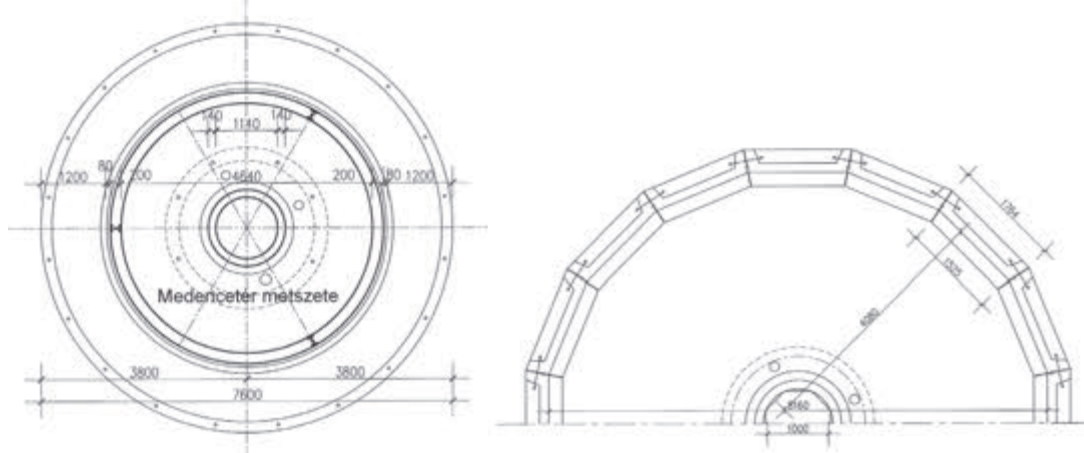


Fig. 4: Tank horizontal sections (Type 1 left, Type 2 right)

The circular tank-wall of Type 1 for smaller capacities consists of prefabricated cylindrical segment elements of 200 mm thickness, and of 1.50 m height connected to form whole circles (rings) at the ground surface. Each ring including three connected segments is lifted up to the bottom plate on the mast (or onto the previous full ring). The 100 m³ capacity tank is of 4.64 m diameter, with a 7.50 m necessary wall height. This height can be reached by five whole rings with four circumferential watertight connections worked up at their final location by special sticking material and welding.

The tank-wall of Type 2 for the bigger capacity is polygonal in layout. It consists of prefabricated vertical plain panels with horizontal and vertical stiffening ribs at the panel-edges. The panels are connected to each-other by bolts along the vertical ribs, while their bottom is welded to steel continuous profiles concreted in the bottom plate. The watertightness at each junction is secured by cement-slurry injection of the designed gaps. Regarding a 200 m³ storage capacity tank, 16 wall-panels of 1.76 m width are needed, arranged around a 9.16 m diameter inner circle of the 16-sided polygon. The height of the panels is 4.60 m, with lowest thickness of 150 mm. (Tanks of similar arrangement with several measures were widely used to build underground water reservoirs a few decades ago.)

The grade of structural concrete to the prefab elements of the water tanks is C40/50-XV2(H)-XC2-XD2. The category of the applied reinforcing steel is B500B.

2.6 Mast and tank element joints

The circular horizontal joints of the mast elements are formed by smooth surfaces (without any notches) compacted by sticking and – obviously – by the prestressing itself.

The watertight joints of tank elements of both Types at the bottom slab are formed by mixing of in-situ welding and concreting.

The wall to wall circumferential joints at tank of Type 1 are notched connections compacted by sticking and welding. The vertical joints along the wall elements of Type 2 are bolted and in-situ cement injected connections.

3. STRUCTURAL ANALYSIS

The following structural models, design principles and analysis methods were applied to the structural design of the water towers:

- *In general:*
Three-dimensional combined structural model on elastic bedding or on discrete elastic springs examined by FEM (Fig. 5).
- *To earthquake load (Modal response spectrum analysis):*
 1. Static model: Reduced at the mass centre (one mass) vertical cantilever. The water load (weight) is considered in the metacentre when determining the mass centre.
 2. Dynamic model: Two mass (M1, M2) vertical cantilever. M1 is the sum of the mass of the tower and of the mass of the impulsive water part (moving together with the structure) acting in the mass centre. M2 is the mass of convective water part (moving separately from the structure) suspended in the metacentre.
- *To stability analysis:*
Elastically supported (walled in) vertical cantilever. (The critical force based on *Föppl-Papkovics* principle.)
- *Prestressing of the mast:*
The effective (applied in two steps) prestressing forces of the mast are increasing from top to bottom to eliminate tension stresses along the mast. The distribution of the considered prestressing forces and of the normal forces due to an ultimate load combination of 200 m³ water tower in Gádoros is presented in Fig. 5.

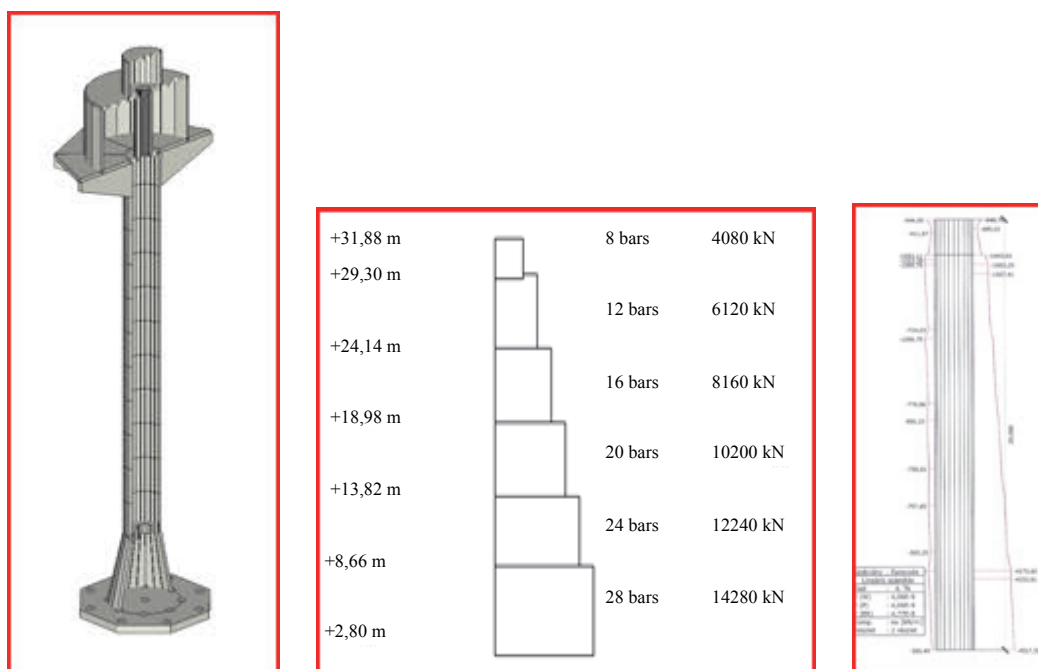


Fig. 5: FEM model of structure, Prestressing- and axial forces of mast

4. CONSTRUCTION ASPECTS

Due to the recent demand for water towers of low and middle range capacities in Hungary the advantages of prefabrication could be considerable because of the next correlating reasons:

- There has been, for long time, a prefabrication capacity for reinforced concrete elements applicable (by not much modification) to build mast and tank of water towers.
- There have been, for long time, building experiences of prefabricated water reservoirs on or under the ground.
- The mounting-like building activity needs low living labour capacity (Fig. 6).
- Possibility of more tower construction at the same time with not multiple recourses. This may reduce multiple costs.
- Possibility of very short building time. After the in-situ concreting works of the substructure have been done the building time of mounting is not more than a few weeks, depending on the storage capacity of the water tower.



Fig. 6: Examples for mounting-like construction (Type 2)

5. CONCLUSIONS

To satisfy the demand for high water storage of lower and middle range capacity in the country, five new types almost fully prefabricated reinforced concrete water towers have been built recently, in Hungary.

The mast of both water tower types is made of vertically post-tensioned prefabricated reinforced concrete pipe elements. The storage tanks above the mast are also fully prefabricated with watertight connections, but the arrangements are slightly different.

The circular tank-wall of the first type for smaller capacities consists of cylindrical segment elements. The tank-wall of the second type for the bigger capacity is polygonal in layout, and consists of vertical plain panels. The only main structural parts of both types made of in-situ reinforced concrete are the foundation and founding of the water-towers.

The experiences with the new type of civil engineering structures (Fig. 7) have been positive so far regarding the aspects of design, building and operation, respectively.



Fig. 7: Views of the new water tower types (Type 1 left, Type 2 right)

Hopefully, the new civil engineering structures, as special kinds of landmarks, satisfy aesthetic considerations, as well.

6. REFERENCES

- Kiss, I. (1973), "Water tower of Balaton Youth-town", *Műszaki Tervezés*, (in Hungarian) March 1973, pp. 27-28.
- Koperniczky, J. (1969), "Construction of small water towers", *Műszaki Tervezés*, (in Hungarian) March 1969, pp. 19-22.
- Márkus, G. (1984), "Reinforced concrete reservoirs", *Mérnöki Kézikönyv, II.*, (in Hungarian) 1984, pp. 920-942.

THE LONGEST INTEGRAL BRIDGE IN AUSTRIA – A5.24 BRIDGE OVER THE SATZENGRABEN

*Robert Schedler, Michael Fritsch, Iztok Arnuga
FCP Fritsch, Chiari & Partner ZT GmbH
Marxergasse 1B, A-1140 Wien*

SUMMARY

On the new highway section of the Austrian northern highway A5, the A5.24 bridge over the Satzengraben is currently being constructed. The bridge with a length of 112 m was designed as an integral bridge, equipped with an innovative road expansion joint, developed by the Technical University of Vienna. Due to the length of the bridge, the constraints of the road expansion joint and the high earth dam made of cement stabilised soil unconventional solutions at the abutment axes had to be implemented. The integral solution with a high superstructure stiffness and robustness of a statically undetermined system also enabled a slender and visually attractive design of the bridge.

1. INTRODUCTION

A new section between Schrick and Poysdorf is currently being built on the Austrian north highway A5. Part of this section, at the chainage 32+347, is also the longest integral bridge in Austria. The highway bridge with a total length of 112 m and with straight geometry crosses in 5 spans the Satzengraben Creek, a local road and a hiking path in 5 spans. The reinforced concrete bridge, designed by the structural consultancy firm Fritsch, Chiari & Partner ZT, is a pilot project of the Austrian highway authority (Asfinag) and will be equipped with a special maintenance-free road expansion joint developed by Univ.Prof. Dr.-Ing. Kolleger and Dr.techn. Eichwalder at the Technical University of Vienna (Kolleger, Eichwalder 2014). The construction of the bridge is carried out by the Joint Venture Strabag-Porr-Habau and began in spring 2016. The completion of the bridge and the expansion joint is scheduled for the second half of 2017.



Fig. 1: View of the bridge

2. INTEGRAL BRIDGES

Today integral bridges present the standard solution for road bridge structures with a total length of up to 60 m in straight geometry. Due to the low life cycle costs they are the

preferred solution by the authorities and therefore there is the tendency to extend the boundaries for integral (and semi-integral) bridges by using and developing special details (e.g. transition slab details, concrete hinges, elastic interfaces etc.) and applying sophisticated calculation methods (e.g. consideration of cracked concrete stiffness, detailed construction stage modelling).

One of the major concerns or limits for integral bridges on road networks presents the detailing of the abutment zone, especially on highways. In order to minimize the differential settlements behind the abutment wall, transition slabs are generally installed. For longer bridges also expansion joints in the road pavement are required. However, due to a large number of heavy vehicles on today's highways, the conventional expansion joints need to be frequently checked, maintained and also replaced.

Therefore, there is a strong initiative on developing maintenance-free road expansion joints or transitions nowadays. In the last couple of years multiple innovative road transition solutions were developed and executed in Austria, e.g. Oberwarter bridge with a rubber concrete transition slab (Geier et al 2017), A5.18 bridge with an anchored stretchable transition slab (IL-Mayer 2015) and the solution applied at the A5.24 Satzengraben.

3. ROAD EXPANSION JOINT

The bridge is equipped with a road expansion joint developed by the Technical University of Vienna (Kolleger & Eichwalder 2014). Below a short description of the system is given, detailed information can be found in (Eichwalder 2017).

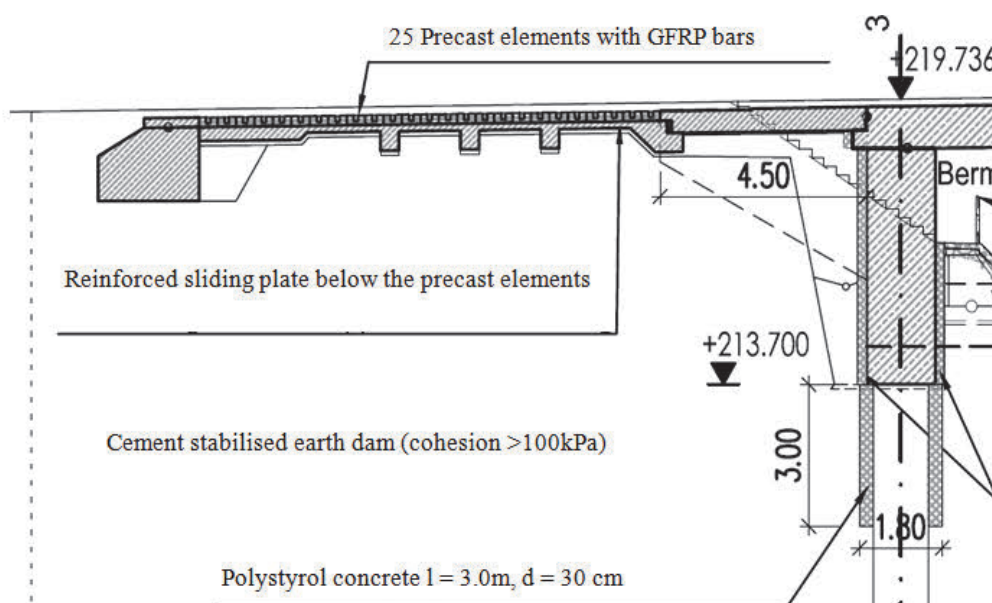


Fig. 2: Road expansion joint

The expansion joint consists of a transition slab, which is monolithically connected to the bridge superstructure; glass fibre bars, which are anchored in the transition slab and in the anchor block; precast elements which are placed between the transition slab and the anchor block and are fixed to the glass fibre bars. The precast elements slide on top of the sliding slab, which is monolithically connected to the anchor block. The anchor block is the fixed point, while the bridge is contracting or expanding. The longitudinal deformation of the bridge is equally distributed to the single gaps between the precast elements. That way the

relative movements between two precast elements are small enough to be resisted by the asphalt. Between the road pavement and the precast elements also a stress absorbing layer is placed to reduce the concentrated loading of the asphalt between the precast element gaps. Therefore the asphalt layer is continuous and should result in lower maintenance costs. The glass fibre bar stiffness results in axial tension forces in the superstructure of the bridge – approx. 4.5 MN, which had to be considered in the design of the bridge.

4. DESIGN OF THE BRIDGE

4.1. Structural Form

The structural form of the bridge was conceptualized together with Dipl.-Ing. Kleiser from the Austrian highway authority (Asfinag) in accordance with the principles stated in the articles (Kleiser 2016) and (Kleiser 2017). The wish was to create a subtle, robust and economic structure. The form and size of the structural elements should reflect the magnitude of forces they are transmitting. To visualize the continuous flow of forces any abrupt cross section and stiffness changes were tried to be avoided.



Fig. 3: View of the superstructure from below



Fig. 4: Detail of the abutment wall

In order to emphasize the integrity of the structure, the cross section of the superstructure was chosen as trapezoidal. The ratio of the span length of 24 m and the superstructure depth of 90 cm in midspan, as well as the 140 cm haunch at the supports, creates a slender appearance of the bridge. The slenderness of the piers is a compromise between the required horizontal stiffness for external loads (e.g. traffic braking) and flexibility to enable an “unconstrained” expansion and contraction of the bridge (temperature, shrinkage).

To visualize the reduced forces at the edges of the superstructure-abutment connection, the abutment wall below the superstructure cantilever is locally drawn in. According to the author’s opinion, the use of such subtle details to “break” the monotony of large flat surfaces contributes to the aesthetic value of the structure and creates an interesting play of light and shadow.

4.2. Foundations

The bridge is supported on pile foundations in all axes, with a maximal pile length of 28.5 m. Six piles reaching through the 15 m high earth dam to the load-bearing soil were executed at the abutment axes, while in the pier axes only four deep piles per axis were cast. For the design of the sub- and the superstructure of the bridge a variation of the soil parameter had to be considered. The mean geotechnical horizontal bedding of the piles was multiplied either by a factor of 2.0 or 0.5. Additional design considerations which are described in the following chapter were taken at the abutment zone.

4.3. Detailing of the Abutment Area

The detailing at the abutment area required a non-conventional solution due to large longitudinal bridge deformations. In order to achieve a decoupling of the abutment from the embankment, the abutment wall is covered with 20 cm of an elastic layer of EPS (Fig. 5) and the top 3 m of the piles are coated with a 30 cm thick elastic layer of polystyrene concrete (Fig. 7). The embankment with a slope of 1:1 has a height of approx. 15 m and is made of cement stabilized gravel. Therefore, any imposed deformation from the piles and the abutment wall due to bridge shortening (temperature and shrinkage), could destabilize the embankment dam, cause large constraining forces or loosen the earth dam behind the abutment wall.



Fig. 5: EPS on the back of the abutment wall

The required depth of the decoupling and the deformation capacity of the embankment were determined with a nonlinear soil-structure analysis (Fig. 6). The following considerations were taken at the abutment axes where the piles are embedded into the cement stabilised earth dam.

Since the dam is made of cement stabilised gravel, it was assumed that due to relatively large horizontal bridge movements, the soil will be compacted by the piles, after a certain number of summer/winter cycles. Therefore, two extreme cases were considered:

- Due to the compaction of the soil, the resistance gets higher – factor 2.0 considered.
- Due to the compaction of the soil, the pile is unsupported in the phases between maximal bridge expansion and contraction – zero horizontal bedding.

The mean horizontal bedding values were calculated with mean geotechnical parameters and with the use of a nonlinear soil-structure 2-dimension interaction model for the abutment area. The maximal horizontal displacement of the pile head was imposed (30 mm) and at every interaction spring, the horizontal reaction and displacement were recorded. On this basis an envelope of the elastic bedding, considered in the general design model, was determined. Additionally, also negative shaft friction had to be considered in the design of the piles since the earth dam had not completely consolidated at the time of pile construction.

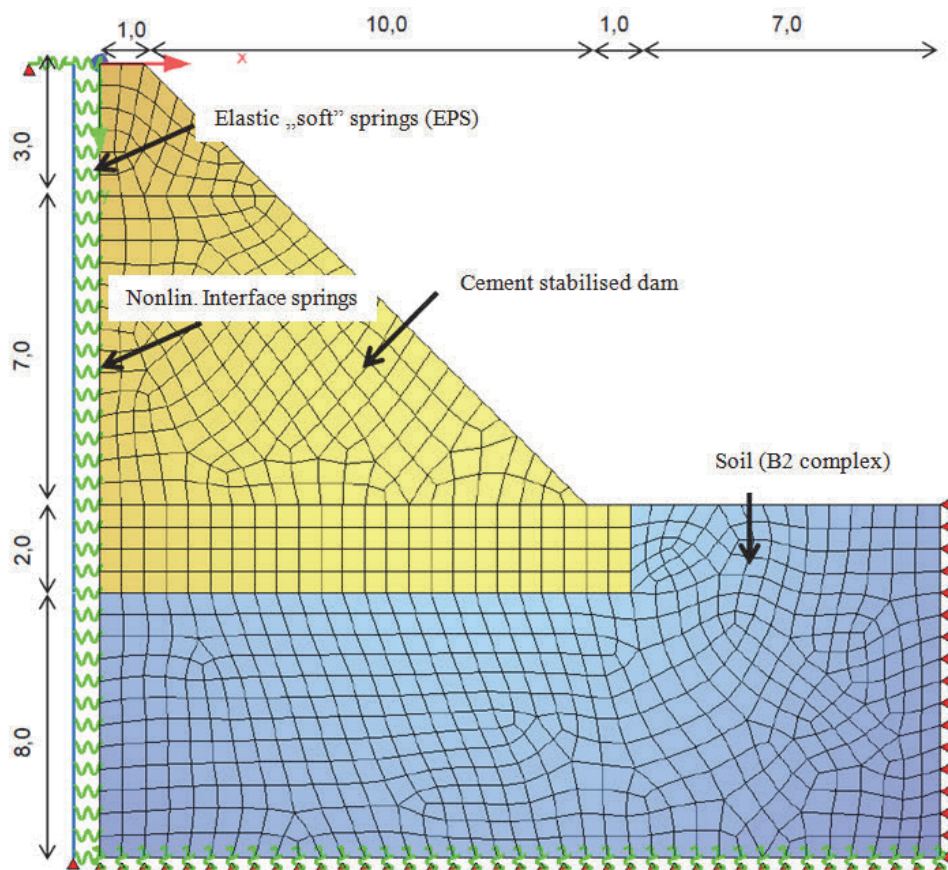


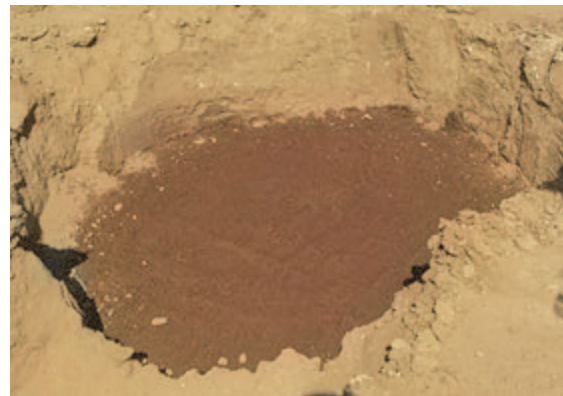
Fig. 6: 2D FE-model of the abutment area

The execution of the partial decoupling of the piles from the earth dam on the top 3 m was planned in the tender design with the use of EPS sheathing as executed at the Seitenhafen bridge in Vienna (Kral, 2012). However, in the detailed design phase, the construction company proposed a simpler solution for execution. In the first stage an approx. 3 m deep borehole with a diameter of 1.8 m was drilled and filled with a polystyrene granulate cement

mixture used for impact sound insulation. After the polystyrene filling hardened, a cased borehole with a diameter of 1.2 m was drilled through the polystyrene to the final depth of the piles and consequently the piles were cast (see Fig. 7).



Filling of the 1.8 m bore hole with the polystyrene granulate cement mixture



Filled bore-hole before the drilling of the piles



Executed piles – earth dam partly removed

Fig. 7: Execution of the piles at the abutment axis

5. CONSTRUCTION

The superstructure of the bridge was erected in 5 construction phases per lane. Due to the height of more than 15 m, the scaffolding with the formwork had to be fixed to the abutment wall or previous construction segment and to the piers, as it can be seen in the figure below. The slender piers (slenderness of $\lambda = 125$ in construction phase) had to be horizontally supported by auxiliary steel columns and struts.



Fig. 8: Temporary support of the scaffolding and formwork of the new superstructure segment on the previous superstructure segment (left) and piers (right)



Fig. 9: Construction phase

6. MONITORING

The average core temperature of the bridge at the moment of "closing" – connecting the bridge with the road expansion joint - is important for the functionality of the expansion joint and magnitude of the constraining forces in the bridge. Therefore, temperature sensors were installed in the superstructure of the bridge.

However, in order to record the performance of the road expansion joint, the structure will be monitored in the following three years of operation. The monitoring is performed by VCE ZT and includes the following monitoring instruments:

- Air temperature sensors.
- Multiple temperature sensors in the superstructure (in three sections, in multiple points over the depth of the deck) and in the abutment.
- Extensometers at every road expansion joint to measure the total extension between the anchor block and the abutment wall.
- Laser sensors to measure the distance between the abutment walls of the bridge.
- Combi-sensors in the asphalt layers for measuring the temperature and strain.
- Fibre-optical strain sensors between the precast elements of the road expansion joint to measure the opening of the gaps between the precast elements.

7. CONCLUSIONS

In the past few decades, many integral bridges were built on the road and railway networks. The positive experience gained with this type of bridge structures encouraged authorities, researchers and designers to develop new solutions and push the boundaries of long integral bridges.

The A5.24 bridge over the Satzengraben with a length of 112 m, equipped with an innovative road expansion joint, is a pilot project setting a step towards maintenance free road expansion

joints on long road bridges. Based on the monitoring results, the actual behaviour of the road expansion joint, the road pavement and the bridge structure new experience will be gained in the following years. This experience will serve as guidance and as a stimulus for further development of integral bridges.

Below the companies involved in the design and realisation of the bridge are listed:

Principal authority:	ASFINAG Bau Management GmbH
Development of the road exp. joint:	Technical University of Vienna – Institute of Structural Engineering and Institute of Transportation
Construction:	Strabag – Porr - Habau JV
Project management:	IGP ZT GmbH
Designer:	FCP ZT GmbH
Design supervision:	KMP ZT GmbH
Site supervision:	IBK ZT GmbH, SPP ZT GmbH
Monitoring:	VCE ZT GmbH

8. REFERENCES

- Eichwalder, B. (2017), “Jointless roadway transition structure for long integral abutment bridges”, doctoral thesis, TU Wien, 2017
- Geier, R. et al (2017), “Integrale Brücken: Entwurf, Berchnung, Ausführung, Monitoring”, Ernst & Sohn, 2017
- IL-Mayer ZT GmbH (2015), “A5 Nordautobahn Ausführungsplanung A5.18”, 2015
- Kleiser, M. (2016), “Form logic at bridges (Part 1) – Considerations on authentic shaping of integral bridge ends”, Bautechnik 2/2016, February 2016
- Kleiser, M. (2017), “Form logic at bridges (Part 2) – Considerations on authentic shaping of jointless column connections”, Bautechnik 2/2017, February 2017
- Kollegger, J. and Eichwalder, B. (2016), “Road expansion joint, applicant: TU Wien, application date: 2014-02-10, granted: 2016-11-16, European patent Nr: EP 2959060”, November 2016
- Kral, H. et al (2012), “Die Seitenhafenbrücke in Wien: Ein Innovationsschritt im integralen Brückenbau”, Beton- und Stahlbetonbau 3/2012, March 2012

MODULUS OF ELASTICITY – SPECIFICATION, ACCEPTANCE CRITERIA AND INFLUENCE ON STRUCTURAL PERFORMANCE

Jan L. Vitek¹, Robert Coufal², Jiří Kolísko³, Radek Vašátko⁴

¹Metrostav, a.s. and Fac. of Civil Engrg. CTU in Prague, Czechhia

²TBG – Metrostav, s.r.o., Prague, Czechhia

³Klokner Institue, CTU in Prague, Czechhia

⁴Faculty of Civil Engrg. CTU in Prague, Czechhia

SUMMARY

Modulus of elasticity of concrete is an important design parameter. It determines the relation between internal forces and deformations, which is important for structural behaviour of concrete structures. Design codes provide only a mean value of the modulus. Significant variability of the modulus is described and the reasons are explained. At some structures, the elastic modulus of concrete has to be specified. Proposed acceptance criteria regard the natural variability of the modulus and simultaneously allow for a reasonable production. The effect of the modulus on deflections of reinforced and prestressed concrete elements is analysed.

1. INTRODUCTION

Modulus of the elasticity is a parameter influencing not only deformations of concrete structures, but also the distribution of internal forces in the structural system. Until recently the modulus was a parameter which was significantly influenced almost only by the concrete strength. The progress in concrete technology made it possible to achieve much larger variety of the modulus of elasticity than it was usual earlier. The concrete strength is not any more a guarantee of a certain range of the modulus of elasticity. Relatively large strength of concrete can be achieved, while the modulus remains rather low. This situation is not regarded in design codes, where the direct dependence of concrete strength and modulus of elasticity is still accepted. No guidelines for specification of modulus of elasticity were published and also any acceptance criteria of the modulus of elasticity do not exist on an international or European level. If a specific value of the modulus is required, the control system checking if it was really achieved is not available. Additionally the excessive deflections of reinforced concrete slabs tend to be justified by low value of the elastic modulus. The example shown here should explain the significance of elastic modulus in deflection analysis. The Czech concrete society analysed this problem and developed a brief document (Vitek et al. 2016), where the scatter of the elastic modulus was discussed and the rules for its specification and acceptance criteria were proposed. In the paper the main ideas of this document are presented. The effect of the modulus on deflection is shown on the example of reinforced and prestressed structure.

2. MODULUS OF ELASTICITY IN STRUCTURAL ANALYSIS

Modulus of elasticity (E-value) defines relation between stress and strain of concrete. In a structural analysis, the assumption of linearity is generally accepted. In a great majority of structures the distribution of internal forces in structural systems is a result of linear analysis in both, ultimate (ULS) and serviceability (SLS) limit states. Later in verification of ULS criteria, the assumption of plasticity is accepted and in verification of SLS cracking is taken

into account. The modulus is therefore an essential value for specification of internal forces. The design codes provide usually only one value of the modulus, which is a mean value. No additional criteria are given for variability of the modulus, with exception of its dependence on the aggregate type e.g. (*fib*, 2013). The modulus of elasticity is defined either as a secant modulus or as a tangent modulus (in dependence on the design code), at a compressive stress level approximately about 0.4 of the mean concrete strength.

At statically determinate structures, the deformations (deflections) are directly dependent on the modulus of elasticity. The internal forces are determined from the conditions of equilibrium and are independent on the modulus of elasticity. At statically indeterminate structures, the both, internal forces and deformations are dependent on the modulus. If only one value of the modulus is defined, it is assumed as a mean value (E_{cm}), e.g. in contrary to the strength, where characteristic and design values are defined. The deviations are not considered according to the existing codes, although they may become important for internal forces and deformation distribution in structural systems. It is important to note, that higher as well as lower value of the modulus may result in unfavourable behaviour of structures. If the modulus is low, the deformations become higher, or the distribution of internal forces may differ from the expected one at non-homogeneous structural systems. If the modulus is high, then the internal forces in systems loaded by imposed deformation are higher than those when the modulus would be lower. This may be a reason for cracking of structures, where higher strength of concrete than originally assumed was used. The role of the modulus is especially important at prestressed structures, where full section is active. Prestressed structures are used for large spans and the value of the modulus of concrete is extremely important for their deflections. Therefore at such important structures it is necessary to specify the modulus of elasticity of concrete in advance so that its actual value would be in accordance with the assumptions of the design calculations.

3. VARIABILITY OF THE MODULUS OF ELASTICITY

Concrete used several decades ago was a mix of aggregate, cement and water. No chemical admixtures and other ingredients were used. The modulus of elasticity and concrete strength were in some relation which is until now used in some design codes. However, during last three decades the composition of concrete changed significantly. Due to application of chemical admixtures (superplasticizers, stabilizers, admixtures for acceleration or delay of hardening, etc.) and due to replacement of a part of aggregate by other constituents (silica fume, flying ash, blast furnace slag, fine stone powder, etc.), the variability of concretes available on the market increased extremely, a value of the modulus may vary more significantly and a relation between strength and modulus of elasticity may be also very different in comparison with a long term experience.

The modulus of elasticity is most often measured on laboratory specimens – cylinders or prisms. There are codes which describe exactly the procedure of testing (ISO 1920-10 or EN 12390-13). The principle of testing is similar, although there are some differences. The specimen is subjected to the prescribed loading process and then the strain under different stress is measured. From the strain and stress increment the elastic modulus is calculated using a Hook's law. The upper loading level is about 30% of the ultimate load which is specified on the basis of the loading test of the specimen cast from the same batch of concrete. There are also other methods, e.g. ultrasonic, which may be suitable for determination of the modulus in existing structures.

The variability of measured values of the modulus has many reasons. Some of them are listed here:

- Method of testing (static, dynamic...)
- Origin of the specimen (cast element, drilled core)
- Shape and size of the specimen (prism, cylinder)
- Arrangement of the ends of the specimen (at cylinders, the surface may be cut, smoothed by a sulphur mortar or some softer elements are placed between the cylinder and the testing machine)
- Influence of the measuring device (measuring gauges)
- Accuracy of the centric loading (avoidance of eccentricity)
- Influence of the upper level of loading
- Velocity of loading process

Some of the items listed above are strongly influenced by persons doing the tests. This is also one of the reasons, why different results may be obtained if the identical specimens are tested in different laboratories.

The variability of the modulus is determined by both, natural variability of material properties and by testing procedures. It is important to take these phenomena into account when designing the structure and decide on the necessity of specification of the modulus and also on site measurements at structures sensitive to deflections, like e.g. cantilever casting of prestressed concrete bridges.

4. MODULUS OF ELASTICITY IN DEPENDENCE ON THE STRENGTH CLASS OF CONCRETE

Variability of the modulus mentioned in the previous section is important for determination of the scatter of the modulus, when an actual production of concrete is considered. The measured moduli at the tests carried out during the production of concrete in different mixing plants were collected and evaluated. Only one diagram is possible to show here (Fig. 1).

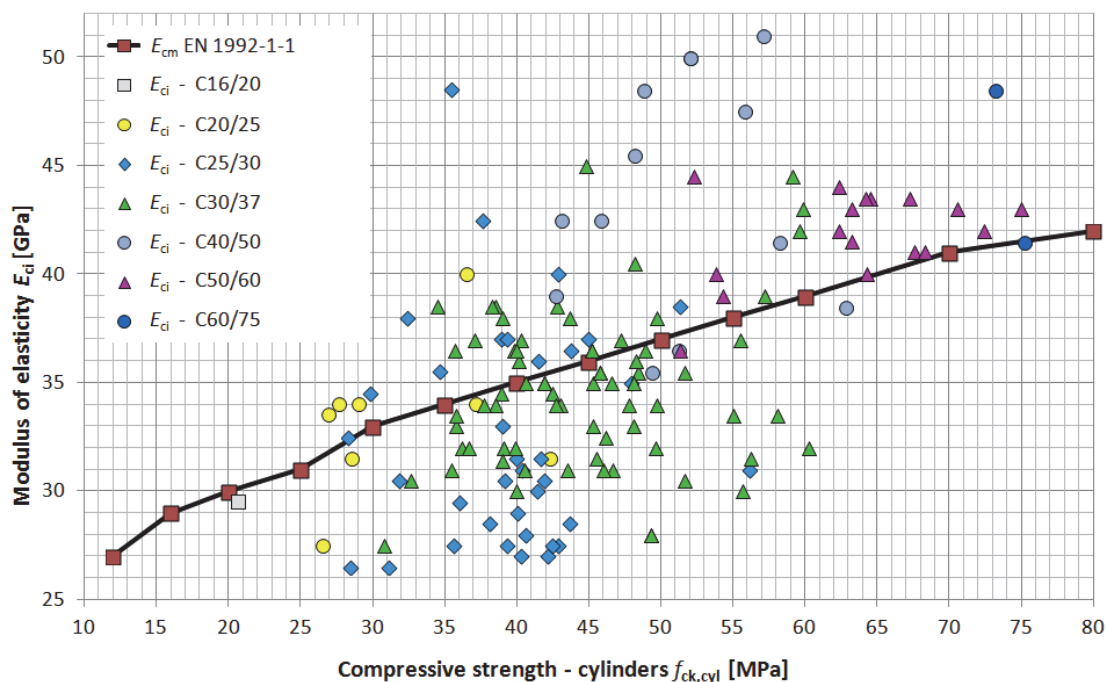


Fig. 1: Measured values of the modulus of elasticity (actual production)

From the diagram the conclusions may be drawn: The measured strength of concrete is higher than that required by the concrete class. It is a natural protection of producers against possible unfavourable test results. The variability of the modulus is extremely high, some values are significantly lower and some higher than the assumption of the design code.

If the production only from one producer and tests from one laboratory were evaluated, the scatter was lower, but still very significant. A long term production of one specific concrete is influenced by variable properties of constituents (cement, aggregate, additional constituents) delivered to the plant during a time period, which makes it impossible to reduce the scatter of the modulus significantly. The variability of the modulus measured on small specimens, does not completely correspond to the variability of the behaviour of a large structure. At important structures it is necessary to check their deformability using measurements on the site and to calculate the representative value of the modulus from the behaviour of the entire structural element.

5. SPECIFICATION AND ACCEPTANCE CRITERIA

At some structures – where the designer is convinced that the value of the modulus of elasticity is important for the structural performance (e.g. prestressed structures) – he may specify the modulus in the concrete specification. It is assumed that the specified value will be a mean value of the modulus. If any value is required, it has to be also checked. According to the document (Vitek et al. 2016), the checking procedure should guarantee that the modulus will not be too low. It was also considered that the procedure which would require satisfying also an upper limit would be too complex. The risk that the modulus will be too high is smaller and it is also assumed that the technologists, who will design the concrete mix are experienced, and will try to approach the specified value as closely as possible. It is also assumed that the designer will specify a reasonable value of the modulus, which is realistic and can be achieved for the designed concrete strength (strength class of concrete). It is recommended that the designer should closely cooperate with the technologist when specifying the concrete properties.

The acceptance criteria were defined separately for initial tests (acceptance tests), before the concrete is approved for application, and for checking tests executed during the concrete production and delivering on site or used in production of precast elements. The acceptance criteria were determined on the basis of evaluation of a large set of measured results collected by the Association of concrete producers. It is expected that the acceptance criteria will help to keep the modulus reasonably close to the assumed values, but contemporarily they will not make the concrete production impossible.

5.1 Acceptance criteria for initial tests

The mean value of the elastic modulus obtained from initial tests (E_{cap}) has to be larger than the specified value plus 1 GPa:

$$E_{cap} > E_{cm} + 1 \quad [GPa]$$

where E_{cm} is a specified mean value of the elastic modulus. The individual value of the measured modulus (E_{ci}) should not be lower than the specified value minus 3 GPa.

$$E_{ci} > E_{cm} - 3 \quad [GPa]$$

If these criteria are satisfied, it may be expected that the concrete will be acceptable for applications where the modulus plays an important role.

5.2 Acceptance criteria for checking tests during production

Checking tests are executed during the production and they should guarantee the stability of a production without any significant deviations. The frequency of checking tests is dependent on the specific structure and should be prescribed in the site documents. Usually the tests are executed after production of every 500 m³ of concrete or at least once in a month.

The acceptance criteria are defined in dependence on the total number of tests (n) which are at the moment available. The average values for acceptance criteria are calculated as an average value from last:

- 3 results of checking tests (E_{ca3}), if the total number of tests (n) is $n \leq 6$,
- 5 results of checking tests (E_{ca5}), if the total number of tests (n) is in the interval ($6 < n < 20$)
- 10 results of checking tests (E_{ca10}), if the total number of tests (n) is $n \geq 20$.

Regarding a relatively large scatter of the elastic modulus obtained from the checking tests there is a criterion for an average value (E_{cai}) and a criterion for a minimum acceptable individual value (E_{ci}). The acceptance criteria are then following:

$$E_{cai} \geq E_{cm} ,$$

$$E_{ci} \geq E_{cm} - 4 \text{ [GPa]}$$

where E_{cai} is an average value calculated from 3 to 10 last test results and E_{ci} is the lowest value measured during the last 3 to 10 tests.

The procedure is illustrated in Fig. 2. The blue line (empty squares) shows the measured values. The black full horizontal line designates the specified value of the elastic modulus. The dashed line designates the lower limit; no measured value should drop under this limit. The yellow line (large squares), green line (triangles) and red line (circles) show the average values when the number of tests is growing from 6 to 29.

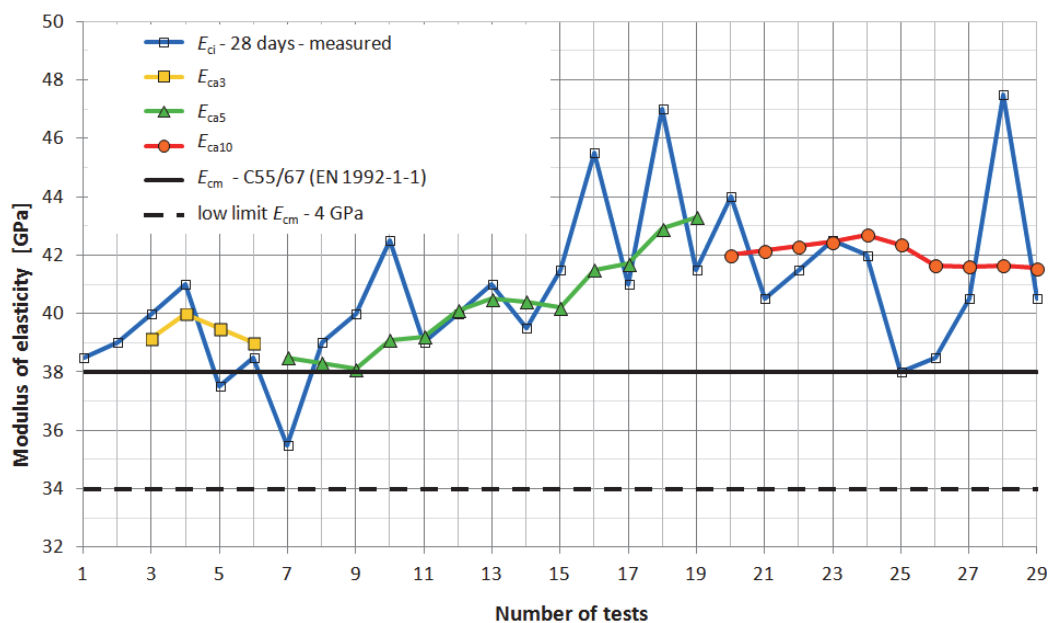


Fig. 2: Results of the checking tests and acceptance criteria

The damping effect of the averaging process may be clearly seen, which makes the acceptance criteria reasonable, since the elastic modulus influences the overall behaviour of the structure in contrary to the strength which may reduce the ultimate loading capacity locally.

6. EXAMPLE OF THE INFLUENCE OF THE MODULUS OF ELASTICITY ON DEFLECTIONS

6.1 Reinforced concrete slab

There are sometimes opinions, that a low value of the elastic modulus may significantly influence deflections of reinforced concrete structures. The following example should illustrate an actual situation. Let's assume a simply supported slab 200 mm thick, with the span of 4.8 m. The slab is made of concrete C30/37. Concrete cover is 30 mm and the slab is reinforced by bars of the profile 16 mm at the distance of 150 mm. The reinforcement ratio is 0.83 which corresponds to the small thickness of the slab. The applied load is 5 kN/m².

First a deterministic analysis was carried out. Modulus of 32.8 GPa was assumed according to the Eurocode. A simple analysis was carried out in two alternatives. a) Deflection analysis under the assumption that no cracks develop. This is an unrealistic assumption; however this analysis is a part of many commercial software products. b) Deflection analysis including cracking and creep. The both analyses were executed twice, once using a modulus according to the Eurocode (32.8 GPa) and second using a reduced modulus lower by 4 GPa (28.8 GPa). This value was considered as a realistic reduction regarding the realistic statistical scatter of the modulus. Results are summarized in the Tab. 1.

Tab. 1: Deterministic analysis of the slab with usual and reduced modulus of elasticity (Full E = 32.8 GPa, Red. E = 28.8 GPa)

	Short-term deflection [mm]		Long-term deflection [mm]		Increase of deflection due to the reduction of the modulus [%]	
	Full E	Red. E	Full E	Red. E	Short-term	Long-term
Uncracked slab	3.01	3.41	8.18	9.13	13.21	11.60
Cracked slab	11.54	11.89	16.32	17.15	3.02	5.08

From the results, following conclusions may be drawn:

- Assumption of uncracked slab provides incorrect results, which is generally known. If cracking is taken into account the short-term deflection increases approximately 4 times, while the long-term deflection increases approximately twice.
- Effect of the lower value of the elastic modulus (here reduction of 4 GPa) has a rather small effect on the deflection. The short-term deflection increases by about 3%, the long term deflection increases by about 5%.
- The deflection is preferably dependent on cracking; the size of the modulus of elasticity has only a minor effect.

As a next step a statistical analysis taking into account variability of the modulus of elasticity and variability of the tensile strength was carried out. The slab which was analysed deterministically became now a subject of the statistical analysis. The slab was divided into 6

elements in the longitudinal direction. In each element the elastic modulus and the tensile strength of concrete were considered to be variable. The Latin Hypercube Sampling method was used. The three alternatives of the analysis were carried out. 1. The elastic modulus was variable, and the tensile strength was constant ($f_{ctm} = 2.9$ MPa). 2. The elastic modulus was constant ($E_c = 34.7$ GPa – mean value taken from a set of measured data) and the tensile strength was variable. 3. The elastic modulus and the tensile strength were variable. In the Tab. 2, statistical data of input parameters (mean value and coefficient of variation) and mean value and coefficient of variation of the calculated deflection are shown.

Tab. 2: Deflections and coefficients of variations (c.o.v.) calculated with variable and constant elastic modulus and tensile strength of concrete.

	Elastic modulus E_c		Tensile strength f_{ctm}		Short-term defl.		Long-term defl.	
	mean v.	c.o.v.	mean v.	c.o.v.	mean v.	c.o.v.	mean v.	c.o.v.
	[GPa]	[%]	[MPa]	[%]	[mm]	[%]	[mm]	[%]
Variable E_c	34.7	10.33	2.90	0	11.43	0.96	16.06	1.63
Variable f_{ctm}	34.7	0	2.90	15.52	11.22	4.53	15.83	3.08
Variable E_c, f_{ctm}	34.7	10.33	2.90	15.52	11.24	4.16	15.88	2.71

The mean value of the modulus of elasticity and its coefficient of variation were obtained from a set of 70 measured values. The tensile strength and its coefficient of variation were assumed according to the Eurocode 2. The results again clearly show that the effect of variable elastic modulus is rather small. While the coefficient of variation of the modulus is 10%, the coefficient of variation of the short-term deflection is only 1% and coefficient of variation of the long-term deflection is only 1.6% (line 1 in the Tab. 2). The effect of variable tensile strength is more significant (line 2 in the Tab. 2).

The obtained results are also plotted in Fig. 3. The diagram shows the distribution of probability of short-term and long-term deflection and also the distribution of probability of variable input parameters – elastic modulus and tensile strength of concrete. It is clearly shown that the deflection, as an integral value has a significantly lower scatter than that of input parameters. It is also shown that the effect of variable modulus is rather low. However, it is necessary to note that these results are valid for a reinforced concrete element with cracks. The Fig. 3 also shows that the long term deflection has a very low scatter. It is a result of the used analysis with a limited number of variable parameters. The creep coefficient is assumed to be constant, which is not definitely the realistic case. If a variability of the creep coefficient was taken into account, much larger scatter would be obtained. The example is illustrative; a quantification of individual parameters is also dependent on the reinforcement ratio and may vary in individual cases. However, the general principles which reduce the variability of concrete properties (here variability of the E- value) due to the relatively strong steel reinforcement will remain valid generally.

6.1 Prestressed concrete elements

At prestressed elements a realistic loading (e.g. frequent combination) does not induce crack opening. It means that full section is under compression. If the bending stiffness is calculated, the effective parameters of the cross-sections are used. The entire area of the cross-section and n -multiple ($n = E_p/E_c$) of the cross-section of the prestressing (and reinforcing) steel are taken

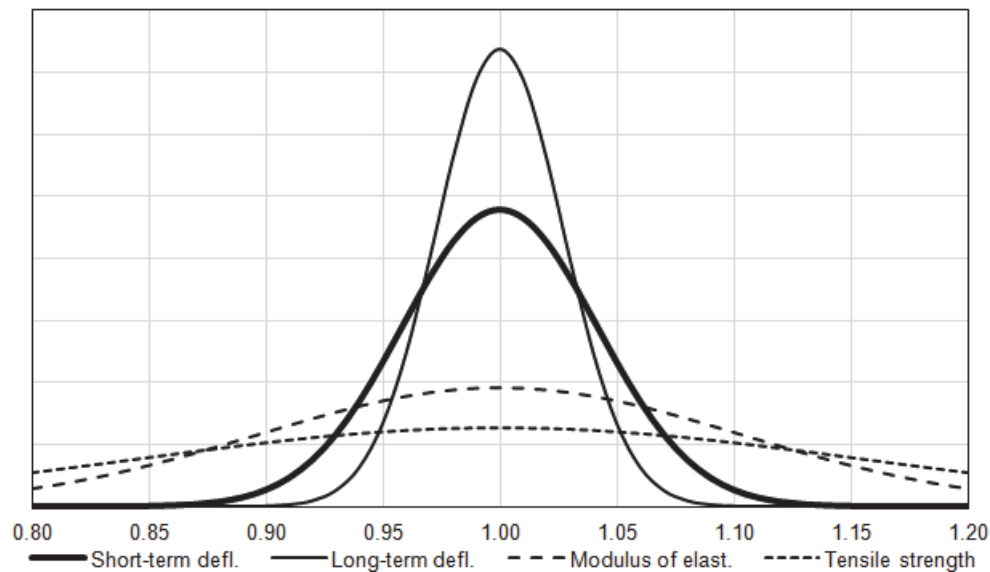


Fig. 3: Probability distribution of the short-term and long-term deflections in dependence on the scatter of the elastic modulus and of the tensile strength of concrete

into account. The reinforcement ratio of prestressed elements is much smaller than that of reinforced elements, since the strength of prestressing steel is much larger than the strength of reinforcing steel. The effect of steel reinforcement of deflections is therefore rather low. Due to the absence of cracking at prestressed structures, the deflection is calculated using the assumption of elasticity. If a simply supported beam loaded by a uniformly distributed load, the deflection may be calculated from a well-known simple formula

$$v = \frac{5}{384} \frac{ql^4}{E_c I_{eff}} \quad (1)$$

It may be clearly seen that the deflection is linearly dependent on the elastic modulus of concrete E_c . It means if there is a coefficient of variation of the elastic modulus about 10%, the deflection will have a similar value of its coefficient of variation (the effect of steel reinforcement, which is here hidden in I_{eff}), is rather small.

If a long-term deflection is calculated, then E_c in Eq. 1 is replaced in a simple analysis by deformation modulus $E_{def} = E_c / (1 + \varphi)$, where φ is a creep coefficient. A linear dependence on the E_c remains, which means that the long-term deflection suffers from approximately a similar scatter as that, which is observed at the elastic modulus E_c , (if a scatter of the creep coefficient is not taken into account). The deflections of prestressed structures are much more sensitive to the scatter of the elastic modulus than reinforced structures. The damping effect of strong reinforcement and cracking, which was observed at reinforced elements, is not applicable at prestressed elements.

7. CONCLUSIONS

Modulus of elasticity is an important parameter for structural performance of concrete structures. It has a significant statistical scatter. This scatter is a result: a) of the nature of concrete and of the developing variability of composition, and b) of testing methods, which are sensitive to many factors. The design codes provide only one (mean) value of the modulus. A variety of advanced compositions of concrete, which are now available, requires a

possibility to specify the value of the modulus for structures, if it is important for their correct structural behaviour. The specified modulus has to be also checked. The described criteria for initial and checking tests were proposed by the Czech concrete society. The examples shows that the influence of the variable modulus of elasticity has only a limited effect to the deflections of reinforced concrete structures, but its effect on deflections of prestressed structures is much more significant.

Acknowledgement

The results presented in the paper were partly achieved under the support of the Technological Agency of the Czech Republic (project no. TE 01020168 – research centre CESTI) and of the Grant Agency of the Czech Republic (project no. 16-04454S). Supports of both agencies are gratefully acknowledged.

8. REFERENCES

- fib* Model Code for Concrete Structures 2010 (2013), *fib*, Ernst und Sohn, 402 pages.
Vitek, J.L., Kolisko, J, Coufal, R., Huňka, P., Števíla, M. (2016), Modulus of elasticity. Technical rules of the Czech Concrete Society No. 5. Czech Concrete Society, 31 pages (in Czech).

CONSTRUCTION AND LOAD TEST OF CABLE-STAYED CONCRETE TRAM BRIDGE IN CRACOW

M. Salamak¹, P. Łaziński¹, A. Salachna²

¹ *Silesian University of Technology, Gliwice, Poland*

² *Mota-Engil Central Europe S.A., Kraków, Poland*

SUMMARY

The paper presents the structural solutions of the cable-stayed bridge along the Cracow Fast Tram (KST). The bridge consists of two separate sections - main extradosed bridge and access in the form of curved in plan cable-stayed structure. Due to its structural solutions, function, size and geometry, these are undoubtedly unique bridges across Europe. The paper discusses different construction technologies of both parts as well as range and results of static and dynamic load tests.

1. CRACOW FAST TRAM

Cracow Fast Tram (Polish: Krakowski Szybki Tramwaj, KST) is one of the examples of the so-called "premetro" or otherwise "light metro". Premetro is a tram line or light railway line that includes high-speed, collision-free connections, especially in city centers. Vehicle gauges and parameters of premetro's engineering structures fit to both tram and metro rolling stocks. Most often, these are specially separated tracks, tunnels and flyovers. Thanks to this, it is possible to turn this section into a real metro network in the future. Premetro is, therefore, something between tram and metro. It is characterised by higher than trams speed (from 24 km/h), more frequent departures during peak hours (3-6 min.) and closer locations of stops than metro languages can be recognized by its spatial, multidimensional objects with defined relations.



Fig. 1: Geometry of KST flyovers in plan

There are many examples of medium-sized cities in the world that decided to build premetro. These are: Volgograd in Russia, Porto in Portugal, Alicante in Spain, Rouen in France and Antwerp in Netherlands. In Poland, this type of communication is being developed mainly in Poznan and Cracow (Cracow Fast Tram). One line of this type is in Warsaw. There are plans to build premetro in Wroclaw and Szczecin. As it turns out, it was rare to transform premetro to a "real metro". So far, this has been the case in Stockholm, Frankfurt and Oslo while in Amsterdam both systems began to function in parallel.

The history of KST dates back to 1974 when the construction of the tunnel under the platforms of Central Station started. Back then it was being constructed with the idea of the first metro line in Cracow. However, only 180 m of this tunnel was built until 1989 and further works were ceased. After the economic transformation, the plans changed and the idea of expensive metro was abandoned in favour of the cheaper premetro. The tunnel was completed and connected to the new tram route as a high-speed tram. In 2015, the longest tram flyovers over Cracow's Plaszow railway station were put into operation. This allowed to connect the previously inaccessible districts in the area of Wielicka and Lipska streets with Rapid Agglomeration Rail: Wieliczka - Cracow Central Station - Cracow Airport.

2. GEOMETRICAL PARAMETERS OF KST BRIDGES

The entire new route connecting Wielicka and Lipska streets is almost 1.5 km long. The bridge consists of two separate structures: 469 m extradosed main flyover and 156 m cable-stayed access flyover. Retaining walls with a ramp for cycles and disabled people are between these two structures (Fig. 1). In addition to the double tram track, the flyovers carry the pedestrian and cycle traffic over the railway station. A wide cycle path with pedestrian walkway runs along the structure.

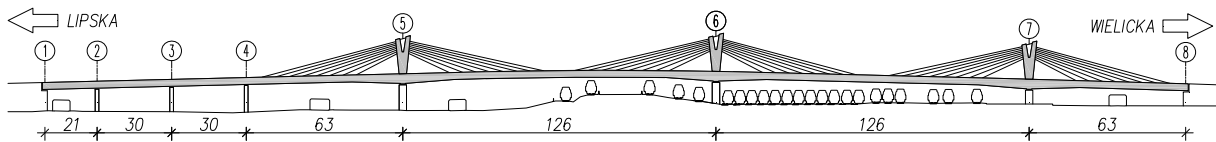


Fig. 2: Side view of the main extradosed bridge

The main bridge (Fig. 2) is a seven-span continuous structure with spans 4÷7 being prestressed with external cable stays (extradosed). The theoretical spans (in the axis of the viaduct) are: $21+2\times 30+63+2\times 126+63$ m. The total width of the bridge is 15.44 m and it increases to 17.30 m on the sections where two tramway platforms are located. There are two tram tracks running along the bridge and 2.5+2.0 m shared path for pedestrians and cyclists. There are balustrades along the outer edges of the flyover and anti-shock guards over the railway lines.

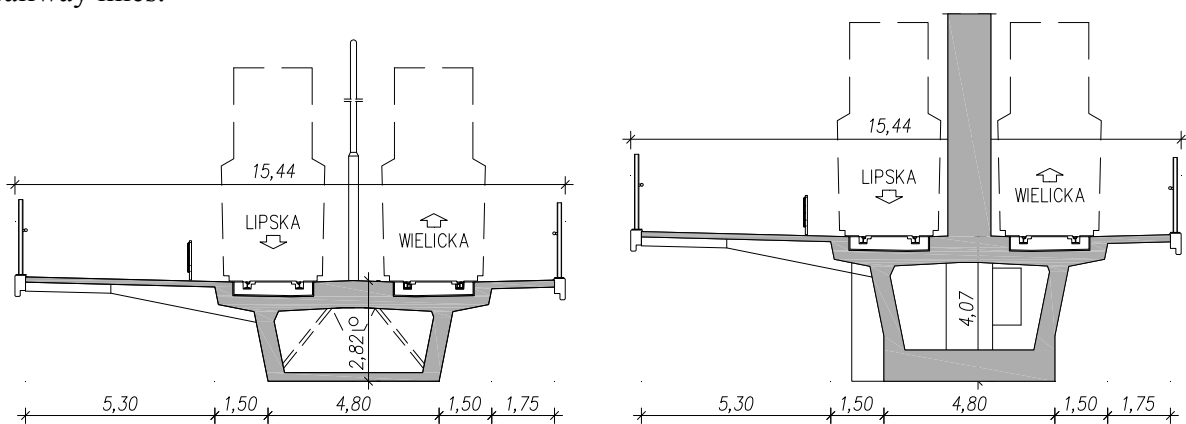


Fig. 3: Cross-section of the main bridge in span section and above the pylon

The pylons are columns with varying width (increasing with height), monolithically connected with the deck over the pillars. Pylons are deviators for external cables. The bridge is supported by pot bearings, two on each support. The bridge rests on reinforced concrete abutments and reinforced pillars. The supports 1÷4 have direct foundations, while supports 5÷8 CFA piles.

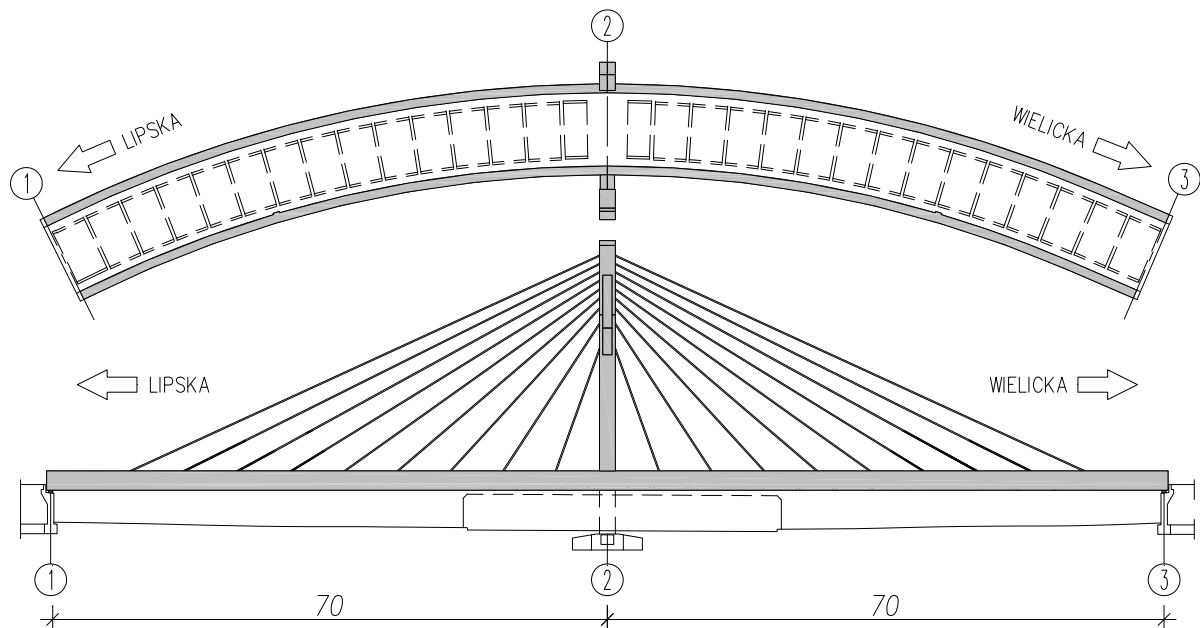


Fig. 4: Access flyover - top view and side view

The access flyover (Fig. 4) is a two-span, continuous, cable-stayed bridge made of prestressed concrete C50/60. The theoretical spans are 2×70 m. The route on the bridge runs in a horizontal arc with radius $R=140$ m. The supports of the bridge are perpendicular to the axis of the route on the object. The total width of the flyover is 11.4 m. The tram line consists of two tracks in axial spacing of 3.9 m. There are also 1.0 m sidewalks on both sides.

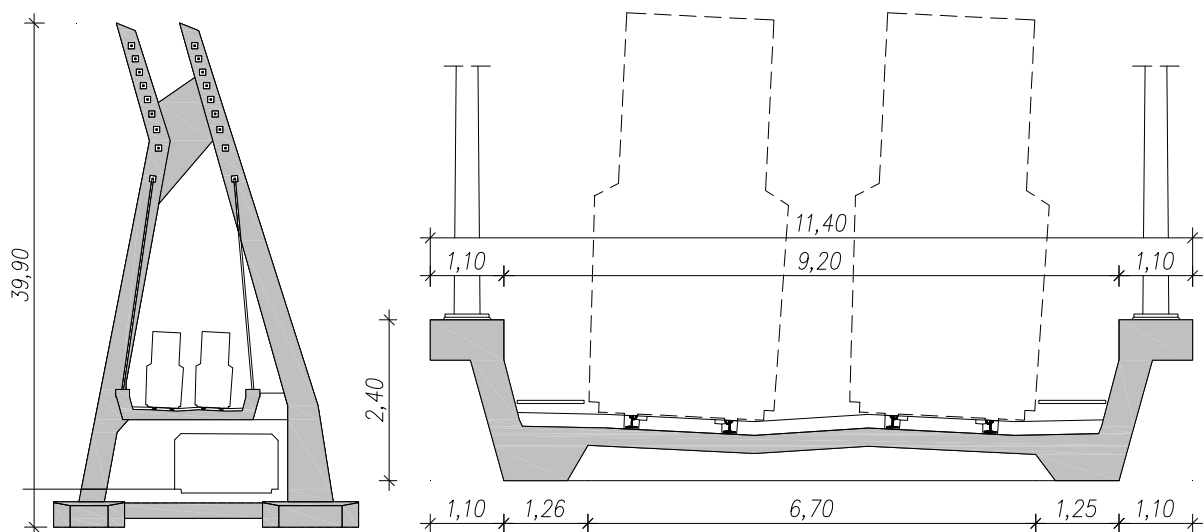


Fig. 5: Access flyover – cross-section

The deck is a concrete plate stiffened with transverse ribs, fixed in the lower part of external main beams (Fig. 5). The deck is suspended to the pylon by 36 cables, 18 for each span. The spans are supported on each of the abutments with two pot bearings. The pillar is a two-legged pylon on separate foundations. All supports are placed indirectly on 800 mm CFA piles.

3. TECHNOLOGY AND STAGES OF CONSTRUCTION

The major problem with the construction of the main flyover was to maintain rail traffic on 21 railway tracks (including 16 electrified) under the bridge being constructed. The same related to the streets on both sides of the station, but the involved difficulties were much smaller than the ones related to the railway. The proposed technology of cantilever concreting method with four travellers helped to ensure uninterrupted rail traffic and complete construction on time. In order to ensure the stability of the starting segments and pendulum, it was necessary to construct temporary supports in the area of supports no. 6 and 7. Fig. 6 shows the main construction stages of the main flyover. They included:

1. Construction of spans from supports no. 1 to 5 (with half of the next span) on stationary scaffolding. Concreting and prestressing of the key block in the area of support no. 4. At the same time, consecutive segments of pendulum from support no. 6 and 7 were concreted.
2. Deconstruction of scaffoldings under spans no. 4 and partly under span no. 5. Further concreting of pendulums from support no. 6 and 7.
3. After completion of the pendulum at the support no. 7, dismantling of two travellers and continuation of concreting of pendulum at the support no. 6.
4. Concreting of the key block in the span between supports no. 6 and 7.
5. Concreting of the key block in the span between supports no. 5 and 6.
6. Concreting of the end key block at the support no. 8.
7. Prestressing of internal (grip) continuity cables.
8. Disassembly of the remaining scaffolding and temporary supports.
9. Prestressing of external (non-grip) continuity cables.
10. Laying tram pavement and equipment elements. Cable tension adjustment.

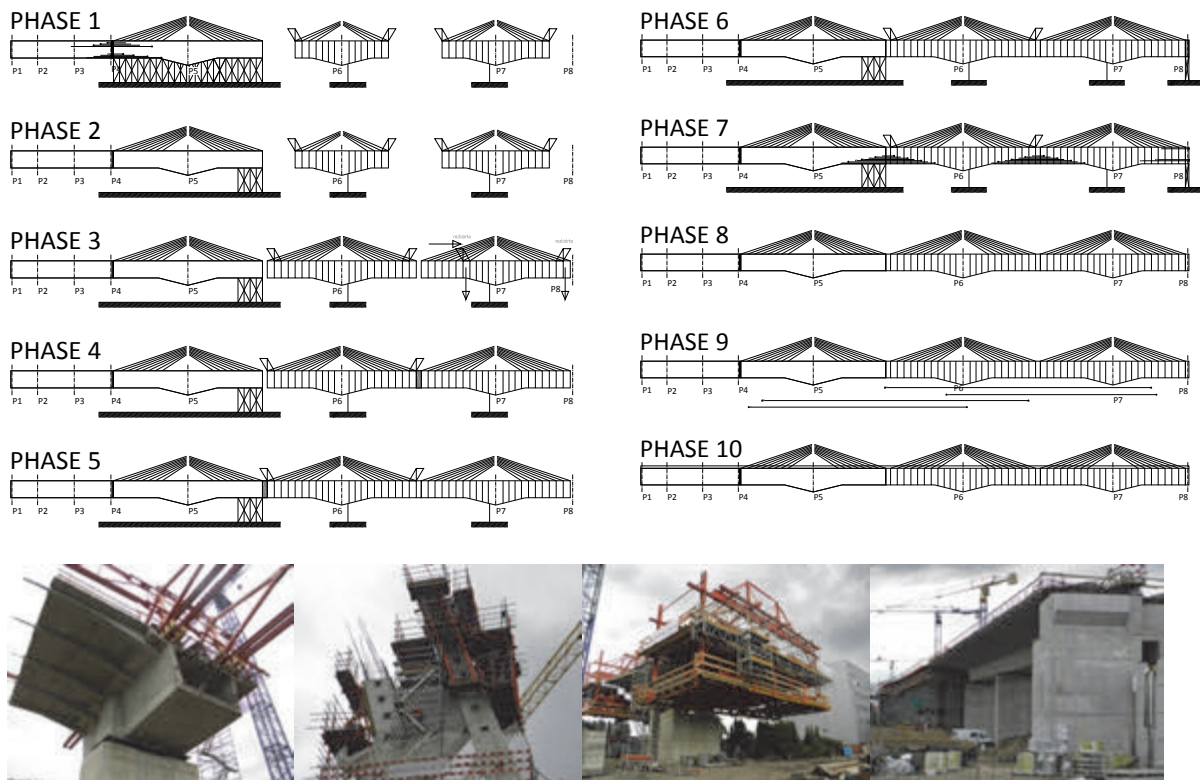


Fig. 6: Construction stages of the main bridge

The asymmetrical cross-section of the bridge with a long cantilever under the pavement and bicycle path was challenging to the contractor. It required a special transverse prestressing. Also, the necessity to connect the flyover with ramps forced the use of an unusual solution in the form of special continuity ramps. Large deformations of the bridge did not allow to use in this place standard expansion joints.

Almost each construction stage of the flyover had many technically complex and organisational aspects. At the construction site, the area was heavily urbanised and full of collisions in the underground infrastructure network. In the field of foundation and support works, the support no. 6 located between the tracks was particularly difficult. It was located in the area of active heating piping, which supplies the southern part of Cracow. Piling was done in winter from the ground level after the earlier protection of the heating piping and the reconstruction of its supports (Koris, 2011). The entire realization was conducted under strict control of the network owner, while the particularly dangerous works were conducted in the presence of MPEC Cracow employees. Any unsealing of active and operating heating piping due to temperature and water pressure could result in a catastrophe with serious consequences.

The access flyover is a demonstration of engineering skills of carpenters from Mota-Engil CE. The cable-stayed and curved flyover with a characteristic inclined pylon is certainly the only bridge of this type in Poland. The complicated shape enriches the architectural form of the bridge and fits into the surrounding industrial part of Cracow. Both flyovers are connected by 12 m high retaining wall. The retaining wall is closed with flyovers' abutments with both ends. This almost record high wall in the form of a "bath" also caused many construction problems.

4. BRIDGES LOAD TESTS

Load tests included static and dynamic parts (Fig. 7), which were conducted by accredited laboratory from the Silesian University of Technology (Łaziński, 2015), (Salamak, 2016), (Markocki, 2012). Due to work schedule and no connection to the track system outside the bridge, static tests were carried out with eight trucks loaded to a total weight of 32 t each. In exceptional cases, on both flyovers, vehicle traffic will be permitted for vehicles or buses, so these tests were almost necessary. In dynamic tests NGT-6 Bombardier trams were used, which mostly run on the tram line in the area.



Fig. 7: Static and dynamic tests

The computational models of both bridges (Fig. 8) were created using bar and panel elements of class (e1+2; p3). They took into account the variable geometry of the bridge and pylon as well as variable plate thickness and cables. Mechanical sensors and precise levelling were

used to measure the displacements under static load test. Vertical span displacements were measured with the use of traditional mechanical sensors and sensors with an electronic display with a range of 50 mm and a reading accuracy of 0.01 mm. Support settlements were observed using optical precise levelling instruments of Koni type with the reading accuracy of 0.1 mm. In addition to this, the deviation of the pylon was observed with the use of electronic tachymeter. Also, non-contact measurement of span deflection was used with the IBIS interferometer radar in places inaccessible due to train traffic (Owerko, 2012), (Kuras, 2012). This scope was realised in cooperation with dr Tomasz Owerko from AGH (University of Science and Technology, Cracow), which was possible thanks to joint comparative research conducted on many other bridges (Salamak, 2016).

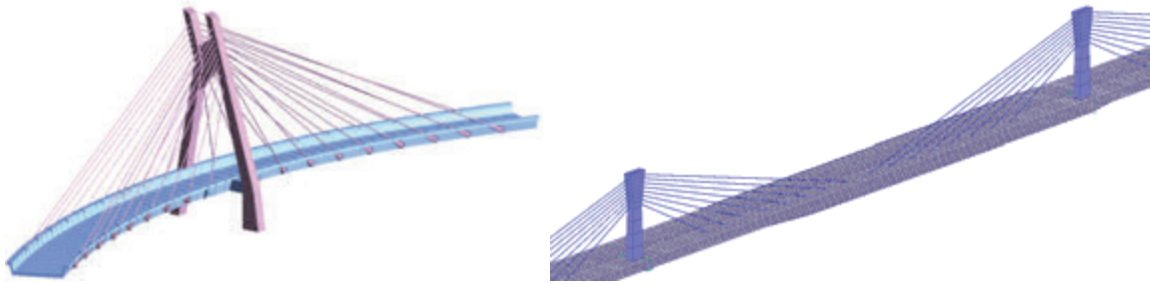


Fig. 8: Computational models consisting of both bridges

Results from dynamic tests were recorded electronically in the form of displacements and vertical accelerations during the tram passages. The speeds were 10, 30, and 50 km/h in both directions. The measuring set consisted of a notebook, LMS SCADAS recorder, measurement card National Instruments, displacement induction sensors (P) and accelerometers (A).

4.1. Load test of the main bridge

On the main bridge, four span schemes were realised (S1, S2, S3, S4) in spans no. 4 ÷ 7, which were selected based on the condition of the maximum span moment and support scheme (P1), selected from the condition of the maximum support moment at the support no. 6. Moreover, asymmetric scheme (N1) was also conducted in span no. 5 (Fig. 9) in order to verify the lateral work of the bridge.

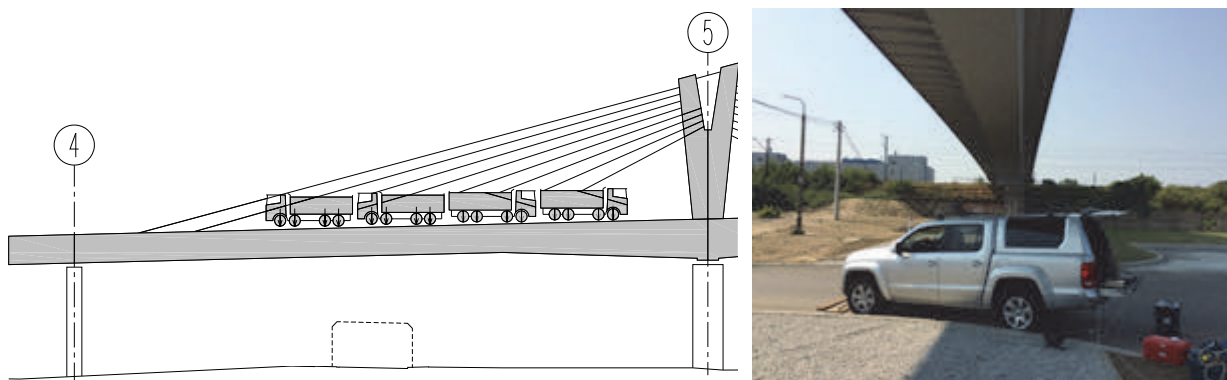


Fig. 9: Selected static scheme on the main bridge

On the basis of results obtained from the settlement measurement, it can be stated that all loaded supports are stable. Foundation settlements were uniform and did not exceed 0.3 mm. The elastic deflections of the bridge were smaller than the deflections calculated theoretically

and ranged from 73% to 87% of their theoretical values calculated for the standard modulus of elasticity. After taking into account the verified concrete age and type of used aggregate, the relationship was, on average, 90%. Such results prove a good stiffness of bridge spans and proper computational model, which gave the results on the safe side (Poprawa, 2016). This indicates also the correct theoretical load capacity. Permanent deflections ranged from 2% to 5% of total deflections and fulfilled the condition of not exceeding 10%. The analysis of results from asymmetrical scheme showed very good agreement of the actual torsional rigidity with the rigidity resulting from the assumed model.

Dynamic amplification factor (DAF) is defined here as the relationship of a maximum deflection at the next passage to the maximum deflection at the same measurement point at the quasi-static passage, i.e. speed of 10 km/h. DAF was determined each time for the entire cross-section, averaging the deflections of both webs. In this way, impact of lateral distribution was omitted (torsion of the box-girder bridge). In general, the flyover is characterised by low susceptibility to dynamic influences. DAF at measured points reached 1.04 and was lower than the standard dynamic factor of 1.10. The lowest identified vertical vibration frequency was 0.62 Hz and was slightly lower than the theoretical value (0.77 Hz). The corresponding damping was 3.85% (Salamak, 2007). The biggest measured accelerations were recorded during additional tests with the tram braking on the flyover. They were at a very low level of 0.15 m/s^2 .

4.2 Load test of the access bridge

Two span schemes (S1, S2), support scheme (P1) and asymmetrical scheme (N1) were conducted on the access bridge (Fig. 10). The largest support settlements were 0.35 mm, which indicates a sufficient stability of the foundation. Compliance of the measured and theoretical deflections was better than for the main flyover and ranged from 88% to 93%, while the permanent deflections did not exceed 2%. After taking into account the verified type of aggregate and the effect of concrete age on the modulus of elasticity, the relationship of theoretical to the measured deflections was, in average, equal to 98%. The torsional rigidity of the bridge was also well estimated, where the differences between the results from measurements and the model in asymmetric scheme were equal to 1%. The measurement of the pylon deviation in the same scheme gave the transverse displacement of the head of only 15 mm.

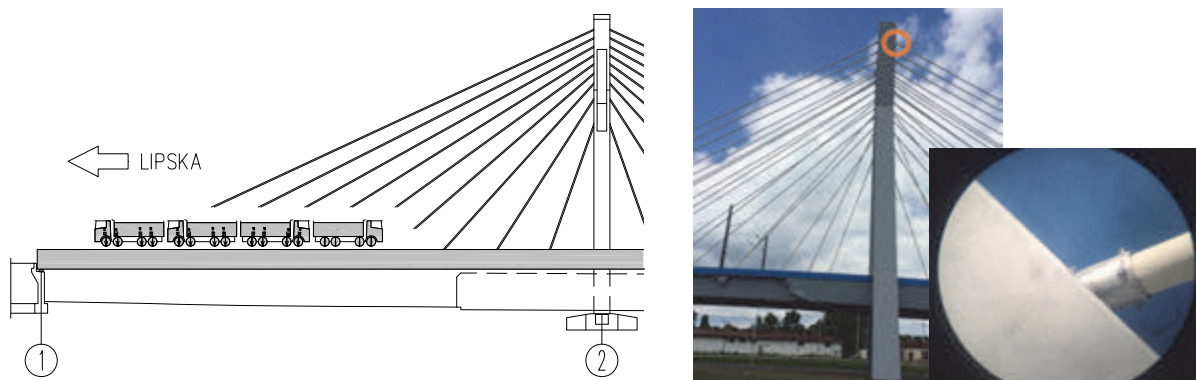


Fig. 10: The chosen scheme of static load of the access flyover

DAF was even lower than in the main flyover, however, due to the arc in plan and slope of the track, it was not possible to achieve a speed higher than 30 km/h. The lowest vertical vibration frequency was 1.05 Hz and was greater than the theoretical vibration (0.85 Hz).

Similar differences were observed in subsequent forms of vibration, which suggests to update the computational model and to correct dynamic parameters. The damping corresponding to the first mode shape was equal to 1.51% and was within the range of values identified for higher forms (from 1.25% to 2.58%). The acceleration was again the biggest in the braking test (0.09 m/s^2). In other cases, values were lower by more than half. It can be stated that the access bridge is also resistant to dynamic influences.

8. CONCLUSIONS

The construction of both bridges from the very beginning was a challenge from an engineering and organisational points of view. Due to the formula of the contract "optimize and build", some changes in the design were possible with the Owner's agreement. It mainly regarded the modifications, which could significantly facilitate the realisation of this extremely difficult investment. General contractor, Mota-Engil Central Europe, decided to construct the spans over the railway tracks with the cantilevered concreting technology. The other spans were constructed with the use of stationary scaffolding technology. Due to the strictly defined contractual time, it was necessary to prepare additional technological documentation, which took into account all modifications and planned exclusions of rail traffic on selected tracks. Thanks to properly organized work among the contractor and design office, the investment was successfully managed and without significant obstacles.

9. REFERENCES

- Koris K., Bódi I. (2011), "Analysis of load carrying capacity of prefabricated concrete pipes", Concrete Engineering for Excellence and Efficiency: fib Symposium Prague 2011, Czech Concrete Society, 2011, pp. 599-602.
- Kuras P., Owerko T., Ortyl Ł., Kocierz R., Sukta O., Pradelok S. (2012), "Advantages of radar interferometry for assessment of dynamic deformation of bridge", Bridge Maintenance, Safety, Management, Resilience and Sustainability: Proceedings of the Sixth International IABMAS Conference, Stresa. Lake Maggiore, 2012, s.885-891.
- Łaziński P., Salamak M. (2015), "Load test of extremely wide extradosed concrete bridge", 11th Central European Congress on Concrete Engineering CCC2015, Hainburg, 2015, pp.302-305.
- Markocki B., Salamak M. (2014), "Durability of stress ribbon bridge checked during load test", Journal of Civil Engineering and Architecture, Apr. 2014, Vol.8, No.4, pp.470-476.
- Miśkiewicz M., Pyrzowski Ł., Wilde K., Chróścielewski J. (2016), "Numerical analysis and in situ tests of the Grot Rowecki Bridge in Warsaw". Advances in Mechanics: Theoretical, Computational and Interdisciplinary Issues – Kleiber et al. (Eds), Taylor & Francis Group, London, 2016, pp. 405-408, DOI: 10.1201/b20057-87
- Owerko T., Ortyl Ł., Kocierz R., Kuras P., Salamak M. (2012), "Investigation of displacements of road bridges under load tests using radar interferometry - case study", Bridge Maintenance, Safety, Management, Resilience and Sustainability: Proceedings of the Sixth International IABMAS Conference, Stresa. Lake Maggiore, 2012, p.181-188.
- Poprawa G., Salamak M. (2016), "Historical Beam Bridge Model Identification after Changing its Structural System into an Arch", Procedia Engineering, 161(2016), pp.523-529.
- Salamak M. (2007), "Vibration damping identification maximizing adjustment to viscous model in civil structures", Archives of Civil Engineering, LIII-3, pp.497-518.
- Salamak M., Owerko T., Łaziński P. (2016), "Displacements of cable-stayed bridge measured with the use of traditional and modern techniques", Journal Architecture Civil Engineering Environment, 4/2016, pp.89-97.

EXAMPLES OF ADVANCED CONCRETE STRUCTURES IN CROATIA

Josip Galic¹, Ivan Klepo²

¹ University of Zagreb, Faculty of Architecture

Kaciceva 26, 10000 Zagreb, Croatia

² Radionica statike Ltd.

Kaciceva 22, 10000 Zagreb, Croatia

SUMMARY

This paper presents some of the high-rise buildings designed in recent years in Zagreb, Croatia. These buildings have been recognized and awarded as the best architectural solutions. Specialties in the design, calculation and construction of concrete load-bearing structures will be briefly presented for each building. Each building has a concrete load-bearing structure.

1. INTRODUCTION

The construction of high-rise buildings in Zagreb started in the 1950s. Oldest skyscraper in Zagreb is Ibler's residential skyscraper (51.0 m) built in 1958 and based on the project of architect D. Ibler. At the same time, the first business skyscraper Ilica 1 (66.5 m) was built on the central square in Zagreb. Architects were S. Jovičić, J. Hitila and I. Žuljević.



Fig. 1: First residential (left) and business (right) skyscraper in Zagreb (1958)

Afterwards, construction of a number of high-rise buildings was followed in Zagreb. A total of 15 business and residential skyscrapers were built in the period from 1968 to 1989. Tallest buildings in Zagreb built in the last century were business skyscrapers: Zagrepčanka (95 m) was built in 1976 and the last skyscraper built in the last century Cibona Tower (92 m) built in 1987.

War and the crisis in the 1990s suspended construction in Croatia and Zagreb in general and therefore also the construction of high-rise buildings. After emerging from a crisis following the Croatian War of Independence and almost 20 years after the last high-rise building was built, the construction of high-rise buildings was again actualized. As it is always with the construction of high-rise buildings, certain companies wanted to show business success and attract customers with attractiveness, hence only business towers were built. In the period from 2004 – 2011 five new business skyscrapers were built: the Hoto Business Tower (2004),

Zagrebtower (2006), Eurotower (2006), the Green Gold Tower (2011) and the Sky Office Tower (2011). For five more high-rise buildings architectural design competitions were conducted. With the coming of new crisis, none of the projects have been realized and in some way construction of high-rise building has again stopped. For the last two buildings construction time was extended due to the financing problems. Also, because of the financial difficulties, Sky Office Tower (81 m) was constructed with several stories less than initially designed. Three largest skyscrapers made from 2004 to 2011 are shown in Fig. 2.

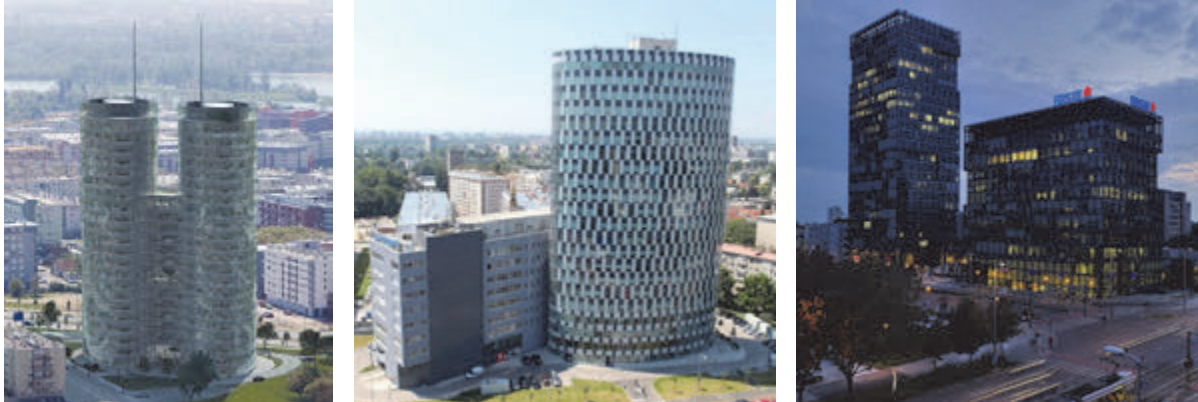


Fig. 2: Sky Office (81 m), Zagrebtower (82.5 m) and Eurotower (96 m)

The reason why even in the period of golden age of construction in Croatia from 2004 to 2009 the height of 100 m was not exceeded and why almost all skyscrapers height is equal to or less than Zagrepčanka skyscraper built in 1976 is the fact that in Zagreb, according to the urban development conditions, the construction of buildings of height over 100 m is not permitted. Also, all high-rise buildings in Croatia have a concrete load-bearing structure.

2. VMD CENTAR

However, in the crisis years with almost no activity in building construction in the period from end-2012 to mid-2015 VMD Center complex has been designed and constructed. Author was Davor Mateković from Proarh d.o.o. With the gross surface area of more than 60.000 m² and thanks to the height of one of its two towers (Tower B), the building represents the highest office building in Croatia, with 97.0 m above ground level height. Due to the aforementioned urban development conditions the height of the building does not exceed 100 m, although this height was later exceeded by the subsequent construction of the antenna column.



Fig. 3: VMD Center in Zagreb

The VMD Center is a business complex consisting of two towers (A and B) and 2 two-story buildings (E and F). Tower A has 17 stories and Tower B has 27 stories above ground level. Also, there are 4 basement stories underneath the entire complex. The VMD Center is business center with office spaces in the upper stories, while the basement stories accommodate garages and technical rooms.

Because of the crisis at that time, the investor requested that the buildings construction is carried out in phases. First phase would include the construction of basement stories with the two-story buildings. Second phase would include simultaneous construction of towers A and B or just the construction of tower A, depending on the possibility of financing. Another requirement was that the basement section, almost three stories in the ground water, is constructed without particular waterproofing system as a "white box". The third requirement was that each tower is built with only one core and one evacuation stairwell, with no fire protection sprinkler system. The fourth requirement was that the facades have only columns and beams of minimum height that fit into the lowered ceiling ($h_b \leq 50$ cm). Because of already constructed construction pit protection depth, problem concerning the thickness of foundation slab has subsequently arisen. The foundation slab could not be more than 200 cm thick. Due to all abovementioned requirements, the load-bearing structure was constructed as a concrete structure (Fig. 4).

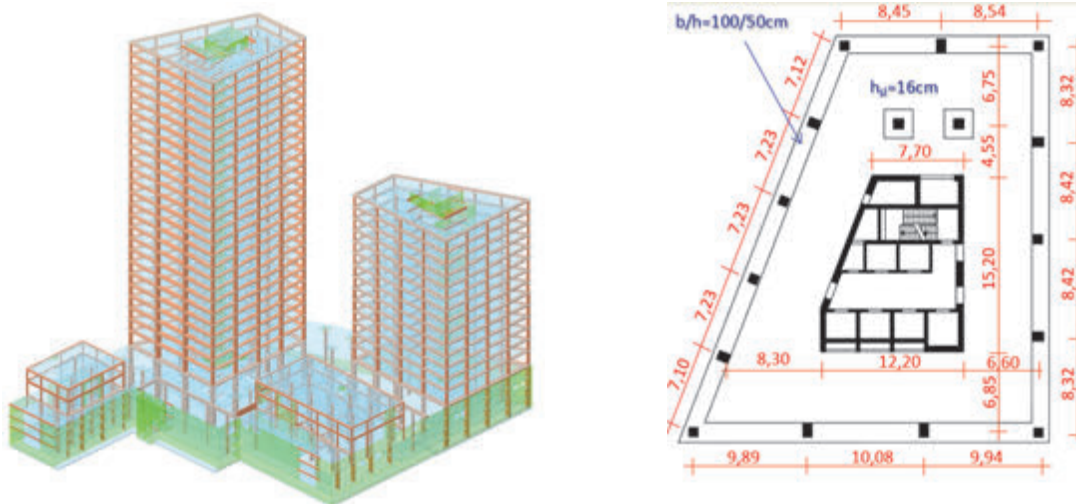


Fig. 4: 3D structural model of concrete load-bearing structure (left) and tower B typical floor plan (right)

Although because of the span itself it was not necessary, but in order to reduce weight and load on the foundation substructure, all floor slabs above ground level were constructed as in situ prestressed slabs supported on the core walls and the prestressed beams of peripheral frames. Slabs are 16 cm thick on the taller tower (tower B) and 18 cm thick on the lower tower (tower A). Pretensioning was carried out with cables without direct contact with concrete. BBR VT CMM 0106 system was used. Cable pattern and the appearance during construction are shown in Fig. 5. Ultimately, the cost of prestressed floor slabs was the same as it would be if they were constructed as reinforced concrete slabs, but 6 cm thicker. The floor slabs of the basement stories were constructed as reinforced concrete slabs directly supported on AB walls and columns. Thickness of the basement floor slabs is 28 cm, except the -1 floor slab, which is 40 cm.

The vertical structure is made of central core and the peripheral frames (Fig. 4). All horizontal forces (wind and seismic action) are transmitted by the core, which accounts for only 18% of

the floor surface ($A_{\text{floor}} \approx 1000 \text{ m}^2$). Peripheral frames transmit only the vertical load and additionally are preventing the torsion of the building. Since it is a high-rise building with a relatively small core, all the walls had to be connected with coupling beams to achieve the required stiffness and core resistance to seismic action ($a_g = 0.25g$, $q = 3.0$).

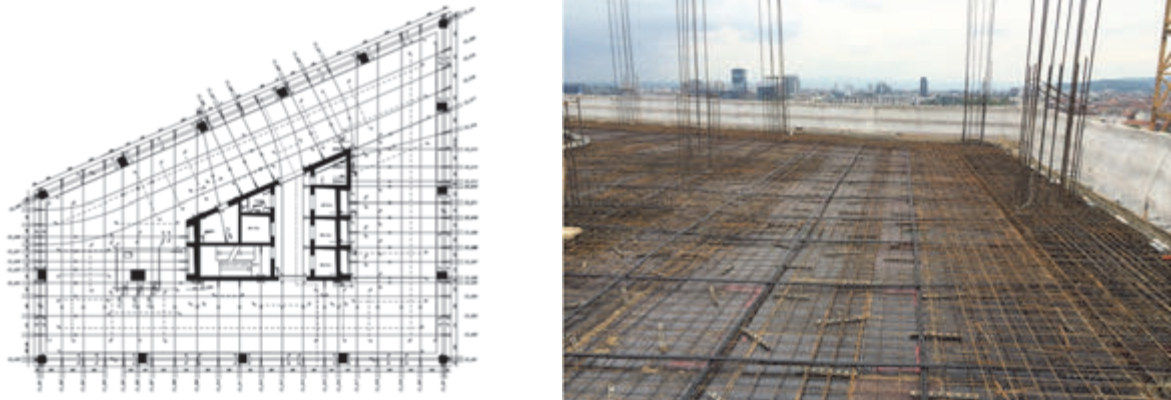


Fig. 5: Cable scheme and construction of above ground level prestressed floor slabs in tower B

Installation of diagonal reinforcement is required according to EN 1998-1 and as shown in Fig. 6a. It has been shown that required diagonal reinforcement cages are impossible to implement. Instead of closed transverse reinforcement around the diagonal reinforcement, an option to enclose entire coupling beams cross-section with transverse reinforcement was applied according to the ACI 318-08 solution as shown in Fig. 6b. In tower B, because of the large amount of required diagonal reinforcement, a solution was applied where diagonal steel plates with shear studs were fitted instead of a regular diagonal reinforcement bars. It proved practical and easy to implement (Fig. 7).

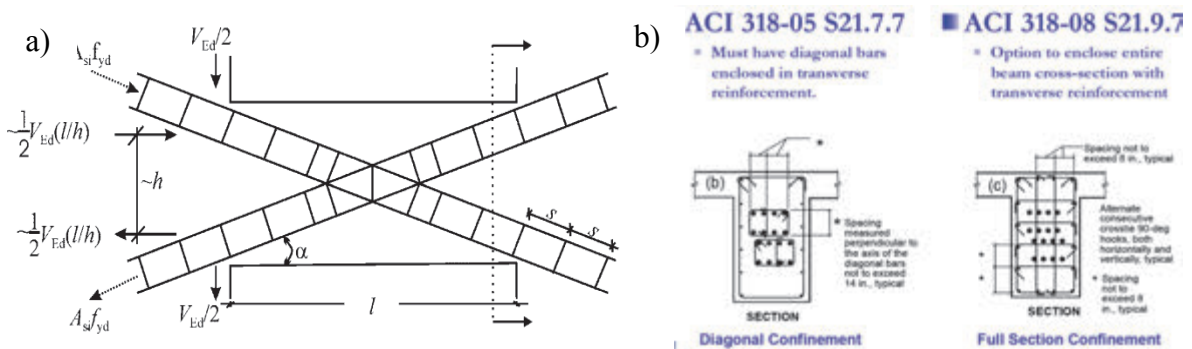


Fig. 6: Coupling beam with diagonal reinforcements



Fig. 7: Coupling beam with diagonal steel plates

Because of the groundwater risk, possible leakage due to differential settlements and the requirement for a singular garage as well as the inability to construct suitable walls in the basement stories, the both towers are designed to be fixed to the basement story. The result of this fixity is the "backstay effect" (Fig. 8). Due to the bending of the tall core fixated in the basement part, high shear forces are appearing in the basement stories. These forces are several times larger than the shear forces in the ground story walls. In the lower buildings shear forces in the ground story walls are usually the largest. Thus, basement stories core walls were necessary to be constructed thicker in relation to the upper core walls and it was necessary to reinforce them according to the capacity of upper part of the core. Also, the floor slabs behave as elastic supports of the core where the ground floor slab is the main backstay diaphragm. Further analysis also determined that by separating the core from the basement floor slabs below the ground floor slab in order to increase the lever arm to the height from the foundation to the ground floor slab, no significant reduction in transverse forces in the core walls nor the reduction of the shear and tensile forces in the main backstay diaphragm is achieved.

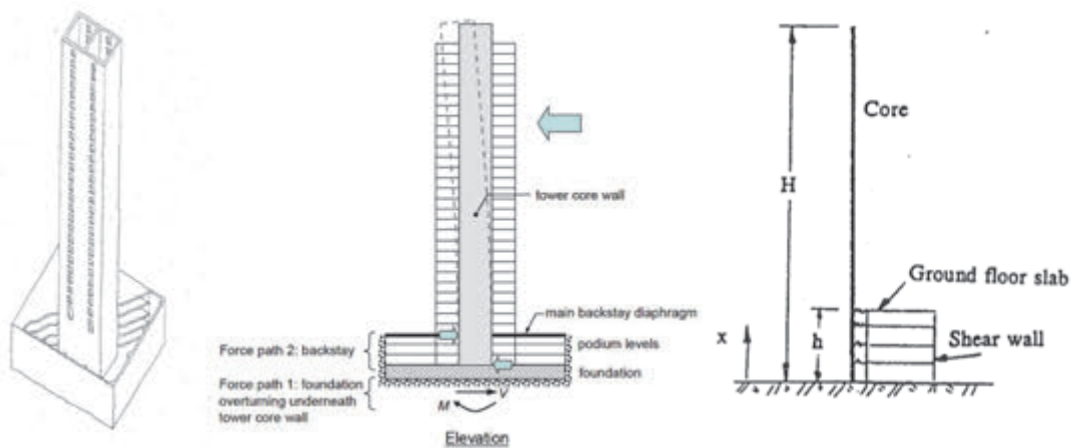


Fig. 8: Backstay effect

Because of all that was mentioned above, tower core walls in the basement stories are thicker than the ground story core walls and were almost twice more reinforced with a transverse reinforcement than the ground story core walls. Besides that, it was also necessary to install diagonal reinforcement in the walls where they are connected with the ground floor slab. Also, due to the unfavorable position of tower B (Fig. 9), it was necessary to transmit large "brake" seismic forces with the core. Original plan was to accept the forces with prestressing. However, earthquake is an alternating action and a problem with the pressure stresses and insufficient thickness of the slabs has appeared. Hence, the structure was designed in such way that the forces are accepted by reinforced concrete.



Fig. 9: Tower B layout, diagonal reinforcement of the walls and ground floor slab reinforcement

Final problem with designing and construction of the building was the foundation work. The foundation was designed as the slab foundation with variable foundation slab thickness depending on the load. Because of the phased construction and high groundwater level, part of the foundation slab had the problem with the uplifting and other part had a problem with large soil settlements and stresses. Therefore, soil improvement with compression – pressure CFA piles on a regular spacing was implemented (Fig 10).

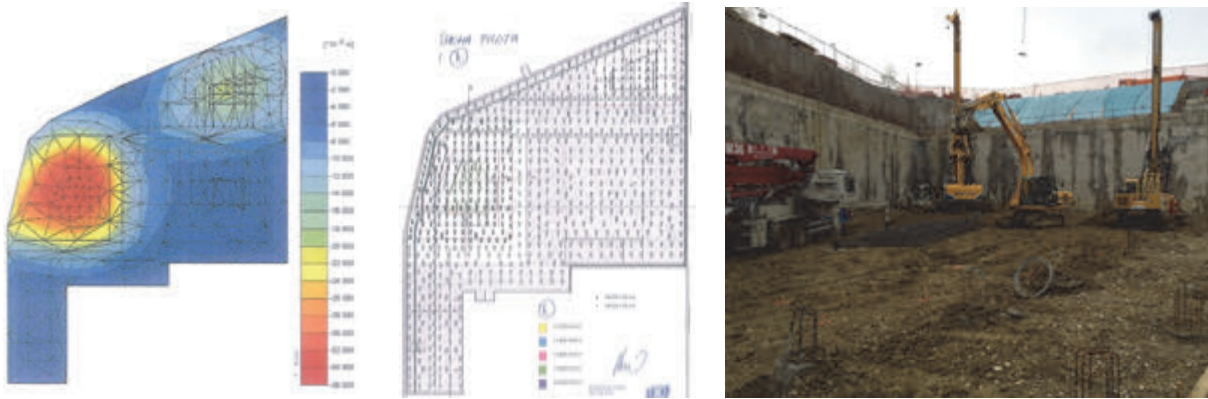


Fig. 10: Soil settlements and piles scheme for soil improvement and uplifting prevention

Incorrectly constructed construction pit protection in one part of the tower A limited the foundation slab thickness to no more than 200 cm, which is extremely small for a 31-story (4+27) building. Also, because of the soil improvement method with small diameter CFA piles (financial reason) and their depth, it was not possible to provide a direct input of the force in the piles. The result was the need for a large transverse reinforcement in the foundation slab and negative effect on peripheral columns. Flexibility of the slab caused rotation of columns fixed ends at the connections with the foundation slab and the occurrence of large bending moments and shear forces (Fig 11). To solve the problem, separation of the towers columns from basement floor slabs was carried out in order to increase the columns flexibility and reduce bending moments and shear forces in the columns.

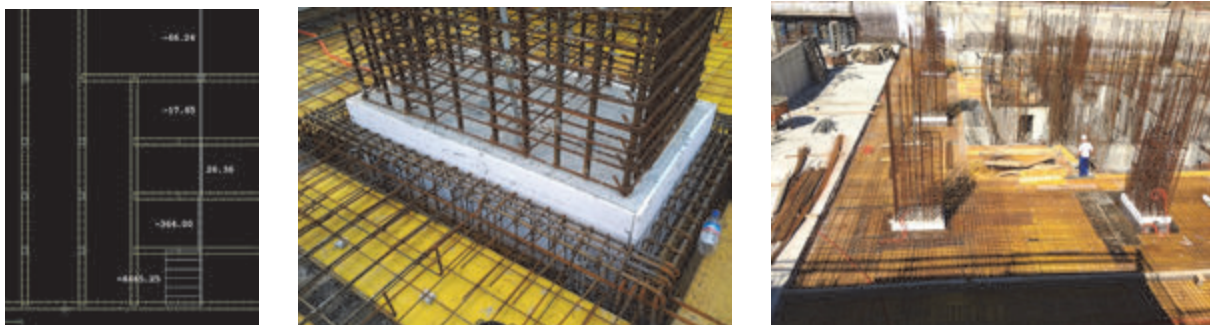


Fig. 11: Large shear force in column and separation of basement floor slabs and columns

Series of request from the investor, mistakes in construction of foundation pit protection and money saving on soil improvement piles have all resulted in a number of negative effects on load-bearing structure. Ultimately, the cost of load-bearing structure was only about 8.700.000,00 €. When reduced to gross surface area, it amounts to only 145 €/m². The load-bearing structure is only 10% more expensive than it is usual for lower buildings with waterproofing system and a number of other advantages. It is certainly interesting that the cost of not so exclusive segment glass façade was the same as the cost of load-bearing structure. One can conclude that the glass and aluminum are more “in” and therefore more profitable than concrete structures.

3. HVU “PETAR ZRINSKI”

In mid-2015 building for the accommodation of military officers HVU “Petar Zrinski” was designed by Davor Mateković. It is located in Ilica Street – the main street in Zagreb. With the gross surface area of 8.500 m², it consists of ground story, 14 stories and technical story on top – total of 16 stories. Building floor plan is rounded and maximum dimensions are 20×20 m (Fig. 12). The basic requirements for the building were high fire resistance (only one evacuation stairwell and no sprinkler system). There are no basement stories and dimensions of foundation substructure are restricted.



Fig. 12: 3D view of a future building, cross – section of the building and typical floor plan

Floor slab structures are reinforced concrete slabs 22 cm thick supported on the central core walls and peripheral frames. All horizontal actions are accepted by the central core with plan dimensions of only 6.0×8.3 m (Fig. 13). Maximum thickness of perimeter walls is 60 cm in the ground story. Peripheral frames transmit only the vertical load and additionally are preventing the torsion of the building. Peripheral walls membrane was designed as a masonry filling and is not used as a load-bearing structure, because a concrete construction would represent a problem due to the uneven and multidirectional curved geometry. In addition, openings on the facades are in irregular arrangement. Also, in the ground story there was a request for a glass façade for business purposes.

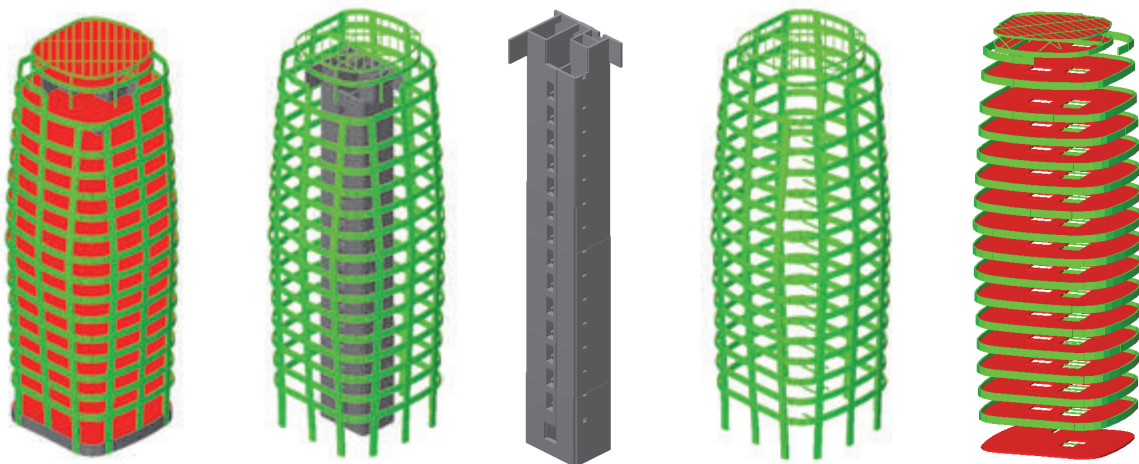


Fig. 13: 3D numerical model with main load-bearing structure elements

Small core and large horizontal seismic forces demanded that the walls are connected with coupling beams and installation of diagonal steel plates as in VMD Center building. In this case, as there were no basement stories and as core was fixed in foundation slab, there was no “backstay effect”. However, the fixation of the tall core in the foundation slab resulted in the foundation slab thickness of 200 cm and the necessity to reinforce the slab in both zones to accept the bending moment of the core (a problem similar to the fixation of wind turbine columns in the foundation). Because of the great load, the 200 cm thick foundation slab is reinforced with 250 kg/m³. Reinforcement in the foundation slab amounts to about 35% of the total reinforcement in the building, which is considerably more than the usual 25%. In addition, it was necessary to reinforce the foundation slab with transverse reinforcement. Also, because of the bad ground the foundation substructure had to be piled foundation. Restricted plan dimensions of foundation slab caused problems and tensile and large pressure forces appeared in the edge piles because of the seismic forces. So, 115 cm embankment was layed on the foundation slab in order to reduce the tensile forces. Also, edge piles were designed to be deeper than the middle ones (Fig. 14). Apart from vertical load, piles transmit a significant part of the horizontal forces to the soil so it was necessary to construct and reinforce the piles according to the EN 1998 standard. In the fixation zone of the core in the foundation slab the transverse reinforcement was compacted. Also, transverse reinforcement and additional reinforcement was implemented at the places of piles in the thickness of the foundation slab. Because of the frequent government changes in Croatia in the last two years, the construction of the building began earlier this year and currently only the ground story is constructed.

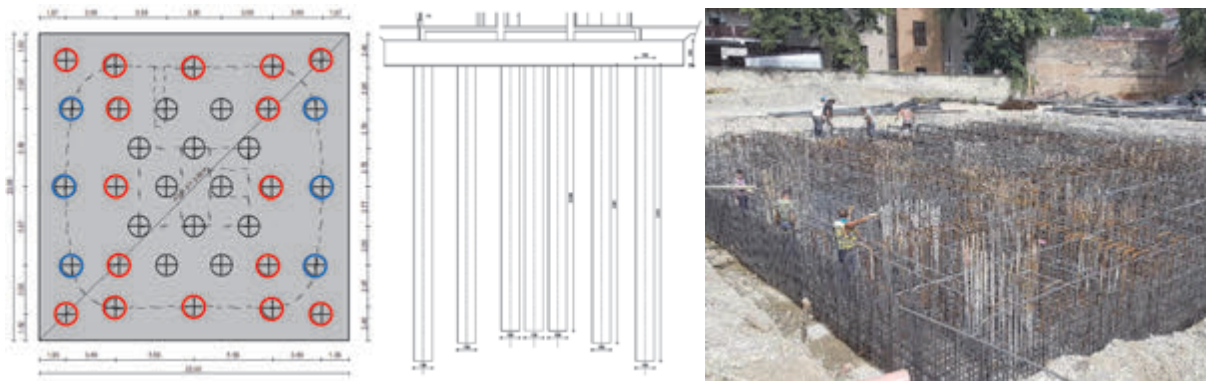


Fig. 14: Foundation slab with piles and the reinforcement in the foundation slab and piles

4. CRYSTAL CENTER

Project for business and residential building CRYSTAL CENTER, also located in the Ilica Street, was developed by Goran Rako in early 2015. It is a building with gross surface area of 22.300 m². It consists of 4 basement stories and two towers with 20 above ground level stories (Fig 15). Garages are located in basement stories, while the -1 story is public with two swimming pools, fitness center and polyvalent hall. Shops are situated in the ground story while offices, polyclinic, kindergarten and hotel are on the stories 1–7. Residential areas are on the stories 8–19. Towers are only functionally connected for evacuation purposes but they are two independent tower constructions that are connected in the single unit at the level of 6th floor slab.



Fig. 15: Crystal Center building

Floor slab structures are reinforced concrete slabs, 20 cm thick on the above ground level stories and 30 cm on the basement stories. They are supported on the core walls, peripheral stiffening walls and AB columns. Horizontal actions are transmitted by the main tower cores together with additional partition walls and façade peripheral walls as can be seen on the floor plan on Fig. 16. Advantage of this building is relatively small floor plan area of the towers stories (500 m^2) and additional walls that are continuous all the way to the foundation substructure. In addition, the towers are centrally positioned in reference to the basement and wider upper part of the structure so “backstay effect” is not present. Since the connection of the towers was designed to be at the level of 6th floor slab and not at the ground floor slab, 13 tower stories are accepted with 10 floors of common structure.

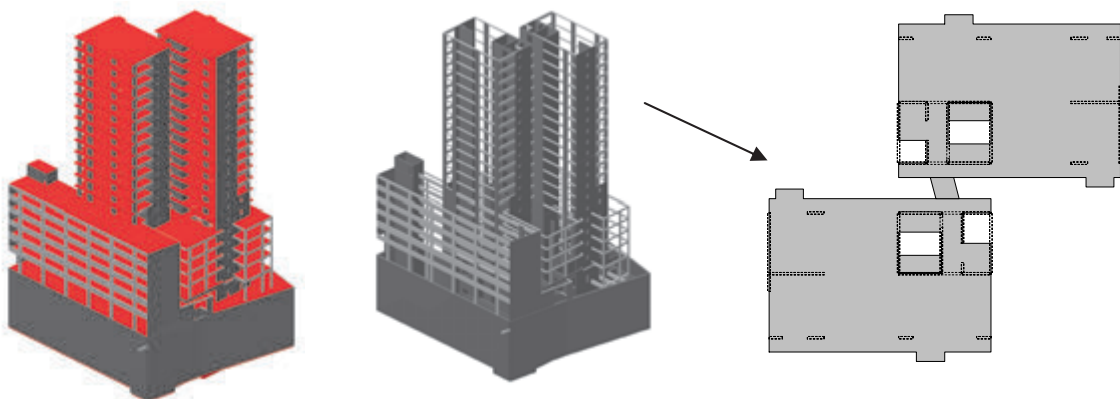


Fig. 16: 3D numerical model with load-bearing structure elements and typical floor plan

The main problem with this building is the construction of the basement part of the building. Since it is an embedded object in the old core of Zagreb, the only way to construct foundation pit protection is the top – down method. However, the problem is that the basement floor slabs are separated and delevelled and intersected with ramps and swimming pools. Also, the tower walls are heavily reinforced and due to the seismic requirements it is imperative that the reinforcement is continuous. Therefore, the solution where the peripheral diaphragm is braced by floor slabs which would be constructed from top to down. The slabs would be supported by the tube section steel columns constructed on the piles. The bracing and the transmitting of the drift force from one slab to another on the delevelled part would be ensured by vertical truss columns which would later be embedded in the wall elements. During construction truss columns would be supported on pilasters. Construction method was based on the construction of the garage in Ljubljana, Slovenia (designer V. Ačanski).

For the later construction of core and stiffening walls, openings at the core position would be left. Bracing slabs would be constructed without openings for the ramps which would be made subsequently by cutting the slabs only after the complete basement construction was constructed (Fig. 17).

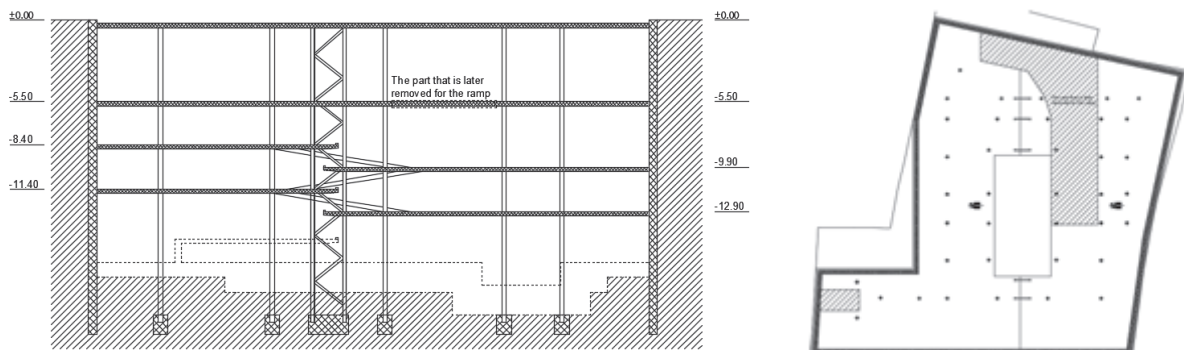


Fig. 17: Scheme of load-bearing structure and implementation of the top – down method

5. POSLOVNO STAMBENA ZGRADA J12

By the end of 2016 a project for business and residential building J12 (Fig. 18) in Zagreb was developed (author Igor Franić). It is a building with gross surface area of 50.000 m² and it has two separate dilatations. South dilatation is a business building and it consists of 2 basement stories and 4 above ground level stories while the north dilatation is a residential building and it consist of two basement stories, 17 above ground level stories and technical story on the building roof. The building is located in the attractive residential area Vrbani. North dilatation was designed as residential building with attractive apartments overlooking Zagreb and its surroundings, while the south dilatation was designed to accommodate shops and offices.



Fig. 18: Future look of the business and residential building J12

At the request of the investor, the entire load-bearing structure, and in particular the residential tower, is fully optimized so that the contracted cost for construction of the load-bearing structure is about 130 €/m². All the issues described previously for other high-rise buildings have been avoided in this project. Floor structure slabs are reinforced concrete slabs 20 cm thick in the above ground level stories and 24 cm thick in basement stories. The slabs are supported on regularly arranged load-bearing walls. Since it is a residential building with a floor area of about 1250 m², it was possible to implement a great number of load-bearing walls between apartments and the stairwell. Hence, it was possible to optimally distribute load-bearing walls in both orthogonal directions (Fig. 19).

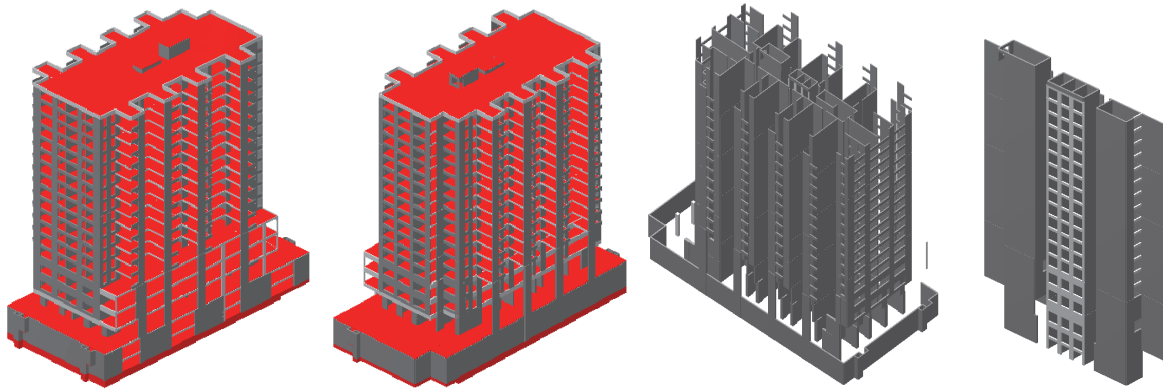


Fig. 19: 3D numerical model and the main vertical structure elements

Because of a large number of load-bearing walls it was not necessary to connect the walls with strong coupling beams, thus complicated reinforcement of coupling beams with diagonal reinforcement was avoided. In addition, by designing the building without coupling beams, positive softening of the structure and the increase in vibration periods was achieved and seismic horizontal load was reduced. It is typically optimal for high-rise buildings that the vibration period is about 2 sec. Since the basement part of the building has only two stories and is not much stiffer than the upper part, “backstay effect” was also avoided. Maximum bending moments and shear forces in the walls are achieved in the ground story, as it is desirable. Ground floor slab is not burdened by large tensile and shear forces. Proper choice of rigidity and load-bearing wall arrangement assured minimum seismic horizontal force and sufficient rigidity without negative influence on critical elements of the building.

Building foundation substructure is a 180 cm foundation slab in the projection of upper part of the building while the rest was designed with a thickness of 100 cm. In order to reduce soil settlement, soil improvement underneath the foundation slab was performed with piles of different depths and diameters of 80 and 50 cm. The goal was to reduce the soil settlement, so the piles were positioned on a regular spacing 3.0×3.0 m with stronger and deeper piles placed where the load is greater and no piles where the load is lower (Fig. 20). This way, except the total soil settlements, differential settlements were also reduced to minimum. Thanks to the underground stories long walls, significant bending of the foundation slab due to the seismic force was also avoided.

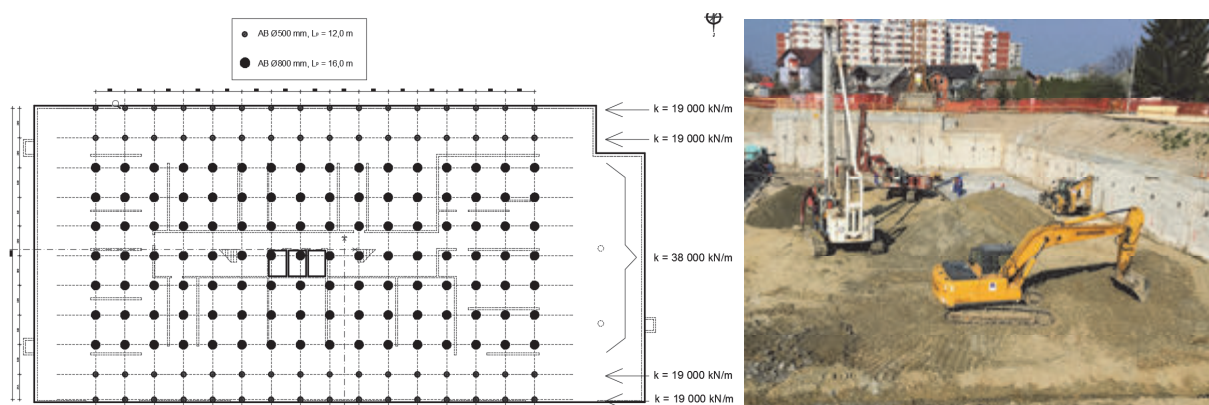


Fig. 20: Piles position for soil improvement

The only and main problem in designing the building was something least to be expected. Even though it is a residential building, it was not possible to design the façades as load-bearing walls with openings. The ground story was designed to be indented and to accommodate offices with glass façades, while in the basement stories the entrances to the garages are located. Therefore, façade walls of the upper walls could not be constructed all the way to the foundation substructure. Although without the façade walls the building has a large number of load-bearing walls properly arranged in two orthogonal directions, the first mode of vibration was torsion. In the longitudinal direction the building walls were concentrated along the longitudinal corridor and the transverse walls did not provide sufficient torsional stiffness due to the small length of the building and transverse walls. The problem was solved by designing wall segments on the façades ending on the 1st floor slab (Fig. 21). These segments provided sufficient torsional rigidity and assured that the first two modes of vibrations are predominantly translational. The construction of the entire façades as reinforced concrete walls was not possible because they would increase the stiffness of the building and therefore the seismic horizontal load would be also increased. Besides that, cantilever wall brackets from transverse walls on which they would be supported could not accept the seismic forces from façade walls.

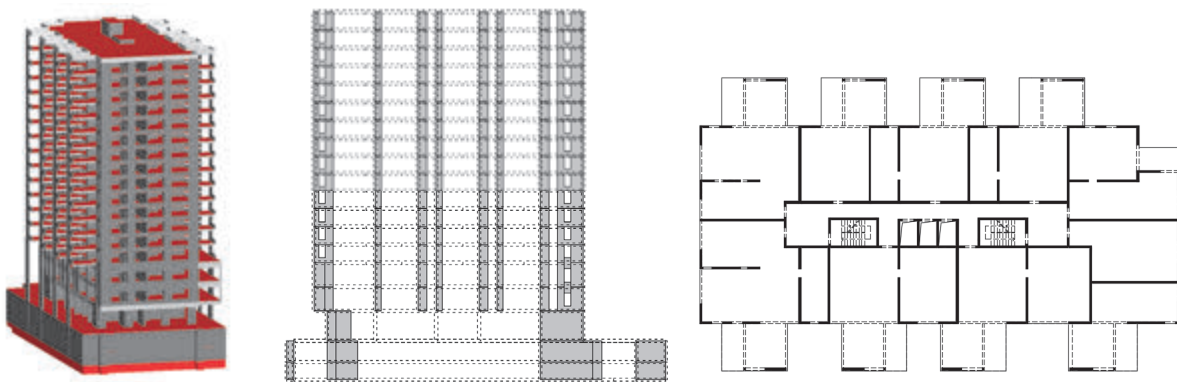


Fig. 21: Display of the wall segments on the façade for ensuring torsional stiffness

The construction of the building began in December 2016 and it should last until mid-2018. Basement stories are already constructed, as well as the south (business) dilatation ground story (Fig. 22).



Fig. 22: J12 building under construction

6. CONCLUSIONS

No matter how many have been designed and implemented, designing high-rise buildings always results in new problems and findings related to their design, behavior and construction. This paper briefly describes some problems in designing high-rise buildings as well as their technical solutions. From the descriptions engineers designing high-rise buildings in seismic areas can see on what they should pay attention to and what measures and technical solutions should be taken to obtain optimal load-bearing structure. Also, from the displayed and described high-rise buildings topics for future scientific research can be obtained, primarily concerning calculation and design of high-rise buildings.

7. REFERENCES

- Ačanski, V., Filipič, V. and Živec, M. (2011), “Design and Implementation of Underground Parking House Congress Square Ljubljana”, *Gradbeni Vestnik*, Vol. 60, No. 9, 2011, pp. 230-236.
- FIB, “Post-tensioning in Buildings” (2005), Technical Report of International Federation for Structural Concrete, Bulletin 31, 2005.
- Galić, J., Vukić, H. and Galić, B. (2014), “Design and Construction of The Tallest Skyscraper in Croatia”, *Izazovi u graditeljstvu 2 - Hrvatski Graditeljski Forum*, Zagreb, Croatia, 18-19 November 2014. HSGI, Zagreb, pp. 187-219.
- Poon, D.C.K., Hsiao, L.E. and Zuo, S. (2009), “ Analysis and Design of a 47-story Reinforced Concrete Structure - Futian Shangri-La Hotel Tower”, *Proceedings of Structures Congress*, American Society of Civil Engineers, Reston 2009, pp. 2751-2764.
- Wallace, J. W. (2007), “Modeling Issues for Tall Reinforced Concrete Core Wall Buildings”, *The Structural Design of Tall and Special Buildings*, Wiley InterScience, No. 16, December 2007, pp. 615-632.

TOPIC 1

TAILORED PROPERTIES OF CONCRETE

AN ADVANCED APPROACH TO DERIVE THE CONSTITUTIVE LAW OF UHPFRC

*Tamás Mészöly, Norbert Randl
Carinthia University of Applied Sciences
Villacherstr. 1, 9800 Spittal an der Drau, Austria*

SUMMARY

More than 200 specimens were tested in a comprehensive test series using ultra-high performance concrete with a mean compressive strength between 150 and 210 MPa and with different amounts of steel fibre reinforcement (0 %, 1 % and 2 % by volume) from the first 2 days to 1.5 years after casting. From the large sets of experimental tests related material parameters were derived. Based on compression tests with strain transducers and laser displacement transducers, the compression side of the constitutive law was derived, and based on the splitting tensile tests and flexural bending tests, the tensile side of the constitutive law was derived and the results are presented. For derivation of the tensile behaviour of ultra-high performance fibre-reinforced concrete an advanced approach was applied by using a photogrammetric camera system with digital image correlation (DIC).

1. INTRODUCTION

Good knowledge of the material parameters, the material behaviour, and an accurate constitutive law for ultra-high performance fibre-reinforced concrete (UHPFRC) are necessary to model or design structures using this composite material. Therefore a large set of test specimens were produced without fibre and with 1 vol% and 2 vol% of fibres. The ultra-high performance concrete (UHPC) concrete matrix was the same for the three mixtures with a maximum grain size of 0.4 mm. The water to cement ratio was 0.23, the water (including 70 % of the superplasticizer) to binder ratio 0.21. For mixtures with fibres the same straight fibre type was used with the length of 15 mm and diameter of 0.2 mm. The tensile strength of the fibres was higher than 2000 N/mm². Size and shape of the specimens, production, storage, curing and testing of the specimens were according to ÖNORM EN 12390 (2012) and ONR 23303 (2010).

2. DENSITY

Fig. 1 shows the average density of the concrete with different fibre contents 28 days after casting based on measurements on more than 100 specimens with different size and geometry (cube and cylinders). The average density of concrete without fibre was 2339 kg/m³. Measured values were between 2324 kg/m³ and 2353 kg/m³. Mean values measured on different types (size or geometry) of specimens were between 2338 kg/m³ and 2342 kg/m³. The average density measured on specimens with 1 vol% of steel fibres was 2403 kg/m³. Measured values varied between 2375 kg/m³ and 2440 kg/m³. Mean values measured on different types of specimens were between 2391 kg/m³ and 2407 kg/m³. The average density measured on specimens with 2 vol% of fibres was 2466 kg/m³. Measured values were between 2442 kg/m³ and 2485 kg/m³. Mean values measured on different types of specimens were between 2453 kg/m³ and 2472 kg/m³. According to these measurements addition of steel

fibres increased the density by 62-64 kg/m³ per % by volume, which is larger than the 55 kg/m³ per % by volume calculated from the density and ratio of the concrete and steel.

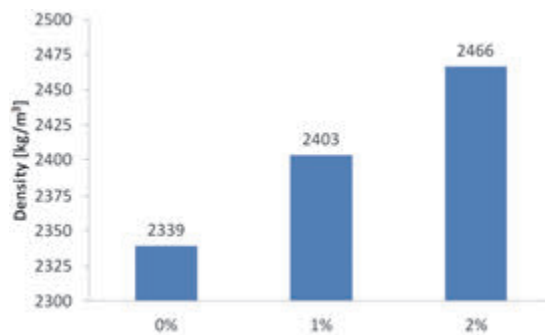


Fig. 1: Density with 0 %, 1 % and 2 % fibres

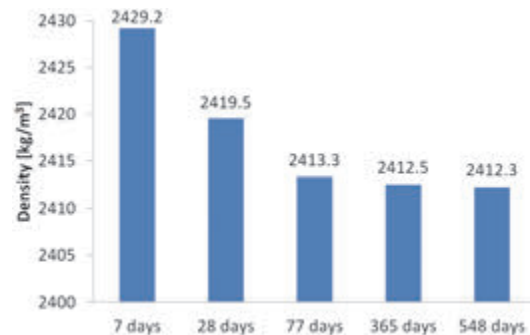


Fig. 2: Density development in time

Fig. 2 shows the development of the density in time between the age of the concrete of 7 days and 1.5 years. Values decreased from 2429 kg/m³ to 2412 kg/m³ by 0.7 % in this time period. Since the specimens spent the first 7 days (between casting and testing) under water, the value related to 7 days age can be considered as fully saturated. Assuming that after 1.5 years the specimens reached the state of equilibrium under laboratory conditions, the average pore ratio of the specimens can be estimated as 1.7 %.

3. COMPRESSIVE STRENGTH

Specimens presented in this chapter did not receive any compacting during casting or any after-treatment (heat or compression) later. Effect of compacting is discussed under chapter 6. The mean value of the 28 days compressive strength on cubes with 100 mm side length was 154.3 N/mm² without fibre, 167.8 N/mm² with 1 % of fibres and 172.5 N/mm² with 2 % of fibres (see Fig. 3 and Fig. 5). 1 vol% of fibres increased the compressive strength of the concrete by 13.5 N/mm² (8.7 %), 2 vol% of fibres increased the compressive strength by 18.2 N/mm² (11.8 %). The increase from 0 to 1 % was around three times higher, than from 1 % to 2 % (4.7 N/mm², 2.8 %). The mean compressive strength values after 28 days on 200 by 100 mm cylinders were 144.2 N/mm² for concrete without fibre, 161.5 N/mm² with 1 % of fibres and 166.0 N/mm² with 2 % of fibres (see Fig. 3). 1 % of fibres increased the compressive strength of the concrete on cylinders by 17.3 N/mm² (12.0 %), 2 % of fibres increased the compressive strength by 21.8 N/mm² (15.1 %). Compared to the strength values measured on cubes, the increase from 0 to 1 % of fibres was significantly higher at cylinders, but the increase from 1 to 2% of fibres was around the same (at cylinders: 4.5 N/mm², 2.8 %).

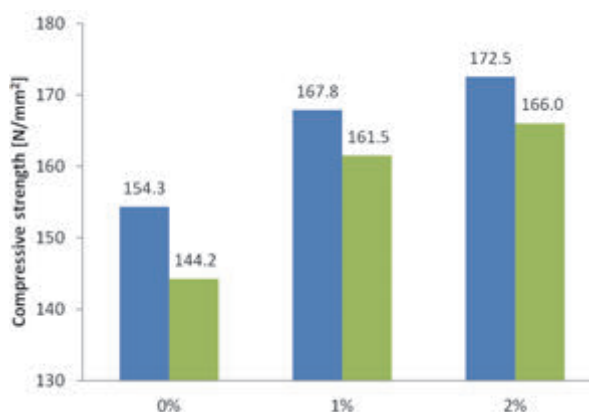


Fig. 3: Compressive strength of the mixtures

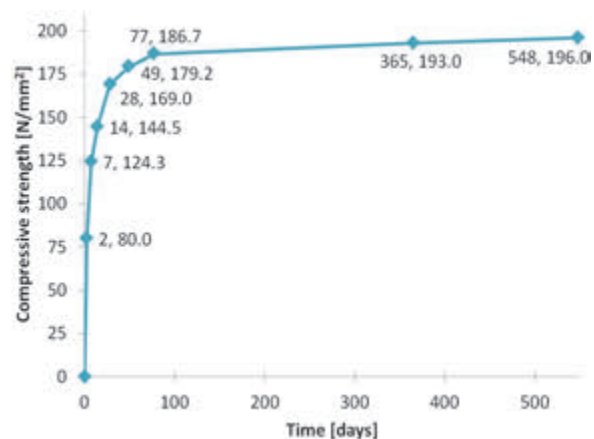


Fig. 4: Compressive strength development

The ratio of the compressive strength measured on 200 by 100 mm cylinders to 100 mm cubes was a slightly above 0.93 without fibres and was around 0.96 with 1 % and with 2 % of fibres. Taking into account all other series (number of batches over the years) with the same recipe and with 1 % or 2 % fibres, the ratios of cylinder to cube strength were between 0.91 and 0.97 with a mean value close to 0.94, and with a tendency that at higher fibre contents the ratio is closer to 1.0. Fig. 5 also depicts the linear regression between compressive strength and density after 28 days with a regression coefficient of 184 kNm/kg.

Fig. 4 shows the development of the mean compressive strength between concrete age of 2 days and 1.5 years. Increase of the compressive strength is especially fast in the first days (80 N/mm² after 2 days and 124 N/mm² after 7 days), but still there is a slight increase after 1 year.

4. MODULUS OF ELASTICITY

The measured modulus of elasticity values on 300 mm by 150 mm cylinders and on a 100 mm base length were 44.7 GPa without fibre, 46.9 GPa with 1 % of fibres and 49.3 GPa with 2 % of fibres. On 200 mm by 100 mm cylinders (with 100 mm base length) the measurements showed slightly (1-3 GPa) smaller values. Measurements were also performed on cubes with 100 mm side length on a base length of 50 mm, and they are resulted in about 5 GPa higher modulus, than the values measured on the 300 mm high cylinders, and in 6-8 GPa higher values than on the 200 mm high cylinders. Specimens tested at the age of 43 days showed 1.0-1.5 GPa higher values than at an age of 28 days. Fig. 6 shows the linear regression between the 28 days modulus of elasticity and density measured on 300 mm by 150 mm cylinders with a regression coefficient of 35.5 MNm/kg.

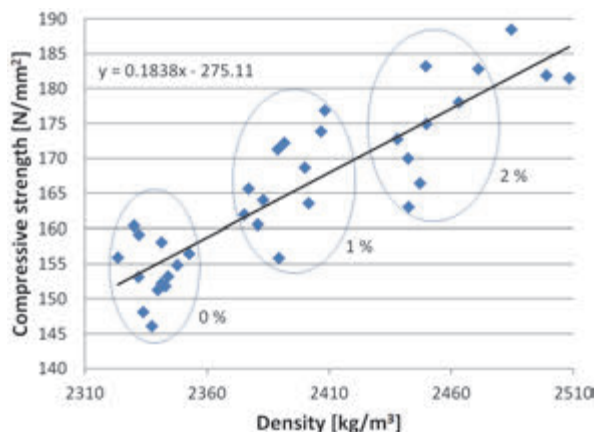


Fig. 5: 28 days comp. strength vs. density

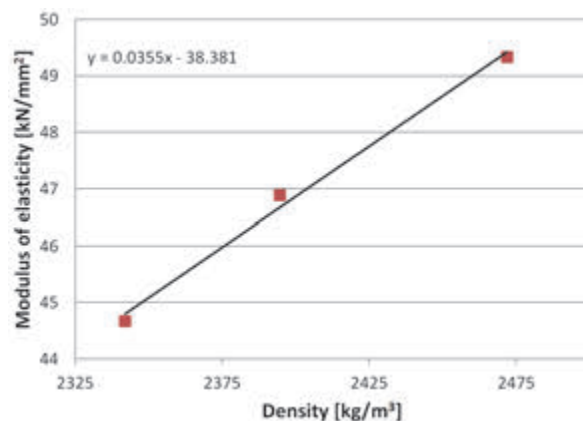


Fig. 6: Modulus of elasticity vs. density

5. SPLITTING TENSILE STRENGTH

The mean value of the 28 days splitting tensile strength on 200 by 100 mm cylinders was 7.9 N/mm² without fibre, 14.1 N/mm² with 1 % of fibres and 16.1 N/mm² with 2 % of fibres (see Fig. 7). At specimens with 1 % fibres, there was a clear sign of the first cracking at a splitting tensile stress of 8.1 N/mm². Fig. 8 shows the linear regression between the 28 days splitting tensile strength and density with a regression coefficient of 63.1 kNm/kg.

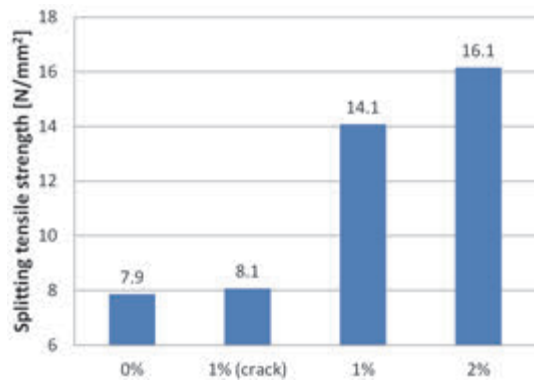


Fig. 7: 28 days splitting tensile strength

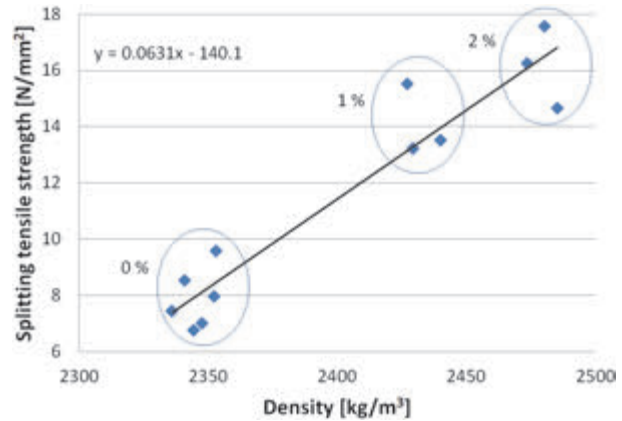


Fig. 8: Splitting tensile strength vs. density

6. EFFECT OF COMPACTING

While most of the specimens from self-compacting UHPC were produced without any compacting treatment during the mixing and casting process of the fresh concrete, some of them were prepared using a hand-compacting method. These specially handled specimens (cubes with 100 mm side length) showed a clear and significant advantage on the measured density and compressive strength (see dashed blue arrows in Fig. 9). According to the measurement, every 10 kg/m^3 density increase enhanced the compressive strength by 2.8 N/mm^2 on average with a range of $1.9\text{-}3.9 \text{ N/mm}^2$; or every 1% increase of density resulted in 3.8% average increase of compressive strength with a range of 2.8 to 4.9%. Fig. 9 also depicts the change of density and compressive strength between ages of 28 days and 1.5 years (continue green arrows). The increase of the compression strength was $26\text{-}29 \text{ N/mm}^2$ in this period, and reached the value of 213 N/mm^2 (compacted specimens with 2% of fibres). The decrease of the density was half (5 kg/m^3) for the compacted specimens in comparison to the non-compacted ones (10 kg/m^3).

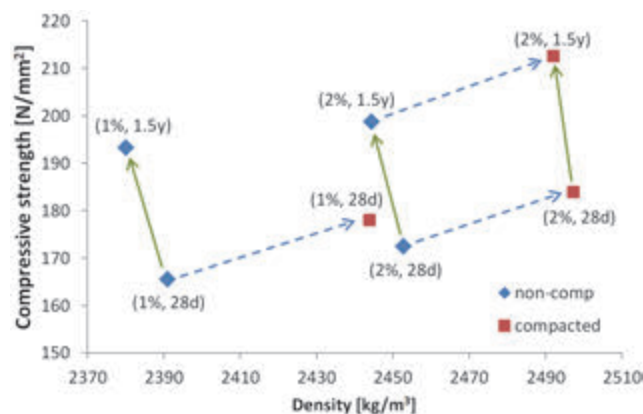


Fig. 9: Effect of the compacting

7. COMPRESSIVE STRESS VS. STRAIN CURVE

The compressive side of the constitutive law was derived from compression tests with deformation measurements. Deformation of the specimens was measured in parallel with strain transducers on the sides of the specimens and with laser (optical) displacement transducers between the two opposition surfaces of the hydraulic press. Strain transducers were used only until about 60% of the expected maximal load because of high risk of their damage during the failure process. Tests were performed on 100 mm cubes, on 200 by

100 mm cylinders and on 300 by 150 mm cylinders. Measured base length of the strain transducers was 50 mm in case of the cubes and 100 mm in case of the cylinders. Measured length of the laser displacement transducers (base length for the strain calculation) was the same as the height of the specimens (100 mm, 200 mm and 300 mm).

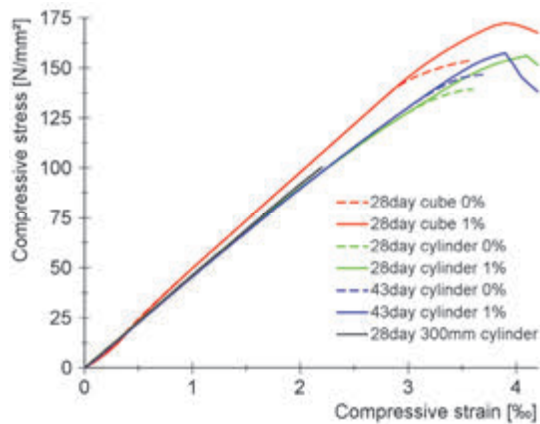


Fig. 10: Compressive stress-strain relation

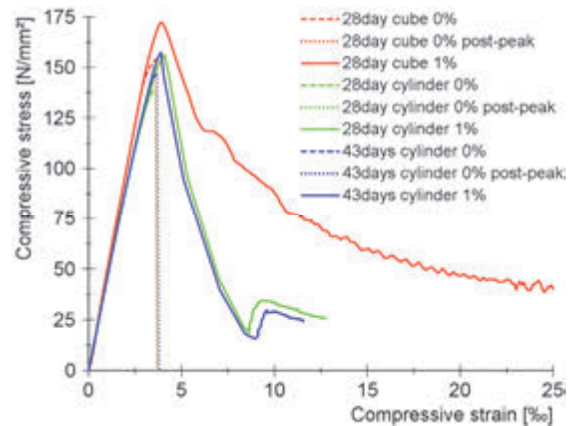


Fig. 11: Post-peak behaviour

Fig. 10 shows the mean curves for the different types of specimens. For this figure the curves from specimens without fibre and with 1 % of fibres were evaluated together in the first, quasi-linear phase (higher number of measurements resulted in straighter and more trustable trend-like curves). As it is described in chapter 3 and 4, curves measured on cubes were steeper and reached a higher strength, than curves measured on cylinders. Curves measured on 300 by 150 mm cylinders showed stiffer behaviour and would have probably reached lower final compressive strength (could not be measured as the failure load exceeded the 3 MN capacity of the hydraulic press). Curves measured after 43 days were slightly steeper and reached slightly higher strength values than curves measured after 28 days. Fig. 10 shows the curves for specimens without fibre and with 1 % of fibres separately from the point where their ratio of steepness started to change. This point was between 125 N/mm² and 140 N/mm², which is around 90 % of the peak values of curves without fibre and around 80 % of the peak values of the curves with 1 % of fibres. Curves from specimens without fibre reach the peak value at 3.5 % strain value on average (3.4-3.6 %), and with 1 % of fibres a value of 3.9 % on average (3.7-4.1 %). Specimens without fibre failed in an explosion at the peak load, and the post-peak part of the curve could not be measured. Cylinders with 1 % of fibres failed quickly, but they did not explode and the post-peak branch of the curve could be measured. Cubes with 1 % of fibres failed slower and the load response dropped gradually. Specimens with 2 % fibres failed slowly and they did not fall apart even at high degradation levels. Fig. 11 depicts the whole curves for specimens without fibre and with 1 % of fibres.

8. TENSILE STRESS VS. STRAIN CURVE

The tensile side of the constitutive law was derived indirectly using flexural bending tests on prismatic specimens. The size of the specimens was 700x150x150 mm and specimens were tested in a four-point bending setup with a span of 600 mm according to the German guidelines (DBV, 2001; DAfStb, 2012). Specimens were measured in parallel using a traditional measurements system (displacement transducers, strain gauges and strain transducers) and a Digital Image Correlation (DIC) system, and the results from the two types of system were compared. The DIC technique is a useful tool to measure and monitor structural deformations. It is possible to directly measure the surface deformations or the crack opening values of every single crack. Based on the DIC measurements it is very easy to

visualise the crack pattern of the measured surface. Fig. 12 shows a typical crack pattern at peak load with 1 % of fibres and with 2 % of fibres. Specimens with 1 % of fibres have fewer cracks (4.2 on average) with sharper edges and with only a few branches. Specimens with 2 % of fibres have more cracks (9.2 on average) with scratchy crack faces and more branching.

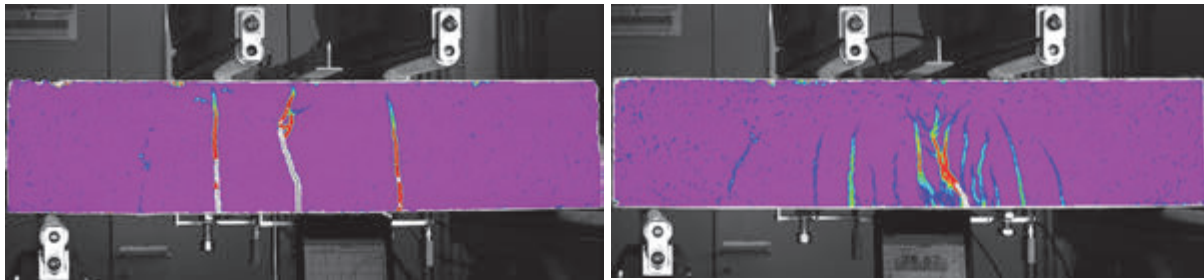


Fig. 12: Crack pattern from the DIC measurement (left: with 1 %, right: with 2 % of fibres)

The basic results from flexural tensile tests are the load vs. deflection curves, and then the flexural tensile stress vs. deflection curves derived from them. The mean values of the maximum load and the flexural strength were 32.6 kN and 5.8 N/mm² for specimens with 1 % of fibres, and 63.5 kN and 11.3 N/mm² with 2 % of fibres (see Fig. 13). Deflection at the peak load was 1.2 mm on average for specimens with 1 % of fibres and 0.9 mm with 2 %. Beside the fibre content, other very important factors of the fibre-reinforced concrete are the fibre distribution and fibre orientation. A well-designed and performed mixing process should provide homogenous fibre distribution, but the casting process has a very big influence on the fibre orientation (and distribution of the fibre orientation inside the specimen). Therefore in this test series one of the specimens was cast differently: generally the fresh concrete was poured into the formwork at several discrete points (later referred to as “unfavourable oriented”), but at one specimen this happened without interruption in continuous longitudinal movement (later referred as “favourable oriented”). The difference was very pronounced: the specimen with favourable oriented fibres showed around double high values than specimens with unfavourable oriented fibres, and the peak value was similar to specimens with 2 % of fibres (see Fig. 13).

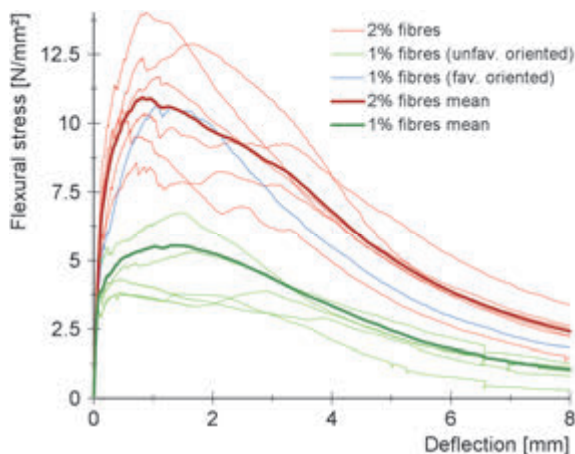


Fig. 13: Flexural stress-deflection curves

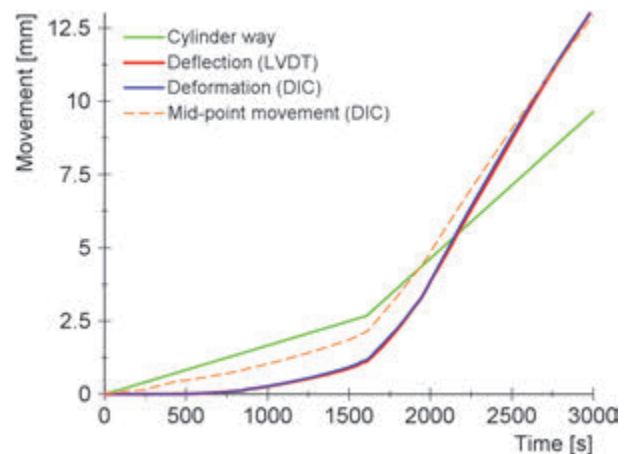


Fig. 14: Movement measurements

Using the DIC system it is possible to follow the movement of any surface point, therefore it was interesting to compare it with the traditional measurement techniques. Fig 14 shows the measured movements of one specimen: way of the cylinder was measured by a built-in sensor of the testing machine; deflection was measured by a displacement transducer fixed on the specimen; and mid-point movement was measured using the DIC system. Deformation from

the DIC system was derived as the subtraction of the mid-point movement and the movement of the fixing point (according to DAfStb, 2012) of the deflection transducers. This method provided the same results as recorded by the displacement transducer (see Fig. 14). Using the DIC system it is not required to fix any sensor on the specimen and it is possible to separate the elastic deformations from the support or rigid body movements.

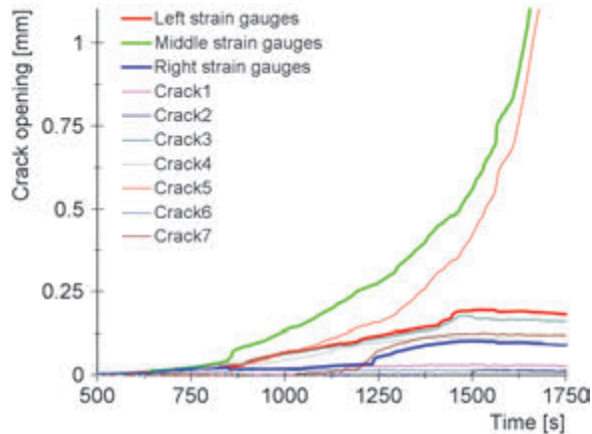


Fig. 15: Crack measurements

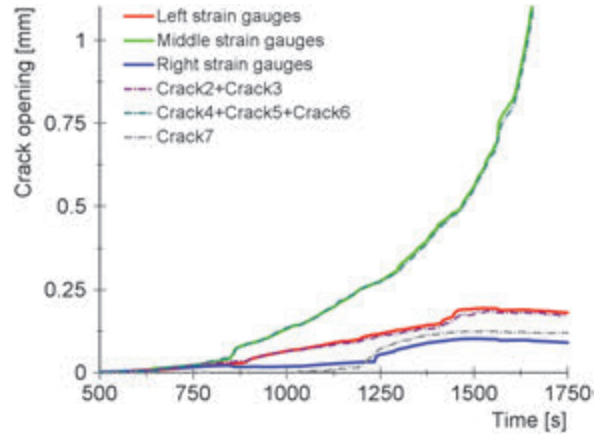


Fig. 16: Crack measurements

Comparison of the crack opening measurements was another field of research. Cracks were measured by three strain transducers with 100 mm base length on the bottom surface of the flexural specimens as well as with virtual extensometers using the DIC system. Fig. 15 shows the crack measurements for one beam. While strain transducers usually measure more cracks together with elongation from the elastic deformation under their base length (300 mm all together), using the DIC system each crack can be measured and it can separate the crack opening and the elastic deformation (base length of the virtual extensometers is 2-5 mm). To check the measurements, the crack opening values under the same strain transducers were summed up. Fig. 16 depicts the result for one beam: 2nd and 3rd crack was under the left strain transducer, 4th, 5th and 6th under the middle transducer and the 7th under the right transducer (1st crack was outside of the 300 mm range of the strain transducers); and the related curves are very similar (small differences came from the asymmetrical failure of the specimen). Other problems which can be avoided using optical measurements are: (a) strain transducers have a tendency to slip on the smooth, sometimes glossy surface of the UHPC; and (b) cracks can be outside of their base length are excluded from the measurement.

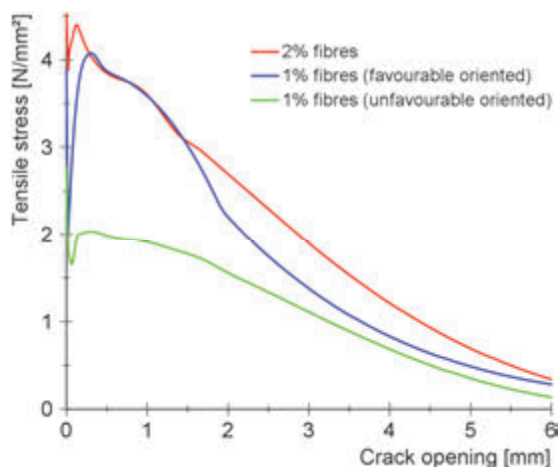


Fig. 17: Tensile stress-crack opening

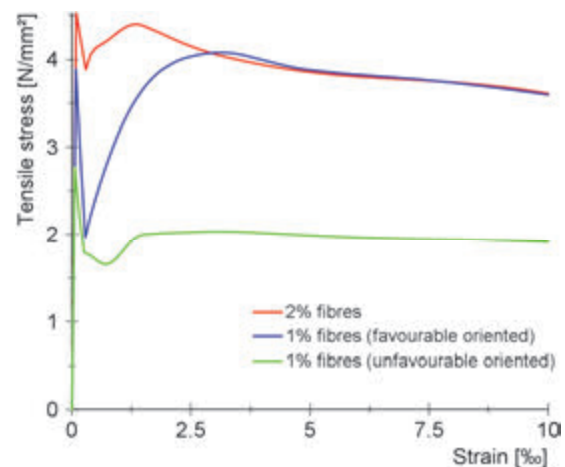


Fig. 18: Tensile stress-strain relation

The mean value of the largest crack opening at the peak load was 1.3 mm with 1 % of fibres and 0.6 mm with 2 % of fibres. Most of the cracks stayed smaller than 0.1 mm and only a few reached the range of 0.1 and 0.5 mm. Close to the peak load one of the largest cracks became the decisive one, and from this point only the decisive crack increased and other cracks partly closed. The tensile stress vs. crack opening and the tensile stress vs. strain curves were derived from the measured load vs. crack opening curves according to AFGC (2013). Fig. 17 and Fig. 18 show the derived curves from the three different types of flexural specimens.

9. CONCLUSIONS

A comprehensive experimental test series with a large number of specimens was performed in order to determine the material parameters, material behaviour and derive the constitutive law on the compressive and on the tensile side of a UHPC mixture without fibre and with a fibre content of 1 % and 2 % by volume, using a new measurement and calculation method:

- The mean density of UHPC after 28 days was 2339 kg/m³ and decreased by time. Addition of steel fibres increased the density of the hardened concrete by 62-64 kg/m³ per % of fibres.
- Increase of the compressive strength by addition of the first % of fibres is significantly higher for cylinders (12.0 %) than for cubes (8.7 %), but around the same for the second % of fibres (2.8 %).
- Ratios of cylinder to cube strength were between 0.91 and 0.97 with a mean value close to 0.94, and with a tendency that at higher fibre contents the ratio is closer to 1.0.
- The splitting tensile strength was 7.9 N/mm² without fibre, 14.1 N/mm² and 16.1 N/mm² with 1 % and with 2 % of fibres, respectively.
- Effect of compacting: 1 % increase of density resulted in 3.8 % increase of compressive strength on average, and decrease of the density by time was half for the compacted specimens in comparison to the non-compacted ones.
- Fibre orientation has a very strong effect on the tensile properties of the concrete: 1 % of “favourable oriented” fibres have a similar effect like 2 % of “unfavourable oriented”, and the tensile properties are about twice that high if the casting process takes care of the final fibre orientation.
- DIC technique allows a continuous optical measurement without interruption of the testing process, and the points of interest in the measured spatial and time range can be chosen later. Results from the traditional and the DIC systems were compared, and the advantageous applicability of the optical system was verified.

6. ACKNOWLEDGEMENTS

The funding of this research by the Austrian Research Promotion Agency (FFG) and support of the Carinthia University of Applied Sciences are gratefully acknowledged.

7. REFERENCES

- AFGC (2013), “Ultra High Performance Fibre-Reinforced Concretes – Recommendation”, Revised ed., Association Francaise de Génie Civil, June 2013.
- DAfStb (2012), “DAfStb-Richtlinie Stahlfaserbeton – Teil 2”, November 2012.
- DBV (2001), “DBV-Merkblatt Stahlfaserbeton”, Deutschen Beton- und Bautechnik-Verein.
- ONR 23303 (2010), “Test methods for concrete – National application of testing standards for concrete and its source materials”, Technical regulation, Austrian Standards, Sept. 2010.
- ÖNORM EN 12390 (2012), “Testing hardened concrete”, Part 1 – Part 7, Austrian Standards.

INFLUENCE OF THE PURITY OF RECYCLED CONCRETE AGGREGATES ON THE MECHANICAL PROPERTIES OF DRY AND SELF-COMPACTING PRECAST CONCRETE

*Miquel Joseph, Zeger Sierens, Jeroen Massaer, Dylan Noppe, Jiabin Li, Luc Boehme
KU Leuven, Technology Campus Bruges, Department of Civil Engineering, Technology
Cluster Construction, Faculty of Engineering Technology
Sporwegstraat 12, 8000 Bruges, Belgium*

SUMMARY

Although different researches have already shown that the creation of concrete with partial replacement of the coarse aggregates by recycled coarse concrete aggregates is feasible with limited effect on the mechanical and durability properties of the concrete, still a lot of questions remain. One of these questions is the influence of the quality of the recycled aggregates. This study takes a closer look at the influence of the purity of the recycled concrete aggregates and its influence on two different precast concrete mixtures: a fast hardening dry mixture used for hollow-core slabs and a self-compacting mixture used for beams and floors. Different parameters which are of importance for precast companies were examined: early age compressive, bending and splitting strength, 28 day compressive and splitting strength and concrete density.

1. INTRODUCTION

According to the Belgian Concrete Industry Federation FEBE, federation of concrete industry, Belgium annually produces 12 million tons of precast concrete (Noterman et al., 2016) of which 5 percent or 600.000 tons are structural elements. To produce these structural elements 250.000 tons of natural coarse aggregates are used. Partially (up to 20%) replacing these natural coarse aggregates by recycled concrete aggregates has different beneficial consequences:

- This replacement could significantly lower the ecological footprint of precast structural elements, which leads to better “Building Research Establishment Environmental Assessment Method” and “Leadership in Energy and Environmental Design” ratings; (Noterman et al., 2016);
- Belgium and more specifically Flanders is depending on the import of aggregates for most of the concrete production. By replacing natural aggregates with recycled aggregates, it could release the pressure on the Belgian market of natural aggregates; (Boehme et al., 2012);
- Recycled aggregates (RA) have a lower market value than natural aggregates and concrete made with recycled aggregates has a lower density (1-2%) than concrete made with natural aggregates. (Boehme et al. 2012; Joseph et al. 2015) These two effects lead to a reduction of the production and transportation costs of precast structural elements.

Although different Flemish researches have already shown that the creation of concrete with partial replacement of the coarse aggregates by recycled coarse concrete aggregates is feasible with limited effect on the mechanical and durability properties of the concrete, still a lot of questions remain. (De Brabandere et al. 2013; Boehme et al., 2011; Noterman et al., 2016) One of these questions is the influence of the quality of the recycled aggregates (Joseph et al., 2012).

2. MATERIALS USED

2.1 Aggregate compositions

24 different recycled concrete aggregate compositions were artificially created in the laboratory. The parameters that were varied are: the amount of recycled concrete particles ranging between 87 and 95 m%, the amount of red brick contamination between 8 and 0 m%, the amount of fines varying between 0 and 3m% and the amount of floating particles between 0 and 2 cm³/kg. The exact compositions and their density and water absorption can be found in Tab. 1.

Tab. 1: Composition of the different purities of recycled concrete aggregates tested

Code	Composition					Mixture	
	Fraction 4/14			Fraction 0/4		ρ_{rd}	Wa ₂₄
	Rcu/FI/f	CRCA	Rb	FI	FRCA		
	[kg/m ³]	[kg/m ³]	[kg/m ³]	[kg/m ³]	[kg/m ³]	[kg/m ³]	[%]
100/0/0	2223	-	-	113	0	2336	4.80
100/0/3	2223	-	-	45	70	2339	4.66
100/2/0	2223	-	0.31	113	0	2336	4.80
99.5/0/1.5	2212	9	-	80	35	2335	4.83
99.5/0/3	2212	9	-	45	71	2336	4.73
99.5/1/1.5	2212	9	0.16	80	35	2335	4.83
99.5/1/3	2212	9	0.16	45	71	2337	4.73
99.5/2/1.5	2212	9	0.31	80	35	2335	4.83
99.5/2/3	2212	9	0.31	45	71	2337	4.73
98/0/1.5	2179	35	-	80	35	2328	4.96
98/0/3	2179	35	-	45	71	2329	4.87
98/1/1.5	2179	35	0.16	80	35	2328	4.96
98/1/3	2179	35	0.16	45	71	2330	4.87
98/2/1.5	2179	35	0.31	80	35	2328	4.96
98/2/3	2179	35	0.31	45	71	2330	4.87
95/0/1.5	2112	88	-	80	35	2314	5.23
95/0/3	2112	88	-	45	71	2315	5.13
95/1/1.5	2112	88	0.16	80	35	2314	5.23
95/1/3	2112	88	0.16	45	71	2316	5.13
95/2/1.5	2112	88	0.31	80	35	2314	5.23
95/2/3	2112	88	0.31	45	71	2316	5.13
90/0/1.5	2001	176	-	80	35	2291	5.68
90/0/3	2001	176	-	45	71	2292	5.58
90/1/1.5	2001	176	0.16	80	35	2291	5.68
90/1/3	2001	176	0.16	45	71	2292	5.58
90/2/1.5	2001	176	0.31	80	35	2291	5.68
90/2/3	2001	176	0.31	45	71	2292	5.58

Recycled Concrete (Rcu) are aggregates with attached mortar originating from the demolition of concrete products like pavement, stones, slabs, walls, and mortar products like sand-cement and screed. According to the Flemish standard PTV 406, which is based on the European standard EN 933-11, CRCA needs to contain at least 70% Rcu in the coarse fraction 4/14. But the combination of Rcu and natural aggregates (Rn) needs to be at least 90% in this fraction. This research focusses on CRCA containing at least 90% Rcu in the coarse fraction and no Rn.

The Rcu used originates 100% from production waste of precast floor slabs, three step crushed with a jaw, percussion and cone crusher. These aggregates have an oven dry density (ρ_{rd}) of 2340 kg/m³ and a water absorption (W_{a24}) of 4.8%.

Floating particles (FL) are aggregates with a size above 4 mm and a density below 1000 kg/m³. While the standard allows up to 5 cm³/kg contamination by floating particles, this is not representative for high quality aggregates found on the Flemish market. This research uses three different rates of contamination: 0, 1 and 2 cm³/kg. The floating particles are a proportional combination of light wood (188 kg/m³), EPS (29,4 kg/m³), PUR (31.1 kg/m³) and PE (23.6 kg/m³). This combination has a density of 70 kg/m³ and their water absorption is negligible.

Red brick (Rb) is besides hydrocarbon (Ra), glass (Rg) and non-stony aggregates (X) one of the other types of coarse aggregates that can be found in CRCA and its presence is limited to 10 m% in the standard PTV 406. Since this research does not use Ra, Rg and X, Rb is the only coarse aggregate used besides Rc. These red brick aggregates are artificially created in the laboratory with a laboratory jaw crusher and have a ρ_{rd} of 1850 kg/m³ and a W_{a24} of 14.2%.

Two types of small aggregate (0/4) impurities are added in this research: fine recycled concrete aggregates and filler. The total amount of 0/4 that can be present in a 4/14 aggregate depends on the standard used. This research uses a constant 5m% contamination by small fraction to create aggregates fulfilling the requirement of a G_C 90/15 according to the NBN EN 12620 -2002.

Fine recycled concrete aggregates (FRCA) are aggregates with an aggregate size below 4 mm. This sand is a by-product of crushing concrete to create coarse aggregates and is often seen as inferior. The FRCA used in this research is a by-product of the production of the Rc and has a ρ_{rd} of 2260 kg/m³ and W_{a24} of 6.4%.

Fines (F) are particles with a size less than 63 μ m. Due to their high specific surface area, these particles demand a high amount of water in concrete mixtures. On the other side, due to their small size, they can easily fill pores and lead to better concrete properties. The fines used in this research were a combination of powdered old concrete and limed clay particles. The exact properties of these fines are not measured.

2.2 Concrete Recipes

Two different types of concrete are tested:

- Self-compacting concrete (SCC), used for columns and beams, with a minimum strength C20/25;
- Fast hardening dry concrete (FHDC), used in pre-stressed hollow-core slab applications, with a minimum strength of C50/60.

The cement used for SCC was CEM I 52,5 R and the one used for FHDC was CEM I 52,5 N. The natural aggregates (NA) used in both mixtures were a combination of different types of sea sand and limestone. Only the SCC-mixture uses a superplasticizer to reach the required workability. The recipes of these concretes can be found in Tab. 2.

Tab. 2: Concrete mixtures

Type	Powders		Aggregates		Liquids	
	Cement	Filler	Limestone 2/14	Sand 0/4	Water	Super Pl.
	[kg/m ³]	[kg/m ³]	[kg/m ³]	[kg/m ³]	[kg/m ³]	[kg/m ³]
SCC	280	290	760	760	200	3.4
FHDC	340	-	1250	712	110	-

The Recycled Aggregate Concrete (RAC) was made by replacing 20 vol% of the Coarse Natural Aggregates (CNA) by the difference qualities of CRCA found in Tab. 1.

All mixtures were produced in a two-step mixing process. This is often used in combination with high absorbing aggregates like CRCA, to give the aggregates the time to absorb the additional water. The procedures can be found in Tab 3.

Tab. 3: Mixing procedures

Type	Step 1		Step 2		Step 3	
	Ingredients	Time	Ingredients	Time	Ingredients	Time
	[-]	[s]	[-]	[s]	[-]	[s]
SCC	Water 20% Aggregates	30	Cement Filler	60	Water 80% Super Pl.	60
FHDC	Aggregates	40	Cement	40	Water	60

3. RESEARCH PROGRAM

All tests were done on beams 100 mm - 100 mm - 600 mm. 29 beams of SCC (27 different purities and 2 reference mixtures) and 27 beams of FHDC (24 difference purities and 3 reference mixtures). Every beam was used for multiple tests. These can be found in Tab. 4.

Tab. 4: Tests

Part beam	Test	Parameter	Standard
Complete beam	Mass and dimensions	Dry Density	NBN B15-221 1989
Complete beam	Three point flexural test	Flexural strength (24h)	NBN B15-214 1984*
Right half	Splitting tensile test	Splitting tensile strength (24h)	NBN B15-218 1986
Right half	2x Compressive test	Compressive strength 10x10x10cm (24h)	NBN B15-220 1990**
Left half	Splitting tensile test	Splitting tensile strength (28d)	NBN B15-218 1986
Left half	2x Compressive test	Compressive strength 10x10x10cm (28d)	NBN B15-220 1990**

* a deviation from the standard is used: beams 100x100x500mm and span 300mm

** a deviation from the standard is used: cubes 100x100x100mm

Some small changed to the standard were used in this test series. These can be found in Tab. 4. The main purpose of these tests was to compare different purities of CRCA and their effect on RAC and not to compare the results to the minimal requirement for concrete elements used in precast elements.

All data results are ordered in minimum-average-maximum graphs. The Y-axis shows the amount of Rcu in the CRCA, while the X-axis is different for every parameter. The top-bar is the minimum-average-maximum of all recycled materials combined, while the bottom-bar is the reference concrete containing no CRCA. These graphs can be used to compare the different purities of CRCA and their influence.

4. TEST RESULTS

4.1 Dry Density

The dry density of NA SCC is 75 kg/m³ higher than the density of RAC SCC with 20 vol% replacement. This can be explained by the lower density of the CRCA. This does not count for FHDC. The exact reason behind this strange effect cannot be explained by the density of the aggregates. One possible explanation could be the difference in aggregate size distribution, which could lead to an increase in density by the presence of additional fine material, while the SCC already contains a lot of fines. The results show an increase in spread of the data results for FHDC. Compaction of these dry mixtures on laboratory scale is a lot harder, than compaction of ordinary concrete. It can be concluded that in case SCC, the use of CRCA leads to a decrease in dry density, while in case of FHDC other parameters play a more important role. The purity of the CRCA does not play any role. Different impurities do increase the scattering of the data in case of FHDC. The data results can be found in Fig. 1 and Fig. 2.

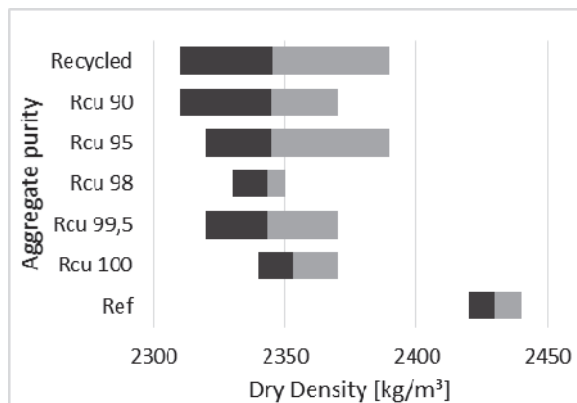


Fig. 1: Dry Density SCC

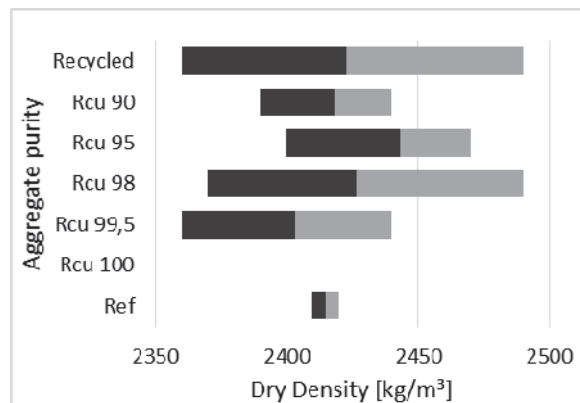


Fig. 2: Dry Density FHDC

4.2 Flexural strength (24h)

The flexural strength of SCC after 24 hours is 0.7 N/mm² lower after replacing 20 vol% CRCA. The influence of the purity of the CRCA does not have any influence. In case of FHDC, the replacement of 20 vol% CNA by CRCA leads to a small increase of 0.3 N/mm² flexural strength. While the purity of the CRCA does not seem to have any influence here either. Impurities do increase the scattering of the data. The data results can be found in Fig. 3 and Fig. 4.

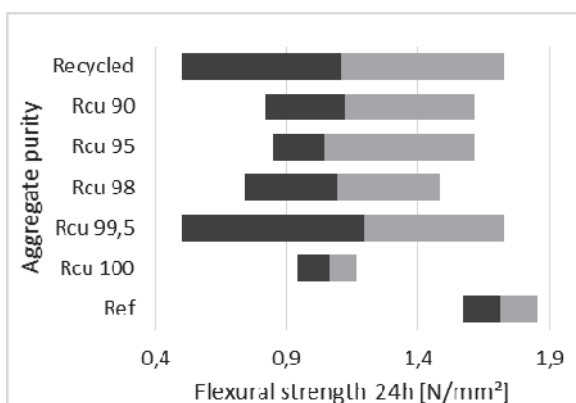


Fig. 3: Flexural strength 24h SCC

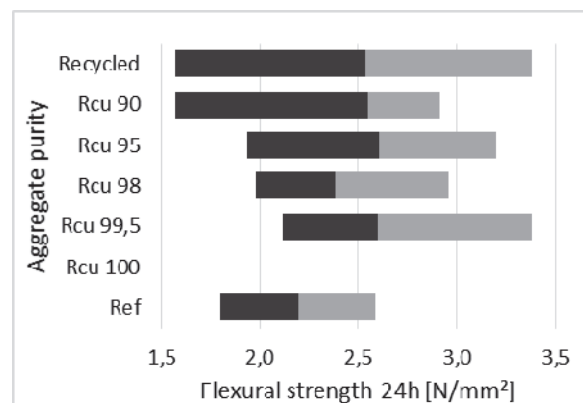


Fig. 4: Flexural strength 24h FHDC

4.1.3 Splitting tensile strength (24h)

The results of the 24h splitting tensile strength are comparable to those of 24h flexural strength. The addition of 20 vol% CRCA to SCC leads to a decrease of 0.4 N/mm², while in case of FHDC a small increase (+0.1 N/mm²) occurs. Impurities also lead to an increase of data scattering. The data results can be found in Fig. 5 and Fig. 6.

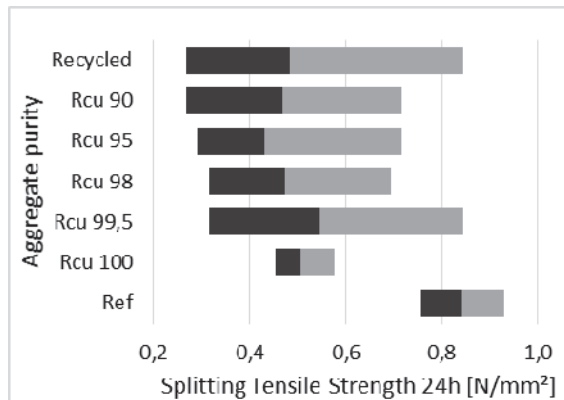


Fig. 5: Splitting tensile strength 24h SCC

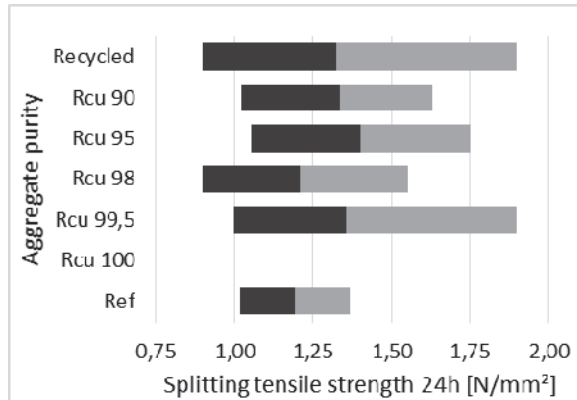


Fig. 6: Splitting tensile strength 24h FHDC

4.1.4 Compressive strength (24h)

Just like in case of the 24h flexural strength and 24h splitting strength, the 24h compressing strength of SCC drops by adding CRCA (-3 N/mm²), while that of FHDC increases(+2 N/mm²). In contrary to the previous tested parameters, the scattering of the data results by adding different types of impurity does not increase. The data results can be found in Fig. 7 and Fig. 8.

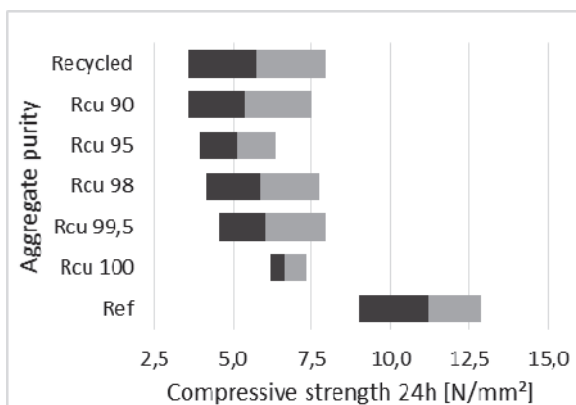


Fig. 7: Compressive strength 24h SCC

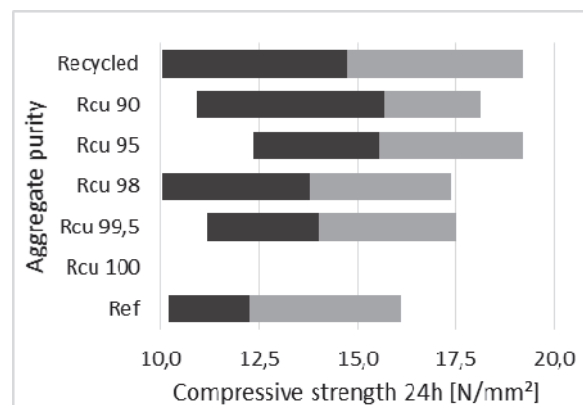


Fig. 8: Compressive strength 24h FHDC

4.1.5 Splitting tensile strength (28d)

The 28h splitting tensile test was the first measured parameter after 28 days of hardening in a climate room (20 °C and 90% humidity). The 0.4 N/mm² decrease in case of SCC enlarged to a difference of 2 N/mm². In case of FHDC, the small increase (+0.1 N/mm²) by the addition of CRCA noticed after 24h, became a small decrease of 0.2 N/mm². The different impurities do again lead to an increase of scattering of the data results found in Fig. 9 and Fig. 10.

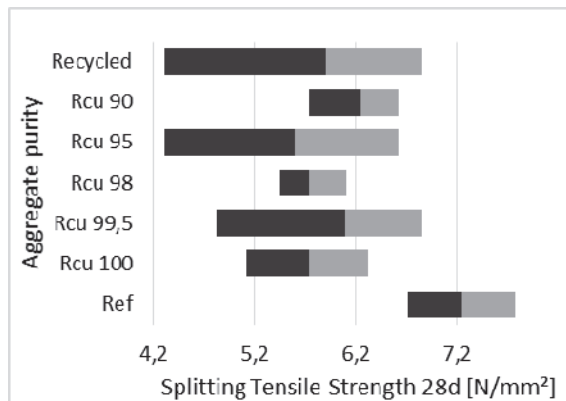


Fig. 9: Splitting tensile strength 28d SCC

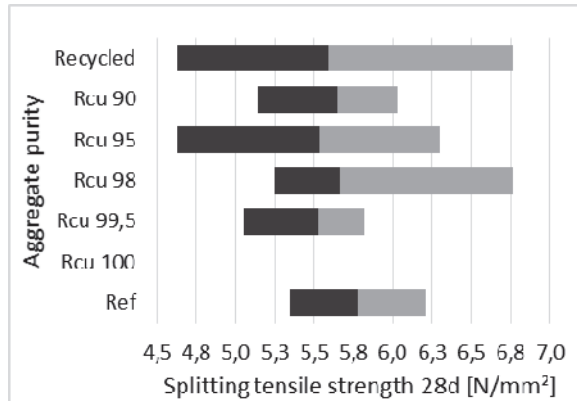


Fig. 10: Splitting tensile strength 28d FHDC

4.1.5 Compressive strength 28d

The addition of CRCA to SCC leads to a small decrease (-3 N/mm^2) of the 28h compressive strength. This decrease is neglectable compared to the scattering of the data. The addition of CRCA to FHDC has no influence at all on the 28h compressive strength. It can be noted that the addition of CRCA to SCC leads to an increase in data scattering, this is less noticeable in case of FHDC, because even the reference shows a rather large scattering. The data results can be found in Fig. 11 and Fig.12.

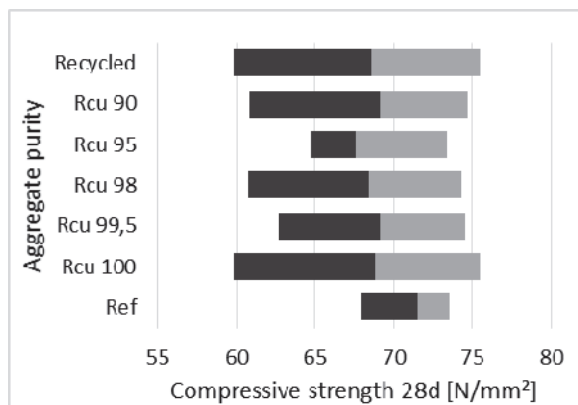


Fig. 11: Compressive strength 28d SCC

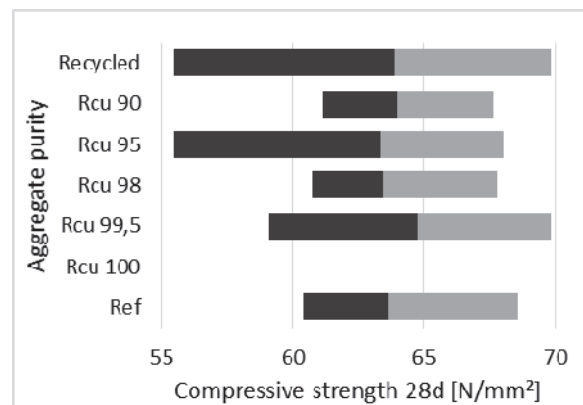


Fig. 12: Compressive strength 28d FHDC

5. CONCLUSIONS

It can be concluded that the amount of impurities in CRCA has no influence on the average mechanical properties of RA SCC and RA FHDC. They do lead to an increase in scattering of data results of most of the measured parameters which is equal to a drop in reliability.

Tab. 5: Average results

Parameter	Unit	SCC		FHDC	
		NA	CRCA	NA	CRCA
Dry Density	kg/m^3	2425	2380	2450	2490
24h Flexural strength	N/mm^2	1,75	1,05	2,20	2,50
24h Splitting tensile strength	N/mm^2	0,85	0,45	1,20	1,30
24h Compressive strength	N/mm^2	11,5	6,0	12,0	14,0
28d Splitting tensile strength	N/mm^2	7,20	5,80	5,80	5,70
28d Compressive strength	N/mm^2	72,0	68,0	64,0	64,0

The influence of replacing 20 vol% of NA by CRCA is most noticeable in the early age mechanical properties of SCC. In case of FHDC and at 28 days compressive strength in case of SCC, the influence of CRCA is neglectable.

The exact reason for slower strength development in the first 24h cannot be concluded by this research. Although literature suggests this is mainly due to the presence of other impurities besides Rcu, this data shows that the decrease is independent of the amount of Rcu present.

6. LIST OF NOTATIONS

CNA	Coarse Natural Aggregatds
CRCA	Coarse Recycled Concrete Aggregates
EPS	Expanded polystyrene
F	Fines fraction in CRCA
FEBE	Belgian Concrete Industry Federation
FHDC	Fast Hardening Dry Concrete
FL	Floating particles fraction in CRCA
FRCA	Fine Recycled Concrete Aggregates
PE	Polyethylene
PTV	Technical Regulations
PUR	Polyurethaan
Ra	Hydrocarbon fraction in CRCA
RA	Recycled Aggregates
RAC	Recycled Aggregate Concrete
Rb	Red Brick fraction in CRCA
RC	Recycled Concrete
Rcu	Recycled Concrete fraction in CRCA
Rn	Natural Aggregates fraction in CRCA
ρ_{rd}	Oven Dry Density of an aggregate
SCC	Self-Compacting Concrete
Wa ₂₄	Water Absorption of an aggregate after 24h submersion
X	Non-stony Aggregates fraction in CRCA

7. REFERENCES

- Boehme, L., Van Gysel, A., Vrijders, J., Joseph, M. and Claes, J. (2011), "ValReCon20: constructief beton met betonpuingranualten", (8 December 2011, Louvain La Neuve, Belgium).
- Boehme, L., Eds, (2012), "ValReCon20: Valorisation of recycled concrete aggregates in concrete C20/25 and C25/30", Oostende. ISBN 9789090265759.
- De Brabandere, P., Boehme, L. and Joseph, M. (2013), "PROJECT in de kijker: Noordmoerstraat, Veurne + Eco-Beton", 2013.
- Joseph, M. and Claes, J. (2012), "De kwaliteit van betongranulaat in functie van betonproductie", 18 Januray 2012, Ingenieurshuis, Antwerpen.
- Joseph, M., Sierens, Z., Boehme, L. and Vandewalle, L. (2015), "Water absorption variability of recycled concrete aggregates", Magazine of Concrete Research, vol. 67, no. 11, 2015, pp. 592-597.
- Noterman, B., Verstraeten, G., Geerts, G., Vrijders, J., Wouters, J., van der Have, J., Van Cauwenberghe, L., Boehme, L., Joseph, M., Schaerlaekens, S. and Moerman, W., (2016) "Recybet Roadmap".

EFFECT OF MIXING TIME TO THE PROPERTIES OF STEEL FIBRES AND SFRC

Olivér CZOBOLY and György L. BALÁZS

Budapest University of Technology and Economics, Department of Construction Materials and Technologies

H-1521 Budapest Hungary

SUMMARY

The mechanical properties of fibre reinforced concrete (FRC) depend on the material properties of fibres, fibre geometry and surface, amount of fibres, matrix properties, interface properties and loading condition. Main purpose of our experimental study was to determine the effect of mixing time (from 5 to 30 min) on the properties of steel fibres and steel fibre reinforced concrete (SFRC), respectively. Separated fibres after mixing were analysed with optical microscope. Pull out tests of hooked end steel fibres with different anchorage length and of steel fibre with shape deformation were carried out. Three-point bending tests were carried out in crack mouth opening displacement (CMOD) control on notched SFRC beams. Results indicated improved properties of FRC in flexure if fibre deform during mixing.

1. INTRODUCTION

Residual flexural strength of FRC is one of the most important parameter both for design and for practice. The bond of fibres mainly depends on material, shape, surface of fibres and the mechanical properties of the matrix, the amount of fibres as well as the loading rate (Balázs, Kovács, 1999; Kovács, Balázs, 2003). Consequently, almost all properties of FRC changes with the changing of the surface and the shape of fibres. Only little information exists on the influence of the mixing procedure on the properties of steel fibres.

The appropriate mixing, preparation and manufacturing of FRC are of high importance. According to Naaman et al. (1996) fibres may even negatively influence the properties of concrete if mixing and casting of concrete are not appropriate. It is of particular importance to reach homogeneous dispersion of fibres. Based on the guidance of European Ready Mixed Concrete Organization (ERMCO, 2012) 100 turns of the mixer are required to ensure good fibre distribution, but in practice it is difficult to monitor. Therefore, a minimum mixing time of 5 minutes (or 1 minute/m³) at the maximum speed of the drum is required. Fibres are often added to the concrete in the concrete plant during mixing or immediately when the concrete was added into the mixer so the concrete can homogeneously disperse in concrete. As a result, the fibres can be mixed for 0.5 to 1.5 hours in concrete with different speed before the casting of FRC.

Testing and modelling of bond behaviour of steel fibres are important to realize the favourable uses of FRC (Kovács, Balázs, 2003, 2004; Zhao, Verstrynge, di Prisco, Vandewalle, 2012; Balázs, 2012; Halvax, Lublóy, 2013; Zile, Zile, 2013; Breitenbücher, Meschke, Song, Zhan, 2014).

Application of steel fibres can be effective in hardened concrete until the fibres fail or are pulled out. Typically steel fibres are pulled out in cross-section of failure. Therefore, pull out tests of steel fibres with different mixing times and fibre shapes were also carried out.

Important question is whether the properties of steel fibres are significantly influenced by the longer mixing time than the minimum? On the other hand, can it significantly influence the final properties of SFRC?

2. EXPERIMENTAL PROGRAMME

Our mix compositions are presented in (Tab. 1). In our experimental programme one type of hooked end steel fibre was tested. The length of the steel fibres was 50 mm and the equivalent diameter 1 mm. The tensile strength of the steel fibres was 1000-1200 N/mm².

Tab. 1: Concrete compositions

Material	Type	Amount [kg/m ³]
Aggregate	sand (45%): (0/4 mm fraction)	824
	coarse aggregate (55%): (4/16 mm fraction)	1008
Cement	CEM I 42.5 N	380
Fibres	steel fibre amount: 0.3, 0.5 V%	
Water	$m_w/m_c=0.43$	163
Admixture	Glenium C300 (max 0.7 m _c %)	max 2.66

Before adding fibres, the mixing process of concrete was 5 minutes with pan type mixer. (The pan type mixer was used every time with activator). The consistence of fresh concrete was checked every 5 minutes and if necessary Glenium C300 type plasticizer admixture was added to the concrete to keep the flow class F4 (to EN 206:2013). Fibres were isolated from the fresh concrete with a magnet. Separated fibres were analysed with optical microscope.

Pull out tests of hooked end steel fibres were carried out (Fig. 1). Effects of mixing time and shape deformation were examined. Concrete with natural sand and gravel aggregate concretes with 0.5 V% steel fibres were used in the pull out test specimens. The pull out tests were carried out on steel fibres with “initial shape”, with “deformed shape” or with “U shape” (Fig. 2). The specimens with different mixing times were prepared at the same time, using the same mixture. The sizes of the specimens were 120×120×360 mm. With this dimensions the possibility of uneven fibre orientation was minimized. Samples with approximately 50×50×360 mm dimensions were cut out from the specimens for the pull out tests. The fibres were placed into the longitudinal axis of the FRC samples. A special loading frame was developed. for these pull out tests with 40×40 mm free surfaces around the tested fibres. 3 pieces of concrete cubes (150 mm) were prepared from each mixture after 5 or 30 minutes mixing for compressive tests and for bulk density tests.

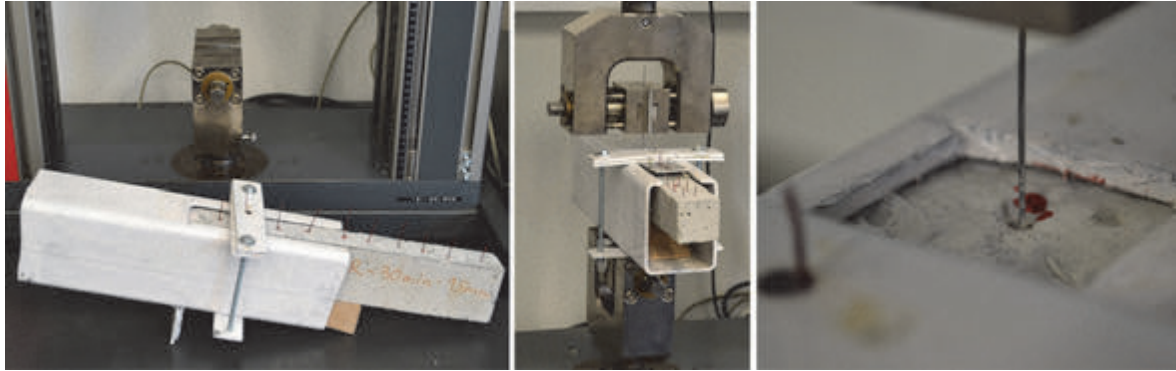


Fig. 1: Pull out tests of steel fibres

Fig. 2: Steel fibres prepared to pull out test,
a) initial shape, b) deformed shape, c) “U” shape

The possible effect on the post-cracking residual flexural strength of SFRC were tested (Fig. 3). Three-point bending tests of notched SFRC beams (with dimensions of 150×150×600 mm) were carried out in crack mouth opening displacement (CMOD) control according to EN 14651:2005+A1:2007 standard. The number of the fibres and the experienced inhomogeneous fibre dispersions were determined in the failed cross-section.

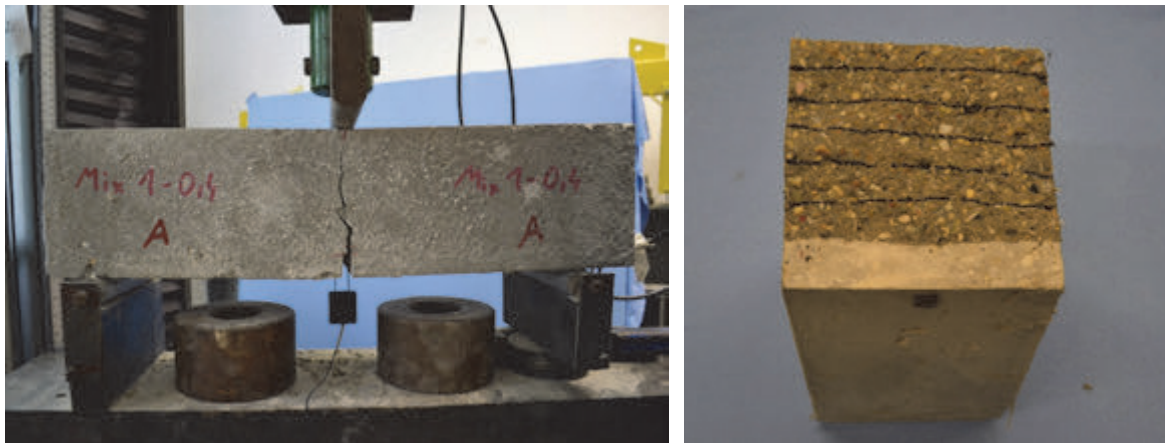


Fig. 3: Three-point bending tests on notched FRC beam

The tested beams were also subjected to compression tests. Compression tests of 90 days old cubes (150x150x150 mm) were carried out according to MSZ EN 12390-3:2009 standard.

The concrete cubes were cut from the undamaged parts of the beams. A part of the tested specimens was pulverized and the fibres were separated. The density of the concrete material (without fibres) were determined with pycnometer according to MSZ EN 1097-7:2008 standard. The porosity of the specimens was calculated from the density and the bulk density of the concrete and fibres for each fibre content.

3. TEST RESULTS

3.1. Type of deterioration of fibres

Shape deformations were observed for hooked end steel fibres during mixing in concrete (Fig. 4). Our tests indicated that the deformation of steel fibres could be observed after 5 minutes long mixing in concrete and the number of deformed fibres and the degree of deformation slightly increased as mixing time increased.

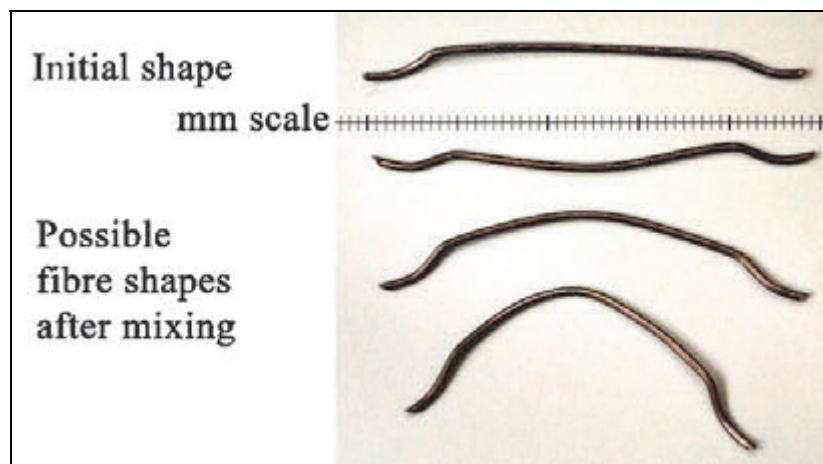


Fig. 4: Deformed steel fibre during mixing in concrete

3.2. Changes of pull out behaviour of steel fibres during mixing in concrete

Probably the shape deformation could slightly improve the anchorage capacity of steel fibres. Therefore, pull out tests were carried out on steel fibres after shape deformation.

According to the tests results the maximum pull out force was higher in case of fibres with shape deformation than in case of fibres with initial shape (Fig. 5-a). Some tested fibres with shape deformation were broken during the test. (The pull out force was higher than the load bearing capacity of the steel fibre.) Break of the steel fibres with initial shape and with similar anchorage length was not observed.

We observed a steel fibre with significantly deformed shape in the failed cross-section of a 30 minutes mixed SFRC beam by three-point bending test. In this case both ends of the fibre were bonded in the same side of the concrete beam (Fig. 6). The fibre could not be pulled out so the concrete crashed around the fibre. In order to analyse such behaviour, pull out tests were carried out on steel fibres with U shape.

According to the tests results the pull out behaviour of fibres with U shape was significantly different from the pull out behaviour of fibres with initial shape (Fig. 5-b). Failure (crashing) of concrete was observed in case of pull out tests of U shape fibres.

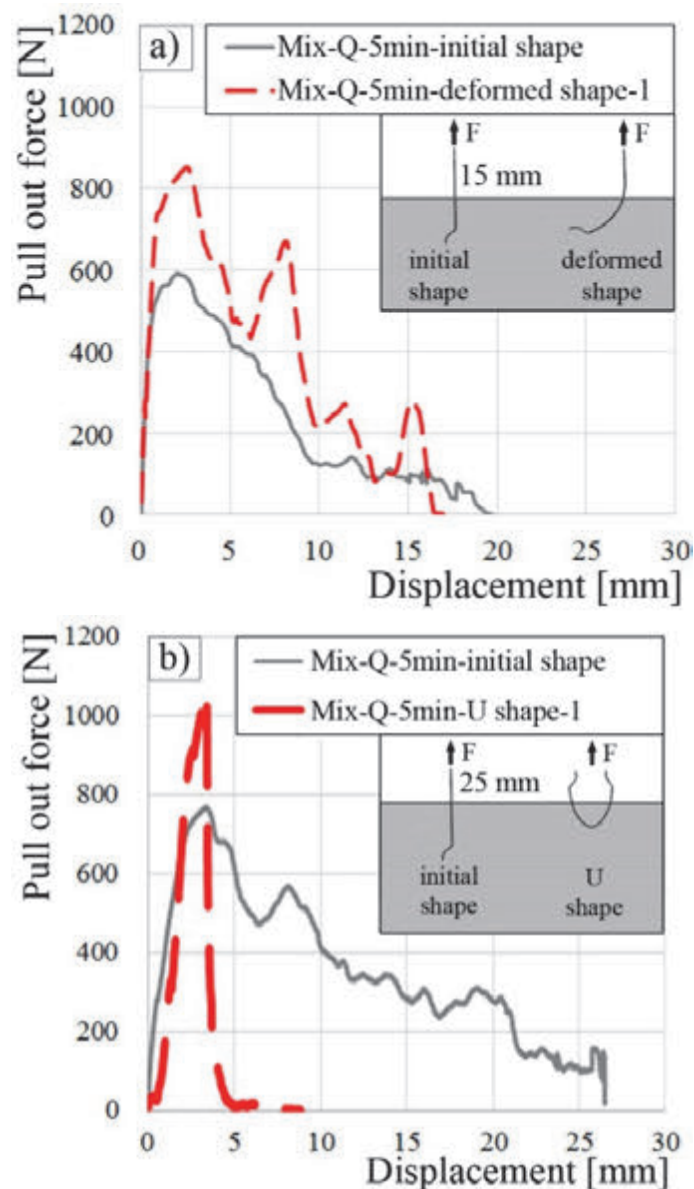


Fig. 5: Pull out force vs. displacement curves of steel fibres used in concrete with natural sand and gravel aggregates (mixing time: 5 minutes after addition of fibre), for better comparison average pull out force vs. displacement curves of intact fibres with 15 or 25 mm anchorage length are also represented,

a) - - - deformed shape fibre, b) - - - U shape fibre



Fig. 6: Deformed shape of steel fibre in cross-section of beam by the 30 min mixed SFRC

3.3. Effect of mixing time on post-cracking residual flexural strength of FRC

Present part of our research was directed to study the possible influence of the mixing time on the post-cracking residual flexural strength of SFRC. The SFRC beams were prepared with two different mixing times (an additional 5 or 30 minutes mixing of concrete after adding the fibres into the concrete).

In the legends of Fig. 7 the applied fibre type (0 → without fibre, S1 → hooked end steel fibre), the mixing time after adding of fibre (5 or 30 min), the planned fibre content in volume fraction (0.3 or 0.5 V%) and the number of fibres counted in the failed cross-section (... pcs) are represented, respectively.

We experimentally verified that the increase of mixing time of steel fibres in concrete from 5 minutes to 30 minutes slightly increases (by maximum 10%, in case of 0.3-0.5 V% fibre content) the post-cracking residual flexural strength of steel fibre reinforced concrete beams (Fig. 7), if the other parameters are constant. According to the test results this positive effect increased as the amount of fibres (0.3 V% to 0.5 V%) increased.

The main reason for this was the increased compressive strength and advantageous behaviour of deformed steel fibres as the mixing time increased (Fig. 8).

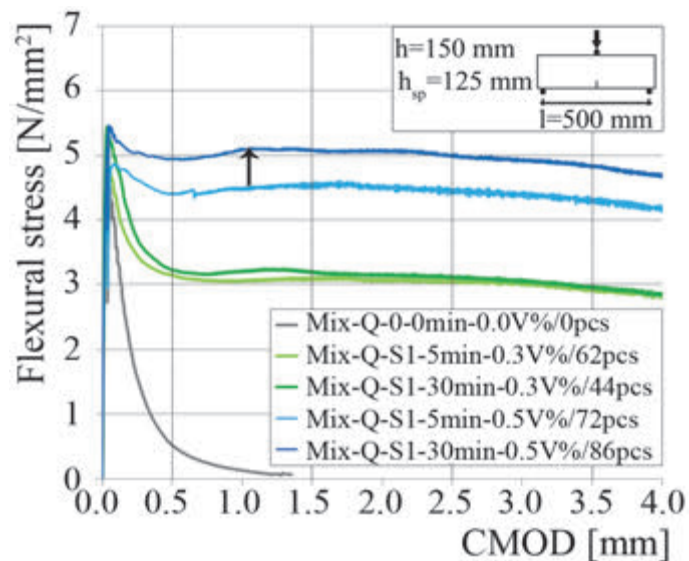


Fig. 7: Flexural stress-CMOD curves of three-point bending tests of SFRC beams mixed in pan type mixer, with 0.3 and 0.5 V% fibre content

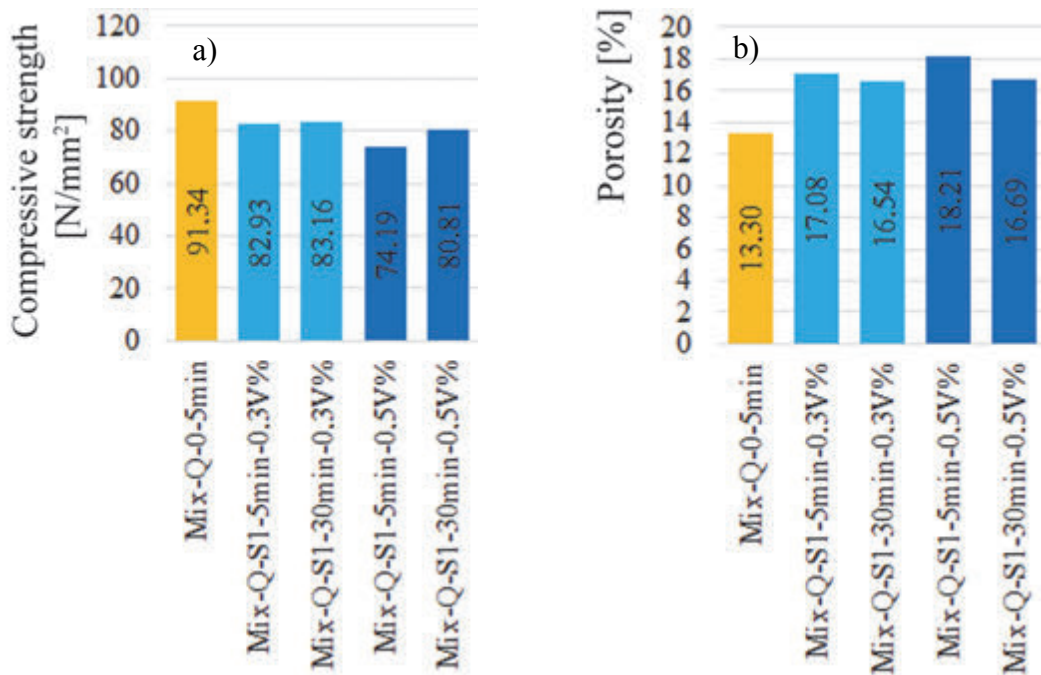


Fig. 8: Properties of SFRC specimens, a) Compressive strength, b) Porosity

4. CONCLUSIONS

Main purpose of our experimental study was to determine the effect of mixing time (from 5 to 30 min) on the properties of steel fibres and SFRC, respectively. We tested two types of steel fibres (without coating or with brass-coating). Results of our experimental study indicated the following:

1. Shape deformations were observed for hooked end steel fibres during mixing in concrete. Our tests indicated that the deformation of steel fibres could be observed after 5 minutes long mixing in concrete and the number of deformed fibres and the degree of deformation slightly increased as mixing time increased.
2. Pull out tests were carried out on hooked end steel fibres with initial shape and with shape deformation. According to our tests the maximum pull out force was higher in case of fibres with shape deformation than in case of fibres with initial shape.
3. Longer mixing times resulted in a slight increase of the post-cracking residual flexural strength of SFRC. The main reason for this was the increased compressive strength and increased number of the deformed steel fibres as the mixing time increased.

5. REFERENCES

- Balázs, G. L. (2012), "Fibres in Concrete Structures", Section of the book: Innovative Materials and Techniques in Concrete Construction (Ed. Fardis, M. N.), Springer-Science+Business Media, Dordrecht, Heidelberg, London, New York, 2012, ISBN 978-94-007-1996-5, pp. 153-165. <http://www.springer.com/us/book/9789400719965>
- Balázs, G. L. and Polgár L. (1999), „Past, present and future of fibre reinforced concrete”, Vasbetonépítés, Vol. 1., No. 1., pp. 3-10.

- Breitenbücher R., Meschke G., Song F., Zhan Y. (2014), "Experimental, analytical and numerical analysis of the pullout behaviour of steel fibres considering different fibre types, inclinations and concrete strengths", *Structural Concrete*, Vol. 15, No. 1, pp. 126–135.
- EN 14651:2005+A1:2007, "Test method for metallic fibre concrete – Measuring the flexural tensile strength (limit of proportionality (LOP), residual)", European Committee for Standardization, 17 p.
- ERMCO (2012), „Guidance to fibre concrete, Properties Specification and Practice in Europe”, European Ready Mixed Concrete Organization, pp. 1-39.
- Halvax K. and Lublóy É. (2013), "Pull-out behaviour of steel fibres", *Fibre Concrete 2013*, Prague, Czech Republic, Sep. 12-13, 2013, pp. 1-10.
- Kovács, I. and Balázs, G. L.,(2003), "Structural behaviour of steel fibre reinforced concrete", *Journal of Structural Concrete*, Vol. 2003, No. 2, pp. 57-63.
- Kovács, I. and Balázs, G. L. (2004), "Structural performance of steel fibre reinforced concrete", Book, Publ. Comp. of Budapest University of Technology and Economics, ISBN 963 410 822 3, 233 p, <http://fib.bme.hu/konyvek/steel-fiber-.pdf>
- Naaman, A. E., Paramasivam, P., Balázs, G. L. et al. (1996), "Reinforced and prestressed concrete using HPRCC matrices". In: *Proc. 2nd Int. RILEM/ACI Workshop*, pp. 291-347.
- Zhao G., Verstryngne E., di Prisco M., Vandewalle L. (2012), "Investigation on single fiber pullout and interfacial debonding mechanisms with acoustic emission techniques", 8th RILEM International Symposium on Fiber Reinforced Concrete: challenges and opportunities (BEFIB 2012), pp. 369-380.
- Zile E. and Zile O. (2013), "Effect of the fiber geometry on the pullout response of mechanically deformed steel fibers", *Cement and Concrete Research*, Vol. 44, No. 1, pp. 18-24.

EFFECT OF SUPPLEMENTARY CEMENTITIOUS MATERIALS ON MORTAR PROPERTIES AND CORROSION OF STEEL IN DIFFERENT ENVIRONMENTS

Egon Milost¹, Tadeja Kosec¹, Aljoša Šajna¹, Irina Stipanović Oslaković¹, Andraž Legat¹, Violeta Bokan Bosiljkov²

*¹ Slovenian National Building and Civil Engineering Institute, Ljubljana / Slovenia
Dimičeva ulica 12, 1000 Ljubljana, Slovenia*

*² Faculty of Civil and Geodetic Engineering, University of Ljubljana, Ljubljana / Slovenia
Jamova cesta 2, 1000 Ljubljana, Slovenia*

SUMMARY

Use of supplementary cementitious materials (SCM), ageing and carbonation significantly impact mortar properties and corrosion of embedded steel. To study the influence of SCMs on mortar properties, specimens from pure Portland cement and three different types of blended cement were prepared. Compressive strength, open porosity and resistance of capillary absorption have been investigated. Further, the impact of SCMs and carbonation on chloride induced corrosion of steel in mortars was monitored with Electrochemical Impedance Spectroscopy (EIS) technique and after the measurements, the specimens were demolished and a visual inspection of the reinforcement surfaces was performed.

1. INTRODUCTION

SCMs are used in concrete for ecological reasons and to improve properties. They generate noticeable changes in hydration process of binder and consequently in properties of cement matrix which determine its durability. The experience of recent decades shows that reinforced concrete structures are not immune to the effects of the environment, but are subject to deterioration processes, where corrosion of concrete reinforcement is the most common cause of reduced service life and reparations (Cox et al., 1996). Carbonation and ingression of aggressive ions are two main causes for corrosion of steel in concrete (Cigna et al., 2003) significantly affected by individual environmental parameters and properties of the cement matrix, thus the nature and intensity of the corrosion processes of embedded steel are highly variable by using various kinds of cements (Mehta and Montero, 2006; Bertolini et al., 2013). Since the intended service life of the new complex concrete buildings can be hundreds of years (Legat et al., 2009), an accurate and reliable investigations in the effects of specific SCM on the properties of the cement matrix are extremely important and challenging.

2. MATERIALS AND SAMPLES

2.1 Materials

Cements used in this study were produced in laboratory by grinding and blending raw materials (Portland cement clinker (K), granulated blast furnace slag (S), siliceous (V) and calcareous (W) fly ash, natural pozzolana ((P) - tuff) provided from local cement plant where are used in regular production. Designation, composition and physical properties of cements are listed in Tab. 1 and are in accordance with SIST EN 197-1:2011.

Tab. 1: Composition, specific gravity and specific surface area of used cements

		Cement type			
		CEM I	CEM III/A	CEM IV/A (W-P)	CEM V/A (S-V-P)
Constituents	Clinker [m. %]	100	50	72	55
	Granulated blast furnace slag [m. %]		50		25
	Flay ash (siliceous) [m. %]				15
	Flay ash (calcareous) [m. %]			20	
	Natural pozzolana (tuff) [m. %]			8	5
Specific gravity [g/cm ³]		3.13	3.02	2.93	2.94
Fineness (Blaine) [cm ² /g]		3870	3593	4950	5510

The tests were performed on four different mortars, each prepared of different cement and in accordance with standard SIST EN 196-1:2005. They were composed of three parts of sand, one part of cement and a half part of water. Consistency of each was determined by flow table according to SIST EN 1015-3:2001. Results are presented in

Tab. 2.

Tab. 2: Consistency of fresh mortar determined by flow table

	Cement type			
	CEM I	CEM III/A	CEM IV/A (W-P)	CEM V/A (S-V-P)
Consistency of fresh mortar [mm]	171	176	174	157

2.2 Samples for determination of physical properties of mortars

Mortar prisms 40×40×160 mm³ to determine physical properties were prepared according to SIST EN 196-1:2005. They were stored in humid chamber at 20 ± 1 °C with RH > 90 % for first 24 h after casting and then demoulded and additionally cured at 20 ± 2 °C with RH > 95 % until the age of 28 days.

2.3 Samples for investigations in corrosion of steel in mortars

Mortar prisms of 30×30×100 mm³ with embedded drawn steel rod (Φ6 mm) as working electrode and carbon fibre yarn as counter and reference electrode were cast for EIS measurements (Fig. 1). The working electrode was properly cleaned before installation by grinding (SiC paper 500) and degreasing with acetone. Perpendicular distance between the axis of the reinforcement and the upper exposed surface was of 10 mm and the thickness of the mortar protective layer was of 7 mm. Specimens were poured in wooden moulds and stored in laboratory conditions at 20 ± 2 °C with RH 20 ± 5 % for first 24 h and then demoulded and cured as those for physical tests.

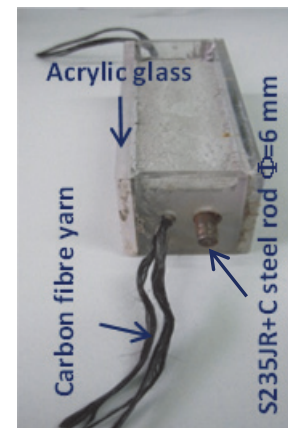


Fig. 1: Specimen for investigations in corrosion of steel in mortar

3. METHODS

3.1 Environments

Investigations were performed in two simulated environments where in the first one the specimens were aged in humid chamber for another 10 months after curing period (28 days) while in the second one they were placed in carbonation chamber till the last mortar was fully

carbonated (10 months). After that period the physical characteristics of mortars were determined and exposure to cyclic wetting and drying began.

3.2 Physical properties of mortar

The following physical properties of the cement mortars were investigated: compressive strength according to standard SIST EN 196-1:2005, open porosity according to standard SIST EN 1936:2007 and resistance of capillary absorption according to standard SIST EN 13057:2002.

3.3 Corrosion resistance

EIS method was used on cyclically wetted and dried mortar prisms to determine the corrosion resistance of mortars. The cycle lasted for a week and began with wetting period when 3.5 % NaCl solution was poured on the specimen surface for 2 days. Then it was removed, the specimen surface dried and EIS (Gamry Reference 600) performed (frequency: 100 kHz - 5 mHz, perturbation: ± 10 mV at 10 points per decade). In order to assess corrosion resistance of the samples the absolute values of the total impedance $|Z|_{tot}$ at lowest frequency were taken into account. The cycle ended by 5 days of drying. At the end of 22 weeks of testing period specimens were demolished and rods visually examined for the forms of corrosion attack.

4. RESULTS AND DISCUSSION

4.1 Physical properties of mortars

4.1.1 Compressive strength

The compressive strength of 28 days old, 10 months aged and fully carbonated mortars are graphically presented in Fig. 2.

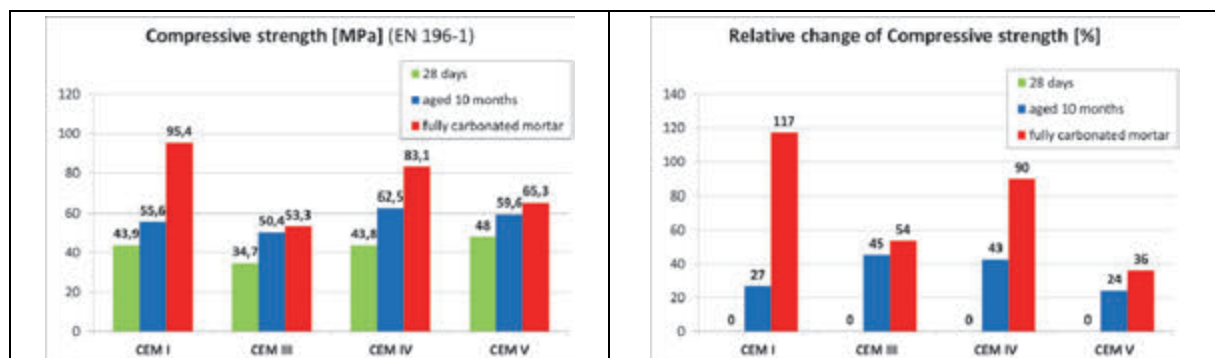


Fig. 2: Comparison of compressive strengths of mortars

Test results show that 28 days compressive strength of mortar from blast furnace cement (CEM III) was 21 % lower, from pozzolanic cement (CEM IV) was approximately the same while from composite cement (CEM V) was 9 % higher than that from Portland cement (CEM I). According to the theoretical background of cement hydration (Mehta and Montero, 2006) and available results in the literature, the highest 28 days compressive strength for mortar from CEM I was expected and a moderately lower for mortars from CEM IV and CEM V. This discrepancy is mostly consequence of differences in specific surface areas of the investigated cements. The lowest compressive strength for mortar from CEM III was expected because of the high content of slag with low reactivity.

10 months of aging has increased the compressive strength of all inspected mortars because prolonged curing raised the rate of hydration and provided additional products of pozzolana reaction to fill the pore structure. The highest increment of compressive strength was expected at CEM III and CEM V because of lower clinker content and higher content of slag and/or pozzolanic material slowing down the hydration and delaying the strength development, followed by CEM IV and CEM I. The results has confirmed expectations for all mortars except for CEM V, where the lowest increment of compressive strength could be related with a lack of lime which is a product of hydration of clinker and is essential for pozzolana reaction.

Carbonation gained the highest compressive strength at all tested mortars. Fully carbonated CEM I mortar yielded a 117 % higher compressive strength in comparison with the 28 days old specimen followed by CEM IV, CEM III and CEM V. It is assumed that the increase in compressive strength is mostly related to the amount of clinker in cement, as portlandite emerging from clinker hydration is primarily carbonated and thus forming compounds that fill the pore structure in cement matrix (Mehta and Montero, 2006). Relatively big difference in compressive strength between CEM III and CEM V, despite almost the same clinker content, can be explained by low reactivity of CEM III delaying the strength development and possible lack of lime for pozzolana reaction at CEM V.

The open porosity and resistance of capillary absorption of cements at 28 days, 10 months aged and fully carbonated are graphically presented on Fig. 3.

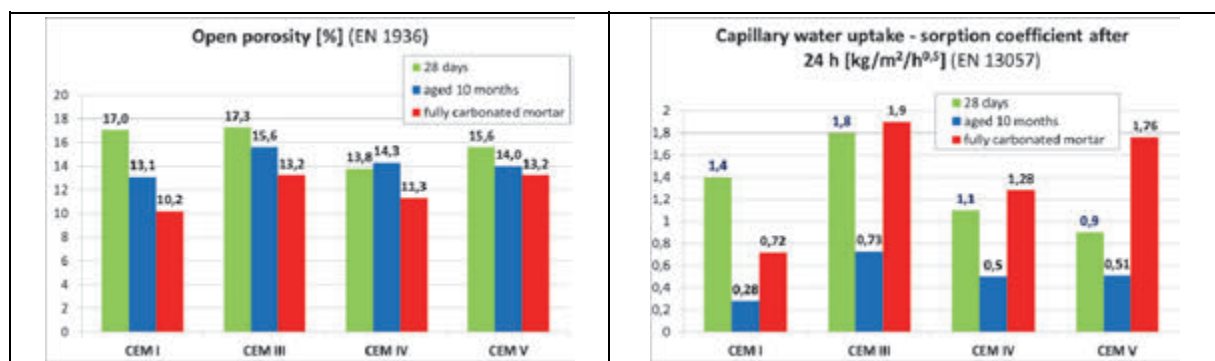


Fig. 3: Graphical comparison of open porosity and water sorption coefficient after 24 hours

According to the theoretical background (Bertolini et al., 2013) lower open porosity on 28 days old specimens was expected for all cements with SCMs as products of pozzolana reaction fill the pore structure but from the results it can be seen that the porosity detected on CEM III was almost the same as on CEM I and was the highest. It seem that before mentioned simultaneous milling of all the components of CEM III and a high content of slag has slowed down the effect of pozzolana reaction which couldn't be detected at this age. A higher open porosity of CEM V in comparison with CEM IV despite the higher content of pozzolanic material can be explained by the lack of lime which is formed by hydration of clinker and is necessary for pozzolana reaction.

10 months of aging has reduced the open porosity of all inspected cements except for CEM IV where a slight rise was detected and we couldn't find the explanation for this phenomenon. A prolonged curing period increased the rate of hydration of cement paste and provided additional products of pozzolana reaction filling the pore structure what reduces open porosity of hydrated cement paste. Relatively high drop in open porosity at CEM I can be explained with low reactivity due to low specific surface of this cement which needs more time to fill the pore structure in cement paste.

As expected, carbonation caused a significant drop in open porosity in comparison with 28 days old samples for all types of cements as its products precipitate on pore surface. Relatively high drop in open porosity for CEM I compared to CEM IV and CEM V can be explained by mutual complementation of effects of lower hydration rate due to low specific surface and high portlandite content which reacts during carbonation. High drop in open porosity for CEM III compared to CEM IV and CEM V is probably the consequence of low reactivity of CEM III and a high content of slag leading to prolonged formation of cement matrix in sense of filling the pore structure.

In theory, capillary action is stronger as the pore dimensions decrease (Bertolini et al., 2013). Therefore, in case of the investigations into the capillary water uptake a higher values of sorption coefficient after 24 hours was expected for all cements with SCMs in comparison with CEM I but from the results it can be seen that the highest sorption coefficient on 28 days old specimens was detected on CEM III followed by CEM I, CEM IV and CEM V. The lower values of sorption coefficient at CEM IV and CEM V could be explained by two phenomena: the pores become so small that friction significantly slowed down the transport of water, the products of pozzolana reaction have reduced interconnections of capillary pores.

10 months of aging has reduced the sorption coefficient after 24 h of all inspected cements. Prolonged curing period has increased the rate of hydration and provided additional products of pozzolana reaction reducing the pore dimensions. That should lead in higher sorption coefficients, but as it seems, aging has also significantly influenced the interconnections of capillary pores. A bit surprising is an extremely high drop in sorption coefficient at CEM I. We can assume that low reactivity due to low specific surface of this cement has slowed down hydration process what has reduced interconnections of capillary pores.

Carbonation has reduced sorption coefficient of CEM I and raised those of blended cements in comparison with 28 days old samples. The reason for reduction of sorption coefficient of CEM I could be the same as in case of ageing. The expected raise of sorption coefficient of specimens with SCMs is related to carbonation products which reduces the pore diameter. A very high increase of sorption coefficient for CEM V could be in relation to occurrence of microcracks as a result of carbonation of Calcium-silicate-hydrate (C-S-H) (Šavija and Luković, 2016).

Generally, by comparing the results of investigations into the capillary water uptake and open porosity it can be noticed that they differs and can't be correlated. This may be attributed to the fact that capillary water uptake is not only related with the total capillary porosity (i. e. the percentage of volume occupied by capillaries) but also with the size and interconnection of capillary pores and that the influence of carbonation on pore structure is very complex (Šavija and Luković, 2016). It is also important to emphasise that investigations in porosity and transport processes can give misleading results in sense of corrosion resistance, because they cannot consider a chloride binding capacity and alkalinity of mortars.

4.2 Corrosion resistance of mortars in different environments

EIS measurements were conducted weekly on cyclically wetted and dried mortar prisms. The total duration was of 22 weeks. Absolute values of total impedance $|Z|_{tot}$ can be related to polarisation resistance which is in correlation with corrosion resistance. The higher is the $|Z|_{tot}$ the lower the corrosion rate. In order to assess the corrosion resistance of the samples the $|Z|_{tot}$ at smallest measured frequency were taken into account.

4.2.1 Cyclically exposed aged mortars

The results of EIS measurements on aged mortars are presented on Fig. 4. Constant values of $|Z|_{tot}$ at lowest frequency during first 19 weeks can be noted for all samples except CEM IV where two significant drops at 9th and 15th week were measured. According to values on the chart the mortar samples exhibit increasing resistance to corrosion in following order: CEM III < CEM IV < CEM V < CEM I.

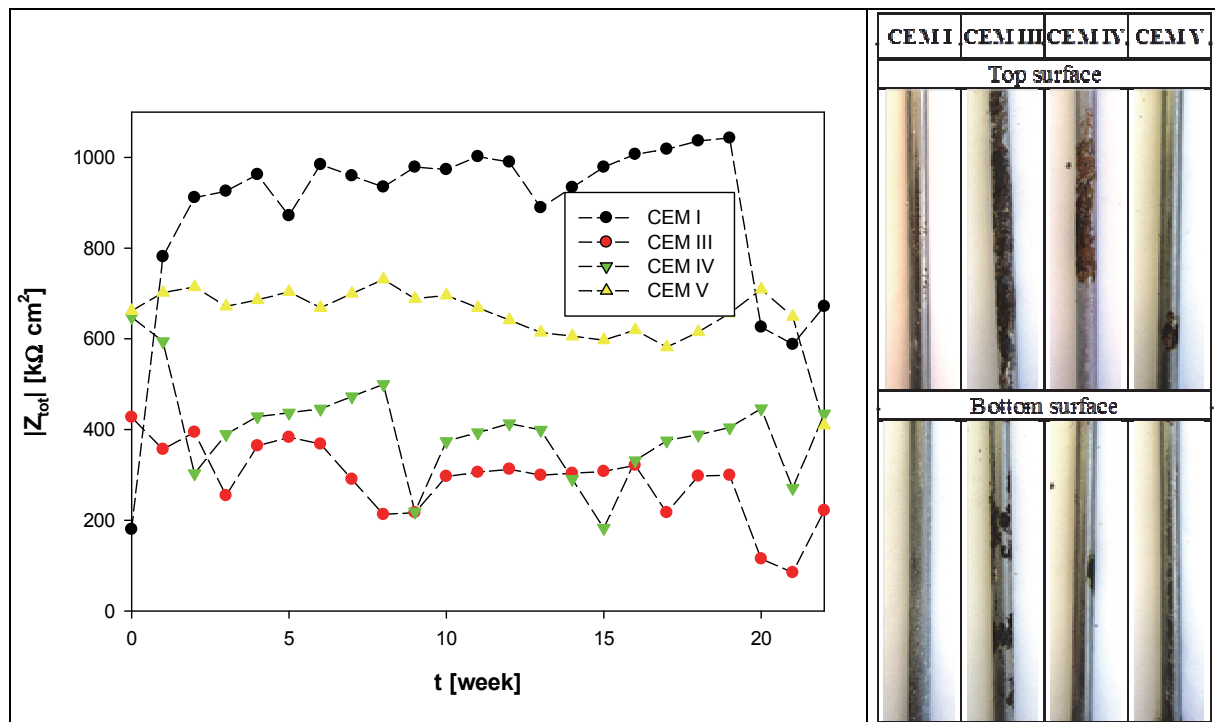


Fig. 4: Total impedance chart for different types of 10 months aged mortars, measured at lowest frequency and photos of the reinforcements after 22-week exposure

Visual inspection of the surfaces of the exposed portion of the reinforcement showed that the intensity of the corrosion damage varied. The most pronounced, general corrosion was observed in the case of CEM III followed by CEM IV. In the case of the CEM V, localized surface corrosion with some pits was observed while on the rod embedded in CEM I only some traces of corrosion products in the form of dots were detected. From a comparison of the estimates of the resistance to corrosion on the basis of the EIS measurements and the visual inspection of the damage to the samples can be seen, that the results are comparable and show the lowest corrosion resistance of CEM III followed by CEM IV and CEM V, while CEM I experienced only slight general corrosion.

4.2.2 Cyclically exposed fully carbonated mortars

The results of EIS measurements on fully carbonated mortars are presented on Fig. 5. Constant values of $|Z|_{tot}$ at lowest frequency during first 11 weeks can be noted for all samples except CEM V where a significant rise at 3rd week was measured. According to values on the chart the mortar samples exhibit increasing resistance to corrosion in following order: CEM III \leq CEM V < CEM IV < CEM I.

Visual inspection of the exposed surfaces of the reinforcement showed that the most pronounced, general corrosion was observed in the case of CEM III mortar followed by

CEM V. Also on the top surface of CEM IV sample general corrosion was observed whilst on the bottom surface only localized surface corrosion was observed. At CEM I only localized general corrosion with some small pits was noticed. From a comparison of the estimates of the resistance to corrosion on the basis of the EIS measurements and the visual inspection of the damage to the samples can be seen, that the results are comparable and show the lowest corrosion resistance of CEM III followed by CEM V and CEM IV, while CEM I experienced only slight general corrosion.

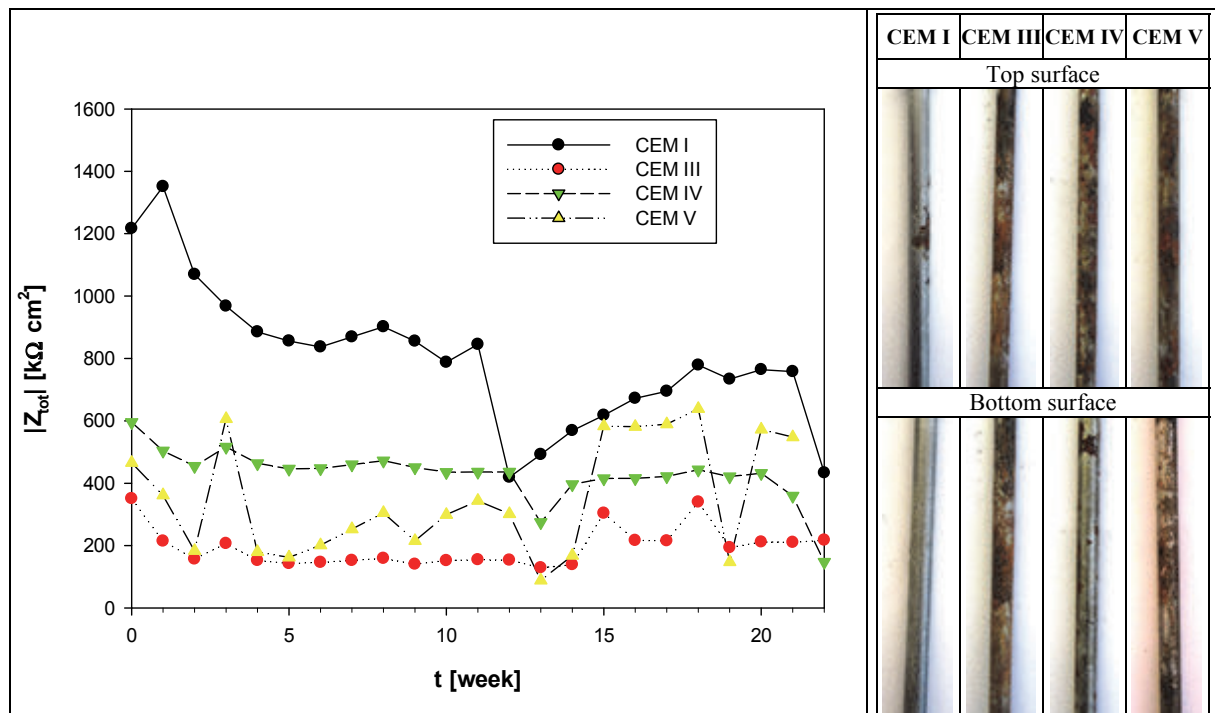


Fig. 5: Total impedance chart for different types of carbonated mortars, measured at lowest frequency and pictures of the reinforcements after the exposure

From a comparison of the results of EIS measurements in different environments it can be seen that carbonation generally reduces values of $|Z|_{tot}$ and shortens the period of constant values. This means that the resistance to chloride induced corrosion of carbonated mortars is lower than that of aged, what is confirmed also by results of visual inspection.

From a comparison between the results of sorption coefficient after 24 hours and resistance to chloride induced corrosion a very good correlation can be found (except for aged CEM IV). The higher is the sorption coefficient the lower the resistance to chloride induced corrosion.

5. CONCLUSIONS

In the 10 months of ageing and fully carbonation and 22 week exposure to cyclic wetting and drying the effect of SCMs on the physical properties of mortar and corrosion of embedded steel was studied. CEM III, CEM IV and CEM V were investigated next to CEM I. The following major conclusions can be drawn:

1. Ageing (prolonged curing) moderately increases compressive strengths of mortars, severely reduces open porosity, except for CEM IV where a slight rise is noticed and extremely decreases sorption coefficient after 24 hours.

2. Carbonation moderately to severely raises compressive strengths of mortars, extremely reduces sorption coefficient after 24 hours for CEM I, slightly rises it for CEM III and CEM IV and extremely increases for CEM V.
3. Testing results on open porosity of carbonated mortars are misleading in sense of corrosion resistance and durability.
4. EIS technique on specimens exposed to cyclic wetting and drying can distinguish between corrosion resistance of mortars prepared from different cements and exposed to different environments, giving results consistent with the visual appearance of corroded steel.
5. Investigation in chloride induced corrosion on specimens prepared from different cement types and aged has shown increasing resistance to corrosion in following order: CEM III < CEM IV < CEM V < CEM I.
6. Investigation in chloride induced corrosion on carbonated specimens prepared from different cement types has shown increasing resistance to corrosion in following order: CEM III \leq CEM V < CEM IV < CEM I.
7. Carbonation reduces resistance to chloride induced corrosion.
8. A very good correlation between sorption coefficient after 24 hours and resistance to chloride induced corrosion is noticed.

6. ACKNOWLEDGEMENTS

This study is supported by research program P2-0273, financed by Slovenian Research Agency.

7. REFERENCES

- Bertolini, L., Elsener, B., Pedferri, P., Redaelli, E., Polder, R. (2013), "Corrosion of Steel in Concrete; Prevention, Diagnosis, Repair", Wiley-VCH Verlag GmbH & Co. KGaA.
- Cigna, R., Andrade, C., Nuernberger, U., Polder, R., Weydert, R., Seitz, E. (2003), "COST 521: Corrosion of Steel in Reinforced Concrete Structures, Final Report," European Communities, Luxembourg.
- Cox, R. N., Cigna, R., Vennesland, Ø., Valente, T. (1996), "COST 509: Corrosion and protection of metals in contact with concrete, Final Report," European Communities, Luxembourg
- Legat, A., Šajna, A., Mladenovič, A., Strupi-Šuput, J., Kuhar, V., Gartner, N., Kosec, T. (2009), "Methodology of monitoring the conditions and development of damages in concrete engineering barriers and metal containers for possible type of LILW repository: research project, 2nd phase". Ljubljana: Slovenian National Building and Civil Engineering Institute,
- Mehta, P. K., Monteiro, P. J. M. (2006), "Concrete: Microstructure, Properties, and Materials", New York: McGraw-Hill Professional.
- Šavija, B., Luković, M. (2016), "Carbonation of cement paste: Understanding, challenges, and opportunities", Construction and Building Materials, Vol. 117, October 2016, pp. 285-301.

EXPERIMENTAL PEDESTRIAN THIN WALLED DOUBLE CURVATURE ARCH FOOTBRIDGE MADE OF UHPFRC

*Jiří Kolísko, David Čítek, Petr Tej, Milan Rydval
Czech Technical University in Prague, Klokner Institute
Šolínova 7, 166 08 Prague 6, Czech Republic*

SUMMARY

Article presents design and production of thin-walled double curved footbridge made from UHPFRC. Parameters of this relatively new cementitious material enables design very thin structures. Article presents complex theoretic-experimental program solving design and real preparation of very specific pedestrian bridge. Single-span bridge with span of 10 m and the clear width of 1.50 m with the total thickness of shell structure 30 - 45 mm was cast as a prefabricated element in one piece. Extensive research was needed to be done before production of arch double curve footbridge. Large scale mock-ups were casted and tested. Casting technology and production of formwork were tested and optimized several times. Results of experiments were compared with numerical analysis.

1. INTRODUCTION

UHPC is very promising material and its very favourable material properties allow to design very thin structures. Experiences with the real UHPFRC applications and results of many experimental research programs in Czech Republic lead to design modern footbridge using new principles and knowledge (AFGC, 2013; Wang, 2015; Vitek, 2013). This article is focused on experimental research in field of material optimization, testing of material properties and preparation of the preliminary mock-up of the part of the construction, testing of load bearing capacity of thin walls and on final mock-up 1:1 of the whole footbridge. Each part of this extensive experimental research is presented in more detail in this article.

The span of the footbridge is 10 m. The bridge is designed with double curvature – horizontal and vertical. In the vertical and transverse direction it is a circular arc with a camber of 0.4 m. The cross section of the bridge has a width of 1.5 m. The bridge load bearing structure consists of a bottom deck with only 45 mm thickness and 30 mm thick side walls. The side walls serve as handrails. Handrails height is 1.1 m in the middle of the bridge span and 1.5 m at the support area. In place of the support area a bridge deck is a little bit thicker because of anchors zones. These zones are reinforced by ordinary reinforcement for reliable transfer of the shear and anchors forces at the end supports. The rest of the bridge has no conventional reinforcement and it is reinforced only by the steel fibre reinforcement.

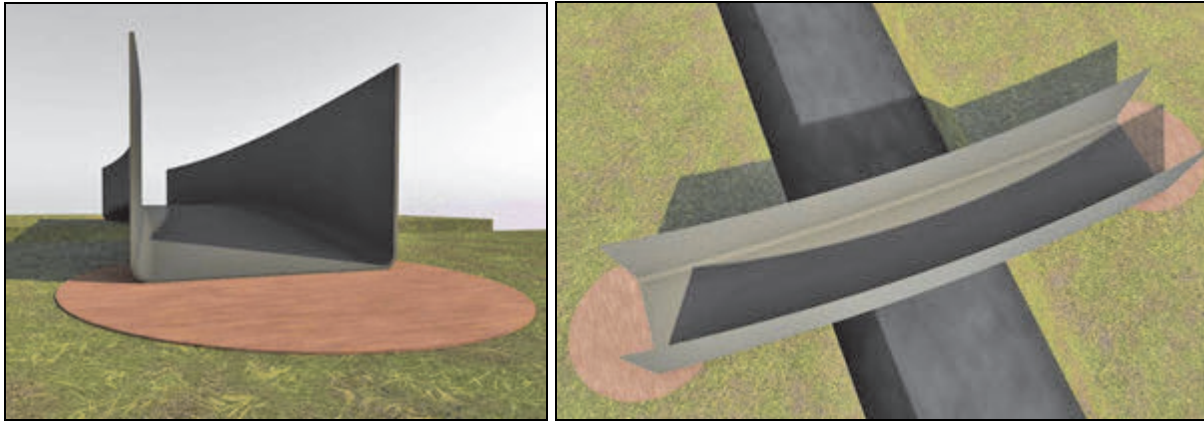


Fig. 1: Visualization of the bridge

The main shape of the footbridge (“U” shape) was taken partly from steel construction and partly from shell construction. Optimized UHPFRC mixture should be able to be cast in such a thin and difficult shape. The main outstanding features of this material are the high compressive strength, high tensile (direct and flexural) strength and very high durability also (JSCE, Kabele, 2013; Kolisko, 2015; Vitek 2013). Favourable durability is caused by a very high density of the cement matrix and by very low level of porosity with unconnected pores. This fact is provided by very fine particles (slag, silica fume) and very low water-cement coefficient. High levels especially of flexural strength are provided by using of the steel fibres. These perfect material properties should be supplemented by high workability (Abbas, 2016; Blank 2016; Shi, 2015).

Production of “U” shaped UHPFRC footbridge is very complex problem. Whole construction need to be cast in one part, one time and design of the structure need be optimized with respect to all factors during casting, demoulding, transporting and using.

2. DESIGN - FIRST STEP

Bridge model was created in a computer program ATENA 3D. Which is materially and geometrically nonlinear simulation program mainly for concrete structures. These macro elements have specified material item 3D Nonlinear Cementitious2. We used parameters of UHPC concrete class C110/130 blended with scattered reinforcement in first static approximation. First calculation were performed on a basis of the experimental data gained in the past research in field of UHPC. Material properties are not yet reduced by material coefficients. The resulting structure is considered using one or two class better concrete.

The bottom plate of the bridge was loaded with whole surface load of 4.2 kN/m^2 , and subsequently up to structural failure, further part with the greatest eccentricity to cause torque to structural failure. Railing was loaded with a force corresponding to 1 kN/m at the top edge and vertical force until failure of the whole structure. The whole bridge was also loaded temperature change of $+40 \text{ }^\circ\text{C}$ and $-35 \text{ }^\circ\text{C}$.

The bearing capacity of the construction achieves satisfactory values (12.6 kN/m^2), which is well above the required load capacity (4.2 kN/m^2). Gained value of bearing capacity is valid for construction in ideal condition. Which means a footbridge in a state where there are no shrinkage cracks. Due to the shape of the construction, it is a very difficult task and the occurrence of these cracks is expected, which will probably lead to a lower load bearing capacity.

A static loading test is planned to be performed to verify design assumption. Deflection in the middle of span on both sides of footbridge and crack development on construction will be observed during loading.

3. “U” PROFILE MOCK-UP

Because of very complex design of the footbridge a preliminary mock-up need to be prepared. The footbridge was casted in the upside-down position because of double curvature and more several reasons that will be describe in more details in this article. The support part of the construction was chosen as a highest part with high of 1.5 m. The wooden formwork of preliminary mock-up was prepared and everything was managed at the same way as for final footbridge was designed. The main reasons of preparing of the mock-up were: verification of the casting process, surface conditions of the element, verification of right consistency of the fresh UHPFRC mixture and ability of the mould to be completely filled. The crucial factor for the element was the time of demoulding, respectively the time of releasing of the formwork. UHPFRC has very high shrinkage that was developed at a very early age of concrete. Developing of the shrinkage cracks is than caused by fixed formwork which is relatively stiff and does not allowed any movement of the casted element. All of these factors need to be considered. Casting of the mock-up was in September 2016.

3.1 Preparation of the mock-up

The wooden formwork was designed and prepared to withstand pressure of the fresh concrete which is the main load during casting (Fig. 2). The technology of the casting was the main issue during whole process of design. Because of double curvature of the bridge and very thin deck and side walls the bridge had to be casted in upside-down position. There was also problem with the surface of the construction which is not in the mould during casting. The formwork was closed from all sides and also the bridge deck (in this position the top deck) was closed. Only three openings were made on the top desk used for pouring of the concrete. Smooth surface of the concrete was achieved in all visible surfaces of the bridge. Only upper side of the casted element in closed formwork has always many pores because of air coming from the UHPC matrix upward from the walls and deck. In this case the position is advantageous because the surface with pores is on the nonvisible bottom part of the bridge in final position. Total volume of used UHPFRC for this element was 0.4 m³.



Fig. 2: Formwork of the preliminary mock-up



Fig. 3: Preliminary mock-up after the demolding

3.2 Optimization of UHPFRC mixture

UHPFRC mixture, used in this construction, need to fulfil very high requirements. Extensive research in the field of material optimization was carried out in Klokner Institute. The key parameter for UHPFRC mixture was high flowability. Because of the upside – down pouring of the footbridge, concrete need to flow inside by the 30 mm thin area and fill both thin walls and upper deck. Usually consistency of the mixture can be adjusted by volume of added water and superplasticizer. In this case (especially for UHPFRC) added water means lower mechanical properties and higher shrinkage. Because of these problems a new UHPFRC mixture were designed and tested. Black pigment was added to the mixture according to requirement of the architect. Many mixtures were tested with a different volume of pigment in dependence to flowability and mechanical properties. The final colour shade was discussed regarding to the material parameters. Final mixture consists of the cement CEM II 52,5 N, fine aggregate with maximum size of 2 mm, slag, silica fume and steel fibres (0.2 mm thick, 13 mm long). Volume fraction of the fibres was 1.5%. The volume of water and superplasticizer depended on the temperature conditions with regard to the workability.

3.3 Material properties of UHPFRC

During casting of the preliminary mock-up the specimens (prisms with dimensions 169x40x40 mm and cubes with 100 mm edge) were prepared. Because of early demoulding age, many specimens were tested for compressive and flexural strength. Flexural strength was tested by 3-points bending test. First tests were carried out 5 hours after casting. Next set of the specimens was tested after 2 hours and the tests continued until the demoulding of the element. The development of material properties at early age is shown in Fig. 4. The crucial value of the compressive strength was set to 30 MPa. At this point the formwork should be released and removed. Preliminary mock-up was demoulded after 11-12 hours after casting. Formwork was completely removed and surfaces of the element were cured by special fluid wax. The surface quality was checked. Element is shown in Fig. 3. No shrinkage cracks and no empty areas without UHPFRC were observed. Only the top surface under top wooden desk was covered by the layer with many pores. Development of material properties at first 10 days after casting shows in Fig. 5.

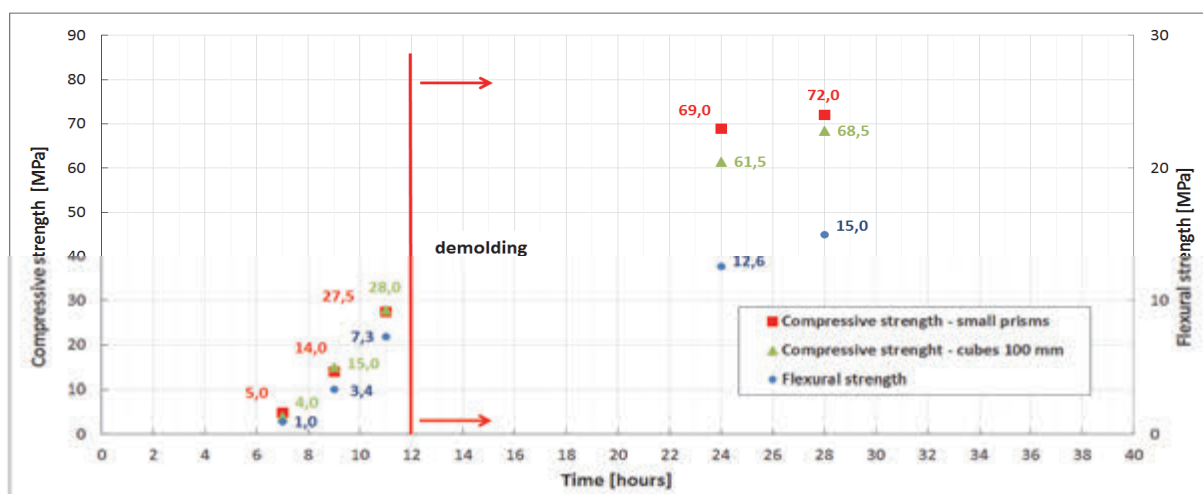


Fig. 4: Development of compressive and flexural strength at first 40 hours after casting

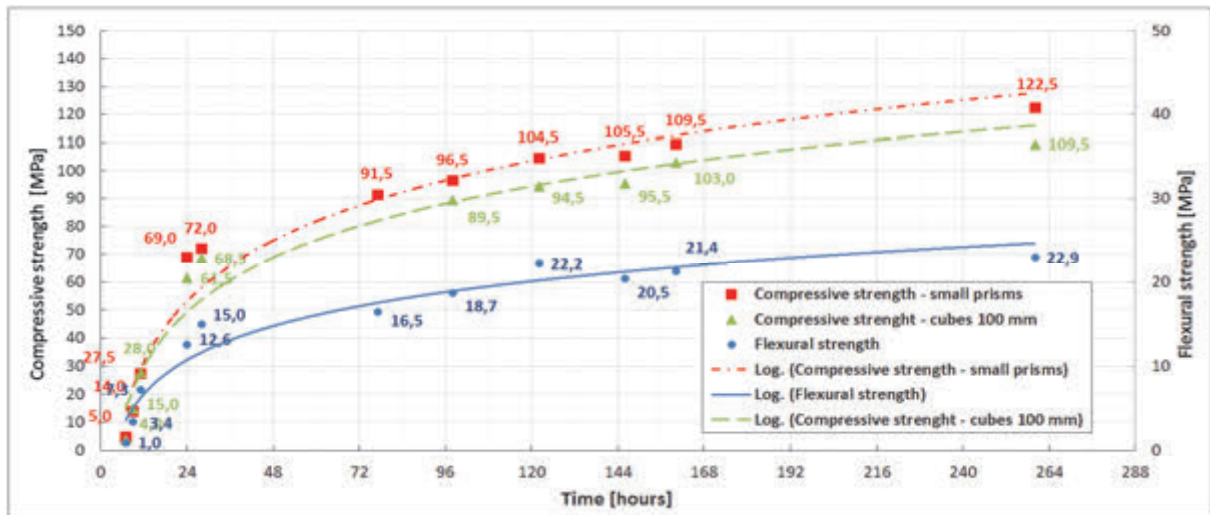


Fig. 5: Development of compressive and flexural strength at first 10 days after casting

3.4 Loading tests of the thin walls

Load bearing capacity of the thin wall was tested by horizontal force at a height 1.3 m. The applied axial force was distributed by steel profile to entire width of the wall. Tests were performed after 35 days after casting.

At first the load bearing capacity of the right thin wall in inward direction were evaluated (Fig. 6). Maximum horizontal force 3.1 kN was reached. It means that force divided by width of the tested wall (1.5 m) was 2.1 kN/m. The second test was performed in opposite direction (a way out direction – Fig. 7) and the maximum force was 3.5 kN (2.3 kN/m). It was concluded that load bearing capacity of the walls (handrails) is sufficient.



Fig. 6: Test of load bearing capacity of the right thin wall – an inward direction



Fig. 7: Test of load bearing capacity of the left thin wall – a way out direction

4. “U” PROFILE FULL SIZE FOOTBRIDGE MOCK-UP

The final formwork was prepared after optimization of many details from preliminary mock-up. Double curvature of the bridge was applied on the top deck and side walls. Two openings for pouring UHPFRC were placed on the edges of the top deck on the ends of the bridge. Development of the material properties and knowledge from casting of the preliminary tests were used for the optimization of formwork and whole construction process.

4.1 Preparation of the final formwork

The formwork was prepared in Klokner Institute. Because of length of the bridge it had to be divided into four parts (Fig. 8). Very complex design of the formwork needed to be optimized in case of fast and easy releasing and demoulding. UHPFRC has early shrinkage so the fast releasing of the screws and desks is needed to enable some movement of construction and prevent cracks development. All formwork beams were reinforced by additional wooden beams (Fig. 9) for safety reasons and to withstand the pressure of the fresh concrete.



Fig. 8: Transport of the 1/4 of the formwork



Fig. 9: Formwork prepared for the casting

4.2 Casting, demoulding and transport of the footbridge

The final volume of the UHPFRC was 1.4 m³. The mould was poured from the top of two edges of the bridge, where the final bearing will be installed. No additional vibrations were applied because of the self-compacting character of the mixture. Casting of the whole element took approximately one hour. Consistency of the fresh concrete was measured in several times after mixing. Cold temperature had a positive effect on consistency so there was not a problem with cold joint between different 3 batches. Development of the compressive and flexural strength was tested at the same way as during preliminary mock-up. The time of releasing of the formwork was set to 11-12 hours after casting. Additional heating was provided for the next 5 days. After 4 days a temperature inside concrete was settled to the same temperature as on wooden desk surfaces, so the formwork should be removed with no additional temperature shock. All sides of the thin walls and especially top deck had very smooth surface with good quality.

Construction was removed from the hall to the storage place outside the hall, after 7 days from casting. Element was transported by two cranes (Fig. 10) and placed on polystyrene desks to allow volumetric changes caused by shrinkage, creep and changes caused by temperature. Temperature measurement was kept during storage.

The final material properties (measured at the age of 28 days) of the UHPFRC were: compressive strength 149.6 MPa (cubes 100 mm), 152 MPa (small prisms), flexural strength 22.6 MPa (small prisms), modulus of elasticity 51 GPa.



Fig. 10: Transport of final 1:1 mock-up of the footbridge in upside-down position

The next step of the program was to turn the footbridge to the final position (see Fig. 11) and prepare static load test. Turning was provided by two cranes. Footbridge was anchored on the edges, to transfer load caused by horizontal curvature in opposite sides of load bearings.



Fig. 11: Storing of the footbridge in correct position

Static load test is in preparation now in the precast plant. Results of the test will be presented in following publications.

5. CONCLUSIONS

Actual paper presents very complex theoretical and experimental program of the design, casting and testing of the “U” shaped thin walled double curvature arche footbridge made from UHPFRC. Single-span bridge with span of 10 m and the clear width 1.50 m with the total thickness of shell structure 30 - 45 mm was cast as a prefabricated element in one piece. Self-compacting character of UHPFRC with high flow ability allowed the production of the final structure. Reinforcement of material of this structure is by randomly distributed steel fibres only without any reinforcement bars. Steel mesh was applied at bearing edges of footbridge, only. An extensive research was carried out in Klokner institute before final foot bridge casting. Based on the requirements of architect and designer a new UHPFRC mixture was developed. Material properties were tested especially at early age of concrete because of releasing of the formwork and demoulding of the mould after 11-12 hours after casting. An extensive numerical analysis was done, too. Preliminary mock-up was produced and technology of casting and many

details of formwork and mould were optimized based on experiences gained. Casting of the full scale foot bridge model was performed with very satisfactory result. Complete shape of complicated shell structure was filled with UHPFRC without any cavern or significant entrapped air bubbles. After demoulding the surface of structure was very smooth with very small amount of entrapped air. Hardened footbridge was easily transported to storage place and turned to final position. No static problems occurred during transport and rotation. Now is this unique double arch foot bridge prepared for load bearing test procedure to prove designers assumptions. According results of tests, possible modification of design will be done to prepare final structure which is planned to install in small town nearby Prague.

ACKNOWLEDGEMENTS

This contribution is the result of the research supported by the research project GAČR 15-22670S and GAČR17-22796S. The tests were carried out in laboratory of Klokner Institut, CTU in Prague.

REFERENCES

- Abbas, S., Nehdi, M.L., Saleem, M.A.: Ultra – High Performance Concrete: Mechanical Performance, Durability, Sustainability and Implementation Challenges, International Journal of Concrete Structures and Materials, Vol.10, No.3, pp. 271-295, September 2016
- AFGC/SETRA: Ultra High Performance Fibre-Reinforced Comcretes, Recommendations (06/2013). Paris CEDEX.
- Blank, M. - Tej, P. - Kolísko, J. - Vráblík, L. Design of Experimental Suspended Footbridge with Deck Made of UHPC, 3rd International Conference on Mechanics and Mechatronics Research, ICMMR 2016; Chongqing; China; 15 June 2016 through 17 June 2016; ISSN: 2261236X MATEC Web of Conferences, Volume 77, 3 October 2016, Article number 08005, Code 124092
- C. Shi, Z. Wu, J. Xiao, D. Wang, Z. Huang, Z. Fang; Review on ultra high performance concrete: Part I. Raw materials and mixture design, Construction and Building Materials 101, p. 741-751, 2015.
- D. Wang, C. Shi, Z. Wu, J. Xiao, Z. Huang, Z. Fang; Review on ultra high performance concrete: Part II. Hydration, microstructure and properties, Construction and Building Mat. 96, p. 368-377, 2015
- Duque, L.F.M, Varga,I., Graybeal, B.A.: Fiber Reinforcement Influence on the Tensile Response of UHPFRC, First International Interactive Symposium on UHPC -2016, Des Moines, IOWA, Jul.18 – 20, 2016
- JSCE-USC; “Recommendations for Design and Construction of Ultra-High Strength Fiber-Reinforced Concrete Structures – Draft.”
- Kabele, P. - Sajdlová, T. - Rydval, M. - Kolísko, J.: Modeling of High-Strength FRC Structural Elements with Spatially Non-Uniform Fiber Volume Fraction. Journal of Advanced Concrete Technology. 2015, vol. 13, no. 6, p. 311-324. ISSN 1346-8014.
- Kolísko, J. - Rydval, M. - Huňka, P.: UHPC - Assessment of Steel Fibre Distribution and Matrix Homogeneity. In fib Symposium TEL-AVIV 2013 Engineering a Concrete Future: Technology, Modeling & Construction - Proceedings. Tel Aviv: IACIE Israeli Association of Construction & Infrastructure Engineers, 2013, p. 113-116. ISBN 978-965-92039-0-1.
- Kolísko J., Rydval M., and Huňka P.: UHPC – Assessing the Distribution of the Steel Fibre and Homogeneity of the Matrix. Tel Aviv, Israel: fib Symposium Tel Aviv, 2013.
- Vítek, J. L., Coufal, R., Čítek, D.: UHPC - Development and Testing on Structural Elements. Concrete and Concrete Structures 2013, Žilina, 2013, University of Žilina, pp. 218-223

EVALUATION OF THE COMPRESSIVE STRENGTH OF CONCRETE

Tibor Kausay, Tamás K. Simon

Budapest University of Technology and Economics, Department of Construction Materials and Technologies

betonopu@t-online.hu, t.simon@eik.bme.hu

SUMMARY

When determining the characteristic compressive strength of any concrete with given composition from its mean compressive strength according to the European product standards (EN 206:2013) compressive strength conformity criteria, there is a big likelihood of that the compressive strength class will come out to be at least one class higher. That is, apparently a better quality will be obtained than in the case if the same concrete composition would be evaluated according to the Eurocode design standards (2006 EN 1990: 2002, EN 1992-1-1: 2004, EN 1992-2: 2005, EN 1992-3).

In order to avoid this risky practice, the new Hungarian standard MSZ 4798:2016 Annex P offers a possibility to use concrete with the same compressive strength class, but having a higher mean strength. The differentiated sign of such concrete is AC₅₀(H), having higher strength – closer to that which was before 2014 –, incorporating bigger safety and from durabilitywise also performing better. The properties of the Hungarian AC₅₀(H) concretes – strength, safety and durability – is close to the expectations of the engineers, when designing reinforced concrete structures according to Eurocode.

However this is also dependent on the conditions of the compressive strength testing methods which is to be in harmony with the threshold compressive strength values. Due to this reason the Hungarian MSZ 4798:2016 standard also regulates the usability of compressive strength results which are obtained on polished samples, stating their unacceptability if the values are not corrected. The Hungarian prestandard regarding concrete gutter manhole elements (MSZE 15612:2014) prohibits the polishing of the cylindrical samples.

1. DETERMINATION OF CHARACTERISTIC STRENGTH

The safety of concrete, reinforced concrete and prestressed concrete structures is endangered by:

- according to the EN 206:2013 product standard and – and the national application document – the MSZ 4798:2016, in general the probability of acceptance of the strength wise not acceptable concrete may be up to 70%. Meanwhile Eurocode 2 (EN 1990:2002, EN 1992-1-1:2004 etc.) design standards state that the acceptance of the strength wise not acceptable concrete may have a probability of 50% as a maximum. The difference of concrete production standards and design standards from the point of critical acceptance probability is expressed in the Operational Characteristic Curves (OC-curves) which are demonstrated on Fig. 1,
- during the evaluation of concretes compressive strength, due to the different OC-curves (Fig. 1) the characteristic strength of the same concrete is to be determined with different relationships, having different underspending.

The underspending according to the MSZ 4798:2016 national application document – which incorporates with standing letters EN 206:2013 product standard also – is a function of either the Taerwe's underspending factor (λ_n) (Taerwe, 1986) or a constant 4 N/mm² according to Eurocode 2 design standard, the function of the Student's underspending factor (t_n) or a constant 8 N/mm² (Tab. 1).

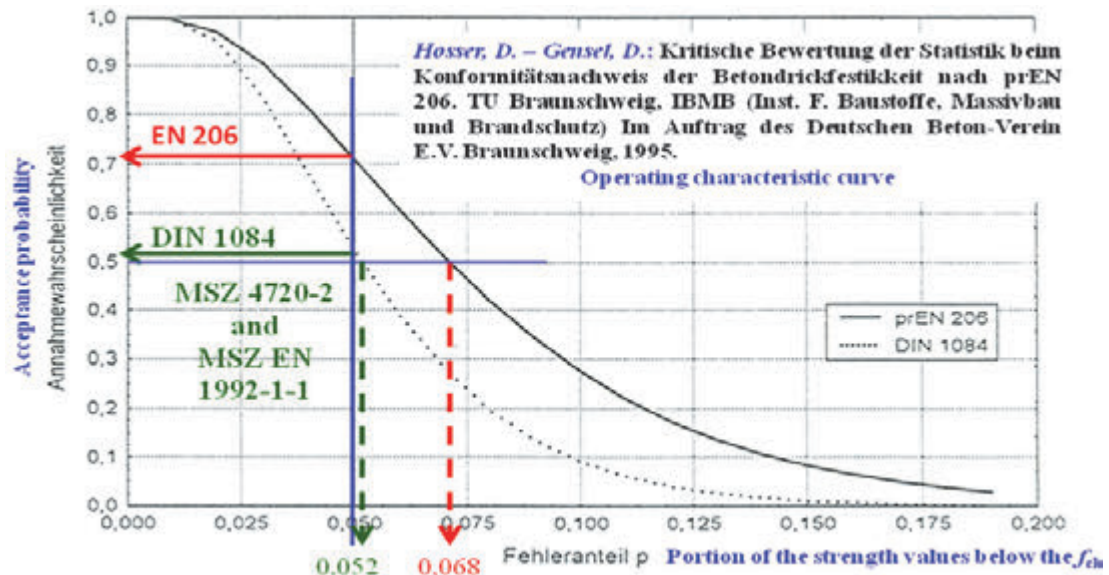


Fig. 1: Acceptance characteristic curve (Operating characteristic curve) for acceptance verification according to EN 206, the DIN 1084 and the MSZ EN 1992-1-1 standards.

Tab. 1: Acceptance factors

Specimen number n	Student's-factor, t_n	Taerwe's-factor, λ_n
	(Stange et al., 1966)	(Taerwe, 1986)
2	6,314	
3	2,920	2,67
4	2,353	2,20
5	2,132	1,99
6	2,015	1,87
7	1,943	1,77
8	1,895	1,72
9	1,860	1,67
10	1,833	1,62
11	1,812	1,58
12	1,796	1,55
13	1,782	1,52
14	1,771	1,50
15	1,761	1,48
20	1,729	
30	1,699	
∞	1,645	

The result of the above is that if evaluating the mean strength of a concrete of a given composition by the product standards, the compressive strength class with big probability will be higher by one. That is a better quality will be obtained (it will be classified higher) than if the evaluation would have been done according to Eurocode 2 design standard. The accepted

compressive strength of concretes according to the product standards are lower than what is expected in the model of Eurocode 2 design standard (Fig. 2).

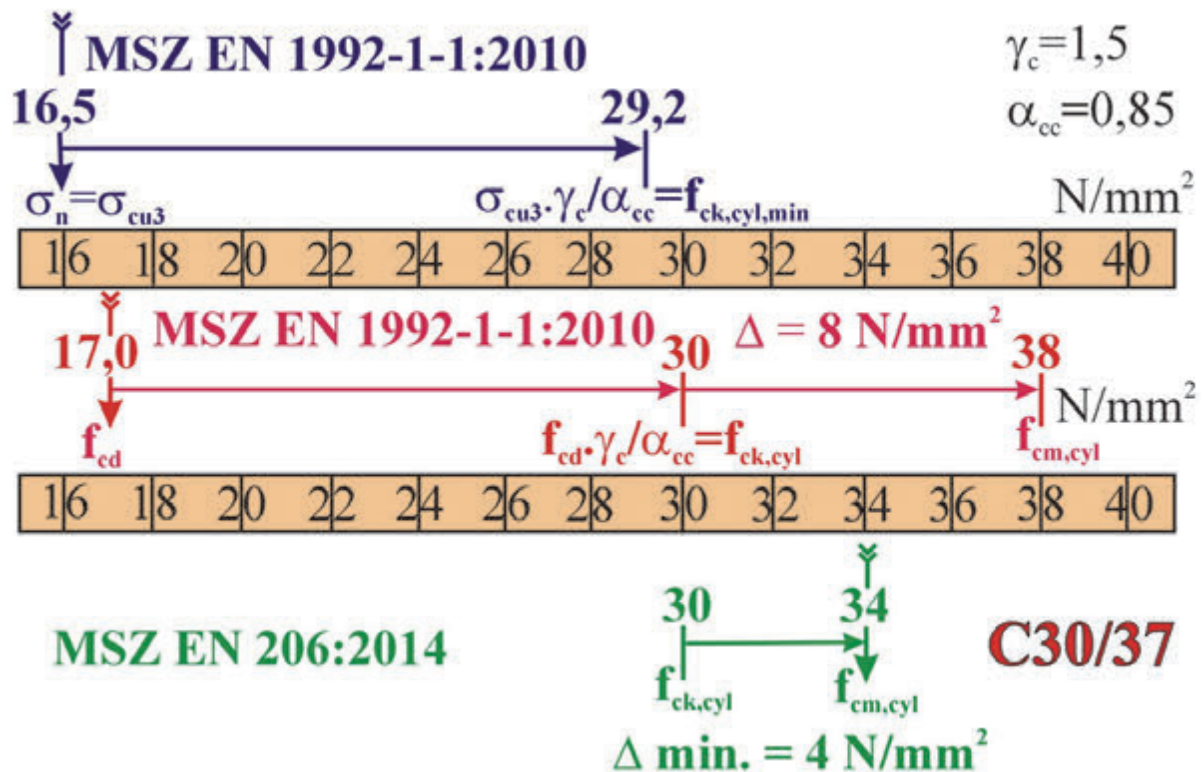


Fig. 2: Comparing the design, characteristic and mean values of concrete compressive strength by taking into consideration the long lasting strength, where: γ_c is the partial factor of the compressive strength of σ_{cu3} , while α_{cc} is the divider of σ_{cu3} compressive strength concrete, which is corresponding to structures of 100 years design life.

In contrary to present, before 2004 there was harmony between the concept of the Hungarian product standard (MSZ 4798:1982 and its predecessors), the design standards of structures (MSZ 15022:1986), the design standard of water management structures (MSZ 15227:1980), the design standard for pavements (MSZ-07-3212-3:1981) etc. At that time both by the product standard and the design standard the characteristic compressive strength of concrete was to be evaluated by using Student's factor as we are doing it today according to the Eurocode 2 design standards (Fig. 3).

The meaning of this is that, all of the structures, which are today constructed according to the main standing characters of the concrete standards EN 206:2013 or MSZ 4798:2016 have most probably a lower mean compressive strength, having a weaker composition, with lower expected lifetime, than the structures constructed out of same compressive strength class concrete before 2004, or the expected compressive strength and durability, what is desired by the Eurocode 2 design standard (Fig. 4 and 5).

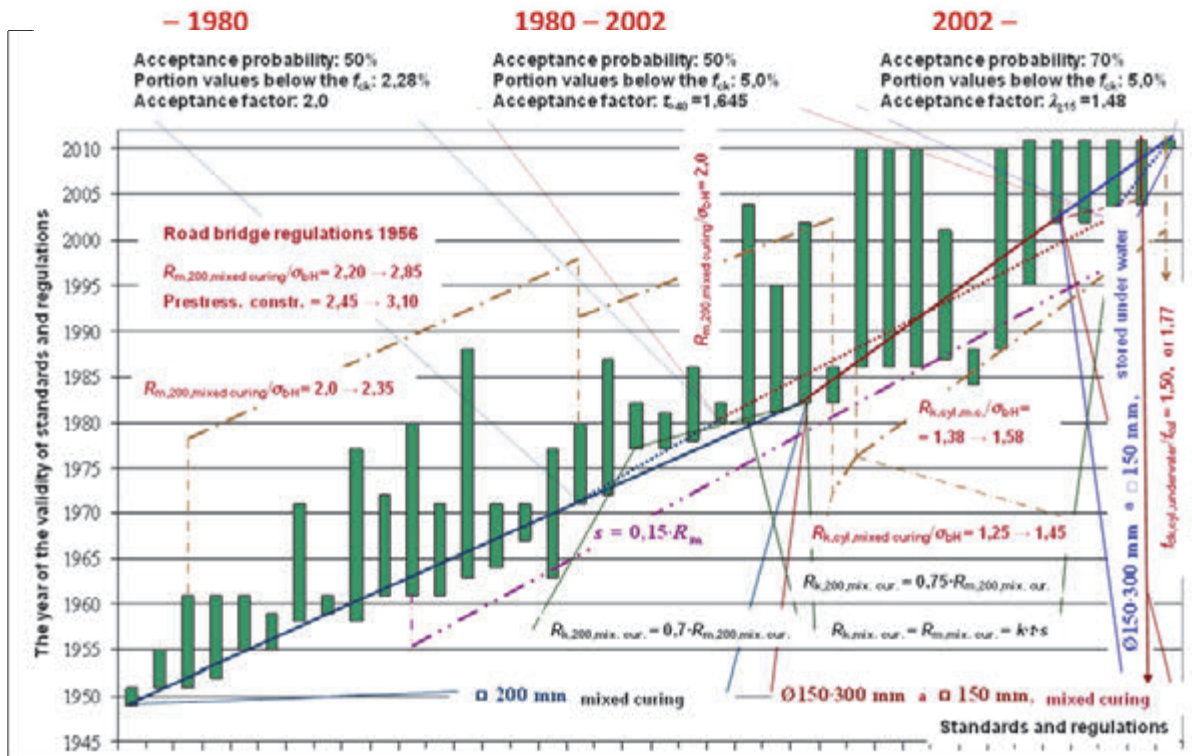


Fig. 3: The changes of concretes compressive strength characterisation in Hungary, during the last 65 years.

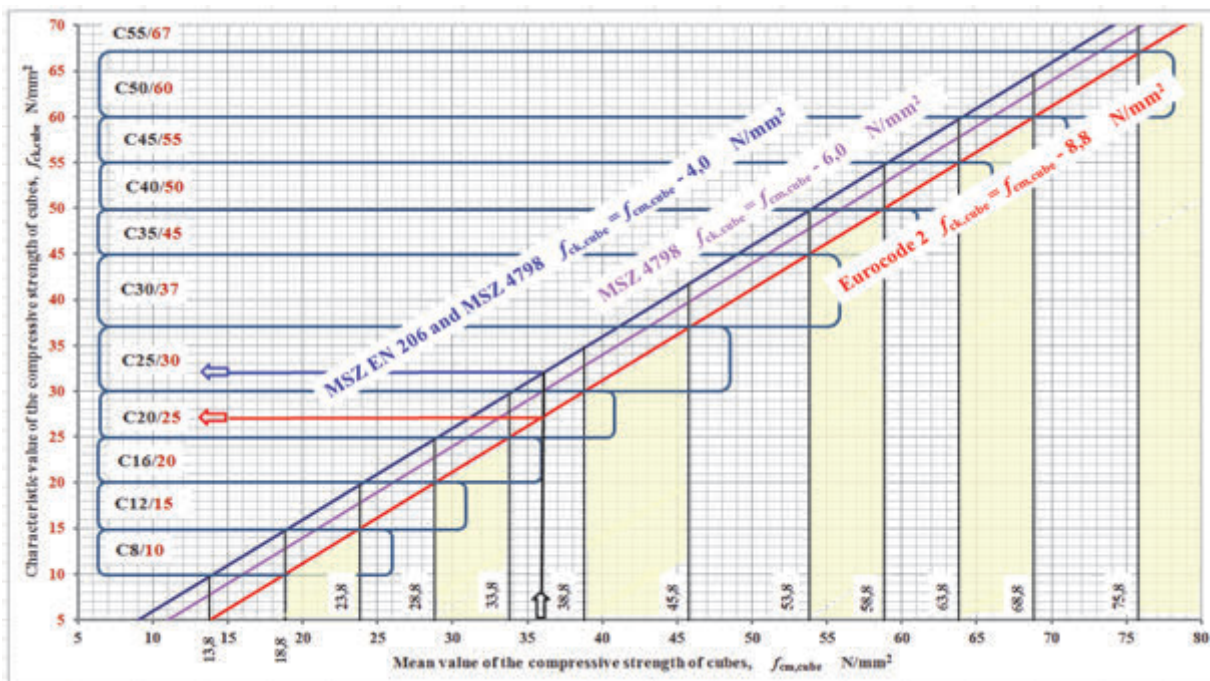


Fig. 4: Comparing the evaluation of concrete compressive strength classes according to concrete standards and Eurocode 2 design standards during the handing over of the material, originating from an unknown standard deviation and mean compressive strength.

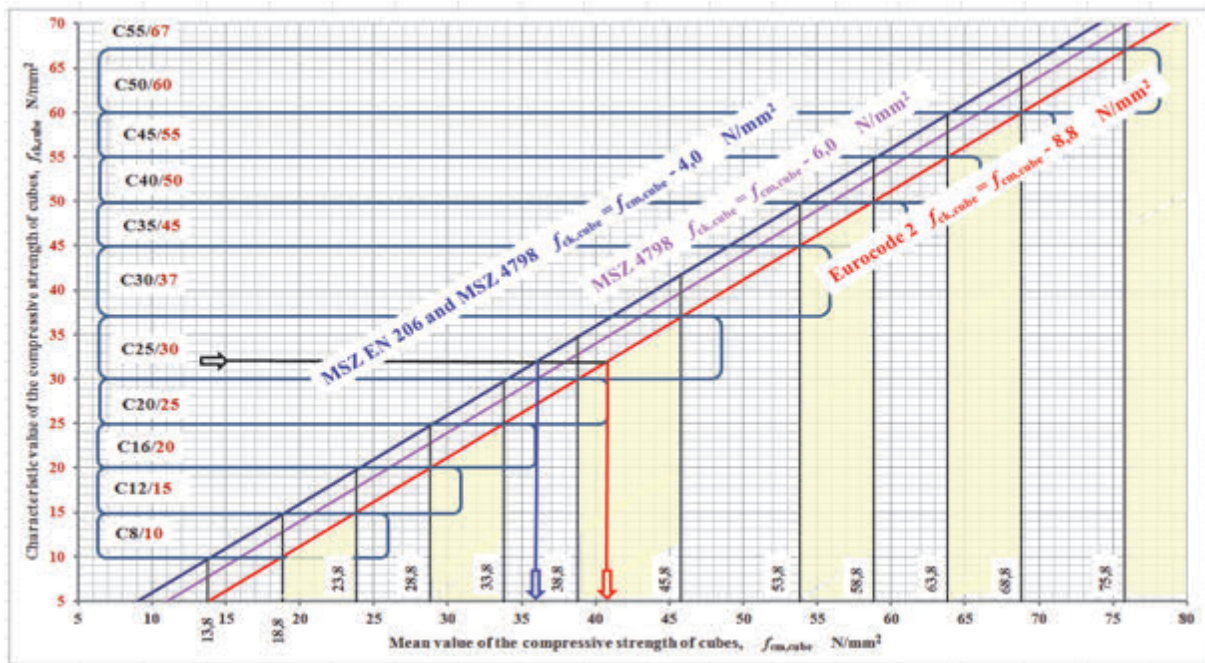


Fig. 5: Comparing the evaluation of concrete compressive strength classes according to concrete standards and Eurocode 2 design standards during the handing over of the material, originating from an unknown standard deviation and characteristic compressive strength.

The danger in the safety and durability of our concrete, reinforced concrete and prestressed concrete may be decreased according to Annex P of MSZ 4798:2016, if during the handing over procedure the mean compressive strength ($f_{cm,cube,test}$, $f_{cm,cube,test,H}$) of the 150 mm cubes would satisfy the following criteria:

- if the concrete's compressive strength class is \leq C50/60 and after stripping the cubes were throughout kept under water, then:
 $f_{cm,cube,test} \geq f_{ck,cube} + 6.0$ [N/mm²],
- if the concrete's compressive strength class is \leq C50/60 and after stripping the cubes were mix cured (7 days under water, then ambient circumstances), then:
 $f_{cm,cube,test,H} \geq f_{ck,cube}/0.92 + 6.5$ [N/mm²],
- if the concrete's compressive strength class is \geq C55/67 (high strength concrete) and after stripping the cubes were throughout kept under water, then:
 $f_{cm,cube,test} \geq f_{ck,cube} + 8.0$ [N/mm²],
- if the concrete's compressive strength class is \geq C55/67 (high strength concrete) and after stripping the cubes were mix cured (7 days under water, then ambient circumstances), then:
 $f_{cm,cube,test,H} \geq f_{ck,cube}/0.95 + 8.5$ [N/mm²].

If the standard deviations $s_{cube,test}$ and $s_{cube,test,H}$ are known, then it is correct to check the compliance of the mean compressive strength by the t_n Student's factor as follows:

- if after stripping the cubes were throughout kept under water, then:
 $f_{cm,cube,test} \geq f_{ck,cube} + t_n \times s_{cube,test}$ [N/mm²],
- if the concrete's compressive strength class is \leq C50/60 and after stripping the cubes were mix cured (7 days under water, then ambient circumstances), then:
 $f_{cm,cube,test,H} \geq f_{ck,cube}/0.92 + t_n \times s_{cube,test,H}$ [N/mm²],

- if the concrete's compressive strength class is $\geq C55/67$ (high strength concrete) and after stripping the cubes were mix cured (7 days under water, then ambient circumstances), then:
 $f_{cm,cube,test,H} \geq f_{ck,cube}/0.95 + t_n \times s_{cube,test,H}$ [N/mm²].

Annex P of MSZ 4798:2016 standard is near to EHE-08:2008 (Spanish national document of Eurocode 2 design standard) No. 14167/2008 Prime Minister's Decree for structural concrete Annex 19, point 5.1, according to which "through statistical criteria must be ensured that the risk of the customer regarding the compressive strength of concrete, that is accepting a faulty delivery, must be lower than 45%" (this is what annex J of EN 206:2013 is referring to).

2. COMPRESSIVE STRENGTH OF SURFACE POLISHED CYLINDERS

The above relationships are only valid, if the tested surfaces of the samples (cubes or cylinders) are not polished. Standards since long are referring to that, the surface of badly shaped specimens are to be corrected by polishing. But the present standards do not take into consideration the development of polishing technology in the last two decades. From sandpaper, slow polishing to the technology of diamond particled high speed polishing brought a huge difference into the quality of the polished surfaces. Those, who are applying the standard are capable to misunderstand the text of the standard.

The recommendations regarding polishing in EN 12390-3:2009, EN 12504-1:2009, EN 13791:2007 és EN 13369:2013 is only for such cases if the specimen is faulty in shape or size. As an example, according to the annexes of EN 12390-3:2009 standard:

- Annex A: „When it is necessary to reduce the size of a specimen, it shall be ground or sawn. The intended load-bearing surfaces shall be prepared by grinding or by capping.”,
- Annex B: „If any dimension is greater, or less than, 3% from the designated size, then the specimen is rejected or adjusted.”,
- And the following regulation of Annex A can not be interpreted: „In cases of dispute, grinding shall be the reference method. Note: Other methods of adjustment may be used if they are validated against grinding.”

A serious imperfection is that, these standards do not talk about the increasing effect of polishing on the measurable compressive strength, and the necessity of conversion. By polishing the compressive strength will increase only virtually, since the structure of concrete does not change by it, only the test circumstances are changed.

According to our experiences the polishing of the compressive planes of the drilled test specimens if compared to the not polished, sawn but not polished, or to those which are prepared in formworks and uncapped or cupped with mortar, will increase the measurable compressive strength even if the compressed planes were perfectly parallel prior to polishing (Tab. 2). The more perfect the polishing of the compressed planes is, it gets closer to the pressing plate during the test, from between the plates the air is totally disclosed, and adhesion between the particles of the planes have bigger and bigger effect. The adhesion frictional force increases in case of polished and clean surface, due to what the measured compressive strength will be bigger. If the compressed plane of a polished specimen is wet, then friction and the measured compressive strength may be less, because the thin film of water may compose a slipping layer.

Tab. 2: Measurable compressive strength of concrete Ø150×300 mm specimens which were prepared in formwork, kept under water for 28 days and the compressed surfaces were differently prepared

Preparation of compressed surface	Top plane is cupped with cement mortar, while the bottom plane is "as stripped"	Top plane is polished, while the bottom plane is "as stripped"	Both planes are polished
Specimens of Ø150×300 mm sizes kept under water till the age of 28 days	When crushing, did not explode	When crushing, exploded	When crushing, exploded
Mean compressive strength, N/mm ²	42.8	51.4	52.7
Compressive strength, %	100.0	120.0	123.1
Standard deviation, N/mm ²	1.68	0.67	1.64
From the spread of standard deviation ($T_{n=3}$) calculating, $s = T_3/3,31\text{N/mm}^2$ (Harter, 1960)	1.95	0.71	1.89
Effective standard deviation, N/mm ²	3.00	3.00	3.00
Student's factor for $n = 3$	2.92	2.92	2.92
Characteristic value, N/mm ²	34.06	42.63	43.94
Strength class:	C30/37	C40/50	C40/50



Fig. 6: Sample cylinders, which have the size of Ø150×300 mm, until the age of 28 days kept under water, cupped with cement mortar or polished on their compressed surface

According to Tab. 2 the cylinders having sizes of Ø150×300 mm:

- have a mean compressive strength with polished compressed surface (52.7 N/mm²) even by 20% higher than that of the mortar surfaced Ø150×300 mm ones (42.8 N/mm²),
- the compressive strength class (C40/50) might even be higher by two classes (C30/37),
- and the characteristic threshold value (40 N/mm²) may reach the characteristic value of the 150 mm cubes, which have the surface of which is prepared by the formwork (37 N/mm²).

Due to the above reasons as an example in case of according to MSZE 15612:2014 standard regarding Precast concrete manhole elements, the polishing of drilled cores is prohibited, while determining the compressive strength. In MSZ 4798:2016 Hungarian standard it is stated: “The correction of sample cylinders by polishing is not advised, since presently there is no accepted correction value for such procedure.

3. CONCLUSIONS

- Technical safety is the guarantee of the durability of structures, which means capital in an economy.
- The level of technical safety is a basic requirement of the design model of structures, what may only be ensured, if the material model can be ensured by the assumed quality of the materials.
- Due to the above reasons it is incorrect to build into reinforced concrete structures such concretes, of which compressive strength class was not evaluated according to the EN 1992-1-1 standard with a maximum of 50% critical acceptance probability, or if the compliance is proved by using polished test specimens. We do not want to talk about the effect of using the two, improper procedures in combination.

4. REFERRED STANDARDS

EN 206:2013 Concrete. Specification, performance, production and conformity

EN 1990:2002 Eurocode: Basis of structural design

EN 1992-1-1:2004/A1:2014 Eurocode 2: Design of concrete structures. Part 1-1: General rules and rules for buildings

EN 1992-2:2005/AC:2008 Eurocode 2: Design of concrete structures. Part 2: Concrete bridges. Design and detailing rules

EN 1992-3:2006 Eurocode 2: Design of concrete structures. Part 3: Liquid retaining and containment structures

EN 13369:2013 Common rules for precast concrete products

EN 12390-3:2009/AC:2011 Testing hardened concrete. Part 3: Compressive strength of test specimens

EN 12504-1:2009 Testing concrete in structures. Part 1: Cored specimens. Taking, examining and testing in compression

EN 13791:2007 Assessment of in-situ compressive strength in structures and precast concrete components

EN 13877-2:2013 Concrete pavements. Part 2: Functional requirements for concrete pavements

MSZ 4719:1982 Betonok (Concretes in Hungarian)

MSZ 4798:2016 Beton. Műszaki követelmények, tulajdonságok, készítés és megfelelés, valamint az EN 206 alkalmazási feltételei Magyarországon (Concrete. Technical

specification, properties and acceptability, and the conditions of usage of EN 206 in Hungary in Hungarian)

MSZ 15022-1:1986/2M:2001 Építmények teherhordó szerkezeteinek erőtani tervezése. Vasbeton szerkezetek (Design of structures, Reinforced concrete structures, in Hungarian)

MSZ 15022-2:1986/1M:1990 Építmények teherhordó szerkezeteinek erőtani tervezése. Feszített vasbeton szerkezetek (Design of structures, Prestressed concrete structures, in Hungarian)

MSZ 15227:1980/1M:1988 Vízépítési műtárgyak vasbeton szerkezeteinek erőtani tervezése (Design of reinforced concrete water management structures, in Hungarian)

MSZ-07-3212-3:1981 Beton pályaburkolatok. Követelmények (Concrete pavements, requirements, in Hungarian)

MSZE 15612:2014 Előregyártott beton csatornázási aknaelemek (Prefabricated concrete gutter elements, in Hungarian)

5. REFERENCES

Harter. H. L. (1960) Tables of range and studentized range. The Annals of Mathematical Statistics. Baltimore, USA. VOL. 31. 1960. No. 4. pp. 1122-1147.

Hosser. D., Gensel. B. (1995) Kritische Bewertung der Statistik beim Konformitätsnachweis der Betondruckfestigkeit nach prEN 206. Schlußbericht DBV 162. Braunschweig.

Stange. K., Henning. H.-J. (1966) Formeln und Tabellen der mathematischen Statistik. Springer-Verlag. Berlin/Heidelberg/New York.

Taerwe. L. (1986) A General Basis for the Selection of Compliance Criteria. IABSE Periodica. Proceedings P-102/86. pp. 113-127. ETH-Hönggerberg, Zürich 3/1986 August.

SURFACE BLAST-CLEANING WASTE AS A REPLACEMENT OF FINE AGGREGATE IN CONCRETE

Wojciech Kubissa^{1}, Roman Jaskulski¹, Tamás Simon²*

¹Warsaw University of Technology, Faculty of Civil Engineering, Mechanics and Petrochemistry

²Budapest University of Technology and Economics, Department of Construction Materials and Technologies

**wojciech.kubissa@pw.edu.pl*

SUMMARY

In the article the possibility of using a surface blast-cleaning waste as a replacement of fine aggregate in concrete manufacturing was presented. Concretes with w/c ratio 0.6 and 300 kg/m³ dosage of cements: CEM I 32.5R and CEM II/B-V 32,5N were tested. The quite high value of the w/c ratio resulted in good compactibility of the mixtures without use of plasticizer. The replacement rate of the fine aggregate (0 – 2 mm) with copper slag (CS) was 33%, 66% and 100% respectively. Concretes of the same composition served for reference except for with river sand as fine aggregate instead of slag. The performed tests focused on: compressive and tensile strength (both after 28 days), sorptivity, free water absorption capacity and abrasion resistance. The obtained results showed that the strength and some other tested properties of concretes with copper slag as sand replacement were similar or even better than that of the control mixtures.

1. INTRODUCTION

Recycling of waste materials, reducing greenhouse gas emission and frugal natural resources management became necessary. This is caused by both climate changes and necessity of the transition to an energy-efficient, low-carbon economy (Holden, Linnerud & Banister, 2016; Broman & Rob, 2015). Copper slag is a by-product, produced besides mill tailing, during the process of copper extraction by smelting. It is an inert material and its physical properties are similar to natural sand (Meenakshi Sudarvizhi, S and Ilangovan, 2011). It is used, among others, as an abradant in the surface blast-cleaning process but after this usage it is considered to be a waste. Despite increasing the rate of reusing copper slag, the huge amount of its annual production is still disposed in landfills or stockpiles. Potential applications were described already (Gorai, Jana & Premchand, 2003; Dhir, de Brito, Mangabhai & Lye, 2017). One of the most promising potential application for reusing copper slag is concrete production (Ayano & Sakata, 2000; Al-Jabri, Al-Saidy & Taha, 2011; Alp, Deveci & Söngün, 2008). It is possible to use copper slag for the production of high-quality concrete, improving its properties compared to concrete, which is mixed with sand (Al-jabri, Hisada, Al-saidy & Al-oraimi, 2009; Ambily et al., 2015). The usage of copper slag in concrete production provides potential benefits both environmentally and economically for all related industries, particularly in such areas where considerable amount of copper slag is produced. Using copper slag with gravel improves the consistency of the mixture (Wu, Zhang & Ma, 2010; Al-Jabri et al., 2011). It has been found that the usage of copper slag instead of sand, without changing the amount of tap water, significantly improves consistency and compressive strength (Al-jabri et al., 2009). However it is possible to reduce the amount of water by 22% and obtain the same consistency. In this case the compressive strength increases up to 20%.

No negative impact of copper slag on concrete contraction was found (Ayano & Sakata, 2000). Copper slag is also used as an abrasive in blast-cleaning processes during corrosion protection. The copper slag particle size after this process is smoother. The content of 0 – 0.125 mm and 0.125 – 0.25 mm fractions is significantly increased. The waste also contains a small amount of corrosion products and corrosion protection coatings [(Rzechuła, 1994)]. The use of blast-cleaning waste as a substitute for sand was tested and described in the article. Since the tested concrete can be used in the production of prefabricated elements, part of the research and evaluation of the results were carried out according to the PN-EN 1340:2004 “Concrete kerb units - Requirements and test methods” standard.

2. MATERIALS AND METHODS

Portland cement CEM I 32.5R and Portland-composite cement CEM II/B-V 32.5N from Ożarów Cement Plant as per PN-EN 197 were used. All concrete mixes contained 300 kg/m³ of cement by 0.6 w/c ratio. Fractions of River sand 0 – 2 mm and natural gravel of 0.5 – 16 mm were used. Aggregates were at laboratory air-dry condition. Copper slag waste from blast cleaning was used as a partial replacement of sand. The ratio of substitution was 33%, 66% and 100% of sand amount by volume. Regular tap water was used as mixing water.

Grading curves of the used aggregates and the waste is shown in Figure 1. Boundary grading curves were adopted according to PN-B-06250:1988. Grading of all mixes of the aggregates were similar. They differed mainly in the amount of finest fractions 0 – 0.125 mm. If only sand and natural gravel were used, the portion of this fraction was about 0.5% while after replacing 100% of the sand with CS it increased to about 5.0%.

Eight concrete mixtures were prepared. Mix IDs and proportions are presented in Tab. 1. The consistency of fresh concrete was measured by slump test, in accordance with PN-EN 12350-2. In the case of mixes CI100 and CII100 also test mixes were prepared with using superplasticizer for concrete with an extended workability Ha-Be PANTARHIT[®] RC540 (FM) according to PN-EN 934-2. For these mixtures only the consistency of the mixture was determined to find the right amount of the necessary amount of plasticizer to provide such a consistency as that of the reference concrete.

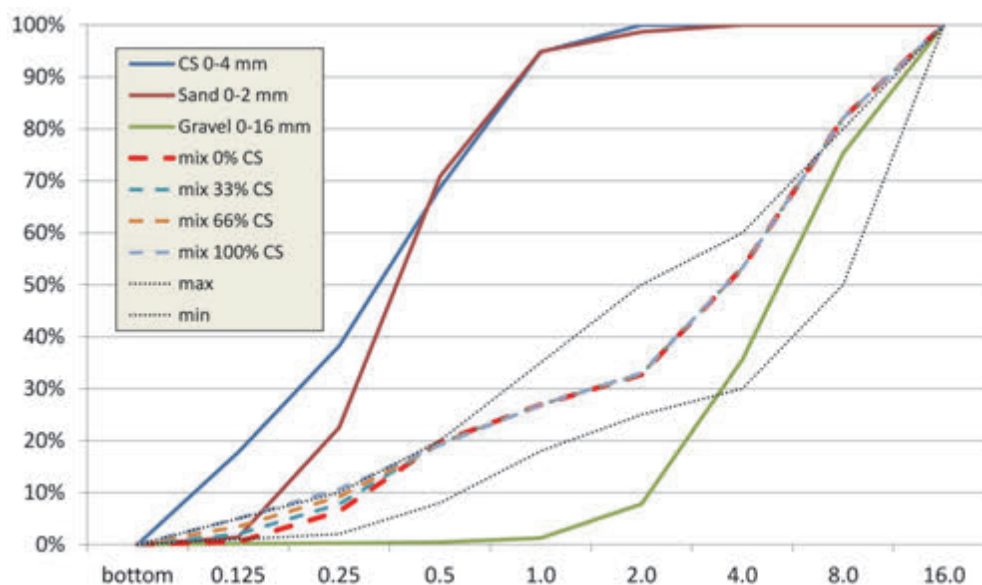


Fig. 1: Grading curves of aggregate fractions and mixtures.

Eight concrete mixtures were prepared. Mix IDs and proportions are presented in Tab. 1. The consistency of fresh concrete was measured by slump test, in accordance with PN-EN 12350-2. In the case of mixes CI100 and CII100 also test mixes were prepared with using superplasticizer for concrete with an extended workability Ha-Be PANTARHIT[®] RC540 (FM) according to PN-EN 934-2. For these mixtures only the consistency of the mixture was determined to find the right amount of the necessary amount of plasticizer to provide such a consistency as that of the reference concrete.

Tab. 1: Proportions of concrete mixtures [kg/m³]

Mixture ID	CI0	CI33	CI66	CI100	CII0	CII33	CII66	CII100
CEM I 32,5	300	300	300	300	0	0	0	0
CEM II/B-V 32,5	0	0	0	0	300	300	300	300
natural sand 0-2	519	346	173	0	524	349	175	0
natural gravel 0-16	1375	1375	1375	1375	1388	1388	1388	1388
copper slag	0	195	390	586	0	197	394	591
water	180	180	180	180	180	180	180	180
W/C	0.60	0.60	0.60	0.60	0.60	0.60	0.60	0.60

Specimens were prepared and cured as per PN-EN 12390-2. They were cast in plastic moulds and compacted by double vibration (half and full) on a vibrating table. After 2 days they were stripped and then water cured in the laboratory for 28 days.

2.1 Compressive and tensile strength test

The compressive strength test was conducted on 100 mm cube specimens on the 28 day of hardening. The test was carried out in accordance with PN-EN 12390-3. The splitting tensile strength test was conducted on the same type of specimens in accordance with PN-EN 12390-6. The strength tests were performed by using a Matest instrument, having 3000 kN compression force capacity. The rate of loading was maintained at 0.5 MPa/s for compressive strength test and 0.05 MPa/s for splitting tensile strength test.

2.2 Free water absorption and sorptivity test

The free water absorption test was conducted on the halves of cubic specimens of 100 mm edge by means of mass method. Specimens after splitting were stored 12 hours in water. Then the surface-dry mass of the specimens m_s were determined. Prior to the sorptivity test, the specimens had been oven-dried to the stable mass at a temperature of 105 °C. The measurements were conducted at the temperature of approximately 20 °C. The specimens were weighed (to determine mass m_d for calculation of free water absorption) and then arranged in a water containing vessel. The specimens were immersed up to the height of 3 mm. In the specific time intervals from the beginning of the test the specimens were weighed again to define their weight gain resulting from water sorption. Subsequent weight measurements were conducted for 6 hours. Sorptivity S in $\text{g}/(\text{cm}^2 \cdot \text{h}^{0.5})$ was defined as a slope of the linear function expressing the dependence of the mass of the water absorbed Δm by the area F on the time root $t^{0.5}$ (Kubissa & Jaskulski, 2013):

$$\frac{\Delta m}{F} = S \cdot t^{0.5} \quad (1)$$

Free water absorption has been calculated using formula (2):

$$n = \frac{m_s - m_d}{m_d} \quad (2)$$

where: n - free water absorption [%];
 m_s - mass of the fully soaked specimen [g];
 m_d - mass of the specimen dried to stable mass [g].

Mass of a specimen dried to stable mass has been the same value as the starting mass in sorptivity test.

2.3 Bohme abrasion test

The abrasion resistance is important to evaluate the durability of concrete produced with waste used as aggregates, especially in cases of such structural elements as pavement slabs or kerb units, which are subjected to abrasion degradation. The test was performed according to PN-EN 1340. For each concrete mix, four 70×70×70 mm specimens were tested. Specimens were obtained by sawing the 150 mm cubes, and the tests were carried out between 40 and 45 days after concreting. Just before the test the specimens were dried in an oven at 105 °C to stable mass. The specimens were then weighed with 0.1 g accuracy and the thickness in four points was measured.

3. RESEARCH RESULTS

Research results are presented in the Tab. 2. Each value in the table is an average of six measurements expect abrasion test result which is an average of four measurements and fresh concrete slump which is an average of three measurements. Due to paper content limitations we can only represent some of the obtained data in figures.

Tab. 2: Test results

Test	ID of mixture	CI0	CI33	CI66	CI100	CI0	CI33	CI66	CI100
	Flow [mm]		140	80	40	20	130	50	20
Compressive strength 28d [MPa]		34.82	37.60	38.08	40.20	28.04	31.58	34.40	35.24
Compressive strength 90d [MPa]		38.12	41.77	48.83	50.01	35.21	41.17	43.95	45.59
Tensile strength 28d [MPa]		3.11	3.27	3.46	3.41	2.72	3.16	3.20	3.16
Water absorption [%]		5.88	5.81	5.87	5.89	6.53	6.74	6.60	6.21
Sorptivity [cm ³ /(cm ² *h ^{0.5})]		0.133	0.129	0.123	0.107	0.136	0.121	0.122	0.121
Bohme abrasion [cm ³ /50 cm ²]		17.08	17.49	15.86	17.52	18.05	19.10	19.26	18.32

3.1 Consistency of concrete

Particle size, finer than in the copper slag is not used for sandblasting and high dust content results in increased water demand of aggregate and lowers the consistency of the mixture. There was a change in the consistency class from S3 to S1 for both cements used when replacing 100% of sand with the waste. There were no problems with compaction and specimen preparation. Obtaining the same consistency like of reference concrete, the ones mixed with the waste required the usage of plasticizer. For concrete with a 100% replacement

ratio it was necessary to add up to 1% of plasticizer on cement base to achieve a consistency such as of the reference concrete.

3.2 Compressive and tensile strength

The compressive strength after 28 days increased as the replacement ratio increased. The difference for 100% replacement rate was 25.7% for CEM I cement and 15.4% for CEM II/B-V one. The compressive strength after 90 days also increased with the increase replacement ratio (Fig. 2). The maximum increase was 31.2% and 29.5% respectively for CEM I100 and CEM II100 concrete. The difference in compressive strength after 28 and 90 days was 9.5% and 11.1% in the CEM I0 and CEM I33 series respectively. In the remaining series, the increase was higher and ranged from 24.4% for CEM I66 to 30.4% for CEM II33. The tensile strength after 28 days for CEM I cement concrete increased with increasing replacement ratio. The difference in comparison with reference concrete was, respectively 5.1%, 11.3% and 9.6% in case of concrete CEM I33, CEM I66 and CEM I100. For concrete with CEM II/B-V all mixes with the waste added had the tensile strength higher by approximately 16.5% compared to the result of the reference mix. The increase in compressive strength and tensile strength was probably due to the higher content of fine particles that could fill the space between the larger aggregate grains.

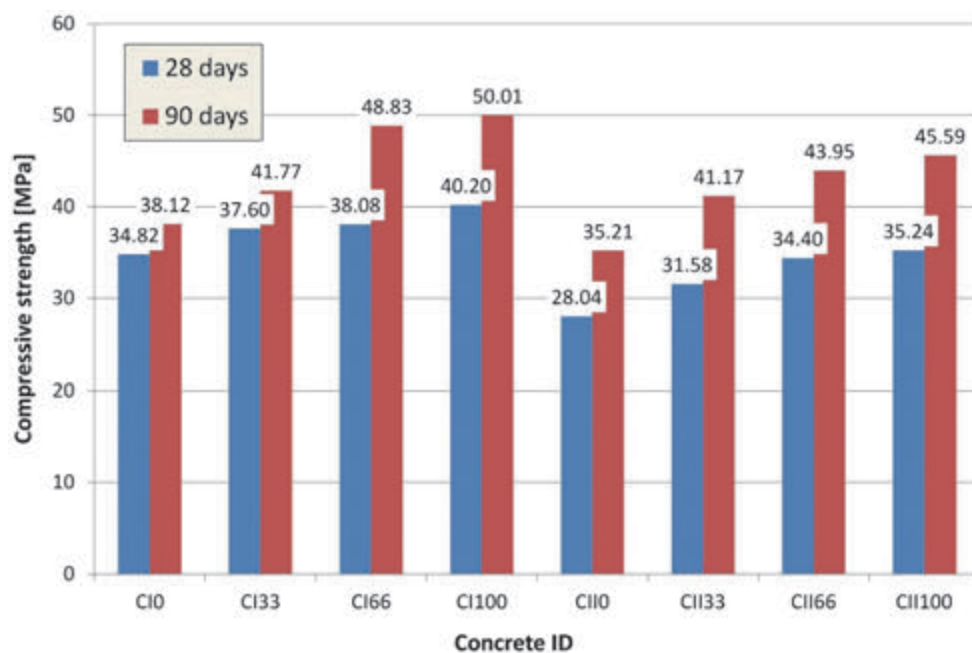


Fig. 2: Presentation of compressive strength test results

3.3 Free water absorption and sorptivity

The water absorption of concrete with a given type of cement was similar regardless of the degree of substitution of sand with the waste. The average water absorption of concrete with cement CEM II/B-V was 11.2% higher than that of CEM I. Concrete with CEM I cement fulfilled the water absorption requirements of class 2 according to EN 1340:2004, whereas concrete with CEM II/B-V had water absorption > 6% and did not meet the requirements for prefabricated elements.

The addition of waste reduced the sorptivity of concrete. In the case of concrete with CEM I cement a gradual decline of sorptivity with increasing replacement ratio was found. Sorptivity

of concrete CEM I100 is 19.5% lower if compared to the reference concrete. The concrete with CEM II/B-V cement, independently of the replacement ratio, had a similar sorptivity of approximately 11% lower than the sorptivity of the reference concrete.

3.4 Bohme abrasion

In the case of concrete with CEM I cement, no significant impact of sand substitution on abrasion was found. The abrasion of concrete with CEM II/B-V cement and replacement ratios 33% and 66% of sand was 5.8% and 6.7% higher than the reference concrete. At 100% replacement the abrasion was 1.5% higher than the abrasion of CII0. The abrasion resistance of all CEM II/B-V concrete meets the requirements of EN 1340: 2004 for abrasion resistance class H. Concrete with CEM I have met the requirements of wear class I.

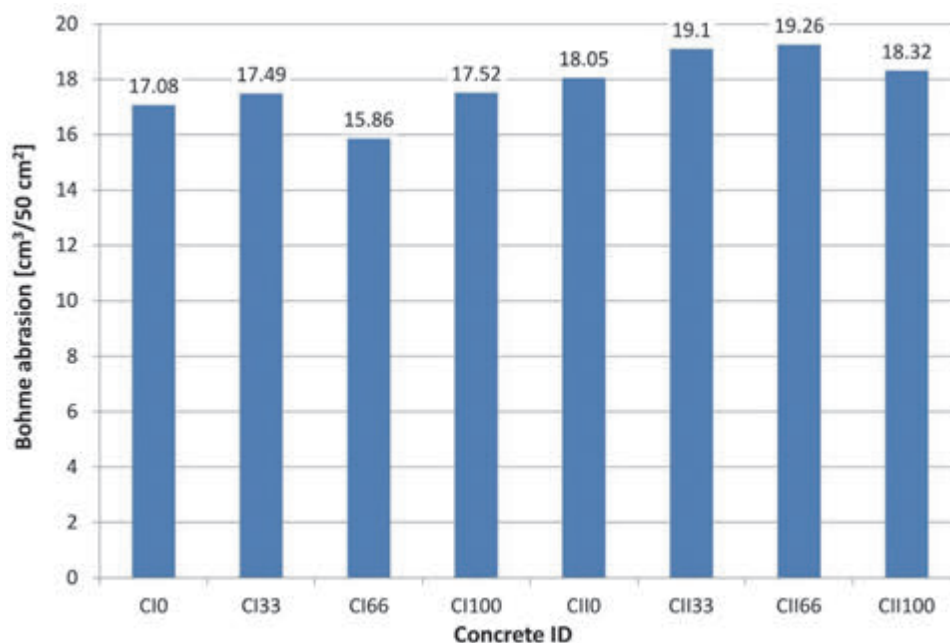


Fig. 3: Presentation of abrasion test results

4. CONCLUSIONS

- Replacing a part or all of the sand with blast-cleaning waste does not aggravate any of the tested properties of concrete.
- The compressive of the concrete with the waste is higher than that of the reference concrete and the higher the slag content is, the higher is the increase in the strength. The reference value for compressive strength is 34.8 MPa for CIn series and 28.4 for CIIIn series and for the concrete with the slag the values are 37.6 – 40.2 MPa and 31.6 – 35.2 MPa respectively.
- The tensile splitting strength of the concrete with the slag is higher than that of the reference concrete. The reference tensile strength is 3.11 MPa for CIn series and 2.72 for CIIIn series. Concrete with the waste achieved values 3.27 – 3.46 MPa and 3.16 – 3.20 MPa respectively.

- Greater content of fine particles in the waste if compared to sand changes the consistency. In the case of 100% sand replacement it changed from S3 to S1.
- Achieving for the concrete with 100% replacement the consistency class such as of the reference concrete requires superplasticizer in an amount of about 1% of cement mass.
- Concrete with 100% of sand replaced with the waste can be used for the production of precast elements. It is possible to properly compact the mixture without the addition of plasticizer. Concrete meets the requirements of abrasion and water absorption.

5. REFERENCES

- Al-Jabri, K. S., Al-Saidy, A. H. & Taha, R. (2011) "Effect of copper slag as a fine aggregate on the properties of cement mortars and concrete", *Construction and Building Materials*. 25(2). 933–938., <https://doi.org/10.1016/j.conbuildmat.2010.06.090>
- Al-jabri, K. S., Hisada, M., Al-saidy, A. H. & Al-oraimi, S. K. (2009) "Performance of high strength concrete made with copper slag as a fine aggregate", *Construction and Building Materials*. 23. 2132–2140., <https://doi.org/10.1016/j.conbuildmat.2008.12.013>
- Alp., I., Deveci, H. & Süngün, H. (2008), "Utilization of flotation wastes of copper slag as raw material in cement production", *Journal of Hazardous Materials*. 159(2–3). 390–395. <https://doi.org/10.1016/j.jhazmat.2008.02.056>
- Ambily, P. S., Umarani, C., Ravisankar, K., Ranjan, P., Bharatkumar, B. H. & Iyer N. R. (2015), "Studies on ultra high performance concrete incorporating copper slag as fine aggregate", *Construction and Building Materials*. 77. 233–240. <https://doi.org/10.1016/j.conbuildmat.2014.12.092>
- Ayano. T. & Sakata. K. (2000). Durability of concrete with copper slag fine aggregate. *Special Publication*. 192. 141–158.
- Broman, I. & Rob, K. (2015), "A framework for strategic sustainable development", *Journal of Cleaner Production Journal*. 140. 17–31., <https://doi.org/10.1016/j.jclepro.2015.10.121>
- Dhir, R. K., de Brito, J., Mangabhai, R. & Lye. C. Q. (2017), "Sustainable Construction Materials-Copper Slag", Cambridge: Woodhead Publishing.
- Gorai, B., Jana, R. K. & Premchand (2003), "Characteristics and utilisation of copper slag - A review", *Resources. Conservation and Recycling*. 39(4). 299–313. [https://doi.org/10.1016/S0921-3449\(02\)00171-4](https://doi.org/10.1016/S0921-3449(02)00171-4)
- Holden, E., Linnerud, K. & Banister, D. (2016), "The Imperatives of Sustainable Development", (I). <https://doi.org/10.1002/sd.1647>
- Kubissa, W. & Jaskulski, R. (2013), "Measuring and Time Variability of The Sorptivity of Concrete", *Procedia Engineering*. 57. 634–641. <https://doi.org/10.1016/j.proeng.2013.04.080>
- Meenakshi Sudarvizhi, S and Ilangovan, R. (2011), "Performance of Copper slag and ferrous slag as partial replacement of sand in Concrete", *International Journal of Civil and Structural Engineering*. 1(4). 918–927.
- Rzechuła, J. (1994), "Gospodarcze wykorzystanie odpadowego ścierniwa z żużła pomiedziowego", In A. Łuszczkiewicz (Ed.). *Fizykochemiczne Problemy Mineralurgii. zeszyt 28* (pp. 207–218). Wrocław: Politechnika Wroclawska.
- Wu, W., Zhang, W. & Ma. G. (2010), "Optimum content of copper slag as a fine aggregate in high strength concrete", *Materials and Design*. 31(6). 2878–2883. <https://doi.org/10.1016/j.matdes.2009.12.037>

PREDICTING RISK OF CORROSION OF BRIDGES MADE OF CONCRETE WITH PORTLAND CEMENT AND LOW ALKALI PORTLAND CEMENT

Szweda Zofia, Śliwka Andrzej

Faculty of Civil Engineering, Silesian University of Technology

Gliwice, Poland ul. Akademicka 5, 44-100

SUMMARY

Chloride ions, a major component of agents for road deicing, are currently the main cause of reinforcement corrosion in bridges due to their depassivating action. As established in codes of recommendations for materials and designs, 100 years is an expected period of bridge durability. After that period, reinforcement corrosion can occur. The required durability of reinforced concrete bridge structures should be achieved by applying concrete cover. Such concrete cover should be made of concrete of adequate waterproofing degree and correct thickness, which impedes the diffusion of very small chloride ions through the pore system of concrete filled with moisture. The required durability can be achieved by increasing the thickness of concrete cover. This has an impact on weight and strength of the structure. Also other solutions can be applied. They involve the use of other types of cement to increase durability. For a bridge made of ordinary concrete with ordinary Portland cement CEM I 42,5 R, and Portland cement with low-alkali content CEM I 42,5 N-SR3/NA, the corrosion risks for reinforced concrete structures was determined on the basis of diffusion coefficient values calibrated with diffusion values. Diffusion values were determined on the basis of a thermodynamic model of ion flow in the concrete pore solution under the influence of electric field. The obtained results show that the selection of a suitable cement type for concrete mix should be the fundamental method for obtaining the required durability of the structures. This method allows reducing thickness of concrete cover.

1. INTRODUCTION

Nowadays, corrosion of reinforcement in bridges is mainly caused by aggressive (depassivating) impact of chloride ions. The applied material and design solutions should guarantee the required durability of bridge structures, which can be defined as the period, after which the risk of chloride corrosion in the reinforcement may occur under typical operating conditions (Zybura, 2003). According to the Polish Regulation, the structure durability is understood as its functional capability within the limit states (Dz.U. Nr 63/2000). Durability of the whole structure is determined as the average durability of its main structural elements. Their service life ranges from 30 to 200 years; for a typical girder or box spans – 80 years, and for supports – depending on their location and construction, from 60 to 200 years. The service life of 100 years is assumed to be guaranteed for the whole structure. The Regulation, in addition to the material and design solutions, allows the additional anti-corrosion, e.g. coating when some difficulties are experienced in achieving the required durability. Due to costs and difficulties in using additional protective treatments, using concrete of adequate waterproofing degree and correct thickness is acceptable to obtain the required durability of reinforced concrete structures in bridges. This may interfere with diffusion of chloride ions, which seem to be very small ($181 \cdot 10^{-12}$ m) in comparison to pores,

through the concrete pore system (the smallest gel pores having a diameter of $1.5 \div 2.0 \cdot 10^{-9}$ m) filled with water. According to the binding Polish Regulation (Dz.U. Nr 63/2000), only low-alkali Portland cement CEM I (Bieńkowski and Wróblewski 2008; Aleksion and Bieńkowski. 2008; Giergiczny, 2014; Giergiczny, 2015; Batog, Giergiczny and Wąsik 2014) can be used for bridge structures. If this criterion is to be met, the use of concrete cover with minimum thickness required by standard PN-91/S-10042 as recommended in the Regulation, will be insufficient to achieve the minimum durability. The minimum durability requires greater thickness of concrete cover which, accordingly, affects the weight and loading capabilities. Other solutions, for example coating, are also acceptable. Alternatively, another type of cement with minimum or slightly increased cover thickness, can be used to guarantee the necessary durability.

The determined values for concrete with Portland cement were in the range from 1.6 to 3.26 10^{-12} m²/s depending on w/c ratio from 0.35 up to 0.6 and cement content from 375 to 280 kg/m³ (Castellote and Andrade 2006). The aim of this paper is to predict the corrosion risk of a bridge with reinforced concrete structures made of ordinary concrete with ordinary Portland cement CEM I 42,5 R and low-alkali Portland cement CEM I 42,5 N-SR3/NA. Concrete without superplasticizers, with w/c = 0.5 (the upper limit value for concrete used in bridges) was used to prevent any possible impact of chemical admixtures on the rate of chloride ion diffusion. The predicted durability of reinforced concrete structures containing the above cement types was used to compare the impact of cement type on diffusion rate of chloride ions. The rate of chloride ion ingress in wet concrete is determined by diffusion coefficients for a given type of concrete. Different test methods produced different values of diffusion coefficients for the same type of concrete. A migration test, that is exposure of chloride ions to electric field accelerating their migration, is used in many methods to measure quicker the migration coefficient (NT BUILD 492; NT BUILD 443; Kurdowski, 2010).

Since the Regulation (Dz.U. Nr 63/2000) does not specify the method of predicting the service life, this paper refers to the values of diffusion coefficients obtained from the thermodynamic model of ion flow in the concrete pore solution exposed to the electric field. The calibration of those values was based on diffusion tests. The distribution of chloride concentration in the concrete cover was determined by means of values of diffusion coefficients for those types of concrete. The corrosion risk – durability of reinforced concrete structures in a bridge was defined as the length of time, after which chloride ion concentration reached the critical value $c_{crit} = 0.4\%$ related to cement weight in concrete at the reinforcement interface. Moreover, the threshold chloride content in the pore solution was found from the Hausman criterion. He suggested that pitting corrosion of steel in pure $\text{Ca}(\text{OH})_2$ and NaOH solutions in the presence of NaCl , is initiated when Cl/OH ions activity ratio exceeds 0.6. The critical content of Cl^- ions is inversely proportional to the concentration of H^+ ions. A change in $\text{pH} = \lg[\text{H}^+]$ from 12 to 11 cause a ten-fold drop in critical chloride content. Thus, decreased concrete pH has a significant impact on corrosion risk of reinforced steel exposed to chlorides. Simultaneous carbonation of concrete raises corrosion risk of reinforcement (Kurdowski, 2010; Alonso et al. 2000). Hobbs found that pH in pores depended on alkali content in cement. For high-alkali cement, pH value is within the range of 13.5-13.9, whereas pH of low-alkali cement is within the range of 12.7-13.1. The pH of fresh grout from Portland cement is 12.5 or higher (Neville, 2012).

2. DETERMINATION OF THE DIFFUSION COEFFICIENT IN MIGRATION TESTS

Diffusion coefficients were determined from the thermodynamic model of chloride penetration into concrete (Szweda and Zybura, 2012; Szweda and Zybura, 2013). On the basis

of experimentally determined distribution of Cl^- ion concentration in concrete samples exposed to the electric field, numerical values of the diffusion coefficient of chloride ions D^1 were calculated from the following expression:

$$D^1 = \frac{\bar{j}^1(a)a\Delta t}{\frac{z^1 F U g}{R T h} [\bar{\rho}_1^1 + \bar{\rho}_2^1 + \dots + \bar{\rho}_n^1] \Delta t - B}, \quad B = \int_0^a Q_x [\rho^1(x, t + \Delta t) - \rho^1(x, t)] dx. \quad (1)$$

where $\bar{j}^1(a)$ means time-averaged Δt mass flux of chloride ions passing through the surface at a distance $x = a$; $\bar{\rho}_1^1$, $\bar{\rho}_2^1$, and $\bar{\rho}_n^1$ are time-averaged averaged Δt mass densities of Cl^- ions at midpoints of the following intervals $[0, g]$, $[g, 2g]$, ..., $[(n-1)g, a]$. In this equation z means ion valence, $F = 96\,487 \text{ C/mol}$ – Faraday constant, U – voltage between electrodes, $R = 8.317 \text{ J/mol}\cdot\text{K}$ – universal gas constant, T – absolute temperature, h – sample height. The first component of denominator defines the steady state of chloride ion diffusion, whereas the second component B defines the non-steady state.

Diffusion coefficients of Portland cement-based concrete were determined in (Szweda, 2016). The tests were performed on cylindrical test elements with a diameter of 100 mm and a height of 50 mm, made of two types of concrete mix. Their content just differed in a type of the cement. C1 concrete contained CEM I 42,5 R Portland cement having high strength at early ages and high heat of hydration. C2 concrete contained cement CEM I 42,5 N-SR3/NA with low content of alkali Na_2O , tricalcium aluminate C_3A and aluminum oxide Al_2O_3 . That cement type is recommended (Dz.U. Nr 63/2000) for bridge structures of high chemical resistance, particularly to sulfate corrosion. Chemical composition of cement types is shown in Table 1. Characteristics of concrete mixes used in the test elements are presented in Table 2. Concrete strength was higher when compared to class B35 (Szweda, 2016), which can be used in all structural elements of bridges in accordance with the Regulation (Dz.U. Nr 63/2000).

Tab. 1: Content of oxides and minerals in tested type of cement (%), (Szweda, 2016)

Concrete	Cement	CaO	SiO ₂	Al ₂ O ₃	Fe ₂ O ₃	SO ₃	K ₂ O	Na ₂ O	MgO	C ₃ A*	C ₄ AF*
C1	CEM I 42.5 R	63.78	19.38	4.57	3.59	3.26	0.58	0.21	1.38	6.04	14.35
C2	CEM I 42.5 N/SR3/NA	63.34	21.15	3.93	5.14	2.61	0.39	0.21	1.28	1.73	15.63

* – acc. to Bogue

Tab. 2: Basic composition of concrete and its compressive strength (%), (Szweda, 2016)

Concrete	Cement	Aggregate	Water	w/c	Compressive strength, f_{cm} MPa	Bulk density, ρ_{cm} kg/m ³ Błąd! Nie można tworzyć obiektów przez edycję kodów pól.
C1					54.2	2271
C2	324.1	1931	166.7	0.5	58.4	2258

The papers (Szweda and Zybur. 2013, Szweda and Zybur 2012) describe the test method for diffusion coefficients. The migration of chlorides in individual sets of three samples was tested over time $t_1 = 24 \text{ h}$ and $t_2 = 48 \text{ h}$. Also diffusion of chlorides was tested in other sets of three samples for $t_3 = 90 \text{ days}$ and $t_4 = 180 \text{ days}$.

The determined results for migration tests were grouped by computational zones within range $a = (n-1)g$ – where $g = 2 \text{ mm}$ is the layer thickness. Those zones were defined according to n layers of collected material weight content of chloride in the concrete volume – Fig. 1.

The averaged mass density values in particular zones and the averaged mass fluxes of chloride ions ρ^{Cl} exceeding limit values of individual computational zones, values of diffusion coefficients were determined assuming in the expression (1) the proportional ratio of component B in the non-steady state to the component expressing the steady state:

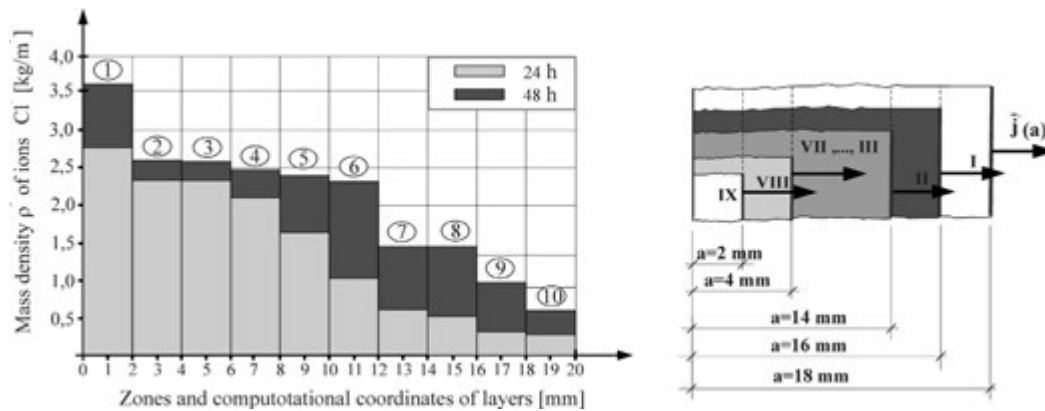


Fig. 1: Computational scheme - concrete C1: a) chloride density in separated layers, b) computational areas

$$B \cong \omega \frac{z^1 F U g}{R T h} (\bar{\rho}_1^1 + \bar{\rho}_2^1 + \dots + \bar{\rho}_n^1) \Delta t \quad (2)$$

where ω is proportionality factor (0.1÷0.5) under conditions similar to the steady state ($B=0$). Then, arithmetic mean value of diffusion coefficients was calculated from all computational zones at two migration times (Szweda et al., 2013; Szweda et al., 2012), Tab. 3.

Such factors as the content of C_3A and C_4AF in cement determine the amount of bound chlorides (Kurdowski, 2010; Kopeckó and Balázs 2007). They affect diffusion rate of chloride ions in concrete. For C2 concrete, diffusion coefficient $D^1=4.73 \cdot 10^{-12}$ m²/s was nearly four times greater than for C1 concrete ($D^1=1.36 \cdot 10^{-12}$ m²/s). This result could indicate that Portland cement CEM I has greater chloride binding capacity than low-alkali Portland cement CEM I/NA with reduced C_3A and C_4AF content (Szweda 2016). The distribution of Friedel's salt described in the paper (Słomka-Słupik and Zybura, 2012) on tests performed on grouts containing those cements, confirmed the obtained result.

Tab. 3: Diffusion coefficient of chloride ions in testing resistance of C1 and C2 concrete against their penetration

Computational area	Diffusion coefficient of chloride ions in testing resistance of concrete against their penetration											
	$D_{ns}^1 \cdot 10^{12}$ m ² /s											
	Impact of non-steady-state process											
	0%		10%		20%		30%		40%		50%	
hours	24	48	24	48	24	48	24	48	24	48	24	48
I	0.02	0.17	0.02	0.19	0.02	0.22	0.02	0.24	0.03	0.29	0.03	0.34
II	0.03	0.31	0.03	0.34	0.04	0.40	0.04	0.43	0.05	0.53	0.06	0.62
III	0.37	0.48	0.40	0.52	0.48	0.62	0.51	0.67	0.62	0.81	0.73	0.95
IV	0.72	0.87	0.79	0.96	0.93	1.14	1.01	1.22	1.22	1.49	1.44	1.75
V	1.05	1.14	1.16	1.25	1.37	1.48	1.47	1.59	1.79	1.93	2.11	2.28
VI	1.68	1.51	1.85	1.66	2.18	1.96	2.35	2.12	2.85	2.57	3.36	3.02
VII	2.09	2.37	2.30	2.61	2.71	3.08	2.92	3.32	3.55	4.03	4.17	4.74
VIII	2.46	3.15	2.71	3.47	3.20	4.10	3.45	4.41	4.19	5.36	4.93	6.31
IX	2.84	3.15	3.12	3.46	3.69	4.09	3.97	4.41	4.82	5.35	5.67	6.30
\bar{D}^1	1.36		1.49		1.76		1.90		2.03		2.71	

I	0.42	0.45	0.46	0.49	0.54	0.58	0.59	0.62	0.71	0.76	0.84	0.89
II	0.75	1.10	0.83	1.20	0.98	1.42	1.06	1.53	1.28	1.86	1.51	2.19
III	1.90	1.98	2.09	2.17	2.47	2.57	2.66	2.77	3.23	3.36	3.80	3.95
IV	2.70	2.72	2.97	3.00	3.51	3.54	3.78	3.81	4.59	4.63	5.39	5.45
V	3.97	4.03	4.37	4.43	5.16	5.23	5.56	5.64	6.75	6.84	7.94	8.05
VI	5.93	5.29	6.52	5.82	7.71	6.88	8.30	7.41	10.08	9.00	11.86	10.51
VII	8.48	6.44	9.33	7.09	11.02	8.37	11.87	9.02	14.42	10.95	16.96	12.88
VIII	11.24	7.41	12.36	8.15	14.61	9.64	15.73	10.38	19.11	12.60	22.48	14.82
IX	12.82	7.51	14.10	8.26	16.67	9.76	17.95	10.51	21.80	12.76	25.64	15.02
\bar{D}^I	4.73		5.20		6.15	6.62	10.45	13.24	4.73	5.20	6.15	6.62

3. PREDICTING THE PROGRESS OF CORROSION RISK

The method of predicting chloride corrosion was described on the example of a bridge structure. The prediction included concrete with strength values corresponding to the average strength of concrete used in typical bridge structures, and to usual cover thickness. Thus, such prediction can be used to profile the rate of chloride corrosion and the effect of cement type in concrete on its diffusion properties, and to determine whether monitoring the boundary condition of durability at the stage of designing and performing bridge structures is necessary. Diffusion properties of concrete depend on many factors. They should be defined for each specific concrete mix. This paper describes how to accelerate the process of their defining. Development of corrosion risk was predicted for those elements of the bridge structure, whose exposure to chlorides was the greatest, that is for the load-carrying structure and lightweight pillars. First symptoms of chloride corrosion could be observed just in those elements. For lightweight pillars, the standard (PN-91/S-10042) specifies the minimal thickness of concrete cover of 40 mm for stirrups, and 50 mm for the main reinforcement. For the load-carrying structure, it is 25 mm and 30 mm, respectively. Changes in protective properties of the concrete cover were determined by calculating an increase in chloride ion concentration on the basis of the diffusion coefficients from (Szweda, 2016) and presented in Tab. 3. Calculations included diffusion coefficients of chlorides in the steady state ($\omega = 0$), shown in Tab. 3, as the tests (Szweda, 2016) have indicated that reliable results for both types of tested cement are obtained after a six-month diffusion, without taking into account the impact of non-steady state ($\omega = 0$) of the process. Critical value of chloride ion concentration at the level value of 0.4% related to cement weight was assumed to pose the risk of reinforcement corrosion.

The changes in chloride concentration at the interface between reinforcement and concrete cover $x = c$ were calculated according to the following relation (Szweda, Ponikiewski and Katzer 2017):

$$\rho_{cal}^I(x,t) = \rho_0^I \left(1 - \operatorname{erf} \frac{x}{2\sqrt{D^I t}} \right) \quad (3)$$

Chloride penetration into concrete is a more complex phenomenon for several reasons. Firstly, the diffusion coefficient is not a constant, but it varies with age, temperature and relative humidity. Secondly, chloride binding has a significant influence on chloride penetration because only free chloride can diffuse into bulk concrete. Thirdly, not only chloride diffusion but also convection flow of chloride ions plays an important role in chloride ion migration in concrete,

especially when exposed to drying–wetting condition. (Castellote and Andrade 2006). The boundary conditions are also more complicated to simulate the real exposure conditions.

Mass density of chloride ions referred to constant mass density of cement ρ_{cem} in concrete to determine the relative concentration of chlorides (Szweda, Ponikiewski and Katzer 2017):

$$C^I(t) = \frac{\rho^I(x=40,t)_{cal}}{\rho_{cem}} 100\% \quad (4)$$

Chloride concentration by cement weight was assumed for concrete boundary value. In real conditions, concentration of chloride ions at the boundary of concrete element may vary over time, e.g. increase as the result of washing out chloride ions by atmospheric precipitation or quite the opposite, decrease due to convection process in alternating dry and wet concrete. The value of boundary concentration was determined experimentally assuming extremely aggressive environmental impact on concrete. However, long-term testing in real conditions is recommended to determine values corresponding to conditions in real structures and verifying the determined value. Such results would be used to determine boundary values for verifying boundary states of the concrete structure durability. Also the coefficient diffusion in real conditions varies over time. It increases at higher moisture content in concrete, temperature increase, and decreases in curing concrete over time (Słomka-Słupik and Zybura 2012). We used the common and simplified method of modelling chloride ion penetration as the purpose of this paper is to compare the effect of used types of cement in concrete on the penetration rate of chloride ions, and not to precisely model the real conditions. Correlation of experimentally determined diffusion coefficients with the real ones requires long-term tests in real conditions.

Changes in chloride concentrations over time at the interface between reinforcing inserts and concrete cover are shown in Fig. 2. By comparing concentration with the critical value, we determined time, after which the risk of reinforcement corrosion could occur. It is equivalent to the expected durability of reinforced concrete structures. For C2 series concrete with cement CEM I 42.5 N/SR3/NA, very fast transport of chlorides was observed. Boundary concentration of chlorides on the stirrup surface in the load-carrying structure was already achieved after five years of its exposure to chlorides. After another two years, chloride concentration reached the limit value on the surface of the main reinforcement. Thus, the real durability was much shorter than specified 80 years (Dz.U. Nr 63/2000). For C1 series concrete, with cement CEM I 42.5 R, the obtained durability was much longer, nearly 3.5 times, but did not exceed ¼ of the required durability. The achieved durability of lightweight pillars was much longer due to the increased minimum thickness of the cover. For C2 series concrete, durability was 12 and 19 years respectively. However, the required 60-year durability for that element was not achieved. C1 series concrete was much more durable, that is its service life was 42 and 66 years respectively. It means that the required durability of the main reinforcement can be ensured without any additional treatments, and the stirrups achieve 2/3 of the defined service life.

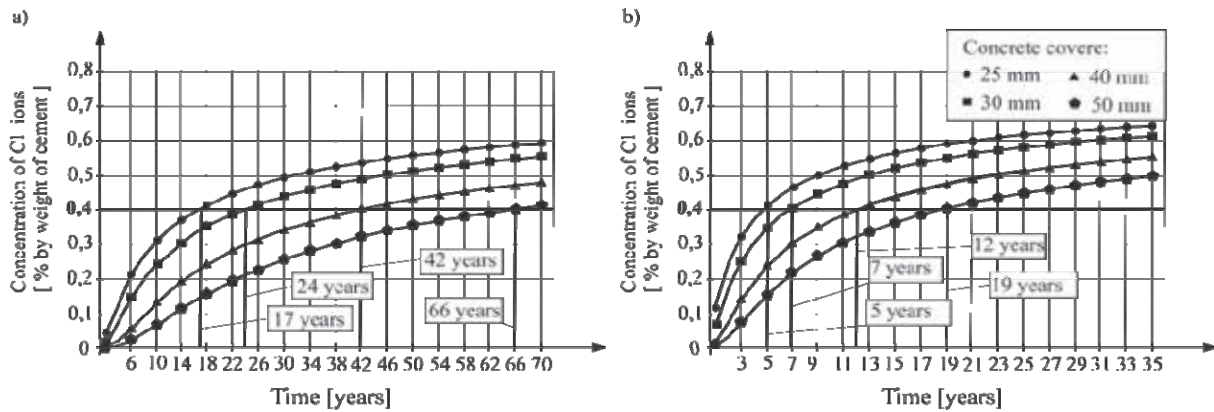


Fig. 2: Increase in ion concentration at the surface of reinforcement protected with concrete cover having thickness of 25, 30, 40 and 50 mm in the following concrete series: (a) C1, (b) C2

The minimum thickness of cover was also determined to achieve required durability (Dz.U. Nr 63/2000) (Fig. 3). For C2 concrete in lightweight pillars and load-carrying structures, the minimum cover thickness should be 90 mm and 105 mm respectively. C1 concrete required the cover thickness of 50 mm and 55 mm respectively. They were nearly half as low as the above values. Thickness required for the specific durability can be reduced by more than 44% just by changing the type of cement for concrete mix. It has a direct impact on material consumption and load-bearing capacity of the structure.

4. CONCLUSIONS

The selection of suitable cement type for the concrete mix should be the basic method of obtaining the required structure durability. It can significantly increase the durability without any change in the concrete cover. Consequently, additional treatments increasing the durability, such as impregnation, cathodic or sacrificial anode protection, can be limited. They increase costs of the construction, and sometimes are ineffective. In the analyzed example, only the change of cement type increased durability over 3.4 times. Currently, there is a tendency to limit additional solutions for increasing durability. Concrete is assumed to ensure the proper protection of reinforcing steel against corrosion. Hence, additional treatments increasing durability should be used only in special cases. Then, the appropriate thickness of concrete cover is important as it prevents aggressive agents and protects reinforcing steel. If the increased thickness of concrete cover is necessary for durability, it increases material costs and affects the load-bearing capacity of the structure. In this case, suitable cement type in concrete can reduce the concrete cover thickness – in the analysed situation, thickness could be reduced by more than 44%. If the critical chloride content acc. to the Hausman criterion:

$$\frac{[Cl^-]}{[OH^-]} \leq 0,6 \text{ where } [OH^-] = 10^{pH-14} \quad (5)$$

The measured concrete pH, and pH = 11.8 typical for possible carbonation of each tested concrete type are considered for durability tests, a substantial drop in critical chloride content can be found in both series of carbonated concrete ($C_{cr} = 0.05$ for C1, $C_{cr} = 0.24$ for C2) (Tab. 4). The prediction, which includes the Hausman criterion, indicates significantly longer durability of C1 concrete with CEM I cement over C2 with CEM I NA cement.

Tab. 4: Calculated critical concentration of chlorides acc. to Hausman criterion - the equation (5)

Concrete	[Cl ⁻]	pH	[Cl ⁻]/[OH ⁻]
C1	0.4	13.0	0.338
C2	0.4	12.5	1.07
C1 and C2	0.4	11.8	5.36
C2	0.24	12.5	0.6
C1 and C2	0.05	11.8	0.6

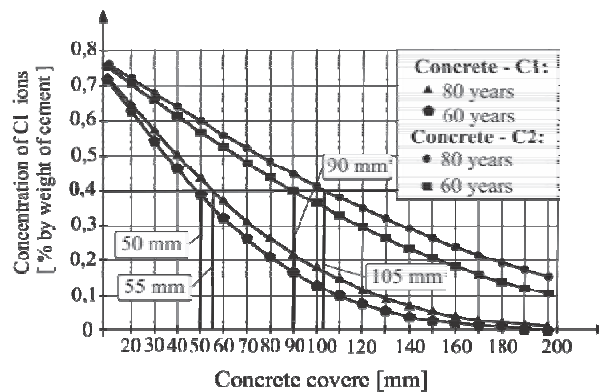


Fig. 3: Decrease in ion concentration at the reinforcement surface protected with variable thickness of concrete cover in concrete of C1 and C2 series

The impact of only two types of cement: CEM I 42.5 R and CEM I 42.5 N/SR3/NA on the protective properties of concrete cover was analysed in the paper. It turned out to be significant. Nowadays, a very broad range of cement types is available. If present in concrete, they can further improve protective properties of concrete for reinforcing steel with reference to chlorides (Giergiczny, 2014; Giergiczny, 2015; Batog et al. 2014 Słomka-Słupik et. al., 2012). Both the cement properties and the adequate composition of concrete mix can result in achieving the required durability of a bridge structure without the increased minimum thickness of the concrete cover and additional protective treatments. That, in turn, will have a direct impact on cost and load-bearing capacity of the structure.

7. REFERENCES

- Aleksion M., Bieńkowski T., (2008) "The highest bridge structure in Poland within the Kwiatkowski Freeway in Gdynia, containing special cement CEM I 42.5 N-HSR/NA for bridge structures. Concrete Days.
- Alonso C., Andrade C., Castellote M., Castro P. (2000) "Chloride threshold values to depassivate reinforcing bars embedded in a standardized OPC mortar". Cement and Concrete Research. 30: 1047-1055.
- Batog, M., Giergiczny, Z., Wąsik, M. (2014) "Cement as a component of concrete in e communication engineering. Journal of Motorways. 8-9, pp. 28-30.
- Bieńkowski, T. Wróblewski, P. (2008) The construction of road bridge over the Warta River in Konin, based on cement CEM I 42.5 N-HSR/NA. Concrete Days 2008.
- Castellote, M. Andrade, C. (2006), "Round-Robin test on methods for determining chloride transport parameters in concrete". Materials and Structures. 99pp. 955-990.
- Decree of Minister of Transport and Maritime Economy of 30 May 2000 on the technical conditions to be met by engineering road structures and their location. (Dz.U. Nr 63/2000, poz. 735).
- Giergiczny Z., (2014) "How to choose cement for specific use in building engineering?" Journal of Motorways. 1-2, pp. 18-23.

- Giergiczny Z., (2015), Slag cement for road and bridge engineering. *Journal of Motorways*. 8-9pp. 26-31.
- Kopecskó K., Balázs Gy. (2007) "Chloride ion binding of steam cured aluminates and cements" *Proceedings of the International Symposium on Concrete Structures – Stimulators of Development*. Cavtat; Dubrovnik, Horvátország, 2007.05.20-2007.05.23. Zagreb: pp. 383-390
- Kurdowski. W. (2010) *Cement and concrete chemistry*. Wydawnictwo Polski Cement. Wydawnictwo naukowe PWN. Kraków.
- Neville A. M., (2012) „Concrete properties” *Polski cement*. Kraków.
- NT BUILD 443. *Concrete, hardened: Accelerated chloride penetration*. Approved 1995–11.
- NT BUILD 492. "Concrete, mortar and cement-based repair materials: chloride migration coefficient from non-steady-state migration experiments." Approved 1999–11
- PN-91/S-10042 *Bridges. Concrete, reinforced concrete and prestressed concrete structures. Design*
- Słomka-Słupik, B. Zybura A. (2012) "Corrosion of Portland cement pastes produced from CEM I 42.5 R and CEM I 42.5 N-HSR/NA in ammonium chloride solution." *Cement Wapno Beton* 3: 144-148.
- Szweda Z., (2016) "Resistance of concrete with ordinary and low-alkali Portland cement to chloride ingress. *Ochrona przed korozją* 5, pp. 148-153.
- Szweda Z., Ponikiewski T., Katzer J. (2017). "A study on replacement of sand by granulated ISP slag in SCC as a factor formatting its durability against chloride ions". *Journal of Cleaner Production*. 156:569-576
- Szweda Z., Zybura A., (2012) "Analysis of chloride diffusion and migration in concrete. Part I – Theoretical model", *Architecture Civil Engineering Environment*.1, pp. 47-54.
- Szweda Z., Zybura A., (2012) "Analysis of chloride diffusion and migration in concrete. Part II – Experimental tests", *Architecture Civil Engineering Environment*.1, pp. 55-62.
- Szweda Z., Zybura A., (2013) "Theoretical model and experimental tests on chloride diffusion and migration processes in concrete". *Procedia Engineering*. Elsevier 57, pp. 1121–1130.
- Zybura A., (2003) "Electrochemical protection of reinforced concrete structures", *Monograph*. Wydawnictwo Politechniki Śląskiej. Gliwice,

THE SIMULATION OF CORROSION DEGRADATION OF CONCRETE SPECIMEN IN STATIONARY HEAT AND MOISTURE CONDITION

*Faustyn Recha, Tomasz Jaśniok, Tomasz Krykowski
Silesian University of Technology, Faculty of Civil Engineering
Akademicka 5, 44-100 Gliwice*

SUMMARY

This paper is focused on the problem of the forecasting of damage in the reinforced concrete specimens as the consequence of chlorides corrosion. The performed numerical calculations take into consideration as well the time that is necessary for filling the empty pores space in the interface transition zone (ITZ) as the time necessary for tightening the products of corrosion. The approach that assumes creation of distortional strains in the ITZ layer that is the result of the mass production of corrosion products and can be described as the function of corrosion current intensity was used.

1. INTRODUCTION

The corrosion phenomenon and the damage of reinforced concrete elements caused by the reinforcement corrosion represent one of the most fundamental problems of the durability of structures. The existing code PN-EN impose the thickness of the concrete cover which should be ensured in the structures subjected to chlorides attack (class XD and XS). These conditions are rather general and do not take into consideration many of complex situation's that can occur in the life time of structures. The evaluation of the overall cost of the exploitation of structures and the forecast of the durability of structures e.g. for the needs of the BIM (building information modeling) or the evaluation of the durability of structures subject to the complex physicochemical attack can be awkward. The degradation of the reinforced concrete elements as the result of reinforcement corrosion can be divided in to several stages. In the first stage there is a transport of aggressive substances, oxygen, moisture and heat through the cover of concrete in to the rebar's surface. This issue is widely discussed and described in the scientific literature (Ožbolt, at al., 2017; Saetta, at al., 1998; Koniorczyk, at al.; 2008). In the successive stage the initiation of electrochemical corrosion processes take place (Dao, at al., 2010). During the process of corrosion the embedding of created products of electrochemical corrosion on the rebar surface and in the structure of pores of the cement paste also known as interface transition zone (ITZ) takes place. The structure of this layer which is characterized by increased porosity is of a fundamental significance for the description of physicochemical processes occurring in the concrete cover (Bentur, at al., 2000; Horne, at al., 2007; Ollivier, at al., 1995; Bentur, at al., 1985). The mechanical interactions of corrosion products on the concrete cover are initiated after filling up the pores in the interface transition zone by the products of corrosion. The time that is necessary to fill tight the structure of pores was analyzed among other things in (Liu, 1996; Chen, at al., 2008; Bhargava, at al., 2005). In (Liu, 1996; Bhargava, at al., 2005; Pantazopoulou, at al., 2001) the problems of damage evolution in the concrete cover caused by the volumetric increase of corrosion products was analyzed. In (Krykowski, 2012; Molina, at al., 1993) the description of effects of the theory of damage that takes into consideration distortional strains that are the result of the volumetric increase of corrosion products was used. It was assumed in (Ožbolt, at al., 2017; Suwito, at al., 2008)

that the process of embedding of corrosion products in the structure of pores can be described by the equations of diffusion. It was also accepted in (Suwito, at al., 2008) that the corrosion products can be transferred from the interface transition layer deep into the cement paste that is surrounding the rebar.

This paper concentrates on the forecasting of damage evolution in the concrete specimen which are the result of carried on experimental analysis. The experimental research presume adding the chlorides into the concrete mix in the phase of formation of concrete specimens. The results that can be obtained in the laboratory was analyzed (constant relative humidity of the air in the concrete pores, constant temperature and chloride ions concentration on the rebar's surface). The mechanism of damage of concrete cover was analyzed as well with taking into account the time of filling of the transition zone as the time that is necessary to tighten the corrosion products in the interface transition zone. This issue was described with taking into account the approach based on the concept similar to the well-known idea from the damage mechanics namely the degradation parameter (Krykowski, at al., 2017). The purpose of the paper is the answer to the question what will look like the time evolution of damage in concrete specimens in the case of the uniform corrosion of reinforcement and the excluded impact of the rheology.

2. THE EVOLUTION OF EQUIVALENT CHANGE OF CORROSION PRODUCTS VOLUME

The structure of the steel-concrete interface transition zone has a crucial impact on the way of evaluation and description of the fracturing of concrete cover. The concrete in the vicinity of reinforcing bars by the reason of impact of solid phase in the cement hydration process has slightly different structure. This layer that is called the interface transition zone has the thickness of about 50-100 μm . Into the composition of this layer come electric double layer of thickness about 1-2 μm , the layer of the cement paste of increased porosity and the layer of large crystals (Bentur, at al. 2000; Zybura, at al. 2011). In the moment of activation of the process of corrosion the accumulation of the products of corrosion in the interface transition zone has place. This products after filling the structure of pores start to impact mechanically on the concrete cover. The very important is here to define what part of the products of corrosion directly contribute to forming of damage in the concrete cover. In the initial stage the process of creation of the corrosion products was not accompanied by the increase of stress in the concrete cover. The corrosion products are located on the corrosion pit surface and fill the empty spaces of pores in the interface transition layer. Along with the increase of pressure exerted through the products of corrosion to the concrete cover the transport of the part of corrosion products from the high porosity ITZ layer can be done. The products are transferred into the characterized by smaller porosity deeper layers of concrete. Analyzing the mechanisms of transfer and production of the products of corrosion in the ITZ layer one can accept that four variables have influence on a function of the rate of change of effective volume \dot{V}_{eff} . This variables are the rate of production of corrosion products \dot{V}_R , the rate of corrosion cavity creation $\dot{V}_{Fe^{2+}}$, the rate of loss of corrosion products as the result of transfer into ITZ layer \dot{V}_{por} and the rate of change of corrosion products volume \dot{V}_{tran} as the result of transfer from high porosity ITZ layer deeper into the layer of concrete cover. The transport of the corrosion products from the ITZ layer deep into concrete cover is the result of the pressure increase which this products exert on the pores structure of concrete. The aforementioned dependence can be formally written (Suwito, at al., 2008) by the use of the equation:

$$\dot{V}_{eff} = \dot{V}_R - \dot{V}_{Fe^{2+}} - \dot{V}_{por} - \dot{V}_{tran} = \dot{V}_{ekw} - \dot{V}_{por} - \dot{V}_{tran}, \quad (1)$$

The first two values in the equation (1) the rate of changes \dot{V}_R and $\dot{V}_{Fe^{2+}}$ can be defined as functions of corrosion current intensity I , (Krykowski, 2012). The determination of next two values \dot{V}_{por} and \dot{V}_{tran} is complex and complicated in the theoretical description. One can however assume (Krykowski, at al. 2017) that this values can be defined as functions of the rate of changes \dot{V}_R and $\dot{V}_{Fe^{2+}}$ and a certain additional variable which was called the parameter of damage of the equivalent volume $\beta = \beta(\tau) \in \langle 0,1 \rangle$ by the analogy to the mechanics of damage:

$$\dot{V}_{por} + \dot{V}_{tran} = \beta(\dot{V}_R - \dot{V}_{Fe^{2+}}) = \beta \dot{V}_{ekw}, \quad (2)$$

The value \dot{V}_{ekw} that exist in equations (1) and (2) can be determined according to the Faraday's law and linear relationship between the amount of ferrous ions transferred to the pore solution and the volume of the products of corrosion. Taking into account the equation (2) in (1) allows for formulation of the relationship between the rate of change of effective volume and the rate of change of equivalent volume in the way that is close to the approach used in the continuum damage mechanics (Krykowski, at al. 2017):

$$\dot{V}_{eff} = (1 - \beta)(\dot{V}_R - \dot{V}_{Fe^{2+}}) = (1 - \beta)\dot{V}_{ekw}, \quad \dot{V}_{ekw} = \frac{(\alpha^{-1}\vartheta - 1)k}{\rho_{Fe^{2+}}} I, \quad (3)$$

where $\rho_{Fe^{2+}}$ is the density of ferrous ions, α and ϑ - parameters, which in the literature are accepted in dependence of composition of corrosion products (Pantazopoulou, at al. 2001; Krykowski, 2012). The β parameter determines the intensity of the interaction with which the developing process of corrosion influence to the structure of the concrete cover. These parameter describe three phases of the interaction of corrosion products on the structure of the concrete cover. In the initial phase that precede the feeling of the empty pores spaces in the ITZ layer which takes place in the time $\tau < \tau_0$, where τ_0 is the assumed time that is necessary to fill the space of pores in the way that is not producing the mechanical effects in the concrete cover $\beta = 1$. The second phase takes place in the imaginary range of time $\tau_0 < \tau < \tau_u$, $0 \leq \beta = \beta(\tau) \leq 1$. In this stage we can observe the progressive increase of the pressure exerted by corrosion products on the walls of pores. The time τ_u that correspond to reaching the tightness by the corrosion products that block the diffusion of these products from the ITZ layer into surrounding concrete is treated as the imaginary time of the second phase of the process of degradation. The creation of the tight layer of the corrosion products is equivalent with accepting the evolution of the volume change in the concrete cover in accordance with the equation (3) $\dot{V}_{eff} = \dot{V}_{ekw}$. These phase of degradation of the concrete cover is the third and the last stage of the process of concrete cover degradation. This stage takes place when $\tau > \tau_u$ and the value of β parameter is equals to zero. The exemplary linear function of degradation β that is applied in this paper can be expressed in the form of the expression (Krykowski, at al. 2017)

$$\beta(\tau) = \begin{cases} \beta = 1 & \tau \leq \tau_0 \\ \beta = \beta(\tau) = \tau_u - \tau / \tau_u - \tau_0 & \tau_0 < \tau < \tau_u \\ \beta = 0 & \tau \geq \tau_u \end{cases} \quad (4)$$

The value τ_0 can be estimated from the Faraday's laws as the time that is necessary to fill the pores in the ITZ layer. The time τ_u is the parameter that must be determined experimentally.

3. THE COMPUTATIONAL MODEL

The analysis of fracture was made using system ATENA. The elastic-plastic-brittle model of concrete implemented in this system uses the Rankine surface for the description of fracturing:

$$F_i^f = \sigma_{ii}^t - f_{ii} \leq 0, \quad (5)$$

where f_{ii} is tensile strength in the material direction i . In the remaining situations the fracture of concrete is defined by the use of the Menetrey - Williams failure surface:

$$F_{3P}^p = \left[\sqrt{1.5} \frac{\rho}{f_c} \right]^2 + m \left[\frac{\rho}{\sqrt{6} f_c} r(\theta, e) + \frac{\xi}{\sqrt{3} f_c} \right] - c = 0, \quad (6)$$

$$m = 3 \frac{f_c^2 - f_t^2}{f_c f_t}, \quad r(\theta, e) = \frac{4(1-e^2)\cos^2 \theta + (2e-1)^2}{2(1-e^2)\cos \theta + (2e-1)[4(1-e^2)\cos^2 \theta + 5e^2 - 4e]^{0.5}}, \quad (7)$$

where ξ , ρ , θ - are Heigh-Vestergard coordinates, f_c - material resistance for compression, f_t - material resistance for tension, e - the parameter defining the shape of the failure surface. The kinetics of the electrode process was described by the use of the function of corrosion current density obtained on the basis of a few years empirical research (Liu, 1996):

$$i_{corr} = 0.9259 \left(8.37 + 0.618 \ln(1.69 C_{fc}) - \frac{3034}{T} - 0.000105 R_{c,res} + 2.25 t^{-0.215} \right), \quad (8)$$

where i_{corr} is the density of corrosion current ($\mu A/cm^2$), C_{fc} - the concentration of the free chlorides on the surface of the rebar (kg/m^3), T - the temperature on the surface of the rebar (K), $R_{c,res}$ - the electrical resistance of concrete (Ω), however t - the time of exposition ($year$). The electrical resistance of concrete in the form of empirical relationship of relative humidity φ (1), (López, at al., 1993) was included as well into this equation:

$$R_{c,res} = 90.537 \varphi^{-7.2548} [1 + \exp(5 - 50(1 - \varphi))]. \quad (9)$$

According to the concept of the increase of the transition layer the tensor of corrosion strain rate $\dot{\boldsymbol{\varepsilon}}^{kor}$ can be formulated in the form of relationship (Krykowski, 2012; Krykowski, at al. 2013):

$$\dot{\boldsymbol{\varepsilon}}^{kor} = \frac{1}{2} \frac{\dot{V}_{eff}}{V_{ini}} \mathbf{1} = \frac{(1-\beta)AI}{2V_{ini}} \mathbf{1}, \quad A = \frac{(\alpha^{-1}\vartheta - 1)k}{\rho_{Fe^{2+}}}, \quad \mathbf{1} = \delta_{ij} \mathbf{e}_i \otimes \mathbf{e}_j. \quad (10)$$

where V_{ini} is the initial volume of the analyzed region. It was assumed in (10) that the nonzero strains appear only in the plane perpendicular to the rebar's axis. The FEM algorithm requires formulation of (3), (10) in the incremental form. Applying the Euler backward algorithm this equations will have the form:

$$\boldsymbol{\varepsilon}_{n+1}^{kor} = \boldsymbol{\varepsilon}_n^{kor} + \frac{(1-\beta_{n+1})A_{n+1}I_{n+1}}{3V_{ini}} \mathbf{1} \Delta t, \quad V_{eff,n+1} = V_{eff,n} + (1-\beta_{n+1})A_{n+1}I_{n+1}\Delta t, \quad \Delta t = t_{n+1} - t_n. \quad (11)$$

The time after which the empty pores space in the ITZ layer will be filled can be determined by the use of Faraday's law. We will have the following incremental form of these equations:

$$\frac{m_{n+1} - m_n}{\Delta t} = \rho_R \frac{V_{n+1} - V_n}{\Delta t} = kI_{n+1}, \quad t_{n+1} = t_n + \Delta t, \quad V_{n+1} \leq V_{por}, \quad (12)$$

where ρ_R is the mass density of corrosion products, V_{por} - the volume of the pores space in the ITZ layer.

4. COMPUTER ANALYSIS OF THE PROBLEM

The test specimen with dimensions 100x100x100 mm³ with unsymmetrically located steel bar with diameter $\phi = 22$ mm subjected to the uniform corrosion on the entire surface was analysed. Three dimensional space FEM model of the test specimen discretized by three-linear solid elements was made using the system ATENA. The FEM model was supported on three mutually perpendicular walls and presented in Fig. 1.

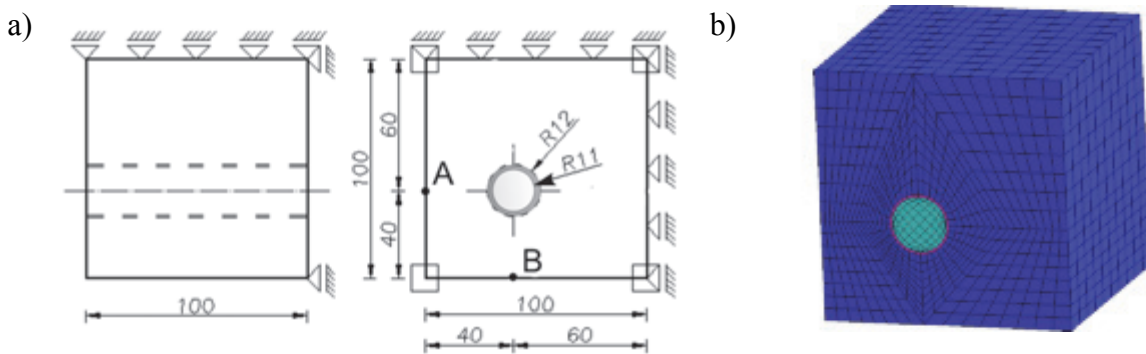


Fig. 1: The model of the reinforced concrete test specimen: a) static scheme, b) FEM model

The mean values of material parameters were assumed according to the ATENA database. For the purpose of the analysis was assumed that the steel rebar as well as the ITZ layer (containing the corrosion products) which is assumed to be 1 mm thick are described by the linear-elastic materials (it is assumed that the concrete cover crack depends only on the increment of the mass of corrosion products). The increments of distortional strains caused by the corrosion products in the ITZ layer in the discrete instants of time was the loadings for this model. The material parameters of the model were compiled in Tab. 1. In Tab. 2 the constants that are required to determine the parameters of corrosion was compiled. It was assumed that the corrosion products are entirely composed of ferrous hydroxide $Fe(OH)_2$. Two computational experiments were made. In the first one the assumption was made that the density of corrosion electric current is a constant value. This value was accepted as $i_{kor} = 3 \mu A/cm^2$ what correspond to the value of corrosion electric current intensity $I_{kor} \cong 207 \mu A$. The numerical values obtained as the result of computations was compiled in Fig 2, depending on the constant $\bar{I} = I/I_{max}$ that express the ratio of the corrosion current intensity I to the maximum value of the corrosion current intensity I_{max} , the parameter of degradation of the equivalent volume β and the time. In Fig. 2a the diagram of changes of effective volume V_{eff} of corrosion products and the diagram of changes of maximum distortional strain in radial directions ε_r is presented, instead on 2b the evolution of the width of the cracks w_c is presented. In the subsequent stage of research the function of corrosion electric current density that is changing in time according to (8) was accepted. The calculations was made under the assumption of constant hygro-thermal conditions (constant temperature $T_{Rf} = 22$ °C and the constant concentration of chlorides on the rebar surface $C_{fc} = 1.8$ kg/m³). For the needs

of the theoretical analysis the relative humidity of the air in the pores of concrete was assumed as 60%, $\varphi = 0.6$.

Tab. 1: The material parameters of concrete, steel and ITZ layer	
<i>Material mean parameters of concrete C20/25</i>	
Young's moduli, E_c [GPa]	30
Poisson coefficient, ν [1]	0.2
Tensile strength, f_{ctm} [MPa]	2.2
Compressive strength, f_{cm} [MPa]	28
Fracture energy, G_F [MN/m]	5.5e-5
<i>Material parameters of steel</i>	
Young's moduli, E [GPa]	200
Poisson coefficient, ν [1]	0.3
<i>Material parameters of transition layer (ITZ)</i>	
Young's moduli, E [GPa]	200
Poisson coefficient, ν [1]	0.3

Tab. 2: Material parameters of the products of corrosion	
Assumed thickness of the ITZ layer, w_{wp} [μm]	100
Porosity, ε [m^3/m^3]	0.5
Effective thickness of the ITZ layer, $w_p = \varepsilon \cdot w_{wp}$ [μm]	50
Length of corrosion active reinforcement, L_a [m]	0.1
Density of corrosion products, ρ_r [kg/m^3]	3600
Electrochemical equivalent of iron, $k \cdot 10^3$ [$\text{g}/(\mu\text{A} \cdot \text{year})$]	9.12
Parameter, $\alpha = m_{\text{Fe}^{2+}} / m_R$ [1]	0.622
Parameter, $\vartheta = \rho_{\text{Fe}^{2+}} / \rho_R$ [1]	2.24
ITZ layer tightening time, $\Delta\tau = \tau_u - \tau_0$ [[month.]]	4

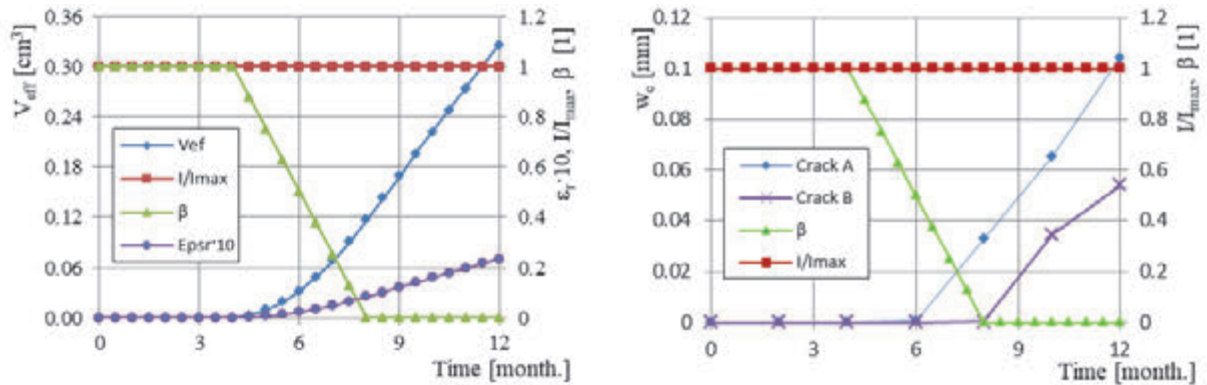


Fig. 2: The diagram of changes of the constant in time function of corrosion current intensity: a) the effective volume of corrosion products V_{eff} and distortional radial strains ε_r , b) the width of cracks w_c

The electrical resistance of concrete was determined by the use of (9). The numerical values obtained as the result of computations are compiled in Fig. 3 according to the constant $\bar{I} = I / I_{max}$, the parameter of degradation β and the time (the value $I_{max} = 300.92 \mu\text{A}$). In these figure the process of changes of the following functions is presented: the effective volume of corrosion products V_{eff} and the diagram of change of maximum distortional strain in radial direction ε_r in Fig. 3a instead in Fig. 3b the evolution of the width of the cracks w_c . The crack pattern in the concrete specimen in the case of constant value of the corrosion current density and the case when the corrosion current density is a time dependent function are presented in Fig. 4a and 4b.

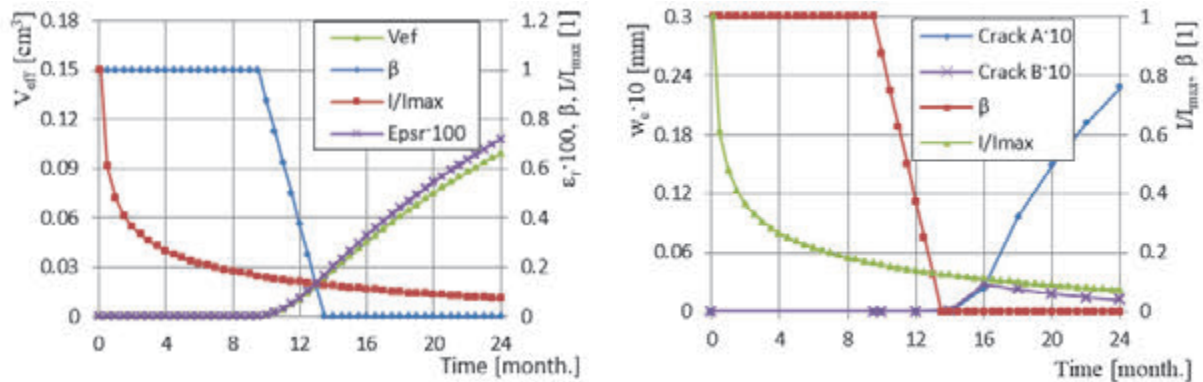


Fig. 3: The diagram of changes of the time dependent function of corrosion current intensity: a) the effective volume of corrosion products V_{eff} and distortional radial strains ϵ_r , b) the width of cracks w_c

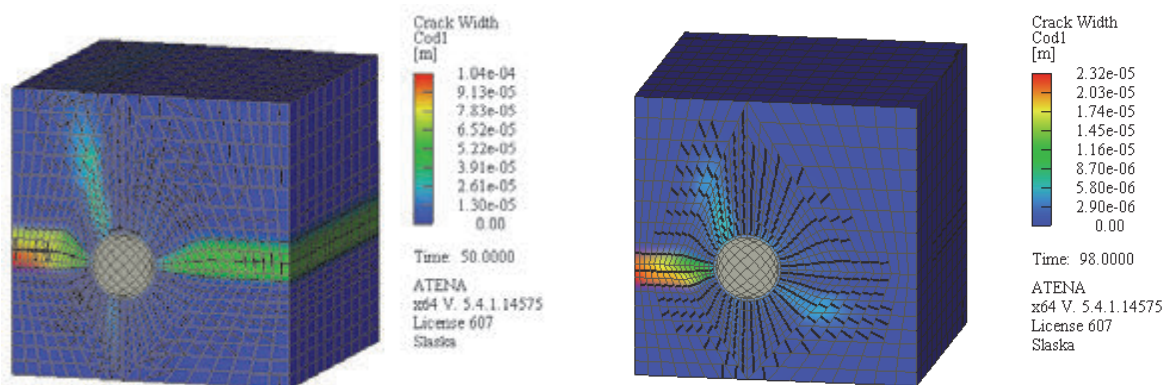


Fig. 4: The crack pattern: a) after 12 month (constant value of corrosion $I = const$), b) after 24 month (variable in time corrosion current intensity function $I = I(t)$).

5. CONCLUSIONS

The purpose of the research that was presented in this paper was to show the application of the approach presented in (Krykowski, et al. 2017) to evaluate the effects of corrosion products influence on the concrete cover. The presented approach takes into consideration the effect of corrosion products tightening. The performed calculations can be used as the support in the proper design of the experiment. The very important information that results from carried out calculations is the expected length of the time of research. Assuming the width of cracks $w_c = 0.1$ mm as the durability limit one can notice that this criterion in the first case (Fig. 2) will be fulfilled approximately after one year. In the model that takes into consideration the variable in time function of corrosion current intensity (Fig. 3) this criterion will be not fulfilled even after two years.

7. REFERENCES

- Bentur, A., Alexander, M. G. (2000). Engineering of the interfacial transition zone in cementitious composites. *Materials and Structures*, 33, 82-87.
- Bentur, A., Diamond, S., Mindess, S. (1985). Cracking processes in steel fiber reinforced cement paste. *Cement and Concrete Research*, 15, 331–342.

- Bhargava, K., Ghosh, A. K., Mori, Y., & Ramanujam, S. (2005) Modeling of time to corrosion-induced cover cracking in reinforced concrete structures. *Cement and Concrete Research*, 35(11), 2203–2218.
- Chen, D., Mahadevan, S. (2008). Chloride-induced reinforcement corrosion and concrete cracking simulation. *Cement & Concrete Composites*, 30, 227–238.
- Dao, L. T. N., Dao, V. T. N., Kim, S-H., & Ann, K, Y. (2010) Modeling Steel Corrosion in Concrete Structures - Part 1: A New Inverse Relation between Current Density and Potential for the Cathodic Reaction. *International Journal of electrochemical science*, 5, 302 – 313.
- Dao, L. T. N., Dao, V. T. N., Kim, S-H., & Ann, K, Y. (2010). Modeling Steel Corrosion in Concrete Structures - Part 2: A Unified Adaptive Finite Element Model for Simulation of Steel Corrosion. *International Journal of electrochemical science*, 5, 314 – 326
- Horne, A.T., Richardson, I.G., & Brydson, R. M. D. (2007). Quantitative analysis of the microstructure of interfaces in steel reinforced concrete. *Cement and Concrete Research* 37, 1613–1623.
- Koniorczyk, M., Gawin, D. (2008). Heat and moisture transport in porous building materials containing salt. *Journal of Building Physics*, 31(4), 279–300.
- Krykowski T. (2012). Modelowanie uszkodzenia otuliny wywołanego korozją zbrojenia w żelbecie. Polska Akademia Nauk, Komitet Inżynierii Lądowej i Wodnej, Warszawa, Studia z Zakresu Inżynierii 78.
- Krykowski, T., Wieczorek, B. (2017). Application of damage mechanics rules to evaluate the growth of corrosive deformations in transition layer. *Corrosion Protection*, 1(60), 3-6.
- Krykowski, T., Zybura, A. (2013). Modelling of reinforced concrete element damage as a result of reinforcement corrosion. *Procedia Engineering* 57, 614 – 623.
- Liu, Y. (1996). Modeling the Time-to-Corrosion Cracking of the Cover Concrete in Chloride Contaminated Reinforced Concrete Structures. Dissertation submitted to the Faculty of the Virginia Polytechnic Institute and State University in partial fulfillment of the requirements for the degree of Doctor of Philosophy in Civil Engineering.
- López, W., González, J. A. (1993). Influence of the degree of pore saturation on the resistivity of concrete and the corrosion rate of steel reinforcement. *Cement and Concrete Research*, 23(2), 368–376.
- Molina, F. J., Alonso, C., & Andrade, C. (1993). Cover cracking as a function of rebar corrosion: Part 2 Numerical model. *Materials and Structures*, 26, 532-548.
- Ollivier, J.P., Maso, J.C., & Bourdette, B. (1995). Interfacial Transition Zone in Concrete. *Journal of Advanced Cement Based Materials*, 2, 30-38.
- Ožbolt, J., Oršanić, F., & Balabanić, G. (2017). Modelling processes related to corrosion of reinforcement in concrete: coupled 3D finite element model. *Structure and Infr. Engin. Maintenance, Management, Life-Cycle Design and Performance*, 13(1), 135-146.
- Pantazopoulou, S. J., Papoulia, K. D. (2001). Modeling cover-cracking due to reinforced corrosion in RC structures. *Journal of Engineering Mechanics*, 127(4), 342–351.
- Saetta, A., Scotta, R., & Vitaliani, R. (1998). Mechanical behavior of concrete under physical-chemical attacks. *Journal of Engineering Mechanics*, 124(10), 1100–1109.
- Suwito, C., Xi, Y. (2008). The effect of chloride-induced steel corrosion on service life of reinforced concrete structures. *Structure and infrastructure engineering: maintenance, management, life-cycle design and performance*, 4(3), 177 – 192.
- Zybura, A., Jaśniok, M., Jaśniok, T. (2011). Diagnostyka konstrukcji żelbetowych, Badania korozji zbrojenia i właściwości ochronnych betonu, t. II. *Warszawa: Wydawnictwo Naukowe PWN*.

COMPRESSIVE AND FLEXURAL STRENGTHS OF HEAT CURED ULTRA-HIGH PERFORMANCE CONCRETE PRODUCED WITH LOCAL MATERIALS

*Ahmed J. Al-Basha, Craig M. Newton, Brad D. Weldon
Department of Civil Engineering at New Mexico State University
P.O. Box 30001, MSC 3CE, Las Cruces, NM, 88003*

SUMMARY

Ultra-high performance concrete (UHPC) was produced using materials local to New Mexico, USA to investigate the effects of elevated temperature curing (greater than 90°C) on compressive and flexural strength. The purpose of this investigation was to develop a mixture and curing regimen that could be used to produce small, high quality modular UHPC elements. Several curing regimens were tested using temperatures of 95°C, 150°C, 200°C, 250°C, and 300°C. Effects of cement type, fine aggregate gradation, and fiber content and type on the strength properties were also investigated. A curing regimen including wet curing at 95°C followed by dry curing at 250°C was selected as the optimal curing regimen. This curing regimen, along with careful material selection, improved compressive and flexural strengths of locally produced UHPC by 38.5% and 54.9%, respectively.

1. INTRODUCTION

Ultra-high performance concrete (UHPC) is concrete exhibiting compressive strength greater than 150 MPa, high ductility, and excellent durability and resistance to chemical and physical attacks (Magureanu et al., 2012). These properties are attained through careful selection of UHPC's constituent materials, the method by which it is prepared, and its curing regimen.

Typical UHPC mixtures consist of cement, fine aggregates, supplementary cementitious materials (SCMs), low water-cementitious materials ratios (w/cm), high-range water reducing admixture (HRWRA), and fibers. Optimal gradation of the dry constituents improves packing density and contributes to the improved workability and densification of UHPC (Droll, 2004). Additionally, applying pressure and heat curing have been used as pre- and post-setting treatments, respectively, to improve UHPC properties (Richard et al., 1994; Shaheen et al., 2006). In the case of heat treatment, it has been shown to accelerate hydration and the reactivity of SCMs such as silica fume and fly ash (Heinz et al., 2012). Heat treatment also helps densify the microstructure of UHPC and encourages the production of more and longer chains of calcium-silicate-hydrate, further improving mechanical and durability properties (Cwirzen et al., 2008).

Previous research at New Mexico State University (NMSU) has demonstrated that UHPC produced with local materials and SCMs that include both silica fume and fly ash has excellent mechanical and durability properties (Lyell, 2012; Villanueva, 2015). Use of local aggregates and fly ash in UHPC produced at NMSU has decreased cost by nearly 70% compared to prepackaged proprietary UHPC mixtures (Lyell, 2012; Montoya, 2010). Additionally, prepackaged proprietary UHPC mixtures are often shipped long distances making them less attractive from a sustainability perspective.

This project used materials local to New Mexico, USA and high curing temperatures to develop a cost effective UHPC for production of small, high quality modular elements. Initial investigations focused on the compressive and flexural strength of the UHPC, while future work will determine its durability against freezing and thawing exposure.

2. EXPERIMENTAL METHODS

Seven UHPC mixtures were prepared with a variety of materials. The initial mixtures consisted of a Type I/II cement, coarse sand, fly ash, silica fume, 13 mm steel fibers, HRWRA, and water.

2.1 Cementitious Materials and Aggregates

The cementitious materials consisted of Type I/II and V cements, fly ash, and silica fume. Working from a reference mixture that used Type I/II cement, subsequent mixtures were produced by replacing the Type I/II cement with a Type V cement and a coarse sand with a finer sand. Tab. 1 presents the physical and chemical properties of the cements, fly ash, and silica fume. The SCM's were Rheomac SF 100 silica fume from BASF and Class F fly ash from Four Corners Generation Station (Villanueva, 2015). Properties of the sands used in this study are presented in Tab. 2.

Tab. 1: Chemical and physical properties of cement, silica fume, and fly ash.

	Cement Type I/II	Cement Type V	Silica Fume	Fly Ash
Chemical Compounds	Percent by Mass			
SiO ₂	20.3	21.9	96.9	61.8
Al ₂ O ₃	4.6	3.8	0.2	24.5
Fe ₂ O ₃	3.4	3.5	0.2	4.22
CaO	63.9	63.9	0.3	1.45
K ₂ O	0.38	0.53	0.3	1.32
Na ₂ O	0.23	0.22	0.2	1.41
MgO	1.91	2.2	0.2	0.74
SO ₃	2.86	2.1	0.1	0.18
Loss on Ignition	2.24	1.1	2.17	0.36
Insoluble Residue	0.38	0.36	-	-
pH	-	-	7.65	10 - 11
Physical Properties				
Specific Gravity	3.15	3.15	2.24	1.96
Spec. Surface Area (m ² /kg)	335	355	26,810	2,500
Autoclave Expansion (%)	0.05	0.05	-	-0.03
Moisture Content (%)	-	-	0.04	0.09

Tab. 2: Properties of fine and coarse sands.

Sand Type	Fineness Modulus	Specific Gravity	Absorption
Fine	1.82	2.69	1.35%
Coarse	3.14	2.56	2.04%

2.2 Other Materials

The steel fibers used were 13 mm Nycon-SF Type I N (straight fibers) fibers with an aspect ratio of 65, and 25 mm Nycon-SSF Type I HE (Hooked-Ends) fibers with an aspect ratio of 50. The HRWRA was a polycarboxylate-based product from BASF (Glenium 3030 NS).

2.3 Materials Preparation

All of the materials used in the UHPC mixtures were ready to use as purchased with the exception of the sand. The coarse and fine sands were sieved through a No. 4 sieve (4750 μm) then washed over a No. 200 sieve (75 μm) to remove fine particles. The washed sand was then oven dried for 24 hours at a temperature of $110\pm 5^\circ\text{C}$ to remove all moisture. The dried sand was stored in airtight buckets for future use. Tab. 3 shows the grain size distribution of the sands used.

Tab. 3: Grain size distribution of the fine and coarse sands (ASTM standard sieves).

Sieve No. (μm)	4 (4750)	8 (2360)	16 (1180)	30 (600)	50 (300)	100 (150)
Fine Sand % Passing	100	98.4	94.7	82.3	43.9	6.9
Coarse Sand % Passing	96.9	73.0	56.5	40.6	16.2	3.1

2.4 Mixture Proportioning and Mixing Process

The reference UHPC mixture adopted from Villanueva (2015) used the coarse sand. To proportion additional mixtures, the mixture was adjusted for the properties of the fine sand and to accommodate different volumes of steel fibers. The amount of fly ash and silica fume in the mixtures was determined by substituting 20% of the weight of cement with an equal weight of SCM. The 20% SCM content was achieved with a blend of 50% fly ash and 50% silica fume by mass. Tab. 4 presents mixture proportions for the seven UHPC mixtures.

To initiate mixing, the materials were weighed out and placed into a 19 L pan mixer. The constituents were dry mixed until the mixture appeared homogenous (approximately one minute). Once the dry mixture was ready, 75% of the water was added, and mixing continued for five minutes. The HRWRA was then added and the batch was mixed for another five minutes. Next, the remainder of the water was added and the batch was mixed for at least 10 more minutes. Steel fibers were added once the mixture appeared to be smooth and consistent. Mixing continued until the fibers seemed to be uniformly distributed throughout the mixture. This usually took about five minutes. Overall, each UHPC batch took between 25 and 35 minutes to mix completely.

2.5 Preparation of Compression and Flexural Strength Specimens

UHPC specimens produced for compressive and flexural strength tests consisted of 51 mm and 102 mm cubes and 76x102x406 mm prisms. The specimens were prepared by filling the cube molds in three lifts and the prism molds in two lifts. The layers were rodded to insure proper consolidation of the concrete in addition to being vibrated using a vibrating table. The finished specimens were covered with plastic sheets for 24 hours before demolding.

Tab. 4: Mixture proportions for all mixtures.

Materials		Mixture Proportions (kg/m ³)						
		1	2	3	4	5	6	7
Cement	Type I/II	750	750	742	-	-	758	758
	Type V	-	-	-	750	742	-	-
Fly Ash		94	94	93	94	93	95	95
Silica Fume		94	94	93	94	93	95	95
Sand	Coarse	1107	-	-	-	-	-	-
	Fine	-	1107	1107	1107	1107	1107	1107
HRWRA (L/m ³)		42	42	42	42	42	42	42
Water		146	146	145	146	145	147	147
Steel	SF	117	117	156	117	156	78	-
Fibers	H	-	-	-	-	-	-	78

2.6 Curing Regimen

A curing regimen used in previous UHPC research at New Mexico State University (Villanueva, 2015) for precast concrete involved four days of wet curing at 95 °C followed by two days of dry curing at 95 °C (CR0). In addition to CR0, five curing regimens were developed for this project. The first three regimens involved only dry curing for six continuous days at temperatures of 150 °C, 200 °C, and 300 °C. These curing regimens are referred to as CR150D, CR200D, and CR300D. The last two regimens included two days of wet curing at 95 °C followed by four days of dry curing at 200 °C and 250 °C, respectively. These curing regimens are referred to as CR95/200, and CR95/250.

2.7 Testing Procedures (compression and flexure)

For compressive strength testing, the cubes were centered on steel plates that were then centered on the load heads of the testing machine. The specimens were then loaded at a constant stress rate of 62.1 MPa/min.

Prism specimens were tested for flexural strength using a four-point flexural test. The supports were placed 51 mm from each end and the load points were spaced 102 mm apart and centered between the supports as shown in Fig. 1.

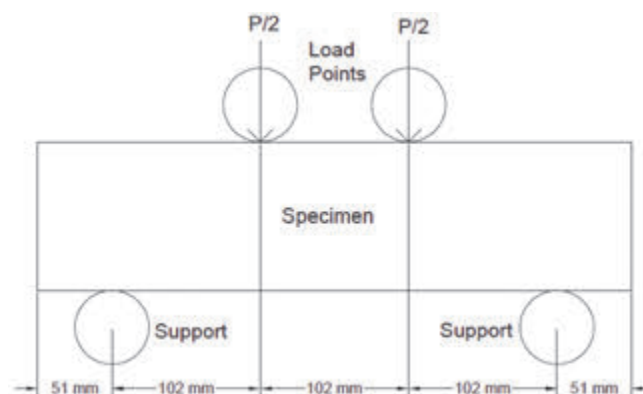


Fig. 1: Four-point flexural strength test schematic.

3. RESULTS AND DISCUSSION

3.1 Compressive Strength

Fig. 2 and Tab. 5 present the compressive strength results for Mixture 1 specimens exposed to CR0 and the dry curing regimens. A 14.9% increase in compressive strength was observed when switching from CR0 to CR150D. Subsequently, there were 15.7% and 4.3% increases in compressive strength from curing using CR150D to CR200D and from curing according to CR200D to CR300D, respectively. The increase in compressive strength is attributed to the accelerated hydration reaction of the SCMs in the UHPC mixtures at the higher temperatures used in the new curing regimens.

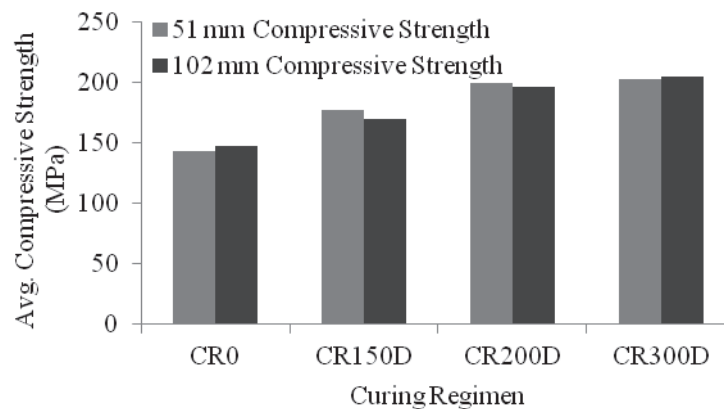


Fig. 2: Average compressive strengths for different curing regimens.

Tab. 5: Average compressive strengths from cube specimens for different curing regimens.

Curing Regimen	Average 51 mm Cube Compressive Strengths, MPa	Average 102 mm Cube Compressive Strengths, MPa
CR0	143.4	148.3
CR150	177.2	170.3
CR200	199.8	197.0
CR300	203.0	205.6

Data from the three dry curing temperatures suggest that dry curing at 300 °C generates the greatest compressive strengths. However, the compressive strength was less than 5% greater than the strength from curing at 200 °C. The additional energy cost for curing at 300 °C likely outweighs the minor strength gain. Therefore, dry curing at 200 °C was selected as the curing temperature for subsequent mixtures.

3.2 Mixture Modification

Another aspect of the investigation focused on incorporating different materials into the UHPC mixtures (Mixtures 2 through 5). Results are presented in Tab. 6 for UHPC mixtures with varying combinations of sand, cement, and volume of steel fibers. The first step in this investigation was to exchange the coarse sand used in the original mixture for a finer sand. Next, a Type V cement was used to study whether the greater C₂S and C₃S contents would provide greater compressive strengths. Each mixture was also produced with two different volumes of steel fibers, 1.5% and 2%, to study the impact that a greater volume of steel fibers had on compressive strength. To accommodate the 2% fiber volume cement, SCM, and water

quantities were decreased while maintaining the w/cm ratio. HRWRA content was held constant with these changes.

Tab. 6: Average compressive strengths for UHPC produced with various combinations of sand, cement type, and volume of steel fibers.

Curing Regimen	Mixture	Avg. Comp. Strength of 51 mm Specimens (MPa)	Avg. Comp. Strength of 102 mm Specimens (MPa)
CR200D	1	199.8	197.0
	2	164.0	201.5
	4	132.3	175.5
	5	146.3	183.2
CR95/200	2	224.8	196.3
	3	226.8	188.1
	4	244.6	206.6
	5	240.9	210.5

Compressive strengths obtained using CR95/200 were compared to a completely dry curing regimen (CR200D). From these results, Type V cement produced lower compressive strengths than Type I/II for the dry curing regimen CR200D but greater compressive strengths than Type I/II cement for CR95/200 that included both wet and dry curing. The decrease in compressive strength using CR200D can be attributed to less hydration occurring when no external water was provided, and shrinkage cracking that may have occurred in the absence of external water. CR95/200 became the standard curing regimen for subsequent mixtures because it showed significant increases in compressive strength for mixtures with Type V cement and had only a small decrease in compressive strength for Type I/II cement mixtures. The data in Tab. 6 also illustrate that a greater volume of steel fibers seemed to have a small influence on compressive strength, providing a 6 MPa increase in compressive strength. This increase is not proportional to the increased cost associated with the increased fiber content. Therefore, future mixtures were all produced with 1.5% steel fiber content by volume.

Previous research (Shaheen et al., 2006) suggested that a curing temperature between 200°C and 300°C proved to be optimal for improving SCM reactivity and densification of UHPC mixtures. Consequently, CR95/250 was developed. Cube specimens were cured using this regimen and the compressive strength results are presented in Tab. 7. This curing regimen showed a significant increase in compressive strength (9.2%) compared to CR95/200 when using Type I/II cement and 1.5% volume of steel fibers (Mixture 2).

Tab. 7: Compressive strength of 51 and 102 mm cubes cured using CR95/250.

Curing Regimen	Specimen, mm	Average Compressive Strength, MPa
CR95/250	51	244.4
	102	205.4

3.3 Flexural Strength

In regards to flexural strength, the investigation concentrated on the effects that fiber content and type had on the flexural strength of UHPC produced using CR95/200. The UHPC mixture that

was investigated consisted of fine sand, Type I/II cement, and a variety of steel fiber volumes and types (Mixtures 1 through 7). Fig. 3 and Tab. 8 illustrate the average flexural strengths of the UHPC mixtures prepared in this work. Four different prism sets were tested that differed in the volume of fibers used and fiber type. Three sets included 1%, 1.5%, and 2% volume of straight fibers (SF) and one set was produced with 1% volume of hooked-end fibers (H).

Tab. 8: Average flexural strength of prisms cured using CR95/200 and CR95/250.

Fiber Volume	Fiber Type	Sand Type	Cement Type	Curing Regimen	Average Flexural Strength, MPa
1.5%	SF	Coarse	I/II	CR0	8.54
1%	SF	Fine	I/II	CR95/200	8.94
1.5%	SF	Fine	I/II	CR95/200	11.08
2%	SF	Fine	I/II	CR95/200	15.32
1%	H	Fine	I/II	CR95/200	10.46
1.5%	SF	Fine	I/II	CR95/250	13.23

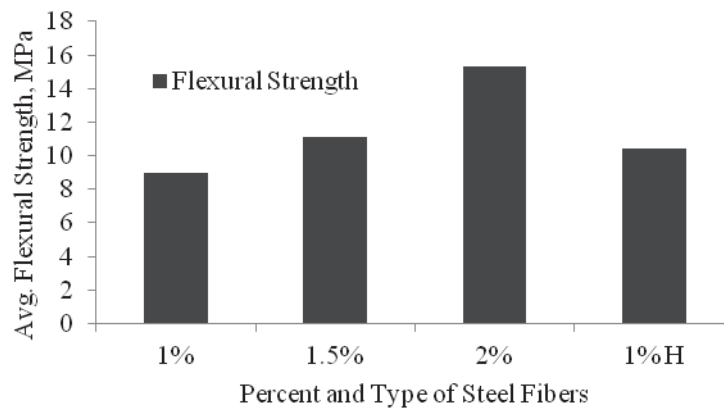


Fig. 3: Average flexural strength of prisms curing using CR95/200 and CR95/250.

Fig. 3 shows that the straight fibers showed an increase in flexural strength with increased fiber volume. However, Tab. 8 indicates that average flexural strengths for CR0 were 8.54 MPa using 1.5% volume of straight fibers (Villanueva, 2015) which is less than the flexural strength achieved using 1% volume of straight fibers and CR95/200 (8.94 MPa). This is attributed to the more complete hydration that is apparent from the improved compressive strengths of CR95/200 specimens.

Mixtures produced with 1% hooked-ends fibers by volume yielded greater average flexural strength than mixtures using straight fibers at the same concentration. There was a 17% increase in flexural strength associated with the hooked end fibers. The volume of H fibers was limited to 1% because workability appeared limited and consolidation required substantial vibration and rodding. Additionally, Mixture 7 seemed to be on the verge of fiber clumping, which would have led to an uneven distribution of the H fibers.

Tab. 8 also illustrates the effect CR95/250 had on the flexural strength. Compared to the mixture with 1.5% volume of steel fibers cured according to CR95/200, CR95/250 produced a 19.4% increase in flexural strength.

4. CONCLUSIONS AND FUTURE WORK

Based on the results of this study, the following conclusions are drawn:

- Mechanical properties of locally produced UHPC were significantly improved using elevated temperature curing regimens. This was especially evident using CR95/200 and CR95/250 which increased compressive strengths by 32.4% and 38.5%, respectively.
- CR95/200 and CR95/250 also improved flexural strengths by 29.7% and 54.9%, respectively, using 1.5% SF by volume.
- The effect of various materials on UHPC's mechanical properties illustrated that switching from the coarse sand to the fine sand, and from the Type I/II cement to Type V cement improved compressive strengths by 35.9% and 39.3%, respectively.

This work is continuing in an effort to determine if small, modular UHPC units cured using CR95/200 can be used as cladding to improve the frost resistance of normal strength concrete elements.

5. REFERENCES

- Cwirzen, A., Habemehl-Cwirzen, K., & Pentala, V. (2008). "*The effect of heat treatment on the salt freeze-thaw durability of UHSC*". Second International Symposium on Ultra High Performance Concrete, pp. 221 - 230.
- Droll, K. (2004). "*Influence of additions on ultra high performance concretes – grain size optimisation*". First International Symposium on Ultra High Performance Concrete, pp. 285 - 301.
- Heinz, D., Urbonas, L., & Gerlicher, T. (2012). "*Effect of Heat Treatment Method on the Properties of UHPC*". Third International Symposium on UHPC and Nanotechnology for High Performance Construction Materials, pp. 283 - 290.
- Lyell, E. (2012). "*Optimization of Ultra High Performance Concrete Mixture Proportions using Locally Available Materials*". New Mexico State University.
- Magureanu, C., Sosa, I., Negrutiu, C., & Heghes, B. (2012). "Mechanical Properties and Durability of Ultra-High-Performance Concrete". *ACI Materials Journal*, pp. 177 - 183.
- Montoya, K. F. (2010). "*Feasibility of Using Ultra High Performance Concrete in New Mexico Bridge Girders*". New Mexico State University.
- Richard, P., & Cheyrezy, M. H. (1994). "Reactive Powder Concrete with High Ductility and 200-800 Mpa Compressive Strength". *Concrete Technology Past, Present, and Future*, pp. 507 - 518.
- Shaheen, E., & Shrive, N. G. (2006). "Optimization of Mechanical Properties and Durability of Reactive Powder Concrete". *ACI Materials Journal*, pp. 444 - 451.
- Villanueva, J. M. (2015). "*Mixture Proportioning and Freezing and Thawing Durability of Ultra High Performance Concrete Using Local Materials*". New Mexico State University.

MATERIAL PROPERTIES STUDY OF SEVEN 100-YEARS OLD CONCRETE BRIDGES IN SLOVAKIA

Peter Paulík¹, Michal Bačuvčík², Katarína Gajdošová¹, Jaroslav Halvoník¹

*¹ Faculty of Civil Engineering, Slovak University of Technology in Bratislava
Radlinského 11, 810 05 Bratislava, Slovakia*

*² Building Testing and Research Institute
Studená 3, 821 04 Bratislava*

SUMMARY

The first major application of concrete in bridge construction at the territory of Slovakia was within the construction of former Franz Joseph Bridge across the Danube River in Bratislava in 1890. The oldest reinforced concrete bridge in Slovakia was built 2 years later, in 1892, in Krásno nad Kysucou. There are many other concrete bridges in daily use in Slovakia, which are already more than 100-years old, even though their real load bearing capacity is unknown. Our research of the oldest concrete bridges in Slovakia, was focused on the material properties of concretes and reinforcements used in bridge construction 100 years ago. Our paper concerns the mechanical properties of concretes measured on drilled core specimens from seven bridges in Slovakia as well as some non-destructive measurement results and mechanical properties of reinforcements. Correlation between mechanical properties of these old concretes, their porosity and results of non-destructive measurements are reported.

1. INTRODUCTION

Research was focused primarily at the oldest reinforced concrete bridges in Slovakia, which are almost 100 years old or older. Many of these bridges are still in service, even though no drawings or information about their structure have been preserved and no relevant standards existed at the time of their construction. For the proper evaluation of their load bearing capacity and their remaining service life it is necessary to know the material properties of their structural materials, as well as the type and progress of their deterioration. Then, if necessary, they have to be reconstructed and strengthened by an appropriate method, such as FRP reinforcement or external prestressing. Thus, for strengthening purposes, especially with FRP reinforcement, it is necessary to know the properties of concrete in the cover zone, which in reality could significantly differ from the properties of the inner concrete (Čech, 2017). By this means, it is questionable if we can correctly correlate the non-destructive measurements of material properties provided at concrete surface with material properties measured on drilled core specimens. As our results show, correlations given in modern standards between non-destructive measurements provided on the cover zone and measurements on drilled core specimens could be misleading when applied to these old concretes.

Our results of the research should also provide at least some general information about the mechanical properties of concretes and reinforcements used in the construction of bridges at the very beginning of applications of concrete in bridge construction in Slovakia. Results show also the uncertainties of the non-destructive methods, when they are used for evaluating the overall material properties of these concretes.

To select representative bridges, we tried to choose those, which are likely to be reconstructed in near future. Results could also serve as a rough estimate of expected material properties of other similar bridges from this construction period. As it turned out, many assumptions made by the designers in Slovakia, when they dealt with the oldest concrete bridges, were quite far from reality. Also many mechanical properties of concretes derived from non-destructive tests only, within various reconstruction projects, were very misleading. However, despite a large scatter of results, some correlation between different material properties and measurement techniques were observed.

The following bridge structures, were selected for detailed research:

- concrete piers of the old bridge in Bratislava (BA), age of the structure: 125 years
- reinforced concrete bridge in Krásno nad Kysucou (KnK), age of the structure: 122 years
- reinforced concrete bridge in Hlohovec (HC), age of the structure: 104 years
- reinforced concrete bridge in Ruzomberok (RK), age of the structure: 102 years
- bridge truss girder from Hungary, near Slovak borders (NY), age of the structure: 100 years
- reinforced concrete bridge in Nižná Myšľa (NM), age is unknown, but more than 96 years
- reinforced concrete bridge in Sládkovičovo (SL), age is unknown, but more than 96 years

Further information about the bridges could be found in book *Bridges in Slovakia* (Paulik, 2014) and some basic information about production and properties of old concretes could be found in book “*Beton és vasbeton I.*” (Balázs, 1994).

2. RESEARCH METHODOLOGY

The overall diagnosis of the old bridges was divided into two main phases. The first phase consisted of in situ diagnostics performed by a team of experts from Slovak University of Technology (STU) and Building and Testing Research Institute (TSÚS). In-situ diagnostics methodology comprised of the following procedures: locating the steel reinforcement and measurement of its cover, non-destructive determination of the concrete strength by Schmidt rebound hammer, ultrasonic measurement of the dynamic modulus of elasticity, pull-off tests and permeability test by the Torrent permeability device.

Concrete core samples of a nominal diameter of 100 mm and steel reinforcement samples were taken from the bridge structures. Immediately after the concrete cores were drilled out the depth of carbonation was measured by the phenolphthalein test.

The second phase consisted of laboratory tests on drilled cores. We have measured the mechanical properties (dynamic and static modulus of elasticity, compressive strength), the mineralogical phase and chemical composition of the concrete (XRD, TG-DTA, SEM/EDS) and the pore size distribution (by mercury intrusion porosimetry - MIP).

The present state of concrete was assessed on the above-mentioned set of obtained results. However, due to the limited length of the article, only some selected data are published here.

3. SELECTED RESULTS OF MEASUREMENTS

The results of the mechanical properties of concrete and reinforcement measured on samples taken from almost 100 years old or older bridge structures are summarized in Tab. 1 and Tab. 2. Compressive strength measured on drilled core specimens has been evaluated by taking into account the slenderness of the specimen in accordance with ČSN 73 1317. Also

the compressive strength measured by Schmidt rebound hammer has been evaluated and recalculated to cylinder strength in accordance with ČSN 73 1373.

Tab. 1: Selected mechanical properties of steel reinforcements

Bridge	Sample	Yield strength [MPa]	Ultimate strength [MPa]
BA	-	-	-
KnK	K1	321	378
	K2	330	389
	K3	363	416
HC	-	-	-
RK	R1	304	364
	R2	296	359
NY (HU)	NY1	238	349
	NY2	236	333
NM	N1	292	315
	N2	299	361
SL	-	-	-

Tab. 2: Average mechanical properties and porosity of concretes

Bridge	Location of the sample within the bridge	Average compressive strength measured on drilled core specimens	Average compressive strength measured by Schmidt rebound hammer.	Average tensile strength of the cover zone	Porosity
		(MPa)	(MPa)	(MPa)	(%)
BA	Above the caisson	18	-	-	25,1
	Caisson	3,7	-	-	39,2
	Pier	12	-	-	-
KnK	Arch and arch overfill	23,1	26,7	2,1	21,8
	Parapet	20,5	16,9	1,1	26,6
HC	Superstructure	6,5	24,9	1,2	22,1
	Abutment	36,4	44,1	-	-
	Pier	17,2	16,9	0,8	24,7
RK	Abutment	15,7	-	-	23,3
	Superstructure	32,5	30,6	1,2	19,3
NY	Girder	17,0	56,3	4,3	16,0
NM	Abutment	11,9	-	-	-
	Superstructure	16,6	33,2	3,2	19,8
SL	Abutment	22,9	16,7	0,8	27,0

4. DISCUSSION

Based on the research results, a high variability of strengths and modulus of elasticity could be seen, not only between various bridges, but also often within a single structural element of the same bridge. The large scattering of material properties we attribute primarily to insufficient compaction of concrete during its pouring, to which only a limited attention was paid at that time (first internal vibration compaction was used in 1932 (Menn, 1986)).

The results, plotted in the graph in Fig. 1, show, that even through there is some relation between the minimum measured modulus of elasticity and the compressive strength of the concrete, there is a relatively large scatter. From X-ray analysis of the concrete we have found that all concretes were made of quartzite aggregates and thus the scatter could probably not be caused by different types of aggregates.

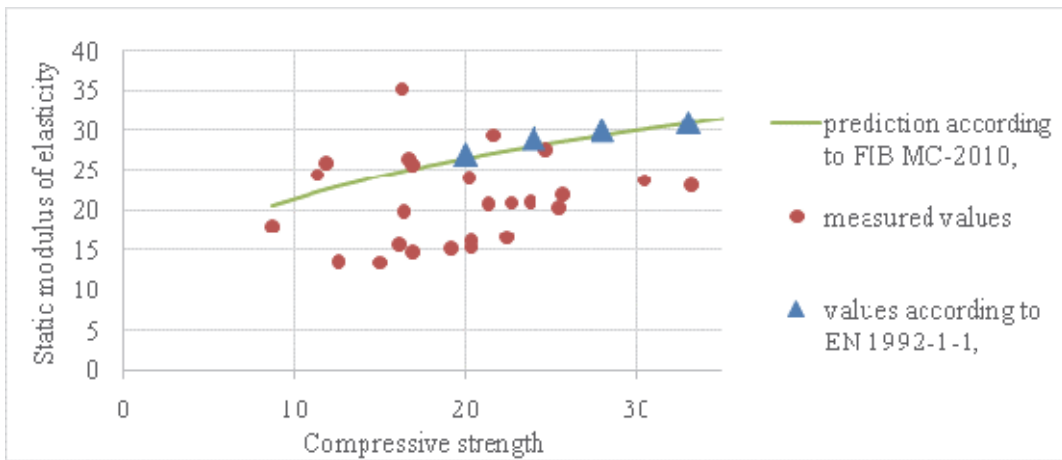


Fig. 1: Correlation between the compressive strength and static modulus of elasticity

On graph in Fig. 2 a certain correlation between the dynamic and static modulus of elasticity could be observed, but once again we could not talk about some strong relationship.

Thus when dealing with more than 100 years old bridges we propose to measure not only the compressive strength of concrete, but also the modulus of elasticity and not to rely on current standards and documents for their conversion.

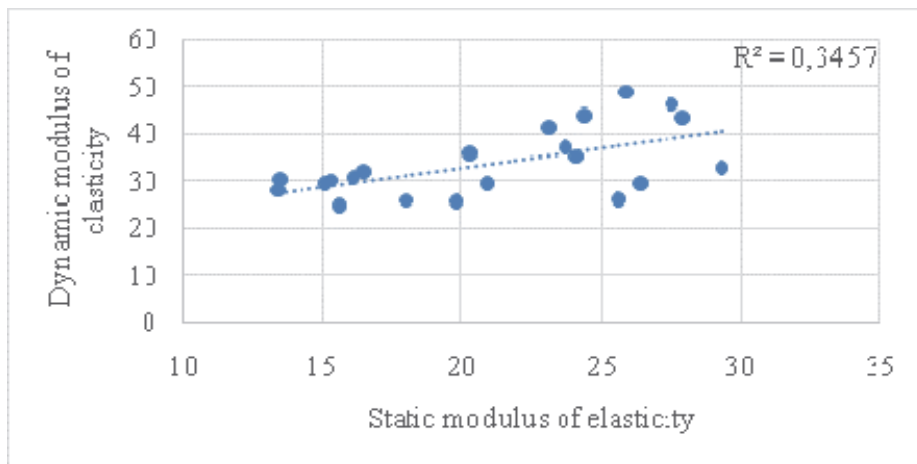


Fig. 2: Correlation between the measured static modulus of elasticity and dynamic modulus of elasticity

Graph in Fig. 3 shows the correlation between the compressive strengths measured by Schmidt rebound hammer and compressive strength measured on drilled core specimens is showed, together with an ideal line representing the theoretical perfect match between the two compressive strength measurement methods.

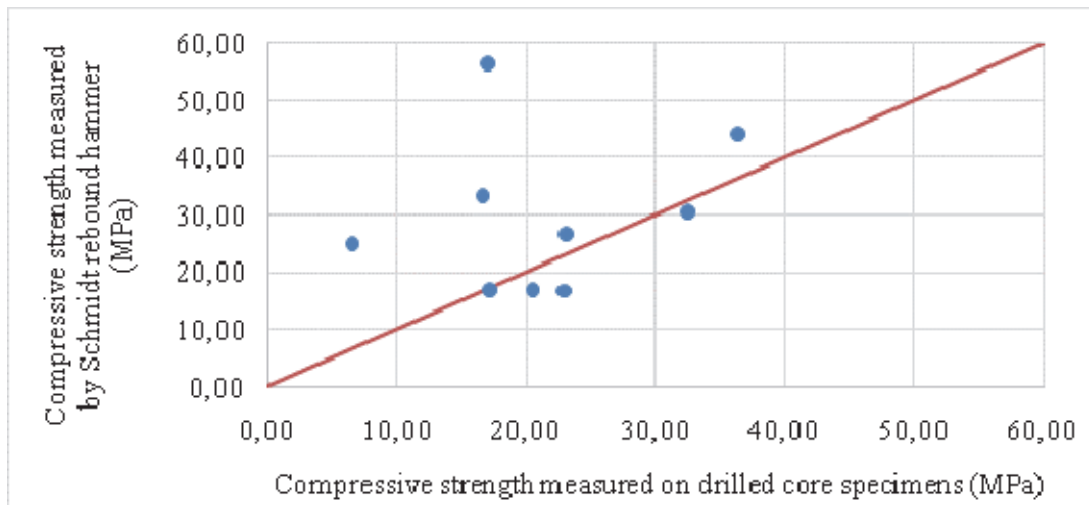


Fig. 3: Correlation between the compressive strengths measured by Schmidt rebound hammer and compressive strength measured on drilled core specimens

Graphs in Fig. 4 and 5 show the correlation between porosity and concrete strength measurements performed on cover zone.

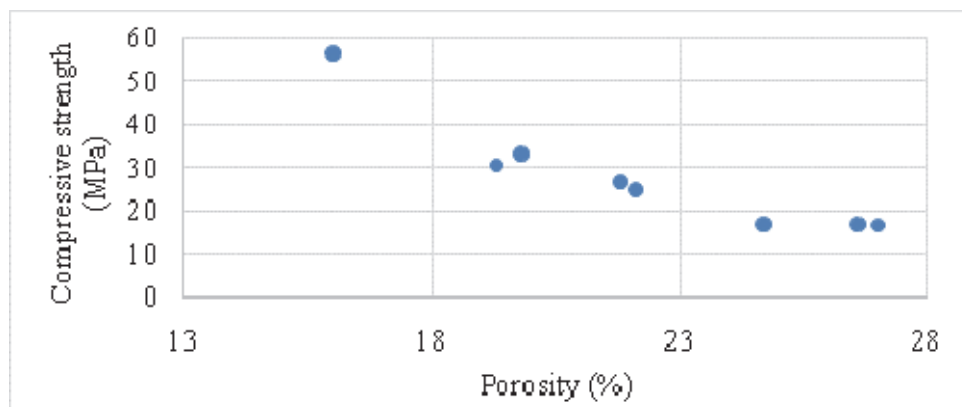


Fig. 4: Correlation between the porosity of the cover zone and compressive strength measured by Schmidt rebound hammer

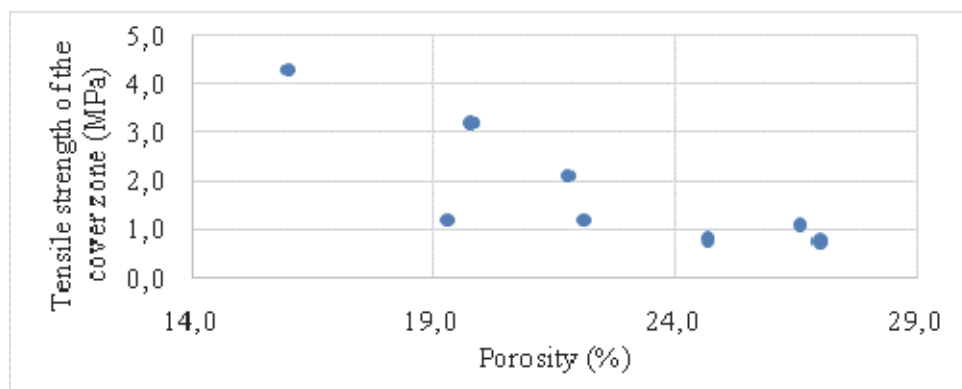


Fig. 5: Correlation between the porosity and tensile strength of the cover zone

5. CONCLUSIONS

From the results of our experimental investigation performed on seven concrete bridges that are almost 100 years old or older, it is possible to formulate the following conclusions:

- 1) The values of compressive strengths and modulus of elasticity shows, that the vast majority of surveyed concretes do not meet the criteria for classification even to the lowest strength class C 12/15 according to EN 1992-1-1.
- 2) Modulus of elasticity had a relatively large scatter, and mostly the real values are much smaller than values derived from compressive strengths according to relevant documents (EN 1992-1-1 and FIB Model Code for Concrete Structures 2010). Overall, there is a great variability in the measured mechanical properties even within a single bridge element. This fact could be attributed to a poor compaction of the concrete during construction, to which only a limited attention was paid at the beginning of 20th century.
- 3) From the measured mechanical properties of reinforcement, it could be stated that the real yield strength of steel reinforcement used for the construction of bridges in Slovakia at the beginning of 20th century was at most cases approximately 30% higher than what was believed and given in most of recommendations and technical papers. Taking into account the real properties of the reinforcement it is possible in many cases to increase the maximum allowed load on the bridge or to reduce the scale of the planned reconstruction.
- 4) Determination of compressive strength of concrete by Schmidt rebound hammer was found to be unreliable for these concretes, since in some cases the results indicated much higher strength than was the real strength measured on concrete core samples.
- 5) Most of the investigated old concrete bridges do not meet strength requirements at concrete surface for strengthening with FRP reinforcement.
- 6) Strong correlation was observed between porosity of surface layers and non-destructive strength measurements. This was in contrast to almost no-correlation between porosity of surface layers and strength measurements on concrete core samples. This result indirectly indicates different properties of concrete in the surface zone when compared to the properties of the inner concrete. Thus, if strengthening with FRP reinforcement is considered to be applied to these old concrete bridges, the required strength values should be always measured by an appropriate method at the surface of concrete element and not derived from results measured on drilled cores only.

6. ACKNOWLEDGEMENTS

This work was supported by the Slovak Research and Development Agency under the contract No. APVV-15-0658 and the University Science Park (USP) of the Slovak University of Technology in Bratislava (ITMS: 26240220084).

7. REFERENCES

- Balázs, G., (1994) “Beton és vasbeton I. – alapismeretek történelme” (en.: Concrete and reinforced concrete I. – History of basic knowledge), Akadémiai Kiadó, Budapest, Hungary, 1994, ISBN 9630567547
- Čech, J., Tej, P., Kolísko, J., Král, J. (2017), “Structural condition assessment of the bridge in Ostrava”, in: Dynamics of Civil Engineering and Transport Structures and Wind Engineering – DYN-WIND’2017, MATEC Web Conf., Vol. 107, 2017
- ČSN 73 1373 (1981): Tvrdoměrné metody zkoušení betonu (en: hardness methods of concrete testing), 1981
- ČSN 73 1317 (1986): Stanovení pevnosti betonu v tlaku (en: evaluation of concrete compressive strength), 1986
- EN 1992-1-1: Design of concrete structures, 2015
- FIB Model Code for Concrete Structures 2010 (2013), Lausanne, Switzerland, 2013
- Menn, C. (1986), “Prestressed Concrete Bridges”, Wien, Austria, 1986, ISBN 9783-7643-2414-7
- Paulík, P. (2014), “Bridges in Slovakia”, Bratislava, Slovakia, 2014, ISBN 978-80-8076-111-0

COMPARISON OF MODULES OF ELASTICITY AND MECHANICAL PROPERTIES OF DIFFERENT CONCRETE TYPES

Vlastimil Bílek^{1,2}, David Pytlík¹, Markéta Bambuchová¹, Sabina Bonczková¹

¹ *VSB - Technical University of Ostrava, L.Podeste 1875/17*

708 33 Ostrava-Poruba, Czech Republic

² *ZPSV a.s., Trebizskeho 207, 687 24 Uherský Ostroh, Czech Republic*

SUMMARY

The topic of this paper is a comparison of the mechanical properties and, in particular, the module of elasticity of concretes based on ordinary portland cement, alkali-activated concrete and concrete based on alkali activated hybrid cement. The latter two types of concretes represent environmentally friendly alternatives of concrete. All these concretes were prepared with a high content of binder and with a low volume of binder. All of these options were also prepared with steel fibres. One of the most frequently discussed mechanical properties is the modulus of elasticity. The values of the modulus of elasticity are discussed with respect to compressive strengths. The influence of the testing procedure – static compression test and three-point bending of notched beams (during fracture tests) – are discussed too.

1. INTRODUCTION

The modulus of elasticity is one of the basic mechanical characteristics of concrete. In general, there is an effort to derive its value from compressive strength, but it appears that this way is not very precise. The reason is different properties of cement composite components - binders and fillers. They play a more significant role in the case of the modulus of elasticity than in measuring the compressive strength, (Cikrle and Bílek, 2010). Already the binder composition itself affects the modulus of elasticity. Various mixtures can be added to Portland cement - for example, microsilica, metakaolin, slag etc. These admixtures influence the composition and abundance of the resulting hydration products as well as the microstructure of the boundary between hardened cement paste and aggregate (Cikrle and Bílek 2010, Kursá and Latif, 2009, Elshafie et al. 2016). However, there are also alternative binders that do not contain Portland cement or only minimal. These include, in addition to a number of others, alkaline activated concretes, or concretes with hybrid cements, whose research has been given much attention both around the world and also in the Czech Republic (Bílek, 2016, Provis and van Deventer 2014). If these concretes are to be usable in practice, we need to know their modules of elasticity. This work brings a little contribution to this issue.

2. EXPERIMENTAL DETAILS

2.1 Materials

CEM I 42.5 R Hranice was used as a cement; the slag was a finely ground blast furnace slag Kotouč Štramberk with a specific surface area above 420 m²/kg. In addition, sodium water glass with a silicate module $M_s \approx 2$ and a dry matter content of 48.5% was used. Na₂CO₃ was used to activate hybrid cement. Besides, drinking water and commonly used aggregates were used - sand Tovačov 0/4 and crushed aggregates 4/8 and 8/16.

12 formulas were designed for three main types of concrete. The first type of concrete was alkali-activated concrete whose binder was a finely ground blast furnace slag. The second type was concrete with traditional Portland cement. The third type of concrete contained as a binder a hybrid cement consisting of 90% blast furnace slag and 10% Portland cement. Each of these three types of concrete was made with a high binder content and a low binder content, mainly due to the study of cohesion of concretes with reinforcement, which is discussed in (Bilek *et al.*, 2017). Concretes containing a high proportion of cement binder were mixed again with the addition of structural synthetic fibres and steel wires. The formulas themselves are shown in Tab. 1.

Tab. 1: Composition of prepared concretes

Raw materials kg/m ³	A1	B1	C1	A2	B2	C2	A3	B3	C3	A4	B4	C4
Slag	308	-	227	450	-	405	450	-	405	450	-	405
CEM I 42.5R	-	308	31	-	450	45	-	450	45	-	450	45
Na VS 2.0	31	-	-	45	-	-	45	-	-	45	-	-
50% KOH	23	-	-	34	-	-	34	-	-	34	-	-
Water	139	169	168	152	180	195	152	180	195	152	180	195
Chrysoplast 760	3.5	3.5	6.7	10	3.5	8	10	3.5	8	10	3.5	8
Aggregates 0/4	645	645	645	855	910	860	855	910	860	855	910	860
Aggregates 4/8	225	225	225	385	410	390	385	410	390	385	410	390
Aggregates 8/16	990	990	990	400	425	405	400	425	405	400	425	405
Na ₂ CO ₃	-	-	21.5	-	-	31.5	-	-	31.5	-	-	31.5
Fibres*	-	-	-	-	-	-	8	8	8	-	-	-
Wires**	-	-	-	-	-	-	-	-	-	40	40	40

*Chryso Fibre S25

**Dramix OL13/20

A – alkali-activated concrete

B – concrete with Portland cement

C – concrete with hybrid cement

1 – low binder content

2 – high binder content

3 – low content of binder, wires

4 – high content of binder, wires

2.2 Experimental procedures

Concrete prisms 100x100x400 mm were prepared for measuring the static compressive modulus as well as prisms 80x80x480 mm for measuring fracture properties by effective crack model (Karihaloo and Nallathambi 1989). Prior to the test, notches were cut in the prisms at a height of 1/3. In addition to fracture properties - fracture toughness K_{IC} and fracture work W_F , is the outcome of the test also the modulus of elasticity in the three-point bend on the beam with notch E_K . The static modulus of elasticity E_C was tested on prisms 100x100x400 mm in accordance with (CSN ISO 1920-10, 2016). Compressive strength was determined using cubes 150 mm according to (CSN EN 12 390-3, 2009).

3. DISCUSSION

3.1 Dependence of the static modulus of compressive elasticity on the compressive strength

The average values of the static modulus of elasticity E_C and the values of the prismatic compressive strength are shown in Tab. 2. These values are also graphically depicted in Fig. 1.

Tab. 2: Values of modules of elasticity and compressive strength

Marking of plain concrete	A1	B1	C1	A2	B2	C2
$f_{c,prism}$ [MPa]	44.9	29.8	26.3	64.8	37.5	23.1
E_c [GPa]	30.5	28.1	28.4	30.2	27.8	24.1
Marking of fibreconcrete	A3	B3	C3	A4	B4	C4
$f_{c,prism}$ [MPa]	51.6	43.9	23.7	63.1	50.6	34.3
E_c [GPa]	26.0	30.1	23.9	29.9	31.0	28.6

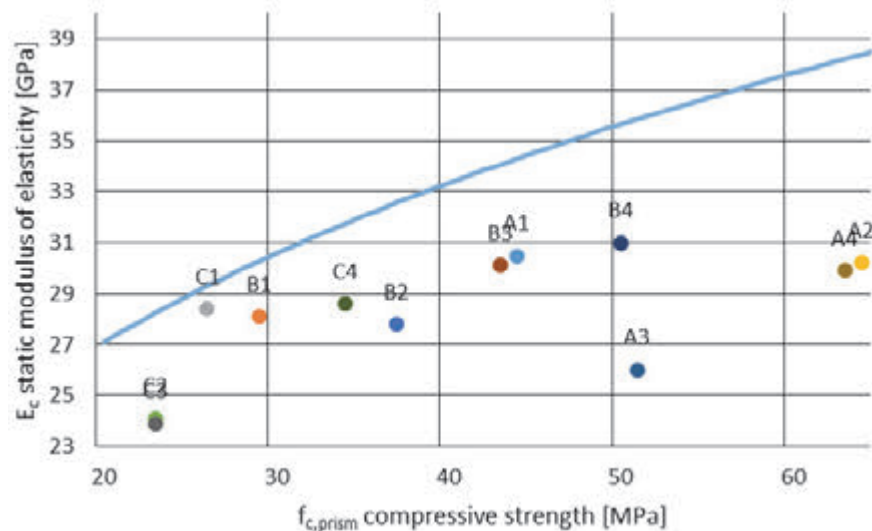


Fig. 1: Modulus of elasticity in compression for different types of concrete (The curve represents the dependence of the modulus of elasticity on compressive strength according to CSN EN 1992-1-1 Eurocode 2, 2006)

The values of the modulus of elasticity for concrete with Portland cement (B1 - B4) essentially copy the course of the theoretical curve *CSN EN 1992-1-1 Eurocode 2* (2006). They are only distributed under this curve, the reasons are discussed, for example, in (Cikrle and Bílek, 2010). Alkali - activated concretes (A1 up to A4) show a different tendency. Elasticity modules with increasing strength values show a decrease. This phenomenon can be explained by the low modulus of elasticity of the matrix - the alkali activated paste - which is probably mainly influenced by higher volume changes and higher microcracking. In the case of concrete with a low content of binder, a larger volume is occupied by aggregates which have a higher modulus of elasticity, and thus the modulus of elasticity of the composite is even higher, although the compressive strength is lower than in the case of high binder concrete. In the case of fibre addition, there was apparently no good cohesion between the fibres and the matrix, and the modulus of elasticity and strength decreased. With steel, however, alkali-activated concrete has excellent cohesion and thus, even the modulus of elasticity reaches similar values as for non-wired concrete.

Higher strengths have not yet been achieved with hybrid cements, the maximum is between 30 MPa and 40 MPa. Interestingly, the strength of concrete with a higher proportion of binder is lower than that of concrete with a higher proportion. The explanation may again be the low strength of the binder. The composition of the binder must be optimized for this type of concrete.

3.2 Dependence of the static modulus of compressive elasticity on the modulus of elasticity during the fracture test

The measured values of static elastic modulus in compression and elastic modulus from the fracture test are shown in Tab. 3 and graphically depicted in the graph in Fig. 2.

Tab. 3: Modules of elasticity in compression E_C and in the test of fracture properties E_K

plain concrete	A1	B1	C1	A2	B2	C2
E_K in t. K_{Ic} [GPa]	29.4	29.9	29.4	29.5	30.9	23.5
E_c [GPa]	30.5	28.1	28.4	30.2	27.8	24.1
fibre-concrete	A3	B3	C3	A4	B4	C4
E_K in t. K_{Ic} [GPa]	25.6	36.1	26.7	27.7	33.4	35.4
E_c [GPa]	26.0	30.1	23.9	29.9	31.0	28.6

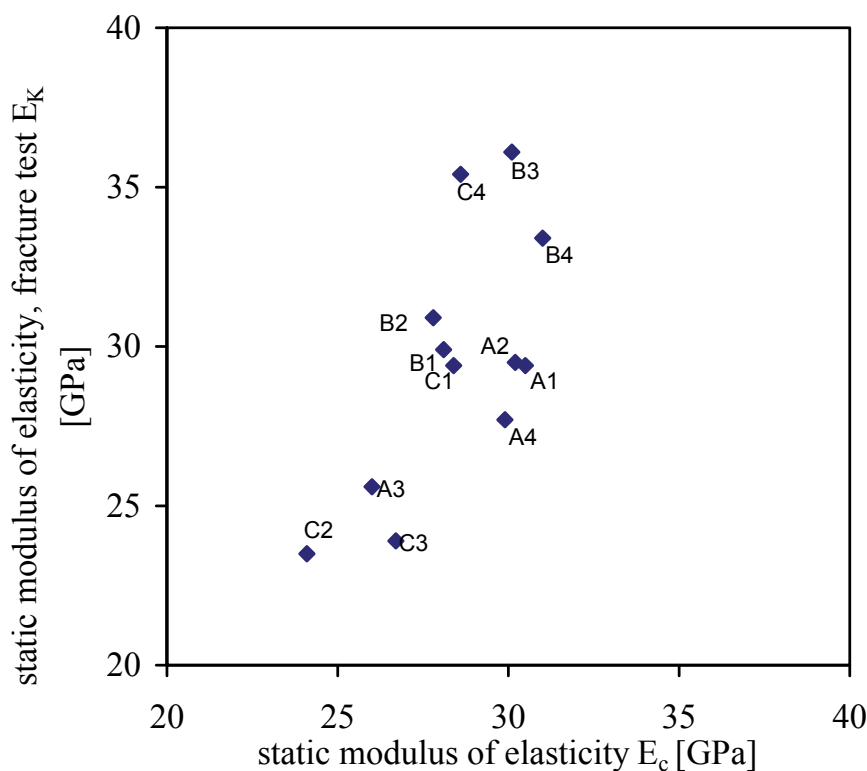


Fig. 2: Comparison of modules of elasticity E_K and E_C

When determining the modulus of elasticity in both ways, the values were similar, especially for lower values. For higher values of the modulus of elasticity, in the case of notched beams, higher values than the static modulus of compressive elasticity are obtained. It is not evident from Figure 2 that any of the types of concrete significantly deviated from this trend. However, more values would be needed for a more objective discussion.

4. CONCLUSION

In this work, the values of static modulus of compressive elasticity on prisms and on the three-point bending on notched prisms were compared for different types of concrete. It can be said that the values of the compressive elastic modulus for Portland cement based concrete correspond to the modulus which are specified by Eurocode 2 for the given compressive strengths.

Alkaline activated concrete and concrete based on hybrid cements behave differently, in their cases the modulus of elasticity sometimes even decreases. This property can be explained by different matrix properties whose modulus of elasticity is probably considerably lower than the modulus of elasticity of hardened cement paste from Portland cement. In the case of concrete with Portland cement, an increase in the modulus of elasticity has occurred due to the addition of fibres, in the other cases the modules are probably influenced by matrix properties and cohesion with fibres.

When measuring the modulus of elasticity on beams with a notch in the three-point bend, higher values are usually achieved than in a test of the modulus of elasticity in pressure.

5. ACKNOWLEDGEMENTS

This work was supported by the project SGS SP2017 / 84, Faculty of Civil Engineering, VŠB-TU Ostrava.

6. REFERENCES

- Bílek, V. (2016) "Development of alkali activated concrete for practical application", habilitation work, Faculty of Civil Engineering, VSB-TU Ostrava (2016)
- Bílek, V., Bonczková S., Hurta, J., Pytlík, D., Mrovec, M. (2017) "Bond Strength Between Reinforcing Steel and Different Types of Concrete", *Procedia engineering*, 190, 243 – 247
- Cikrle, P., Bílek, V. (2010) "Modulus of elasticity of high strength concretes of different composition (Modul pružnosti vysokopevných betonů různého složení), *BETON TKS*, No.5, s. 40-45 (in Czech)
- CSN EN 12 390-3 (2009) Testing of hardened concrete - Part 3: Compressive strength
- CSN EN 1992-1-1 Eurokód 2(2006) Design of concrete structures - Part 1-1: General regulation and regulation for buildings
- CSN ISO 1920-10 (2016) Testing of concrete - Part 10: Testing of static modulus of elasticity in compression
- Elshafie, S., Boulbibane, M., Whittleston, G.(2016) "Influence of mineral admixtures on the mechanical properties of fresh and hardened concrete", *Construction Science*, December 2016, Vol. 19, 4-12, ISSN 2255-8551
- Karihaloo, B.L., Nallathambi, P.(1989) An improved effective crack model for determination of fracture toughness of concrete. *Cem. Concr. Res.*, 19, 603-610
- Kursat, Y., Latif, O.U. (2009) "The effect of mineral admixture type on the modulus of elasticity of high strength concrete", *Scientific Research and Essay*, Vol.4 (8) August 2009, pp. 791-798
- Provis, J.L., van Deventer, J.S.J. (2014), *Alkali-Activated Materials*, RILEM State-of-the-art-reports TC 224 AAM, RILEM, ISBN 978-94-007-7671-5, 379 p.

VALUE-ADDED RECYCLING AND REUSE OF WASTE CONCRETE ON A CONSTRUCTION SITE

Yupeng Yang

The fifth Engineering Co., Ltd., China Railway 16th Bureau Group

Guanghua Road 2, 064000 Tangshan, Hebei, China

SUMMARY

During the construction of high speed rail from Wuzhong to Yinchuan in China, a huge amount of concrete wastes was generated. Driven by the saving of transportation cost and environment protection, it is proposed to recycle and reuse of the concrete wastes. This paper examines the economical and technical feasibility of this proposal considering the actual conditions on the construction site. A simplified economic analysis is firstly performed. It is found that the high transportation cost makes the recycling and reuse concrete wastes economical viable. Then, the concrete wastes were crushed in a plant, which produces natural coarse aggregates. Laboratory tests on the properties of the RCAs have been carried out. It is found that that the physical and mechanical properties of the RCAs can meet the requirements in various standards. Intensive research work on the use of the RCAs is currently ongoing.

1. ENGINEERING BACKGROUND

A large number of high speed rail projects are currently ongoing in China. The rail between Wuzhong and Yinchuan, which has a length of 39.6 km, belongs to a part of the Yinchuan-Xi'an high speed rail. The total budget is about 212 million Euros and this project is planned to be completed to the end of 2018. During the construction work, a huge amount of concrete waste has been produced. More and more waste concrete will be further generated. These concrete wastes are mainly resulted from the following sources:

- The cut (removal) of the heads of plain concrete drilled piles. In this project, a lot of plain concrete piles are used as deep foundations. The strength class of the pile concrete is mainly C16/20.
- The demolition of many concrete and reinforced concrete structures and infrastructures. Fig. 1(a) presents a reinforced concrete bridge near the Yinchuan International Airport, which will be demolished soon. This bridge is still at a relatively young age and the strength class of the bridge concrete is C40/50.
- Laboratory – cast concrete specimens. Owing to the high requirements on the quality of the rail concrete, numerous specimens were cast in the laboratory to ensure the quality of the concrete. Fig. 1(b) shows some concrete cubes and prisms after mechanical or durability tests. In addition, there are also some rejected structural precast elements, which accounts for a relatively small part of the concrete wastes.



(a) A concrete bridge to be demolished



(b) Laboratory –cast concrete specimens after tests

Fig.1: some sources for generating concrete wastes on the construction site

2. IDEA TO RECYCLE CONCRETE WASTES AND SOME CHALLENGES

The idea to recycle and reuse the concrete wastes on the construction site of this project is put forward mainly driven by the incentives to reduce the cost for the disposal of the concrete wastes and to decrease the environmental impact.

At present, landfilling of construction and demolition wastes in China is still allowed, unlike in some European countries such as Belgium, the Nederland and the UK. Therefore, the principal cost for disposing the concrete wastes is the transportation cost. To check the economic feasibility of this idea of recycling and reuse the generated concrete wastes, a comprehensive economic analysis is required. However, such an analysis is very difficult since a lot of factors need to be taken into account. Therefore, in this paper a simplified economic analysis is carried out. In this analysis, only the transportation cost for the concrete pile heads is considered, since it accounts for the largest cost, as mentioned above.

In this project, two types of concrete piles are used:

- Type I: diameter 400 mm, cut length 500 mm, number of piles: 60000;
- Type II: diameter 1500 mm, cut length 1500 mm, number of piles: 6000.

The volume of the cut concrete heads is 3768 m³ for Type I pile and 15904 m³ for Type II pile, respectively. The cost for the transportation of the concrete heads to the closest place where they can be landfilled is about € 2.0 /m³ for Type I pile and € 6.7 /m³ for Type II pile. This means the total transportation cost for the concrete pile heads is approximately €114 092.8. Hence, if the concrete pile heads can be recycled and reused on the construction site, the high transportation cost can be saved. Another consideration is that the cut concrete piles have nearly no contaminations, which greatly facilitates the reuse of the crushed concrete as new aggregates. Obviously, a better economic benefit can be achieved when the reduction of the cost for purchasing natural aggregates is considered. This indicates the economic viability of the idea for the recycling and reuse of the concrete wastes in this project. Evidently, a more detailed economic analysis should be performed considering the cost for the crushing of the concrete waste and the actual amount of the recycled concrete aggregates (RCAs) that can be obtained.

It is well known that idea of recycling of old concrete as recycled concrete aggregates (RCAs) and then reuse of the RCAs to manufacture of concrete is not new. The research work on this topic can be traced to just after the World War II (Nixon 1978). In the past several decades,

numerous studies have been carried out in Belgium, Germany, the Nederland, Japan, the UK and later Canada, USA, China, Italy, Spain, France and other countries. Many studies on the crushing and processing technology of old concrete, the mixing proportion of concrete with RCAs, often called recycled aggregate concrete (RAC), the mechanical properties and durability of RAC as well as the behaviour and design of structural elements with RAC (De Brito and Saikia 2013; Pacheco-Torgal et al. 2013). These intensive research efforts have successfully demonstrated that the utilisation of RCAs and RAC is technical feasible, even in structural applications (Messari-Becker et al. 2014; Xiao 2017). In many cases, an economical benefit can also be achieved. This has opened many potential markets for RCAs and RAC.

Despite the technology is becoming more and more mature, the implementation of the idea of recycling and reuse of concrete wastes in this project still meets some big challenges. These challenges include:

- No special designed recycling plants for crushing construction and demolition wastes are available in the area where the construction work locates;
- It is not easy to install mobile crushers on the construction site due to the possible noise and dust during the processing of the concrete wastes;
- Adequate knowledge such as the processing and the quality of RCAs, the mix design procedure of RAC and the effect of RCAs on the concrete properties, are missing;
- The construction schedule is very tight, which means that the recycling and reuse of concrete wastes should not disturb the work plan and not add too much additional work, for instance, to the laboratory technicians and construction workers.

To overcome these challenges, it was decided to carry out the work under the consulting of an experienced academic institution for recycling and reuse of concrete materials. The research group RecyCon - Recycling in Construction at KU Leuven (Belgium) was then commissioned to this end. Based on the advices of the consultants, the following procedures were (or will be) taken:

- Processing the concrete wastes in a crushing plant for natural coarse aggregates;
- Only using coarse RCAs in manufacturing new concrete to make sure that the quality of the concrete can meet the code requirements;
- Testing the produced RCAs by using of the Chinese Standard for natural aggregates and imposing the requirements for RCAs in the European Standard EN 12620: 2013 *Aggregates for Concrete* and the Belgian Standard NBN B-001: 2017 *Concrete: Specification, Performance, Production and Conformity*;
- Firstly utilising of RCAs in secondary or non-load bearing elements and then considering for structural use.

3. PROCESSING AND PROPERTIES OF RECYCLED CONCRETE AGGREGATES

3.1 Processing of concrete wastes for RCAs

A plant for crushing natural stones (rocks) as coarse aggregates for concrete was used to crush the concrete. This the closest plant to the collection site of the concrete wastes, with a distance of around 80 km. Fig. 2 shows the crushing plant.

Since the crushing procedure has a very important influence on the properties of RCAs, the quality of the processing of the crushing plant must be checked. For this aim, the laboratory

– cast concrete specimens were crushed in this crushing plant and the properties of the produced RCAs were examined. The parent concrete has a maximum aggregate size of 31.5 mm with a strength class of C30/37 to C35/45. The concrete specimens were firstly subjected to a jaw crusher and then a hammer crusher for further shaping the RCAs. Finally, the RCAs were sieved according to three sizes: 5 – 10 mm, 10 – 20 mm and 16 - 31.5 mm. The whole procedure does not differ from that for producing coarse natural aggregates. The produced RCAs of different sizes are illustrated in Fig. 3. It can be seen from the figure that the RCAs have an angular and rough surface, irrespective of the sizes. The RCAs are in general original natural aggregates with old mortar attached on them. This is quite consistent with many previous findings, such as Hansen (1986), Xiao et al. (2005), Li et al. (2006) and Boehme et al. (2012).



Fig. 2: Crushing plant for concrete aggregates



(a) 5-10mm



(b) 10-20mm



(c) 16-31.5mm

Fig. 3: Recycled concrete aggregates (of different sizes)

3.2 Properties of produced RCAs

The laboratory tests on the properties of the RCAs were carried out according to the Chinese Standard *GB/T 14685 -2011 Pebble and Crushed Stone for Construction*. The tested items included: the grading, apparent density, tight density, tight void ratio, flakiness index, and the water absorption as well as the impact value.

The grading curves of the RCAs are presented in Fig. 4. In Fig. 4(a) to (c), the curves are for the aggregates directly obtained from the crushing plant. It can be seen that the grading curves for all the three sizes of aggregates fall within the maximum and minimum limits given in the Chinese Standard *GB/T 14685 -2011*. This means the RCAs can meet the grading requirement for aggregates used in concrete. Fig. 4(d) shows the grading curve of a recomposed aggregate, in which the proportion of the aggregates of 5-10 mm, 10-20 mm and 16-31.5 mm is 20%, 50% and 30%, respectively. It can be seen that the grading curve of the recomposed aggregate also falls within the envelope for coarse aggregate for using in concrete.

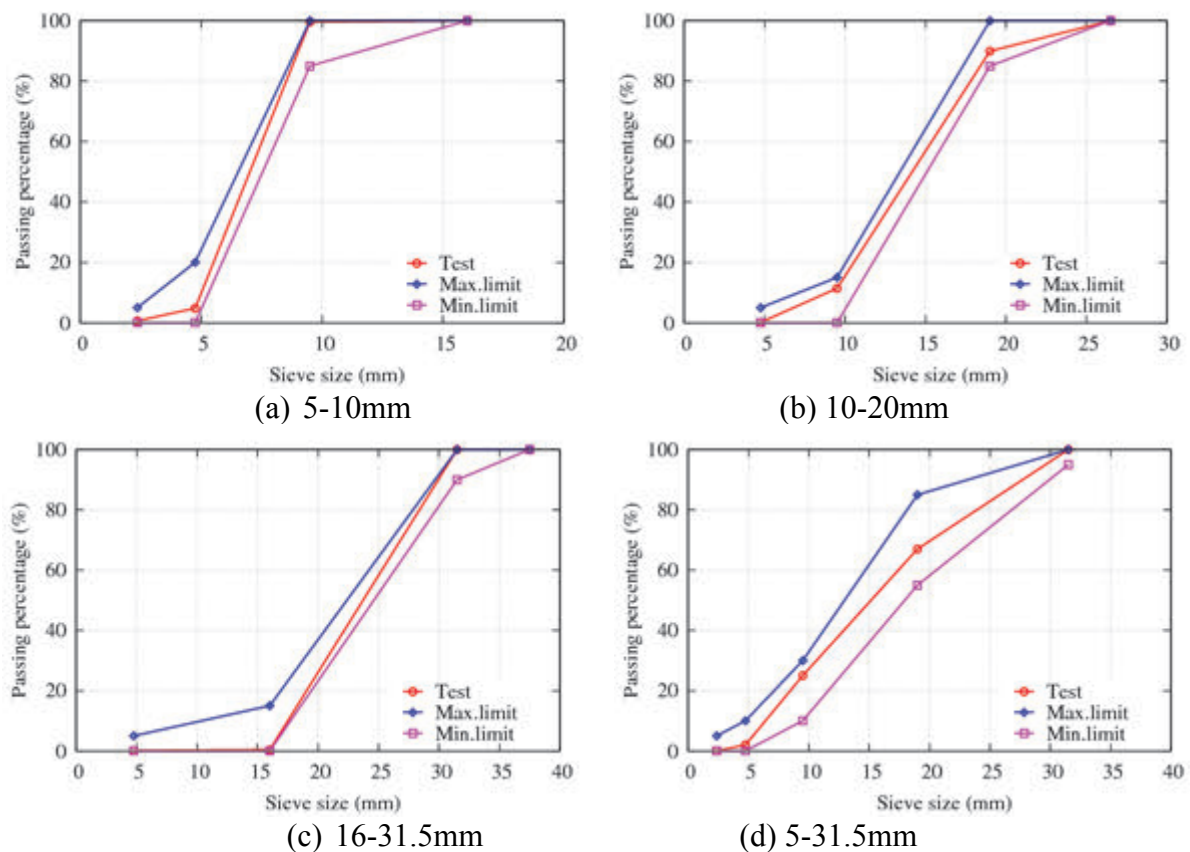


Fig.4: Grading curves of the RCAs

The test data for the other physical and mechanical properties of the RCAs are presented in Tab. 1. From this table, it can be seen that the RCAs obtained in this work are able to meet the requirements for RCAs in the standards EN 206 12620: 2013 and NBN B-001: 2017 as well as the Chinese Standard *GB/T 25177 - 2010 Recycle Coarse Aggregate for Concrete*.

Tab. 1: Physical and mechanical properties of the RCAs

Properties	Requirement		Test results		
	EN 206 12620 + NBN B-001	GB/T 25177	5-10mm	10-20mm	16-31.5mm
Apparent density (kg/m ³)	≥ 2200	>2450 (Type I)	2630	2600	2600
Tight density (kg/m ³)	-	-	1510	1530	1550
Tight void ratio (%)	-	< 47 (Type I)	43	41	40
Flakiness index (%)	≤ 20	<10	-	2.5	1.8
Water absorption 24h (%)	≤ 10	< 5 (Type II)	4.5	4.6	4.4
Crushing index (%)	-	< 12 (Type I)	-	12	-

4. PLANNED UTILIZATION OF RECYCLED CONCRETE AGGREGATES

As described above, the produced RCAs from the concrete wastes on this construction site and using the crushing plant for natural coarse aggregates have high quality and can meet the code requirements. Therefore, it is possible to use the RCAs for manufacturing concrete. Based on actual conditions and taking into account the relatively insufficient knowledge and experiences of the construction team, it was decided to firstly utilise the RCAs in precast concrete blocks for highway bank protection revetments, as illustrated in Fig. 5. As a first step, hexagonal hollow blocks shown in Fig. 6 will be made. Considering the wall thickness of the block, which is 5cm, only RCA of 5-10mm will be used to make this type of blocks. Currently, the research work is being carried out in collaboration with the research group RecyCon at KU Leuven, Belgium.



Fig. 5: Highway bank protection revetment

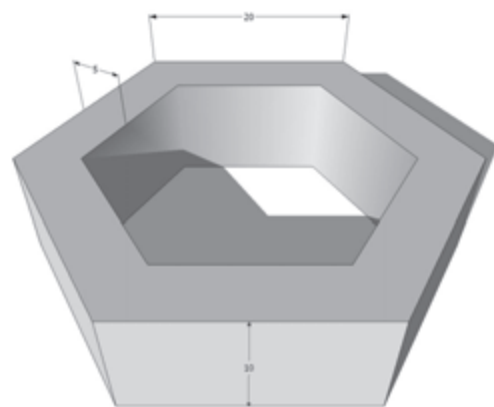


Fig. 6: Hexagonal concrete hollow blocks

In a next step, the RCAs will be utilised to produce other types of blocks for highway bank protection revetments and also to manufacture precast concrete parapet elements for the high-speed rail, see Fig.7. Finally, attempts to use RCAs in large scale structural elements, such as precast concrete bridge decks, as presented in Fig. 8 will also be made. For this work, the recomposed RCA will be used.

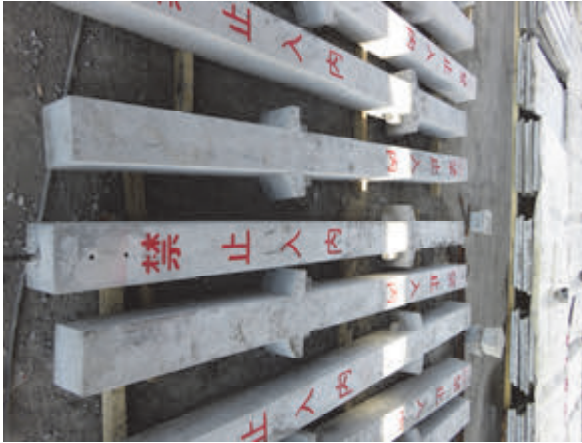


Fig. 7: Precast concrete parapet beams

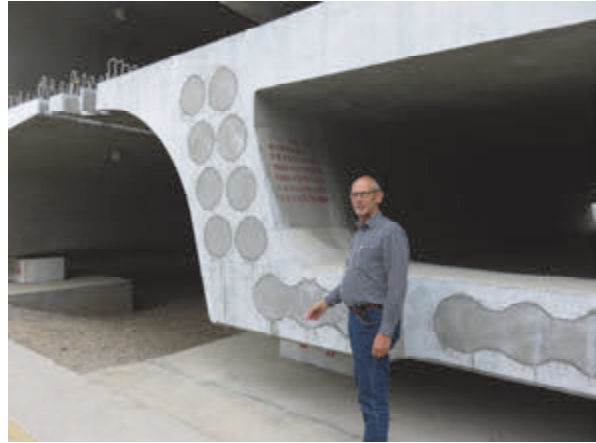


Fig. 8: Precast concrete bridge decks (with L. Boehme)

5. CONCLUSIONS AND REMARKS

This paper provides an attempt to recycle and reuse concrete wastes on a construction site, which were generated due to the construction of a high-speed rail. Instead of being used in sub-bases for road works and similar applications, the crushed concrete – recycled concrete aggregates (RCAs) are planned to be used for manufacture concrete, representing a value-added application. In spite of several big challenges, the first efforts for producing and testing the RCAs are successful. The following conclusions can be drawn from this work:

- The transportation costs accounts for the largest part of the disposal cost of the concrete wastes under the current conditions in China, where lanfilling of construction and demolition wastes is still permitted;
- Recycling and reuse of the concrete wastes are economically viable in this project owing to the decrease of the high transportation costs;
- It is possible to obtain recycled concrete aggregates with good grading by using of the crushing plant for natural coarse aggregates, where the concrete wastes are firstly crushed by a jaw crusher and then further shaped by a hammer crusher;
- The physical and mechanical properties of the recycled concrete aggregates can meet the requirements in different standards, demonstrating the viability of using this material for producing concrete. Since the parent concrete is generally young and contains nearly no contamination, the effect of the recycled concrete aggregates on the durability of concrete should not be a big concern;
- Research work on the utilisation of the recycled concrete aggregates for manufacturing precast concrete non-structural and structural elements are ongoing at this time. The results will be published later in another paper.

6. ACKNOWLEDGEMENTS

During the research work presented in this paper, Professor Jiabin Li and Professor Luc Boehme (KU Leuven – University of Leuven, Belgium) provided many useful information and advices. The author would like to express his sincere acknowledgement for their kind help.

7. REFERENCES

- Boehme, L., Van Gysel, A., Vrijders, J., Joseph, M., Claes, J. (2012), "Valorisation of Recycled Concrete Aggregates in Concrete C20/25 & C25/30", ACCO, Leuven, 199pp.
- De Brito, J. and Saikia, N. (2013), "Recycled Aggregate in Concrete", Springer-Verlag London, 448pp.
- Fernando Pacheco-Torgal, F., Tam, V., Labrincha, J., Ding, Y. and De Brito, J. (2013), "Handbook of Recycled Concrete and Demolition Waste", Woodhead Publishing 2013, 672pp.
- Hansen, T. C. (1986), "Recycled Aggregates and Recycled Aggregate Concrete: Second State-of-the-Art Report Developments 1945–1985", *Materials and Structures*, Vol. 19, No. 3, May 1986, pp 201-246.
- Li, J., Xiao, J. and Huang, J. (2006), "Influence of Recycled Coarse Aggregate Replacement Percentages on Compressive Strength of Concrete", *Chinese Journal of Building Materials*, Vol. 9, No. 3, June 2006, pp. 297-301.
- Messari-Becker, L., Mettke, A., Knappe, F., Storck, U., Bollinger, K. and Grohmann, M. (2014), "Recycling Concrete in Practice – A Chance for Sustainable Resource Management", *Structural Concrete*, Vol. 15, No. 4, December 2014, pp 556-562.
- Nixon P. J. (1978), "Recycled Concrete as An Aggregate for Concrete—A Review", *Materials and Structures*, Vol.11, No.65, September–October 1978, pp.371-378.
- Xiao, J. (2017), "Recycled Aggregate Concrete Structures", Springer-Verlag Berlin Heidelberg, 666pp.
- Xiao, J., Li, J and Zhang, Ch. (2005), "Mechanical Properties of Recycled Aggregate Concrete under Uniaxial Loading", *Cement and Concrete Research*, Vol. 35, No. 6, June 2005, pp. 1187-1194.

FEASIBILITY OF ON-SITE RECYCLING AND REUSE OF WASTE CONCRETE IN CHINA – A CASE STUDY

Daguang Han¹, Yongwang Geng², Jianfeng Bai², Yupeng Yang², Chunli Ying¹, Hongyuan Li³, Jiabin Li⁴

¹College of Civil Engineering, Chongqing Jiaotong University, Xuefu Road 66, 400074 Chongqing, China.

²The fifth Engineering Co., Ltd., China Railway 16th Bureau Group., Guanghua Road 2, 064000 Tangshan, Hebei, China.

³Department of Civil Engineering, Lushan College, Guangxi University of Science and Technology, New Road 99, Liu Zhou, Guangxi, China.

⁴KU Leuven, Technology Cluster Construction, Technology Campus Bruges, Spoorwegstraat 12, 8000 Bruges, Belgium.

SUMMARY

This paper examines the feasibility of the on-site recycling and reuse of waste concrete in China through a case study. Based on the up-to-date research, an overview of the properties of the recycled concrete aggregates (RCAs), the performance of the concrete with RCAs, often referred as recycled aggregate concrete (RAC) in the fresh and hardened states, and the structural behaviour of RAC as well as the international utilisation of RAC and the gained experiences, is presented. It is found that the recycling and reuse of the waste concrete on the construction site is feasible. Tests the properties of the RCAs illustrate that they can meet the requirements in the standards. It is therefore possible to use the RCAs in producing concrete. Some preliminary tests on the mix design and performance of RAC demonstrate that the RAC can meet the mechanical and durability requirements for railway concrete structures.

1. INTRODUCTION

The rapid urbanisation in recent decades in China has led to a large amount of demolitions of structures and infrastructures. These demolitions, together with the construction of new structures and the renovations of old buildings, have resulted in a great deal of construction and demolition (C&D) wastes. Presently, the amount of C&D wastes generated in China is approximately 2 billion tons, which reaches around 40% of the whole city solid wastes. Amongst the C&D wastes, old or end-of-life (EOL) concrete accounts for about 30-40% of the streams. Therefore, the quantity of concrete waste is rather huge. It is estimated that 638 million tons waste concrete will be produced in 2020 (Shi and Xu 2006).

In recent years, China has built an extensive number of high-speed rail lines. At present, there are still many lines are under construction, especially in the western part of the country. The fifth Engineering Co., Ltd. of the China Railway 16th Bureau Group is principal contractor of the high-speed rail from Yinchuan to Wuzhong (Yin-Wu), which has a length of about 40 km. During the construction of the Yin-Wu high-speed rail, many concrete infrastructures have to be demolished, even though most of which are still young. Fig. 1 shows a prestressed concrete bridge close to the Yinchuan international airport and a mobile precast concrete plant that need to be demolished. The bridge is far from its service life. A lot of waste concrete will be resulted from the demolitions.



(a) A prestressed concrete bridge



(b) A precast concrete plant

Fig. 1: Concrete structures to be demolished

How to deal with the large amount of demolished concrete is obviously a big problem facing the contractor since the cost for the disposal of the wastes is rather high. Motivated by saving the disposal cost for the waste concrete and protecting the environment, it is decided to recycle the demolished concrete on the construction site, that is, to crush the waste concrete as new aggregates, often referred as recycled concrete aggregates (RCAs) for producing concrete.

2. FEASIBILITY STUDY OF WASTE CONCRETE RECYCLING

To examine the feasibility of on-site recycling of the waste concrete, both the economic and technical feasibility of this idea need to be investigated. The former is determined in the light of a complexity of parameters, such as the availability of natural (virgin) aggregates, the transportation cost for the waste concrete as well as the RCAs, the cost for the manufacture of RCAs, the incentive and disincentive policy intervention, the cost of alternative aggregates, as well as know-how and skilled labor; while the latter is related to the short-term and long-term technical properties of concrete with RCAs, often called recycled aggregate concrete (RAC). A preliminary analysis on the economical viability of recycling of the waste concrete in this work has been presented in Yang (2017). It was found that the main cost of the disposal of the waste concrete is due to the transportation to the landfill site. The cost for the transportation of the waste concrete to the recycling plant and the production of the RCAs can be easily offset by saving the disposal cost. Therefore, the on-site recycling of waste concrete in this work shows its economical viability.

In the present paper, the feasibility study is therefore focused on the technical characteristics of concrete with RCAs. In the following, an overview of the physical and mechanical properties of RCAs as well as the technical characteristics of RAC in the fresh, hardened short-term and long-term states based on up-to-date research, such as Boehme et al. (2012), De Brito and Saikia (2013), Pacheco-Torgal et al. (2013), Li et al. (2006), McNeil and Kang (2013), Yehia et al. (2015), Said et al. (2017), Barros et al. (2017) as well as Xiao (2017) is presented.

Recycled concrete aggregates (RCAs)

- RCAs produced from waste concrete via conventional crushing technology can generally fulfil the size distribution requirements for natural aggregate, indicating there is no special difficulty in mixing concrete with RCAs (Hansen 1992; Li 2004; Li 2008);

- The density of RCAs is somewhat lower than that of natural (virgin) aggregates. The decrease is up to 10% (Hansen 1992; Li 2004; Xiao et al. 2006);
- The water absorption of RCAs is significantly higher than that of natural aggregates. The former is normally in the range of 2 to 10% while the latter is typically 0.5-1.0%. The high porosity of RCAs is mainly attributed to the attached mortar to the original aggregates (Boehme et al, 2012; Li 2004; Xiao et al. 2005a; De Brito and Saikia 2013; Pacheco-Torgal et al. 2013; Xiao 2017);
- The resistances of RCAs to mechanical actions and environmental loads are generally inferior to that of natural aggregates, for instance, the Los Angeles abrasion loss of RCAs is considerably increased in comparison with natural aggregates (Boehme et al, 2012; Li 2004; De Brito and Saikia 2013, Pacheco-Torgal et al. 2013).

Fresh concrete

- Due to a sharp irregular shape, rough surface and high water absorption of RCAs, RAC often yields inferior workability (Hansen 1992; Boehme et al, 2012; Li 2004; De Brito and Saikia 2013, Pacheco-Torgal et al. 2013);
- To achieve desired workability, compensation water is required. It is also possible to increase the workability of RAC through pre-wetting RCAs or the use of water reducing admixtures (super plasticizers) (Hansen 1992; Boehme et al, 2012; De Brito and Saikia 2013) ;
- RAC often exhibits consistency retention than conventional concrete with natural aggregates. This needs to be considered when transporting RAC for relatively long distances (Abou-Zeid and McCabe 2002; Boehme et al. 2012);
- The unit weight of RAC is slightly less (about 5 to 10%) than conventional concrete, which falls in the range between 2100 and 2250 kg/m³ (Hansen 1992; Li 2004).

Short-term hardened concrete

In the case of the same water-to-cement (w/c) ratio, RAC exhibits the following material properties compared to conventional concrete:

- The water absorption of RAC is higher than of concrete made with virgin aggregates (Boehme et al. 2012);
- The compressive strength of RAC decreases with the increase of amount of RCAs. When natural aggregates are fully replaced with RCAs, the reduction in the compressive strength is up to 25% (Hansen 1992; Li 2004; Yehia et al. 2015; Xiao 2017);
- Provided that the quality of the RCAs is uniform, the scattering of the compressive strength of RAC does not differ much from that of conventional concrete (Li 2004; Xiao et al. 2005b; Li et al. 2006; Li 2008);
- The direct and splitting tensile strength as well as the flexural tensile strength decreases with the increase of RCAs with a reduction rate up to 10% (Hansen 1992; Xiao 2017);
- The modulus of elasticity of RAC decreases in comparison that of conventional concrete, with a decrease ratio up to 45% (Hansen 1992; Li 2004; Xiao et al. 2005a; Xiao et al. 2006; Boehme et al. 2012);
- The drying shrinkage of RAC increases up to 70% compared to that of conventional concrete (Hansen 1992; Safiuddin et al. 2013; Xiao et al. 2014).

Long-term hardened concrete

- The creep of RAC increases up to 50% in comparison with conventional concrete. This needs to be considered when RAC is used in prestressed concrete (Hansen 1992; Safiuddin et al. 2013; Xiao et al. 2014);
- The flexural fatigue of RAC is superior than conventional concrete due to a stronger bond between cement paste and RCAs (Abou-Zeid and McCabe 2002);
- The abrasion resistance of RAC is inferior to that of conventional concrete, which limits its use in applications involving wear and heavy frictional loads (Hansen 1992; Abou-Zeid and McCabe 2002; De Brito and Saikia 2013);
- Due to higher internal voids and enhanced bond, RAC has a somewhat enhanced performance in fire and elevated temperatures (Abou-Zeid and McCabe 2002; Xiao et al. 2013; Said et al. 2017; Xiao 2007);
- The carbonation resistance of RAC is comparable to that of conventional concrete (Xiao et al. 2013; Messari-Becker et al. 2014);
- The freezing - thawing resistance of RAC can be superior or inferior to that of conventional concrete, depending on the quality of the RCAs (Hansen 1992; Xiao et al. 2013; Said et al. 2017);
- The chloride penetration of RAC is the same or slightly increased compared to that of conventional concrete (Abou-Zeid and McCabe 2002; Xiao et al. 2013).

Structural behaviour

- The bond between reinforcing steel and RAC is comparable or even superior to conventional concrete made with RCAs (Xiao and Falkner 2007; Sadati et al. 2017);
- The flexural capacity of RAC beams slightly reduces with increase of RCA. However, the reinforcement decreases the effect of RCA on ultimate load (Li 2009; Tošić et al. 2016; Xiao 2017);
- The failure modes of RAC members subjected to shear and punching are similar to that of conventional concrete components (Tošić et al. 2016);
- The shear and punching capacities of RAC beams decrease with the increase of RCAs when no shear reinforcement is used. However, the use of RCAs has only a minor effect when shear reinforcement is provided (Li 2009; Tošić et al. 2016; Xiao 2017);
- The cracking pattern and load-deformation behaviour of RAC compressive members are similar to that of members made of conventional concrete. However, the load-carrying capacity of RAC columns decreases as the amount of RCAs increases (Li 2009; Xiao et al. 2012; Choi and Yun 2012);
- The deflections of RAC components and structures increase in comparison with that of beams made of conventional concrete (Xiao et al. 2012; Choi and Yun 2012);
- The seismic properties of RAC structural components and structures are comparable to that of members made of conventional concrete when properly designed (Corinaldesi et al. 2011; Xiao et al. 2012; Xiao 2017).

From the above overview, it can be seen that the material and structural behaviour of RAC are different from that of conventional concrete. It should be noted that some properties of RAC are inferior to conventional concrete. This needs to be adequately considered, especially when RAC is used as structural concrete. However, there are techniques that can be used to enhance the properties of RAC to a comparable level as conventional concrete with virgin aggregates. For instance, the use of equivalent mortar volume (EMV) mix proportion method can reduce

the creep strain of RAC greatly. Nevertheless, this method results in a loss of the workability and freezing-thawing resistance. This means that performance-based mix design methodology for RAC is required.

International utilisation of RCAs in concrete and gained experience

Although some properties of RAC are generally inferior to that of conventional concrete and this limits the application field of this material, there were many successful implementations of RCAs in concrete, mainly for road constructions. At present, the technology for the use of RAC in rigid pavements is becoming more and more mature. A number of pavements with RAC have been constructed, which have shown satisfactory performance after more than several decades of service.

In addition, there are also several successful practical applications of RAC in structures. Typical examples include the Berendrecht lock in the port of Antwerpen (Belgium), the RecyHouse in Brussels (Belgium), the Environmental Building of BRE (UK), the Waldspirale residential building in Darmstadt (Germany) and the Vilbeler Weg office in Darmstadt (Germany).

The successful application examples indicate that the use of RAC in engineering practice is technically feasible. However, the difference between RAC and conventional concrete must be adequately taken into account. Therefore, a strict quality insurance and control of the RCAs and the RAC is necessary because of the complexity, qualitative and quantitative aspects of RCAs and the presence of wide arrays of parameters.

3. CHALLENGES OF ON-SITE RECYCLING OF WASTE CONCRETE

From the technical and economic points of view, it is highly feasible to recycle waste concrete and to use the crushed concrete as RCAs in the manufacture of concrete. The recycling of the demolished concrete in this work is considered to be additionally more attractive because the purity of the concrete is fairly high, in other words, the amount of the contaminants in the concrete is quite low. In spite of this, there are some challenges in recycling of the concrete on the construction site, as addressed in Yang (2017). The most challenging issue is the lack of sufficient knowledge. Due to this, the research group RecyCon at KU Leuven, Belgium, has been commissioned to provide necessary supervisions for this work. This group has fairly rich experiences in both academic research and practical applications of RAC.

4. SOME PRELIMINARY RESULTS AND FUTURE WORK

With the guidance of the research group of RecyCon, KU Leuven, the following work has been done so far:

- The crushing of waste concrete in a local production plant for natural (virgin) stone aggregates;
- Test the physical and mechanical properties of RCAs according to the Chinese Standard and the European Standard;
- Check whether the RCAs can meet the related requirements in the Chinese and European Standards, especially the apparent density and the water absorption;
- Decide the suitable use of the RCAs based on their properties.

It is found that the technical characteristics of the RCAs can meet the requirements for RCAs in the standards EN 206 12620: 2013 and NBN B-001: 2017 as well as the Chinese Standard GB/T 25177 - 2010 *Recycle Coarse Aggregate for Concrete*. More details about the RCAs, including the grading curve, apparent density, tight void ratio, Flakiness index, crushing index and water absorption can be found in Yang (2017).

Based on the properties of the RCAs, it is decided to use RCAs firstly in concrete blocks for bank protection revetment for highway. Some preliminary laboratory studies on the mix proportioning of concrete with the RCAs have been carried out. The test results indicate that the produced concrete with the RCAs can meet the mechanical and durability requirements in the Chinese Code for Durability Design of Concrete Structures for Railway (TB 1005-2010).

Some attempts to use RCAs in other non-structural products and even in full scale precast prestressed concrete bridge decks will also be made in the future.

5. CONCLUSIONS AND REMARKS

This paper examines the feasibility of the on-site recycling and reuse of waste concrete in China through a case study during the construction of the Yin-Wu high speed rail. Based on the up-to-date research, it is found that the recycling and reuse of the waste concrete on the construction site is feasible. Tests on the manufacture of the RCAs and the physical as well as mechanical properties of RCAs illustrate that the RCAs can meet the requirements in different standards. It is therefore possible to use the RCAs in producing concrete. Some preliminary tests on the mix design and performance of concrete with the RCAs demonstrate that the RAC can meet the mechanical and durability requirements for railway concrete structures.

6. LIST OF NOTATIONS

C&D	Construction and demolition
EMV	Equivalent mortar volume
EOL	End of life
RCA	Recycled concrete aggregates
RAC	Recycled aggregate concrete

7. ACKNOWLEDGEMENTS

During the research work presented in this paper, Professor Luc Boehme at KU Leuven – University of Leuven, Belgium provided many useful information and advices. The authors would like to express their sincere acknowledgements to him for his kind help.

8. REFERENCES

- Abou-Zeid, M. N., McCabe, S. L. (2002), “Feasibility of Waste Concrete As Recycled Aggregates In Construction”, *Waste Management and the Environment*, Vol. 56, pp. 537-546.
- Barros, J. A.O., Ferrara, L., Martinelli, E. (2017), “Recent Advances on Green Concrete for Structural Purposes”, Springer International Publishing AG, 427pp.
- Boehme, L., Van Gysel, A., Vrijders, J., Joseph, M., Claes, J. (2012), “Valorisation of Recycled Concrete Aggregates in Concrete C20/25 & C25/30”, ACCO, Leuven, 199pp.

- Choi, W.-C., Yun, H.-D. (2012), "Compressive Behaviour of Reinforced Concrete Columns with Recycled Aggregate under Uniaxial Loading", *Engineering Structures*, Vol.41, August 2012, pp.285-293.
- Corinaldesi, V., Letelier, V., Moriconi, G. (2011), "Behaviour of Beam-Column Joints made of Recycled-Aggregate Concrete under Cyclic Loading", *Construction and Building Materials*, Vol. 25, No. 4, April 2011, pp. 1877-1882.
- De Brito, J. and Saikia, N. (2013), "Recycled Aggregate in Concrete", Springer-Verlag London, 448pp.
- Fernando Pacheco-Torgal, F., Tam, V., Labrincha, J., Ding, Y. and De Brito, J. (2013), "Handbook of Recycled Concrete and Demolition Waste", Woodhead Publishing 2013, 672pp.
- Hansen, T.C. (1992), "Recycling of Demolished Concrete and Masonry", Chapman and Hall, London, 336pp.
- Li, J. (2004), "Study on Mechanical Behaviour of Recycled Aggregate Concrete", Master Thesis, Tongji University, Shanghai, 122pp.
- Li, J., Xiao, J. and Huang, J. (2006), "Influence of Recycled Coarse Aggregate Replacement Percentages on Compressive Strength of Concrete", *Chinese Journal of Building Materials*, Vol. 9, No. 3, June 2006, pp. 297-301.
- Li, X. (2008), "Recycling and Reuse of Waste Concrete in China: Part I. Material Behaviour of Recycled Aggregate Concrete", *Resources, Conservation and Recycling*, Vol. 53, No. 1-2, December 2008, pp.36-44.
- Li, X. (2009), "Recycling and Reuse of Waste Concrete in China: Part II. Structural Behaviour of Recycled Aggregate Concrete and Engineering Applications", *Resources, Conservation and Recycling*, Vol.53, No.3, January 2009, pp.107-112.
- McNeil, K., Kang, T. H.K. (2013), "Recycled Concrete Aggregates: A Review", *International Journal of Concrete Structures and Materials*, Vol. 7, No.1, March 2013, pp 61-69.
- Messari-Becker, L., Mettke, A., Knappe, F., Storck, U., Bollinger, K. and Grohmann, M. (2014), "Recycling Concrete in Practice – A Chance for Sustainable Resource Management", *Structural Concrete*, Vol. 15, No. 4, December 2014, pp 556-562.
- Safiuddin, M., Alengaram, U.J., Rahman, M. M., Salam, M.A. Jumaat, M. Z. (2013), "Use of Recycled Concrete Aggregate in Concrete: a Review", *Journal of Civil Engineering and Management*, Vol. 19, No.6, pp. 796-810.
- Said, A.M., Ayad, A., Talebi, E., Ilagan, A.C. (2017), "Durability of Recycled Aggregate Concrete: A Review", *ACI Special Publication*. Vol. 314, March 2017, pp. 1-18.
- Sadati, S., Arezoumandi, M., Khayat, K.H., Volz, Jeffery S. (2017), "Bond Performance of Sustainable Reinforced Concrete Beams", *ACI Materials Journal*, Vol. 114, No.4, July 2017, pp. 537-547.
- Shi, J., Xu, Y. (2006), "Estimation and Forecasting of Concrete Debris Amount in China", *Resources, Conservation and Recycling*, Vol. 49, No.2, December 2006, pp.147-158.
- Tošić N., Marinković, S., Ignjatović, I. (2016), "A Database on Flexural and Shear Strength of Reinforced Recycled Aggregate Concrete Beams and Comparison to Eurocode 2 Predictions", *Construction and Building Materials*, Vol. 127, November 2016, pp. 932-944.
- Xiao, J. (2017), "Recycled Aggregate Concrete Structures", Springer-Verlag Berlin Heidelberg, 666pp.
- Xiao, J. Falkner, H., (2007), "Bond Behaviour between Recycled Aggregate Concrete and Steel Rebars", *Construction and Building Materials*, Vol. 21, No. 2, February 2007, pp.395-401.
- Xiao, J., Li, J and Zhang, Ch. (2005a), "Mechanical Properties of Recycled Aggregate Concrete under Uniaxial Loading", *Cement and Concrete Research*, Vol. 35, No. 6, June 2005, pp. 1187-1194.

- Xiao, J., Li, J and Zhang, Ch. (2005b), “On Statistical Characteristics of the Compressive Strength of Recycled Aggregate Concrete”, *Structural Concrete*, Vol. 6, No. 4, October 2005, pp. 149-153.
- Xiao, J., Li, J and Zhang, Ch. (2006), “On Relationships between the Mechanical Properties of Recycled Aggregate Concrete: An Overview”, *Materials and Structures*, Vol.39, No.6, July 2006, pp.655–664.
- Xiao, J., Li, L., Tam, V. W.Y., Li, H. (2014), “The State of the Art Regarding the Long-Term Properties of Recycled Aggregate Concrete”, *Structural Concrete*, Vol.15, No.1, March 2014, pp. 3–12.
- Xiao, J., Li, W., Fan, Y., Huang, X. (2012), “An Overview of Study on Recycled Aggregate Concrete in China (1996–2011)”, *Construction and Building Materials*, Vol.31, June 2012, pp.364-383.
- Xiao, J., Lu, D., Ying, J. (2013), “Durability of recycled aggregate concrete: An overview”, *Journal of Advanced Concrete Technology*, Vol. 11, December 2013, pp. 347-359.
- Yang, Y. H. (2017), “Value-added Recycling and Reuse of Waste Concrete on a Construction Site”, *Proceedings of CCC 2017 - Innovative Materials and Technologies for Concrete Structures*, 31 August - 1 September 2017, Tokaj, Hungary, 8pp.
- Yehia, S., Helal, K., Abusharkh, A., Zaher, A., Istaitiyeh, H. (2015), “Strength and Durability Evaluation of Recycled Aggregate Concrete”, *International Journal of Concrete Structures and Materials*, Vol. 9, No.2, June 2015, pp. 219-239.

FRESH AND HARDENED STATE OF FIBRE CONCRETE

*Čechmánek René, Drdlová Martina, Boháč Martin
Výzkumný ústav stavebních hmot, a.s. (Research Institute for Building Materials)
Hněvkovského 30/65, 61700 Brno, Czech Republic*

SUMMARY

The Research Institute for Building Materials has designed new experimental devices for the Discovery Hybrid Rheometer to measure rheological properties of fresh cement-based mixtures. They are 3-blade and 3-ball agitators with a complementary role for absolute measurements using a system of coaxial cylinders. For slurries with low viscosity blade agitators are used and for higher viscosity suspensions ball agitators or a board-to-board system with roughened surface may be used. The aim of research works was to find suitable homogenization techniques, design of mixing process and optimal dosing of individual components. By means of these actions it is possible to achieve the best dispersion of selected fibre types in fine-grained cementitious matrixes, which is subsequently verified in hardened composites at first by non-destructive and then by destructive methods.

1. INTRODUCTION

Fibre-cement composites have a long and abundant history of their use. Their role in the building industry has gradually progressed, but their use is not still ending even in the 21st century. With a growing knowledge on their physico-mechanical properties, taking into account demands on health and environment in these days, the fibre-cement composites represent a material with a high potential.

Fibre reinforcement does not play the full role of steel reinforcement. Its role is to create a ductile structural material with limited deformation shrinkage.

Fibre reinforcement is characterized by the following properties (Pytlík, 2000):

- increases tensile strength and bending strength of concrete;
- reduces deformation of concrete due to shrinkage, increases the modulus of elasticity;
- reduces brittleness and increases toughness of concrete;
- increases temperature resistance and reduces water permeability.
-

Design, preparation and testing of fibre-cement composites are a task of wide range of research workplaces and universities in our country and abroad. However, a question on homogeneity of all cement matrix components and mainly optimal dispersion of fibre reinforcement in a mixture has not been yet solved sufficiently. Within testing of properties of such designed composites there is usually a realized fact, that variability of these properties is distinctive mainly for the reason of uneven dispersion of commonly used fibres in a whole matrix volume. Elimination of this phenomenon could be achieved by means of a design of the optimal homogenization process of dry mixture components with fibre reinforcement. Properties of fibre reinforced concrete (FRC) are mostly influenced by the fibre type and the amount of fibres. The bond of fibres mainly depends on material, shape and surface of fibres and mechanical properties of a matrix, the amount of fibres as well as the loading rate

(Kovacs, Balazs, 2003). Consequently, almost all properties of FRC changes with the changing of the surface and the shape of fibres. Only little information exists on the influence of the mixing procedure on the properties of fibres.

Residual tensile strength of FRC is one of the most important parameters both for design and for practice. Appropriate method and mixing time are required to reach random distribution of fibres and acceptable properties of concrete. The research conducted in Budapest University of Technology and Economics was directed to the possible influences of mixing time on the tensile properties of fibres and the flexural properties of FRC. The research team realized that some of the fibres may suffer from too long mixing time of concrete mixture (Czoboly, Balazs, 2015).

Several research works have been aimed to monitoring of fibre dispersion and orientation in cementitious composites, e.g. a magnetic method could be employed for this purpose, but only for composites reinforced with steel fibres (Ferrara, Faifer, Toscani, 2012). Other techniques could be used for cracking assessment of concrete structures by means of electric resistivity measurement (Lataste, Sirieix, Breyse, Frappa, 2003), including the research conducted by the authors' team from the Research Institute for Building Materials using electrically conductive elements with modified cement matrix (Čechmánek, Junek, Šteffan, Macháň, 2016; Junek, Čechmánek, Nešpor, Šteffan, 2014). The aim of the further works is to find a method for monitoring homogeneity of cement composites reinforced with both metal and non-metal fibres before being subjected to mechanical loading.

2. RHEOLOGICAL PROPERTIES OF MIXTURES

The Research Institute for Building Materials has designed new experimental devices for the Discovery Hybrid Rheometer (DHR-1) to measure rheological properties of fresh cement-based mixtures. They are three-blade and three-ball agitators with a complementary role for absolute measurements using a system of coaxial cylinders. For slurries with low viscosity blade agitators are used and for higher viscosity suspensions ball agitators or a board-to-board system with roughened surface may be used (Kuder, Ozyurt, Mu, Shah, 2007). Results of the measurements of cement mixtures with non-metallic fibres are depicted in Fig. 1.

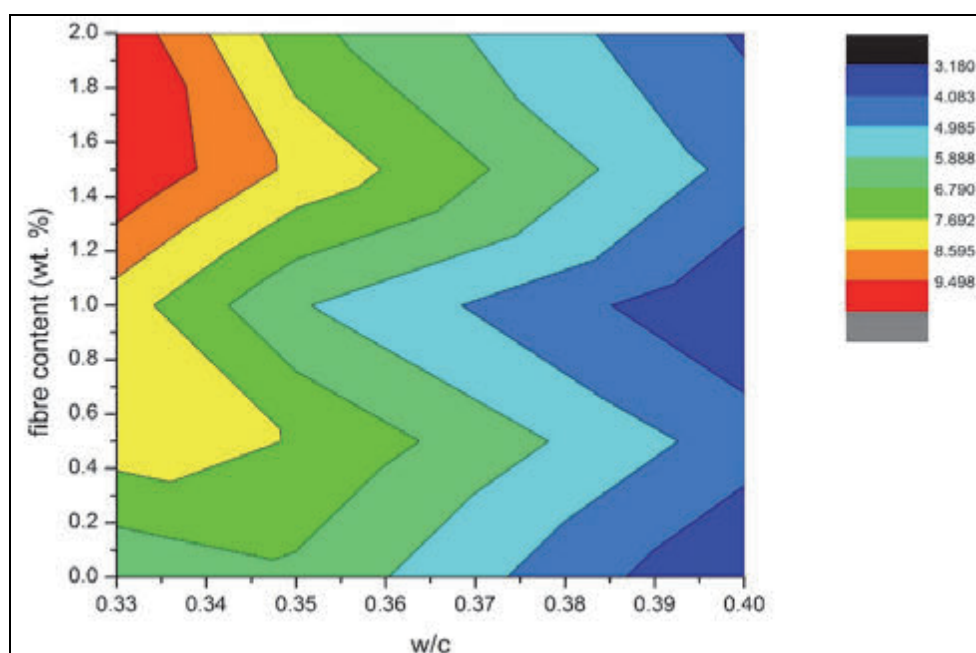


Fig. 1: Plastic viscosity of fibre-cement fresh mixtures

The size of the ball depends on the viscosity of the material. A suitable approach how to obtain rheological parameters is to use a ball agitator and take measurements of one revolution only. As to cement mortar, the structure is broken and does not retrieve its original state even after material relaxation.

Watery mortars close up, however, water is separated into a groove formed by the passing ball and thick mortars create a permanent groove. It means that repeated passage of the ball shows misleading values.

In order to measure highly heterogeneous suspensions, such as cement paste and mortar, a helical rotor was designed and manufactured. The advantage of its use is that during measurements the material is carried by the rotor and heavier particles do not settle which avoids slippage like when coaxial cylinders or bladed rotors are used.

3. GLASS FIBRE REINFORCED CONCRETE (GFRC)

Massive use of glass fibre reinforced concrete started with the development of prefabricated skeleton structures in the second half of the 20th century. The thin-walled elements with a matrix based on the high-value Portland cement with dispersed reinforcement in the form of alkali-resistant glass fibres are used in a range of applications. They include elements used for exterior cladding, various landscape architecture elements or elements for technical applications. Thanks to its durability, low basic weight, colouring ability and shape diversity, glass fibre reinforced concrete may properly replace certain natural materials (Vavrušková, Chromková, Čechmánek, Zavřel, 2016). Thin-walled fibre-cement elements are widely used in residential and industrial buildings for their appearance and durability. Because they are made of light-weight materials, they are mostly used as cladding elements for façades of multi-storey buildings exposed to hard external conditions.

Within a preparation of these fibre-cement composites an exact amount of alkali-resistant glass fibres with length of 12 mm is added into fine-grained matrix consisting of cement, aggregate and admixtures in the last stage of a mixing process and in this way properly dispersed in the whole volume of the mixture. This technology requires the use of highly flowable mixtures free from bleeding and sedimentation of heavier mixture components (Čechmánek, Prachař, Lederer, Loskot, 2015; Čechmánek, Prachař, Loskot, 2014).

4. SLURRY INFILTRATED FIBRE CONCRETE (SIFCON)

SIFCON was first developed in 1979 by Lankard Materials Laboratory, Columbus, Ohio, USA, by incorporating large amounts of steel fibres in steel fibre reinforced cement-based composites (Lankard, 1984). It possesses excellent mechanical properties coupled with very good energy-absorption characteristics. The fibre volume fraction of traditional fibre reinforced concrete is limited, because excessive amount of the fibres affects the workability of the fresh concrete in a negative way. This fact limits the fibre volume V_f to 1 - 5%, depending on the fibre type used and the required workability of the mixture. SIFCON specimens can be produced with V_f 5% up to 30% (Lankard, 1984; Homrich, Naaman, 1987). The fibre volume depends on the fibre geometry, length and diameter and vibration of the fibres during their placement process. The other major difference is in the composition and casting process of the composite. SIFCON is prepared by infiltrating pre-placed fibres with fine grain aggregate mortar. It has been reported that SIFCON slab elements exhibit excellent behaviour in flexure and punching shear when compared to HPFRC, reinforced

cement concrete (RCC) and plain cement concrete (PCC) slabs (Sudarsana, Ramana, 2005; Sudarsana, Gnaneswar, Ramana, 2008).

Due to extraordinary ductility of SIFCON, it seems to be very promising material for applications in structures subjected to impact load, but the literature review reveals only a few studies dealing with the SIFCON under dynamic loading. The results of our own investigation carried out on SIFCON slab panels under impact loading can bring significant contribution to the current knowledge in the field (Drdlová, Buchar, Řídký, Krátký, 2015; Drdlová, Čechmánek, Řídký, 2015).

5. PREPARATION OF FIBRE REINFORCED CONCRETE SPECIMENS

5.1 Fibre reinforced concrete boards

4 formulas representing different types of fibre reinforcement used in fine-grained cement composites were selected: glass fibre reinforced concrete (GFRC), composite reinforced with PVA fibres (PVA), composite reinforced with steel fibres (SFRC) and composite with a high content of steel fibres infiltrated in a slurry (SIFCON). In the first stage, all formulas were prepared according to the standard procedures recommended for the respective composite and fibre reinforcement using a standard agitator, always three test boards for each formula.

5.2 Test specimens

Each 500 x 500 x 40 mm test board was divided by cutting into a total of 22 specimens with dimensions 250 x 40 x 40 mm according to the proposed scheme in order to allow identification of the position of each test specimen of the test board. The end of the test specimen directed towards the edge of the board was labelled "A" and the end of the test specimen directed towards the centre of the board was labelled "B".

6. TESTS PERFORMED

6.1 Ultrasound measurement theory

Ultrasound is a mechanical wave motion which the human ear is incapable of perceiving; the frequency of wave motion exceeds 20 kHz; some literature sources mention 16 kHz. Ultrasound wave motion for testing and research of material properties in the construction industry uses frequencies exceeding 20 kHz. Ultrasound wave motion is based on the general principles for oscillating motion, in particular Hooke's law, Huygens principle, the law of reflection and refraction, Doppler effect, the principle of interference, law of absorption and others. Ultrasonic wave motion in solids transmits from the source to the surrounding space as a progressive longitudinal and transverse wave motion, in gases and liquids only as a longitudinal wave motion.

Oscillation is gradually spreading from the source by gradual transfer of energy from one particle to another. Generated elastic waves are transferred at speeds based on the elasticity parameters (e.g. Young's modulus of elasticity and Poisson's ratio) and the density of the surrounding space. The basic relations describing transmission of ultrasound wave motion are the same as for mechanical oscillation.

$$V_p = \sqrt{\frac{E \cdot (1 - \nu)}{\rho_0 \cdot (1 + \nu) \cdot (1 - 2\nu)}} \quad (1)$$

$$V_s = \sqrt{\frac{E}{2 \cdot \rho_0 \cdot (1 + \nu)}} \quad (2)$$

where: V_p is the speed of transmission of longitudinal wave [$\text{m} \cdot \text{s}^{-1}$]
 V_s is the speed of transmission of transverse wave [$\text{m} \cdot \text{s}^{-1}$]
 ρ_0 is the density of the surrounding space [$\text{kg} \cdot \text{m}^{-3}$]
 ν is Poisson's ratio [-]
 E is Young's modulus of elasticity [Pa]

The aforementioned relations show that the speed of wave transmission is not dependant on the wave frequency but on the material parameters of the environment only. Therefore, selection of the source frequency for measurements does not affect the absolute results but the quality of the measurement only. The transmitted energy disappears (absorbs) in the given environment which significantly depends particularly on the wave motion frequency but also on humidity, temperature and other parameters.

The so-called ultrasonic impulse method is used for non-destructive testing of concrete. Our goal is to use this method for testing of a cement composite material. The principle of concrete testing using the aforementioned method is described in the ČSN 73 1371 standard - Ultrasonic impulse concrete testing method. Ultrasonic impulses are repeatedly transmitted into the test material and subsequently registered while measuring the transmission time of these impulses; knowing the path along which the impulse transmits, we can calculate the impulse rate.

6.2 Ultrasound measurements

For ultrasound measurements we use a portable measuring apparatus – TICO – made by Proceq (Switzerland) which is intended to test concrete (detection of cavities, cracks, identifying concrete strength, modulus of elasticity, evenness of compaction, etc.). The apparatus consists of an indicating unit and a pair of audio probes, i.e. a transmitter and a receiver of ultrasonic impulses. To calibrate the apparatus, a calibration rod is used (a metal cylinder of the respective length with a precisely defined time of passage of ultrasonic waves).

In our case, the only parameter monitored is the passage time of ultrasonic waves; knowing the length of the impulse transmission path, the speed of impulse transmission can be calculated. The first task was to ensure perfect contact between the measuring probes and the surface of the composite for transmission of ultrasonic waves. When the probes contacted the surface of the tested material, a small air gap formed, causing a considerable distortion of the passing time of the ultrasound impulses (wave reflection created at the interface) or even preventing transmission of the ultrasound waves from the probe into the composite. When measuring ultrasound in the laboratory using specimens with flat surface, the so-called acoustic binder can be used. Unfortunately, when measuring rough surface of composites, this binding paste cannot be used (inappropriate consistency), so a different sonic bonding agent – plasticine – was used as recommended by the available literature.

The passage time of ultrasonic wave motion using 54 kHz probes was measured and automatically converted using the TICO apparatus with a preset distance of the probes to

the speed of passage of the ultrasonic wave. The measurement was performed twice – in A-B and B-A directions.

At the first stage non-destructive testing by means of ultrasound waves was carried out at first on a compact test slab with dimensions 500 x 500 x 40 mm and subsequently on individual test specimens with dimensions 250 x 40 x 40 mm, cut from the test slab according to a designed pattern.

6.3 Determination of flexural strength

At the second stage destructive testing of test specimens was performed, mainly evaluation of flexural strength with 4-point bending. A purpose of all these research works is finding of correlation between testing by means of destructive and non-destructive methods. A tensile test with four-point bending and loading perpendicular to the direction of compaction was performed using 250 x 40 x 40 mm test specimens. The distance between the lower supports was 210 mm, the distance between the loads was 100 mm. The flexural strength is defined:

$$R_f = \frac{3 \cdot F \cdot (l - l_1)}{b \cdot h^2} \quad (3)$$

where: R_f is the flexural strength [MPa]
 F is the maximum load [N]
 l is the distance between the supports [mm]
 l_1 is the distance between the loads [mm]
 b is the specimen width [mm]
 h is the specimen height [mm]

The measured values of the ultrasound passing speed and the tensile strength with four-point bending of the individual sets of test specimens (cut from the manufactured boards) were tabulated and plotted for mutual comparison. Already at this stage of the research it is possible to derive some relations between destructive and non-destructive testing. The higher values of the flexural strength correspond to the longer time of ultrasonic waves passing through the measured specimen thanks to the higher degree of fibre reinforcement as it is depicted in the graph in Fig. 2.

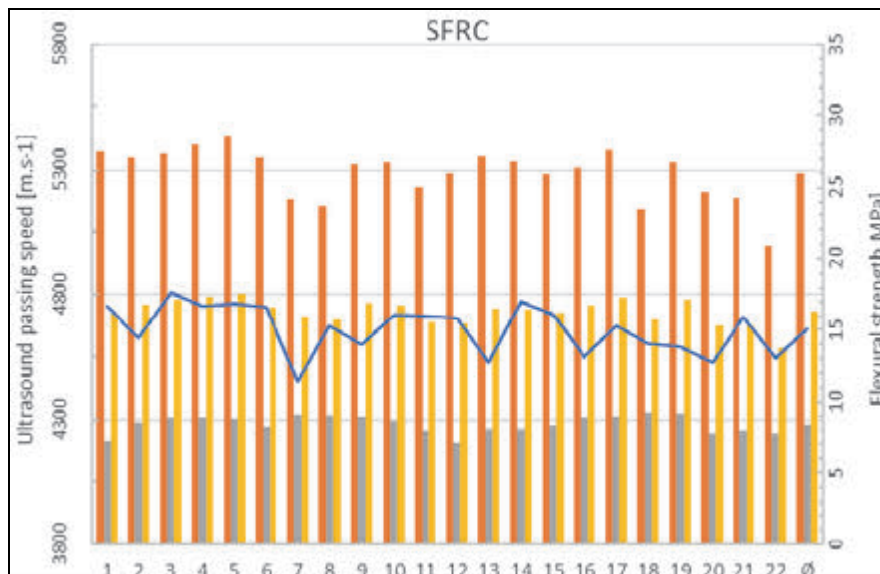


Fig. 2: Relation between destructive and non-destructive testing for SFRC specimens (blue line – flexural strength, individual columns – US passing speed A-B, B-A and average)

6.4 Fracture surface

The fracture surface of the individual specimens and the degree of the cross-section reinforcement in relation to the obtained flexural strength were also observed similarly and the position of a crack relative to the length of the specimen was documented.

While in the samples of glass fibre reinforced concrete the degree of fibre reinforcement in the cross section may be observed by the naked eye, in the composites reinforced with PVA fibres monitoring will be based mainly on polarization and 3D microscopy.

The standard steel fibre reinforced concrete shows considerable uneven distribution of steel fibres in the cross section. The sections of SIFCON specimens are heavily reinforced with steel fibres. Insufficient reinforcement can be observed only at the upper side of the test board where only a cement slurry was added and also in some places where the individual fibres locked into each other and created an empty space.

6.5 Microscopic analysis

Thin sections were prepared from the cracked area of the selected samples for polarizing and 3D microscopy in order to observe the proportion of the individual elements in the given cross section and, in particular, the distribution of the individual reinforcing fibres in correlation with the achieved flexural strength. Only one thin section of optimally reinforced and insufficiently reinforced cross section of the prepared formula of fibre reinforced concrete is assumed. The main attention will be paid to the stressed bottom side of each specimen, i.e. the side perpendicular to the direction of compaction.

7. CONCLUSIONS

For measurement of rheological properties of fresh cement-based mixtures there were designed new experimental devices for the Discovery Hybrid Rheometer. In order to measure highly heterogeneous suspensions, such as cement paste and mortar, a helical rotor was designed and manufactured. The advantage of its use is that during measurements the material is carried by the rotor and heavier particles do not settle which avoids slippage like when coaxial cylinders or bladed rotors are used.

A total of 4 formulas of different types of fibre reinforced concrete were prepared and subjected to non-destructive and destructive testing. Currently, the dependence on the values measured using ultrasound and flexural strength is being identified. It is necessary to evaluate other several sets of specimens and the results should be subjected to a correlation analysis again. After this, optimization of the process of preparation of selected fibre reinforced concrete and the related measurements will be carried out.

8. ACKNOWLEDGEMENTS

This research has been supported by institutional support for the long-term strategic development of a research organization provided by the Ministry of Industry and Trade of the Czech Republic.

9. REFERENCES

- Čechmánek, R., Junek, J., Šteffan, P. and Macháň, L. (2016), "Monitoring of concrete structures by means of composite tensometers", Monograph 537 Mechanics, Diagnosis and material issues in the 20th century architecture, Cracow University of Technology Press, 2016, pp. 123-139.
- Čechmánek, R., Prachař, V., Lederer, L. and Loskot J. (2015), "Benefits of using light-weight elements in building industry", Innovative, cost effective and eco-friendly fibre-based materials for construction industry, Cracow University of Technology Press, 2015, pp. 79-91.
- Čechmánek, R., Prachař, V. and Loskot J. (2014), "Filler from expanded glass as a light-weighting component of the cement composite with fiber reinforcement", Advanced Materials Research, Vol. 1000, August 2014, pp. 102-105.
- Czoboly, O. A. and Balazs G. L. (2015), "Can too long mixing time negatively influence properties of FRC?", The 11th Central European Congress on Concrete Engineering. Innovative Concrete Technology in Practice, October 2015, pp. 31-34.
- Drdlová, M., Buchar, J., Řídký, R. and Krátký, J. (2015), "Blast resistance characteristics of concrete with different types of fibre reinforcement", Journal of Structural Concrete, Vol. 16, Issue 4, December 2015, pp. 508-517.
- Drdlová, M., Čechmánek, R. and Řídký, R. (2015), "Blast impact behaviour of concrete with different fibre reinforcement", EPJ Web of Conferences, Vol. 94, September 2015.
- Ferrara, L., Faifer, M. and Toscani, S. (2012), "A magnetic method for non destructive monitoring of fiber dispersion and orientation in steel fiber reinforced cementitious composites – part 1: method calibration", Materials and Structures, Vol. 45, Issue 4, April 2012, pp. 575-589.
- Homrich, J. R. and Naaman, A. E. (1987), "Stress-Strain Properties of SIFCON in Compression", Fiber Reinforced Concrete – Properties and Applications, ACI SP-105, American Concrete Institute, Detroit, Michigan, 1987, pp. 283-304.
- Junek, J., Čechmánek R., Nešpor B. and Šteffan P. (2014), "Use of composite elements for monitoring of concrete under loading", Advanced Materials Research, Vol. 1000, August 2014, pp. 326-329.
- Kovacs, I. and Balazs, G. L. (2003), "Structural behaviour of steel fibre reinforced concrete", Journal of Structural Concrete, Vol. 4, Issue 2, June 2003, pp. 57-63.
- Kuder, K. G., Ozyurt, N., Mu, E. B. and Shah, S. P. (2007), "Rheology of fiber-reinforced cementitious materials", Cement and Concrete Research, Vol. 37, October 2006, pp. 191-199.
- Lankard, D. R. (1984), "Preparation, Applications: Slurry Infiltrated Fiber Concrete (SIFCON)", Concrete International, Vol. 6, Issue 12, 1984, pp. 44-47.
- Lataste, J. F., Sirieix, C., Breysse, D. and Frappa, M. (2003), "Electrical Resistivity Measurement Applied to Cracking Assessment on Reinforced Concrete Structures in Civil Engineering", NDT & E International, Vol. 36, Issue 6, September 2003, pp. 383-394.
- Pytlík, P. (2000), "Concrete Technology" (in Czech), VUTIUM Brno, 2000.
- Sudarsana, R. H., Gnaneswar K. and Ramana N. V. (2008), "Behaviour of steel reinforced slurry infiltrated fibrous concrete (SIFCON) two way slabs in punching shear", Indian Journal of Engineering Material Science, Vol. 15, August 2008, pp. 326-333.
- Sudarsana, R. H. and Ramana, N. V. (2005), "Behaviour of slurry infiltrated fibrous concrete (SIFCON) on simply supported two way slabs in flexure", Indian Journal of Engineering Material Science, Vol. 12, October 2005, pp. 427-433.
- Vavrušková, L., Čechmánek, R., Chromková, I. and Zavřel, L. (2016), "Fibre cement composites that have significantly influenced global architecture", Monograph 537 Mechanics, Diagnosis and material issues in the 20th century architecture, Cracow University of Technology Press, 2016, pp. 57-82.

EFFECT OF CELLULAR CONCRETE POWDER ON DURABILITY OF NORMAL STRENGTH CONCRETE

*Zoltán Gyurkó, Anna Szijártó, Mohammed Abed, Rita Nemes
Budapest University of Technology and Economics
Műegyetem rkp. 3, Budapest 1111, Hungary*

SUMMARY

Present research program is dealing with the effects of cellular concrete powder (CCP) on the compressive strength and durability of concrete. CCP is an industrial by-product, which was applied as supplementary cementitious material (SCM) in the concrete mix. In the previous research of the authors of this article, it was found that the cellular concrete powder, applied as an additive to the concrete mix, can increase the compressive strength and the resistance against freezing of concrete (Gyurkó, Szijártó, Nemes, 2017). In that paper, the results were compared to a reference mix and a mix that contains air-entraining agent, which is a typical solution to increase concrete durability. Increasing of durability can be done by the application of supplementary materials, like silica-fume or metakaolin. Present paper is dealing with the comparison of concrete with metakaolin and cellular concrete powder, on the basis of compressive strength and freeze resistance, using them as a cement substituting material. Different amount of metakaolin and CCP were added to the concrete mix, by substituting a given percentage (3, 10 or 17%) of cement with them. The results show the positive effect of both supplementary materials and based on present research the maximum amount of useful CCP can be approximated for the given concrete mix.

1. LITERATURE REVIEW

Concrete structures, that are exposed to the effect of the environment, have to be designed for durability as well. Normal concrete structures, without any external protection system, are sensitive for environmental effects, like freezing. There are different solutions that are applied, when one would like to improve the durability of concrete structures. One possibility is to add air-entraining agent to the concrete mix, which produces air bubbles in the concrete mix. It was found in the literature that is highly increasing freeze resistance of concrete (He *et al*, 2016). However, the price of air-entraining agent is high compared to the total price of concrete. Besides that, air-entraining agents have negative effect on the compressive strength of concrete and usage is not allowed in case of some application area (Łazniewska-Piekarczyk, 2013). Another solution is the application of supplementary cementitious materials (SCMs, like metakaolin and silica-fume), which lowers the porosity of the cement stone. It was shown that the lower the porosity of the cement stone, the better the durability performance of concrete (Nemes, Fenyvesi, 2013). Since cement is the most expensive component of the concrete mixture and major ingredient of the concrete mixture, partial or full replacement of it is considered as a sustainable solution toward enhancing the properties of concrete, decreasing the environmental impact of cement production and will also contribute to sustainable concrete (Abed, Nemes, 2017). Among of these typical SCMs, there is metakaolin, which lowers the porosity of the cement stone. When some portion of cement is replaced with metakaolin for manufacturing concrete, the compressive strength and durability (water absorption, water tightness, air permeability, chloride ion migration, freeze/thaw

resistance, damage by acidic solutions, abrasion resistance) of the concrete can be improved (Siddique and Klaus, 2009 and Gruber *et al.*, 2001).

Kaolinite clay (the raw material of metakaolin) can be locally available in large amounts in many countries (Cassagnabère *et al.* 2010). Metakaolin thus also holds promise for use in locations, where silica-fume cannot be produced. There are many researchers, who investigated the effect of metakaolin on the properties of concrete. It was found, that the optimal dosage of metakaolin as additive in high performance concrete is between 0 to 25% by mass of cement (Zeníšek *et al.*, 2017).

By using cement supplementary materials in the aggregate, small particles are introduced in the mix, which strengthens the material and increases its durability as well (Borosnyói, 2016). It was revealed that some new waste materials have the ability to improve various properties of concrete, which make them a suitable alternative of the traditional SCMs (Nehme, 2015; Abed, Nemes 2017).

As it was shown in the previous paper of present authors, a waste material that proved to be advantageous is cellular concrete powder (CCP), which is the result of the cutting process of cellular concrete bricks (Gyurkó, Szijártó, Nemes, 2017; Fenyvesi, Jankus, 2015). Another solution, which can be applied to increase durability is the decrease of water to cement ratio of the concrete mix).

2. PRELIMINARIES

Present paper is relies on a previous research of the authors (Gyurkó, Szijártó, Nemes, 2017), where the effect of different waste materials was discussed on the durability of normal strength concrete. Among those materials, the cellular concrete powder showed good performance in both strength and durability as well. There CCP was added to the concrete mix as an additive material with 10% amount compared to the cement in the mix. CCP increased the compressive strength of the reference mix significantly (+37%) and based on a freeze–thaw resistance test, the weight loss is decreased to the half. Present paper is dealing with the comparison of CCP and metakaolin as supplementary materials. Among the different kind of supplementary cementing materials (SCMs) the metakaolin was chosen, because it activates more Portlandite for the pozzolanic reactions, than silica fume (Borosnyói, 2016). However, the combined use of SCMs did not result in better performance neither in compressive strength, nor in durability.

3. LABORATORY EXPERIMENTS

3.1 Concrete mix design

The concrete mix applied in this research was designed to have a relatively low resistance against freezing. The aimed strength class was C25/30 in case of the reference mix, which is a typically used concrete strength in the industry. The aggregate was normal quartz gravel with the following distribution:

- **0/4 mm:** 47% (936 kg/m³),
- **4/8 mm:** 25% (498 kg/m³),
- and **8/16 mm:** 28% (557 kg/m³).

The maximum aggregate size was 16 mm. The applied cement was a CEM I 42.5 N type cement (270 kg/m^3), while the water to cement ratio was 0.57 in case of the reference mix. The above described mix was used as the reference mix, in which a given amount of cement was substituted by CCP or metakaolin in the other mixes. Finally, there were six different mixes:

- Reference: reference mix, as it described above,
- Y3: 3% of cement was substituted by CCP,
- Y10: 10% of cement was substituted by CCP,
- Y17: 17% of cement was substituted by CCP,
- MK10: 10% of cement was substituted by metakaolin,
- MK/Y 7/3: 10% of cement was substituted 7 % by metakaolin and 3% by CCP.

As it can be seen in the above list, in the present research it was intended to investigate the effect of CCP with different proportions as well as the interaction of metakaolin with CCP. It is important to mention that the aggregate size of the CCP is belonging to the 0/0.25 fraction, while the metakaolin is to the 0/0.018 fraction.

From the above-described mixes, 100 mm and 150 mm edge length cubes were casted and used during the laboratory experiments.

3.2 Test descriptions

The compressive strength of the mixes was determined at 28 days of age after wet curing of the 150 mm edge length specimens. The uniaxial compressive strength test was performed in an Alpha 3-3000 S hydraulic press with 5 kN/s (static) loading rate. The test was also done on samples, which were subjected to 50, 100 or 150 freezing cycles to determine their frost resistance. This type of test is typically applied to determine the frost resistance of vertical structures, like walls, pillars. The duration of a freezing cycle is 8 hours in a laboratory freezer, where after 2 hours of cooling the samples are kept on $-20 \text{ }^\circ\text{C}$ for another 2 hours, then after 2 hours of melting they are kept in $20 \text{ }^\circ\text{C}$ (\sim room temperature) for 2 hours. After the given number of cycles, compressive strength test is applied on the samples and the differences from the standard test results is observed.

Besides these the samples were subjected to freeze-thaw resistance test, which was performed based on the recommendations of the CEN/TS 12390-9:2007 standard (CEN, 2009). The samples were saw to half and on their sawn surface was the test performed. The other surfaces of the specimen were isolated and then in 5 mm thickness a test liquid (in our case 3 m% NaCl solution) was placed on the sawn surface. On the specimens in total 56 freeze-thaw cycles were applied. The freezing cycle is similar to the one previously described, but here every step lasts 6 hours instead of 2. After 7, 14, 28 and 56 cycles the samples were taken out from the freezer and the scaled material from the tested surface was removed and weighed. The higher amount of scaled material means lower resistance against freeze-thaw.

4. RESULTS AND DISCUSSION

4.1 Compressive strength test

As it can be seen in Fig. 1 the compressive strength of all mixes is higher, than the compressive strength of the reference mix. By applying more and more percentage of CCP the compressive strength is increasing until a given point (around 10%), after that it is decreasing. Fig. 1 shows that even the 3% of CCP is increasing the compressive strength.

At 10% of CCP content the strength increase was 34%. In the present research the maximum applied amount of CCP was 17% and until that point the compressive strength of the mix with CCP was higher than it was in case of the reference mix. It is important to see, that here the cement is substituted by a waste material, which means a significant cost reduction (in case of the higher dosages of CCP (10 and 17%)) without losing strength performance.

The highest increase was done by the 10% of metakaolin, which increased the compressive strength of the concrete with 61%. As it can be seen it is almost the double of the strength increase done by the 10% CCP, however it should be considered that CCP has no production cost because it is fully a waste material. Thus, by applying CCP instead of metakaolin, the material cost of concrete and the CO₂ emission caused by the metakaolin production process can be decreased (Szijártó, 2016). The mix that contained both CCP and metakaolin performed well, its value was between the Y10 and MK10 mixes. It means that the two materials can be mixed.

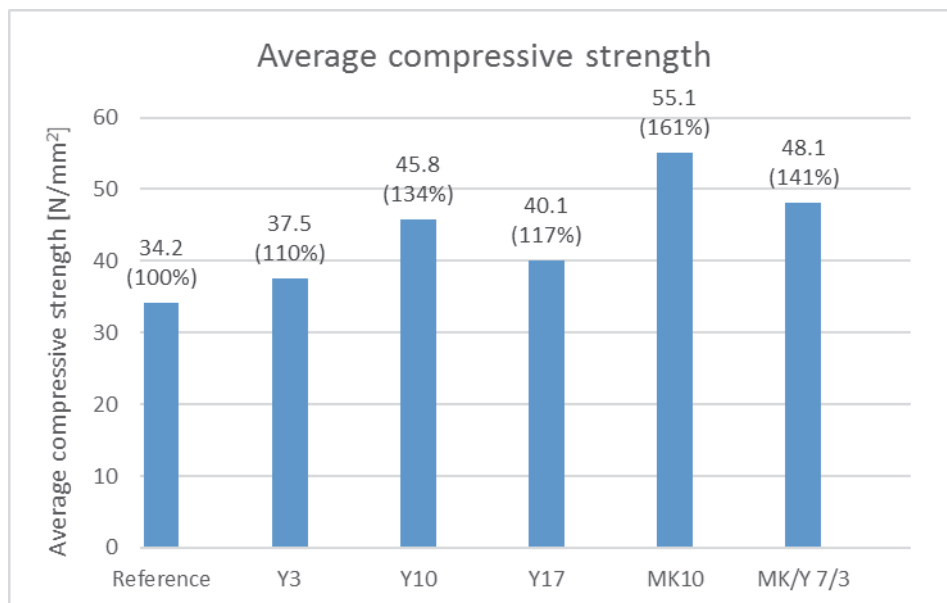


Fig. 1: Average compressive strength of the different mixes

4.2 Frost resistance test

In the Easter-European countries the most hazardous durability failure mode is freezing of the structures, therefore the specimens were subjected to the two most well-known freezing tests. Tab 1. and Fig. 2. show the results of the frost resistance tests applied in our samples. In the table the compressive strength of the samples after a given number of freezing cycles is shown. In the figure the compressive strength of the concrete before freezing (indicated by 0 number of cycles) and after 150 cycles of freezing can be seen. It is shown that how large strength drop was caused by the freezing cycles.

Tab. 1: Compressive strength before and after a given number of freezing cycles

Number of cycles	Compressive strength [N/mm ²]					
	R	Y3	Y10	Y17	MK10	MK/Y 7/3
0	35.1	40.0	47.0	36.6	58.6	51.4
50	32.8	33.3	39.9	33.4	45.6	43.7
100	32.8	34.9	41.3	33.0	40.1	42.3
150	25.0	32.3	35.6	18.6	35.0	43.0

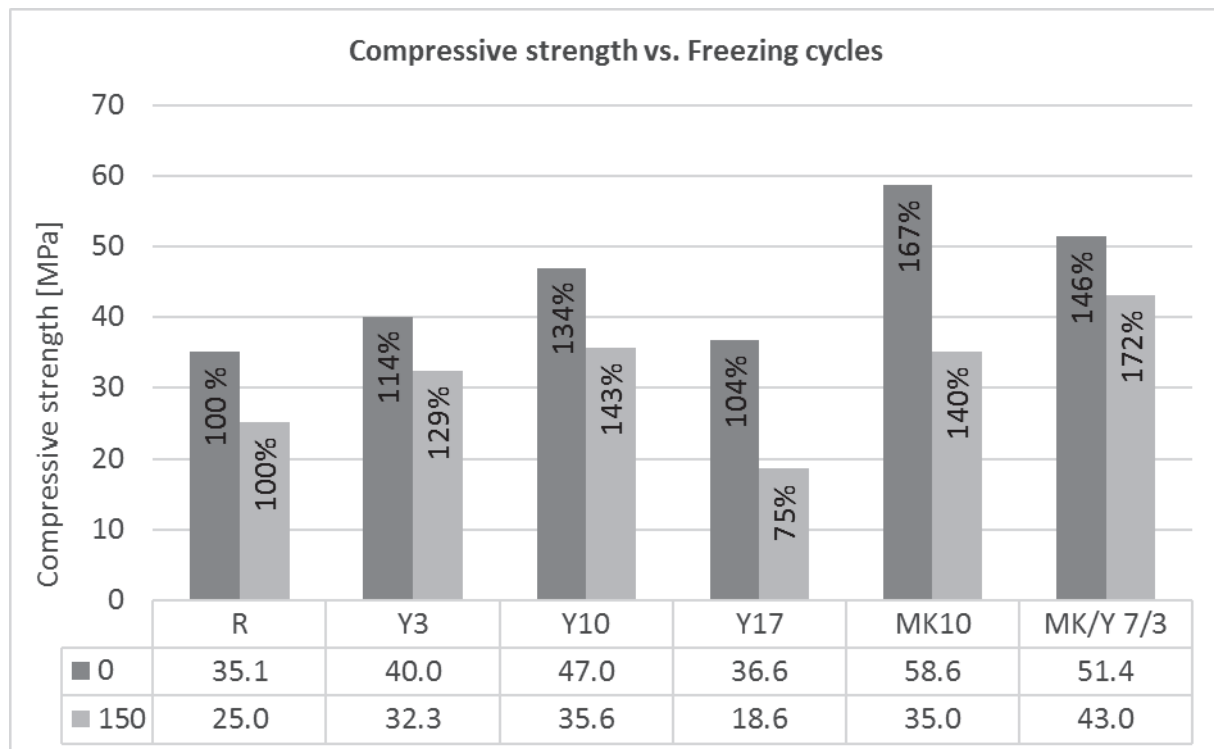


Fig. 2: Compressive strength before freezing and after 150 freeze cycles

In Fig. 2 it can be seen that the best performances were done by the mix with 3% of CCP and the mix, where the metakaolin and the CCP were combined. In case of those two mixes the strength drop (the difference between the value belonging 0 and 150 freezing cycles) was the lowest. The figure shows that the compressive strength (after 150 cycles) of the mix with 3% of CCP was almost equal to the mix with 10% of CCP. It can be seen as well, that by applying too much of CCP (Y17) the strength drop can be even higher, than it was in case of the reference mix. After the freezing cycles the MK10 mix showed a significant strength drop and it can be seen that the mix with 10% of CCP performed slightly better, which indicates that metakaolin can be substituted by CCP.

4.3 Freeze-thaw test

The deterioration of the concrete surface was determined by freeze-thaw test and the weight loss of the material was measured. Fig. 3 shows the results, where it can be seen that the reference mix had the highest amount of scaled material, while the mix with 3% of CCP and the mix, where the metakaolin and the CCP were combined, have the least. In case of this test all the mixes performed better, than the reference mix, as it was planned at the mix design phase. The worst performance, among the mixes with supplementary material, was achieved by the mix with 17% of CCP. The mix with 10% of metakaolin and with 10% of CCP were between the previously mentioned mixes. By comparing these two mixes with 10% of supplementary material, it can be seen that the CCP performed better, than the metakaolin in this test too.

Despite of the decrease of the scaled material non of the mixes reached the limits of the XF2 environmental class (max 2000 g/m²), but this was not expected from a C25/30 strength class concrete. It would be also useful to see the effect of CCP for a higher strength concrete with higher cement content as well.

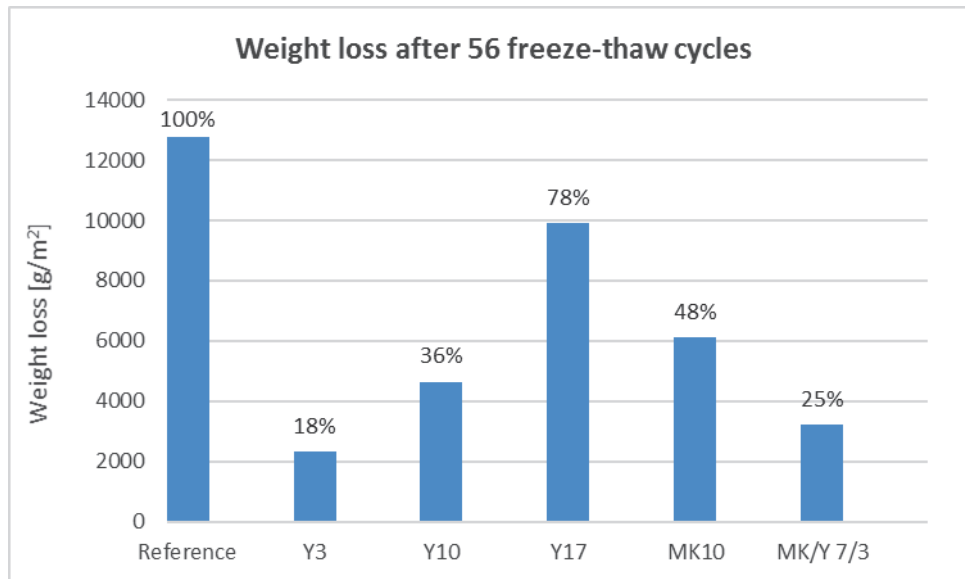


Fig. 3: Weight loss of the samples after 56 freeze-thaw cycles

5. CONCLUSIONS

In a previous study it was shown, that cellular concrete powder (CCP) as an additive can have a positive effect on both compressive strength and durability as well. Present study introduced the application of CCP as a supplementary material (a given amount of cement was substituted by waste material), aiming to increase the durability of normal strength concrete. Compared to the other possibilities the application of a waste material can significantly decrease the cost of a concrete mix. Three different mixes containing CCP, one containing metakaolin, one with both CCP and metakaolin and a reference mix were casted. The reference mix was designed to have low frost resistance. The specimens were subjected to compressive strength test, frost test and freeze-thaw test and the effect of the additives was observed.

Based on the results, it can be seen that a given amount of CCP can increase the strength and durability of concrete as well (~10%), however too much of it can cause detrimental effects, especially in compressive strength (~17%). It was also shown, that the correct amount of CCP can have a better performance, than the metakaolin has on the durability of concrete, despite that metakaolin increases the compressive strength more, than CCP. However, it is also important to see that CCP is completely a waste material without any need of production and preparation, which means a significant decrease in cost and in CO₂ emission as well.

The results indicate that the combination of the two investigated supplementary material can be advantageous for many applications. The combined mix performed well on the durability tests and it increased significantly the compressive strength. It was not as advantageous in the freeze-thaw test as the mix with 3% of CCP and it did not increase the compressive strength as the 10% of metakaolin, however it had the best performance on the frost resistance test.

Lastly, it can be proved that the correct amount of CCP or the combination of CCP and metakaolin can increase both the strength and the durability of normal concrete, without highly influencing the cost of the material.

6. FUTURE STUDIES

As a continuation of the present research, authors are intending to widen the investigations for concretes with higher cement amount and with different types of cement. Presented studies dealt with concrete mixes, which were less than 60 days old. Thus the authors are intending to investigate samples, which were stored for longer time.

7. ACKNOWLEDGEMENTS

Authors are grateful to the Hungarian Scientific Research Fund (OTKA) for the financial support of the OTKA K 109233 research project.

Special thanks to Bengineer House Kft., Duna-Dráva Cement Kft., SIKÁ Hungária Kft., MC-Bauchemie Kft. and BASF Hungária Kft. for providing the materials used in the experiments.

8. REFERENCES

- Abed, M., Nemes, R. (2017), „Possibility of Producing Green, Self-Compacting, High Performance Concrete (GSCHPC), Concrete Structures, Vol. 18, pp. 21-29.
- Borosnyói, A. (2016), “Long term durability performance and mechanical properties of high performance concretes with combined use of supplementary cementing materials”, Construction and Building Materials, Vol. 112, pp. 307–324.
- Cassagnabère, F., Mouret, M., Escadeillas, G., Broilliard, P., Bertrand, A. (2010), „Metakaolin, a solution for the precast industry to limit the clinker content in concrete: mechanical aspects”, Construction and Building Materials, Vol. 24(7), pp.1109–1118.
- European Committee for Standardization (CEN), CEN/TS 12390-9 Testing hardened concrete - Part 9: Freeze-thaw resistance - Scaling, p 24.
- Fenyvesi, O., Jankus, B. (2015), “Opportunities in recycling AAC waste as aggregate for lightweight concrete”, Építőanyag - Journal of Silicate Based and Composite Materials, Vol. 67, pp. 66–70.
- Gruber, K. A., Ramlochan, T., Boddy, A., Hooton, R. D., Thomas, M. D. A. (2001), “Increasing concrete durability with high-reactivity metakaolin”, Cement and Concrete Composites, Vol. 23(6), pp. 479–84.
- Gyurkó, Z., Szijártó, A., Nemes, R. (2017), “Increasing freeze-thaw resistance of concrete by additions of powdered cellular concrete and clay bricks”, Procedia Engineering, Vol.193C, pp. 11-18.
- He, Z., Tang, S. W., Zhao, G. S., Chen, E. (2016), “Comparison of three and one dimensional attacks of freeze-thaw and carbonation for concrete samples”, Construction and Building Materials, Vol. 127, pp. 596–606.
- Łazniewska-Piekarczyk, B. (2013), “The frost resistance versus air voids parameters of high performance self-compacting concrete modified by non-air-entrained admixtures”, Construction and Building Materials, Vol. 48, pp. 1209–1220.
- Nehme, S. G. (2015), „Kiegészítőanyagok hatása a szokványos és az öntömörödő betonokra 2. rész. Laboratóriumi vizsgálatok”, Építőanyag – Journal of Silicate Based and Composite Materials, Vol. 67 (2), pp. 72-78.
- Nemes, R., Fenyvesi, O. (2013), Frost resistance of LWAC made with different lightweight aggregates in urban environment, CCC 2013 – Concrete Structures in Urban Areas, Wrocław, Poland. pp. 478–481.
- Siddique, R., Klaus, J. (2009), “Influence of metakaolin on the properties of mortar and concrete: a review”, Applied Clay Science, Vol. 43(3–4), pp. 392–400.

Szijártó, A. (2016), "Performance studies of concretes containing perlite supplementary cementitious material", Bachelor Thesis, Budapest University of Technology and Economics, Budapest, Hungary.

Zeníšek, M., Vlach, T., Laiblová, L. (2017), „Dosage of Metakaolin in high performance concrete”, Key Engineering Materials, Vol. 722, pp. 311–315.

EARLY-AGE MECHANICAL PROPERTIES OF RECYCLED AGGREGATE CONCRETE

Zeger Sierens, Miquel Joseph, Luc Boehme, Jiabin Li

*KU Leuven, Technology Campus Bruges, Faculty of Engineering Technology, Department of Civil Engineering, Technology Cluster Construction
Sporwegstraat 12, 8000 Bruges, Belgium*

SUMMARY

The use of small amounts of recycled concrete aggregates (RCAs) is frequently asked in the precast industry in many European countries to enhance the sustainability of the products. The early age and time-dependent properties of concrete with RCAs, often called recycled aggregate concrete (RAC), are of crucial importance to examine the feasibility of the utilisation of RCAs in precast concrete components. This paper provides a study on the mechanical properties of RAC at early ages, including the compressive strength, the splitting tensile strength and the modulus of elasticity, based on available data in literature and recent test results by the authors. The developments of the mechanical properties of RAC with time are studied. The suitability of the equations given in EN 1992-1-1:2004 (which are developed for conventional concrete) for RAC is also examined.

1. INTRODUCTION

The protection of natural resources and sustainable development play an essential role in the modern requirement of construction works. The use of recycled concrete aggregates (RCAs) has increased due to extensive research and the regulations, which allow the use of more and more RCAs. A large amount of studies has reduced the uncertainty related to the performance of concrete with RCAs, which is often called recycled aggregate concrete (RAC). Many researches have shown that the use of RCAs in non-structural concrete is both technically feasible and economically viable. However, more research is required for new and high-grade applications of RCAs and RAC.

One promising application of RCAs is in precast/prestressed concrete. Precast manufacturers and clients are frequently asking about the improvements of the carbon footprint of building products, as sustainability is an important issue in today's construction projects. Sustainable materials and waste management are the key to reduce the carbon footprint of constructions.

Systematic research on the use of RCAs is necessary to determine the viability of this material in precast concrete. Precast concrete requires different and generally stricter quality control in comparison with on-site cast concrete. To examine the feasibility of using RCAs in precast concrete, information about the time-dependent material properties of RAC at early ages is needed. This paper presents a study on the development of the strength and stiffness of RAC in the period between 1 to 28 days. The effect of RCAs on the strength and stiffness gain of concrete is investigated. In addition, the suitability of the code equations given in EN 1992-1-1:2004 (which are developed for concrete with natural aggregates) for RAC is examined.

2. EARLY-AGE PROPERTIES

There is no widely accepted definition on the early-age period for concrete. It depends mostly on the investigated property. In other words, the time required to achieve a certain level of a desired property is perceived as the early age (Nehdi and Soliman, 2011). For the use of concrete in precast components, the development of the compressive strength, tensile strength and elastic modulus with time is very important for the quality insurance and the safety of the precast products.

Compressive strength

The compressive strength of concrete generally increases with time. In the early age (prior to 28 days), the strength gain is rapid. This gain is depended by different factors such as the cement type and curing condition as well as the water-cement ratio, air entrainment, aggregate, admixtures, etc. Many experiments have been carried out on the influence of the RCAs on the compressive strength (Silva et al., 2014). It was found that the replacement percentage and the quality of the RCAs can have an important influence on the compressive strength of concrete. However, most of the studies are often based on the compressive strength at an age of 28 days.

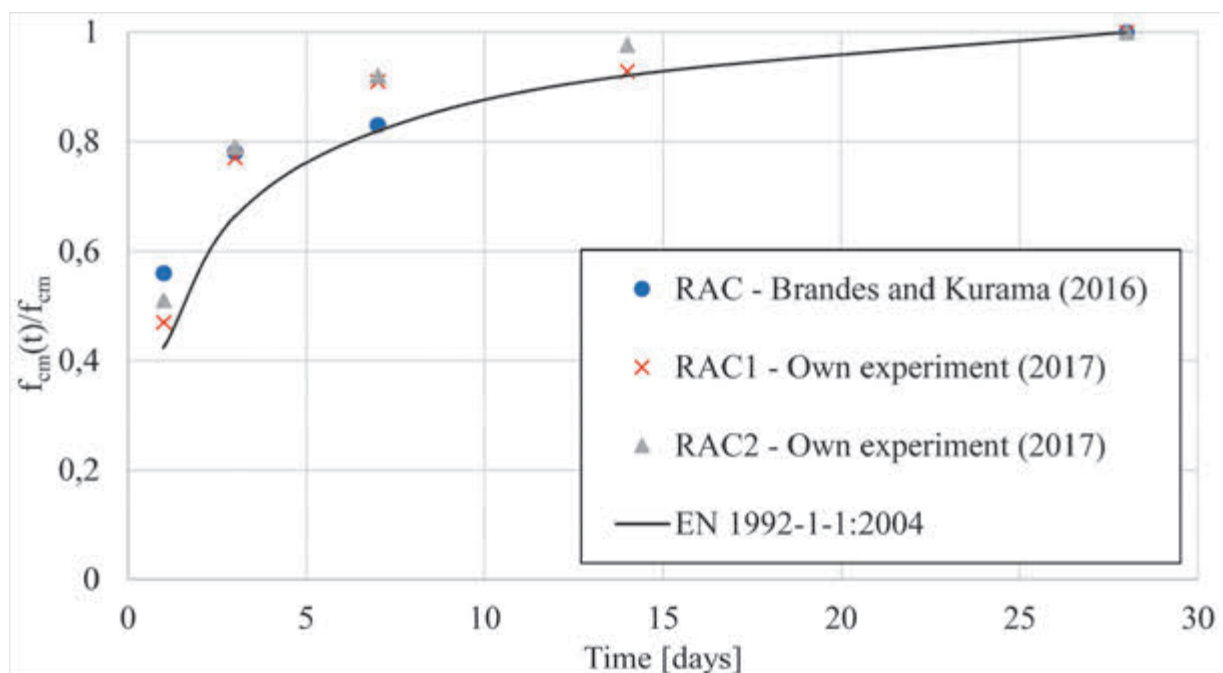


Fig. 1: Compressive strength development of RAC

Fig. 1 shows some test data on the development of the compressive strength of concrete with RCAs. These include the test results reported by Brandes and Kurama (2016) and the recent data by the authors of this paper. In the experiments of Brandes and Kurama (2016), the used cement was type III cement according to ASTM, which is high early strength cement. The natural coarse aggregates were completely replaced with RCAs, which had a water absorption of 8.16%. In the tests by the authors, CEM I 52.5 R cement according to European Standards was used. The RCAs had a water absorption of 4.4%, which replace 10% (RAC1) and 20% (RAC2) of the natural coarse aggregates by volume. The two groups of test data were selected since both tests used rapid hardening cement, which is commonly used in the precast industry in Flanders.

It can be seen from the figure that the concretes with RCA exhibit a rapid concrete gain in the early age, especially prior to 7 days, irrespective of the RCA replacement percentage. After that, the rate of the strength gain decreases. This is, in fact, in consistent with the compressive strength development of conventional concrete, that is, natural aggregate concrete (NAC). The difference between the strength developments of the two groups of test data is due to the difference in the used cement, the quantity and quality of the RCAs and water reducing admixtures.

In EN 1992-1-1:2004, the following equation (1) is recommended to predict the compressive strength of natural aggregate concrete (NAC) at various ages.

$$f_{cm}(t) = [\beta_{cc}(t)] f_{cm}$$

$$\beta_{cc}(t) = \exp \left\{ s \left[1 - \left(\frac{28}{t} \right)^{1/2} \right] \right\} \quad (1)$$

where: $f_{cm}(t)$ compressive strength of concrete at time t
 f_{cm} compressive strength of concrete at 28 days
 $\beta_{cc}(t)$ is a coefficient which depends on the age of the concrete t
 t is the age of the concrete in days
 s is a coefficient, which depends on the type of cement.

Fig. 1 shows a comparison of the predictions of equation (1) (with $s = 0.20$ for rapid hardening cement) with the test data. It can be seen the equation (1) yields somewhat underestimations of the strength development of the RACs prior to 7 days. More data is required to develop a more accurate equation to estimate the compressive strength development of concrete with RCAs.

The 7 day compressive strength of concrete is an important parameter to check the quality of the concrete in the construction site. Due to this reason, many tests on the 7 day compressive strength of RAC were carried out in literature. In Tab. 1, some test data are presented. In this table, results on both specimens with normal hardening cement and rapid hardening cement are included. Compared to NAC, the $f_{cm}(7)/f_{cm}$ ratio for RAC is slightly smaller, indicating a slightly slower development of the compressive strength of RAC. This might be due to a later reaction of unhydrated cement of the adhered mortar present on the surface of RCAs and/or retarded absorption of water by RCAs (Manzi et al., 2013). However, the difference between the strength development of RAC and NAC is rather small.

Tensile strength

Knowledge about the early age tensile strength of concrete is needed to assess the early-age loading and cracking in concrete, which can affect the strength and stiffness of the structure. There are different methods to test the tensile strength of concrete: uniaxial tensile strength, splitting strength and flexural tests. The use of RCAs can influence of the tensile behaviour of concrete (Silva et al., 2015), especially the flexural strength of concrete since RCAs normally have an angular shape, which leads to a higher flexural strength than natural coarse aggregates.

Tab. 1: $f_{cm}(7)/f_{cm}$ of RAC

Reference	Replacement ratio [%]	Cement Type	Curing condition	WA ₂₄ RCAs [%]	$f_{cm}(7)$ [MPa]	f_{cm} [MPa]	$\frac{f_{cm}(7)}{f_{cm}}$
Brandes and Kurama (2016)	0	Rapid hardening	un-known	-	unknown	unknown	0.90
	100			8.16			0.89
Own experiments (2017)	0	Rapid hardening	20°C 95% RH	-	70.47	76.67	0.92
	10			4.4	68.00	75.46	0.90
	20			4.4	68.08	73.87	0.92
Rahal (2007)	0	Rapid hardening	un-known	-	21.2	32.3	0.66
	100			3.47	18.9	30.7	0.62
	0			-	32.5	46.0	0.71
Gonzales and Etxeberria (2014)	100	Rapid hardening	un-known	3.47	26.5	39.4	0.67
	0			-	91.19	102.09	0.89
	20			Rapid hardening	18-23°C 95% RH	5.91	91.73
Adnan et al. (2007)	50	Normal hardening	un-known	5.91	84.39	96.84	0.87
	100			5.91	79.88	91.23	0.88
	0			-	34.4	56.6	0.61
Santos et al. (2002)	25	Normal hardening	un-known	3.34	29.9	44.2	0.68
	50			3.34	27.1	43.2	0.63
	75			3.34	23.2	32.1	0.72
	100			3.34	21.8	38.1	0.57
Schoppe (2011)	0	Normal hardening	23°C 52% RH	-	37.1	42.8	0.87
	50			4.9	31.8	39.3	0.81

In Fig. 2, the test data for the relative tensile strength development of RAC in two studies are presented. The data are from the tests of Adjukiewicz and Kliszczewicz (2002) and recent tests of the authors of this paper. In the former, a rapid hardening cement PC30 was used and the natural coarse aggregates were completely replaced by RCAs; while in the latter, a CEM I 52.5 R cement was used and the RCAs replaced 10% (RAC1) and 20% (RAC2) of the natural coarse aggregates, as mentioned in section 2.1. Both groups of data are derived from splitting tensile tests. It can be seen from the figure that the tensile (splitting) strength of the RACs increases with time, similar to the compressive strength, as shown in Fig. 1. This is also in consistent with NAC. In addition, the data from the two tests are fairly comparable.

In EN 1992-1-1:2004, the following equation (2) is utilised to describe the time dependent tensile strength of NAC.

$$f_{ct,sp}(t) = [\beta_{cc}(t)]^a f_{ct,sp} \quad (2)$$

where: $f_{ct,sp}(t)$ splitting tensile strength of concrete at time t
 $f_{ct,sp}$ splitting tensile strength of concrete at 28 days
 $\beta_{cc}(t)$ is defined in equation (1)
 t, s are defined in equation (1)
 a is a coefficient; $a = 1$ for $t < 28$ days

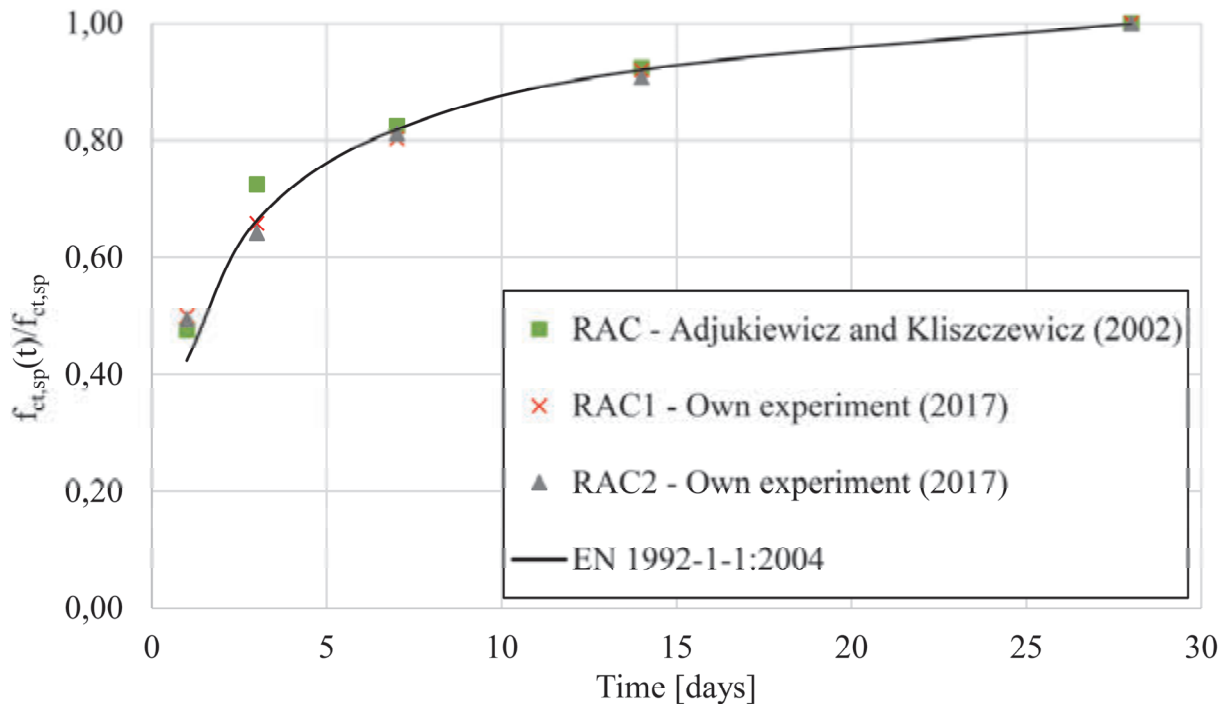


Fig. 2: Development of tensile (splitting) strength of RAC

A comparison of the predictions of equation (2) (with $a = 1$, $s = 0.20$) is also illustrated in Fig. 2. It is evident from the figure that the predictions are in good agreement with the test data. The largest difference between the predicted and test data is the tensile strength at 1 day. The equation gives a slight underestimation of this value.

Modulus of elasticity

The modulus of elasticity indicates the concrete's capability to deform elastically. It is obtained from the stress-strain curve at a certain stress level relative to the ultimate strength (Mang et al., 2005). The use of RCAs results in a more pronounced influence on the modulus of elasticity of concrete, in comparison to the compressive and tensile strength. The test data indicated that a 5% to 20% decrease of the 28 day modulus of elasticity of concrete when the RCAs replaced up to 50% of the natural coarse aggregates (Boehme and Joseph, 2016; Gonzalez and Etxeberria, 2014; Kou et al., 2012).

Laboratory tests on the modulus of elasticity of RAC at various ages are very limited in the literature. In Fig. 3, the test data by Brandes and Kurama (2016) as well as that by the authors of this paper are illustrated. Some details of the tests, such as the cement type and the information of the RCAs are given in Section 2.1.

It can be seen from the figure that the data from the two tests show quite consistent trend, that is, the modulus of elasticity of RAC increases with time. There are some small discrepancies in the test data between the two sources. This is caused by the different quantity and quality of the RCAs.

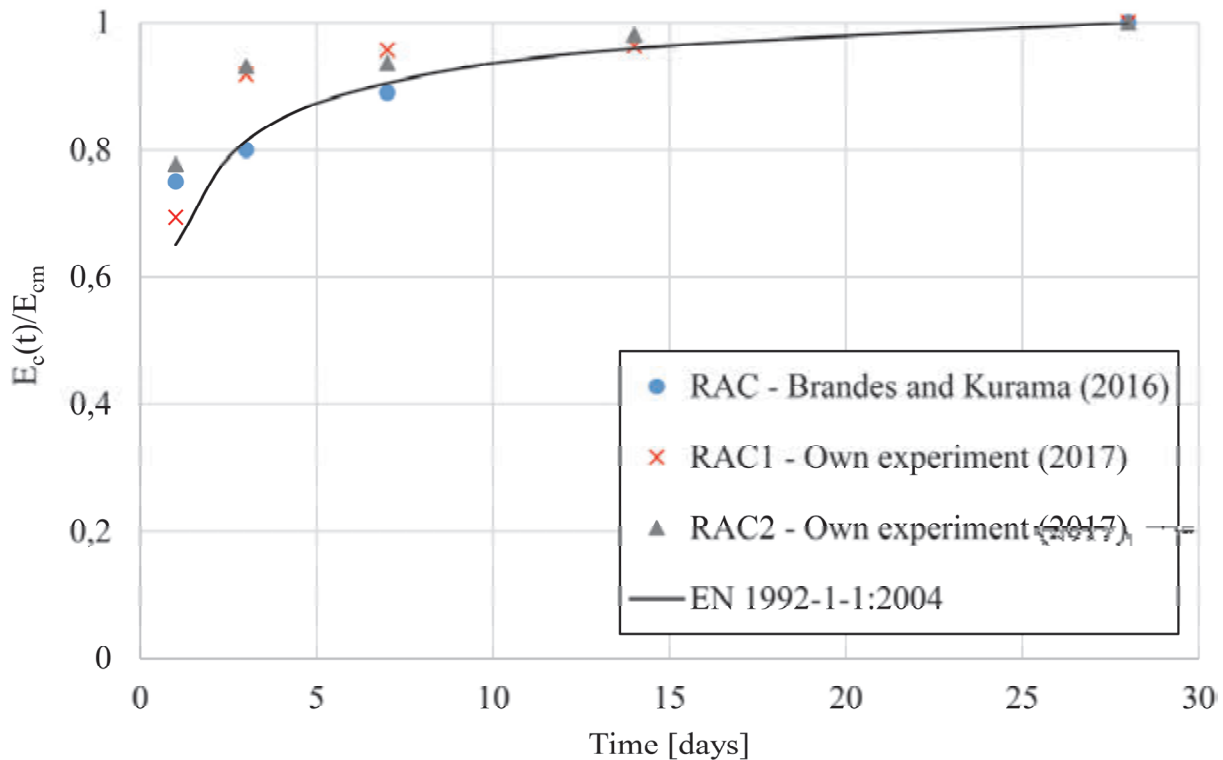


Fig. 3: Development of modulus of elasticity of RAC

The following equation, i.e., equation (3) is used in EN 1992-1-1:2004 for estimating the development of the modulus of elasticity of NAC with time.

$$E_c(t) = [\beta_{cc}(t)]^{1/2} E_{cm} \quad (3)$$

Where: $E_c(t)$ elastic modulus of concrete at time t
 E_{cm} elastic modulus of concrete at 28 days
 $\beta_{cc}(t)$ is defined in equation (1)
 t, s are defined in equation (1)

The predictions of equation (3) are also presented in Fig. 3. It can be observed from the figure that the predictions are in fairly good agreement with the test data. However, due to the limited test data, it is difficult to quantify clearly the influence of the quantity and quality of the RCAs on the development of the modulus of elasticity of concrete in the early ages.

3. CONCLUSIONS AND REMARKS

This paper presents a study on the compressive strength, tensile strength and modulus of elasticity of RAC at early ages. Based on discussions of the test data in the literature and that of recent tests by the authors, the following conclusions can be drawn:

- (1) The compressive strength, tensile (splitting) strength and elastic modulus of RAC at early ages increase with the curing time. The increase rate of the mechanical properties is larger in the first 7 days in comparison to that after 7 days;
- (2) The equations in EN 1992-1-1:2004 for the time-dependent compressive strength, tensile (splitting) strength and modulus of elasticity of NAC, can generally provide a satisfactory description of the properties of RAC at early ages;

- (3) Due to the limited test data, it is not yet possible to accurately investigate the effect of the quantity and quality of RCAs on the strength and modulus of elasticity developments of concrete. More test data are obviously required;
- (4) In addition to the strength and modulus of elasticity, knowledge about the shrinkage and creep behaviour of RAC at early ages is also required to examine the feasibility of the use of RCAs in precast concrete.

4. LIST OF NOTATIONS

NAC	Natural aggregate concrete
RCA	Recycled concrete aggregates
RAC	Recycled aggregate concrete
WA ₂₄	Water absorption of the aggregates after 24h submersion

5. ACKNOWLEDGEMENTS

This research work herein has been supported by a start-up funding at KU Leuven – University of Leuven, Belgium (No. STG/16/011). This financial support is gratefully acknowledged.

6. REFERENCES

- Adnan, S. H., Loon, L. Y., Rahman, I. A., Saman, H. M., and Soejoso, M. V. (2007), “Compressive strength of recycled aggregate to concrete with various percentage of recycled aggregate”, National seminar on civil engineering research, Skudai.
- Ajdukiewicz, A., and Kliszczewicz, A. (2002), “Influence of recycled aggregates on mechanical properties of HS/HPC”, *Cement & Concrete Composites*, Vol. 24, No.2, pp. 269-279.
- Boehme, L., and Joseph, M. (2016). “Assessment of the E-modulus of recycling concrete with different replacement rate”, CESB16; Materials, Technologies and Components for Sustainable Building, Prague.
- Brandes, M. R., and Kurama, Y. C. (2016). “Use of recycled concrete aggregates in precast/prestressed concrete”, *Procedia Engineering*, Vol.145, pp. 1338-1345.
- Gonzalez, A., and Etxeberria, M. (2014), “Experimental analysis of properties of high performance recycled aggregate concrete”, *Construction and Building Materials*, Vol. 52, pp. 227-235
- Kou, S.-C., Poon, C.-S., and Wan, H.-W. (2012), “Properties of concrete prepared with low-grade recycled aggregate”, *Construction and Building materials*, Vol.36, pp. 881-889.
- Mang, T., Liu, Y., and Brown, D. (2005), “Modulus of elasticity, creep and shrinkage of concrete”, Research Report, Florida, USA.
- Manzi, S., Mazzotti, C., and Bignozzi, M. (2013), “Short and long-term behavior of structural concrete with recycled concrete aggregate”. *Cement & Concrete Composites*, Vol. 37, pp. 312-318.
- Nehdi, M. L., and Soliman, A. (2011), “Early-age properties of concrete: Overview of fundamental concepts and state-of the art research”, *Proceedings of the Institution of Civil Engineers - Construction Materials*, Vol. 164, No. 2, April 2011, pp. 57-77.
- Rahal, K. (2007), “Mechanical properties of concrete with recycled coarse aggregate”, *Building and Environment*, Vol. 42, pp. 407-415.

- Santos, J. R., Branco, F. A., and de Brito, J. (2002), "Compressive strength, modulus of elasticity and drying shrinkage of concrete with coarse recycled concrete", World Congress on Housing, Portugal.
- Schoppe, B. M. (2011), "Shrinkage & Modulus of Elasticity in Concrete with Recycled Aggregates", Dissertation, California Polytechnic State University, USA.
- Silva, R., de Brito, J., and Dhir, R. (2014), "The influence of the use of recycled aggregates on the compressive strength of concrete: a review", European Journal of Environmental and Civil Engineering, Vol. 19, No.7, pp. 825-849.
- Silva, R., Dhir, R., and de Brito, J. (2015), "Tensile strength behaviour of recycled aggregate concrete", Construction and Building Materials, Vol.83, 15 May 2015, pp. 108-118.

CHARACTERIZATION OF PORTLAND CEMENT COMPOSITES PREPARED BY A DISPERSION OF CARBON NANOTUBES ON CEMENT PARTICLES

Vanessa V. Rocha¹, Péter Ludvig²

¹ Masters Student in Civil Engineering, Department of Civil Engineering, Federal Centre for Technological Education of Minas Gerais, Campus II, Av. Amazonas, 7675, Nova Gameleira, Belo Horizonte, Brazil

² Professor, Department of Civil Engineering, Federal Centre for Technological Education of Minas Gerais, Campus II, Av. Amazonas, 7675, Nova Gameleira, Belo Horizonte, Brazil
peter@civil.cefetmg.br

SUMMARY

The hydrophobic behaviour of CNTs is a main challenge to the incorporation on cement composites. In this paper, MWCNTs at proportion of 0%, 0.05% and 0.10% of cement weigh, without any surface treatment, were mixed in a non-aqueous isopropanol media and unhydrated Portland cement and were sonificated during 2 hours. After that, the isopropanol was evaporated, water was added to the mixture of cement and CNTs, and pastes were prepared and moulded. Completed 28 days, the cement pastes were tested by the compression and splitting tensile strengths method. Results indicated a better performance of cement nanocomposites. Incorporation of 0.05% of CNTs achieved gains of approximately 50% in both compressive and splitting tensile strengths. The results suggests a reinforcement due to the presence of CNTs and/or the nanomaterial acted as nucleation sites for cement hydration product formation leading to a matrix densification.

1. INTRODUCTION

Carbon nanotubes (CNTs) are hollow tubular channels, formed by graphene laminated sheets. They can be classified as single-walled (SWCNTs) when they have a simple cylindrical layer of graphene or as multiple-walled (MWCNTs) formed by the joining of two or more single cylindrical layers.

Due to the extraordinary properties, as a high tensile strength, the incorporation of the CNTs in civil construction materials has been studied. Recent research has shown that the incorporation of this nanomaterial allows improvements in the mechanical properties of cementitious compounds (REFs). However, the hydrophobic nature of CNTs makes the dispersion a challenge to the cement pastes production. CNTs tend to agglomerate and form granules in presence of water, and those clusters contribute to weaken the cement pastes mechanical properties. A good dispersion is crucial for the improvement of cement composites mechanical strength.

According to (MELO *et al.*, 2011) there is an optimal range for the incorporation of CNTs in Portland cement particles. For a given dispersion technique there is an optimum CNT content and the excess of nanomaterial lead to granules formation that compromise the mechanical performance and durability of cement pastes. All optimal CNT contents in cement paste or

mortar composites found in the literature were in the order of 0.01-0.5% in mass with respect to cement weight (REFs).

The CNTs can be surface-treated to achieve a better dispersion, resulting in an increase of the dispersive properties. According to FILHO and FAGAN (2007) there is a treatment through noncovalent and covalent interactions, the so-called functionalization. The noncovalent interactions are weak bonds with CNTs, conversely, the covalent interactions are strong and can cause modifications in the CNTs properties. Non-covalent functionalization of CNTs can be achieved by the use of surfactants such as concrete admixtures (COLLINS *et al.*, 2012). However, the amount of surfactant necessary to achieve a good dispersion of CNTs has negative effects on cement hydration which limits the quantity of CNTs to be incorporated in cement matrixes (LIU *et al.*, 2007). On the other side, the most common covalent functionalization involves the use of strong acids in processes that are not suitable for large scale production that is needed for the application in cement based materials (YU *et al.*, 2007).

According to PAULA *et al.* (2014), researchers have studied two methods of dispersion currently. The first one involves a previous dispersion in sonicating surfactant, allowing covalent interaction between the materials. The other method is an attempt to spread the CNTs in the cement or other grain particles. There are two known methods for this dispersion: or by the in situ synthesis of the CNTs on ground Portland cement clinker particles (LUDVIG *et al.* 2011) or by suspending the CNTs in a non-aqueous medium, to avoid hydration of the cement, also with ultrasonic frequencies (MAKAR and CHAN, 2009).

The in-situ synthesis on clinker produces lower quality nanotubes, but can be easily upgraded to industrial scale. The addition of this nanostructured clinker resulted in similar effects on the rheology of fresh paste (PAULA *et al.*, 2014), on the mechanical behaviour (LUDVIG *et al.*, 2011), and on the microstructure (LUDVIG *et al.*, 2017) as the addition of high quality CNTs.

The research published by MAKAR and CHAN (2009), using images obtained from a high resolution electron microscope, indicated good dispersion of SWCNTs on Portland cement grains, after 2 hours sonication in non-aqueous isopropanol media. The authors also observed that the dispersed CNTs in the cement matrix act as nucleation sites for calcium silicate hydrate (C-S-H) formation, which is responsible for the strength and durability of cement pastes, suggesting a good interaction between the C-S-H and CNTs.

Currently, there is no accepted method able to quantify the dispersion of carbon nanotubes in the cement matrix. An indirect method adopted by some researchers is the analysis of the mechanical behaviour of cementitious composites. Considering this information and the results obtained by (MAKAR and CHAN, 2009), the present paper aims to evaluate the mechanical performance of cement pastes with 0%, 0.05% and 0.10% of non-functionalized MWCNTs in a non-aqueous isopropanol media and sonification for 2 hours.

2. MATERIALS AND METHODS

2.1. Materials

The nanotubes used were multi-walled type (MWCNTs), with estimated tube lengths between 5 μm and 30 μm , 99% of external diameter between 10 nm and 50 nm, and purity greater than 93%. CNTs were produced in the Nanomaterials Laboratory of the Physics Department of the

Federal University of Minas Gerais (UFMG). Brazilian Type CP-V Portland cement, produced by Holcim, was used because of the low percentage of mineral additions. The isopropanol used was absolute grade of EMFAL brand.

2.2. CNTs dispersion

The dispersion process began with the mix of CNTs and approximately 30 ml of isopropanol. The mixture was shaken and sonicated on ultrasonic apparatus with 42 Hz frequency during 30 minutes. In sequence, 300 grams of cement was added with further isopropanol (approximately 200 ml). The suspension was mechanically shaken at 500 rpm and sonicated for additional 2 hours. Fig. 1 illustrates this process.



Fig. 1: Mixture of cement, CNTs and isopropanol in the ultrasonic bath being mechanically agitated

After 24 hours, the isopropanol was completely evaporated, and the dry mixture of cement and CNTs were used for cement paste preparation.

2.3. Cement Paste Preparation

The cement paste was prepared in a mortar blender, as described in the Brazilian National Standard for the determination of consistency of cement pastes (ABNT NBR NM 43: 2003). First the mixing water was placed in the batch, the CNTs dispersed on cement particles together with the remaining cement were added subsequently. Tab. 1 describes the proportion of materials used for the production of pastes with and without CNTs dispersed on unhydrated Portland cement particles. Three cement paste types were mixed with water cement ratio of 0.33. The first paste was the reference, using only cement and water (0% of CNTs). The second, in addition to cement and water, contained a proportion of 0.05% carbon nanotubes with respect to cement weight. The third type incorporated 0.10% of carbon nanotubes.

Tab. 1: Proportions of materials used to prepare cement pastes with CNTs dispersed on cement particles

Identification	Materials	Weight Composition (g)
REF-ISO-P	CP-V Cement	3.000,00
	Water	990
0.05%-ISO-P	CP-V Cement	3.000,00
	Water	990
	CNTs	1,5
0.10%-ISO-P	CP-V Cement	3.000,00
	Water	990
	CNTs	3

Following the paste preparation, prismatic specimen with 5 cm of diameter and 10 cm height were moulded and vibrated on a vibrating table for 1 minute. The moulds were demoulded after 24 hours and bathed in a tank of lime saturated water until reaching the age of 28 days. For each type, 8 cylindrical specimens were moulded: 4 for compressive strength test and 4 for splitting tensile strength test.

2.4. Compressive strength test and splitting tensile strength test

After 28 days, the test specimens' surfaces were regularized for uniform stress distribution in compressive strength test. After that, they were measured and tested on a universal EMIC brand test equipment with load cell of 300 kN for compressive strength test and 20 kN for splitting tensile strength test. The load increment was 0.20 MPa/sec and 1mm/min respectively. Fig. 2 a) and Fig. 2 b) illustrate the compressive strength test and splitting tensile strength test setups, respectively.

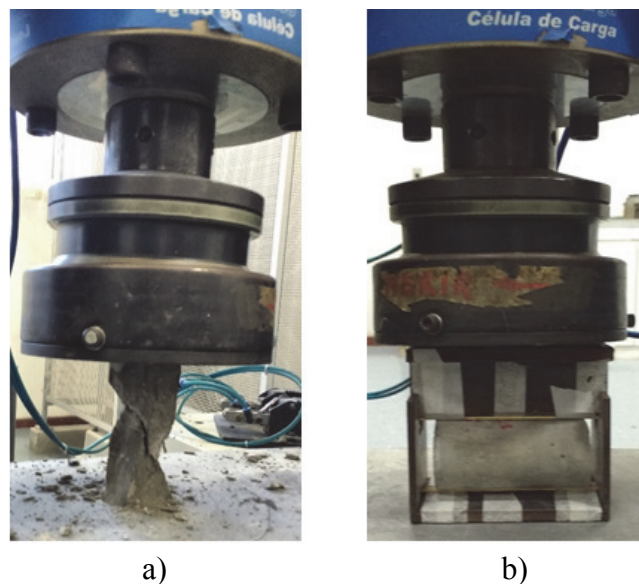


Fig. 2: a) compressive strength test setup; b) splitting tensile strength test using an apparatus specially developed for the test

The results of compressive strength test and splitting tensile strength test were obtained by the followed equations:

$$f_c = \frac{F}{\pi r^2} \quad (1)$$

f_c = compressive strength (MPa);
 F = maximum load applied (N);
 r = test piece average radius (mm);

$$f_t = \frac{2F}{\pi d h} \quad (2)$$

f_t = splitting tensile strength (MPa);
 F = maximum load applied (N);
 d = test piece diameter (mm);
 h = test piece height (mm).

For analysis, the one with the higher deviation among the 4 results of the same paste was discarded and the mean value of the remaining 3 results was considered.

3. RESULTS AND ANALYSIS

The dispersion process of CNTs on the cement particles surface using isopropanol resulted in visually homogenous dispersion. While in suspension, the CNTs were apparently well dispersed, without formation of clumps.

During the paste preparation no significant effect of the CNT addition on paste workability was noticed.

Tab. 2, Fig. 3 and Fig. 4 describe the results obtained in the compressive and splitting tensile strength tests.

Tab. 2: Results obtained in the compressive and splitting tensile strength tests

Identification	Compressive strength			Splitting tensile strength		
	Average strength (MPa)	Standard deviation (MPa)	Strength gain	Average strength (MPa)	Standard deviation (MPa)	Strength gain
REF - ISO - P	38.24	6.84	-	2.13	0.18	-
0,05 - ISO - P	55.44	9.27	45%	3.17	0.47	49%
0,10 - ISO - P	51.74	5.91	35%	2.55	0.09	20%

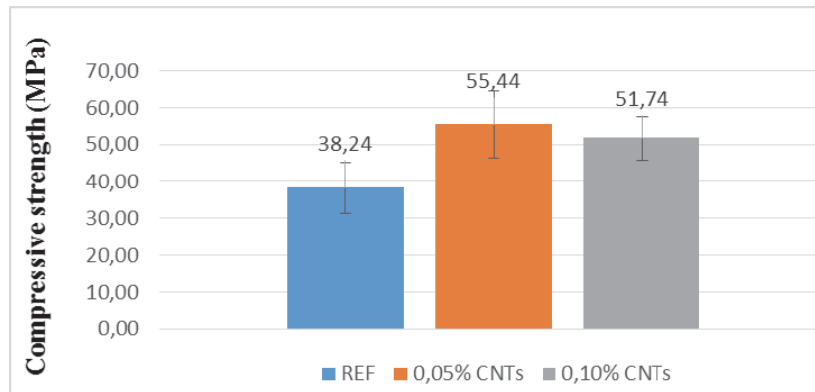


Fig. 3: Compressive strength test results

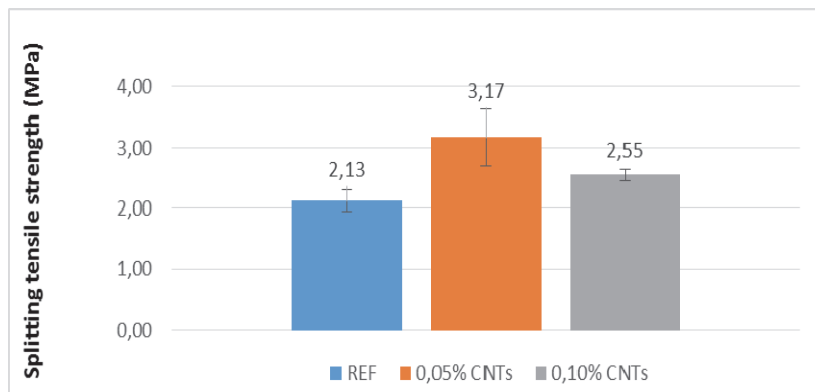


Fig. 4: Splitting tensile strength test results

The presence of CNTs at the cement composites in both concentrations resulted in a better performance, when compared to the reference paste. 0.05-ISO-P paste had 45% higher compressive and 49% higher tensile strength than the reference. At the same time the gains for the 0.10-ISO-P paste were 35% and 20%, respectively. For an addition of 0.05% CNTs, however, the gain was greater than 0.10% in both compressive and splitting tensile tests.

A difference between the relation of gain in compressive and tensile strength was also observed. For 0.05-ISO-P paste the gain in tensile strength was slightly higher (49%) than in compressive strength (45%), meanwhile for 0.10% CNT content the relation was the opposite: higher compressive strength gain (35%) than tensile (20%). This phenomenon may be explained by the CNTs working more like fibre reinforcement when used in smaller content. The higher gain in compressive strength for the 0.10-ISO-P paste indicates that the CNTs in this case have less fibre reinforcement effect, acting rather as nucleation sites for cement hydration products.

These results may also indicate the existence of a dispersion limit of CNTs by this methodology between 0.05 and 0.10% pf CNT content. Despite the visually good results using isopropanol, the dispersion of contents higher than 0.05% was less effective, which may have caused the agglomeration of CNTs and worse strength performance.

4. CONCLUSIONS

A method for the production of cement pastes based on the previous dispersion of CNTs on cement particles was presented in this work. A visually good dispersion was achieved without using any surfactant, nor was covalent functionalization of the nanotubes performed.

The described dispersion method allowed the incorporation of MWCNTs in cement matrix, at 0.05% and 0.10% proportion. The addition of CNTs resulted in improvement of the cement pastes' mechanical strength properties. Gains of up to 45% in compressive strength and up to 49% in splitting tensile strength were observed in the case of 0.05% CNT content. For higher CNT addition the gains were lower, but still had better behaviour than the reference paste without nanotubes.

The better performance of 0.05% than 0.10% CNTs incorporation may indicate a possible accumulation of nanomaterial at sites of cement hydration nucleation, compromising the good reaction. This fact corroborates the hypothesis that there is an optimal range for the incorporation of CNTs, and for the present method the ideal range is close to the 0.05% ratio.

5. ACKNOWLEDGEMENTS

The authors would like to thank to CAPES, CEFET-MG, CNPq, FAPEMIG and UFMG for the financial and technical help provided for this work.

6. REFERENCES

- ABNT NBR NM 43: 2003 - Cimento Portland - Determinação da pasta de consistência normal, Rio de Janeiro, 2003.
- Collins, F.; Lambert, J.; Duan, W. H. (2012), "The influences of admixtures on the dispersion, workability, and strength of carbon nanotube – OPC paste mixtures", *Cement & Concrete Composites*, Vol. 34, No. 2, February 2012, pp. 201-207.
- Filho, A. G. d. S.; Fagan, S. B. (2007), "Funcionalização de Nanotubos de Carbono", *Química Nova*, Vol. 30, No. 7, pp. 1695-1703
- Liu, Y.; Gao, L.; Sun, J. (2007), "Noncovalent Functionalization of Carbon Nanotubes with Sodium Lignosulfonate and Subsequent Quantum Dot Decoration", *Journal of Physical Chemistry*, Vol. 111, No. 3, pp. 1223–1229.
- Ludvig, P.; Calixto, J. M. F.; Ladeira, L. O.; Souza, T. C. C. (2017), "Analysis of Cementitious Composites Prepared with Carbon Nanotubes and Nanofibers Synthesized Directly on Clinker and Silica Fume", *Journal of Materials in Civil Engineering*, Vol. 29, June 2017, No. 6, pp. 06017001.
- Ludvig, P.; Calixto, J. M. F.; Ladeira, L. O.; Gaspar, I. C. P. (2011), "Using converter dust to produce low cost cementitious composites by in situ carbon nanotube and nanofiber synthesis", *Materials*, Vol. 4, No. 3, pp. 575-584.
- Makar, J. M.; Chan, G. W. (2009), "Growth of Cement Hydration Products on Single-Walled Carbon Nanotubes", *The American Ceramic Society*, Vol. 92, No. 6, June 2009, pp.1303–1310.
- Melo, V. S.; Calixto, J. M. F.; Ladeira, L. O.; Silva, A. P. (2011), "Macro-and Micro-Characterization of Mortars Produced with Carbon Nanotubes", *ACI Materials Journal*, Vol. 108, No. 3, May/June 2011, pp. 327-332.
- Paula, J. N.d.; Calixto, J. M. F.; Ladeira, L. O.; Ludvig, P.; Souza, T. C. C.; Rocha, J. M.; Melo, A. A. V. d. (2014), "Mechanical and rheological behavior of oil-well cement slurries produced with clinker containing carbon nanotubes", *Journal of Petroleum Science and Engineering*, Vol. 122, October 2014, pp. 274-279.
- Yu, J.; Grossiord, N.; Koning, C. E.; Loos, J. (2007), "Controlling the dispersion of multi-wall carbon nanotubes in aqueous surfactant solution", *Carbon* 45, Vol. 45, No. 3, March 2007, pp. 618-623.

ESTIMATION OF MODULUS OF ELASTICITY OF CONCRETE ON GRANITE AGGREGATE WITH THE CONSIDERATION OF MECHANICAL PARAMETERS OF AGGREGATE

P. Łaziński, J. Krzakała

Silesian University of Technology, Gliwice, Poland

SUMMARY

The modulus of elasticity of concrete with the known geometry of the concrete bridge significantly influences the stiffness, i.e. values of deformation and erection lifts. Nowadays, recipes of concrete mixtures in bridge construction more and more often contain granite aggregate, which is characterized by large differences in mechanical properties depending on the origin. Consequently, the modulus of elasticity of concrete may vary by up to 20% due to mechanical properties of the granite rock. Eurocodes exclude granite aggregates for estimation of the modulus of elasticity of concrete. The article proposes the value of the coefficient on the example of analysis of granite aggregates from different mines and the results from load tests.

1. INTRODUCTION

In the identification of stiffness of concrete bridge spans, it is necessary to properly determine the modulus of elasticity of concrete. Its value depends on the type of aggregate and age of concrete. The elastic deformation of concrete according to the standard PN-EN 1992-1:2008 may vary by up to 50% for the same concrete strength. This is due to large dispersion of mechanical properties of aggregates.

Different values of mechanical properties of concretes are assumed throughout the design, construction and operation phases. In the design phase, the value of modulus of elasticity is taken from PN-EN 1992-1:2008 based on the adopted concrete class and type of aggregate. The standard allows the reduction of modulus by 30% for sandstone aggregate and the increase by 20% for basalt aggregate. At the same time, it does not take into account the values of modulus of granite aggregate. In paper (Seruga, 2012) authors propose to reduce the elastic modulus of concrete by 20% for granite aggregate. At this stage, designers initially specify the value of modulus of elasticity.

During the construction phase, the contractor knows the characteristics of the approved concrete mixture. With the given composition, the relationship σ - ε is determined in concrete strength tests. Not often the contractor knows the value of modulus of elasticity of concrete from the conducted tests. This is due to the need to conduct such tests in the research laboratory. In practice, the value of the modulus of elasticity of concrete is determined using the formulas given in various standards and publications. The calculated modulus may not be correct due to the mechanical properties of the aggregate depending on its origin. At this stage, the assumed value of the modulus results in proper prestressing of the concrete, proper calculation of erection lifts and the correct determination of the vertical alignment on the bridge.

The operation phase is preceded by the load test of the bridge. These tests, through displacement and deformation measurements, allow to assess the real characteristics of the bridge and verify the computational model. This makes it possible to determine the final modulus of elasticity in the verified computational model and to use it in the decision-making process during the operation. The author discussed this problem in detail in the paper (Łaziński, 2009).

The paper presents the comparative analyses of two concrete mixtures, in which granite aggregates from mines in Strzelin and Rogoźnica were used. The obtained during load tests stiffnesses confirmed the lower modulus of elasticity of concretes in relation to standard values and differences in mechanical properties of granite aggregates in Poland.

The results from load tests carried out by an accredited laboratory from the Silesian University of Technology in Gliwice (Report, 2015) were used in the analysis.

2. ANALYSIS OF LOAD TEST RESULTS

The analysis of results from load tests was conducted for two bridges on A2 motorway on section Stryków - Tuszyn. The bridge WD-247 is a four-span, continuous, prestressed structure made of B45 (C35/45) concrete. The theoretical spans are $18.5+2\times 28.0+18.5=93.0$ m. The cross-section consists of two trapezoidal girders with an axial spacing of 5.90 m, connected by a 0.27 m thick reinforced concrete slab and clear distance between girders equal to 4.13 m. The girders are 1.40 m (at the bottom) and 1.40 m high. The cantilevers on both sides are 1.65 m long with a thickness ranging from 0.35 m to 0.21 m at ends (Fig. 1, Fig. 3).

The bridge WD-267 is a two-span, continuous, prestressed structure made of B50 (C40/50) concrete. The theoretical spans are $37.5+37.5=75.0$ m. The cross-section consists of two trapezoidal girders with an axial spacing of 5.03 m, connected by a 0.25 m thick reinforced concrete slab and clear distance between girders equal to 3.35 m. The girders are 1.20 m wide (at the bottom) and 1.70 m high. The cantilevers on both sides are 1.31 m long with a thickness ranging from 0.35 m to 0.18 m at ends. (Fig. 2, Fig. 3).



Fig. 1: Static scheme and view on bridge WD-247 (A1 motorway; section Stryków - Tuszyn)



Fig. 2: Static scheme and view on bridge WD-267 (A1 motorway; section Stryków-Tuszyn)

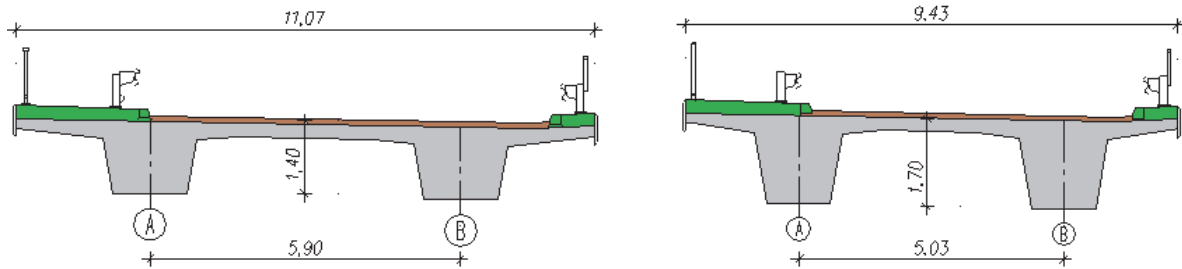


Fig. 3: Cross-sections of bridges: WD-247 (left side) and WD-267 (right side)

Load tests of both bridges were conducted in accordance with uniform procedures. Bridges were modeled as flat bar-panel structures (e1+2;p2). The material includes standard values of modulus of elasticity of concrete equal to 37.8 GPa (bridge WD-247) and 39.0 GPa (bridge WD-267). The load test of bridge WD-247 was conducted on 03.11.2015 after 217 days from concreting of the deck and load test of WD-267 was conducted on 01.10.2015 after 125 days from concreting.

The asymmetrical span schemes realized for both bridges allowed to verify the flexural and torsional stiffness of concrete girder-slab structures. The measured deflections were compared with deflections calculated theoretically. The deflections of girders are shown in (Fig. 4). In addition, (Fig. 5) presents elastic deflections and deflections calculated theoretically for both bridges.

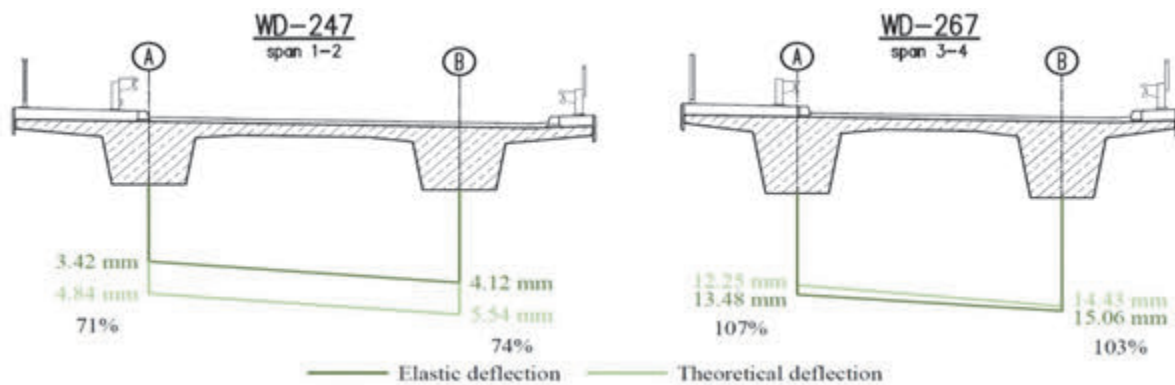


Fig. 4: The deflections of girders for bridge WD247 (left side) and bridge WD267 (right side)

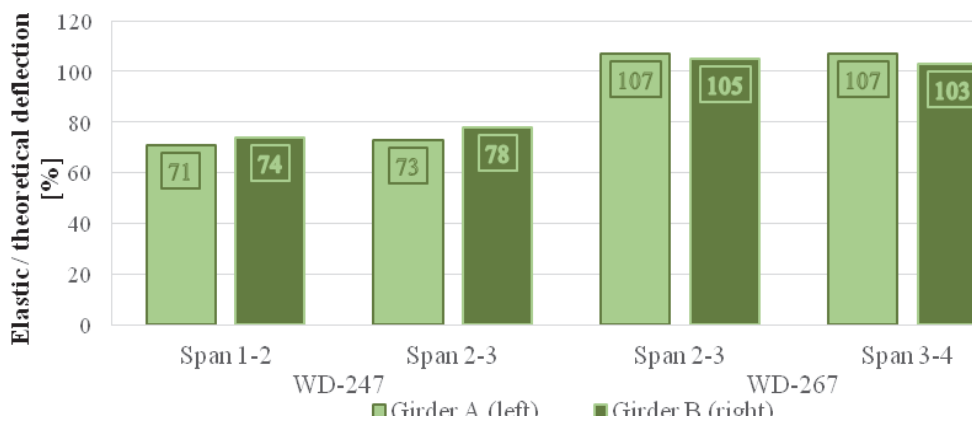


Fig. 5: The comparison of elastic deflections with deflections calculated theoretically for both bridges

The average deflections of tested spans were equal to 74% for bridge WD-247 and 105% for bridge WD-267. Such large differences in stiffness of spans in relation to theoretical stiffness indicate the significant influence of mechanical properties of granite aggregates. The causes of underestimated values of the modulus of elasticity of concrete were explained using the analysis of the composition of concrete mixtures and concrete strength tests after 28 days of curing.

3. ANALYSIS OF THE COMPOSITION OF CONCRETE MIXTURES

The recipes of both concrete mixtures were prepared in accordance with the PN-EN 206:2013. The basic parameters of mixtures are summarized in (Tab. 1). Portland cement of the same class, low alkali, sulfate resistant, in the amount that meets the requirements for exposure class XF4 ($C \geq 340 \text{ kg/m}^3$) was used. The same fine aggregate content (sand of 0-2 mm fraction) in the cubic meter of the mixture was assumed. Granite boulders with similar grain curves were used as coarse aggregate. The total mass of coarse aggregate in 1 m^3 was similar and was equal to 1125 kg (49% of mass per m^3) for bridge WD-247 and 1110 kg (48% of mass per m^3) for bridge WD-267. Water-cement ratios met the requirements for class XD3, XF4 and XS3 ($w/c \leq 0.45$). The aeration admixture was used in both mixtures. The average air content was 6.6% and 5.0% for WD-247 and WD-267, respectively. The composition of the concrete mixture is shown in (Tab. 2).

Tab. 1: Basic parameters of concrete mixtures

Parameter	WD-247	WD-267
Producer	CEMEX Poland Ltd. -WBT Łódź	P.P.M.B. Bosta Beton Ltd.
Strength class	C35/45	C40/50
W/c ratio	0.41	0.40
D_{\max}	16 mm	16 mm
Exposure class	XC4, XD3, XF4	XC4, XD3, XF4, XS3, XA1, XM1
Consistency	S3	S3

Tab. 2: Composition of concrete mixtures

Parameter	Unit	WD-247	WD-267
Fine aggregate - sand 0-2			
Origin	-	Święcice	Koluszki
Amount in m^3 of batch of concrete	kg/m^3	640	640
Coarse aggregate - granite grit 2-8 and 8-16			
Origin	-	Strzelin	Rogoźnica II
Fraction 2-8 - amount in m^3 of batch of concrete	kg/m^3	445	490
Fraction 8-16 - amount in m^3 of batch of concrete	kg/m^3	680	620
Water			
Origin	-	Municipal waterworks	Municipal waterworks
Amount in m^3 of mixture	kg/m^3	155	160
Cement			
Type	-	CEM I 42,5 N-SR 3/NA	CEM I 42,5 N-SR 3/NA
Producer	-	Cement Plant Chełm	Cement Plant Warta
Amount in m^3 of mixture	kg/m^3	375	400
Concrete admixtures			
Plasticizer	Producer	-	Plastiment BV 3 M
	% of mass of cement	-	Sika AG
	Amount in m^3 of mixture	kg/m^3	0.40
Superplasticizer	Producer	-	1.60
	% of mass of cement	-	Viscocrete 3088
	Amount in m^3 of mixture	kg/m^3	0.36*
Aerator	Producer	-	1.35*
	% of mass of cement	-	2.40
	Amount in m^3 of mixture	kg/m^3	0.10*
Aerator	Producer	-	0.20
	% of mass of cement	-	0.38*
	Amount in m^3 of mixture	kg/m^3	0.80
Together	kg/m^3	2297	2315

Tab. 3 presents test results of hardened concrete. The calculated characteristic strength allowed to classify the concretes to strength class of C35/45 (WD-247, as assumed in the recipe) and C45/55 (WD-267, class C40/50 - higher than assumed). Both absorbency and water tightness were very similar. The relatively high average strength reduction achieved for concrete from WD-267 in the frost-resistance test is worth attention.

In addition, a small mass increment, instead of, characteristic for this type of test, loss of mass was recorded for every sample. This occurs when additional products swell in concrete due to the presence of water or when the water fills the internal microcracks caused by shrinkage stresses and disintegrating action of freezing water in concrete pores.

Tab. 3: Characteristics of hardened concretes

Characteristic	Unit	Standard	WD-247	WD-267
Compressive strength after 28 days				
Average f_{cm}	MPa		54.0	61.0
Characteristic f_{ck}	MPa	PN-EN 12390-3	49.4	57.0
Corresponding f_{ck} concrete class	-	-	C35/45	C45/55
Mass water absorption	%	PN-88/B-06250	4.6	4.5*
Penetration depth of water under pressure	mm	PN-EN 12390-8	29	30*
Frost resistance F150				
Average strength loss ΔR	%		6.3	13.0
Average weight loss ΔG	%	PN-88/B-06250	0.0	-0.06

* Based on the data provided by the concrete producer

Coarse, granite, crushed-stoned aggregate was used in the production of concrete for bridges WD-247 and WD-267. It came from two mines: Strzelin (WD-247) and Rogoźnica II (WD-267). The locations of both mines are marked in Fig. 6. They are located in south-western Poland in the Lower Silesian Voivodeship. The dashed line indicates the probable boundaries of granite massifs. Rogoźnica is located in the area of Strzegom-Sobótka massif and Strzelin in the area of Strzelin-Żulów massif. This is due to the differences in the properties of rocks and aggregates from these regions.

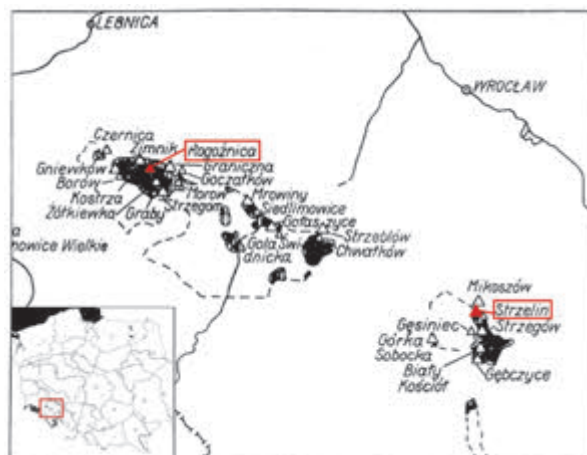


Fig. 6: Location of granite mines and granite massifs in Lower Silesia.

Comparison of the physical characteristics of granite rocks exploited in mines Strzelin and Rogoźnica II is shown in (Tab. 4). Information in the table were taken from MIDAS operated by the Polish Geological Institute and several publications. Despite various origins, the information are coherent and correspond to the relationships between rock properties described in the paper (Kozłowski, 1986).

Granite rocks from both mines are characterized by low absorption and belong to a group of very heavy rocks. There is a distinct difference in mechanical characteristics of both rocks. The granite from Strzelin exhibits greater resistance to abrasion tested in Deval drum and Boehm's shield. The compressive and tensile strength as well as the modulus of elasticity of rock are significant from the point of deformability of concrete with granite aggregate. According to (Tab. 4), the tensile strength of granite from Strzelin is two times higher, which corresponds to the results from load tests. Moreover, bridge WD-247 made of concrete from aggregate from Strzelin had deflections lower by approx. 30% than the bridge WD-267, in which the aggregate from Rogoźnica II was used. The paper (Ziętkowski, 2007) presents ranges of mechanical characteristics of Polish granites. The compressive strength varies from 120 to 280 MPa and the value of modulus of elasticity ranges from 26 to 70 GPa. The levels of these characteristics obtained for granites from the area of Strzegom are therefore below the average.

Tab. 4: Characteristics of granite rocks

Characteristic	Unit	WD-247	WD-267
Mine	-	Strzelin	Rogoźnica II
Massif	-	Strzelin-Żulowa	Strzegom-Sobótka
Bulk density	g/cm ³	2.64	2.61
Water absorption by weight	%	0.40	0.48
Watertightness	%	0.985*	0.98
Abrasiveness in Deval drum	%	3.00	4.80
Abrasiveness on Boehm's shield (dry)	cm	0.19	0.33
Compressive strength in air-dry condition	MPa	210÷217*	149.7
Tensile strength**	MPa	10.62÷10.73	3.65÷5.46
Modulus of elasticity	GPa	44.8***	28.0****
Modulus of elasticity calculated in accordance with equation (3) based on compressive strength	GPa	59.2	43.2
Modulus of elasticity (in a comparative scale)**	-	1.47÷3.86 (average 3.03)	0.96÷2.38 (average 2.38)

* based on Parrott

** Based on information for Rogoźnica II obtained for Strzegom-Sobótka massif.

**** Based on the data for Graniczna quarry located in the Strzegom-Sobótka massif; (granites from Graniczna and Rogoźnica II have similar mechanical properties)

The influence of the aggregate on the modulus of elasticity of concrete can be taken into account by mechanical properties of aggregate and even rock from which it is made. Parrott formulated the following relationship:

$$E_{cm} = 0.38 \cdot E_a + 200 \cdot f_{cm} \quad (1)$$

where: E_{cm} [MPa], f_{cm} [MPa], E_a is the modulus of elasticity of rock [MPa].

Arioglu modified the relationship:

$$E_{cm} = 0.7075 \cdot E_a^{0.838} + 200 \cdot f_{cm} \quad (2)$$

where: E_{cm} [MPa], f_{cm} [MPa], E_a is the modulus of elasticity of rock [MPa] in accordance with the formula:

$$E_a = 0.41 \cdot \sigma_a^{0.93} \quad (3)$$

where: σ_a is the compressive strength of rock [MPa].

Gutierrez and Canovas presented another approach:

$$E_{cm} = 8.48 \cdot \alpha_\beta \cdot f_{cm}^{1/3} \quad (4)$$

where: E_{cm} [GPa], f_{cm} [MPa], α_β is the coefficient determined from the formula:

$$\alpha_\beta = 0.1485 \cdot \sqrt{E_a} \tag{5}$$

where: E_a is the modulus of elasticity of rock [MPa].

Baalbaki, when mathematically analyzing numerous research results of the influence of aggregate on the modulus of elasticity of concrete, developed the following equation:

$$E_{cm} = -52 + 41.6 \cdot \log E_a + 0.2 \cdot f_{cm} \tag{6}$$

where: E_{cm} [GPa], E_a [GPa], f_{cm} [MPa].

The values of moduli for analyzed bridges were calculated based on the above equations describing the influence of rock properties on the modulus of elasticity of concrete, The values of the compressive strength of rocks and their moduli of elasticity, determined from the equation (3), were used in calculations (Tab. 4). These relationships allowed to obtain the modulus of elasticity of concrete for bridge WD-267 lower than for WD-247, which was not achieved by any of the methods described above, including Eurocode 2. The influence of concrete age t was taken into account in the results, which for WD-247 was 217 days, increasing the additional modulus by approx. 5%. In the case of bridge WD-267, concrete was 125 days old, increasing the modulus by approx. 4%.

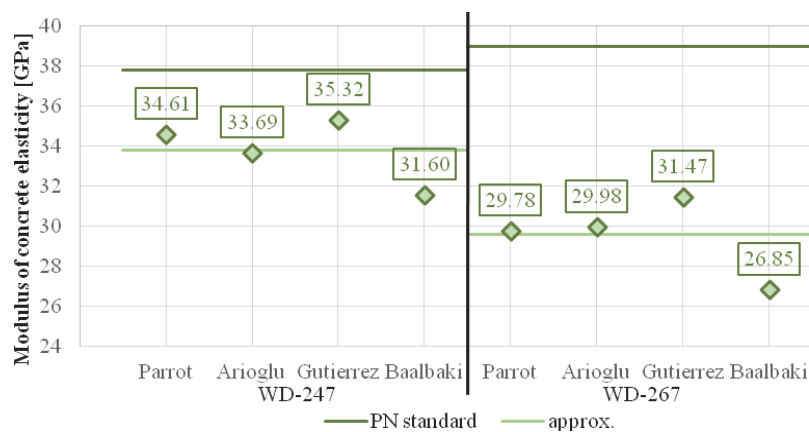


Fig. 7: The values of modulus of elasticity based on the relationships that take into account the aggregate characteristics and age of concrete.

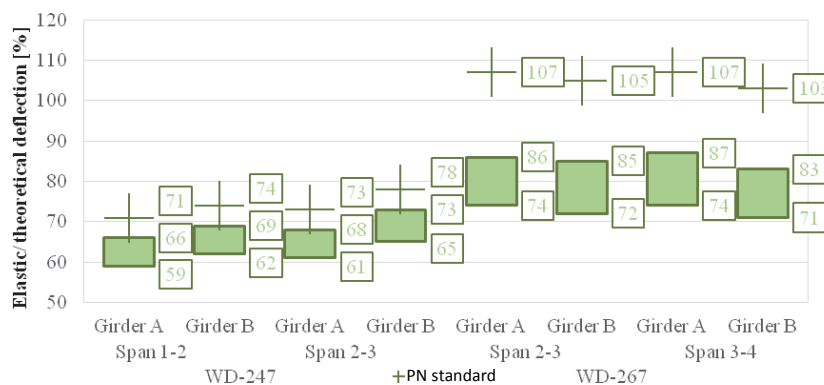


Fig. 8: Range of values of relationship of elastic deflections to calculated deflections with taking into account the mechanical properties of aggregate and age of concrete.

Load tests confirmed the underestimated values of the secant moduli of elasticity in relation to the standard values for granite aggregates. For bridge WD-247, the calculated secant modulus of elasticity from four relationships was equal to an average of 33.8 GPa and was lower by approx. 10% in relation to the standard value. In the case of bridge WD-267, the obtained secant modulus of elasticity was equal to an average of 29.6 GPa, reducing the value of modulus by approx. 24%. At the same time, tests revealed that granite aggregates are characterized by a variety of mechanical characteristics, depending on their origin. When using concretes with granite aggregate, the authors (Seruga, 2012) propose to introduce the reduction factor of 0.8 in relation to the standard value. The conducted load tests of concrete bridges confirm this relationship.

4. PROCEDURE FOR DETERMINING THE MODULUS OF ELASTICITY OF CONCRETE

The algorithm was developed using the analysis of methods of determining the modulus of elasticity of concrete and results described in the paper (Łaziński, 2009) (Fig. 9). It is an instruction to determine the modulus depending on available information and possibilities to conduct specific tests. The additional relationships described in PN-EN 1992-1:2008 were also used as they give results close to the average of the described, particular groups of methods. The Arioglu method was used in order to take into account the mechanical properties of aggregates.

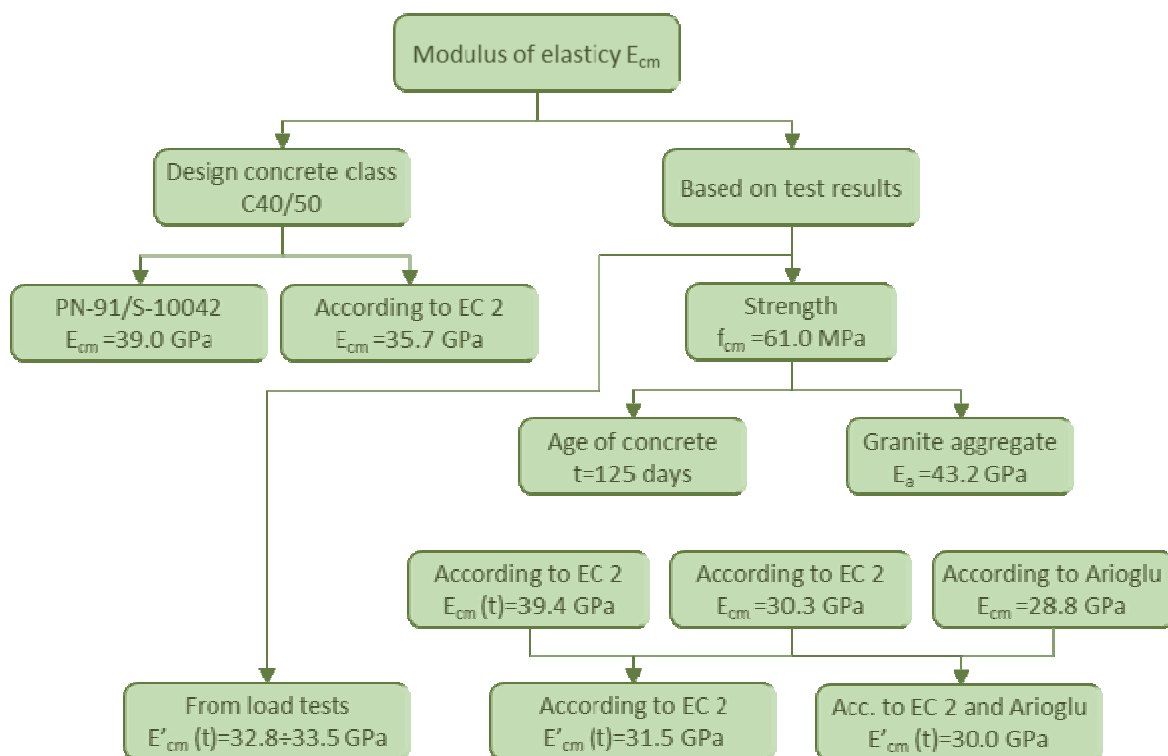


Fig. 9: Scheme of determination of modulus of elasticity of concrete on the example of WD 267

5. CONCLUSIONS

The modulus of elasticity of concrete with the known geometry of concrete bridge significantly influences its stiffness, i.e. values of deformations or erection lifts. The currently used concrete recipes in bridge engineering more and more often contain granite aggregate, which is characterized by large differences depending on the origin. The conducted analyses

of estimation of the modulus of elasticity of concretes with granite aggregate verified by the load tests confirm the underestimation the value of modulus in relation to standard values. It is generally advisable to individually determine this parameter within the conducted quality control of the concrete. However, it should be noted that the test of the modulus of elasticity of concrete is actually a one-axis compression test, whereas the concrete conditions of concrete correspond to a complex state of stress in cooperation with the reinforcing steel.

In the absence of test results of the modulus of elasticity of concrete, a procedure for determining its values was proposed. It assumes design situations when we adopt a given class of concrete and those when we have the results of strength tests of concrete or aggregates.

Based on the analyses conducted in this paper, it seems reasonable to take into account the mechanical parameters of aggregate, especially in the analyses from which high accuracy is expected. This, however, involved the need to carry out the strength tests of the aggregate and, above all, the rock from which it was obtained.

In the absence of results of strength tests of aggregate, the generalization of its effect on the modulus of elasticity of concrete only based on its type is the most accurate and predictable method of estimation of this value. Therefore, the modulus of elasticity of concrete of granite aggregate should be multiplied by a factor α_E equal to 0.8 as proposed by the authors (Seruga, 2012).

The research works that allow the mathematical representation of mechanical properties of the aggregate are reasonable, including the resistance to crushing or more common abrasion with the use of Los Angeles drum, in relation to its deformability or directly to the modulus of elasticity of concrete with a given aggregate. This would be significant due to the need to test the aggregate, hence the producers would know the modulus of elasticity of concrete, which is not the case for compressive strength or modulus of elasticity of rock.

6. REFERENCES

- Łaziński P.: Procedure for modeling objects in the form of a certain type of bridges. PhD thesis, Gliwice: Silesian University of Technology Civil Engineering, 2009
- Seruga A., Kańka S., Lisowicz T.: Moduli of elasticity of concrete on granite aggregate in the light of experimental research. Technical Journal of Cracow University of Technology, 2012, p. 103-117.
- PN-EN 1992-1:2008. Design of concrete structures.
- PN-EN 206:2013 Concrete - Requirements, properties, production and compatibility
- Ajdukiewicz A. and Mames J., Prestressed concrete structures, Cracow: Polish Cement, 2004.
- Kozłowski S., Rock raw materials in Poland, Warsaw: Geological Publisher, 1986.
- Ziętkowski L., Rock and concrete blasting tests by electrohydraulic method, Cracow: University of Science and Technology Publisher, 2007.
- Parrott L., "The Production and Properties of High-Strength Concrete," Concrete, pp. 443-448, 11 1969.
- Arioglu E., Arioglu N. and Yilmaz A. O., "Discussion on In-place modulus of elasticity of high-performance concrete bridge," ACI Materials Journal, pp. 397-399, 2006
- Report from the load test of bridge WD-247 and WD-267. A1 motorway Stryków - intersection Tuszyn on the section from km 295+850 to km 335+937,65,. Field Tests Team - Silesian University of Technology, 2015.

APPLICATION OF POTENTIOSTATIC MEASUREMENTS ACCORDING TO PN-EN 480-14 IN ASSESSMENT OF THE EFFICIENCY OF REINFORCEMENT PROTECTION AGAINST CORROSION BY CONCRETE WITH ADDITION OF FLY ASHES

*Katarzyna Domagała, Andrzej Śliwka
Faculty of Civil Engineering, Silesian University of Technology
Akademicka 5, 44-100 Gliwice, Poland*

SUMMARY

The paper presents a comparison of the results of the tests of the effectiveness of corrosion protection of reinforced concrete with the addition of calcareous fly ash. Tests were conducted by two electrochemical methods. Results obtained by potentiostatic measurement on reinforcement inserts deposited in cylindrical specimens in accordance with EN 480-14 standard were compared with studies investigating the progress of reinforcement corrosion caused by chlorides in loaded and cracked test elements made of these concretes. Tests of the cracked elements reflect the behaviour of reinforced concrete construction during operation in adverse environmental conditions, classified as standard XD and XS exposure classes. Comparison of the tests indicates the potential for potentiostatic measurement to be used to current assessment of protective properties of concrete with mineral additives.

1. INTRODUCTION

Manage of solid fuel burning products - mostly hard coal and brown coal - is an important economic and technical problem. One of the products of combustion are fly ashes, which can be a useful mineral additive to concrete. Ashes that do not meet the standard criteria are secondary materials but research is undertaken on the wider implementation of them for the production of concrete. Replacing part of the cement in the concrete with fly ash requires testing, including the degree of the reinforcement protection against corrosion provided by concrete. Determination of these characteristics allows for predicting the durability of reinforced concrete structures made from materials modified with coal combustion products. The results of published studies are not directly comparable due to the different types of ash used and the percentage of cement used as well as the different concrete recipes, curing conditions, and the way the experiment is conducted. Most of the results confirmed that the use of ashes in appropriate proportions does not impair the protective properties of concrete to reinforcing steel (Ampadu K.O., Torii K., 2002; Saraswathy V., Muralidharan S., Thangavel K., Srinivasan S., 2003; Jiang L., Liu Z., Ye Y., 2004; Kayali O., Zhu B., 2005; Pacewska B., Bukowska M., Wilińska I., Swat M., 2002) and improves the tightness of concrete (Hossain K.M.A., Lachemi M., 2004; Kayali O., Zhu B., 2005). In some studies conducted in the environment heavily contaminated with carbon dioxide and chlorides, accelerated corrosion of reinforcement by the introduction of silica fly ash replacing part of the cement was found (Montemor M.F., Simões A.M., Salta M.M., 2000; Montemor M.F., Cunha M.P., Ferreira M.G., Simões A.M., 2002; Jiang L., Liu Z., Ye Y., 2004). In addition, the use of common building chemicals poses a risk of antagonistic action and, as a consequence, deterioration of protective properties to reinforcing steel. Composition of fly-ashes can also vary considerably - depending on the source and fuel

used. Due to this should be conducted current control of protective properties. In the case of control tests, the speed of obtaining results is important.

Potentiostatic test according to PN-EN 480-14 allows for fast results, but test conditions deviate from the natural conditions in which the construction works. This can have an impact on the proper reasoning about proper protection in real construction. It should answer the question whether these tests are reliable and can be to draw conclusions about the protective properties of concrete containing fly ash cement.

Therefore, in order to verify the protective properties of concretes containing fly ash cements were examined (Śliwka A., Domagała K., Zybura A., 2013). Rapid selection tests were performed on standard test elements according to standard (PN-EN 480-14: 2008). Then corrosion rate of reinforcing steel caused by the impact of a 3% solution of sodium chloride on reinforced beam elements was determined by linear polarization. Samples for both tests were made of concrete on cement with different contents of high calcium fly ash (Tab. 1). Concrete test elements made of Portland cement were also tested, which were reference level during the study.

Tab. 1: Types of cement towards electrochemical measurements used in the experiments

Series	Cement	High calcium fly ash [% by weight]
I	CEM I 42,5R	–
II	CEM II/A-W	15
III	CEM II/B-W	30
IV	CEM IV/B-W+	50
V	CEM IV/B-W	50

2. CORROSION SUSCEPTIBILITY OF THE REINFORCEMENT IN CONCRETE – POTENTIOSTATIC TESTS

2.1. Technique of potentiostatic tests

Specimens for potentiostatic tests were prepared in accordance with PN-EN 480-14 in the form of cylinders 110 mm in height and 50 mm in diameter, centrally reinforced with a ribbed rod of 6 mm diameter class B steel – Fig. 1a. Research began 88 days after sample preparation – after maturation and completion of hydration of cement (Śliwka A., Domagała K., Zybura A., 2013).

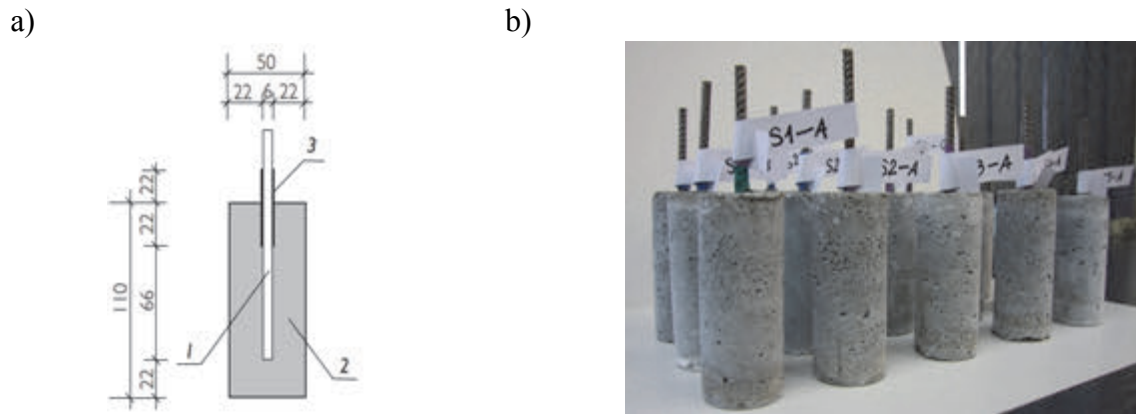


Fig. 1: Potentiostatic measurements: a) the test element scheme: 1 – working electrode (reinforcing bar), 2 – concrete, 3 – protective coating of plastic, b) photography of test elements

Potentiostatic studies were carried out in accordance with standard (PN-EN 480-14: 2008) – Fig. 1b. The reference electrode was a silver chloride electrode and an auxiliary electrode made of stainless steel. Based on the measurements, a maximum current value I between 1 and 24 hours was determined. Taking into account the active area of the test electrode, the current density i was calculated.

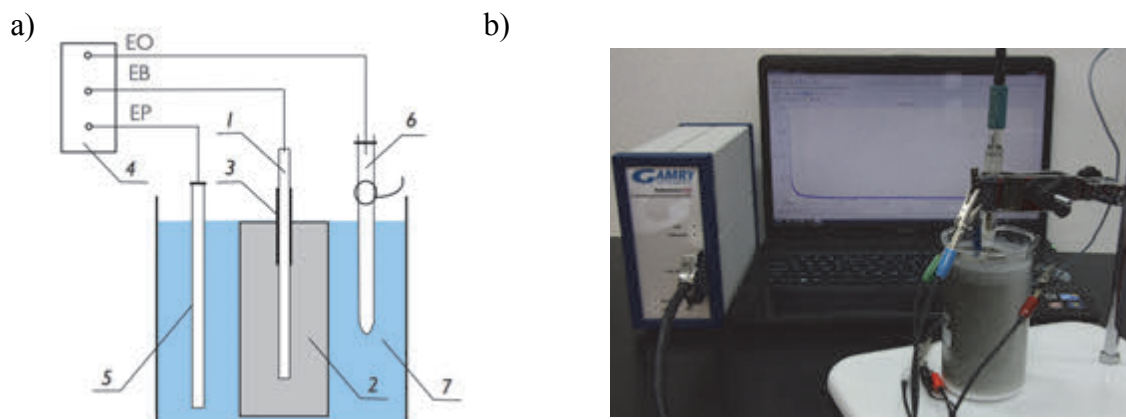


Fig. 2: Potentiostatic measurements: a) diagram of the measuring system: 1 – working electrode (reinforcing bar), 2 – concrete, 3 – protective coating of plastic, 4 – potentiostat, 5 – counter electrode, 6 – reference electrode, 7 – electrolyte (saturated solution of calcium hydroxide), b) view of the test stand

2.2. Results of potentiostatic testing of corrosion susceptibility

The results of potentiostatic measurements are current intensity changes, which are shown in Fig. 3 for elements of series I ÷ V.

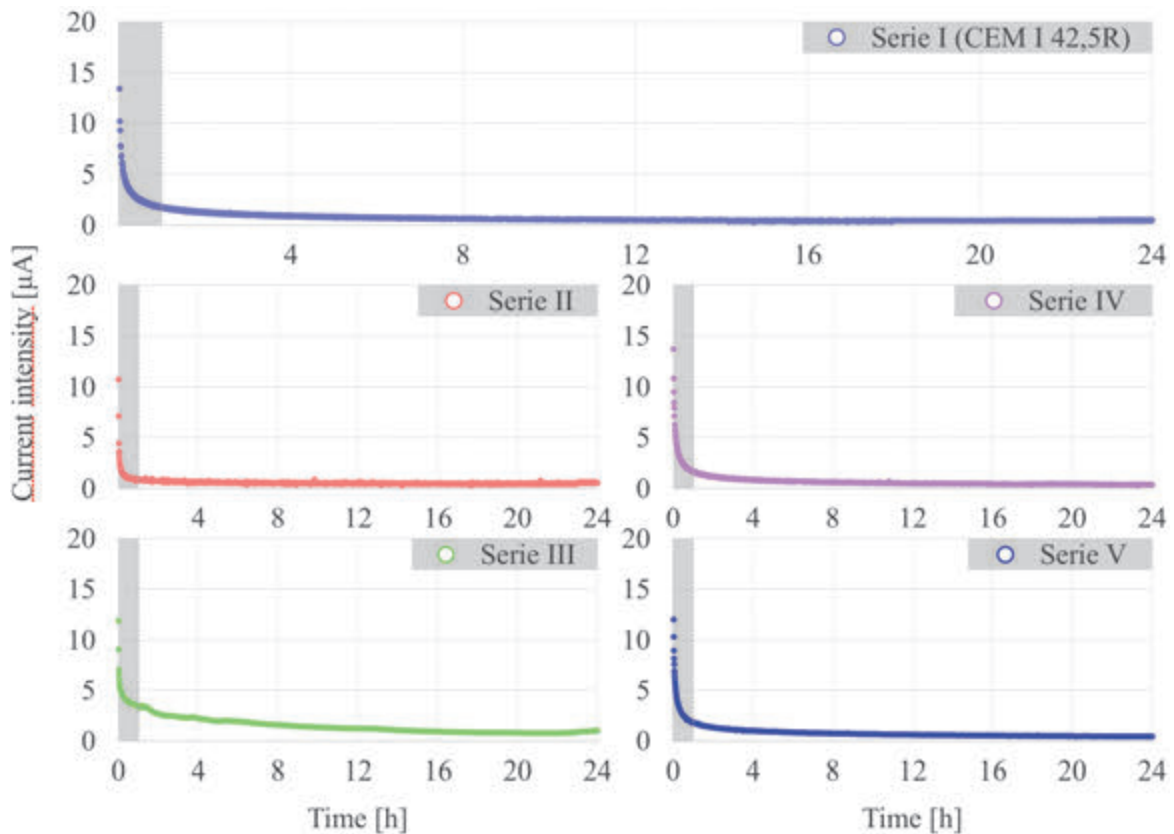


Fig. 3: The current intensity changes in representative element of all series

The values of current density for the specimens of series II ÷ V were compared with the results for the reference specimens of series I. The overall results from the potentiostatic testing of corrosion susceptibility are presented in Fig. 4.



Fig. 4: The values of corrosion current density obtained from results of all types of the analyzed concrete

The average values of current density for the specimens of series II ÷ V, made of concrete with cement containing high calcium fly ash were found to be lower than the average values of current density for the specimens of the reference series I referred to as the comparative level.

After the measurements were completed, the test elements were split. The surface of the reinforcement in each case showed no signs of corrosion. Photos of representative splitted elements are shown in Fig. 5.

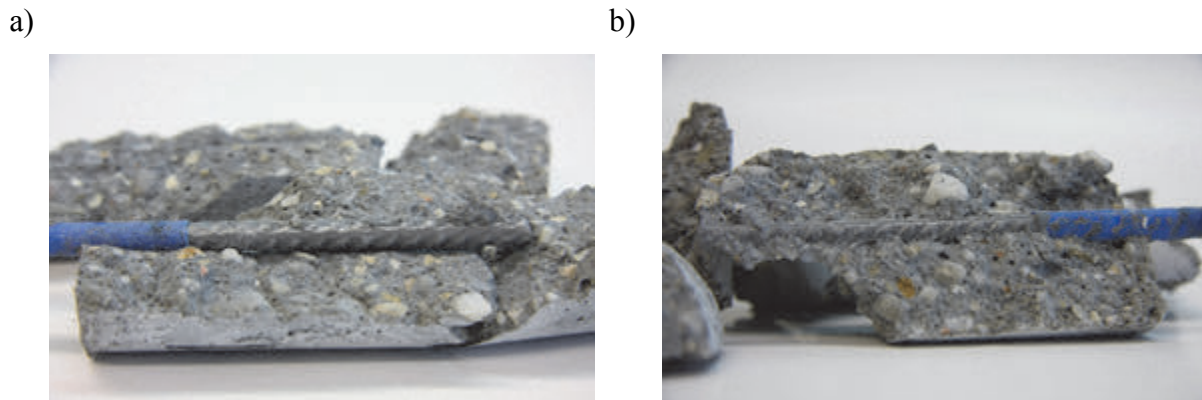


Fig. 5: Photos of representatives elements after tests: a) series I, b) series III

It was observed that using high calcium fly ash of different content (series II ÷ V) in cement did not result in reduction of the protective properties of concrete to the reinforcement.

3. TESTS OF PROGRESS OF REINFORCEMENT CORROSION CAUSED BY CHLORIDES

3.1. Test elements and the course of measurements of reinforcement corrosion rate

The development of reinforcement corrosion was determined in loaded and cracked test elements. Test elements were made of concrete containing high calcium fly ash. To induce corrosion of reinforcement to determine the rate of corrosion processes the elements were periodically wetted with 3% solution of sodium chloride. The measurements were performed under conditions similar to the original conditions existing in the structure exposed to chlorides. Beams of 50x100x600 mm dimensions were prepared to determine the rate of corrosion processes. They were reinforced with ribbed bar of 6 mm diameter of steel class B. Concrete made of multi-component cement containing high calcium fly ash in 3 following proportions – 15% (series II), 30% (series III) and 50% (series IV and V) by mass of cement were used in the test elements. The test results were compared to the values of measurements of test elements of reference concrete made of Portland cement (series I). Platinised titanium rod of 1.6 mm diameter was embedded in each test element as the counter electrode.

The measurements were carried out using the polarization method. The corrosion rate was determined as the corrosion current density. The corrosion density was measured every few weeks in the crack and in the selected uncracked points along the reinforcement axis. The measuring points were so located along the beams to consider the differences in the migration of aggressive substance through the cover between cracked tension zone and loaded and unloaded zones of elements – Fig. 6. Cracks were obtained by loading the simply supported beam elements with a concentrated force. The elements were loaded using the individually prepared tie-beam system (Domagała K., Śliwka A., Zybura A., 2013). The load was increasing until the crack from 0.05 to 0.1 mm in width appeared on the element surface.

On every test element were located 5 measurement points – one in the crack – most exposed to the effort and to aggressive substances section, two on both sides of the crack – zone, in which reinforcement is protected by stretched but uncracked concrete, and two in no loaded zone.

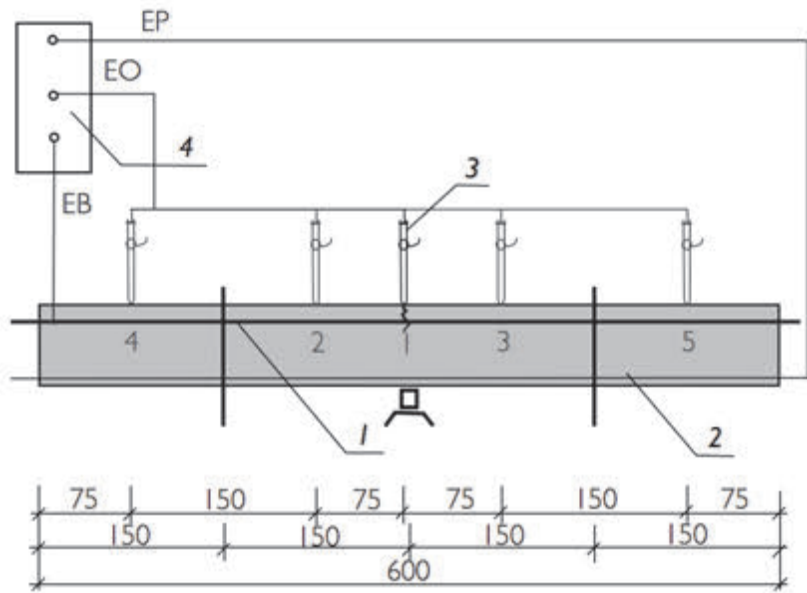


Fig. 6: Diagram of polarization measurement performed in selected points of the test element:
 1 – working electrode (reinforcing bar), 2 – counter electrode (titanium rod covered with platinum), 3 – reference electrode (Ag/AgCl), 4 – potentiostat

The full way of inducing corrosion and measuring is described in (Śliwka A., Domagała K., Zybura A., 2013; Domagała K., Śliwka A., Zybura A., 2013; Domagała K., Śliwka A., Zybura A., 2014). The wetting was conducted till the corrosion current density reached the value of $i_{cor} 2 \div 3 \mu\text{A}/\text{cm}^2$ in the crack of test elements made of reference concrete of series I with Portland cement. This value indicated the moderate level of the reinforcement corrosion according to the paper (Kayali O., Zhu B., 2005). From that moment, only the electrochemical measurements were conducted under conditions of developing corrosion of the reinforcement without the impact of the aggressive solution. The tests were conducted for 40 weeks.

3.2. Test results of reinforcement corrosion rate

The results of each electrochemical measurement were obtained in the form of computer printouts of cathodic and anodic polarization, as well as the values of corrosion potential E_{cor} and corrosion current density i_{cor} determined in Echem Analyst software, using the method of polarization resistance. The main results are presented in Tab. 2.

The results obtained in series II \div V were referred to the values estimated on reference series I – made of Portland cement. For cracked elements, the obtained values of corrosion current density in the crack (Tab. 2) indicate that concrete of series II \div V maintained its protective properties with respect to reinforcing steel. The measurement results of points 2 and 3 confirmed as well the good protective properties of concrete with cement containing high calcium fly ash. The developed corrosion was found in the reinforcement inserts embedded in reference concrete of series I, while the reinforcement present in concrete of series II \div V made of cement containing high calcium fly ash was well protected. The values of corrosion current density usually did not exceed the assumed threshold value $0.20 \mu\text{A}/\text{cm}^2$. Very good protective properties of the analyzed types of concrete were also confirmed by the results of points 4 and 5 in the specimens.

Tab. 2: The fundamental results of the electrochemical measurements

Series	Stage	Time [week]	i_{cor} [$\mu\text{A}/\text{cm}^2$]														
			Point 1			Point 2			Point 3			Point 4			Point 5		
			Elements														
			1	2	3	1	2	3	1	2	3	1	2	3	1	2	3
I	0	1	0.01	0.06	0.03	0.46	0.06	0.35	0.38	0.01	0.52	–	–	0.00	–	–	0.00
	I	2	0.65	–	0.13	0.08	0.14	0.35	0.46	0.22	0.54	0.00	0.00	0.07	0.00	–	0.00
	R	23	–	2.03	3.06	2.12	–	3.18	1.44	2.10	2.89	2.01	2.11	2.05	–	2.05	2.79
	R	40	1.46	1.60	1.16	0.84	1.73	–	–	2.01	2.71	0.73	0.98	0.47	2.07	2.05	–
II	0	1	0.02	0.03	0.01	0.01	0.03	0.02	0.03	0.06	0.03	0.01	0.01	0.01	0.05	0.05	0.02
	I	2	0.01	–	0.02	–	–	0.00	0.01	0.03	0.02	0.06	–	0.01	–	–	–
	R	23	–	0.10	0.01	–	0.06	–	–	0.03	–	–	0.01	–	–	0.03	–
	R	40	0.07	–	–	0.17	0.05	–	–	0.05	0.05	–	0.04	–	0.03	–	–
III	0	1	0.04	–	–	–	–	–	0.03	0.01	–	0.05	–	0.01	0.02	0.03	–
	I	2	0.01	0.01	0.01	0.04	–	0.03	0.03	0.02	0.01	–	0.01	–	0.01	0.05	0.01
	R	23	0.24	–	0.02	0.13	0.25	–	0.17	–	–	0.04	0.06	–	0.02	–	–
	R	40	0.05	–	0.26	0.09	–	–	0.14	0.08	0.19	0.01	–	–	0.06	–	–
IV	0	1	0.01	0.09	0.01	0.01	0.02	0.03	0.01	0.02	0.06	–	0.00	0.05	0.02	0.01	0.02
	I	2	0.07	0.05	0.04	0.00	0.01	–	0.00	0.01	0.05	0.21	0.01	0.03	0.11	–	–
	R	23	0.13	0.09	0.01	–	0.05	–	–	0.05	–	0.06	0.04	–	–	0.08	–
	R	40	0.04	0.06	0.08	0.10	–	–	0.13	0.03	–	0.04	0.09	–	–	–	0.02
V	0	1	0.01	0.02	0.04	0.05	0.03	0.02	0.09	0.04	0.09	–	–	0.11	0.18	–	0.16
	I	2	0.06	–	0.07	0.10	0.02	–	–	0.05	–	0.05	0.01	–	0.28	–	–
	R	23	0.02	0.02	0.10	0.02	–	0.08	–	–	0.05	0.15	–	0.01	0.02	0.34	0.09
	R	40	0.03	–	0.09	0.03	0.36	0.20	0.04	–	0.23	0.04	–	0.02	0.34	–	0.08

4. CONCLUSIONS

The efficiency of reinforcement protection against corrosion by concrete with addition of fly ashes were conducted using two individual methods: (i) the potentiostatic method for the cylindrical concrete specimens with the centrally located rebar and (ii) the method of polarization resistance conducted during 40 weeks of corrosion rate induced by chlorides on the loaded and cracked beam elements.

On the basis of the both conducted electrochemical tests and the analysis of obtained results it can be concluded that high calcium fly ash used as the component of cement didn't get worse the protective properties of concrete with respect to the reinforcement in comparison to reference concrete with Portland cement.

In case of tests carried out according to standard method, cements containing high calcium fly ash have been reported to improve the protective properties of concrete to reinforcing steel in comparison to Portland cement concrete. As the fly ash content increases, the protective properties slightly deteriorate but are not worse than in case of Portland cement. Corrosion-induced chloride rate measurements made on beam elements by linear polarization method also showed better protective properties of concrete on cement containing fly ash. Due to the very high variability of the linear polarization results, it is much more difficult to observe the effect of the ash content on the protective properties and thus the corrosion rate, but there is a tendency to increase the corrosion current density value in case of higher ash content in the cement.

The obtained results indicate the possibility of using a fast method, such as the standard method (PN-EN 480-14: (2008)), for the current assessment of the protective properties of concrete. Both applied research methods allowed the same conclusions to be drawn, indicating the possibility of their replacement. Of course, the number of tested samples is not great and further studies are needed, taking into account other factors, to verify presented conclusions.

6. REFERENCES

- Ampadu K.O., Torii K., (2002), "Chloride ingress and steel corrosion in cement mortars incorporating low-quality fly ashes", *Cement and Concrete Research*, Vol. 32 (2002), pp. 893-901.
- Domagała K., Śliwka A., Zybura A., (2013), „Protective properties of reinforcing steel in concrete containing fly ash”, *Central European Congress on Concrete Engineering „Concrete Structures in Urban Areas”*, Wrocław, Poland, September 4-6, 2013, pp. 292-295.
- Domagała K., Śliwka A., Zybura A., (2014), „Przebieg korozji zbrojenia chronionego betonem na cemencie zawierającym popiół wapienny (The proces of corrosion of the reinforcement protected with concrete made of cement containing high calcium fly ash)”, *Ochrona przed Korozją*, Vol 57, Nr 1/2014, pp. 21-27.
- Hossain K.M.A., Lachemi M., (2004), "Corrosion resistance and chloride diffusivity of volcanic ash blended cement mortar", *Cement and Concrete Research*, Vol. 34 (2004), pp. 695-702.
- Jiang L., Liu Z., Ye Y., (2004), "Durability of concrete incorporating large volumes of low-quality fly ash", *Cement and Concrete Research*, Vol. 34 (2004), pp. 1411-1413.
- Kayali O., Zhu B., (2005), "Chloride induced reinforcement corrosion in lightweight aggregate high-strength fly ash concrete", *Construction and Building Materials*, Vol. 19 (2005), pp. 327-336.
- Montemor M.F., Cunha M.P., Ferreira M.G., Simões A.M., (2002), "Corrosion behaviour of rebars in fly ash mortar exposed to carbon dioxide and chlorides", *Cement and Concrete Composites*, Vol. 24 (2002), pp. 45-53.
- Montemor M.F., Simões A.M., Salta M.M., (2000), "Effect of fly ash on concrete reinforcement corrosion studied by EIS", *Cement and Concrete Composites*, Vol. 22 (2000), pp. 175-185.
- Pacewska B., Bukowska M., Wilińska I., Swat M., (2002), "Modification of the properties of concrete by a new pozzolan. A waste catalyst from the catalytic process in a fluidized bed", *Cement and Concrete Research*, Vol. 32 (2002), pp. 145-152.
- PN-EN 480-14: (2008), „Domieszki do betonu, zaprawy i zaczynu. Metody badań. Część 14: Oznaczanie podatności korozyjnej stali zbrojeniowej w betonie za pomocą potencjostatycznego badania elektrochemicznego”.
- Saraswathy V., Muralidharan S., Thangavel K., Srinivasan S., (2003), "Influence of activated fly ash on corrosion-resistance and strength of concrete", *Cement and Concrete Composites*, Vol. 25 (2003), pp. 113-120.
- Śliwka A., Domagała K., Zybura A., (2013), „Evaluation of protective properties of concretes made of cements with calcareous fly ash with respect to reinforcing steel”, *Roads and Bridges – Drogi i Mosty*, Vol. 12, No. 2/2013, pp. 237-250.

THE EFFECT OF STEEL FIBRES FOR CRACK WIDTH LIMITATION

*Andreas Haus
Bekaert GmbH
Siemensstraße 24, 61267 Neu-Anspach, Germany*

SUMMARY

Combined reinforcement, a combination of traditional concrete reinforcement and steel fibres, is an effective and economical alternative for heavy reinforced foundation systems. Next to the significant contribution to the flexural-, shear- and punching-capacity, the effect of combined reinforcement can also be used for the crack width limitation. After decades of research, development and practical experiences, not only recommendations but also compulsory codes are available. The German Guideline as one example is an addition to the structural concrete code DIN EN 1992 (Eurocode 2) of Germany and is taken up by the building authority in the list of official building materials. The following paper will show the theoretical effect of steel fibres to the crack width limitation in the design as well as the use of steel fibres for real project.

1. INTRODUCTION

With the introduction of the Eurocodes, especially the EN 1992, designers have become more and more aware of serviceability limit state (SLS) requirements. For concrete structures, in addition to deformation and rotation checks, the crack width limitation is a major point for the SLS design. Even optimized design methods, like the direct calculation of the crack width, will result in heavy reinforcement. Especially when it comes to fully restrained structures, the reinforcement layout is often governed by requirements from crack width design. In many cases it is possible to simplify traditionally reinforced solutions by using hybrid reinforcement.

Steel fibres can transfer stresses already at small crack openings, so that ductility and post crack strength are provided to a concrete matrix. Practical experience for applications like industrial flooring, precast elements and tunnelling is available worldwide. With the upcoming of design standards like the DAFStb Guideline “Steel Fibre Concrete”, a national annex to EN 1992 in Germany, or the fib Model Code 2010, new options for designing with SFRC were given. The focus in this paper to one of the new possibilities is the use of steel fibres in combination with traditional reinforcement for crack width design in serviceability limit state.

2. THE EFFECT OF STEEL FIBRES ON COMBINED REINFORCEMENT

It is well known that steel fibres provide post-crack strength to concrete by transferring forces from one side of the crack to the other. Usually steel fibres bridge a crack at a non-perpendicular angle. Therefore, the fibre will be slightly bent, already at small crack widths. Due to the locally increased friction, compressive stresses parallel to the crack surface are induced. As a consequence, cracks become more curved, more irregular or they may split. Resistance to intruding substances, especially liquids, is substantially increased. Aggregate interlock is improved and friction is enhanced.

For regular fibre dosages, the uniaxial post-crack strength is always lower than the uniaxial first crack strength. Therefore conventional applications of steel fibre reinforced concrete apply special design, construction and detailing rules in order to benefit from the superior cracking properties of steel fibre concrete for ULS and SLS.

Elastic bedded, jointless steel fibre reinforced industrial floors have become a major application in huge parts of the world, e.g. Europe and Australia / New Zealand. Yield line theory is applied for the strength design of the steel fibre reinforced concrete slabs. The required serviceability is achieved through the excellent cracking properties provided by the SFRC together with advanced detailing and execution techniques which are tailored to limit restraint stresses to a minimum. A specific crack width design is usually not required and the whole concept aims at the avoiding of cracks, by reducing the friction between the floor and the subbase. Even though this cannot be avoided in all cases, it is known from experience that due to the suitable dosages of high performing steel fibres, cracks won't exceed the accepted crack widths of 0.3 – 0.5 mm. Such cracks do not affect the load-bearing capacity nor serviceability of regular industrial floors.

Especially for floors with special requirements like large field sizes (>50 m), seamless and restrained floors, as well as floor with requirements to the tightness, the reduction of friction alone is not sufficient to guarantee the characteristics of a crack free floor. In such cases, the crack widths can be calculated by considering the post crack strength provided by steel fibres in the crack width design.

One major factor in the calculation of crack width is the force, released when the concrete is cracking. As the steel fibres will carry a part of the released force, only the remaining force has to be handled by the traditional reinforcement. Assuming a uniaxial concrete tensile strength of 3 MPa for example, while providing a post crack tensile strength of 1 MPa when using steel fibres, only 2/3 of the dissipated force has now to be transferred by the reinforcement. The reduction by 1/3 leads to a saving of 50% on the required reinforcement for crack control because the effect accounts by the power of 2 according to expressions (2) ($2/3 \times 2/3 \approx 50\%$).

As the calculated crack width w_{cal} is a function of the concrete tensile strength, the formula in EN 1992 or other standards can be adapted by subtracting the uniaxial post crack strength $f_{ct,res}$ from the concrete tensile strength f_{ct} .

$$w_{cal} = \text{function of } (f_{ct} - f_{ct,res}) \quad (1)$$

It is important to apply the same concrete age to both f_{ct} and $f_{ct,res}$, for instance when young concrete is considered for the calculation dissipation of hydration heat.

3. EXAMPLE: CRACK WIDTH CONTROL OF COMBINED REINFORCEMENT IN THE DAFSTB GUIDELINE STEEL FIBRE CONCRETE

In the actual EN 1992, the effect of steel fibres is not yet considered. Therefore different countries have created guidelines for steel fibre concrete. With the DAfStb guideline Steel Fibre Concrete, an official document on code level is available for the design of steel fibre reinforced concrete structures in Germany. This document is fully synched with EN 1992 and its main concepts have been used in the industry for about ten years.

The approach for the calculation of the crack width w_k can be found in chapter 7.3.4 of the DAfStb guideline:

$$w_k = s_{r,max} \cdot (\varepsilon_{sm}^f - \varepsilon_{cm}) \quad (2)$$

$$s_{r,max} = (1 - \alpha_f) \cdot \varnothing_s / (3.6 \cdot \rho_{p,eff}) \leq (1 - \alpha_f) (\sigma_s \cdot \varnothing_s) / (3.6 \cdot f_{ct,eff}) \quad (3)$$

$$\varepsilon_{sm}^f - \varepsilon_{cm} = (1 - \alpha_f) \cdot (\sigma_s - 0.4 \cdot f_{ct,eff} \cdot 1/\rho_{p,eff}) / E_s \geq 0.6 \cdot (1 - \alpha_f) \cdot \sigma_s / E_s \quad (4)$$

The effect of steel fibres is accounted for by the normalized factor α_f :

$$\alpha_f = f_{ctR,s} / f_{ctm} \quad (5)$$

where: $f_{ctR,s}$ uniaxial post crack tensile strength of fibre reinforced concrete for SLS design at 28 days

f_{ctm} mean uniaxial tensile strength of concrete at 28 days

$f_{ct,eff}$ mean value of the uniaxial tensile strength of the concrete effective at the time of cracking

$s_{r,max}$ maximum crack spacing

ε_{sm}^f mean strain in the reinforcing steel, including the effect from the steel fibres

ε_{cm} mean strain in the concrete between cracks

\varnothing_s reinforcing bar diameter

$\rho_{s,eff}$ effective reinforcement ratio

σ_s stress in the tension reinforcement without the effect from the steel fibre

E_s Modulus of elasticity of the reinforcement

4. PRACTICE OF SFRC COMBINED REINFORCEMENT

Australian Container Freight Services at the Port of Brisbane – The world's largest combi slab joint free pavement

The challenge was to construct a 50,000 m² container yard without any saw-cut joints or other contractions / expansion joints. The solution was a 290 mm thick seamless "Combi Slab" slab, reinforced with hybrid reinforcement. The SLS design required the use of Dramix[®] 4D 65/60BG fibres and one layer of mesh at the top to achieve a calculated crack width of 0.25 mm. Due to pouring limitations (temporary) construction joints were required but all panels were continuously connected by reinforcement so that finally one seamless slab was achieved. Figure 1 shows the final slab; former construction joints are visible but they do not act as joints anymore. By using hybrid reinforcement the building process could be significantly increased, joints which would require permanent maintenance could be avoided and the serviceability requirements were met.



Fig. 1: 50,000 m² seamless slab with hybrid reinforcement

Elastic bedded slab as a secondary barrier against hazardous goods – A liquid tight slab

The German guideline “Concrete as secondary barrier against hazardous goods” allows the construction of liquid tight slabs without any additional sealing. The project owner, one of the largest chemical companies of the world, wanted to increase the production for synthetic lubes with a new storage tank. In accordance with the German guideline “Concrete as secondary barrier against hazardous goods” a calculated crack width of ≤ 0.1 mm was required and designed in accordance with the German guideline steel fibre concrete. The technical solution for this project was carried out as a “Combi Slab” with 25 kg/m³ high performing Dramix® 5D 65/60BG fibres and conventional reinforcement of about 23.50 cm²/m at top and 15.28 cm²/m at bottom. The raft foundation was cast with C35/45 concrete and is up to 1.55 m thick. Walls were partially pre-stressed. Major time savings could be achieved due to simplifying the complex reinforcement layout which would have been required without the steel fibres.



Fig. 2: Pouring of the liquid tight raft foundation

Raft foundation with slab thickness up to 2.00 m

The new production plant of Carl Zeiss SMT was erected in 2012. Because of a very high sensitivity of the production to vibrations, the foundation of the plant had to be designed for

compensating vibrations. To reach this requirement, a monolithic slab of about 2.00 m thickness had to be cast. Both ULS and SLS design were based on the DAfStb guideline steel fibre concrete. Crack width design had to be based on the material properties of mature concrete. The maximum crack width of 0.3 mm was achieved by using a C25/30 concrete, reinforced with 30 kg/m³ Dramix® 3D 80/60BG fibres and traditional bar reinforcement of Ø14 mm at 100 mm spacing at top and bottom. Figure 4 gives an impression of the slab. Thanks to the steel fibres, Bamtec rolled reinforcement could be used instead of single bars so that construction time was drastically reduced, only in that way the very challenging time schedule could be met.



Fig. 4: The 2.00 m slab with the traditional reinforcement

5. CONCLUSIONS

Steel fibre reinforced concrete has proven to be a reliable construction material. After years of research and experience new possibilities in regards to combined reinforcement are feasible, and are already built. Particularly the effectiveness for crack control has proven outstanding well. In the case of combined reinforcement, durability and serviceability are improved while the required reinforcement layout can be simplified. Significant savings of maintenance cost may be achieved in addition.

Meanwhile a number of design guidelines or codes are available for steel fibre reinforced concrete to calculate the crack width for combined reinforcement. The use of combined reinforcement will certainly increase in fields of application which are currently dominated by solely use of traditional reinforcement, such as large jointless structures, floors with special coatings and water- / liquid-tight structures. Very good experience from carried out projects is available, confirming the concept of combined reinforcement and pointing out its advantages. Practical experiences together with the available theoretical bases strongly supports an increasing use of steel fibres in combination with combined reinforcement.

6. REFERENCES

- A. Haus, (2017), "From Theory to Practice – 15 Years of Applying SFRC for Crack Control in Design", American Concrete Institute, SP-319-8 (Reduction of Crack Width with Fiber), June 2017.

- A. Haus, P. Guirguis, (2015), "Flüssigkeitsdichte Bauteile in Kombinationsbewehrung" (Fluid tight sections in combined reinforcement), Bauingenieur Heft 11/2015, Springer VDI Verlag, Düsseldorf, Germany, November 2015.
- Deutscher Ausschuss für Stahlbeton (DAfStb) (2012), "German Committee for Structural Concrete, guideline steel fibre concrete", Beuth-Verlag, Berlin, Germany, November 2012.
- Deutscher Ausschuss für Stahlbeton (DAfStb), (2011), „Richtlinie für Betonbau beim Umgang mit wassergefährdenden Stoffen“ (German Committee for Structural Concrete, guideline concrete as secondary barrier against hazardous goods), Beuth-Verlag, Berlin, Germany, March 2011.
- European Committee for Standardization (CEN), (2004), "EN 1992-1-1 Eurocode 2: Design of concrete structures – Part 1-1: General rules and rules for buildings", Brussels, Belgium, December 2004.
- fib Model Code for Concrete Structures 2010 (2010), International Federation for Structural Concrete (fib), 2013, Lausanne, Switzerland.
- G. Vitt, (2005), „Crack control with combined reinforcement: from theory into practice“, Concrete Engineering International, April 2005.
- P. Guirguis (2009), "Combined Reinforcement – Effect of Steel Fibers in a Crack Width Design", Fiber Concrete 2009, Prague, Czech Republik, September 2009.

THAUMASITE FORMATION IN CEMENT PASTE EXPOSED FOR 4 DAYS TO AMMONIUM CHLORIDE SATURATED WATER SOLUTION AT AMBIENT TEMPERATURE AND PRESSURE

Barbara Słomka-Słupik, Adam Zybura

Faculty of Civil Engineering, Silesian University of Technology
Akademicka 5 Street, 44-100 Gliwice, Poland

SUMMARY

The thaumasite is a very dangerous, non binding product of concrete corrosion. There was a conviction that the conditions required for the formation of thaumasite in concrete are: source of calcium silicate, sulfate ions, carbonate ions and a very wet, cold (below 15 °C) environment. While the TSA (thaumasite sulphate attack) is recognized, the thaumasite non-sulphate attack (TnSA) must be highlighted, because is also possible. The purpose of this work is to show that thaumasite, or solid solutions of Ett-Th (ettringite with thaumasite) are able to form in hardened cement paste without external source of sulphate ions, at ambient temperature and pressure (25±2°C (298.15 K) and 102±1 kPa). The experiment appeared on thaumasite formation in corroded specimen made of CEM I (Portland cement) and of CEM III (slag cement) after 4 days of immersion in saturated water solution of NH₄Cl.

1. INTRODUCTION

In conventional sulphate attack, diffusing into concrete sulphate ions react with calcium aluminate phases and calcium hydroxide in hardened cement pastes to form either ettringite (3CaO·Al₂O₃·3CaSO₄·32H₂O) or gypsum (CaSO₄·2H₂O). The effects are usually expansion, cracking and spalling. Formation of thaumasite (CaSiO₃·CaCO₃·CaSO₄·15H₂O) does not need aluminate phases, but necessary is the source of carbonate ions, SO₄²⁻ ions, SiO₃²⁻ and water, as well. The calcium silicate hydrates (C-S-H gel) are attacked by external sulphates. Replacement of C-S-H by thaumasite results in the softening of the cement paste matrix into a white, mushy incohesive mass, what destroys the cementitious binding ability (Bensted, 2007; Crammond, 2003; Małolepszy and Mróz, 2006; Révay and Gável, 2003; Thaumasite Expert Group, 2000). In addition:

- the strength of the concrete started to gradually and significantly decrease (Fig. 1);
- the cross section of concrete construction was reduced due loss of cover with exposition of reinforcement.

Many works indicate, that the formation of thaumasite prefers wet and cold conditions. This kind of corrosion appeared mainly in burried construction, where groundwaters containing dissolved sulphates can lead to chemical attack on concrete. It was observed in concrete foundations, columns, pillars, tunnels, slabs of foundations of buildings, sewer pipes, road pavements, drainage construction, concrete anchors, in a grout in a mine, in the base of slab-on-grade pavement, in historical buildings, water dams (Crammond, 2003; Czerewko and Cripps and Reid, 2003; Maingyu and Fumei and Mingshu, 2006; Małolepszy and Mróz, 2006; Stark, 2003; Thaumasite Expert Group, 2000).

Not in Tokaj, but in Budapest, the structural concrete of the largest Hungarian Ferenc Puskás Sports Stadium suffered significant damages due to carbonation and sulphation causing

thaumasite crystallization. This construction was under the effect of waste gases from the nearby railway station and rubber plant (Révay and Gável, 2003) – Fig. 1.

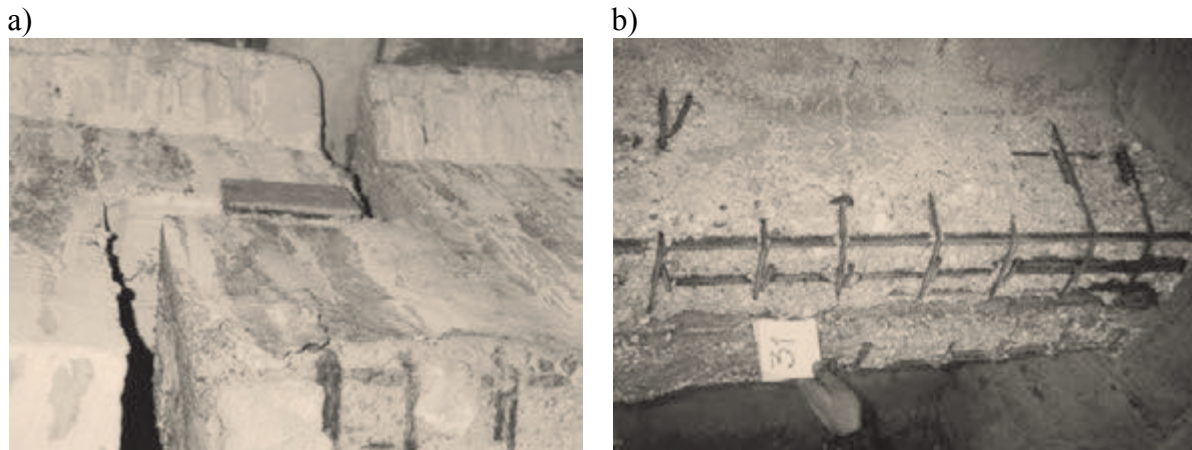


Fig. 1: Corroded reinforced concrete elements from Ferenc Puskás Sports Stadium – a) mushy concrete, b) exhibited steel bars (Révay and Gável, 2003)

The thaumasite form of sulphate attack have come to light on the M5 motorway in Gloucestershire, UK (Crammond, 2003; Czerewko and Cripps and Reid, 2003; Wimpenny and Slater, 2003; Thaumasite Expert Group, 2000), but the first case of thaumasite occurrence in concrete products in the United States were identified in the 1960s (Stark, 2003).

During microscopic observation, thaumasite easily can be confused with ettringite. Morphologically, both appear as needle-like and sometimes columnar crystals and can overgrowth with each other. Also the X-ray diffraction patterns of both phases are quite similar. The main peak of ettringite is by the angle of $9.091^{\circ} 2\Theta(\text{Cu})K\alpha$, and the main peak of thaumasite is by the angle of $9.242^{\circ} 2\Theta(\text{Cu})K\alpha$ (Bensted, 2007; Edge and Taylor, 1969; Nielsen and Nicolai and Darimont, 2014; Słomka-Słupik, 2009; Stark, 2003).

Examinations presented in this work are not concerning conventional sulphate corrosion. During decalcification caused by ammonium chloride penetrated into cement paste and its reactions with hydrated phases, pH of cement matrix was lowered. Due pH changes, stability of different pristine and not pristine hydrated cement phases was disturbed, some of them started to dissolve, and other started to crystallize, depending on substrate accessibility (Biczók, 1972; Słomka-Słupik and Zybyra, 2010 and 2015). Portlandite, as the first one, starts to react with ammonium and chloride ions and releases calcium free ions necessary to reactions in further transformations of phases. The formation of thaumasite needs also source of carbonate which can be supplied from the limestone contained in the cement, from carbonate contained in aggregates, ground waters, soils or the air, from monocarbonate ($\text{C}_3\text{A} \cdot \text{CaCO}_3 \cdot 11\text{H}_2\text{O}$) or calcite. According to Schmidt et. al. (2008), thaumasite is forming from pH 12.5 and is leaching at low pH levels, below 8.0. Then gypsum became the dominant sulphate phase and the amount of thaumasite is decreasing.

The purpose of this work was to highlight thaumasite formation in hydrated cement paste in non-sulphate-bearing environment – in saturated water solution of NH_4Cl , after very short, because 4 days, of immersion in normal (temperature and pressure) conditions.

2. MATERIALS AND METHODS

The samples made of cement paste, which is the most reactive component of concrete, were used for experiments. Samples were separately produced from two industrial cements. The

first one was CEM I 42.5R (Portland cement), and two specimens named „B” was made from it. Also 2 specimens from slag cement CEM III/A 32.5 N-LH/HSR/NA with low heat of hydration, marked as „C”, prepared. Both with $w/c = 0.4$. Chemical compositions of cements and their phases composition, according to Bogue’s method, are presented in Tab. 1.

Tab. 1: Chemical and phase composition of cements, mass %

component cement	CaO	SiO ₂	Al ₂ O ₃	Fe ₂ O ₃	SO ₃	K ₂ O	Na ₂ O	MgO	C ₃ A	C ₄ AF	C ₃ S	slag
B: CEM I 42,5 R	62.63	19.03	5.60	2.89	3.14	0.98	0.16	-	10.0	8.8	59.56	-
C: CEM III/A 32.5 N-LH/HSR/NA	51.95	27.87	5.55	1.63	2.56	0.71	-	4.21	5	4	30	50

The paste samples of dimensions 60×250×250 mm were cured for 2 weeks in moulds, in laboratory conditions, and after demoulding – 3 months in lime-saturated water, in temperature 20 ± 2 °C. Afterwards one sample of each cement: B and C, was immersed in saturated water solution of ammonium chloride, of pH equal to 5. To keep on constant level the concentration of NH₄Cl in the solution, the salt addition was in excess to saturation and remained undissolved on the bottom of the container, in which the samples were immersed. Hydrated cement samples were taken away from the solution after 4 days and designated as B-4 and C-4. Reference samples (B-0 and C-0) were also prepared. They were cured during 3 months in saturated solution of Ca(OH)₂ to avoid leaching effects. Before examination, samples were dried in laboratory conditions – in air, during 2 days.

The changes of phases content with reference to the pH and microstructure are discussed in this article. For this purpose specimens to examination under SEM and XRD were collected as fractures, polished sections and powders. Fractures were used to determine corrosion fronts, roughly, and to microscopic observations with a Zeiss Supra 25 high-resolution scanning electron microscope with smartSEM and Leo32 software. Several specimens were collected by abrasion from consecutive layers of thickness: 0.5; 1.0; 1.5 or 2.0 mm with known distance from external surface of suitable sample. Powder specimens were stored in hermetically closed glass containers. Granulation of powder samples was in correct range for X-ray analysis: 2 – 10 μm. X-ray patterns were collected using Cu-K α radiation (45 kV, 35 mA) with PANalytical X’PERT PRO MPD diffractometer. For peaks identification, the HighScore software package of the PANalytical and PDF4+(2008) ICDD database was used. In order to investigate the changes of contents of main phases in the consecutive layers collected from the outer surfaces of samples, the intensity of strongest peaks was measured. In addition, after one minute from mixing of powder with distilled water (in mass relation: $p/w = 1/100$), the pH measurement was also carried out using an pH electrode for wastewater.

3. RESULTS AND DISCUSSION

In Fig. 2 presented the XRD patterns illustrating crystalline phases changes of samples exposed to the NH₄Cl attack (B-4 and C-4) together with the reference (B-0 and C-0) samples. The localization of particular layers of powdered paste are indicated, as well. In Tab. 2 compiled the presence of phases in various layers.

Portlandite started to dissolve in external layers. At his expense arose ettringite, thaumasite and vaterite. Gypsum crystallized due ettringite, thaumasite and theirs solid solution (SS) decomposition. Calcite in both samples was present everywhere. Even vaterite occurred in the external layers, probably because of carbonation reaction of atmospheric CO₂ with calcium ions diffusing from decalcificated internal parts of samples, or because of thaumasite dissolution.

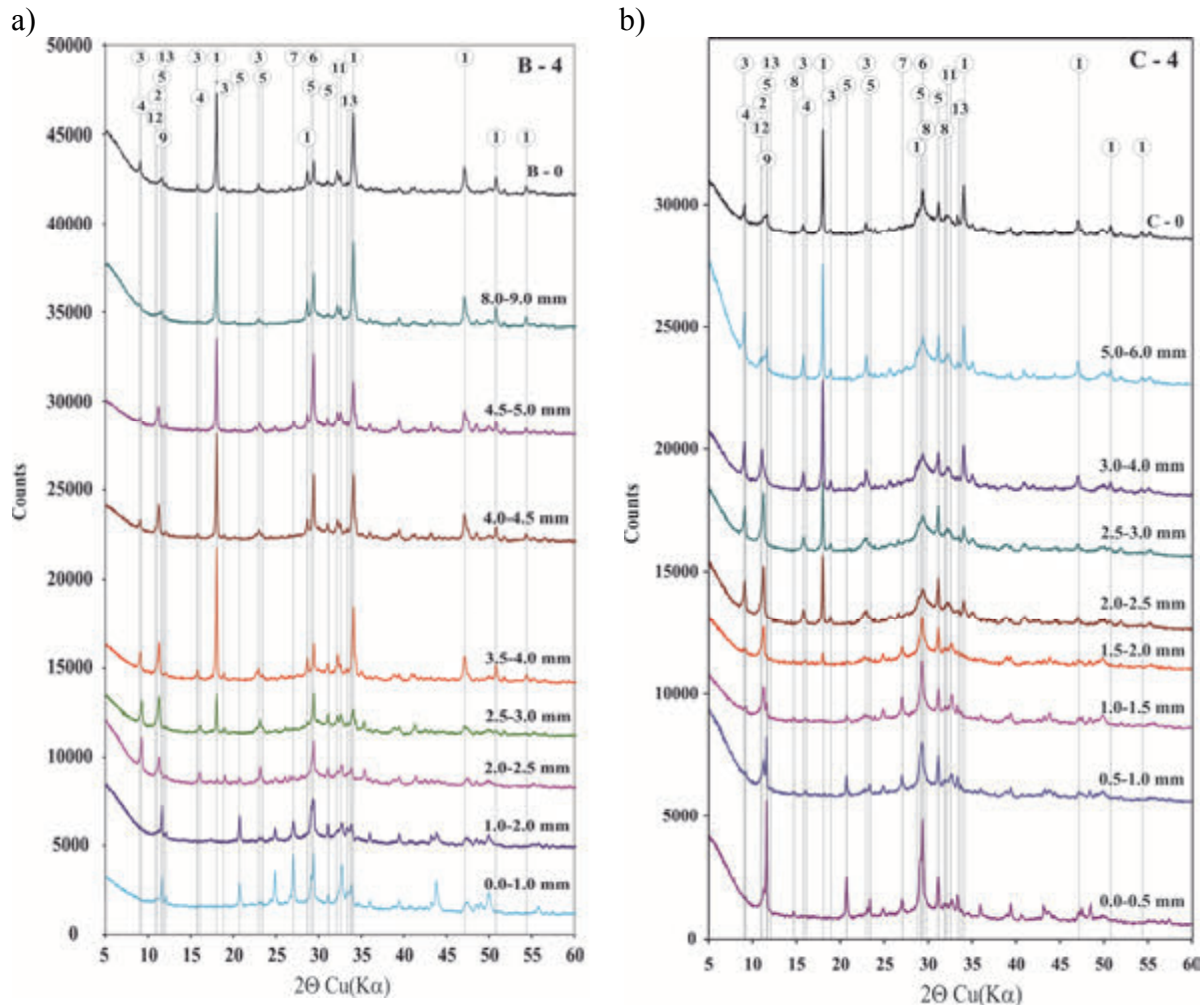


Fig. 2: The diffraction patterns of hardened cement pastes: corroded and comparison a) B-0, B-4 and b) C-0, C-4. Notation: 1 – portlandite, 2- Friedel's salt, 3 – ettringite, 4 – thaumasite, 5 – gypsum, 6 – calcite, 7 – vaterite, 8 – bassanite, 9 – carboaluminate, 11 – belite, 12 – calcium aluminate, 13 – brownmillerite

In corroded specimen made of CEM I (B-4) thaumasite was identified mainly as solid solution with ettringite in layers at the depth of 2.0 to 4.0 mm from external surface of the specimen, while in C-4 (corroded specimen made of CEM III) thaumasite was found as a separate phase (in layers from 0 to 2.5 mm) and in solid solution with ettringite (in layers from 1.0 to 1.5 mm), as well – Tab. 2. The thaumasite dissolution, during pH lowering, is accompanied with the release of carbonate ions. Carbonate ions formed calcite with the free calcium ions derived from phases decalcification, also thaumasite. The changes in the amount of ettringite and thaumasite, compared to pH values showed in Fig. 3.

After portlandite dissolution, calcium ions released from the subsequent phases, to maintain the balance of calcium content in liquid pore solution and in the solid phase, acc. to Carde and François (1997). Finally, the C-S-H phase dissolution occurred, because the Ca/Si ratio in solid phase also depends on the calcium ions concentration in pore solution remaining in equilibrium with this phase. On the basis of the discontinuity in this molar ratio, three kinds of C-S-H phases can be distinguished (Nonat, 2010; Kurdowski, 2008). The results of changes in the content of particular elements in C-S-H phase, presented in Fig. 4, show the relation: as the distance from the B-4 sample surface increased, the ratio of Ca/Si also increased. This is the evidence of C-S-H decalcification in the external layers after 4 days of NH_4Cl water solution action.

Tab. 2: Selected phases identified in the layers of the B-4 and C-4 specimens

Specimen	Depth [mm]	Phases					pH	
		Gypsum CaSO ₄ ·2H ₂ O	Thaumasite	Thaumasite- SS-Ettringite	Ettringite	Vaterite CaCO ₃		Portlandite Ca(OH) ₂
B-4	0.0 – 1.0	+				+		8.48
	1.0 – 2.0	+				+		8.68
	2.0 – 2.5	+	+	+	traces	+		8.78
	2.5 – 3.0		+	+	traces		+	8.81
	3.5 – 4.0			+			+	9.12
	4.0 – 4.5				+		+	12.21
	4.5 – 5.0				+		+	12.08
	8.0 – 9.0				+		+	11.58
C-4	0.0 – 0.5	+	traces			+		8.45
	0.5 – 1.0	+	traces		traces	+		9.20
	1.0 – 1.5	+	+	traces		+		10.20
	1.5 – 2.0	+	+		+			10.19
	2.0 – 2.5	traces	+		+		traces	11.70
	2.5 – 3.0				+		+	11.93
	3.0 – 4.0				+		+	12.13
	5.0 – 6.0				+		+	12.05

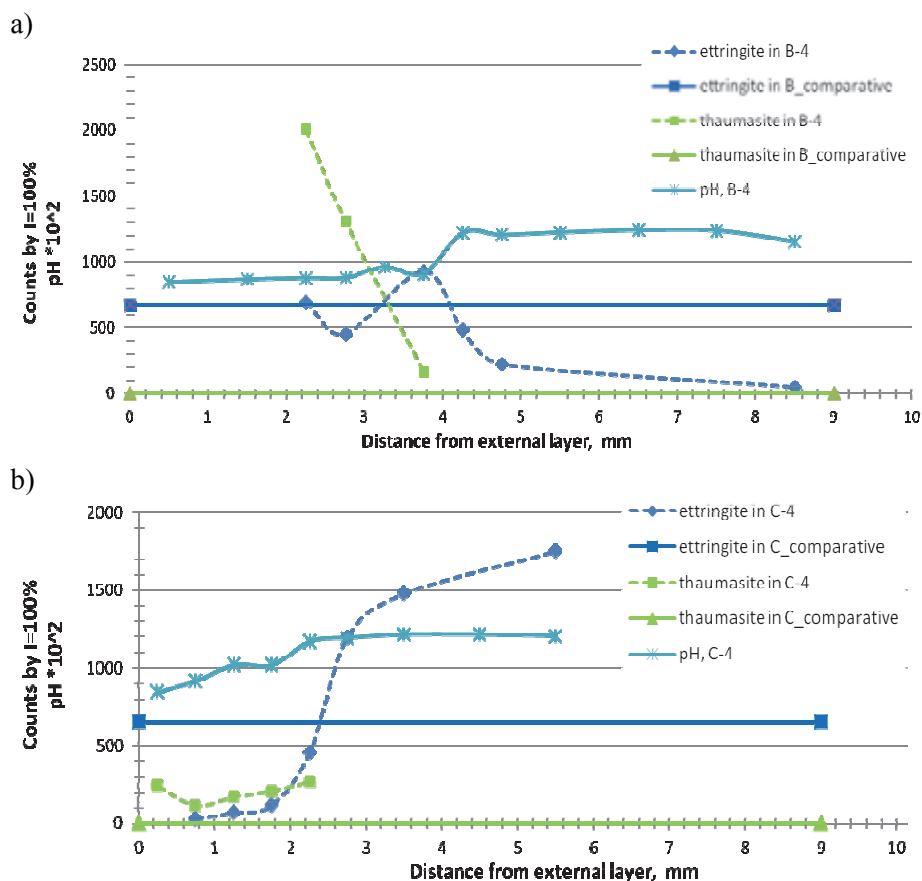


Fig. 3: The comparison of pH, thaumasite and ettringite content in: a) B-4 and b) C-4 specimen as a number of counts by the peaks of the highest intensity, based on XRD patterns

By carrying out a chemical analysis of the micro-area of a crystallized phase located at a distance of 2.2 mm from the surface of the B-4, the presence of thaumasite in solid solution with ettringite has been confirmed – Fig. 5.

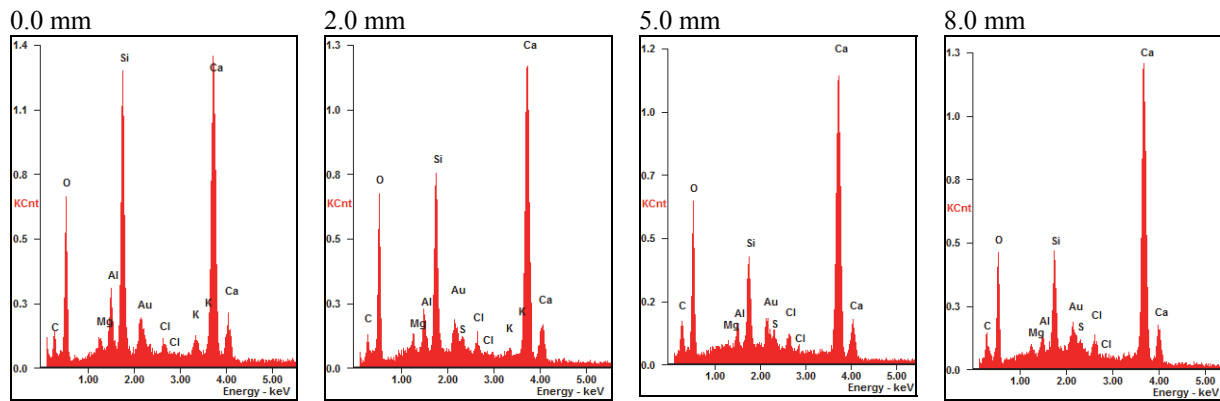


Fig. 4: X-ray microanalysis of the fracture at a certain distance from the surface of B-4 sample

In Fig. 6 is shown the SEM-BSE image of the polished section of C-4 specimen with measured distance from external surface to the microcrack equal to 2.57 mm. There is a suspicion that occurred microcrack is the boundary between external zone – rich and internal zone – lack of thaumasite. At this depth also a boundary of ettringite amount appeared, above and under its comparative line. Ettringite formation can lead to increase in the volume of reaction products from 0.48 to 2.83 times even – during formation from tricalcium aluminate and portlandite (Sarkar and Mahadevan and Meeussen, 2010), what probably caused crack at this depth, as well.

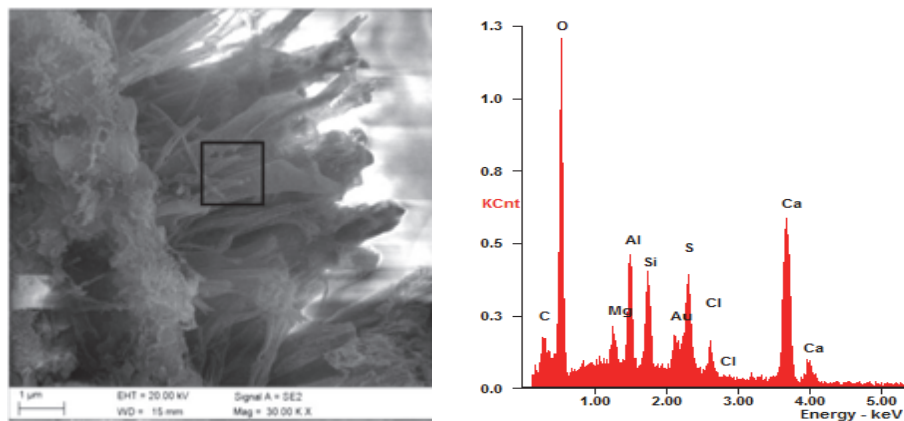


Fig. 5: Solid solution of thaumasite with ettringite in a pore in the depth of 2200 μm from external layer of B-4 sample with X-ray microanalysis in selected area

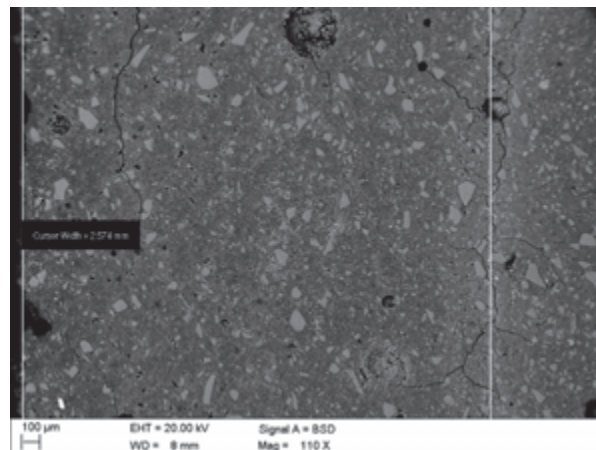


Fig. 6: SEM-BSE image of the microstructure of C-4 sample near external layer, with the microcracks at 2570 μm and 500 μm depth

From sulphate ions releasing during thaumasite dissolution, gypsum crystallized. It was observed at a small depth of 0.5 mm from the external surface of C-4 sample, on the pore wall in form of needle-like crystallites – Fig. 7. The reaction of gypsum formation from thaumasite decreases the volume of sulphate products (Słomka-Słupik and Zybura, 2010), and this dependence probably caused the microcrack formation at the depth of 0.5 mm – Fig. 6.

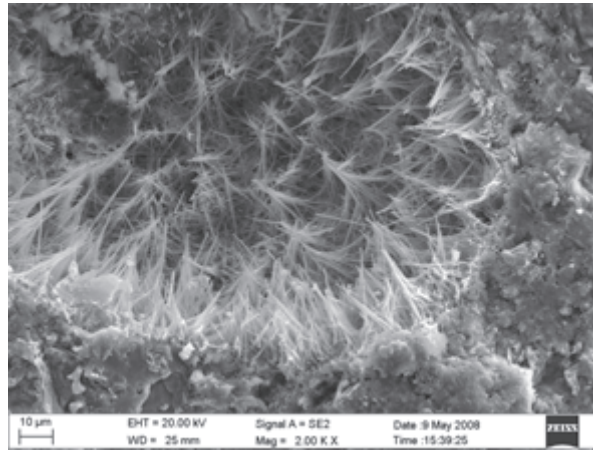


Fig. 7: Gypsum crystals on the pore wall. Sample C-4, $\times = 500 \mu\text{m}$

4. CONCLUSIONS

The diffusion of aggressive ions into and pristine cement ions out of the concrete accompanied chemical reactions, which lead to dissolution and precipitation of solids or even to mechanical damage. Obtained results confirmed that ettringite is unstable, in lower pH underwent dissolution. Thaumasite and gypsum formed from released sulphate ions. Moreover, the formation of thaumasite in specimen attacked by non sulphate medium can cause an astonishment, also the way of thaumasite formation is a little surprising. It seems, thaumasite was formed from solid solution in case of Portland cement paste, but in case of slag cement paste it crystallized directly at the expense of C-S-H phase. Combination of slag with cement (to produce CEM III) extended the scope of thaumasite presence. Whereas in Portland cement sample thaumasite crystallized in a greater amount, but in smaller width of the depth. Thaumasite is stable at a certain pH range, but this is not the only important factor. As can be seen, in case of the sample B-4 (CEM I) thaumasite was noticed from 8.78 – 9.12 pH and in sample C-4 (CEM III) thaumasite was durable from 8.45 to 11.70 pH. Very important was also presence of portlandite, which was consumed in favor of thaumasite formation. The formation of thaumasite accompanied the drop of pH value, more significant in case of Portland cement sample after 4 days of NH_4Cl aggressive immersion.

This article has shown that thaumasite corrosion of concrete is possible even if the corrosive medium is not a sulphate salt solution, in normal conditions. Has also shown that many factors contribute to corrosion effects that need to be adequately determined prior to construction. A new term: „thaumasite non sulphate attack”, shortly TnSA, was introduced in this article.

5. REFERENCES

- Bensted, J. (2007), “Thaumasite - part 2: origins, ramifications and discussions related to the thaumasite expert group report” Cement-Lime-Concrete, Vol. XII/LXXIV, No. 5, September-October 2007, pp. 245-260.

- Biczók, I. (1972) "Concrete corrosion. Concrete protection", Akadémiai Kiadó, Budapest, 1972.
- Carde, C. and François, R. (1997), "Effect of the leaching of calcium hydroxide from cement paste on mechanical and physical properties", *Cement and Concrete Research*, Vol. 27, No. 4, 1997, pp. 539-550.
- Crammond, N. J. (2003), "The thaumasite form of sulfate attack in the UK", *Cement and Concrete Composites*, Vol. 25, Issue 8, December 2003, pp. 809-818
- Czerewko, M. A. and Cripps, J. C. and Reid, J. M. and Duffell, C. G. (2003), "Sulfur species in geological materials—sources and quantification", *Cement and Concrete Composites*, Vol. 25, Issue 7, October 2003, pp. 657-671.
- Edge, R.A., Taylor, H.F.W. (1969), "Crystal structure of thaumasite, a mineral containing $[\text{Si}(\text{OH})_6]^{2-}$ groups", *Nature* 224, 25 October 1969; pp. 363-364, doi:10.1038/224363a0
- Kurdowski, W. (2008), "C-S-H phase - state of the problem. Part 1", *Cement-Lime-Concrete*, No. III/LXXV, July-August 2008, pp. 216-222.
- Maingyu, H. and Fumei, L. and Mingshu, T. (2006), "The thaumasite form of sulfate attack in concrete of Yongan Dam" *Cement and Concrete Research*, Vol. 36, Issue 10, October 2006, pp. 2006-2008.
- Małolepszy, J. and Mróz, R. (2006), "Conditions of thaumasite formation", *Cement-Lime-Concrete*", No. XI/LXXIII, March-April 2006, pp. 93-101.
- Nielsen, P. and Nicolai, S. and Darimont, A. and Kestemont, X. (2014), "Influence of cement and aggregate type on thaumasite formation in concrete", *Cement and Concrete Composites*, Vol. 53, 2014, pp. 115-126.
- Nonat, A. (2010), "C-S-H phase and concrete properties", *Cement-Lime-Concrete*, Vol. 15, No. 6, November 2010, pp. 315-326.
- Révay, M. and Gábel V. (2003), "Thaumasite sulphate attack at the concrete structures of the Ferenc Puskás stadium in Budapest", *Cement and Concrete Composites*, Vol. 25, Issue 8, December 2003, pp. 1151-1155.
- Sarkar, S. and Mahadevan, S. and Meeussen, J.C.L. and van der Sloot, H. and Kosson, D.S. (2010), "Numerical simulation of cementitious materials degradation under external sulfate attack", *Cement and Concrete Composites*, Vol. 32, No. 3, March 2010, pp. 241-252.
- Schmidt, T. and Lothenbach, B. and Romer, M. and Scrivener, K. and Rentsch, D. and Figi, R. (2008), "A thermodynamic and experimental study of the conditions of thaumasite formation", *Cement and Concrete Research*, Vol. 38, 2008, pp. 337-349.
- Słomka-Słupik, B. (2009), "The changes of phases composition of the paste from cement CEM III/A under the influence of NH_4Cl water solution", *Cement-Lime-Concrete*, Vol. XIII/LXXV, No. 2, March-April 2009, pp. 61-66.
- Słomka-Słupik, B. and Zybura, A. (2010), "Microstructure of decalcified cement paste", *Cement-Lime-Concrete*, Vol. 15, No. 6, November 2010, pp. 333-339.
- Słomka-Słupik, B. and Zybura, A. (2015), "Corrosion of hardened cement paste in concrete used for building coke wastewater treatment plant tanks", *Pol. J. Environ. Stud.* Vol. 24, No. 3, May 2015, pp. 1309-1316.
- Stark, D. C. (2003), "Occurrence of thaumasite in deteriorated concrete", *Cement and Concrete Composites*, Vol. 25, Issue 8, December 2003, pp. 1119-1121.
- Thaumasite Expert Group (2000), "One-Year Review", Prepared by Professor L A Clark and BRE in consultation with The Thaumasite Expert Group, March 2000.
- Wimpenny, D., Slater, D. (2003), "Evidence from the highways agency thaumasite investigation in Gloucestershire to support or contradict postulated mechanisms of thaumasite formation (TF) and thaumasite sulfate attack (TSA)", *Cement and Concrete Composites*, Vol. 25, No. 8, December 2003, pp. 879-888.

EFFECT OF MAXIMUM AGGREGATE SIZE ON MECHANICAL PROPERTIES OF HIGH-STRENGTH CONCRETE

Abdulkader El Mir, Ágnes Péity, Salem G. Nehme

Budapest University of Technology and Economics, Budapest, Hungary

1111 Budapest, Műegyetem rkp 3. Main building I. floor 85.

SUMMARY

This study aims to investigate the effect of maximum aggregate size (d_{\max}) on the mechanical properties of high-strength concrete (HSC). The constant parameters were the following: Shrinkage reducing admixture (SRA) to cement weight ratio (1.5%), metakaolin to cement weight ratio (10%), silica fume to cement weight ratio (5%) and water to cement weight ratio ($w/c = 0.3$). The variable parameters were the cement type (CEM I 52.5, CEM II A-S 42.5 R), cement content (500 kg/m^3 , 600 kg/m^3 , 700 kg/m^3 , 800 kg/m^3) and d_{\max} (5 mm, 8 mm). Several mechanical tests (compressive strength, flexural tensile strength, watertightness and drying shrinkage) were carried out to evaluate the influence of d_{\max} on the concrete properties. Thereby, an objective evaluation between studied parameters could be reached to achieve HSC with the least possible shrinkage behavior.

1. INTRODUCTION

Properties of high-strength concrete (HSC) depend on the type of aggregate, both on a qualitative selection as well as grading. The influence of maximum aggregate size (d_{\max}) on concrete strength has been stated by several authors in the literature. Aïtcin (1998) and Venkateswara et al. (2010) agreed that, if smaller aggregate particles size were used, higher concrete strength would be obtained. (Aïtcin, 1998) stated that the increase of d_{\max} may evoke some problems with the quality of the interfacial transition zone in which it could be larger and more heterogeneous. According to Chen and Liu (2006), aggregate size significantly affects the fracture behavior of high performance concrete. The fracture energy of concrete will increase with the increase of the d_{\max} , and by that, the larger the size of the aggregate, the more significant the crack propagating and the greater the fracture process zone can form.

The undertaken study aims to investigate the effect of alumino-silicate supplementary cementitious material (SCM) metakaolin (MK) and silica fume (SF), along with the d_{\max} , on the mechanical and durability aspect of HSC. Several concrete batches were designed and arranged based on the combined effect of these materials.

2. EXPERIMENTAL PROCEDURE

2.1. Materials and mixtures proportions

Two types of cement were used (CEM II A-S 42.5 RS and CEM I 52.5) for the production of HSC mixtures. A commercially locally produced MK was used as alumino-silicate based SCM. Also, SF in the form of slurry was implemented as silica based SCM. Mixtures were developed with two separate d_{\max} (5 mm and 8 mm) groups. The aggregate grading size distribution for $d_{\max} = 5$ mm was arranged into 30% very fine sand (0.2-0.6 mm), 10% fine sand (0.4-1 mm), 25% medium sand (1-2.5 mm) and 35% coarse sand (2-5 mm) with fineness

modulus value of 4.7. Also natural quartz sand was added as aggregate with mean size diameter of 2.36 mm. On the other hand, the aggregate grading size distribution corresponding to $d_{\max} = 8$ mm was arranged into 45% river sand (0-4 mm) and 55% coarse aggregate (4-8 mm) with fineness modulus value of 5.72. As for the chemical admixtures, “Glenium 300” superplasticizer and “Sika Control-40” shrinkage reducing admixture (SRA) were added to the fresh mixture for adequate rheological properties. Note that a constant dosage of SRA was added for all mixtures (1.5 % of the cement weight). The water-cement ratio was selected to be constant ($w/c = 0.3$). Regarding SCMs, the cement weight replacement percentages by MK and SF were 10% and 5% respectively. Tap water was used for mixing. The detailed composition of mixtures is presented in Tab. 1.

Tab. 1: Mixtures compositions

Concrete ID	Cement Content [kg/m ³]	Cement Type	Maximum aggregate size	Paste content [m ³ /m ³]
8	500	CEM II	$d_{\max}=5$ mm	0.4175
1	600	CEM II	$d_{\max}=5$ mm	0.5440
2	700	CEM II	$d_{\max}=5$ mm	0.6127
3	800	CEM II	$d_{\max}=5$ mm	0.6864
4	500	CEM II	$d_{\max}=8$ mm	0.3570
5	600	CEM II	$d_{\max}=8$ mm	0.3888
6	700	CEM II	$d_{\max}=8$ mm	0.4969
7	800	CEM II	$d_{\max}=8$ mm	0.4518
VIII	500	CEM I	$d_{\max}=5$ mm	0.4165
I	600	CEM I	$d_{\max}=5$ mm	0.5441
II	700	CEM I	$d_{\max}=5$ mm	0.6131
III	800	CEM I	$d_{\max}=5$ mm	0.6862
IV	500	CEM I	$d_{\max}=8$ mm	0.3569
V	600	CEM I	$d_{\max}=8$ mm	0.3876
VI	700	CEM I	$d_{\max}=8$ mm	0.4958
VII	800	CEM I	$d_{\max}=8$ mm	0.4509

2.2. Test methods

The density of hardened concrete was measured in accordance with to European Standards (MSZ, 2009a).

Cubic sized specimens (150 mm) were tested for compressive strength by a universal closed-loop hydraulic testing machine performed based on European Standard (MSZ, 2009b) at a constant loading rate of 11.25 kN/s and at the age of 28 days. As for the flexural strength test, it was in compliance with the American standards (ASTM, 1994). Prismatic specimens (75 × 75 × 250 mm) were tested at 28 days.

In accordance with the European Standard (MSZ, 2009c), watertightness test was performed on 150 mm cubic sized specimens at the age of 28 days.

As for the drying shrinkage, prismatic specimens (75 × 75 × 250 mm) were tested for multiple time offset. After removal from their steel molds, studs were glued on the four longitudinal surface sides of concrete prism by applying a special adhesive. Demountable mechanical strain gauge (DEMEC), that could read up to 0.001 mm, was the shrinkage measurement tool. Therefore, the change in length of the specimens could be measured until 35 days of curing time.

3. RESULTS AND DISCUSSION

3.1 Body density

Body densities of HSC mixtures are illustrated in Fig. 1. The highest density was recorded for mixtures corresponding to $d_{\max} = 8$ mm with the lowest cement content of 500 kg/m^3 reaching a density value of 2418 kg/m^3 . In general, the body density of concrete mixtures decreases with the increase of cement content, keeping a constant water to cement ratio. Therefore, the lowest value of density (2253 kg/m^3) was recorded for the mixture corresponding to $d_{\max} = 5$ mm with the highest cement content (800 kg/m^3). That could be attributed to the increase of the cement paste keeping in mind that a constant water to cement ratio was applied.

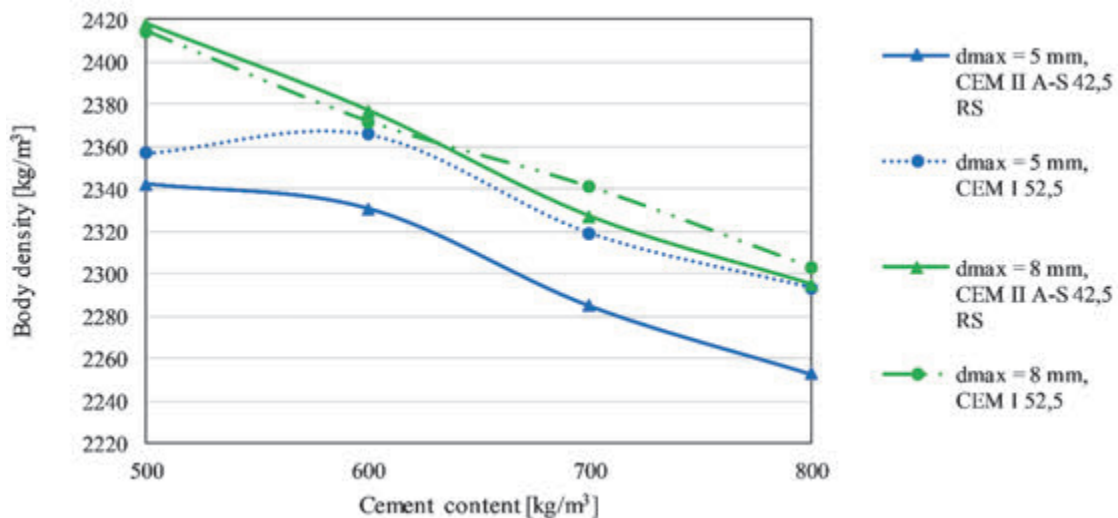


Fig. 1: Variation of the body density of HSC mixtures in terms of their cement content, cement type and maximum aggregate size (d_{\max})

3.2 Compressive and flexural strength

To test the hydraulic activity of binders in the present examination, HSC mixtures consisting of various cement contents were produced with constant amount of SCMs replacement by weight of cement. The cement content ranged between 500 - 800 kg/m^3 with constant cement weight replacement by 10% of MK and 5% of SF. According to Fig. 2, HSC mixture corresponding to $d_{\max} = 5$ mm, with 600 kg/m^3 cement content and “CEM I 52.5” cement type showed the highest compressive strength value of 136 MPa from all produced mixtures. However, other HSC mixtures in the same conditions but with higher cement content (700 kg/m^3 , 800 kg/m^3) and with similar $w/c = 0.3$ revealed that the optimum level of cement use was 600 kg/m^3 . This behavior could be attributed to the effect of the paste variation on the failure pattern in compression. The effect of paste content is more pronounced for low values cement content for which the rate of strength change is higher. It is usually attributed to the longer path for the crack needs to follow when the aggregate volume in the concrete is higher, thus having to move around greater number of aggregates, a fact that makes the energy absorbed higher. When the volume of paste is higher and the volume of aggregates is smaller, the length of the path becomes straighter, thus smaller, and the amount of energy absorbed becomes less (Kolias and Georgiou, 2005). On the other hand, considering the effect of d_{\max} , lower d_{\max} contributed to higher values of compressive strength. For instance, when the same cement type and content (CEM I 52.5, 500 kg/m^3) were selected, mixture that corresponds to

$d_{\max} = 5$ mm showed an increase of 14.6 % of compressive strength value than of the mixture corresponding to $d_{\max} = 8$ mm.

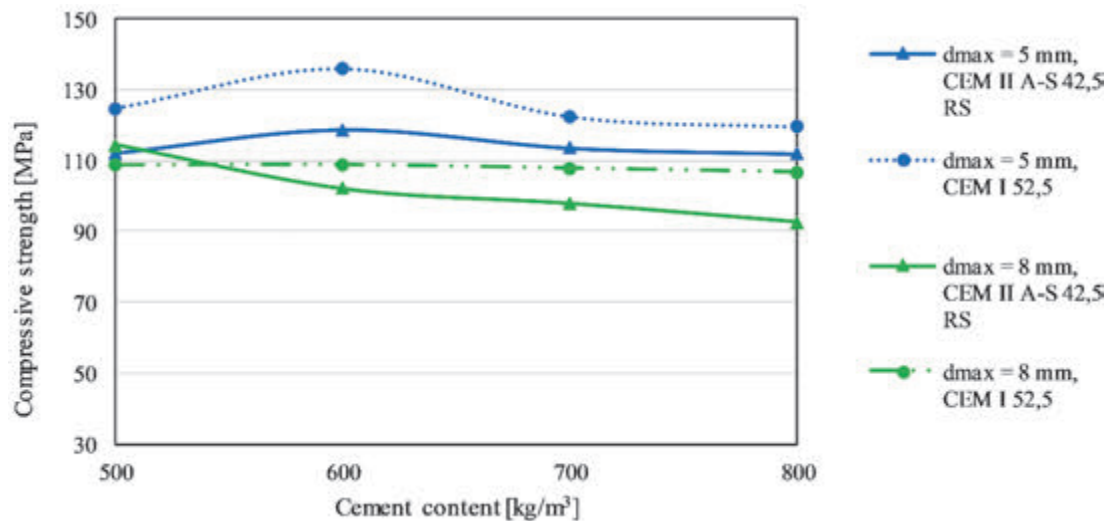


Fig. 2: Variation of the compressive strength of HSC mixtures in terms of their cement content, cement type and maximum aggregate size (d_{\max}).

Fig. 3 shows the flexural strength results of all HSC mixtures at the age of 28 days. Quite different trends were observed in the flexural strength of concrete, whose compressive strength showed a slight decrease along with the paste increase. It is clearly noticeable that in case of smaller d_{\max} (5 mm), the flexural strength significantly decreases with higher cement content of 800 kg/m³. This behavior could be explained by the increase of the paste volume, reaching the lowest flexural tensile strength value of 3.8 MPa at 800 kg/m³ of cement content.

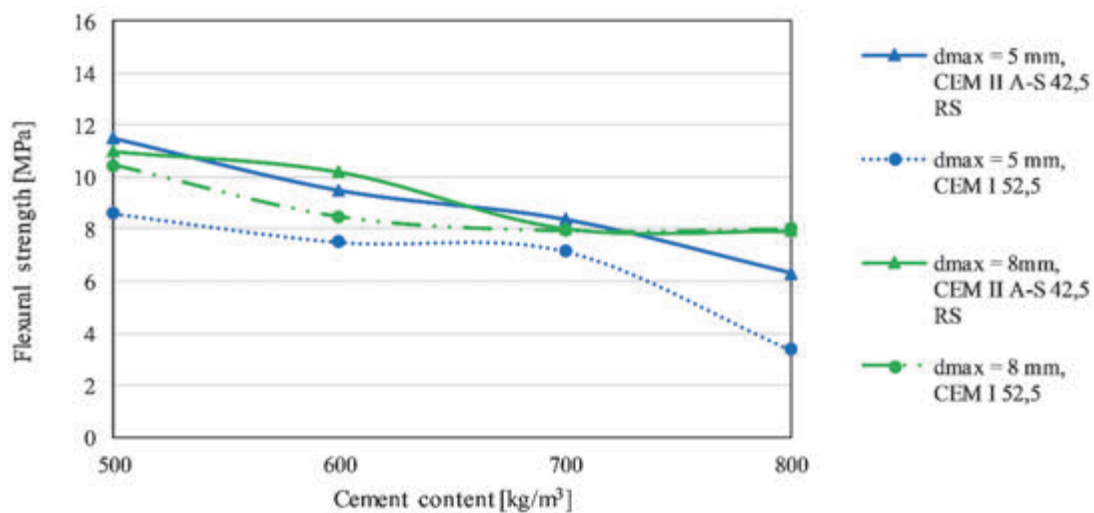


Fig. 3: Variation of the flexural strength of HSC mixtures in terms of their cement content, cement type and maximum aggregate size (d_{\max}).

3.3 Water penetration depth

Watertightness test results are shown in Fig. 4. The individual maximum penetration depth value of each mixture was recorded at 28 days. Evaluating the penetration depth results in terms of d_{\max} variation (5 or 8 mm), it can be noticed that for the highest d_{\max} (8 mm), higher water penetration depth values were attained (18.5 mm) in comparison with the lowest d_{\max}

value (5 mm). On the other hand, a decreasing pattern of water penetration depth is observed as the cement content increases. This behavior is attributed to the effect of the paste volume in decreasing the concrete permeability. Yet, the general response of all HSC mixtures still considered to be very high in terms of permeability resistance (Saheed et al., 2014).

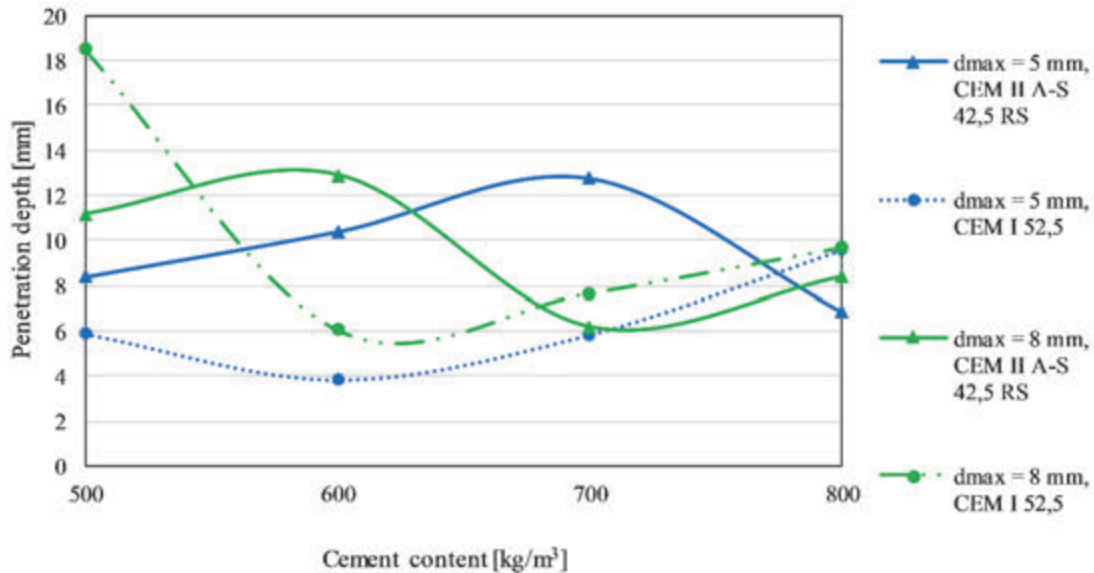


Fig. 4: Variation of the water penetration depth of HSC mixtures in terms of their cement content, cement type and maximum aggregate size (d_{max}).

3.4 Drying shrinkage

Cracking is a sensitive phenomenon resulting by variation in the concrete volume, thereby, shrinkage hazards could occur, in which are directly connected to corrosion and deterioration of the reinforcements. Fig. 5 and 6 show the development of the drying shrinkage of HSC mixtures over time. Test results showed that the drying shrinkage values of mixtures, which were recorded up to 35 days, fell below 900 microstrains.

At earlier ages, shrinkage rates were observed to be different and directly dependent on the cement type, content, and d_{max} . Obviously, it could be noticed the dramatic increase of the drying shrinkage in case of $d_{max} = 5$ mm (with the corresponding cement type and content, CEM I 52.5; 800 kg/m³). However, if d_{max} was changed to 8 mm for the same previous conditions, the shrinkage value dropped significantly from 0.566 to 0.133 microstrains at 3 days. The same pattern is observed when “CEM I 52.5” type is replaced by “CEM II A-S 42.5 RS”. The shrinkage values increase continuously until the 25 day, and then gradually after 30 days. The combined effect of MK and SF along with the main cement binder highly stimulate the hydration reaction, especially, the effect of SF in fast hydraulic activity, thus higher shrinkage values were observed. For mixtures corresponding to $d_{max} = 8$ mm, lower shrinkage values were observed at the 30 day. This behavior is due to the lower volume of paste as compared to $d_{max} = 5$ mm mixtures. At high paste volume, higher drying shrinkage values were observed. Undoubtedly, explanation of this behavior must be sought to the variation of aggregates proportions in which the fraction of paste is lower.

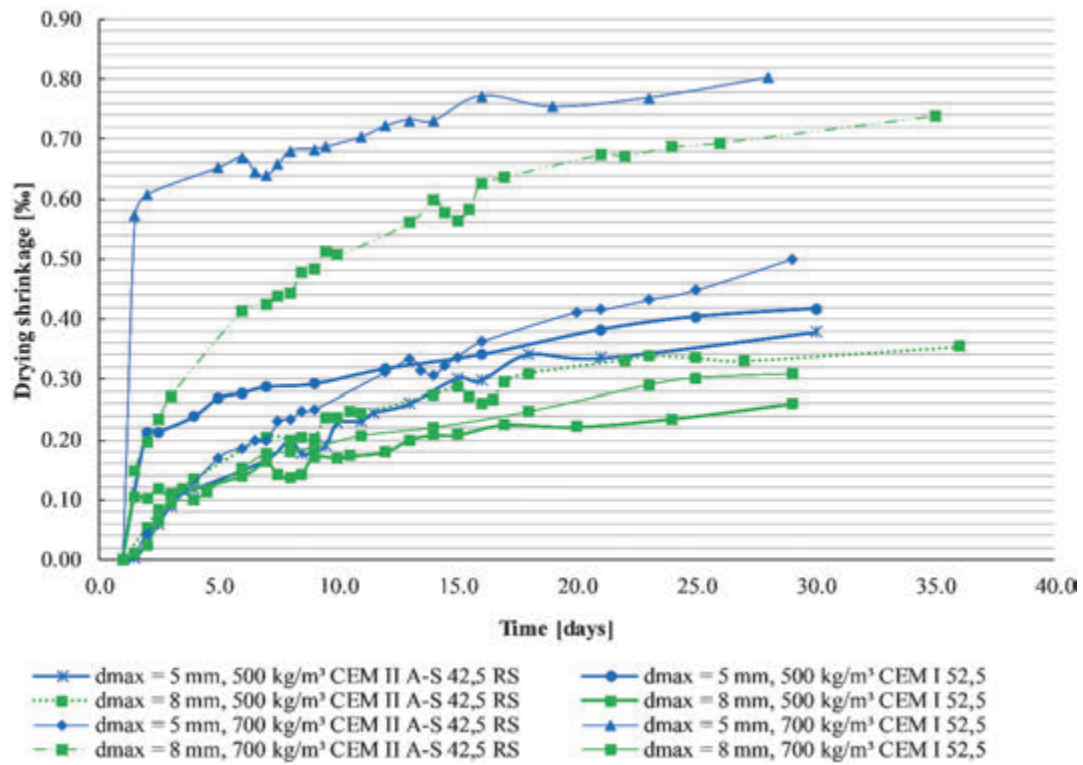


Fig. 5: Drying shrinkage of HSC mixtures over drying time for 500 and 700 kg/m³ cement content.

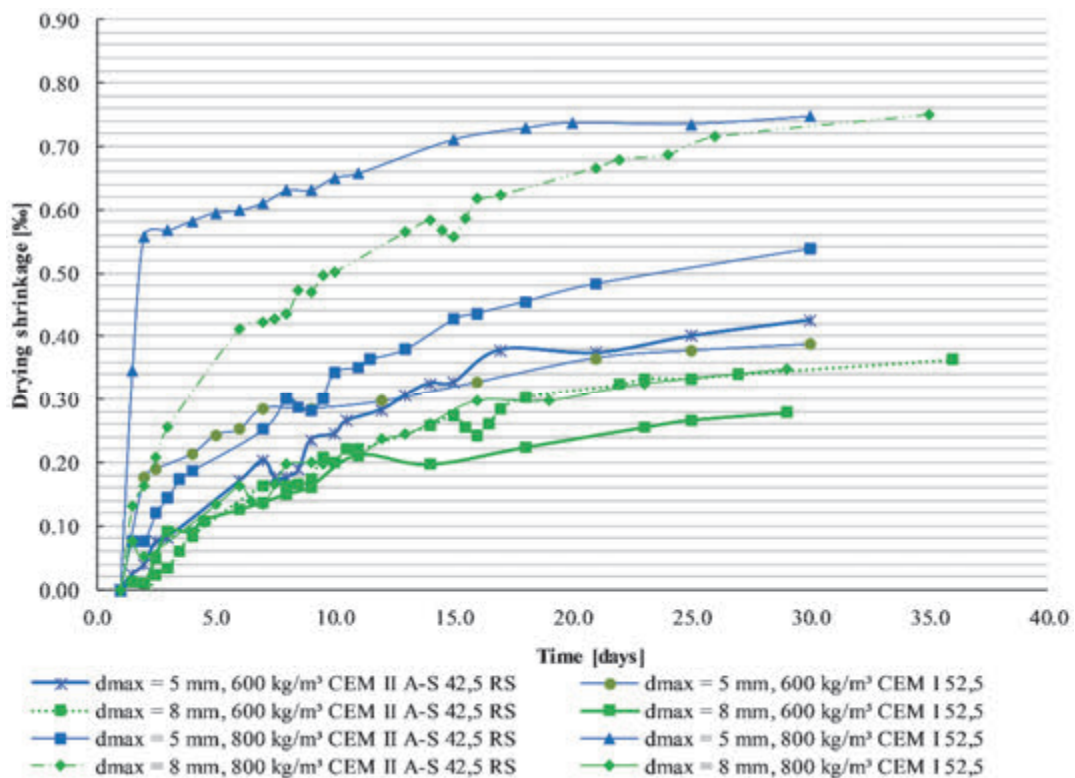


Fig. 6: Drying shrinkage of HSC mixtures over drying time for 600 and 800 kg/m³ cement content.

4. CONCLUSIONS

The most important aim of this work was to reveal the response of HSC concrete to the combined use of SCMs at optimum level of cement substitution ratio with different maximum aggregate sizes. Taking into consideration the limitations of the work concerning primarily the maximum aggregate size used (5 and 8 mm), the following conclusions can be drawn on the mechanical and durability characteristics of HSC:

- The use of 5 mm maximum aggregate size and “CEM I 52.5” type showed to have the best performance for the compressive strength and watertightness properties among other mixtures.
- As the maximum aggregate size increased from 5 to 8 mm, lower compressive strength values were obtained for the same w/c ratio.
- For the mixtures with the same maximum aggregate size, the increase of the paste volume decreased the flexural strength, keeping a constant w/c ratio.
- The drying shrinkage values of HSC mixtures with smaller maximum aggregate size were higher than those of HSC mixtures with higher maximum aggregate size.

5. REFERENCES

- Aïtcin, P.-C. (1998), “High-performance concrete”, E and FN Spon, London and New York
- ASTM International, ASTM C 293-94, “Standard Test Method for Flexural Strength of Concrete (Using Simple Beam With Center-Point Loading)”. ASTM Standards 1994
- Chen, B. and Liu, J. (2006), “Investigation of effects of aggregate size on the fracture behavior of high performance concrete by acoustic emission”, *Construction and Building Materials*, Vol. 21, pp. 1696–1701
- Kolias, S and Georgiou, C. (2005), “The effect of paste volume and of water content on the strength and water absorption of concrete”. *Cement and Concrete Composites*, Vol. 27, pp. 211-216
- MSZ, 2009a. Testing Hardened Concrete – Part 7: Density of hardened concrete, MSZ EN 12390-7. Hungarian Standards Institution, Hungary
- MSZ, 2009b. Testing Hardened Concrete – Part 3: Compressive Strength of Test Specimens, MSZ EN 12390-3. Hungarian Standards Institution, Hungary
- MSZ, 2009c. Testing Hardened Concrete – Part 8: Depth of Penetration of Water Under Pressure, MSZ EN 12390-8. Hungarian Standards Institution, Hungary
- Rao, S. V, Rao, M.V. and Kumar, P.R. (2010), “Effect of Size of Aggregate and Fines on Standard and High Strength Self Compacting Concrete”, *Journal of Applied Science Research*, Vol. 6, No. 5, pp. 433-442
- Saheed, A., Shamsad, A., Mohammed, M., Husain, J. A. (2014), “Properties of SCC prepared using Natural Pozzolana and Industrial Wastes as Mineral Fillers”, *Journal of Cement and Concrete Composites*, Vol. 62, pp. 125-133

IMPROVED FIRE RESISTANCE BY USING DIFFERENT DOSAGES OF METAKAOLIN

Abdelmelek Nabil¹, Éva Lubláy²

¹ *nabil3c@gmail.com*

² *Corresponding author; lubloy.eva@epito.bme.hu*

Budapest University of Technology and Economics, Department of Construction Materials and Technologies, H-1521 Budapest, Hungary)

SUMMARY

Concrete is a composite material that consists mainly of mineral aggregates bound by a matrix of hardened cement paste. Strength reduction of high strength concrete during and after fire may be different from that of normal strength concrete. The use of metakaolin as a recent material in the construction industry proves to be very useful to modify the properties of concrete. An extensive experimental study was carried out to analyse the post-heating characteristics of hardened cement paste subjected to temperatures up to 800 °C. Major parameters of our study were the content (0, 3, 6, 9 or 12 m%) of one type supplementary material (metakaolin) as a replacement of cement, as well as the value of maximum temperature of exposure (50, 150, 300, 400, 500, 800 and 900°C). In the experiments specimens were exposed to the given maximal temperatures and then cooled down to room temperature. Present studies included analysis of compressive strength.

1. INTRODUCTION

Concrete can be exposed to elevated temperatures during fire or when it is applied by furnaces and reactors. The behaviour of a concrete structural members exposed to fire is dependent on physical, thermal, and mechanical deformation properties of concrete of which the member is composed. The deterioration processes influence the durability of concrete structures and may result in undesirable structural failures. Therefore, preventative measures such as choosing the right materials should be taken to minimize the harmful effects of high temperature on concrete. The high temperature behaviour of concrete is greatly affected by material properties, such as the properties of the aggregate, the cement paste, and the bond between the aggregate and cement paste, as well as the thermal compatibility of the aggregate and cement paste.

2. BEHAVIOUR OF CONCRETE IN FIRE

2.1 Physical behaviour

It is generally agreed (Short, Purkiss and Guise, 2001; Colombo and Felicetti, 2007) that concrete containing siliceous aggregates when heated between 300 °C and 600 °C it will turn red; between 600 °C and 900 °C, whitish-grey; and between 900 °C and 1000 °C, a buff colour is present. The colour change of heated concrete results from the gradual water removal, dehydration of the cement paste, and transformations occurring within the aggregate, respectively. The most intense colour change, the appearance of red colouration, is observed for siliceous riverbed aggregates containing iron. This colouration is caused by the oxidation of mineral components. While siliceous aggregates turn red when heated, the aggregates

containing calcium carbonate get whitish. Due to calcination process CaCO_3 turns to lime and give pale shades of white and grey (Hager, 2013a).

2.2 Thermal behaviour

Thermal properties that govern temperature dependent properties in concrete structures are thermal conductivity, specific heat (or heat capacity) and mass loss (Kodur, 2014). The density of concrete shows only slight temperature dependence, which is mostly due to moisture losses during heating. However limestone concretes show a significant decrease of density at about 800 °C due to the decomposition of the calcareous aggregate. The thermal conductivity of concrete depends on the conductivities of its constituents. The major factors are the moisture content, the type of aggregate and the mix proportions. The conductivity of any given concrete varies approximately linearly with the moisture content (Schneider, 1988).

2.3 Mechanical behaviour

The mechanical properties that are of primary interest in fire resistance design are compressive strength, tensile strength, elastic modulus and stress-strain response in compression (Kodur, 2014). The mechanical response of concrete is usually expressed in the form of stress-strain relations, which are often used as input data in mathematical models for evaluating the fire resistance of concrete structural members (Hager, 2013b).

Generally, because of a decrease in compressive strength and increase in ductility of concrete, the slope of stress-strain curve decreases with increasing temperature. The strength of concrete has a significant influence on stress-strain response both at room and elevated temperatures.

3. METAKAOLIN

Metakaolin (MK) is a recent addition in the list of pozzolanic materials. It is a thermally activated alumino- silicate produced from kaolinite clay through a calcining process. Unlike other pozzolans, MK is a primary product, not a secondary product or by-product. This allows the manufacturing process to be structured to produce the optimum characteristics for the MK, ensuring the production of a consistent product and a consistent supply. The white color of MK results in a concrete with lighter color, another advantage making it popular (Mlinárik and Kopeckó, 2013; Kopeckó and Mlinárik, 2014).

MK enhances the strength and durability of concrete through three primary actions which are the filler effect, the acceleration of ordinary Portland cement (OPC) hydration and the pozzolanic reaction with calcium hydroxide (CH). Wild, Khatib and Jones (1996) found that the filler effect is immediate, the acceleration of OPC hydration has its major impact within the first 24 h and the maximum effect of pozzolanic reaction occurs between 7 and 14 days. It was concluded that the optimum replacement level of OPC by MK to give maximum long term strength is about 20% by weight.

Kostuch, Walter and Jones (2000) discovered that a 10% replacement of cement with MK reduced the CH content in concrete by 70%, and a 20% replacement reduced it to almost zero after 28 days. However, the amount of MK required for complete elimination of CH depends on a number of factors such as purity of MK, Portland cement composition, water/binder ratio and curing conditions (Oriol and Pera, 1995). The reduction in CH content results in superior

strength and durability performance, even at elevated temperatures (Lin, Lin and Powers-Couche, 1996). Poon, Kou and Lam (2000) prepared normal and high strength concrete (HSC) mixes incorporating 5%, 10% and 20% MK and compared their performance with the equivalent silica fume (SF) and fly ash (FA) mixes. They observed that the MK concrete possessed higher strength, lower permeability and less porosity as compared to the corresponding SF and FA concretes. In another study in the case of the mortar samples prepared with 10 or 17 m% MK, the smaller substitution (10 m%) was found more effective, than the higher substitution of the cement (17 m%). The compressive strength of the samples with 17 m% substitution is very similar to that of the reference samples (specimens made without metakaolin addition). The higher dosage of MK is expectedly resulted in the aggregation of the particles, which could not completely disperse during mixing. The results of the samples made with SF were the opposite; the higher substitution ratio (10 m%) was found to be more effective than the smaller substitution ratio (5 m%) (Mlinárik, Kopecskó and Borosnyói, 2016).

It was observed that the fire resistance of concrete is highly dependent on its constituent materials, particularly the pozzolans. A number of research studies (Phan, 1996) indicated that the addition of pozzolanic SCM highly densifies the pore structure of concrete, which can result in explosive spalling due to the build-up of pore pressure by steam. Since the evaporation of physically absorbed water starts at 80 °C which induces thermal cracks, such concretes may show inferior performance as compared to pure OPC concretes at elevated temperatures.

4. EXPERIMENTAL DETAILS

An experimental program was designed to analyse the post-heating characteristics of hardened cement paste subjected to temperatures up to 800 °C. Major parameters of our study were the different dosages (0, 3, 6, 9, 12 or 15 m%) of supplementary material (metakaolin) of the binder (as replacement of cement) and the value of maximum temperature (50, 150, 300, 400, 500, 800 °C). In the experiments specimens were exposed to the given maximal temperatures and then cooled down to room temperature. Tests were carried out at room temperature. Present studies included analysis of compressive strength.

4.1. Materials

Preparing the specimens OPC (CEM I 42,5 N) and metakaolin supplementary material was used. The water cement-ratio was 0.35. 2 g/kg liquid superplasticizer was applied. Cubic form cement paste specimens were cast with the size of 30 mm.

4.2. Curing and heating regimes

The specimens were demolded 24 h after the casting and placed in a water tank at 20 °C. After 7 days of water curing, they were transferred to an environmental chamber maintained at 20 °C and normal humidity. At an age of 90 days, the specimens were heated in a furnace (20, 50, 150, 300, 400, 500, 800 and 900 °C). Our experimentally applied heating curve was similar to the standard fire curve up to 800 °C. Specimens were kept for two hours at the actual maximum temperature levels. Specimens were then slowly cooled down in laboratory conditions for further observations. During the heat load a program controlled electric furnace was used. The compressive strength was measured on the heat loaded and, than

cooled down specimens and the average values of the measurements were analysed. The specimens were allowed to cool naturally to room temperature, and tested.

5. RESULTS AND DISCUSSIONS

The development of compressive strength as a function of temperature is presented in Fig. 1.

Residual compressive strength of cement stone specimens is shown in Fig. 2 relating to the concrete composition and the maximum temperature of thermal load, from which the following conclusions can be drawn: the relative residual compressive strength decreases up to 150 °C heat loading, then increases up to 300 °C. In the case of higher temperatures than 300 °C the residual relative compressive strength decreases again. Specimens loaded up to 300 °C show higher residual strength comparing with the average strengths measured on specimens loaded up to 150 °C because the intensive dehydration in the temperature interval between 60 and 180 °C probably causes the hydration of the unhydrated cement grains in the microstructure. To sum up these results, the temperature load at 900 °C caused increasing residual relative compressive strength with the increase of content of supplementary materials.

In case of cement stone prepared with metakaolin containing binder (to 12 m% related to the mass of cement) the strength increased due to the temperature load of 800 °C. Addition of metakaolin was found to be unfavourable for fire resistance of concrete at the age of test (thermal load was applied at the age of 90 days).

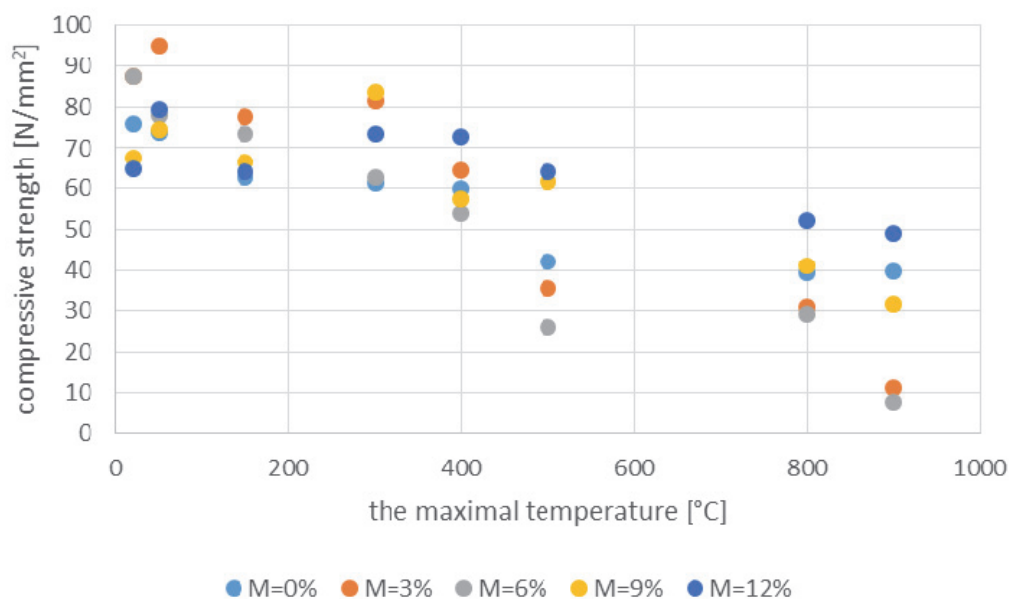


Fig. 1: The compressive strength for the different mixes as a function of maximum temperature (averages of 5 measurements)

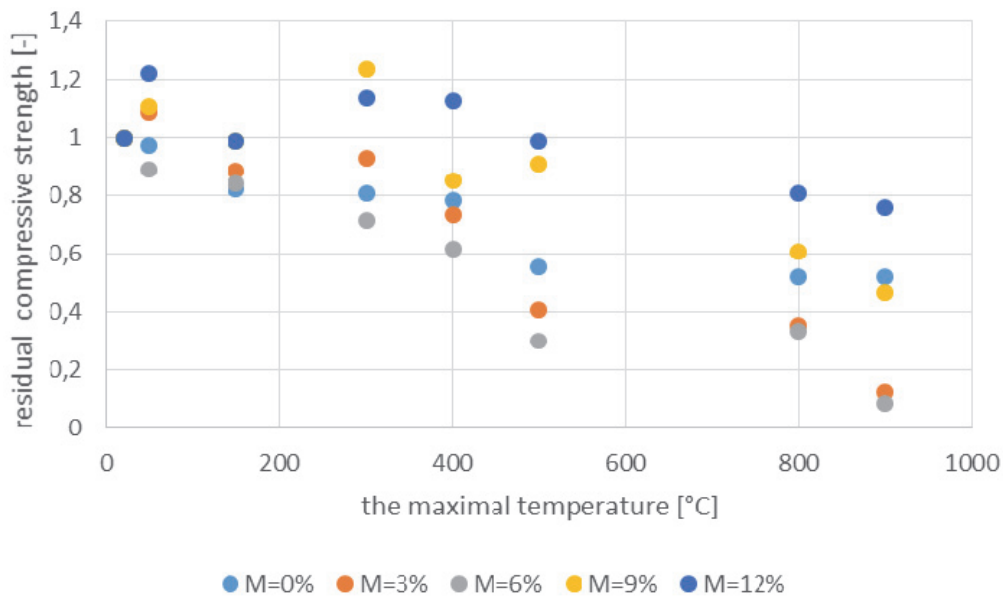


Fig. 2: Relative residual compressive strength for the different mixes as a function of maximum temperature (averages of 5 measurements)

6. CONCLUSIONS

Concrete is a composite material that consists mainly of mineral aggregates bound by a matrix of hardened cement paste. Strength reduction of high strength concrete during and after fire may be different from that of normal strength concrete. The use of metakaolin as a recent material in the construction industry proves to be very useful to modify the properties of concrete. An extensive experimental study was carried out to analyse the post-heating characteristics of hardened cement paste subjected to temperatures up to 800 °C. Major parameters of our study were the content (0, 3, 6, 9 or 12 m%) of supplementary material (metakaolin) of cement and the value of maximum temperature (50, 150, 300, 400, 500, 800 and 900°C). In the experiments specimens were exposed to the given maximal temperatures and then cooled down to room temperature.

The relative residual compressive strength decreases up to 150 °C heat loading, then increases up to 300 °C. In the case of higher temperatures than 300 °C the residual relative compressive strength decreases again. Specimens loaded up to 300 °C show higher residual strength comparing with the average strengths measured on specimens loaded up to 150 °C because the intensive dehydration in the temperature interval between 60 and 180 °C probably causes the hydration of the unhydrated cement grains in the microstructure. To sum up these results, the temperature load at 900 °C caused increasing residual relative compressive strength with the increase of content of supplementary materials.

In case of cement stone prepared with metakaolin containing binder (to 12 m% related to the mass of cement) the strength increased due to the temperature load of 800 °C. Addition of metakaolin was found to be unfavourable for fire resistance of concrete at early ages (thermal load was applied at the age of 28 days). This could be explained by the different rate of pozzolanic reaction of the SCMs.

7. ACKNOWLEDGEMENTS

Authors acknowledge the support by the Hungarian Research Grant NVKP_16-1-0019 “Development of concrete products with improved resistance to chemical corrosion, fire or freeze-thaw”. Second author acknowledges the support by the János Bolyai Resarch Scholarship of the Hungarian Academy of Sciences.

8. REFERENCES

- Colombo, M., Felicetti, R. (2007), “New NDT techniques for the assessment of fire-damaged concrete structures”, *Fire Safety Journal* 42 (6–7), pp. 461-472
- Hager, I. (2013a), “Colour change in heated concrete”, *Fire Technology*, 50, pp. 945–958.
- Hager, I. (2013b), “Behaviour of cement concrete at high temperature”. *The Journal of Polish Academy of Sciences*. Vol 61, Issue 1, Mar 2013. Poland
- Kodur, V.R. (2014), “Properties of Concrete at Elevated Temperatures”, *Civil Engineering Volume Hindawi Publishing Corporation ISRN*, Article ID 468510, 15 p.
- Kostuch J.A., Walter G.V., Jones T.R. (2000), “High performance concretes containing metakaolin – A review” In: *Proceedings of the International Conference – Concrete 2000*, Dundee, vol. 2. 2000. pp. 1799–811.
- Kopecskó, K., Mlinárik, L. (2014), "Metakaolin a betonban (in English: Metakaolin in concrete)", *BETON XXII.:(3-4.)* pp. 18-21.
- Lin W.M., Lin T.D., Powers-Couche L.J. (1996), “Microstructures of firedamaged concrete” *ACI Mater J* 93 (3), pp. 199–205.
- Mlinárik, L., Kopecskó, K. (2013), "Impact of metakaolin - a new supplementary material - on the hydration mechanism of cements", *Acta Technica Napocensis - Civil Engineering & Architecture* 56 (2) pp. 100-110.
- Mlinárik, L., Kopecskó, K., Borosnyói, A. (2016), "Properties of cement mortars in fresh and hardened condition influenced by combined application of SCM, "Építőanyag – Journal of Silicate Based and Composite Materials, Vol. 68, No. 2 (2016), pp. 62–66. <http://dx.doi.org/10.14382/epitoanyag-jsbcm.2016.11>
- Oriel M., Pera J. (1995), “Pozzolanic activity of metakaolin under microwave treatment”, *Cem Concr Res* 25 (2), pp. 265–70.
- Phan L.T. (1996), “Fire performance of high strength concrete: A report of the state-of-the art” Maryland: Building and Fire Research Laboratory, National Institute of Standards and Technology
- Poon C.S, Kou S.C, Lam L. (2000), “Compressive strength development, chloride-ions resistance and pore size distribution of metakaolin concrete”, *The Hong Kong Polytechnic University, Hong Kong*
- Schneider., U. (1988), “Concrete at high temperatures - a general review,” *Fire Safety Journal*, vol. 13, no. 1.
- Short, N.R., Purkiss, J.A., Guise, S.E. (2001), “Assessment of fire damaged concrete using colour image analysis”, *Constr. Buil. Mater.* 15, pp. 9-15
- Wild S., Khatib J.M., Jones A. (1996), “Relative strength pozzolanic activity and cement hydration in superplasticised metakaolin concrete” *Cem Concr Res* 26 (10):1537 44.

BONDED ANCHORS IN THERMALLY-DAMAGED CONCRETE

Viktor Hlavička, Éva Lubláy

Budapest University of Technology and Economics, Department of Construction Materials and Technologies

H-1521 Budapest, Hungary

SUMMARY

In our paper we analyzed the load bearing capacity of bonded anchors placed in thermally-damaged reinforced concrete. Our primary goal was to facilitate the reinforcing techniques of reinforced concrete structural elements damaged in fire events. For the tests, 8 mm diameter threaded rods installed with epoxy adhesive were used, with an embedment depth of 50 mm. Three levels of thermal loading (200, 300, 400 °C) were applied to the concrete specimens, with respect to the embedment depth. The mean value of the compressive strength of the concrete used in the tests was $f_c = 45.29 \text{ N/mm}^2$.

1. INTRODUCTION

In case of thermally damaged buildings, fastening elements should be occasionally inserted in reinforced concrete structures damaged by the fire. This may be required due to the replacement of the existing fasteners that have been damaged in the fire or to ensure a combined function of the additional elements together with the existing thermally damaged reinforced concrete structural elements (e.g. column jacketing, strengthening of the tension boom, and reinforcement of the slab with sprayed concrete). There are very few experiments dealing with the determination of the load-bearing capacity of fasteners placed in thermally-damaged reinforced concrete (Bamonte et al, 2004; Bamonte et al, 2007; Bamonte, Gambarova, 2005; Bamonte et al, 2012), which became our topic of interest.

1.1 Fire resistance of concrete

The mechanical properties of concrete are changed by the effects of fire. Related research has been carried out since the 1940s (Schneider, 1988) and it is still actual. Previous studies indicated that changes in the mechanical properties of concrete are caused by a variety of chemical and physical changes that occur at different temperatures (Niels, 2005). The extent of such changes is highly affected by the composition of the concrete.

The change in volume of the various components of concrete varies as a function of temperature. The cement stone and the aggregate react to temperature increase in completely different ways (*fib* bulletin 38, 2007). Consequently, the primary reason for the change in the strength of concrete is the deterioration of the connection between the aggregate and the cement stone. This effect is amplified by the dehydration of calcium dioxide and ettringite deposited on the surface of the aggregate particles (Balázs, Lubláy, 2012). During thermal loading, as the temperature increases, the compressive strength of concrete is reduced together with the load bearing capacity.

In *EN 1992-1-2:2004*, reduction of concrete strength in case of high temperatures is characterized by a reduction factor. The evaluation of this factor as a function of temperature is represented in Fig. 1.

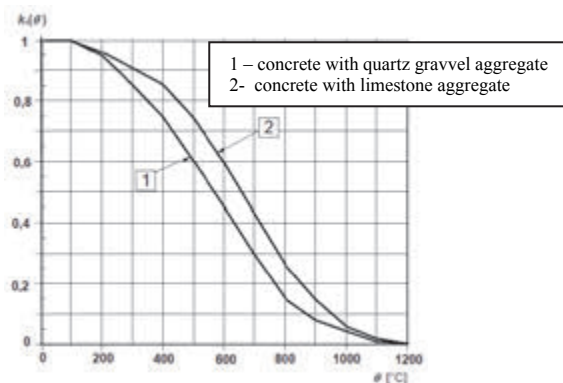


Fig. 1: Reduction factor for characteristic compressive strength as a function of the temperature (*EN 1992-1-2:2004*)

1.2 Fastening systems

Several post-installed anchors are available with different methods of load-transfer. The commercially available fastenings can transfer the load to the host material via the following mechanisms: mechanical interlock, friction or bond (Fig. 2). Furthermore, the most recent techniques use combined bond and friction (e.g. bonded expansion anchors). In the case of expansion anchors, the load is transferred by friction. Generally, an expansion sleeve is expanded by an exact displacement or torque applied on the anchor head during the installation process. Chemical fastenings are anchored by bond. Bonded anchors can be divided into two subgroups: capsule or injection systems. The bond material can be either organic, inorganic or a mixture of them. In this case the loads are transferred from the steel (normally a threaded rod, rebar) into the bonding material and are anchored by bond between the bonding material and the sides of the drilled holes (*fib* MC 2010; Eligehausen et al, 2001; Eligehausen et al, 2006; CEB, 1994; Mallée et al, 2013; Balázs, Józsa, Liptay, 1976; *fib* bulletin 58, 2011).

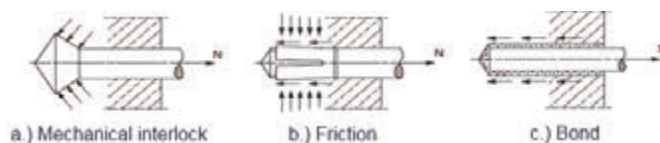


Fig. 2: Load transfer mechanisms (Eligehausen et al, 2001)

Load bearing of fastenings can be determined by taking the minimum of ultimate loads corresponding to different failure modes. In case of tensioned anchors steel failure, concrete cone failure, pull-out failure and splitting can occur (Fig. 3).

The properties of concrete cone failure mostly depend on the effective embedment depth (h_{ef}) and concrete strength (f_{ck}). Cone failure is the optimal failure type, because concrete strength is completely utilized. It can be either a full cone type or a partial cone type. The ultimate tensile force corresponding to full cone failure can be calculated as:

$$N_{u,k} = k * \sqrt{f_{ck}} * h_{ef}^{1,5} \quad (1)$$

where coefficient k shows whether concrete is uncracked ($k = 10.1$) or cracked ($k = 7.2$).

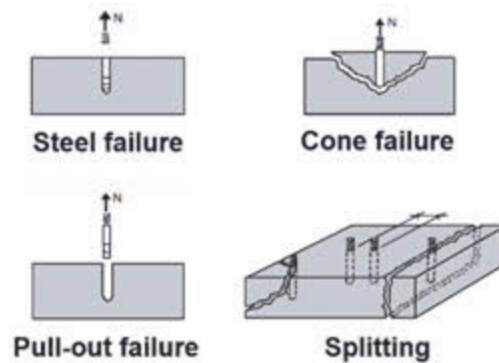


Fig. 3: Failure modes (fischer, 2010)

2. EXPERIMENTAL PROGRAM

In our experiments, we analyzed the load bearing capacity of anchors placed in thermally damaged reinforced concrete as a function of thermal load. In the tests carried out earlier (Bamonte et al, 2004; Bamonte et al, 2007; Bamonte, Gambarova, 2005) undercut fasteners were used. These studies did not address the behaviour of other types of fasteners, and that is why we used bonded anchors in our investigations to test the load bearing capacity of the bonded connection and its damage. During the experiments, the specimens were exposed to fire load on one side until they reached the desired temperature, then they were allowed to cool down at laboratory temperature (20 °C). The day after the fire load, typically after 24 hours, when the specimen had been cooled down, the fastener was inserted in the thermally damaged specimen. In order to allow the cross-linking of the adhesive, loading of the fasteners took place after a further 24 hours.

2.1 Tested anchors

One type of bonded anchor systems (epoxy resin) was tested. Bonded anchors were installed according to the MPII (Manufacturer's Printed Installation Instructions). The embedment depth was $h_{ef} = 50$ mm ($\sim 6d$, where “ d ” is the diameter of the anchor), and the diameter of the threaded rods was 8 mm, the strength class of threaded rods was 10.9.

2.2 Concrete mixture

The concrete mixtures were made by Portland cement (CEM I 42.5 N). The aggregates were natural quartz sand and quartz gravel and a superplasticiser of BASF Glenium C323 Mix was also used (Tab. 1). The specimens were held under water for 7 days and then kept at laboratory temperature (20 °C) for an additional 21 days.

Tab. 1: Concrete mixture

Materials		[kg/m ³]	[l/m ³]
Aggregate	0/4 mm	0,45	833
	4/8 mm	0,25	463
	8/16 mm	0,30	556
	SUM	1,00	1852
Cement	CEM I 42,5 N	290	93,5
Water	mw/mc=	0,675	196
Superplasticizer cem. %	Glenium C300	0,002	0,58
Air		-	10
SUM		2338	1000

Compressive strength properties were tested on additional 3 cubes of 150x150x150 mm. Uniaxial compressive strength tests were carried out on concrete cubes 28 days after casting. The results were evaluated in accordance with *EN 12390-3:2009* for concrete. The mean value of the mixture was $f_c = 45.29 \text{ N/mm}^2$.

The dimensions of concrete specimens for pull-out tests were 300x300x150 mm.

2.3 Thermal loading

In laboratory tests, the concrete specimens were exposed to thermal load on one side. An electric furnace was used to produce this thermal load, with a heating curve shown on Fig. 4. Based on the measurement data, the curve of the furnace is different from the standard fire curve according to *ISO 834-1*, so the experiments cannot be called a standard test. However, the heating curve of the furnace remained unchanged even after several checks, so it was well suited for the comparison of the specimens with varying degrees of thermal load, as well as for the preparation of a possible future standard test.

Thermal loading of the specimens was carried out in three different thermal steps relative to the embedment depth: 200 °C (Test 1), 300 °C (Test 2), 400 °C (Test 3) (Fig. 4). Three specimens were tested after being subjected to each of the thermal steps. Temperature was measured in the face of specimen (T2) and in the embedment depth (T1) by a thermocouple. In case of the embedment depth, the thermocouple had been placed from the “cold” side of the specimen through an inspection hole ($\varnothing 6 \text{ mm}$). Fig. 4 shows that the specimen is gradually warmed, with a significantly slower tendency than the furnace. After reaching 100 °C the temperature increases for a short time, then water in the concrete vaporizes and starts flowing out from the concrete. The temperature does not rise because the heat energy is entirely devoted to the change of state of the water. The arrangement for the thermal loading test is shown on Fig. 5.

We did not observe spalling of the concrete in any of the specimens during the tests. This may be due to fact that water vapor generated in the concrete was not accumulated due to the dimension of the specimen and the arrangement of the measurement, thus no moisture barrier was created. The steam was able to flow out freely through the test hole made for temperature measurement and the sides of the specimen. Therefore, the results of the test can be used only in cases where spalling does not occur in the reinforced concrete structure during the fire.

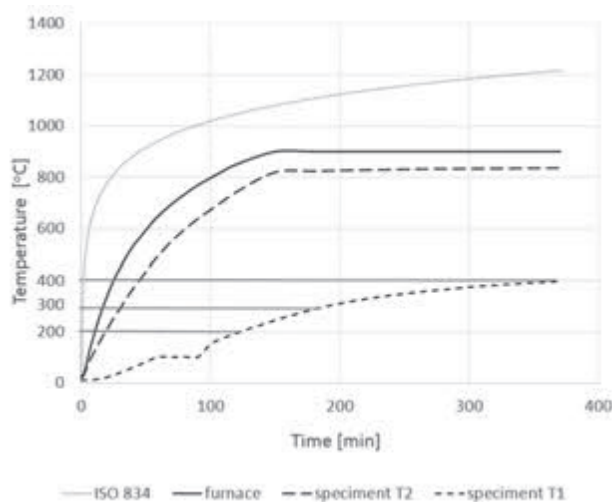


Fig. 4: Temperature increase

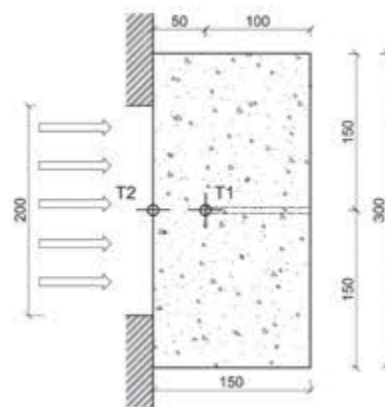


Fig. 5: Arrangement of heating for the specimen

2.4 Pull-out tests

Our unconfined test setup is shown in Fig. 6. The loading device was displacement controlled test apparatus, which allowed the recording of residual strength. This setup enabled the formation of all possible failure modes, the results were not affected by the geometry of the investigated samples (thickness of the test member, critical edge, placing). The measurement setup was capable to measure, record and show the applied load and related displacement of the anchor in real-time. The perpendicular pin-joints ensured the centrality of the acting force. The displacement was measured by two electronic transducers. Three additional independent displacement transducers were used to record the deformation of the surface. The load was measured by a calibrated load cell. The tests were carried out in accordance with the instructions given in *ETAG 001 Annex A*. The support distance was greater than $4h_{ef}$.

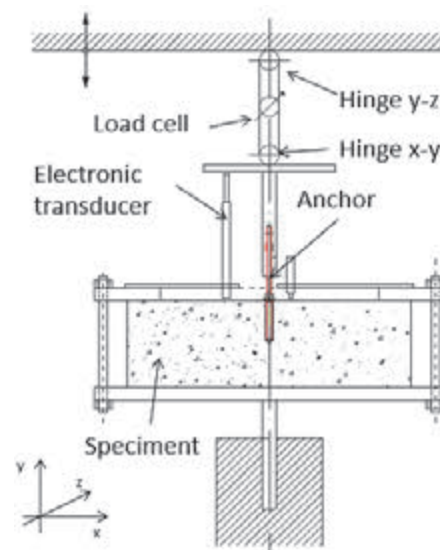


Fig. 6: Arrangement of pull-out test

3. THERMAL ANALYSIS

Finite element analysis was used to calculate the change of temperature in the concrete specimens. The analyses were made in ANSYS Workbench 16.2 software. We used material properties (temperature dependent density, heat capacity and thermal conductivities) taken from the current *Eurocode standards*. Full-size finite element models of one quarter of the specimens were created by using axis-symmetric boundary conditions. Temperature values were measured at 11 points (on the surface of the specimen, at the embedment depth, and in 9 points between the surface and the point at the embedment depth).

4. RESULTS

During the experiment, anchors have failed in all cases with pure concrete cone failure. These failures illustrate that an adhesive bond can be created between the adhesive and the thermally stressed concrete with a strength that caused a concrete cone failure.

Fig. 7 shows the tensile resistance of the anchors, while Fig 8 indicates the relative residual resistance values in function of the temperature. In Fig 8 each point of the curve means the average of three measurements, that are connected by spline fit.

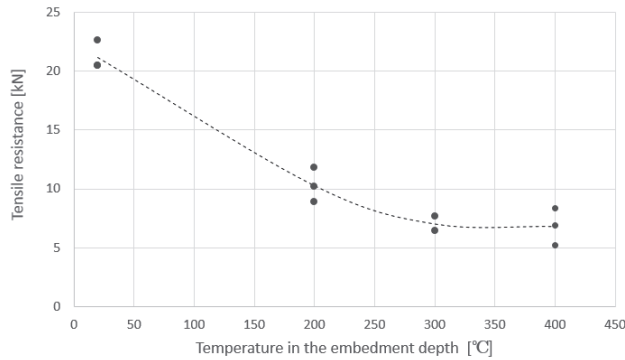


Fig. 7: Relationship between the tensile resistance and the temperature in the embedment depth

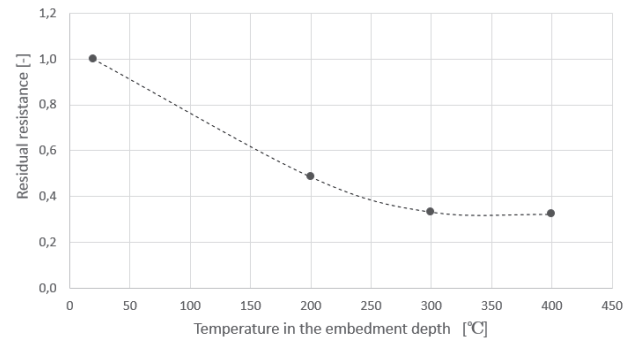


Fig. 8: Relationship between the residual resistance and the temperature in the embedment depth

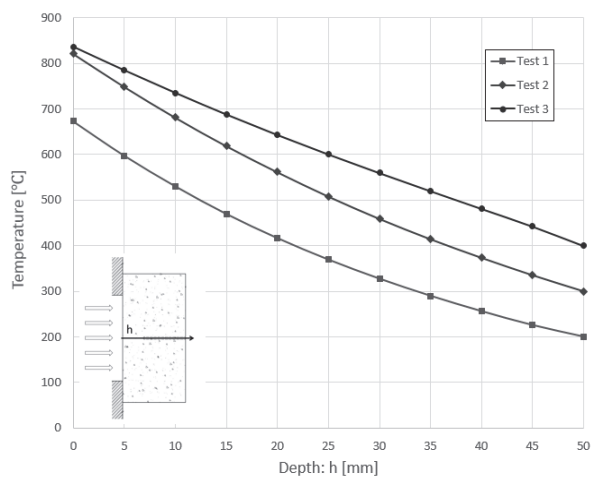


Fig. 9: Temperature distribution between the surface of the concrete specimen and the embedment depth (50 mm)

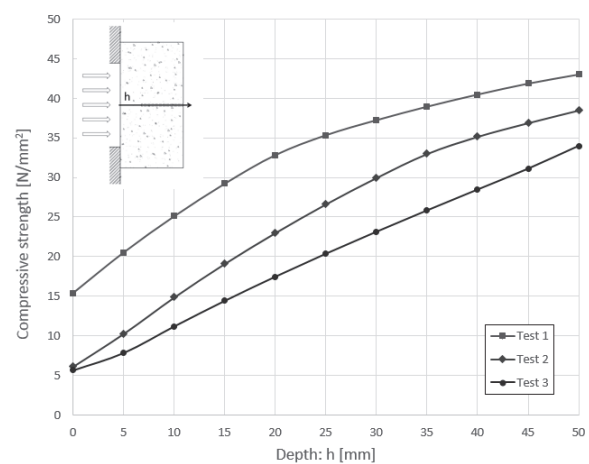


Fig. 10: Compressive strength distribution between the surface of the concrete specimen and the embedment depth (50 mm)

Based on the results of the numerical analyses, the isotherm lines can be determined. Changes in temperature in the layers between the surface and the embedment depth (50 mm) are represented in Fig. 9. Based on the reduction factors taken from *EN 1992-1-2:2004* (see Fig. 1), reduced compressive strength distribution can also be determined from the temperature distribution (Fig. 10).

Our aim was to develop an analytic method that can follow the results of our tests, therefore resistance of anchors installed in thermally-damaged concrete was estimated in different ways. During our tests, concrete cone failure was the general failure mode. In this case Eq. (1) calculates the resistance in case of normal concretes, therefore we tried to modify this formula for the case of thermally-damaged concretes. In Eq. (1) the compressive strength was calculated in two ways. In the first case, residual compressive strength values at ten points in different depth measured from the surface were calculated according to the Eurocode. Then their weighted average was determined by using lateral surface areas of truncated cones as weights, that we go by cutting the original concrete cone by planes parallel to the surface. In the second case, residual strength of zones where maximum temperature was above 500°C were neglected, because based on the Eurocode, load bearing capacity of concrete subjected to temperature loads higher than 500°C should not be taken into account. The value of parameter k in Eq. (1) is also questionable. Due to high temperatures the matrix loosens, and cracks also

occur, therefore application of $k=7.2$ that corresponds to cracked concretes may be needed. To see the effect of the different calculation methods, in Fig. 11 our experimental results are represented together with the four calculated curves (with $k=10.1$ or 7.2 , and average residual strength with or without the zones subjected to temperatures higher than $500\text{ }^{\circ}\text{C}$).

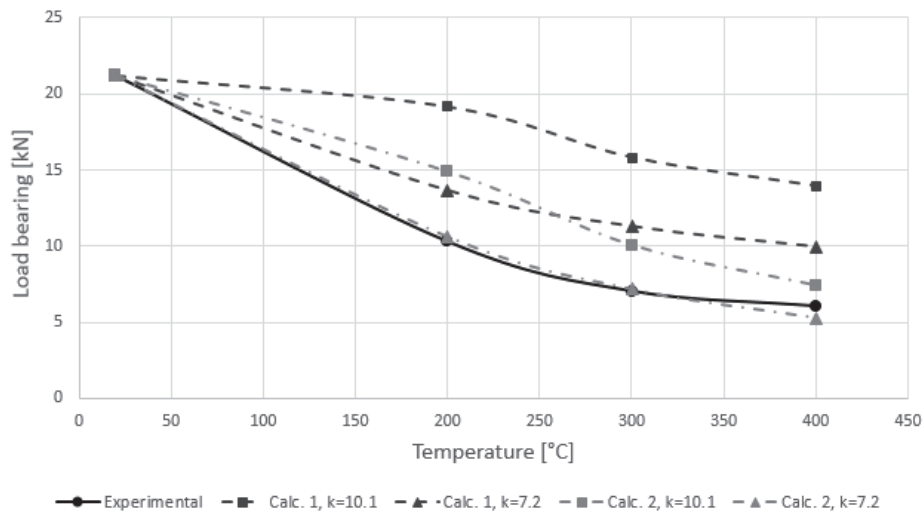


Fig. 11: Results of the tests and the different calculation methods

5. CONCLUSIONS

In our work we analyzed the load bearing capacity of anchors placed in thermally damaged reinforced concrete. Our primary goal was to assist the reinforcement work of reinforced concrete structural members damaged in fire events.

In all pull-out tests, concrete cone failure was observed. Among the failures, no specimen showed either a pull-out failure or the combination of concrete cone failure and pull-out failure. This means that the adhesive can create a bond of sufficient quality even in thermally damaged concrete. The load capacity of anchors created with epoxy adhesive decreased with increasing temperature during thermal loading.

Load bearing capacity of anchors installed in thermally-damaged concretes were calculated in different ways. In case of concrete cone failure, we saw that calculated values were closest to the experimental results if strength of zones that were subjected to temperatures higher than $500\text{ }^{\circ}\text{C}$ were neglected and $k=7.2$ that corresponds to cracked concrete were applied.

6. ACKNOWLEDGEMENTS

The authors wish to thank Szabolcs Kovács-Sebestény and Fischer Hungary for providing the necessary anchors.

7. REFERENCES

- Balázs, Gy.; Józsa, Zs.; Liptay, A. (1976): Ragasztott és terpesztett csapos kapcsolat. MAGYAR ÉPÍTŐIPAR XXV.:(6-7.) pp. 374-393.
- Balázs, L. Gy., Lublóy, É.: Post-heating strength of fiber-reinforced concretes, Fire Safety Journal, Volume 49, April 2012, pp. 100-106.

- Bamonte P. F., Bruni M., Gambarova P.G.: On the application of fracture mechanics to undercut fasteners installed in thermally-damaged concrete, *Befestigungstechnik* *Bewerungstechnik und ... II* (Rolf Eligehausen zum 70. Geburtstag) (Edited by: Fuchs W., Hofmann J.), Stuttgart 2012, pp. 79-93. ISBN-13:978-3-8382-0397-3
- Bamonte P. F., Gambarova P. G., D'agostino L.; Genoni A.: Preliminary pull-out test on post-installed mechanical fasteners embedded in thermally-damaged concrete, *Fire Design of Concrete Structures: What now? What next?*, (Edited by: Gambarova G. P., Felicetti R., Meda A., Riva P.), Milan, Italy, December 2-3, 2004, pp. 199-207.
- Bamonte P. F., Gambarova P.G.: Residual behavior of undercut fasteners subjected to high temperatures, *fib* Symposium "Keep Concrete Attractive" (Edited by: Balazs L. Gy.; Borosnyói A.), Budapest, Hungary, May 23-25, 2005, pp. 1156-1163. ISBN: 963-420-839-8
- Bamonte P.F., Gambarova P.G., Bruni M., Rossini L.: Ultimate Capacity of Undercut Fasteners Installed in Thermally-Damaged High-Performance Concrete, Proc. 6th Int. Conf. on Fracture Mechanics of Concrete Structures – FraMCoS-6, Catania (Italy), June 18-21, 2007.
- Comité Euro-International du Béton (CEB) (1994): Fastenings to Concrete and Masonry Structures: State-of-the-art report. Bulletin D'Information No. 216, Lausanne, published by Thomas Telford Services Ltd, London, 1994.
- Eligehausen R., Hofacker I., Lettow S.: Fastening technique – current status and future trends, *International Symposium on Connections between Steel and Concrete, Volume One*, Stuttgart, Germany, 2001, pp. 11-27.
- Eligehausen R., Mallée R., Silva J. F.: *Anchorage in Concrete Construction*, Ernst&Sohn 2006, ISBN: 978-3-433-01143-0
- EN 12390-3:2009 Testing hardened concrete – Part 3: Compressive strength of test specimens
- EN 1992-1-2:2004 Eurocode 2: Design of concrete structures. Part 1-2: General rules. Structural fire design, CEN, Brussels, 2004.
- ETAG 001: Guideline for european technical approval of metal anchors for use in concrete, EOTA, Avenue des Arts 40 Kunslaan, B – 1040 Brussels, 2013.
- fib* BULLETIN 38: Fire design of concrete structures – materials, structures and modelling, 2007, ISBN: 978-2-88394-078-9
- fib* BULLETIN 58: Design of anchorages in concrete, 2011, ISBN: 978-2-88394-098-7
- fib* Model Code 2010. pp. 282-285. ISBN: 978-3433-03061-5
- fischer: Technical Handbook. Stuttgart: fischerwerke GmbH, 2010
- ISO 834-1: Fire-resistance Tests – Elements of building construction, Part 1: General requirements, 1999.
- Mallée R., Fuchs W., Eligehausen R. (2013): Design of Fastenings for Use in Concrete – the CEN/TS 1992-4 Provisions. *BetonKalender*, Ernst&Sohn, ISBN: 978-3-433-03044-8
- Niels, H. P.: Fire Design of Concrete Structures, Proceedings of *fib* symposium on Keep concrete attractive, (Edited by: Gy. L. Balázs, A. Borosnyói), 23-25 May 2005, Budapest, pp. 1097-1105.
- Schneider, U.: Concrete at high temperatures-a general review, *Fire Safety Journal*, vol 13, 1988, pp. 55-68.
- Thielen, K. Ch.: Strength and Deformation of Concrete Subjected to high Temperature and Biaxial Stress-Test and Modeling (*Festigkeit und Verformung von Beton bei hoher Temperatur und biaxialer Beanspruchung – Versuche und Modellbildung*), 1994, Deutscher Ausschuss für Stahlbeton, Heft 437, ISSN: 0171-7197, Beuth Verlag GmbH, Berlin.

TOPIC 2
ADVANCED REINFORCING AND
PRESTRESSING MATERIALS AND
TECHNOLOGIES

ADJUSTMENT OF INTERNAL PRESTRESSING IN EXISTING STRUCTURES – A CASE STUDY

Vazul Boros¹, Balthasar Novák²

¹ Schömig-Plan Consulting Engineers

63801 Kleinostheim, Germany Saaläckerstr. 8.

² Institut für Leichtbau Entwerfen und Konstruieren, University of Stuttgart

70569 Stuttgart, Germany Pfaffenwaldring 7.

SUMMARY

To improve the access of disabled citizens to a subway station in the city centre of Stuttgart new elevators have been installed. The construction required the trimming of the existing prestressed reinforced concrete beams that were kept intact throughout the construction as they carry one of the city's main traffic arteries. Both the re-anchorage and the deactivation of prestressing tendons were monitored by strain gauges in order to verify that the intended modifications in the prestressing forces were realized successfully. In addition the project provided insights into the aspects that need to be considered during the casting of additional concrete layers and how superfluous prestressing tendons can be deactivated effectively. Finally results for the long-time monitoring of the bond behaviour for a ribbed tendon without anchorage device in a neighbouring subway tunnel are shown.

1. INTRODUCTION

The construction industry faces increasing challenges concerning the maintenance, upgrading and conversion of existing infrastructure. For newly erected structures prestressed reinforced concrete generally provides a favourable and economic structural solution, as the tendon profiles and the prestressing forces can be optimized according to the loadbearing and serviceability requirements. If however at a later stage an alteration in load or support conditions arises, the subsequent adjustment of the internal prestressing is a demanding task. The present case study provides some insights into a project where such an undertaking could be solved effectively. Due to the lack of experience in this field, the changes in prestressing during construction were monitored with strain gauges. The insights gained through these measurements and during the long-time monitoring of the bond behaviour for a ribbed tendon in a neighbouring subway tunnel are shared in the paper.

2. INSTALLATION OF ELEVATORS AT ÖSTERREICHISCHER PLATZ

2.1 Project description

The subway station Österreichischer Platz in the city centre of Stuttgart had to be equipped with elevators to enable the accessibility by disabled citizens (Novák et. al., 2016). The cross section of the subway station is displayed in Fig. 1. The precast, prestressed reinforced concrete hollow beams span across a distance of approximately 17.0 m between the two drilled pile walls which they are supported by. The station is located at the crossroad of a pedestrian underpass, a subway tunnel and a federal highway. The prestressed concrete beams

carry the road that serves as one of the main arterial roads of the city. Therefore they had to be trimmed while maintaining the traffic on them throughout the entire time of the construction.

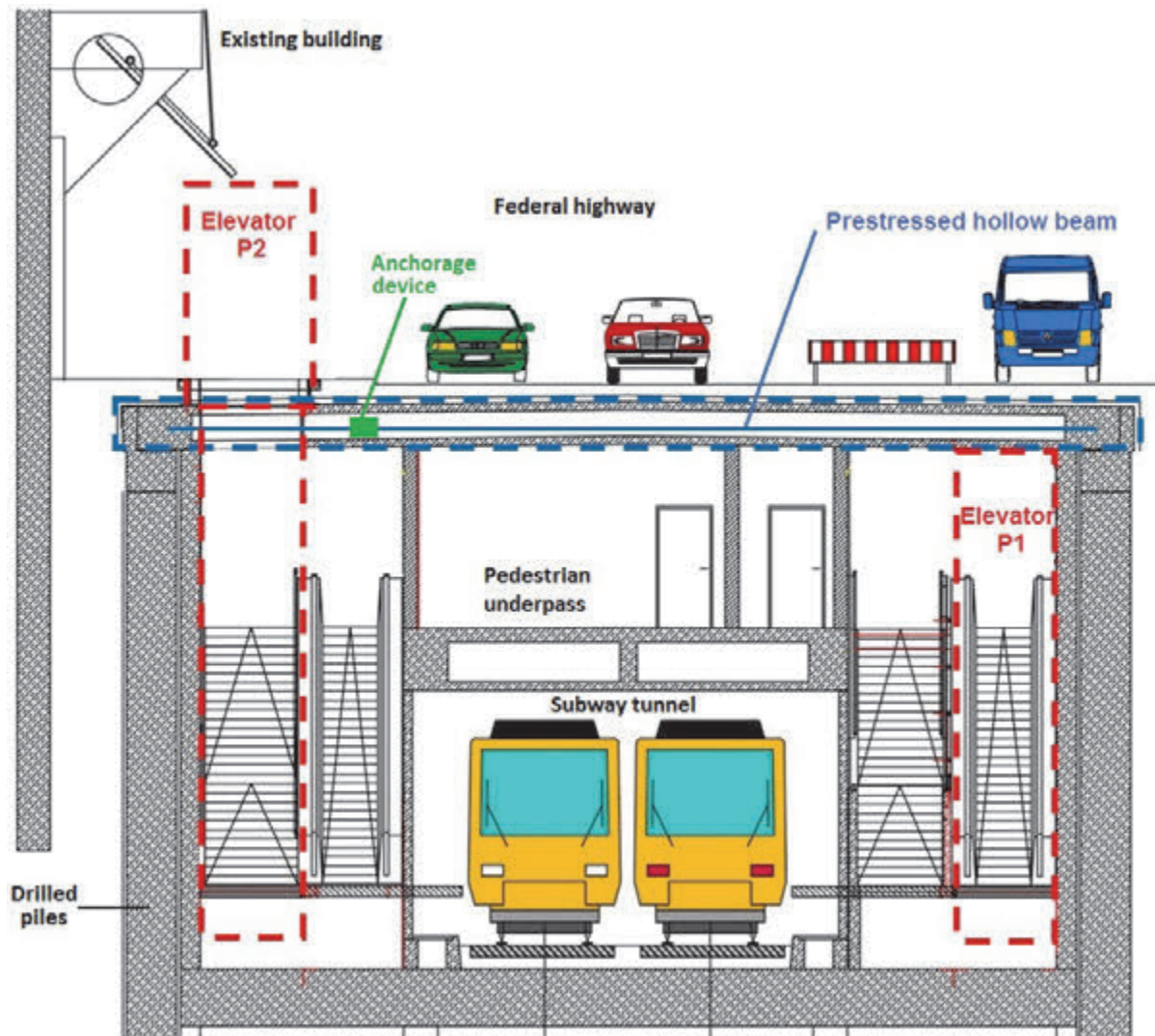


Fig. 1: Cross section of the Subway station at Österreichischer Platz in Stuttgart

The beams are prestressed with four Dywidag tendons of 32 mm diameter and an additional one with 18 mm diameter. The cables run horizontally in the bottom flange of the hollow section until they are diverted towards the centre of the cross section nearby the supports, where they end in plate anchorages. Due to the changed support conditions the prestressing cables had to be re-anchored in a way corresponding to the altered circumstances. Already in 2008 the Civil Engineering Department of the city of Stuttgart, with Prof. Novák from the University of Stuttgart, initiated a research project, where a special anchorage device for re-anchoring the smooth prestressing cables had been investigated by laboratory tests under static and cyclic loading (Novák et. al., 2008). The new anchorage device consists of steel wedges which clamp onto the cables, thus ensuring low slippage.

A part of the prestressing cables had to be deactivated, since they would have had adverse effects on the internal stresses in the section due to the reduced span. The surface of the tendons is smooth, without ribs, therefore a reliable assessment of the bond behaviour is extremely difficult. On the one hand the successful anchorage by the installed anchorage devices needed to be confirmed, not solely under laboratory conditions but in the actual

structure. On the other hand it had to be examined at the same time, whether the superfluous cables could be deactivated effectively. To achieve these two goals a monitoring concept accompanying the construction was developed and implemented.

2.2 Monitoring setup

In order to monitor the prestressing losses in the cables that were to be deactivated, three strain gauges were installed on a cable in distances of approximately 30 cm from the drill hole and each other (D0V, D0M and D0H). The successful anchorage mechanism was to be verified by four strain gauges mounted on four different cables respectively just before the anchorage devices (D1V, D2V, D3V and D4V). Finally on two of the cables additional strain gauges were installed behind the anchorage device to investigate the losses in strain without the anchorage (D1H and D3H). The sampling rate of the measurements was 0.1 s. The layout plan with the position of deactivation drill holes, strain gauges and anchorage devices is shown in Fig. 2. The prestressing cables were first exposed by high pressure water jetting. Thereafter the new special anchorage devices were mounted on the tendons. The strain gauges were installed before an additional 10 cm concrete layer beneath the beams was casted. The additional concrete provided the bond between the anchorage elements and the beams.

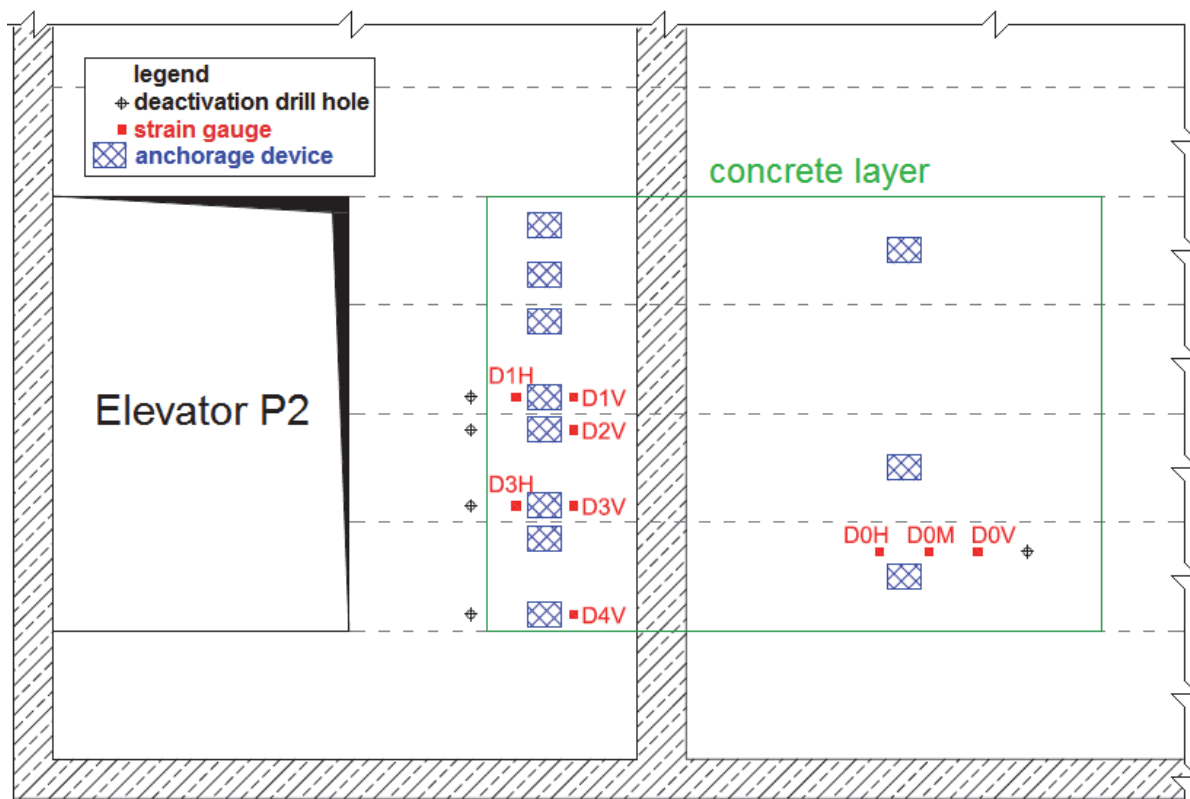


Fig. 2: Monitoring setup showing the position of deactivation drill holes, strain gauges and anchorage devices in the layout plan

2.3 Results

The first measurements were carried out on the 12th of February 2015. In this test the prestressing losses in the deactivated cables had been investigated. The strain gauge with the identification D0V did not deliver any readings, as it had probably been damaged during the casting of the concrete. The other two strain gauges which had been positioned even further

from the drill hole have shown however significant loss in strain. On the 17th of September 2015 the second test was performed, investigating the stresses during the activation of the anchorage devices as shown in Fig. 3. The four prestressing cables equipped with strain gauges were in decreasing order successively deactivated with a drill hole each behind the anchorage device. Around 25 minutes a small decrease in strain at the strain gauge D4V indicates the moment when the first cable was severed. At roughly 55 minutes a significant drop in strain of the D3H shows the deactivation of the second tendon, while the strain gauge D3V positioned in front of the anchorage device only experiences a minor loss. A light decrease around 77 minutes after the start of the test in the readings of the strain gauge D2V marks the moment, when the third cable was separated. Finally starting from approximately 100 minutes the last tendon is drilled through, snapping just before 110 minutes followed by a loud bang. As can be seen despite the large losses of D1H, its counterpart D1V in front of the anchorage device shows only a minor decrease in strain.

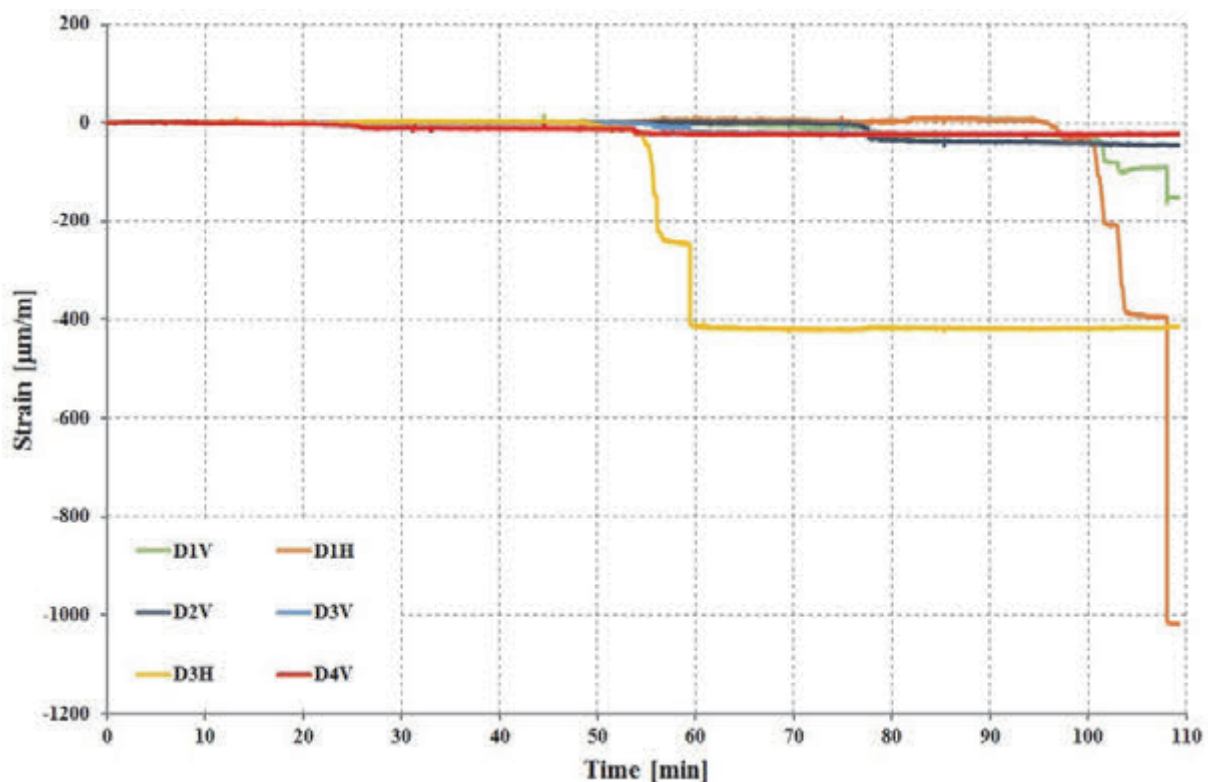


Fig. 3: Measurements during the activation of the anchorage devices

The German Standard DIN 4227-1 (1979), that was in effect at the time of the construction of the original structure, limited the permissible stresses to the lower of 75 % of the yield strength or 55 % of the tensile strength of the prestressing steel. Assuming this limit and using the material properties provided by the Guideline for the calculation of existing bridges (Nachrechnungsrichtlinie, 2011), the initial prestress strain can be calculated to approximately 2900 $\mu\text{m}/\text{m}$. The estimated prestressing losses based on this assumption are calculated in Tab. 1 for both measurements. The results show, that the anchorage devices proved effective in reintroducing the prestressing force.

Tab. 1: Estimated prestressing losses at the strain gauges

Strain gauge	Strain in $\mu\text{m/m}$	Estimated prestressing loss in %
D0M (drillhole, 60 cm)	-2439.2	84.1
D0H (drillhole, 90 cm)	-1985.2	68.5
D1V (anchorage)	-152.1	5.2
D1H (drillhole)	-1017.4	35.1
D2V (anchorage)	-44.9	1.5
D3V (anchorage)	-21.6	0.7
D3H (drillhole)	-413.8	14.3
D4V (anchorage)	-21.8	0.8

2.4 Experiences gained during construction

As the alteration of existing structures requires special care and considerations a few insights gained during the construction are worth to be discussed. To ensure the bond between the existing and newly casted concrete generally an indented interface according to DIN EN 1992-1-1 (2011) is required. Applications for the retrofitting of bridges via external prestressing have already shown, that these surface requirements can be met by high pressure water jetting using a rotating jet, yet they require qualified personal and close supervision (Novák et. al., 2015). Casting a concrete layer beneath, represents however a special challenge. It proved essential to pump in the concrete from beneath while providing sufficient ventilation shafts for the air to escape, especially in cavities i.e. around the anchorage devices. It is also advisable to monitor the progress in observation windows and with endoscope cameras.

Another difficult task was the deactivation of the tendons, since the prestressing steel is fairly hard and submitted to high tension. Moreover the tensile forces should be released as smoothly as possible to avoid dynamic effects. In addition the almost 100 drill holes required a straightforward technique. Eventually the most suitable approach proved to be to drill a concrete core of a minimum of 80 mm diameter until the tendon is reached and thereafter drilling holes of increasing diameter into the cable. Fig. 4 shows the described observation window and a deactivation drill hole with the severed tendon.



Fig. 4: Observation window with Perspex cover (left) and severed prestressing tendon at deactivation drill hole (right)

3. LONG-TERM MEASUREMENTS AT VIERKERHALLE

In a nearby tunnel along the same subway line a similar project had been considered for a while, yet up until now it has not been launched. Nevertheless in an attempt to assess whether the trimming of the beams would be possible, long-term measurements have been carried out already in 2008. The prestressing cables installed in these beams had a parabolic layout and were of the type 55,5 t by Züblin, consisting of six oval, ribbed strands of 120 mm² each. In contrast to the previously described project, a better bond behaviour could be expected due to the higher roughness. In this case the tendon was severed by drilling a concrete core sample of a larger diameter through it. The two bottom strands of each tendon had been equipped with strain gauges in approximately 50 cm distances from each other, with DMS1 and DMS2 located next to the deactivation point and DMS7 and DMS8 positioned furthest away. The ribbed strands with the mounted strain gauges are shown in Fig. 5.



Fig. 5: Strain gauges mounted on the ribbed prestressing cables

Whereas the DMS8 failed unfortunately, for the remaining seven strain gauges readings were recorded for a period of up to almost 210 days. The results of this long-term test are displayed in Fig. 6. It is apparent, that the two strain gauges DMS1 and DSM2 next to the core bore show significant losses immediately during the drilling. These increase further during the first three months approximately, thereafter however no additional decrease can be detected. The strain gauges further away did not experience any significant losses and also after more than half a year no adverse changes can be observed on them.

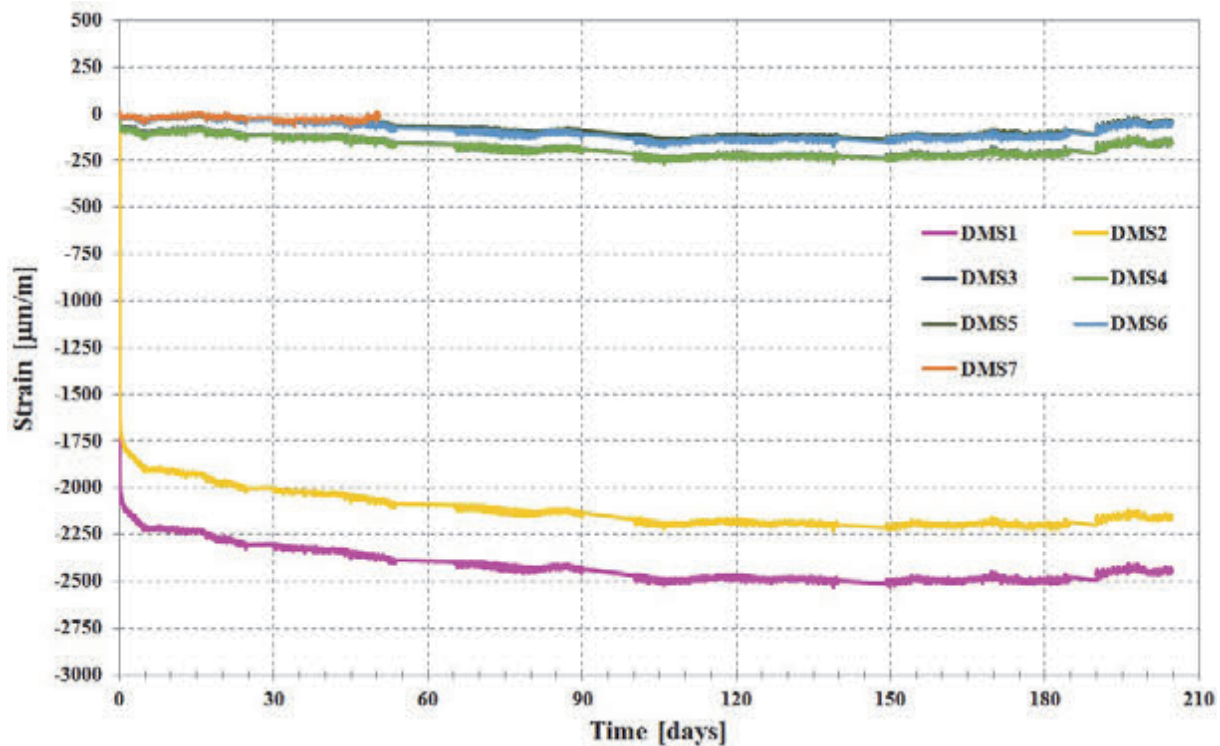


Fig. 6: Long-term measurements recorded after the deactivation of the cables

4. CONCLUSIONS

The construction industry is faced with the task of retrofitting or altering existing constructions. In case of prestressed concrete structures however special considerations are necessary, in order to adjust the cable profile and anchorage points to the altered conditions as far as it is possible. The paper presents a project, where with a new anchorage device smooth tendons could be re-anchored, while at the same time superfluous cables could be deactivated. Long-term measurements of another project show, that in case of ribbed strands even a relatively short bond development length might suffice to re-anchor the prestressing force.

5. ACKNOWLEDGMENTS

The authors would like to gratefully acknowledge the support of the main investor, the Stuttgart public transport operating company “Stuttgarter Straßenbahnen AG (SSB)”, as well as the Civil Engineering Department of the city of Stuttgart, which accompanied the technical realization of the project.

6. REFERENCES

- Bundesministerium für Verkehr, Bau und Stadtentwicklung (2011), „Nachrechnungsrichtlinie: Richtlinie zur Nachrechnung von Straßenbrücken im Bestand“.
- DIN 4227-1 (1979), „Spannbeton Bauteile aus Normalbeton mit beschränkter oder voller Vorspannung“.
- DIN EN 1992-1-1 (2011), „Eurocode 2: Design of concrete structures – Part 1-1: General rules and rules for buildings“.

- Novák, B., Sasmal, S., Röhm, C., Schnabel, T., Becker, R. (2008), „Zum nachträglichen Kürzen und Verankern von glatten Spanngliedern im Verbund“, Beton- und Stahlbetonbau Vol. 103, No. 8, August 2008, pp. 522-529.
- Novák, B., Pelke, E., Boros, V., Reinhard, J., Berger, D. (2015), „Endverankerungen bei Ertüchtigung von Brücken mit externer Vorspannung“, Beton- und Stahlbetonbau Vol. 110, No. 2, February 2015, pp. 138-154.
- Novák, B., Boros, V., Hauck, C.-D., Hermann, H., Koster, G. (2016), „Aufzugsnachrüstung Österreichischer Platz - Ein Beispiel für die Herausforderungen beim Bauen im Bestand“, Bautechnik Vol. 93, No. 7, July 2016, pp. 490-496.

INNOVATIVE STEEL FIBERS AND THEIR EFFECT ON FIBER DISTRIBUTION IN BEAMS – EXPERIMENTAL INVESTIGATIONS

Michael Huss, Viet Tue Nguyen
Graz University of Technology
Lessingstraße 25
8010 Graz, Austria

SUMMARY

This contribution presents experimental investigations on fiber reinforced concrete (FRC). A new type of straight steel fibers (company Feel Fiber) with a length of 60 mm was used. 12 beams with a length of 6 m, a height of 0.4 m and a width of 0.5 m were produced, in order to determine the fiber distribution along them. The beams differ in the manufacturing method (cast in layers or from one side), the fiber content and the way of fiber addition. After concretes hardening, slices were cut of the beams to determine the number of fibers in the cross section. The results showed that the number of fibers per unit area scatters about 10 %, independent of manufacturing method and type of fiber addition. Finally, the results are discussed and a proposal to modify certain factors in the German and Austrian guideline for fiber reinforced concrete is made, to take the advantages of this new fiber type into account.

1. INTRODUCTION

The post cracking tensile behaviour of fiber reinforced concrete (FRC) scatters with about 20 – 25% as generally known. The large scattering influences the characteristic material properties as well as the safety factor negatively. As a result, fiber reinforced concrete is mainly used in components with high rearrangement capacity and relatively low load, such as floor slabs or tunnel shells. Investigations by (Müller, 2015; Erdem, 2002 and Gröger et al., 2012) have shown that the large scattering in the post cracking tensile strength occurs in normal strength concrete and ultra high performance concrete, independent of fresh concrete properties. In (Lin, 1996; Holschemacher et al., 2006; Leutbecher, 2007 and Fehling et al., 2013), the fiber distribution and the fiber orientation are mentioned as reason for the large scattering. Especially the fiber orientation has been focused in the last years, as can be seen in (Leutbecher, 2007; Fehling, 2013 and Freytag, 2014). Different methods for positive influencing the of fiber orientation have been tested by (Bonzel et al., 1984 and Linsel, 2005). However these methods have proved to be unpractical. Recent findings have shown that the inhomogeneous fiber distribution is mainly responsible for the large scattering in the post cracking tensile behaviour.

In this work, the influence of a new fiber type (company *Feel Fiber*) on the fiber distribution has been investigated. Fig. 1 demonstrates the *Feel Fiber* geometry schematically. It is characterized by anchorages at the end of the fiber and two rough sides as a consequence of the production process. The number, position and size of these anchors can be adapted according to the requirements.

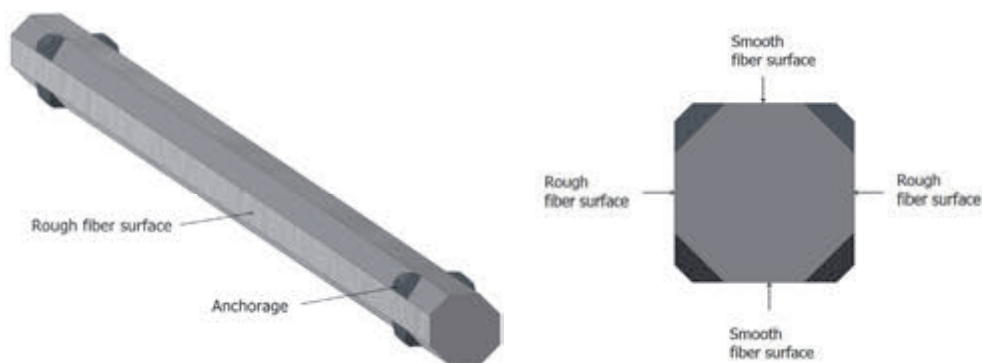


Fig. 1: Shape of the fiber

One of the main advantages of this fiber is the straight fiber design. Thus, the influence on the fresh concrete properties should be smaller compared to hooked fibers. Consequently a more homogenous fiber distribution is expected and greater amounts of fibers can be used.

2. EXPERIMENTAL PROGRAM

The aim of the experiments was to investigate the fiber distribution in beams, depending on type of fiber addition, fiber content and manufacturing process. Beams with a length of 6 m, a width of 0.5 m and a height of ≈ 0.4 m were produced. The experimental program is shown schematically in Fig. 2.

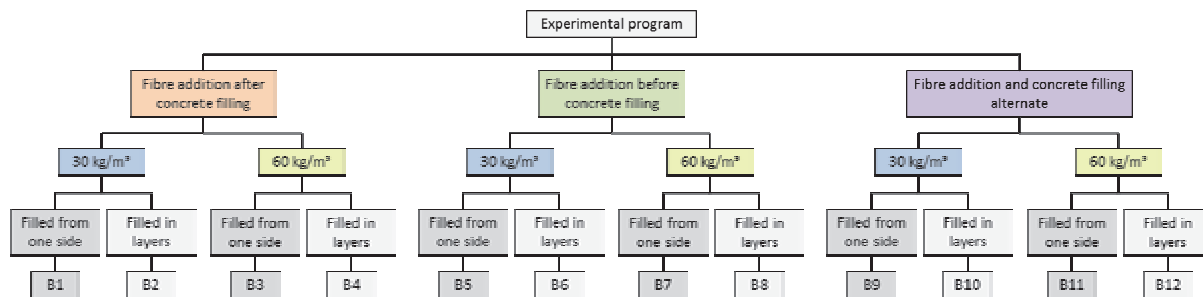


Fig. 2: Experimental program

Straight steel fibers with a length of 60 mm ($d_f \approx 0.75$ mm) and fiber contents of 30 and 60 kg/m³, respectively, were used. Half of the beams were filled from one side, the other half was filled in layers. The fibers were added into a truck mixer by conveyor belt but varying the time of fiber addition. For the beams B1 to B4, the concrete was added in the truck mixer in advance and the fibers were added afterwards. In contrast to this, the steel fibers for beams B5 to B8 were completely added in the mixer before the concrete was filled. Beams B9 to B12 present a third fiber addition procedure. In this process the fibers and the concrete were alternately added in several steps. One beam was produced for each fiber addition procedure, fiber content and filling method.



Fig. 3: Fiber addition via conveyor belt (left) and filling of the beam from one side (right)

3. EXPERIMENTAL SETUP AND PROCEDURE

The used concrete is classified as a C30/37 with a maximum grain size of 16 mm. The amount of paste got increased for the mixtures with a fiber content of 60 kg/m^3 , in order to keep the consistency constant for all test series. The mixing time of the truck mixer was always 8 min. Two beams were produced with one load of the truck mixer. All beams were compacted with an internal vibrator at predefined points (distance between points 30 cm).

Six slices were cut from each beam to determine the number of fibers in different cross sections. The thickness of the slices was 70 mm, in order to get two independent cuts by using 60 mm fibers. The number of fibers was counted on the front side and on the back side of the slices. Hence, a total of 12 cross sections were investigated for each beam. Fig. 4 shows the configuration of the cuts as well as the vibration points.

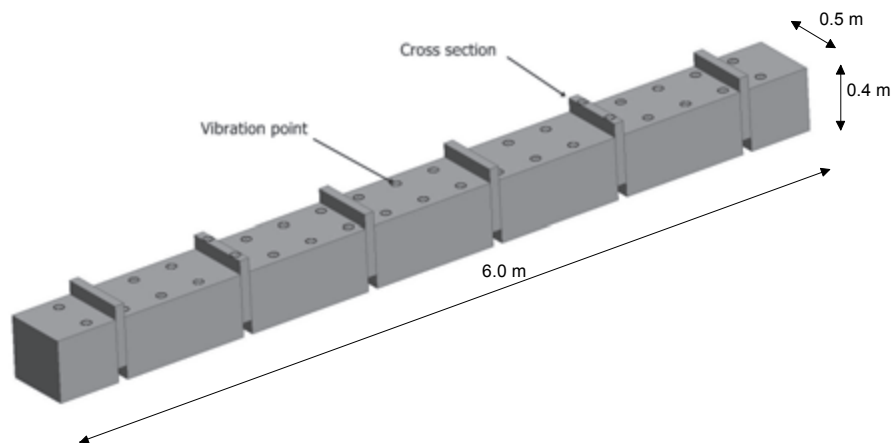


Fig. 4: Beam and configuration of the cuts

The fresh concrete properties were tested parallel to the casting of the beams. The flow spread was determined accordingly to DIN EN 12350-5. Furthermore, the fiber distribution in the fresh concrete was carried out accordingly to the German guideline for steel fiber reinforced concrete (washout-test). Three fresh concrete samples (10 – 15 liters) were taken from the truck mixer (one of every third of the batch). By measuring the fresh concrete density, according to DIN EN 12350-4 and the weight of the partial samples, it is possible to determine the volume of the partial sample. After separating the fibers from the fresh concrete by magnet, the mass of the steel fiber as well as the steel fiber content of the sample could be determined.



Fig. 5: Determination of the flow spread (left) and separation of steel fibers from the fresh concrete (right)

4. EXPERIMENTAL RESULTS

4.1 Properties of fresh concrete

The mixtures with a fiber content of 30 kg/m³ as well as those with 60 kg/m³ showed a good flowability of the fresh concrete. The flow spread was in a range of 540 to 630 mm. The results of the washout-test are shown in Tab. 1. According to the DAfStb guideline for steel fiber reinforced concrete, the following conformity criteria must be observed:

- Single value criteria: $m_{f,i} \geq 0.80 \times m_{f,ziel}$
- Mean value criteria: $\bar{m}_f \geq 0.85 \times m_{f,ziel}$

Tab. 1: Fiber distribution in the fresh concrete

		Fiber content $m_{f,i}$ [kg/m ³]	Mean value criteria \bar{m}_f [kg/m ³]	Variation coefficient [%]	Fiber content $m_{f,i}$ [kg/m ³]	Mean value criteria \bar{m}_f [kg/m ³]	Variation coefficient [%]
		$m_{f,ziel} = 30$ [kg/m ³]			$m_{f,ziel} = 60$ [kg/m ³]		
Fiber addition after concrete filling	1. sample	30.3	30.6	0.9	63.1	65.4	4.5
	2. sample	30.7			68.7		
	3. sample	30.8			64.4		
Fiber addition before concrete filling	1. sample	31.0	31.2	6.8	60.9	65.1	5.9
	2. sample	33.4			65.9		
	3. sample	29.2			68.5		
Fiber addition and concrete filling alternate	1. sample	30.9	31.4	1.9	68.9	64.8	5.6
	2. sample	32.1			63.1		
	3. sample	31.3			62.3		

The criteria according to (Deutscher Ausschuss für Stahlbeton, 2010) were fulfilled for all mixtures. Furthermore, the coefficient of variation ($V = \text{standard deviation} / \text{mean value}$) has been determined, as it can be seen in Tab. 1. The scattering is in a range of 1 – 7 %. On the basis of these small scatterings, a good fiber distribution in the mixer can be expected for all fiber addition procedures.

It is worth mentioning that the sample quantity of 15 litres corresponds to one entire standard bending beam. Therefore this method does not make it possible to reproduce the scattering in the local bearing behaviour of standard beams. Due to this fact, it is proposed in (Hadl, 2017) to determine the sample quantity as a function of the component geometry.

4.2 Fiber distribution in beams

The number of fibers was counted in each cross section of the beam. The mean number of fibers per cross section [number of fibers / dm²] is shown in Fig. 6 for each beam.

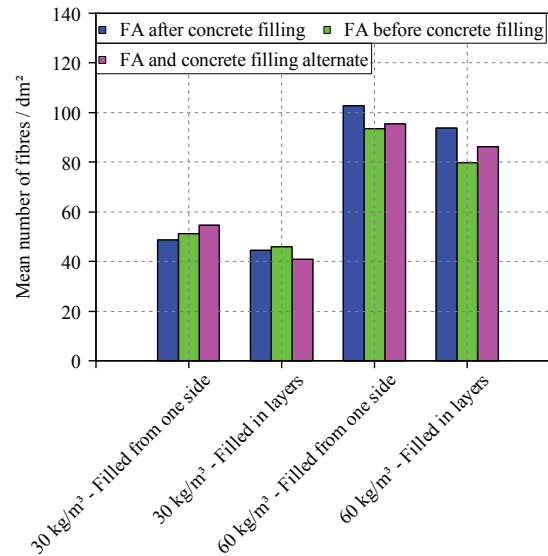


Fig. 6: Mean number of fibers in the cross sections

It has to be mentioned that the number of fibers in the cross section depends essentially on the fiber orientation in the component. As shown in Fig. 6, a smaller mean number of fibers was determined in beams which were filled in layers, compared to beams, which were filled from one side. This indicates that the fibers align along the flow direction. Consequently, more fibers cross the beam section. A mean fiber orientation $\eta \approx 0.55 - 0.60$ could be determined in beams filled from one side, according to the equation of (Hilsdorf et al., 1985) and the model of (Hadl, 2017). For beams, which are filled in layers, a three-dimensional fiber orientation of about $\eta \approx 0.50$ was obtained. The determined values corresponds to the statements, which are given by (Hadl et al., 2015), (Lin, 1996) and (Hadl et al., 2016).

The fiber distribution was calculated, based on the number of fibers in the 12 cross sections. Therefore, the coefficient of variation was determined as shown in Fig. 7. It can be seen that the number of crossing fibers scatters in a range of 7 – 12 %. This constitutes a low scattering in view of test series by (Hadl et al., 2016) and (Hadl, 2017) with comparable fiber addition procedures, where variation coefficients of $\approx 15\%$ could be determined.

Fig. 7 shows that no fiber addition procedure tends to a larger scattering. But they show a tendency, that beams which are filled in layers, lead to a more homogenous fiber distribution than beams cast in layers.

As demonstrated, the new fiber type leads to a relatively low scattering of the fiber distribution, independent of fiber content, filling method and type of fiber addition.

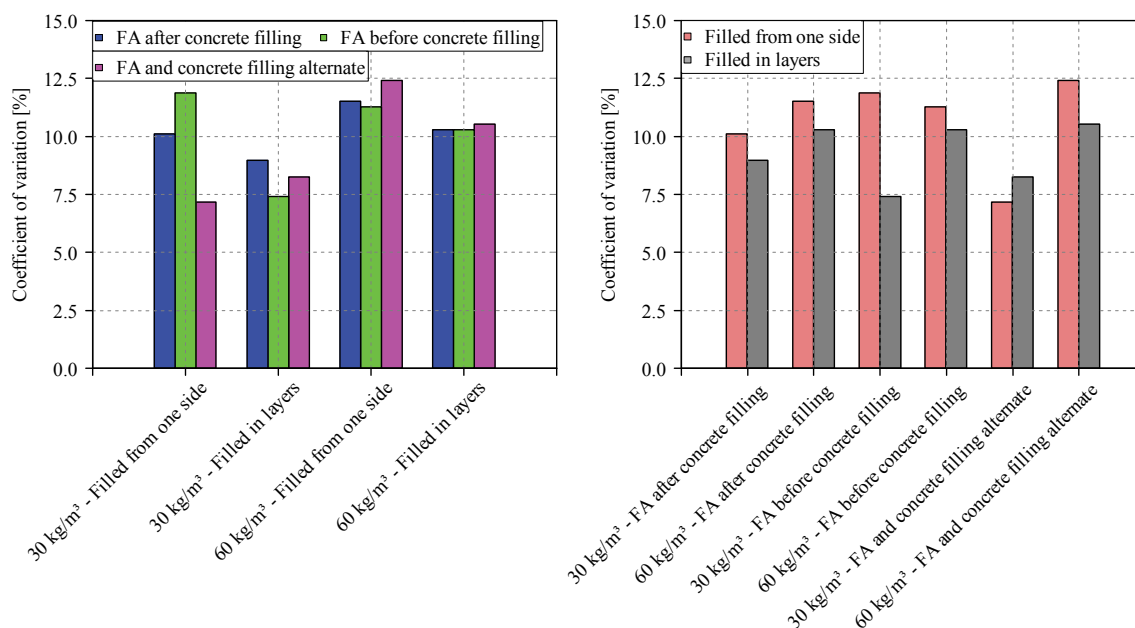


Fig. 7: Scattering of the number of crossing fibers – Comparison of the fiber addition procedures (left) and the filling method (right)

5. CONCLUSIONS AND FUTURE PROSPECTS

This contribution presents the results from an investigation on the effect of a new straight fiber type on the fiber distribution in beams. The influence of the fiber addition procedure, the fiber content and the filling method were additionally investigated. The presented results show that the number of fibers in the cross section of the beams, scatters about 10%, independent of the manufacturing procedure.

The German as well as the Austrian guideline for fiber reinforced concrete, define 4-point-bending tests for the determination of the material properties. In order to obtain the characteristic value of the flexural tensile strength (5% – quantile), the mean value is reduced by a factor of 0.51, which corresponds to a variation coefficient of about 25%. However, the advantage of a more homogenous fiber distribution cannot be taken into account with this limitation. As shown in (Hadl, 2017), a scattering of 15 % increases the factor from 0.51 to 0.7, which means that the design value of the post-cracking tensile strength is increased by the factor 1.4.

Regarding the further development of this steel fiber type and its influence on the fiber distribution, an additional experimental program is planned. The future program includes beams, basements and rising walls in order to consider realistic conditions. Small specimens according to the German guideline for fiber reinforced concrete will be cut from beams, basements and walls after casting. Subsequently 4-point-bending tests will be performed, to obtain the realistic load bearing behaviour of the component. To gather information on the fiber orientation and distribution, slices will be cut from selected specimens after its bending test. By using an opto-analytic method the fiber orientation and distribution will be determined.

6. REFERENCES

- Deutscher Ausschuss für Stahlbeton (2010), DAfStb - Richtlinie Stahlfaserbeton, Beuth Verlag.
- Hadl, P. (2017), "Zum besseren Verständnis der Streuung des Zugtragverhaltens von stahlfaserbewehrtem Normalbeton und Ultra-Hochleistungsbeton", Dissertation, TU Graz.
- Hadl, P., Gröger, J., Tue, N.-V. (2015), "Experimentelle Untersuchungen zur Streuung im Zugtragverhalten von Stahlfaserbeton", Bautechnik, 92. S. 385-393.
- Müller, T. (2015), "Untersuchungen zum Biegetragverhalten von Stahlfaserbeton und betonstahlbewehrtem Stahlfaserbeton unter Berücksichtigung des Einflusses von Stahlfaserart und Betonzusammensetzung", Dissertation, HTWK Leipzig.
- Erdem, E. (2002), "Probabilistisch basierte Auslegung stahlfasermodifizierter Betonbauteile auf experimenteller Grundlage", Dissertation, Ruhr-Universität Bochum.
- Gröger, J., Tue, N.-V., Wille, K. (2012), "Bending Behaviour and Variation of Flexural Parameters in UHPFRC", In Proceedings of 3rd International Symposium on Ultra-High Performance Concrete, Kassel University Press.
- Lin, Y.-Z. (1996), "Tragverhalten von Stahlfaserbeton", Schriftenreihe des Instituts für Massivbau und Baustofftechnologie der TU Karlsruhe.
- Holschemacher, K., Klug, Y., Dehn, F., Wörner, J.-D. (2006), "Beton-Kalender, Kapitel X: Faserbeton", Ernst & Sohn.
- Leutbecher, T. (2007), "Zum Tragverhalten von zugbeanspruchten Bauteilen aus Ultra-Hochleistungs-Faserbeton", Dissertation, Universität Kassel.
- Fehling, E., Schmidt, M., Walraven, J., Leutbecher, T., Fröhlich, S. (2013), "Betonkalender", Kapitel IX, Ultrahochfester Beton – UHPC, Ernst & Sohn.
- Freytag, B. (2014), "UHPC im konstruktiven Ingenieurbau", Habilitationsschrift, TU Graz.
- Bonzel, J., Schmidt, M. (1984), "Verteilung und Orientierung von Stahlfasern im Beton und ihr Einfluss auf die Eigenschaften von Stahlfaserbeton", Teil 1 + 2, Beton, 34 + 35.
- Linsel, S. (2005), "Magnetische Positionierung von Stahlfasern in zementösen Medien", Dissertation, TU Berlin.
- Hilsdorf, H., Brameshuber, W., Kottas, R. (1985), "Weiterentwicklung und Optimierung der Materialeigenschaften faserbewehrten Betons und Spritzbetons als Stabilisierungselemente der Felssicherung", Abschlussbericht zum Forschungsvorhaben, Universität Karlsruhe.
- Hadl, P., Tue, N.-V. (2016), "Einfluss der Faserzugabe auf die Streuung im Zugtragverhalten von Stahlfaserbeton", Beton- und Stahlbetonbau, 111. S. 310-318.

RESEARCH ON THE LIGHTWEIGHT CONCRETE BRIDGE DECK SLABS REINFORCED WITH GFRP COMPOSITE BARS

Agnieszka Wiater

Rzeszow University of Technology

al. Powstańców Warszawy 12, 35-959 Rzeszów PL

SUMMARY

The main goal of the paper is the presentation of research works on static and fatigue behaviour of LWC (*lightweight concrete*) deck slab reinforced with GFRP (*glass fibre reinforced polymer*) rebars. The structural LWC with *lytag* type aggregate has been used for slab casting. The carrying capacity of the slabs as well as fatigue durability have been checked during experimental tests on three full-scale deck slabs. All slabs were 5,2 m long, 1,9 m wide and 0,18 m deep. One- and two-span arrangements have been applied for static and fatigue tests in shear and flexure. The research has clearly revealed that bridge deck slabs made of LWC concrete and GFRP rebars could be viable alternative for conventional concrete bridge decks with steel rebars. Following the research the first Polish application of LWC bridge deck slab reinforced with GFRP bars took place on a medium-size road bridge.

1. INTRODUCTION

Corrosion of steel reinforcement is a major durability problem in concrete structures which leads to shorten the service time of concrete construction such as bridge decks and increases the maintenance cost. In road bridge system, concrete bridge decks deteriorate faster than any other bridge components due to de-icing salts and increasing traffic load. Corrosion of steel rebars causes structural degradation and constant costly repairs. In order to avoid steel corrosion problem, concrete structures can be reinforced with non-corroding reinforcement such as GFRP (*glass fiber reinforced polymers*) rebars. The use of GFRP bars in concrete structures can lead to increase a service life of bridge, decrease the maintenance cost and improve effectiveness cost in life-cycle of construction. GFRP reinforcement, as compared to steel, is resistant to corrosion, lighter and has a higher tensile strength. Moreover, GFRP rebars are transparent to magnetic fields and electrically non-conductive. Due to their advantages GFRP rebars are a promising alternative for conventional steel reinforcement (El-Salakawy et al., 2005; Benmokrane et al., 2006; Benmokrane et al., 2007; Holden et al., 2014).

Another issue, which is considered in bridge deck construction is a lightweight concrete (LWC) application. When lightweight concrete is used, the extra decrease of self-weight of deck (about 30%) which means bridge strengthening in redecking cases, might be obtained. So far, a major obstacle of application LWC in bridge decks is highly absorptive concrete. When steel reinforcement is used, it usually leads to faster steel corrosion following by concrete deterioration. However, when using LWC and GFRP reinforcement, this problem is solved owing to non-corrosive properties of rebars. Combination of LWC and GFRP offers synergy of advantages of both materials and leads to more durable, less-weight and cheaper in terms of LCC (*life cycle cost*) bridge decks.

The paper presents the research works on static and fatigue behaviour of LWC deck slab reinforced with GFRP rebars, which results enabled the first Polish application of LWC-GFRP deck slab on medium-size road bridge.

2. EXPERIMENTAL PROGRAM

A total of three full-scale concrete deck slab of 5.14 m long, 1.90 m wide and 0.18 m deep, were constructed and tested. All slabs were reinforced with top and bottom grids of 12 mm diameter GFRP rebars spaced at 80 mm in both directions, with concrete cover of 30 mm. The rebars were fabricated using pultrusion process. The GFRP bars had a sand-coated surface to enhance the bond performance between the rebars and surrounding concrete. The tensile strength of GFRP rebars were obtained from appropriate standard test (ACI 440.1R-06) and amount to about 810 MPa. The structural LWC with *lytag* type aggregate has been used with target class LC35/38. The density of fresh mix concrete was 1970 kg/m³.

One simply and two continuously GFRP reinforced LWC slabs were tested in shear and flexure. The continuous slabs comprised of two equal spans, each of 2.4 m, while the simply supported slab has a span of 4.8 m, as show in Fig. 1.

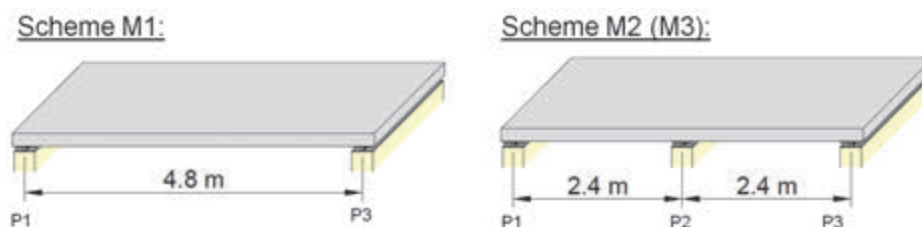


Fig. 1: Test arrangements - scheme M1, M2 (M3)

The load was applied through a 400x400 mm steel plates at places that represent the LM1 traffic load models as specified by Eurocode 1 (EN 1991-2) (Fig. 2). The static test was carried out on slab M1 and M2, and fatigue test was carried out on M3 slab.

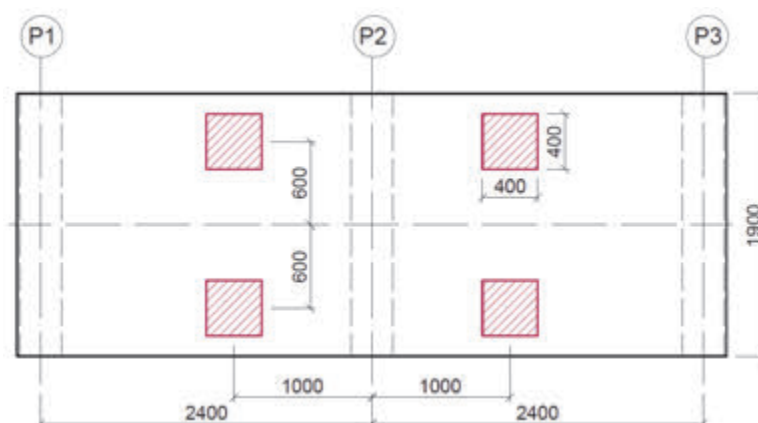


Fig. 2: Loading scheme LM1

The slab testing was a part of research works on the first Polish road bridge made of FRP composites, so applied loads corresponded to bending moments induced by the traffic load in deck slab of the bridge with 1.7 m spaced main girders (Siwowski et al., 2015). According to this assumption two load levels had been specified for each test scheme, unit force P_k and P_d characteristic and design load value respectively, see Tab. 1.

Tab. 1: Load levels for static test

Test scheme	Characteristic load value	Design load value
	P_k [kN]	P_d [kN]
M1	34.9	94.5
M2	155.5	324.0

Slab M3 was subjected to constant amplitude of fatigue loading. The cyclic load with frequency 2 Hz (up 500 000 cycles) and 1.5 Hz (after 500 000 cycles) was applied to test specimen. The maximum load level $F_{max} = 222.2$ kN (2×111.1 kN) correspond to bending moment caused by weight 210 kN for each axle, as specified in Eurocode 1 (EN 1991-2). The minimum load level was set as $F_{min} = 22.2$ kN (2×11.1 kN).

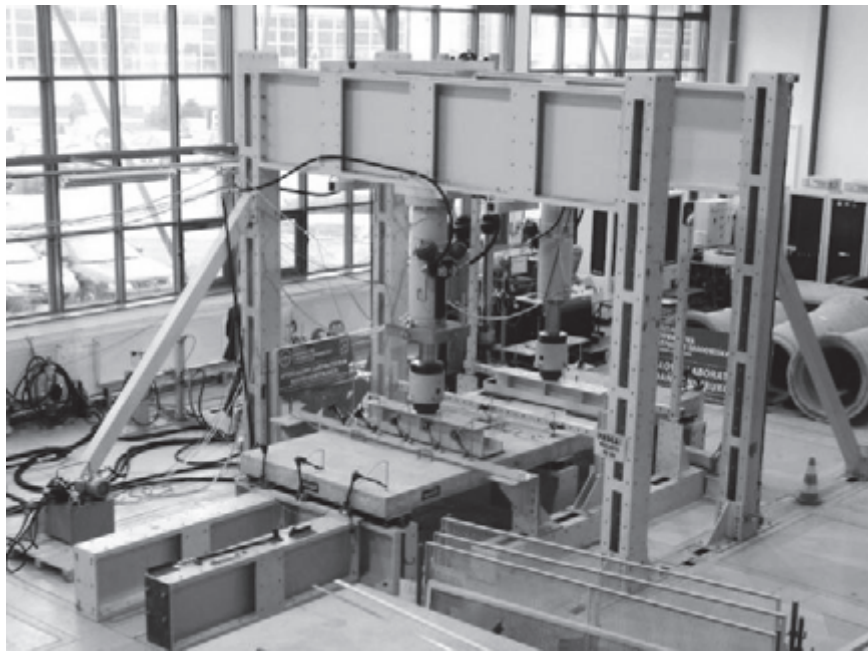


Fig. 3: Slab specimen M3 under testing

During static and fatigue tests, the deflection, concrete strains and formation of cracks were recorded and marked.

3. TEST RESULTS AND DISCUSSION

Two different failure modes were observed in the experimental static tests as shown in Fig. 4 and Fig. 5. The M1 slab (simply supported scheme) showed flexure failure (concrete crushing) at $P_{M1,ul} = 220$ kN load level, while the M2 slab (continuous scheme) failure in shear at $P_{M2,ul} = 880$ kN. Shear crack started at loading point and propagated to middle support.

Basing on static test, the global safety coefficient for ultimate limit state (ULS) were specified as ultimate to characteristic load ratio. The value of this coefficient for tasted slabs were over 5.0 what seems to be the satisfactory result in terms of bridge safety.

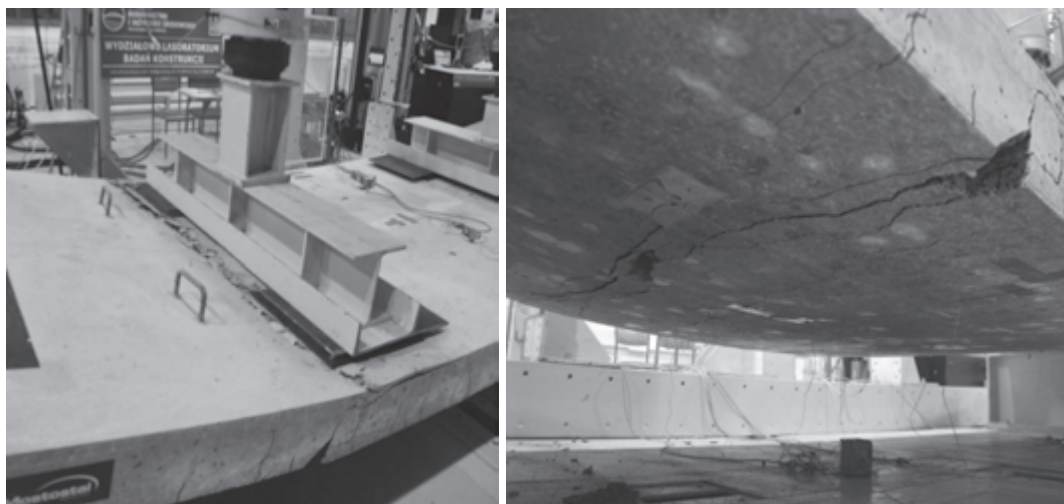


Fig.4: Flexure failure of M1 slab specimen

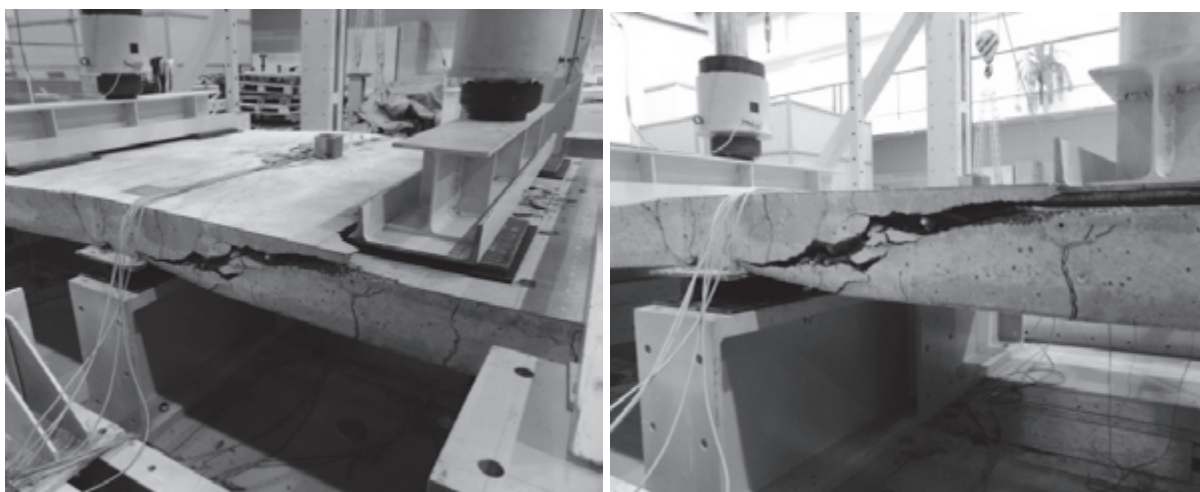


Fig. 5: Shear failure of M2 slab specimen

Similar analysis were performed for serviceability limit state (SLS). The experimental value of deflection and crack width at characteristic load level was compared with allowable value (Tab. 2). As allowable deflection of slab the value of $l_t/250$ was adopted, where l_t is center to center space between supports and as allowable crack width the value of 0.5 mm was assumed according to ACI guide (ACI 440.1R-06).

Tab. 2: Comparison of experimental and allowable values for SLS

	Crack width [mm]		Deflection [mm]	
	M1	M2	M1	M2
Maximum test value (a)	0.3	0.3	13.4	1.8
Allowable value (b)	0.5	0.5	19.2	9.6
(a)/(b) [%]	60 %	60 %	70 %	19 %

In fatigue test after 980 500 cycles, there was observed a considerable increase of slab deflection amplitude. Due to large value of deflection and rapid crack propagation in concrete the test was stopped (Fig. 6). The main reason of fast increase of crack width and slab deflection was bond failure between GFRP rebars and concrete. Due to the fact that the service load of the real bridge will be much lower than applied in fatigue test, the results of this experiment were accepted as satisfactory.



Fig. 6: Slab failure pattern after the fatigue test

The full presentation of static and fatigue tests of LWC-GFRP bridge deck slabs is presented elsewhere (Wiater et al., 2015).

4. APPLICATION ON A ROAD BRIDGE

The prototype LWC-GFRP bridge deck slab exhibited satisfying structural behaviour during the static and fatigue test, therefore it was decided to implement it for the first time in Poland on a medium-size road bridge. The bridge was built in Błażowa (south-eastern Poland) along the local road over Ryjak stream. The bridge superstructure with a simple span of 22.00 m and a width of 10.44 m, is formed by four simply supported U-shape FRP girders with an overlying 0.18 m thick lightweight concrete slab reinforced longitudinally and transversely with two grids of GFRP rebars. The cross-section of the bridge and reinforcement details are shown in Fig. 7. The deck slab was made from LC35/38 lightweight concrete with *lytag* type aggregate and reinforced with two grids of GFRP rebars of 12 mm diameter, spaced at 120 mm in transverse and 150 mm in longitudinal direction. The GFRP reinforcement using in bridge deck slab was the product of ComRebars Company, the only Polish FRP rebar manufacturer. The GFRP rebars are made of epoxy-resin and fiber content 75-80% by weight with braided proces for fiber spiral ribs on the outer surface. The guarantee tensile strength and elastic modulus of GFRP rebars were 1000-1100 MPa and 50 ± 5 GPa, respectively. The concrete deck slab was designed using an ACI guide (ACI 440.1R-06).

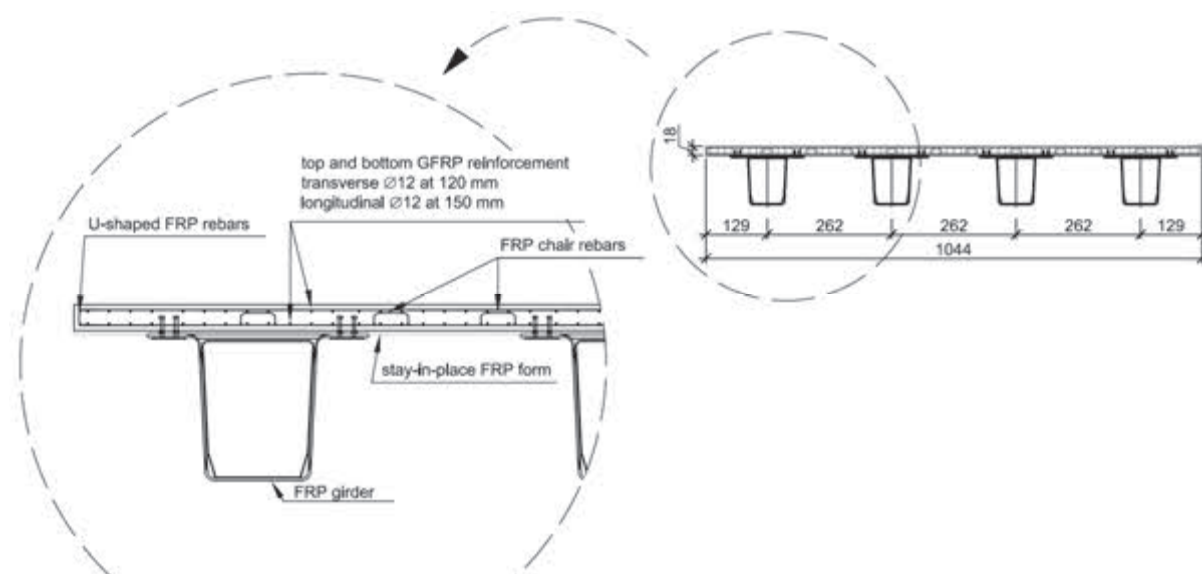


Fig. 7: Cross section of deck slab of the Błażowa bridge

The concrete mixture volume of 53 m³ was used for casting entire bridge deck slab in one-stage continuous process. Concrete mixture was lifted and placed using basket by mobile crane, what prevented from the damage of lightweight aggregate (Fig. 8).



Fig. 8: Installation and construction of a lightweight concrete bridge deck slab reinforced with GFRP rebars

The experience from the first Polish application of LWC-GFRP bridge deck slab is very promising. Technology of casting was similar to one used for the conventional steel reinforced concrete bridge deck slabs. One of the differences was stiffness of GFRP grids, which were significantly deflecting under workers, comparing to steel reinforcement. To ensure the right position of reinforcement during concreting, the extra space elements made of PVC tubes were used. The other difference was the method of connecting rebars together, which in case of GFRP rebars was realized by using zip ties (clamping bands).

The bridge construction was completed in November 2015 (Fig. 9). The general characteristic of the bridge and construction process is described in (Siwowski et al., 2017)



Fig. 9: Completed bridge in Błazowa with LWC-GFRP deck slab

5. CONCLUSIONS

Recent progress in material engineering, allowed for the application of a new, technology-advanced construction materials, such as high-performance lightweight concrete and FRP composite. Due to excellent physical and mechanical characteristic in comparison to the

conventional materials, each of these materials has its field applications in bridge construction. The main advantage of the lightweight concrete is relatively small density of hardened concrete, what allows for construction of less-weight and smaller elements. GFRP reinforcement is used due to high strength and high durability in aggressive environment. Synergy of LWC and GFRP rebar advantages was motivation to start of aforementioned research on combination of both materials for bridge decking. Preliminary works showed that the application of LWC-GFRP deck slab is possible and even advisable. The behaviour of lightweight concrete slab reinforced with GFRP rebar is similar to conventional steel reinforced deck slab.

Besides of the first application there is a constant need to test the behaviour of this kind of bridge structural elements under the service loading. These tests are planned to be carried out by the Rzeszow University of Technology in the near future. Following the further tests the verification and modification of design procedure when lightweight concrete is used are going to be done. These works allow for wider application of LWC-GFRP bridge deck slabs and optimization of amount of construction material used. The latter is highly expected due to higher material price in comparison with conventional materials. However, the output of the research project presented in this paper gives a very promising future for LWC-GFRP deck slab as application in road bridge construction.

6. ACKNOWLEDGEMENTS

This research was supported by the National Centre of Research and Development (NCBiR), Poland, in the frame of DEMONSTATOR+ programme, the project title: "ComBridge: Innovative road bridge with FRP composites" (No. UOD-DEM-1-041-/001).

7. REFERENCES

- ACI 440.1R-06. "Guide for the design and construction of concrete reinforced with FRP bars", American Concrete Institute (ACI), USA, 2006.
- Benmokrane B., El-Salakawy E., El-Ragaby A., El-Gamal S. (2007): "Performance evaluation of innovative concrete bridge deck slabs reinforced with fibre-reinforced-polymer bars", *Canadian Journal of Civil Engineerin*g, vol.34, no. 3, 2007, pp. 298-310.
- Benmokrane B., El-Salakawy E., El-Ragaby A., Lackey T. (2006): "Designing and testing of concrete bridge decks reinforced with glass FRP bars", *Journal of Bridge Engineering*, vol.11, no. 2, pp. 217-229.
- El-Salakawy E., Benmokrane B., El-Ragaby A., Nadeau D. (2005): "Field investigation on the first bridge deck slab reinforced with glass FRP bars constructed in Canada", *Journal of Composites in Construction*, vol.9, no. 6, 2005, pp. 470-479.
- EN 1991-2. "Eurocode 1 - Actions On Structures - Part 2: Traffic Loads On Bridges", European Committee for Standardisation, 2003.
- Holden K., Pantelides C., Reaveley L. (2014): "Bridge constructed with GFRP-reinforced precast concrete deck panels: case study", *Journal of Bridge Engineering*, vol.19, no. 5, 2014.
- Siwowski T., Rajchel M., Kaleta D., Własak L. (2016): "The first Polish road bridge made of FRP composites", *Civil Engineering and Building*, no. 10, 2016, pp. 465-470 (in Polish).
- Siwowski T., Rajchel M., Wiater A. (2017): "The first Polish composite bridge in research", *Builder*, no. 04, May 2017, pp. 98-102 (in Polish).
- Wiater A., Rajchel M., Siwowski T. (2015): "Research on deck slabs made of lightwiegth concrete and reinfroced with GFRP bars". *Journal of Civil Engineering, Environment and Architecture*, vol. XXXII, no. 62 (4/15), 2015, pp. 469-492 (in Polish).

HYBRID STEEL-CONCRETE SHEAR WALLS STRENGTHENED USING HIGH PERFORMANCE STEEL FIBRE REINFORCED COMPOSITES

Viorel Constantin Todea, Valeriu Stoian, Daniel Dan, Tamás Nagy-György, Sorin Codruț Floruț, Emanuela Boita

*Politehnica University of Timișoara, Faculty of Civil Engineering
2nd T. Lalescu street, 3000223 Timișoara, Romania*

SUMMARY

Post-earthquake strengthening of damaged structural elements represents an important issue for all structures placed in seismic areas. In most cases, the lateral resisting system of mid- and high-rise buildings comprises of Reinforced Concrete (RC) and composite steel-concrete shear walls, which are prone to damage during earthquakes of high magnitude. The current paper proposes a modern approach for strengthening of such elements, using high performance steel Fibre Reinforced Cementitious Composite (FRCC) materials, a technique that has not been thoroughly investigate and documented. This material was applied in the shape of thin jacketing for three composite steel-concrete shear walls that had previously been tested up to failure, in a cyclic loading procedure, simulating the effects of earthquake. The results for one strengthened specimen are presented hereinafter.

1. INTRODUCTION

In the last decade, some of the modern materials which are being studied extensively in concrete technology and strengthening solutions, are Fibre Reinforced Concrete (FRC) and high-performance steel fibre grouts, materials which could replace the arranged longitudinal and transversal reinforcements made from steel bars, of reinforced concrete structural members, if the minimum percentage of steel fibres embedded in mass of this kind of materials are satisfied. FRCC is a modern material, which was developed and used mostly to increase the mechanical performances and durability of damaged structural members. In most common studies, after strengthening structural elements, this material has proved significant increases in bearing capacity, at least 30% higher compared to the initial situation. The research is limited on this topic, several results being highly visible, dealing with strengthening of slabs, beams, columns and masonry elements. For reinforced concrete or composite walls strengthened using FRCC the available research is quite scarce. Most studies concerning the strengthening of RC structural elements with FRCC approach the benefits provided by the high tension strength of the material, applying a relatively thin layer of mortar in sections with the largest stress rate. A study like this was performed by (Lampropoulos et al., 2016) whose experimental program has proven the high efficiency of strengthening of concrete beams subject to bending and shear with FRCC. The strengthening of the concrete beam was accomplished in several ways, placing the mortar in a simple layer of material, about 50 mm thickness, at the bottom of the tensioned area of beam, on the both sides, and last at the top in compression zone. After that, the results obtained show a significant increase of the bearing capacity by up to 30%, practically the material having great potential in strengthening of such elements. Another important research (Xiuling et al., 2016), studied the nonlinear behaviour of some concrete columns strengthened with FRCC. The results obtained

after testing 4 specimens shown an important increase of bearing capacity with 30% higher than the initial performances of the columns.

2. EXPERIMENTAL PROGRAM

The present study is a continuation of a research performed on steel-concrete hybrid walls with the intention of studying their performance with that of similar reinforced concrete shear walls (the latter representing the generally applied solution for mid- and high-rise buildings placed in seismic areas). The main objective of the current research is to investigate the behaviour of three steel-concrete hybrid shear walls which were tested up to failure, strengthened with 2x25 mm thin jacket of FRCC, and then retested to full failure. The results obtained by completing the experimental research are encouraging, highlighting an enhanced behaviour of the strengthened walls, especially in comparison to the original FRC.

2.1. Wall specimen characteristics

The experimental specimens are 1:3 scale reinforced concrete and steel-concrete hybrid elements, with 3000 mm height, 1000 mm width and 100 mm thickness, simulating a three storey and one bay element from the base in a lateral resisting system of a building structure. For some of these elements, the traditional steel reinforced concrete has been replaced by FRC (using longer and thicker steel fibres in comparison to the solution presented hereinafter). For this type of structural walls, the Composite Steel Fibre Reinforced Concrete Wall (CSFRCW) notation is used. The thin walls, including the reinforcements and steel profiles, were build-in a heavily reinforced concrete foundation with 1500 mm length, 400 mm height and 350 mm width. The foundation block was highly reinforced in order to avoid any circumstances regarding the failure at this level of embedded specimens in testing procedure. Steel profiles embedded in the core of specimens, have assured the connection with the concrete by welded headed shear stud connectors placed at every 150 mm on the length/height of the profiles. The reinforcement placed on the edges of the web panel consist of 8Ø10 mm vertical bars and Ø8/75 mm horizontal stirrups. Details of the experimental specimens tested in the laboratory are presented in Fig. 1 and the sectional characteristics of steel profiles are shown in Tab. 1.

All the specimens were designed in accordance with the principles of existing codes, Eurocode 2, Eurocode 4 and Eurocode 8. The investigations and specifications for composite FRC walls are poor and the knowledge related to the nonlinear behaviour of such elements is limited.

2.2. Material properties

Steel profiles were manufactured by welding steel plates which correspond to S355 steel quality. The used reinforcements are made from S500C steel grade. To determine mechanical properties of the steel fibre mixed concrete some cubes and prismatic elements were provided. After the samples were tested, the established strength class of the concrete was C30/37. For disperse reinforcement of the concrete, hooked steel fibres were used with a minimum tensile strength of 1100 MPa, based on the supplier's data. The steel fibres had 60 mm length and 0.8 mm diameter. For strengthening the damaged specimens, free-flowing high ductility fibre-reinforced cementitious mortar with steel fibres (FRCC) material was used. FRCC is a bi-component material, component A is brass coated steel fibres defined by 13-15 mm length and 0.2 mm diameter while component B is pre-dosed powder grout made from high-strength

cement, selected aggregates and special additives. The steel fibres correspond to a maximum of 6.5% weight of component B.

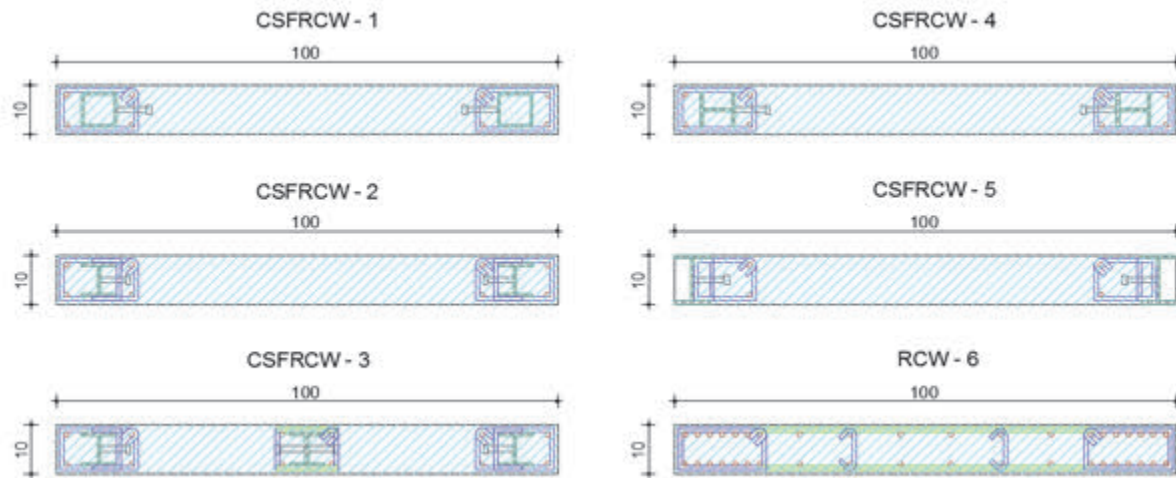


Fig. 1: Details of experimental specimens before and after strengthening with FRCC

Tab. 1: Sectional parameters of encased steel profiles

Specimen label	Steel shape	Encasement level	b_f [mm]	t_f [mm]	h_w [mm]	t_w [mm]
CSFRCW-1	2□	fully	70	5	70	5
CSFRCW-2	2I	fully	70	7	56	7
CSFRCW-3	3I	fully	70	7	56	7
CSFRCW-4	2H	fully	70	7	56	7
CSFRCW-5	2I	partially	70	7	86	7

After testing some samples made from FRCC (3 cubes and 6 prismatic elements) the mechanical properties of this material indicate higher net values than a usually mortar or concrete used predominantly for building structural elements. The compression strength of the material was close to 121 MPa. In case of tensile strength, values from 5.46 MPa up to 9.57 MPa were obtained.

2.3. Test set-up and loading procedure

The composite shear walls were tested under constant vertical load (100 kN, corresponding to a normalised axial force of 1.5%) and quasi-static reversed cyclic lateral loads. The specimens were anchored with some steel bolts and connecting steel devices in a reaction floor. The lateral loads were applied alternatively left-right, using two 400 kN hydraulic jacks placed at 400 mm below the top of the specimens. The vertical force was provided by a 250 kN hydraulic jack placed at the top of the walls. In the Fig.2 experimental testing frame can be observed.

The recommended ECCS [6] short testing procedure was used for cyclic tests. All the cyclic load steps, horizontal forces, were applied in displacement control model. Four cycles were performed before the elastic limit of the specimens was reached. Horizontal forces were applied until the strength of the specimens decreased to 85% of the peak horizontal load. For monitoring the behaviour of the specimens, displacements transducers and pressure transducers were used.

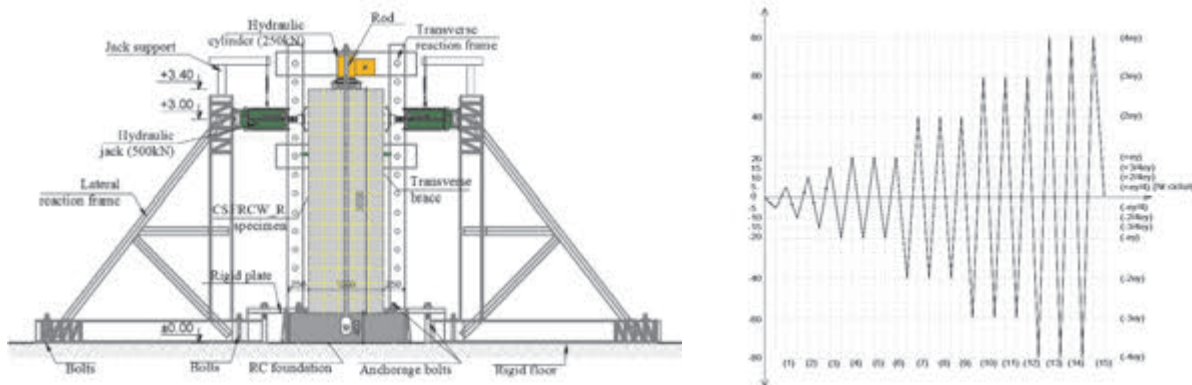


Fig. 2: Test set-up and loading history diagram

3. EXPERIMENTAL RESULTS AND OBSERVATIONS

3.1. General behaviour and failure modes of elements

The main objectives of this experimental program, in the first part, were to investigate the possibility to totally replace the traditional reinforcement (steel rebar) placed in the central area of the composite walls with steel fibres and then, to evaluate the main parameters of the behaviour, i.e. strength, ductility and stiffness and make some comparisons with the behaviour of common RC walls and composite shear walls with steel encased profiles. The aim of the second part of the experimental program, was to retrofit and strengthen (using FRCC) the specimens which had already been tested up to failure and to investigate if the initial performance of elements i.e. those before testing can be restored.

Some of the studies performed on the composite steel-concrete walls with traditional reinforcements placed in the central area of the wall, shown a good behaviour under cyclic lateral loads, failure modes being ductile, with more than 25% bearing capacity than RC traditional walls. The failure mode is characterised by yielding of the steel profiles in tension, plastic deformations in concrete, crushing of the compressed concrete zone and tearing the tensioned steel profiles. Specimens reach up to 100 mm in drift prior to failure.

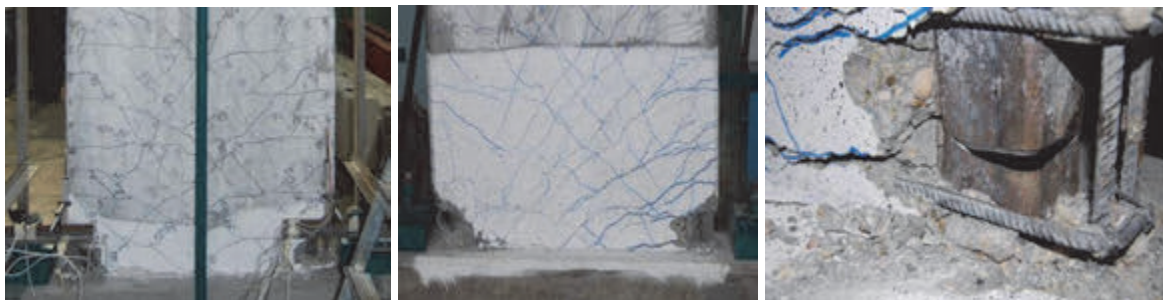


Fig. 3: Type of failure modes of steel-concrete composite walls

In the case of the composite FRC walls, which were tested up to failure, the results shown the brittle failure modes of the elements, which occurred with a diagonal crack and without yielding of vertical reinforcement and structural steel. Almost all cracks start developing at 15 cm from the edge of the wall, corresponding to the internal face of the steel profiles embedded in the core of the walls. The cracks appear when the tensile strength of the concrete is exceeded. Before the elastic limit was reached, only diffused cracks have

developed. All the specimens (CSFRCW) reach failure at 30-40 mm value of the drift. No crushing of the compressed concrete zone and tearing the tensioned steel profiles was observed.

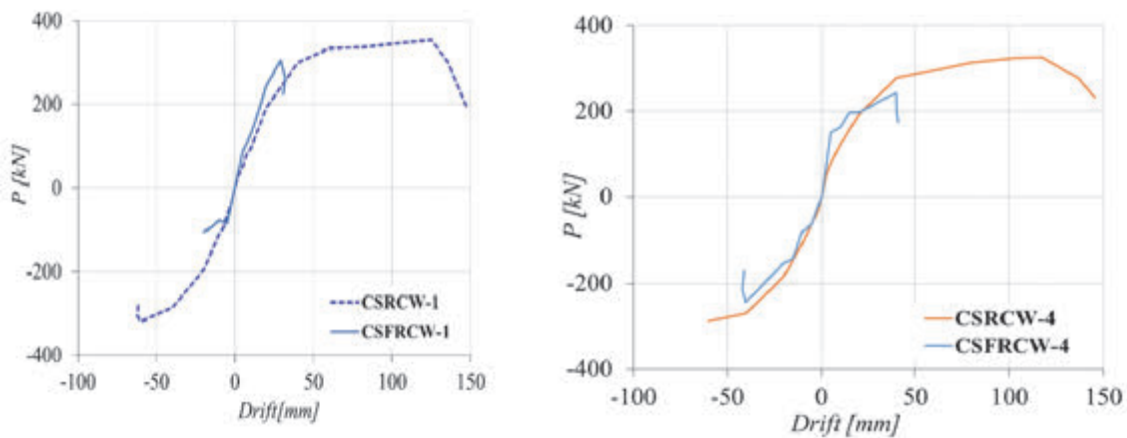


Fig. 4: Specific envelope curves for two tested specimens



Fig. 5: Type of failure modes of steel-concrete composite walls

In terms of bearing capacity, the values registered of the lateral forces applied are quite similar in both cases and the stiffness of the specimens is slightly similar. The big difference in behaviour of the elements is represented by their capacity to dissipate energy and their ductility. In fact, the series of investigations carried out on the composite walls show their net superior performance in comparison to the specimens which have the traditional reinforcement replaced by steel fibres. In case of dispersed FRC walls, the observed failure modes are characteristic of a fragile behaviour, without enabling the yielding capacity of the steel profiles placed at the extremities, and, compared to the reinforced concrete walls or steel-concrete composite walls with traditional reinforcement in the central area the overall behaviour is net inferior. This kind of behaviour is not accepted in seismic area. At the end of the tests, the specimens before strengthening showed an advanced state of degradation as illustrated in the figures below.



Fig. 6: Level of degradation stage, retrofitting and strengthening walls with FRCC

Upon a quick investigation, tested specimens had multiple cracks on the surface oriented in a random direction, completed by destruction of the concrete in the corners and the buckling of the steel profiles and reinforcements. After that, retrofitting with high performance mortars and epoxy materials was done, and walls were strengthened with FRCC in a 2x25 mm thin jacket. The last step was retesting the strengthened specimens. As can see in the illustrated figures, many cracks were developed on the FRCC surface, defined by small openings at different level of encountered drift.

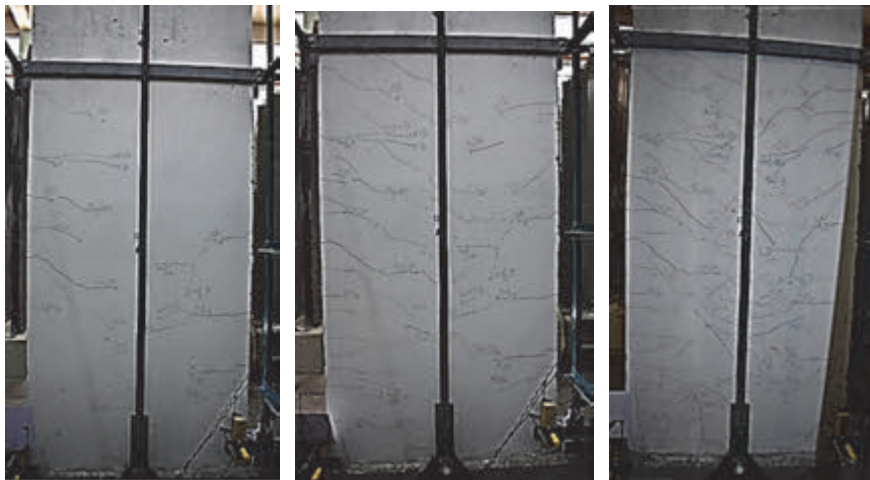


Fig. 7: Cracks developed on the surface of thin jacket FRCC (10–40–90 mm drift)

It was register a maximum 94.5 mm drift and 395.6 kN peak value of lateral induced force. Specimens before strengthening with FRCC has failed at 30...40 mm value of drift, while after strengthening, elements do not reach the elastic limit of bearing capacity at this level of drift, as can see. The failure mode of strengthened specimens has changed, becoming a ductile one, steel profiles was reaching the plastic capacity in tension and walls registered a high rate of dissipated energy.

After the tests were done, structural steel profiles were discovered, to observe the level of plastic strain developed. No pronounced plastic deformation was encountered, steel profiles had not reach the ultimate state limit under the lateral load, which mean the strengthening was

successful. Since this is an ongoing project, the conclusions are limited, the available results could be presented as it is in Tab. 2.

Tab. 2 – Results of tested specimens

Specimen	Steel shape	Testing phase	Maximum load [kN]	Maximum drift [mm]	Failure mode
CSFRCW-1	2□	Baseline	305.6	32.18	Shear
CSFRCW-2	2工	Baseline	N/A	N/A	N/A
CSFRCW-2	2工	Strengthened	N/A	N/A	N/A
CSFRCW-3	3工	Baseline	332.6	60.57	Shear
CSFRCW-3	3工	Strengthened	395.6	94.5	Bending
CSFRCW-4	2H	Baseline	244	40.95	Shear
CSFRCW-4	2H	Strengthened	N/A	N/A	N/A
CSFRCW-5	2工	Baseline	245.6	33.47	Shear
RCW-6	N/A	Baseline	280	108.1	Bending

4. CONCLUSIONS

The performed studies show that initial failure mode of the CSFRCW tested specimens in bending was fragile, the concrete crushed before plastic capacity of steel profiles was reached and after strengthening with FRCC applied in a thin layer, rate of dissipated energy and ductility was increased. The performances of strengthened specimens have to be compared with performances of traditional reinforced concrete walls. As can see the proposed strengthening solution was successfully and it could be a possible option at choosing the best solutions for retrofitting damaged structural members.

5. REFERENCES

- Lampropoulos, A. P., Paschalis S. A., Tsioulou O. T. and Dritsos S. E. (2016), “Strengthening of reinforced concrete beams using ultra high fibre reinforced concrete (UHPFRC)”, *Engineering Structures*, Vol. 106, January 2016, pp. 370-384.
- Xiuling, L., Juan, W., Yi, B. and Genda, C. (2017), “Cyclic behavior of damaged reinforced concrete columns repaired with high-performance Fibre-reinforced cementitious composite”, *Engineering Structures*, Vol. 136, April 2017, pp. 26-35.
- Dan, D., Fabian, A. and Stoian, V. (2011), “Theoretical and experimental study on composite steel–concrete shear walls with vertical steel encased profiles”, *Journal of Constructional Steel Research*, Vol. 67, May 2011, pp. 800-813.
- Dan, D., Fabian, A. and Stoian, V. (2011), “Nonlinear behaviour of composite shear walls with vertical steel encased profiles”, *Engineering Structures*, Vol. 33, October 2011, pp. 2794-2804.
- Boita, I. E., Dan, D., Stoian, V. A., Florut, S. C. and Todea, V. C. (2017), “Composite Steel Fibber Reinforced Concrete Shear Walls with Vertical Encased Profiles. Experimental Study”, *Conference: 16th National Technical-Scientific Conference on Modern Technologies for the 3rd Millennium*, March 2017.
- ECCS. Recommended testing procedure for assessing the behaviour of structural steel elements under cyclic loads, *European Convention for Constructional Steelwork*, 1999.

INNOVATIVE PERFORATED STEEL SHEET REINFORCEMENT: CORBEL APPROACH

*E. Apostolidi¹, K. Bergmeister¹, A. Strauss¹, P. Winkler¹, P. Kremnitzer², C. Rauch²,
B. Schembera³*

¹ *Institute for Structural Engineering, University of Natural Resources & Life Sciences,
Vienna, Austria*

Peter-Jordan-Strasse 82, A-1190, Vienna, Austria

² *PORR AG*

Absberggasse 47, A-1100, Vienna, Austria

³ *FCP – Fritsch, Chiari & Partner ZT GmbH*

Marxergasse 1 B, A-1030, Vienna, Austria

SUMMARY

Concrete planar structural elements (plates, walls, etc.) are normally reinforced by perpendicularly arranged bars in two directions. An alternative innovative perforated steel sheet reinforcement layout is developed with comparable mechanical properties. Steel sheet reinforcement is designed with certain layout, size and shape of perforations, a) to allow concrete flow within the steel sheet and b) to secure a better interaction between sheet and concrete. Within the steel sheet's perforations small concrete elements are formed, which are assumed to act as corbels. In the present paper, more than 30 (2D and 3D) numerical models of the corbels are calculated and evaluated, as part of a parametrical study. Results indicated the existence of an optimum correlation of the corbel height (h) to the corbel depth (a), considering the current numerical results and certain simplifications.

1. INTRODUCTION

Reinforced concrete is one of the most commonly used structural materials in the last decades, as steel reinforcement achieved to increase significantly the tensile capacity of concrete, which only had high compressive strength. Initially, steel bars were used as reinforcement for concrete, but recently, steel in form of fibres, grids, cables, etc. has also been introduced in reinforced concrete elements. For planar structural elements (such as slabs, walls, etc.) it is common to place two layers of steel bars, arranged perpendicularly to one another, to achieve a biaxial load bearing capacity of the element. An innovative idea is that steel reinforcement in form of a planar reinforcing element could be embedded in concrete and replace common steel reinforcing bars (Wille, 2008), as indicatively shown in Fig. 1(a).



Fig. 1: Reinforcing system of a perforated steel sheet (a) in 3D view, (b) detail of a bulged perforation, & (c) concrete corbel formed within the bulged openings of the steel sheet (Apostolidi & Strauss, 2014)

This novel reinforcing system is designed to have similar load bearing capacity with the reinforcing bars, minimizing the thickness of the composite element and particularly the steel to a final thickness of around 1 to 2 mm (Wille and Tue, 2013). To ensure an efficient interaction between the two materials, openings with bulged edges (Fig. 1(b)), are introduced in the steel sheet (Mucha, 2003). The bulged perforations facilitate the concreting procedure, allowing the concrete to pour through the openings. More importantly, within the bulged perforations a concrete element is formed, assumed to act as a corbel and is considered as the main shear transfer mechanism between steel and concrete (Fig. 1(c)). The bond behaviour between steel sheet and concrete is mainly governed by mechanical interlock and bond action has only a small contribution. For the steel sheet to have a sufficient load bearing capacity, some main influential parameters should be defined, such as the steel tensile strength, the layout and shape of perforation and the sheet thickness. Based on a decision making process, a certain perforation system is developed and briefly presented.

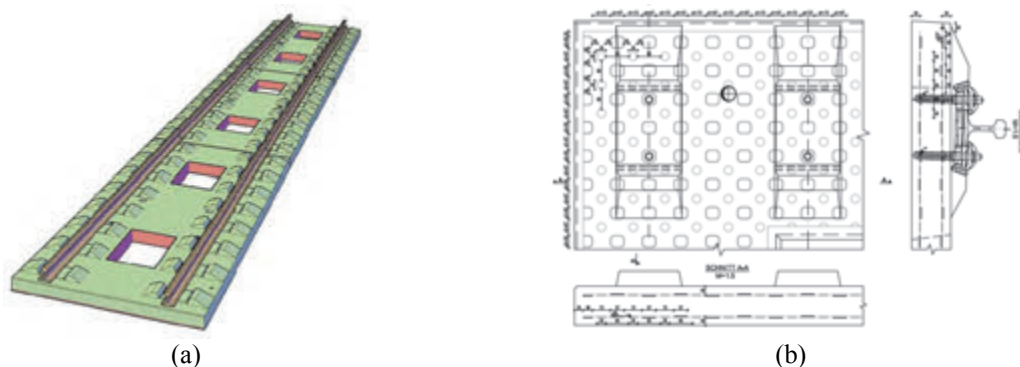


Fig. 2: Railway supporting RC Slabs to be reinforced with the innovative steel sheet reinforcement. (a) 3D view, and (b) constructional detail for the placement of the sheet reinforcement (Rauch, 2014)

The target of the development of this innovative reinforcement is to replace conventional bar reinforcement in prefabricated railway slabs, shown in Fig. 2(a). This slab track system, where the train rails are fixed on, is developed and patented by the construction company PORR AG and in order to optimize and accelerate the slab production, the idea of the steel sheet reinforcement placement, as presented in Fig. 2(b) is investigated. A national and international patent of this perforated steel sheet as reinforcement is available.

In the present paper, the focus will lean on the shear transfer mechanism between the two materials, the steel and the concrete, which is assumed to be achieved through the mechanical interlock of concrete corbels. Case specific assumptions, limitations and constraints are discussed, through the development of a 3D finite element model of the corbel. A parametric study, considering several geometrical properties of the corbel, is presented and leads to an optimum correlation between the corbel's height and depth that will further facilitate the overall development of the perforated steel sheet layout.

2. DESIGN OF THE STEEL SHEET

The design process of the innovative sheet reinforcement is a rather complex task and is based on consecutive decision-making steps, trying to combine theoretical and practical aspects, as well as findings from previous researchers (Mucha, 2003; Wille, 2008; Wille and Tue, 2013). The development of this innovative perforated steel sheet was initially based on the concept of replacing the minimum bar reinforcement ($\text{Ø}10/100\text{mm}$) in a 1 m^2 reinforced concrete slab (Fig. 3). Therefore, the thickness of the steel sheet, the size and position of the perforations

and the steel material properties had to be defined. To facilitate the production and the placement on site, the sheet should be as thin as possible, however the maximum tensile resistance decreases proportionally with the thickness (Wille and Tue, 2013). Also, the size and shape of the openings further affects the overall bearing capacity of the sheet, along with the layout and the orientation of openings on the steel sheet. Finally, the bulging of the openings is achieved through mechanical deformation, therefore it should be smooth to avoid plastic deformation of steel and provide sufficient area for the pouring of the concrete.

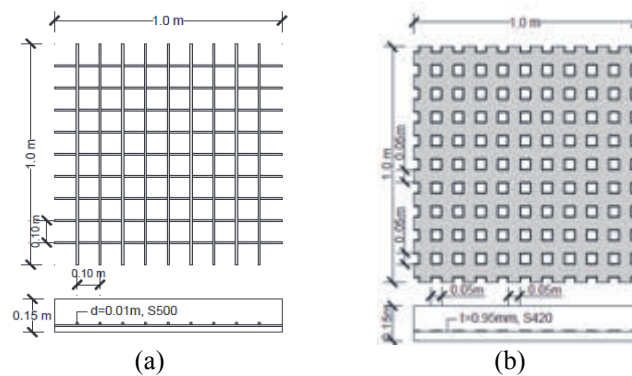


Fig. 3: Schematic depiction of a 1 m² slab with thickness of 0.15m, (a) minimum bar reinforcement (Ø10/100mm), & (b) indicative equivalent steel reinforcement (perforation 50 x 50mm, every 50 mm) (Apostolidi & Strauss, 2014)

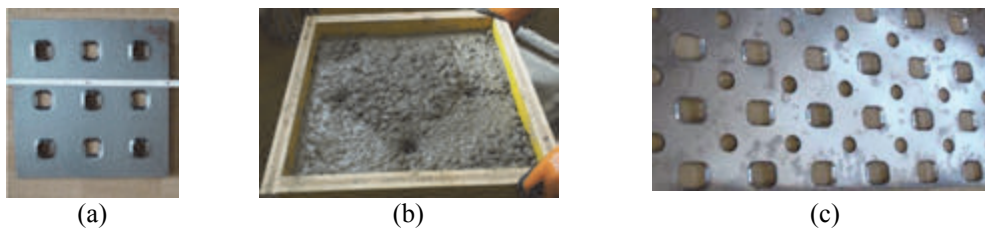


Fig. 4: (a) Initial sheet specimen (750 x 750 mm), (b) sheet fixed in wooden mould during concreting procedure. (Apostolidi et al., 2014). (c) Steel sheet layout after preliminary numerical and experimental investigations (Rauch, 2014)

Through a series of preliminary numerical investigations, correlating the sheet thickness (varying between 0.7 mm and 1.5 mm) with the steel grade (tensile strength varying between 260 MPa and 520 MPa), shape of openings (parametric studies between circular, elliptical and quadratic openings with rounded edges) and size of openings (diameter and width/length varying between 35 mm and 65 mm), a first steel sheet layout with bulged quadratic openings that have rounded edges, positioned in parallel to the main axes of the steel sheet was produced, as shown in Fig. 4(a). A series of preliminary experimental tests followed, in an effort to determine an appropriate concrete type for the final composite element and to consider some practical aspects during the production of the steel sheet and of the composite RC element. As shown in Fig. 4(b), the initial steel sheet was used for the first production of a RC element and through this process an appropriate concrete type of C45/55 with maximum aggregate size of 1.6 cm was chosen. After these tests, the introduction of secondary openings to facilitate the air path coming out of the mould during concreting was decided. These ventilating openings were positioned between the main bulged openings and placed parallel to the main axis of the steel sheet, leading to the layout presented in Fig. 4(c). Considering the procedure described above and given these specific geometrical and material limitations, a series of 3D finite element models is going to be developed in an effort to verify the shear transfer mechanism between sheet and concrete and to chose the optimal dimensions and inclination angle of the bulged edges around the steel perforations.

3. CORBEL APPROACH – MECHANICAL INTERLOCK

The introduction of bulged edges around the openings of the steel sheet serves mainly to the shear transfer between the steel and concrete, as already mentioned above. Therefore the inclination angle (γ°) of the bulged part around the openings is important for even stress distribution in concrete, when a force is transferred from steel to concrete. In the present paper, the concrete elements formed within the bulged edges of the perforations, are assumed to behave as unreinforced concrete corbels (Fig. 1(b), 1(c)). The composite element should be designed in such a way, so that brittle failure in these concrete bulges is avoided. Therefore, the shear and tensile capacity of these concrete elements needs to be verified for the maximum horizontal shear force to be applied from the sheet to each concrete corbel. Corbel is usually a short cantilever, with a ratio of depth over height (t/h) less than 1.0 (see Fig. 5). In this case of an unreinforced corbel, the transfer of the shear force (F_{sd}) from the steel to the concrete depends on the geometrical properties of the corbel and on the concrete's material properties (Heydel et al., 1995). Fig. 5 presents the forces acting on the corbel based on the simple strut-tie model, along with the stress (σ) and strain (ϵ) distribution on the section along the face of the main concrete core. F_{sd} is the shear force, H_{sd} is the tension force applied on corbel along with shear load ($\geq 0.2 F_{sd}$) and Z_{sd} is the tensile reaction force. The target is to define the maximum values of the horizontal shear force $F_{sd,max}$ and the maximum tension force $Z_{sd,max}$ that simultaneously develop on each corbel without any type of failure to occur in the concrete.

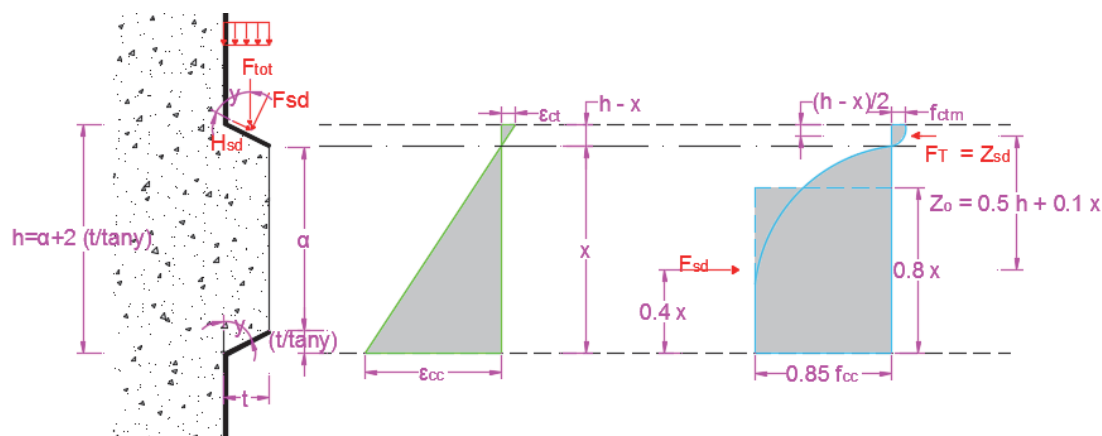


Fig. 5: Shear force transfer from steel sheet to concrete. Stress (σ) and strain (ϵ) distribution on the section, where the corbel starts projecting from the face of the main concrete core

Based on the design compressive strength of the concrete, the maximum shear force ($F_{sd,max}$) to be received by the concrete corbel is given by Eq. (1) and it is equal to V_{Rd2} , which is the maximum design value of the shear force without any compression failure in the element (Heyden et al., 1995):

$$F_{sd} = V_{Rd2} = \frac{1}{2} \cdot v \cdot f_{cd} \cdot b_w \cdot 0,90 \cdot d \quad (1)$$

Where: $v = 0.7 \cdot f_{ck} / 200 \geq 0.5$ (reduction factor), f_{ck} is concrete's characteristic compressive strength, f_{cd} is concrete's design compressive strength, b_w is the corbel's width and d is the effective depth of the corbel, which due to the absence of tensile reinforcement is equal to the overall depth of the corbel h . The maximum tensile force to be received by the concrete is given by Eq. (2):

$$Z_{sd,max} = A_{Tension} \cdot f_{ctm} = b_w \cdot \frac{(h-x)}{2} \cdot f_{ctm} \quad (2)$$

Where A_{Tension} is the corbel's cross sectional area in tension, f_{ctm} is concrete's mean tensile strength and x is the height of the compression zone (shown in Fig. 5). According to the simple strut-tie model, the tensile strength Z_{sd} is given as a function of F_{sd} and $H_{\text{sd}} (\geq 0.2 F_{\text{sd}})$, through Eq. (3) (Heyden et al., 1995):

$$Z_{\text{sd}} = F_{\text{sd}} \cdot \frac{a_c}{z_o} + H_{\text{sd}} \cdot \frac{a_h + z_o}{z_o} \quad (3)$$

Where a_c is the distance from the centre of load to the nearest face of concrete's main core, a_h is usually the distance between the centre of reinforcement and the load application face, but in the present case it is equal to the sheet thickness and z_o is the height of the lever arm given by Eq. (4) (Heyden et al., 1995):

$$z_o = d \cdot \left(1 - 0,4 \cdot \frac{F_{\text{sd}}}{V_{\text{Rd2}}} \right) \quad (4)$$

Based on Eq. (3), one could calculate the shear force value F_{sd}^* that corresponds to the maximum tensile force to be received by the concrete corbel, with the aid of Eq. (5):

$$Z_{\text{sd,max}} = F_{\text{sd}}^* \cdot \frac{a_c}{z_o} + H_{\text{sd}} \cdot \frac{a_h + z_o}{z_o} = F_{\text{sd}}^* \cdot \frac{a_c}{z_o} + 0,20 \cdot F_{\text{sd}}^* \cdot \frac{a_h + z_o}{z_o} \rightarrow F_{\text{sd}}^* \quad (5)$$

To enable the use of these basic equations about the force transfer in these concrete corbels, the target of this work is to create a 3D finite element model, that will assist the definition of: a) an optimum correlation between the depth and the height of a corbel, b) the approximate height of the tension zone in an unreinforced corbel and c) an optimum inclination angle around the openings.

4. MODEL GENERATION & PARAMETRICAL STUDIES

Considering the corbel approach described above, a series of numerical models were created with the support of the FE software ATENA 3D (Beneš et al., 2016; Červenka and Červenka, 2017), see Fig. 6(c). The parametrical studies of the models include the investigation of the maximum shear load (F_{sd}), the height of the tensile zone ($h-x$), the optimum correlation between the height (h) and depth (t) of the corbel and finally, the influence of the inclination angle (y), as shown in Fig. 6(a).

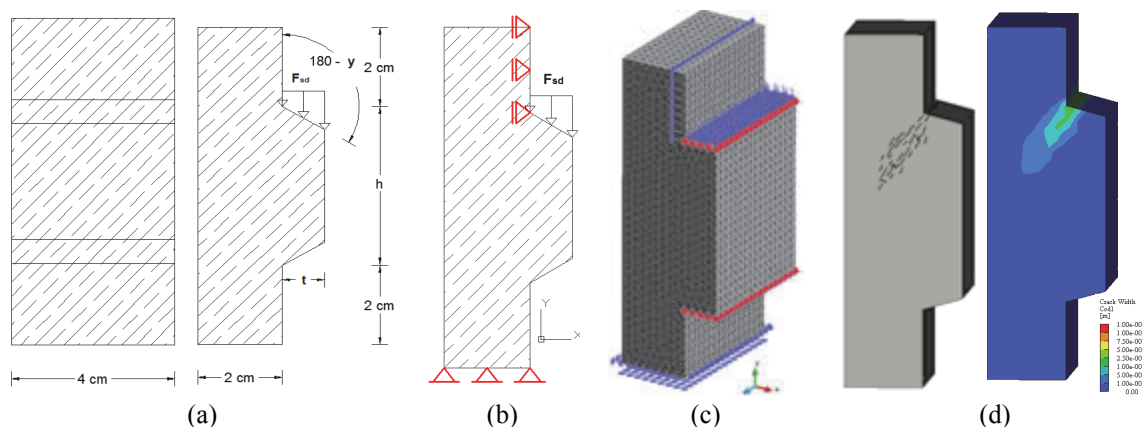


Fig. 6: (a) Constant dimensional properties and investigated parameters of the model, (b) support and loading conditions in the models, (c) sectional and 3D view of a meshed model, and (d) Different 3D view presentation of the maximum crack width of 0.1 mm

For comparison purposes between the various models, some dimensional properties were kept constant, such as a model width of 4 cm, a concrete core depth of 2 cm (regardless of the corbel's depth) and a concrete stripes' height above and below the corbel of 2cm each (Fig. 6(a)). Further constant properties throughout the model were: (a) the concrete type of C45/55, as it was defined in the preliminary experiments, (b) the boundary conditions of the model, as shown in Fig. 6(b), and (c) the meshing in tetrahedral elements of 2.5 mm side size, automatically generated by the software. A characteristic model with the aforementioned, meshing and boundary conditions is presented in Fig. 6(c). The load was uniformly distributed on the top area of the corbel, along the y direction (Fig. 6(b) and (c)), and it was increased stepwise until failure. The failure criterion was a maximum crack width of 0.1 mm, so the loading step, where the maximum accepted crack width is measured, leads to the maximum failure load $F_{0.1\text{mm}}$ of each model.

Tab 1: Values of the investigated parameters used in the models

Parameter	Units	Values
h (Corbel's height)	mm	30; 40; 50; 60; 100
t (Corbel's depth)	mm	2,5; 5; 10; 15
y (Inclination angle)	°	45; 60; 75; 90

Based on the geometrical restrictions of the corbels (mentioned in §2), the chosen values of the parameters under investigation are presented in Tab. 1. The combination of all these values led to the simulation of 80 different FE Models. The most characteristic results and their evaluation follows in the next section.

5. RESULTS & EVALUATION

In each of the simulated models, the results to be evaluated are the crack width, the stress distribution and the failure load $F_{0.1\text{mm}}$. The crack propagation in each model can be schematically presented in various ways, with the aid of the ATENA Studio interface (Beneš et al., 2016). In Fig. 6(d), different 3D views of a cracked model, with crack width up to 0.1 mm are presented. Based on the failure criterion described above, the failure load $F_{0.1\text{mm}}$ is calculated as a concentrated load in kN and the effect of the corbel's height, depth and inclination on these load is evaluated.

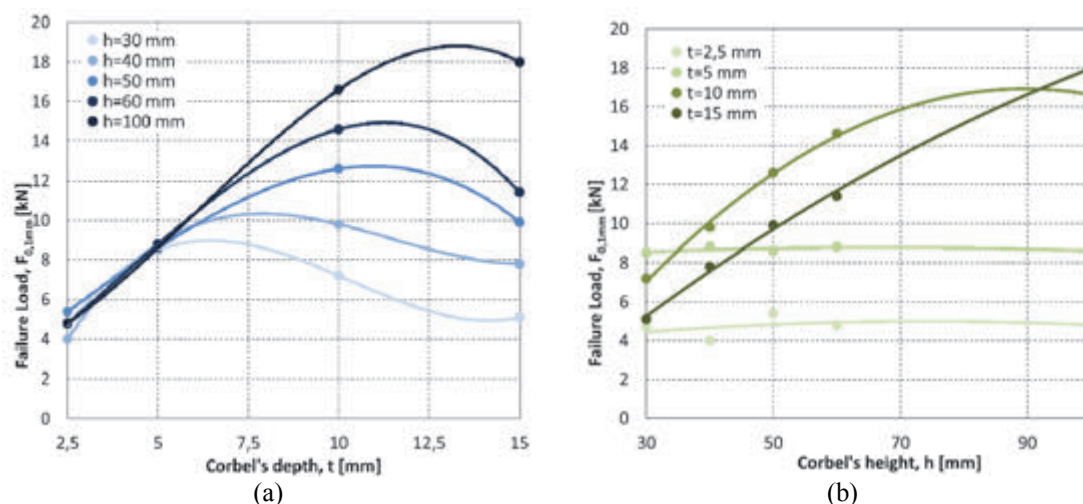


Fig. 7: (a) Calculated failure load ($F_{0.1\text{mm}}$) over corbel's depth (t), for increasing corbel's height (h), and (b) Calculated failure load ($F_{0.1\text{mm}}$) over corbel's height (h), for increasing corbel's depth (t). Constant $y=75^\circ$

In Fig. 7, a correlation of the failure load ($F_{0.1mm}$) with the corbel's depth (t) and height (h) for a constant inclination angle of 75° is presented. Fig. 7(a) shows the results of the failure load over corbel's depth and the curves with darker blue colour correspond to higher corbel height values. Fig. 7(b) presents an inversed correlation, where the values of the corbel's height are along the x-axis and the curves with darker green colour represent higher corbel's depth values. In both Figures, it can be noticed that for a corbel depth $t = 2.5$ and 5 mm, the height of the corbel h has no impact on the failure load. For values of t between 5 mm and 11 - 12.5 mm, the failure load reaches a maximum value, which is different for each corbel height h . So, each curve or corbel height corresponds to a specific corbel depth that leads to the maximum failure load and this increases with the corbel height.

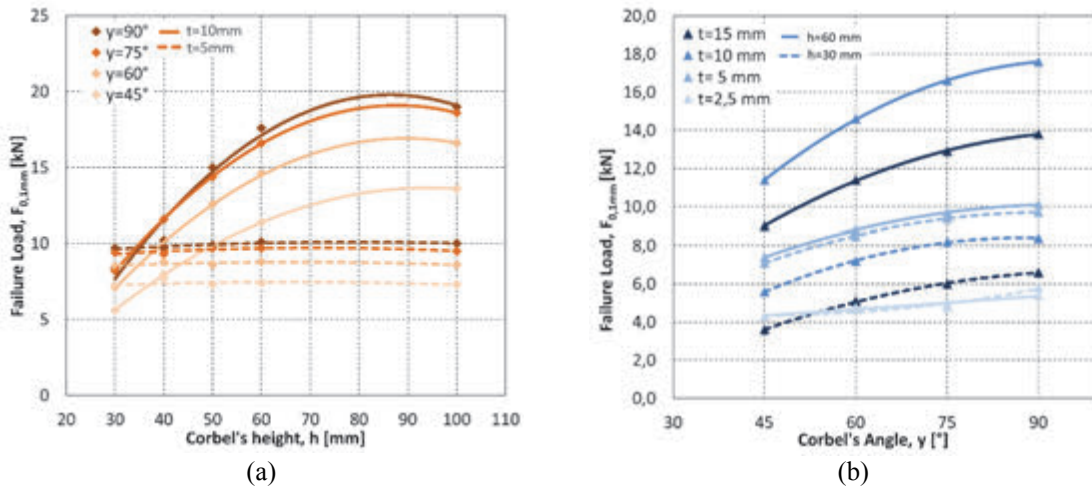


Fig. 8: Correlation of corbel's height with the inclination angle: Calculated failure load ($F_{0.1mm}$) over corbel's height (h), (a) for $t=10$ mm and (b) for $t=5$ mm.

In Fig. 8, there is an effort to correlate all the investigated parameters t , h and y , and their impact on the failure load. Fig. 8(a) is a diagram of the corbel's height over the corresponding failure load, where the curves with darker orange colour represent higher inclination angles. Solid and dashed lines correspond to a corbel depth of $t=10$ and 5 mm, respectively. Regardless of the t value, it is noticed that the resulting failure load values for $y=75^\circ$ and 90° are almost the same. However, it seems that the impact of the y is higher for a corbel depth of $t=10$ mm, as the distances between the solid curves are larger than the respective dashed ones. Again, Fig. 8(b) is an inversed depiction of Fig. 8(a), where the corbel angle's values are along the x-axis. The darker blue colour corresponds to higher t values and solid and dashed lines represent a corbel height of $h=60$ and 30 mm, respectively. In Fig. 8(b), it is worth noting that for $t=2.5$ and 5 mm, the height has almost no impact on the failure load values, as solid and dashed lines almost overlap. Another observation would be that for both $h=60$ and 30 mm, the maximum failure loads occurred for $t=10$ mm, while for the highest corbel depth $t=15$ mm, the $F_{0.1mm}$ values were much lower.

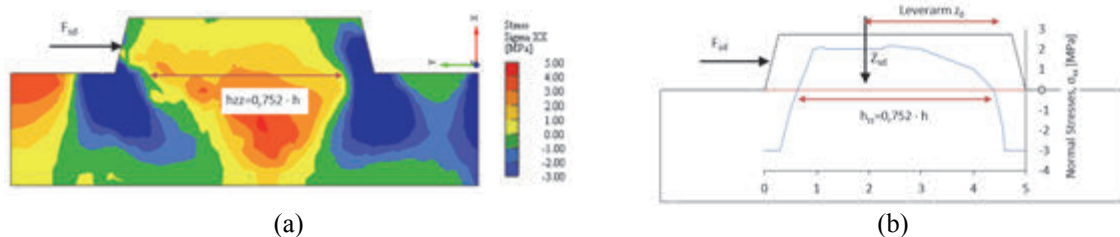


Fig. 9: FE model with $h=50$ mm, $t=10$ mm and $y=75^\circ$, (a) Stress distribution, (b) definition of the tension zone based on the stress distribution

The last Fig. 9(a) presents the stress distribution in a model with $h=50$ mm, $t=10$ mm and $\gamma=75^\circ$. Compression and tension in the model are depicted with blue and red-yellow colours, respectively. To be able and use the corbel assumption equations presented in §3 and to further compare analytical with numerical results, the height of the tension zone should be defined. In Fig. 9(b), the height of the tensile zone can be defined as a percentage of the corbel's height and for this specific model was found equal to $0.752 h$.

6. DISCUSSION

A novel perforated steel sheet reinforcement element has been developed to be adopted in structural elements and undertake the existing forces. Through the bulged perforations in the steel sheet and the concrete corbels, that are assumed to be formed within the openings, a mechanical interlock between the steel sheet and the concrete has been developed. A parametrical study on a series of 3D FE models leads to optimum pairs values for corbel height and depth that resulted to the maximum failure load (e.g. for $h=50$ mm the optimum $t=11$ mm, leading to $F_{0.1mm}=14.4$ kN and an inclination angle of $\gamma=75^\circ$). The results presented above can serve as a solid ground for further comparison between analytical and numerical results, which will lead to generalisation of the use of corbel equations in structural elements reinforced with this innovative perforated steel sheet.

7. ACKNOWLEDGEMENTS

This work has been supported by the Project “InnoFLAB, No. 839869”, financed by the FFG “The Austrian Research Promotion Agency” and the company PORR AG. This support is gratefully acknowledged.

8. REFERENCES

- Apostolidi, E. and Strauss, A. (2014), “Final scientific report on the progress of the FFG Project: InnoFLAB; Development of steel sheet reinforcement”, University of Natural Resources and Life Sciences, Vienna, Austria, Internal Report No. 875-14-003.
- Apostolidi, E. et al. (2015), “Integrative monitoring measurements of perforated steel sheets”, Fourth International Symposium in Life Cycle Engineering, IALCCE 2014, Tokyo, Japan, November 2014, pp. 908-914.
- Beneš, S., Mikolášková, J. and Altman, T. (2016), “ATENA Program Documentation Part 12: User's manual for ATENA Studio”, Červenka Consulting s.r.o., Prague.
- Červenka, V. and Červenka, J. (2017), “ATENA Program Documentation Part 2-2: User's manual for ATENA 3D”, Červenka Consulting s.r.o., Prague.
- Heydel, G., Krings, W. and Herrmann, H. (1995). “Stahlbeton im Hochbau nach EC2: Einführung und Anwendungsbeispiele”, Ernst und Sohn, Berlin (in German).
- Mucha, S. (2003), “Development of reinforced system made of sheet steel”, Leipzig Annual Civil Engineering, Report No. 8 165.
- Rauch, C. (2014). “InnoFLAB: Innovatives flächiges Bewehrungssystem für effizientere Produktion von hochwertigen Stahlbetonteilen; Dokumentation des bisherigen Versuchsprogramms”, PORR A.G., Vienna, Austria, Internal Report (in German).
- Wille, K. (2008), “Load carrying behaviour of novel composite structures using two dimensional reinforcing elements”, University of Leipzig, Germany, Doctoral Thesis 222. ISBN: 978-3-8370-1029-98 (in German).
- Wille, K. and Tue, V. T. (2013), “Tensile load capacity analysis of perforated reinforcement sheet”, Materials and Structures, Vol. 48, No. 1-2, September 2013, pp. 77-91.

BEHAVIOUR OF MULTI-DIRECTIONAL CFRP AND UNIDIRECTIONAL CFRP PLATE BONDED TO CONCRETE BY MEANS OF EPOXY AND A COMBINATION OF EPOXY AND MECHANICAL ANCHORS

Cronje Bruwer

*University of Johannesburg, Department of Civil Engineering Technology
PO Box 17011, Doornfontein, 2028 South Africa*

SUMMARY

The flexural capacity of reinforced concrete structural elements can be increased by bonding carbon fiber reinforced polymer (CFRP) plates to the tension surface creating a composite structural element. Debonding of the CFRP plate from the concrete surface is the most likely failure mechanism of the composite structural element. This research study compares the bond strength between a multi-directional CFRP (MD-CFRP) plate and a unidirectional CFRP (UD-CFRP) plate to the concrete surface. A single shear pull off test is used to establish if additional mechanical anchorage to epoxy bonded MD-CFRP or UD-CFRP plates to concrete would have a combining capacity. The testing was conducted for the following three conditions (1) CFRP plate epoxy bonded to a concrete block; (2) CFRP plate mechanically bonded to a concrete block; (3) CFRP plate epoxy and mechanically bonded to a concrete block.

1. INTRODUCTION

Bonding plates externally to the tension surface of reinforced concrete structural elements, by means of epoxy, to resist tension forces larger than derived from applied loads is referred to as composite structural elements. Multi-directional carbon fiber reinforced polymer (MD-CFRP) or unidirectional carbon fiber reinforced polymer (UD-CFRP) plates can be used for this purpose. Debonding of the plate from the concrete surface is the most likely failure mechanism and it occurs instantaneously without prior warning. Mechanical anchors can be installed, in addition to the epoxy bonding, which would (1) prevent instantaneous debonding; (2) increase the ductility of the CFRP plate to the concrete surface; (3) increase the bond strength between the CFRP plate and the concrete.

This research study compares the influence of additional mechanical anchors to the strength of epoxy bonded MD-CFRP and UD-CRFP plates to the concrete surface. The following experimental single shear pull off tests are presented to establish the basis for the combining capacities of an epoxy bonded CFRP plate with additional mechanical anchorage: (1) CFRP plates epoxy bonded to a concrete block; (2) CFRP plates mechanically bonded to the concrete block; (3) CFRP plates epoxy and mechanically bonded to the concrete block.

2. EXPERIMENTAL PROGRAM

To determine the differences in bond strength between the MD-CFRP and UD-CFRP plates and the surface of the concrete block, the single shear pull off test with near end supported CFRP plates were utilized as described by Yao et al. (2004). Due to the available laboratory

equipment the setup of the single shear pull off test was done in a vertical plane, as indicated in Fig. 1, instead of a horizontal plane as described by Yao et al. (2004).

Concrete blocks, 150 mm wide, 150 mm high and 750 mm long were used as test specimens onto which the MD-CFRP (1.2 mm wide x 50 mm thick) and UD-CFRP (1.2 mm wide x 50 mm thick) plates were bonded. The concrete blocks, bonded to the MD-CFRP plates, had an average concrete cube strength (f_{cu}) of 25.4 MPa and the concrete blocks bonded to the MD-CFRP plates, had an average cube strength (f_{cu}) of 45.7 MPa. The surface of the concrete blocks were prepared for bonding by removing the cement laitance by means of scabbling to expose the well bonded large aggregate. Pro-Struct 617LV primer was applied to the concrete blocks which penetrates the concrete surface and Pro-Struct617NS epoxy was applied to the surface of the CFRP plates, which were then firmly pressed onto the concrete blocks to obtain a good bond. The bonded length for both the MD-CFRP and UD-CFRP plates was 550 mm. The mechanical bond was achieved by drilling holes into the concrete block and installing Hilti M10 HAS-(E) chemical anchors. Epoxy was placed between the washer (50 mm diameter and 4 mm thick) and the nut was torqued to 20 Nm to provide a friction connection.

The CFRP plate was pulled from the concrete block at a rate of 0.02 mm/s. The slip was measured by means of two linear resistive positive transducers (LRPT) which were bolted to the CFRP plate and measured to the loaded surface of the concrete block.

Fig. 1 indicates the layout of single shear pull off test, with the near end supported CFRP plates.

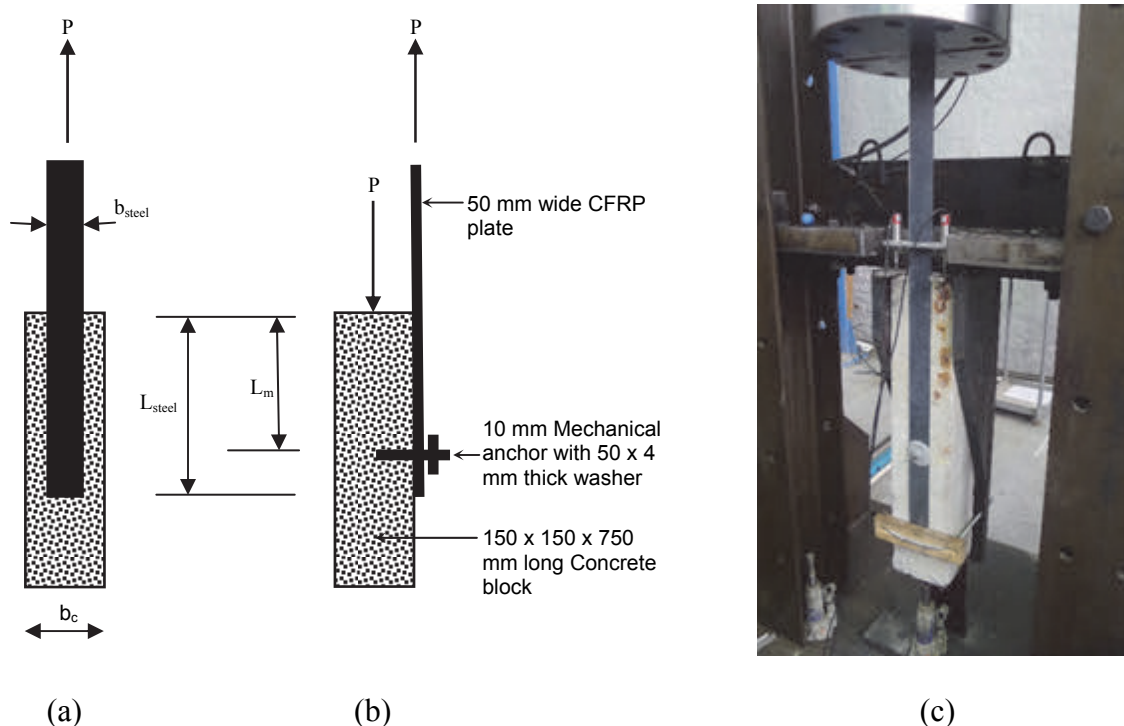


Fig. 1: Single shear pull off test with the near end supported (a) Schematic front view (b) Schematic side view (c) Image of complete set-up

Tab. 1 indicates the number of prepared experimental pull-off test samples and the type of bond between the MD-CFRP and UD-CFRP plates and the concrete block.

Tab. 1: Number of pull-off specimens constructed

Specimen Name, MD-CFRP Plate Bonded to Concrete Block	Specimen Name, UD-CFRP Plate Bonded to Concrete Block	Type of Bond Between CFRP Plate and the Concrete Surface
EB1(MD-CFRP)	EB1(UD-CFRP)	Epoxy bonded
EB2(MD-CFRP)	EB2(UD-CFRP)	
EB3(MD-CFRP)	EB3(UD-CFRP)	
EB4(MD-CFRP)	EB4(UD-CFRP)	
EB5(MD-CFRP)	EB5(UD-CFRP)	
EB6(MD-CFRP)	EB6(UD-CFRP)	
MB1(MD-CFRP)	MB1(UD-CFRP)	Mechanically bonded
MB2(MD-CFRP)	MB2(UD-CFRP)	
MB3(MD-CFRP)	MB3(UD-CFRP)	
MB4(MD-CFRP)	-	
EMB1(MD-CFRP)	EMB1(UD-CFRP)	Epoxy and mechanically bonded
EMB2(MD-CFRP)	EMB2(UD-CFRP)	
EMB3(MD-CFRP)	EMB3(UD-CFRP)	
EMB4(MD-CFRP)	EMB4(UD-CFRP)	
-	EMB5(UD-CFRP)	
-	EMB6(UD-CFRP)	

3. EXPERIMENTAL RESULTS

Experimental results obtained from the single shear pull off tests of CFRP plates from the concrete blocks (1) epoxy bonded, (2) mechanical bonded and (3) a combination of epoxy and mechanical bond are indicated as load-deflection graphs in Fig. 2, 3 and 4 below:

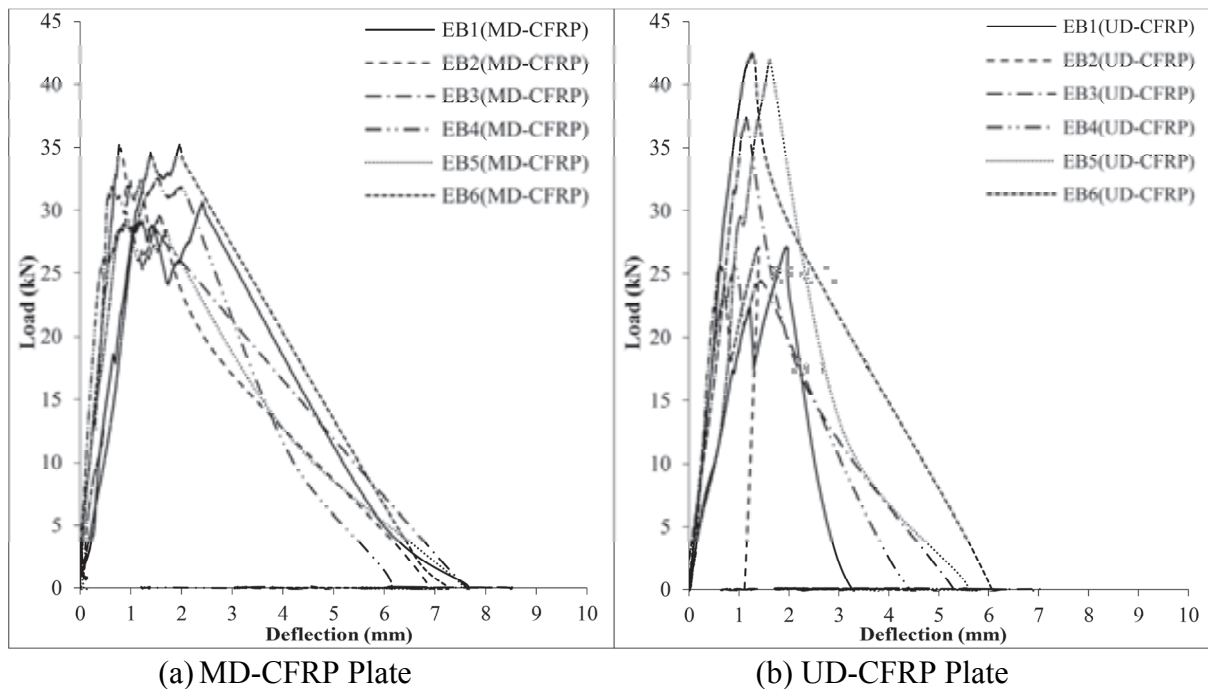


Fig. 2: Load deflection graphs of single shear pull off tests of MD-CFRP and UD-CFRP plates epoxy bonded to the concrete block

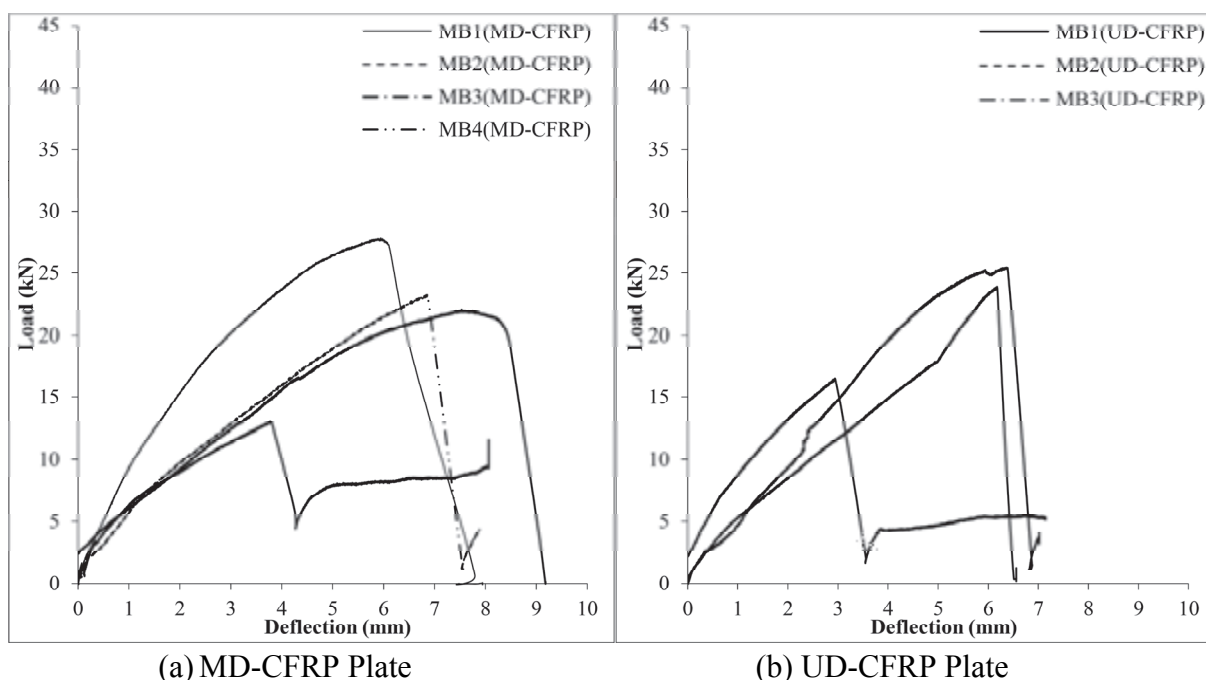


Fig. 3: Load deflection graphs of single shear pull off tests of MD-CFRP and UD-CFRP plates mechanically bonded to the concrete block

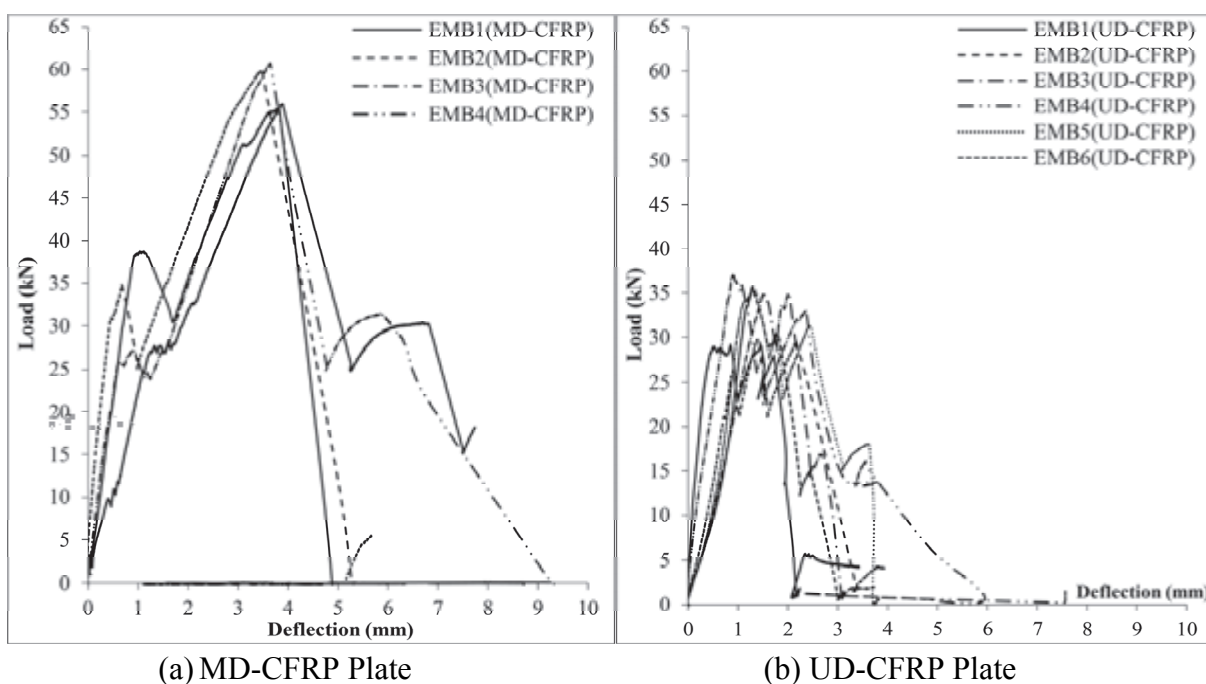


Fig. 4: Load deflection graphs of single shear pull off tests of MD-CFRP and UD-CFRP plate's epoxy and mechanically bonded to the concrete block

4. DISCUSSION OF THE EXPERIMENTAL RESULTS

Single shear pull off tests with the near end supported CFRP plates were performed for both MD-CFRP and UD-CFRP plates attached to the concrete blocks with the following bonding mechanisms: (1) CFRP plate epoxy bonded to a concrete block; (2) CFRP plate mechanically bonded to a concrete block; (3) CFRP plate epoxy and mechanically bonded to a concrete block. The maximum single shear pull-off forces are listed in Tab. 2.

Tab. 2: Maximum single shear pull off forces

MD-CFRP Plates			UD-CFRP Plates		
Specimen Name	P_{exper} (kN)	P_{exper} Average (kN)	Specimen Name, Bonded to Concrete Block	P_{exper} (kN)	P_{exper} Average (kN)
EB1(MD-CFRP)	30.6	32.5	EB1(UD-CFRP)	27.2	33.7
EB2(MD-CFRP)	35.2		EB2(UD-CFRP)	27.2	
EB3(MD-CFRP)	31.9		EB3(UD-CFRP)	37.4	
EB4(MD-CFRP)	32.5		EB4(UD-CFRP)	25.7	
EB5(MD-CFRP)	29.3		EB5(UD-CFRP)	42.1	
EB6(MD-CFRP)	35.2		EB6(UD-CFRP)	42.5	
MB1(MD-CFRP)	27.8	21.6	MB1(UD-CFRP)	23.9	21.9
MB2(MD-CFRP)	13.1		MB2(UD-CFRP)	16.5	
MB3(MD-CFRP)	22.1		MB3(UD-CFRP)	25.4	
MB4(MD-CFRP)	23.3		-	-	
EMB1(MD-CFRP)	55.5	58.0	EMB1(UD-CFRP)	29.2	33.7
EMB2(MD-CFRP)	59.9		EMB2(UD-CFRP)	29.8	
EMB3(MD-CFRP)	55.9		EMB3(UD-CFRP)	35.0	
EMB4(MD-CFRP)	60.7		EMB4(UD-CFRP)	37.0	
-	-		EMB5(UD-CFRP)	35.4	
-	-		EMB6(UD-CFRP)	35.7	

The maximum average single shear pull-off force for MD-CFRP plates (32.5 kN) epoxy bonded to concrete is 3.6% lower than the maximum force for UD-CFRP plates (33.7 kN). This difference is insignificant and the shear pull off forces of MD-CFRP and UD-CFRP plates are considered the same.

The maximum average single shear pull-off force for MD-CFRP plates (21.6 kN) mechanically bonded to concrete is 1.4% lower than the maximum force for the UD-CFRP plates (21.9 kN). This difference is not significant and the shear pull off forces of MD-CFRP and UD-CFRP plates can also be considered the same.

Comparing the difference between mechanical and epoxy bonding, the maximum average single shear pull-off force for CFRP plates mechanically bonded to concrete (21.6 kN for MD-CFRP and 21.9 kN for UD-CFRP) is 21.8 kN and for epoxy bonded CFRP plates (32.5 kN for MD-CFRP and 33.7 kN for UD-CFRP) is 33.1 kN. The epoxy bonded plate yield a significantly stronger bond (52% stronger) than a mechanical only bond.

MD-CFRP plates bonded to concrete by means of epoxy bonding (32.5 kN) and mechanical bonding (21.6 kN) yield a total pull-off force of 54.1 kN (32.5 kN + 21.6 kN). This total pull-off force (54.1 kN) compare well to the experimentally measured combined epoxy and mechanical pull-off force of 58.0 kN. It could therefore be concluded that the epoxy and the mechanical bonding mechanisms of MD-CFRP plates to concrete have a combined effect.

UD-CFRP plates bonded to concrete by means of epoxy bonding (33.7 kN) and mechanical bonding (21.9 kN) yield a total pull-off force of 55.6 kN (33.7 kN + 21.9 kN). This total pull-off force (55.6 kN) does not compare well to the experimentally measured combined epoxy and mechanical pull-off force of 33.7 kN. It could therefore be concluded that the

epoxy and the mechanical bonding mechanisms of UD-CFRP plates to concrete does not have a combined effect.

5. CONCLUSIONS

The data collected from this experimental study, comparing the combined epoxy and mechanical pull-off force of a bonded UD-CFRP plate to a bonded MD-CFRP plate by means of a single shear pull off test, disclose the following: (1) No significant difference could be found in the pull-off forces between the MD-CFRP plates (32.5 kN) and the UD-CFRP plates (33.7 kN), both epoxy bonded to the concrete. (2) The pull-off forces of MD-CFRP plates (21.6 kN) and UD-CFRP plates (21.9 kN) from concrete can also be considered the same. (3) Epoxy bonded CFRP plate yields to a significantly stronger bond than a mechanical only bond. (4) The pull-off forces of epoxy and mechanically bonded UD-CFRP plates, does not show a composite action. (5) The pull-off forces of MD-CFRP plates show composite action.

6. REFERENCES

- Bruwer, C.P.C. (2016), "Experimental Study to Determine if the Strength of an Epoxy Based Joint of CFRP Plates to Concrete Can Be Increased by Adding Mechanical Anchors" Performance-Based Approaches for Concrete Structures, fib Symposium 2016, Cape Town, November 2016, pp. 619-620
- Cheng, J.F., Teng (2001), J.G. "Anchorage Strength Models for FRP and Steel Plates bonded to Concrete" J Struct Eng, ASCE 2001;127(7):784-91
- HILTI HVU with HAS/HAS-E rod Adhesive anchor brochure.
- Yao, J., Teng, J.G., et al. (2005), "Experimental Study on FRP-to- Concrete Bonded Joints", Composites: Part B 36 (2005) 99-113

EXPERIMENTAL INVESTIGATIONS OF PULL-OUT BEHAVIOUR OF SYNTHETIC FIBRES

Mária Erdélyiné Tóth, Anikó Pluzsik, Tamás Pluzsik, Bálint Morlin
Technical University of Budapest
1111 Budepest, Műegyetem rkp. 3.

SUMMARY

The pull-out behaviour is one of the distinctive features of fibre reinforced concrete. Few analytical models for the pull-out of synthetic fibres can be found in the literature. Moreover, the existing models are not supported by comprehensive experimental investigations. In this research experimental investigations were made. First, the one-sided and two-sided pull-out phenomena were compared to each other. Then the effect of the mortar strength, fibre surface and the anchored fibre length were examined for one-side anchored samples. None of the available analytical models for synthetic fibres could be fitted well to the experimental data. A model suggested for steel fibres with a modified friction law (τ - s relation) was used to gain the most precise approximation for the pull-out of synthetic fibres. After specifying the appropriate model the critical anchorage length was determined.

1. INTRODUCTION

There are well-based, theoretical, smeared models for designing FRC beams (ACI 1998; ACI 2002; CNR-DT 2006; Lee et al. 2011; ÖVBB 2008; Vandewalle et al. 2002), however, these models cannot be used well in the analysis of experimental results because of the high deviation of the data. The existing, smeared models can provide only the approximate average of the load-displacement curves which does not fit well to the discrete results of the experimental samples. Another disadvantage of the existing models is that because of the high deviation of the input data numerous experiments have to be carried out to gain an appropriate approximation for the real load-displacement curves. To overcome these drawbacks of the existing models a new analytical beam model was suggested according to Tóth, Pluzsik and Juhász (2017) which takes into consideration the real distribution of the fibres in the cross-section of the FRC beam. With the help of this new model experimental beam results can be compared to each other by a fictive pull-out force eliminating the high deviation caused by the different amounts and distribution of fibres in the critical cross-section. The pull-out behaviour is one of the distinctive features of fibre reinforced concrete. The more we know the phenomenon of the pulling out the better we understand the mechanical behaviour of the FRC material. It can usually be observed that fibres are mainly pulled out rather than torn in the cracked cross-section of a FRC beam (Tóth, Pluzsik and Juhász, 2017). The higher ductility of FRC compared to plain concrete and the residual tensional strength after the first crack is due to the frictional stresses acting on the interface of the fibres and the concrete during the slipping of the fibres in the cracked zone.

In the new beam model according to Tóth, Pluzsik and Juhász (2017) the fictive pull-out force was assumed to be constant. The aim of this work is to choose a more appropriate analytical model for the pull-out of synthetic fibres which can be built in the beam model to improve it and to gain a more precise approximation of the experimental load-displacement curves for FRC beams.

Few analytical models for the pull-out of synthetic fibres can be found in the literature (Wang and Backer, 1988; Lin, Kanda and Li, 1999). The existing models are not supported by comprehensive experimental investigations. A more detailed analysis can be found for steel fibres (Zhan and Meschke, 2014), however, the question arises whether the existing models can be applied for synthetic fibres.

2. TESTING METHOD, EXPERIMENTAL RESULTS

Although the pull-out of fibres in a FRC beam is determined mainly by the bonding of the fibre surface and the mortar in the concrete, it is affected by a lot of other factors (aggregate type, porosity, efficiency of the compaction, chemical admixtures, etc.). Thus, there is no simple, determinable relation between the concrete strength and the maximum pull-out force. To eliminate the uncertainties mentioned above, mortar samples were used in the experiments. The samples were prepared based on the requirements of EN 196-1 standards in the Miskolc Cement Laboratory of CRH. Two series of the samples were prepared with five different cement contents in both. The standard cement content was changed in the samples by refilling the missing cement part with limestone powder (Tab. 1). The water-mix ratio (mix means cement and limestone) was held on 0.5 (standard value) in all samples while the water-cement ratio changed proportionally with the reducing of the cement content. In the first series five two-side anchored and five one-side anchored samples were made for each different cement content and for both fibre types, respectively. In the second series one-sided samples were made with three different anchored lengths, five different cement contents and two fibre types, respectively. Five pieces of samples were made from every similar case (similar anchored length, cement content and fibre type).

Tab. 1: Experimental samples

Experimental samples - five pieces of every similar case					
All of the mix prepared from 1250 g standard sand (according to EN 196-1), sum total 450 g CEM I 42,5 R cement and limestone powder and 225 g water, water-mix (cement and limestone) ratio 0.5					
Sign of the sample	Cement content of the mix [g]	Limestone powder content of the mix [g]	Fibre type	Anchored length [mm]	Anchorage type
150_20	150	300	waved/ribbed	20	one-sided/ two-sided
225_20	225	225	waved/ribbed	20	one-sided/ two-sided
300_20	300	150	waved/ribbed	20	one-sided/ two-sided
375_20	375	75	waved/ribbed	20	one-sided/ two-sided
450_20	450	-	waved/ribbed	20	one-sided/ two-sided
150_15/ 150_20/150_25	150	300	waved/ribbed	15/20/25	one-sided
225_15/ 225_20/225_25	225	225	waved/ribbed	15/20/25	one-sided
300_15/ 300_20/300_25	300	150	waved/ribbed	15/20/25	one-sided
375_15/ 375_20/375_25	375	75	waved/ribbed	15/20/25	one-sided
450_15/ 450_20/450_25	450	-	waved/ribbed	15/20/25	one-sided

The experiments took place in the polymer laboratory of TUB according to the measure method used in case of fibre reinforced plastic. The speed of the pull-out was 10 mm/min. The pull-out tester was the ZWICK/ROELL Z005 universal material testing machine. Because of the restriction of the length of this paper not all the experimental results are presented here, only representative samples are shown. The curves in the following figures are calculated as an average of 3-5 similar samples.

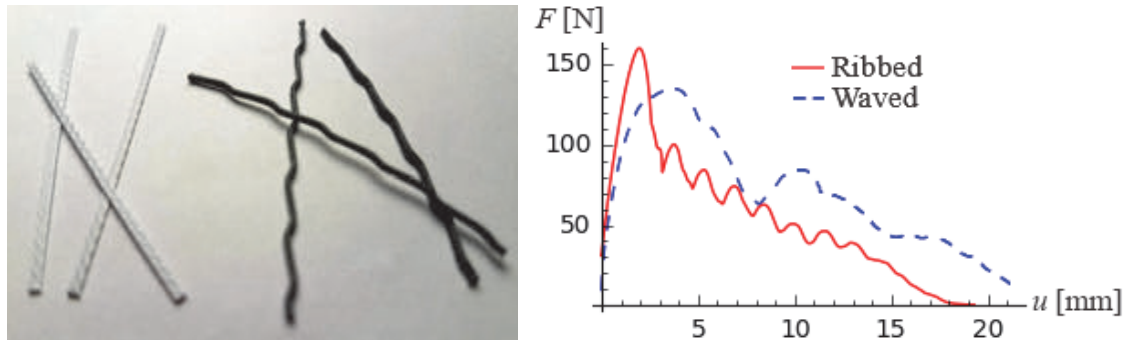


Fig. 1: Ribbed and waved fibres and experimental F - u curves for one-sided case, cement content: 300 g, anchored length: 20 mm

Two fibre types which had different surface characteristics (ribbed, waved) were examined (Fig. 1). In Fig. 1 the pull-out curves of the two types of fibres are compared in case of one-sided samples, with 300 g cement content and 20 mm anchored length. Although the ribbed fibres had higher maximal force in all cases, after the maximum force the waved fibres behaved more favourably in the descending part of the pull-out function. The speciality of ribbed fibres furthermore was the systematic jumps in the descending part of the curves as a result of the surface shaping. Aside from the above differences the curves for both fibre-types had similar main features in all examined cases. Ultimately, these fibre-types can be modelled by the same theoretical model.

A one-side anchored sample can more easily be carried out in the laboratory, however, according to the literature (Wang and Backer, 1988) the phenomenon of the two-sided pull-out, which really occurs in the cracked cross-section of an FRC beam, has significantly different features. In the present experiment fifty two-sided and fifty one-sided samples were made with various cement contents as well (Tab. 1, Fig. 2) to examine the differences between the one-sided and two-sided phenomena.

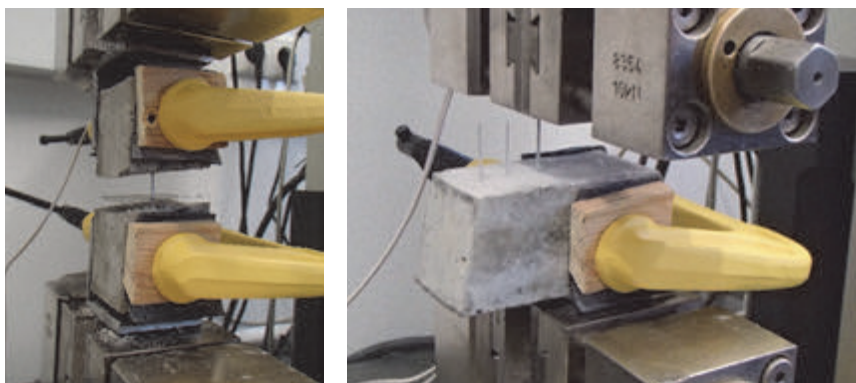


Fig. 2: One- and two-sided samples in pull-out tester

In Fig. 3 as a typical example the one-sided and two-sided samples with 300 g cement content and 20 mm anchored length are compared to each other for both ribbed and waved fibres.

The maximal forces of one-sided samples were higher, which can be caused by the eccentric pull-out. However, the main features of the curves were similar in all examined cases. Contrary to Wang and Backer (1988) the results of the present experiments show that the two-sided pull-out phenomenon can be modelled by using one-sided pull-out samples with the reduction of the maximum force.

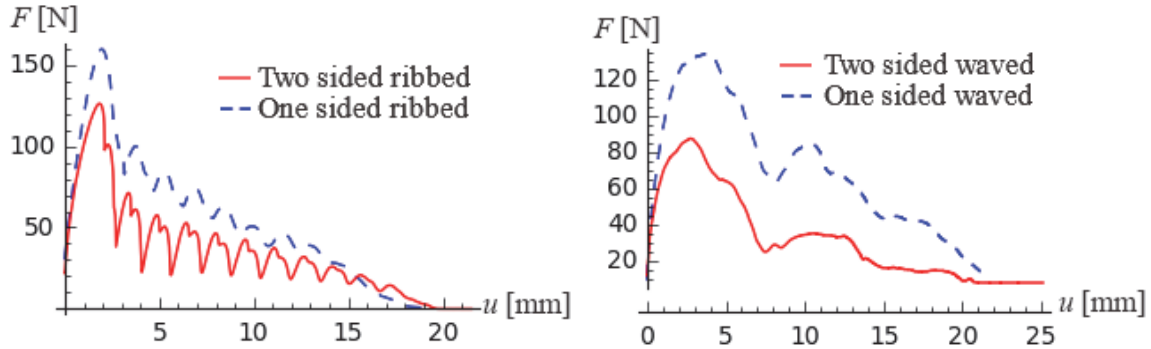


Fig. 3: One- and two-sided pull-out with 300 g cement content and 20 mm anchored length

Then the effect of the mortar strength (compressive strength) was examined.

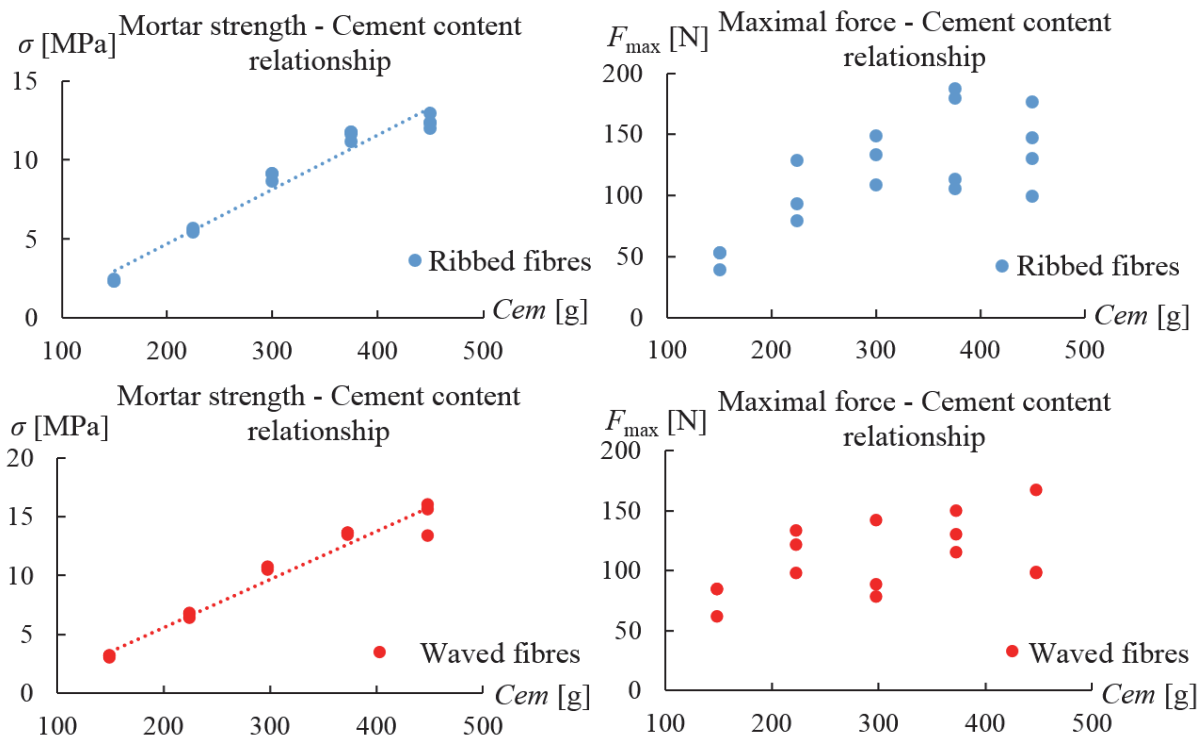


Fig. 4: Mortar strength/Maximal slipping force – Cement content relationship of two-sided pull-out tests, anchored length: 20 mm

Increasing the amount of cement in the mortar resulted in higher mortar strength (Fig. 4). The increasement was approximately linear for lower cement content. (In case of higher cement content the increasement in the strength was less.) However, the relationship between the maximal slipping force and the cement content (or the mortar strength as well) cannot be modelled linearly (Fig. 4). Moreover, in case of high cement content adding more cement resulted in lower maximal slipping force. The dispersion of the samples was high. In this experiment mortar samples were made in laboratory circumstances. In case of not mortar but concrete matrix the dispersion of the results would be even higher. So, there is no general rule

to describe the relationship between the maximal slipping force and the cement content, laboratory test is required in all cases.

To examine the applicability of the existing theoretical models 150 one-side anchored samples were made with different mortar strength, fibre surface and anchored fibre length (Tab. 1).

3. THEORETICAL MODEL

Few analytical models for the pull-out of synthetic fibres can be found in the literature (Wang and Backer, 1988; Lin, Kanda and Li, 1999). A more detailed analysis can be found for steel fibres (Zhan and Meschke, 2014). In Fig. 7 the existing models are compared to the experimental results for the one-sided case, with 300 g cement content and 20 mm anchored length.

To choose the appropriate model, the relation of the maximal slipping force and the length of the anchored fibre segment were examined in Fig. 5 by comparing the theoretical curves with the experimental results. It can be seen in Fig. 5 that the suggestion of (Lin, Kanda and Li, 1999) did not predict well the maximal slipping forces.

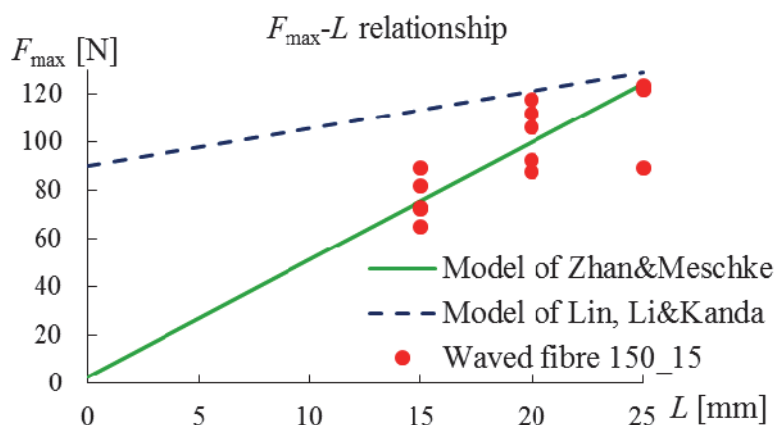


Fig. 5: Maximal slipping force – Anchored length relationship

The model of (Zhan and Meschke, 2014) gave a better approximation for the maximal force (first part of the slipping). However, none of the existing analytical models could be fitted well to the descending part (second part of the slipping) of the experimental curves (an example is shown in Fig. 7). The theoretical curve of (Zhan and Meschke, 2014) was calculated by solving the differential equation (1).

$$dF(u) = \pi d \tau(u) du, \quad \frac{F(u)}{AE} = \frac{ds(u)}{du} \quad (1)$$

The feature of the resulting $F-u$ curve depends on the friction law ($\tau-s$ relation) which is substituted in the differential equation in (1). The friction law for steel fibres according to Zhan and Meschke (2014) is given in (2,4) and in Fig. 6. In (Lin, Kanda and Li, 1999) a constant τ_0 is assumed while in (Wang and Backer, 1988) the function of the slipping stress is a second order parabola. Instead of these friction laws a modified model of Zhan and Meschke (2014) is suggested in (3,4). Substituting (3) to (1), the resulted $F-u$ curve fit better the experimental curves (Fig. 7).

$$\tau(s) = Gu, \text{ if } s \leq s_0;$$

$$\begin{aligned} \tau(s) &= \tau_{\max}, \text{ if } s_0 < s \leq s_1 \text{ and} \\ \tau(s) &= \tau_0 + (\tau_{\max} - \tau_0) \exp\left(\frac{s_1-s}{s_{\text{ref}}}\right), \text{ if } s > s_1 \end{aligned} \quad (2)$$

$$\begin{aligned} \tau(s) &= Gu, \text{ if } s \leq s_0; \\ \tau(s) &= \tau_{\max}, \text{ if } s_0 < s \leq s_1 \text{ and} \\ \tau(s) &= \left(1 + \frac{s_1-s}{L}\right) [\tau_{\max} - (s - s_1)a], \text{ if } s > s_1 \end{aligned} \quad (3)$$

where:

$$\begin{aligned} s_0 &= \frac{\tau_{\max}}{G} \\ G &= \frac{E_m}{d_f(1 + \nu_m) \ln(R/r)} \\ s_1 &= s_0 + \frac{\pi d_f \tau_{\max} L^2}{2AE} + \frac{F_0 L}{AE} \end{aligned} \quad (4)$$

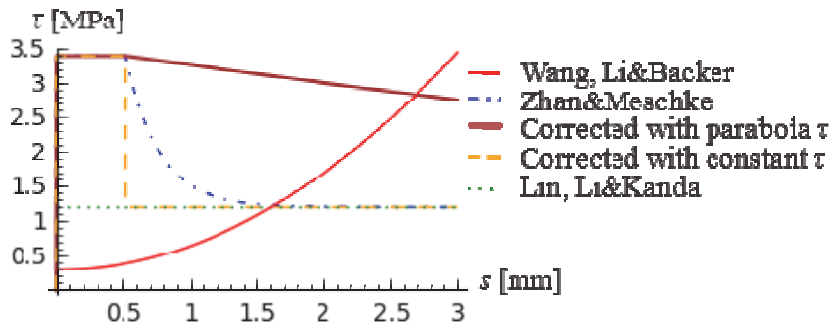


Fig. 6: Frictional stress – relative displacement relationship

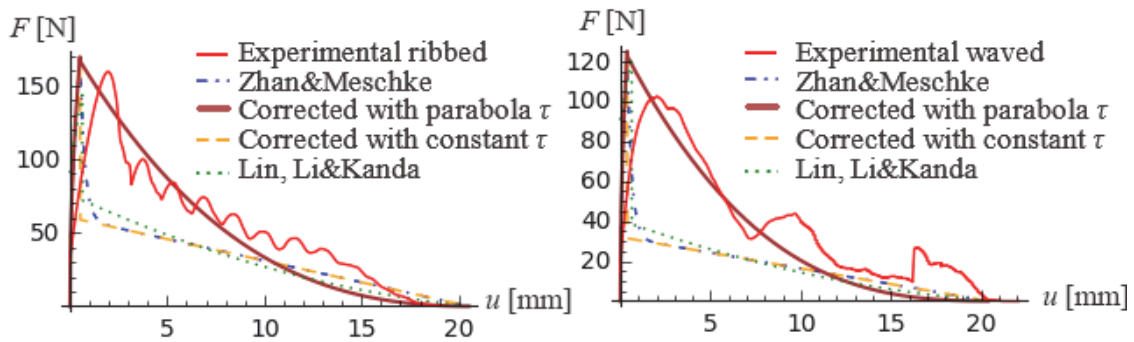


Fig.7: Modelling experimental curves (cement content: 150/300 g, anchored length: 20 mm) with analytical models

Tab. 2 Non-changeable parameters

E_m	30000 Mpa
ν_m	0.2
E	7000 Mpa
d_f	0.78 mm
R/r	50.8
s_{ref}	0.25 mm
a	0.1

Tab. 2 contains the parameters used in the calculation.

In the experiments some fibres were torn (Fig. 8). With the help of the modified theoretical model, the critical length of anchorage could be calculated (Tab. 3) from equation (5):

$$L_{\text{crit}} = \frac{F_{\text{max}} - F_0}{\pi d_f \tau_{\text{max}}} \quad (5)$$

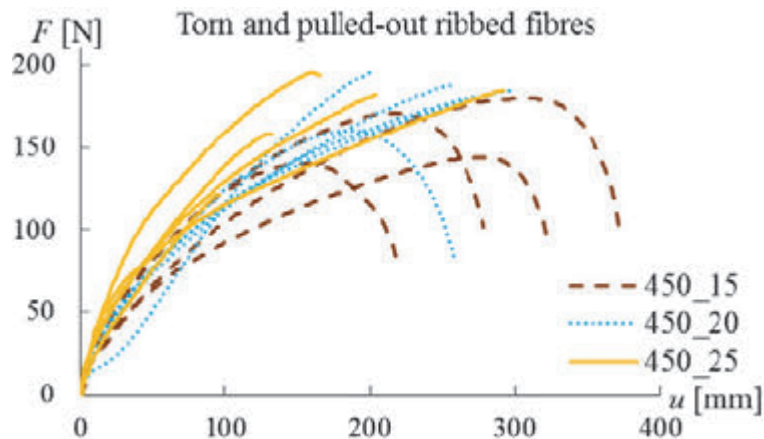


Fig. 8: Torn and pulled out ribbed fibres of samples with 450 g cement content

Tab. 3: Critical length of anchorage

Fibre types	Cement content [g]	F_{max} [N]	τ [MPa]	L_{crit} [mm]
Waved fibre	150	280	2.5	45
	225		3.4	33
	300		4	28
	375		4	28
	450		4	28
Ribbed fibre	150	180	2	37
	225		3	24
	300		3.4	21
	375		3.8	19
	450		3.8	19

4. CONCLUSIONS

Detailed experimental investigation was performed to examine the pull-out phenomenon of synthetic fibres. Contrary to the literature, the experiments revealed that the two-sided pull-out problem has the same features as the one-sided pull-out one, but the maximum pull-out force is bigger in the one-sided case. None of the available analytical models for synthetic fibres (Wang and Backer, 1988; Lin, Kanda and Li, 1999) could be fitted well to the experimental data. The model suggested for steel fibres according to Zhan and Meschke (2014) also failed the prediction of the experimental results. This model (Zhan and Meschke, 2014) with a modified friction law (τ - s relation) is suggested to use in beam modelling (Tóth, Pluzsik and Juhász, 2017) to gain the most precise approximation not only for the pull-out of synthetic fibres but for the load-displacement curves for FRC beams. The suggested model

gave acceptable approximation in all examined cases for different mortar strength, fibre surface and anchored fibre length.

5. LIST OF NOTATIONS

a [-]:	free parameter of parabola
A [mm ²]:	cross sectional area of fibre
d_f [mm]:	diameter of fibre
E [MPa]:	elastic modulus of fibre
E_m [MPa]:	elastic modulus of mortar matrix
F_{\max} [N]:	maximal force
G [N/mm ³]:	relative bond modulus
L [mm]:	embedment length
L_{crit} [mm]:	critical length of embedment
R/r [-]:	matrix-fibre size ratio
s [mm]:	slip (relative displacement)
s_{ref} [mm]:	reference slip
u [mm]:	displacement of the fibre
ν_m [-]:	Poisson's ratio
τ_0 [MPa]:	asymptotic frictional strength
τ_{\max} [MPa]:	bond strength

6. REFERENCES

- ACI Committee 544. (1998). "Design Considerations for Steel Fiber Reinforced Concrete." ACI Structural Journal, Vol. 85, No. 5, Sept.-Oct. 1998, pp. 563-580.
- ACI Committee 544. (2002). "State-of-the-Art Report on Fiber Reinforced Concrete." ACI Structural Journal, 544.1R-96.
- CNR-DT 204/2006. (2006). "Guide for the Design and Construction of Fiber-Reinforced Concrete Structures", Advisory Committee on Technical Recommendations for Construction, Rome, 2006
- Lee, S.C., Cho, J.Y., and Vecchio, F. J. (2011). „Diverse Embedment Model for Steel Fiber-Reinforced Concrete in Tension: Model Development." ACI Materials Journal, V. 108, No. 5, Sept.-Oct. 2011, pp. 516-525.
- Lin, Z., Kanda, T., and Li, V. C. (1999) "On Interface Characterization and Performance of Fiber-reinforced Cementitious Composites." Concrete Science and Engineering, Vol. 1, pp 173-174
- Österreichische Vereinigung für Beton- und Bautechnik. (2008). Richtlinie Faserbeton ÖVBB, Vienna, 2008
- Tóth, M. Pluzsik, A. and Juhász, K. P. (2017) "Effect of Mixed Fibers on the Ductility of Concrete." Journal of Materials in Civil Engineering, Vol., 29 Issue 9, September 2017
- Vandewalle, L., et al. (2002). "RILEM TC 162-TDF: Test and Design Methods for Steel Fibre Reinforced Concrete." Materials and Structures, Vol. 33, January-February, 3-5.
- Wang, Y., Li, V. C., and Backer, S. (1988) "Modelling of Fibre Pull-out from a Cement Matrix." The International Journal of Cement Composites and Lightweight Concrete, Vol. 10/3
- Zhan, Y., Meschke, G., (2014) "Analytical Model for the Pullout Behaviour of Straight and Hooked-end Steel Fibers." Journal of Engineering Mechanics, 140(12), 04014091(1-13)

INFLUENCE OF UNIDIRECTIONAL CFRP PLATE PULL-OFF STRENGTH BONDED TO CONCRETE BY MEANS OF EPOXY AND A COMBINATION OF EPOXY AND MECHANICAL ANCHORS

Cronje Bruwer

University of Johannesburg, Department of Civil Engineering Technology

PO Box 17011, Doornfontein, 2028, South Africa

SUMMARY

The flexural capacity of reinforced concrete structural elements can be increased by epoxy bonding external reinforcement in the form of unidirectional carbon fiber reinforced polymer (UD-CFRP) plate/s to the tension surface, thus creating a composite element. Debonding of the UD-CFRP plate from the concrete surface is the most common failure mode. This experimental study investigates if additional mechanical anchorage to the epoxy bonded UD-CFRP plate will have a combining effect. Single shear pull off tests was conducted for the following three bonding mechanisms (1) UD-CFRP plate epoxy bonded to a concrete block; (2) UD-CFRP plate mechanically bonded to a concrete block; (3) UD-CFRP plate epoxy and mechanically bonded to a concrete block. The experimentally determined pull-off forces is also compared to the theoretically calculated forces.

1. INTRODUCTION

The technique of externally bonding steel plates to the tension surface of a reinforced concrete structural element by means of epoxy, creating a composite element was developed in the 1960's. In recent years UD-CFRP plates instead of steel plates are used due to better rust resistance and lighter weight.

A structural composite member's capacity is based on the interaction between the bonded plate and the concrete surface. Debonding of the plate, occurs instantaneous due to cracks in the tension zone of the concrete, obliterate this interaction between the bonded plate and the concrete. This experimental study investigate if additional mechanical anchorage to the epoxy bonded UD-CFRP plate will have a combining effect, therefore (1) prevent instantaneous debonding of the plate from the concrete surface; (2) increase the ductility of the bond between the plate and the concrete surface; (3) increase the bond strength between the plate and the concrete surface.

The following experimental single shear pull off tests was conducted to establish the basis for the combining bonding capacities of epoxy and mechanical anchorage of the UD-CFRP plates to the concrete surface (1) plate epoxy bonded to a concrete block; (2) plate mechanically bonded to a concrete block; (3) plate epoxy and mechanically bonded to the concrete block.

Yao et al. (2004) theory was used to compare the theoretically calculated forces to the experimental pull-off forces of the UD-CFRP plates epoxy bonded to the concrete block.

2. EXPERIMENTAL PROGRAM

The single shear pull-off test, with the near end supported, as described by Yao et al. (2004) was used to determine the differences in bond strength between the UD-CFRP plate and the concrete block. The available laboratory equipment compel the setup of the single shear pull-off test to be done in a vertical plane, as indicated in Figure 1, instead of a horizontal plane as described by Yao et al. (2004).

Concrete blocks, 150 x 150 x 750 mm long, were constructed and used as test specimens onto which the UD-CFRP plates were bonded. The average cube strength (f_{cu}) of the concrete blocks is 45.7 MPa with a cylinder strength (f'_c) of 36.6 MPa.

The concrete surface was prepared by removing the cement laitance by means of scabbling to expose the well bonded large aggregate. Pro-Struct 617LV primer was applied which penetrate the concrete surface onto which the Pro-Struct617NS epoxy could bind. The epoxy was applied to the UD-CFRP plate and firmly pressed to the concrete block for 24 hours to provide a good bond.

The mechanical bond was established by drilling a 12 mm hole through the UD-CFRP plate into the concrete block to install a Hilti M10 HAS-(E) chemical anchor. Epoxy was placed between the washer, 50 mm diameter and 4 mm thick, and the nut of the mechanical anchor was torqued to 20 Nm to ensure a friction connection between the UD-CFRP plate and the concrete surface.

The pull off rate of the UD-CFRP plate from the concrete block, for the single shear pull-off test, was 0.02 mm/s. The slip was measured by means of two linear resistive positive transducers (LRPT) which were bolted to the UD-CFRP plate and measured to the loaded surface of the concrete block as indicated in Fig. 1.

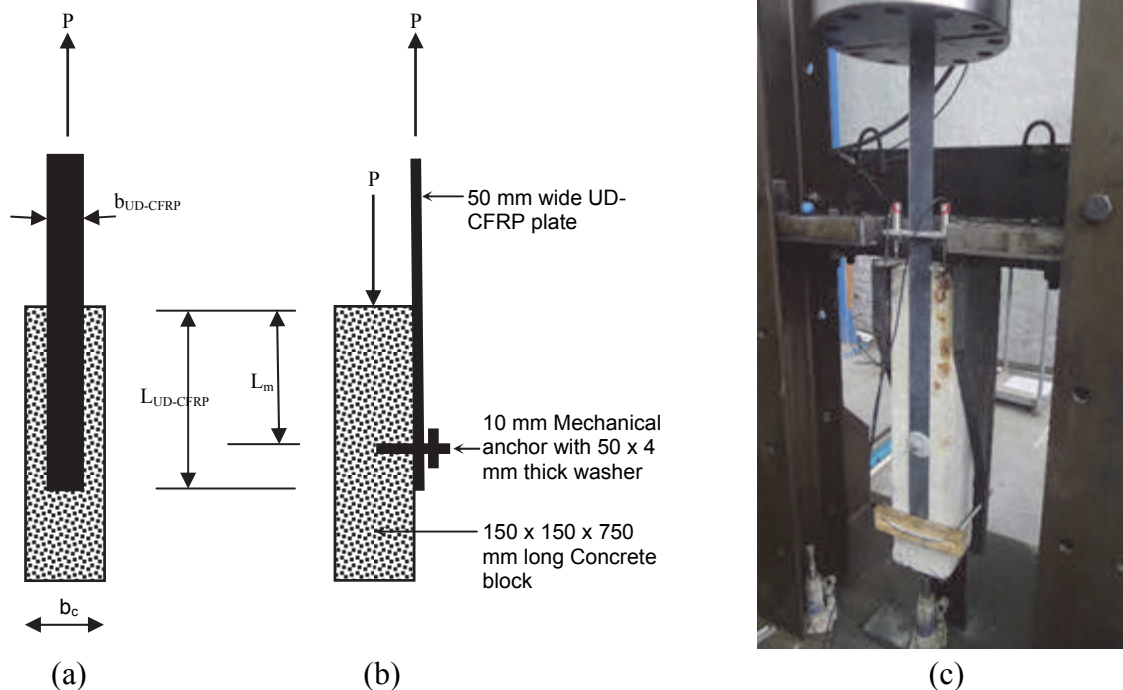


Fig. 1: Single shear pull-off test with the near end supported (a) Schematic front view (b) Schematic side view (c) Image of complete set-up

Tab. 1 indicates the number of specimens prepared to be tested by means of the single shear pull-off test and the type of the type of bond between the UD-CFRP plate and the concrete block.

Tab. 1: Number of pull off specimens prepared

Specimen name	Bonded UD-CFRP plate			Type of bonding
	Plate Thickness ($t_{UD-CFRP}$) (mm)	Plate Width ($b_{UD-CFRP}$) (mm)	Bonded Length ($L_{UD-CFRP}$) (mm)	
EB1	1.2	50	550	Epoxy bonded
EB2	1.2	50	550	Epoxy bonded
EB3	1.2	50	550	Epoxy bonded
EB4	1.2	50	550	Epoxy bonded
EB5	1.2	50	550	Epoxy bonded
EB6	1.2	50	550	Epoxy bonded
MB1	1.2	50	550	Mechanically bonded
MB2	1.2	50	550	Mechanically bonded
MB3	1.2	50	550	Mechanically bonded
EMB1	1.2	50	550	Epoxy and mechanically bonded
EMB2	1.2	50	550	Epoxy and mechanically bonded
EMB3	1.2	50	550	Epoxy and mechanically bonded
EMB4	1.2	50	550	Epoxy and mechanically bonded
EMB5	1.2	50	550	Epoxy and mechanically bonded
EMB6	1.2	50	550	Epoxy and mechanically bonded

3. TEST RESULTS AND DISCUSSIONS

The experimental results obtained from the single shear pull-off tests (1) epoxy bonded, (2) mechanical bonded and (3) combined epoxy and mechanically bonded UD-CFRP plates to the concrete is indicated in the load-deflection graphs in Fig 2, 3 and 4 below:

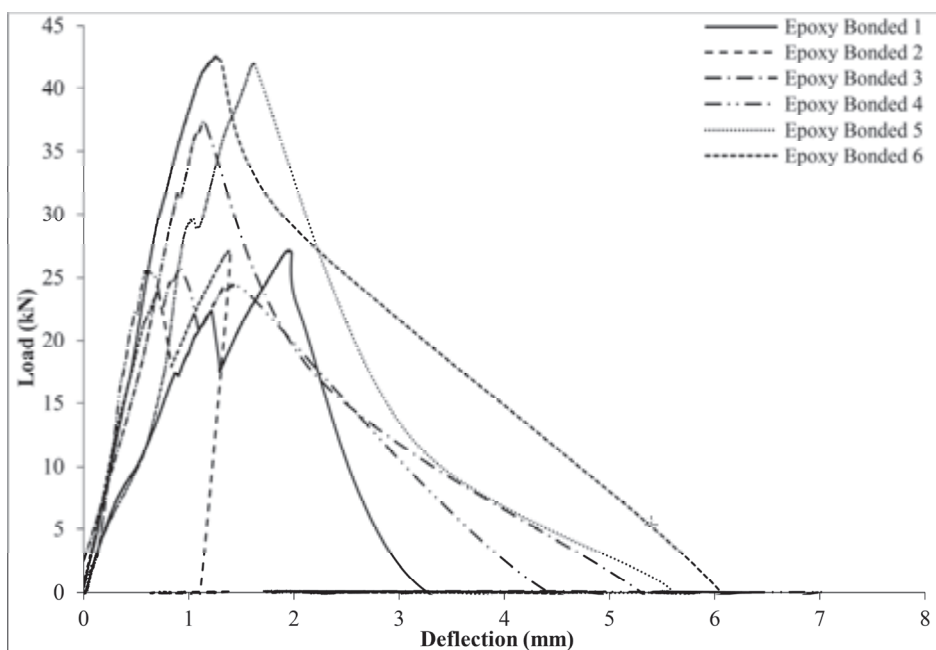


Fig. 2: Load deflection graph for single shear pull-off test, 50 x 1.2 mm UD-CFRP plate epoxy bonded to concrete

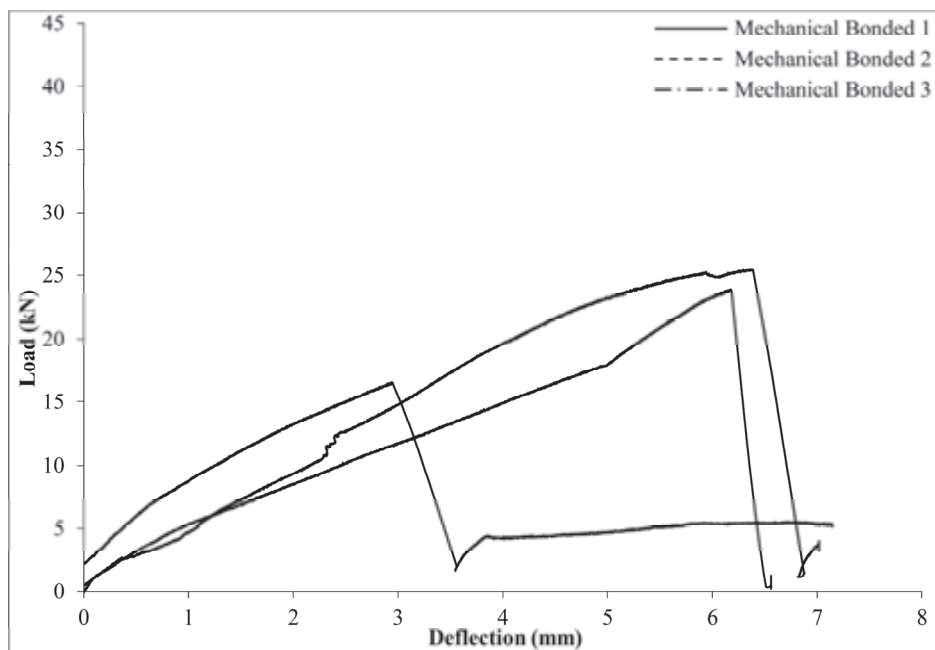


Fig. 3: Load deflection graph for single shear pull-off test for 50 x 1.2 mm UD-CFRP plate mechanically bonded to concrete

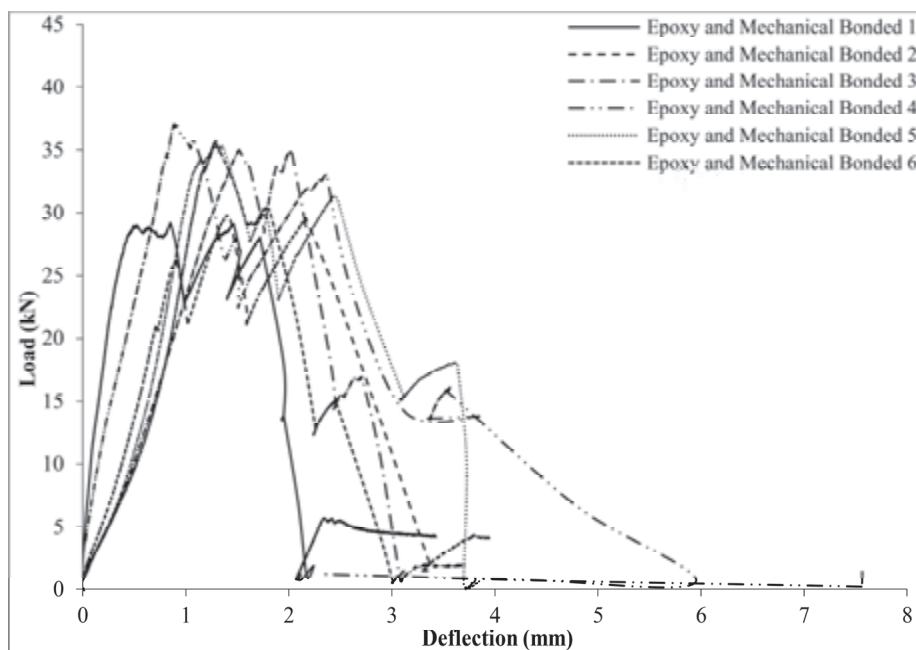


Fig. 4: Load deflection graph for single shear pull-off test for 50 x 1.2 mm UD-CFRP plate epoxy and mechanically bonded to concrete

The maximum pull-off forces and deflections for (1) epoxy bond ($P_{exper,EB}$); (2) mechanical bond ($P_{exper,MB}$) and (3) combined epoxy and mechanical bond ($P_{exper,EMB}$) obtained from the single shear pull-off test are listed in Tab. 2.

Tab. 2: Maximum single shear pull-off forces and deflections

Name	Epoxy Bond		Mechanical Bond		Combined Epoxy And Mechanical Bond	
	$P_{exper,EB}$ (kN)	$y_{exper,EB}$ (mm)	$P_{exper,MB}$ (kN)	$y_{exper,MB}$ (mm)	$P_{exper,EMB}$ (kN)	$y_{exper,EMB}$ (mm)
EB1	27.2	1.97				
EB2	27.2	1.39				
EB3	37.4	1.14				
EB4	25.7	1.45				
EB5	42.1	1.61				
EB6	42.5	1.27				
MB1			23.9	6.18		
MB2			16.5	2.94		
MB3			25.4	6.37		
EMB1					29.2	1.71
EMB2					29.8	2.17
EMB3					35	2.03
EMB4					37	2.36
EMB5					35.4	2.46
EMB6					35.7	1.26

The average pull-off forces at which debonding of the UD-CFRP plates from the concrete surface occur is (1) $P_{exper,EB}$ is 33.7 kN for epoxy bonding,, (2) $P_{exper,MB}$ is 21.9 kN for mechanical bonding and (3) $P_{exper,EMB}$ is 33.7 kN for combined epoxy and mechanical bonding. The epoxy bond is 54% stronger than the mechanical bond indicating that an epoxy bond create a stronger bond than a mechanical bond. The combined of epoxy and mechanical bond yield a maximum pull-off force of ($P_{exper,EMB}$) is 33.7 kN, almost the same as for an epoxy only bonding ($P_{exper,EB}$) 33.7 kN. It is therefore evident that no increase in the pull-off force could be obtained by combining the epoxy and mechanical bond even if a 50 mm diameter washer providing a friction connection was used.

The average deflection at which debonding of the UD-CFRP plate from the concrete surface occur is (1) $y_{exper,EB}$ is 1.47 mm for epoxy bonding; (2) $y_{exper,MB}$ is 5.16 mm for mechanical bonding and (3) $y_{exper,EMB}$ is 2.00 mm for combined epoxy and mechanical bonding. Since debonding occur at 2.00 mm ($y_{exper,EMB}$) for a combined epoxy and mechanical bond and at 1.47 mm ($y_{exper,EB}$) for an epoxy bond it is evident that the combined epoxy and mechanical bond have a more ductile failure mode.

4. COMPARING THE MAXIMUM EXPERIMENTALLY TESTED PULL-OFF FORCES TO THE THEORETICALLY CALCULATED FORCES

Comparing the experimental pull-off forces of the UD-CFRP plates ($P_{exper,EB}$), epoxy bonded to the concrete block, to the theoretically calculated forces ($P_{theory,EB}$), Yao et al. (2004) theory was used. Equations 1, 2, 3 and 4 makes provision for both fiber reinforced polymer (FRP) and steel plates.

$$P_u = b_{CFRP} \alpha \beta_w \beta_l L_e \sqrt{f'_c} \quad (1)$$

$\alpha = 0.427$ for best fit value

$\alpha = 0.315$ for 95th percentile

$$\beta_w = \sqrt{\frac{2 - b_{CFRP}/b_c}{1 + b_{CFRP}/b_c}} \quad (2)$$

$$\beta_l = \begin{cases} 1.0 & \text{if } L_{CFRP} \geq L_e \\ \sin \frac{\pi L_{CFRP}}{2 L_e} & \text{if } L_{CFRP} < L_e \end{cases} \quad (3)$$

$$L_e = \sqrt{\frac{E_{CFRP} t_{CFRP}}{\sqrt{f'_c}}} \quad (4)$$

in which E_{CFRP} and f'_c are in MPa, t_{CFRP} and L_e are in mm.

The comparison of the experimental pull-off forces ($P_{exper,EB}$) of the UD-CFRP plates, epoxy bonded to the concrete block, to the theoretically calculated forces ($P_{theory,EB}$) is indicated in Tab 3.

Tab. 3: Comparing the experimentally tested ($P_{exper,EB}$) to the theoretically calculated ($P_{theory,EB}$) pull-off forces.

Name	UD-CFRP plate			β_w	f'_c (Mpa)	L_e (mm)	β_l	α	$P_{theory,EB}$ (kN)	$P_{exper,EB}$ (kN)	$\frac{P_{theory,EB}}{P_{exper,EB}}$
	t_{CFRP} (mm)	b_{CFRP} (mm)	L_{CFRP} (mm)								
EB1	1.2	50	550	1.1 2	36.6	181. 0	1.0	0.42 7	26.1	27.2	0.96
EB2	1.2	50	550	1.1 2	36.6	181. 0	1.0	0.42 7	26.1	27.2	0.96
EB3	1.2	50	550	1.1 2	36.6	181. 0	1.0	0.42 7	26.1	37.4	0.70
EB4	1.2	50	550	1.1 2	36.6	181. 0	1.0	0.42 7	26.1	25.7	1.02
EB5	1.2	50	550	1.1 2	36.6	181. 0	1.0	0.42 7	26.1	42.1	0.62
EB6	1.2	50	550	1.1 2	36.6	181. 0	1.0	0.42 7	26.1	42.5	0.61

The theoretical calculated pull-off force ($P_{theory,EB}$) produce the best comparison to the experimentally tested pull-off force ($P_{exper,EB}$) with the best fit value (α) of 0.427). The experimental test results ($P_{exper,EB}$) for UD-CFRP plates yield average pull-off forces 18.8% higher than the theoretically calculated results.

The comparison of the experimental pull-off forces ($P_{exper,MB}$) of the UD-CFRP plates, epoxy bonded to the concrete block, to the theoretically calculated pull-off forces ($V_{Rd,s}$) is indicated in Tab. 4.

Tab. 4: Comparing the experimentally tested ($P_{exper,MB}$) to the theoretically calculated ($V_{Rd,s}$) pull-off forces.

Name	Bolt Diameter	$V_{Rd,s}$ (kN)	$P_{exper,MB}$ (kN)	Failure Mode	$\frac{P_{theory,MB}}{P_{exper,MB}}$
MB1	M10	13.70	23.90	UD-CFRP plate bearing failure	0.57
MB2	M10	13.70	16.50	UD-CFRP plate bearing failure	0.83
MB3	M10	13.70	25.40	UD-CFRP plate bearing failure	0.54

The experimental tested pull-off forces ($P_{exper,MB}$) of UD-CFRP plates from concrete, mechanically bonded, yield average forces of 60.1% higher than the shear strength ($V_{Rd,s}$), as per the Hilti catalogue. Since the CFRP plates is uniformly directional weaved it have no shear resistance, the only shear resistance provided is from the friction connection provided by the 50 mm washer torqued onto the UD-CFRP plate.

5. CONCLUSIONS

The data collected from this experimental study disclose that: (1) The combination of epoxy and mechanical bond ($P_{exper,EMB}$) to concrete yield pull-off results similar as to epoxy bonding ($P_{exper,EB}$) only. It is therefore evident that no increase in the pull-off force could be obtained by combining the epoxy and mechanical bond. (2) Debonding for combined epoxy and mechanical bond ($y_{exper,EMB}$) occur at a larger deflection as for an epoxy bond ($y_{exper,EB}$) only, which indicate that a more ductile failure mode can be achieved by adding mechanical anchors to an UD-CFRP plate bonded by means of epoxy only. (3) The experimental test results ($P_{exper,EB}$) for UD-CFRP plates yield average pull-off forces 18.8% higher than the theoretically calculated results. (4) The experimental tested pull-off forces ($P_{exper,MB}$) of UD-CFRP plates from concrete, mechanically bonded, yield average forces of 60.1% higher than the shear strength ($V_{Rd,s}$), indicating that the only shear resistance is provided from the 50mm washer torqued onto the UD-CFRP plate providing a friction connection.

6. REFERENCES

- Cheng, J.F., Teng, J.G. "Anchorage Strength Models for FRP and Steel Plates bonded to Concrete" J Struct Eng, ASCE 2001;127(7):784-91
 HILTI HVU with HAS/HAS-E rod Adhesive anchor brochure.
 Yao, J., Teng, J.G., et al., "Experimental Study on FRP-to- Concrete Bonded Joints", Composites: Part B 36 (2005) 99-113

LONG-TERM PROPERTIES OF FRP REINFORCEMENT

*Katarína Gajdošová, Róbert Sonnenschein, Peter Paulík, Jaroslav Halvonik
Faculty of Civil Engineering, Slovak University of Technology in Bratislava
Radlinského 11, 810 05 Bratislava, Slovakia*

SUMMARY

Mechanical properties of FRP reinforcement significantly change in time. Results of previous experimental programs showed the ratios of stress level at creep rupture to the initial strength to be in range of 0.18 to 0.93 for different types of FRP reinforcement. The reduction as a result of environmental action on durability is in the range of 0.5 – 1.0 of the initial tensile strength. The unfavourable change in properties limits the use of these materials. Reduction of the initial tensile strength according to durability and creep rupture significantly reduces the final cross-section resistance of a structural member reinforced with FRP reinforcement. This change in properties is only extrapolated from short-term tests. Long-term measurements are needed to verify these statements.

1. INTRODUCTION

FRP (Fibre Reinforced Polymer) reinforcement becomes widely used for strengthening structures with insufficient reliability level and for reinforcing new structures in special conditions, where traditional steel reinforcement is not suitable, e.g. in environment with chloride ions, when non-conductivity is needed or when the reinforcement in concrete should not affect magnetic fields.

The characteristics of FRP reinforcement are dependent on factors such as fibre volume, type of fibre, type of resin, fibre orientation, dimensional effects and quality control during manufacturing (ACI 440.1R-03). The resin acts as a matrix bonding the fibres together and transferring the load applied to the composite between each of the individual fibres. The resin also protects the fibres from abrasion and impact damage as well as severe environmental conditions (water, salts, alkalis) which affect the durability of FRP products (Benmokrane, 2015). The commonly used fibres are carbon (that form Carbon Fibre Reinforced Polymer – CFRP), glass (forming GFRP), aramid (forming AFRP) and basalt (forming BFRP) fibres.

Glass fibres are the cheapest ones but the less durable due to high chemical sensibility to alkali environment. Carbon fibres tend to show the best resistance. CFRP and AFRP reinforcement is also insensitive to chloride ions. Carbon and glass fibres do not absorb water which affects in better fatigue strength. The most discussed problem of non-metallic reinforcement is the behaviour during elevated temperature – which is the problem of resin. Carbon fibres themselves are not sensitive to high temperature and that is why CFRP shows the most favourable behaviour. CFRPs are in addition not affected by ultraviolet rays.

Durability of FRP reinforcement is not only influenced by component properties but also by the interface between them. The transfer of shear and transverse forces at the interface between reinforcement and concrete, influencing the bond, and between individual fibres within the composite are the resin-dominated mechanisms. Fibre-dominated mechanisms

control properties such as longitudinal strength and stiffness of FRP reinforcement (Ceroni, 2006).

2. LONG-TERM PROPERTIES

To date, there is not enough information about long-term behaviour of FRP reinforcement, because they are not used for a long time and structures with FRP reinforcement or strengthening systems do not reach their service life, yet.

From long-term properties of FRP reinforcement, the next three are the most important: durability, creep rupture and fatigue. The durability of FRP reinforcement is affected by alkali environment in concrete and moisture access. The creep rupture phenomenon appears after a period of time when FRP is subjected to a constant load and suddenly fails. The creep rupture and the fatigue strength both depend on fibre type in FRP reinforcement.

Long-term properties of FRP reinforcement are, according to various standards, calculated from short-term properties by introduction of reduction factors. Properties reduced according to these requirements are very low and the use of FRP reinforcement seems not to be effective. It has to be stated, that reduction factors for long-term properties were not yet measured experimentally, they are only extrapolated in time from short-term tests. Some experimental investigation ten years after application of FRP reinforcement does not contribute these assumptions.

2.1 Durability

The lack of design rules for the use of FRP for reinforcing and strengthening of concrete structures is also related to durability design. Thus the experimental tests for durability have long duration, accelerated methods are usually used. To this date, no real-time test data exist for the conversion of accelerated test results. The specification of durability characteristics of FRP reinforcement is also complicated by its structure, because it depends on the characteristics of fibres, matrix and their interface.

The influences on durability are divided to the effects of external environment and to the effects of concrete environments (applicable for the use of FRP for reinforcing).

The most important effects of external environment are thermal conditions, ultraviolet rays and chemical attacks. The elastic modulus and strength of FRP reinforcement decrease with high temperatures and sustained load. Under service temperature of concrete structures (from -20 to +60 °C) the reduction of modulus of elasticity is negligible for CFRP, however slight reduction occurs for AFRP and GFRP. After exposure of ultraviolet rays, AFRP reinforcement showed 13 % reduction of tensile strength, GFRP 8% reduction and CFRP no reduction. The combined effect of ultraviolet and moisture exposure showed even greater reduction in material characteristics. From chemical effects, the acid attack is the most dangerous, but there is a lack of data in this field (*fib* Bulletin 40).

In comparison with steel reinforcement the effect of concrete environment can harm FRP reinforcement. The usual benefit of concrete in protecting steel reinforcement could cause FRP reinforcement degradation. Carbon fibres tend to show the best resistance to alkali environment followed by aramid and glass fibres, the deterioration in alkali environment of which is well known (Ceroni, 2006). Here is the importance of the matrix in the role of

protection agent. The summary of results from Sweden for tensile strength reductions obtained for GFRP bars in alkaline solutions, concrete and water at 60 °C and 20 °C is shown in Fig. 1 (Dejke, 2001). It can be seen that after one year, the reduction in tensile strength starts steady in case of alkali environment. Also monitoring of bridge decks in Canada shows smaller degradation of GFRP rebars as assumed according to accelerated test methods. Another effect of the concrete environment to fibres is the presence of moisture. Carbon and glass fibres cannot absorb water, while water absorption in aramid fibres causes reversible decrease in tensile strength, the modulus of elasticity and fatigue strength (Ceroni, 2006).

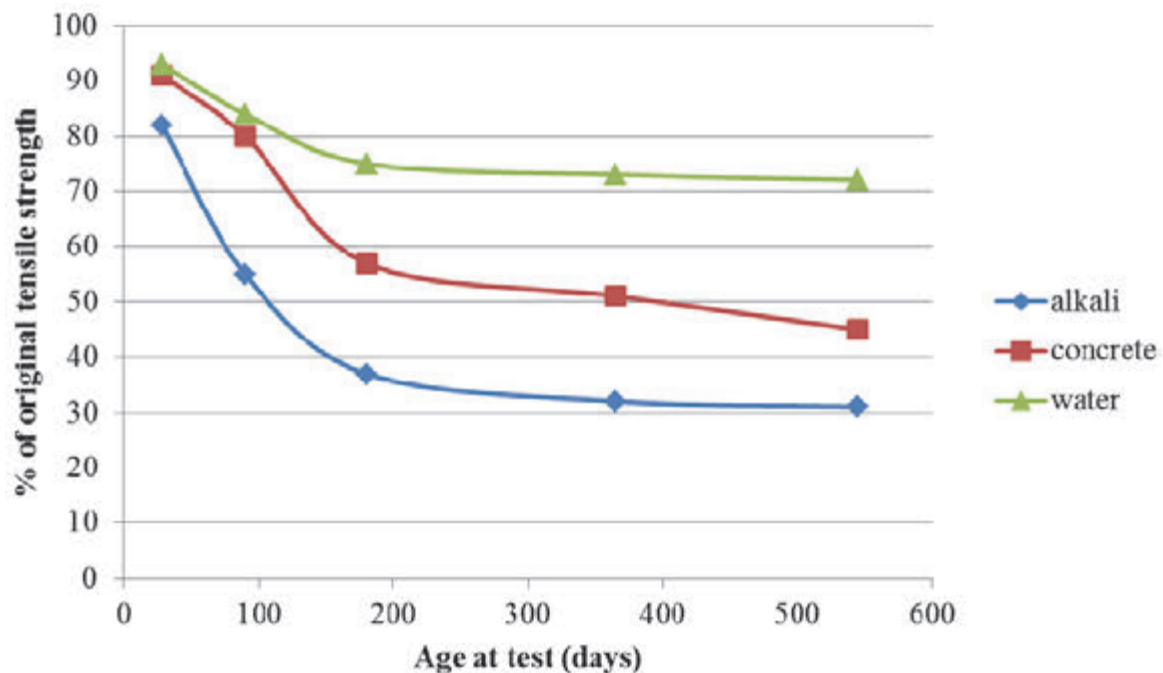


Fig. 1: Effect of environment on GFRP exposed to alkali, concrete and water

To take account of tensile strength reduction due to environmental actions, the reduction factors are used in existing guidelines.

2.2 Creep rupture

FRP reinforcement subjected to a constant load over time can suddenly fail after a time period called the endurance time. This phenomenon is known as creep rupture. The endurance time of FRP reinforcement decreases as the ratio of the sustained tensile stress to the short-term strength increases. The endurance time also decreases with the effects of high temperature, ultraviolet radiation exposure, high alkalinity, wet and dry cycles, and freezing-thawing cycles (ACI 440.1R-03). Carbon fibres have a very good resistance to creep rupture. Aramid fibres are more susceptible to this phenomenon and glass and basalt fibres are the most susceptible ones. Nevertheless, the susceptibility of the resin is the biggest problem.

A few series of creep rupture tests were conducted on FRP reinforcement with different fibres (carbon, aramid, glass, basalt). Usually the tests lasted for a time of 100 h and the results were linearly extrapolated to 500,000 h (more than 50 years).

Results of the experimental program of Yamaguchi et al. (1997) showed the ratios of stress level at creep rupture to the initial strength to be 0.29 for GFRP, 0.47 for AFRP and 0.93 for CFRP. In another extensive investigation (Ando et al. 1997) the percentage of stress at creep

rupture versus the initial strength after 50 years was found to be 0.79 for CFRP and 0.66 for AFRP. Seki et al. (1997) reported the ratio of 0.55 for GFRP. A 50-year ultimate creep rupture strength coefficient of 0.18 was found by Banibayat and Patnaik (2014) to be suitable for BFRP reinforcement (*fib* Bulletin 40).

There are two possibilities to avoid creep rupture – adjust the material resistance of FRP reinforcement or limit the stress level in FRP reinforcement under sustained stresses.

2.3 Fatigue

The fatigue stress limit is the stress level below which a material can be stressed cyclically for an infinite number of times without failure. Glass fibres individually are not prone to fatigue failure. GFRP reinforcement may lose about 10 % of the initial static strength per decade of logarithmic lifetime in presence of cyclic tensile loading. CFRP composites are at least vulnerable to fatigue failure. Their fatigue strength is 3-4 times higher than that of prestressing steel. At one million cycles, the fatigue strength is usually between 50 and 70 % of the initial static strength. For AFRP, the fatigue strength after 2 million cycles was reported of about 54 and 73 % of the initial static strength (Ceroni, 2006), (*fib* Bulletin 40).

3. REDUCTION OF MATERIAL PROPERTIES DUE TO LONG-TERM EFFECTS

The durability properties and environmental conditions consideration are established by reduction factors summarized in Tab. 1.

Limitations according to sustained load and creep rupture phenomenon are summarized in Tab. 2.

Tab. 1: Durability reduction factors (*fib* Bulletin 40)

	CFRP	GFRP	AFRP
ACI 440.1R-06	$0.95 f_{fu}$	$0.75 f_{fu}$	$0.85 f_{fu}$
NS3473	$1.00 f_{fu}$	$0.50 f_{fu}$	$0.90 f_{fu}$
CSA-S806-02 CHBDC-2006	$0.75 f_{fu}$	$0.50 f_{fu}$	$0.60 f_{fu}$
JSCE	$0.87 f_{fu}$	$0.77 f_{fu}$	$0.87 f_{fu}$

Tab. 2: Long-term stress limitation factors

	CFRP	GFRP	AFRP	BFRP
ACI 440.1R-06	$0.55 f_{fu}$	$0.20 f_{fu}$	$0.30 f_{fu}$	-
Yamaguchi et al. (1997)	$0.93 f_{fu}$	$0.29 f_{fu}$	$0.47 f_{fu}$	-
Ando et al. 1997	$0.79 f_{fu}$	-	$0.66 f_{fu}$	-
Seki et. al (1997)	-	$0.55 f_{fu}$	-	-
Banibayat and Patnaik (2014)	-	-	-	$0.18 f_{fu}$

For illustration of FRP composite reinforcement action in a simply supported one-way reinforced concrete slab, the example shown in Fig. 2 was chosen. FRP reinforcement characteristics are shown in Tab. 3.

Tab. 3: Properties of FRP reinforcing bars

	CFRP	GFRP	AFRP	BFRP
Tensile strength [MPa]	3100	1000	2100	1500
Modulus of elasticity [GPa]	170	50	83	41
Limit strain [%]	1.20	2.20	2.90	2.50

The input parameters of a chosen example:

- slab thickness: 250 mm
- reinforcement bars diameter: 6 mm
- reinforcement characteristics: see Tab. 3
- concrete cover: 20 mm
- concrete class: C25/30
- effective span of a slab: 6000 mm

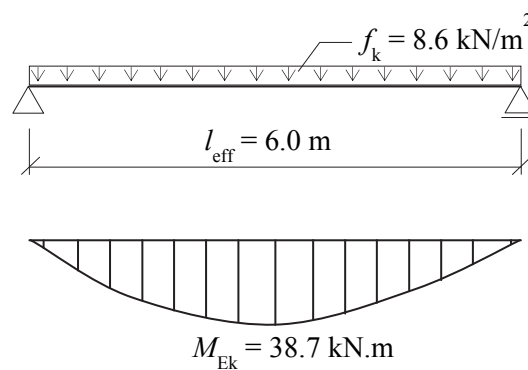


Fig. 2: Example of a one-way slab

Tab. 4: Comparison of calculated resistance moments with consideration of durability and long-term reduction factors

	CFRP		GFRP		AFRP		BFRP	
Calculated short-term resistance (M_{Rd} [kNm]):	63.7		56.8		54.3		54.3	
	Resistance including durability [kNm]							
ACI 440.1R-06	60.7	-4.8%	43.0	-24.3%	46.4	-14.6%	-	
NS3473	63.7	0%	28.9	-49.1%	49.0	-9.8%	-	
CSA-S806-02 CHBDC-2006	48.3	-24.3%	28.9	-49.1%	33.0	-39.2%	-	
JSCE	55.7	-12.6%	44.1	-22.4%	47.5	-12.5%	-	
assumption	-	-	-	-	-	-	33.02	60.8%
average	57.1	-10.4%	36.2	-36.3%	44.0	-19%	-	
	Resistance including durability and long-term effects [kNm]							
ACI 440.1R-03 (2003)	31.9	-49.9%	7.4	-87.0%	13.5	-75.1%	-	
Yamaguchi et al. (1997)	53.3	-16.3%	10.7	-81.2%	21.0	-61.3%	-	
Ando et al. (1997)	45.5	-28.6%	-		29.3	-46.1%	-	
Seki et. al (1997)	-		20.1	-64.6%	-		-	
Banibayat and Patnaik (2014)	-		-		-		6.04	-88.9%

4. CONCLUSIONS

According to reduction factors summarized in Tab. 1 and Tab. 2 it can be concluded, that the existing design guidelines for FRP reinforcement strictly limit their usability according to durability effects and creep rupture phenomenon.

The results from the calculated example of a one-way slab (Tab. 4) show the reduction of cross-section resistance in the range of 5 – 50 % for durability and 20 – 90 % for additional long-term properties depending on the used FRP reinforcement type.

Nevertheless, it cannot be stated that FRP composites will not reliably satisfy their function in the structure and that structures with FRP reinforcement will fail before reaching their service life because the values of residual stresses are only extrapolated from short-term tests and we need real experience in time to decide about real long-term degradation of these materials.

5. ACKNOWLEDGEMENTS

This work was supported by the Slovak Research and Development Agency under the contract No. APVV-15-0658 and the University Science Park (USP) of the Slovak University of Technology in Bratislava (ITMS: 26240220084).

6. REFERENCES

- ACI 440.1R-03 “Guide for the Design and Construction of Concrete Reinforced with FRP Bars”, 2003.
- Banibayat, P., Patnaik, A. (2014) “Creep Rupture Performance of Basalt Fiber-Reinforced Polymer Bars”, *Journal of Aerospace Engineering*, 2014, Vol.04014074, pp.1-6.
- Benmokrane, B., Elgabbas, F., Ahmed, E., Cousin, P. (2015) “Characterization and Comparative Durability Study of Glass/Vinylester, Basalt/Vinylester, and Basalt/Epoxy FRP bars”. *J Compos Const* 2015. ASCE ISSN 1090e0268/04015008(12).
- Ceroni, F., Cosenza, E., Gaetano, M., Pecce, M. (2006) “Durability Issues of FRP Rebars in Reinforced Concrete Members”, *Cement & Concrete Composites*, Vol. 28 (2006), pp: 857.
- Dejke, V. (2001), “Durability of FRP reinforcement in Concrete”, PhD. Thesis at Dept of Building Materials, Chalmers University of Technology, Goteborg, Sweden.
- fib Bulletin* 40: FRP reinforcement in RC structures, 2007.

RESEARCH ON THE NEW CFRP PRESTRESSING SYSTEM FOR STRENGTHENING OF RC STRUCTURES

*Bartosz Piątek, Tomasz Siwowski
Rzeszow University of Technology
al. Powstańców Warszawy 12, 35-959 Rzeszów*

SUMMARY

The paper presents a research on the new Polish CFRP prestressing system for strengthening of reinforced concrete structures. The system is called Neoxe Prestressing System II (NPS II). NPS II consists of two main elements: a special steel anchorages mounted on both ends of a single CFRP strip and a tensioning device. The anchorage is made of two steel plates. CFRP strip end is fixed between steel plates through bonding by epoxy resin and gripping by bolts. The tensioning device compatible with anchorages can generate maximum prestressing force of 170 kN. The research on NPS II comprised a series of static and fatigue tests on anchorages themselves, system mounted on strengthened beams as well as on-site, i.e. on actual RC bridge. The system has been examined, its efficiency has been confirmed in laboratory and in-field tests and now it is ready for use in strengthening purposes.

1. INTRODUCTION

One of the best method to increase load bearing capacity and stiffness of reinforced concrete structures subjected to bending is the external prestressing with CFRP strips. Thanks to great mechanical parameters of CFRP strips and high efficiency of prestressing effects, this technology can be a good alternative to conventional strengthening methods and it has recently been more often used for practical application. Tensioning of CFRP strips allows to increase load bearing capacity and stiffness of strengthened structural elements and enhances composite material utilisation in comparison with passive externally bonding technique. The first externally bonded prestressing system has been developed by Leonhardt, Andrä & Partners. This system is known as Sika Leoba Carbodur II. The first on-site application of externally bonded prestressed CFRP strips was carried out using this system on a prestressed concrete bridge in Germany in 1998 (Andrä, Maier, 2000). Nowadays we can observed a dynamic development of CFRP prestressing systems worldwide. There is a lot of systems available on the market, for instance Sika StressHead (Berset et al., 2002) , S&P systems (Suter, Jungo, 2001; Michels et al., 2013) or Tenroc (Haghani et al., 2015). Still a great number of solutions have been currently testing and developing in laboratories all over the world (Aslam et al., 2015). This technology is also fast developing in Poland. The first Polish system has been developed in Road and Bridges Research Institute based on Sika Leoba Carbodur II idea (Łagoda, 2004). The next Polish system, Neoxe Prestressing System (NPS), has been developed by Neoxe company and tested in laboratories of Rzeszow University of Technology (Siwowski et al., 2010). This paper presents the results of a research programme on the second generation of the Neoxe Prestressing System (NPS II). The main goal of creating a new system was increasing of tensioning force, which could be applied on the strips. For this purpose many research have been conducted. During this study the new types of anchorages and tensioning device have been developed.

2. DESCRIPTION OF THE NEW SYSTEM

The Neoxe Prestressing System II consists of two main elements: a special steel anchorages mounted on both ends of a single CFRP strip and a relevant tensioning device. The system uses high-strength UHS 614 strips of cross-section 1.4×60 mm with the ultimate tensile strength 3200 MPa, modulus of elasticity 160 GPa and the strain at failure about 2%. There are two kinds of anchorages: an active anchorage combining with a tensioning device and a passive one. The strips with determined length are delivered on site as ready-to-install, i.e. with two steel anchorages mounted on both strips ends. The anchorage is made of two 2 mm thick steel plates welded together along edges to create a pocket, in which CFRP strip end is fixed. The end of the strip is placed in the steel anchorage pocket and bonded with special epoxy-based glue. It is followed by gripping of both materials (steel plates and CFRP strip in-between) with small high-strength bolts with 6 mm diameter. The anchorages transfer the tension force from tensioning device to the strip by internal bonding, screw gripping and friction simultaneously. The anchorage has two functional areas: external and internal (Fig. 1). The strip is clamped, bonded and gripped within the internal area. The external area comprises small holes for attaching the plate to the concrete surface by anchors and threaded holes for mounting the tensioning device (in the active anchorage only).

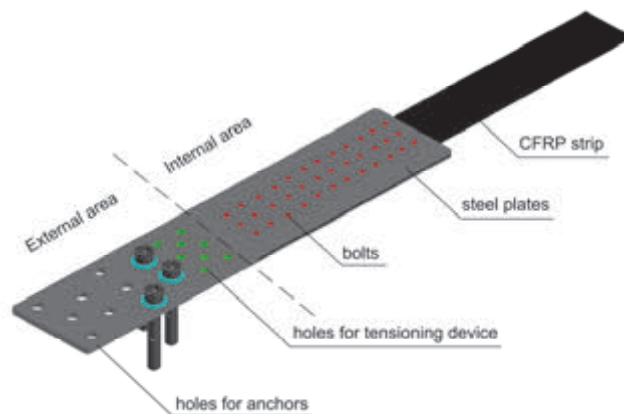


Fig. 1: Active anchorage

The tensioning device comprises three separately installed components: guide rails, carriage (bolted to the active anchorage) and hydraulic jack (Fig. 2). The hydraulic jack can generate maximum prestressing force of 170 kN. Thanks to device body division to three small and light parts (the heaviest element weights 37 kg) its installation on-site is very fast and easy.

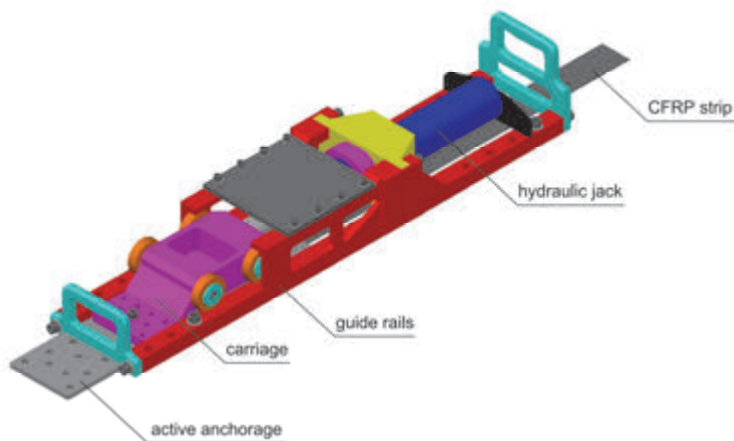


Fig. 2: Tensioning device

3. TESTS OF ANCHORAGES

In order to develop steel anchorages with required carrying capacity many research have been conducted. In the first phase tests on small specimens have been performed in order to find optimal method of preparing steel surface, composition of epoxy-based glue and type and arrangement of mechanical fasteners. The second phase concerned full scale anchorage specimens. Technology of performing anchorages was developed based on first phase tests. The tests of static carrying capacity were conducted in five series (two or three specimens in each of them). Specimens tested in subsequent series were subjected to small modifications aimed at increasing the carrying capacity of anchorages. The modifications mainly comprised several attempts to enhance the bonding shear capacity of both glued steel surfaces and to check the different arrangement small bolts. In the final solution CFRP strip is overlaid by epoxy adhesive before mounting between steel plates and the arrangement of bolts as presented in the Fig. 3 is used. All specimens were made as a one-sided anchorage and the free ends of strip were protected by aluminium plates and placed in the jaws of the testing machine (Fig. 4).

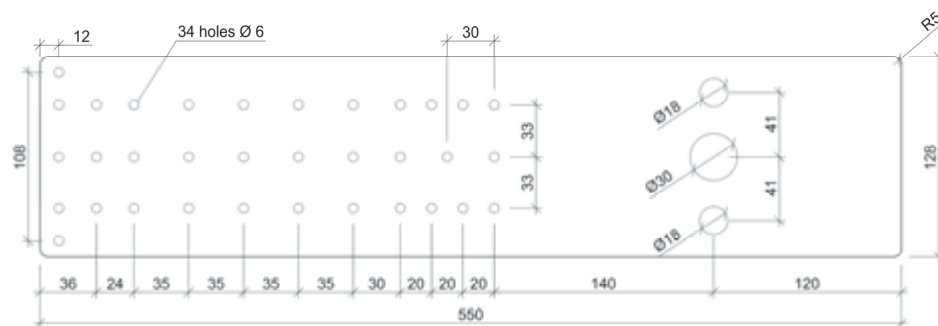


Fig. 3: Final arrangement of the holes in the anchorage



Fig. 4: Anchorage specimen view

The anchorage specimens were subjected to axial tensile test in testing machine Instron J1D 1200 kN. The tests were conducted under displacement control at a rate of 2 mm/min. During the tests increment of force and displacement were measured. The measurement of these values was provided by using the set of sensors built in the testing machine.

Fig. 5 shows the load – displacement plots for the maximum value of the failure force of each series. Thanks to successive modifications in manufacturing anchorages the noticeable increase of failure force was obtained. Still development of anchoring technology for followed specimens allowed to obtain value of failure force of almost 200 kN in the last two series. Variability coefficients equal to 1.7% and 0.4% in the last two series indicate that the tested anchorage specimens had a high level of homogeneity. The collected results of static tests were presented in Tab. 1. The value of the failure force is applied to establish the efficiency of the anchorages defined as ratio of maximum failure force of the anchorage to the CFRP characteristic tensile strength (force), which is 276 kN for the UHS 614 CFRP strips. Thanks to applied modifications repeatable anchorage efficiency higher than 70% could be obtained. It is a sufficient value for post-tensioning system for strengthening concrete structures because optimal strengthening effects are obtained with strip prestressing level equals about 60% of CFRP tensile strength (Meier, 1995).

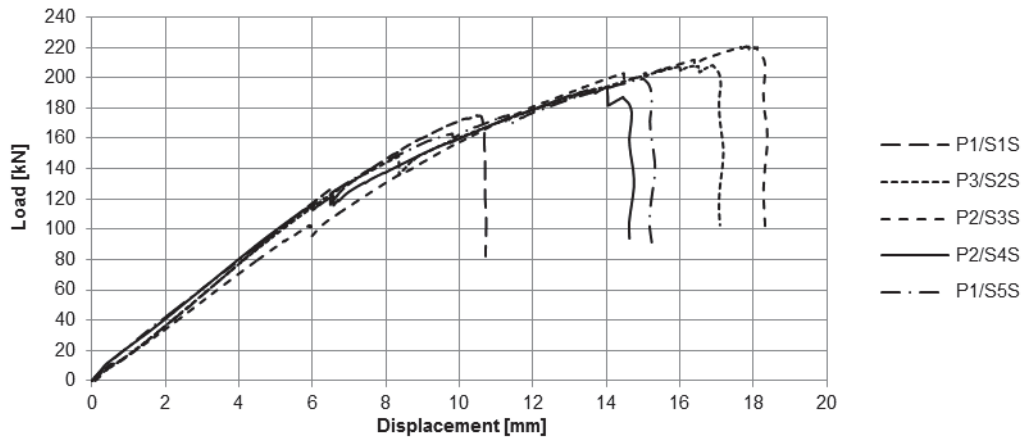


Fig. 5: Maximum load – displacement plots for five series

Tab. 1: Collective testing results of five series of anchorages

Series No.	Failure load of each specimen:			Mean failure load	Standard deviation	Variability coefficient	CFRP efficiency
	P1	P2	P3				
	[kN]	[kN]	[kN]	[kN]	[kN]	[-]	[-]
S1S	175	174	166	171	5,2	3,0%	62%
S2S	147	161	208	-	-	-	-
S3S	177	221	-	199	31,3	15,7%	72%
S4S	189	194	188	190	3,2	1,7%	69%
S5S	199	198	-	199	0,8	0,4%	72%

4. TESTS OF STRENGTHENED RC BEAMS

In order to verify of system efficiency tests on the strengthened reinforced concrete beams were conducted. Beams had a rectangular cross-section with dimensions of 0.50×0.42 m and 6.0 m length. They were made of C45/55 concrete and B500SP steel. Longitudinal reinforcement bars were the 25-mm-diameter and stirrups the 12-mm-diameter. The scope of the study included six beams. The first of them was the reference beam (B1). The second beam (B2) was strengthened with two CFRP strips with dimensions of 60×1.4 mm, which were passively glued to beam's tensioned surface. The third beam (B3) was strengthened with the same strips but additionally anchored by system anchorages. The next three beams (B4-B6) were strengthened with pre-tensioned strips with various prestressing level and anchored by system anchorages (Tab. 2).

Tab. 2: Specification of tested beams

Beam	Prestressing level	Prestressing force	Initial CFRP strain	Initial CFRP stress	Anchorage
	[-]	[kN]	[-]	[MPa]	[-]
B1	-	-	-	-	-
B2	-	-	-	-	No
B3	0% f_{tu}	-	-	-	Yes
B4	30% f_{tu}	81	6,0‰	960	Yes
B5	40% f_{tu}	108	8,0‰	1280	Yes
B6	50% f_{tu}	134	10,0‰	1600	Yes

f_{tu} – CFRP tensile strength (for the Neoxeplate UHS 614 strips $f_{tu}=3200$ MPa)

The studies were conducted on a special test stand. The span length of beams was 5.6 m. Loading was carried by a hydraulic actuator Instron Schenck with maximum pressure force 630 kN. Four point bending scheme was applied by means of spreading the load from the actuator by steel traverse beam. During the tests continuous measurement of load, displacements of beams, strains of upper and lower surfaces of concrete and steel bars in the constant bending moment range, as well as strains along CFRP strips, were measured. In the subsequent steps of loading cracking of concrete was controlled. The failure modes were checked and identified in detail.

The results of beam tests were collected in Tab. 3. For each beam values of cracking, yielding and ultimate load as well as strengthening efficiency were noted. The strengthening efficiency is defined as ratio of increase of ultimate load of strengthened beam to ultimate load of reference beam. The ultimate load is defined as the maximum value of bending moment occurred during the test. In the strengthened beams ultimate load is connected with failure of strengthening system. Moreover, in the table maximum CFRP strains at failure and CFRP utility level were given. CFRP utility level is ratio of maximum stress occurred in CFRP strip to ultimate strength of CFRP. In the last column ductility of the beams was presented. Ductility is calculated as ratio of deflection at failure to deflection at yielding.

Tab. 3: The results of tested beams

Beam	Cracking moment [kNm]	Yielding moment [kNm]	Ultimate moment [kNm]	Strengthening efficiency [-]	CFRP strain at failure [-]	CFRP utilization [-]	Ductility [-]
B1	55	266	272	-	-	-	1,84
B2	70	318	332	22%	5,9‰	30%	1,35
B3	72	321	361	33%	7,8‰	39%	2,78
B4	111	371	424	56%	15,8‰	79%	3,52
B5	120	394	415	53%	16,4‰	82%	2,17
B6	136	419	428	57%	16,7‰	84%	1,15

Strengthening of the beams caused increasing of cracking and yielding moment as well as ultimate moment. It influences the improving of serviceability parameters of beams: a reduction of deflection and cracking. Deflection reduction can be observed in Fig. 6, where load-deflection plots in the middle of span for each beam were presented.

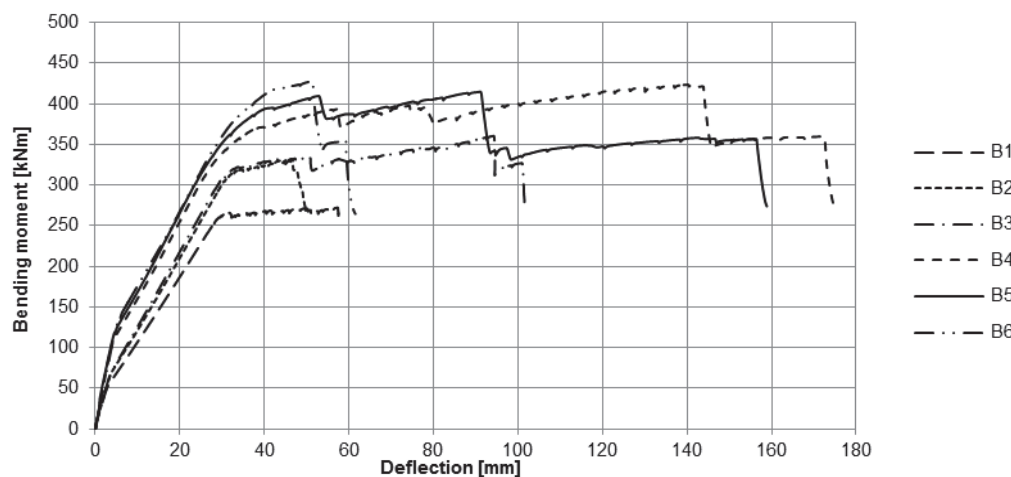


Fig. 6: Load – deflection plots for all tested beams

Beams strengthening by the passive strips resulted in a small reduction of deflection of the beams and increase of these ultimate load by 22% and 33% for beams B2 and B3 respectively. The usage of the anchorages in beam B3 effects on appearance of additional, emergency phase of work (after debonding up to failure). The anchorages caused increasing the ultimate load of 9% compared to beam without anchorages, increasing the CFRP utilities level and changing the failure mode. Thanks to the use of tensioned CFRP strips ultimate load of tested beams was increased about 55% in relation to reference beam. Value of ultimate load was similar for each prestressed beam. Prestressing level has therefore no important effect on increase of ultimate carrying capacity. However, it significantly affects the yielding moment (Tab. 3) and ductility of the beams. With increasing prestressing level increases the value of yielding moment. Increase of this value compared to reference beam was 39% and 58% for beams B4 and B6, respectively. Beams with higher prestressing level exhibited lower ductility. It is connected with behaviour of beam during failure. When the prestressing level is higher, then failure is more abrupt. Failure mode of each prestressed beam was similar. Failure was caused by debonding of CFRP strips from concrete surface followed by slipping from anchorages. In certain cases slipping CFRP strips from anchorages was accompanied by CFRP failure.

The most important results from the point of view of strengthening system are significant increase of ultimate load (strengthening efficiency about 55%) and improving of serviceability: reduction of deflection and cracking. The system is characterized by a high level of utilization of the composite material. In the prestressed beams utilization of CFRP strips was about 80%. The results of the tests of beams, strengthened by Neoxe Prestressing System II, confirm generally known conclusions about the behaviour of reinforced concrete beams strengthened with prestressed CFRP strips. Therefore, they proved that the new system works properly.

5. APPLICATION ON-SITE

The last stage of research on the new strengthening system was practical on-site application at the existing RC bridge. The bridge is simply supported beam with cantilevers. The length of the middle span is 16.0 m and the length of both cantilevers is 5.5 m. Superstructure consists of four main RC beams braced by crossbeams and deck slab, all of them cast monolithically. The girders have a rectangular cross section with dimensions of 0.5×1.2 m. An angle between longitudinal axis of the bridge and the river is 50°.

In order to increase the bridge carrying capacity, the strengthening by prestressed CFRP strips of main RC beams in tension regions was designed. The strips were located at the bottom surfaces of beams in the main span and at the top surfaces of slab deck above beams over the supports and in the cantilevers. The location of strips in both cross-sections was presented in Fig. 7. Each strip was tensioned with force of 75 kN, which corresponded to strains equal about 5.6‰. A total of 48 CFRP strips were used to strengthen of the bridge.

The strips with the anchorages were prepared at the factory and delivered for the construction site in a bobbins. Installation was started following preparation of concrete and strips surfaces. For each strip at first passive anchorage was mounted to the concrete surface, then the tensioning device was installed at active side, adhesive was applied on the CFRP strip and the strip was tensioned up to designed value of prestressing force. After tensioning, active anchorage was mounted and the tensioning device could be removed. In the last step strip was pressed to the concrete surface and excess of adhesive was removed.

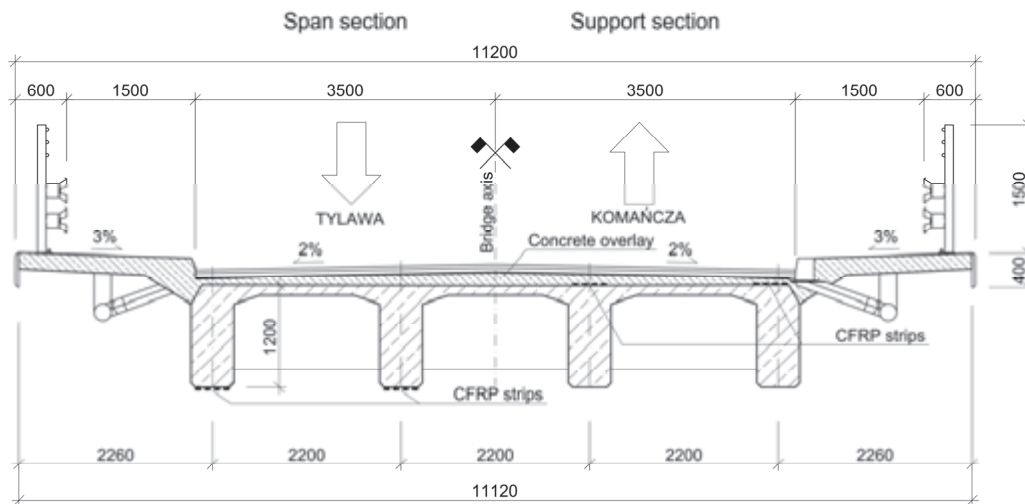


Fig. 7: Cross-section of strengthened bridge

The bridge was subjected to static load tests before and after strengthening works. The aim of the test was to evaluate the efficiency of strengthening the existing RC bridge using the NPS II system. During the tests beam's deflection in the middle span were measured along with strains of concrete, reinforcing bars and CFRP strips in the middle section of the span. Two trucks with a weight of 38 tons each were used for the tests.

There were no significant changes of the beam deflections due to strengthening with prestressed strips. The deflection in the first stage (performed before strengthening) and the second stage (after strengthening) was equal to 2.0 and 1.8 mm for beam B1 (outer) and B2 (inner) respectively. Such a result could be expected, because strengthening of RC beams (with quite large cross-section) by CFRP strips has negligible effect on their stiffness. The strip in fact cannot improve beam's moment of inertia and thus the stiffness of the beam. No reduction of beam deflection could be explained by the fact that the capacity utilization of the beams under applied load was very small. The beams were not cracked and in I phase of RC beam work the deflection change may be imperceptible. However, inducing a larger utilization of the beams was unreachable due to bridge geometry (span length of 16.0 m and angle 50°). The detailed analysis of the results was performed by comparison of the strains (stresses) measured under load. The effectiveness of the strengthening of the bridge beams can be checked based mainly on reducing the stress in the reinforcing steel. The mean value of tensile stress in the steel reinforcement bars obtained in the first stage was on average 28.3 MPa. In the second stage this stress was reduced to 21.8 MPa. Therefore, the average reduction of the stresses in the reinforcing steel due to strengthening was equal 23%.

The test results indicate that despite a slight utilization of the beam's carrying capacity, it was possible to observe the effects of the strengthening. In the second stage, after beams prestressing by the CFRP strips, there were significantly lower stresses in reinforcing bars than before strengthening. Moreover, strains noted in CFRP strips indicate that the strips were effectively incorporated into the cooperation in carrying loads. Based on the results it can be concluded that the strengthening of the bridge by NPS II system was performed properly, and its use was quite effective (at least at the expected level). The installation of the strips on the bridge was performed very efficiently. All elements of the system, both anchorages and tensioning device, passed the exam on the construction site. Strengthening was carried out at a rate of approximately 4 strips daily.

6. CONCLUSIONS

The new Polish CFRP prestressing system for strengthening reinforced concrete structures was shortly presented in the paper. After examination on RC beams in the laboratory and practical application on-site the system is ready to use for strengthening purposes.

Comparing the NPS II system to another CFRP prestressing solutions available on the market authors observe the following advantages of the new system thanks to applied strip anchorage method:

- the method comprises adhesive bonding with bolt gripping and friction action and thus sums up the advantages of these three joining methods;
- effects of prestressing are transferred to the strengthened structure just after mounting of active anchorage, without need to wait for adhesive curing;
- anchorages are mounted in factory and fully tested before delivering to construction site;
- geometry of steel anchorages can be designed to suit existing rebar layout and strip type;
- cutting the grooves in concrete is not required with this method;
- the method eliminates risk of the strip slippage during strengthening on-site and guarantees constant strip tension during setting of adhesive.

7. REFERENCES

- Andrä, H. P. and Maier, M. (2000), "Post-strengthening with Externally Bonded Prestressed CFRP Strips". In IABSE Congress Report, Vol. 16, No. 7, pp. 1507-1514.
- Aslam, M., Shafiq, P., Jumaat, M. Z. and Shah, S. N. R. (2015), "Strengthening of RC Beams Using Prestressed Fiber Reinforced Polymers – a Review", *Construction and Building Materials*, Vol. 82, pp. 235-256.
- Berset, T., Schwegler, G. and Trausch, L. (2002), "Verstärkung einer Autobahnbrücke mit vorgespannten CFK-Lamellen", *tec21*, Vol. 128, No. 22, pp. 27-29.
- Haghani, R., Al-Emrani, M. and Kliger, R. (2015), "A New Method for Strengthening Concrete Structures Using Prestressed FRP Laminates", In: Saha, S., Lloyd, N., Yazdani, S. and Singh, A. (ed.), *Implementing Innovative Ideas in Structural Engineering and Project Management*, ISEC Press.
- Łagoda, M. (2004), "Element Strengthening by Stressed Composite Strip – an Example of Experimental Investigation", *Archives of Civil Engineering*, Vol. 50 No. 4, pp. 599-623.
- Meier U. (1995). "Strengthening of structures using carbon fibre/epoxy composites", *Construction and Building Materials*, Vol. 9, No. 6, pp. 341-351.
- Michels, J., Sena-Cruz, J., Czaderski, C. and Motavalli, M. (2013), "Structural Strengthening with Prestressed CFRP Strips with Gradient Anchorage", *Journal of Composites for Construction*, Vol. 17, No. 5, pp. 651-661.
- Siwowski, T., Michałowski, J. and Błażewicz, S. (2010), "The New CFRP Prestressing System for Strengthening Concrete Structures", *Inżynieria i Budownictwo*, Vol. 66, pp. 152-156 (in Polish).
- Suter, R. and Jungo, D. (2001), "Vorgespannte CFK-Lamellen zur Verstärkung von Bauwerken", *Beton- und Stahlbetonbau*, Vol. 96, No. 5, pp. 350-358.

NON-METALLIC REINFORCEMENTS WITH DIFFERENT MODULI OF ELASTICITY AND SURFACES FOR CONCRETE STRUCTURES

Sándor Sólyom, Anna Szijártó and György L. Balázs

Department of Construction Materials and Technologies, Budapest University of Technology and Economics

1111 Budapest, Műegyetem rkp., 3, Hungary

solyom.sandor@epito.bme.hu, balazs.gyorgy@epito.bme.hu

SUMMARY

The use of Fibre Reinforced Polymer (FRP) bars as internal reinforcement for concrete structures is increasing in civil engineering, due to their advantageous properties, e.g. being insensitive to electrolytic corrosion. In this paper two experimental studies are presented, investigating the bond development of FRP bars. The first series aimed to study the effect of modulus of elasticity of FRP bars on the bond behavior with concrete. Two types of FRP bars were used with similar properties (surface and diameter), but with different modulus of elasticity. Four different concrete compositions were prepared. The second series meant to study the effect of surface characteristics of FRP bars. Three types of GFRP bars were used with the same nominal diameter of 16 mm and similar tensile strength and modulus of elasticity, however with different surface characteristics: sand coated and two types of indented surfaces.

1. INTRODUCTION

Over the last centuries steel reinforced concrete was the most widely used structural material in construction. Nevertheless, it is well known that, under certain environmental conditions, the corrosion of steel reinforcement can lead to the deterioration or even to the collapse of structural elements, requesting expensive repairing and strengthening. This detrimental property of the steel reinforcement directed the interest on alternative reinforcing materials (Cosenza et al., 1995; Focacci et al., 2000; Lublók et al., 2005; Guadagnini et al., 2004; Balázs, 2008; Račić et al., 2015; Veljković et al., 2017).

Using FRP material can be one possible way to replace the corrodible steel reinforcement. FRP bars have various advantageous properties, such as high tensile strength and resistance to electrochemical corrosion.

To manufacture FRP bars different fibres (glass, carbon, aramid and recently basalt) are used. Fibres are bound together with diverse resins (polyester, vinyl ester and epoxy). Mechanical properties as well as their surface characteristics of FRP rebars can be considerably different from that of the conventional steel reinforcements. Such non ferrous rebars provide excellent resistance to environmental factors such as freeze-thaw cycles, chemical attack etc.

Tensile strength and elastic modulus of FRP bars are governed mainly by the type of fibre, the volumetric ratio of fibres (usually 60-70 V%) and the angle between the fibres and the longitudinal axis of the rebar. Tensile strengths of FRP rebars are in the range of 450 to 3 500 N/mm², between 35 000 and 580 000 N/mm² in terms of Young's moduli and in the range

of 0.5 to 4.4% in terms of failure strains (fib, 2007). Furthermore, the mechanical and physical properties of FRP bars can be tailor made to fit any specific application the best. The most important difference between FRP and steel rebars is that FRP bars have linear elastic behavior up to failure without any plasticity and considerable release of elastic energy (fib, 2007).

There are many examples of structural applications indicating the speed and convenience of strengthening and repairing of concrete structures using advanced composites as cost effective solutions (Balázs and Borosnyói, 2001b). Furthermore, there are structures reinforced with FRP rebars that have been in service in aggressive environments in various parts of the world for more than 20 years, without considerable structural problems (Nanni et al., 2014).

One of the fundamental aspects of structural behavior of RC elements which are reinforced with FRP bars is the bond development. The bond stress transfer between reinforcement and the surrounding concrete is the basis of the theory of reinforced concrete (Robert and Benmokrane, 2010; Borosnyói, 2014). Without a proper transfer of stresses between concrete and rebar, reinforced concrete structures would not be viable (Balázs and Borosnyói 2001a; fib 2007; Baena et al., 2009). This paper presents two experimental series to study the bond behavior of FRP bars in concrete.

Bond strength calculation in CSA S806-12

In CSA-S806-12 (CSA, 2012) the following equation (Eq. 1) is proposed for bond stress calculation, that takes into account different factors:

$$\tau_{b,max} = \frac{d_{cs} \sqrt{f'_c}}{1.15(k_1 k_2 k_3 k_4 k_5) \pi d_b} \quad (1)$$

where: k_1 - bar location factor, k_2 - concrete density factor, k_3 - bar size factor, k_4 - bar fibre factor, k_5 - bar surface profile factor, d_{cs} - the smaller of the distance from the closest concrete surface to the center of the bar being developed; or two-thirds of the center-to-center spacing of the bars being developed, f'_c - compressive strength of concrete, d_b - nominal diameter of FRP.

The recommended values for k_4 parameter are: 1.0 for CFRP and GFRP; 1.25 for AFRP bars. The proposed values for k_5 parameter are: 1.0 for surface-roughened or sand-coated surfaces; 1.05 for spiral pattern surfaces; 1.0 for braided surfaces; 1.05 for ribbed surfaces; 1.80 for indented surfaces.

Based on authors' previous experimental studies and available data in literature from various researchers, the proposed values seem to be not totally appropriate in all cases. Present study has directed to verify and if needed to propose new values of k_4 and k_5 parameters, based on the experimental results.

2. EXPERIMENTAL PROGRAM

Pull-out test was chosen to compare the bond behavior of different FRP rebars in various concrete compositions. Although, the stress condition developed in concrete during pull-out tests can differ from that developed in reinforced concrete elements, pull-out test is a powerful method to study and compare the effect of diverse factors on bond behavior, owing to its simplicity and ease of application.

150 mm edge length, metallic cubic molds were used to produce the pull-out specimens. The bars were vertically placed in the molds as that the bond length of rebars was in the lower part of the molds. Concrete was poured with the FRP bars in position inside the mold. After concreting, the specimens were kept in the molds in laboratory ambient condition for one day. Thereafter, the concrete cubes were stripped, marked and placed under water for 6 days. After this period of time the concrete specimens were taken out of water and kept under laboratory ambient conditions until testing.

In Fig. 1 (left) the rebars are presented with the prepared embedment (bond) length, being five times the rebar diameter (5ϕ) in all cases. In Fig. 1 (right) a photo of the pull-out test setup is visible. The FRP bars are placed into a metal frame and gripped into testing machine (lower part of the pictures). This part is considered as the loaded end of the concrete test specimen and the relative displacement between the FRP rebar and concrete is measured with three Linear Variable Differential Transducers (LVDT). At the other end, which is usually referred to as free end, the slip is measured with one LVDT.

The pull-out tests were performed by using a servo-hydraulic testing machine with a capacity of 600 kN. Displacement control was selected to capture post-peak behavior. The load was applied at a rate of 1 mm/min and measured with the electronic load cell of the testing machine. An automatic data acquisition system was used to record the data transmitted by LVDTs. Three nominally identical specimens for each configuration were tested (Sólyom and Balázs, 2016).

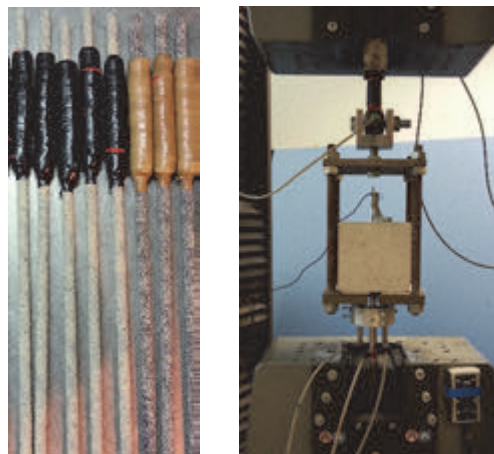


Fig. 1: Left: CFRP and GFRP bars prepared with 5ϕ embedment length. Right: pull-out test setup

Two different experimental series were performed and described herein. The first series aimed to study the effect of modulus of elasticity of FRP bars on the bond behavior in concrete.

Two types of FRP bars were used in current experimental work. They have similar properties (sand coated surface, 9.5 mm in diameter), however owing to the different fibre types (carbon and glass) their modulus of elasticity and tensile strength differs. Manufacturer's specification of the FRP bars include a minimum guaranteed tensile strength of 880 MPa for Glass Fiber Reinforced Polymer (GFRP) and 1356 MPa for Carbon Fiber Reinforced Polymer (CFRP) and a nominal tensile modulus of elasticity of 42.5 GPa for GFRP and 127 GPa for CFRP respectively (VRod, 2013).

Four different concrete compositions were prepared (symbols: C1, C2, C3 and S1). The mean value of the concrete properties at the day of testing (28 days) varied from 40.3 to 67.2 MPa in regards of compressive and 2.91 to 4.13 MPa in regards of tensile splitting strength. The values were obtained by testing three similar specimens (150 mm cubes and both in diameter

and height 150 mm cylinders, respectively). C1 concrete composition gave the lowest concrete strength, while S1 provided the highest. C stands for traditional, whereas S represents self-compacting concrete.

The second series meant to study the effect of surface characteristics of FRP bars on the bond behavior in concrete.

Three types of GFRP bars were used in current experimental work. They have the same nominal diameter (16 mm), characteristic tensile strength over 1000 MPa and a modulus of elasticity between 55-60 GPa (Schöck, 2013). However, they possess different surface characteristics: sand coated and two types with indented surface.

C2 concrete composition (47.2 MPa compressive and 3.40 MPa splitting tensile strength, respectively) was used to prepare the concrete for the second series.

3. RESULTS AND DISCUSSION

Experimental results are summarized in Tab. 1 to Tab. 3, including the individual and the mean of individual bond strength values, the loaded and free end slips at maximum bond stress, as well as standard deviations and coefficient of variations for the previously mentioned properties. The bond stiffness is also presented in the last column. In particular, each of the individual bond strength values ($\tau_{b,max}$) are calculated by dividing the maximum load (F_{ult}) by the sheared surface (Eq. 2), considering a uniform bond stress distribution along the bond length (l_b) of the FRP bars.

$$\tau_{b,max} = \frac{F_{ult}}{\pi \cdot \phi \cdot l_b} \quad (2)$$

3.1. Effect of modulus of elasticity of FRP bars on bond behavior in concrete

CFRP and GFRP bars (Fig. 1 left) were used to study the effect of modulus of elasticity of FRP bars on bond behavior. FRP bars had similar properties (such as 9.5 mm diameter and sand coated surface characteristics) but the moduli of elasticity differed due to the different fibre types.

Tab. 1: Pull-out test results, CFRP SC #3 (Ø10) bars

Symbol	Bond strength				Loaded end slip				Free end slip				Bond stiffness	
	$\tau_{b,max}$	Average	St.Dev	Coef. of Variation	Slip	Average	St.Dev	Coef. of Variation	Slip	Average	St.Dev	Coef. of Variation		
	[MPa]	[MPa]	[MPa]	[%]	[mm]	[mm]	[MPa]	[%]	[mm]	[mm]	[MPa]	[%]	[N/mm ²]	
C1	1	19.82			0.261				0.130				82.61	
	2	20.25	19.31	1.27	6.58%	0.196	0.234	0.034	14.50%	0.112	0.100	0.038		38.16%
	3	17.86				0.245				0.057				
C2	1	14.30			0.163				0.038				60.18	
	2	17.29	15.57	1.54	9.90%	0.213	0.259	0.125	48.13%	0.054	0.051	0.011		22.45%
	3	15.14				0.400				0.060				
C3	1	12.60			0.291				0.067				65.15	
	2	19.30	15.95	4.74	29.72%	0.199	0.245	0.065	26.50%	0.062	0.065	0.004		5.48%
S1	1	16.47			0.358				0.036				62.58	
	2	15.25	16.30	0.97	5.98%	0.254	0.260	0.095	36.43%	0.039	0.038	0.002		5.43%
	3	17.18				0.169				0.040				

Owing to the size of pull-out specimen, the centric placement and diameter of the FRP bars, bond failure always happened by “pull-out” of the FRP bar, no splitting cracks were observed. The bond failure in most of the cases was brittle at relatively low slip values, by interlaminar shear failure at the surface between fibres and sand coating. However, for higher strength concrete compositions in case of GFRP bars, bond failure happened also through gradual pull-out of the bars, reaching high slip values.

In Fig. 2 it can be observed that CFRP bars have higher bond strength regardless the concrete mix or type. The ratio between bond strength of CFRP and GFRP sand coated bars varies between 1.22 and 1.70. Furthermore, the bond stiffness of CFRP bars are always higher (about double) than in case of GFRP bars (Tab. 1 and Tab. 2). The bond stiffness is defined by calculating the inclination of the ascending branch of the bond stress-slip diagram (which was assumed linear) considering the loaded and slip diagrams. This can be particularly important in Serviceability Limit State (SLS) design, since crack opening is dependent on the slip value associated to the bond stress level.

Higher bond strength values associated with higher modulus of elasticity can be explained with the fact that higher modulus involves less elongation at the loaded end of the bond length, consequently lower will be the damage at the bond surface, which can result in higher average bond strength.

Tab. 2: Pull-out test results, GFRP SC #3 (Ø10) bars

Symbol	Bond strength				Loaded end slip				Free end slip				Bond stiffness
	$\tau_{b,max}$	Average	St.Dev	Coef. of Variation	Slip	Average	St.Dev	Coef. of Variation	Slip	Average	St.Dev	Coef. of Variation	
	[MPa]	[MPa]	[MPa]	[%]	[mm]	[mm]	[MPa]	[%]	[mm]	[mm]	[MPa]	[%]	[N/mm ³]
C1	1	12.87			0.397				0.038				
	2	18.85	14.11	4.26	30.21%	0.566	0.406	0.156	38.34%	0.134	0.075	0.052	69.45%
	3	10.60				0.255				0.052			
C2	1	9.54			0.255				0.040				
	2	8.30	9.16	0.74	8.08%	0.188	0.256	0.069	27.03%	0.022	0.026	0.012	48.04%
	3	9.63				0.326				0.016			
C3	1	8.21			0.238				0.034				
	2	17.86	13.03	6.82	52.33%	0.509	0.374	0.192	51.36%	0.074	0.054	0.028	52.38%
S1	1	9.24			0.297				0.044				
	2	12.70	10.97	2.44	22.26%	0.296	0.297	0.001	0.20%	0.070	0.057	0.018	32.25%

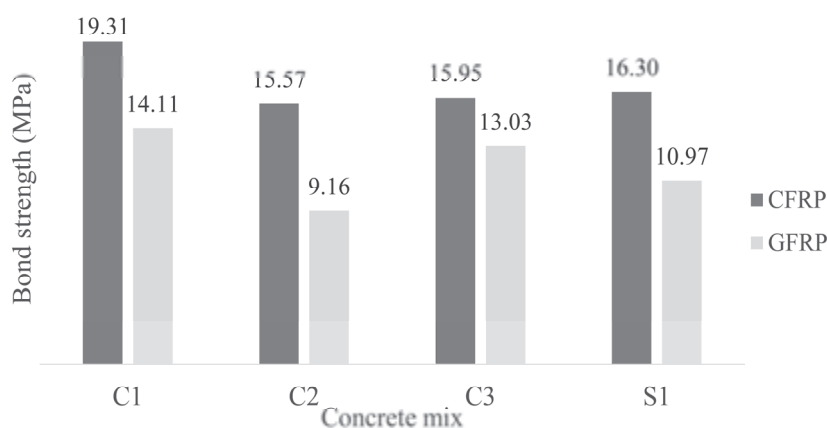


Fig. 2: Effect of modulus of elasticity of FRP bars (CFRP: 127 GPa, GFRP: 42.5 GPa, with same diameter, surface pattern and producer) on bond strength in concrete

3.2. Effect of surface characteristics of FRP on bond behavior in concrete

The surface of FRP bars can be considerably different from that of steel, furthermore, mechanical properties are different also. Various surface types involves different bond mechanisms and failure modes. While in case of steel bars bond failure happens by crushing the concrete in front of the ribs, this is usually not the case for FRP bars. Bond failure can happen either at the surface of FRP and concrete, or inside the FRP (interlaminar shear between fibres and outer surface) (*fib*, 2007).

Results of the experimental work, performed to study the effect of surface characteristics (sand coated and two types of indented surface finishing) are summarized in Tab. 3. Furthermore, for better visualization the bond characteristics of GFRP bars, with different surface characteristics are presented in terms of bond strength values (Fig. 3) and bond stress-slip diagram (Fig. 4) as well.

The ratio between the bond strength of GFRP sand coated and differently indented bars varies between 1.22 and 1.88. Furthermore, the bond stiffness of GFRP bars also varies depending on the surface characteristics.

Bond failure happened through pull-out of the FRP bar in case of centrally placed bars (Fig. 3 right), however, when the bars were placed eccentrically to the concrete cover $1\varnothing$ (bar diameter) splitting failure was observed (Fig. 3 left). Furthermore, bond failure mode was significantly affected by the surface type: sand coated bars failed in a brittle manner at low slip values, while indented bars failed in a gradual manner. In terms of bond strength, highest values were reached when sand coated bars are considered (Fig. 3).

In case of sand coated bars, the surface of the FRP bars sheared off, while the concrete failed in case of indented bars (owing to the geometry of the FRP indentation).

Tab. 3: Pull-out test results, GFRP sand coated and indented 16 mm diameter bars

Symbol	Bond strength				Loaded end slip				Free end slip				Bond stiffness	
	$\tau_{b,max}$	Average	St.Dev	Coef. of Variation	Slip	Average	St.Dev	Coef. of Variation	Slip	Average	St.Dev	Coef. of Variation		
	[MPa]	[MPa]	[MPa]	[%]	[mm]	[mm]	[MPa]	[%]	[mm]	[mm]	[MPa]	[%]	[N/mm ³]	
Sand c.	1	23.24			0.718				0.266					
	2	22.36	23.01	0.57	2.47%	0.545	0.638	0.088	13.71%	0.256	0.247	0.024	9.78%	36.05
	3	23.43				0.652				0.220				
Indented 1	1	20.02			0.581				0.317					
	2	17.69	18.91	1.17	6.18%	0.473	0.606	0.148	24.38%	0.252	0.319	0.068	21.32%	31.19
	3	19.03				0.765				0.388				
Indented 2	1	11.21			1.138				0.957					
	2	11.84	12.25	1.29	10.53%	1.138	1.198	0.103	8.59%	0.957	0.917	0.069	7.49%	10.23
	3	13.69				1.316				0.838				

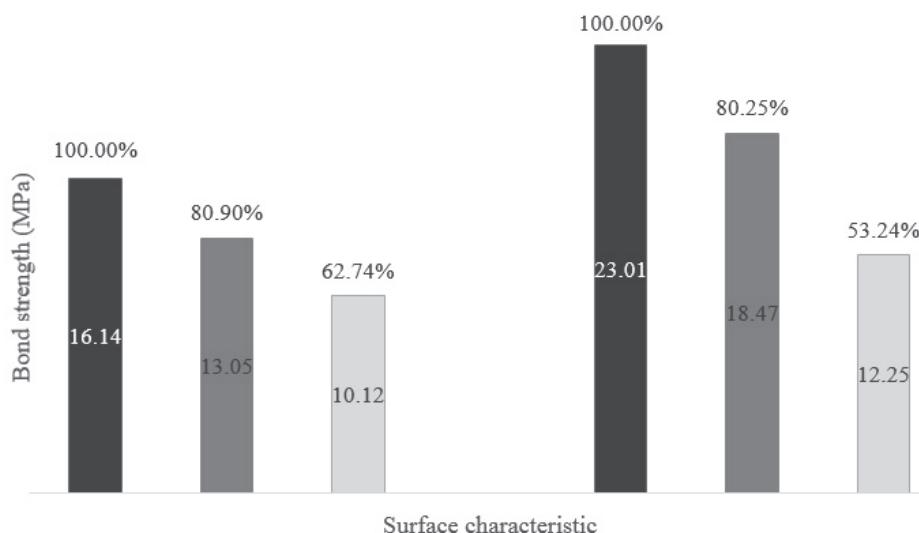


Fig. 3: Effect of surface characteristics of GFRP bars on bond strength. Eccentric (left) and centric (right) pull-out tests. Surface types from left to right: sand coated; indented type 1 and indented type 2

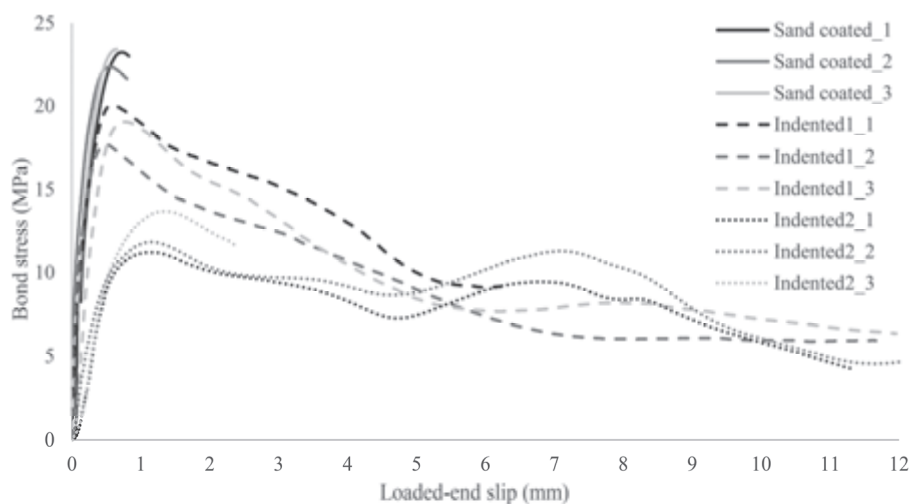


Fig. 4: Bond stress-slip diagrams for GFRP bars with different surfaces

4. CONCLUSIONS

This paper presents two experimental series to study the bond behavior of CFRP and GFRP bars in concrete, focusing on the effect of two factors: modulus of elasticity and surface characteristics of FRP bars, respectively. Different concrete compositions and different FRP bars (See Ch. 2) have been used in the study. Based on the test results the following conclusions can be drawn.

Effect of modulus of elasticity

- Bond strength was always higher for the bars with higher modulus of elasticity (CFRP). It highlights the importance of the need for revision of parameters proposed to take into account the effect fibre type of FRP bars in available guidelines (i.e.: k_4 in CSA S806-12).
- Bond stiffness is also affected by the modulus of elasticity of FRP bars, and it increases with the increase of E_f .

Effect of surface characteristics

- The bond strength of sand coated GFRP bars was higher than the ones for indented surfaces. Furthermore, bond strength was considerably different in case of two indented surface types. This leads to a conclusion that generalization of parameters taking into consideration only the surface type might not be straight forward. Subgroups within the same surface types might be necessary, or a standardized test method should be defined to be used for determination of such a parameter (i.e.: k_5 in CSA S806-12).
- The slope of the ascending branch (bond stiffness) of the bond stress-slip diagrams varies when similar FRP bars with different surface characteristics are used. However, the variation within the same surface type (with different finishing materials) can be even larger than among different surface types.
- Failure mode is affected by the surface characteristics. In case of sand coated bars the most common failure is through a sudden shearing off of the whole FRP surface, however in case of indented bars the bond failure happens by gradually pulling out the FRP bar reaching high slip values.

5. ACKNOWLEDGEMENTS

Authors gratefully acknowledge the financial support of European Union by Marie Curie ITN: European Network for Durable Reinforcement and Rehabilitation Solutions (endure), Grant: PITN-GA-2013-607851. The authors wish to thank to senior lecturer Dr. Tamás K. Simon for the help and advices. A part of the GFRP bars were provided by Schöck Germany, special thanks to Dr. André Weber.

6. REFERENCES

- Baena, M. et al. (2009) "Experimental study of bond behaviour between concrete and FRP bars using a pull-out test", *Composites Part B: Engineering*, 40(8), pp.784–797..
- Balázs, G.L. (2008), "Innovative materials and technologies for concrete structures", In *Betontag*. Wien: 24-25 April 2008, pp. 183–186.
- Balázs, G.L. & Borosnyói, A., (2001a), "Long-term behavior of FRP" *Int. Workshop Composites in Construction A Reality*.Capri, Italy: 20-21 July 2001, pp. 84–91.
- Balázs, G.L., Borosnyói, A. (2001b), "New construction materials in bridges", *Roads and Bridges in Europe*, 8th Int. Road Conference. Budapest-Esztergom: 21-23 May 2001.
- Borosnyói, A. (2014), "Use of corrosion resistant Fibre Reinforced Polymer (FRP) reinforcements for the substitution of steel bars in concrete"*Korróziósfigyelő*,54, pp.3–15.
- Cosenza, E., Manfredi, G., Realfonzo, R. (1995), "Analytical modelling of bond between FRP reinforcing bars and concrete", *Non-metallic (FRP) reinforcement for concrete structures*. London: E & FN Spon, pp. 164–171.
- CSA-S806-12 (2012), "Design and construction of building structures with fibre-reinforced polymers", Mississauga, Ontario, Canada: Canadian Standards Association.
- fib* (2007), "Bulletin 40: FRP reinforcement for RC structures", International Federation for Structural Concrete (*fib*).
- Focacci, F., Nanni, A., Bakis, C.E. (2000), "Local bond-slip relationship for FRP reinforcement in concrete",*Journal of Composites for Construction*, (February), pp.24–31.
- Guadagnini, M. et al. (2004), "Tests for the evaluation of bond properties of FRP bars in concrete", 2nd Int. Conf. on FRP Composites in Civ. Eng. (CICE 2004). Adelaide, pp.343–350.

- Lublóy, É. et al. (2005), "Bond of CFRP wires under elevated temperature", Bond Behaviour of FRP in Structures. 7-9 Dec. 2005, pp. 163–167.
- Nanni, A., De Luca, A., Zadeh, H. (2014), "Reinforced Concrete with FRP Bars", CRC Press - Taylor, Francis Group.
- Raicic, V. et al. (2015), "Behaviour of Deep Embedded FRP / Steel bars". SMAR 2015 - The 3rd Conf. on Smart Monitoring, Assessment and Rehab. of St. Antalya, Turkey, pp. 1–8.
- Robert, M., Benmokrane, B. (2010), "Effect of aging on bond of GFRP bars embedded in concrete", Cement and Concrete Composites, 32(6), pp.461–467.
- Schöck, 2013. "Schöck ComBAR Technical Information", Available at: <http://www.schoeck-combar.com/comb/download-combar1?type=7&filter=1>. Downloaded: June 2017.
- Sólyom, S., Balázs, G.L. (2016), "Influence of FRC on bond characteristics of FRP reinforcement", In 11th fib Int. PhD Symp. in Civil Engineering. Tokyo, J, pp. 271–278.
- Veljkovic, A. et al. (2017), "Concrete cover effect on the bond of GFRP bar and concrete under static loading", Composites Part B: Engineering, 124, pp.40–53.
- VRod (2013), "V-Rod standard straight bars", Available at: <http://www.vrodcanada.com/product-data/gfrp/v-rod-40gpa-gi-technical-specifications>. Downloaded: June 2017.

TOPIC 3
ADVANCED PRODUCTION AND
CONSTRUCTION TECHNOLOGIES

SMALL BRIDGES UP TO 32.5 M SPAN IN UHPC-CONSTRUCTION – BRIDGE SYSTEMS WITH AESTHETIC REQUIREMENTS

*Michael Olipitz
SDO ZT GmbH
Sporgasse 32/2/14
A-8010 Graz
E-Mail: olipitz@olipitz.com*

SUMMARY

Due to its durability and resource-conserving use, the UHPC building material is the ideal prerequisite for infrastructure construction. Due to the high degree of pre-fabrication, system bridges with spans of up to 35 m can be realized. The focus is on construction-specific design and the aesthetic shape language. In cooperation with the SDO ZT GmbH and the concrete precast elements manufacturer Franz Oberndorfer GmbH & CO KG, the bridge system construction is to be developed and implemented in three stages. The described system design attempts to make the enormous advantages of the material UHPC noticeable to the observer through material-compatible design. This development work is to contribute positively to the image of this new building material and to further applications.

1. GENERAL

Bridge systems, which are currently offered on the market by various manufacturers, are offered in the materials steel, aluminum and wood. Fig. 1 shows various bridge systems customary on the market. In addition to the material, the truss-like building block system represents the primary characteristic of these bridges.



Fig. 1: On the market available bridge systems with steel and aluminium

The present paper deals with the project idea, with the specifics in the prefabrication of the components, with the examples already carried out. It deals with system bridge development with ultra-high performance concrete (UHPC) and the special properties derived from the material in terms of material efficiency and durability. The idea and approach of this type of bridge has arisen through the implementation of an interesting solution of a UHPC-shell bridge (Olipitz, 2015 a) in Carinthia (Austria). Starting from this implementation, which essentially corresponds to the UHPC 325 type, simplifications were made in the manufacture and assembly, and a system bridge series UHPC 125, UHPC 225 and UHPC 325 were developed, whereby the combination of numbers always had the maximum achievable span L_{sp} (12.5 m, 22.5 m and 32.5 m) of this bridge type (Fig. 2 and Fig. 3). As the span widens, the type of prestressing and the geometrical stiffness are changed, resulting in high-slender and elegant designs. The bridge form is always an open bridge solution with 15 ° inclination of the UHPC-walls to the outside and on the other hand has the advantage that there are small heights of the constructions, on the other hand, the construction can be experienced by the user on the bridge and thus the performance of this material becomes noticeable. This first advantage also leads to the fact that due to the low constructional heights, no ramps on the abutments are required. Furthermore, the trough shape offers the advantage that the railing construction is an integral part of the load-bearing structure and is used for design purposes. In the case of the UHPC 325, the high slenderness can only be achieved by utilizing geometric stiffnesses from the shell-bearing effect. The system design allows modular construction with almost the same formwork geometry. This provides the prerequisite for mass production and competitiveness against conventional bridge systems. The static mode of operation is based on the principle of an arch-tie-model (Fig. 3) and can be ideally implemented by flat UHPC-boards in ideal combination with prestressing cables.

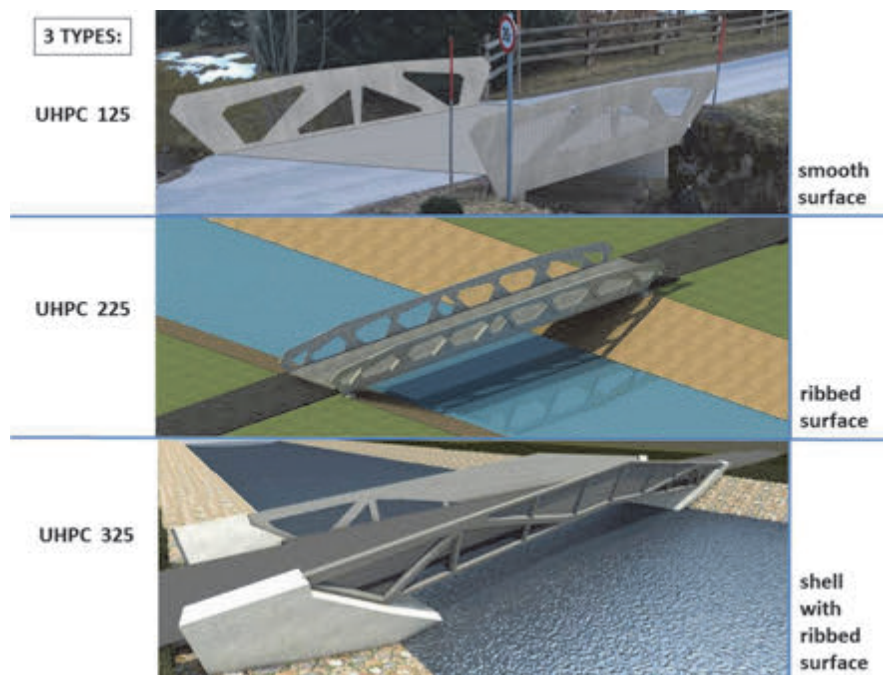


Fig. 2: UHPC bridge system series open bridges (trough shaped) with variable spans

The UHPC system bridges are characterized by the fact that they are integral bridge systems without bearings and transition structures, which avoids expensive maintenance parts. The increasing span leads to static measures of the UHPC-walls, which are reflected in the different shapes and assemblies. The type UHPC 125, which is designed up to a span of 12.5 m, has a plane-parallel surface (without ribs) with a thickness of 50 mm. The low wall

thicknesses are possible due to the favorable load-bearing capacity as an arch-tie-model. The openings are arranged in such a way that the printing sheet (see Fig. 3 in green) can be formed with slenderness ratio $L/H = 4$ to 8 . Only in the case of a span of more than 12.5 m, in the UHPC 225 type, ribs with a thickness of 100 mm arranged on the outer side of the UHPC walls are required, resulting in a total thickness of 150 mm. The rib arrangement follows the strut arrangement of a truss. The slenderness ratio of the truss are for this type $L/H = 7-13$. The arrangement of the bearing nose is identical to all three types on the inside of the UHPC-walls, which has a thickness of 100 mm and has a height of 300 mm for UHPC 125, and a height of 400 mm for UHPC 225 and UHPC 325. The roadway slaps (decking see subchapter 2.2 and 2.3) are placed on the inside of the bearing nose acting as support platform.

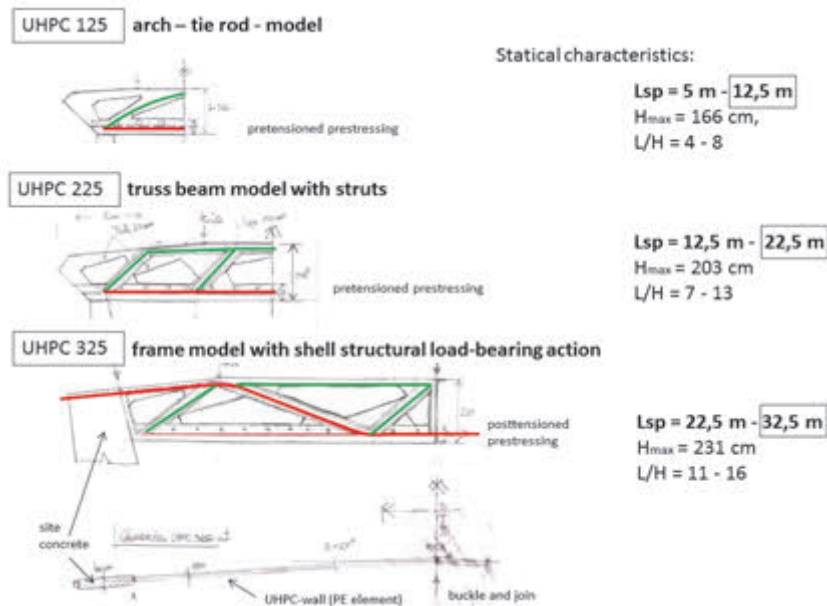


Fig. 3: Statical mode of functioning and exterior logic of the bridge system types

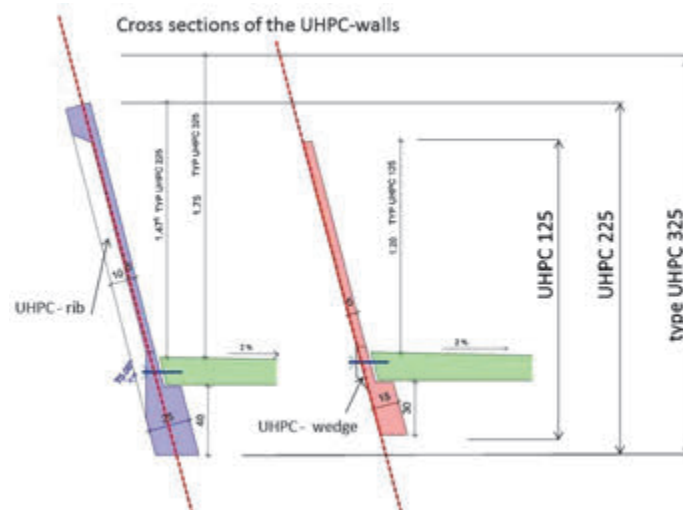


Fig. 4: Development of the cross sections per type

The ribs with a thickness of 100 mm arranged on the outside are executed with UHPC 225 and UHPC 325, the rib on the bottom flange of the UHPC-walls forming a fusion of the rib arranged on the outside and the bearing nose as base on the inside. The plane-parallel overall thickness of the bottom flange for these two types is 250 mm and is used for the

accommodation of the strands in the immediate bond (UHPC 225) or for the insertion of sheaths for the post-bond (UHPC 325). In the case of UHPC 325, the arrangement of the outer-side ribs corresponds to the static requirement of a frame support. The frame leg is made of a slab with in-situ concrete ($d = 40$ cm, see subchapter 3.1.) with a positive pitch, which is also used as a prestressing block for the load introduction of the pretension forces during assembly. The UHPC 325 consists of two UHPC-wall elements per longitudinal side which are subsequently joined together on the construction site by pretensioning over wet joints and successfully applied at the Paulifurt bridge (Olipitz, 2015 a). The buckle arranged in the plan view in the axis of symmetry with an angle of $\beta = 2.7^\circ$ leads to the positive mode of action of a space shell of the beam of frame. This ensures the buckling stability of the UHPC-walls. The slenderness ratios of the UHPC 325-walls are $L/H = 11-16$.

2. ELEMENTS OF THE BRIDGE SYSTEMS

In the following text the individual components of the system bridges, which are essentially repeated for all three types, are described. Chapter 3 discusses some special features of the UHPC 325 type. These are due to the changed static mode of operation and the multipart as well as for the UHPC walls and for the abutment situation.

2.1 UHPC-walls

As can be seen in Fig. 4, differences in the cross section between UHPC 125, UHPC 225 and UHPC 325 result in that the two at least mentioned types have additional reinforcing ribs arranged on the outer side according to the static requirement in the longitudinal direction (see fig. 3). The cubatures per meter ($[m^3/lm]$ per profile) are for UHPC 125 on average (o.a.) $0.08 m^3/lm$, for UHPC 225 o.a. $0.16 m^3/lm$ and for UHPC 325 o.a. $0.19 m^3/lm$. The material of the UHPC-walls is chosen for all types with C 130/155, whereby the fiber lengths should be $l_f = 12$ or 16 mm, respectively, in order to ensure post-fracture resistance of $\sigma_{cf,d} = 10$ to $14 N/mm^2$. The elements are only provided there with reinforcement, where tensile forces from lifting forces occur.

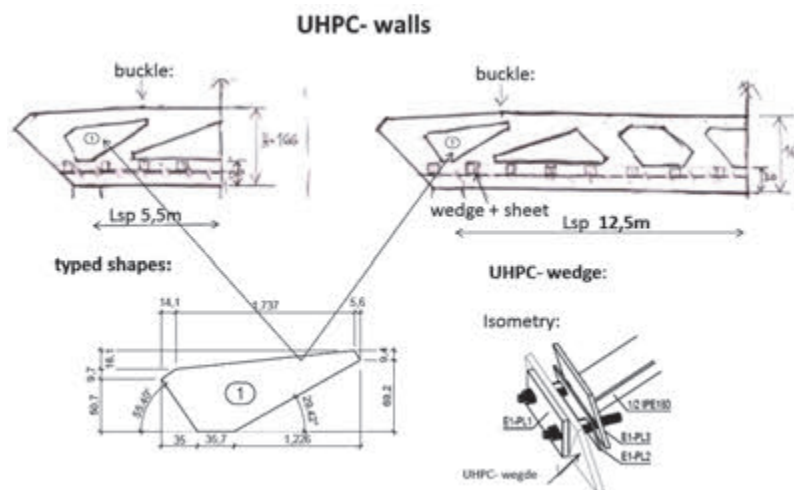


Fig. 5: UHPC-wall elements

The UHPC walls have a thickness of 50 mm outside the ribs and are provided with corresponding openings through the load flow. These opening geometries duplicate within one type, so that with a small number of typed shapes for frameworks, the opening is found

and can be accommodated flexibly into the formwork geometry for different bridge lengths L_w . The UHPC-elements are concreted in the vertical position, whereby the outer and inner surfaces have a smooth structure. Plan-parallel vertical formwork edges with distances of 150 mm (UHPC 125) and 250 mm (UHPC 225 and UHPC 325) allow simple manufacture in the factory. For the UHPC 125, specially shaped UHPC wedges are required due to the 15° inclined and smooth outer surfaces in the installed state for the attachment of the roadway elements (decking). This permits a horizontal arrangement of the screw position. The total number of UHPC-wedges or the built in parts for the mounting of the roadway boards results in a road width of $b = 3.5$ m with $n = 1.4$ pcs per m^2 of bridge area. For UHPC 225 and UHPC 325 types, UHPC-wedges are not required due to the vertical rib geometry in the region of the screws.

2.2 Decking elements

The roadway panels (Fig. 6) are full precast element parts with system widths of $b = 2.40$ m and are mounted on the system dependent supporting nose of the UHPC-walls. The roadway panels are bolted to the UHPC-walls, with the screwing joint at a distance of $e = 80$ cm. The road surface is with a roof-shaped drainage axis extending in the road axis, the plate thickness being in the roadway axis $d = 12$ cm and at the edges $d = 16$ cm. The quality of the concrete of the elements is C50/60. In order to ensure a steel connection, a ½ IPE 180 carrier is potted into the precast panel and is closed at both ends by a flange plate with welded threat nut.

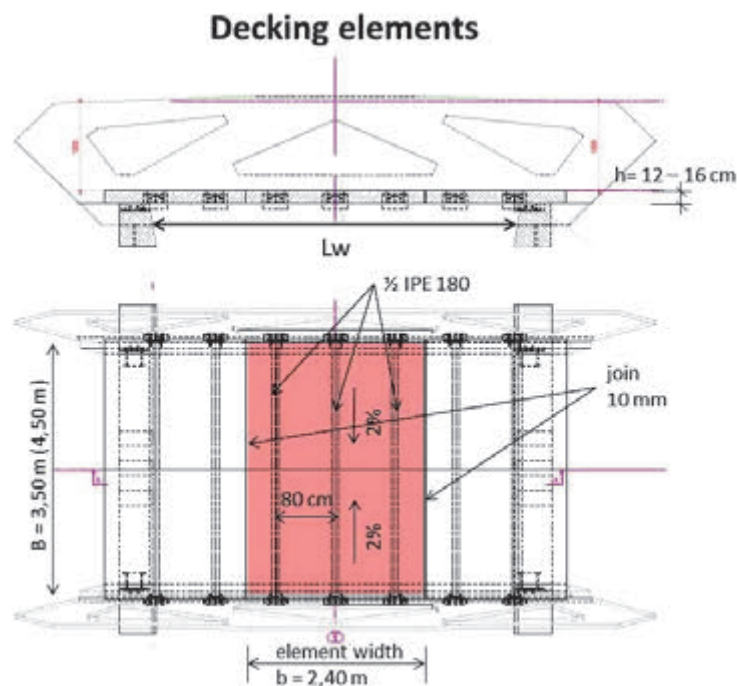


Fig. 6: Decking elements with HPC

In addition to the bridge length L_w (Fig. 6), the angle of intersection α between the abutment axis and the bridge axis can also be arbitrarily adapted. The angular adjustment is geometrically accomplished by longitudinally displacing a UHPC-wall side along the longitudinal axis of the bridge and leads to parallelogram-shaped roadway plate geometries. The axial dimension $e = 80$ cm of the bolted connection of the pavement panels with the UHPC-walls is maintained with an oblique-angled arrangement.

2.3 Abutment beam

The abutment beam (Fig. 7) is produced as a trapezoidal cross section with air inclination with concrete HPC 50/60. The task of the abutment beam consists, on the one hand, of establishing a rigid connection with the substructure, on the other hand, by means of specially provided built in parts, to ensure the stabilization of the UHPC-walls in the assembly process. For fixing the abutment beam with the substructure, sheaths for the grouting of steel mandrels $\varnothing 30$ mm are provided.

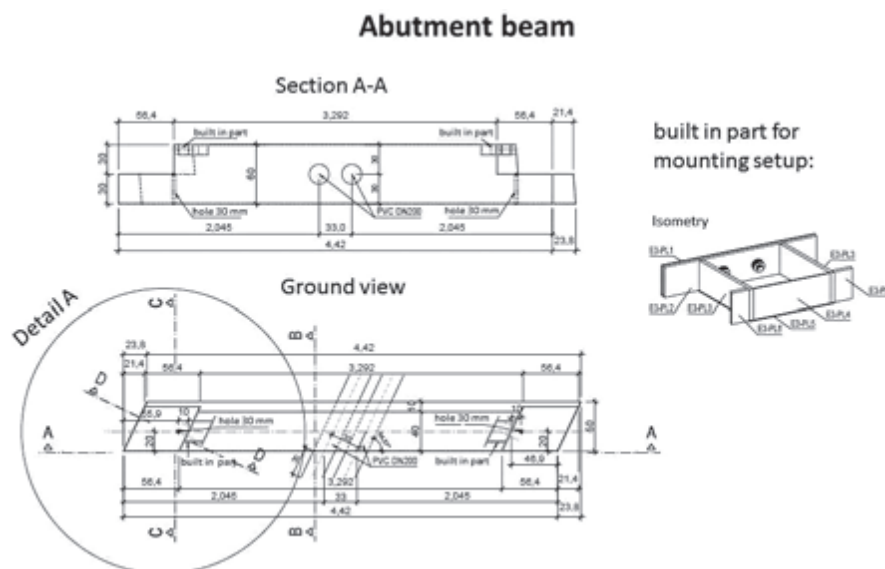


Fig. 7: Geometry of the abutment beam for a skew bridge

3. SPECIFICS ON UHPC 325 AND THE TRANSFER TO UHPC-SHELL CONSTRUCTION

3.1 Frame leg with in-situ concrete

Due to the static design of a frame construction and the two-part design of the UHPC-walls, (Fig. 8) the side abutment walls, which have a positive pitch, are made with in-situ concrete. In contrast to the other two embodiments, the prestressing is selected with a subsequent bond (posttensioned prestressing). This makes it possible to manufacture the UHPC-walls as two-part elements and to interlock them on site. The required prestressing force to absorb the frame moment is introduced into the UHPC-precast elements via the frame leg with in-situ concrete, thus enabling the controlled load introduction.

The positive inclination of the frame leg leads tendency compared with frame constructions without a pitch to lower horizontal forces and thus to the possibility of flat foundations. The transition of the frame leg into the foundation should be articulated, but a connection with conventional reinforcement with plug-in rings is sufficiently ductile to accommodate the bearing rotations.

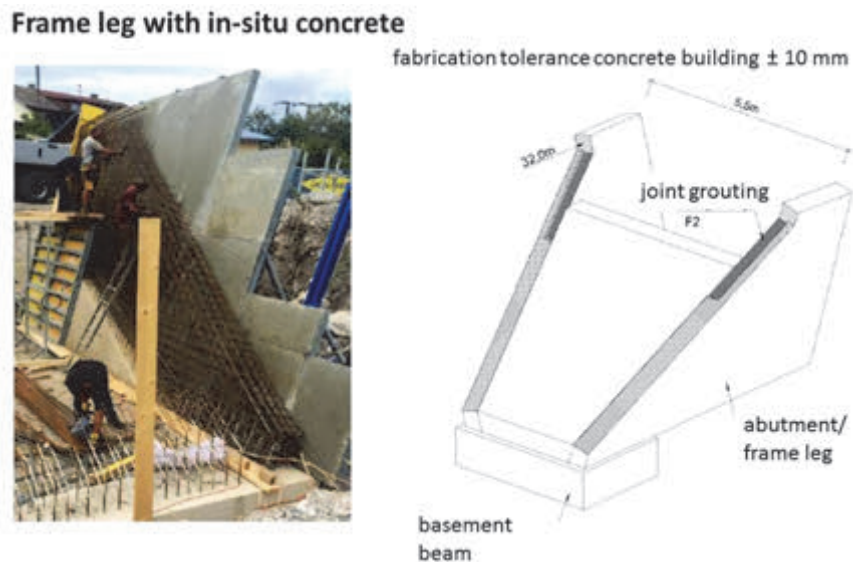


Fig. 8: Fabrication and design of the frame leg with in-situ concrete

3.2 Joint design

A further special feature of this type is the formation of the system-dependent joints, which is to be developed from the experience of the project Paulifurt (Olipitz, 2015 a) as a wet joint (Fig. 9). The design of dry joints allows almost no tolerances and is more cost-intensive to manufacture. The wet joint allows the tolerance compensation, whereby a corresponding post-limit stiffness has to be taken into account.

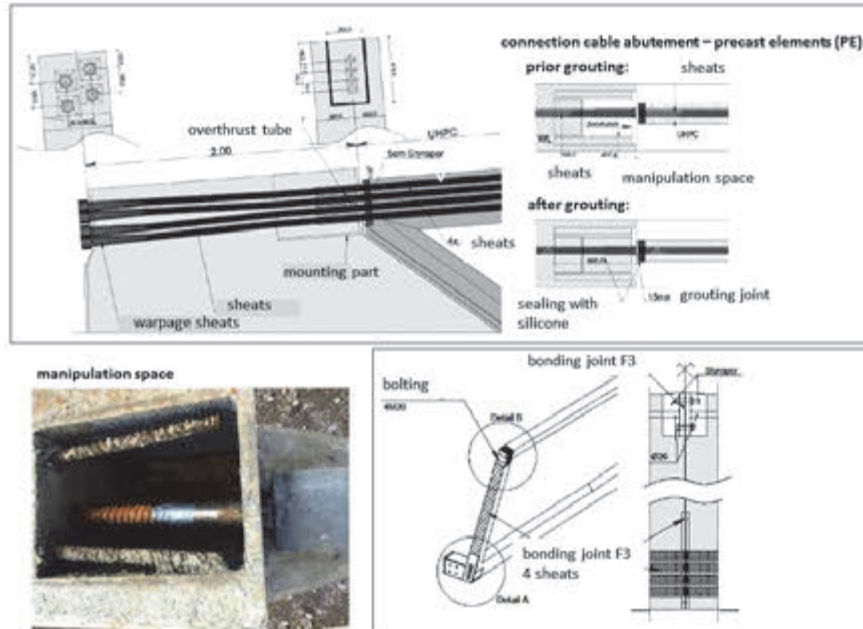


Fig. 9: Design of the wet joints and coupling joints for prestressing

A further special feature is the type of prestressing with subsequent bonding (posttensioned prestressing). This is preferable to pre-stress without bonding (pretensioned prestressing). The joints and transitions of the sheaths must be tested for leak tightness for the later grouting with the cement matrix. The project Paulifurt (Olipitz, 2015 a; Olipitz, 2015 b) (Fig. 11) has shown that expensive sealing rings can be dispensed with due to the high prestressing. A particularly

neuralgic point is the transition of the sheats from the frame leg with in-situ concrete to the UHPC-precast element section, which has been solved only by a specially designed overlapping construction. The insertion of the strands into the casing should be carried out symmetrically from both sides, as is the tensioning of the litz wires so as to obtain a minimum of prestressing losses from friction.

3.3 Geometrical stiffness through shell effect

UHPC components are very thin-walled components whose high slenderness (ratio) can only be achieved by utilizing geometric stiffnesses. Thus, the buckling stability of the upper flange in the UHPC 325-walls in the field center can only be achieved by the buckle (bend) in the ground plan. This possibility of geometrical stiffness can also be achieved in the case of spatial shell elements with flat UHPC-plates. In Fig. 10, on the basis of a cantilever construction, rotationally symmetrical roof structures, such as those known e.g. can be provided for canopies. The challenge lies in the joining of the UHPC-plate elements, which can be solved from the author's point of view by means of steel elements with grouting.

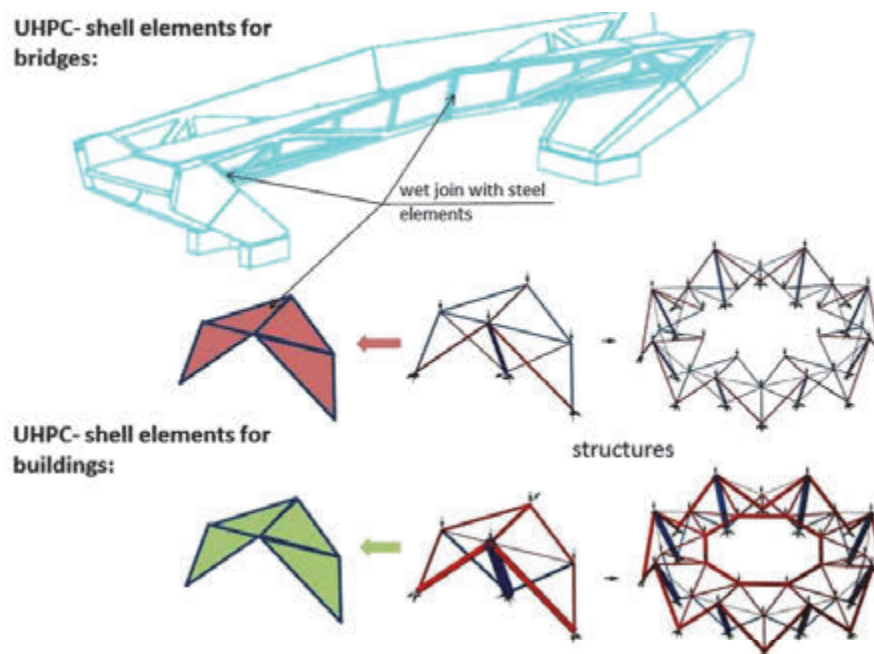


Fig. 10: Shell effect (geodesics) of the frame and other tiled slaps in buildings

4. CONCLUSIONS

Due to their characteristics bridge systems with UHPC represent a quite competitive alternative to previously implemented bridge system solutions. They offer the advantage of a resource-saving efficiency when used in a material specific correct application and also enable sustainable infrastructure projects. In the case of material specific correct application and utilization of the static advantages, beautiful shaped system bridges and buildings can be created by expressing the inner logic through the external appearance. This is perceived by the viewer as a harmonious building structure (e.g. in Fig. 11).



Fig. 11: Paulifurt bridge in Carinthia in Austria

5. REFERENCES

- Cooperation with the Austrian company Franz Oberndorfer GmbH & Co KG, Lambacher Strasse 14, A-4623 Gunskirchen (2016). Link: <http://www.oberndorfer.at> [cited 19 June 2017]
- Olipitz, Michael (2015 a): „Paulifurtbrücke – Entwurf, Planung und Ausführung einer UHPC – Schalenbrücke in Kärnten“, Beton und Stahlbeton, May 2015, Ernst und Sohn Verlag Berlin. Link: <http://www.olipitz.com> [cited 19 June 2017]
- Olipitz, Michael (2015 b): „Innovationen an Beispielen einer Bogen-, Balken-, und Schalenbrücke“, article in the anniversary publication for Professor Dr. Lutz Sparowitz (75): Innovation und Ästhetik im Ingenieurbau, ISBN: 978-3-85125-431-0, December 2015, Graz.

AN ASFINAG PILOT PROJECT FOR A WATERTIGHT STRUCTURE WITHOUT REINFORCEMENT FOR CRACK WIDTH CONTROL

Michael Kleiser¹, Wolfgang Lindlbauer², Helmut Huber³

¹ ASFINAG Baumanagement GmbH
Modecenterstrasse 16, 1030 Vienna

² Ingenieurbuero Dr. Lindlbauer
Garnisongasse 7, 1090 Vienna

³ Birgitz, Tirol

SUMMARY

The ASFINAG took the opportunity to propose constructing a trough on the planned new section of the S7 Fürstenfeld expressway as a pilot project for testing new modified forms of concrete with increased AHWD components in a practical situation. The basic motivation was to significantly reduce the surface reinforcement previously used to distribute any potential cracks at an early stage. Reinforcement employed for crack control will largely be dispensed with and considerable costs saved by using a suitable indexing procedure which specifies a required crack index that errs on the safe side, using modern concrete concepts and obtaining appropriate guidance from concrete specialists.

1. INTRODUCTION

Sufficient protection against water penetration in watertight trough structures without seals, in German shortly called “Weiße Wannen”, is currently regulated through the provision of a corresponding minimum surface reinforcement in the current guidelines of the Austrian Society for Construction Technology. The reinforcement regulations were determined in the revised version in 2009 in accordance with Eurocode 2 with the help of measurement diagrams with the goal of reducing the crack width in the case of early restraint cracking to between 0.15 mm and 0.25 mm depending upon the construction class (OeVBB 2009).

Simultaneously with the publication of the revised guideline “Weiße Wanne”, a research project with the Austrian Research Promotion Agency FFG with the title “Optimisation Weiße Wanne West” was proposed in order to investigate the influence of modified concrete with increased amounts of AHWZ (effective additives prepared hydraulically) to reduce hydration heat on early restraint cracking. The material behaviour of modified concrete during the setting process was tested using large samples and the results verified by means of a numerical, thermo-mechanical 3D FEM simulation (Nietner, Schmid 2003). Through the introduction of a crack index, which showed the ratio of the tensile stress present in the component to the permitted tensile stress at marked points, the aim was to calculate a corresponding safety criterion for preventing crack using modified sorts of concrete and therefore to dispense with the reinforcement normally employed for crack control in accordance with the principle “avoidance instead of limitation of cracks”. In addition, material cooling costs in Austria can be reduced with this new process alongside the savings in reinforcing steel. Reducing the clinker component can also make a considerable contribution to reducing CO₂ emissions, thus supporting more sustainable construction. The results were correspondingly published following

the completion of the research project in December 2011 (OeBV 2011). Additional publications have been released, e.g. (Huber 2012).

In order to incorporate new knowledge into practice in a timely manner, the Austrian motorway and expressway operator ASFINAG provided a trough structure as a pilot project for the new Fürstenfelder Schnellstraße S7 project. The planned trough structure at the Rudersdorf-West intersection provides the ideal preconditions for testing the new procedure thanks to the nearly reinforcement-free type of construction, short block lengths and the challenging local aggregates.

2. PROJECT DESCRIPTION

The previous project, the routing, began in January 2003 with the aim of achieving a primary street connection from the current A2 South motorway to the Hungarian border. The civil engineering works planning was given the go-ahead in 2005.

The western section of the S7 Fürstenfelder Schnellstraße between Riegersdorf (A2) and Dobersdorf branches off from the A2 Southern motorway near the planned Riegersdorf intersection. The route runs eastward north of the communities of Großwilfersdorf, Altenmarkt and Fürstenfeld to the intersection with Rudersdorf West, leading to the approximately 2.9 km long Rudersdorf tunnel via a trough structure. The eastern section of the S7 to be realised later is located there and leads to the border (see Fig. 1).

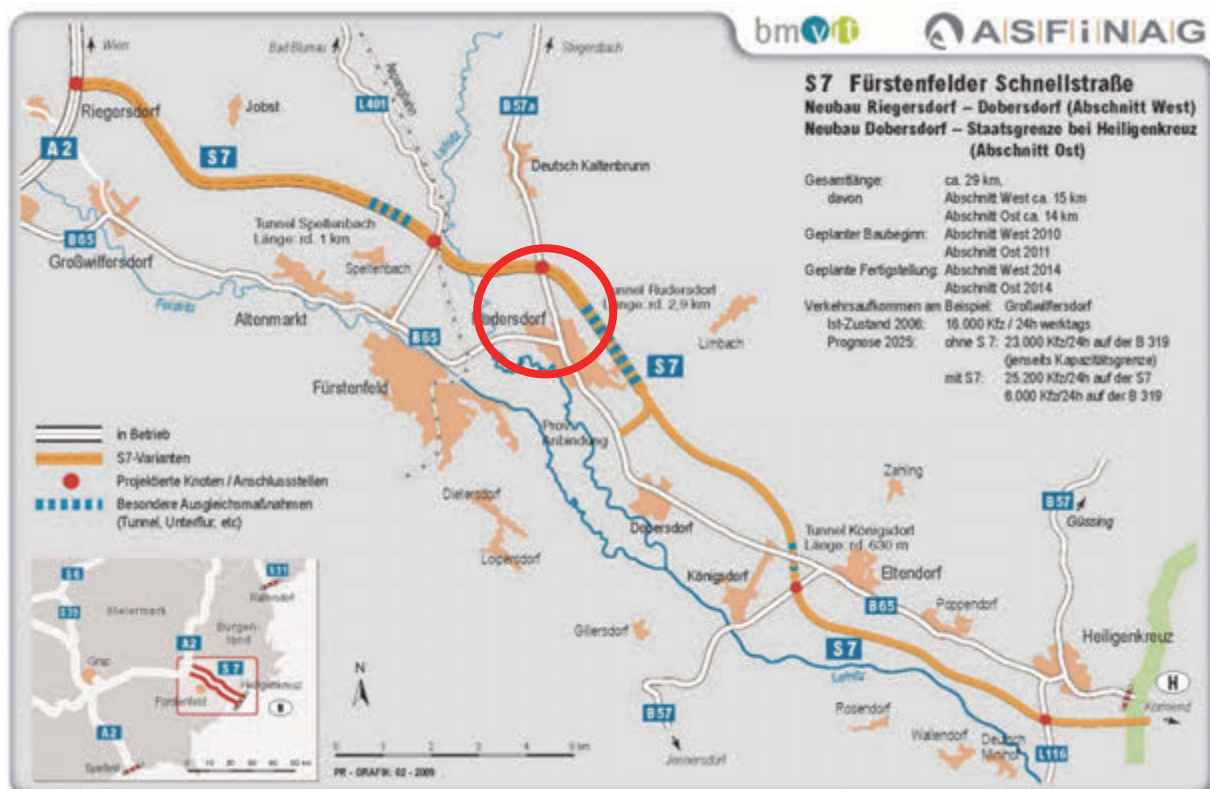


Fig. 1: Planned route S7 Fürstenfelder Schnellstraße

The trough structure as a pilot project is located at the Rudersdorf West intersection (see the red circle in Fig. 1). The Rudersdorf West intersection to be newly established is planned as a roundabout with two bridge constructions, corresponding to the ramp constructions connected

to the main roadway. The trough structure for the main roadway with the object name S7.24b will be approx. 845 m long and extend to the western portal of the Rudersdorf tunnel. It is an average of 32 m wide in the centre and immersed in the groundwater up to the tunnel portal to a depth of approx. 6.30 m in blocks measuring 12.50 m in length. The water level measurement was determined in geotechnical-hydrogeological reports under consideration of a safety margin of approx. 2.00 m and the height of the existing upper edge of the site. The bottom slab will be up to 1.80 m thick in order to withstand the high groundwater pressure. The walls of the trough structure are generally 80 cm thick and taper above the measurement water level. The overview of the trough structure and a standard profile are visible in Fig. 2, 3 and 4.

In general, an optimised concrete called BS1COPT should be used in the entire trough structure with the exception of the trough blocks under the roundabout. An initial inspection and the key figures to calculate the crack index for BS1COPT are requested from the contractor. It is presumed that the procedure for the required testing of BS1COPT will take approx. six months. As a result, the contractor must submit their planned concrete composition for the optimised concrete BS1COPT to the client for approval at latest six months before the first installation of BS1COPT and prior to the first inspection. This will provide the contractor with sufficient time for the optimal composition of the concrete based upon the guidelines.

In order to ensure the construction process mandated by the client, the first sections of the trough structure (roundabout bridges, block KV-1 to KV-5, see Fig. 3) will be produced using conventional construction methods with concrete in accordance with (OeVBB 2009). The optimised concrete BS1COPT will be used for the additional blocks (B1 to B21 as well as B22 to B64). Possible colour differences due to the change in construction material will be accepted and/or welcomed as a visible comparison of various procedures.

Certain delays must be tolerated over the course of the approval process for this construction. This pilot project is unique in Austria and is expected to be realised as soon as the remaining legal conditions are satisfied.

3. VERIFICATION OF THE PROCEDURE

In the course of revising the guideline of “Weiße Wanne”, a new analytical verification method on the basis of the deformation compatibility for measuring watertight constructions was presented (Schlicke 2014). A Master’s thesis verified the procedure for the S7 Rudersdorf-West trough structure with reduced surface reinforcement. A measurement-relevant macro crack formation was ruled out, which under certain circumstances could have resulted in leaks in the structure (Kainer 2015).



Fig. 2: Map of project area S7.24b trough structure Rudersdorf West

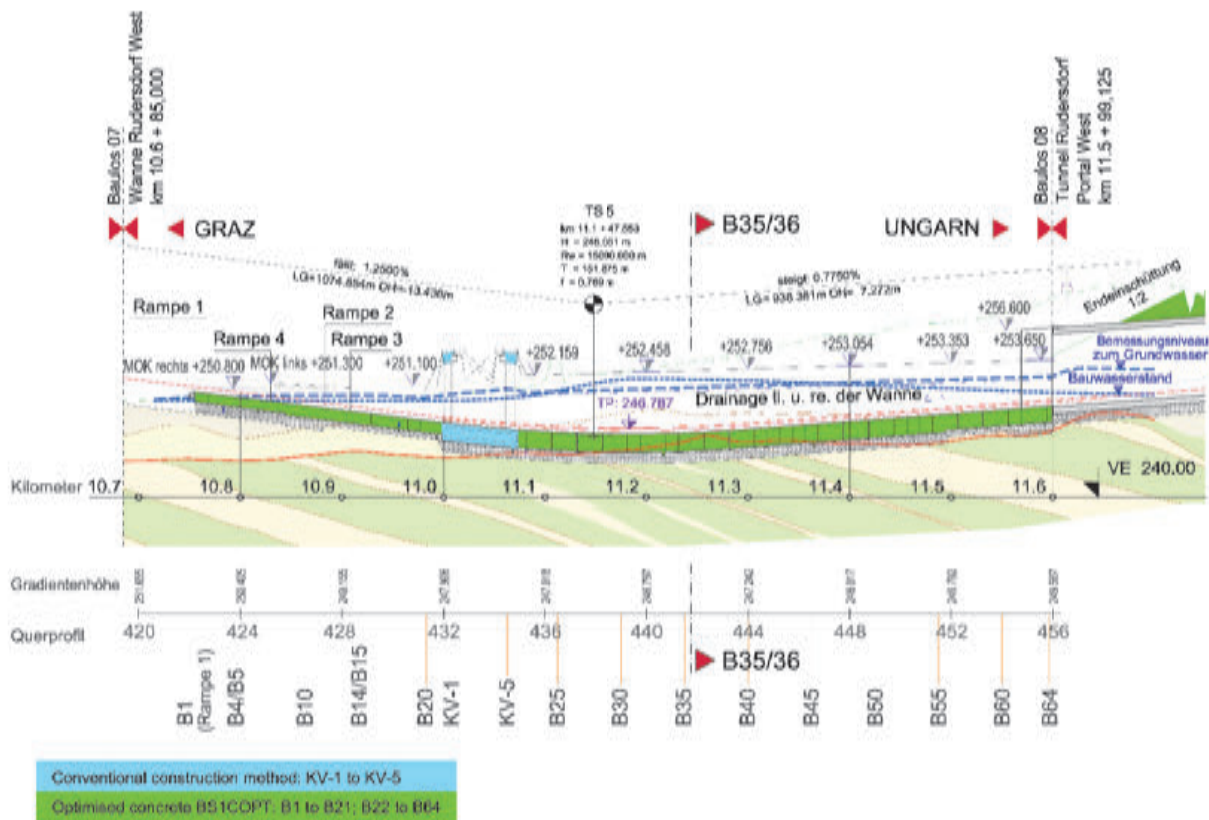


Fig. 3: Longitudinal section S7.24b trough structure Rudersdorf West

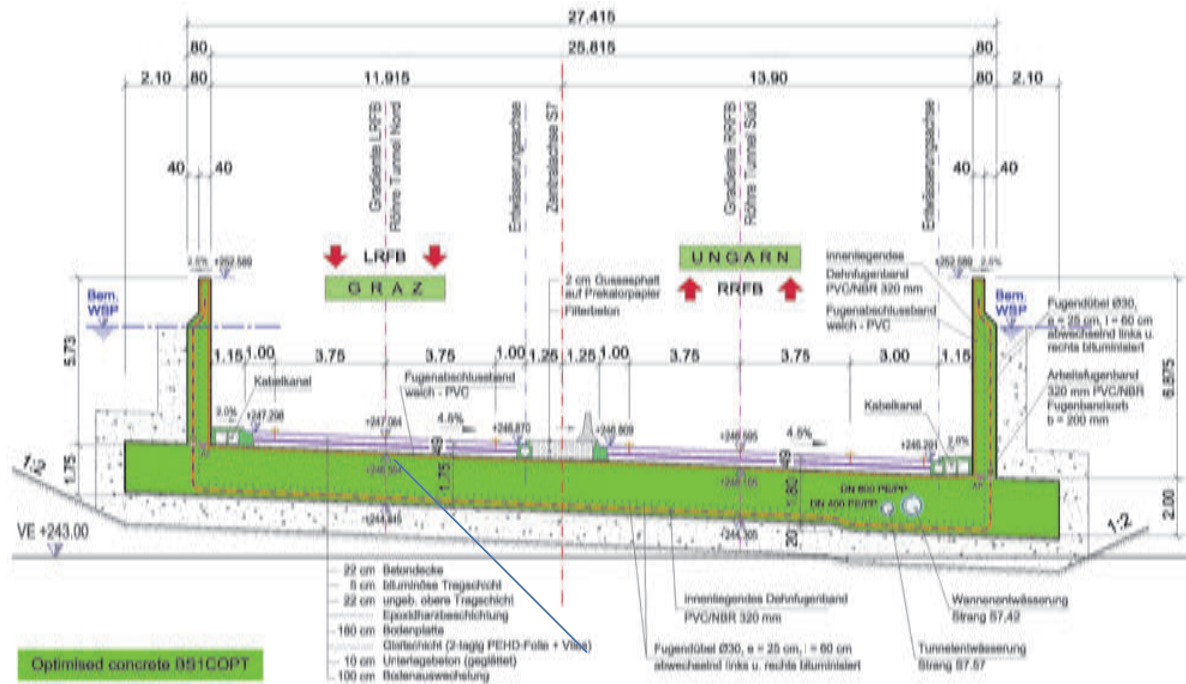


Fig. 4: Cross section S7.24b - block joint B35/36 km 11+244,000

4. S7 PILOT PROJECT – TENDER DESIGN

In 2012, the planning of the Rudersdorf West trough was completed on the basis of the March 2009 edition of the OeVBB-guideline, to the extent that tender design with the creation of the services directory was possible. Due to the conditions with ASFINAG, beginning in February 2012, ASFINAG decided in autumn 2012 to conduct the Rudersdorf West trough as a pilot project.

The basis for the decision of ASFINAG to plan, tender and realise “Weiße Wanne Rudersdorf West” as a pilot project with the optimised concrete C25/30(56)/BS1COPT were comprehensive investigations into optimised concrete including the related reinforcement savings which resulted from numerical verification of the calculated crack index. The presumptive tender requirements, subject to changes, with regard to the use of the optimised concrete will be described in the following subchapters:

4.1 Concrete - Supplemental information in the tendering project

Directly following the awarding of the order, the contractor must present the planned concrete composition, the implementation and the entire inspection schedule for the first inspections for BS1COPT to the client for approval. The key figures necessary to calculate the crack index are to be presented to the client at latest 6 weeks after the beginning of the first inspection or at latest 3 months after the awarding of the order. The client will then conduct the calculation of the crack index. The permissible crack index is determined with a max. 0.70. The temperature increase based on ONR 23303 in the concrete may amount to a maximum of 16 K at variance with the OeVBB-guideline, point 5.1.3, Tab. 5/2.

The maximum fresh concrete temperature is limited to 22°C, the maximum concrete structure temperature is limited to 45 °C (walls) and 50 °C (concrete slab). These requirements are valid for the use of all “Weiße Wanne” concrete of the Rudersdorf West trough structure.

In the course of making the offer and prior to the awarding of the order, the contractor must present to the client a concept for the measures regarding the cooling of the fresh concrete. In order to determine the cooling measures, the annual figures for the daily air temperature (measuring point Fürstenfeld of the Zentralanstalt für Meteorologie und Geodynamik) will be added to the tender as supplements for the years 2002 to 2015. For the optimised concrete C25/30(56)/BS1COPT, the verification of the exposure class XF4 in hardened concrete (beginning of inspection after 28 days and after 90 days) is to be conducted by an accredited testing institution. If the verification has been provided after 28 days, the inspection after 90 days is no longer necessary.

An internal verification of the XA2L exposure class can be omitted due to the selection of a concrete coverage that is 10 mm higher on the earth side (“sacrificial layer”) and the verification of the XC4 exposure class. In accordance with ÖNORM B 1992-1-1, there is a minimum concrete coverage $c_{\min,dur} = 40$ mm and $c_{\min,dur} = 30$ mm for the exposure class XD1 (earth side) for exposure class XD3 (roadway side). This value will be increased by 5 mm for the planned usage duration of 100 years. The tolerance allowance amounts to $c_{dev} = 5$ mm. The nominal mass of the concrete coverage thus amounts to 50 mm for the entire object. Defects (wet areas, cracks, etc.) that can occur despite compliance with the requirements of the OeVBB-guideline and those of the client are to be remedied by the contractor at their expense up to the extent indicated in table 3/1 of the OeVBB-guideline.

4.2 Reference concrete, guidelines and quality assurance

4.2.1 Composition of reference concrete

The following raw materials were selected for the composition of the reference concrete, whereby the lowest content of cement is to be selected in order to limit the crack widths with BS1COPT.

- Cement CEM I 42.5 N C3A-free, *Lafarge, Retznei plant* 215 kg/m³
- AHWZ Flumix C, *Lafarge, Retznei plant* 115 kg/m³
- Total water quantity 150 l/m³
- Aggregates quarzitic 0/4, 4/16, 16/32 *Holler gravel plant, Königsdorf*
- Additives FM, LP, *Mapei-Betontechnik*

With this concrete composition, the most favourable values for the stability and safety against temperature stress cracks were achieved. Due to the test results, this concrete composition will be used as “reference concrete” against which other concrete compositions with other raw materials can be compared.

4.2.2 Initial assessment and conformity checks BS1C and BS1COPT

For all concrete sorts and concrete of exposure class XF4, the creation of a concrete concept with a comprehensive test procedure will be required in conjunction with the initial assessment and for the verification of the crack limitation. Due to lack of space a detailed listing of all tests will not be provided.

4.3 Calculation of the crack index

The finite element modelling (see Fig. 5) with the calculation of the crack index for the pilot project “Wanne Rudersdorf West” will be conducted by the client. The theoretical frameworks for the verification are described in (Nietner, Schmid 2003) as well as in (Schlicke 2014) and (Kainer 2015) in expanded form. The calculation values for the crack index are herein not described in detail. The temperature development will be determined on the basis of the initial values, the development of tension as well as the maximum crack index and the development of tension for various conditions (see Fig. 6 and 7). The temperature criteria for the avoidance of separating cracks are defined depending upon the required crack index.

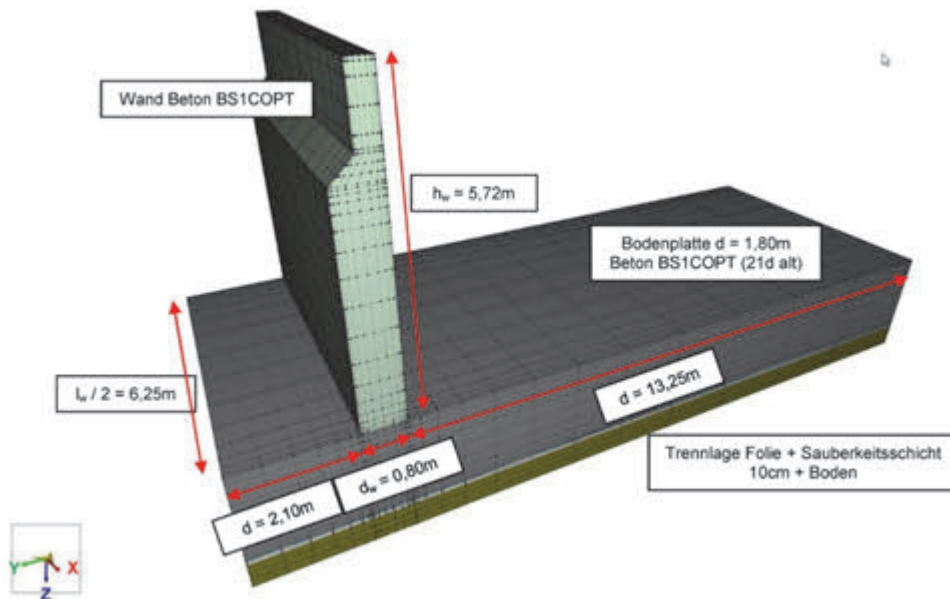


Fig. 5: Calculation model (foundation block 35)

Auswertungspunkte	#1	#2	#3	#4
Max. Temperatur [°C]	38,9 (32)	45,3 (36)	38,9 (32)	43,5 (32)
Normalepannung [N/mm ²]	Max	0,75 (42)	1,10 (318)	0,72 (42)
	Min	-0,36 (318)	-0,71 (42)	-0,31 (318)
Max. Rissindex [-]	0,47 (42)	0,40 (246)	0,47 (42)	0,59 (318)

Die Werte in Klammern geben den Zeitpunkt des Eintretens des Ereignisses in Stunden an.

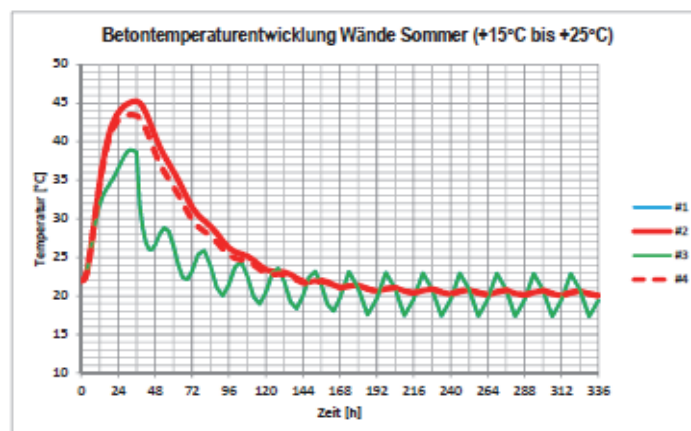


Fig. 6: Concrete temperature summer

Auswertepunkte		#1	#2	#3	#4
Max. Temperatur [°C]		16,80 (40)	22,49	16,80	21,06
Normalspannung [N/mm ²]	Max	0,38	0,70	0,45	0,89
	Min	-0,40	-0,24	-0,30	-0,28
Max. Rissindex [-]		0,54	0,29	0,53	0,38

Die Werte in Klammern geben den Zeitpunkt des Eintretens des Ereignisses in Stunden an.

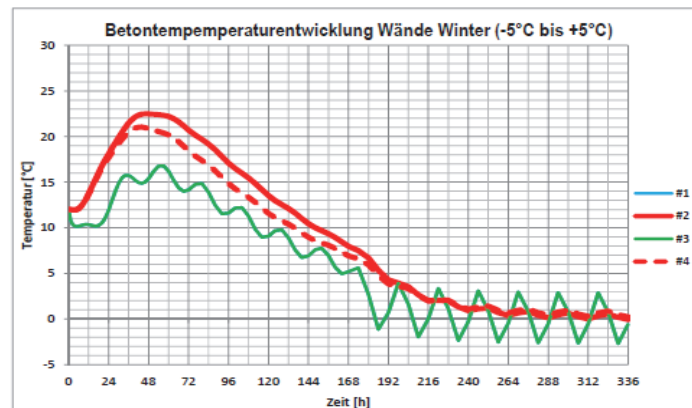


Fig. 7: Concrete temperature winter

4.4 Comparison of the reinforcements

Reinforcement drawings for conventional BS1C concrete and optimised concrete BS1COPT were created for standard cross sections in order to reach a decision for the “Weiße Wanne Rudersdorf West” pilot project. The reinforcement plans are the object of the tender and offer a savings potential of approx. 15% for BS1COPT in comparison with an execution with BS1C in accordance with the guideline.

5. CONCLUSIONS

The Wanne Rudersdorf West pilot project of the S7, Fürstenfelder Schnellstraße should be the basis for the fourth revision of the guideline conducted by the Austrian Society for Construction Technology. The experience gained from this project, including the additional investigations (Schlicke 2014), and verification calculations (Kainer 2015) should contribute to the formation of an economical, high-value and sustainable construction method.

6. REFERENCES

- OeVBB (2009), „Wasserundurchlässige Betonbauwerke - Weiße Wannen“, Österreichische Vereinigung für Beton- und Bautechnik (Austrian Association for Concrete and Construction Technology), Vienna, March 2019.
- Nietner, L., Schmid, L. D. (2003), „Temperatur- und Festigkeitsmodellierungen durch Praxiswerkzeuge.“ Beton- und Stahlbetonbau, 12/2003.
- OeBV (2011), „Optimierung Weiße Wanne West“, Österreichische Bautechnik Vereinigung, Vienna, 2011.
- Huber, H. (2012), „Rezepte für mehr Wirtschaftlichkeit“, Österreichische Bautechnik Vereinigung, Bautechnik, Vienna, 2012.
- Schlicke, D. (2014), „Mindestbewehrung für zwangsbeanspruchten Beton - Festlegung unter Berücksichtigung der erhärtungsbedingten Spannungsgeschichte und der Bauteilgeometrie“, Dissertation, Graz Technical University, 2014.
- Kainer, B. (2015), „Bemessung von WU-Konstruktionen unter Berücksichtigung des tatsächlichen Bauteilverhaltens“, Master's thesis, Graz Technical University, 2015.

EFFECT OF DESIGN AND EXECUTION ON QUALITY AND DURABILITY OF MULTI-STOREY REINFORCED CONCRETE PARKING GARAGES

Vítězslav Vacek¹, Miroslav Sýkora¹, Jiří Kolisko¹, Vladimír Vančík²

¹ *Czech Technical University in Prague, Klokner Institute*

Šolínova 7, 166 08 Prague 6, Czech Republic

² *VIN Consult s.r.o.*

Jeremenkova 763/88, 140 00 Prague 4, Czech Republic

SUMMARY

The contribution discusses the difference between quality and durability of monolithic and prefabricated reinforced concrete elevated parking garages. The concept of a composite concrete to concrete structure makes it possible to reduce the total volume of the structure and thus its price when compared to a monolithic building. Other benefits of the prefabricated structure include reduced execution time, smaller construction site area, and increased quality and durability of the completed building. It appears that prefabrication helps to reduce scatter in basic variables including material and geometrical properties as well as durability-related characteristics. After six years of operation the garages show no major defects and serve well their purpose.

1. DURABILITY OF REINFORCED CONCRETE GARAGES

Durability of building structures is significantly affected by the quality of used materials and quality of the workmanship. Good quality execution is therefore necessary in conjunction with the optimum project with respect to structural and technological solution. Concept of the whole structure and its key details must be designed optimally with regards to structural but also to operational costs, both in the context of designed durability of the building.

The principal factor in design is purpose of the building determined by requirements and conditions of the client. This implies loading of the structure during execution and operation. It is not only stress by static or dynamic mechanical actions due to self-weight and imposed loading, but also actions caused by changes of temperature or humidity and impacts of surrounding environment, which often leads to deterioration of construction materials.

Garages (parking houses) represent rather a specific type of civil engineering structures. Though methods of their construction have been significantly improved over the last two decades in the Czech Republic, serious defects are quite frequently observed and expensive repairs or upgrades are needed.

One of the causes of such difficulties is attributable to insufficient initial costs allocated for execution, resulting in numerous complications when execution fails to fully comply with structural design. The most important issue which finally draws interest of the owner of the building is damage to vehicles caused by leakage from cracks in floor structures (Vacek et al., 2016).

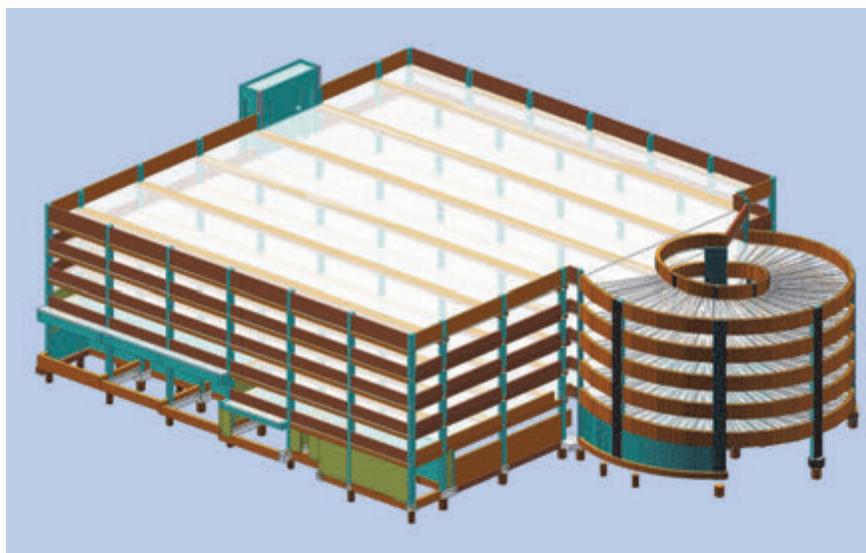


Fig. 1: View of optimized garages

2. CASE STUDY AND CONCEPT OF TECHNOLOGICAL OPTIMISATION

Parking house was designed as a six-floor building (one basement and five floors, including the roof) of ground plan dimension 52×69 m. Structural height of the floor level is 2850 mm, clearance under beams 2250mm and clearance for walking by the column under the edge of cantilever is 2100 mm.

Entrances, exit and arrival to the building are located next to the staircase core. Separate closed garages and storage room were designed in the area of underground atypical floor level. Internal vertical communication for vehicles between individual parking levels is provided by a two-lane ramp in the shape of helix – rondel, with new cylindrical fire reservoir designed in its centre. The parking house with a capacity of 450 vehicles was initially designed in the tender documentation as a monolithic system.

After the tender, the structural design including foundation system was changed, preserving the original layout, but aiming to optimize life-cycle costs, use of technologies and reduce structural volume. The height of the building was reduced (smaller floor depths, lower heights of continuous girders). Originally designed horizontal floor structures were changed to slabs with slope (Fig. 1) even at the price of increased initial costs of both the contractor and the designer.

Special attention was paid to designing execution phases in order to minimise time and allow for assembly in restricted building site conditions. Design of the building consisting of monolithic and precast parts required careful attention to connections. Execution time was significantly reduced as the structural concept made it possible to execute the monolithic and precast components in parallel.

3. DESIGN OPTIMISATION

3.1 Foundations

Originally designed foundation had insufficient resistance for an additional load of 500 kN/m^2 – characteristic value – required for the new monolithic-precast structure. Strengthening was not feasible due to insufficient information from engineering and

geological surveys made during the previous phases of the project. Additional geological survey revealed a layer of loose backfills of remarkably variable thickness up to 7 m. Alternatives to provide for foundations with enhanced load-bearing capacity included:

- Flat foundations on footing of increased dimensions allowing for a 300 kN/m² additional load
- Deep foundations on bored piles with grillage

The critical comparison of the two alternatives suggested that the deep foundations be more appropriate in the case under consideration. The main reasons included insufficient resistance of soils for flat foundations and expected excessive uneven settlements.

3.2 Structural system

Structural solution of the parking house was revised taking into consideration technological optimisation for a contractor selected for execution. The change to a hybrid concrete-concrete (monolithic-precast) system included the following:

- Ribs of floor slabs were replaced by continuous girders.
- Grid structures in the area of connection to the rondel were simplified – two columns were replaced by prestressed girders.
- The rondel – columns with girders and external parapets – was cylindrically shaped with opening.
- Horizontal floor structures were modified to slabs with slope.

The change of monolithic to prestressed components and inclination of floor slabs were crucial for the increased quality of building (Fig. 2).

3.3 Final design

Vertical bearing structure of the parking house is formed by the module system with dimensions of 8.25 × 7.60 m. Horizontal structures were designed as a composite hybrid concrete-concrete structure; a major part of the structure is precast while the ramp is mostly monolithic. Impermeable concretes for structures of peripheral underground wall along the access communication, fire tank and underground collector for connection of fire tank to the main office building were applied.



Fig. 2: The finished structure with apparently inclined floors

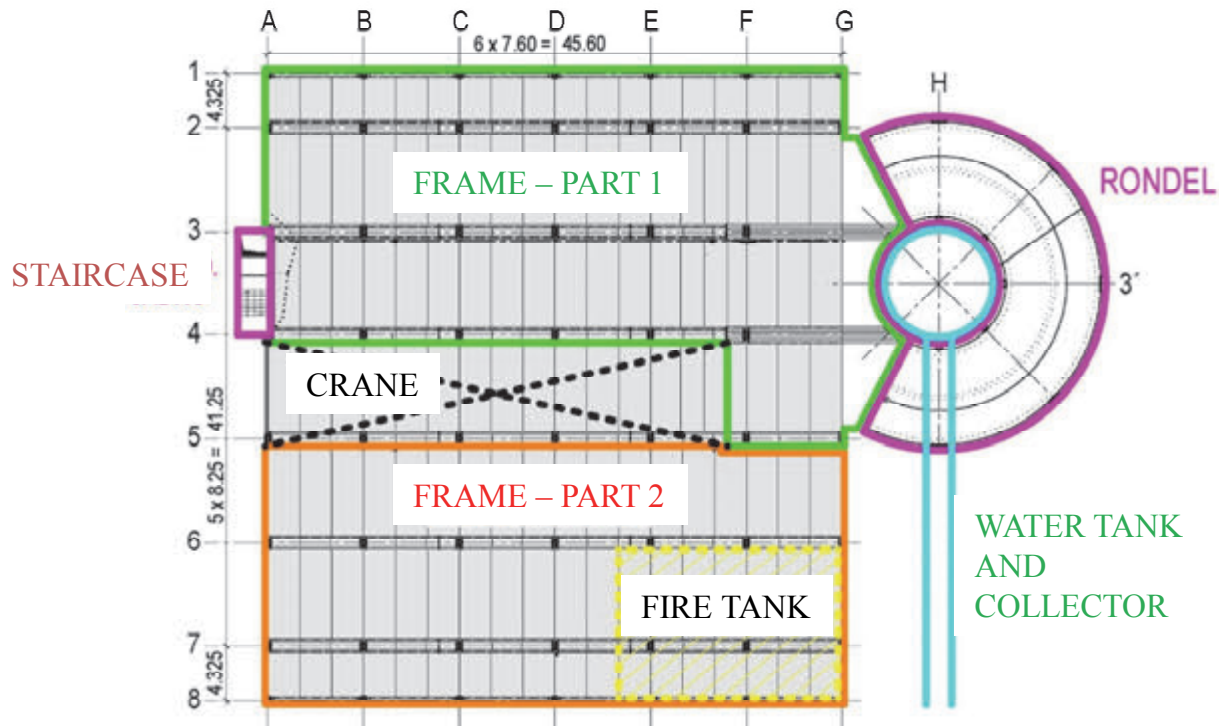


Fig. 3: Layout of the building

Basic components of the structural system include (Fig. 3):

- Parking house frame structure
- Continuous five-storey columns with cantilevers
- Double inner continuous girders 250×600 mm with span of 7.6 m
- Main prestressed girders 350×600 mm with span of 12.3 m
- Simply supported girders 600×575 mm with integrated parapets
- Continuous filigreed floors of height of 200 mm, spanning 8.25 m
- Precast parapets of the slab in Axes A and G
- Crossing ramp (rondel): floor slab of depth of 240 mm spanning 7.95 m and girders of height of 1390 mm spanning 10.4 m

Tab. 1 provides comparison of concrete volumes of the structure above foundations for the different design strategies.

Tab. 1: Comparison of volumes of the above-foundation structure [m³]

Component	Original	Monolith	Precast	Total
Frame columns	530	227	212	439
Frame horizontal members	3500	1682	1196	2878
Rondel vertical	280	180	8	188
Rondel horizontal	630	546	0	546
Total	4940	2635	1416	4051

4. EXECUTION

Construction procedure was strongly influenced by restricted conditions on site with the only access communication, very limited possibilities of material storage and necessity to

keep the fire tank (Fig. 3) in operation – first the existing one and then the new one. Possibility of space division and therefore also independent realisation of technologically and functionally separated parts of the structure were necessary to meet the time frame. Execution was divided into the following phases (see also Figs. 3 to 5):

- Construction of the collector of buried services and substructure of the water tank
- Planking and strutting of excavation pit (first part), underground foundation for rondel and first part of frame
- Assembly of the crane
- Construction of staircase core and substructure of internal part of rondel
- Assembly of the first part of frame and independent construction of water tank and monolithic rondel
- Reconnection of the original fire tank to a new water reservoir
- Demolition of fire tank, planking and strutting of excavation pit second part and underground foundations for the second part of the frame
- Assembly of the second part of the frame
- Dismantling of the crane and completing of all floors between axes 4 and 5 (Fig. 3)

Interesting technological part was the execution of additional concrete works in the field 4-5 after dismantling of rail crane at the end of shell construction. Time for execution of this section was limited to one week under adverse weather conditions disabling use of common filigree slabs with assembly supports for relevant technological periods. Therefore, filigree girder beams Montaquick with pressed concrete line were additionally designed and used and individual floors were concreted within two days working step. Shell construction under condition of uninterrupted operation of the fire tank was executed within only four months in a winter period.

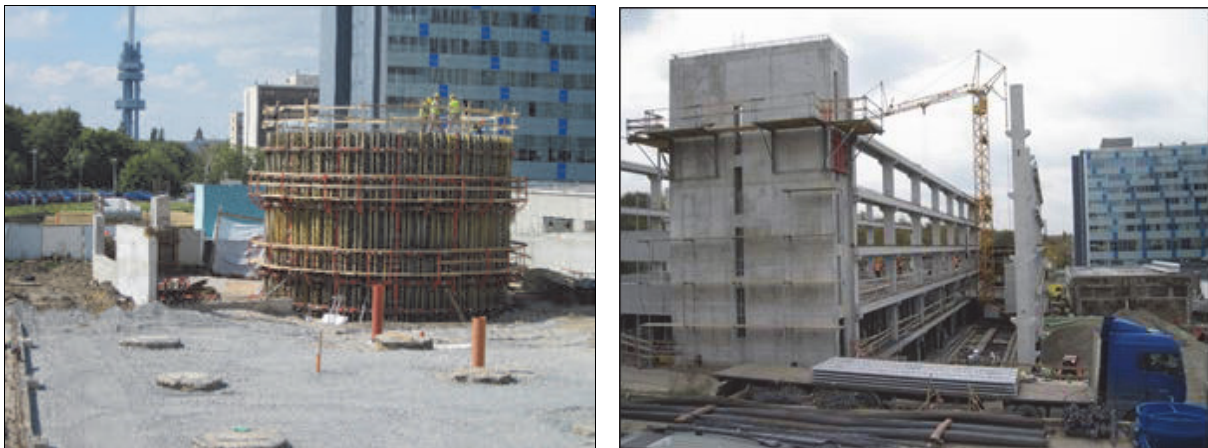


Fig. 4: The new fire water tank (left); execution of the precast frame (right)



Fig. 5: View of prefabricated structures and reinforcement before concreting floors

5. IMPLICATIONS FOR PARTIAL FACTOR DESIGN AND FORESEEN DURABILITY

The quality of execution has a substantial effect on reliability verifications with respect to Ultimate Limit States ULS, Serviceability Limit States SLS and Initiation (Durability) Limit States ILS. Following the basic standards for such verification (EN 1990, 2002; EN 1992-1-1, 2004; ISO 13823, 2008), the distinction between monolithic and precast concrete can be made:

- ULS: Detailed guidance on how to apply the reduced factors for concrete and reinforcing steel γ_c and γ_s , respectively, considering reduced uncertainty in geometry and reduced variability of concrete strength is provided in Annex A of (EN 1992-1-1, 2004). Detailed numerical procedure for updating partial factors was recently provided in (Caspéele et al., 2013 and 2017; Sykora et al. 2013). (EN 1992-1-1, 2004) makes it possible to reduce the partial factors up to $\gamma_c = 1.30$ and $\gamma_s = 1.05$, tacitly assuming a common target reliability level for medium consequence class (EN 1990, 2002). However, such reductions should be adopted with caution as it can lead to low reliability levels (Holický et al., 2016).
- SLS: For garages, a limiting crack width is assumed to be 0.2 mm in (EN 1992 -1-1, 2004; *fib*, 2013). The structure was designed to meet this criterion under a quasi-permanent load combination; this has been achieved by additional reinforcement. Overall structural performance with respect to crack widths is considerably enhanced by use of prestressed elements (reduced effects of constrained shrinkage, improved curing).
- DLS: increased quality of precast members is recognised in (EN 1992-1-1, 2004) by allowing reducing a minimum concrete cover. Moreover, concrete cover of precast members is mostly of better quality compared to monolithic members and is more resistant against ingress of unfavourable agents (Malioka, 2009).

6. CONCLUSIONS

The parking house is serving after 5 years of daily operation successfully its purpose. During inspection, no defects or failures were found, even no tear and wear of for example pavements, which might have impact on reduction of its durability or which might call for

need of premature construction maintenance or repairs. Current conditions of the structure are demonstrated by Figs. 2, 6 and 7.



Fig. 6: Roof of garage with the parking floor after five years of service

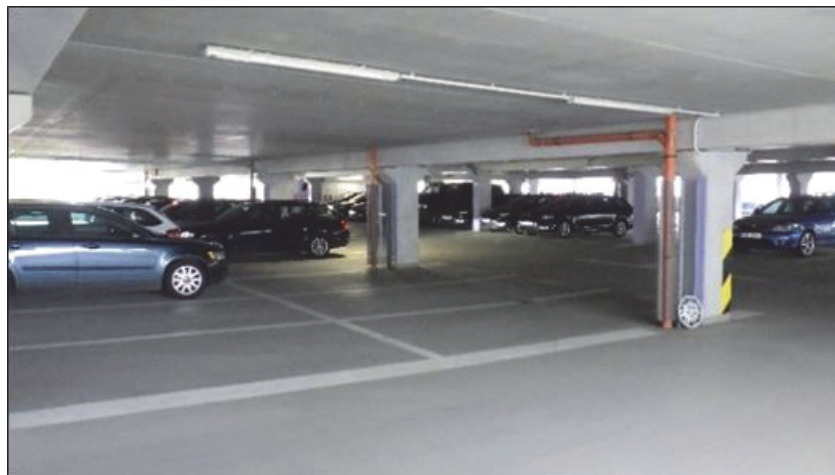


Fig. 7: The floor surface of the third floor of the garage after five years of service

Exceptionally successful outcomes resulted mainly from close cooperation of the designer and contractor during the design phase and by execution of compact, aesthetic and highly economical structure. The gained experience suggests that in structural design, it is beneficial to:

- Respect operating requirements and site conditions
- Suitably modify shape of the structure as was demonstrated here by the inclined surface of parking areas
- Divide the building into functionally and technologically different parts that may then be executed in parallel
- Increase durability and serviceability of the structure by using prestressed elements (to avoid leakages) and ensure structural robustness by monolithic concrete.

When compared to the originally designed monolithic structure, the case study shows the following benefits of the monolithic-precast system:

- a) The hybrid system made it possible to reduce a total volume of concrete and thus weight of the structure (in particular slender precast columns and floor monolithic-precast structures with lower depths), see Tab. 1.

b) Reduced time of execution in a constrained construction site:

- Simultaneous execution of precast and monolithic structures
- Precast structural members with large volumes of concrete decreased an amount of on-site operations
- Hybrid floor structures executed without additional supports.

c) Increased durability and serviceability:

- Inclined floor structures ensure proper drainage
- Minimised constrained shrinkage by segmentation of staircases and of the rondel that support the hybrid floor structures.

7. ACKNOWLEDGEMENTS

This work has been supported by the Czech Science Foundation under Grant P105/12/G059.

8. REFERENCES

- Caspeele, R., Sykora, M., Allaix, D. and Steenbergen, R. (2013), “The Design Value Method and Adjusted Partial Factor Approach for Existing Structures”, *Structural Engineering International* 23/4, pp. 386-393.
- Caspeele, R. et al. (2017), “Partial Factor Methods for Existing Concrete Structures”, *fib bulletin* 80, Fédération internationale du béton (*fib*), *fib* COM3 TG3.1. 129 p.
- EN 1990 (2002), “Basis of structural design”, CEN, Brussels.
- EN 1992-1-1 (2004), “Design of concrete structures – General rules and rules for buildings”, CEN, Brussels.
- fib* (2013), “*fib* Model Code for Concrete Structures 2010”, Lausanne: *fib*, p. 402
- Holicky, M., Diamantidis D. and Sykora, M. (2016), “Effect of Quality Control on Reliability of Reinforced Concrete Structures according to Eurocodes”, *Performance-based Approaches for Concrete Structures - Proceedings of the fib Symposium 2016*, 21-23 November 2016, Cape Town. Lausanne: *fib*, p. 103-104.
- ISO 13823 (2008), “General principles on the design of structures for durability”, ISO, Geneva.
- Malioka, V. (2009), “Condition indicators for the assessment of local and spatial deterioration of concrete structures (doctoral thesis)”, Zurich: ETH, p. 235.
- Sykora, M., Holicky, M. and Markova, J. (2013), “Verification of Existing Reinforced Concrete Bridges using a Semi-Probabilistic Approach”, *Engineering Structures* 56(November 2013), p. 1419-1426.
- Vacek, V., Sýkora, M. and Vančík, V. (2016), “Impact of structural and technological optimisation on quality and durability of concrete car garages”, *Proc. Advances and Trends in Engineering Sciences and Technologies II*, Tatranské Matliare, Slovak Republic, 29 June – 1 July 2016. Boca Raton/ CRC Press, p. 661-666.

THE SANNA-BRIDGE – “TEMPORARILY SUSPENDED” SUPER-STRUCTURE SAFELY LANDED

Herbert Weier

Swietelsky Baugesellschaft m.b.H.

A- 1040 Wien, Wiedner Hauptstrasse 56

SUMMARY

In order to ensure proper access for construction of the Perjen tunnel, it was necessary to erect the 166 m long Sanna bridge in the region of the western portal. The construction company Swietelsky Baugesellschaft m.b.H. won the tender with an alternative offer. The alternative offer consisted of a post-tensioned box girder bridge, rather than a composite bridge, with a total weight of 5,400 tonnes. The superstructure was constructed 2.35 m above the final position and was then lowered within 9 days.

1. GEOGRAPHICAL POSITION



Fig. 1: Route Diagram ASF INAG

In the federal states of Tyrol and Vorarlberg, the route of the S16 Arlberg expressway runs from the Zams interchange following the A12 Inn valley motorway up to the Bludenz-Montafon interchange where the S16 expressway merges into the A14 Rhine valley motorway. The project area is located in the federal state of Tyrol between the Zams interchange and the Landeck West interchange, in the municipal areas of Zams, Stanz, Grins and Landeck.

2. CONSTRUCTION OF THE WORKS

2.1 Site conditions and construction period

The Sanna bridge, with a total length of 166 metres and only 2 support columns, is nevertheless a very complex structure. The extremely short construction period, restricted space conditions and the need to maintain the traffic flows, combined with headroom conditions that were reduced to a minimum, made it into the kind of challenge that we technicians are so fond of.

Once the access date for developing the Perjen tunnel structure had been irrevocably confirmed we were left with barely 10 months of construction time. Another constraint was the requirement in the water law decision that all work in the river Sanna's runoff area had to be completed by the end of March at the latest. This virtual halving of the construction period for the entire substructure, therefore, made it necessary to work on all the building axes simultaneously.

2.2 Reinforced concrete bridge version

A clear headroom of at least 4.70 m in the final state is ensured for the roads passing underneath. When construction of the bridge is in progress, compact protective scaffolding will be installed for the roads passing underneath, ensuring a clear headroom of at least 4.30 m under the protective scaffolding.

Our choice of executing a reinforced concrete bridge in an elevated position, including lowering of the supporting structure, had already been examined at the tendering stage. The planners, however, felt that this type of execution was too cost-intensive and, moreover, the higher weight would lead to problems with the foundations.

Thus the following description was defined in the tender specification for construction of the new Sanna Bridge: "The bridge will be executed as a composite supporting structure made of steel and concrete. The bridge's static system will be formed by a three-span beam which is supported on spherical bearings on the two centre supports and the abutments".

Fortunately, we did not share this view so, on the one hand, we were able to build a post-tensioned box girder bridge appropriate to the existing bridge and, on the other hand, we offered the client a cost saving. The indisputably higher weight of the supporting structure is counterbalanced by the fact that, contrary to the original proposal, we chose large drilled piles for the foundations of the river piers as well as for the eastern abutment. This was also associated with a reduction in the geological risk as the excavation pits no longer had to extend under the riverbed.

2.3 Static system and construction

The static system of our post-tensioned box girder superstructure is formed by a three-span beam with the width between supports being 2 x 51.0 m in the outer spans and 64.0 m in the centre span.

The supporting structure consists of a haunched reinforced steel deck slab ($h=50$ cm above the webs and 28 cm in midspan) and a single-cell box girder. The overall height of the supporting structure, in this case, is 3.0 m.

Geometry:

Outer edge beam	1.25 m
Hard shoulder	1.00 m
Carriageway	3.50 m
Carriageway	3.50 m
Carriageway	3.50 m
Hard shoulder	1.00 m
Inner edge beam	1.25 m
Total	15.00 m

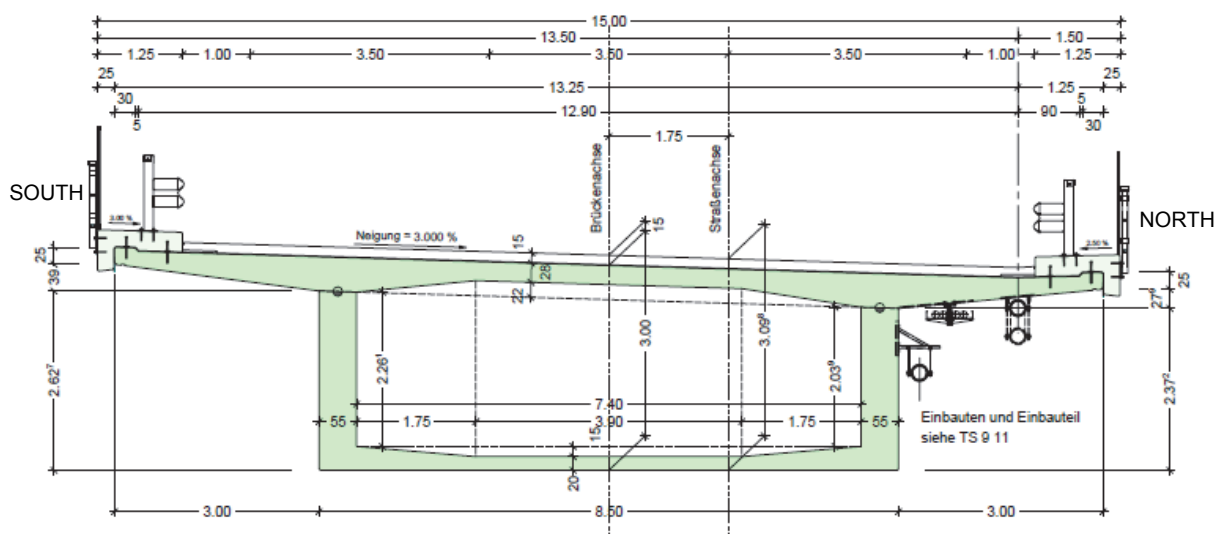


Fig. 2: Cross-section



Fig.3: Longitudinal section

The supporting structure was basically divided into 3 construction phases; priority was given first to the two outer spans, each equipped with a 10 m cantilever arm. After finishing the outer spans, the construction of the suspended centre span was done.

The centre support columns are formed by cylindrical reinforced concrete columns (2.5 m diameter) on which crossheads with a width of 8.5 m and a height of 2.75 m are situated. As the bridge's visual appearance had to meet the tender criteria in its dimensions, we equipped these crossheads with transverse prestressing in order to absorb the higher weight of the supporting structure.



Fig. 4: Crosshead



Fig. 5: Concreting of section 1 superstructure

Of course, the key feature of our alternative was that the entire 166 m long bridge superstructure was constructed in an elevated position and our “Big Bertha” was subsequently lowered by 2.35 m (!!). Even if the title of our presentation speaks of a “temporarily suspended superstructure”, we’re not really talking about levitation when the total weight is 5,000 metric tonnes.

2.4 Falsework

Rolled girders, which were supported on sloping yokes (due to the traffic flows which had to be maintained), were used to execute the scaffolding of the outer spans. The varying levels of deflection arising, as a result, were the subject of many long discussions. In the 64 m long centre span, 2.40 m high and 32 m long lattice girders were used. On the one side, they were supported on the crossheads of the piers and on the other side on an auxiliary yoke situated in the middle of the Sanna.



Fig. 6: Falsework

2.5 Lowering operation

After completion of the supporting structure, where in the individual sections the trough structure and deck slab were concreted separately to reduce the loads on the scaffolding, and after removal of the formwork, the structure rested on the previously installed set-down

stacks. These stacks are formed mainly by concrete-lined 10 cm thick steel pipes of seamlessly drawn piping with a diameter of 50 cm. Due to the great height and reduction of the buckling risk, precast concrete elements measuring 1.00 x 1.00 x 0.35 m were used up to a height of 1.75 m. Press stacks, on which the hydraulic presses were situated, were constructed in the same way next to the set-down stacks.



Fig. 7: Finished superstructure



Fig. 8: Lowering stack

Support of the finished supporting structure provides for fixed bearings in the area of pier 1. This support was also retained in the elevated position. To dissipate the horizontal forces, plain bearings which were movable in the longitudinal direction and fixed in the lateral direction were installed in the set-down stacks in all the other bearing axes. Of course, these plain bearings were removed again during the lowering process. The 24 hydraulic presses used were controlled via a path- and force-controlled synchronised hydraulic system with PC-control. This system is accurate to within +/- 1 mm.

The lowering process took place axis by axis, with 2 axes always being lowered simultaneously by 4 cm at a time. At the same time, in a path-controlled manner, the presses raised the superstructure in the corresponding bearing axes by 3 mm, lining material with a thickness of 4 cm was removed from the set-down stacks, and the structure was set down again on the set-down stacks. This process started on the abutments, with both piers always following subsequently. The friction on the remaining axes was so high due to the heavy weight of the superstructure that it was possible to dispense completely with guide girders. The press stacks had to be progressively and appropriately dismantled prior to reaching the maximum travel distance of 200 mm.

Since with a lowering height of more than 2 metres it cannot reliably be assumed that the lowering process will be 100% vertical, we had made provision for any need to move the supporting structure longitudinally and transversely. However, as the positional deviation at the end of the 9-day lowering process was only 1.5 cm, this corrective action was dispensed with.

2.6 Completion

Subsequently, it was only necessary to install the spherical bearings, weighing up to 1,200 kg, to weld them to the already concrete-embedded anchor plates and to construct the bearing pedestals.

On 04.12.2015, after a construction period of only 10 months, the bridge was opened to the client on time so that construction site traffic had access for construction of the 2nd tunnel tube of the Perjen tunnel.

3. CONCLUSION

At this point, I would like to say that it was only possible to achieve this target due to the fact that all the parties involved, starting with the project management of Asfinag, the local site supervision, representatives of the authorities not to mention the labourers and employees of the construction companies, all pulled together from start to finish of the construction site.

I would like to conclude our presentation with a quote from the French artist Francis-Marie Picabia which sums up how the project was handled and the structure's success:

“Our heads are round so that our thoughts can change direction!”

With this in mind, ladies and gentlemen, may I propose that you too look for unconventional solutions and also allow their use. Success will justify your decision.

FOUNDATION SLABS SUPPORTED BY SPOT FOOTING

Árpád Orosz, János Nagy, Ernő Zábrádi, Aliz Horváth, Imre Répáczki
SWIETELSKY Hungary Ltd.
42 Rákóczi Road, Budapest 1072

SUMMARY

The essay presents the foundation systems of underground garages, drain systems with one- and two shell breast walls, advantages and disadvantages of raft and deep foundation methods and supported foundation slabs evolved through their combination. It submits in detail the simplified technical calculating method of the supported foundation slabs, and the determination of the bending moment and punching load. It introduces the bending and punching reinforcement systems used successfully in practice, called “torus” reinforcement which ensures the load distribution getting to the spot footing besides conveying punching.

1. INTRODUCTION

Through the development of the urban traffic and the spread of motor vehicles, it has become necessarily to create parking areas. The needs cannot be satisfied by building parking lots, therefore it is required to create so-called underground garages, even though the cost of the construction of a parking place is the highest. This essay is concerned only with the approximate determination of the forces in play for foundation slabs supported by deep foundation, applied only in underground garages.

2. STRUCTURAL SYSTEM OF UNDERGROUND GARAGES

2.1. Structural system of underground garages designed with diaphragm wall

The structural system of underground garages built with diaphragm wall bordering can be sorted into three groups:

- single-layer, single-shell,
- double-layer, double-shell breast wall,
- double-layer breast wall with drainage systems.

Instead of detailed review, – at this point – only the most important, typical properties are presented.

2.1.1. Single-layer system

The most important features of this structural system (Fig. 1a) are the undermentioned:

- the diaphragm walls ensure the mass insulation and water tightness on their own,
- the surface about the inner space of the diaphragm wall remains free,
- the foundation slab and the intermediate slabs join to the slot created in the diaphragm wall.

The groove created by additional slotting in the diaphragm wall is highly unfavorable, regarding both the water tightness and the bearing capacity of the diaphragm wall. The water seeping through the concrete must be handled. Finally, it is found that the single-layer system makes a cracking sensitive structure, therefore its application is not recommended (Orosz, 2005).

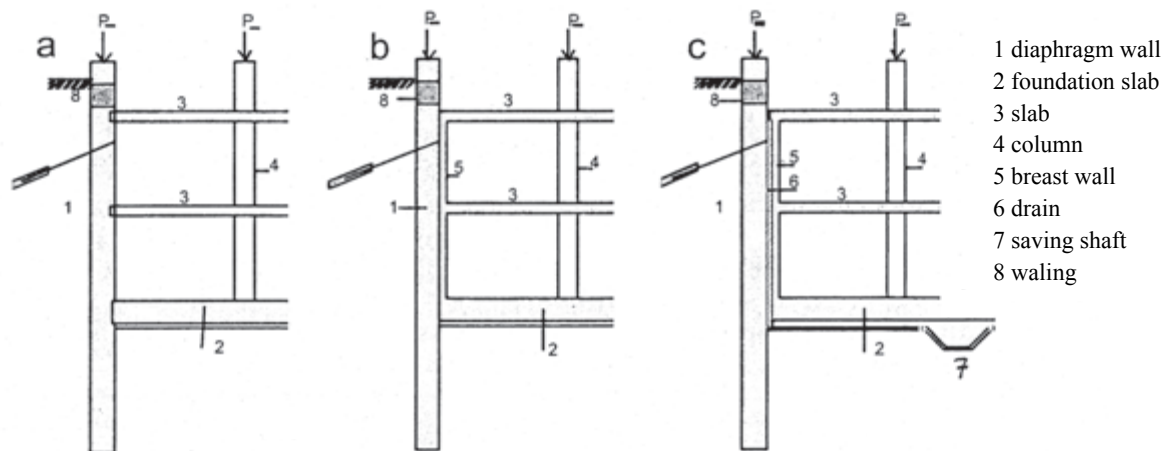


Fig. 1: Underground garages with diaphragm wall

2.1.2. Double-layer breast wall system

The particularity of this system (Fig. 1b) is that a so-called breast wall is created inside the diaphragm wall, so in this case it is unnecessary to form a slot in the diaphragm wall, because the foundation and intermediate slabs join to the breast wall. The connection between the diaphragm wall and the breast wall can be ensured by reinforcement, then the two structural elements bear the loads together because of their co-working.

It can be ascertained that the structure is crack sensitive also in the case of multi-layer systems because of the presence of restrained deformations, regarding both the bed plate and the intermediate slabs.

2.1.3. Double-layer breast wall system with drainage

The watertight foundation system with drainage (Fig. 1c) has been developed through the improvement of the breast wall system, which can be applied when the diaphragm walls bordering the foundation system can be stood into an impermeable soil stratum. In this case the amount of water seeping through the side and bottom of the diaphragm wall is small, it can be collected by drainage and wiped away by pumping out or rather utilized. The drainage between the diaphragm wall and breast wall such as Dörken plate collects water seeping through the side of diaphragm wall, in turn the drainage system created under the bed plate collects water seeping from beneath. We mention that in the case of approximately 70 underground garages built with this system some hairline cracks only appeared in few cases near the working joints in the course of concreting in the summer, and their spaciousness not exceeding 0.3 mm.

Finally, it can be stated that the breast wall system with drainage provides an optimal solution regarding both cracking sensitivity and water tightness.

2.2. Foundation system of underground garages

Through choosing the foundation system of underground garages it is possible to choose from the undermentioned opportunities (Fig. 2):

- deep foundation,
- raft foundation,
- foundation slab supported by spot foundation.

It can be decided for the optimal solution out of these by taking into consideration the current circumstances.

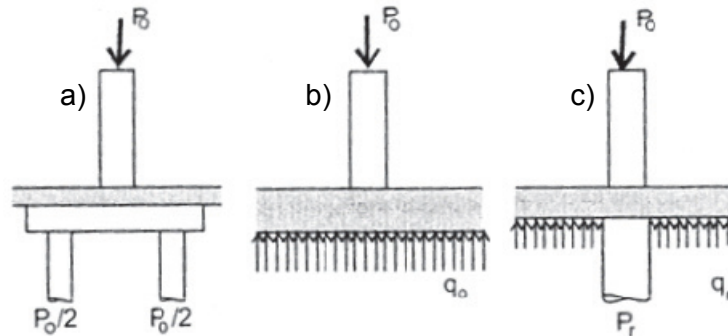


Fig. 2: Foundation systems

2.2.1. Deep foundation

At this method the deep foundation bears the whole pillar forces, and the foundation slab is only loaded by the water pressure impressing upwards from beneath, and uplifting has to be analysed (Fig. 2a).

The advantage of deep foundation is that the extent of settlement is low and the settlement differences can be kept down also in the case of significantly diverse pillar forces.

2.2.2. Raft foundation

In this case the whole pillar forces, pillars are born by the raft foundation or rather conveyed to the soil (Fig. 2b). The advantage of the slab foundation is that its construction, the reinforcement assembling and concreting can be executed the easiest and its costs are low. The disadvantage is in case of stiff plates the concrete technology requires special respect because of the effect of shrinkage and heat-on-hydration. The settlements are bigger than in case of deep foundation and the settlement differences can be significant in the case of substantially diverse pillar forces. It is explicable with the above mentioned that the cracks and failures in case of such structures appear after the structure of the building has been constructed and last for years.

2.2.3. Foundation slabs supported by spot footing

The total pillar load is born by the deep foundation and bed plate together (Fig. 2c). The principles regarding static working of the bearing foundation system developed by combining the spot footing and bed plate can be summarized in the undermentioned:

- part, e.g. 50% of the pillar forces is conveyed to the spot footing,
- the other part gets into the bed plate, as the bed plate tightened to the soil bears soil stresses and water pressure as a bent structure because of the deformation of the spot footing,
- in the case of system with drainage the water pressure is not present.

The greatest advantage of the system of supported foundation slabs is that in case of significantly different pillar forces – e.g. buildings with back yard – the settlement differences can be reduced with spot footing, sufficiently choosing their number, size and depth.

Comparing with the raft foundation – as a consequence of load distribution – the thickness of bed plate can be reduced to almost half of it. The concrete saved this way gets to be used in spot footing, thus the amount of concrete built in basically does not decrease, however the material gets to the place where it is mechanically needed the most, so it results a much better structure. It is not necessary to fit the spot footing with reinforcement, because only pressure is delivered.

The greatest settlement difference measured on the constructed structures has not exceeded 10 millimeters, furthermore the crack width is within prescribed limits.

The advantage of the foundation system is also that the stiffness of the foundation and the upper structure is increasing gradually providing accordingly the circumstances of the optimal co-working of soil, foundation and structure.

3. QUESTIONS IN CONNECTION WITH THE STRUCTURAL ANALYSIS OF FOUNDATION SLABS SUPPORTED BY SPOT FOOTING

3.1. General principals, load distribution

It is easy to see reason that the foundation slab tightens to the soil due to the settlement of spot footing and it takes part in bearing of pillar forces, and the utilization of load bearing capacity of the bed plate is natural, mechanically and technically reasonable, and the load distribution makes it possible to create an economic, optimal foundation system. Certainly the problem is raised that in which extent the spot footing and bed plate take part in load bearing. In our home country, first Arpád Kézdi suggested and applied the joint load bearing of the deep foundation and bed plate through strengthening of the grain elevator in Kaposvár (Kézdi, 1963; Mahler, 2008). The successful of execution gave incentive to János Nagy, senior engineer at VÍZÉP company to improve and apply more expansively the supported foundation system. Since the beginning the problem was the determination of the load distribution ratio. Therefore, in default of precise theoretical methods the load distribution ratio has been determined through loading tests and measurements. Results of measurements carried out in natural size are reliable, so the practical application has been approved (VÍZÉP, 2000).

Several structures have been constructed with the method initially defended, and nowadays this advantageous foundation system is more and more expansively prevalent, especially the breast wall drainage system called watertight version. The factors influencing the load distribution ratio are the undermentioned: the quality and stratification of subsoil, the size and depth of the spot footing, the distance and size of the columns, the thickness of bed plate. Such calculating method, which determines the load distribution ratio between spot footing and bed plate more precisely, theoretically well-founded and practically appropriate, is not processed today. However, investigations regarding this have been begun (Józsa, Móczár, 2011).

3.2. Principals of the early calculating methods

At the time of the first application of foundation slabs supported by spot footing, the loading of bed plate was determined through the generally known and applied method at that time which had been worked out for slab plates besides the supposal of consistently distributed soil stresses (Pfaffinger, Thürlimann, 1967; Eisenbiegler, Lieb, 1979; CEB, 1985). On checking this method rested on theory of elasticity, Bertalan Juhász worked out a yield-line theoretical method rested on theory of plasticity, applied easily in practice which determines the critical condition for failure. The reinforcement system came to configure through comparing and weighing up the state determined in two ways.

3.3. Trends of specifying the calculating method

3.3.1. Effects of soil stresses bearing the foundation slab

The distribution of soil stresses bearing the foundation slab is varying in time. Under construction it increases from zero and changes consistently because of soil consolidation. Its initial distribution is shown in Fig. 3 by continuous line. After the building is ready the variation keeps going on the way that the stress under the column is decreasing, contrarily in the pane increasing. As a consequence, the bending moments in pane are increasing compared to the initial phase, in turn the bending moment under column is decreasing. On calculating precisely this temporal variation there is no well worked out method today, but the increase of the bending moment in pane is obvious.

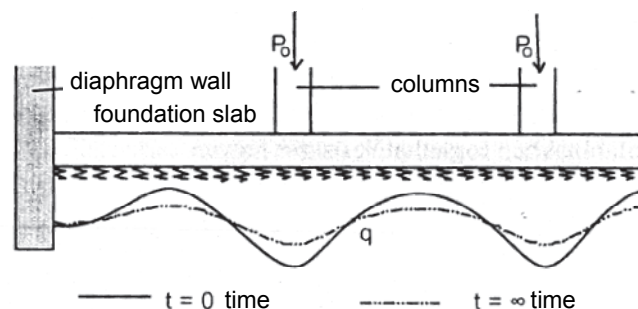


Fig. 3: Soil stresses bearing the foundation slab

3.3.2. Contrasting crack-free and cracked phase

Methods rested on theory of elasticity assume the crack exemption of reinforced concrete elements. Because of the crack of the bent structure the stiffness decreases to almost half, and the realignment of loading occurs. Due to the phenomenon the bending moment is decreasing in the more rigid parts, under the columns, but in piers it is increasing. Precise calculating method on this realignment of loading, which is also come in useful in practice does not exist today (Fig. 4).

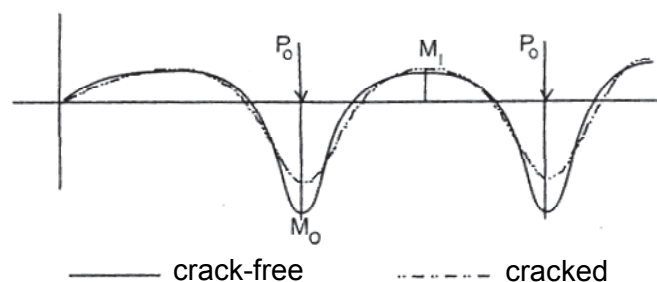


Fig. 4: Realignment of loading due to crazing

3.3.3. Issues regarding computer analysis

Along practical application of methods worked out for slab plates, there appeared computational methods, for this foundation system too. In connection with the calculated loading, the problem was principally the ratio of bending moments under the columns and in pane. Since the ratio of bending moments evolving in pane and under columns is 1:4, or rather 1:5, which caused by that the fillet of bending moment diagram is not determined properly. The bending moment peaks are high because of the pointwise support, which discharge significantly on the cracked structure.

4. TECHNICAL ANALYSIS OF FOUNDATION SLAB

4.1. Necessity of technical calculating method

In the previous chapter we pointed out the issues that make the exact determination of the stress of the foundation slabs supported by spot footing more difficult. The experience gained during the first few occasions of applying such architectural system proved its advantages, economic efficiency and reliable functioning. Thus, the development of a simple calculation method that makes the practical implementation of the system possible in a safe way became necessary. The requirements related to the calculation method applicable in practice are summarised as follows. It shall

- be simple, clear
- provide proper safety.

4.2. The definition of load distribution

In case of spot footing sizes applied in practice, base slab thickness of 40-60 cm, less than 10 meters of distance between pillars, average soil conditions. Based on the deformation measurements carried out during load tests on foundation structures built by VÍZÉP and also based on theoretical consideration, the load distribution could be uniform for the whole foundation system; but the structure will be economically more efficient and more favourable if at the high-load pillars more load is placed on spot footing, thus flexibly adapting to each - and even every single - pillar load. The proportions of load distribution can most reliably be determined through test load, but nowadays neither contracting prices nor time limits allow for that. In the course of dynamics check, usually it is the basic 50-50% load distribution that is used as a basis, which then can be fine adjusted considering the circumstances.

4.3. The calculation of bending moments

4.3.1. Principles

As mentioned earlier, the load distribution between the spot footing and the base slab can be uniformly the same on the entire base slab or it can vary at each pillar. The disadvantage of uniform load distribution is that in case of higher pillar loads the plate thickness needs to be increased in order to bear bending moments and punching. This local thickening unfavourably affects both the establishment and the reinforcement of the base slab. It is more expedient and economical to determine the load distribution pillar by pillar in a way that the thickness of the base slab remains the same and adapting to varying stress is done by making changes in the reinforcement. If we determine load distribution for individual pillars, then it is advisable to

develop the practical calculation method in a way that stress can be calculated directly from the pillar loads as follows:

Pillar load P_o [kN] is distributed between the spot footing and the base slab,

load on the spot footing: $P_r = \alpha \cdot P_o$

load on the base slab: $P_1 = (1 - \alpha) \cdot P_o$

The coefficient α may vary between 0.3 and 0.7; we usually consider $\alpha = 0.5$ value as a basis.

Ground reaction effect on the base slab is calculated from: $q = \frac{P_1}{l_x \cdot l_y}$

The bending moments can therefore be determined with the formula from the pillar load directly affecting the base slab. $m = c \cdot q \cdot l_x \cdot l_y = c \cdot P_1$

The c values are recorded on the basis of table-values for solid flat plates from relevant literature, but we modified them according to the followings (Pfaffinger, Thürlimann, 1967; Eisenbiegler, Lieb, 1979; CEB, 1985).

Estimating the cracked fake base in the plate strip and the change caused by the consolidation of ground stress to result an increase of 20%, we increased the values from the relevant literature by this percentage. The coefficient $c = 0.05$ proposed in the plate strip includes this increase.

At the moments under the pillars we ignored the same 20% decrease because of the effects mentioned above. The rounding, reduction of the moment-tips may even result a decrease of 30-40%. The effect of difference in the subsidence of pillars is considered in a way that we recommend the quasi average of the values that can be determined for the stationary supported plate and for the flexibly embedded plate. Based on this, the coefficient under the pillars can be applied with the value of $c=0.15$. The proportion of the moments calculated in the field and under the pillars is 1:3 which is realistic and incorporates the effects of both the rounding and the settlement differences.

4.3.2. Determining the moments

The moments under the pillars can be calculated directly from the pillar loads according to the above mentioned. The moments of the plate fields can be determined by considering the heavier pillar load from those of two identical pillars, for safety reasons. The result will be closer to reality if we calculate with the average of the two pillar loads. The moment generated in the middle of the field is also advisable to be determined with the average of the four pillar loads.

Tab. 1: Comparison of calculating methods

Moment [kNm/m]	CEB	Eisenbiegler	AXIS	Orosz	c
m_0^-	1265	1008	1956	741	-0.15
m_0^+	265	252	287	247	0.05
m_m^-	213	94	95	198	-0.04
m_m^+	91	163	180	248	0.05

$P_o = 12350$ kN $\alpha = 0,6$ $l = 7.50$ m



For information purposes, in Tab. 1, we present the moments that can be calculated with the different calculation methods for a simple case. It is clear that the deviations are significant, which is to be considered during planning.

4.3.3. Forming the reinforcement

Based on the experience gained in building more than 50 structures, it is advisable to establish the reinforcement system according to the followings; Lower, upper base mesh reinforcement in two directions with equal spacing during reinforcement. The minimum percentage of reinforcement should be 0.3% since this amount of reinforcement is enough for practically any field moment and the crack limitation requirements are also fulfilled. Its advantage is simple installation and flexibility in connection with construction joints and concrete modules. Ø16/15 cm size base netting is advised. Supplementary netting under the pillars, applying compression using reinforcing steel bars with bigger diameter than that of the base netting.

The identical reinforcement in both directions is also justified by the rotationally symmetric load distribution. The rotationally symmetric load distribution is acceptable up to the 1:2 lateral pillars; and only in case of larger, oblong shear walls is local, more accurate investigation needed.

4.4. The analysis of punching

4.4.1. Punching issues of reinforced concrete

In case of substructures supported by spot footing the establishment of punching shear reinforcement is of crucial importance. The reinforcement system applied here has dual purpose; first, it has to bear the punching force, and also it has to ensure the reliable transfer of pillar load to the differently arranged spot footing. The failure of the punching shear reinforcement, the brittle breach, may occur suddenly without previous sign; and also, its repair is extremely difficult and costly. This is why extraordinary safety is reasonable (Orosz, 2004-2005).

In case of reinforced concrete base slabs, several special influences, which do not occur in case of flooring systems, must be considered. The most important of these are summarised below.

Pillar loads that cause punching reach their planned values as a result of continuous increase in the course of building. In case of monolithic structures, the bracing effect of the superstructure is continuously present, which, in part, can also have an effect on the values of the pillar loads because of the unequal subsidence. The distribution of ground stress is changing during the construction phase because of the consolidation. The peak-stress under the pillars decreases by time but increases in the fields.

4.4.2. Applying torus reinforcement

Because of the problems related to punching failures, in order to improve safety, we recommend handling all the punching force by applying reinforcement. The reinforcement applied to avoid punching comprises only a few percent of the entire reinforcement applied on the structure, therefore the extra reinforcement here does not affect the economic efficiency of the structure but it provides significant protection against a bothersome type of failure.

The punching shear reinforcement can be seen in Fig. 5, with ring-oriented reinforcing bars and hoops, with a reinforcement system characteristic for beams, the lower and the upper base netting; and, with the so-called bridging reinforcing bars that connect the supplementary nettings, a densely reinforced plate section is formed above the spot footing, which, as a beam, ensures the reliable transfer of pillar loads onto the spot footing. The bridging reinforcing bars, by connecting the lower and the upper reinforcement, due to the pin-effect involve these reinforcements into bearing the shear force providing extra safety.

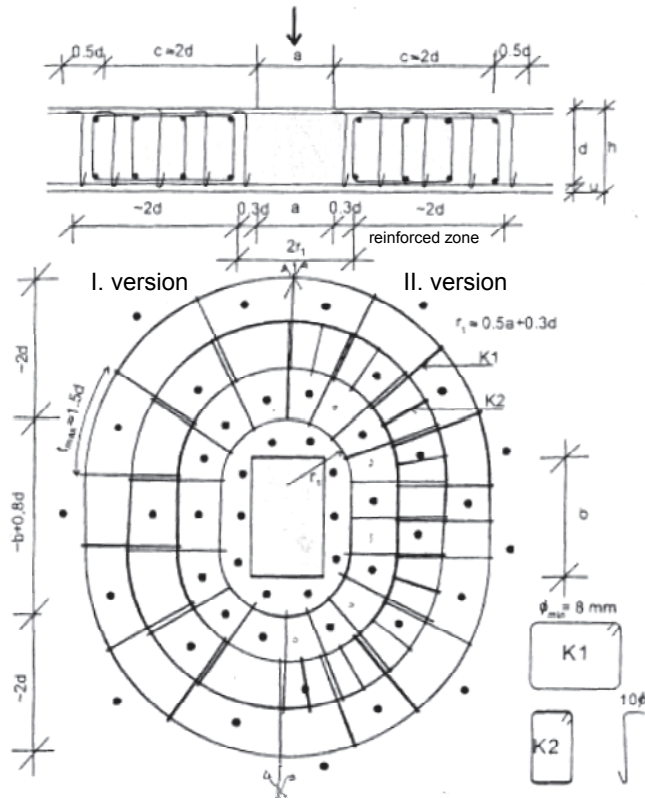


Fig. 5: Design of the torus reinforcement

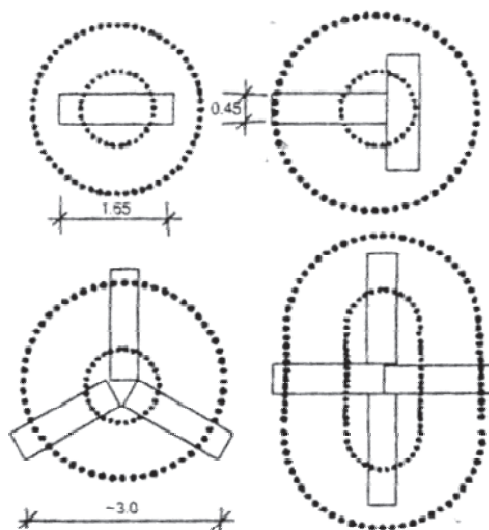


Fig. 6: The arrangement of spot footing and torus reinforcements

5. SUMMARY

Foundation slabs supported by spot footing - where loads on the base slab are jointly held by the spot footing, as deep foundation, and the flat plate - have been applied with success in the past decades. The proportions of load distribution have been determined through measurements carried out in realistic dimensions, which proved proportions between 0.3-0.7 to be appropriate. Initially, loads were calculated with methods applied to flat plates in a condition without cracks. A modified and simplified method had to be developed for considering cracked condition and the changes of ground stress over time. Besides the dynamics calculations, a new, easily mountable reinforcement system has been formed, which considers the nearly rotationally symmetric forces around the pillars by applying both the bending moments and the special “torus” reinforcement developed for punching shear reinforcement. The advantage of the system is that by choosing the number and size of the spot footing, we can adapt to different amounts of load and therefore unequal subsidence can be reduced. Subsidence measured in finished construction projects can be reduced. Subsidence measured in finished construction projects and subsidence differences were below 1 cm. Considering the load distribution and the reinforcement method itself together form a uniform system developed by Hungarian engineers, therefore it can be regarded as a Hungarian construction system.

The most important components and features of the system:

- securing the excavation pit with diaphragm wall,
- supporting the foundation slab with spot footing,
- binding the foundation and intermediate slabs to the breast wall,
- method of load distribution, starting off the load bearing capacity of the base slab,
- reinforcing system of the foundation slab, lower-upper base netting with supplementary netting,
- applying torus reinforcement for punching.

If the bordering diaphragm walls bind to impermeable subsoil it is possible to create a watertight system with drainage, its advantages are:

- perfect water tightness,
- no water pressure loads the foundation slab, no uplifting.

The components of the system cohere, changing of them reduces the reliability and efficiency. The arrangement of the spot footing and torus reinforcements is shown in *Figure 6*.

6. ACKNOWLEDGEMENTS

The authors of present summarising study are fortunate and feel grateful for that - on the basis of experience gained by the engineers of VÍZÉP - they had the opportunity to participate in the construction of the reinforced foundation systems of some 60 underground garages, they could participate in developing the practical calculation method and, further developing Árpád Kézdi's principle of applying reinforced foundation systems, they could implement it in the foundation systems of underground garages. Of course, engineering work is team work, and therefore special thanks to the participants: engineers Bertalan Juhász, Csaba Bancsik and Ernő Zábrádi who played a very important role in the fine adjustment and development of the system.

7. REFERENCES

- Kézdi Á.: *Szakvélemény a kaposvári 1000 vagonos gabonasiló cölöpalapozásáról*, (Kézirat) 1963.
- Pfaffinger, D. – Thürlimann, B.: *Tabellen für unterzuglose Decken*, Verlag AG, Zürich 1967.
- Eisenbiegler, G. – Lieb, H.: *Schnittgrößen und Verformungen von Pilzdecken mit Stützen Kopfverstärkungen infolge von Gleichlast*, Beton – und Stahlbetonbau Heft. 9. 1979. S. 219-225,
- CEB Manual, *Cracking an Deformations*, Lausanne, Suisse 1985.
- Orosz Á.: *Parkolóházak általános tervezési irányelvei*, BME Vasbetonszerkezetek Tanszéke, Vízügyi építő Vállalat - OMFB tanulmány. Kézirat 1997.
- Mélygarázsok tervezése*, Tervezési Útmutató. Magyar Vízügyi Társaság 1998.
- Armuth M. - Deák Gy.: Repedések mélygarázsok födémein, *Vasbetonépítés* 3. 85-91. old. 1999.
- Összefoglaló jelentés a VÍZÉP megbízásából az ÓBUDA GATE Irodaház fenéklemezein mért talpfeszültségekről és alakváltozásokról*, Kézirat 2000.
- Wasserundurchlässige Betonbauwerke - Weisse Wannen*. Richtlinie Österreichische Vereinigung für Beton-und Bautechnik, Wien 2002.
- Dichte Schlitzwände*, Richtlinie. Österreichische Vereinigung für Beton- und Bautechnik. Wien 2002.
- Orosz Á.: Konstruktív elvek az alaplemezek átszűrődésének vizsgálatához - átszűrődés elleni kialakításhoz, *Síklemes födémek átlukadás elleni méretezése*, Tervezési segédlet 1. füzet 2004, 2. füzet 2005., Magyar Mérnöki Kamara, Tartószerkezeti Tagozat
- Orosz Á.: Részfalba befogott alaplemezek és födémlemezek - az alapozási mód megválasztásának következményei. *Geotechnikai Konferencia*, Ráckeve 2005.
- MSZ En 1992-1-1 Eurocode - 2 Betonszerkezetek tervezése, Általános és az épületekre vonatkozó szabályok, 2006.
- Farkas Gy. - Huszár Zs. - Kovács T. Szalai K.: *Betonszerkezetek méretezése az Eurocode alapján*, Közúti Hidak, Épületek. TERC Kft. 2006.
- Mahler A.: Kaposvári gabonasiló alapozásának véges elemes modellezése, *Kézdi Árpád Emlékkonferencia*, 77 - 86. old. 2008.
- Józsa V. - Móczár B.: *Talaj és szerkezetek kölcsönhatása* Elektronikus jegyzet (HEFOP) Budapest. 2011.
- Orosz Á.: Réspillérekkel gyámolított vasbeton alaplemez átszűrődésének egyszerűsített vizsgálata, a tóruszvasalás alkalmazása. *Erdélyi Magyar Műszaki Tudományos Társaság XVIII. Nemzetközi Építéstudományi Konferencia*, Csíksomlyó 248 - 252. old. 2014.
- Orosz Á.: *Mélylappal gyámolított alaplemezek*. A BME Hidak és Szerkezetek Tanszék Tudományos Közleményei. 2016.
- Nagy J.: *Vízmentes, gyámolított alaplemezzel épített munkagödrök*. A BME Hidak és Szerkezetek Tanszék Tudományos Közlemény 2016.

APPLICATION OF MACRO-SYNTHETIC-FIBER-REINFORCED SPRAYED CONCRETE FOR PRIMARY LINING SUPPORT ON HIGHWAY TUNNEL PROJECT IN BOSNIA AND HERZEGOVINA

Vedad Terzić, Reuf Kadrić

Motorways of Federation of Bosnia and Herzegovina Ltd.

Dubrovačka 6, 71000 Sarajevo, Bosnia and Herzegovina

t.vedad@jpautoceste.ba; k.reuf@jpautoceste.ba

SUMMARY

The application of macro synthetic fiber reinforced sprayed concrete is seen by many design engineers as the alternative to steel reinforced sprayed concrete. The first applications of macro synthetic fiber reinforced sprayed concrete in Bosnia and Herzegovina were applied during the construction of the Sarajevo By-pass Motorway. The Project included a Motorway tunnel-system of three (3) double tubed, two-lane tunnels receptively 860 m, 2776 m and 402 m in length, passing through an extensive and diverse geology. In this work application of macro synthetic fiber reinforced sprayed concrete will be presented, giving an inside in the underground condition, the concrete testing, measurements and calculations. The aspects related to the excavation work-cycles and time savings applying fiber reinforced sprayed concrete in the primary lining will also be presented.

1. THE HIGHWAY TUNNEL PROJECT

The Motorway Project is located on the route of the Pan European Corridor 5c: Budapest - Osijek - Ploče and is the most important Project for Bosnia and Herzegovina in the last decade. The construction works on the 20 km long motorway section passing the capital city Sarajevo were significant for the city traffic itself.

The Project started in May 2012 and the construction time was 28 months. The length of the subsection “Lepenica-Tarčin” (Fig. 1) was approximately 10 km and included a number of different structures, whilst the construction of tunnels T2, T3 and T4 was the most significant part of the project. Especially the construction of the Tunnel T3 (later renamed as “Tunnel 25th of November”) with an average length of 2776 m being potentially on the “critical path”. The construction of Tunnel T3 on the subsection “Lepenica-Tarčin” will be the subject of this work.

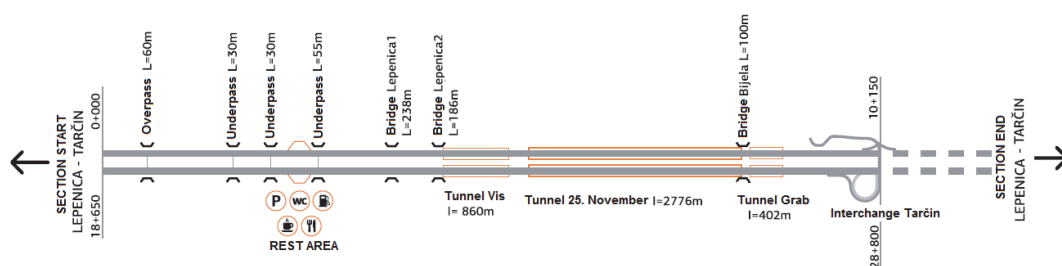


Fig. 1: Motorway Section

1.1 Geometric Elements of Tunnel T3

Right tunnel tube length: 2802 m;

Left tunnel tube length: 2743 m;

Max. Altitude: 664.7 m; max. Longitudinal gradient 3.59 % at north portal;

The carriageway width is 7.0 m, and consists of two lanes of 3.50 m.

The tunnel height is 4,70m.

2. UNDERGROUND CONDITIONS

The Underground conditions (geological formations) on the location of Tunnel T3 were diverse and complex. Three (3) basic types of rock were found (Sedimentary, Metamorphic and Magmatic rocks). The Metamorphic rock were from Paleozoic and the Dolomites were from Devon. In-between two Magmatic layers of Quartz Porphyries were also found (Fig. 2).

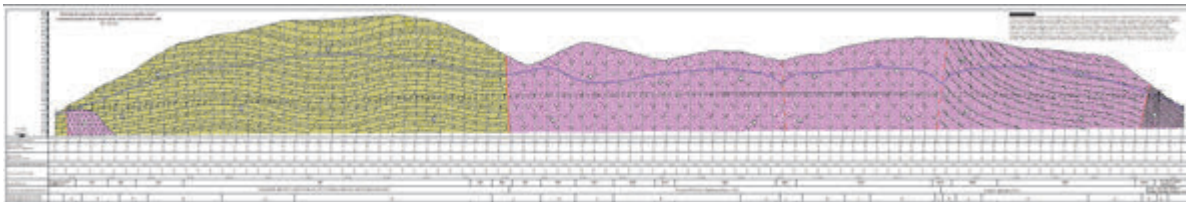


Fig. 2: Longitudinal tunnel section

3. TUNNEL EXCAVATION AND SUPPORT

3.1 Tunnel Excavation and Support Elements (Main Design of the Project)

In accordance to the Main Design documentation in the Project the excavation works were divided into three (3) phases. The top heading, bench and the invert arch excavation phase. In better underground conditions the excavation works were divided in top heading and bench phases only. The Main Design defined rock categories, predicting the round lengths and defining support elements (system) for each of the rock category respectively (Tab. 1).

Tab.1: Rock categories and support elements (systems) in accordance with the Main Design

TUNNEL T3					TUNNEL T3				
LEFT TUNNEL TUBE - DESIGN					RIGHT TUNNEL TUBE - DESIGN				
ROCK CATEGORY	ROUND LENGHT (m)	SUPPORT SYSTEM	LENGTH (m)	PERCENTAGE (%)	ROCK CATEGORY	ROUND LENGHT (m)	SUPPORT SYSTEM	LENGTH (m)	PERCENTAGE (%)
IV	1.5	C2 + S	201	7%	IV	1.5	C2 + S	201	7%
IV/III	2.5	B1	118	4%	IV/III	2.5	B1	299	11%
III	3	B1	600	22%	III	3	B1	630	23%
III/II	3.5	B1	1491	55%	III/II	3.5	B1	1005	37%
II	4	B1	291	11%	II	4	B1	609	22%
TOTAL			2700	100.00%	TOTAL			2744	100.00%

The following support elements were installed according to the rock mass categorization:

B1 - rock mass category

Sprayed concrete C25/30, 10 cm in thickness;
Reinforcement - Mesh Q189, 1 layer;
SN anchors 4 m, 250 kN

C2+S - rock mass category

3 cm thick layer of sprayed concrete and mesh Q131 at tunnel face;
Sprayed concrete C25/30, 20 cm in thickness;
Steel arch TH21;
Reinforcement - Mesh Q189, 1 layer;
SN or IBO anchors 4 m, 250kN;
Concrete invert arch

3.2 Tunnel T3 excavation works

At the early beginning of the Tunnel T3 Project it was obvious that the predicted rock mass categories given in the Main Design are different compared to the actual underground conditions on site. At the entrance portal and the tunnel precut it was identified that the Main Design was predicting 4th (IV) rock mass category and actually 5th (V) rock mass category was present.

Consequently it was necessary to apply other support elements, demanding more time (require longer installation time) than predicted. Due to the underestimation of underground conditions inevitably delays in the excavation works in Tunnel 3 were going to occur.

Only undertaking appropriate measures it was possible to mitigate delays and finish the Project within the expected program of work.

According to the geological predictions approximately two thirds of the Tunnel T3 was located either in dolomitic limestone (approx. 900 m) or quartz-porphyrific metamorphic rock (approx. 900 m). In such underground conditions it was possible to modify the conventional support elements (systems) and apply fiber reinforced sprayed concrete instead of mesh reinforced sprayed concrete. It has been estimated that the changes in these support elements would probably save 2 to 3 hours per round length (step of excavation).

The length of the tunnel rock mass categories where fiber reinforced sprayed concrete could be used was estimated to be 1800 m in length. Average round length (step of excavation) was estimated to be 2.5 m.

Calculating:

$1800 \text{ m} / 2.5 \text{ m} = 720 \text{ steps}$

$720 \text{ (steps)} \times (2\text{--}3 \text{ hours} - \text{shorter installation time}) = \text{makes up to } 1440 \text{ to } 2160 \text{ hours}$

$(1440 \text{ h} - 2160 \text{ h}) / 24 \text{ hours} = 60 - 90 \text{ days}$

In order to implement this idea a 60 m’ test field in Tunnel T3 was formed to compare the behavior of the support elements in real underground conditions. The behavior of mesh reinforced sprayed concrete (cross section 24.300-24.330; 30 m’) and fiber reinforced sprayed concrete (cross section from 24.330 m to 24.360 m ; 30 m’) lining had to be tested.

Measurement profiles were installed (measuring the movements in the primary lining for a period of time until the settlements stabilize) at 24.315 m’ (cross section with mesh reinforced sprayed concrete) and 24.345 m’ (cross section with fiber reinforced sprayed concrete).

4. TUNNEL SUPPORT SYSTEMS USING FIBER REINFORCED SPRAYED CONCRETE

4.1 The updated Q-System

The relation between the rock-mass quality and the support elements (supporting system) using fiber reinforced sprayed concrete is defined by the updated Q-System by Grimstad and Barton (Fig. 3). Identifying the rock-mass quality (Q) for certain rocks the supporting elements (system) can be predicted using the updated Q-System.

For the intended underground conditions in Tunnel T3 where fiber reinforced sprayed concrete could have been used, the rock-mass quality index was ranging between 1 and 10 (D-Poor, C-Fair, B-Good). Considering the Span or Height ratio (for ESR = 1) being 10 the expected reinforcement categories 4, 5 and 6 would need energy absorption capacity between E = 500 - 700 J (see Fig. 3).

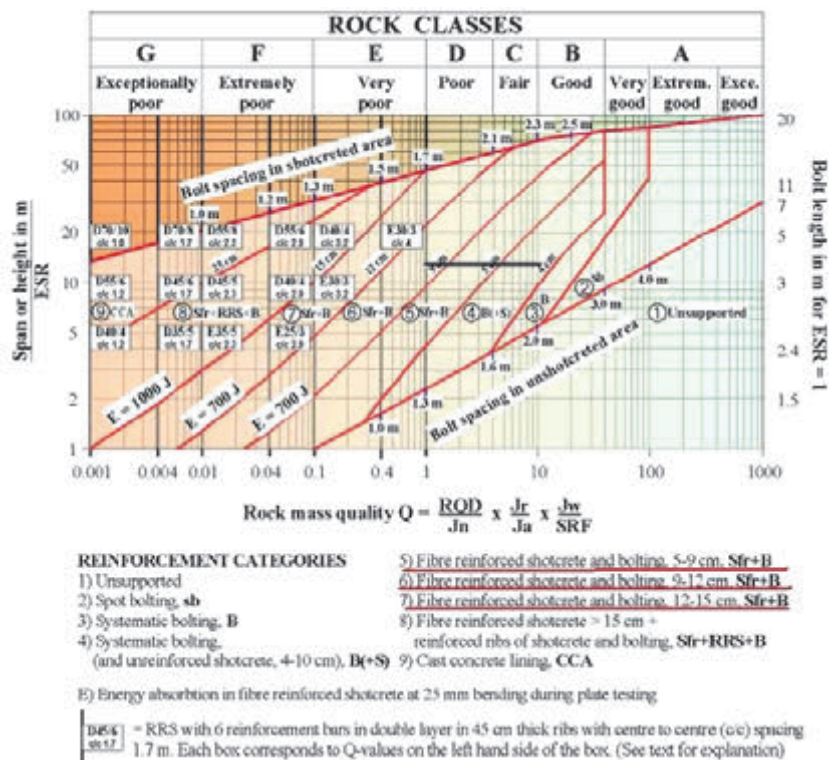


Fig. 3: Updated Q-System (Grimstad and Barton, 1993)

4.2 The Test field of macro-synthetic fiber reinforced sprayed concrete in Tunnel T3

The interaction of the rock-mass and the tunnel primary lining could be observed during the construction, making real scale measurements. Measuring the displacements of the rock-mass the impact on the tunnel support elements could be observed in real time. According to the NATM concept, measurement profiles are installed systematically at characteristic sections along the tunnel. The aim of the monitoring is to predict and to prove the adequacy of the supporting system. This approach was also applied in the test field with the aim to confirm the adequacy of the fiber reinforced sprayed concrete lining in Tunnel T3. The back calculation analysis was used to determine the relevant mechanical characteristics of the rock-mass and to refine the support measures. The test field of a 60 m' section of the both mesh and fiber-reinforced sprayed concrete lining was installed to examine if the fiber reinforced sprayed concrete primary lining could be equally efficient as the conventional primary lining when used in similar geological conditions. In particular the bending capacity had to be assessed this way.

To quantify the efficiency of the fiber reinforced sprayed concrete primary lining, the results from the test section had to be compared with the results of the measurement profiles featuring the conventional primary lining for the same overburden, and very similar geological conditions.

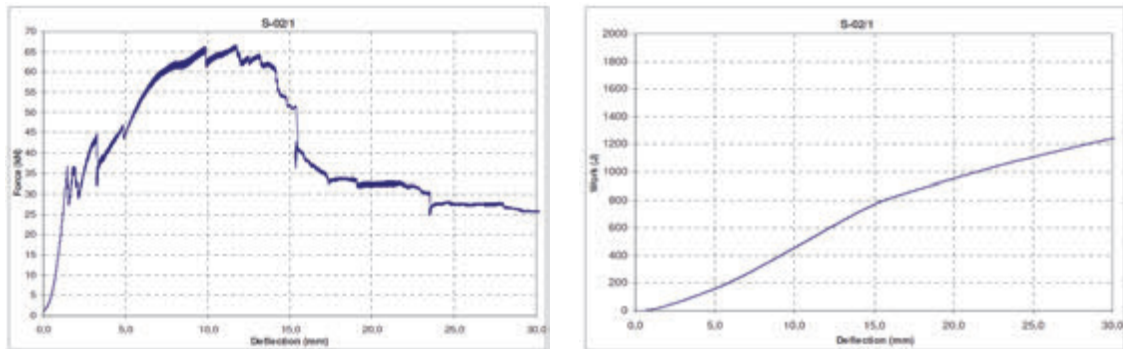
4.3 The Test Setup

The test setup was as follows:

- In to the already used sprayed concrete mixture 4 kg of polypropylene fibers were added. Properties of the "Barchip 54" fibers: length 54 mm; tensile strength 640 MPa; Specific Gravity 0.90 – 0.92; Elastic modulus 10 GPa; Number of fibers per kg 37,000.
- Determination of energy absorption capacity - EFNARC plate test (EN 14485-5;2006) mesh reinforced concrete samples.
- Determination of energy absorption capacity - EFNARC plate test (EN 14485-5;2006) macro-synthetic fiber reinforced sprayed concrete samples.
- Back-calculation for the underground conditions and support measures installed at 24.315 m' (mesh reinforced sprayed concrete).
- Measuring the profiles on cross sections at 24.315 m' (mesh reinforced sprayed concrete) and 24.345 m' (cross section- fiber reinforced sprayed concrete).

4.4 Results of the Testing and Measurements

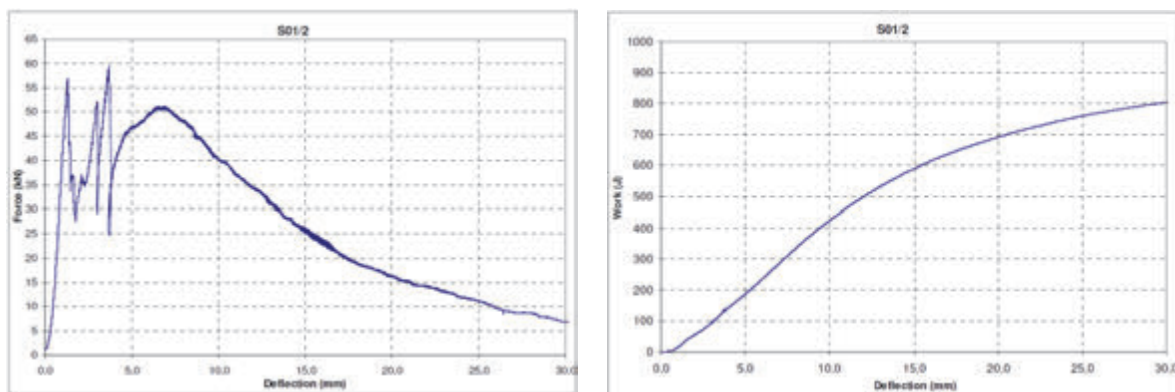
4.4.1 Plate test - (EFNARC, EN 14485-5;2006) mesh reinforced concrete (Fig. 4)



Specimen identification		Average slab dimensions			Maximum load	Energy absorption capacity (for deflection 25 mm)
Laboratory	Client	L (mm)	W (mm)	H (mm)	F_{max} (kN)	E (J)
S-02/1	1	606	607	104	64,4	1110

Fig. 4: Plate test (EN 14485-5) – mesh reinforced sprayed concrete

4.4.2 Plate test - (EFNARC, EN 14485-5;2006) fiber reinforced sprayed concrete (Fig. 5)



Specimen identification		Average slab dimensions			Maximum load	Energy absorption capacity (for deflection 25 mm)
Laboratory	Client	L (mm)	W (mm)	H (mm)	F_{max} (kN)	E (J)
S-01/2	2	597	596	99	43,5	740

Fig. 5: Plate test (EN 14485-5) – fiber reinforced sprayed concrete

4.4.3 Back calculation of the support elements at 24.315 (mesh reinforced lining)

The estimation of geotechnical parameters was based on the geological mapping and data collected by the geologist on the site (RMR = 47). The geotechnical parameters were assumed using the Hoek & Marinos method taking into account all the relevant indicators of the rock mass behavior including the favorableness of the rock layering. Relevant parameters ($\sigma_{ci} = 40$ MPa, GSI = 42, $m_i = 10$, $D = 0.5$, $MR = 500$, $\gamma = 0.025$ MN/m³, Tunnel Depth = 65 m) where

analyzed using the software (“RocLab”) to acquire Mohr-Coulomb strength parameters for numerical analysis ($c = 0.274$ MPa; $\phi = 42, 86$ deg; $E = 1744.22$ MPa). After the back-calculation the following results were computed (Fig. 6 and Fig. 7).

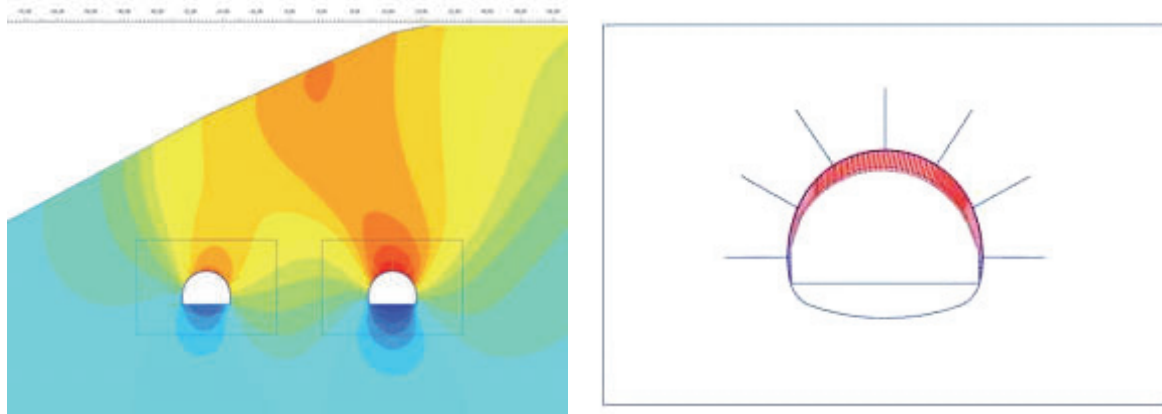


Fig. 6: Computed results – displacements

Total displacement was 10 mm. The bending moments ($M_{d,max} = 8.78$ kNm/m²) and axial forces ($N_{d,max} = 489.80$ N/m²) are plotted on the interaction diagrams (Fig. 7) of the mesh reinforced sprayed concrete for the installed sprayed concrete C25/30 and reinforcement steel mesh type - Q 188.

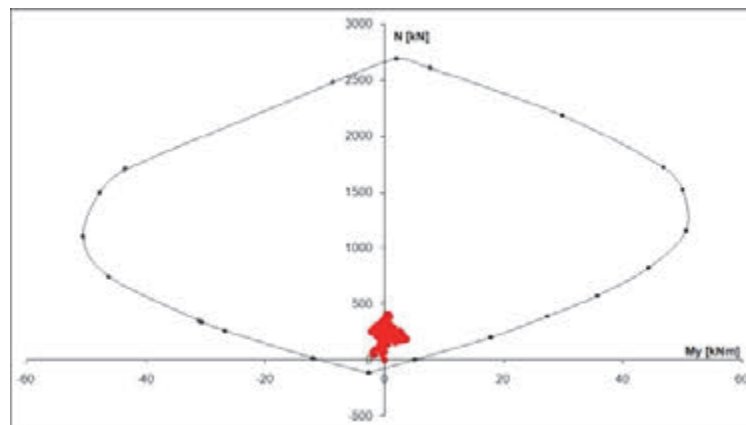


Fig. 7: Computed results – interaction diagram

The predicted bending capacity of the primary lining in the B1 rock mass category should not exceed 20 kNm/m².

4.4.4 Measurement profiles on cross sections at 24.315 m' and 24.345 m'

Maximum displacement at 24.315 m' – mesh reinforced sprayed concrete: 11 mm (Fig. 8)

Maximum displacement at 24.345 m' – fiber reinforced sprayed concrete: 9 mm (Fig. 9)

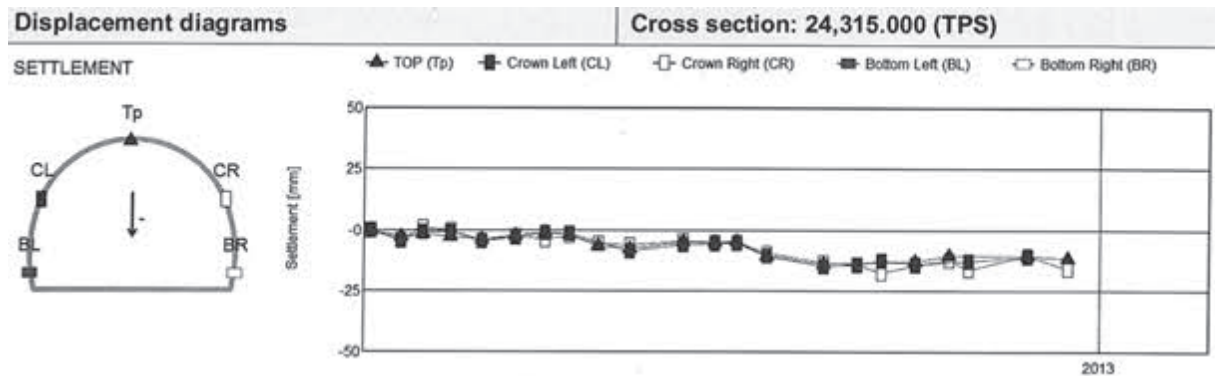


Fig. 8: Movements in the primary lining – mesh reinforced sprayed concrete

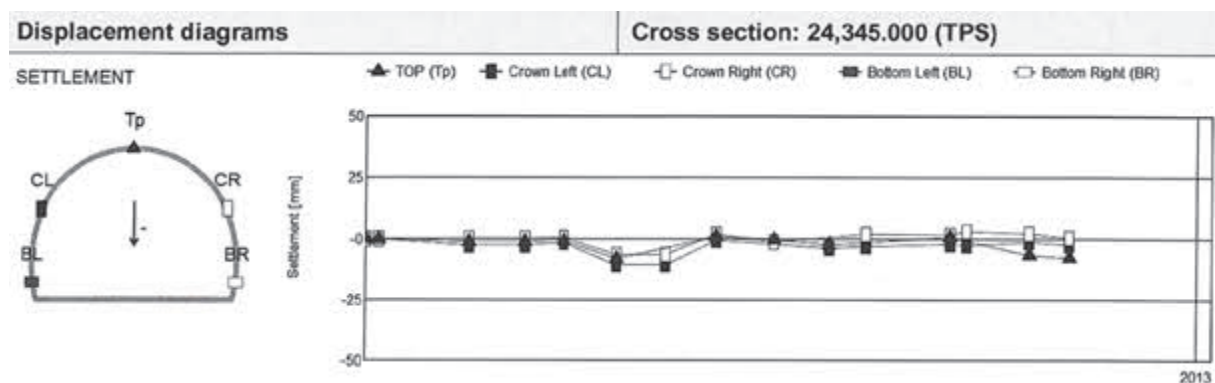


Fig. 9: Movements in the primary lining – fiber reinforced sprayed concrete

5. CONCLUSION

The macro-synthetic fiber reinforced sprayed concrete samples have shown less energy absorption capacity in comparison with the mesh reinforced sprayed concrete samples determined by the EFNARC plate test (EN 14485-5; 2006). The required energy absorption capacity according to the updated Q-System rock classification by Grimstad and Barton was between $E = 500-700$ J (see Fig. 3) and the tested energy absorption capacity of tested specimens using macro-synthetic fiber in the test field was of an average of $E = 740$ J (see Fig. 5). It could be concluded that the energy absorption capacity of the macro-synthetic fiber reinforced sprayed concrete was still of satisfactory capacity and could be applied for the support system in category B1.

The test field results show a very good post cracking performance of the macro-synthetic fiber reinforced sprayed concrete at deflections of about 5 mm. It was measured that the deflections of 5 mm usually occur during the first hours after excavation.

Analyzing the energy absorption test results at the deflection of 5 mm it can be concluded that both the mesh and fiber sprayed concrete capacity absorb almost the same force $F = 45$ kN (see Fig. 4 and 5). Considering these results the fiber sprayed concrete provides more safety during the first hours of excavation due to simple installation.

Analyzing the results of the back calculation the $M_{d,max} = 8.78 \text{ kNm/m'}$ at the total displacement of 10 mm is much more smaller compared to the predicted bending capacity of 20 kNm/m' in the primary lining for B1 rock mass according to ÖNORM B2203.

The measurement profiles on cross sections at 24.315 m' and 24.345 m' showed almost the same deflections for both the mesh and fiber sprayed concrete primary lining. So it can be concluded that the fiber sprayed concrete lining can be equally efficient.

The in-situ identified geological rock mass categories and the applied support systems are shown in Tab.2. Comparing the geological rock mass categories from the Main Design (Tab.1) and the categories identified during the excavation obviously shows that the share of 4th (IV.) rock category was increased and on the other hand, the shares of 2nd (II.) and 3th (III.) geological rock mass categories were reduced.

Tab. 2: Rock mass categorization and executed support systems

TUNNEL T3					TUNNEL T3				
LEFT TUNNEL TUBE - EXECUTED					RIGHT TUNNEL TUBE - EXECUTED				
ROCK CATEGORY	ROUND LENGHT (m)	SUPPORT SYSTEM	LENGTH (m)	PERCENTAGE (%)	ROCK CATEGORY	ROUND LENGHT (m)	SUPPORT SYSTEM	LENGTH (m)	PERCENTAGE (%)
V	1	PC	32	1%	V	1	PC	0	0%
IV	1.5	C2 + S	1077	40%	IV	1.5	C2 + S	975	36%
IV/III	2.5	B1	0	0%	IV/III	2.5	B1	15	1%
III	3	B1	890	33%	III	3	B1	1048	39%
III/II	3.5	B1	702	26%	III/II	3.5	B1	670	25%
II	4	B1	0	0%	II	4	B1	0	0%
TOTAL			2701	100.00%	TOTAL			2708	100.00%

After all, in Tunnel T3 almost 1600 m' of fiber reinforced sprayed concrete was applied. The net saving time using macro synthetic fiber in the sprayed concrete lining was 70 days. This fully compensated the lost time for the increased length of 4th (IV.) rock category that was not predicted by the Main Design. The Project was successful accomplished on time, with no delays. The application of fiber sprayed concrete using engineering know-how and experience played a dominant role in this successful construction project. Macro synthetic fiber sprayed concrete and fiber sprayed concrete in general should be considered as a powerful tool in tunnel engineering projects.

6. REFERENCES

- Hrvatović, H. (2006), "Geological Guidebook trough Bosnia and Herzegovina"
- Grimstad, E. and Barton, N. (1993), "Updating the Q-system for NMT", Fagernes, Norway
- Barton, N. (1991), "Geotechnical Design", World Tunneling
- Barton, N., R. Lien and J. Lunde (1974), "Engineering Classification of Rock Mass for the Design of Tunnel Support", Oslo 1974
- European specifications for sprayed concrete (1996)
- Marinos, P., Hoek, E. (2001), "Estimating the geotechnical properties of heterogeneous rock masses of Flysch", Bull. Eng. Geol. Env., 60: 85–92

SHEAR CAPACITY OF PRESTRESSED FRC BEAMS WITH SPARSE STIRRUP SPACING

Kálmán Koris, István Bódi

*Budapest University of Technology and Economics, Department of Structural Engineering
1111 Budapest, Műegyetem rkp. 3-9. Hungary*

SUMMARY

The assembly of conventional shear reinforcement in concrete beams is usually a time and labour-intensive process which may reduce the effectiveness of the mass production of prefabricated elements. In addition to the application of stirrups, the shear strength of reinforced concrete beams can also be increased by using fibre reinforcement. The objective of our research was to find out, whether the use of appropriate fibre reinforcement could partially or fully replace the conventional shear reinforcement in prefabricated beams. Shear strength of several steel fibre reinforced, prestressed concrete beams with sparse stirrup spacing was tested. Analytical and numerical analysis of these beams were also carried out to investigate the effect of fibre dosage on their shear capacity, and the amount of steel fibre reinforcement that could replace conventional shear reinforcement was determined for the examined beams.

1. INTRODUCTION

Current tendencies in Hungary show a shortage of labour in the construction industry which requires the application of less labour-intensive structural solutions. The application of fibre reinforced concrete for prefabricated structural members is a promising way to reduce the demand for labour of reinforcement assembly and speed up the construction process. Results of the monitoring of existing structures (Klikowicz, Salamak, Poprawa, 2016) show the advantages of fibre reinforcement in the field of structural durability, too. According to the detailing rules of EN 1992-1-1 standard (EC2), a minimum amount of stirrups must be applied as shear reinforcement in reinforced concrete beams. This kind of “conventional” shear reinforcement can be, however, decreased below the required minimum, or it may be even completely neglected by the application of proper fibre reinforcement. The objective of our research was to find out whether the use of fibre reinforced concrete mixture could partially or fully replace the conventional shear reinforcement in prefabricated beams for industrial halls. The concept of using fibres as reinforcement is not new, they have been used as reinforcement since ancient times. Fibres are usually used to increase ductile behaviour of concrete, control cracking due to plastic and drying shrinkage, reduce bleeding of water and permeability of concrete, and produce a better resistance against dynamic impacts. Generally, fibres do not increase the flexural strength of concrete beams, however, shear strength can be significantly improved as tensile strength of the concrete is increased by the application of fibre reinforcement (Balázs, Kovács, 1997; Dulácska, 1999; Kovács, Balázs, 2003; Kovács, Balázs, 2004; Grunert, Strobach, Teutsch, 2004). The present research was preceded by previous studies. To find the fibre type that is best suited to the objective set in terms of performance, workability and efficiency an extensive experimental program was carried out at the Laboratory of Materials and Structures, Budapest University of Technology and Economics (Kovács, 2014). Another experimental program was also carried out at the Structural Laboratory of Budapest University of Technology and Economics between 2014

and 2015. In this experimental program the shear strength of small span (6 m), prefabricated, prestressed beams without stirrups, but with variable fibre type and content were tested (Koris, Bódi, Polgár, Mansour, 2015). During the current research, we focused on the shear capacity of larger span (12-25 m) prefabricated, prestressed FRC beams with sparse stirrup spacing (applying stirrups at the ends of the beams only) or without shear reinforcement. Within the frames of the research, the shear strength of several beam specimens was tested, and the analytical and numerical analyses of these beams were also performed.

2. INTRODUCTION OF THE TESTS

2.1 Tested beam specimens

In frames of the research four different prefabricated, prestressed FRC floor beams were studied. Beam types T70 and T140 have variable height T sections, beam type T90 has constant height T section and beam type R70 has constant height rectangular cross-section that works together with an in-situ reinforced concrete slab in the final state. Shear reinforcement was completely neglected for beam type T90 while other beams included stirrups with partially sparse spacing (compared to the requirements of EC2) at their support region only. In each beam, Dramix steel fibre reinforcement was applied. Typical shapes, cross-sections and main dimensions of analysed beams are illustrated in Fig. 1. Applied concrete grade, longitudinal reinforcement and fibre dosage of different beams are shown in Tab. 1.

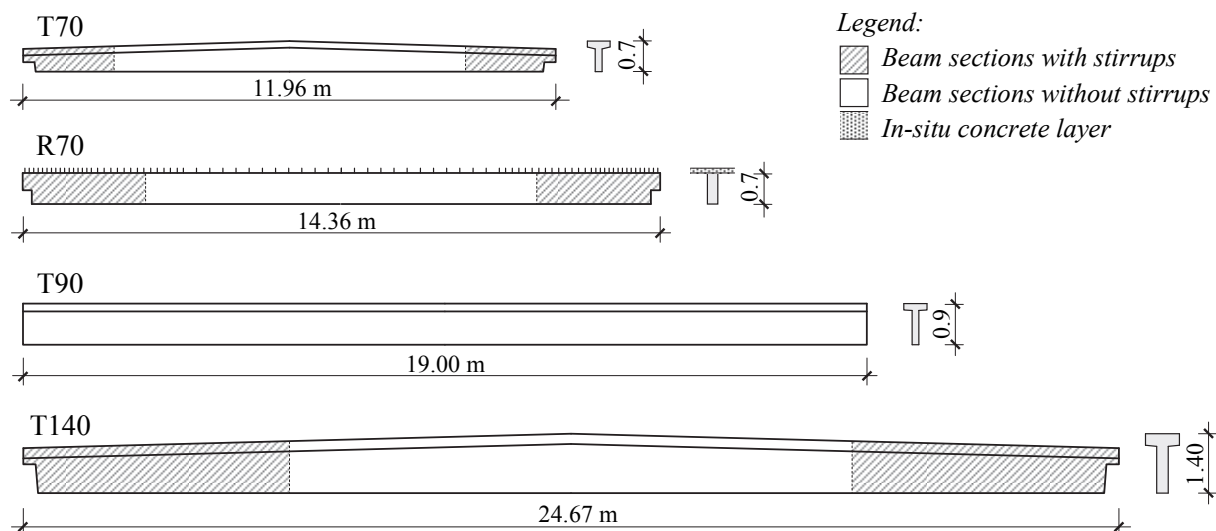


Fig. 1: Side view and cross-section of tested beams

During the tests, fork supports were used at both ends of the beams according to the usual construction solution. For beam types T70, R70 and T140 the load was applied step-by-step using verified weights that were put on the beams in predetermined points. In each load step, the deflection of the examined beam was measured by mechanical dial indicator placed in the middle of the span. To avoid the complete destruction of the beams they were loaded only up to ~80% of their load carrying capacity calculated on the mean level. Beam type T90 was tested on a test stand. In this case the asymmetrically applied concentrated force (Fig. 2) was produced by a hydraulic jack and the deflection of the beam was measured in the middle of the span as well as under the acting force. This beam was also loaded up to ~80% of its calculated carrying capacity only to avoid the collapse. Before performing the load test on the beam, its concrete strength was determined by conducting non-destructive Schmidt hammer tests in 10 locations

along the web and in 5 locations along the flange. The measured concrete compressive strength values were considered for the numerical analysis of the beam (Karimi, 2016).

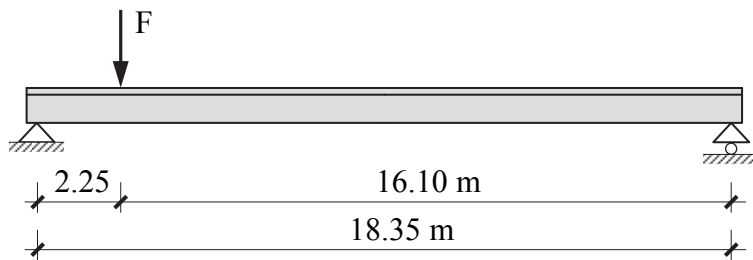


Fig. 2: Shear loading arrangement of beam T90 and picture of the T90 beam on the test stand

Tab. 1: Dimensions, material grades and longitudinal reinforcement of tested beams

		Type of beam			
		T70	R70	T90	T140
Total length L [m]		11.96	14.36	19.00	24.67
Heigh (at midspan) h [m]		0.70	0.70	0.90	1.40
Concrete grade (prefabricated girder)		C40/50	C40/50	C50/60	C50/60
Dramix fibre volume [kg/m ³]		20	20	30	20
Longitudinal reinforcement	Bottom	2Ø16 + 2×Fp93-1860	3×4Fp93-1860	6×2Fp93-1860	4×4Fp93-1860
	Top	2Ø16 + 2×Fp52-1860	4×Fp52-1860	4×Fp52-1860	2×Fp52-1860
Design load p _d [kN/m]		25.34	38.28	18.97	32.92

2.2 Results of the tests

Measured shear force – displacement diagrams are presented in Fig. 3. The shear force acting at the support was always calculated from the actual load arrangement and intensity in each load step.

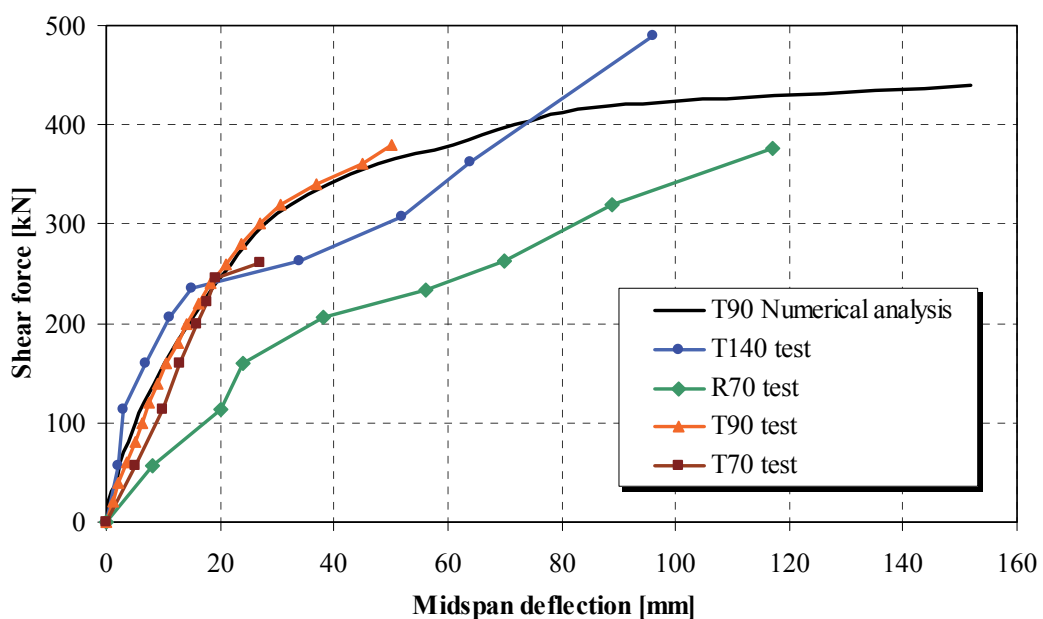


Fig. 3: Measured and numerically calculated shear force – displacement diagrams

In case of the tested beams the measured shear capacities were higher than the corresponding design shear forces. However, it does not automatically mean that the shear strength of FRC beams is satisfactory on the same reliability level as the beams with conventional shear reinforcement. According to our previous studies (Koris, Bódi, Polgár, Mansour, 2015), FRC beams with even higher fibre content (35 kg/m^3) have a higher probability of shear failure than the control beam containing stirrups as shear reinforcement. Because of the insufficient number of specimens, the shear reliability of the tested beams could not be directly determined. It is planned to test further beams in the future so statistical evaluation of the results can be also carried out. The results of current tests were nevertheless used, on the one hand, to verify the results of analytical calculations and, on the other hand, to calibrate the numerical model.

3. ANALYTICAL VERIFICATION OF THE BEAMS

3.1. Shear strength of FRC beams

EC2 does not provide guidance on the detailed analysis of fibre reinforced concrete structures, therefore the effect of fibre reinforcement on shear strength was considered on the basis of the Steel Fibre Concrete Directives from German Committee on Reinforced Concrete (DAfStb-Richtlinie Stahlfaserbeton, 2012), which also conforms to the Eurocode standard system. According to the DAfStb directives, steel fibre reinforced concrete beams can be classified into the strength classes L1 and L2 based on the characteristic bending-tensile strength that can be measured after the cracking of the concrete. The L1 performance class delivers the characteristic post-cracking bending-tensile strength of concrete in serviceability limit state, while class L2 stands for post-cracking bending-tensile strength in the ultimate limit state. The additional shear strength that is provided by the steel fibres can be calculated from the $f_{\text{ctd},i}^f$ design centric tensile strength:

$$V_{\text{Rd},cf} = f_{\text{ctd},i}^f \cdot b_w \cdot h$$

where b_w is the web thickness and h is the overall height of the beam. The additional shear strength provided by the fibres can be summarised with the shear strength of concrete to obtain the total shear strength of the concrete cross section. The shear resistance of the member without shear reinforcement is satisfactory if the following criterion is fulfilled (Gödde, Strack, Mark, 2010):

$$V_{\text{Rd},c} + V_{\text{Rd},cf} \geq V_{\text{Ed}}$$

where $V_{\text{Rd},c}$ is the design shear resistance of the member without shear reinforcement calculated according to EC2, and V_{Ed} is the design value of the applied shear force.

The performance class of an FRC beam is influenced by several factors (Rosenbusch, 2003) and it can be determined by the evaluation of appropriate test results according to DAfStb directives. However, in our situation, the performance class of the tested beams was not determined by the manufacturer, only the amount and type of applied fibres were known. Therefore, the performance class of the tested beams was determined based on empirical data available in the relevant literature (Schwarz, 2002). The centric tensile strength was calculated for the tested beams according to the DAfStb directives, considering the appropriate concrete grades and fibre volumes (Koris, Bódi, 2017). The calculated values of centric tensile strength are displayed in Tab. 2.

Tab. 2: Values of centric tensile strength in case of the tested beams

Beam type	Concrete grade	Fibre volume fraction [kg/m ³]	Performance class (L2) [N/mm ²]		Centric tensile strength [N/mm ²]
			C25/30	Actual concrete	
T70	C40/50	20	0.488	0.631	0.233
R70	C40/50	20	0.488	0.631	0.233
T90	C50/60	30	1.001	1.564	0.579
T140	C50/60	20	0.488	0.736	0.272

3.2. Results of analytical calculations

Compliance of the tested beams was verified by analytical calculations according to EC2. Initial prestress in the tendons was calculated from the 110 kN tensioning force that was applied by the manufacturer for the construction of the members. Concrete and steel stresses were verified in the initial state ($t=0$). The loss of prestressing force due to shrinkage, creep and relaxation was calculated and the distribution of effective prestress was determined in the final state ($t=\infty$). Bending moment resistances of different beams were verified considering the calculated effective prestress values. In case of beam type R70, a 15 cm thick in-situ concrete (grade C30/37) slab was also taken into account for the determination of bending moment resistance. For the verification of shear resistance, the effect of fibre reinforcement was also taken into account. The anchorage region of the tendons was verified for transverse tension taking the shear utilization of the stirrups into consideration. Serviceability limit states, as well as transition states, were also verified (Koris, Bódi, 2017).

According to the comprehensive study of the beams, we may conclude that despite the reduced amount of conventional shear reinforcement they still meet the requirements in most design situations. However, we encountered some problems with the shear strength, as well as with the transverse tensile strength at the ends of the beams. Fig. 4 illustrates the utilization of shear strength ($v = \max[V_{Rd,c}; V_{Rd,s}]/V_{Ed}$) along the length of beam T70. The end of the beam is satisfactory for shear, but there are regions along the length where design shear force slightly exceeds the design shear resistance. Shear strength of the concrete, the fibres and the shear reinforcement together would be able to provide appropriate resistance, but EC2 does not allow the summary of concrete and steel strength values in a shear design situation as an approximation to the safe side.

In order to have satisfactory structural elements also for shear and transverse tension, the concrete grade, the diameter or spacing of the stirrups and/or the applied fibre volume may be modified. For the studied beams, the concrete grade and the amount of stirrups were left unchanged but an increased fibre volume was assumed (we considered 40 kg/m³ fibres for beams T70, R70, T90 and 60 kg/m³ fibres for beam T140). According to the analytical calculations, all beam types would be satisfactory for shear and transverse tension with the increased fibre volumes. Fig. 4 illustrates the utilization of shear strength for beam type T70 with the initial and increased fibre volumes. Results of the analysis showed that the application of the right type and amount of fibres can partially replace the conventional shear reinforcement in prefabricated floor beams. If we want to completely neglect the stirrups from the beams, the fibre volume must be significantly increased, as it will be shown in the next chapter. However, concrete mixing and casting in case of high fibre volumes is still a challenge for the domestic concrete industry.

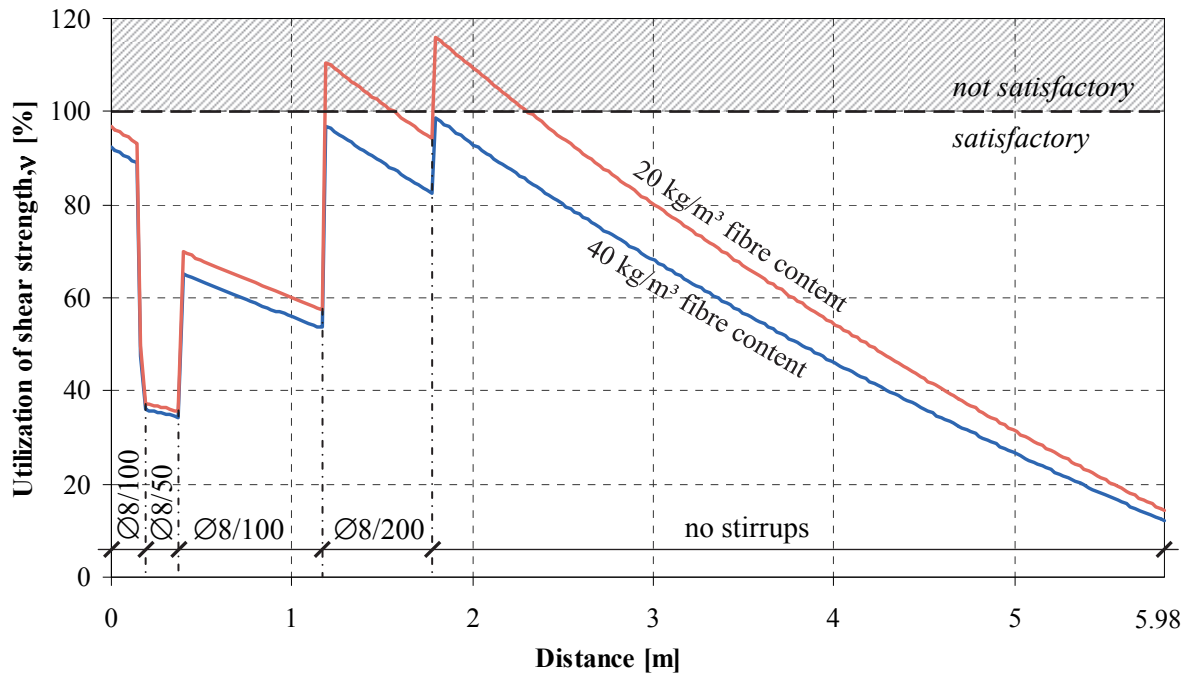


Fig. 4: Shear strength utilization of beam T70 in case of different fibre contents

4. NUMERICAL ANALYSIS

The effect of applied steel fibre volume on the shear strength of prestressed beams was analysed using the ATENA v5.1.1 nonlinear finite element software (Karimi, 2016). This software allows the consideration of both conventional and fibre reinforcement, as well as geometric and material nonlinearity for the calculation of structural behaviour. The numerical analysis intended to compare the shear strength of prestressed FRC beams with different amount of steel fibres and also to compare these values to the shear strength of a beam containing the amount of stirrups required by EC2. In the followings, the modelling of beam type T90 will be briefly presented.

In the numerical model, fork support was applied according to the usual construction solution. The analyzed beam was symmetrical so it was possible to analyze only the symmetrical half, thus the running time could be speeded up. In the calculations, the *CC3DNonLinCementitious2* material model built into ATENA was used to describe concrete behaviour. The beam was modelled by tetrahedral and brick elements, the average mesh size was 0.1 m (0.2 m mesh with 0.5 length coefficient). To have constant shear force distribution on the beam, a concentrated force was applied 2.25 m from the support like in case of the test. The load was applied in 20 kN steps to the structure. In ATENA software the widely known AKC-model (Aveston, Cooper and Kelly, 1971) is used to predict the stress and strain for the concrete containing fibres. The amount of applied fibres was entered as certain reinforcement ratios in 7 directions. The beam was analysed in 6 different situations. In the first case stirrups fulfilling the requirements of EC2 were applied in the beam. In five more cases the beam was modelled without stirrups, but with variable fibre contents (0, 20, 30, 40, 110 kg/m³). During the numerical analysis the shear force – deflection diagrams and the corresponding shear capacities were determined for each shear reinforcement type. The results of the shear strength are shown in Fig. 5. Based on these results, the shear capacity of the beam increases by increasing

the amount of fibre reinforcement, however, 30 kg/m³ fibre content applied in beam T90 is not able to provide the same shear resistance as the stirrups.

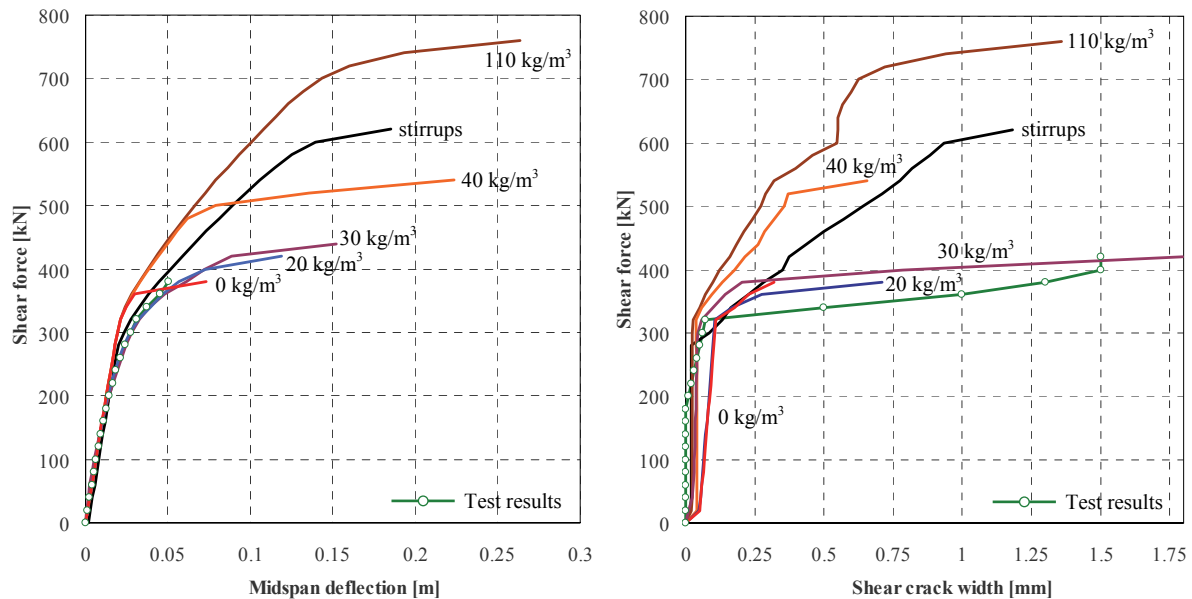


Fig. 5: Shear force – deflection and shear crack width diagrams of beam T90 in case of different fibre volumes

It can be seen from Fig. 5 that only a significantly higher fibre dosage (about 75 kg/m³) can provide the shear strength that is equivalent to the shear strength of stirrups. Thanks to the crack bridging effect of the steel fibres, the ductility of the beam significantly increases by the increase of fibre dosage but the width of shear cracks will be still larger than in the case of the beam with stirrups as shear reinforcement (Fig. 5). This phenomenon is mainly caused by the fibres being pulled out from the concrete due to their relatively small anchorage length. Similarly to the shear resistance of the beam, the shear crack width can be efficiently limited by the significant increase of the fibre content. It was also observed during the numerical modelling, that while shear strength can be efficiently increased by the application of proper fibre dosage, the bending moment resistance does not increase considerably even if the amount of fibres is significantly increased. If we increase the fibre dosage from 20 kg/m³ to 110 kg/m³ for the beam T90, the bending capacity is increased by 20% only, while the increase in shear capacity is 81%.

5. CONCLUSIONS

The purpose of our study was to find out whether the use of fibre reinforced concrete mixture could partially or fully replace the conventional shear reinforcement in prefabricated beams for industrial halls. We can conclude that steel fibre reinforcement significantly increases the shear strength of prestressed concrete beams. However, in case of the studied beams, only a significant amount of steel fibre reinforcement (75 kg/m³ or greater) could completely replace the conventional shear reinforcement. The mixing and casting of concrete with such high fibre content can be, however, technologically problematic with the use of the currently available pre-casting technologies. According to the analytical and numerical calculations, it could be a suitable and economical production alternative for prestressed concrete floor beams to provide the shear strength by the mixed application of about 40 kg/m³ steel fibre content and conventional stirrups with sparse

spacing only at places that are most utilized for shear. As it is also shown by some foreign approaches (Grunert, Strobach, Teutsch, 2004), a more economical production of such structural elements may be achieved if we completely neglect the stirrups from prestressed concrete floor beams by using high strength concrete mixtures and by significantly increasing the fibre content, which of course requires the development of manufacturing technologies, too.

7. REFERENCES

- Aveston, J., Cooper, G. A. and Kelly, A. (1971), "The Properties of Fibre Composites", Conference Proceedings, National Physical Laboratory (IPC Science and Technology Press Ltd, Paper I, 15. p.
- Balázs, L. Gy. and Kovács, I. (1997), "Increase in shear strength of beams by applying fiber reinforcement", Proceedings, Symposium organized for the 65th birthday of Prof. G. Mehlhorn „Materialmodelle und Methoden zur wirklichkeitsnahen Berechnung von Beton-, Stahlbeton- und Spannbetonbauteilen" (eds. F. Blaschke, G. Günther, J. Kollegger), ISBN 3-88122-903-5, Kassel, pp. 10-17.
- Dulácska, E. (1999), "Design theory of steel fibre reinforced concrete and reinforced concrete" (in Hungarian), Proceedings of the Conference: Fibre reinforced concrete – from the research till the application, Hungarian Group of *fib*, Budapest, ISBN 963-420-589-5.
- Kovács, I. and Balázs, L., Gy. (2003), "Structural behaviour of steel fibre reinforced concrete", Journal of Structural Concrete, 2003/2, pp. 57-63.
- Rosenbusch, J. (2003), "Shear force capacity of steel fibre reinforced beams", (in German), Dissertation, Technische Universität Braunschweig, Department of civil engineering, 199. p.
- Grunert, J., P., Strobach, C. and Teutsch, M. (2004), "Prestressed steel fibre reinforced SCC beams without steel reinforcement", (in German), BFT International 2004/04, Bauverlag BV GmbH, Gütersloh, pp. 50-55.
- Kovács, I. and Balázs, L., Gy. (2004), "Structural performance of steel fibre reinforced concrete", Book, Publ. Comp. of Budapest University of Technology and Economics, ISBN 963-410-822-3, 233. p.
- Gödde, L., Strack, M. and Mark, P. (2010), "Structural elements made of steel fibre reinforced concrete and steel fibre strengthened concrete", (in German), Beton- und Stahlbetonbau 105 (2010), Heft, 2 Ernst & Sohn Verlag für Architektur und technische Wissenschaften GmbH & Co. KG, Berlin, pp. 78-91.
- Deutscher Ausschuss für Stahlbeton (2012), "DAfStb-Steel Fibre Concrete Directives" (in German) 47. p.
- Kovács, G. (2014), "Partial replacement of reinforcement with fibre reinforced traditional concrete. Report 1: Fibre comparison and selection", ASA Construction Ltd. – Consolis Group Material Development Centre, Budapest.
- Koris, K., Bódi, I., Polgár, L. and Mansour, K. (2015) "Experimental analysis of the shear capacity of prestressed FRC beams", Proceedings of the 8th International Conference Fibre Concrete 2015 - Technology, Design, Application, Prague, 529. p.
- Karimi, R. (2016), "DEM and FEM analysis of fibre-reinforced prefabricated concrete beams", MSc Thesis at the Budapest University of Technology, Faculty of Civil Engineering, Budapest.
- Klikowicz, P., Salamak, M. and Poprawa, G. (2016) "Structural Health Monitoring of Urban Structure", Procedia Engineering, 161(2016), pp. 958–962.
- Koris, K. and Bódi, I. (2017) "Shear strength of FRC beams with reduced shear reinforcement", Concrete Structures Vol. 18 (2017), Hungarian Group of *fib*, Budapest, pp. 36-44.

VARIOUS ASPECTS OF BRIDGE HEALTH MONITORING SYSTEMS IN POLAND

*Piotr Klikowicz, Marek Salamak, Mateusz Smolana
Silesian University of Technology
Akademicka 5, 44-100 Gliwice, Poland*

SUMMARY

This paper discusses Polish bridges on which Structural Health Monitoring was installed. SHM benefits were taken into consideration. The difficulties in data analysis and interpretation were described as well as probable development aim and evolution of measurement systems, algorithms and software.

1. INTRODUCTION

Monitoring systems provide continuous measurement of specific parameters of the bridge. They combine electronics and information technology with civil engineering, introducing new techniques into classical engineering. The beginnings of SHM in civil engineering date back to the 70s of the previous century when it was used on drilling platforms. The first monitoring systems in transport infrastructure engineering were installed in the 80s (Farrar Ch. R., Worden K., 2013). In Poland, the first system on a large bridge was installed in 2007. In recent years, there has been a rapid development of SHM (Klikowicz P., et-al, 2016). This is due to the continuous miniaturisation and reduction of costs of electronic equipment with the increasing demand in the construction industry.

Tab. 1: List of SHM system installed on Polish bridges

#	Name and city	Obstacle	Structure system	Max span	No. of sensors	Year	SHM
1	Redzinski Bridge in Wroclaw	Oder River	Cable-stayed	256	222	2011	2011
2	John Paul II Bridge in Pulawy	Vistula River	Arch	212	96	2008	2009
3	Solidarnosc Bridge in Plock	Vistula River	Cable-stayed	375	23	2007	2007
4	Kwidzyn Bridge	Vistula River	Extradosed	204	71	2013	2014
5	Bridge over Brda in Bydgoszcz	Brda River	Cable-stayed	110	38	2013	2013
6	Main tram flyover in Cracow	Rail terrain	Extradosed	126	18	2015	2016
6	Access tram flyover in Cracow	road	Cable-stayed	70	18	2015	2016
7	Mazowiecki Bridge in Rzeszow	Wislok River	Cable-stayed	240	74*	2015	2015

* - information received from official documents during tender for the construction

According to the maintenance policy of the transport infrastructure administration, the most of the recently constructed bridges in Poland are made of concrete. This material has been used for most of the medium and small span bridges. In Poland, most long bridges were

constructed in recent times. Among 20 longest bridges, the Swietokrzyski Bridge built in 2001 is the oldest, however, unlike short span bridge, these are usually built of steel due to larger spans. Due to the significant contribution of dead weight in long span bridges, among seven bridges with active structural health monitoring in Poland, only three have spans made of concrete (Tab. 1 presents bridges with installed monitoring system, bridges with the concrete deck are marked in grey). They all were built after 2000 (Mariak A. et-al, 2016). There are also few “special” installations eg. made on objects erected on the terrain affected by the influence of mining industry on bridges (Salamak M. et-al, 2007), tunnelling (Dulacska E., Bodi I., Koris K., 2016) and even on some sections of motorway (Salamak M., Klikowicz P., 2014), in the assumption made for a particular reason and temporary.

2. EXAMPLES OF CONCRETE BRIDGES IN POLAND WITH SHM

One of the first installations of SHM in Poland was the monitoring on Redzinski Bridge in Wroclaw (Fig. 2). It is the bridge with a total length of 1744 m with 2 x 256 m spans over Oder River. Two independent box-girder bridges are cable-stayed to the H-shaped pylon. The bridge, when constructed, broke several engineering records, including the longest reinforced concrete span, the highest pylon and the most extensive structural monitoring system in Poland. A total of 222 sensors were installed on the bridge (Fig. 1).

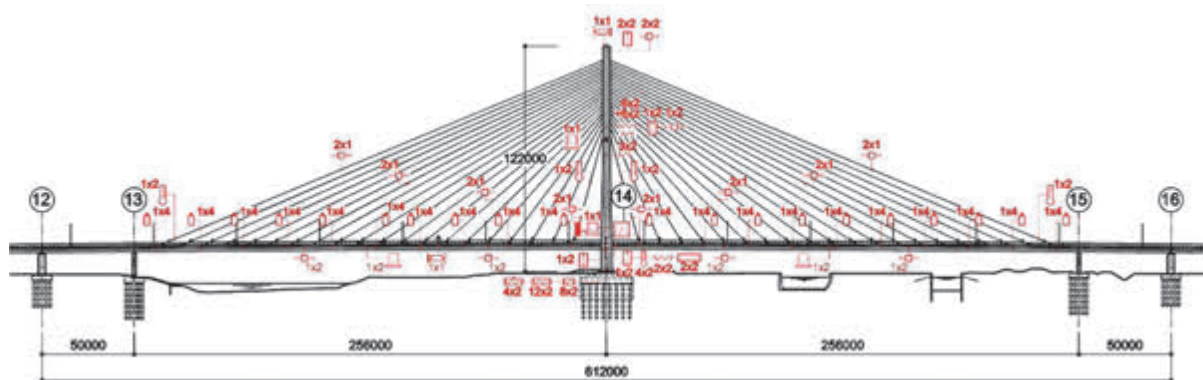


Fig. 1: Diagram of the bridge with location of sensors

Force sensors were installed in the active anchorage in every second cable in the deck, in 4 suspension planes on each of the 2 spans. Inclinometers (total of 10) were installed on the pylon - at the top and at the level of the top and bottom transverse stiffeners. Displacement sensors, in this case, are used to measure the torsion of the bridge. Two sensors measuring the distance from the edge of the bridge to the support were installed under each girder. The accelerations are measured on the pylon (6), in span (6) and on selected cables (16). The strains are measured in 90 selected points, mainly in the foundation of the pylon (48). The number of sensors is justified by the fact that it is a prototype bridge and one of the first implementations of the monitoring system on this type of structure in Poland.

Thanks to the information obtained from the monitoring, several scientific publications have been written that enriched the knowledge about cable-stayed bridges. This system was also used in the preparation of the expert opinion after a traffic accident during which a car burned down near one of the cables.

The bridge near Kwidzyn over Vistula River is an example of the landmark (Fig. 3), which, in addition to its basic transport infrastructure function, aims to delight in beauty and harmony with the surrounding area. The bridge with the longest span of 204 m is one of the longest

extradosed bridges in Europe and one of the longest in the world. It is a reinforced concrete box-girder bridge prestressed in transverse and longitudinal directions.



Fig. 2: View on Rędziński Bridge in Wrocław



Fig. 3: Bridge over Vistula River near Kwidzyn (photo: www.kwidzyn.pl, photo A. Łubiński)

Due to the record-breaking spans and innovative design, the decision was made to install the monitoring system. It consists of dynamic inclinometers located at the top of all pylons, strain sensors in the superstructure near the supports and in the center of the cable-stayed spans (Fig. 4). The hydraulic displacement sensors and accelerometers were installed in the middle of all spans (not only extradosed). The width of the expansion joint with the use of the displacement sensors (at the ends of the superstructure) is also measured. The forces are measured (with the use of force meters) only in active anchorages of the longest cables.

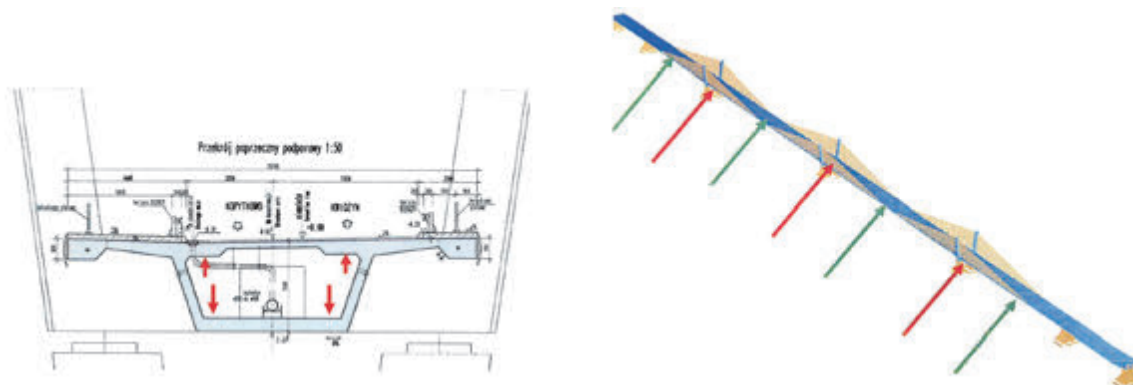


Fig. 4: Localization of strain sensors in Kwidzyń Bridge **Hiba! A hivatkozási forrás nem található.** K, 2015)

In 2016, a part of the tram line in Cracow was put into operation, which incorporates two spectacular bridges within a short distance - cable-stayed viaduct and three-span extradosed flyover. The first of them is plate girder bridge with two 70 meters long spans, which are cable-stayed to the asymmetric pylon. Interesting architecture of the bridge emphasizes the artistic effect achieved by a horizontal arc with the stay cable system. Another bridge is the first in Poland extradosed tram flyover. It was built over operating railway lines, making the construction technology a big challenge and a particular achievement. The flyover is a single box-girder and the main spans are 126 m long.

Monitoring of bridges is done by measuring the forces calculated on the basis of the vibration frequencies. They were installed on 12 cables on the cable-stayed flyover and on 18 cables on the extradosed flyover within tram line in Cracow (Fig. 5).

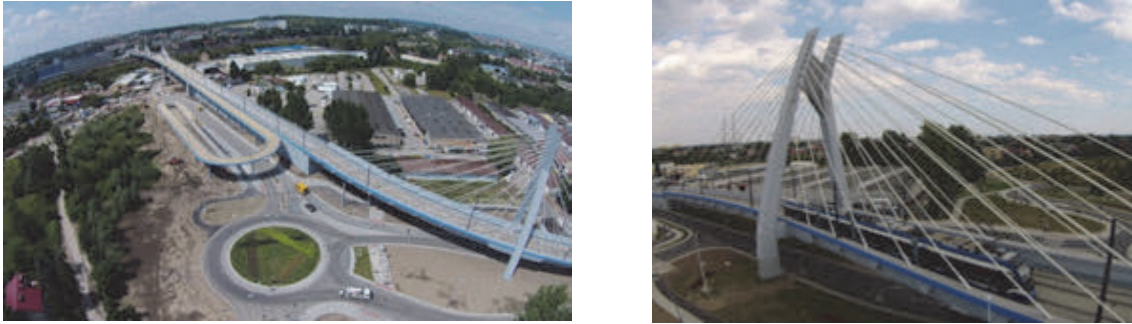


Fig. 5: Viaducts within tram line in Kraków (photo ZIKIT Kraków)

2. DIFFICULTIES WITH STRAIN MEASUREMENT

The presented examples show that strains are most often measured on bridges. This is because the civil engineers mainly deal with stresses and internal forces. These values define clearly and unambiguously the parameters of the structure, however, their direct measurement is impossible. In determining these values, Hooke's law is used by multiplying the measured strains by the coefficient of elasticity of a given material. These measurements are done with strain sensors among which the most popular are a string, electrical resistance and fiber optic sensors.

Strain sensors operate directionally, so if we want to measure the spatial state of stresses, it is necessary to use at least 3 sensors. In addition, the measured value is the sum of all the influences that act on the structure, therefore, it is necessary to determine them independently in order to determine one of them. For example, in order to determine the load acting on the beam subjected to bending, temperature effect, in addition to external loads, should be taken into account. Therefore, most of the strain sensors are equipped with temperature sensors. The problem with defining thermal strains may be the characterization of the structure and material.

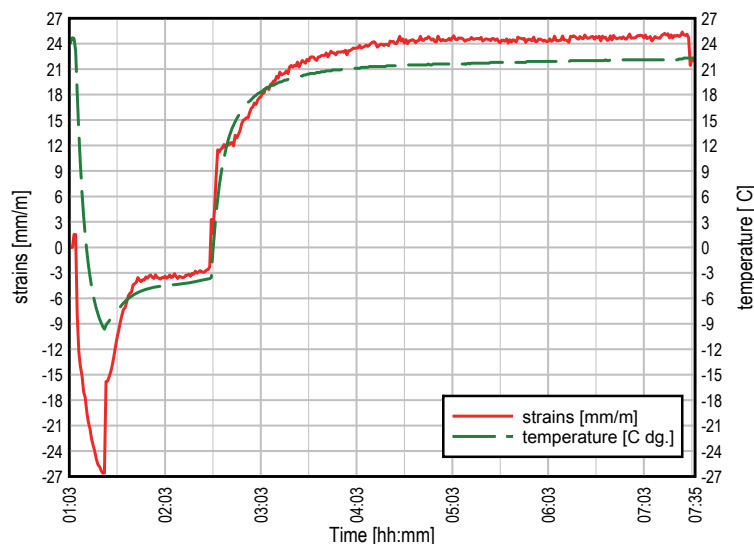
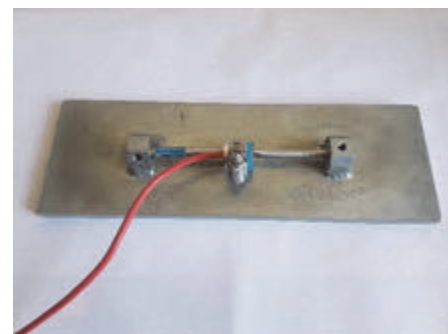


Fig. 6: Graph representing relationship strain - temperature on the steel sample



The thermal expansion coefficient is determined based on the relationship of strains and temperature for each material. This relationship, closest to linear, is characterised by crystalline materials (e.g. quartz). Although steel is an alloy of several elements of building

materials, it is an isotropic material of homogeneous structure that exhibits a relationship temperature - strain close to linear in theory. The first graph (Fig. 6 - left) shows the reading from the sensor fixed to the $5 \times 20 \times 2$ cm steel sheet (Fig. 6 - right) subjected to varying temperature (from +24 to -6 °C). Linear relationship strain - temperature in the sample can be seen on this graph with almost immediate dependence.

Another graph (Fig. 7 - left) was obtained from the strain sensor placed in the $0.52 \times 0.52 \times 0.3$ m concrete cube (Fig. 7 - right). The graph shows the delay (about 15 minutes) with which the temperature is read in relation to strains. The sensor is placed inside the sample; concrete covering the sensor delays the reading of temperature. The strains, which are greater on the side of the heat source, are transferred deep into the sample, "overtaking" the temperature change. As a consequence, the relationship strain - temperature is shifted in time and it depends on many factors, causing considerable difficulties in interpreting the readings.

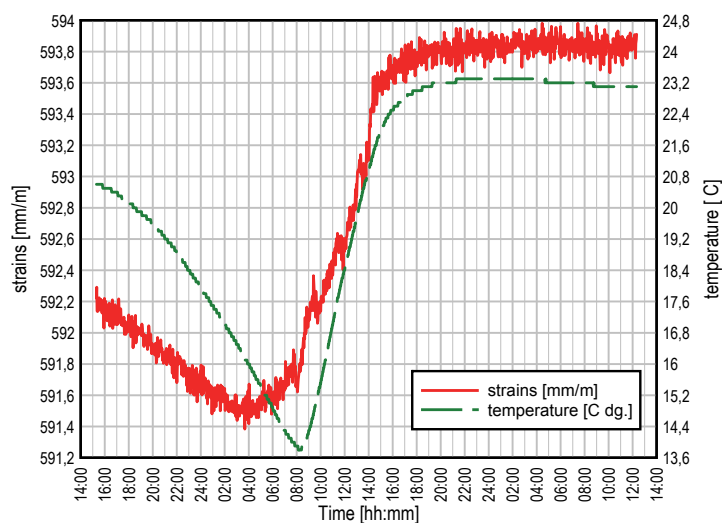


Fig. 7: Graph representing a relationship strain - temperature in the concrete sample

The graph in the Fig. 8 (left) shows the results from the measurement of the unloaded steel girder (Fig. 8 - right) with the static scheme of the frame with the bowstring. The rafter of the frame is at the angle in the middle of the span, creating a cross-fall of the hall's roof. The sensor was placed in the top rafter of a rolled I steel section. Despite the material from which the structure is made, we can observe the delay of strains in relation to the temperature. Deformation increments are not proportional to temperature changes in subsequent 24-h cycles. The probable cause of such situation is the friction that arises in the connections of the rafter with column, bowstring and purlins.

Forces in cables, usually every second cable, are measured in all Polish arch, cable-stayed and suspension bridges with installed monitoring system. The force is determined based on the strains of anchoring elements. Tests on several bridges with cables showed low effectiveness in force or strain measurements of the superstructure at the failure of one of the cables. The numerical calculations of the bridge over Wislok River showed that the force reduction in the cable by 10%, depending on the number of strands in the cable and stiffness of the cross-section, changes the tension in adjacent cables by 0.5% to 4% (Żółtowski, K., 2015). It can, therefore, be concluded that the general measurement system of forces in cables is correct. A good alternative for this measurement is to check deflections by measuring the displacements of the respective points of the structure.

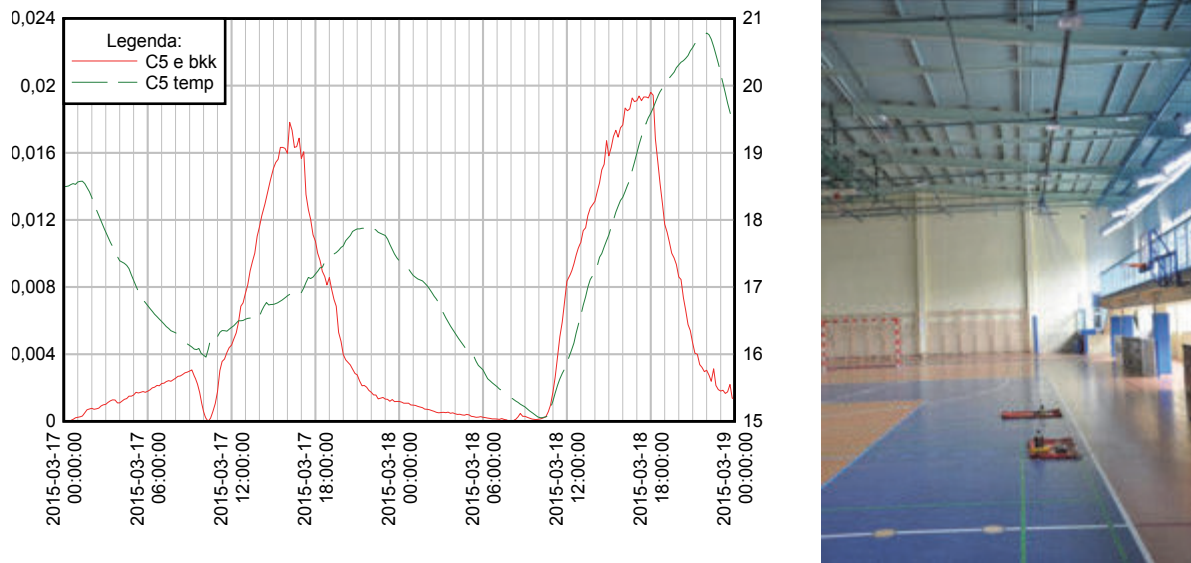


Fig. 8: Results from the monitoring system of storage hall

3. DIFFICULTIES WITH DISPLACEMENT MEASUREMENT

The displacements, depending on the range, can be measured in a variety of ways by different sensors and methods. It is divided into "relative" when the distance from one point to another is measured within the structure and "absolute", when the result of measurements are the displacements referred to the global coordinate system. The example of relative measurement in bridges is the measurement of the width of expansion joints, most often with inductive or electro-resistive sensors. The deflection of span in "relative" manner can be measured with the use of hydraulic sensors (Fig. 9 – left). They operate on the principle of connected vessels. A sensor, i.e. liquid container (usually with a glycerine solution) is installed in the middle of the span, while a similar sensor is installed in a reference point (e.g. at the support), which measures pressure changes in the container, defining a change of its location. The disadvantage of this measurement is the assumption that the reference point does not move. Also, on bridges with spans exceeding 100 m, the slope of vertical alignment is usually so large that the difference in levels between the sensor and the reference point affects the measurement accuracy. Due to the need to stabilise the level of liquid in containers, the hydraulic displacement sensors can only be used in static measurements (no more than 1 per minute).



Fig. 9: Devices used to measure displacement

"Absolute" measurement can be realized using photogrammetry (Fig. 9 – right), radar interferometry (Owerko and others, 2012), GPS and optic geodetic techniques (Fig. 9 – middle). Each of the techniques has specific limitations. GPS accuracy depends on the range of satellites while geodetic equipment with cyclic rotation and change of measured points can

wear at an accelerated pace. In addition, the space between the theodolite and the measuring prism must not be obscured.

4. VIBRATION MEASUREMENTS

Accelerometers are present on most bridges with installed monitoring. They are used to measure the accelerations of particular elements and to calculate vibration frequencies. The analysis of these data is ambiguous as there are no limit values in the standards. The calculated frequency can be compared with the frequencies of the first mode shapes to check whether the structure gets into a resonance. There are also ways of calculating the internal forces in the tendon elements on the basis of the vibration frequency. However, the accuracy of these methods so far leaves much to be desired.

5. ELECTRONICS AND SOFTWARE

The monitoring system also consists of an electronic part, i.e. industrial computers, acquisition and data transmission components, which may also introduce limits, for example, the sampling frequency or measurement range. The reading of one value may take 2 bytes of data. This means that a one-minute measurement with one sensor with the frequency of 300 Hz will generate 36 MB of data. Assuming an average (from Tab. 1) of 60 sensors per bridge, it can be calculated that in the system working dynamically generates 2.16 GB of data per minute.

Another issue is the software, mean as application with appropriate algorithms implemented. Most of them are the web pages with picture containing layout of sensors and a table with list of sensors and appropriate readings. All the algorithms of the SHM systems in Poland including examples listed in this paper are the „warning systems” based on simple thresholds calculated using FEM model of the structure. Example of expanded analysis may be the SHM system implemented on the National Stadium in Warsaw. It is based on accelerometers and geodesian displacement measurement. The FEM model of the stadium is connected with the SHM system, so using the readings from the sensors we can calculate other properties of structure (e.g. internal forces) not only there, where sensor is placed, but on the whole structure. The application connected with FEM model is not working simultaneously, because of insufficient computing power of nowadays computers.

6. SUMMARY

The monitoring system for the engineer is a repository of additional knowledge, properly designed and constructed may lengthen the life of the facility and support administration in maintenance works. However, it must be properly planned. The quantity, location and type of sensors, sampling frequency and measuring range, resolution and accuracy are parameters that must be strictly defined in the project prior to the installation. And the system should be installed during the construction works.

Sensors state of the art is fully sufficient for civil engineering needs. Latest sensors development, is just like electronics in general, focused on dimensions miniaturisation and reducing costs. Although we are still working on developing new measure techniques like Fibre Optic and trying to shift some measure techniques and sensors from others branches of knowledge like Acoustic Emission from geophysics.

Much more to do is on the field of data analysis. So far the SHM system application are quite simple, based on thresholds. In the near future first to do is to implement data fusion algorithms in order to use all scope of sensor installed on the structures e.g. temperature strains compensation using thermistors. Observations described in 2 paragraph reveal the difficulty level of this task. The strain – temperature dependence is far from linear and depends on many factors like material and joints that must be included. The future of SHM in civil engineering is damage detection and responding on it – evolution to smart structures that react on environment influence. Although there is long way to smart structures, and we have to take it step by step, through learning and decision making algorithms.

7. ACKNOWLEDGEMENTS

Authors would like to thank NeoStrain ltd. for all help, especially data from SHM and other materials granted.

8. REFERENCES

- Dulacska E., Bodi I., Koris K. (2016), Damage prediction of historical buildings in connection to subsidence caused by underground tunnelling, 16th International Multidisciplinary Scientific Geoconference SGEM 2016: Book 6: Nano, Bio and Green Technologies dor a Sustainable Future Conference Proceedings Vol. III, 692 p.
- Farrar, Ch. R. and Worden, K. (2013), Structural Health Monitoring a machine perspective, John Wiley & Sons Ltd. ISBN 987-1-119-99433-6.
- Klikowicz P., Salamak M., Poprawa G.: Structural Health Monitoring of Urban Structure, Procedia Engineering, 161(2016), pp.958–962.
- Mariak A., Miśkiewicz M, Meronk B., Pyrzowski Ł. and Wilde K. (2016), “Reference FEM model for SHM system of cable-stayed bridge in Rzeszów,” Advances in Mechanics: Theoretical, Computational and Interdisciplinary Issues – Kleiber et al. (Eds), Taylor & Francis Group, London, 2016, pp. 383-387, DOI:10.1201/b20057-82.
- Owerko T., Ortyl Ł., Kocierz R., Kuras P., Salamak M. (2012), Investigation of displacements of road bridges under test loads using radar interferometry - case study, Bridge Maintenance, Safety, Management, Resilience and Sustainability: Proceedings of the Sixth International IABMAS Conference, Stresa. Lake Maggiore, 2012, s.181-188.
- Salamak M., Weseli J., Radziecki R. (2007), Monitoring of highway bridges in areas under mining exploitation influence, 5th International Conference on Current and Future Trends in Bridge Design, Construction and Maintenance, Beijing, 2007, s.469-478.
- Salamak M., Klikowicz P. (2014), Protections and monitoring of European transportation routes in Upper Silesia mining area, 14th International Multidisciplinary Scientific Conference SGEM 2014, Albena, 2014, Vol. 2, pp.403-410.
- Żółtowski, K. (2015), Concept design of Structural Health Monitoring of Bridge in Kwidzyn
- Żółtowski, K. (2015), Structural Health Monitoring. Assesment of multistrand cable stays in bridges, Archivers of Institute of Civil Engineering, no.19/2015. p.261-271.

DIGITAL IMAGE CORRELATION SYSTEMS IN THE EXPERIMENTAL INVESTIGATIONS: CAPABILITIES AND LIMITATIONS

*Lukasz Krawczyk, Michał Goldyn, Tadeusz Urban
Lodz University of Technology, Department of Concrete Structures
90-924 Łódź, al. Politechniki 6, Poland
E-mail of corresponding author: lukasz.krawczyk@p.lodz.pl*

SUMMARY

The aim of the paper is to present the possibilities and limitations of using the Digital Image Correlation systems. In order to assess the measurement inaccuracies the measuring volume 1250×1100 mm was analyzed. It was stated very good accuracy of the line segment length change. It causes that observation of crack widths can be considered as precisely. Some practical information concern how determine the compatibility between crack width measured traditionally and by using DIC are written. In the second part of the paper the results of the tests concerning capacity of interface between two concrete casting at the same time were presented. Use of the optical measurement system Aramis enables the analysis of the deformation, determination of failure mode of the tested specimens and limit displacement between edges of the interface.

1. INTRODUCTION

Modern measuring devices became more popular, one type of them is Digital Image Correlation system (DIC). That kind of tools gives new research capabilities. Using DIC during the test is much safer, because testing element is observed from a distance. It is important especially if sudden failure is expected. Besides indubitable advantages, using DIC is connected with limitations, which are specified in the paper. Measuring errors of strains under some conditions could represent an order of magnitude for ultimate concrete strain. Examples of experimental investigations of concrete structures conducted in Department of Concrete Structures of Lodz University of Technology by authors are presented in the paper. Discussion of obtained results can be used by other researchers to make interpretation of their experiments easier.

2. UNCERTAINTY ANALYSIS

Essential issue is to determine the uncertainties of measurements. It is very complex task, for analytical approach. Kneć (2015) and Revilock et al. (2007) keep a record of measurement noise then they deduced about inaccuracies. That method requires to take many photos of surface. It is assumed that unloaded specimen, not subjected to temperature changes should look identically in the each image. If any changes are observed they are classified as measurement noise. That procedure can be easily make and all impacts are considered. Very important is to keep constant light condition during the test.

In order to determine inaccuracies 400 measurements (800 pictures) of surface have been made. Deviation value and frequency of its occurrence are presented in Fig. 1 (length) and in Fig. 2 (strain). The readings from -0.013 mm to +0.013 mm for 200 mm and from -0.009 mm to +0.008 mm for 20 mm base were recorded. Statistical analysis for that data

were made. Standard errors were calculated. Their value are equal to 0.005 mm and 0.003 mm for longer and shorter base, respectively. These measurements can be considered as precise – the typical scale division for optic compactor is 0.05 mm.

The linear strains can be also measured by using Digital Image Correlation. Noise values for strain are in range from -0.068% to 0.068% for 200 mm and from -0.441% to 0.363% for 20 mm base. The standard errors values are 0.024% and 0.150% . The longer base the smaller error is. Both values are much higher than error of strain gauges.

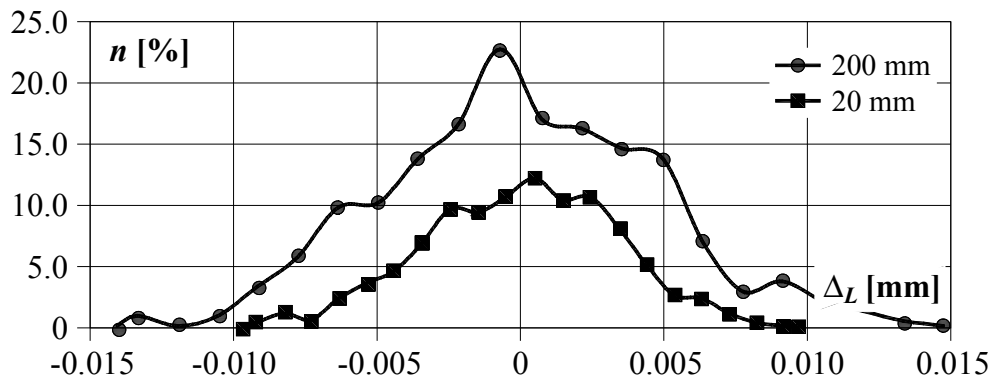


Fig. 1: Deviation of length of virtual measuring bases and frequency of its occurrence – base length 20 mm and 200 mm (unloaded specimen).

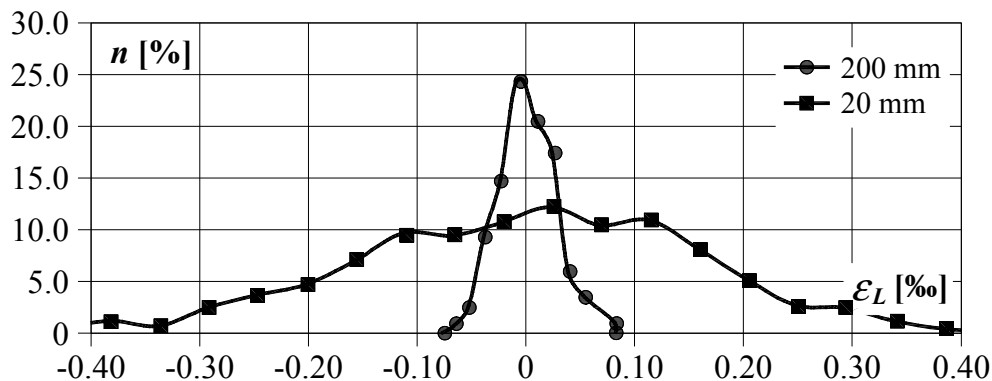


Fig. 2: Deviation of strains for linear measuring bases and frequency of its occurrence – base length 20 mm and 200 mm (unloaded specimen)

3. MEASUREMENTS OF CRACK WIDTH

Measuring crack width is possible by using Aramis system. However it is not easy to make it properly. Aramis creates maps where accumulation of strains can be find – regions where the cracks are occurring. The way of determining the crack width is presented in an example of corbel tested in Lodz. In the Fig. 3b measuring bases for crack 3 and 3' are presented. It was initially assumed that anchor points of measuring base should be outside of the strain accumulation area (crack 3). It is according to the method presented by Goszczyńska et al. (2014) or Goszczyńska and Tworzewska, (2014a). Authors stated that discussed approach gives higher width of crack than values obtained using optical compactor (3 opt.) – see Fig. 3a. It was found that measurements carried out by using base (Crack 3') ensure good compatibility with measurement (3 opt.). In the presented example length of strain accumulation area is about 42 mm while the dimension of the (Crack 3') base is only 12 mm.

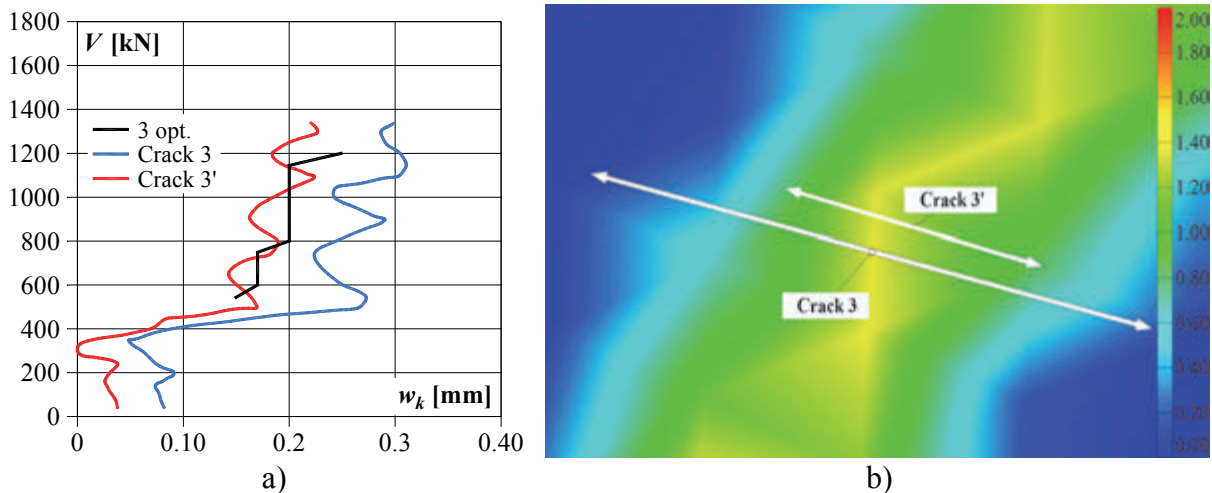


Fig. 3: Crack no. 3 a) comparison of crack widths measured traditionally (3 opt.) and by Aramis, b) measuring bases used by Aramis: (Crack 3) and (Crack 3')

For correct measurements of crack width reference length of base have to be found. It is easy to have correct results if some optical measurements for chosen load level are made. It is necessary to find length of base which gives values similar to reference value, then the rest of the results will be trustworthy.

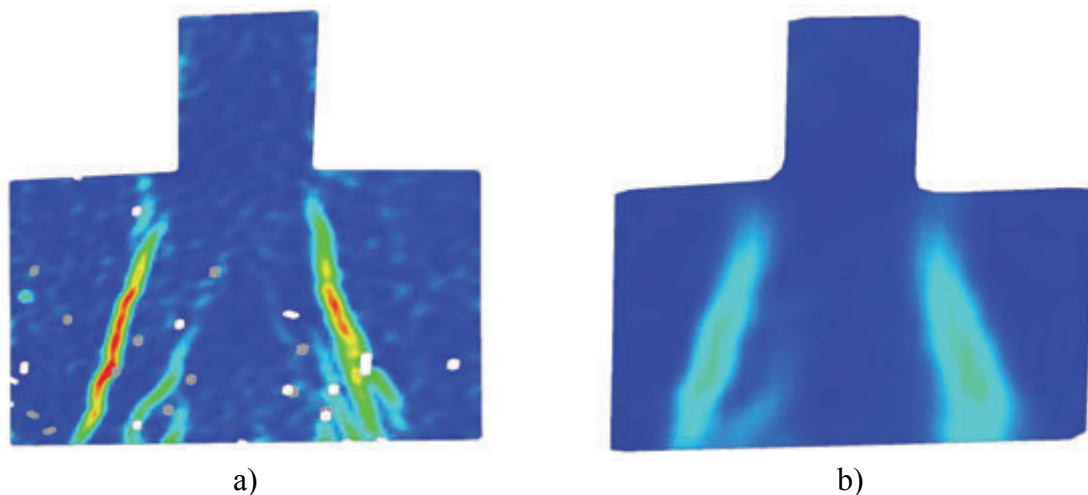


Fig. 4: Comparison of principal strain maps for corbel E – II at load equal to 1300 kN. Surface divided into facets a) 15×15 ; b) 45×45

Measurements provided by using Digital Image Correlation are possible by dividing the test surface into fixed-size fields called facets. The standard facet features is 21×21 pixels. Based on the comparison between reference image and images recorded during the test it is possible to determine the displacement of selected points on the surface. On this basis, the deformation can be calculated. The facet density affects the results in a manner analogous to the grid of the finite element method. To illustrate this phenomenon two different sizes of facets were considered: 15×15 and 45×45 pixels. The image of major deformation of the E-II corbel for the dense and thinning arrangement of facets is shown in Fig. 4. The deformation maps refer to the same element at a load level of 1300 kN. Comparing Fig. 4a and 4b, it can be stated that for larger facets, the features of the cracks were considerably more blurred and the deformation images were less detailed.

4. DIC IN THE TESTS OF SPECIMENS SUBJECTED TO SHEAR CUTTING

The investigations were intended to qualitatively assess the problem of shear cutting of concrete. This phenomenon can occur for elements with low shear slenderness $\lambda = a_c/h$ (where a_c is the distance between point of load and the edge of the support and h is the height of the element) such as very short reinforced concrete corbels. For this purpose, three "Z" shaped specimens made of the same concrete as a whole, were tested – see Fig. 5. The only variable parameter was the area of reinforcement transverse to the contact surface (A_{sw}). During loading the images were recorded by using cameras included in the Digital Image Correlation system Aramis (10 frames per second). The load was increased gradually at 30 kN, however at higher load level (about 60 ÷ 70% of ultimate load) the force was applied in uniform manner.

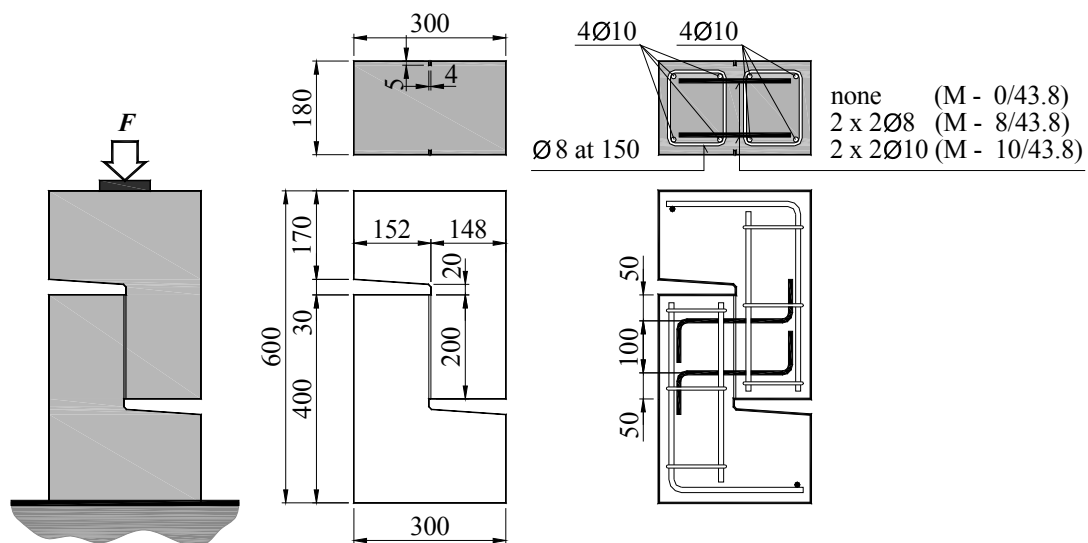


Fig. 5: Dimensions, shape and reinforcement of the test specimens

The use of the DIC system ARAMIS enabled for accurate registration of the destruction process in case of all models. The failure of M – 0/43.8 specimen with unreinforced interface was violent. The splitting of the element occurred within 0.1 s and was preceded by the appearance of a vertical crack, visible in Fig. 6.

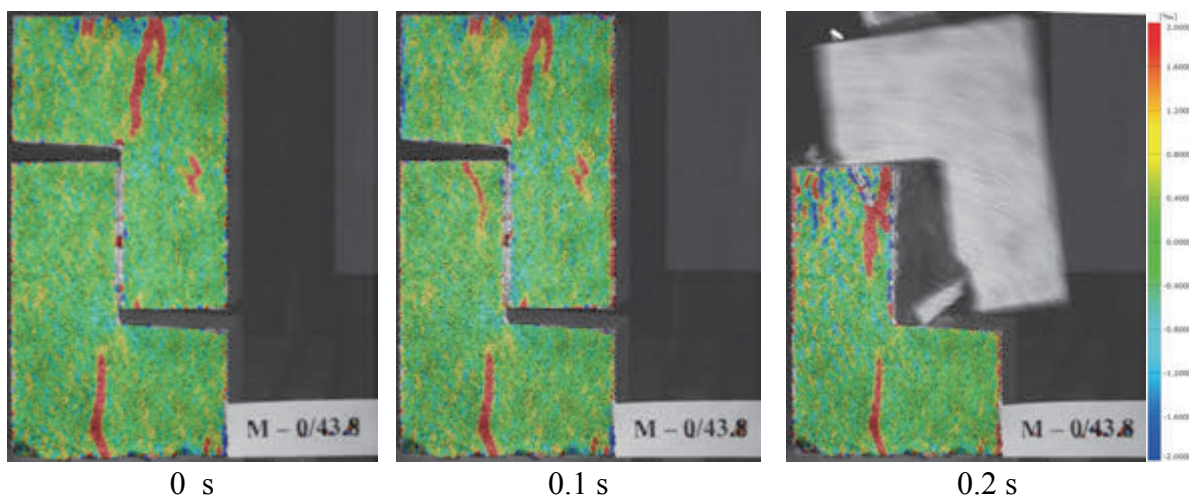


Fig. 6: Course of destruction of M – 0/43.8 specimen

Analysis of the strain maps based on recorded images allowed the qualitative assessment of the distribution of internal forces within the elements. Maps of deformation fields made possible to indicate the potential cracked zones and to determine the probable course of cracks. Comparing Fig. 7a and 7b with Fig. 7c a clear correlation between the zones of tensile strain accumulation (marked with red) and the cracks indicated during the tests can be seen. In the middle of the interface the compressive stress pass from one part of the element to the other. This is accompanied by the splitting forces visible on the maps of horizontal strains. Zones of tensile strain accumulation, visible in internal part of specimens, resulted from pulling as well as bending of transverse reinforcement (kinking effect).

The differences between the extent of the cumulative deformation zones and the course of the cracks marked during the test were due to the accuracy of human eye. The Digital Image Correlation allowed for much earlier prediction of zones of expected cracking.

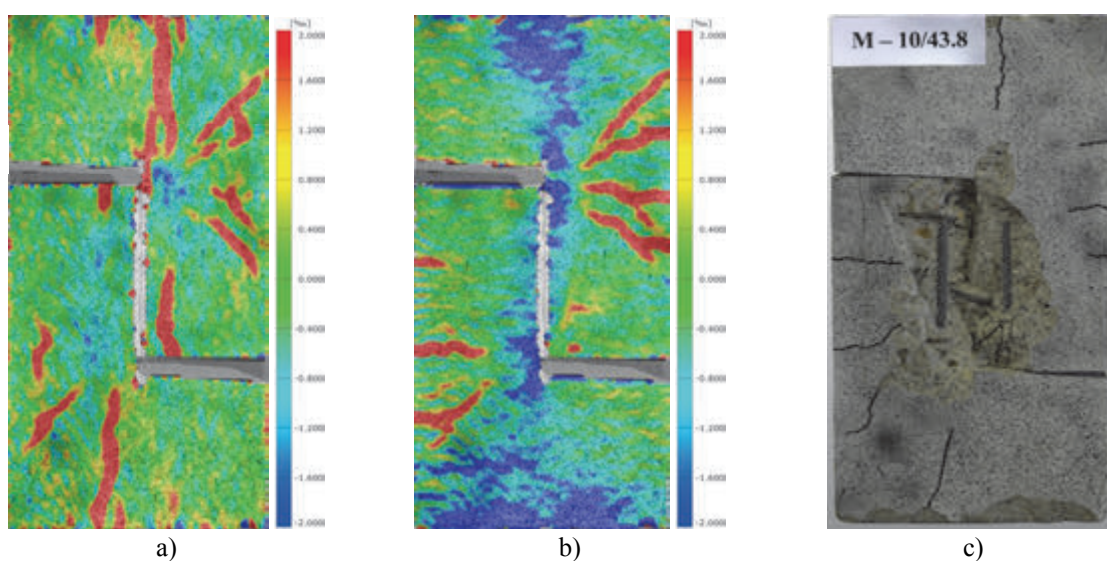


Fig. 7: Specimen M – 10/43.8: a) horizontal, b) vertical strains recorded immediately before failure, c) front view after failure

Due to the lack of interface reinforcement and stress acting perpendicular to the contact surface, the load carrying capacity of the M – 0/43.8 specimen was dependent solely on the adhesion forces. Their disappearance was violent and occurred when the mutual movement of the edges of the interface was about 0.15 mm. Such displacement was about three times higher with respect to values recorded during the tests conducted by Randl and Wicke (2000) who concerned interfaces between concrete cast at different times.

The introduction of transverse reinforcement made it possible to change the mechanism of interface failure – from brittle to ductile, and at the same time to increase the load capacity by 163% and 180% (M – 8/43.8 and M – 10/43.8 respectively) with respect to the reference element M – 0/43.8. It resulted from two additional mechanisms: aggregate interlock and dowel action that could not work in the case of unreinforced interface. Registered images allowed for accurate determination of the displacements associated with achieving the ultimate load – see Fig. 8.

At the further stage of the test, intense increase in deformation, which lead to rupture of the transverse reinforcement, was observed. The appearance of each “step” in the load – deformation curves was accompanied by a characteristic thwacks, hearable during the test. This allows to state that the measurements carried out by using the DIC system made possible to determinate accurately the moment of rupture of interface reinforcement.

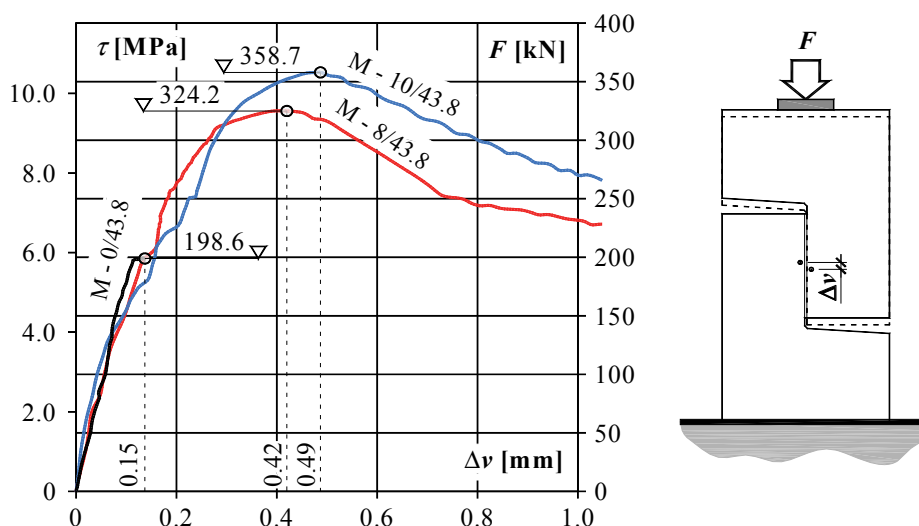


Fig. 8: Comparison of the mean displacements between edges of the interface at ultimate load

5. CONCLUSIONS

According to results of the tests concerning corbels and “Z” shaped specimens many advantages of using Digital Image Correlation system can be seen. It enables to predict location of zones of potential cracking, to estimate the width of the cracks as well as to follow the development of model deformation (eg. by using the virtual extensometers). The biggest advantage of using DIC is no need to install the necessary measuring devices before the tests. The analysis of recorded images can be carried out later, when the test is over. The virtual measuring equipment (eg. extensometers) can be placed wherever it is need. The use of the optical measuring device has allowed to record the deformations of M – 0/43.8 specimen even after the maximum load has been exceeded – without damaging of the transducers as would be in case of direct contact measuring methods.

However, it should be borne in mind that the results of measurements carried out by Digital Image Correlation systems can be flawed. Measurement errors are strongly dependent on the: size of the measuring area, inaccuracies of averaging the results of calculations, light condition changes during the test, noises of digital camera, angle between cameras and analyzed surface, quality of the lenses as well as preparation of the test surface.

6. REFERENCES

- Goszczyńska B., Trąmpczyński W., Tworzewska J., Tworzewski P. (2014), “Doświadczalna analiza odkształceń przestrzennych belek żelbetowych z zastosowaniem skanera optycznego 3D”, *Inżynieria i Budownictwo*, Vol. 70, No. 3, pp. 156-159.
- Goszczyńska B., Tworzewska J. (2014a), “Określenie rysy na potrzeby analizy wyników badania procesu powstawania i rozwoju rys w belkach żelbetowych z zastosowaniem systemu Aramis”, *Przegląd Budowlany*, Vol. 85, No. 12, pp. 24-29.
- Kneć M. (2015), „Technika cyfrowej korelacji obrazów w analizie deformacji połączeń elementów konstrukcji stosowanych w lotnictwie”. Doctoral Thesis. RUT, pp. 37.
- Randl, N. and Wicke, M. (2000), „Schubübertragung zwischen Alt- und Neubeton. Experimentelle Untersuchungen, theoretischer Hintergrund und Bemessungsansatz“, *Beton- und Stahlbetonbau*, H. 95, pp. 461– 473.
- Revilock D.M., Thesken J.C., Schmidt T.E. and Forsythe B.S. (2007), “Three-Dimensional Digital Image Correlation of a Composite Overwrapped Pressure Vessel During Hydrostatic Pressure Test” Technical Report NASA, pp. 15.

CHANGE OF THE GRADE LINE OF BRIDGES CONSTRUCTED WITH CANTILEVER CONCRETING TECHNOLOGY

Czesław Machelski¹, Bartosz Pisarek²

¹ Department of Bridge and Railway, Wrocław University of Science and Technology

² HOCHTIEF Infrastructure GmbH Deutschland Nord

czeslaw.machelski@pwr.edu.pl, bartosz.pisarek@hochtief.de

SUMMARY

The cantilever concreting technology is one of modern methods of constructing the concrete long-span bridges. The fundamental features of this method are saving of materials and of construction costs (especially of scaffolding and of formwork) and first of all a possibility of carrying out the construction of the span in many spots at the same time. The negative feature of these bridges is a large long-term deflection of the bridge, as a result of rheological processes in the concrete and in the pre-tensioning steel. Deflection measurements at the mid-span indicate a visible lowering of the grade line of the bridge span, already after few years of service. In this paper the deflection $w(t)$ is represented as a function of the service time of the bridge structure, calibrated by the results of monitoring of the bridge deflection. Analyses presented in this paper will be used to develop rheological models of behavior of the concrete and of the pre-tensioning steel.

1. INTRODUCTION

The cantilever concreting technology was used first time in 1951 by U. Finsterwalder to construct the bridge over the Lahn Bulduinstein River. Hence most of bridges constructed with this technology have not exceeded half of the expected service life of 100 years. Until present thousands of such bridges were made in the world. In Poland between 1963 and 1973 the cantilever method was for construction of three (in two cases the prefabricated assembly was used). The next big groups of those bridges were built after the bridge in Torun (1998). It seems, that Polish experience of that technology is in initial phase.

The cantilever concreting (or assembly) technology is one of present techniques of bridge construction. The fundamental features of this method are saving of materials and construction costs (especially of scaffolding and of formwork) and first of all a possibility of carrying out the construction of the span in many spots at the same time. The latter, especially the cyclical concreting of bridge segments result in a shorter construction time. This technology is effective for the bridges, whose span length is between 50 and 250 meters.

The characteristic feature of those bridges is the external appearance, which is showed in the Figures 1 and 2. The geometrical profiles are determined by the applied technology and by the distribution of loads - especially, in the construction phase. In such long-span pre-tensioned concrete bridges the distribution of internal forces is mainly influenced by static behaviour pattern of cantilevers in construction phase.

Characteristic feature of post-tensioned long-span concrete bridges are excessive deflections. The excessive deflections are meant those exceeding the deflection coefficient $\omega = 1.250\%$. That coefficient is calculated from the following expression:

$$\omega = \frac{w}{L} \quad [\%], \quad (1)$$

w [mm] is a displacement at the mid-point of the bridge span L [m].

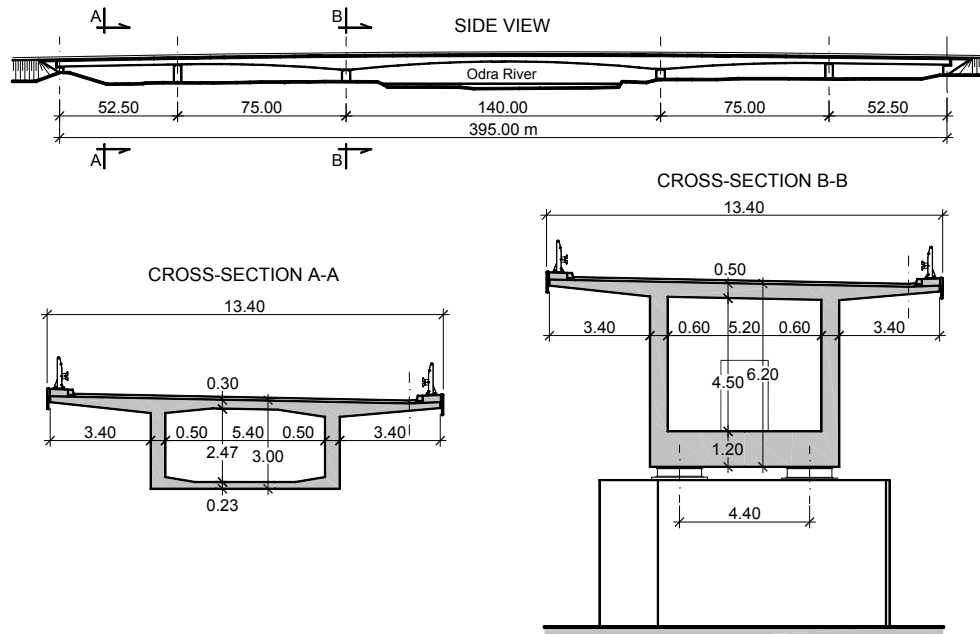


Fig. 1: Geometry of the Kedzierzyn-Kozle Bridge (Poland)

Problem of excessive deflections considered in this paper is a common one. One of the best documented examples of the analyzed problem is the bridge Støvset (Takacs, 2002), Fig. 2. The designer used in the middle of the span *light* concrete LC55, like in the Stolma Bridge, which spans an amazing length $L = 301$ m. Hence, this method could be used to build long-span bridges. Nevertheless, already 8 years after the completion of the structure, the deflection w was over the design value 200 mm! It was believed that the main reason was underestimation of the deformation of the light concrete, used to build that bridge (Takacs, 2002).

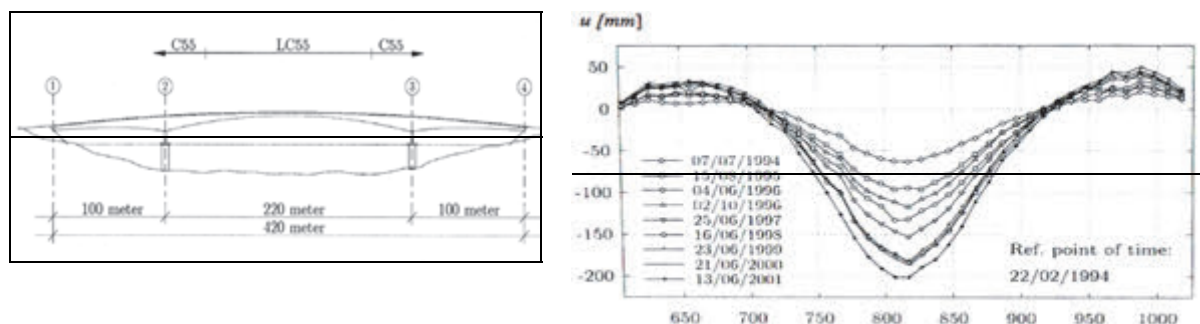


Fig. 2: Scheme of the Støvset Bridge incl. the development of deflections during the service time (Takacs, 2002)

One of negative examples of reduction of excessive deflections is the Koro-Babelthaupt Bridge: span $L = 241$ m. After 12 years of service, the deflections of this bridge were measured, which reached the value $w = 1200$ mm, corresponding to $\omega = 4.98\%$. After 18 years the span deflection increased to $w = 1390$ mm, so now $\omega = 5.77\%$. It follows, that the deflection coefficient very much exceeded the allowable value (1). The reinforcing of the bridge – post-tensioning – did not help and after short service the structural failure occurred.

In spite of the fact, that the rheological behaviour of the concrete was studied over the whole 20th century, the problem of excessive deflections of post-tensioned concrete bridges remains unsolved. It seems, that during the designed service time of 100-years the rheological effects do not reach any final, constant value. The excessive deflections problem is quite well recognized by monitoring of the span-bridge deflection (Bažant, Hubler, Glang, 2011). In this paper the deflection $w(t)$ is represented as a function of the service time of the bridge structure, calibrated by the results of monitoring of the bridge deflection for the cantilever concreting constructions. However the experience from a number of bridges shows that some bridges show excessive deflections, but a great majority of bridges work very well.

2. UPLIFT OF THE BRIDGE SPAN

During the construction process of the cantilever spans the uplift is used, which is the initial elevation of the longitudinal axis of the bridge with respect to the grade line of the bridge. The purpose of that initial elevation is the reduction of deflection, which results from sustained loads after connection of spans, especially from the forced deflection during the cantilever span connection, post-tensioning for river span, equipment loads. In some cases the rheological processes occurring during the service time are taken into account. Because of relatively big own weight of the structure, as compared with service loads, in this paper the arising span deformations are regarded as rheological effects, rather than as the results from variable loads.

In the Tab. 1 as well as in the Fig. 3 two different examples of bridges over Odra River (in Poland) are compared. In comparison with similar bridge structures, these bridges have more varying height of the box girder. Because of the used construction technology - concrete scaffolding, the bridge spans over the river usually have constant height of box girder. Along the bridge, the grade line is a circle of radius R , where the highest value occurs in the longest span.

Tab. 1: Geometrical characteristic of bridges over the Odra River

Location of the bridge	Geometrical parameters of bridges [m]				
	L	h	H	R	Span spread
Opole	100	2.35	5.80	10000	45+55+ 100 +55+45+45+40
Kędzierzyn-Koźle	140	3.00	6.20	10000	52.5+75+ 140 +75+52.5

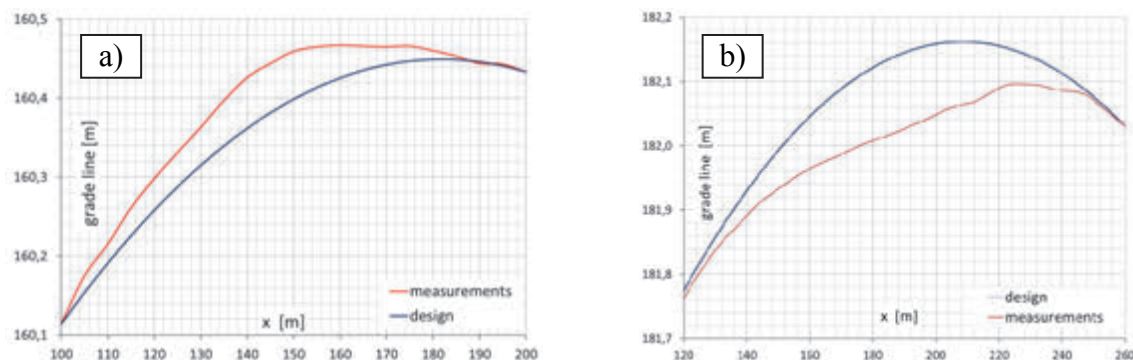


Fig. 3: Grade line of bridge a) Opole Bridge after 15 years of service time
b) Kedzierzyn- Kozle Bridge 3 years after connection of cantilevers

The technology – uplift of span – which was applied in the structure located in Opole Fig. 3a is usually used to erect the structure with the cantilever concreting technology. In the Fig. 3a. two curves of the bridge grade line are presented, the first one - planning phase, which is determined as the section of the circle of the radius R and the second one - the curve, which is the result of the surveying measurements during service. These curves show that after 10 years of service, the bridge elevation of 60 mm remaining from the applied uplift still existed, the span length being 150 m. The difference, which is seen between both lines (design phase - surveying measurement) is the provided excess, which was designed to minimize the rheological processes occurring in the bridge structure.

In the Fig. 3b the case is presented, where the designer did not apply the uplift of the span, in the middle of that ($x = 190$ m) the recess occurred, which amounted to 130 mm. It turned out that the allowable deflection coefficient for this type of bridges is $\omega = 1.25\text{‰}$, was reached already after 8 years of service. Comparison of those deflections (rheological process) with the deflection due to service loads, which were measured during the commissioning loading test of the Kedzierzyn-Kozle Bridge showed that the ω coefficient from the rheological processes is bigger than the ω coefficient from service loads, where deflection $w = 59.9$ mm, which gives $\omega = 0.43\text{‰}$.

3. CHANGE OF THE DEFLECTION COEFFICIENTS DURING THE BRIDGE SERVICE LIFE

Characteristic feature of these bridges are large long-term deflections of span, especially during the initial phase of service life. Some measurement results of the deflections for the bridge structures in Japan are shown in Fig. 4. On the basis of these, the equation (2) is given, which can be used to determine the deflection coefficient dependent on time t [years] for bridges constructed with cantilever concreting technology.

$$\omega(t) = \frac{9}{20} \sqrt{t} \quad [\text{‰}], \quad (2)$$

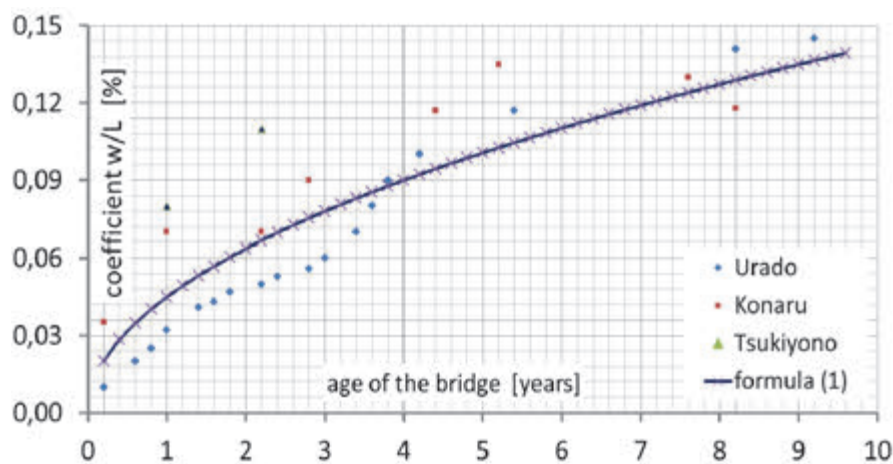


Fig. 4: Change of deflection of cantilever spans vs. time

Development of the deflection of a span constructed with the cantilever technology may be regarded in 3 different ranges of time. At the beginning – few years after putting into service – the increase of deflections is the biggest. From the curve in Fig. 4 it follows, that in the first year the increase of the deflection is the largest, and during the subsequent years the deflec-

tions get stabilized. During the second period in Fig. 5, the development of deflections is more balanced. The third, the longest period of bridge service life (75% of service time) could be only forecast (predicted), because of lack of measurement results.

In the paper (Bažant, Hubler, Glang, 2011) results of deflection measurements of 56 bridges constructed with cantilever concrete method are presented. These bridges were made from different concretes as well as in various climatic zones. Also the static schemes (mainly the span length L) of these bridges are diverse. Therefore the deflection coefficient, as given by equation (1), rather than the deflection itself is presented.

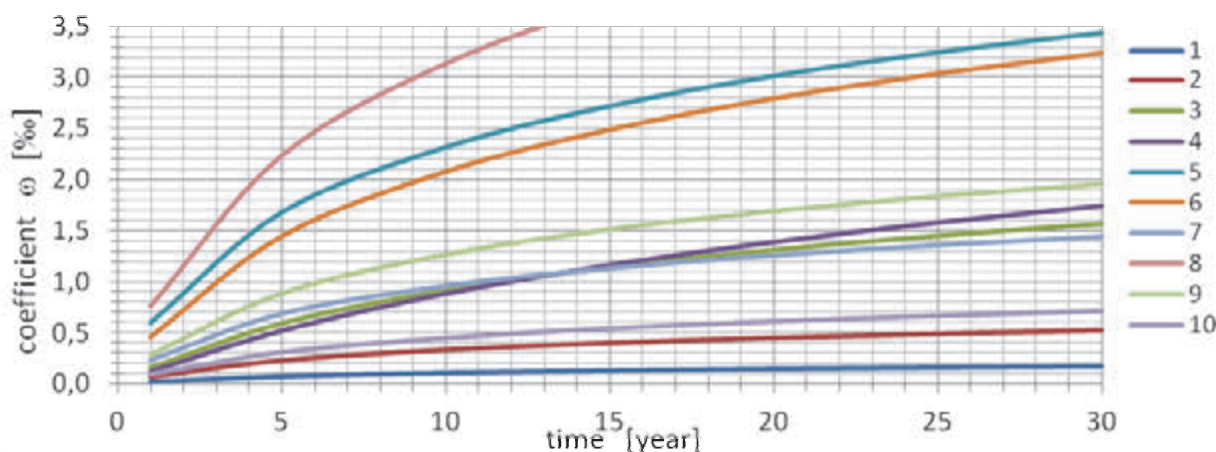


Fig. 5: Change of deflection coefficient for the analysed bridges

Tab. 2: Parameters of bridges spans

Location of the bridge		Parameters			Coefficients [‰]	
Groups	nr	L [m]	a	b	ω_{10}	ω_{100}
1	31	102	0.061	0.4596	0.0105	0.2359
2	35	130	0.194	0.4612	0.3343	0.7467
3	8	112	0.724	0.2545	0.9116	2.3592
4	25	131	1.200	0.1092	0.8880	2.9813
5	3	142	1.111	0.7045	2.3165	4.7429
6	22	101.5	1.190	0.4750	2.099	4.6579
7	32	125	0.475	0.6500	0.9571	1.9901
8	39	95	1.620	0.5952	3.1412	6.6468
9	37	84.5	0.700	0.5130	1.2711	2.7739
10	21	104	0.271	0.4246	0.4492	1.0222

With the aid of the results given in (Bažant, Hubler, Glang, 2011) 10 groups of coefficients were made depending on the time evolution of $\omega(t)$. In the Tab. 2 the characteristics of chosen structures for these groups are listed, where the range of span length was $95 \text{ m} < L < 142 \text{ m}$. On the grounds of the results of measurements (for short service time) the following approximate equation was established:

$$\omega(t) = a \ln(1+bt) \quad [\text{‰}] \quad (3)$$

where a and b are coefficients listed in Tab. 2 and t denotes time (in years), measured from completion of the construction process. These functions are plotted in Fig. 5.

4. CALIBRATION OF DEFLECTION FUNCTION

The result presented in the Tab. 2 as well as in the Fig. 5 show, that the deflection equation results are scattered. It means, that many approximate functions $\omega(t)$ could be proposed. In this paper some selected examples of these equations referring to four-span Zvikov-Otava Bridge (nr 7), $L = 84$ m are given. For this bridge, similar plots of deflection were obtained from equation (3) for each span. The values of parameters in equation (3) are listed in the Tab. 3, the graphs are shown in the Fig. 6.

Tab. 3: Span parameters of Zvikov-Otava Bridge

Number of span	Parameters	
	a	b
B7	0.547	0.2819
8B	0.629	0.1819
B9	0.498	0.4205
B10	0.552	0.4200
7-10	0.554	0.3086

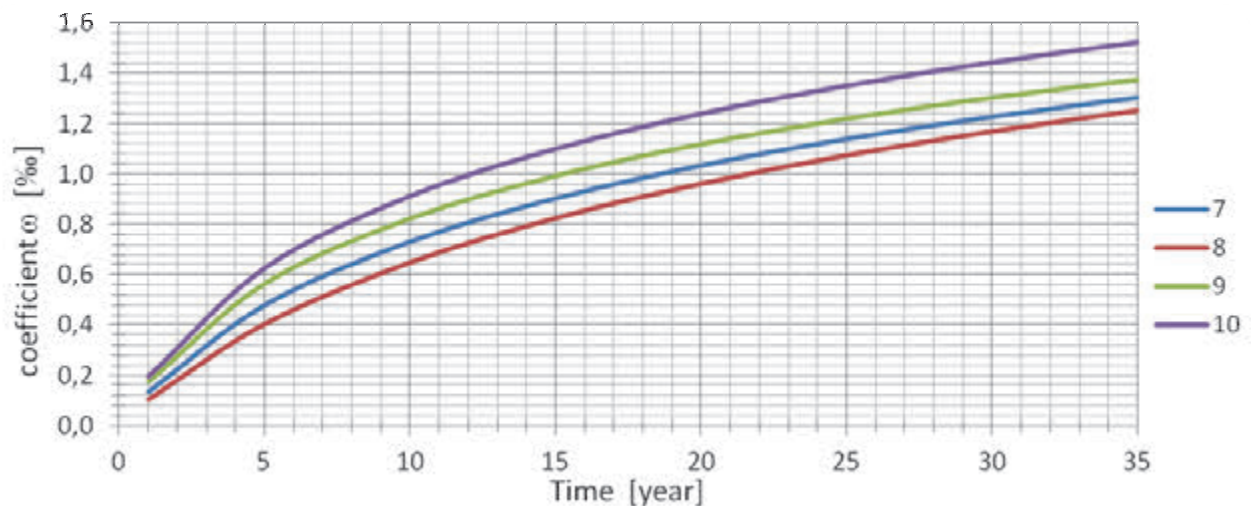


Fig. 6: Change of deflection coefficient during the service time – equation (3)

The equation (3) is regarded as the initial equation. As the approximation of deflection, during first 30 years, $t < 30$ years also the following function can be used:

$$\omega(t) = c\sqrt{t} \quad [\text{‰}] \quad (4)$$

For example, for the Zvikov-Okava Bridge good results are obtained for $c = 0.24$, as compared with the Japan bridges (analyzed before in Fig. 3), magnitude of deflection coefficient c is two times smaller.

As next example, the equation (5) is given, which is more complex than (3). The results obtained from that equation are equally accurate as from (3):

$$\omega(t) = d \left[\ln(e+t) + e^{-f \cdot t} \right] \quad (5)$$

where $d = 0.003701$ and $f = 0.06994$.

The simple equation (6) given below:

$$\omega(t) = \frac{\ln(t) - g}{h} \quad (6)$$

where $g = 0.3023$ and $h = 2413$ is not useful.

The effectiveness of approximate equations (3) to (6) is compared in Fig. 7. The data was taken from the measurements of Zvikov-Otava Bridge.

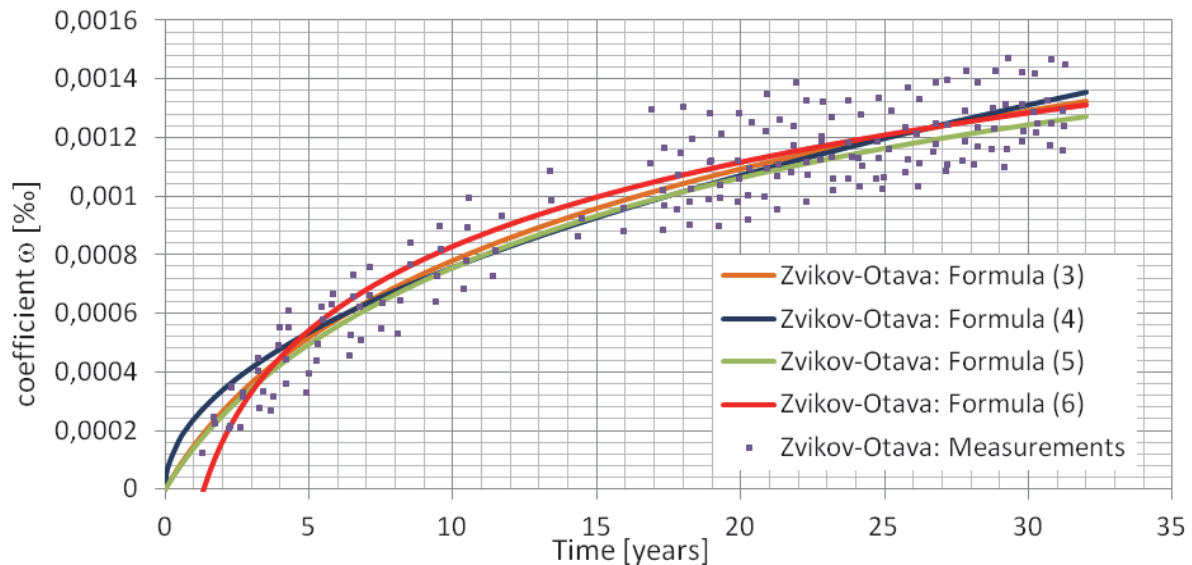


Fig. 7: Analysis of approximate deflection equation for Zvikov-Otava Bridge

5. PROGNOSIS OF FINAL VALUE OF DEFLECTION

The purpose of establishing equation for $\omega(t)$ is to estimate the deflection of the span during the whole service time of the structure, assumed usually as, 100 years. The functions useful for an early phase of bridge service time are not necessarily so useful for long-term deflection. For example, if the value of coefficient deflection for $t = 10$ years was equal, the results obtained from equation (3) and (4) would be the same, i.e. $w_{10}(3) = w_{10}(4)$. Then for $t = 100$ it would be:

$$w_{100}(3) = \frac{\ln(1+30,86)}{\ln(1+3,086)} w_{10} = 2,46 w_{10}$$

where $a = 0,554$ and $b = 0,3086$.

From the equation (4) it is obtained:

$$w_{100}(4) = \frac{\sqrt{100}}{\sqrt{10}} w_{10} = \sqrt{10} w_{10} = 3,16 w_{10}$$

If we assume, that the equation (3) is a reliable deflection extrapolation, the results in the Tab. 2 can be taken as final results after service time $t = 100$. As we can see the coefficient ω_{100} , that means for $t = 100$ year, for the groups 3 – 9 (Tab. 2) has exceeded the allowable

value $\omega(t) < 1.25\%$. For bridges of groups 5, 6, 8, 9 the values of coefficients have reached very high levels, which is comparable with the Koror-Bablthaupt deflection.

6. CONCLUSION

Characteristic feature of behaviour of bridges constructed with cantilever concreting method, resulting from large span lengths, are excessive long-term deflections of the bridge ($w > L/800$), due to of rheological processes in the concrete and in the pre-tensioning steel. For example, if we take the results from Fig. 6, it can be easily said, that the deflection increase is not proportional to the final value $w_{100} = 155$ mm, $t = 100$ years: 25% of the value is already reached after 4 yers of service; $w_4 = 38.75$ mm, 50 % of final results after 13 years; $w_{13} = 77.50$ mm, 75% after 32 years; $w_{32} = 116.25$ m. It follows that, the reological processes (as regards deflections) do not approach any final value after 100 years predicted service life, these processes continue.

Fundamental feature of the cantilever bridges is the large scatter of the measurements results, which is caused by many random factors like: construction technology, duration of construction process, concreting time, climate, concrete strength, used aggregate, quantity of reinforced steel and the important / rheological processes. In this paper the equation (3) for deflection depending on service time of the structure is proposed, which is based on the measurements of bridges constructed with cantilever concreting method. Analyses presented in the paper are going to be used to establish rheological models of reinforced steel and concrete. The current aim of the paper is not the assessment of rheological models of concrete and of reinforced steel, but the demonstration of complexity of the problems of large long-term deflections. It should be pointed out, that the bridges with hinges at the midspan are much more sensitive to long-deflections then continuous bridges, that knowledge should be used during the design phase of bridges. The problem of maintaining of the grade line of reinforced concrete bridges in appropriate-designed line is still not solved.

7. REFERENCES

- Bazant Z., Hubler M.H., Glang Y.: “*Excessive Creep Deflections: An Awakening*”. Concrete International, 8(33), 2011, p. 44-46.
- Takacs P.F.: “*Deflections in Concrete Cantilever Bridges: Observation and Theoretical Modeling*”. Doctoral Thesis, Trondheim 2002.
- Mutsuyoshi H., Duc Hai N., Kasuga A.: “*Recent technology of prestressed concrete bridges in Japan*”, IABSE-JSCE Joint Conference on Advances in Bridge Engineering-II, August 8-10, 2010, Dhaka, Bangladesh.
- Burdet O., and Badoux M.: “*Deflection monitoring of prestressed concrete bridges retrofitted by external post-tensioning*”, IABSSE SYMPOSIUM RIO DE JANEIRO 1999.
- Kalny M., Soucek P., Kvasnicka V.: “*Long-term behavior of balanced cantilever bridges*”, ACEB Workshop, Corfu 2010.
- Bazant Z., Guang-Hua Li, Qiang Yu, Klein G., Kristek V.: “*Explanation of Excessive Long-Time Deflections of Collapsed Record-Span Box Girder Bridge in Palau*”, Preliminary report, presented and distributed on September 30, 2008, at the 8th International Conference on Creep and Shrinkage of Concrete.

TOPIC 4

ADVANCED CONCRETE STRUCTURES

MATERIAL DEVELOPMENT FOR THE QUICKWAY SYSTEM

Johannes Oppeneder¹, Lutz Sparowitz¹, Bernhard Freytag², Nguyen Viet Tue¹

¹ Institute of Structural Concrete, Graz University of Technology, Austria

² Laboratory for Structural Engineering, Graz University of Technology

SUMMARY

QUICKWAY is a traffic system above existing roads for passenger and freight transport in "green cities", for new and existing Megacities. The system consists of slender, cross-free, high-speed ways for autonomous vehicles. Additionally, new paths for cycling and pedestrian emerge at the existing roads. In addition to the roadways in different levels, a roof construction is integrated to protect the traffic from environmental influences and collect rainwater and or solar energy. This article deals with the material development for QUICKWAY. The prefabricated components of the modular construction are produced of Ultra high performance fibre reinforced concrete UHPFRC. The challenges of the usage as well as the wide-spanned construction places high demands on the fresh and hardened concrete properties of the material.

1. INTRODUCTION

QUICKWAY is a new transport concept for urban and freight transport in cities. The system consists of slender, wide-span roadways along common traffic routes see *Fig. 1*. Especially for "green cities" or for cities with high traffic volumes, QUICKWAY offers a solution to the traffic problem. For this, QUICKWAY consists of different roadway routes, which are connected to each other. The linking of the different routes, create a new road network for the city. QUICKWAY is to be completed by a transparent roof construction. This provides protection against environmental influences, and allows gaining energy and or rainwater. These are increasingly important raw materials for such cities.



Fig. 1: QUICKWAY System

Furthermore, grade separated junctions and central navigation, as well as use of autonomous vehicles, create a very efficient traffic system for existing megacities. Particularly in the junctions, as well as for ramps and descents from the roadways, different types of road elements are necessary. In order to ensure fast and easy production, as well as assembly of the innovative modular structure, a sustainable, durable and easy manufacture able material is necessary.

This paper deals with the concrete development, whereby on the one hand the fresh concrete properties are of great importance for the production, casting and hardening, and on the other hand, the hardened concrete properties are important for the usage and verification of stability.

2. QUICKWAY ROADWAY SYSTEM

The QUICKWAY system consists of three different traffic networks, which are interconnected. The primary and secondary network, see Fig. 2, consists of roadways (height at least 5.5 m) above the normal road network of existing or new cities and serve as main routes for long and short connections. An essential design principle is, that the turning lanes for the entire network each contain either only left curves (left hand traffic system) or right curves (right hand traffic system). A left turn in a right hand traffic system is made through three times right turns in a mesh of the network. By means of a meaningful route selection in the QUICKWAY network, depending on the traffic situation, each point can be reached in the shortest amount of time.

Tab. 1: Grade separated junction

transit lane 1	transit lane 2	r [m]	V transit lane [km/h]	V transfer lane [km/h]
Sekundary	Sekundary	15 / 30	40 / 50	22.5 / 30
Primary	Sekundary	15 / 30 50 / 80	50 / 80	22.5 / 30 40 / 50
Primary	Primary	50 / 80	80 / 80	40 / 50

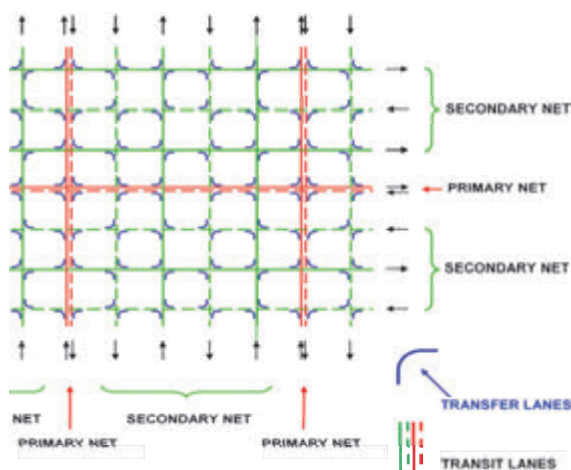


Fig. 2: QUICKWAY NETWORK (schematic)

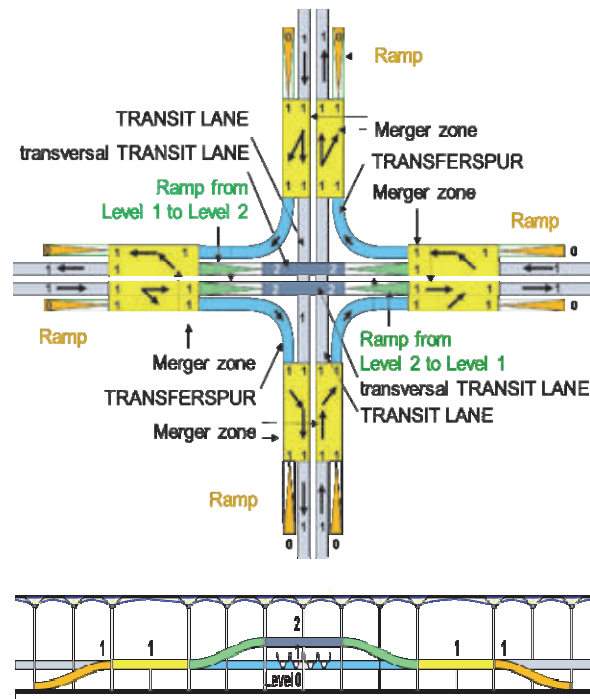


Fig. 3: Grade separated junction, primary QUICKWAY network, ground plan / elevation

The Tertiary network consists of the existing road network and is mainly used for traffic routes in the source and destination areas. With these three network types QUICKWAY enables efficient and targeted public and private traffic from door to door as well as freight transport.

2.1 QUICKWAY network

The primary network is designed for a speed of 80 km/h with paths in both directions. The mesh size in the primary network is ~ 4 km. The paths of the mesh can be divided in transit lanes for the main routes and transfer lanes. The transfer lanes are part of the grade separated junctions, which are introduced in the system for a fluent road traffic. The transfer lane can be traversed with a maximum speed, as shown in Tab. 1, depending on the curve radii and network type. The primary network is directly connected to the secondary network via transfer lanes.

The secondary network is much more subdivided and is executed as a one-way system. Thereby it is suitable for streets with less space. In order to obtain an efficient system, the distance between the various roadways is arranged narrower and has a distance of 600 to 900 m. For this purpose, grade-separated junctions with tighter curves and slower speed are available, see Tab. 1. Due to the network design, a lower speed of 50 km/h appears to be useful for the secondary network. The secondary network is connected to the primary network and allows to exit to the tertiary, existing network via ramps.

For a flexible powerful roadway mesh in smart cities, many junctions are necessary in the primary and secondary roadway network. To increase the traffic flow especially at the crossing points of the roads, exclusively grade separated junctions are introduced in the QUICKWAY network. Fig. 3 show a junction in the primary network. In the secondary network the junctions are constructed according to the same functional principle, see (Oppeneder, September 2016). For a grade-separated junction, the tracks of the transversal transit lanes are ramped across the transit lanes. Vehicles from the transit lane, which change the roadway, are guided over merger zones and transfer lanes to the transversal transit lane. In the merger zone a direct connection via ramps to the tertiary network is located. This type of intersection provides a simple and sleek design for the transit lanes and for the right-turning transfer lanes. An overview of the required roadway elements for the QUICKWAY system can be found in Fig. 3.

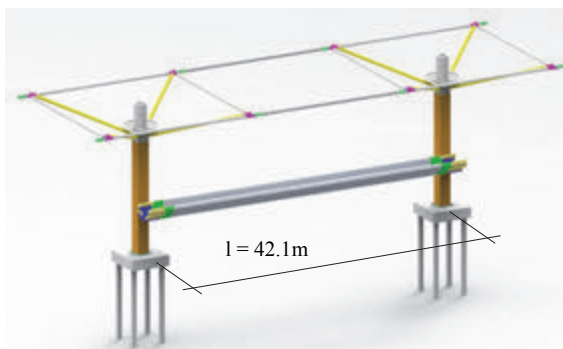


Fig. 4: Standard QUICKWAY structure

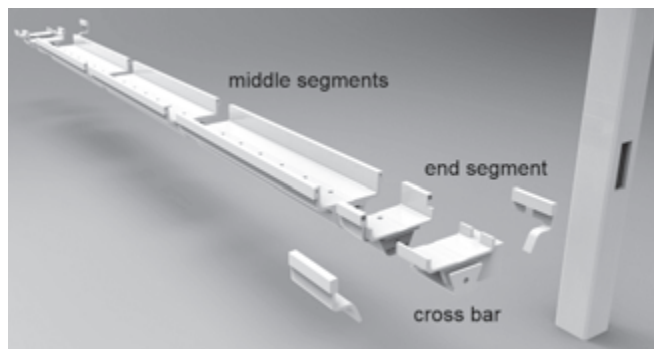


Fig. 5: Segmental construction straight element

2.2 Modular construction kit QUICKWAY structure

Fig. 4 gives an overview of the standard QUICKWAY structure. It consists of the foundation, the pole, the roof construction and the roadway. The standardized centre distance of the poles of 42.1 m results from the verification of stability of the straight roadway elements. The roadway elements are executed as single span girders. For the realization of the transfer and transit lanes in the QUICKWAY network, various elements for the roadways are necessary. In order to enable a flexible, simple system, as well as a fast assembly and a rapid exchange of individual

components, the elements are based on the segment construction method, with a connection through dry joints and external tendons. A structural element consists of two end segments and different standard middle segments see Fig. 5. The prefabricated elements will be delivered in preassembled segments, connected on site and positioned by lifting the whole member. For this purpose, a modular system for the various segments of the roadways, supports and roof construction, was created (Oppeneder, September 2016). Criteria are maximum, as well as minimum dimensions of the segment lengths, curve radii and cross sectional types.

2.3 Cross section

The cross section for the roadways consists of a hollow box girder, which is monolithically connected to the handrails. Hereby the hollow box girder increases the torsional stiffness whereby the handrails increase the bending stiffness and serve as guardrails.

As mentioned before, various elements and segments are required. Therefore five different cross sections exist, see Tab. 2. The height for all girders is 1.80 m, although the construction height is only 1.00 m. The position of the webs of the hollow box takes into account the position of the vehicle wheels. For the QUICKWAY network, a limitation of the maximum vehicle dimension of 2 x 7 m was chosen. The minimum width of the roadway is set including a safety distance to 2.50 m. In curves with a radius $R < 60$ m, a wider travel path is defined as a function of the vehicle width in the curve.

The maximum section thickness for the production is 12 cm, the connection of the webs to the roadway panel is produced with cuffs. Fig. 6 shows the cross-section of a produced box girder.

Tab. 2: Dimensions of the cross section

cross section	curve radius r_k [m]	width [m]	area [m ²]	t_1 [cm]	t_2 [cm]	t_3 [cm]	t_4 [cm]
QS 1	∞	2.50	0.76	8	6	8	10
QS 2	15	3.10	1.06	10	10	12	12
	50	3.10	1.06	10	10	12	12
QS 3	30	2.75	1.05	12	12	12	12
	50	2.75	1.05	12	12	12	12
QS 4	≥ 50	2.50	0.91	10	8	12	12
QS 5	∞	7.30	-	8	10	8	10

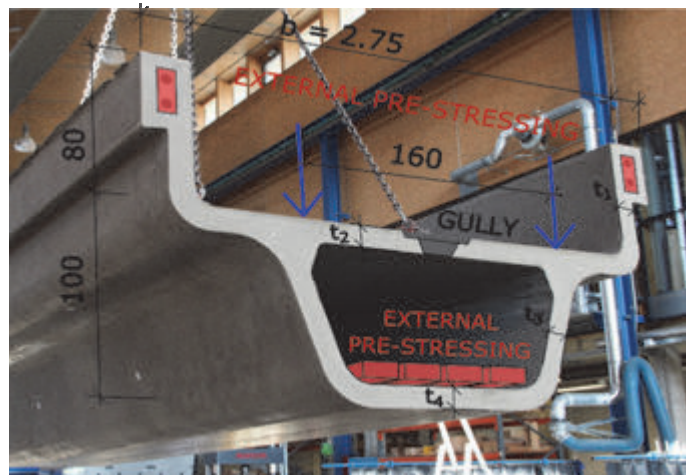


Fig. 6: Cross section

2.4 Design concept

The basic structural concept for the design is based on straight or slightly curved single-span beams, which are mounted on bearing brackets with elastomer bearings. These allow non-constraining bearing in the longitudinal direction, however torsion for the curved beams is fully constrained. The permanent loads for the construction result from the dead weight with a density of the UHPFRC of $\gamma = 26$ kN/m³ and an additional load of 2 kN/m². A limitation of the maximum load for vehicles of 5 tons is chosen for the QUICKWAY network. The various segments are connected with straight tendons and dry joints. The load bearing capacity for

bending and shear in longitudinal and transversal direction have to be verified by the UHPFRC cross section in combination with longitudinal tendons. Additional reinforcement should be avoided with regard to an easy prefabrication.

3. UHPFRC AS MATERIAL FOR QUICKWAY

Due to the high requirements of the slender QUICKWAY construction, fibre reinforced UHPC as a durable material for the required fast and easy production was chosen. In the following part, the requirements and the finally chosen material is shown. A full scale casting test was done to show the feasibility.

Tab. 3: Required and achieved fresh and hardened UHPFRC properties

	required	achieved
slump flow (Hoang, 2017) on dry steel plate	750 – 850 mm	✓
flow time t_{500}	6 – 12 s	✓
cylinder compressive strength	$f_{ck} = 150$ MPa	$f_{ck} = 170$ MPa; $f_{cm} = 180$ MPa
tensile strength of UHPC matrix	$f_{ct,el,k} = 6.0$ MPa	$f_{ct,el,k} = 6.5$ MPa; $f_{ct,el,m} = 8.4$ MPa
post cracking tensile strength	$f_{ctk,r} = 6.0$ MPa	$f_{ctk,r} = 7.3$ MPa; $f_{ctm,r} = 10.4$ MPa
young's modulus	$E_c \geq 50\,000$ MPa	$E_c = 52\,000$ MPa
final shrinkage	≤ 0.7 mm/m	≈ 0.65 mm/m

3.1 Required fresh concrete properties for casting

As a result of the cross-sectional geometry, the production is demanding. On the one hand, the process must ensure the high quality requirements for UHPFRC with regard to the mixing procedure, the fibre distribution and orientation. On the other hand, the self-compacting behaviour with a good flow ability should be achieved for a fast and economical use in the plant. In Tab. 3 the required fresh concrete properties are shown.

A further special requirement is placed on the formwork. For the casting of a QUICKWAY segment, the formwork was placed in an upright position (Mosinz, 2016). The following points were analysed in the casting test:

- One-sided filling of a "lying" formwork
- Robust formwork made of coated concrete
- Internal formwork with reducible cross-section
- Ordered air distribution on the counter-shell instead of venting via expensive drain sheets
- Fibre distribution and orientation

3.2 Required hardened concrete properties

The required hardened properties of the UHPFRC are defined in the design concept and verification of stability. The design concept is based on fibre reinforced UHPFRC segments, which are connected with dry joints and external tendons in longitudinal direction. The required number of pre-stressing wires for the bending bearing capacity is determined by the decompression criteria in the rare load combination. Criteria for the maximum concrete compressive and tensile stress have to be achieved. Additional reinforcement for bending in longitudinal and transverse direction and for shear forces should be avoided for the main

segments. There for the main tensile stresses have to be equal or smaller than the design tensile strength of the fibre reinforced UHPC. Only in rare cases, additional reinforcement should be added. In Tab. 3 the required hardened concrete properties for the UHPFRC without reinforcement are shown. Further detailed information on the verification of stability is given in (Oppeneder, March 2016).

3.3 Fresh and hardened UHPFRC material properties

According to the challenging requirements of design and static verification of the components of QUICKWAY, as material UHPFRC was chosen. For the production of the 6 to 12cm thick structural elements, a concrete recipe of self-compacting UHPFRC was developed at Graz University of Technology. Based on a theoretical optimization of the packing density, a suitable concrete formulation was developed by experimental small-scale tests. Investigations were carried out on mixing stability, aeration capability, flow ability, shrinkage and tensile strength. Details can be found in (Hadl, 2016; Hoang, 2016).

Due to the small thickness of the hollow box girder cross-section parts and the required fast production steps, a renouncement of conventional reinforcement is useful. By using 2 % volume of fibres and a grain size of 0.8 mm the required fresh and hardened concrete properties could be achieved without any restriction on the self-compacting behaviour and without heat treatment that can also be seen in Tab. 3.

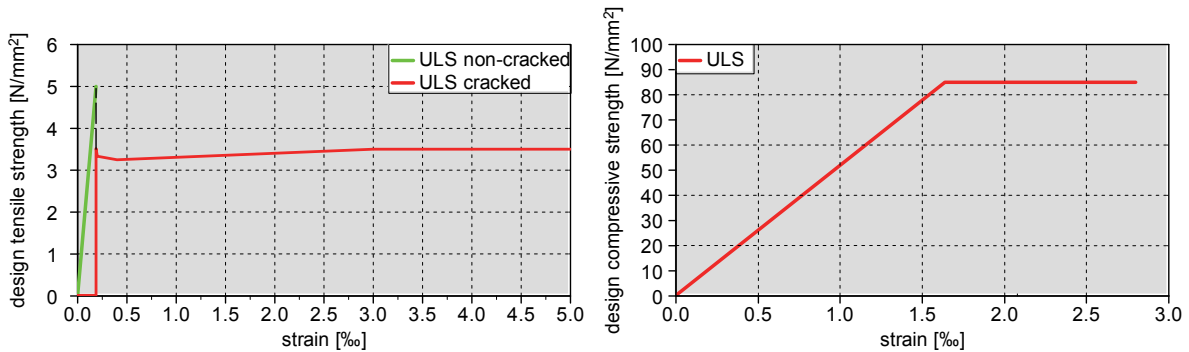


Fig. 7: Design stress- strain behaviour under tension (left) and under compression (right)

$$\text{tension, uncracked state : } f_{ct,el,d} = \alpha_{ct} \cdot \frac{f_{ctk,el}}{\gamma_{ct}} \quad (1)$$

$$\text{tension, cracked state : } f_{ctd} = \alpha_{ct} \cdot \frac{f_{ctk}}{\gamma_{ct} \cdot K} \quad (2)$$

$$\text{compression : } f_{cd} = \alpha_{cc} \cdot \frac{f_{ck}}{\gamma_c} \quad (3)$$

The stress strain behaviour under tension is derived from the measurements on 6 four-point bending tests. The tensile strength for a design of uncracked UHPC is determined by the point of the first load drop in the experiment and a safety factor independent of fibre content and orientation. However, the post peak behaviour under tension will be described according to (Hadl, 2016). Beginning from the first load drop a constant stress level is expected up to 5%, which decreases linearly to zero until a crack opening w reach value of $l_f / 4$ (l_f = fibre length). In that case, the safety factor has to take fibre content and orientation into account. The design values are calculated with equation (1), (2) and (3) with a fibre orientation factor

$K_{\text{Global}} = 1.25$ and $K_{\text{local}} = 1.75$ as well as safety factors of $\gamma_{\text{ct}} = 1.3$; $\gamma_c = 1.5$; $\alpha_{\text{cc}} = \alpha_{\text{ct}} = 0.85$. Further details on this procedure are given in (AFGC 2013; DAfStb 2008).

When selecting the starting materials required for the UHPFRC formulation, particular attention was paid to the availability and cost of the materials. The concrete optimization was primarily carried out with starting materials available in Austria and Germany, whereby the formulation of QUICKWAY is to be adapted to locally available raw materials.

3.4 Full-scale casting test

Tests with the developed UHPFRC segment with a length of 0.5 m in scale 1:1 was planned as it can be seen in Fig. 8. Accordingly, one side of the formwork was made of Perspex® to show the flow behaviour of the fresh concrete during casting.

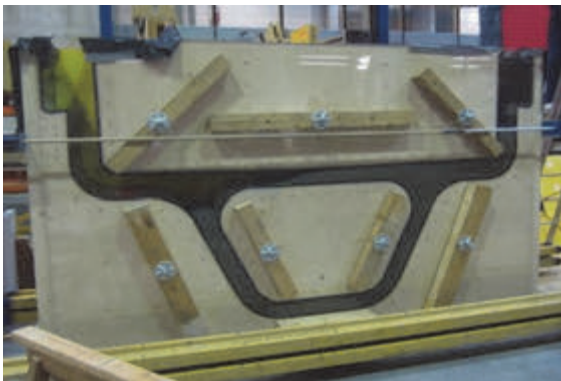


Fig. 8: Casting test



Fig. 9: Formwork / QUICKWAY Segment

At the casting test it has been shown that the desired flow behaviour of the developed UHPFRC could be adjusted well. The self-compacting UHPC balanced independently, and there were no air inclusions at discontinuities. Small problems of air inclusions occurred in horizontal places, which could be eliminated by a controlled air distribution (Marius, 2017), a slightly inclined arrangement of the formwork or by drain sheets.

In a further investigation with the FiberScan method (Freytag, 2013), the fiber distribution and orientation was shown in the cross-section. A homogeneous distribution of fibers, as well as orientation, could be seen. A fibre deposition was not visible.

4. CONCLUSIONS

This paper describes the QUICKWAY system with focus to the primary network. The paper specifically deals with the material development for the precast modular construction kit.

With the investigations of the fresh concrete properties, it can be shown that the segments with different cross sections and shapes could be casted with the self-compacting UHPFRC specially developed for QUICKWAY. A full scale casting test was carried out to show the feasibility. In addition, the desired fixed concrete properties, in particular the compressive and tensile properties of the concrete could be achieved and detected at the relevant points on the cross-section. With the material the design of the different hollow box girders can be executed.

Through this approach, all components of the modular system for the QUICKWAY system can be manufactured and dimensioned in their shape. The development of QUICKWAY has thus advanced so far that a first construction project can get started.

5. ACKNOWLEDGEMENTS

The studies described, are carried out in the framework of a Federal funded joint research project under the auspices of the Austrian Research Promotion Agency (FFG): 840397. The joint research is carried out in cooperation with S+W Wörle Sparowitz Ingenieure ZT GmbH, Hans Lechner ZT GmbH and Graz University of Technology represented by the Institute of Construction Management and Economics, the Laboratory for Structural Engineering as well as the Institute of Structural Concrete.

6. REFERENCES

- Association Francaise de Génie Civil (AFGC) Documents scientifiques et techniques (2013) "Bétons fibres a ultra-hautes performances", Recommandations.
- Deutscher Ausschuss für Stahlbetonbau DAfStb (2008): „Sachstandsbericht Ultrahochfester Beton“, Heft 561, Beuth Verlag GmbH, Berlin, Wien, Zürich, 1. Auflage.
- Freytag, B., Heinzle, G., Santner, G. (2013) Fibre Scan A3-22.F-10/2009/6 Zerstörungsfreie Bestimmung der richtungsabhängigen Zugtrageigenschaften von stahlfaserbewehrten Bauteilen aus UHPC. Endbericht, TU Graz
- Hadl, P.; Henner, S.; Kim, H.; Tue, N.V. (2016): "Experimental investigations on the scattering in the post cracking tensile behaviour of UHPFRC", Kassel University Press, Kassel March 2016
- Hoang, K., Dissertationsvorhaben, A Systematic Mix Design Approach for Ultra-High Performance Fibre Reinforced Concrete, TU Graz, Institut für Betonbau.
- Marius, R (2017): Interaktion Schalldhaut-Betonoberfläche beim Produktionsverfahren QUICKWAY, Masterarbeit, Graz, in preparation
- Mosinz C. (2016): Verfahren zur Herstellung der Fahrbahnträger – Fertigteile aus UHPFRC im Projekt QUICKWAY. Graz Universität of Technology: Diplomarbeit.
- Oppeneder J., Sparowitz L., Tue N.V. (2016): "Structural Design for the QUICKWAY System". Kassel University Press, March 2016.
- Oppeneder J., Sparowitz L., Hadl P., Freytag B., Tue N.V. (2016): "Modular construction kit for the QUICKWAY system", Proceedings SEMC 2016, Captown September 2016.
- Reichl, M. (2010): „Dünnwandige Segmentfertigteilm Bauweisen im Brückenbau aus gefasertem Ultrahochleistungsbeton (UHFB) – Tragverhalten, Bemessung und Konstruktion“, Graz Universität of Technology, Dissertation.

STRUCTURAL HEALTH MONITORING SYSTEM OF A CONCRETE CABLE-STAYED BRIDGE

*Jan Biliszczyk, Paweł Hawryszków, Marco Teichgraber
Wrocław University of Science and Technology, Poland
Wybrzeże Stanisława Wyspiańskiego 27, 50-370 Wrocław, Poland*

SUMMARY

In this paper a system of the Rędziński bridge will be described. The Rędziński bridge is the biggest object along the A8 motorway around the city of Wrocław and the biggest concrete cable-stayed bridge in Poland. For the purposes of the bridge monitoring a system of 222 sensors was installed. Results from the first 5 years of work of the SHM will be presented below.

1. STRUCTURAL HEALTH MONITORING SYSTEMS IN POLAND

For over the last decade an intensive development of SHM systems has appeared in Poland and some of them are installed in the following bridges:

- the Solidarity Bridge over the Vistula River in Płock (2007), which is the biggest cable-stayed bridge in Poland, made of steel;
- the John Paul II Bridge over the Vistula River in Puławy (2008) – one of the largest arch bridges in Poland, made of steel;
- the Rędziński Bridge (Fig. 1) over the Odra River in Wrocław (2011), which is the biggest concrete cable-stayed bridge in Poland, constructed along the motorway A8.

Furthermore SHM systems are not only installed on bridges. Under a constant observation is also the roof structure of the National Football Stadium in Warsaw or the road surface on motorway A4 which is built in the region of underground mine damages.



Fig. 1: View of the Rędziński Bridge [www.golowersilesia.pl]

2. DESCRIPTION OF THE RĘDZIŃSKI BRIDGE AND ITS SHM SYSTEM

The Rędziński Bridge (Biliszczyk et al. 2011) was open to traffic on 31st August 2011 and is the biggest bridge along the motorway ring-road of Wrocław. It is a four-span cable-stayed bridge situated over the Odra River. The spans are 50 m + 2 x 256 m + 50 m long (Fig. 2).

The two separated concrete decks are connected to a single 122 m high concrete pylon located on the Rędziński Island. The stay cable system consists of 160 stays. The decks were built with the longitudinal launching method (Hawryszków, Hildebrand, 2012).

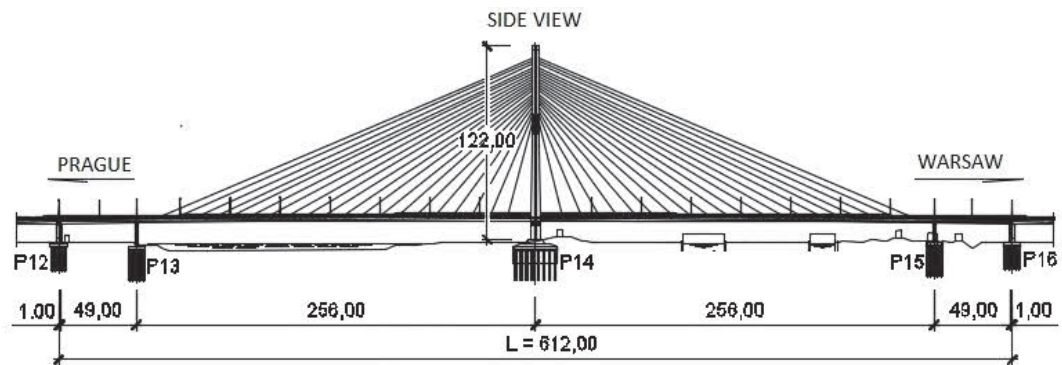


Fig. 2: General view of the Rędziński Bridge

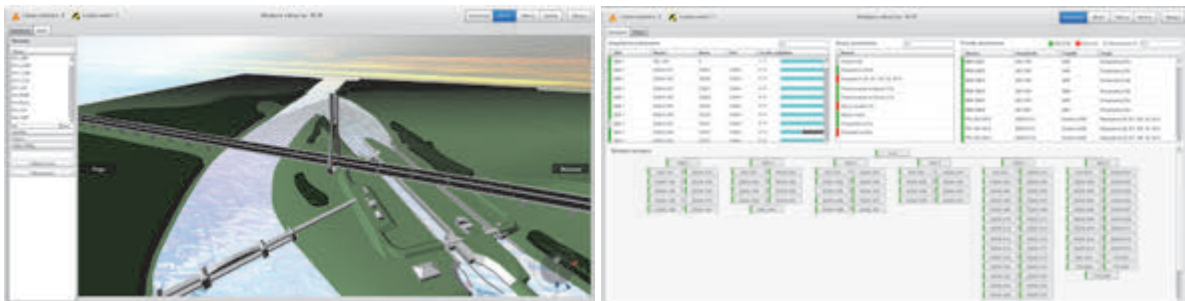


Fig. 3: View of the Rędziński Bridge model in the SHM application. It shows a virtual location of each sensor (NEOSTRAIN A)

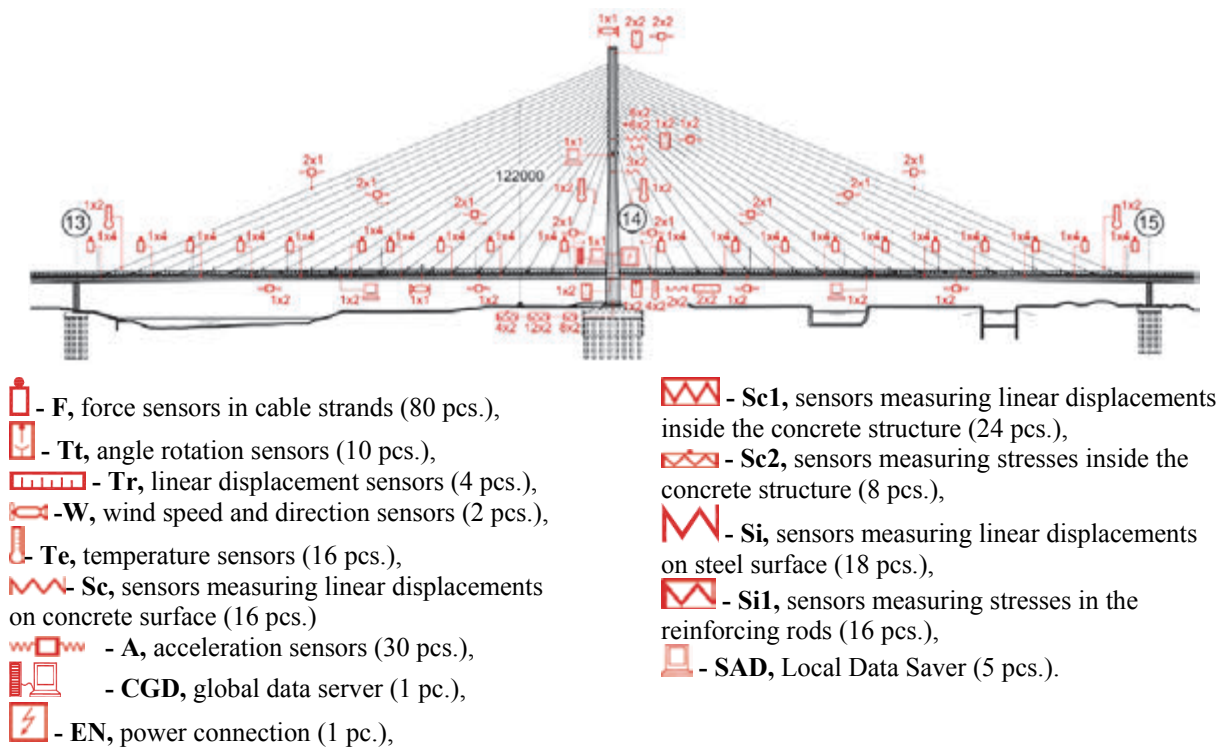


Fig. 4: Measuring scheme of the Rędziński Bridge (Barcik, Sieńko, Biliszczuk, 2011)

For the purposes of the bridge monitoring a system of 222 sensors was installed (Fig. 4). The system is saving data concerning stresses in the concrete elements like the pylon and the decks, it is measuring the forces and accelerations in 80 cable-stays, furthermore it is collecting data about the temperature in the bridge elements with comparison of the current weather conditions. All parameters are measured at the same time and saved in 6 local servers. The dynamic values are registered with the frequency of 100 Hz. The database is available via internet through a professional application. The application (Fig. 5) is equipped with an alert module that informs the user about some dangerous or strange behaviours of the bridge elements. Moreover, it is equipped with a 3D-model of the bridge, where the user can check the precise location of each sensor.

3. MEASUREMENT ANALYSIS

In 2016 a first overview of the registered data from August 2011 till December 2015 was made (Biliszczuk, Onysyk, Teichgraeber, 2016). The analysed sensors were divided into 3 groups:

- for the cable stayed system: forces, temperatures and acceleration sensors,
- for the deck: stresses, temperatures and acceleration sensors,
- for the pylon: stresses, temperatures, acceleration and displacements sensors.

Some of the results are presented below in detail.

3.1 Cables – forces in strands

The cable stayed system is equipped in 80 force sensors (NEOSTRAIN b). Over each single deck 20 cables are under the SHM observation. In Tab. 1 a comparison between the beginning average and the last average force value is presented. Each sensor has its number and code which informs the SHM user about its location. Numbers of the sensors W1-W20 are for the cables from the southern side of the pylon (Prague direction) and numbers W21-W40 are for the northern cables (Warsaw direction; see Fig. 2). The letter L in the sensor code means the left deck, and the P letter means the right deck. Then the letter W means that the sensor is located on the internal cable row of the deck, the letter Z refers to the external cables. The sensor is installed on the reference strand in each cable. The cables were installed using the Isotension method, which guarantees the same force in each strand. If the number of strands in cable is known – a simple calculation allows to define the force in a whole cable.

During the analysis for each measured cable the maximum, minimum and average monthly force value was saved. It was the basis for creating a global overview how the forces in 80 cables have been changing for the first 5 years. Generally a decrease of the force has place. Moreover, during summer the force is increasing, and in winter it is lower again. Fig. 6 shows an example how the force in the longest stay-cable is changing. Fig. 7 shows the same for the shortest cables.

According to the Figures 5 and 6 and Tab. 1 it is visible, that the decrease of the force in the longest cables is between 6.4% and 11.8%, whereas in the shortest the differences are between 7.0% and 16.8%. The biggest change had place in the middle cable W12-PW and was about 21.7%. In cables W12-LZ and W28-PZ the change was about 0.2 %. Some sensors are not working properly, like W24-PZ/F and W32-PZ/F.

Tab. 1: Comparison of average monthly forces

Sensor	Average force, August 2011 [kN]	Average force, December 2015 [kN]	Difference [kN]	Percent change
W1-LZ/F	1784	1658	-126	-7.0%
W1-LW/F	1433	1237	-196	-13.7%
W4-LZ/F	3121	3007	-114	-3.6%
W4-LW/F	3001	2921	-80	-2.7%
W6-LZ/F	3290	2756	-533	-16.2%
W6-LW/F	3229	3254	24	0.8%
W8-LZ/F	3669	3590	-79	-2.2%
W8-LW/F	3771	3758	-13	-0.4%
W10-LZ/F	4572	4675	103	2.3%
W10-LW/F	4482	4419	-62	-1.4%
W12-LZ/F	4898	4907	9	0.2%
W12-LW/F	4441	4384	-57	-1.3%
W14-LZ/F	5781	5580	-200	-3.5%
W14-LW/F	5493	5362	-131	-2.4%
W16-LZ/F	5262	4972	-290	-5.5%
W16-LW/F	5428	5220	-208	-3.8%
W18-LZ/F	5253	4932	-322	-6.1%
W18-LW/F	5018	4681	-337	-6.7%
W20-LZ/F	3135	2934	-202	-6.4%
W20-LW/F	2966	2716	-250	-8.4%
W21-LZ/F	1740	1528	-212	-12.2%
W21-LW/F	1380	1185	-196	-14.2%
W24-LZ/F	3111	3033	-78	-2.5%
W24-LW/F	3025	2930	-95	-3.1%
W26-LZ/F	3305	3206	-99	-3.0%
W26-LW/F	3229	3006	-223	-6.9%
W28-LZ/F	3714	3572	-142	-3.8%
W28-LW/F	3670	3614	-56	-1.5%
W30-LZ/F	4744	4658	-86	-1.8%
W30-LW/F	4570	4438	-132	-2.9%
W32-LZ/F	4918	4697	-221	-4.5%
W32-LW/F	-	-	-	-
W34-LZ/F	-	-	-	-
W34-LW/F	5759	5448	-310	-5.4%
W36-LZ/F	5263	5005	-258	-4.9%
W36-LW/F	5614	5233	-381	-6.8%
W38-LZ/F	5254	4832	-421	-8.0%
W38-LW/F	5281	4928	-353	-6.7%
W40-LZ/F	3202	2825	-376	-11.8%
W40-LW/F	3448	3041	-408	-11.8%

Sensor	Average force, August 2011 [kN]	Average force, December 2015 [kN]	Difference [kN]	Percent change
W1-PZ/F	-	1524	-	-
W1-PW/F	-	1304	-	-
W4-PZ/F	3051.3	3001	-50.1	-1.6%
W4-PW/F	3069.3	2993	-76.5	-2.5%
W6-PZ/F	3591.8	3625	33.7	0.9%
W6-PW/F	3253.1	3116	-136.7	-4.2%
W8-PZ/F	3596.8	3643	46.4	1.3%
W8-PW/F	3550.4	3595	44.8	1.3%
W10-PZ/F	4794.7	4823	27.8	0.6%
W10-PW/F	4448.6	4368	-81.1	-1.8%
W12-PZ/F	4869.1	4764	-104.6	-2.1%
W12-PW/F	4722.2	3696	-1026.7	-21.7%
W14-PZ/F	5579.0	5599	20.2	0.4%
W14-PW/F	5598.2	5455	-143.5	-2.6%
W16-PZ/F	5183.5	4987	-196.8	-3.8%
W16-PW/F	5374.6	5241	-133.9	-2.5%
W18-PZ/F	5285.3	5022	-263.5	-5.0%
W18-PW/F	5323.7	5072	-251.5	-4.7%
W20-PZ/F	3199.6	2959	-240.4	-7.5%
W20-PW/F	2952.4	2701	-251.6	-8.5%
W21-PZ/F	1279	1064	-215	-16.8%
W21-PW/F	1455	1266	-189	-13.0%
W24-PZ/F	3088	603	-2485	-80.5%
W24-PW/F	3028	2954	-74	-2.4%
W26-PZ/F	3458	3316	-141	-4.1%
W26-PW/F	3426	3443	17	0.5%
W28-PZ/F	3610	3619	9	0.2%
W28-PW/F	3614	3679	65	1.8%
W30-PZ/F	4532	4641	108	2.4%
W30-PW/F	4745	4650	-96	-2.0%
W32-PZ/F	904	4893	3988	441.0%
W32-PW/F	4942	4849	-93	-1.9%
W34-PZ/F	5664	5497	-167	-2.9%
W34-PW/F	5668	5460	-208	-3.7%
W36-PZ/F	5437	5172	-265	-4.9%
W36-PW/F	5352	4726	-626	-11.7%
W38-PZ/F	5220	4981	-239	-4.6%
W38-PW/F	5134	4979	-155	-3.0%
W40-PZ/F	3029	2718	-312	-10.3%
W40-PW/F	3303	3010	-293	-8.9%



Fig. 5: The monthly average forces in case of the longest stay-cables W40-PZ/F and W40-PW/F

The decrease of forces in cables is a natural process caused by shrinking and creeping of the concrete elements of the bridge. Furthermore, the temperature changes of the whole construction in summer and winter are seen as the local extreme values on the diagrams. A similar change is visible in a day/night cycle, which is shown on Fig. 8. The change of forces for each cable row is shown in the Fig. 7.

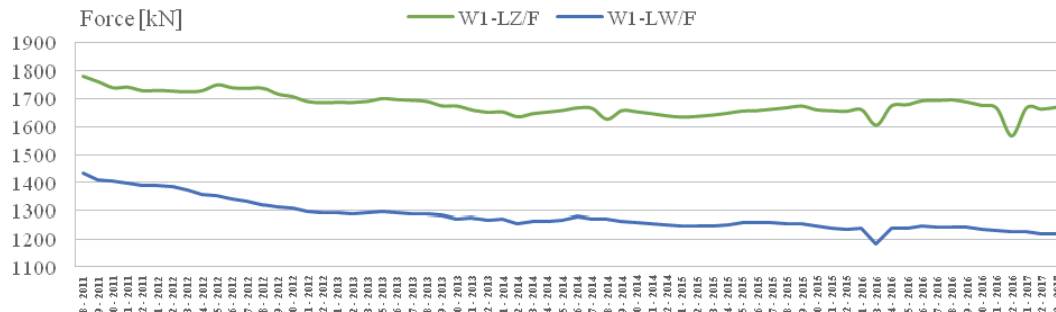


Fig. 6: The monthly average forces in case of the shortest stay-cables W1-LW/F and W1-LZ/F

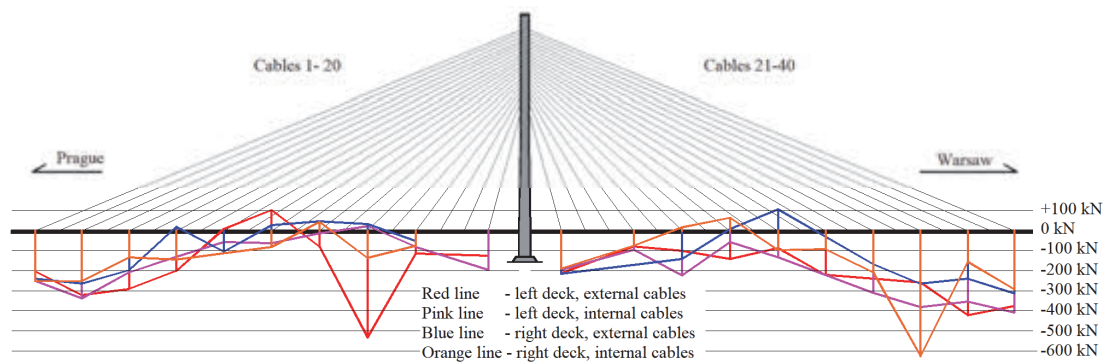


Fig. 7: Change of the monthly average force in cables, in each row

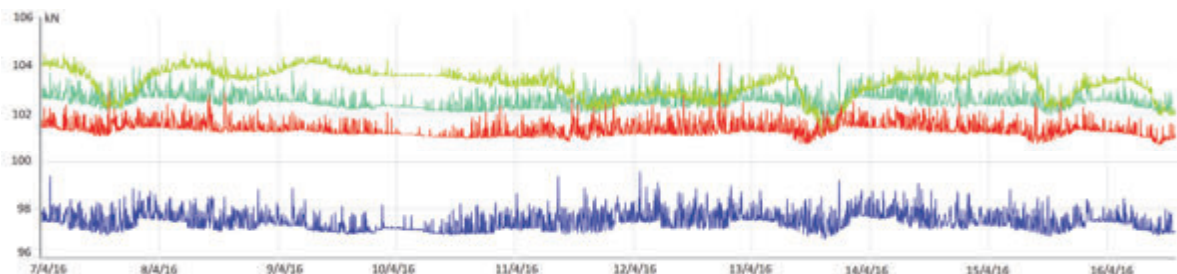


Fig. 8: Forces change between 3/04/2016 and 16/4/2016 in four random cable-stays – a diagram generated using the SHM application

The measurements from the first 5 years are a basis for an advanced durability assessment of the cable stays in bridges under live loads.

3.2 Pylon – angular displacements

Between August 2011 and December 2015 the extreme monthly values of the angular displacements were measured. In the orthogonal direction (Y in the sensor code) to the pylon surfaces the displacement were measured on 3 levels (Fig. 10):

- on the bottom of the pylon, sensors: P0-L/Tt/Y, P0-P/Tt/Y,
- on the pylon's cross-beam, sensors P17-L/Tt/Y, P17-P/Tt/Y,
- on the top of the pylon, sensors: P30-L/Tt/Y, P30-P/Tt/Y.

In the pylon surface (X in the sensor code) only rotation on the top were measured:

- sensors: P30-L/Tt/X, P30-P/Tt/X.

Tab. 2 shows the comparison with the allowed values. Measured angular displacements are below maximum designed values.

Tab. 2: Measured and allowed angular displacements

Sensor	Minimum displacement	Maximum displacement	Maximum designed displacement
P0-L/Tt/Y	-0,01°	0,10°	1,09°
P0-P/Tt/Y	-0,01°	0,05°	1,09°
P17-L/Tt/Y	-0,06°	0,08°	2,74°
P17-P/Tt/Y	-0,06°	0,08°	2,74°
P30-L/Tt/X	-0,09°	0,09°	0,85°
P30-L/Tt/Y	-0,06°	0,04°	1,47°
P30-P/Tt/X	-0,11°	0,08°	0,85°
P30-P/Tt/Y	-0,12°	0,12°	1,47°

3.3 Pylon – stresses in the cross-beam

The upper cross-beam of the H-ptylon of the Rędziński Bridge is exposed to a big torsion moment. The designer of the bridge decided to construct a steel box inside (Biliszczuk et al. 2011). Moreover, the cross-beam was pre-stressed with 18 cables. To have a constant overview of the stresses in the structure, sensors were installed inside and outside the box, at the steel and concrete surface. Fig. 9 shows the localization of each sensor set. The diagrams in Fig. 10 and 11 show, that stresses are slowly increasing in the structure – minus means compressing. The yellow and blue lines describe the values of sensors installed under 60 degrees to the bolt axis. The green line is for the sensor installed in the direction of the cross-beam axis.

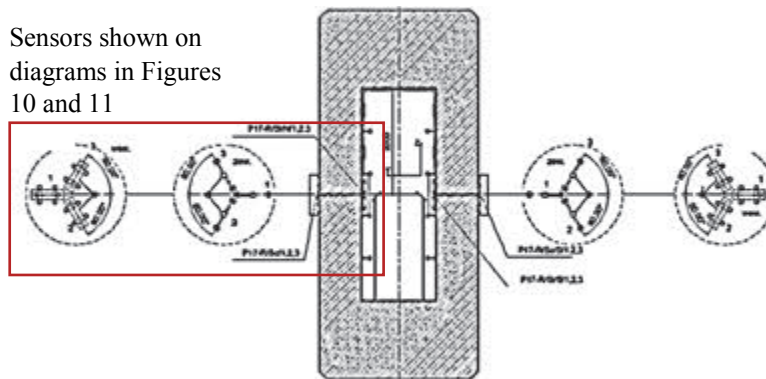


Fig. 9: Sensors in the pylon's cross-beam

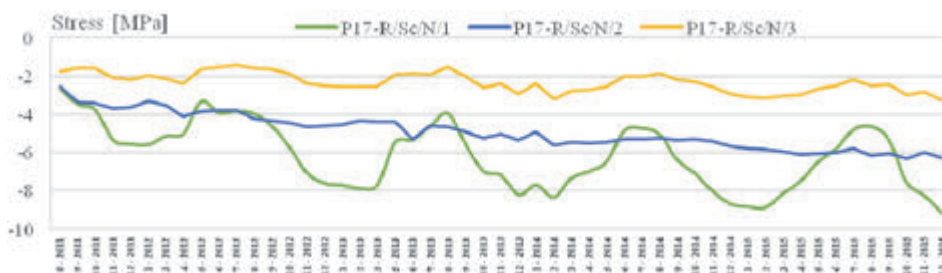


Fig. 10: Monthly average values of stress in concrete for the northern outside cross-beam surface

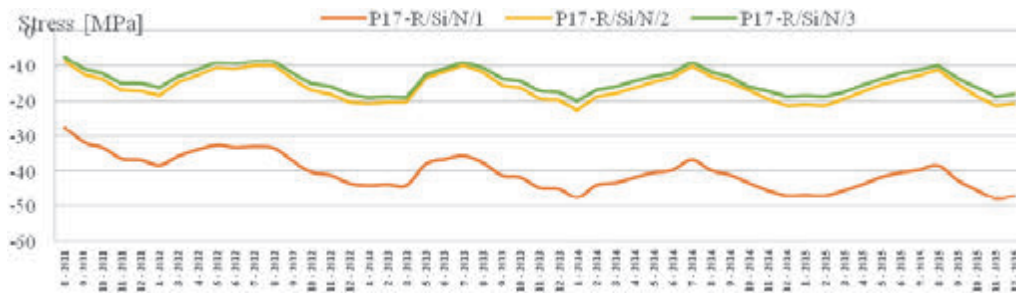


Fig. 11: Monthly average values of stress in steel for the northern outside cross-beam surface

3.4 Temperature comparison between pylon, deck and cables

The 5 years analysis enables a comparison between temperatures in the main structural elements of the bridge. It is an important issue to the Polish Standards, because there is no information about temperature distribution for cable-stayed bridges. Information from the SHM system can be in this case a basis for creating the national attachments for the upcoming Eurocode edition.

A diagram in Fig. 12 how the average temperature changed in the cables, deck and pylon. A period of improper work of sensor is visible – the orange line.

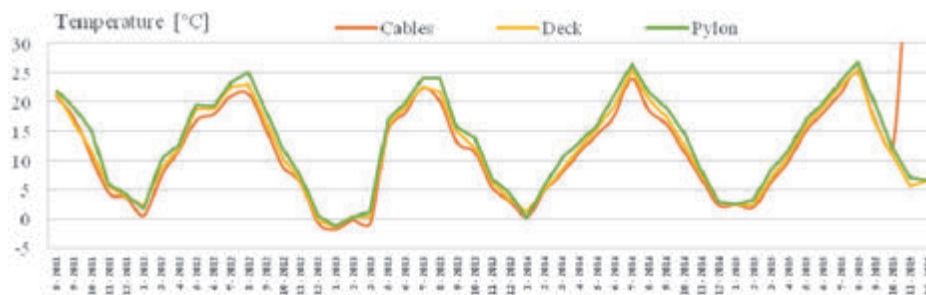


Fig. 12: The monthly average temperature in cables, deck and pylon

Tab. 3: Extreme temperatures in each element.

Element	Minimum temperature [°C] (February 2015)	Maximum temperature [°C] (August 2015)
Cables	-20.89	44.37
Pylon	-9.05	36.03
Deck	-12.72	33.97

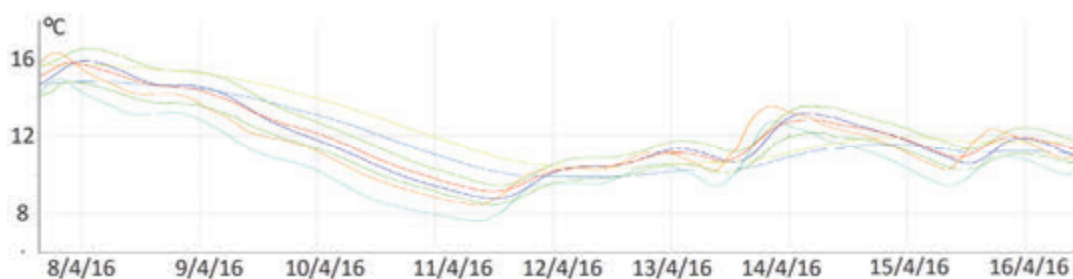


Fig. 13: Two weeks temperature changes in the concrete deck sensors

In the Polish Standard PN-85/S-10030 Bridges – the temperature changes for steel elements are from -25°C till 55°C and for the concrete elements from -15°C till 30°C. The Tab. 3 shows that the temperatures in deck and pylon were higher than allowed. Furthermore short-term

temperature changes are also well visible. The diagrams below show how the temperature is changing in the deck structure and pylon between 3rd of April 2016 and 16th of April 2016.

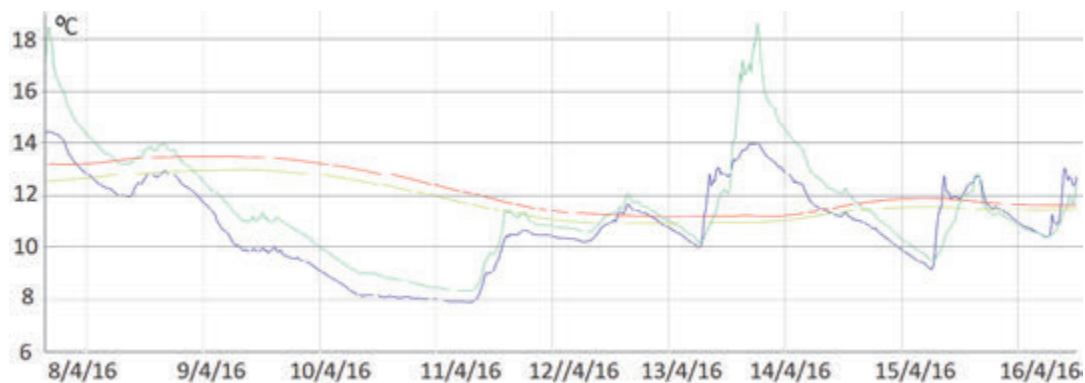


Fig. 14: Two weeks temperature changes in the pylon's cross-beam (in concrete and in steel elements)

4. CONCLUSION

All measurements were taken in real weather conditions and under real loads by the SHM system. Such an overview gives the opportunity to compare the measured values (stresses in concrete and steel elements, the displacements of the pylon and the deck, the change of forces in cable stays) with each other. A long term observation of the force in cable stays with an additional dynamic analysis made with an FEM-model can be a first assessment of the fatigue durability of steel in these structural elements. SHM systems are an innovative research method, because they not only give the opportunity to a constant supervision of the bridges, but also enable the engineers and researches to work with reliable measured data. Such investigations are a valuable contribution to modern civil engineering.

5. REFERENCES

- NEOSTRAIN (a), SHM Application „Inspector”.
- Biliszczuk J., Onysyk J., Barcik W., Prabucki P., Sułkowski M., Szczepański J., Toczkiwicz R., Tomiczek M., Tukendorf A., Tukendorf K., Ast A., Rędziński Bridge along the Wrocław Ringroad. Wrocław Bridge Days, Wrocław 24th-25th November 2011, DWE, Wrocław; p. 203-222, (in Polish).
- Hawryszków P., Hildebrand M.: Installation of the largest stay cable system in Poland – the Rędziński bridge in Wrocław. Proceeding of the 18th IABSE Congress “Innovative Infrastructures – Toward Human Urbanism”. Seoul, Korea, September 19-21, 2012.
- Barcik W., Sieńko R., Biliszczuk J., SHM System of the Rędziński Bridge in Wrocław, Wrocław Bridge Days, Wrocław 24th-25th November 2011, DWE, Wrocław; p. (in Polish).
- Biliszczuk J., Onysyk J., Teichgraber M., Data analysis of the SHM System of the Rędziński Bridge. 1st Rapport from the period August 2011 – January 2016, Wrocław, 2016.
- NEOSTRAIN (b), Instruction of the SHM Application for the bridge along the Wrocław Ringroad.

CONSTRUCTION OF A THIN WALLED CONCRETE SHELL EVENT CANOPY

*Benjamin Kromoser, Johann Kollegger
TU Wien, Institute for Structural Engineering
Karlsplatz 13/ E212-2
1040 Vienna*

SUMMARY

Shells are efficient structures, which enable a very high utilization of the construction material concrete. Unfortunately, most formwork technologies required for the construction of concrete shells are labor and material intensive. A very resource efficient alternative construction method invented at TU Wien is called “Pneumatic Forming of Hardened Concrete (PFHC)” as described in Kromoser and Kollegger (2014, 2015). A flat concrete plate is transformed into a double curved shell by inflating an air cushion placed under the concrete plate and by tensioning additional post-tensioning tendons mounted at the circumference. Currently the construction method is first practically applied for the construction of an event canopy with the plan measurements of 26.5 x 19.1 m and a height of 4.2 m. The present contribution describes the functionality of the construction method, the design process and the construction process of the structure.

1. INTRODUCTION

The utilization of concrete as construction material can be increased sharply by optimizing the form of the structure according to the applied loads. The particular forms found can exemplarily be concrete shells and have a free formed geometry in most cases requiring a complex formwork and falsework to be produced. To address this problem, a new shell construction method was invented at the TU Wien with the name Pneumatic Forming of Hardened Concrete (PFHC). The idea is to simplify the production of such concrete shell structures by bending a thin flat hardened concrete plate to a double curved shell structure. The flat hardened concrete plate is lifted by inflating an air cushion placed underneath the concrete plate and by tensioning post-tensioning tendons mounted at the circumference as shown in Fig. 1. The core of the construction method is the “cold” bending process of concrete itself. The bending behaviour of hardened concrete plates with 50 mm, 100 mm and 120 mm thickness, with different reinforcement types and reinforcement ratios could already be tested in extensive preliminary experiments. In detail, centric tensile tests and bending tests were performed as described in Kromoser and Kollegger (2014, 2015, 2017). The functionality of the complete construction method could already be tested in two large scale experiments where a spherical concrete shell with 10.8 m diameter and 3.2 m height as well as a free formed concrete shell with the plan measurements of 17.6x10.8 m and a height of 2.9 m were erected as explained in Kromoser and Huber (2016). Both shells had a thickness of 50 mm. Currently, in the course of developing the construction method, the next step is to apply the method for the construction of a first building. On behalf of the Austrian Railways (ÖBB infrastructure) a first shell with the plan measurements of 26.5x19.1 m, a height of 4.2 m and a thickness of 50 mm is built in Carinthia in the south of Austria. The building is used to test



Fig. 1: Construction of a concrete shell originating from a thin flat hardened concrete plate by the aid of an air cushion placed underneath the plate and tensioning a post-tensioning tendon mounted at the circumference

and to improve the building technique for the construction of a deer pass over the twin-track railway line Koralmbahn.

2. PROJECT SCHEDULE

The shape of the presented concrete shell is optimized for the shell bridge, which is currently built as second building and main structure. An additional development step, described in the present paper, in terms of the construction of a shell exactly in scale 1:2 was introduced to further improve the production process, to avoid procedural problems and to evaluate the accuracy of the built concrete shell on site. The two shells are shown in Fig. 2. Both buildings, the event canopy and the shell bridge, were awarded within one tendering procedure to ensure that one company receives the order to build both structures. The reason for this is to avoid a loss of knowledge between the construction of the first and the second main shell. The complete construction process, the accuracy of the finished shell and all details of the test structure were evaluated after the erection of the test structure was completed and were used to improve the production process and the construction planning of the bridge.

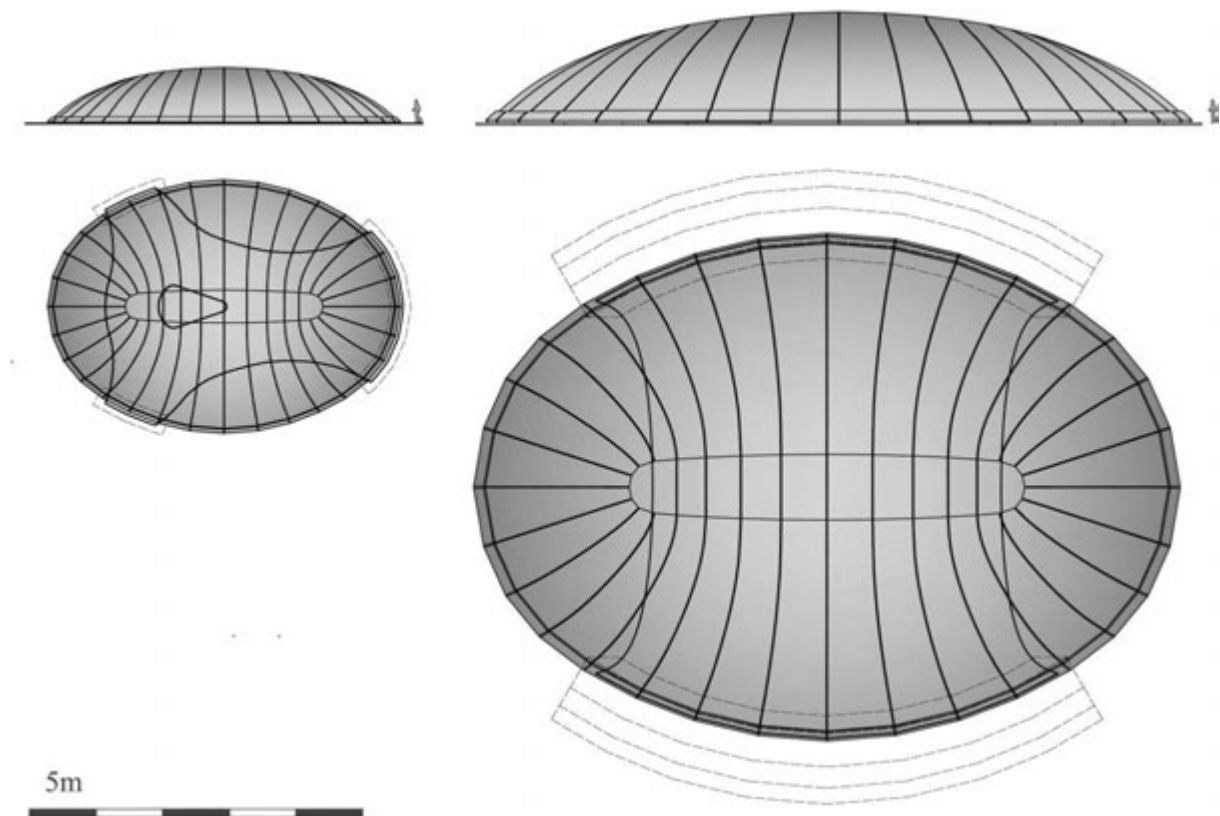


Fig. 2: Concrete shell of the event canopy (left) and the shell bridge serving as deer pass (right)

3. DESIGN OF THE SHELLS

3.1 Design of the shell bridge

The shape of the complete shell for the shell bridge is mainly affected by three factors (1) the applied loads (dead weight of the shell and the vertical and horizontal forces from the earth covering), (2) the minimization of the construction material needed and (3) the procedural requirements from the PFHC-method. The complete optimization process is described in Pachner and Kromoser (2016). A particle-spring system was chosen as basis for the optimization. Considering the diversity of existing requirements the optimization process of the bridge has been split into four steps as shown in Fig. 3. After finding the optimal geometry for the reference geometry of the bridge, two surface patches were added to complete the cupola. In a third step the resulting geometry consisting of a Non-Uniform Rational B-Spline Surface (NURBS) undergoes a discretization process resulting in semi-discrete segments that will finally be unrolled. The special form of the segments found enables a good approximation of the optimized smooth concrete shell geometry.

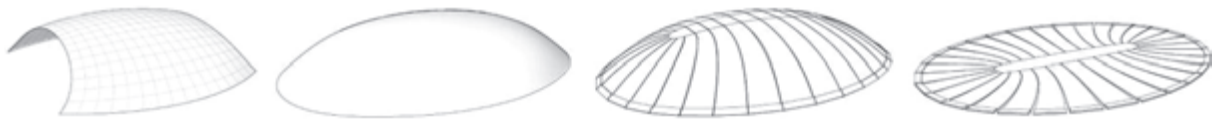


Fig. 3: Design process of the shell bridge serving as deer pass

3.2 Design of the event canopy

The geometry of the complete concrete shell for the construction of the event canopy conforms with the found geometry of the bridge in the scale 1:2 as shown in Fig. 2 to be able to measure the shape and to compare it with the designed geometry. Generous cut-outs adjusted to the static behaviour were designed for the further use of the structure. The ready inflated 50 mm thick concrete shell serves as formwork and is part of the final structure. After the joints between the elements are filled additional reinforcement and an additional shotcrete layer are applied in the relevant areas. The total thickness of the final event canopy is constantly decreasing from 220 mm at foundation connection to 150 mm at the vertex. Fig. 5 shows the dimensions of the designed structure. A detailed static analysis showed maximal elastic deformations of 17 mm under self-weight as shown in Fig. 6. The modulus of elasticity was reduced to 2080 – 8810 MPa according to the occurring stresses in the shell. A stability analysis showed a buckling load factor of 8.4 for the first eigenmode for a non-linear load increase until buckling. The first eigenmode is shown in Fig. 7. In addition, the authors performed a parameter study for the impact of imperfections from 0 – 300 mm. The first eigenmode (Fig. 7) was chosen as form for the imperfection. A second parameter study was performed to determine the impact of a decreasing stiffness of the shell on the buckling behaviour. For this study, the modulus of elasticity was chosen constant for the complete structure in contrast to the first stability study explained above.



Fig. 4: Design process of the event canopy: (1) design of the event canopy, (2) completion of the structure to a full dome, (3) discretization to single curved strips, (4) unrolling to a flat plate

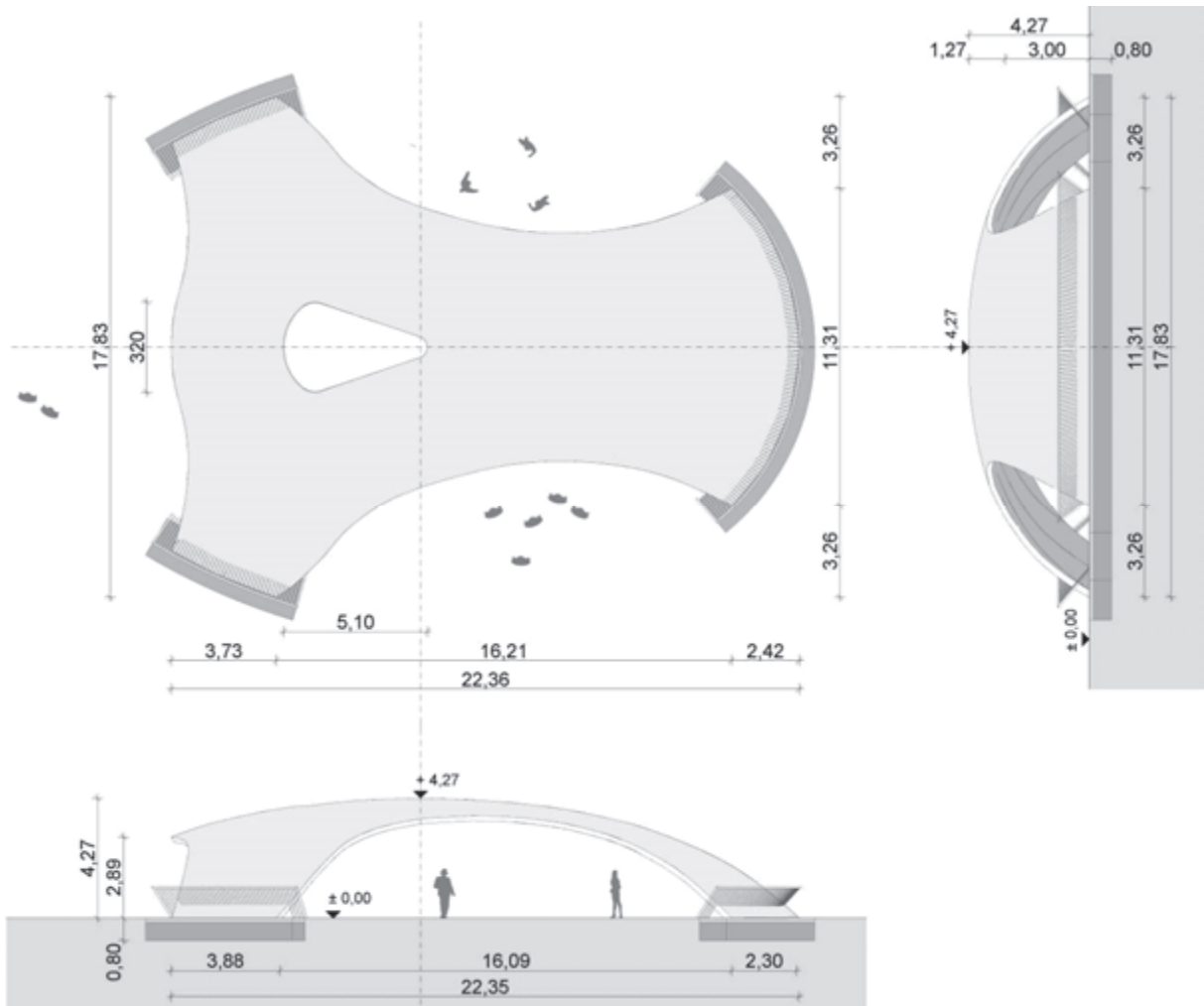


Fig. 5: Design of the event canopy

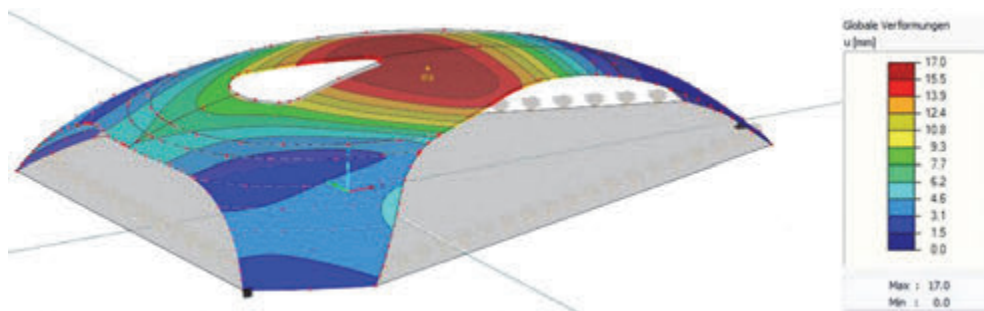


Fig. 6: Elastic deformations under self-weight

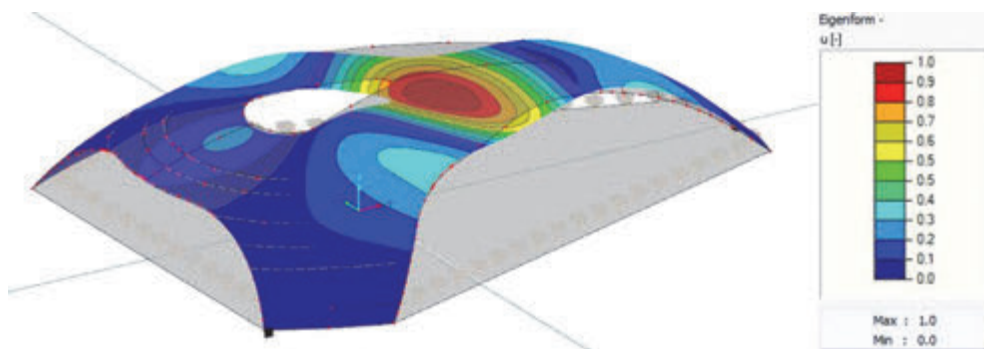


Fig. 7: First eigenmode of the event canopy

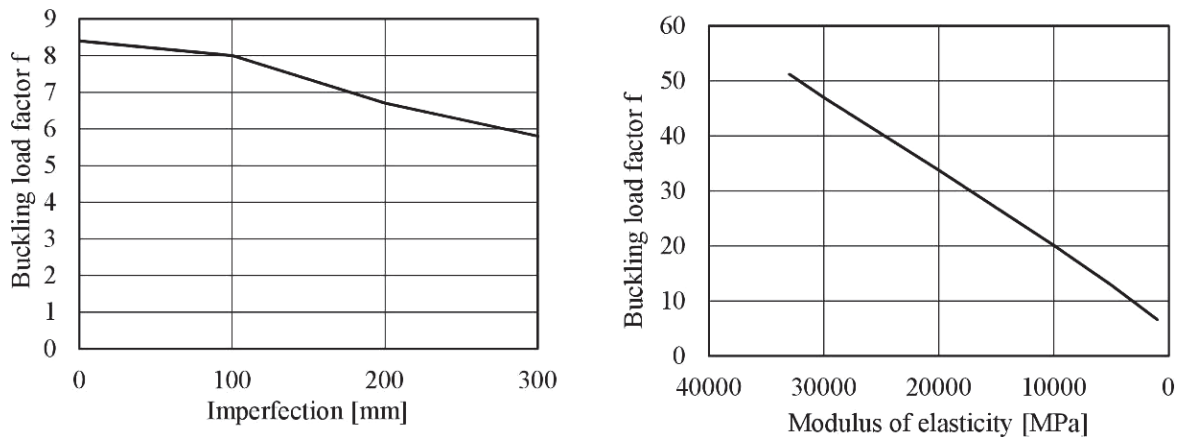


Fig. 8: Buckling load factor – imperfections diagram (left) and Buckling load factor – Modulus of elasticity diagram (right)

Glass-fibre rods are used as reinforcement for the flat plate to absorb the occurring strains during the bending process. A conventional steel reinforcement is used for the secondary reinforcement of the flat plate and as reinforcement for the additional applied concrete layer.

4. CONSTRUCTION PROCEDURE

The complete production process of the event canopy is shown in Fig. 9.

4.1 Preparatory works

In the first step of the preparatory works, the drainage and the foundations are built. In the second step a granular subbase and a flat smoothed concrete plate as operation level above is manufactured. In the third step, the foil serving as pneumatic formwork and the single curved formwork as well as the reinforcement are placed on top (see Fig. 10) before the concrete plate is cast. The single curved formwork for the flat plate was produced by using a numerical controlled mill to comply with the specified accuracy. A very accurate production of the flat plate is very important as the flat plate directly reflects the accuracy of the final shell structure. Spacers are mounted between the elements after stripping the formwork of the flat plate. These spacers were made of a mixture out of epoxy resin and sand. This material combination showed a favourable behaviour with elastic properties to absorb peak stresses caused by grains. The compressive strength was determined in compression tests to

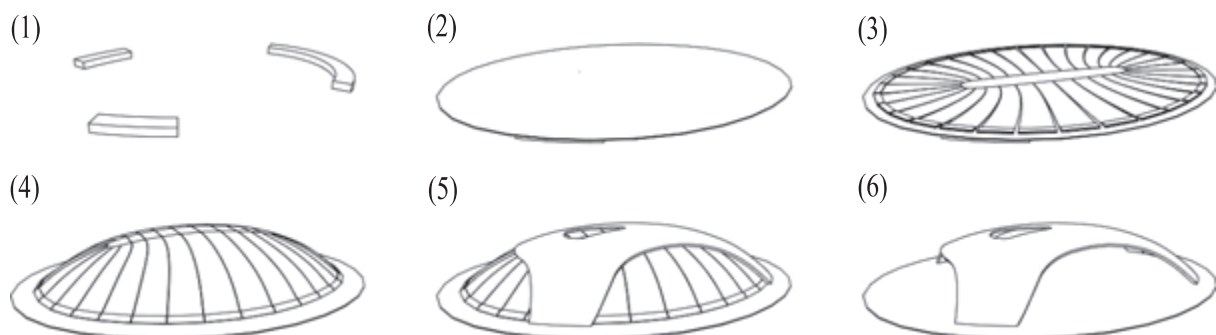


Fig. 9: Construction procedure for the event canopy: (1) foundation, (2) flat smoothed concrete plate as operation level, (3) flat starting plate with wedge shaped outlets, (4) transformed shell, (5) application of the additional reinforcement and the additional concrete layer in the relevant areas, (6) production of the cut-outs



Fig. 10: Air cushion (left) and ready mounted reinforcement of the flat plate (right)

83.3 MPa as a mean value of three experiments. Additional temporary steel profiles are fixed at the elements to avoid a transversal displacement of the elements in the course of the lifting process from the flat plate to the designed double curved shell. These profiles were rented parts and were returned to the formwork company after completion of the transformation process.

4.2 Transformation from a flat plate to a double curved shell

In the next step as shown in Fig. 11, the shell is erected with the PFHC construction principle by inflation of the pneumatic formwork and by tensioning the post-tensioning tendons with four jacks at two anchor blocks placed at the circumference. Subsequently the joints are filled with grout and the tendons are post-tensioned to a calculated force afterwards. Furthermore, a 175 mm wide area at the floor connection was roughened and a small abutment was cast to secure the thin shell against horizontal displacements. Fig. 12 (left) shows the ready transformed shell from inside.

4.3 Finalizing work

The surface of the shell was high-pressure water jetted to ensure a good bonding between the concrete layers. Then additional reinforcement is placed on top of the shell in the relevant areas as shown in Fig. 12. A special reinforcement is drilled into the foundation to absorb the bending forces and the horizontal forces at the intersection of the shell and the foundation. The additional concrete layer was applied in three steps by using shotcrete of the type SpC 30/37/III/XC4/XF4/HZ1,5/GK4. At first, the reinforcement at the edges of the shell was encased in concrete in the lower parts. In the next step, the first layer was applied in the upper parts of the shell. In the last step, the final 50 mm thick layer shotcrete was sprayed on top of the event canopy and was smoothed afterwards. The air cushion initially serving as



Fig. 11: Initially flat plate (left) and finished concrete shell (right) (© webcam of Dipl.-Ing. Wolfgang Reinisch - <http://reinisch.at/> on behalf of the Austrian railways (ÖBB))



Fig. 12: View from inside of the shell for the event canopy after inflation (left) and ready mounted reinforcement for the additional concrete layer

lifting device was inflated again during the concreting work to support the 50 mm thin concrete shell (span 19.1 x 26.5 m). In the following work steps, the cut-outs were made and the edges of the shell were smoothed with repair mortar to avoid a corrosion of the constructive conventional reinforcement of the 50 mm thin shell. Finally, the flat concrete floor is high-pressure water jetted and an inclining concrete is applied.

5. ACCOMPANYING MEASUREMENTS AND SUBSEQUENT STRUCTURAL ANALYSIS

The form of the shell was steadily supervised by 3D laser scans from inside to be able to assess the changes during the complete construction process. The measured 3D point cloud was approximated by a B-spline surface for the import into a FEM structural analysis software. Thus, it was possible to analyse the static behaviour of the really built structure. The results showed that only small changes with a very minor impact at the static behaviour could be observed after the erection of the shell.



Fig. 13: Event canopy during the cutting process with view from above (left) and view from inside (right)

6. CONCLUSIONS

Concrete shells are efficient structures. The PFHC construction principle provides an alternative way to build these kind of structures with high accuracy without requiring the labour and material intensive formwork. The core of the construction method, bending hardened concrete plates, could be optimized within numerous preliminary tests and the

functionality could be tested within two large scale experiments. Currently the construction method is first practically applied on behalf of the Austrian Railways (ÖBB). A two-step way was chosen for a first practical application of the construction method. At first, an event canopy, described in the present contribution, was built as test structure for the construction of a shell bridge over the two-rail track Koralmbahn. A detailed 3D laser scan of the shell showed minor deviations to the designed reference geometry. The construction process and all details of the construction were analysed and improved for the design and construction of the bridge. Summarizing, the construction of the event canopy proved the good applicability of the construction method on site and delivered valuable new findings for a further improvement.

6. ACKNOWLEDGEMENTS

The presented project is designed by TU Wien in collaboration with the engineering office Öhlinger+Partner ZT Ges.m.b.H. and is built by the construction company Kostmann GesmbH. The inspecting structural analysis was done by the engineering office ZKP ZT GmbH and the tendering was prepared by the engineering office Tecton Consult Baumanagement ZT GmbH. The project is realized on behalf of the Austrian Railways (ÖBB). The authors gratefully acknowledge to all partners for the good cooperation.

7. REFERENCES

- Kromoser B and Kollegger J. (2014), „Herstellung von Schalentragerwerken aus Beton mit der „Pneumatic Wedge Method“ - Ein neues Bauverfahren für den Bau von zweifach gekrümmten Betonflächen”, Beton- und Stahlbetonbau 109, Heft 8, 2014, p. 557–565.
- Kromoser B and Kollegger J. (2015), „Application areas for pneumatic forming of hardened concrete”, Journal of the International Association for Shell and Spatial structures (IASS) Vol. 56, No. 3, 2015, p. 187-198.
- Kromoser B, Kollegger J. (2015), „Pneumatic Forming of Hardened Concrete – building shells in the 21st century”, Structural Concrete, Volume 16, Issue 2, 2015.
- Kromoser B and Kollegger J. (2017), „Aktives Verformen von ausgehärteten Betonelementen zur Herstellung von räumlich gekrümmten Betonflächen”, Beton- und Stahlbetonbau 112, Issue 2, 2014, p. 106–115.
- Kromoser B and Huber P. (2016), „Pneumatic Formwork Systems in Structural Engineering”, Advances in Materials Science and Engineering, vol. 2016, 13 pages.
- Pachner T., Kromoser B. (2016), „Structural optimization of a shell bridge built with the Pneumatic Forming of Hardened Concrete construction method”, Proceedings of the IASS Annual Symposium 2016, “Spatial Structures in the 21st Century”, 26–30 September, 2016, Tokyo, Japan.

DESIGN AND CONSTRUCTION OF TILTED WALLS IN ACCORDANCE WITH CODES' PROVISIONS ON THE EXAMPLE OF THE CONSTRUCTION OF THE MUSEUM OF THE SECOND WORLD WAR IN GDAŃSK

*Krystyna Nagrodzka-Godycka, Marta Wiśniowska
Gdańsk University of Technology
Gabriela Narutowicza 11/12, 80-233 Gdańsk, Poland*

SUMMARY

The purpose of this article was to introduce the design and construction process of tilted walls in accordance to codes' rules. The construction of the Museum of the Second World War in Gdańsk (Fig. 1) was chosen to be an example of its successful use in practice. Theoretical knowledge was based on European Standards (EN 1990, EN 1991, EN 1992) and *fib* Model Code for Concrete Structures. Both designing and building process was taken into consideration. One of the Authors was working as a site engineer on the construction of the Museum what provided an inside view on the matter.



Fig. 1: Building of the Museum of the Second World War in Gdańsk- visualization

1. MUSEUM OF THE SECOND WORLD WAR IN GDAŃSK

1.1 Characteristics of the building

The design of the building of the Museum of the Second World War in Gdańsk was chosen in the international architectural competition. The winning architecture has been

described as "a new symbol of Gdańsk", "a new icon" or a "sculptural design". Building site started in July 2012 with building of a dry pit and Museum's first level which is over 14 meters underground. Museum, which floor surface reaches over 30 000 m², is divided into three parts: the underground - which is devoted to the exhibitions, car parks and technical background, the administrative building which is an isolated structure for administrative purposes and the last part, reaching over 40 meters above the ground - the leaning "tower" mainly for education and leisure.

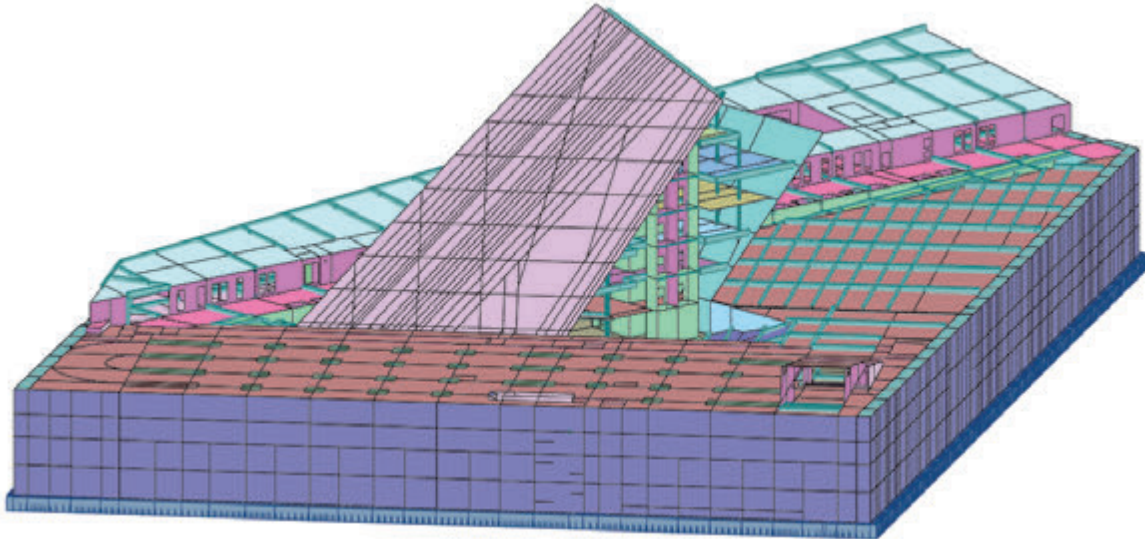


Fig. 2: FEM model of the building

The structure of the building has a complicated, varying geometry on each floor. To provide structure stability and analyse all impacts such as environmental loads (snow, wind) and live loads on the structure, an exact 3D model of the whole building was made to conduct FEM analysis which is presented in Fig. 2.

1.2 Tilted walls

The above-ground section is a leaning triangular prism with all the walls being inclined on different angles. The most tilted wall is constructed on the angle of 56 degrees, the others - 65, 72 and 75 degrees. Among many challenges during the construction of the Museum the most spectacular, in Authors' opinion, was the construction of the falling off wall. An example of a stress distribution in the falling off wall is presented in Fig. 3.

Concrete class for most construction elements was designed as C30/37, yet in case of walls it was increased to C35/45. In addition architectural concrete was used what required special treatment and technology. In case of compacting concrete internal vibrators were used, the time of removing formworks was also restricted, as keeping it too long may change the color of concrete. Reinforcement bars were made of steel BSt 500/AIIN.

Structural stability of the tilted walls was reached mainly by monolithic connections with interfloor slabs. An exemplary construction of the connection between the two elements is presented in Fig. 4.

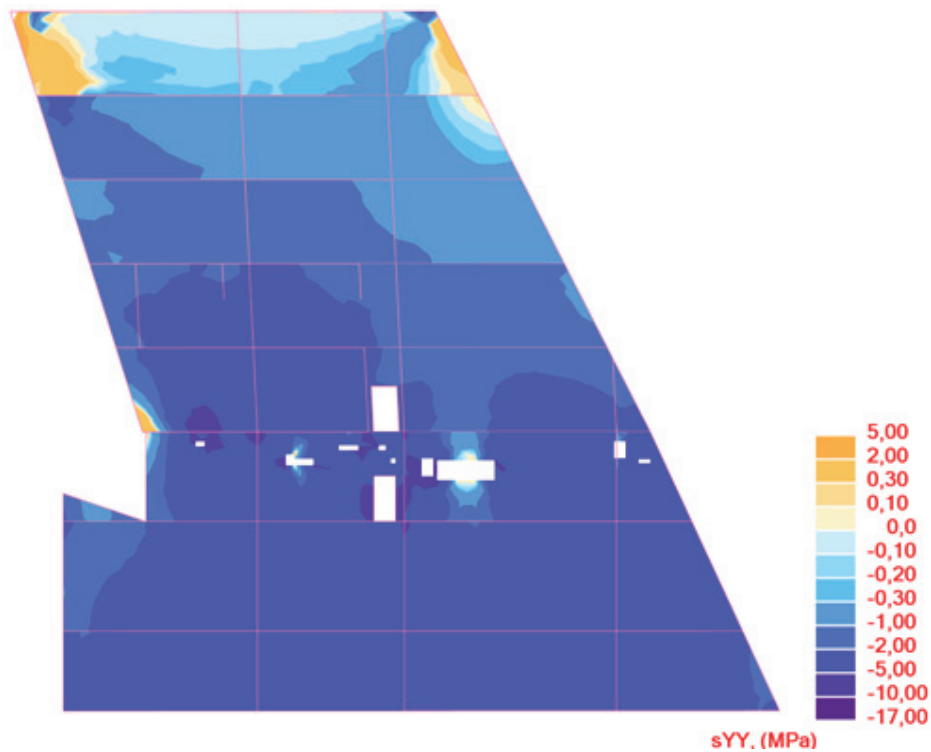


Fig. 3: Map of a stress distribution in a fall off wall

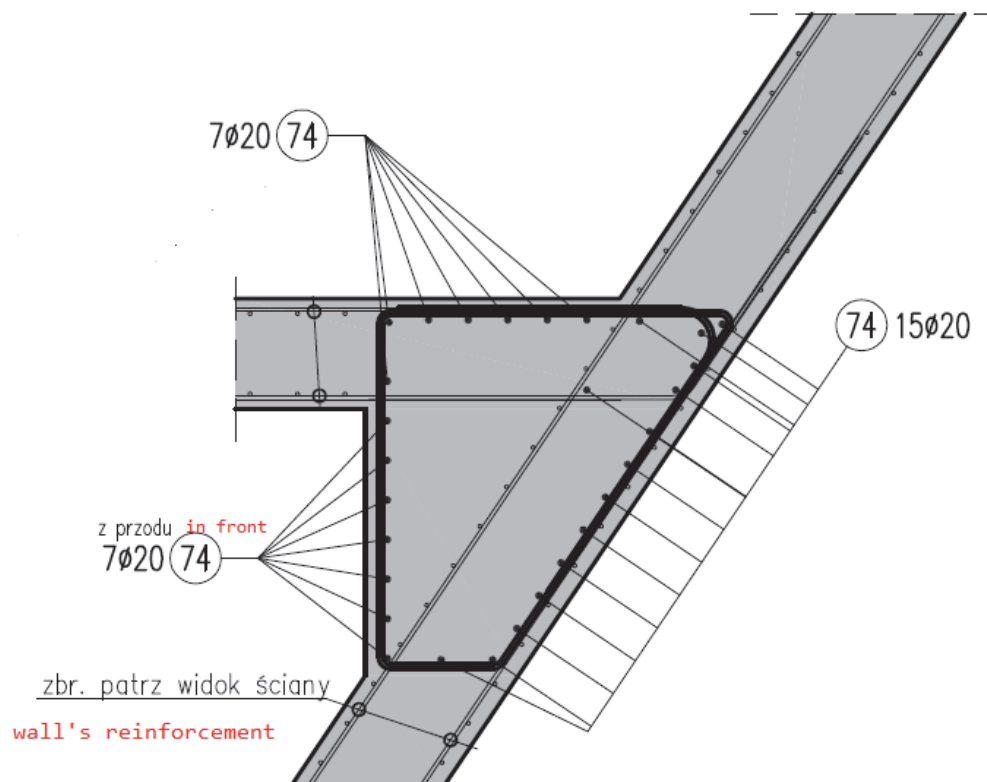


Fig. 4: Monolithic connection between tilted wall and slab.

Looking back at Fig. 2 it can be seen that on the highest floors there were no slabs connected to the falling off wall. To prevent distortions a special reinforced concrete beam was constructed that connected the falling off wall with a wall on the opposite side of the building (see Fig. 5). The beam reaching from one corner to another is supported by a column in the middle of its span.

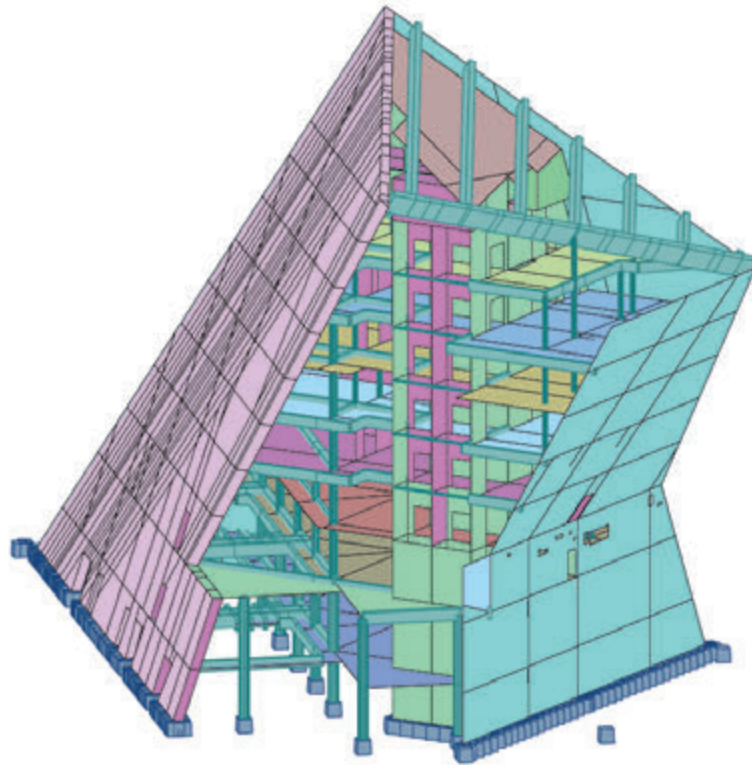


Fig. 5: FEM model with a view on the "connecting beam"

2. CODES' PROVISIONS REGARDING WALLS

2.1 Detailing of members

Both EN 1992-1-1:2004 and *fib* Model Code for Concrete Structures (*fib*, 2010) give rather curt provisions regarding the construction of walls. There is a minimum and maximum areas for vertical reinforcement ($A_{s,vmin} = 0.002A_c$; $A_{s,vmax} = 0.4A_c$) and minimum area for horizontal reinforcement ($A_{s,hmin} = \max(0.25A_{sv}; 0.001A_c)$) specified as well as distances between two adjacent bars (EN: $s_v \leq \min(3t; 400 \text{ mm})$; $s_h \leq 400 \text{ mm}$, MC: $s_v \leq \min(2t; 300 \text{ mm})$). Eurocode 2 also suggests that the amount and proper detailing of reinforcement may be derived from strut-and-tie model, yet it seems unlikely to use it properly in such a complicated case of a tilted wall.

2.2. Durability and concrete cover to reinforcement

EN 1990:2002 specifies five design working life categories lasting from 10 to 100 years. The design working life is the assumed period for which a structure is to be used for its intended purpose with anticipated maintenance but without major repair being necessary. Selection of one category affects later analysis including the choice of material properties (fatigue, creep, shrinkage) or required concrete cover. Although it is recommended in EN 1990 to assume a design working life of 50 years for building structures, Museum was classified as a monumental building with a design working life of 100 years.

The concrete cover is the distance between the surface of the reinforcement closest to the nearest concrete surface. The nominal cover, according to EN 1992-1-1 is a sum of a minimum cover (c_{min}) and an allowance in design for deviation (Δc_{dev}). While calculating the required concrete cover, Eurocode gives us a choice to decide on the value of Δc_{dev}

between 0 and 10 mm. In case of such a complicated structures as tilted walls Engineers have a possibility to choose higher value for safety reasons.

2.3 Wind

The most unfavorable case of wind load on the fall off wall is suction which causes the increase of tensile. In Authors opinion wind load analysis that would specify pressure caused by suction was crucial. Yet modelling of wind actions presented in EN 1991-1-4:2005 does not cover a case of a wind acting on a falling off wall. As the value of pressure differs depending on the angle of the roof construction, the same should be assumed in case of a tilted wall. Therefore to complete code's requirements, solutions proposed in literature were used (Flaga, 2008).

2.4 Load arrangements

EN 1991-1-1:2002 suggests that where imposed loads from several storeys act on walls, the total imposed loads may be reduced by a factor $\alpha_n = [2+(n-2)\psi_0]/n$, where n is the number of storeys ($n>2$) and ψ_0 is in accordance with EN 1990, Annex A1, Table A1.1. In case of Museum the reduction factor, α_n , on the highest, 7th floor could be about 0.7 – 0.8. Yet for safety reasons there was barely no reduction made in case of tilted walls.

3. CONCLUSIONS

The aim of the article was to assess to what extend are Codes helpful while dealing with non - standard elements. Unlike structural advance, Standards seem to analyse only basic cases and elements. It is Structural Engineers' job to use their knowledge and experience to fit those basic guidelines for more complicated forms. Fortunately although codes' recommendations seem curt, practice prove structural advance.



Fig. 6: Museum of the Second World War under construction. pict. R. Jocher



Fig. 7: Museum of the Second World War under construction. pict. R. Jocher

4. ACKNOWLEDGEMENTS

Authors wish to express their gratitude to the extensive help they got from the main constructor Paweł Gębka and his construction office PG-Projekt (<http://www.pg-projekt.pl/>).

5. REFERENCES

- EN 1990:2002/A1:2005 Basis of structural design, 2005
- EN 1991-1-1:2002 Actions on structures - Part 1-1: General actions - Wind actions, 2005
- EN 1991-1-4:2005 Actions on structures - Part 1-4: General actions - Densities, self-weight, imposed loads for buildings, 2002
- EN 1992-1-1:2004 - Design of concrete structures. General rules and rules for buildings, 2004
- fib* Model Code for Concrete Structures 2010, Ernst und Sohn, Berlin, 2013; polish version: Ajdukiewicz A.: Pre - Norma Konstrukcji Betonowych *fib* Model Code 2010, tom 2, Stowarzyszenie Producentów Cementu, Polska Grupa Narodowa *fib*, 2014
- Flaga A. "Inżynieria wiatrowa. Podstawy i zastosowania" Arkady, 2008

PRECAST BRIDGE GIRDERS TO SPAN 44 M

Gábor Durovsky, Eörs Henrik Thék
Ferrobeton Zrt.
H-2400 Dunaújváros, 18-22. Papírgyári str.

SUMMARY

During the implementation of the bridge projects in Hungary in the early 2000s there was a need to use 36-38 m girders, instead of the max. 34.8 m (34 m span) precast concrete bridge girders, which were used before.

The following needs were conceived:

- in the case of single road bridges (even pointed angle crossing)
- and during motorway construction there was a need for a single span bridge above highways (2x2 lanes + 2 emergency lanes + separating lane), and this solution has economic and traffic safety advantages (removing the middle support for better visibility during driving)

To meet the above needs, Ferrobeton Zrt. developed the FI-150/44.80 type bridge girder with the cooperation of the Department of Structural Engineering of the Budapest University of Technology and Economics and the design experts of Uvaterv Zrt.

1. BACKGROUND

Ferrobeton Zrt. manufactured and transported precast concrete bridge girders for hundreds of bridges for motorway constructions in Hungary from the mid 1990s until the mid 2000s. It also developed the above-mentioned increased span bridge beams between 2003 and 2005. We cooperated during the implementation of development projects with the following partners:

- Department of Structural Engineering at the Budapest University of Technology and Economics:
 - preliminary tests were carried out using high strength concrete (C90/105) in pre-stressed concrete bridge girders. As a result of the tests the Hungarian bridge structure requirements have been supplemented by Technical Delivery Terms for using high strength concrete at road works (Fig. 1),
 - the university department performed the independent structural verification of the developed product.
- Uvaterv Zrt. experts created the shop drawings of the new girder type in close cooperation with the professionals of Ferrobeton Zrt. to specify the technological implementation opportunities.

2. GIRDER DEVELOPMENT

Ferrobeton Zrt. generally uses the following strategies and principles during the development of bridge girders:

- Professional cooperation with a wide range of well-established design organisations offices
- Investigating and recognising the needs of the clients, contractors and managers, and adapting the technical solution to their needs
- Cooperation with research projects, implementing the results during development

2.1 General requirements for bridges constructed by precast bridge girders

- Enough durability
- Sustainable structural details: accessibility without enclosed spaces
- Adequate concrete cover
- Adequate concrete quality
- Provide solutions with structural advantages

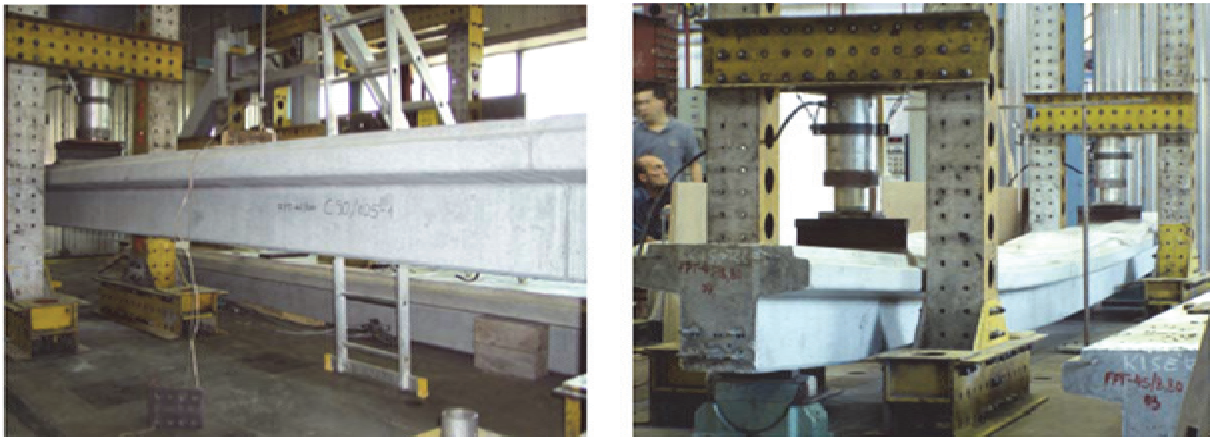


Fig. 1: Load tests of the C90/105 concrete quality test bridge girders at the Budapest University of Technology and Economics

The result of this development is the FI-150/44.80 type bridge girder with the cross-section shown in Fig. 2.

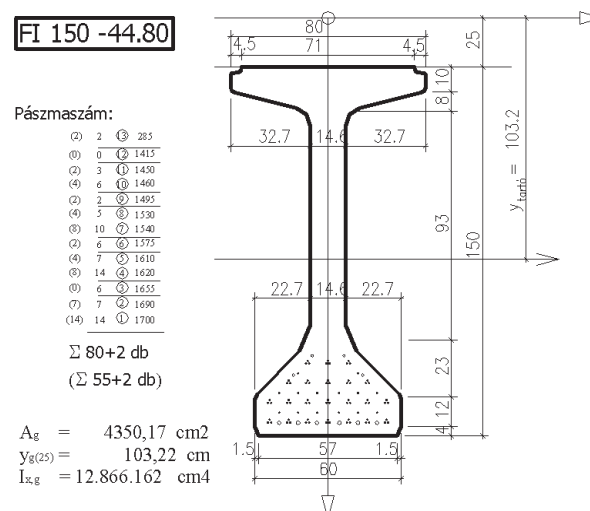


Fig. 2: The developed support structure

In the case of the bridge girders, the composite action is ensured by a 25 cm thick cast in situ bridge deck. Therefore, the combined total structure from the 1.75 m high precast bridge girder and the cast in situ slab in the case of 44.8 m long girders and 60 cm - 60 cm support results in an especially thin load-bearing superstructure with a 43.6 m span. An interesting characteristic of the bridge girder is the 430 kg/m³ specific steel content (normal reinforcement + strands – 82 strands with 115 kN pre-stressing force per strand), with the significant specific steel content and the crushed basalt, the specific density of the girder is 28.5 kN/m³.

3. LOCATION OF THE MANUFACTURING, CAPACITY, OTHER MANUFACTURING CHARACTERISTICS

- Location:
 - Ferrobeton Zrt., Dunaújváros factory
 - 25 ha manufacturing hall + storage area with crane
 - all production takes place in the manufacturing halls
- Concrete factory:
 - two separate concrete plants
 - each plant has a 2 m³ mixer with a 1.1 m³ backup mixer
 - suitable for winter operation
 - 2000 T closed additive storage capacity (18 bunkers)
 - suitable for handling special aggregates (e.g. crushed basalt)
- Steel frame preparation:
 - with own capacity
 - curving reinforcement
 - spot welded mesh production
- Manufacturing hall (parameters of the manufacturing stations suitable for the production of the given girder type):
 - 6x100 m and 2x110 m production table
 - Pre-stress posts with 10 000 kN bearing capacity
 - Radio remote controlled bridge crane with 2x300 kN load bearing capacity
 - complete steam generate and spread system.

The realised production technology is suitable for the production of FI-150/44,80 of precast pre-stressed concrete bridge girders (height: 1.5 m, length: 44.8m, own weight: 565 kN, pre-stressing force: 9430 kN, concrete grade: C60/75) (Figs. 3 and 4).

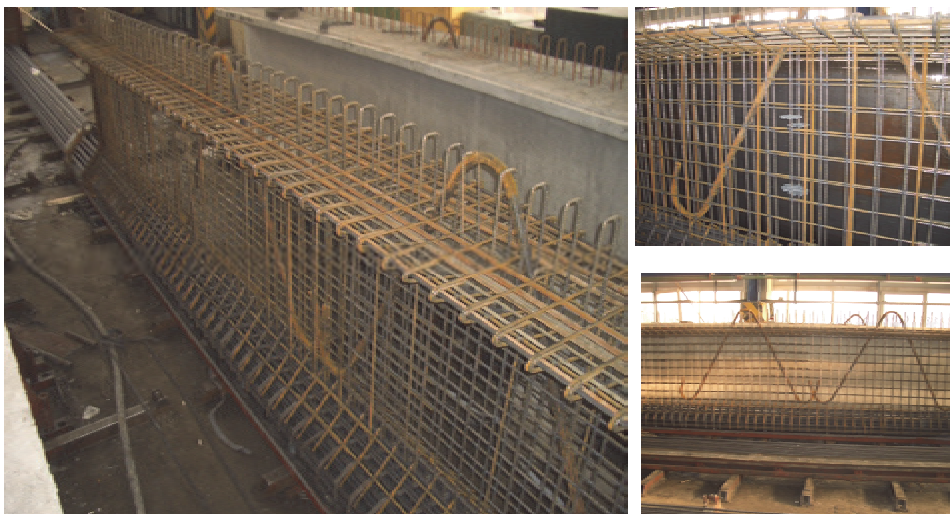


Fig. 3: Bridge girder production (reinforced construction)



Fig. 4: Bridge girder production, transportation within the plant

The material transportation options available in the plant are suitable for the professional storage of the long span bridge girders, which is an important factor in the viability in the execution of construction projects (Fig. 5).

The plant has industrial railways, so the girders can be transported to the constructing site by combined transportation means (railway + road transport).



Fig. 5: Transportation of bridge girders within the Dunaújváros plant

4. COMPLETED CONSTRUCTION PROJECTS

4.1 M7 motorway Z-15 bridge (Fig. 5):

- Motorway overpass above state road 7
- Year of construction: 2007
- FI-150/42.80 type girders: $2 \times 12 = 24$ pieces
- Total: 1027.2 m
- Dual-support structure with a 41.6 m open space



Fig. 5: M7 motorway Z-15 bridge

4.2 M6 motorway

Tab. 1 shows the type and amount of built-in bridge girders for the 5 M6 motorway viaducts on the Dunaújváros-Szekszárd section.

A significant construction project resulted in the extended use of girders, there were 6 viaducts on the project section, and in the case of 4 of them the superstructure were redesigned for precast FI-150 type girders.

Viaducts built with FI-150 girders (Fig. 6, 7, 8, 9):

- 4 viaducts built with FI-150 girders
- Total: 27.026 m
- 687 girders, including 441 with a length over 44.0 m built into superstructures with multiple supports.

Tab. 1: M6 motorway viaducts on the Dunaújváros-Szekszárd section

6 viaducts of Dunaújváros – Szekszárd section					
763	FI-150/ 20,80	38	790,40	3 246,40	
	FI-150/ 32,80	38	1 246,40		
	FI-150/ 44,80	27	1 209,60		
774	FI-150/ 30,80	38	1 170,40	7 467,60	
	FI-150/ 44,20	108	4 773,60		
	FI-150/ 44,80	34	1 523,60		
1019	FI-150/ 30,80	36	1 108,80	5 705,60	
	FI-150/ 44,20	104	4 596,80		
1040	FI-150/ 30,80	40	1 232,00	10 606,40	
	FI-150/ 34,80	56	1 948,80		
	FI-150/ 44,20	168	7 425,60		
B31425	FCI-120/ 31,80	140	4 452,00	6 666,40	
	FCI-120/ 28,80	48	1 382,40		
	FCI-120/ 20,80	40	832,00		
Sum:		915		33 692,40	

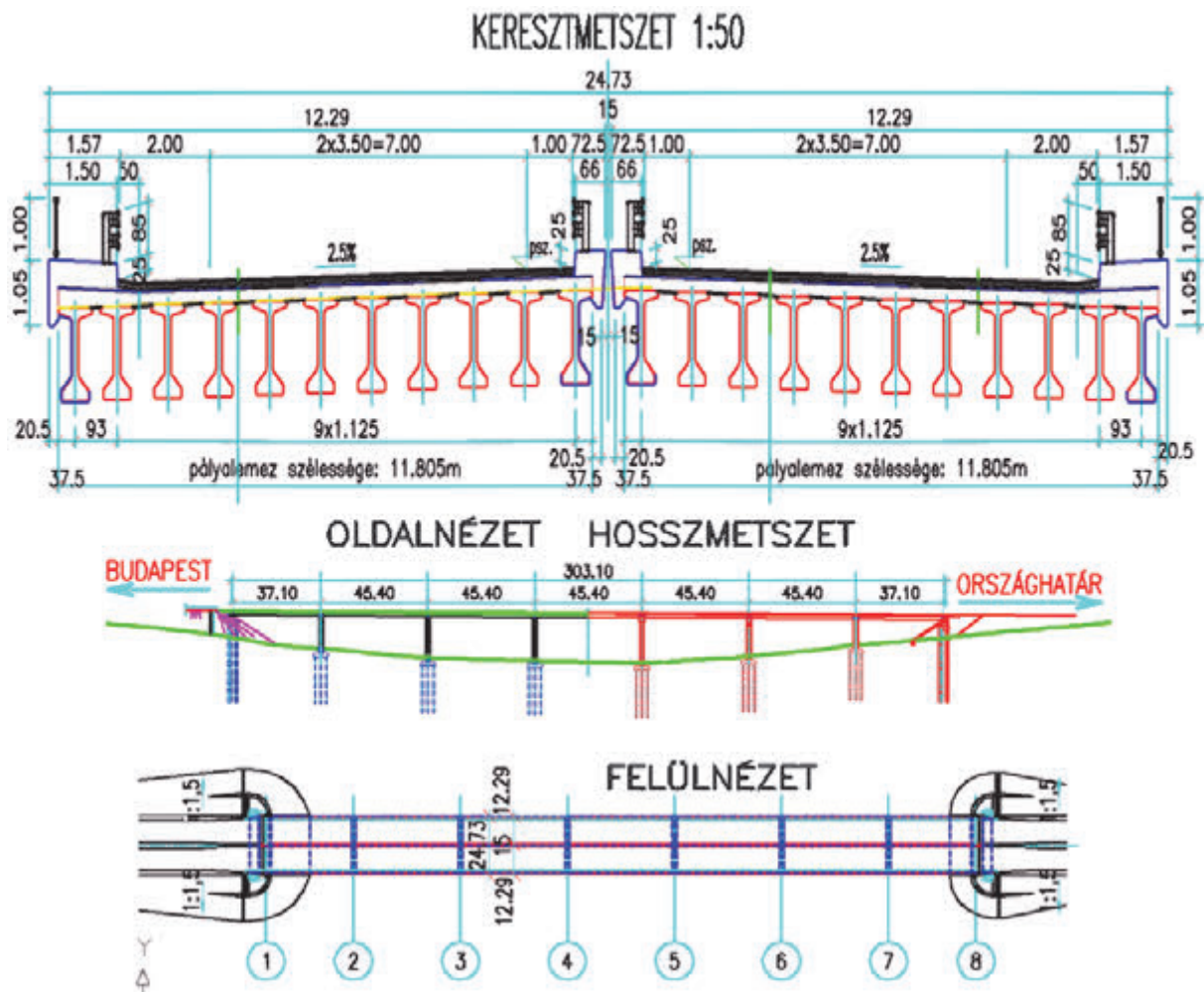


Fig. 6: FI-150 girder cross-section, longitudinal section, view from above



Fig. 7: FI-150 girder



Fig. 8: FI-150 girder



Fig. 9: FI-150 girder

4.3 M3 motorway (Fig. 10, 11)

- 22 bridge structures in total: 14109.4 m bridge girders of which, in the case of 10 bridges (underpasses) FI-150 type girders
- FI-150/41.80 m - 44.80m: 115 girders
- Total length of girders: 4974 m



Fig. 10



Fig. 11

Significant bridge construction projects implemented using these girders:

- M6 motorway between Dunaújváros and Szekszárd, 4 new highway overpasses (built with approx. 25000 m girders of overall length, including 470 girders with a length of 44 m)
- single span motorway underpass bridges in the Vásárosnamény area of the M3 motorway.

A significant project in the near future focuses on the floodplain bridge above the river Kőrös on the M44 motorway (producing and installing 176xFI-150/42.80 girders)

Logistical tasks when using large girders in such a large number:

- relocation and storage tasks in the factory (possible temporary storage at the site).
- craning

5. INDUSTRY RECOGNITIONS FOR THE FI-150 BRIDGE GIRDERS IN HUNGARY

Professional recognitions for the implemented development project:

- Uvaterv Zrt. received the Tierny Clark award for shop drawing (also involved: Ferrobeton Zrt., Department of Structural Engineering and Structures of the Budapest University of Technology and Economics) (Fig. 12)
- Ferrobeton Zrt. received the Innovation Award from the Hungarian Intellectual Property Office in 2010 for the realisation of the developed structure in a significant volume (collaborators: Department of Structural Engineering of the Budapest University of Technology and Economics, Uvaterv Zrt) (Fig. 13).



Fig. 12



Fig. 13

6. CONCLUSIONS

From the perspective of 10 years we can say that:

Although this business seemed presumptuous – thanks to the successful developments – this FI-150 prestressed precast bridge girders with extraordinary high span resulted in a really useful product.

We produced this kind of prestressed precast bridge girder 100 km long.

Designers and customers also use it willingly, so in the near future we have a good chance of use this bridge girder for more bridges.

VTR[®] - MODULAR BRIDGE CONCEPT FOR SKEW INTERSECTIONS

Dragoş Alupoai¹, Elena Metes², Sergiu Enache³, Gavril Köllö⁴, Edward Petzek²

¹ EUROCONSTRUCT TRADING 98 & Technical University Cluj Napoca, Romania

² SSF-RO & University Politehnica Timișoara, Romania

³ SSF-RO, Timișoara, Romania

⁴ Technical University Cluj Napoca, Romania

SUMMARY

An effective bridge solution should take into account many important aspects: reduced costs, fast and simple erection, modularity, durability and robustness, low maintenance costs and pleasant appearance. Their competitiveness depends on several circumstances such as site conditions, local costs of material and staff, and the contractor's experience.

A new construction concept called VTR was applied in Romania for several motorway bridges, structures which do not stand out because of their size or because of their complexity. But the VTR solution is characterized by premises, which could be remarkable for beneficiaries as well as for contractors: a steel-concrete composite girder system, based on a high degree of prefabrication, which can be realized economically and in short time. The article provides details about this solution and case studies.

1. INTRODUCTION – THE VTR SYSTEM

Finding the best solution for a large bridge is challenging, as factors such as integrity of the structure, fastness in execution, cost-effectiveness have to be considered. The VTR[®] modular solution (the name comes from the German “VerbundTrägerRost”) was designed to offer both the beneficiary and the constructor an advantageous structure. The concept is based on a steel-concrete composite girder system using a high degree of prefabrication. No formwork carriage, minimal formworks on site, light and simple shaped parts for easy manoeuvre – these are some of the objectives set out to improve and accelerate the work on site. On the other hand the structure must be durable, robust, slender and low maintenance (Petzek et al. 2016).

The taking over of the earthquake and the breaking forces for bridges with large lengths is an important aspect during the design process. The adequate solutions in this case are bridges with continuous girders or integral bridges. In case of the continuous girders, because of the big seismic forces and the displacements, seismic isolators must be used. The monolithic bounding of the piers to the superstructure, therefore usage of an integral bridge solution offers increased structural stiffness and restricts the displacements.

Advantageous structures result by applying the VTR modular construction method for integral or semi-integral bridges. The number of bearings and expansion joints is reduced or eliminated, simplifying the construction process and future maintenance. This system can also be applied for structures with a curved alignment or structures with skew intersections. In case of the skew intersections, the infrastructure can follow the skew, by maintaining a simple, regular deck conformation.

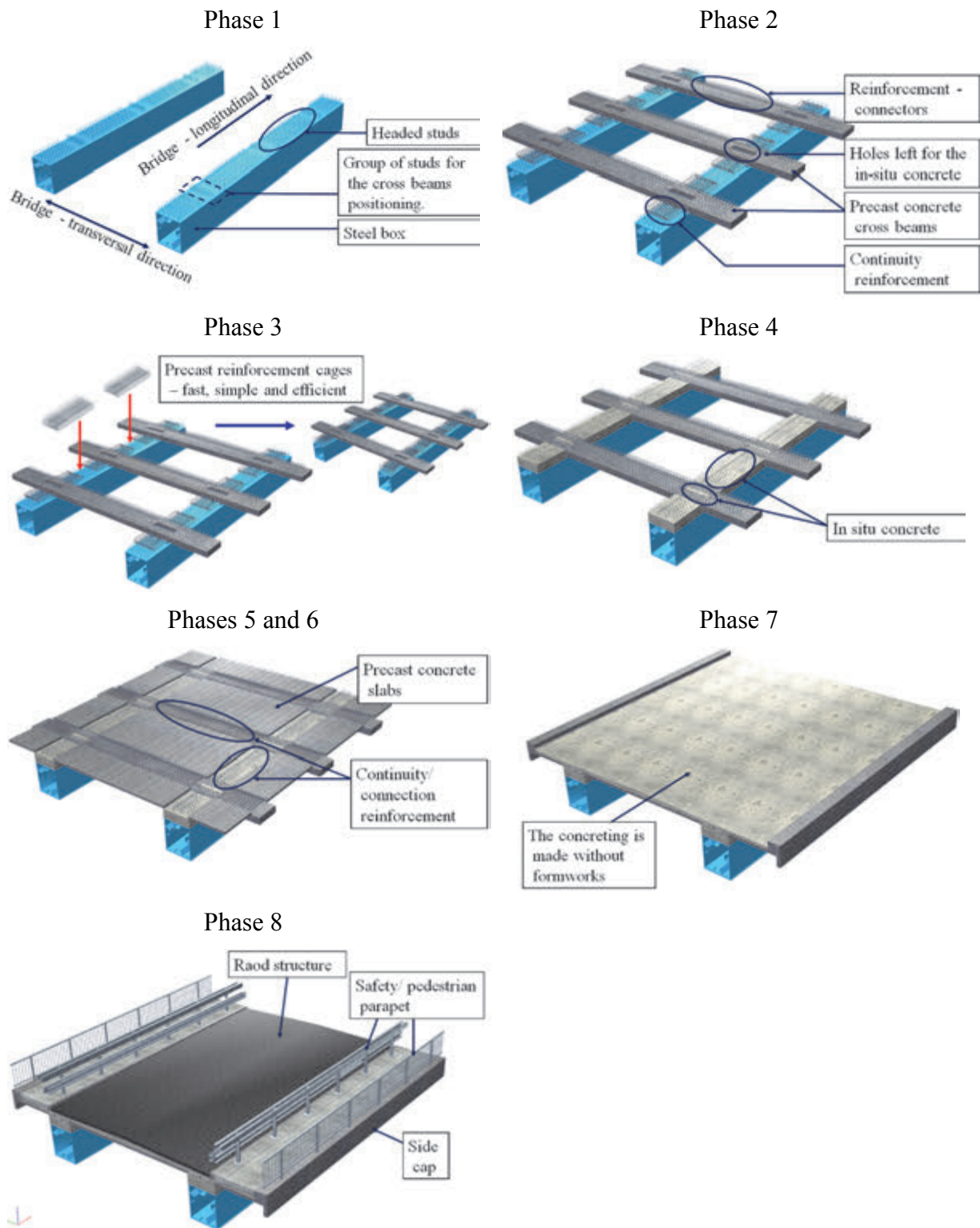


Fig. 1: The VTR[®] modular bridge solution

A VTR superstructure is made out of modules, like a 3D puzzle game (Petzek et al. 2016). Construction stages (Fig. 1):

- 1) The steel main girders are manufactured in the workshop and brought on site. On the upper flange shear stud connectors ensure the composite action between the girders and the slab.
- 2) Prefabricated concrete cross beams are placed on top of the steel girders. For the connection to the steel girders, the cross beams are provided with longitudinal connection reinforcement and with openings in which the studs can reach through.
- 3) Prefabricated reinforcement modules are mounted between the cross beams, on the steel girders.
- 4) The longitudinal connecting areas are concreted. Thus an initial bond – a composite steel-concrete girder system – is created:
 - in longitudinal direction the steel boxes and the first in-situ concrete phase and
 - in transversal direction the prefabricated beams.
- 5) Prefabricated concrete slabs are placed on the composite girder system. The slabs may have the final height of the deck, or they may be half-plates.
- 6) Connection reinforcement in the slab is added and it may as well be designed as prefabricated cages. The geometry permits wide concrete joints and large overlapping lengths of the reinforcement bars.
- 7) The bridge deck is concreted, connecting all separate prefabricated elements. Minimal formwork for the deck is needed.
- 8) In the final phase the structure is equipped with waterproofing, asphalt layers, parapets.

2. CASE STUDY: MOTORWAY BRIDGE OVER THREE RAILWAY LINES CF300 AND CF201

The Sebeş – Turda Motorway provides the link between the A1 Motorway and A3 Motorway in Romania, ensuring a traffic flow from the north-west to the south-east of the country, through the capital Bucharest. The entire section is under construction by a design and build contract. In case of the second lot, three bridges with lengths over 200 m were redesigned using the VTR system. The change was made taking into consideration the short erection time, but also economic aspects.

One of these bridges is situated at km 26+350 over three electrified, main railway lines, the CF300 and the double CF201. Because the VTR solution is well suited for skew bridges, the middle span could be reduced from the initial 80 m length, to 48 m length. The main advantage in this case is that the main girders can be lifted and mounted at once, without the use of temporary supporting towers. This is especially important when working near electrified railway lines. At the time the article was written, works have started at the foundations and substructure.

2.1 Design elements

The bridge has a length of 217.00 m (Fig. 2), with 6 spans (28.00 m + 32.00 m + 48.00 m + 40.00 m + 28.00 m + 28 m). The substructure follows the skew of 31 ° between the motorway axis and the railways. The bridge is made of two parallel structures, each 13.60 m wide (Fig. 3). The structure is integral with rigid connection between the sub- and superstructure. Most of the longitudinal deformation is taken over by pendulum-like columns in the abutment area. No bearings are used and expansion joints are needed only at the abutments.

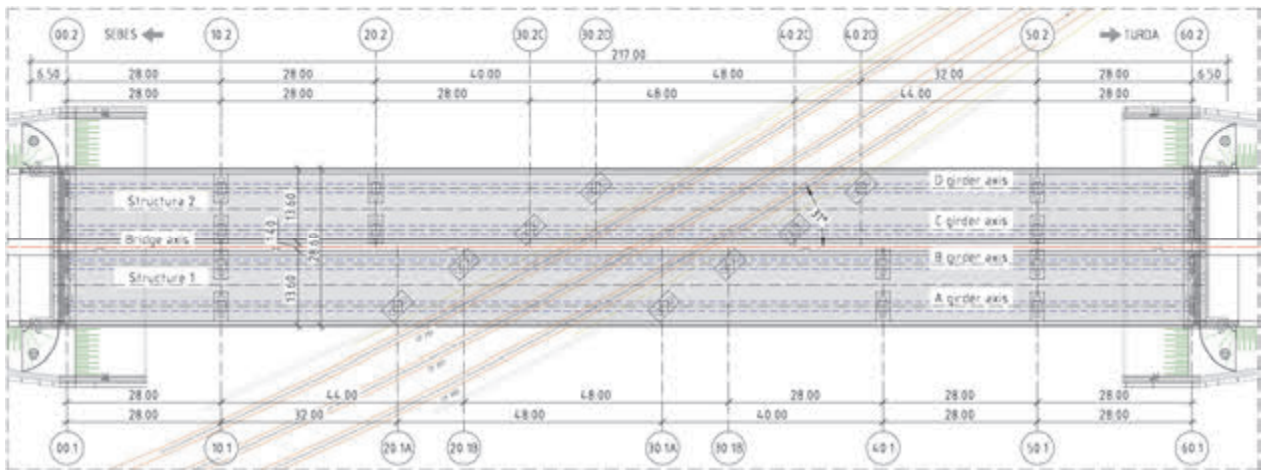


Fig. 2: Plan view

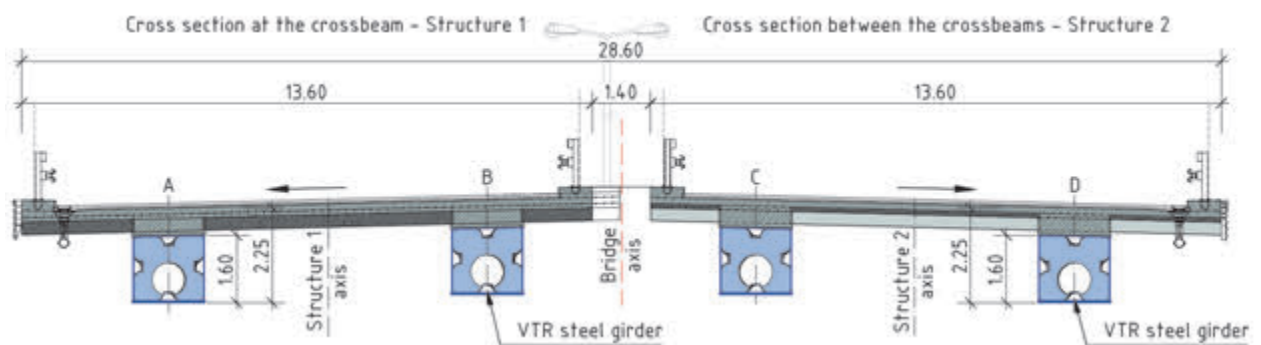


Fig. 3: General cross section

The indirect foundation is made of $\text{Ø}1.20$ m piles and pile caps for the abutments, as well as for the piers. The abutments (Fig. 4, left) are made of a back wall, back wings and also of the pendulum like connection for the superstructure. The pendulum effect results from the small thickness of 40 cm of the columns on which the end girders will rest. Under each girder, piers (Fig. 4, right) with a the rectangular section of $1.80 \text{ m} \times 1.50 \text{ m}$ were designed. The rigid connection of the substructure to the superstructure is made by concreting of the pier nodes.

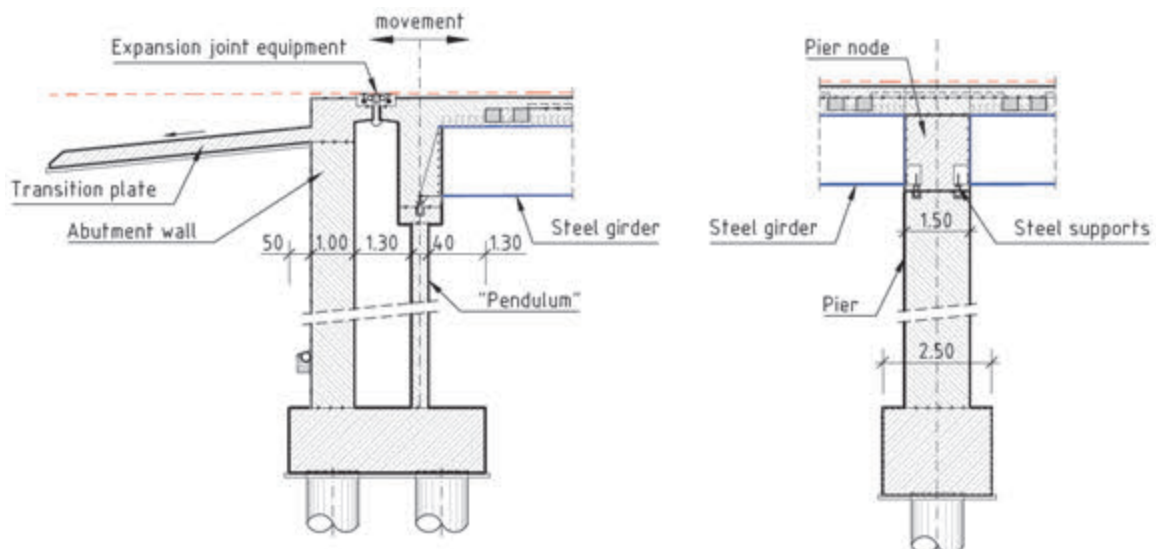


Fig. 4: Sub- to superstructure connection: abutment/ pendulum (left) and pier (right) in longitudinal direction

For the superstructure the VTR solution was chosen. Each of the two decks has 2 longitudinal, steel main girders and precast concrete cross beams every 4 m. The first in situ concrete is poured over the top flange of the steel girders up to the cross beams level, thus realizing an intermediary girder system. A solution with full precast slabs with the total height of 25 cm was analysed, but instead the slab is made out of 10 cm precast slabs and of 15 cm in situ concrete. This allows a better control of the gradient, when taking into consideration the precambering of the steel girders in case of a skew bridge and the different construction stages.

Using a crane, the steel girders with the length of 48 m will be lifted over the railway lines and put on the piers. Only during this operation shall the railway traffic be interrupted. After securing the steel girders, all other construction phases can be done without other interruptions: placing the precast elements, pouring the in situ concrete in the pier nodes and on the bridge deck.

2.2 Static evaluation overview

The bridge model for the static evaluation was carried out with the program system Sofistik. The indirect foundation was modelled by creating bore profiles using data from the geotechnical study. The piles, pile caps, piers and pendulums were introduced as structural line elements, with circular respectively rectangular concrete cross section. The bridge deck was introduced as a girders system, having in longitudinal direction two structural line elements with composite section (Fig. 5) consisting of the steel girder and the concrete slab, and in transversal direction structural lines with rectangular concrete section every 4 m, representing the cross beams (Fig. 6). In addition an orthotropic slab was defined, which will distribute the loads in transversal direction together with the cross beams.

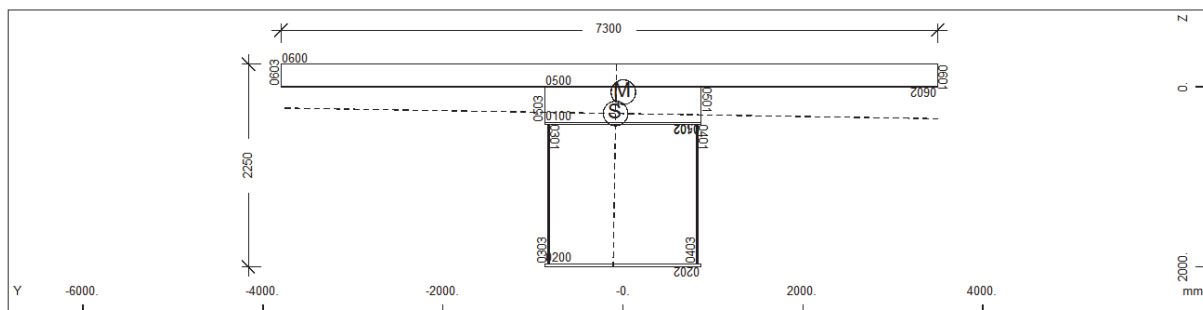


Fig. 5: Composite cross-section in longitudinal direction (final phase)



Fig. 6: Concrete cross-section in transversal direction (final phase: cross beam and slab)

Construction stages for loads and structural elements were defined in accordance with the VTR system principle (chapter 1). The arrangement of nodes and beams show realistically the positions of the erecting sequences and the casting segments as well as the positions of the cross beams (Fig. 8). By defining the main girders as a composite section, the cross load carrying action of the deck is also included. The material distribution is ensured by a close basic grid. In Fig. 7 a general view of the finite element model can be seen. The calculation was made respecting the European norms.



Fig. 7: FE-Model

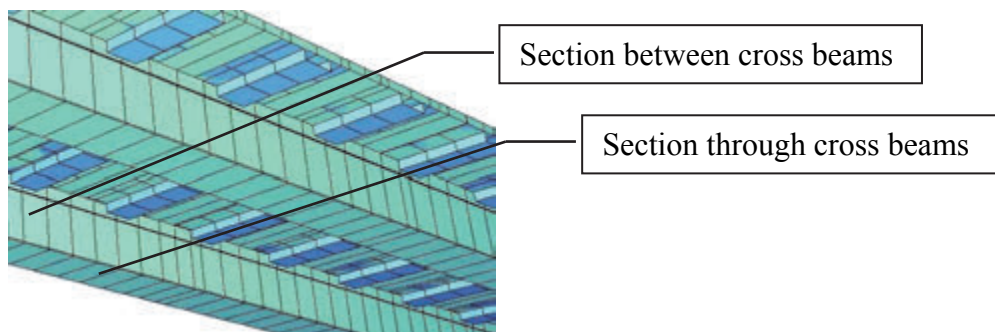


Fig. 8: The FE-Model - cross beams position

The main particularity of this integral structure is represented by the 31° sharp angle between the railway axis and the road axis which makes it sensitive to torsion effects and seismic action (Fig. 9).



Fig. 9: The FE-Model – seismic evaluation

Left eigenvalue in longitudinal direction; right eigenvalue in transversal direction

The structure has a good behaviour in case of all load combinations, both in ULS (ultimate limit state) and SLS (serviceability limit state). The steel consumption indices is 171 kg/m² (kg/ bridge area) resulted.

3. VTR[®] bridges in Romania

This concept was successfully applied on two motorway bridges in Romania. This first bridge is 720 m long and crosses over the Mures River, on the motorway sector Deva – Orăștie (Fig. 10). It has 12 spans, each of 60 m; the static system is semi-integral, with three of the middle piers fixed to the superstructure. The deadline for completing the structure in 16 months was

met; it took only 4 months to finish the entire deck of the bridge, which has a total surface of approximately 2 ha. For the entire structure 4100 tons of steel were used, which led to a consumption indices of 199 t/m².



Fig. 10: Mureș Viaduct (2012)

The second structure is the Orăștie Viaduct, part of the Orăștie-Sibiu Motorway, lot 1. Its geometry is similar to the bridge over the railway on Sebeș-Turda Motorway having a slightly smaller middle span (40 m instead of 48 m). All piers are fixed to the superstructure and bearings are placed only at the abutments. The 240 m long viaduct (Fig. 11) crosses at a skew a double railway line and the National Road DN7, having the piers lined up to the 34° angle.

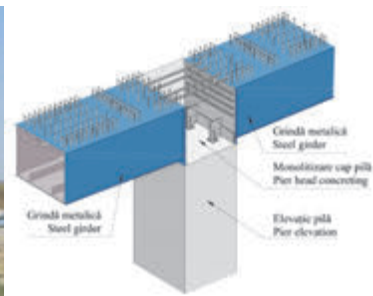


Fig. 11: Orăștie Viaduct (2013)

Fig. 12 shows different working phases developed on the bridge's length. The execution firm had permanently assured a working field, so that there was no interruption throughout the execution.



Fig. 12: Construction phases

A few years have passed since the two bridges were built and up until now the structural behaviour is according to our calculations. The experience gained from the two VTR structures has demonstrated the method is indeed effective, in terms of time and resources management, but at the same time robust.

4. CONCLUSIONS

The motorway bridge over three railway lines CF300 and CF201 stands out because of the pronounced skew alignment of the pier columns at the intersection between the motorway axis and the railway axes. By using the VTR system, a slender, robust and modular structure could be designed. The bridge is currently under construction, but the experience gained through the two motorway bridges, which are already built, lets us believe that the construction process will be fast and easy and that the structure will have a good behaviour in time.

The VTR[®] system is meant to simplify works on site, especially for long bridges. At the same time robustness and aesthetics of the structure is ensured. These are some of its advantages (Petzek et al. 2013):

- High degree of prefabrication - modular system.
- Material consumption savings.
- Light steel/ prefabricated concrete elements for easy manoeuvre.
- Quick construction times.
- Low costs, clean site, low environmental impact.

5. REFERENCES

- Petzek, E. et al. (2013), "VTR[®] a modern composite bridge concept", Springer Vieweg, ISBN 978-3-658-03713-0, pp. 315-338.
- Petzek, E et al. (2016), "New Integral and Semi-integral Bridge Solutions for the Romanian Highways and Motorways", Bridges in Danube Basin, EDIS, University of Zilina, ISBN 978-80-554-1249-8, pp. 111-112.

QUANTIFYING THE EFFECT OF MIXTURE PROPERTIES OF HIGH PERFORMANCE CONCRETE OVERLAYS ON ADHESIVE BOND TO NSC SUBSTRATES ON THE BASIS OF AXIAL TENSILE TESTS

*Martin Schneider, Norbert Randl, Bernhard K. Hofer
Carinthia University of Applied Sciences
Villacher Strasse 1, 9800 Spittal, Austria*

SUMMARY

Based on former studies (Lenz and Zilch, 2010), it was seen that the adhesive bond in concrete-concrete-joints can be significantly affected by the properties of the overlay concrete. Therefore an appropriate HPC mixture was designed and varied in terms of cement type, water-to-binder ratio, inert lime content, reactive components and amount of micro silica to identify the decisive parameters with respect to the adhesive bond strength. The roughness of the substrate surface was fixed by around 1.0 mm which is a quite common value in construction practice. After 28 days hardening of the HPC overlay, axial tensile tests were performed to determine the adhesive bond strength in direct tension. The test results allow for the identification of the decisive parameters of the HPC mixture on the adhesive bond strength. Especially the impact of the type and composition of the fine grain particles on the development of the interface bond capacity was clearly verified.

1. INTRODUCTION

During the maintenance phase of existing structures such as bridges it may become necessary to increase the load bearing capacity. This can be partly due to changing requirements from codes, but also to increase of the traffic loads. Thereby bonded concrete overlays, with optimum adhesive bonding to NSC substrates, provide a well-established solution. Apart from surface preparation, the quality of the overlays can be different and has an effect on the bond strength; for example some studies at the Technical University of Munich (Lenz and Zilch, 2010; Reinecke, 2004 and Mueller, 2009) have shown that much higher tensile bond strength subsists between HPC overlay and NSC substrate than in the case of NSC overlays.

Based on these promising test results recently a research project has been conducted together with the Austrian Society for Construction Technology (ÖBV) and Smart Minerals to investigate the behaviour of HPC overlays on the basis of comprehensive small scale and large scale testing (Randl; Steiner and Peyerl, 2016a and 2016b). The project was funded by the Austrian Research Promotion Agency (FFG), the Austrian motorway (ASFINAG) and railway operators (ÖBB) and the companies Porr, STRABAG and Rohrdorfer and in fact confirmed that an appropriate HPC mixture may lead to significantly higher interface bond strength than an NSC overlay. However, it was also seen that certain modifications of the HPC mixture proportions can significantly affect the adhesive bond.

In order to clarify this question, a follow-up project was conducted where a number of different mixtures of HPC overlays were examined in order to investigate the possible effect of the different ingredients on the adhesive bond strength along the interface. An appropriate

HPC mixture was varied in terms of cement type, water-to-binder ratio, inert lime content, reactive components, amount of micro silica and type of superplasticizer to identify the decisive parameters with respect to the adhesive bond strength. The roughness and preparation of the substrate surface is another very important factor for the adhesive bond strength. The roughness was produced by means of high pressure water jetting (HPWJ). The target roughness was 1.0 mm, verified by the sand patch method.

2. OVERVIEW OF THE TEST PROGRAM AND THE TEST SETUP

The main focus of the parametric study was the variation of the overlay concrete mixture. The target concrete strength of the substrate was between 50 and 60 MPa, being conform to strength class C40/50 requirements. The surfaces of the substrates were slightly wetted before applying the concrete overlays. At the age of 28 days of the substrates, the casting of the concrete overlays started. The compressive strength of the concrete overlay was aimed at a minimum value of 75 MPa. Each variation of the concrete ended up in three composite slab specimens 300x300x130mm. The variation of the production parameters can be seen in Tab. 1.

Tab. 1: Overview of varied parameters

Cement	CEM I 52,5 N	CEM I 42,5 N	CEM II 32,5R
w/b ratio	0.34	0.38	0.42
Mortar content (inert)	600 kg	500 kg	*
Slurry content (cement)	500 kg	450 kg	425 kg
Slurry content (fly ash mixture)	100 kg	75 kg	50 kg
Slurry content (microsilica)	60 kg	20 kg	*

* Reference mixture contains 550 kg mortar and 40 kg microsilica

Tab. 1 shows a summary of the modified ingredients in comparison to the reference mix given in Table 3. The produced test specimens were stored for 28 days curing after preparation of the overlays. Three core holes were drilled into each test specimen to test the axial tensile strength with the test setup according to the following sketch. Between the two layers a 0.5 cm notch was cut along the circumference of the core to ensure failure at the interface, see the sketch in Fig.1. This method was chosen after performing in the first phase a number of standard pull-off tests which frequently led to tensile failure in the substrate or overlay (Schneider; Randl and Hofer, 2017).

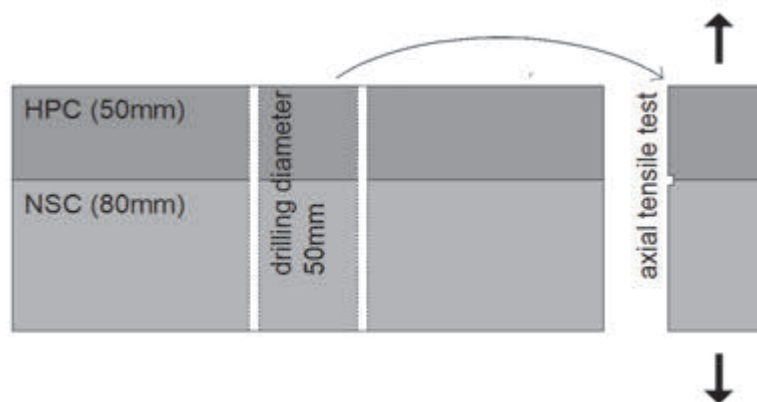


Fig. 1: Sketch of the produced specimen 300x300x130 mm and the test set up

3. CONCRETE AND SURFACE PROPERTIES

3.1 Substrate concrete

The substrate concrete C40/50 was produced with specimen dimensions 300x300x80 mm. A total of 120 test specimens were made. A number of concrete cylinders, 150 mm cubes and prisms were produced to test the tensile strength, the compressive strength and Young's modulus. The splitting tensile strength was multiplied with 0.9 to estimate the uniaxial tensile strength according to Eurocode 2. The results are presented as an average of 3 specimens each. Tab. 2 shows the mix design and the main properties of the substrate concrete.

Tab 2: Mix design and properties of the substrate concrete

Water/cement-ratio	0.42	
Cement content	420	kg/m ³
Largest grain	16	mm
Air content	1.5	%
Fresh concrete density	2409	kg/m ³
Consistency	555	mm

The compressive strength after 28 days tested on at least 3 150 mm cubes each was in the range of 50 to 60 MPa, the tensile strength after 28 days of the substrate concrete reached between 3.1 and 3.9 MPa, an average is given by 3.6 MPa.

3.2 Mix design of the concrete overlays

The consistency of the fresh concrete was determined by the slump-flow test, with a targeted spread of the fresh concrete of 550 mm. The viscosity of fluids influences the penetration into the substrate surface; therefore this parameter was kept constant in the experimental campaign as much as possible.

Tab. 3: Mix design and properties of the reference overlay concrete

Mixture ingredients per m ³		
Water	170	kg/m ³
CEM I 52,5N	475	kg/m ³
Microsilica	40	kg/m ³
Superplasticizer	5.46	kg/m ³
Largest grain	16	mm
Air content	1.5	%
Water/cement-ratio	0.31	
Mortar content	553	dm ³ /m ³
Powder content	500	kg/m ³
Compressive strength	87.6	MPa
Tensile strength	4.5	MPa

The amount of superplasticizer is thereby an important variable. The reference mixture had a compressive strength of 87.6 MPa with a w/b-ratio (water/binder-ratio) of 0.31. The used aggregates sand, gravel and greenstone had a maximum size of 16 mm. Tab. 3 gives the reference mixture for the overlay concrete.

4. RESULTS OF THE EXPERIMENTS

4.1 General description

The adhesive bond was tested by a tensile test device to determine the tensile bond strength of each core drill. In the following figures the tensile strength of the substrate and overlay concrete variations, derived from splitting tensile tests with a factor 0.9, is compared to the uniaxial tension tests with failure at the joints.

4.2 Variation of type of cement

This series has been performed with a constant w/c-ratio (water/cement-ratio) and with the same amount of cement. The first variation is the reference concrete mix. Tab. 4 shows the variation of cement types and the results of compressive strength and tensile strength tests and the slump flow of the fresh concrete. Fig. 2 shows the results of the variation of cement. No significant influence of the cement type on the adhesive bond strength can be detected.

Tab. 4: Overlay properties (test series with variation of type of cement)

Type of cement	CEM I 52.5 N	CEM I 42.5 N	CEM II 32.5 R
Compressive strength [MPa]	87.6	84.5	81.3
Tensile strength [MPa]	4.5	4.6	3.9
Superplasticizer [% by weight]	0.89	0.67	0.77
Slump flow [mm]	610	535	565

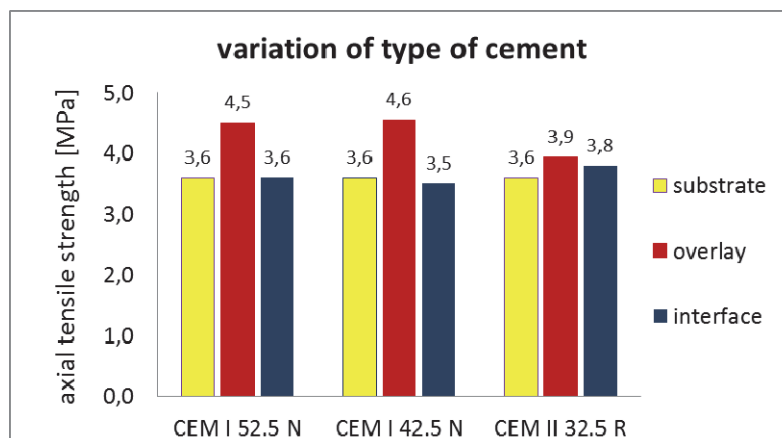


Fig. 2: Results of variation of cement compared to tensile strength of the substrate and overlay concrete

4.3 Variation of water/cement-value

The reference overlay concrete was mixed with a w/c-ratio of 0.31. The results of the variation of the w/c-ratio are shown in Tab. 5 and the comparison of the tensile strength is given in Fig. 3.

Tab. 5: Overlay properties (test series with variation of w/c value)

w/c ratio	0.34	0.38	0.42
Compressive strength [MPa]	76.4	71.2	61.1
Tensile strength [MPa]	4.6	4.5	3.9
Superplasticizer [% by weight]	0.53	0.44	0.18
Slump flow [mm]	580	545	480

The trend of the compressive strength coincides with the increased w/c values. The tendency shows at a higher w/c-ratio a lower bond between the two layers of the concrete. This result is not surprising because the tensile strength of the overlays decreases with increasing w/c-ratio.

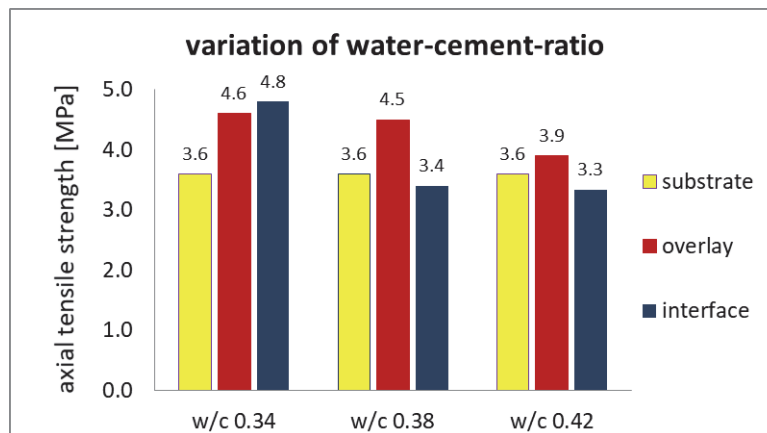


Fig. 3: Results of the w/c series compared with tensile strength of substrate and overlay concrete

4.4 Variation of (inert) mortar content

The mortar content in the reference mix was 550 kg/m³. The following table shows only the results of the variation. The target of this variation was the detection of any influence of the inert components.

Tab 6: Overlay properties (test series with variation of mortar content (inert))

Mortar content (inert)	600 kg	500 kg
Compressive strength [MPa]	82.0	86.5
Tensile strength [MPa]	4.6	4.2
Superplasticizer [% by weight]	0.79	0.67
Slump flow [mm]	570	530

Fig. 4 shows the probability of the failure in the joint between the overlays and the substrates and it is compared with the results of the tensile strength of each concrete. At a lower mortar content frequently joint failure was observed. A significant influence of the inert mortar content can therefore be identified.

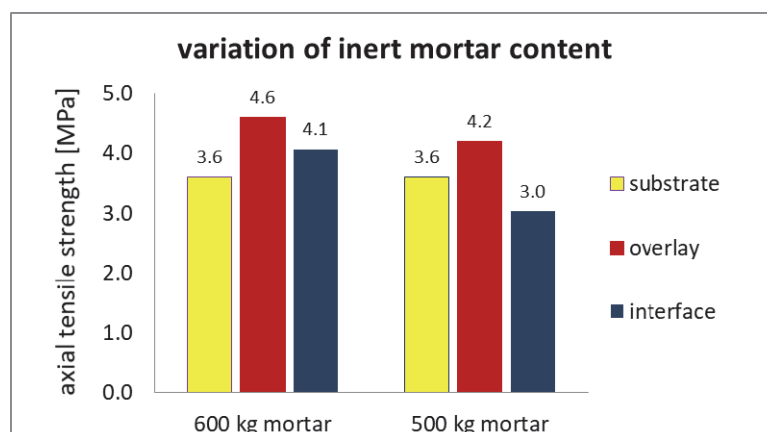


Fig. 4: Results of the mortar content (inert)-series compared with tensile strength of substrate and overlay concrete

4.5 Variation of slurry content (cement related)

This series was focusing on variation of the slurry content (related to cement). In Tab. 7 the variation parameters are presented. The reference concrete had a cement content of 475 kg/m³.

Tab. 7: Overlay properties (test series with variation of slurry content)

Slurry content (cement)	500 kg	450 kg	425 kg
Compressive strength [MPa]	86.9	90.7	88.9
Tensile strength [MPa]	5.2	4.5	4.4
Superplasticizer [% by weight]	0.74	0.92	0.90
Slump flow [mm]	555	535	615

Fig. 5 shows the results of the variation of cement related slurry. The difference of the slurry content between 425 kg and 500 kg shows an opposing trend compared to the series of inert mortar. The lower the content of cement slurry, the higher was the bond strength.

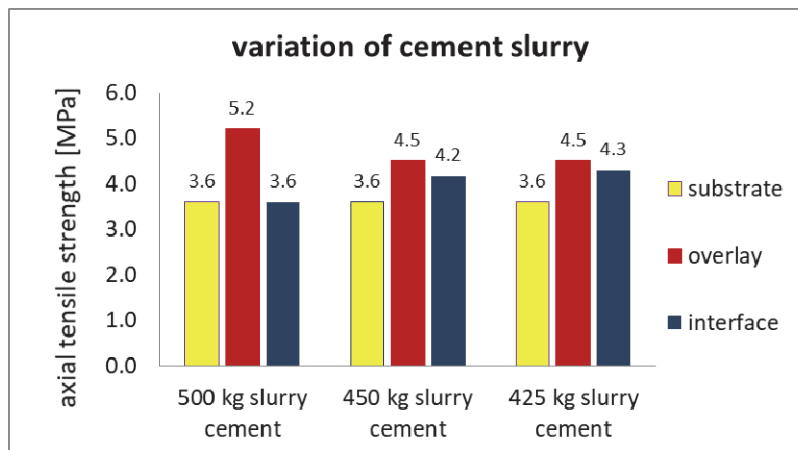


Fig. 5: Results of the slurry content (cement)-series compared with tensile strength of substrate and overlay concrete

4.6 Slurry content (fly ash component mixture)

The original reference mix did not contain fly ash. All variations were produced using the same w/b-ratio. The factor of reactivity of the fly ash component mixture is 0.8. The results are shown in the next Table and Figure. The ordinary dosage of fly ash component mixture is between 25 kg and 75 kg. A dosage of 100 kg is rather high for practical use.

Tab. 8: Overlay properties (test series with variation of slurry content (fly ash component mixture))

Slurry content (fly ash component mixture)	100 kg	75 kg	50 kg
Compressive strength [MPa]	78.8	80.3	83.0
Tensile strength [MPa]	3.7	4.5	4.1
Superplasticizer [% by weight]	0.64	0.73	0.78
Slump flow [mm]	550 (6 minutes)	530 (7 minutes)	520 (7 minutes)

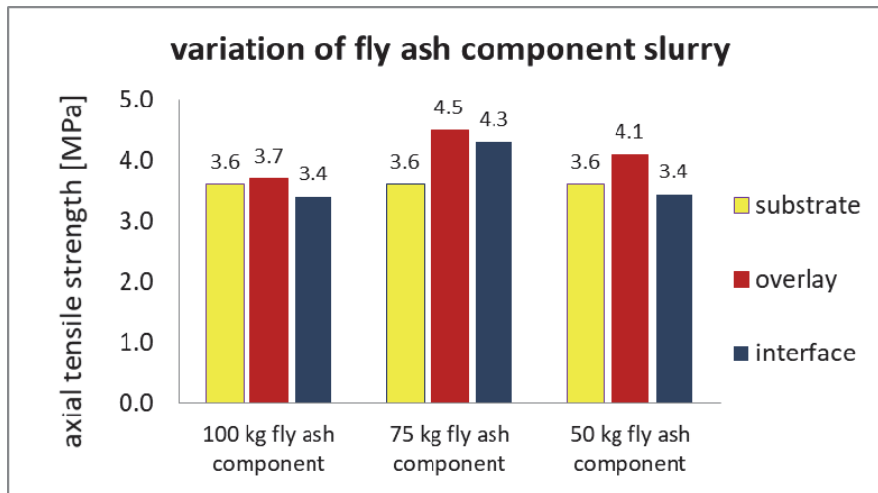


Fig. 6: Results of variation of slurry content (fly ash component mixture) compared with tensile strength of substrate and overlay concrete

4.7 Slurry content (microsilica)

The reference mix includes a microsilica of 40 kg/m³. It has to be mentioned that a part of the specimens in this series had been contaminated and slightly damaged after HPWJ during the storage process; therefore the slabs had to be cleaned. The results are given in Tab. 9.

Tab. 9: Overlay properties (test series with variation of slurry content (microsilica))

Slurry content (Microsilica)	60 kg	20 kg
Compressive strength [MPa]	84.1	84.3
Tensile strength [MPa]	4.8	5.2
Superplasticizer [% by weight]	0.86	0.78
Slump flow [mm]	590	520

In Fig. 7 the results of the variation of microsilica content are shown.

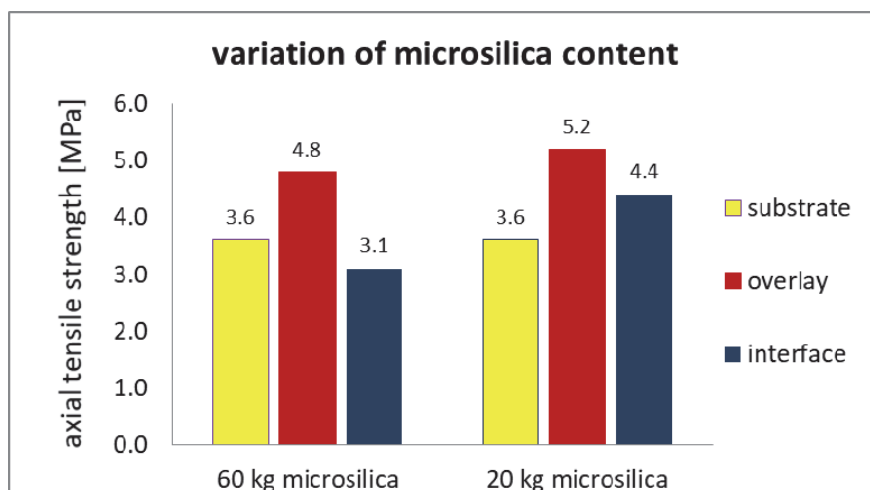


Fig. 7: Variation of slurry content (microsilica) – results compared with tensile strength of substrate and overlay concrete

Compared to the results of the reference mixture, a significant effect is observed. A decrease of the microsilica content leads to an improvement of the adhesive bond in the joint.

5. CONCLUSIONS AND OUTLOOK

In the frame of an experimental campaign investigating the influence of different mixture properties of high-performance concrete overlays on the adhesive bonding with NSC substrates, some interesting correlations are observed. Concerning the HPC mixture properties, the adhesive bond depends clearly on the mortar content and the content of slurry (cement, fly ash and microsilica related). Another factor might be the w/c-ratio, however, increasing the w/c-ratio leads to a strong drop of the compressive and tensile strength of the overlay concrete and in consequence thereby also affects the bonding.

In general a high quality of the cleaning process after HPWJ is necessary and shall be part of the quality management system on the construction site.

6. ACKNOWLEDGEMENT

This experimental campaign was following and linked to a research project supported by the Austrian Research Promotion Agency, Austrian Society for Construction Technology, Austrian Railway Company ÖBB, Austrian motorway operator ASFINAG, Rohrdorfer company and the building contractors PORR and STRABAG which is greatly acknowledged.

7. REFERENCES

- Lenz, P. and Zilch, K. (2010), "Concrete-to-Concrete Bonds - Potentials for new Structures and Rehabilitation", Proceedings of Third International fib Congress, Washington, 2010.
- Mueller, A. (2009), "Zum Zug- und Schubtragverhalten von Betonfugen", Doctoral Thesis, University of Technology Munich, 2009.
- Randl, N.; Steiner, M. and Peyerl, M. (2016a), "Sustainable strengthening of RC members with High Performance Concrete overlays", Proceedings IABMAS 2016, pp. 1308-1315
- Randl, N., Steiner, M., Peyerl, M. (2016b), "Endbericht FFG-Projekt 853509 „Hochfester Aufbeton“, http://bautechnik.pro/pdf/FFG/FFG_konst_Aufbeton_kurz_Endb_23-12-2016.pdf.
- Reinecke, R. (2004), "Haftverbund und Rissverzahnung in unbewehrten Betonschubfugen", Doctoral Thesis, University of Technology Munich, 2004.
- Schneider, M., Randl, N., Hofer, B. (2017), "Effect of mixture properties of High-Performance Concrete overlays on adhesive bonding with NSC substrates", Proceedings of High Performance concrete (11th HPC) and Concrete Innovation Conference (2nd CIC), March 2017.

OPTIMIZING OF UHPC RAILING PANELS AND THEIR PRACTICAL APPLICATION

Jan Tichý, Bohuslav Slánský, Stanislav Ševčík

Skanska a.s.

Křižíkova 682/34a, 18600 Praha 8, Czech Republic, jan.tichy@skanska.cz

SUMMARY

In the Bridge center (Skanska a.s.) premises in Brno, Czech Republic, a series of thin railing panels from UHPC were manufactured in the recent two years. The purpose was both shape and material optimization of mentioned panels. Some of the panels employed also a non-metallic GFRP reinforcement bars. These measures were carried out in order to increase the competitiveness against ordinary steel railing in the terms of durability, strength and economy. The results of both static and dynamic tests are presented. Also, a latest practical application of the mentioned railing panels is mentioned.

1. INTRODUCTION

The UHPC material is a modern cement-based material with outstanding characteristics in the terms of mechanic and durability aspects. It is intensively researched all around the world and it has been employed in many structures, mainly in North America, Japan, Australia and Western Europe. First applications were also achieved in the Czech Republic, Namely, renovation of a bridge over highway R10 near Benátky nad Jizerou (Tichý et al., 2012), or a unique footbridge across Labe river in Čelákovice (Kalný et al., 2015).

Mostly, the UHPC is employed in the bridge structures, preferably for footbridges. Some applications in the building industry are also known, e.g. facade panels of the Kontor building in Malmö, Sweden, manufactured also in Czech Republic (Tichý et al., 2014).

2. BENEFITS OF UHPC RAILING PANELS COMPARED TO A ORDINARY STEEL RAILING

Nowadays, the bridge railing usually consists of a steel frame and a steel pane (either bars or web). The disadvantage of this design is the fact that it cannot prevent air corrosion and thus the corrosion-preventive measures need to be applied several times during the life cycle. Also, unfortunately, the steel can attract thieves.

The main advantage of the UHPC railing panels is the fact that it needs no maintenance during its lifespan. Also, high durability against the weather conditions and long service life may be named out as benefits. High strength of the material allows making the panels very thin (several centimetres).

The panel is then clamped in a steel frame and tighten by a set of bolts and nuts. The panel is lighten with a several openings and can be coloured to a desired shade.

3. MATERIAL AND SHAPE OPTIMIZATION

3.1 Material optimization

The major part of the research in recent year was the material optimization of the UHPC. It was realized in two levels – economical optimization of the UHPC mixture and replacement of the ordinary steel reinforcement bars.

The optimization of the mixture went out of the requirement to lower the price of the panel to make it economically comparable with the steel railing. From the original mixture, derived from the mixture for facade panels (Tichý et al., 2014) the most expensive components were either replaced with cheaper material or (in one case) removed completely (after evaluation of its real contribution). Further on, the possibility of lowering the volume of fibers was examined. As a result, a set of 2 new mixtures were tested both on panels and on testing specimens (cubes and prisms). Both mixture were prepared in two modifications (lower and higher volume of PVA fibres). The comparison of the original mixture (Tichý et al., 2014) and the new mixtures gives some 35-55% cost reduction. This comparison is visible in Fig. 1, where the original mixture is marked R1, the mixture derived from the original is R2 and the above mentioned new mixtures are marked R3 and R4. Mixtures R3.1 and R4.1 consist lower volume of fibres, but otherwise are identical with R3 and R4, respectively.

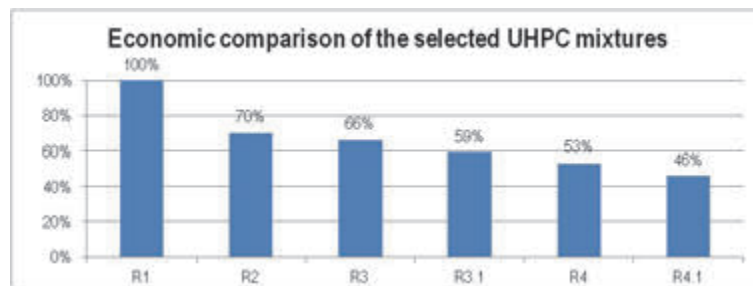


Fig. 1: Economic comparison of the mixtures

According to the newly published regulation of the Ministry of Transport, an impulse have arisen to find an alternative for common steel reinforcement bars. The regulation set up a request for concrete cover for ordinary steel rebars in similar dimensions of the railing panel. Thus, the research team needed to choose from either non-metallic or corrosion-proof rebars. Further on, the GFRP non-metallic rebars from a local manufacturer were used. Panels applying these rebars were tested too.

3.2 Shape optimization

The original shape of the panels on the beginning of the research (autumn 2014) was just a simple full plate. A set of plates with thickness of 13-20 mm in different colours were manufactured. These panels were mounted into a steel frames and loaded in the static tests. As they weren't able to bear the required load (ca. 1.75 kN) and were heavier then the criterion was set (<60 kg for a 2 m long panel, so that two workers can lift it), another shape was sought after.

In the next design, the panel was thicker (33 mm), but a set of polygonal openings were made in order to lighten the panel. This shape was checked during static and dynamic tests and the results were promising. Following changes of the shape were made to find the static, dynamic

and economic satisfactory minimal amount of UHPC. Thus, the panel with different thickness was made (54 mm on the longer edge, 24 mm in between them), see Fig. 2. This panel also performed well during the tests.



Fig. 2: UHPC panel with longitudinal reinforcement

4. STATIC AND DYNAMIC TESTS

Static and dynamic tests were performed according to the CEN/TR 1317-6 standard. The tests were just slightly modified to ease their execution in the Skanska a.s. premises.

4.1 Static tests

Static tests performed in 2016 and 2017 verified that the shape optimizing was justified. For comparison, two panels were made with common rebars (mixture R1 and R3). Another panel was made of R3.1 mixture with GFRP rebars. The mixture marked R4 has shown poor plasticity during casting and was later abandoned (so has the R4.1 mixture). The results from the mentioned tests are visible in Fig. 3. The panels were loaded with 2.50 kN (what represent about 140% of the required load according to the standard) and slowly unloaded. The deformations were kept for both loading and unloading.

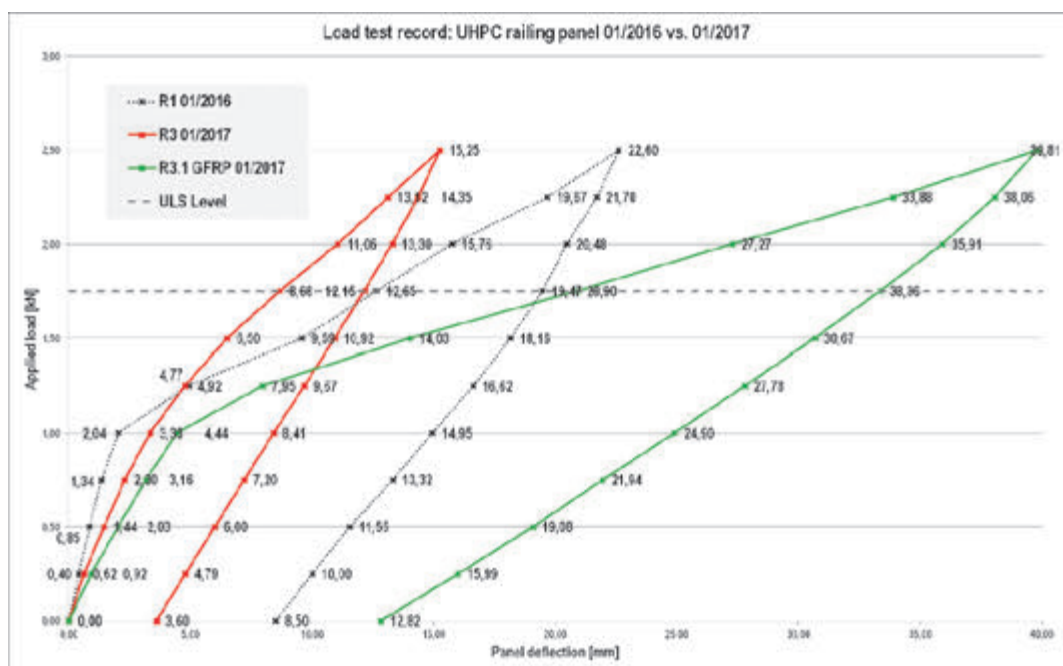


Fig. 3: Load test record

One may see from the results that all the panels passed the requirements for a static load tests. The panel with GFRP rebars showed higher total and plastic deflections. However, this does not affect its quality.

4.2 Dynamic tests

The dynamic test performed on the panels with longitudinal reinforcement also came out well (also according to TNI CEN/TR 1317-6: 50 kg soft body on a pendulum, energy 600 J). All the panels were undivided, although there were cracks visible across whole thickness (in the joint of the longitudinal reinforcement and vertical ribs). After the above mentioned optimizing, a set of panels were manufactured for a practical application on a renovation of a bridge in Sázava municipality. Their static, dynamic and other needed tests will be performed in the certified laboratory (TZÚS Brno) during the spring and summer 2017. Some of the tests are already performed and results may be found in chapter 6.

5. MANUFACTURING OF UHPC PANELS FOR PRACTICAL APPLICATION

In this year, an opportunity to use the UHPC railing panels for a renovation of a bridge in Sázava municipality. This will be already the second application in the Czech Republic of UHPC railing panels as the first application was built up in village of Čeperka (Tichý et al., 2016 & Tichý et al., 2017). The panels were also precast in the premises of the Bridge center of Skanska a.s. A new mixture was developed for this particular production (R3.1.1 – higher amount of plasticiser, part of the cement used was white in order to gain a lighter shade of the panels). A concrete mixer with planetary motion M125/4kW VP were used to mix the materials. The materials needed to be weighted with one-gram-accuracy. The fresh concrete was poured into buckets from the mixer and then smoothly poured into clean and oiled plywood forms. When the UHPC reached half of the height, the rebar mesh was put inside the form and then, the remaining fresh concrete was poured, see Fig. 4 and Fig. 5. Rebar mesh used for these panels was composite (metallic in the longitudinal reinforcements and GFRP in the vertical ribs).

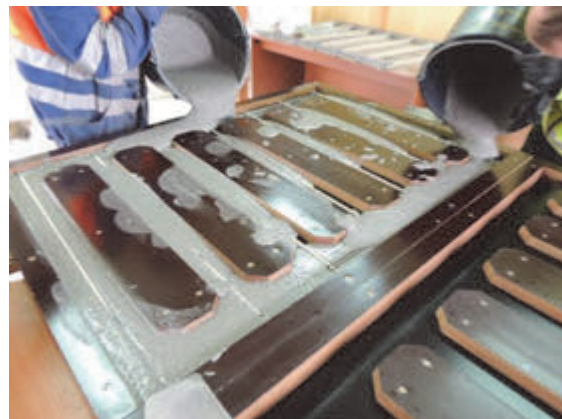


Fig. 4: Fresh UHPC poured into a bucket Fig. 5: Fresh UHPC poured into a form

6. RESULTS OF THE MATERIAL TESTS OF UHPC FOR SÁZAVA BRIDGE

The material tests were performed on prismatic (40x40x160 mm) and cube (150 mm) specimens. The specimens were sampled during the manufacture of the panels. The tests performed on prisms were informative and were used mainly to set up the unforming time.

During the first two castings, a set of cube specimens were also created in order to get results from a credited laboratory for following tests:

- compressive strength EN 12390-3 (1 day, 28 days)
- cubic density of the hardened concrete EN 12390-7
- water absorption capacity EN 14614-1
- freeze/thaw resistance and resistance to defrosting chemicals ČSN 73 1326, cycle A

The results are to be found in Tab. 1.

Tab. 1: Results of the R3.1.1 mixture material tests, cube specimens

Performed test		Unit	Results for mixture R3.1.1	
Compressive strength		<i>MPa</i>	1 day	28 days
			76.6	116.3
Cubic density		<i>kg/m³</i>	2360	2380
Water abs. capacity		<i>%</i>	0.89	
Freeze/thaw resistance	No. of cycles	<i>g/m²</i>		
	25		25.00	
	50		38.17	
	75		57.87	
	100		65.80	
	125		73.67	
	150		78.93	

7. RENOVATION OF THE BRIDGE IN SÁZAVA

The renovation of a bridge in Sázava was carried out by Silmex a.s. company, the railing was delivered by Skanska a.s. The renovation of a bridge from 1960 consists also of the replacement of the bridge deck. The damaged steel-concrete deck was demolished and new fibre-concrete deck was erected on its place (Fládr et al., 2015). Also, new side beams were casted and the railing was mounted on them. It consists of the UHPC panels and steel columns and handrail. Detailed view on the railing is presented in Fig. 6, while the comparison of the bridge before and after the renovation may be seen in Fig. 7.



Fig. 6: Detailed view on the UHPC railing panel on the bridge in Sázava

8. CONCLUSION

The UHPC railing panels is a modern alternative for an ordinary steel railing and it brings up couple of advantages, namely durability, high strength, no need of maintenance and last but not least an interesting aesthetic view. Its manufacture is a precise activity and it needs to keep take serious focus from the workers, this also applies for the erecting on site.

The bridge in Sázava municipality is a second practical application of these panels. Modern railing contributes to a good result of the bridge renovation.



Fig. 7: Comparison of the bridge in Sázava before / after the renovation

9. ACKNOWLEDGEMENTS

These results and experiences were gathered thanks to solving of grant project no. TE01020168 CESTI (Centre for effective and sustainable transport infrastructure), work package WP3 – Bridges – Effective structures with higher reliability and longer serviceability, with financial aid of Technology Agency of Czech Republic (TAČR).

10. REFERENCES

- Fládr, J., Bílý, P., Ryjáček, P. and Vodička, J. (2015), “Development of special fibre-reinforced concrete for exposed concrete pavements on bridges”, Proceedings of the International conference FIBRE CONCRETE, January 2015, pp.141-148.
- Kalný, V., Kvasnička, J., Komanec, J., Vítek, J. L., Brož, P. and Koukolík, P. (2015), “Cable-Stayed Footbridge with UHPC Segmental Deck”, Key Engineering Materials, Vols. 629-630, pp. 64-70, October 2015.
- Tichý, J., Kolísko, J., Kalný, M. and Huňka, P. (2012), “First Practical Implementation of UHPC in Czech Republic”, 8th CCC Durability of Concrete Structures Plitvice Lakes 2012 – Proceedings, 2012.
- Tichý, J., Kolísko, J., Trefil, V. and Huňka P. (2014), “Production of Thin-walled Facade Panels of White UHPC with reinforcement membrane (in Czech)”, 12th Conference Technology of Concrete – Jihlava, 2014.
- Tichý, J., et al. (2016) “UHPC Footbridge over the Opatovický Canal“, Solid State Phenomena, Vol. 249, April 2016, pp. 320-324.
- Tichý, J., Čítek, D., Slánský, B. and Ševčík, S. (2017), “Long-Term Monitoring of a UHPC Footbridge”, Solid State Phenomena, Vol. 259, May 2017, pp. 119-124.
- TNI CEN/TR 1317-6 (2012), “Road restraint systems – pedestrian restraint system – Part 6: Pedestrian Parapet”, November 2012.

CHARACTERIZATION OF OLD/REPAIRING STRUCTURAL CONCRETE THROUGH MECHANICAL FRACTURE PARAMETERS

*Hana Šimonová, Petr Daněk, Petr Frantík, Martin Sedlmajer, Zbyněk Keršner
Brno University of Technology, Faculty of Civil Engineering
Veveří 331/95, 602 00 Brno, Czech Republic*

SUMMARY

Structural concrete of the building of Vítkovice railway station from 1970s and repairing concrete are characterized via mechanical fracture parameters. Together twelve core-drilled cylindrical specimens with diameter of 75 mm were provided by a Chevron type notch of depth of 12 mm. Three-point bending fracture tests were conducted on these specimens supported as beams with the span of 170/180 mm. Load vs. deflection and load vs. crack mouth opening displacement diagrams were recorded from which modulus of elasticity (E), fracture toughness (K_{Ic}) and fracture energy (G_F) were determined using linear elastic fracture mechanics approach and work-of-fracture method. Mean values (coefficient of variation) of these parameters for old/repairing concrete were obtained as follows: $E = 39.4/39.9$ GPa (29/15 %), $K_{Ic} = 0.90/1.38$ MPa·m^{1/2} (19/13 %), $G_F = 174.0/116.4$ J/m² (26/19 %).

1. INTRODUCTION

Among the most frequently used building materials one can primarily name silicate-based, particularly cement-based composites (Neville, 2011). Thanks to their character and to the production technology, these materials are very adaptable and utilizable for a wide range of applications. Thus, from the perspective of the modern construction concepts of the last almost two centuries, concrete can be definitely regarded as a traditional material. Many reinforced concrete buildings are, therefore, already designated as cultural monuments, several ones also in the Czech Republic. Within the project “Analysis and presentation of the values of modern architecture of the 1960s and 1970s as part of the national and cultural identity of the Czech Republic” a particular attention is paid to diagnostics of selected reinforced concrete structures and heritage procedures for restoration of building cores. In this paper, structural concrete of the building of Vítkovice railway station from 1970s (Šimonová et al., 2016) as well as new repairing concrete are characterized using standard fracture test and described via parameters of selected relevant mechanical fracture models. These parameters are important indicators of the material behaviour, although common contemporary engineering practise is usually limited to elastic and strength characteristics only which can be derived from ‘simple’ compressive tests. However, the material brittleness vs. ductility can’t be expressed by these classical parameters and thus characteristics describing the resistance of the material against the crack propagation are becoming important for many types of analyses and assessments of the structures nowadays. The main objective of this paper is to compare the values of these parameters of old and new repairing concrete.

2. SPECIMENS

An analysis of old concrete was first carried out on parts of the samples taken from the structure. The composition of old concrete was found and new concrete test specimens were

produced to determine the concrete properties observed. The effort was to produce concrete comparable to those originally used to respect the original design material.

2.1 Old structural concrete

Six cylindrical specimens were obtained as cores drilled out from the above mentioned building. These samples were geometrically adjusted to create regular beam-shaped specimens with circular cross-section and then provided by the Chevron type notch. Tab. 1 introduces specimen dimensions used in further calculations. The test configuration and meaning of individual dimensions can be found e.g. in (Šimonová et al., 2016). Note, this shape of specimen and notch type is typically used for determination of mechanical fracture properties of rocks – see Ouchterlony (1988), Backers (2004), Vavro (2014).

Tab. 1: Dimensions of old concrete tested cylindrical specimens

	Symbol	Unit	Specimen ID					
			V7	V9	V13	V15	V17	V18
Diameter	D	mm	74.09	74.16	74.97	75.05	74.99	74.68
Length	L	mm	215	237	211	224	196	194
Notch tip depth	a_0	mm	11.28	11.46	11.98	11.77	11.94	12.55
Notch depth	h_0	mm	18.54	18.59	19.00	19.30	18.90	19.12
Ligament	A_{lig}	mm ²	2743	2749	2791	2751	2807	2763

2.2 Repairing structural concrete

During the development of new concrete, the raw materials used were respected. By analyzing the old concrete, the amount of cement and aggregate contained in concrete was determined. The aggregate was separated and the amount was determined by dividing it into individual grain sizes. Also, the location and type of aggregate used was determined. Based on this knowledge, the composition of repairing concrete was based on the original composition of the concrete. The new concrete had the composition listed in Tab. 2.

Tab. 2: Composition of the new concrete mixture

	Unit	Amount
Ordinary Portland cement CEM I 42,5 R	kg	350
Aggregate grain size 0/4 mm	kg	810
Aggregate grain size 4/8 mm	kg	230
Aggregate grain size 8/16 mm	kg	790
Water	kg	170
Plasticizer based lignosulfonates	kg	3.15

For concrete from the period around 1960, simple lignosulfonate based plasticizers were used. Three fractions of aggregate were used: sand, fine gravel and coarse gravel. The problem is in cement, which varies considerably compared to the currently used cement. Today, the cement is very finely ground, previously a larger grain cement has been used, and the hydration of individual grains has gone very slowly over a longer period of time. Today's cements are very reactive and have a great fineness of milling, and a milling intensifier is used to obtain a high level of fineness. There is a different degree of hydration. The design of the new concrete was based on compressive strength and for old concrete was compressive strength about 38 MPa. The new concrete had a compressive strength of 38 MPa after 28 days of ripening and after 60 days of aging the compressive strength was 42 MPa.

Six cylindrical specimens for fracture tests were obtained as cores drilled out from beams of nominal dimensions $100 \times 100 \times 200$ mm. These samples were provided by the Chevron type notch. Tab. 3 introduces specimen dimensions.

Tab. 3: Dimensions of repairing concrete tested cylindrical specimens

	Symbol	Unit	Specimen ID					
			T4 A	T4 B	T5 A	T5 B	T6 A	T6 B
Diameter	D	mm	75.12	75.14	75.20	75.08	75.08	75.05
Length	L	mm	199	199	201	197	198	199
Notch tip depth	a_0	mm	11.46	10.14	10.97	10.28	10.88	10.90
Notch depth	h_0	mm	17.96	18.18	17.88	18.06	18.06	18.03
Ligament	$A_{l_{ig}}$	mm ²	2939	2874	2944	2887	2904	2905

Three reference beam specimens for fracture tests were also prepared with nominal dimensions $100 \times 100 \times 400$ mm – see Tab. 4 for details.

Tab. 4: Repairing concrete tested beam specimens with central edge notch

	Symbol	Unit	Specimen ID		
			T7	T8	T9
Width	W	mm	100.6	100.5	100.7
Breadth	B	mm	99.1	99.7	100.3
Length	L	mm	399.7	399.8	399.0
Notch depth	a_0	mm	32.8	32.7	33.0
Notch to width ratio	a_0/W	–	0.327	0.325	0.328
Weight	m	kg	8.895	9.149	9.120
Density	γ	kg/m ³	2240	2280	2280

3. FRACTURE TESTS

The mechanical fracture parameters of concrete (Karihaloo, 1995; Veselý and Frantík 2014) were determined from experiments on specimens in three-point bending test configurations. Specimens were loaded under displacement control; therefore, it was possible to record the load vs. displacement and also the load vs. crack mouth opening displacement curves ($F-d$ and $F-CMOD$ diagrams) during the course of the test. The load span was set to 170/180 mm in case of cylindrical specimens and 300 mm in case of prismatic beams. The initial Chevron type/edge notch was made before testing with a diamond blade saw. The fracture tests were carried out using a Heckert FPZ 100/1 testing machine with measuring range of 0–10 kN; the speed of the induced displacement of the upper support was equal to 0.02 mm/min. Selected illustrative pictures are shown in Fig. 1.

The *GTDiPS* software (Frantík and Mašek, 2015) was used to correct the raw recorded $F-d$ and $F-CMOD$ diagrams which essentially represent data points registered by the acquisition system at the same time. The correction consisted of elimination of duplicated data points and substantial reduction of the number of the recorded data points). A selected section of the ascending part of each individual diagram (a linear portion of the steady elastic response) was used for its approximation using a linear regression function. Subsequently, the point of intersection of this straight line with the horizontal axis was determined and denoted as the beginning of the loading; then all points on the diagram were shifted by the same distance so that the point of intersection of the straight line belonged to the origin of the coordinate system. Similarly, the next data modification is motivated by the nature of the experimental

system. The configuration of the used experimental system may result in a sudden event, which does not satisfy the requirements of a quasi-static test progress/measurement. During the performed transformations, the violation of such requirements was detected by analyzing the point sequences in time domain which resulted in removing the unsuitable points (the snap-down phenomenon). Then, the resulting gaps in the data sequences were filled with new points generated using an interpolation (gap filling) method based on polynomial approximation.

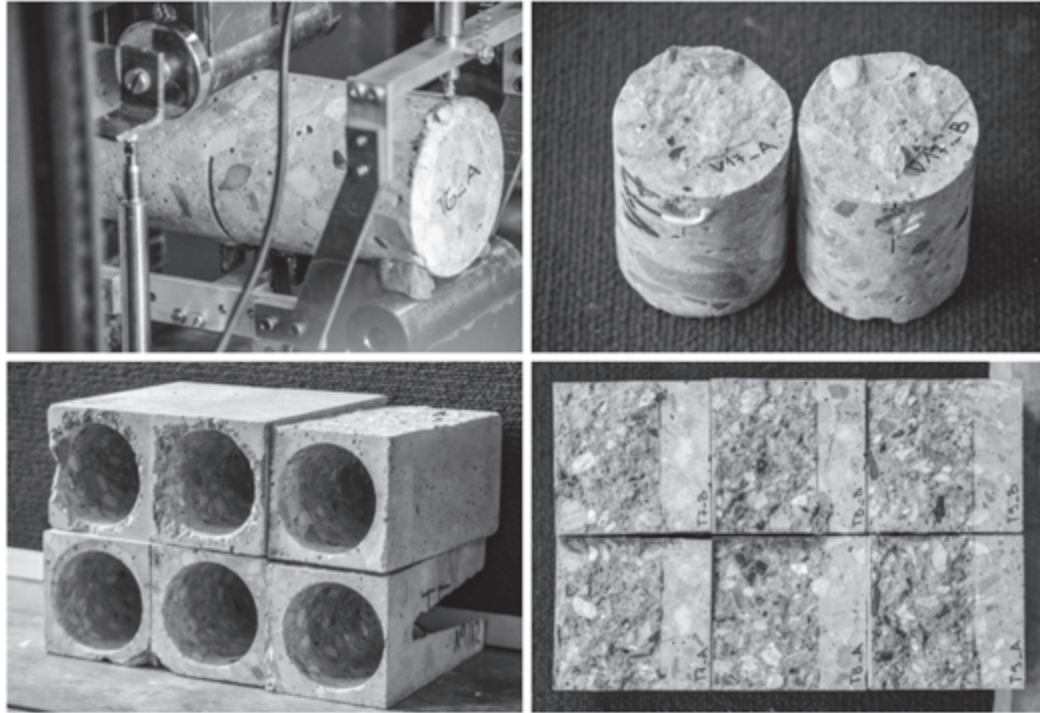


Fig. 1: Illustration related to old/repairing concrete specimens with central Chevron type/edge notch and fracture test

4. METHODS

The mechanical fracture parameters of concrete are calculated from corrected F - $CMOD$ and F - d diagrams using academic software *CheF* (Koryčanská et al., 2017). The first, almost linear part of the F - $CMOD$ diagram (determined by a selected point with values F_i , $CMOD_i$) is used to estimate modulus of elasticity (E) value with help of geometrical factor g_0 (Backers, 2004):

$$E = g_0 \cdot \frac{F_i}{CMOD_i} \cdot \frac{1}{D}, \quad g_0 = 20.8 - 19.4 \cdot \frac{a_0}{D} + 142.3 \cdot \left(\frac{a_0}{D}\right)^2 \quad (1)$$

Afterwards, maximal load F_{\max} is used for fracture toughness K_{Ic} assessment with help of geometrical factor A_{\min} (Ouchterlony, 1988) and span length S :

$$K_{Ic} = A_{\min} \cdot \frac{F_{\max}}{D^{1.5}}, \quad A_{\min} = \frac{S}{D} \cdot \left[1.835 + 7.15 \cdot \frac{a_0}{D} + 9.85 \cdot \left(\frac{a_0}{D}\right)^2 \right] \quad (2)$$

The toughness G_{Ic} is then calculated as follows:

$$G_{Ic} = \frac{(K_{Ic})^2}{E} \quad (3)$$

The work of fracture value W_F , and then the specific fracture energy G_F value, is assessed from the complete $F-d$ diagrams (RILEM TC-50 FMC Recommendation, 1985):

$$W_F = \int F(d)dd, G_F = \frac{W_F}{A_{lig}} \quad (4)$$

Mechanical fracture parameters of concrete of prismatic beams are calculated in similar way using effective crack model (Karihaloo, 1995); academic software *StiCrack* (Stibor, 2004) was used.

5. RESULTS

All mechanical fracture properties (modulus of elasticity, effective fracture toughness, effective toughness, and specific fracture energy) of old/repairing concrete evaluated using Eq. (1) to (5) are summarized in Tab. 5 – results obtained for each specimen and corresponding basic statistics, i.e. mean values and coefficients of variation, are shown.

Tab. 5: Mechanical fracture parameters of concrete of each tested cylindrical specimen: mean values (coefficient of variation in %)

		Specimen							
	Symbol	Unit	V7	V9	V13	V15	V17	V18	Mean (CoV)
Old concrete	E	GPa	57.6	30.2	43.7	29.2	30.3	45.3	39.4 (29.1)
	K_{Ic}	MPa·m ^{1/2}	1.15	0.92	0.79	0.73	0.79	1.06	0.90 (18.5)
	G_{Ic}	J/m ²	22.8	28.0	14.4	18.0	20.4	24.8	21.4 (22.8)
	G_F	J/m ²	224.9	211.3	169.8	149.7	100.1	187.9	174.0 (26.0)
			T4 A	T4 B	T5 A	T5 B	T6 A	T6 B	
New concrete	E	GPa	37.4	30.6	37.9	43.4	42.4	47.5	39.9 (14.7)
	K_{Ic}	MPa·m ^{1/2}	1.21	1.24	1.25	1.47	1.59	1.56	1.38 (12.5)
	G_{Ic}	J/m ²	39.2	49.9	41.0	49.5	59.3	51.3	48.4 (15.1)
	G_F	J/m ²	91.9	114.8	91.7	124.7	148.1	127.4	116.4 (18.8)

Tab. 6: Mechanical fracture parameters of concrete of tested beam specimens: mean values (coefficient of variation in %)

		Specimens				
	Symbol	Unit	T7	T8	T9	Mean (CoV)
New concrete	E	GPa	32.0	28.7	26.2	28.9 (10.0)
	K_{Ic}	MPa·m ^{1/2}	1.35	1.44	1.62	1.47 (9.5)
	G_{Ic}	J/m ²	57.0	72.2	100.7	76.6 (18.1)
	G_F	J/m ²	260.4	213.5	–	237.0 (14.0)

6. CONCLUSIONS

Structural concrete of the building of Vítkovice railway station from 1970s and new repairing concrete are characterized via mechanical fracture parameters. Three-point bending fracture tests were conducted on specimens with Chevron type/edge notch tip. Load vs. deflection and vs. crack mouth opening displacement diagrams were recorded, corrected and processed using linear elastic fracture mechanics approach and work-of-fracture method. Parameters describing the materials ability to resist the deformation and failure propagation, i.e. modulus of elasticity, fracture toughness, toughness and fracture energy were estimated. Comparable results were obtained for old and repairing concrete from point of view fracture parameters

and almost identical in case of modulus of elasticity. Variability of the determined parameter values was also comparable for both materials – it was between 13 to almost 30 %. Comparison of the results from the tests of specimens of different cross-sections and notch types shown that in the case of a Chevron type notch, the modulus of elasticity was evidently overestimated, whereas the fracture toughness and fracture energy values were underestimated.

7. ACKNOWLEDGEMENTS

This outcome has been achieved with the financial support of the Czech Science Foundation, project No. 16-18702S (AMIRI), and supported by the Ministry of Education, Youth and Sports of the Czech Republic under the “National Sustainability Programme I” (project No. LO1408 AdMaS UP). Thanks are also expressed to colleagues from Brno University of Technology, Faculty of Civil Engineering, Tomáš Vymazal and Petr Cikrle for obtaining and adjustment of the drilled cores, as well as to Miroslav Friedl (ditto) for careful preparation of specimens to tests.

8. REFERENCES

- Backers, T. (2004), “Fracture toughness determination and micromechanics of rock under mode I and mode II loading”, dissertation, University of Potsdam.
- Frantík, P. and Mašek, J. (2015), “GTDiPS software”, <http://gtdips.kitnarf.cz/>.
- Karihaloo, B. L. (1995), “Fracture Mechanics and Structural Concrete”, Longman Scientific & Technical, New York.
- Koryčanská, B., Šimonová, H. and Keršner, Z. (2017), “Software support of fracture test evaluation of cylindrical specimens with Chevron type notch”, Proceedings JUNIORSTAV 2017, Brno: Brno University of Technology, Faculty of Civil Engineering, pp. 1–6. In Czech.
- Nevile, A. M. (2011), “Properties of Concrete”, Pearson Education Limited, Harlow.
- Ouchterlony, F. (1988), “Suggested methods for determining the fracture toughness of rock”, International Journal of Rock Mechanics and Mining Sciences and Geomechanics Abstracts, Vol. 25, 1988, pp. 71–96.
- RILEM TC-50 FMC Recommendation (1985), “Determination of the fracture energy of mortar and concrete by means of three-point bend test on notched beams”, Materials & Structures, Vol. 18, 1985, pp. 285–290.
- Stibor, M. (2004), „Fracture Parameters of Quasi-Brittle Materials and Their Determination”, dissertation, Brno University of Technology. In Czech.
- Šimonová, H., Daněk, P., Frantík, P., Keršner, Z. and Veselý, V. (2016), “Tentative Characterization of Old Structural Concrete through Mechanical Fracture Parameters”, Procedia Engineering: Structural and Physical Aspects of Construction Engineering, Netherlands: Elsevier, pp. 414–418.
- Vavro, L. (2014), “Fracture toughness of rock and its determination for geomechanical evaluation of rock and rock mass”, dissertation, VŠB–Technical University of Ostrava. In Czech.
- Veselý, V. and Frantík, P. (2014), “An application for the fracture characterisation of quasi-brittle materials taking into account fracture process zone influence”, Advances in Engineering Software, Vol. 72, 2014, pp. 66–76.

EXPERIMENTAL PRESTRESSED SHELL BY WACLAW ZALEWSKI

Waldemar Bober

University Professor at the Faculty of Architecture

Wroclaw University of Science and Technology

Wroclaw, Poland

waldemar.bober@pwr.edu.pl

SUMMARY

In the 1965 Waclaw Zalewski (1917-2016) designed an experimental structure consisting of compressed concrete shell hung on a hexagonal system of steel arches. Since at that time advance research tools were unavailable, the structure, considerably complicated from the static and technological point of view, had to be built in an experimental manner, based entirely on conceptual assumptions of Zalewski. Dynamic technical research accompanying the process of erecting the construction may be perceived as an early stage of the so called “form finding” - recently developing movement, which places the form of structures in the centre of interest. In the following consideration the technology and technical premises of the structure are going to be analysed. In the absence of documentation the author establish the present report on the information obtained directly from Waclaw Zalewski and on archival photographs made available by the designer.



Fig. 1: View on the experimental shell by W. Zalewski

1. THE TOPOGRAPHY

The experimental structure designed by Waclaw Zalewski at the University of Merida (Venezuela) drew significantly on the research models by Honoracio Caminos, devised as rubber membranes stretched over an artificial ring and upthrust by different configurations of internal support system distorting the flat rubber membrane.

Inspired by these shapes, Waclaw Zalewski proposed to cover an exposition space at the University campus by a structure of a circular projection 36 m in diameter. According to the design the shell was supported by a system of six steel arches forming a regular hexagon. The external perimeter ring was situated 3 m above the ground level. In order to remove the ring away from the support arches in the lines of their topmost point, a circle in the horizontal projection was deformed by a system of six arches ending in the circle line, whose radius was smaller than the circle.

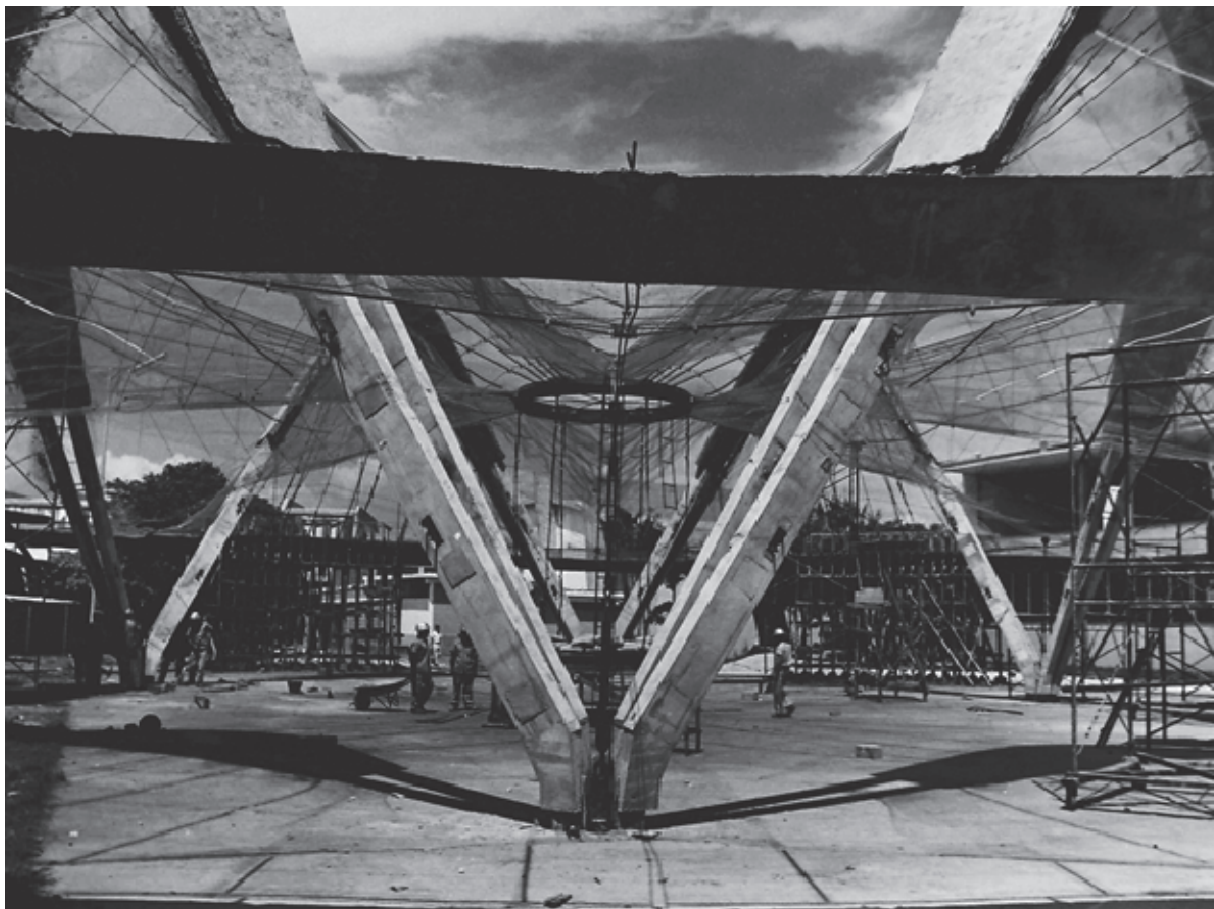


Fig. 2: Supporting on steel arches

The external ring lacked any secondary support and was elevated in its entirety to the sling system of the hanging shell. The internal ring was designed in the circular projection of approx. 3 m in diameter. The load bearing slings of the shell were attached to the rim of this ring. The shape of the shell was adjusted to the sling system attached to the hexagon framed by the steel arches connecting the two rings: the external and internal.

In order to balance the internal ring, the breaklines between the rings of the shell were run along the diagonals of the hexagon, so that rainwater could flow down the breaklines.

The upper parts of the steel arches in the hexagonal system served at the same time as the breaking edge of the hang slings. Sectional roofing bent parallel to the curvature of the arches was added in order to shield this edge from the atmospheric conditions. The lower sections of the steel arches projecting in an open space beneath the surface of the shell formed a hexagonal system of V-shaped columns supported in the corners of the hexagon. The arches of the hexagonal system were constructed from two bifurcating steel arches connected by steel elements assembled in a truss system. From the outside the structure formed a hanging shell, flowing down from the upper sections of the six arches towards the internal and external ring. The spacing between the load bearing slings influenced the shape of the shell, which was not continuous in terms of bicurvature of geometrical surface, but flattened between the lines of load-bearing slings.

2. STRUCTURAL SYSTEM

Concrete blocks situated in support points of the steel arches in the apexes of the hexagon served as the foundations of the experimental structure. While the horizontal forces of support reactions between the adjacent arches were to a large extent counterbalanced, only the vertical component of this reaction force needed to be transferred to the ground. Parabolic arches in the hexagonal system were double arches composed of C-shaped steel profiles. The parabolic shape was also rendered by the straight sections of steel beams welded together. The middle walls of C-profiles were situated on the external surface of the arches. The arches bifurcating upwards were connected by a spatial truss of steel bars, on whose lower rim the load-bearing slings were hung. The points of sling attachment were adjusted to the nodes of the truss structure. The roofing of the upper section of the steel arches was made by laying out concrete on the truss branches of the arches supplemented by a margin placed outside of the arches. The external perimetral ring of the shell was made as a concrete trough. The sections of the ring between the steel arches were prefabricated. The sections facing the arches were cast in situ.

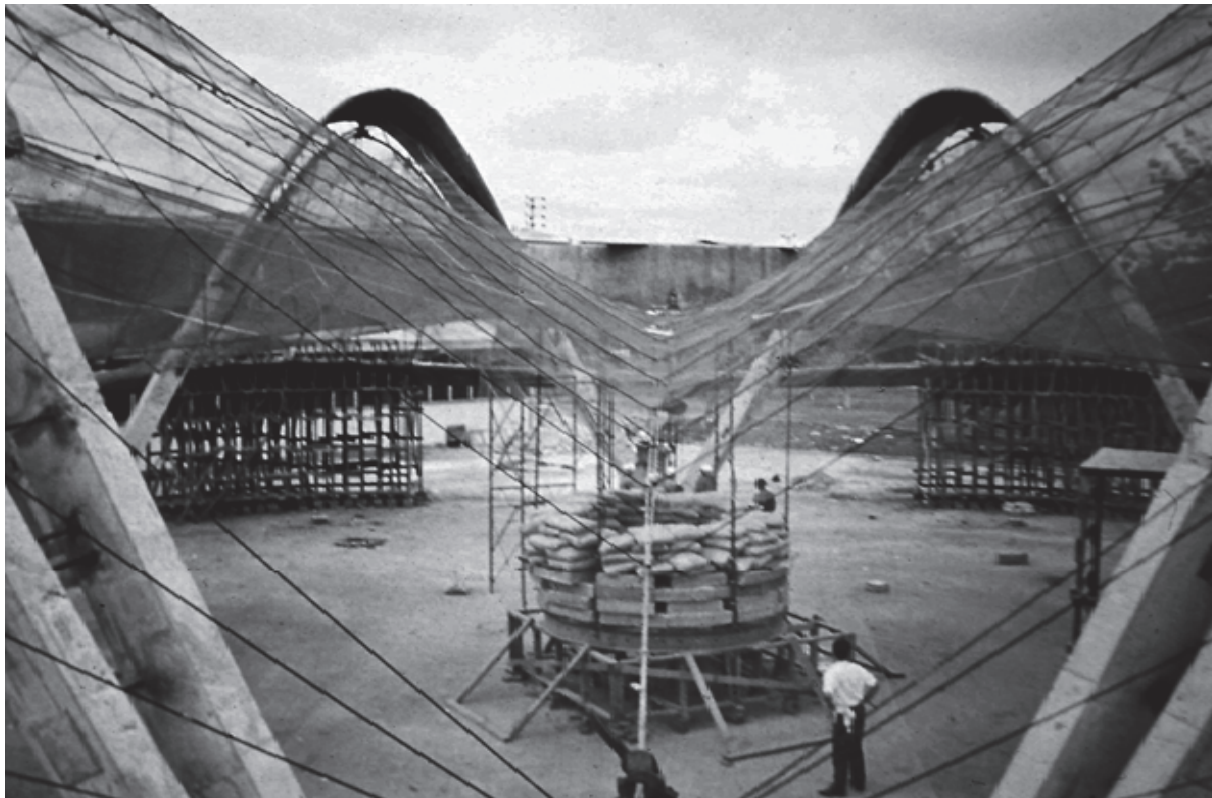


Fig. 3: Configuration of cable net

Steel load-bearing slings of a profile diameter of approx. 4cm were hung with an initial bent against the string length of the overhang. While the adopted length of a bent vertically measured inside the structure was 1m long, for the internal bent of the sling 0,75m was assumed.

Spanning slings were placed perpendicularly to the load-bearing slings, forming fields of linear system resembling regular quadrangles. In the system of slings, it was possible to distinguish radial directions convergent to the middle ring of the shell. The connectors of the obtained sling mesh were made with the help of steel clamps joined together by screws. In order to position the concrete shell, a steel mesh of small openings was unfolded on the sling system. Since the concrete mass had been hand-laid, its layer varied in terms of thickness on each of its sections. A crucial role in preserving the form of the structure was played by dynamic changes of weight of both the external and internal perimetral ring, which helped to maintain a force balance in the whole structure. After concrete had solidified, the shell functioned as a rigid load-bearing surface. Bicurvate form of the shell had a positive influence on the compensation of deformations caused by wind-load or thermal load resulting from insolation of the external surface. The influence of insolation was minimized by covering the shell with silver paint.

3. ADOPTED TECHNOLOGIES

The roofing structure was executed by a renovation group of the University in Merida. The elements of the structure were made with the use of locally available materials, such as steel beams, steel slings, steel meshes and concrete obtained from fine-grained gravel. Elements of the arches were connected by welding. The arches tapering towards the support in joints were balanced in the hexagonal position with the help of the sling system. The external ring was partly prefabricated as a concrete trough of variable cross-section. The ring lying opposite the arches was made as a monolithic structure, unfolded on wooden boarding. In order to maintain a tension of the load-bearing slings during concreting the shell, the internal ring was additionally loaded with sand sacks until the internal part of the shell was made. The shape of the shell was corrected by relieving the load from the slings with hand-winches affixed to the steel arches. Concreting the shell was executed by hand-laying of consecutive layers of concrete, beginning with the perimeter ring of the shell. Suitable tension of the load-bearing slings was continuously corrected by increasing the degree of concreting in the trough of the internal ring. The long-lasting process of hand-concreting was performed without any technological breaks, which helped to obtain a monolithic concrete shell.

4. THE USE OF THE STRUCTURE

The experimental structure of hanging shell was executed in order to cover a space used by the university students for work on models. The covering shielded the space from atmospheric conditions, especially from intense insolation typical of this geographical zone. Unfortunately, during the few years of its use, the technical condition of the structure was not examined. According to the statement of Waclaw Zalewski no cracking or delamination on the concrete shell was noted. It should be stressed that in the subtropical climate the structure was not exposed to the destructive effect of freezing and defrosting or snow load. Due to the changes in the investment plans of the University after a few years of usage the structure was disassembled. Apart from photographic material, neither technical nor research documentation of this original structure was preserved.



Fig. 4: Outside balancing ring

5. CONCLUSIONS FROM THE EXPERIMENT

The experimental structure was one of the first hanging concrete shells ever executed. The spatial bicurvate shape of the shell was obtained in accordance with a logical application of static qualities of steel arches characterised by complex diametral profile. Introducing an active counterbalancing of the shell load to the structural system was an innovative solution, both in terms of form and technology. The correctness of theoretical assumptions adopted in the design phase was confirmed by the period of safe usage. Such a structure could be employed in the public spaces as a cover of expositional objects. Further research on structures of similar kind is planned. Modern technologies employing compressed reinforced concrete or 3D concrete printing could be adopted in the execution of such structures. To this end material research on new concrete formulas is being conducted.

6. RECONSTRUCTION OF THE STRUCTURE

In order to carry out detailed research on the structure of the article, it is designed to reconstruct the shape of the structure using modern technology. It is planned to use the reconstructed construction as an auditorium named prof. Waclaw Zalewski. Reinforced concrete is expected to be made as a compressed material on rope nets. The surface coverage of the nets will be made using a special thin-layer printing of concrete laid automatically by means of mechanical devices designed for this purpose. The addition of the outer cylinder will be made of glazed curtain walls.

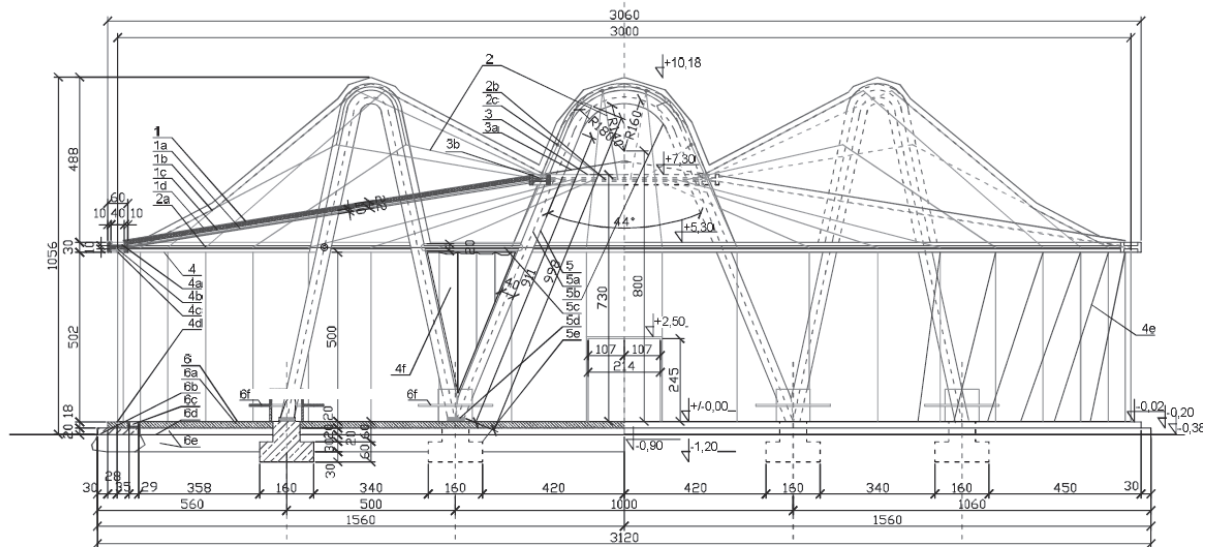


Fig. 5: Cross section of the structure

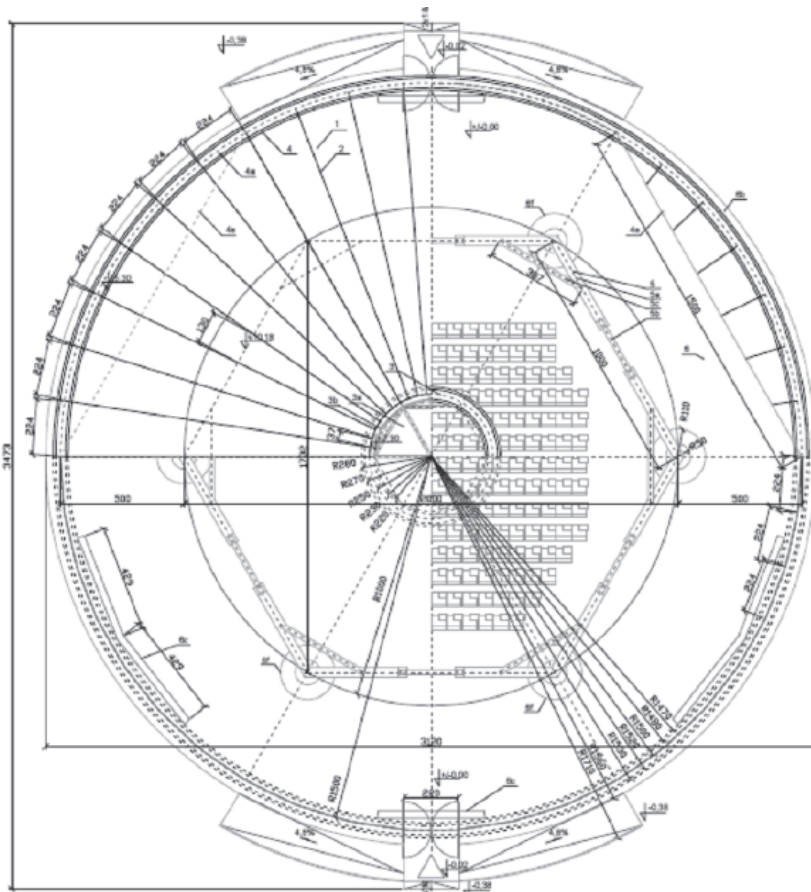


Fig. 6: Perspective view of the plane

7. REFERENCES

Archives of prof. Wacław Zalewski, Boston, 2015
 R. Castellano, students workshop MIT, 1972

SPECTACULAR STRUCTURE IN AN ECONOMICAL WAY

Zoltán Teiter

UVATERV Zrt. / Széchenyi István University

H-1537 Budapest 114. Pf. 453/421 / H-9026 Győr, Egyetem tér 1.

SUMMARY

This paper is to present how a proposal for a Hungarian river bridge is forming from the first idea until the approval design in the case of a given project. The main aspects taking into consideration while deciding, and the circumstances like the flow and the back up of water; the alignments of the linear infrastructure; how the views of the existing bridges of the river effect the selection of the bridge type are discussed. The visualizations of several bridges that would be possible to build are shown detailing their advantages and drawbacks. The economies of the probable superstructures are also dealt with, analyzing not only their construction but also their maintenance costs. Thereafter it is reasoned why that bridge was chosen for designing further on, and some details of the drawings are presented that are already parts of the approval design of the future bridge.

1. INITIAL DATA

1.1 Call for tender

The National Infrastructure Development Plc. had given an order to the ÚT-TESZT Ltd. to make the approval design of the motorway M44 between the town Kecskemét and the village Tizsakürt. The road would cross Tisza, the second largest river of the country flowing from upper eastern to the middle southern part of Hungary. This demands a new bridge that is under design at UVATERV Ltd.. This company has a great experience on designing river bridges (Kovacs et al., 2008), especially with composite superstructures (Teiter, 2008, 2015). Till this time study and approval design phases has been finished (Teiter, 2016).

1.2 Design conditions

The task of the bridge designers was to lead the 2×2 main lanes of the cross-section of the motorway (Fig. 1) over the river. Design speed was 110 km/h. The application of additional paths (e.g. cycle tracks) to the bridge superstructure was under consideration.

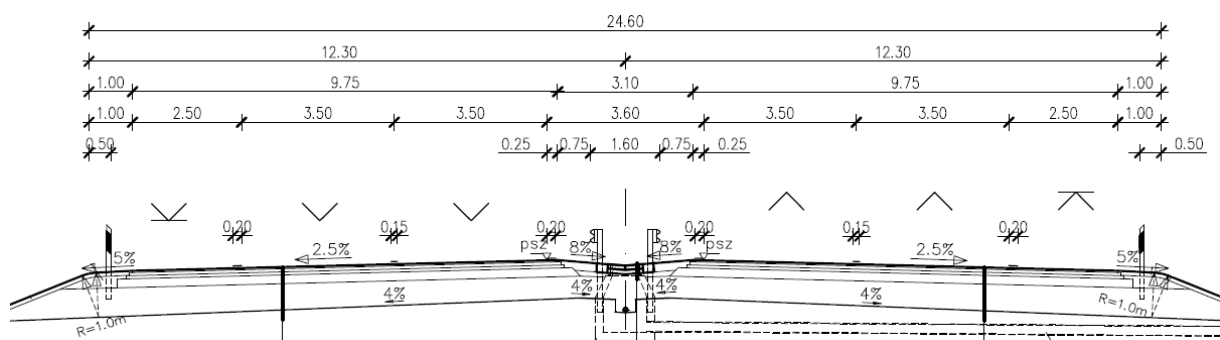


Fig. 1: Typical cross-section of the motorway

The horizontal alignment of the road was favourable, because on both sides of the river it had a curve so the future bridge could be recognized quite well when someone is getting closer to the river (Fig. 2). The top of the vertical alignment situated in the middle of the main span.



Fig. 2: Horizontal alignment of the motorway at crossing the river

The local water authority provided the data of the river (governing water levels, section of the river bed etc.). They specified that the piers of the river bed could not be in the mean water level and the abutment could not be on the inner side of the embankment. To verify the number and the distances of the substructures of the designed bridge there was a need to simulate the back up of water caused by the piers intended to place within the flood area. For this purpose a 2D model was applied. In Fig. 3 it can be seen that river Tisza has two narrow curves above the bridge (flowing direction is from up to down). Flood area is the networked one and the greenish-bluish thick line stands for the river bed.

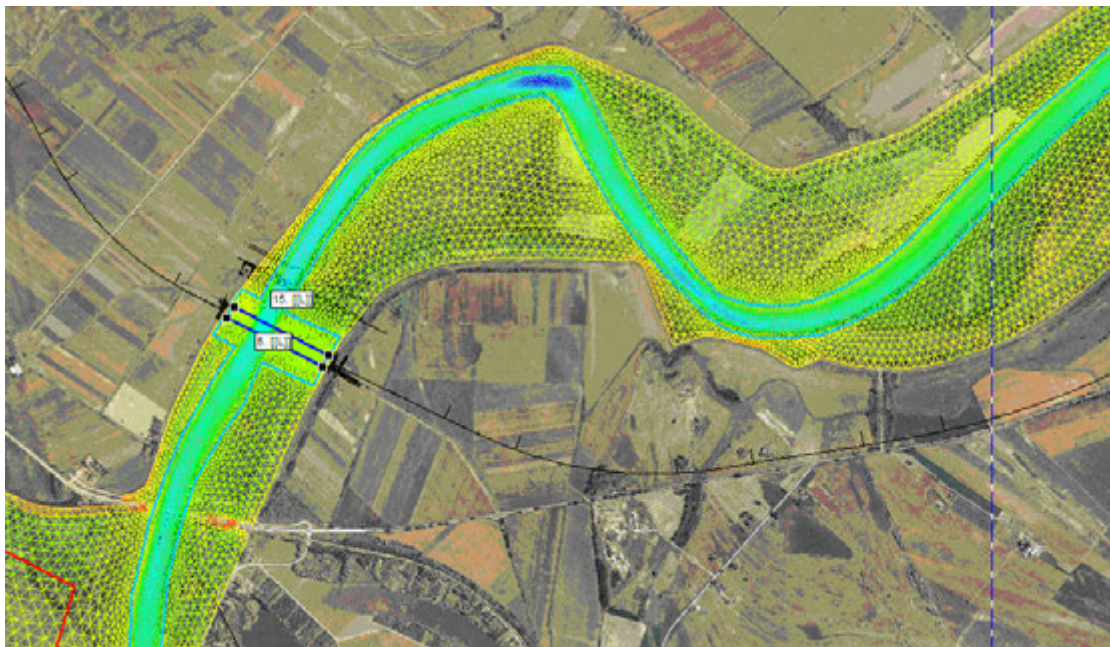


Fig. 3: 2D model simulation of the flowing of water

The most important prescription was given by the environmental authority. They limited the pier distances to a minimum of 50 m in the flood area with no reason (Fig. 4). This made the

usage of regular PPC girders almost impossible as the longest Hungarian ones are for 44.0 m span. To keep the possibility of the comparison of different structure types the pier cap beams were widened to be able to hold the longest girders. Thus the spans were taken as fixed 50 m.

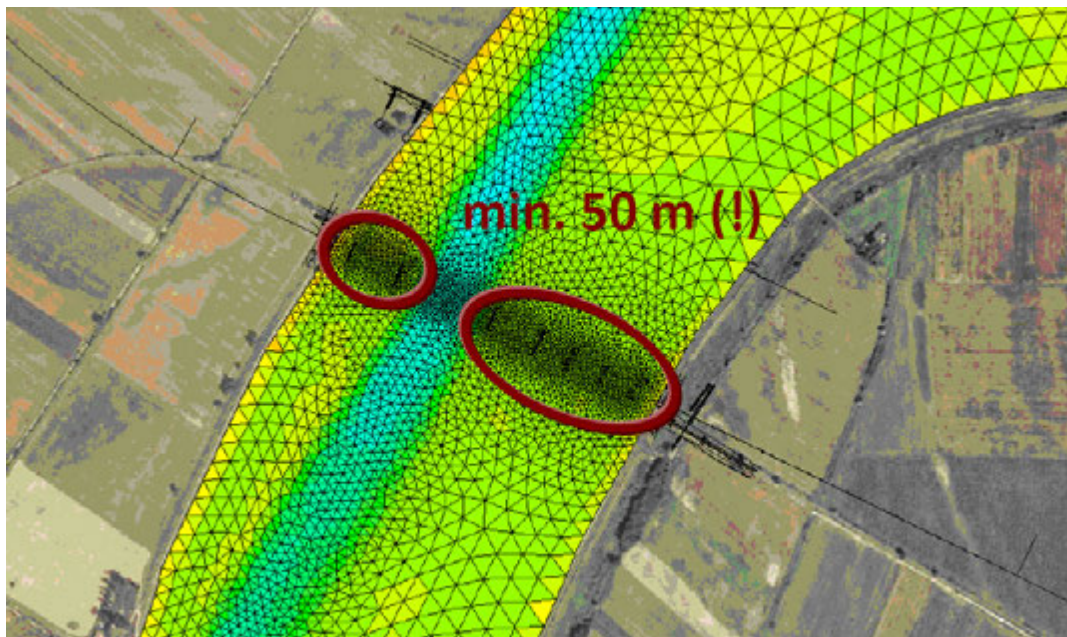


Fig. 4: The restriction for the minimum span in the flood area

1.3 Review of the existing bridges on the river Tisza

Looking for ideas and to be informed, we reviewed all the Hungarian bridges over Tisza. We could also see if there were any trends regarding their types, form etc. There were 26 bridges, most of them were beam structures with truss or opened, haunched, plated web, steel main girders. There were some exceptions: a steel arched footbridge at the town Szolnok and an extradosed prestressed concrete road bridge with corrugated steel webs (Fig. 5)



Fig. 5: The most unique bridges over the river Tisza

Finally the conclusion was that if any kind of bridge being different from a single beam bridge had been built that would not have followed the tradition, which was not a need anyway. According to the call for tender the investor would have seen a bridge here, which is a notable structure and has some sort of attraction for the people happened to be nearby. Our decision was to find a superstructure which is interesting and able to call the attention but it is not difficult to construct and economical. To get closer to the solution we made a study.

2. STUDY VARIANTS

2.1 Bridge types

By the rules of the contract there had to be at least three worked out variants. We made five variants (v1-v5 of Fig. 6). For the request of the involved experts and the future operator we added three more bridges (v6-v9 of Fig. 6).

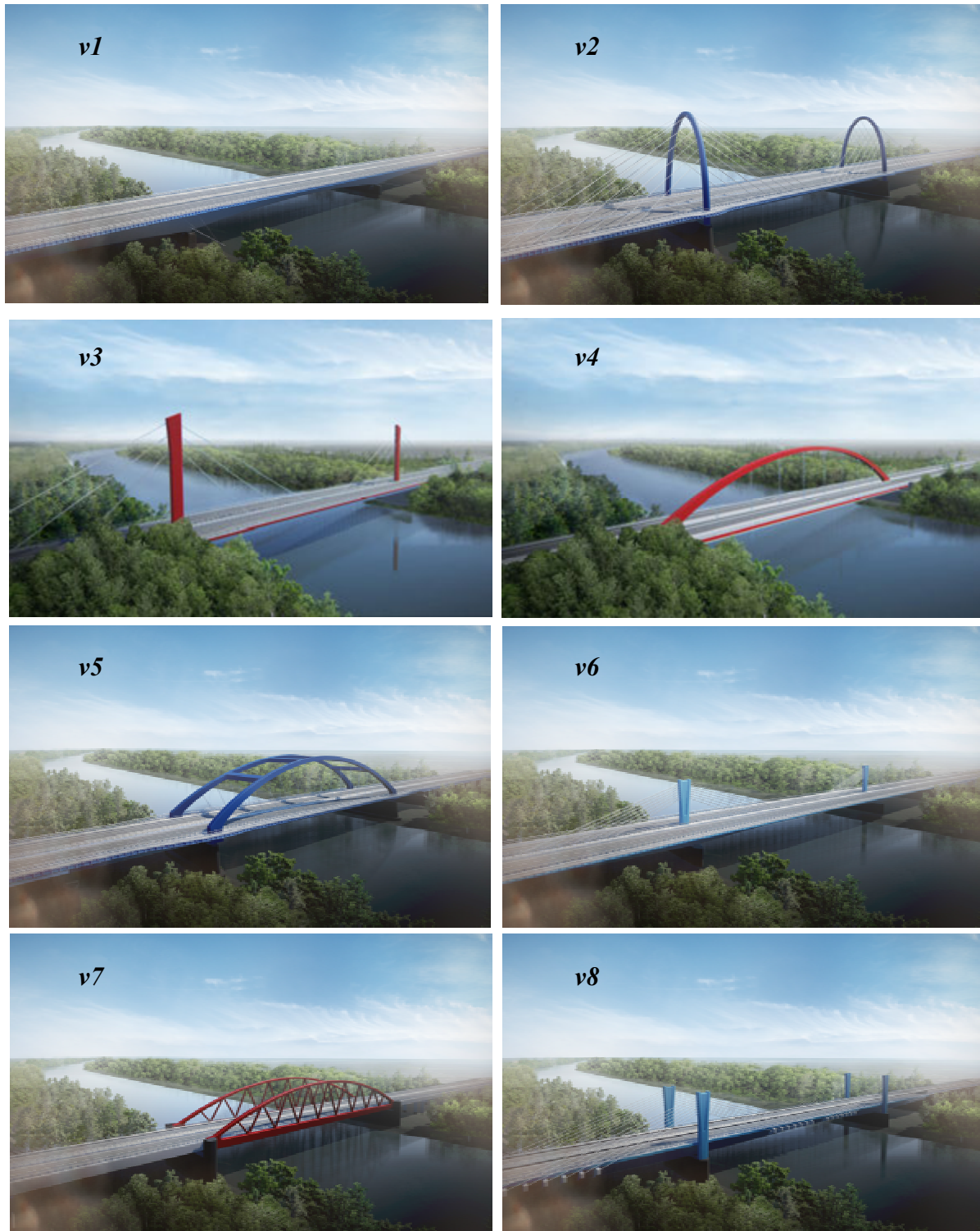










Fig. 6: Bridge variants made for consideration

According to the restrictions mentioned in 1.2., it got clear that a bridge with about 150 m main span would be needed. In Tab. 1 there is a summation of the proposed bridge variants. In the upper part there are some details of the bridges, and in the lower parts we emphasized the advantages of the actual structure.

Because of the flatland around the river we preferred simple beams and/or arches in the appearance. Arch bridges are conventional structures in that part of the country. In our opinion a through bridge was more favourable, even if it had an upper part which could be seen well from a passing car. Constructions of an orthotropic plate deck with hanging up between the middle lanes were considered more complicated. The ease of calculation was less important but that of the inspection and maintenance were.

Tab. 1: Main data and aspects of comparison of the variants

(+ advantage)	 v1	 v2	 v3	 v4	 v5	 v6	 v7	 v8
Main span	148	152	152	152	152	150	152	150
Deck	orthotropic	concrete	orthotropic	orthotropic	orthotropic	concrete	orthotropic	concrete
Beam type	steel box	steel box	steel box	steel box	steel box	conc. box	steel box	conc. box
Beam depth	haunched	constant	constant	constant	constant	haunched	constant	haunched
Pylon / Arch		concrete	steel	steel	steel	concrete	steel	concrete
Spectacle		++	+	+	++	+	++	++
Landscaping	+	+		++	++			
Cost	+	+					++	+
Construction	+	+			+	+	+	+
Calculation	++			+	+		++	
Maintenance	+	+				++		++
Inspection	+	+	+			+		+

2.2 Cost analysis

A complete cost analysis was attached to the study, taking into account not only the construction but also the later maintenance costs of the bridge variants. The calculation was based on general price per square meter data belonging to the materials and the types of the bridges. Due to lack of space we cannot publish the whole cost table but we can show the simplified result of that in Fig. 7.

The lowest rate was represented by the simple beam girder and the arched truss girder variants while the cable stayed bridge and the one with double arches proved to be the most expensive. Because of the relatively moderate cost together with the unique appearance the jury chose the second variant which was also preferred by us. With the arched pylons the stay cables provides a spectacle which is depending on the point of the viewer. From the river the bridge

looks like a usual cable stayed bridge while from the deck the arch with the cables seems to give a hug (Fig. 10).

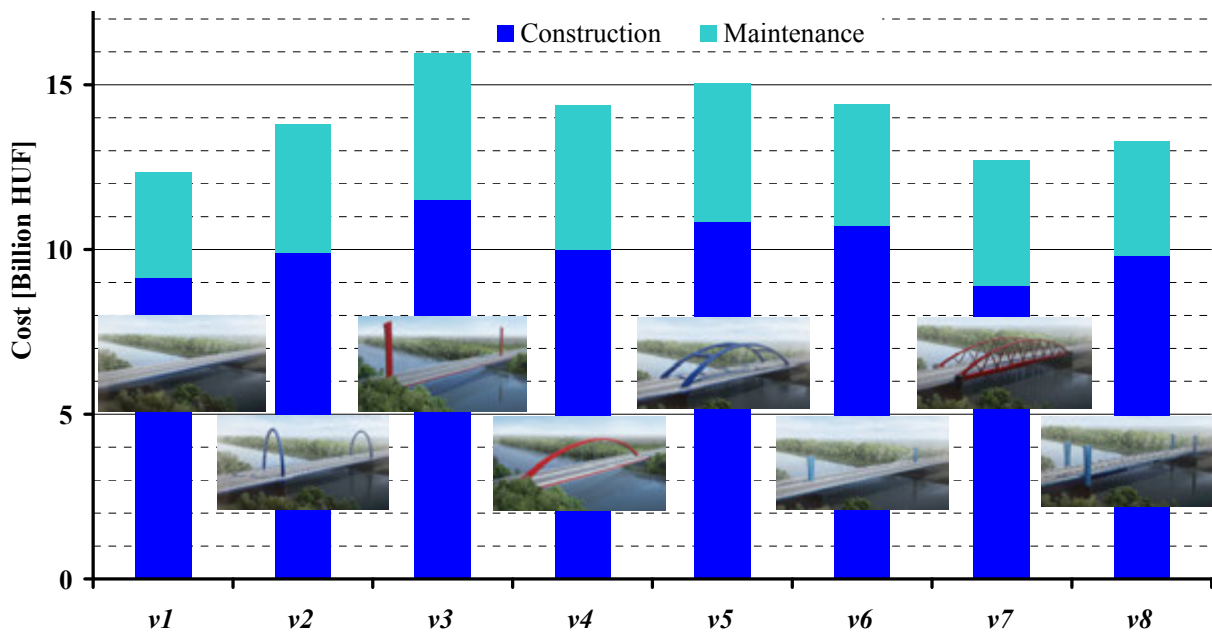


Fig. 7: Costs of the examined bridge variants

3. APPROVAL DESIGN OF THE CHOSEN BRIDGE

As the bridge was chosen we had to make the approval designs for it. That meant making general layout drawings, technical report, and force analysis of the structure with proving that the main sizes were adequate for building and the functioning of the bridge.

To keep the costs lower and to ease the construction procedure we recommended that only the steel part of the main girder should be placed and hanged up by the cables, and only after its completion the concrete deck should be cast. In this way the parts to be moved could be lighter and with the usage of the ready steel parts the pouring of the heavier concrete could be possible. In this way there would be no need of temporary supports for the formworks under the bridge. The pylons were planned to be made of concrete.

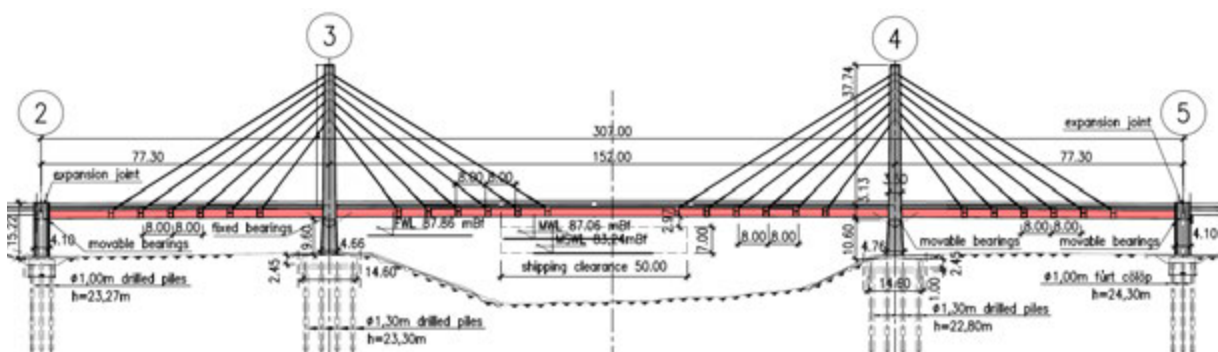


Fig. 8: Lateral view of the designed bridge

The lateral view, that part of the general layout drawing can be seen on Fig. 8. The span is quite close or even a little under the usual range of the cable stayed bridges, so the weight of concrete deck favourable in this point of view as well. Because of aesthetic aspects the pylon

is wider down at the pier wall and thinner on the top sideward (Fig. 8), however its depth are constant transversally (Fig. 9, left side). It has a half elliptic shape and the shape of the top of the pier walls tries to balance it. The cross section of the stiffening girder consists of two steel stiffening boxes which are connected transversally by opened I profiled steel cross beams (Fig. 9, right side).

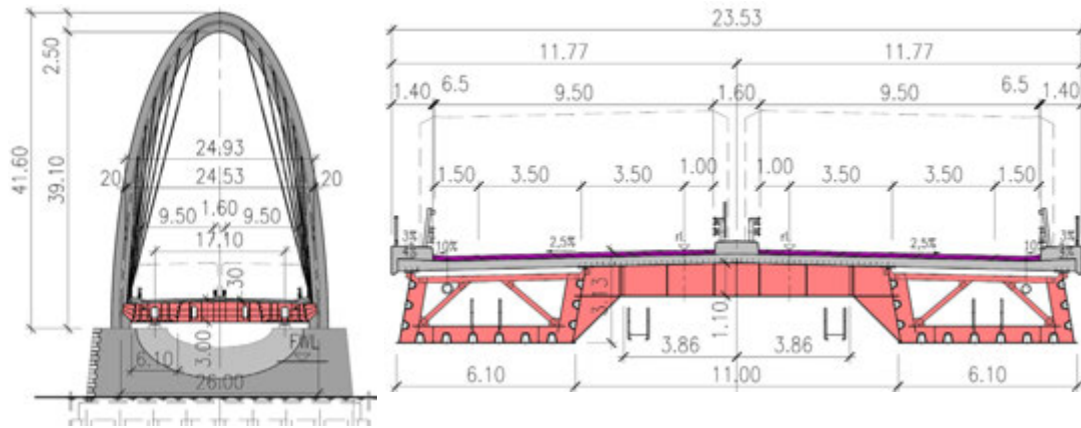


Fig. 9: View of the pier with pylon and the cross-section of the bridge

5. CONCLUSIONS

In this paper it was aimed to show that even a more spectacular superstructure could be competitive in economy point of view. Taking into consideration the maintenance and other additional circumstances finally a decision could be made with which, for a little more cost, such a bridge could be built that might be interesting enough for the public and the contributors might be proud of (Fig. 10).



Fig. 10: The sight of the lit up bridge at sunset

6. REFERENCES

- Kovacs, Zs., Ivanyi Jr., M., Teiter, Z. (2008), "New Motorway Bridge over the Border River Mura", 4th Central European Congress on Concrete Engineering, Opatija
- Teiter, Z. (2008), "Hints for Designing Composite Beam Bridges - Summary and Conclusions of Composite Bridge Designs in Hungary", Eurosteel 2008: 5th European Conference on Steel and Composite Structures, Graz
- Teiter, Z. (2015), "The Effect of the Construction Method of Reinforced Concrete Deck Slab on the Behaviour of Composite Superstructure", 11th Central European Congress on Concrete Engineering, Hainburg
- Teiter, Z. (2016), "Bridge over Tisza of Motorway M44", Days of Bridges Conference, 15-17 Jun 2016, Balatonfüred, Hungary (in Hungarian)

MONITORING OF RC STRUCTURES WITH INTEGRATED SENSORS

Dalibor Sekulić, Mario Ille, Igor Džajić

Institut IGH d.d.

J. Rakuše 1,

HR10000 Zagreb

SUMMARY

Timely observation of damages and degradation of concrete and reinforcement is very important for planning of repair works on the RC structures. Common practice is assessment of the state of RC structures, based on the visual inspection and specimens sampling in the phase when damages are already significant. By the monitoring techniques it is possible to notice damages in the early phase when there are no visible from the outside. This can make possible repair work planning on time which lowering maintenance costs.

Paper emphasize importance of the monitoring of RC structures and gives description of monitoring techniques used in Institut IGH d.d. Monitoring of the state of the advanced RC structures is performing by different sensors embedded into concrete. From monitoring data, it is possible to estimate remaining service life.

1. INTRODUCTION

State of the RC structures estimation is of great importance to insure determination of degree of structure deterioration and remaining load carrying capacity when damages aren't visible yet. For this purpose, use of efficient monitoring methods is necessary.

Main aspects of the advanced monitoring methods are early detection of developing damages, accurate determination of damage type and extent and increased objectivity of assessment. Advanced monitoring techniques based on measurement data minimize the subjective human factor.

Continuous monitoring systems equipped with mobile data transmission units provide information that are always up-to-date and represent advantage over the traditional periodic inspection approach (Spencer, B.F. at al., 2017).

The goal of monitoring techniques is to provide assessment tools with such capabilities that would allow maintenance strategies to improve from reactive to proactive approaches.

2. CORROSION MONITORING

Corrosion of steel reinforcement in structures made of reinforced concrete is the major reason for their deterioration and lifetime shortening and therefore very well studied and known (Broomfield, J. P., 2007; Tuutti, K., 1982; Songl, H-W and Saraswathy V., 2007).

The Krk Bridge was built in 1980 with the largest reinforced concrete arch span (390m) in the world. Bridge is situated in the aggressive maritime environment. Strong wind cause salted water

spraying on the bridge structure, which governed by mechanisms of Cl⁻ diffusion through thin protective concrete layer of only 2 cm caused reinforcement corrosion. As a consequence of corrosion, spalling and deterioration of concrete cover occurred. This is a reason for the extensive repair of bridge elements, especially of columns during past decades (Ille, M. et al., 2011).

After repair works, a group of in-house manufactured sensors was installed on the structural elements of the small arch of Krk bridge, at island Krk side. Sensors 4 and 5 were installed in 1998 at the column S29 (Fig 1). Three groups of sensors were installed in January 2014: one in a zone of sea water splashing (height 2 m above sea level); second group into arch at 10 m height; and third group in a Column S26 at the 20 m height (Fig. 1).



Fig. 1: Positions of the corrosion sensors on the small arch of the Krk bridge

Sensors are fixed to exposed reinforcement of diameter 14 mm, which was at the depth of 7-8 cm as shown in Fig. 2a. Each group of sensors consists of MnO₂ half-cell sensor, corrosion rate sensor installed at the reinforcement depth and anode ladder corrosion current sensor (Fig. 2a).

Concrete is repaired with reprofiling mortar and afterwards covered with protective coating. At that way part of construction surrounding sensor acts as a new rehabilitated structure as shown in Fig. 2b.

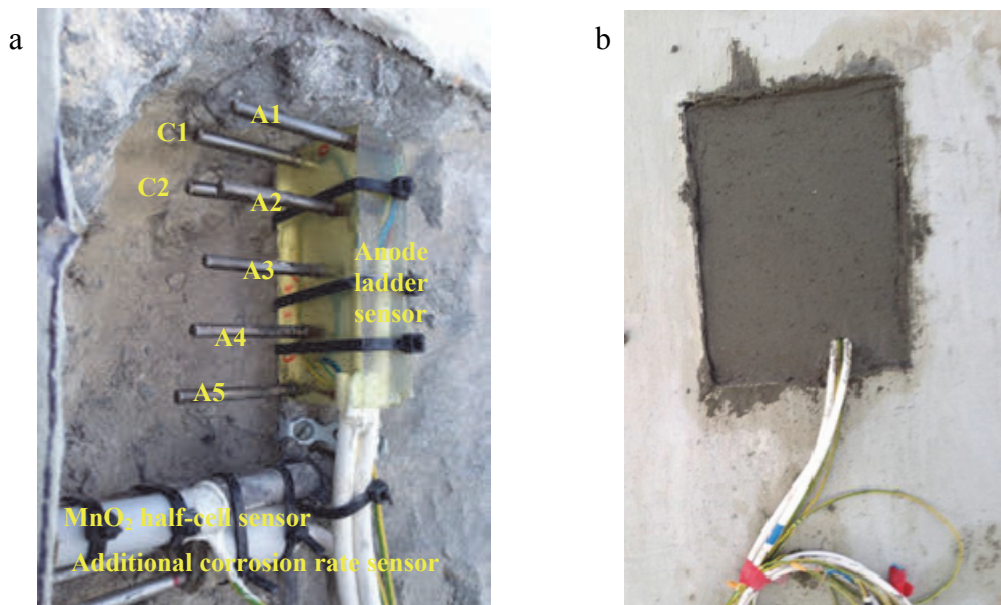


Fig. 2: In-house produced sensor installed in the column of the bridge, a) sensor, b) sensor coated with reprofiling mortar

Self-made anode ladder are composed of 5 rebars of black steel (A1 to A5) that act as anodes and two rebars made of stainless steel acting as a cathodes as shown in Fig. 2a. First electrode of anode ladder is at the depth of 2 cm and 5th electrode at the reinforcement depth. Additional to anodes there is a direct connection to reinforcement. Potential and current are measured between each of the anodes versus the cathode. Concrete electrical resistivity is measured between the each pair of adjacent anodes. Therefore, with these sensors it is possible to detect corrosion through different depths of concrete cover and at the end to evaluate corrosion on the level of reinforcement. Half-cell potential is also measured by the MnO₂ sensor, and concrete resistivity by the AC method using two stainless steel electrodes (Sekulić, D. and Gabrijel, I. 2016).

Corrosion current density for all sensors was above the corrosion initiation limit, indicating that there was no corrosion. Potential measurements also indicated that there was no corrosion except for the anode of Column S26 at the depth of 20 mm. Electrical resistivity of concrete was between 500 Ωm and 1500 Ωm for sensors installed in January 2014. For sensors installed 16 years ago on column S29, electrical resistivity of concrete is lower (100 Ωm – 200 Ωm). Despite of the low electrical resistivity of concrete there is no corrosion activity. Protective coating on concrete prevents drying of concrete, which causes low electrical resistivity. Ingress of chlorides and oxygen is also prevented by the protective coating, which does not enable any corrosion activity. So, low resistivity of concrete does not necessarily mean that there is corrosion activity. Rehabilitation procedures at this site included removal of concrete contaminated with chlorides, application of new protective layer and protective coating, therefore presence of corrosion activators is not likely.

It is important to emphasize that the multidepth sensor monitoring technique has the ability to predict future corrosion of the reinforcement. As multidepth sensors measure initiation of corrosion by anodes placed at the depths lower than reinforcement, the time for the initiation of corrosion at the reinforcement level can be predicted by the extrapolation of measurement results, as shown in Fig. 3a. For example, reinforcement is placed at the 80 mm depth it will start to corrode after 300 days, which is predicted from the measurements during the first 160 days (Fig. 3a).

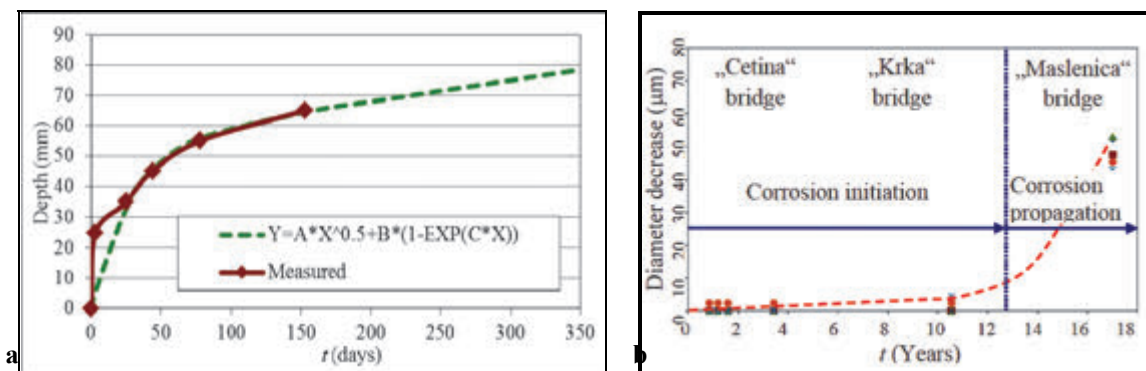


Fig. 3: a) Example for the corrosion front prediction – laboratory measurements, b) Results of reinforcement diameter decrease – measurements on the real structures.

For corrosion prediction the following function is proposed (Equation 1):

$$D = A \cdot \sqrt{t} + B \cdot (1 - e^{Ct}) \quad (1)$$

where, D is the corrosion front depth, t is the time and A , B , C are fitting parameters. In real structures we have a combination of chloride diffusion (first part of eq. 1), and capillary absorption process (second part of eq. 1). (Sekulić and Gabrijel, 2016).

Fig. 3b shows reinforcement cross section decrease in time obtained from measurements at three Croatian coastal bridges, where corrosion measurement data is available during 4 years after construction for “Cetina” bridge, at 11 years for “Krka” bridge and at 17 years for “Maslenica” bridge (right) (Sekulic, Serdar, 2017.). From Fig. 3.b it is visible that first 13 years we have corrosion initiation phase, and after that corrosion propagation phase occurs. For these bridges similar commercially available multidepth sensor systems are used (Raupach, M. and Schießel, P. 2001).

3. DEFORMATION MONITORING

During last years an extensive repair works on the Krk bridge was conducted, consisting of hydro-demolition of chloride contaminated protective layer from columns, reinforcement cleaning, and application of new protective coating (Wurth, et al., 2006). World experiences are that about a half of repair works were poorly performed, from which 75% repairs are attributed to poor durability properties, and 25% to structural failures (Mavar, K. et al., 2007). So, during the repair work design some important questions and open issues arouse: the stress increase rate in the rest of the concrete after hydro demolition of the concrete cover, the rate of elastic deformation and plastic creeping caused by disburdening of column S26, the rate of influence of the new concrete shrinkage on additional longitudinal loading and how the new layers (of repairing concrete) affect loading capacity of the repaired columns - when and in which rate will new concrete participate in useful freight bearing.

In order to find out what really happens during repair phases and afterwards, during further exploitation of the bridge columns, it was decided to perform deformation measurement on two characteristic columns S20 and S26. Different deformation measurement techniques was considered, among that monitoring with interferometric fibre optic sensors was selected as the most appropriate measurement method.

Among several different commercially available fibre optical sensors (FOS) which is based on different principles (Sekulić, D. et al., 2006), interferometric FOS are chosen as the most suitable measurement technique (Inaudi, D. et al., 1994). Used sensors characterise long measurement base of 2 m, which enable averaged deformation measurement without influence of local phenomena as a cracking and concrete non-homogeneity. Another advantage of used FOS is possibility of embedding into concrete which makes sensors insensitive to mechanical influences during operation, unlike conventional extensometers. FOS is insensitive to temperature changes, chemical influences, and to electrical fields. Measurement stability is estimated to about 20 years. Tab. 1 shows main characteristics of used fibre optical sensors.

Tab. 1: Characteristics of used fibre optical sensors

Measurement base	2 m
Resolution	2 μ m
Working temperature range	-50 °C to +110 °C (sensor) -40 °C to +80 °C (optical cable) 20 °C to +60 °C (measurement device))
Linearity, accuracy	< 0.002 % of measured deformation
Maximal length of optical connection between sensor and measuring unit	5 km

Fig. 4 shows mounted sensors on the column S 26 before new protective layer application. Column S 26 above Small arch are disburdened during reparation by help of load bearing scaffolding and hydraulic presses, as shown in Fig. 5.

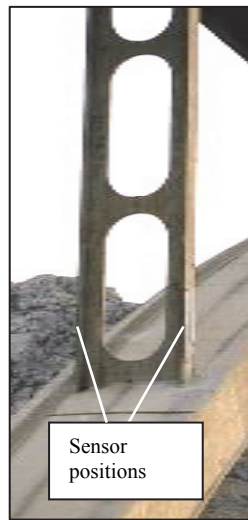


Fig. 4: Mounted sensors



Fig. 5: Disburdening of the column S 26

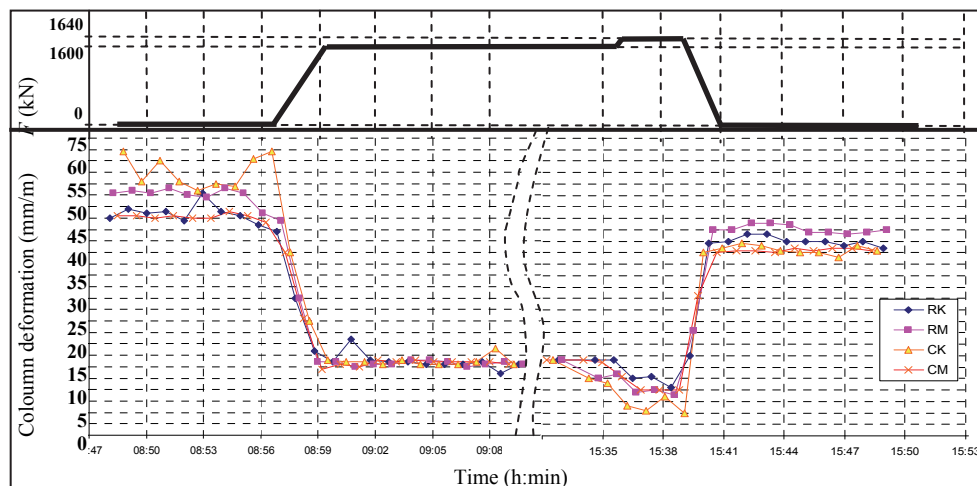


Fig. 6: Measurement results for load application and load removal for column S 26 before new concrete layer application

Measurements with disburdened and loaded column was conducted, before and after new protective layer application.

Fig. 6 shows measurement results for 4 sensors on a column S 26 before new concrete layer application. At the beginning of measurement session a column was loaded by road construction, and after that it was unloaded by reclining of road construction on scaffolding, by hydraulic presses. Pressure reading on hydraulic presses corresponded to 1600 kN at the beginning, and to 1640 kN at the end of measurement in unloaded state, which give column stress of 1.39 MPa and 1.43 MPa respectively. After unloaded phase column was loaded again.

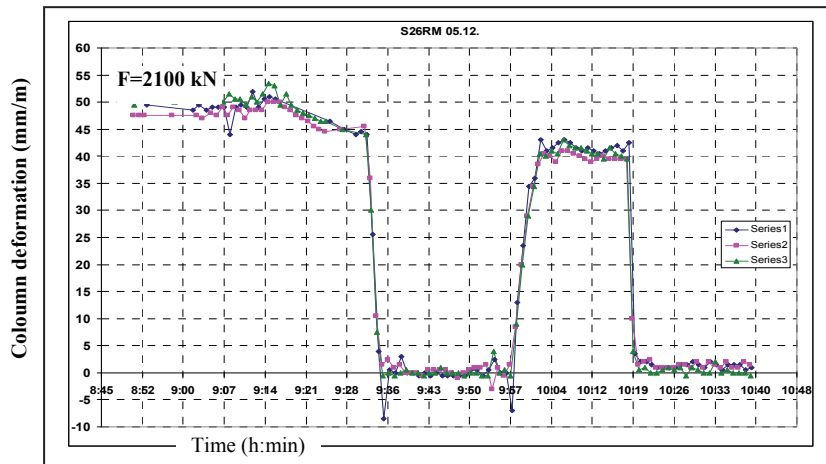


Fig. 7: Measurement results for load application and load removal for column S 26 after new concrete layer application.

Few months later, after new concrete layer application, measurements were repeated, for the same states of loading and unloading, but this time column was more unloaded and force was 2100 kN. Taking into account larger force and larger column cross section due with thicker new concrete layer, column stress of 1.46 MPa was calculated. Deformation measuring results exhibit similar relative deformations, as before refurbishment of columns, as shown in Fig. 7 (Mavar, K. et al., 2007). It leads to conclusion that concrete used for repair exhibit satisfactory mechanical properties and acts as a load bearing layer coupled with old concrete. It is planning to repeat measurements after more than 10 years after repair works to prove deformation state of the columns.

Similar projects with deformation measurements on bridges are conducted worldwide (Inaudi, D., 2009).

4. CONCLUSIONS

Paper emphasizes importance of the monitoring of RC structures and gives description of some monitoring techniques used in Institut IGH d.d.

By the corrosion monitoring techniques it is possible to notice degradation of chloride exposed RC structures when there are no visible degradation yet. It is shown that corrosion monitoring is very useful for proactive repair works planning.

Measurement results of deformations give practical evidence of usability and advantages of fibre optical sensor measurement technique. Measurements after and before refurbishment of Krk bridge columns show similar deformations under load application, which leads to conclusion that concrete used for repair exhibit satisfactory mechanical properties and acts as a load bearing layer coupled with old concrete. Fibre optic sensors have many years stability, which is the main advantage compared with traditional deformation measuring techniques.

Paper also shows that it is possible to predict future degradation of structure from monitoring data to determine remaining service life and to prescribe maintenance actions. This is a complex issue, requiring accurate measurements, optimal number of installed sensors at representative places to obtain relevant conclusions about state of the structure.

5. NOTATIONS

Corrosion monitoring system development, testing and application is funded by the European Commission FP7 project Tomorrow's Road Infrastructure Monitoring and Management (TRIMM), 1st December 2011 to 31st November 2014).

6. REFERENCES

- Broomfield, J. P. (2007), "Corrosion of steel in concrete - understanding, investigation and repair" 2 ed. Oxford, United Kingdom: Taylor & Francis.
- Tuutti, K. (1982), "Corrosion of Steel in Concrete", Swedish Cement and Concrete Research Institute.
- Spencer, B.F.Jr., Park, J.W., Mechitov, K.A., Agha, G. (2017), "Next Generation Wireless Smart Sensors Toward Sustainable Civil Infrastructure", *Procedia Engineering* Volume 171, pp. 5-13
- Song, H-W., Saraswathy V., (2007), "Corrosion Monitoring of Reinforced Concrete Structures – A Review" *Int. J. Electrochem. Sci.*, 2, pp. 1- 28.
- Sekulić, D. and Gabrijel, I. (2016) "Multidepth corrosion monitoring corrosion monitoring system evaluation and application", *Proceedings of the International RILEM Conference Materials, Systems and Structures in Civil Engineering, Segment on Service Life of Cement-Based Materials and Structures Vol.2 / Azenha Miguel ; Gabrijel, Ivan ; Schlicke, Dirk ; Kanstad Terje ; Jensen, Ole Mejlhede (ed.)*.
- Raupach, M., Schießel, P. (2001) "Macrocell sensor systems for monitoring of the corrosion risk of the reinforcement in concrete structures" *Materials and Structures*, 31, pp. 435-441.
- Sekulic, D., Serdar, M., (2017) "Experience with corrosion monitoring using embedded sensors in three bridges on the Adriatic coast", *Proceedings of the 1st International Conference on construction materials for sustainable future (CoMS 2017)*, Zadar, Croatia, 19 - 21 April 2017.
- Ille, M., Bleiziffer, J. Beslač, J. (2011), "Continuation of repair and protection works on the Krk bridge", *Sustainable arch bridges*, Radić, J. ; Chen, B. (ed.), Zagreb: SECON - CSSE, pp. 301-308.
- Mavar, K., Sekulić, D. and Wurth, D. (2007), "Monitoring of Krk Bridge Columns with Interferometric Fibre Optic Sensors", *Fib Symposium Dubrovnik 2007 - Concrete Structures - Simulators of Development*, Proceedings, prof. dr. sc. Jure Radić, ed., Zagreb : Secon HDGK, pp. 709-716.
- Würth, D., Sekulić, D., Štemberga, K. (2006), "Properties of protective coating applied on concrete bridge", *Bridges - International conference proceedings*, Dubrovnik.
- Sekulić, D., Tkalčić, D. Banić, D. (2006), "Principles of Fiber optic Sensors and Applications to Structural Monitoring", *Proceedings of the International Conference on Bridges*, Jure Radić (ed.), Zagreb: Secon HDGK, 2006. pp. 1035-1042
- Inaudi D., Elamari A., Pflug L., Gisin N., Breguet J., Vurpillot S. (1994), "Low-coherence deformation sensors for the monitoring of civil-engineering structures", *Sensor and Actuators A*, Vol 44, p 125-130.
- Inaudi, D. (2009) Overview of 40 Bridge Structural Health Monitoring Projects, *International Bridge Conference, IBC 2010: June 15–17, 2009, Pittsburgh, USA*.

TOPIC 5

MODELLING, DESIGN AND CODIFICATION

ADVANCES IN BRIDGE MANAGEMENT SYSTEMS

Jelena Bleiziffer¹, Ivana Milić

*¹University of Zagreb, Faculty of Civil Engineering
Kaciceva 26, 10000 Zagreb, Croatia*

SUMMARY

The paper provides an overview of some current developments in bridge management systems and discuss prospects of further advances – incorporation of new monitoring techniques and especially implementation of bridge information modelling (BrIM) in an asset management system. There are constant advances in the health monitoring techniques, and increase in number of applications of health monitoring on road structures such as bridges. However, the capabilities of the measurement systems themselves are not always targeted at the key input requirements of an asset management system. A methodology developed to integrate the monitoring data in asset management systems is discussed. The possibilities of implementing bridge information modelling in a bridge management system are discussed using the asset management system of Croatian Motorways authority as an example.

1. INTRODUCTION

World Road Association clearly underlines the importance of road maintenance (PIARC, 2014) stating that “Road infrastructure provides a fundamental foundation to the performance of all national economies, delivering a wide range of economic and social benefits. Adequately maintaining road infrastructure is essential to preserve and enhance those benefits. Road network performance is a result of, among other things, road and bridge conditions, road design, and traffic regulations. Information on condition and performance of bridge and road assets are crucial to ensure proper service to road users and society but also to strengthen management”. Within the transportation networks, bridges are key elements for connecting people and delivering goods (Casas, 2015).

Faced with limited resources, the authorities must prioritize the work. It has long been generally accepted that the only rational way to do so is to determine the inherent risk levels in structures so that those at most risk can be dealt with first (Hearn, 2002). For this purpose, it is necessary that structures are inspected and assessed at regular time intervals, according to prescribed procedures. Asset management systems are developed to assist in reaching decisions related to carrying out management activities.

According to ISO 55000, “asset management involves the balancing of costs, opportunities and risks against the desired performance of assets, to achieve the organizational objectives”, and “enables an organization to examine the need for, and performance of, assets and asset systems at different levels. Additionally, it enables the application of analytical approaches towards managing an asset over the different stages of its life cycle (which can start with the conception of the need for the asset, through to its disposal, and includes the managing of any potential post disposal liabilities).” Furthermore, it identifies the potential benefits of asset management as improved financial performance, informed asset investment decisions, managed risk, improved services and outputs, demonstrated social responsibility,

demonstrated compliance, enhanced reputation, improved organizational sustainability and improved efficiency and effectiveness.

2. ROAD BRIDGE MANAGEMENT IN CROATIA

The road network of Republic of Croatia is managed by several companies. Public roads authority (Hrvatske ceste d.o.o. – HC) is responsible for operation, construction and maintenance of state roads (6,890 km). There are also 20 county road authorities responsible for county (9,650 km) and local (9,080 km) roads. The 1,313-km long motorway network is operated by 4 companies (Drazenovic, 2017a): 925 km by Hrvatske autoceste d.o.o. – HAC, 187 km by Autocesta Rijeka-Zagreb d.d., 141 km by BINA-ISTRA d.d. and 60 km by Autocesta Zagreb-Macelj d.o.o. The latter three, are concession societies for the construction, maintenance and operation of motorways and structures for toll collection. The motorway network comprises 219 bridges, totalling 40 km in length (Drazenovic, 2017b) i.e. 3 % of the motorway.

The project of modernization and restructuring of the Croatian road sector was launched with the objective of strengthening the institutional effectiveness, enhancing the operational efficiency and increasing the debt service capacity of Croatia's road sector (Marteau, 2017). One of the indicators for the results achieved is the implementation of Road Asset Management System (RAMS). It has been identified that road sector agencies and companies do not have integrated RAMS, and the end target is to have RAMS inputs incorporated in rolling plan by the end of 2021.

Sector reorganization is described in a Letter of Sector Policy, announced in March 2017 by the Ministry of Sea, Transport and Infrastructure (MMPI, 2017). It specifies that RAMS will use all available asset management systems from public companies within the road sector. It will ensure availability of current data on the condition of the network and serve as the basis for continuous updating of motorway and state road periodic maintenance estimates. It will also be available for county-managed roads, namely for data-entry on road inventory and road condition, and to generate their own future maintenance programs. It will allow rehabilitation and periodic maintenance to be programmed, based on actual road conditions and not based on predefined standards.

It is recognized that Croatian public road sector companies have existing systems for managing elements of the road infrastructure (e.g. structures at HAC; pavement at HC) and are in the process of expanding such systems (Dimitropoulos, 2017). Thus, the RAMS development will include review of existing RAMS elements, support to implementation and integration of missing elements including data collection.

One of those existing systems is asset management system SGG implemented by HAC (Bleiziffer, Juric and Kuvacic, 2012). It is focusing on civil engineering aspects of maintenance and management of motorway structures (support for data collection, condition assessment based on inspection results, and planning of execution of appropriate and timely maintenance measures, within the prescribed budget). SGG provides the list of priorities with the approximate bill of quantities of maintenance works required. This asset management system includes all types of motorway structures, categorized as: bridges (incl. viaducts, overpasses, underpasses, animal crossings), tunnels, pavements (incl. all paved surfaces), drainage (gutters, ditches, drains, separators, overflow structures etc.), geotechnical structures (retaining walls, embankment and cut slopes), other roadway components (safety barriers,

wind barriers, sound barriers) and buildings (roadside service facilities, maintenance and traffic control centres). The general framework and guidelines on subsequent development were set out in 2006, followed by staged development of modules for bridges, drainage, pavement, tunnels, and data collection on the inventory and condition of inventory, which is still undergoing.

It is very important that restructuring of Croatian road sector clearly identified the goal of an integrated asset management system for the entire network and all responsible authorities. That is a very welcoming objective. Still, asset management worldwide is facing new challenges and developments, and it would be beneficial to consider incorporation of new monitoring techniques and especially implementation of BIM from the earliest stages of development of road asset management system. The following chapters discuss these two elements focusing on road bridges.

2. BRIDGE MONITORING AND BRIDGE MANAGEMENT

Any asset management system requires collecting the data on inventory and on inventory condition. The condition is usually described using the condition indicators.

The calculation of condition indicators is based on evaluation of defects of an asset, detected during manual inspection of the asset and/or measurements that are routinely carried out during prescribed inspections/ condition assessment. The manual inspections are carried out in regular time intervals, prescribed in regulations/ guidelines of the country and/ or road authority. The major prerequisite for a manual inspection to serve as a basis for calculation of a condition indicator that is usable in an asset management system, is that inspection addresses *all* elements of an asset, and is focused on detecting *all* damage that occurred on any part of an asset. This is of major importance when considering incorporation of monitoring data in an asset management system, because monitoring techniques are often focused on only a fraction of elements and/ or only a fraction of parameters that indicate damage/ defects. However, there is a huge advantage of some advanced monitoring techniques that it may indicate damage/ defects even if they are not apparently visible on the external surfaces of an asset, and as such may go unnoticed during manual inspections. Thus, some advanced monitoring techniques are especially important for proper preventive maintenance management.

Part of the research carried out in FP7 Project Tomorrow's Road Infrastructure Monitoring and Management was to provide the methodology on how to utilise the monitoring data in decision making processes of a road asset management system, for which it is essential to establish relationship from monitoring data to condition indicators and maintenance measures.

The methodology developed addressed the following specific barriers to inclusion of monitoring data into road asset management systems:

- difficulty of systematic handling and interpretation of the monitoring data (by establishing relationship between measurable data and condition indicators),
- practicality of the monitoring data within asset management systems (by allowing to combine the information from monitoring and manual inspections in an asset management system),
- the fact that the capabilities of the measurement systems themselves are not always targeted to the key input requirements of an asset management system.

The guiding idea of this task was to break down all damage/defects that may occur on an asset into technical parameters and measurable data. Required data may then be measured by a simple technique during manual inspections (e.g. crack width), or by an advanced monitoring technique (e.g. corrosion rate). If no measurements are available, the condition indicator related to a specific damage/defect may be added manually, based on engineering judgment of damage identified by manual inspection. If certain condition indicators are not readily available, the proposed methodology is still working, as the missing condition indicators are simply neglected, just as is the case in manual inspections. However, there is a risk that resulting planned maintenance measures may not be adequate due to missing information on all condition indicators. But, if there is a health monitoring system installed on a bridge, this valuable data is also included in the calculation of the condition indicator.

In order to implement monitoring information, all condition indicators needed to be related to measurable data in quantitative terms. Referenced document (van Kantén Roos et al., 2013) details the proposed set of bridge condition indicators and transfer functions to calculate each condition indicator from the value of technical parameter. Transfer functions are provided in separate sheet, with indication which measurable data from monitoring is required for calculating values of condition indicators. The report also provides the relationship from monitoring data, through bridge condition indicator to choosing an appropriate maintenance measure.

Flowchart showing how bridge condition index is derived from element single condition index is shown in Fig. 1.

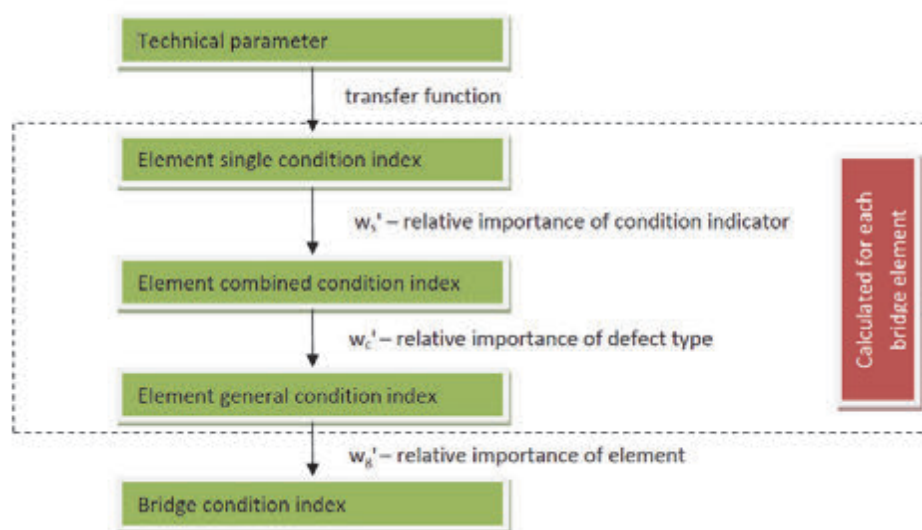


Fig. 1: Flowchart for calculating bridge condition index

Since a bridge is composed of a series of elements, relationship between condition indicators and defects (monitoring data) is done on an element level (element single condition indicators). Single element condition indicator is calculated from the value of technical parameter, using an appropriate transfer function. Then, relative importance of single element condition indicators is introduced to calculate the values of 6 combined condition indicators which correspond to 6 defect types (contamination, deformation, deterioration, loss of material, discontinuity and displacement). Subsequently, relative importance of combined condition indicators (relative importance of defect type) is introduced to calculate the value of general element condition indicator. Finally, general condition indicator for the entire bridge

is calculated considering the relative importance of an element for the entire bridge. The urgency of the maintenance measures was defined by considering only the aspect of asset condition. When deciding on priorities on a network level, other aspects need to be considered (importance of a bridge for the functioning of the network).

3. BRIDGE INFORMATION MODELLING AND BRIDGE MANAGEMENT

Building information modelling (BIM) is a huge topic and causing true digital revolution in the construction sector. This was especially emphasized with the adoption of European directive 2014/24/EU on public procurement stipulating that for public works contracts and design contests, Member States may require the use of specific electronic tools, such as of building information electronic modelling tools or similar. Many countries have turned to developing appropriate strategies for the implementation of BIM. For instance, BIM will be mandatory for all transportation projects by the end of 2020 in Germany (Bramann & May, 2015).

In Croatia, general guidelines for BIM approach in construction sector were recently published by the Croatian Chamber of Civil Engineers (Jurcevic, Pavlovic and Solman, 2017). It acknowledges that the motivation to develop the guidelines was to encourage the application of BIM in Croatian construction sector as the proportion of Croatian design engineers that apply any of BIM technologies is much lower than in the countries of the Western Europe, and if one looks at the proportion of design offices that use BIM processes to encompass the work of different engineering disciplines, the situation is even poorer. These guidelines are not obligatory, but a recommendation. The guidelines cover the following topics: organization and BIM project management, design, construction, maintenance and management, thus encompassing the entire life-cycle of a building. This document clearly identifies that to gain the maximum benefit from BIM approach, it is necessary to incorporate information created during design and construction stages into asset and maintenance management systems, and use them throughout the life-cycle.

The joint ICE – ICES – IAM position paper (Shetty et al., 2014) defines the relationship between asset management systems and BIM as “mutually supportive”, and emphasises the need to “mitigate the danger of treating BIM and asset management as isolated practices”. The paper clearly points to how BIM supports asset management: “The availability of appropriate and reliable information about assets is vital for effective asset management as it supports decision making, planning and execution of activities on assets. By providing a structured framework for the creation, collation and exchange of information about assets, BIM supports effective asset management. However, to enable this BIM must provide information covering the whole life cycle of assets.” In this sense, new standard PAS 1192-3:2014 “Specification for information management for the operational phase of assets using building information modelling” was developed to extend BIM to cover the in-service phase of assets. As specified in its forward, it is a companion document of, and refers heavily to PAS 1192-2:2013, Specification for information management for the capital/delivery phase of construction projects using building information modelling. It applies to both building and infrastructure assets.

There are many advantages of BIM over traditional design, the interrupted flow of information from one stage of the project to another being particularly important for asset management.

Asset management systems require first a database on inventory that is being managed, and for BIM projects these are already readily available in the BIM model. The SGG asset management system used by Croatian motorway authority HAC stores inventory data through combined graphical and textual / numerical inputs (Fig. 2). These may be easily adapted to BIM data, and substantially simplified due to parametric definition of elements in BIM models that inherently comprise material and other properties. Using BIM model in design and construction stages assures that all inventory data is up to date and representative of the structure at the beginning of its service life. Since the asset management system database is already populated by a large number of data, one should carefully consider how to treat the existing information by making appropriate adaptation of procedures for the new projects delivered in BIM first, and then taking a phased approach to extending BIM to existing assets, prioritised by their importance / criticality. The implementation of BIM in asset management systems in this sense is rather straightforward, but requires substantial work on standardization of both BIM and asset management to be mutually supportive, and to consider the entire life cycle of an asset, as well as very clear client requirements for the entire processes, including data specification, information systems, roles and responsibilities.

Fig. 2: Screenshot from SGG with bridge inventory data

More research work is required for collecting inventory condition data in BIM environment, although there are clear advantages both for the carrying out on-site inspection (Turkan et al., 2015), and subsequently storing data on observed damage and defects by introducing changes to the BIM model (McGuire et al., 2016).

4. CONCLUSIONS

Asset management systems are used worldwide to support the decision-making process related to carrying out appropriate maintenance actions on structures within the budget constraints. They rely on inventory data and inventory condition data; the latter being usually collected by manual inspections. The advances in monitoring techniques and building information modelling should be incorporated in the existing asset management systems, as

they provide more accurate data and thus more informed and efficient maintenance management.

5. REFERENCES

- Bleiziffer, J.; Juric, S.; Kuvacic, B. (2012), "Current developments in asset management system for Croatian Motorways", Durability of concrete structures – Proceedings of the 8th Central European Congresses on Concrete Engineering, Plitvicka jezera, Croatia, October 2012, pp. 93-98.
- Bramann, H.; May, I. (2015), "Stufenplan Digitales Planen und Bauen, Einführung moderner, IT-gestützter Prozesse und Technologien bei Planung, Bau und Betrieb von Bauwerken", Berlin : Bundesministerium für Verkehr und digitale Infrastruktur (in German).
- Casas, J.R. (2015), "The bridges of the future or the future of bridges?", *Frontiers in Built Environment*, Vol, 1, No. 3, April 2015, pp. 1-3.
- Hearn, G.; Purvis R., L.; Thompson, P.; Bushman, W. H.; McGhee, K. K.; McKeel, W. T. Jr. (2002), "Bridge Maintenance and Management – A Look to the Future", Proceedings of IABSE Symposium, Melbourne, Australia, September 2002.
- HRN ISO 55000:2016 Upravljanje imovinom -- Pregled, načela i nazivlje (ISO 55000:2014) / Asset management -- Overview, principles and terminology (ISO 55000:2014), Croatian Standards Institute.
- Dimitropoulos, I. (2017), "Reorganization of the Road Sector in Croatia with the Emphasis on Maintenance", Presentation at the International Seminar "Asphalt Pavements 2017", organized by the Croatian Asphalt Association, http://www.h-a-d.hr/ak2017/5.%20Ioannis%20Dimitropoulos_Reorganizacija%20cestovnog%20sektora%20u%20Hrvatskoj%20s%20naglaskom%20na%20ucinkovito%20od.pdf.
- Directive 2014/24/EU of the European Parliament and of the Council of 26 February 2014 on public procurement and repealing Directive 2004/18/EC, Official Journal of the European Union, L 94/65
- Drazenovic, J. (Ed.) (2017), "Key Figures 2016", HUKA – The Croatian Association of Toll Motorways Concessionaires, Zagreb.
- Drazenovic, J. (Ed.) (2017), "Croatian National Report on Motorways 2016", HUKA – The Croatian Association of Toll Motorways Concessionaires, Zagreb.
- Jurcevic, M.; Pavlovic, M.; Solman, H. (2017), "Opće smjernice za BIM pristup u graditeljstvu" /General guidelines for BIM approach in construction sector/, Hrvatska komora inženjera građevinarstva /Croatian Chamber of Civil Engineers/, Zagreb, Croatia.
- Marteau, J.-F. (2017), "Croatia - Modernization and restructuring of the road sector : P155842 - Implementation Status Results Report : Sequence 01". Washington, D.C. : World Bank.
- McGuire, B.; Atadero, R.; Clevenger, C.; Ozbek, M. (2016) "Bridge Information Modeling for Inspection and Evaluation", *Journal of Bridge Engineering*, Vol. 21, Issue 4 (April 2016).
- Ministarstvo mora, prometa i infrastrukture (MMPI) / Ministry of Sea, Transport and Infrastructure (2017), "Poslovno i financijsko restrukturiranje cestovnog sektora / Operational and financial restructuring of road sector" (in Croatian), http://www.mppi.hr/UserDocsImages/2_Tekst%20poslovnog%20i%20financijskog%20restrukturiranja%20cestovnog%20sektora_VRH%20prilog%20ODLUCI_24032017.pdf.
- PAS 1192-3:2014 "Specification for information management for the operational phase of assets using building information modelling", British Standards Institution.
- Shetty, N.; Hayes, A.; Pocock, D.; Watts, J. et al. (2014), "Leveraging the Relationship between BIM and Asset Management", Joint ICE - ICES - IAM Position Paper, <https://www.ice.org.uk/getattachment/knowledge-and-resources/best-practice/relationship->

between-bim-and-asset-management/BIM_Modelling-and-Asset-Management_Position-Paper.pdf.aspx.

Turkan, Y.; Laflamme, S.; Al-Shalabi, F. (2015), "Digital Documentation of Element Condition for Bridge Evaluation", Iowa State University, A Cooperative Research Project sponsored by U.S. Department of Transportation-Research and Innovative Technology Administration, Final Report.

van Kantén Roos, W.; Bleiziffer, J.; Juric, S. (2013), Deliverable D2.1: List of condition indicators and monitoring data requirements including a matrix with relations between maintenance measures and condition indicators

World Road Association (PIARC) (2014), "The importance of road maintenance", <http://www.piarc.org>

NEW CONCEPT FOR DESIGN OF CONCRETE STRUCTURES

Andor Windisch

BMGE Department of Structural Engineering

Schwarzhölzlstrasse 19A, 85757 Karlsfeld, Germany

SUMMARY

Structural Concrete (SC) consists of concrete, reinforcement, cracks and bond. Besides of these four constituents at dimensioning of SC structures equilibrium- and compatibility conditions, kinematics and physically correct material characteristics must be considered. SC structural elements shall not be modelled as trusses, stress fields, strut-and ties but as continuums with discrete, not rotating cracks. Shear and torsion are “products” of the orthogonal global coordinate system only. The structural members do not “know” them concrete. The dimensioning for bending and shear must not be carried out separately. The “concrete contribution” is the “shear component” of the load bearing capacity of the concrete compression zone. A slab is not a sandwich at all. Theoretically really sound dimensioning of SC structures in the XXIth century is a big challenge for all of us.

1. INTRODUCTION

“International and national codes must be transparent, easy to apply for designers and should result in safe but economical structures. Meanwhile codes are significantly more complicated. This is partly due to the development of more scientific background knowledge, nevertheless also due to a lot of unfortunate developments” (Walraven, 2017).

At the beginning of the XXth century it was found/accepted that the dimensioning for bending and shear should be performed independently of each other. For bending in a beam the top and bottom flanges are included whereas for shear the web is “responsible”. This presumption was practical and most inconsistencies which occurred and were perceived by the engineers during practice were smoothed out during the last decades with more and more sophisticated models, concepts, e.g.:

- Varying angle truss model
- Aggregate interlock
- Size effect underlined with the theory of fracture energy
- Strut and tie model
- Modified Compression Field Theory,
- Compressive Force Path-Model.

Windisch (2016) evaluated these models, revealed their shortages. Most of these models disregard basic requirements of equilibrium, compatibility and kinematics.

In this paper the concept of a revised dimensioning model is outlined. The transparency and applicability of the model will be presented on two examples.

2. NEW MODEL FOR DIMENSIONING

2.1 Dimensioning for bending and shear are interrelated

The most fundamental –hence diametrical to habitual– principle of this model is that dimensioning for bending and shear is carried out interdependently.

Structural Concrete (SC) consists of concrete, reinforcement, cracks and bond. Besides of these four constituents at dimensioning of SC members equilibrium- and compatibility conditions, kinematics and physically correct material characteristics must be considered. SC is at macrolevel a “simple”, user-friendly and transparent material for those who understand and feel it.

2.2 SC members fail along a discrete, critical section

Properly dimensioned SC members fail along a critical section which consists of a discrete crack along the tensile zone and an attaching sliding surface along the compression zone. The form of the critical section depends on the local geometry of the member and the action effects in the given section and can be deduced from the elastic trajectories: in case of pure bending it is a plane perpendicular to the member’s axis; at bending + shear it is a cylindrical surface (bending-shear crack, see Fig. 1, in case of punching –depending on the cross section of the column- a pyramidal or conical surface, see Fig. 2; when torsion, too, is acting then the surface performs a “warped” surface (Fig. 3). The inclined shape of the critical section reveals the real physical character of the staggering: it is a length along the longitudinal reinforcement and no plus/minus force supplement in a vertical section.

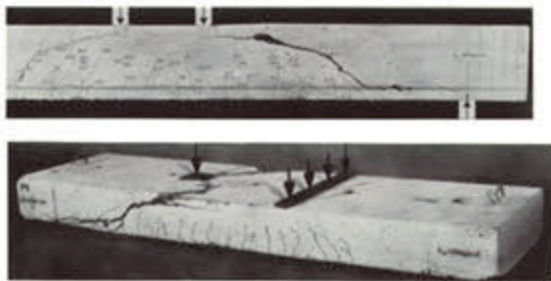


Fig. 1: Critical section in case of bending and shear



Fig. 2: Punching cone (Menétrey, 1995)

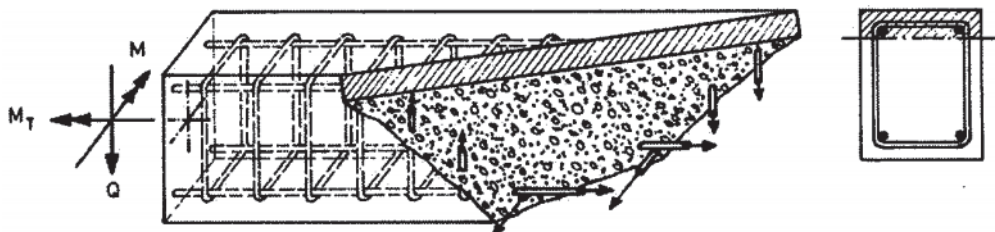


Fig. 3: “Warped” failure section in case of bending + shear + torsion (Gvozdev et al. 1968)

2.3 The location and form of the possible critical sections in ‘D-regions’

The location and form of the possible critical sections can be easily predicted in ‘D-regions’, too. If the tensile zone has a kink, the corner point is always the starting point of a crack. It is inclined with respect to the member’s axis and to the direction of the flexural reinforcement. The inclination of this crack depends on the geometric conditions of the ‘D-region’ and / or

on the ratio of the concrete tensile stresses in the two edge fibers joining in the corner point. The laws of the crack directions can be determined by linear elastic FE calculations. Examples see in Chapter 3.

If the compression zone has a kink or the direction of the compressive force has to change for other reasons, tensile stresses occur transversely to the compressive stresses, which can lead to cracks (e.g. in opening corners). These cracks have the same characteristic features as the "shear cracks"; they are inclined to the respective axis of the member. The tensile force, which is necessary for the equilibrium of the region separated by such a transverse crack, must be taken by reinforcing bars, which are crossing the crack and are properly anchored on its both sides.

2.4 In the shear resistance the aggregate interlock has no influence

In the shear resistance the aggregate interlock has no influence, the "concrete contribution" is the "shear component" of the load bearing capacity of the concrete compression zone. Applying recent advanced measurement technics the relative displacements of the crack faces was traced during the loading procedure: no relative displacements which could activate the aggregate interlock were detected, see Fig. 4 (Völgyi et al. 2017). Moreover, hindering the eventual development of the aggregate interlock with plastic sheets did not change the failure load at all.

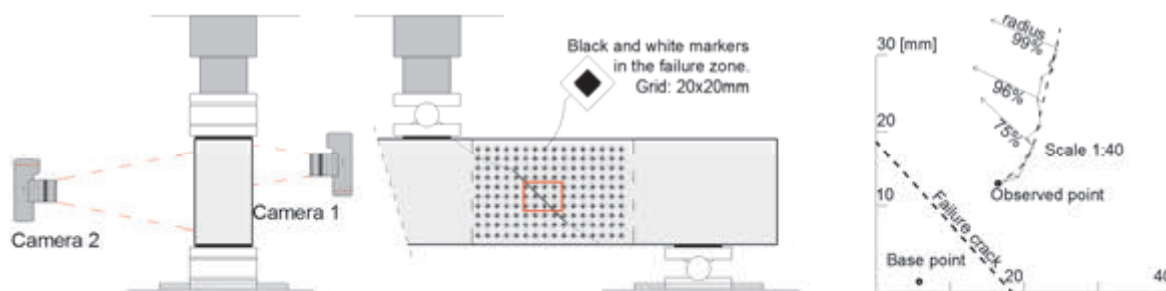


Fig. 4: Optical detection of relative displacement and measured magnified relative displacements between the faces of the failure shear crack at different percentages of the failure load (Völgyi et al. 2017)

2.5 The concrete contribution is the 'shear' component of the compressive zone stresses

The dimensioning for bending and shear must not be carried out separately. In a beam the web has not that fundamental role as attributed to it during the last century. The size effect is the result of an erroneous model for the shear resistance. The size of the 'concrete contribution' equals with the flexural tensile force. Dividing this constant value with the increasing web depth of beams with constant longitudinal tensile reinforcement a decreasing 'concrete web shear strength' is obtained. Recently a "side size effect" was detected which arises from similar reasons.

A slab is not a sandwich at all. Its core (like a web, too) transmits inclined compressive stresses, acts as spacer, controls the deformation of the bonded shear reinforcement (if it exists) and increases the member's stiffness.

2.6 Efficiency factor of inclined rebars

It is known that rebars placed along the compressive trajectories (i.e. perpendicular to the cracks) are more efficient than inclined rebars. This shall be considered at dimensioning. This reduced efficiency is taken into account through the efficiency factor, ψ , introduced/deduced by Windisch (2000).

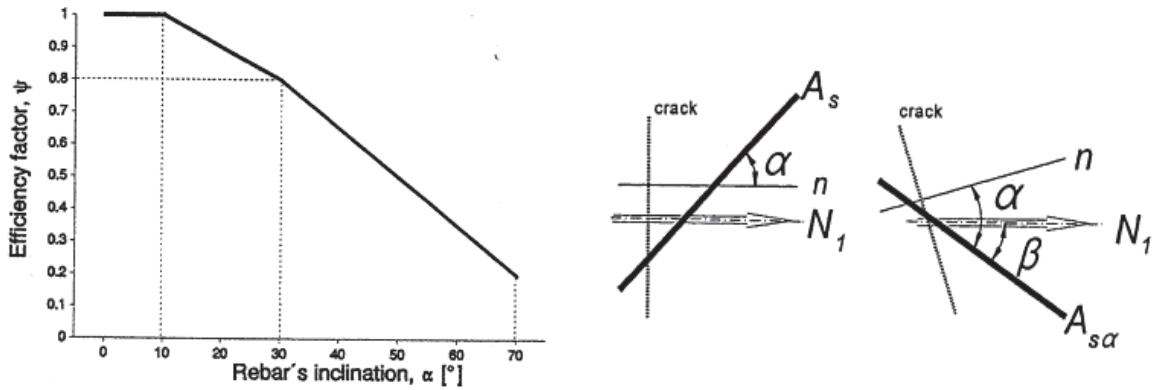


Fig. 5: Efficiency factor, ψ , of an inclined/skew rebar, legend (Windisch, 2000)

Applying the legend shown in Fig. 5

$$A_{s\alpha} = N_1 / (\psi_\alpha \cdot \sigma_{s0} \cdot \cos\alpha)$$

Windisch (2010) pointed out that the specimens of the well-known Toronto panel tests are in principle skew reinforced panels which failed as the weaker band of rebars begun to yield. The failures cannot be attributed to any kind of failure of concrete, Fig. 6. Accordingly the validity of the Modified Compression Field Theory and the shear design methods in MC2010 are questionable.

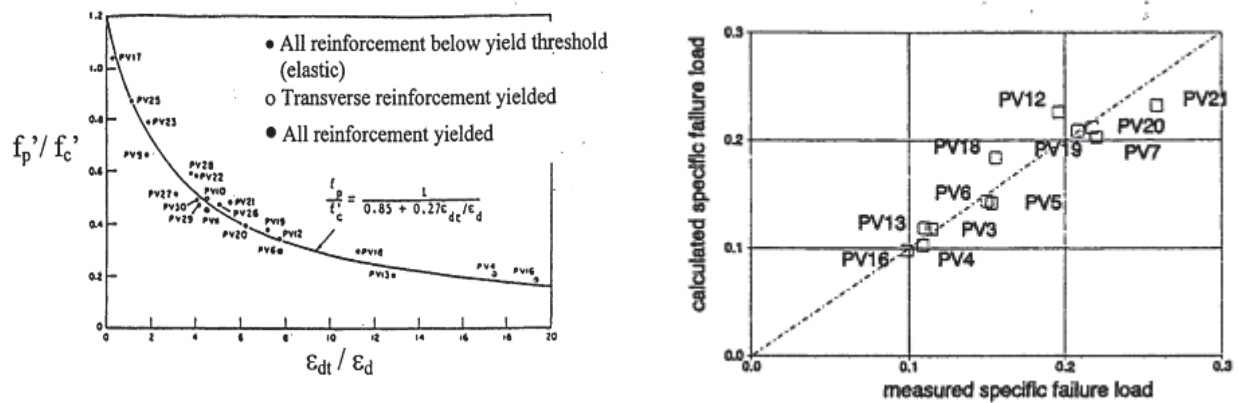


Fig. 6: a) Effective compressive concrete strength as function of the transverse tensile strain (Vecchio and Collins, 1986); b) Evaluation of the Toronto test (biaxial loading) results as skew reinforced panels (Windisch, 2000)

3. APPLICATIONS, EXAMPLES

3.1 Dapped end

The cracks of the two dapped ends shown in the Fig. 7 can be classified as follows:

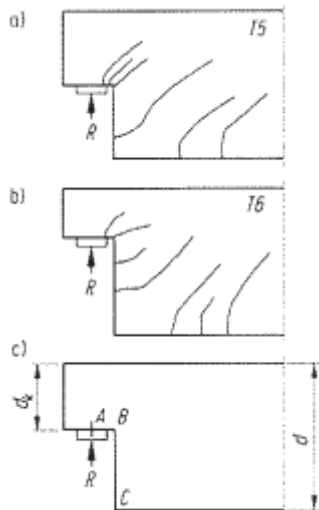


Fig. 7: a) and b) crack patterns of test specimens of Steinle (1975)
c) legend

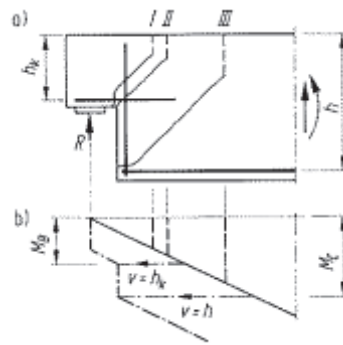


Fig. 8: Dimensioning of the characteristic critical sections

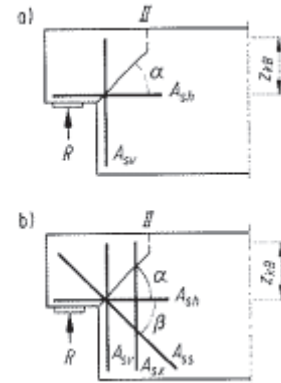


Fig. 9: Dimensioning
a) with orthogonal rebars,
b) with supplementary inclined rebars

To the left of the corner point B and to the right of the lower corner point C, the cracks are conventional bending-shear cracks. Also the cracks occurring between the points B and C show the usual form of a bending-shear crack; the flexural parts of the cracks are perpendicular to the edge BC. The critical section at corner point B has an initial inclination which depends on the ratio d_k/d .

On the basis of linear elastic FE calculations, the inclination angle of the corner crack can be estimated with good approximation for the practice to:

$$\alpha = 90 \cdot \frac{d_k}{d} \quad [^\circ]$$

The necessary reinforcement quantities can be determined by the dimensioning of the sections shown in Fig. 9. The course of these critical sections also determines the size of the moments for which the rebar there should be dimensioned. The horizontal distance between the point where the crack crosses the rebar and the compression zone, resp. is the staggering v .

In case of the critical section II, the inclined position of the rebars relative to the direction of the crack must be taken into account. According to the legend given in Fig. 9 a):

$$M_{II} = A_{sh,II} \cdot \Psi_\alpha \cdot f_{sy} \cdot z_{kB} + A_{sv,II} \cdot \Psi_{(90^\circ - \alpha)} \cdot f_{sy} \cdot z_{kB} \cdot \cot \alpha$$

If an supplementary inclined rebar with A_{ss} is applied, it should be taken into account with its efficiency factor corresponding to the angle β . Accordingly:

$$M_{II} = A_{sh,II} \cdot \Psi_{\alpha} \cdot f_{sy} \cdot z_{kB} + A_{ss} \cdot \Psi_{\beta} \cdot f_{sy} \cdot \cos\beta \cdot z_{kB} + A_{sv,II} \cdot \Psi_{(90^{\circ}-\alpha)} \cdot f_{sy} \cdot z_{kB} \cdot \cot\alpha$$

In the case of the bending dimensioning of the cross-sections, the bearing capacity of all the rebars which cross the crack may be considered. For further details (e.g. proper anchorage of the different rebars) see Windisch (1988).

3.2 Opening corner

The opening corner is a very instructive example of the fact that the usual dimensioning at the adjoining vertical- and horizontal cross sections or in the diagonal section, without a supplementary inclined reinforcement in the corner area, led to corners which failed significantly below the calculated breaking load. The reason for this is to be seen in the fact that the compressive and tensile forces from the adjoining components in the frame corner are forced to change their direction. (Note: until today no practicable Strut-and-Tie model was found.)

Properly dimensioned and reinforced corners can fail in two ways (Fig. 10):

- The corner crack a opens strongly; The transverse crack b , which adjoins the corner crack a , also opens too strong, and it constricts the compression zones of the adjoining sections that fails.
- During loading a further transverse crack (crack c in Fig. 10) develops in the outer corner region.

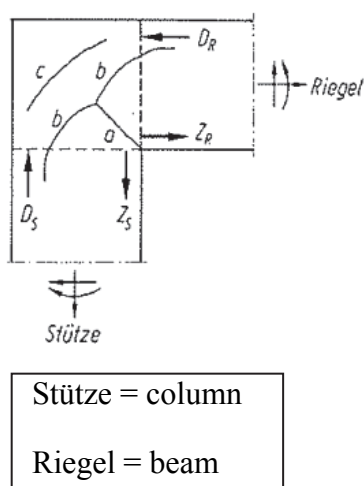


Fig. 10: Typical cracks of an opening corner

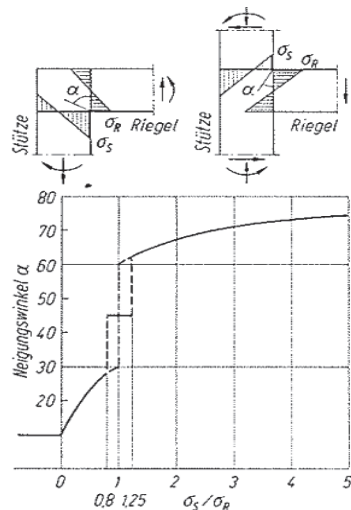


Fig. 11: Course of the angle of inclination of the corner cracks at 90° opening corners

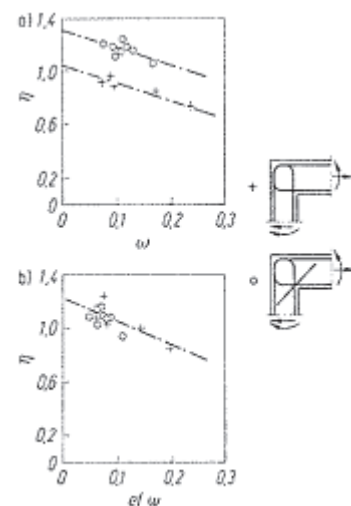


Fig. 12: η -values a) acc. to Nilsson (1973); b) acc. to the new concept

The evaluation of very extensive linear-elastic FE calculations of opening corners with different cross-section depths and stress ratios in the corner revealed that the direction of the tensile stress and thus the direction of the first bending crack at the corner depends only on the ratio of the inner edge stresses, σ_R and σ_S , resp. (Fig. 11).

$$\alpha = 30^\circ - 20^\circ \left(1 - \frac{\sigma_S}{\sigma_R} \right)^{1.5} \quad \text{for } \sigma_S/\sigma_R < 1.0$$

$$\alpha = 45^\circ \quad \text{for } \sigma_S/\sigma_R = 1.0$$

$$\alpha = 60^\circ + 20^\circ \left(1 - \frac{1}{\sigma_S/\sigma_R} \right)^{1.5} \quad \text{for } \sigma_S/\sigma_R > 1.0$$

The jumps in the course of this relationship can be explained as follows: the corner crack is actually the last crack of the beam or the column.

The corner can be loaded in such a way that, despite the positive moment, in the inner edge on the column section a small compressive stress occurs ($\sigma_S/\sigma_R < 0$). Then the crack, beginning practically from the inner corner, will proceed at an angle of $\alpha < 10^\circ$. In case of the stress ratio $\sigma_S/\sigma_R = 0.5$, it is practically still the beam that first cracks at the inner corner; But the inclination angle becomes larger ($\sim 23^\circ$). This crack, as it is known, relieves the concrete tension zone on its both sides, thereby fundamentally changing the conditions of the occurrence of another crack in the corner which could be a crack of the column. Practically, the occurrence of a second corner crack needs not be taken into account in the design.

In the vicinity of the stress ratio $\sigma_S/\sigma_R \approx 1.0$, the distribution of the local tensile strength of the concrete with respect to the first corner crack is decisive. The angle can be practically of any value between 30° and 60° . In this case 45° is decisive for the design of both cross-sections joining the corner region. For further details see Windisch (1988).

As verification in Fig. 12 the efficiency of the reinforcement pattern:

$$\eta = M_{\text{test}} / M_{\text{calc}}$$

is plotted as function of the mechanical rate of reinforcement

$$\omega = \mu f_{\text{sy}} / f_c'$$

with μ – geometrical rate of beam- and column tensile reinforcement, resp. for typical reinforcement patterns with and without additional corner reinforcement. It is striking that the two reinforcement patterns lead to two independent point groups. Fig. 12 b) shows the η -values calculated according to the methods presented here as function of the effective mechanical rate of reinforcement:

$$e_{f\omega} = \frac{\mu_L \Psi_L f_{\text{sy}L} + \mu_S \Psi_S f_{\text{sy}S} \cos \beta - \frac{N}{bh}}{f_c'}$$

It is noteworthy that in Fig. 12 b) all η -values form a single set of points.

4. CONCLUSIONS

A new concept of design of SC members was presented:

- Dimensioning for bending and shear are interrelated
- SC members fail along a discrete, critical section
- The location and form of the possible critical sections in ‘D-regions’ can be predicted
- In the shear resistance the aggregate interlock has no influence
- The concrete contribution is the ‘shear’ component of the compressive zone stresses
- Efficiency factor of inclined rebars must be taken into account.

The straightforward applicability of the proposed method is presented on two examples: dapped end and opening corner. The results are more than promising. Theoretically really sound dimensioning of SC structures in the XXIth century is a big challenge for all of us.

5. REFERENCES

- Gvozdev, A.A., Lessig, N.N. and Rulle, L.K., (1968) “Research on Reinforced Concrete Beams Under Combined Bending and Torsion in the Soviet Union”, American Concrete Institute Special Publication Sp18-11 “Torsion of structural concrete” 1968, pp. 307-336.
- Menétrey, Ph. (1995), “Flexural and punching failure experiments in r.c. slabs”, EPFL, March 1995, p. 36.
- Nilsson, I. H. E., (1973) “Reinforced Concrete Corners and Joints Subjected to Bending Moment. D7. National Swedish Building Research, 1973, p. 249.
- Sneed L.H. and Ramirez J. A. (2014), “Influence of Cracking on Behavior and Shear Strength of R/C Beams” ACI Structural Journal, March-April 2014, No. 111-S15
- Steinle, A. and Rostásy, P., (1975), “Zum Tragverhalten ausgeklinkter Trägerenden”, Betonwerk + Fertigteiltechnik 41 (1975), H. 6, pp. 270-277, H. 7, pp. 337-341.
- Völgyi, I., Windisch, A. and Farkas Gy., (2014), “Resistance of reinforced concrete members with hollow circular cross-section under combined bending and shear - Part I: Experimental Investigation”, Structural Concrete, Vol. 15/1, January 2014, pp. 13-20.
- Völgyi, I. and Windisch, A.: Resistance of reinforced concrete members with hollow circular cross-section under combined bending and shear - Part II: New calculation model”, Structural Concrete, Vol. 15/1, January 2014, pp. 21-29.
- Völgyi, I. Windisch, A., (2017), “Experimental investigation of the role of aggregate interlock in the shear resistance of rc beams”, Structural Concrete, Vol. 18/3, 2017
- Walraven, J., (2017), “Codes of practice: burden or inspiration?”, fib Symposium 2017, keynote lecture, Maastricht, The Netherlands, 2017
- Windisch, A. (1988), „Das Modell der charakteristischen Bruchquerschnitte – Ein Beitrag zur Bemessung der Sonderbereiche von Stahlbetontragwerken“, Beton- und Stahlbetonbau Vol. 83, 1988, H. 9, pp. 251-255., H. 10, pp. 271-274. Ernst & Sohn
- Windisch, A. (1994), „Zur Bemessung von Rahmenendknoten“, Beton- und Stahlbetonbau Vol. 89, 1994, H. 11, pp. 294-303., H. 12, pp. 340-343, Ernst & Sohn
- Windisch, A. (2000), “On the design of two-way reinforcements in R/C.”, Studi e Ricerche Scuola die Specializzazione in Costruzioni in Cemento Armato Fratelli Pesenti, Vol . 21, Italcementi Bergamo 2000, pp. 283-302.
- Windisch, A. (2000), “Towards a consistent design model for punching shear capacity”, International Workshop on Punching Shear Capacity of RC Slabs – Proceedings TRITA-BKN. Bulletin 57, 2000, pp. 293-302
- Windisch, A. (2002), “Reinforcement pattern of reinforced concrete members in pure torsion”, Befestigungstechnik, Bewehrungstechnik und ..., Festschrift Eligehausen, ibidem-Verlag, Stuttgart, 2002, pp. 293-302.
- Windisch, A. (2016) “Unified dimensioning for bending and shear“, Concrete Structures 2016, pp. 2-7.

PROBABILISTIC STUDY ABOUT UNCERTAINTIES IN PREDICTING SHEAR BEAM CRACKING AND FAILURE

Radomír Pukl¹, Vladimír Červenka¹, Tereza Sajdlová¹, Jan Červenka¹, Drahomír Novák²

¹ *Červenka Consulting, s.r.o.*

Na Hřebenkách 55, 150 00 Prague 5, Czech Republic

² *Inst. of Structural Mechanics, Faculty of Civil Engineering, Brno University of Technology
Veveří 95, 662 37 Brno, Czech Republic*

SUMMARY

Deep beam with large dimensions was investigated experimentally at University of Toronto, Canada. A competition for blind prediction of the beam failure was organized with more than 60 participants worldwide. The shear behaviour, cracking and strength of the beam was significantly affected by the large beam size. The best results were achieved and submitted by Červenka Consulting with ATENA deterministic numerical analysis based on nonlinear constitutive model of concrete using fracture mechanics. After the predictive contest authors performed several studies about input parameters of the material models, FE-mesh size etc. and their influence to the beam capacity, response and cracking. An advanced probabilistic analysis based on LHS method with random fields and random variables approaches has been consequently applied and evaluated.

1. INTRODUCTION

Theories are best validated on laboratory experiments in competitions, where experimental results are not known to competitors, because experiments are performed after the predictions are submitted. Recently, the “Prediction contest for strength of four meter deep reinforced concrete slab strip” organized by M.P. Collins and E.C. Bentz from University of Toronto (Collins et al., 2015) was aimed to large structures, where size becomes an important factor. The strength prediction submitted by the authors was selected as the best among 66 participants. The Toronto contest included two tests, one without shear reinforcement and other with stirrups.

The authors simulated the specimen behavior, namely the crack propagation, by the finite element method with a constitutive model based on the smeared crack approach with crack band regularization. At the prediction phase when the experimental response was not known a sensitivity to model parameters was experienced. This poses a problem for the right choice of model parameters relevant for the fracture analysis. The laboratory test provided the concrete compressive strength as the only parameter describing concrete properties. The other parameters such as tensile strength or fracture energy were not tested. In this situation, which is typical in practice, one has to rely on derivation of these parameters from generally known relationships from codes and other research sources. Further on, an effect of the finite element size should be minimized. At the prediction phase authors based these choices on experience gained from other validations (Galmarini et al., 2015), (Červenka et al., 2014). After publication of the contest results (Collins et al., 2015) an investigation of parameter sensitivity was conducted with the aim to describe the model uncertainty of the simulation method.

2. NUMERICAL MODEL

The specimen representing a 0.25 m wide strip of a 4 m deep slab shown in Fig. 1 has the support span of 19 m, is loaded by the force positioned non-symmetrically and provided by shear reinforcement in the left shear span only. The left span is reinforced by vertical T-head bars $\text{Ø}20$ mm at spacing 1.5 m. The bottom bending reinforcement is realized by 9 bars of 30 mm diameter in 3 layers. Material properties were described by concrete strength 40 MPa, reinforcement yield strength 573 MPa, ultimate steel strength 685 MPa and ultimate strain 18%. It is designed so that it would fail first in the right shear span denoted as the “east test”, with a/d ratio 3.12 while that of the left span denoted as the “west test” with a/d ratio 1.82 is expected to have an increased strength.

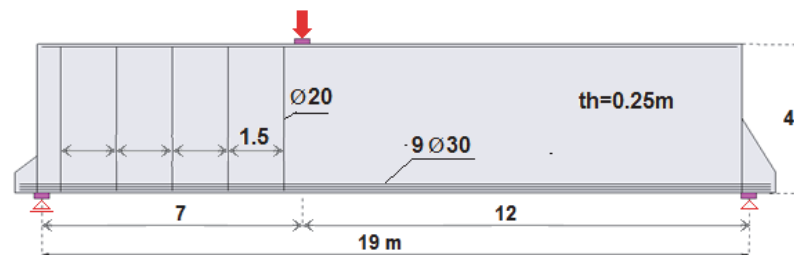


Fig. 1: Test specimen geometry

The smeared crack analyses performed in this investigation were made with the program ATENA (Cervenka et al., 2015) using the combined fracture-plastic model for concrete of Červenka & Papanikolaou (Cervenka & Papanikolaou, 2008). Model principles can be described as follows:

- strain decomposition into components of damage (elastic, plastic, fracture and others),
- smeared crack model, crack band localization limiter, fixed cracks,
- fracture modes I and II, due to crack opening and sliding,
- reduction of compressive strength due to tensile cracks,
- multi-axial behavior in compression by the Menetrey-Willam model (Cervenka & Papanikolaou, 2008),
- Rankine criterion for tensile fracture with exponential softening of Hordijk (Hordijk, 1991),
- determination of stress softening in tension using the crack band approach of Bažant & Oh (Bažant & Oh, 1983) and analogically in compression according to Cervenka et al (Cervenka et al., 2014).

The nonlinear solution is incremental with iterations in each load step by Newton-Raphson method until restoring equilibrium. The finite element model is made for a plane stress simplification, with low order quadrilateral isoparametric elements with 2×2 integration scheme, with the square elements shape and size of 100 mm, i.e. 20 elements through the height. In addition, in a case study a quadratic element with eight nodes and nine integration points was used. The loading is applied by the imposed displacement on the top loading plate and the force is obtained as a reaction. Reinforcement was modelled by truss elements embedded into concrete elements. A perfect bond is assumed for interaction between reinforcing bars and concrete.

Based on previous experience (Cervenka, 2013), (Cervenka & Papanikolaou, 2008) it was assumed that the basic material parameters (such as concrete elastic modulus, Poisson ratio,

compressive and tensile strengths and fracture energy) can be considered by standard values, see Tab. 1. The attention was devoted to shear behavior of crack face, described often as “aggregate interlock”, which is characterized by the shear factor S_F . It relates the shear fracture Mode II to the crack opening fracture Mode I. Shear factor $S_F = 50$ was used in the prediction stage.

Tab. 1: Concrete material parameters

<i>Parameter</i>	<i>Value</i>
Elastic modulus initial E [MPa]	34129
Poisson ratio	0.2
Compressive strength f_c [MPa]	40.0
Tensile strength f_{ct} [MPa]	3.0
Fracture energy G_f [N/m] (MC90)	78
Plastic disp. in compression w_d [mm]	5
Fixed cracks	1.0
Strength reduction r_c^{lim}	0.8
Shear factor S_F	50

3. PREDICTION AND EXPERIMENT

The loading test was performed in two phases. In Phase I loading was increased till failure, which occurred in east span. After this the east span was strengthened by external bars and the west test was performed. This allowed to obtain two shear tests on one test specimen. Both tests were simulated in the ATENA software; load-displacement diagrams are compared in Fig. 2. Average error from two predictions is only 1% indicating extremely good prediction. A source of individual errors can be attributed to the random effects of material properties and also to model uncertainties. Detailed information about the prediction results can be found in (Cervenka et al., 2016b).

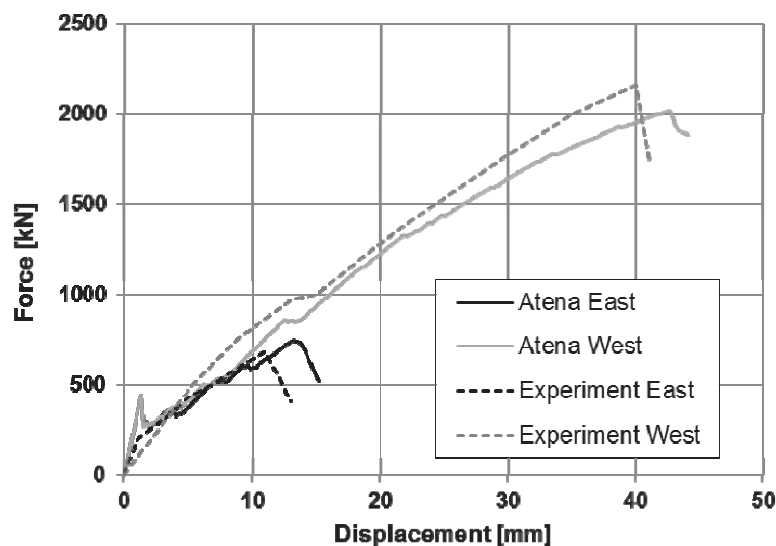


Fig. 2: Load-displacement diagrams - comparison of prediction by ATENA with experiment

Failure mode is described by crack patterns shown in Fig. 3. In the east test without shear reinforcement a distinct diagonal crack formed, which can be attributed to a brittle tensile failure in concrete. In the west test with shear reinforcement and also with lower shear span

ratio the failure was due to the simultaneous contribution of tensile crack, vertical reinforcement yielding and compressive crushing of concrete at the top root of diagonal crack near the loading point. The yield stress of the main horizontal reinforcement was not reached in any of the tests. It could be concluded that predicted strength as well as failure modes agreed very well with experiments, as documented in Fig. 3.

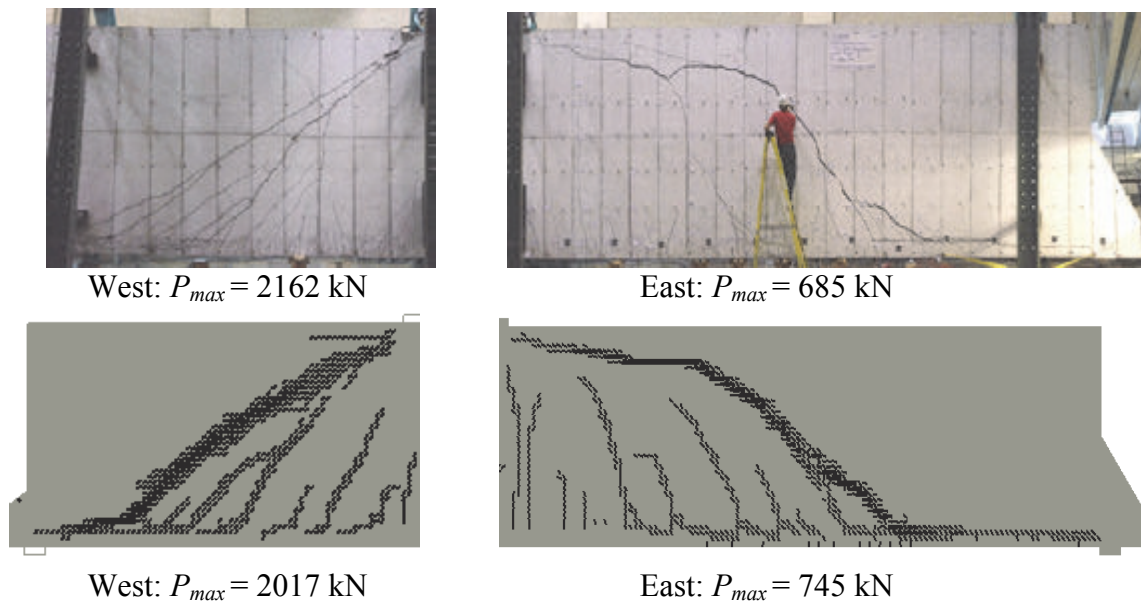


Fig. 3: Crack patterns: above – experiment (Collins et al., 2015), below - ATENA prediction

4. PARAMETER STUDY

After the test results were made public, the authors performed a sensitivity study on the selected model parameters (Červenka et al., 2016a). First, the mesh size effect was investigated for the element sizes 50, 100, 200 and 400 mm. The load-displacement diagrams are shown for low order square elements with 2x2 integration scheme in Fig. 4 (left) and for high order quadratic elements with 3x3 integration scheme in Fig. 4 (right).

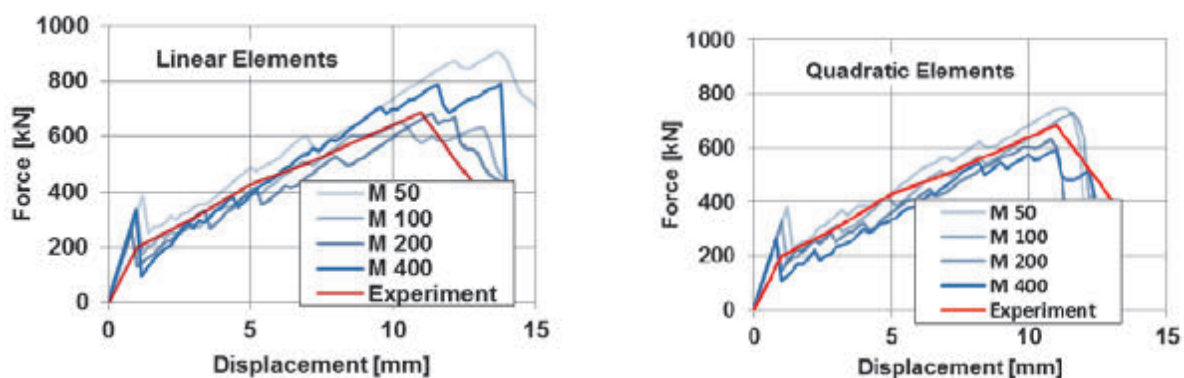


Fig. 4: Mesh size effect – (left) low order elements, (right) quadratic elements

The shear factor was found to be an essential parameter for the study. Low shear factor may produce a change of failure mode. Instead of a diagonal crack a system of strut and tie can be formed. Consequently, the tensile failure due to a diagonal crack is changed to the compressive failure and may lead to a high resistance. Therefore the shear factor $S_F = 200$ was used for this study.

Both element types indicate systematic increase of stiffness with the mesh refinement. The response curves are almost parallel but shifted to higher resistance. This trend can be attributed to the concrete tension stiffening, i.e. contribution of the cracked concrete to the reinforcement stiffness. Apparently, in large meshes the concrete contribution is less due to large volume of the cracked concrete. The crack patterns after failure shown in Fig. 5 reproduce very well the experimental behavior and are consistent for both element types and all mesh sizes. Visible cracks larger than 0.2 mm are denoted by lines showing crack orientation in elements.

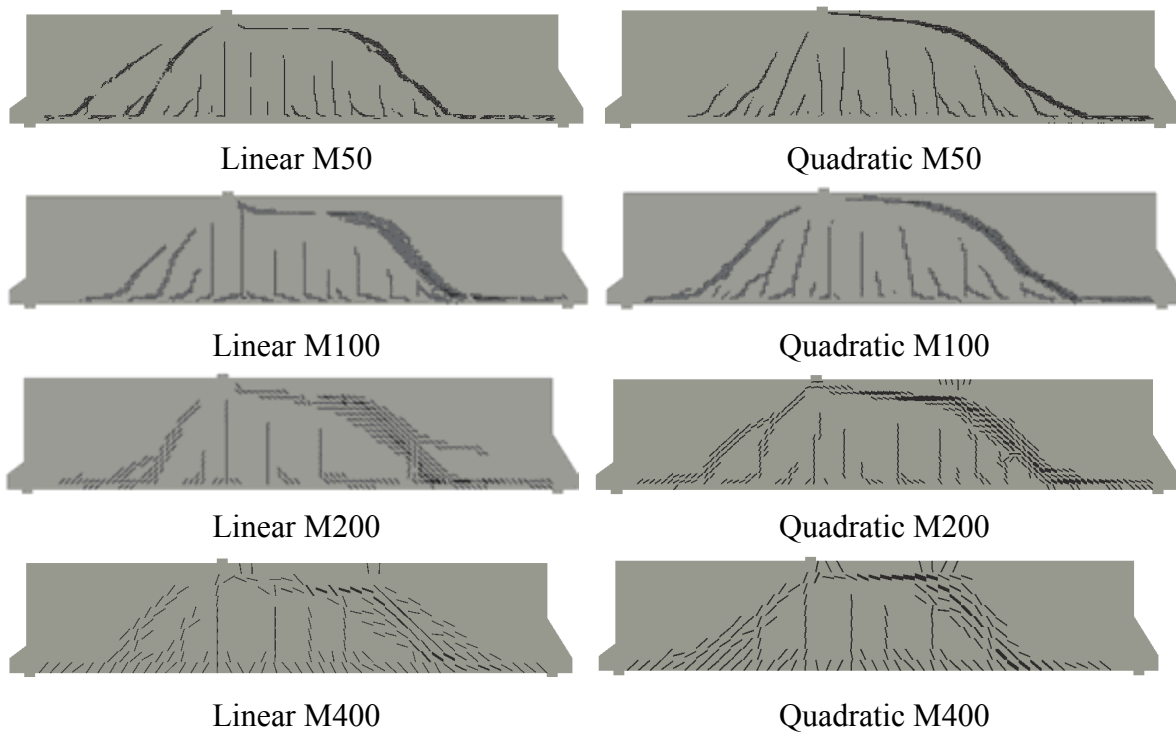


Fig. 5: Crack patterns for low order meshes (left) and quadratic meshes (right)

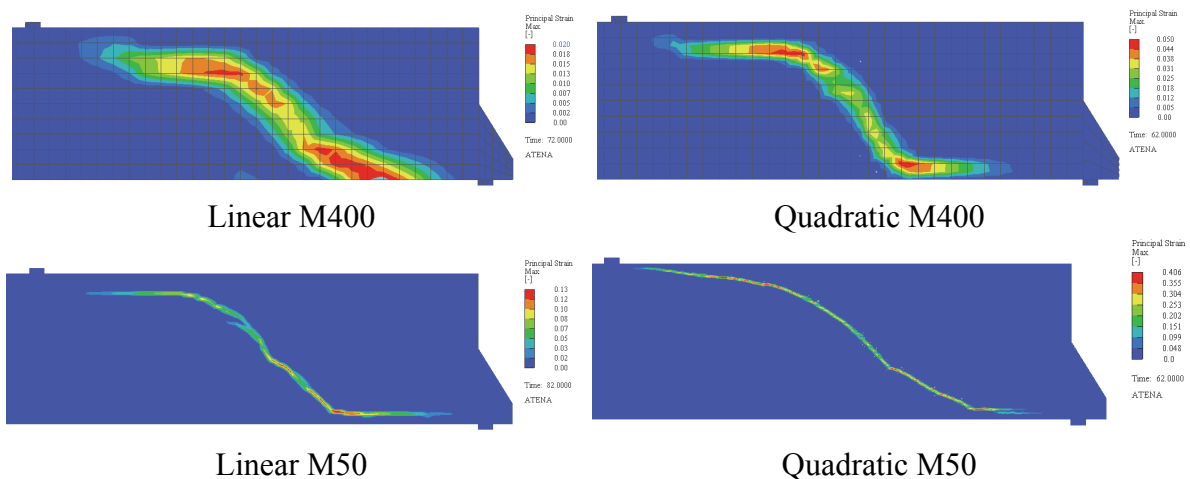


Fig. 6: Strain localization for different meshes

The mesh size effect on the shear strength is stronger in linear elements. The strength range for linear elements is 260 kN (from 646 to 906 kN), for quadratic elements it is 181 kN (from 603 to 784 kN). This is probably caused by different crack paths, which are the result of a strain localization in different meshes and element types. This is illustrated in Fig. 6, where

iso-areas of strains indicating the crack paths in early post-failure stages are compared for two meshes M400 and M50 and two element types. Such a difference can be observed, for example, between the linear and quadratic elements in mesh M400 near the bottom edge and in the mesh M50 near the top and bottom edges.

5. PROBABILISTIC ANALYSIS

A discrepancy between prediction and experiment was observed at the stage of crack initiation. It is believed that this is due to inability of the deterministic model to capture the non-homogeneity of concrete. This is illustrated in Fig. 7, where a “jump” in the simulated response diagram at point A is caused by a sudden propagation of a vertical crack at point B. This can be explained by the instability of the softening solution in the nearly uniform field of smeared cracks with a sudden strain localization. Such response was not observed in the experiment. It is believed that in a real material the localization is triggered by imperfections in early stages of cracking and large zone with almost homogenous strains does not appear. This can be addressed by the application of the spatial probabilistic distribution of material properties. The effect of two fracture parameters, tensile strength f_t and fracture energy G_f , was investigated using the probabilistic model.

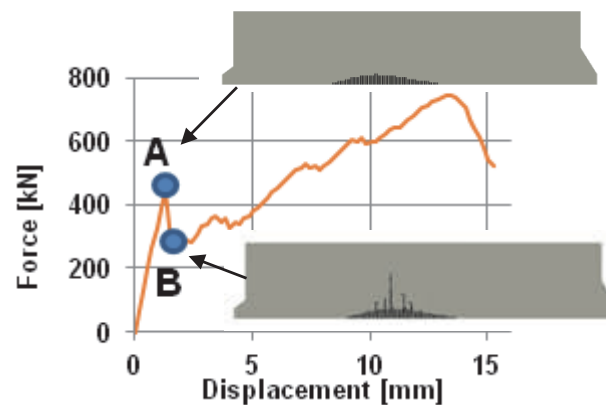


Fig. 7: Strain localization at the crack initiation

In attempt to explain this behavior a probabilistic model was developed using the software SARA, which is based on the work of research group in Brno Technical University reported by Vorechovsky (Vorechovsky & Novak, 2005).

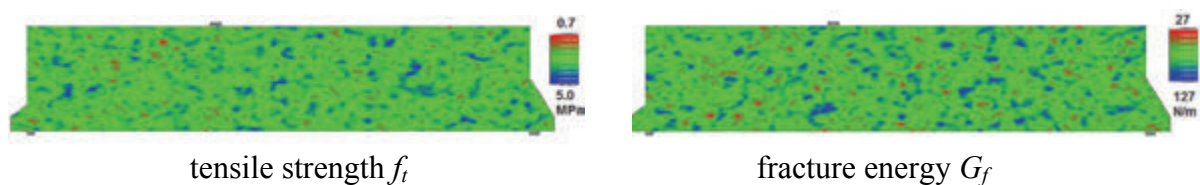


Fig. 8: Example of random fields

In the probabilistic model, two material parameters deciding about the fracture response, namely tensile strength and fracture energy, are modeled as random fields over the two-dimensional domain of the strip as shown in Fig. 8. The fields are generated under the assumption of normal distribution with average values of parameters given in Tab. 1, coefficient of variation 0.2 and two correlation lengths, 0.2 and 0.1 m for horizontal and vertical directions respectively.

A set of 32 simulations was generated using the LHS sampling resulting in load-displacement diagrams shown in Fig. 9 (left).

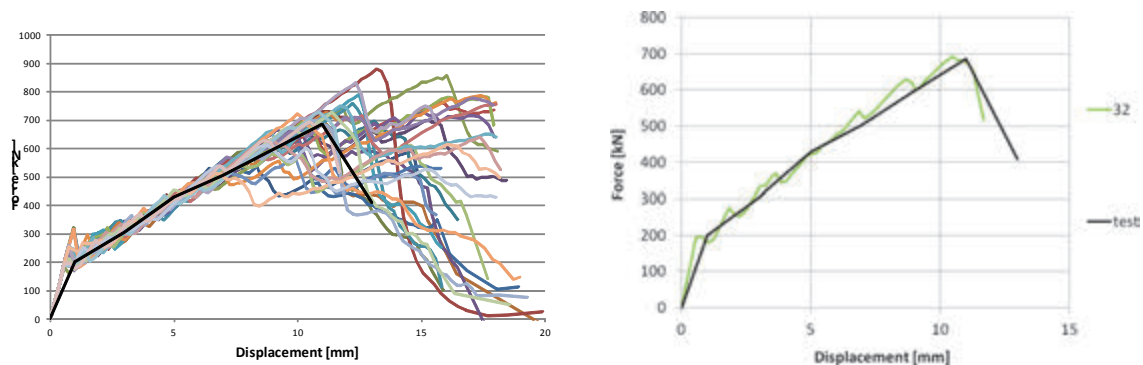


Fig. 9: (left) response diagrams generated by random fields, (right) best fitting sample No. 32

It can be observed that for many simulations the stability jump at the crack initiation does not happen and thus the agreement with the experimental response is even better, as documented by comparison of the test response and the best fitting random field sample (Fig. 9 left).

The average strength of 715 kN from random simulations corresponds well with the strength of the experiment 685 kN. The range of random strength values is quite large, 306 kN (from 573 to 879 kN). The scatter is obviously directly dependent on the assumed variability of random fields. More data describing the non-homogeneity distribution in real structures are required for further improvement of this exercise.

6. CONCLUSIONS

The finite element analysis based on the smeared crack approach and fracture mechanics provided a realistic prediction of slab strip behavior tested experimentally in Toronto shear contest. However, significant uncertainties are involved and should be considered in result interpretation.

The model uncertainties were investigated for two element types, linear and quadratic, and for four mesh sizes. The experimental response described by a load-displacement curve was located approximately in the average of all simulations. The uncertainty of strength due to mesh size effect described by the range of strengths was 38% (i.e. +/- 19% about average) for linear elements and 26% (i.e. +/- 13%) for quadratic elements (with reference to the experimental strength).

Considering strength prediction the mesh sizes of 100 and 200 mm provided the best results close to mean (and also to experiment), while the extreme sizes 50 and 400 mm gave worse results. Thus, element sizes close to sizes of usual material test specimen (150 mm) seems to be optimal.

The probabilistic model revealed, that a “jump” during the initial crack propagation can be explained by the homogenous material assumed in the model. An introduction of randomly distributed material properties helped to avoid this discrepancy. The probabilistic study indicated also an effect of material random variability on strength, which was in the range of 42% (or +/- 21%) of the shear strength.

The present study offered interesting answers to many questions related to the Toronto contest, while it also opened many questions. It is a motivation for a future research to derive partial safety factors for large structures for material and model uncertainties based on probabilistic safety formats.

7. ACKNOWLEDGEMENTS

Background for the paper was gained under financial support of the Czech Grant Agency project 16-04132S „Epistemic uncertainties of crack models in RC structures“.

8. REFERENCES

- Bazant, Z.P., Oh, B.H. (1983), “Crack band theory for fracture of concrete”, *Materials and Structures*, RILEM 16 (3), pp. 155–177.
- Cervenka, J., Cervenka, V., Laserna, S. (2014), “On finite element modelling of compressive failure in brittle materials”, *Computational Modeling of Concrete Structures*, Euro-C 2014, St. Anton, Austria, ISBN 978-1-138-00145-9, pp. 273-281.
- Cervenka, J., Jendele, L., Cervenka, V. (2015), “ATENA Program documentation”, Cervenka Consulting, www.cervenka.cz.
- Cervenka, J., Papanikolaou, V.K. (2008), “Three dimensional combined fracture-plastic material model for concrete”, *Int. J. Plast.*, 2008, 24:2192–220, doi:10.1016/j.ijplas.2008.01.004.
- Cervenka, V. (2013), “Reliability-based non-linear analysis according to *fib* ModelCode 2010”, *Structural Concrete*, Journal of the *fib*, Vol. 14, March 2013, ISSN 1464-4177, pp. 19-28.
- Cervenka, V., Cervenka, J., Jendele, L., Smilauer, V. (2014), “ATENA simulation of crack propagation in CONCRACK benchmark”, *European Journal of Environmental and Civil Engineering*, Taylor Francis, Vol. 18, No.7, 2014, pp. 828-844.
- Cervenka, V., Cervenka, J., Pukl, R., Sajdlová, T. (2016a), “Prediction of shear failure of large beam based on fracture mechanics”, *FraMCoS-9*, Berkeley, California, USA, 2016.
- Cervenka, V., Cervenka, J., Sajdlová, T., Pukl, R. (2016b), “Uncertainty of Predicting Shear Strength”, 23rd Czech Concrete Days, Litomyšl, Czech Republic, 2016.
- Collins, M.P., et al. (2015), “Challenge of Predicting the Shear Strength of Very Thick Slabs”, *Concrete International*, Vol. 37, No. 11, November 2015, pp. 29-37.
- Galmarini, A., Lochner, D., Marti, P. (2015), “Predicting the response of reinforced concrete slab strips subjected to axial tension and transverse load: a competition”, *Structural Concrete* Volume 16, Issue 2, June 2015, pp. 172–183.
- Hordijk, D.A. (1991), “Local approach to fatigue of concrete”, PhD Thesis, Delft University of Technology, 1991, The Netherlands.
- Vorechovsky, M., Novak, D. (2005), “Simulation of random fields for stochastic finite element analysis”. *ICOSSAR 2005*, Millpress, Rotterdam, ISBN 90 5966 040 4.

SHEAR LOAD ASSESSMENT OF EXISTING CONCRETE BRIDGES BY NONLINEAR FE-MODELLING

Michaela Kopp¹, Markus Vill
Vienna University of Applied Sciences, Department for Building and Design
Favoritenstraße 226
1100 Vienna
¹ *Michaela.kopp@fh-campuswien.ac.at*

SUMMARY

This research paper deals with different concrete slab railway bridges, which were built in the years 1930 to 1990 and should be used in their current mode of operation at least until the end of their expected economic lifetime or even further.

Due to the conservative approaches in terms of design, it is not possible to provide documented evidence of conformity for slab bridges of the last century 0. But for all that, these structures are still in use and do not show many noticeable damages. Hence, it was important to represent the interacting load bearing capacity, or rather the remaining safety, with the use of nonlinear FE modeling. The main target of this research was to display structural reserves of existing slab bridges within the context of the bridge management system nowadays. To ensure the quality of the results, all investigations are verified by numerical analysis, which use the current Eurocode 1 for the design action referring to load model 71, the operation trains D4 and the limits of the V_{Ek} values of B2302 (ÖNORM B2302, 1931) from the year 1936. The shear resistance values were compared with different design methods like EC2 (ÖNORM EN 1992-1-1), the *fib* Model Code 2010 and the results of the nonlinear FE- modeling of ATENA 2D and 3D (Cervenka et al. 2015). The calculation of ATENA 2D (Cervenka et al. 2015) used single span girders, which were bonded at the threefold of their effective depth.

Finally the investigations pointed out that 50% of the design value of the reinforcing steel in addition to the concrete contribution according to EC2 should be used by the verification of existing slab bridges with bent-up bars. Furthermore, with the consideration of these calculatory assumptions, the normative safety of bridge structures could be achieved and many bridges are still safe to use in their mode of operation, if the maintenance conditions are adequate.

1. INTRODUCTION

According to the recalculation using current standards 0, some bridge structures do not need any strengthening whereas others may need to be strengthened or even completely replaced. In addition to that, the Eurocode 2 prescribes that bent-up bars should cover only fifty percent of the entire shear load. In this way, there is often no option to fulfil the requirements of the current standards for the assessment of the existing bridges, which has to be done if there is a change due to enlargement of the load. This high level of safety, which happens due to neglected load bearing effects, was investigated for existing concrete slab bridges with bent-up bars.

The calculation, respectively the assumptions, was generated referring to the proof of perforation. Contrary to bent-up bars in slab bridges, the provision for bent-up bars in the

ceiling refers to the thickness of the slab. The results of the numerical simulation and the suggestion in this research paper are to consider fifty percent contribution of the yield strength of the bent-up bars.

The most important facts concerning the investigated bridge structures are:

- the static system of each bridge is a single span girder with a span width from ten to nearly thirteen meters,
- the statically effective depth varies between 69 cm and 87 cm,
- the steel types are B500A and B550A,
- the longitudinal reinforcement area varies between $39.1\text{cm}^2/\text{m}$ to $72.75\text{cm}^2/\text{m}$.

1.1 Investigations of bridge structures

For the analysis of the ultimate load, a cross-sectional area of the existing reinforcement of the total span was used. The span has a length of 7.2 m; the height of the slab varies between 0.66 m and 0.8 m in the middle of the bridge. The concrete class was C30/37 and the thickness of the concrete cover was about 3 cm. To induce the force into half of the bridge's structure due to symmetric boundary conditions, steel plates were used. The dimensions of the steel plates are about 20 cm in length and 3 cm in thickness and are positioned at the distance of 3.5 times of the effective depth of the section. All results are listed in table 1. The reinforcement of the beam was calculated in relation to the whole slab. The analysis is separated in two load cases, load case 1, the support of the beam with the steel plates and load case 2, the load which was applied by prescribed deformation which presses the slab downwards. The load steps, which have different multipliers, were calculated step by step. The first 40 load steps have a coefficient of 1.0, the next 40 steps work with a coefficient of 0.1 and the next steps are continuously levelled till 120 analysis steps are remaining.

2. NONLINEAR FINITE-ELEMENT INVESTIGATION OF BRIDGES

2.1 Dimensions and reinforcement of bridge structure B05

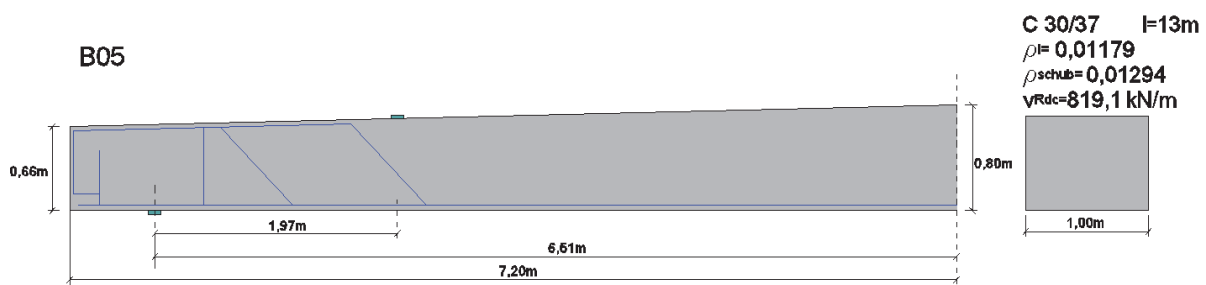


Fig. 1: Dimensions of the beam B05

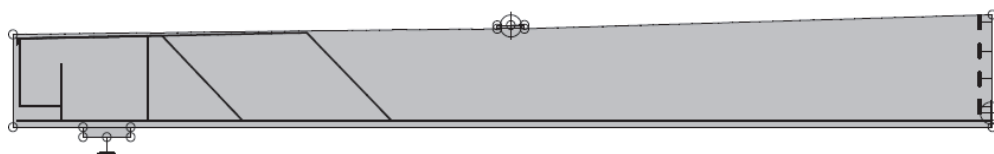


Fig. 2: Reinforcement of the 2D structural model

In comparison with the other bridge structures, B05 pictures the highest shear resistance, as shown in Figure 3 excepting B09 bridge structure, which was a post-tensioning bridge structure. The stated reasons are the lean beam and the high graduated shear reinforcement ratio of about $\rho_w=0.013$. Also, the good concrete quality of C30/37 influences the load-bearing behaviour positively.

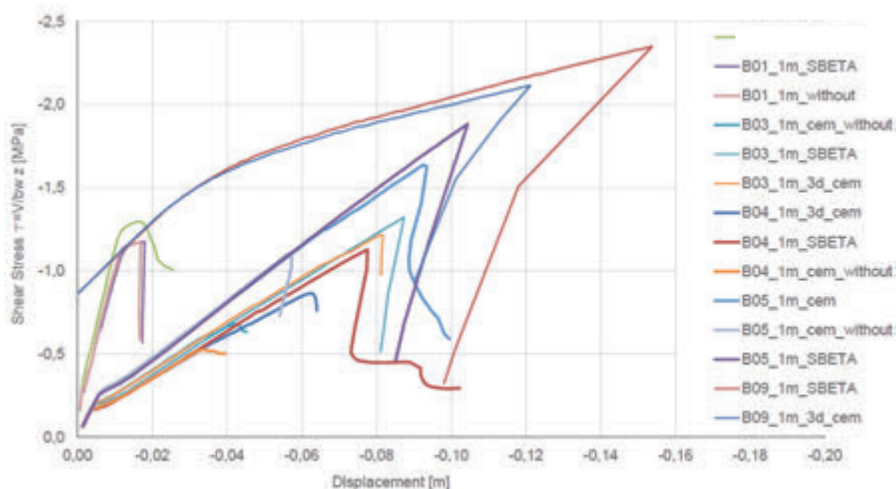


Fig. 3: overview of the parameter study 2D and 3D

3. 2D – MODEL ANALYSIS

The nonlinear-finite-element simulation was carried out with the software ATENA (Cervenka et al. 2015). Therefore, different material models were used to calculate the bridge structures. In total, 5 bridge structures, built between the 1940s and the 1990s were investigated. For the simulation, the SBETA Model, as well as a Fracture Plastic Constitutive Model (CC3DNonLin Cementitious2), were used to investigate the influence of the material model.

3.1 Parameter study 2D beam

Fig. 4 shows the ultimate load of 819 kN/m, which comes to failure at a displacement of 92 mm. After achieving the maximum load, the iterative calculation process is stopped due to discontinuity. Fig. 4 significantly marks the higher shear resistance of the SBETA 0 material. Furthermore, the chart describes a shear failure, which can be seen in the big difference between the shear resistance of the structure with and without bent-up bars. The design shear resistance achieved by the concrete without shear reinforcement according to EC2 is about 246 kN/m, which points out existing reserves of the load-bearing behaviour in contrast to the FE-model of about 560 kN/m. This would mean in further consequence, that EC2 shows additional safety. The simulation of the slab without bent-up bars was limited by an ultimate load of 550 kN.

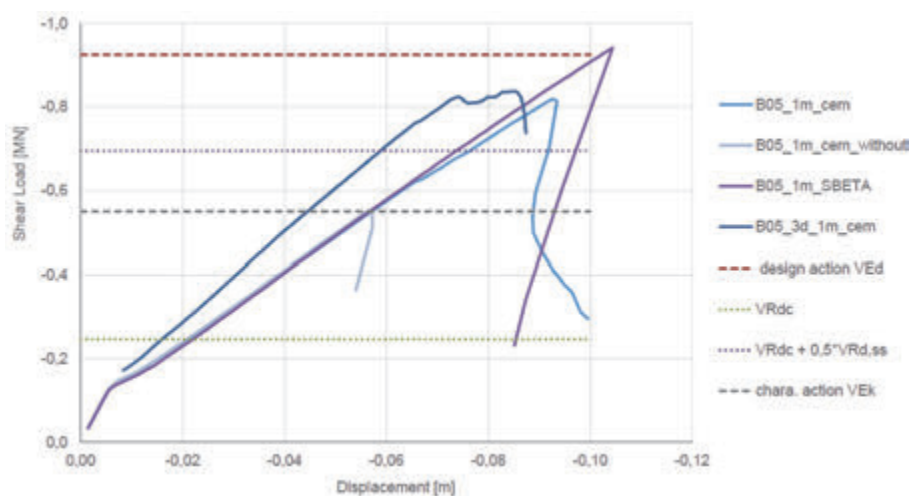


Fig. 4: Depiction of the differences between the shear-load displacement course with and without bent-up bars and different material parameters like the 3D – cementitious and SBETA

3.2 Required characteristic action of shear (V_{Ek}) under the terms of LM71, Eurocode 1 for railway bridges

The plot significantly marks the higher shear resistance of the SBETA material. Furthermore, the chart describes a shear failure, which can be seen in the big difference between the shear resistance of the structure with and without bent-up bars. The design shear resistance achieved by the concrete without shear reinforcement according to EC2 is about 278 kN/m, which points out existing reserves of the load-bearing behaviour in contrast to the FE-model of about 540 kN/m. This would mean in further consequence, that EC2 shows additional safety.

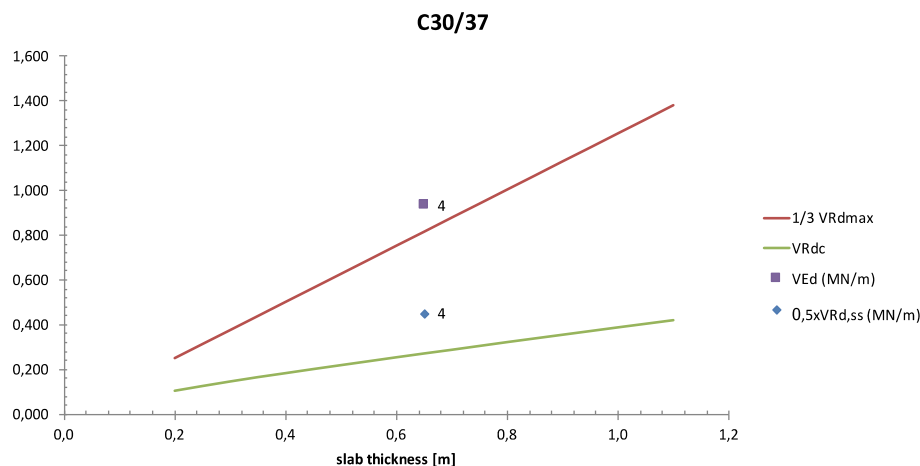


Fig. 5: Comparison of shear resistance over slab thickness for bridge structure B05 according to EC2 and EC1

As Fig. 5 shows, the calculations illustrate that an ultimate load level of 819 kN/m could be achieved by nonlinear-finite-element modeling, whereby the required design load for railways should consider a load level of about 925 kN/m as a result of all load combinations and additional load class factors. This implies that the value of the FE-model overruns the characteristic value of the load model 71 according to the EC1, which correlates with the other findings of the research. The current standards allow taking into account 50% of the shear contribution of the bent-up bars in addition to the shear stirrups. A combination of the contributions of bent-up bars and concrete without shear reinforcement is not allowed in the current standards.

3.3 Detailed results of the 2D model

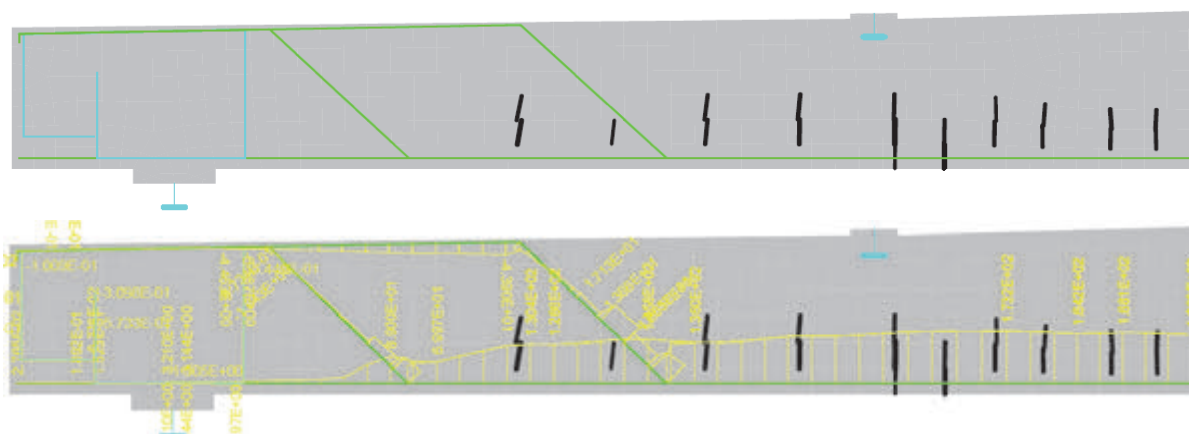


Fig. 6: The progress of steel stress σ_{xx} [MPa] at the load concrete resistance level V_{Rd} of EC2 with a flexural crack width starting from 0.1 mm

The maximal stress of the reinforcement at the load concrete resistance V_{Rdc} level of EC2 faces a force of 374 kN/m, which was achieved at load step 26. This resistance causes a stress of 146 N/mm² in the reinforcement. The concrete starts cracking once a stress of 60 N/mm² is achieved in the reinforcement, which is set at load step 6. This confirms the assumption that the bent-up bars can only be activated if there is an increase of the strain in the concrete and a crack crosses the shear reinforcement.

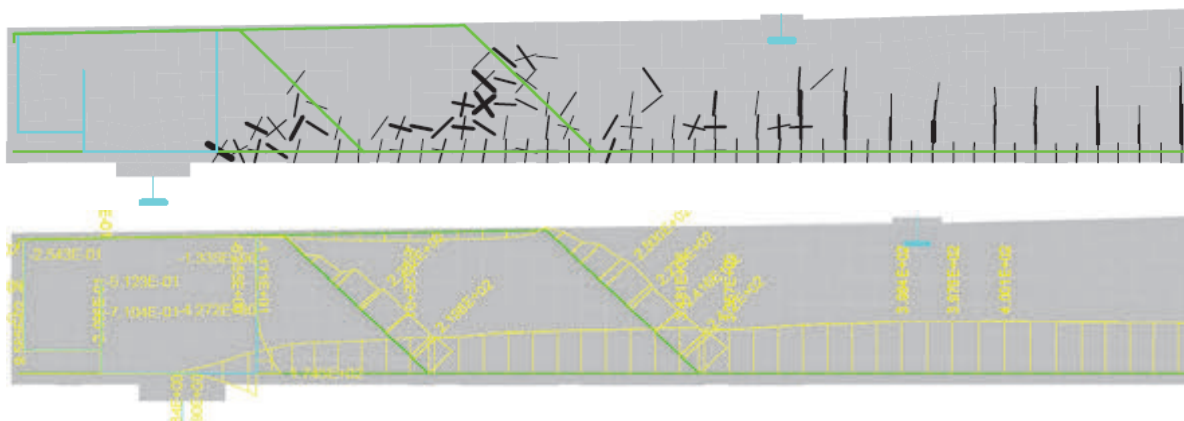


Fig. 7: The progress of steel stress σ_{xx} [MPa] at the ultimate load level

In ultimate load level condition, which starts at load step 68, the bent-up bars face a shear stress of 250 MPa. Fig. 7 shows that the concrete is cracking through the shear reinforcement area accordingly to the rising shear stress. In this connection, the shear reinforcement operates at 50% of its capacity.

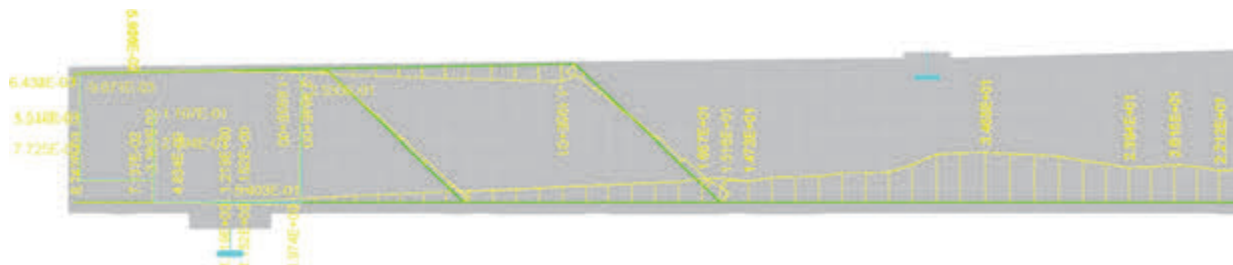


Fig. 8: The progress of steel stress σ_{xx} [MPa] of B05 at the transition of condition I to condition II

At the transition of condition I to condition II the maximum stress of the reinforcement before cracking is about 15 N/mm², which is achieved at load step five.

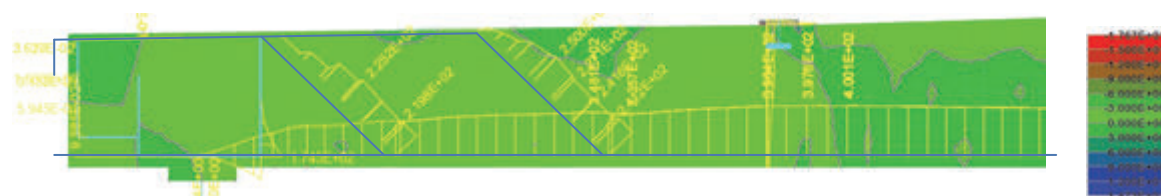


Fig. 9: Progress of stress τ_{xy} at ultimate load [MPa]

The area of stress includes shear stress from τ_{xy} -3.0 N/mm² to +3.0 MPa at maximum or minimum loaded elements.

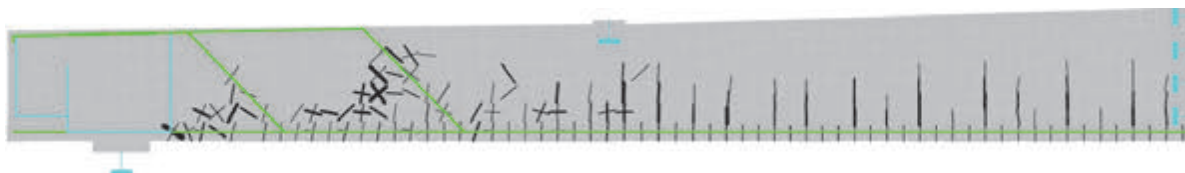


Fig. 10: Crack configuration and crack openings of structure B05 at the ultimate load level faces crack patterns at ultimate load, which visualizes cracks at a width of more than 0.1 mm

The maximum crack width is about 0.8 mm, which starts at a stress level of $\sigma_T = 2.75$ MPa. The simulation shows that the concrete starts cracking at load step 6, which equals a deflection of about 1 mm.



Fig. 11: Principal tensile stress [MPa], shear reinforcement stress of structure B05

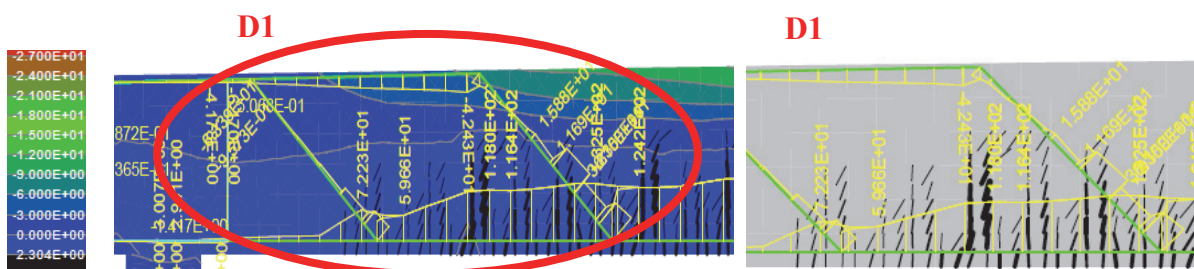


Fig. 12: 2D girder modeling – quasi-continuous load $V_{Ek} = 350$ kN/m, above displayed with crack pattern

Figure 12 displays the results of the quasi-continuous load, which is about 44% of the ultimate load. The chart illustrates the different load levels and points out that there is no exceeding of the ultimate load. The stress in the longitudinal flexure reinforcement has a value of 160 MPa, and the stress in the bent-up bars show values of 38 MPa after cracking. The results show that the shear forces are covered mostly by the concrete contribution.

Tab. 1: Overview of the comparison between different design standardizations and the numerical analysis

structure	shear resistance [kN/m]			shear stress [N/mm ²]	performance ratio []	
	EC 2	MC 10 LoA II	ATENA 3D	τ_{test}	ATENA/EC 2	ATENA/MC10
B05	$V_{Rd,c}$			$V_{R,test}$	2.17	2.43
	374	335	819	1.61		

4. COMPARISON OF THE DIFFERENT TEST SERIES

Fig. 13 displays the shear stress of the different samples as a function of the inner lever arm. The described bridge structure is noted as B05. The approach exemplifies that the 2D and 3D analysis picture quite similar results. The overview makes clear that the numerical results of this investigation conform to the results of other researchers. Further, this work deals with the question of a realistic bent-up bar calculation and how it could be represented in an appropriate calculation model for Eurocode 2 or *fib* Model Code 2010. To adapt the currently valid standards for assessment of existing structures, continuing test series have to be carried out. The analysis of five different slab bridges in Austria was carried out by using 2D and 3D nonlinear FE modeling. These FE models vary between two different conditions, one condition uses bent-up bars, the other does not have any kind of shear reinforcement, consequently, there are two kinds of material parameters.

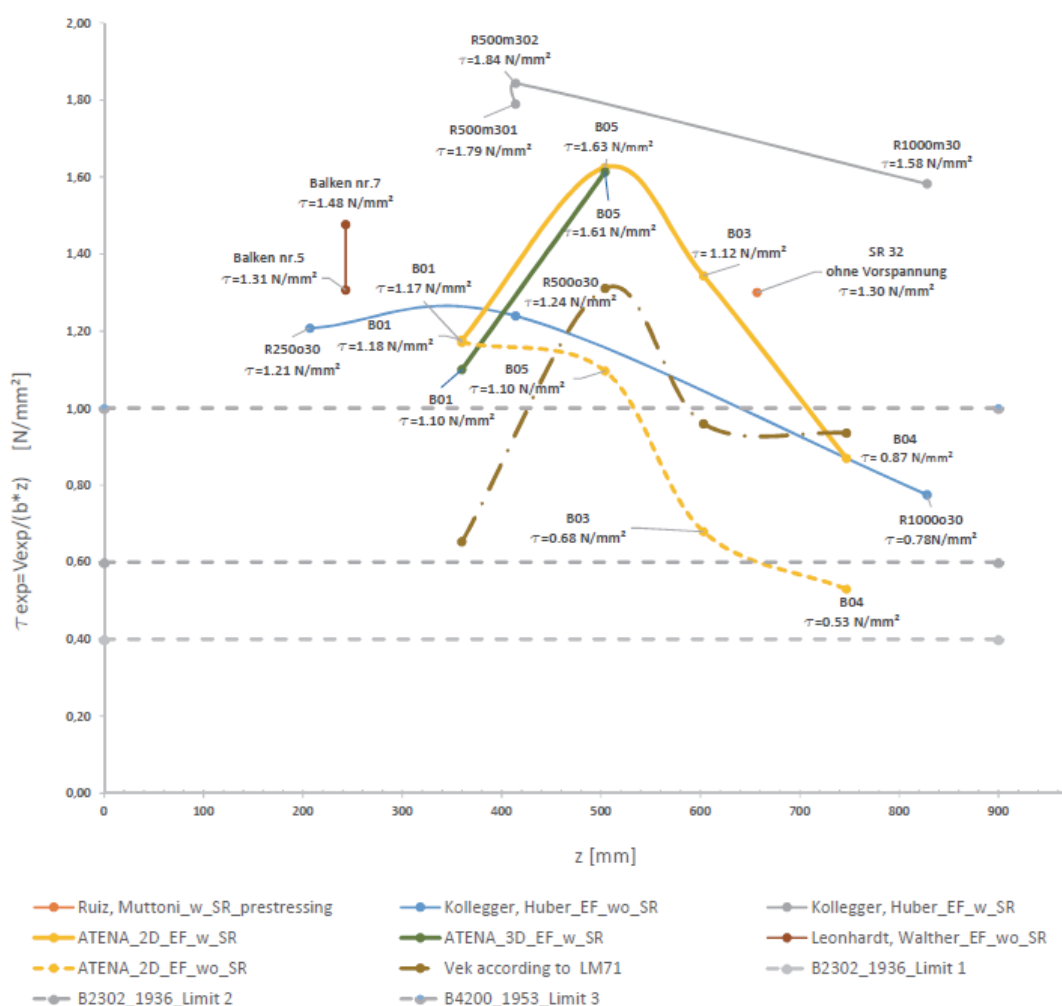


Fig. 13: 2D girder modeling – comparison of shear stress as a function of the inner lever arm

The calculation displays the bridges with shear failure and the bridges with bending failure and it also gives advice for the right use of the different material parameters. Nowadays, the most important design specification insists on the verification of existing bridges and giving a statement about their load-bearing behaviour. Through the use of the currently valid design standards, it is not possible to get positive, documented evidence of conformity, so this approach uses nonlinear FE modelling to expose load bearing reserves. To get a good overview, the complementary shear stress of the analysed slabs is compared with the limits of B2302 (ÖNORM B2302, 1931) and the V_{EK} values of load model 71. The design concept of

B2302 from the year 1936 deals with a high level of loads for beams without any shear reinforcement. As opposed to this, one-third of the shear reinforcement is needed compared to current requirements. The analysed models also contain a pre-stressed concrete bridge, which shows the threefold concrete design ultimate load of the EC2 provisions.

The sensitivity analysis of this research describes that the bent-up bars can only be activated if a shear crack crosses the shear reinforcement. If this crack does not cross the shear reinforcement, the activation of the bent-up bars would not happen.

As a threshold matter, there was no exceedance of the yield strength of bent-up bars during the simulation at ultimate load. Neither was there total utilization of the stress in the steel. Therefore only a specific percentage of the yield strength of bent-up bars in addition to the shear contribution of concrete should be used in the calculatory approach. Conformable to the study, the bent-up bar's consideration is limited to 50% of the yield strength of steel, because the strain of the shear reinforcement inclination would cause a distinctive crack pattern, which further causes a reduced shear contribution of concrete. According to design standards, the shear resistance provided by bent-up bars is only permitted to be considered if the concrete struts display an underutilization. Furthermore, it is important to mention, that the maximum space between the bent-up bars of the existing bridges exceed the defined design limits in many cases. It becomes apparent, that the contribution of the bent-up bars of beams or slab without required shear reinforcement significantly influences the shear behaviour.

This fact would represent the good conditions of the existing bridges, which are not confirmable with the shear design standards nowadays. Therefore, a new simplified verification model for existing bridges is urgently needed, which also involves the continuously rising traffic impact. Last but not least it's important to say, that the analysed bridges last the impact of the actual traffic, because of the actual lower traffic loads in comparison to the values of Eurocode 1, which should be mainly used for designing bridges and not for verification. Finally, it's important to have bridge inspections need to be condensed in terms of time to fulfil the whole criteria of the bridge management guidelines. In the case of doubt, the structure has to be verified by numerical, respectively extended methods.

5. CONCLUSION

Due to the different investigations, results of both models 2D and 3D (not published in this paper) showed free reserves in the load bearing capacity compared to EC2 (ÖNORM EN 1992-1-1) and fib model code (fib 2010). Referring to the live load trains according to the current ONR 24008, a high level of safety still remains. In accordance with the defined assessment proposal of this paper and in consideration of the ratio of the concrete contribution, a positive verification could be achieved. Many parameters depend on the load capacity of slab bridges, so no general guidance could be listed. Only by taking each parameter such as the aggregate interlock, dowel effective, arch effect and the shear contribution of concrete into account, could realistic conditions be simulated. An established theory in the field of structural engineering makes clear that the aggregate interlocking resistance of the cracked tension zone is considered an additional shear resistance mechanism. To get an efficient output for slabs with a low level of shear reinforcement, the research results were compared to the conservative approach of EC2 and the *fib* Model Code 2010.

This comparison points out that the beams without shear reinforcement do not show any differences between using EC2 and Model Code for the level of approximation II. The nonlinear finite element simulation showed that the bent-up bars contribution could be taken into account with 50% of the design value of reinforcing steel in addition to the concrete

contribution according to EC2. The limit of 50 % is caused by the limitation of the crack pattern, which would further reduce the concrete contribution.

Moreover, it is suggested to have additional bridge inspections to get a reliable projection about the structural behaviour due to actual loading.

With the help of frequent surveying and inspections of the existing structures, it becomes clear that there is no current demand for strengthening or replacement of many structures. Thus, adjusting the engineering standards for the assessment of existing concrete bridge structures, and especially for shear load capacity, appears to be necessary.

Finally, the investigations pointed out that the normative safety of bridge structures could be achieved by considering a reduced resistance of the bent-up bars in combination with the load bearing capacity of the concrete contribution. The results of the FE modeling and the comparison of the different test series from different universities and different researchers (Huber et al. 2012; Leonhardt, Walther, 1962; Rumpf et al. 2013; Weilharter et al. 2015) confirm that the structures are still safe to use for the current load classes, if the maintenance condition of the bridge structure is adequate.

6. LIST OF NOTATIONS

V	shear force	ϵ	strain
V_{Ed}	shear design load	f_{yk}	yield strength
V_{Rdc}	shear resistance of concrete without shear resistance	f_u	fracture strength
V_s	shear bar	w_k	crack opening
V_{test}	Shear force of test	$w_{k,b}$	bending crack
F	load	$w_{k,s}$	shear crack
a_s	longitudinal reinforcement	V_d	dowel action
σ	stress	V_{ca}	aggregate interlock

7. REFERENCES

- Huber, P., Schweighofer, A., Kollegger, J., Brunner, H., Karigl, W.: Vergleich der rechnerischen Quertragfähigkeit von Bestandsbrücken nach Eurocode 2 und fib Model Code 2010, Beton- und Stahlbetonbau. - Wien: Verlag Ernst & Sohn 2012, pp. 451-462.
- Jäger T., Marti P.: Versuche zum Querkraftwiderstand und zum Verformungsvermögen von Stahlbetonplatten. - Zürich: Hochschulverlag AG an der ETH Zürich 2006. pp. 89-292.
- ÖNORM EN 1992-1-1: Eurocode 2: Bemessung und Konstruktion von Stahlbeton- und Spannbetontragwerken.
- ÖNORM B2302: 1931 01 01: Eisenbeton; Berechnung und Bemessung von Tragwerken.
- International Federation for Structural Concrete: *fib* Model Code for Concrete Structures 2010. Lausanne 2010.
- Leonhardt, F., Walther R.: Schubversuche an einfeldrigen Stahlbetonbalken mit und ohne Schubbewehrung. In: Deutscher Ausschuss für Stahlbeton. Heft 151. Berlin 1962.
- Rumpf, M., Ruiz, M., Muttoni, A.: Assessment of Shear Strength for Existing Bridges with Low Amounts of Shear Reinforcement. In: fib Symposium. Tel - Aviv 2013. pp. 1-5.
- Weilharter, J., Huber, P., Kollegger, J.: Experimentelle Untersuchungen zur Schubtragfähigkeit von Stahlbeton- und Spannbetonträgern.- Wien: Technische Universität Wien, Dipl. Arbeit, 2015, pp. 57-76.
- Cervenka, J. and Cervenka, V., ATENA Program Documentation, Part 2-1, User's Manual for ATENA 2D, Prague, 2015.

ADOPTION OF A RHEOLOGICAL BODY FOR THE SIMULATION OF VISCOELASTIC EFFECTS IN HARDENING CONCRETE

Peter Joachim Heinrich, Dirk Schlicke, Nguyen Viet Tue
University of Technology, Institute for Structural Concrete
Lessingstraße 25/I, 8010 Graz

SUMMARY

The simulation of viscoelastic effects in hardening concrete is in general a challenging task. The main reason is the significant dependency of the viscoelastic behaviour on time. This refers to both the influence of the age of concrete at loading as well as the fact that viscoelastic strains occur only in the course of time. In hardening concrete, this is additionally affected by a significant evolution of stiffness in this course of time as well as a variable stress history due to the hydration-induced temperature history in combination with shrinkage.

The modelling of viscoelastic strains in hardening concrete over the course of time on basis of rheological bodies can provide an efficient solution, however, the calibration of these rheological bodies as well as their application is not trivial. This contribution presents the implementation of a rheological body in form of a generalized Maxwell-model in a time step based Finite element simulation. In detail, the model was calibrated against the creep curves given in (Eurocode 2, 2012) with consideration of a modified creep under tension according to the proposal of (Schlicke, 2014). This model was then applied for the simulation of experimental studies with restraining frames of (Turner *et al.*, 2017), whereby a satisfying agreement between experiments and simulation could be achieved.

1. INTRODUCTION

In structural design, viscoelasticity of concrete is usually considered in form of two limit cases according to the restraining situation: (i) creep in case of free deformability (degree of restraint $a = 0.0$) and (ii) relaxation in case of perfect restraint ($a = 1.0$). In case of hardening concrete a common scenario is also the partial restraint ($0.0 < a < 1.0$) where creep and relaxation occur simultaneously. Fig. 1 illustrates these three cases with respect to applied forces F and imposed deformations ε_0 as well as resulting concrete stresses σ_c and strains ε_c .

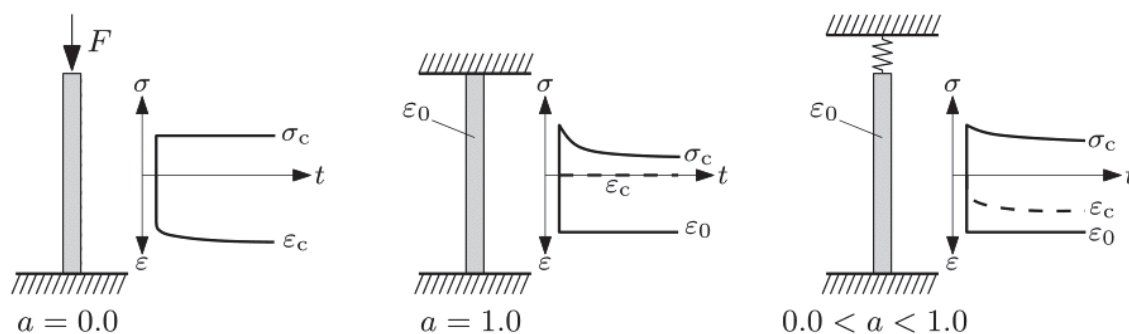


Fig. 1: Viscoelastic behaviour related to the degree of restraint a

The simulation of viscoelastic effects in hardening concrete is in general a challenging task. The main reason is the significant dependency of the viscoelastic behaviour on time. This refers to both the influence of the age of concrete at loading as well as the fact that viscoelastic strains occur only in the course of time. In linear viscoelasticity, a conventional solution can be provided by the discrete superposition of viscoelastic strain increments with respect to the viscoelastic potential of each stress change in each time step, as shown in (Schlicke, 2013). However, such a solution requires a holistic recording of the stress history in each element which becomes costly in computational-time with increasing size or fineness of the calculation model as well as the size of the simulated period.

On the contrary, rheological bodies can provide an efficient solution since they do not require such stress recording because the viscoelastic strain of a certain time step can be determined by the initial conditions of each element in the actual time step. The challenge in the application of rheological bodies is their calibration as well as their application in terms of solving their differential equations for each element in each time step.

This contribution presents the implementation of a rheological body in form of a generalized Maxwell-model in a time step based Finite-Element-simulation and shows its calibration. In detail, the model was calibrated against the creep curves given in (Eurocode 2, 2012) with consideration of a modified creep under tension according to the proposal of (Schlicke, 2014). This model was then implemented in a FE-solution and applied for the simulation of experimental studies with restraining frames of (Turner *et al.*, 2017), whereby a satisfying agreement between experiments and simulation could be achieved.

2. APPLIED RHEOLOGICAL BODY AND SOLUTION OF ITS DIFFERENTIAL EQUATION

2.1 Basic principle

In the present contribution, the rheological body for the determination of viscoelastic effects is a so-called generalized MAXWELL-model (also known as ZENER_m-body). This body consists of four parallel Maxwell-elements (series of a HOOKEAN spring and a NEWTONIAN dashpot) and a parallel single Hookean spring, as shown in Fig. 2.

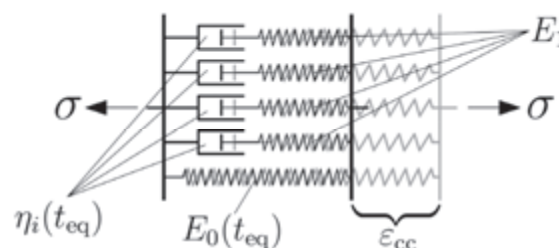


Fig. 2: Generalized Maxwell-model and resulting creep strain ϵ_{cc} caused by σ

In order to represent the effects of aging viscoelasticity, the applied generalized Maxwell-model consists of elements that develop their properties according to the concrete age. In detail, these are the four dashpots of the Maxwell-elements which have variable viscosities (η_i) whereas the stiffness of the springs (E_1) of the Maxwell-elements remain constant. The single spring, however, has also a variable stiffness (E_0).

According to the current state of the art the concrete age is considered by the equivalent age t_{eq} depending on the real time as well as additional aging due to the present concrete temperature (maturity / concept of aging). This equivalent age is implicitly provided by the thermo-mechanical material model for temperature and stress simulation, see e.g. (Schlicke, 2014).

Altogether, the generalized Maxwell-model leads to the inhomogeneous fourth-order (stiff) differential equation eq. (1) with time-dependent coefficients. This equation describes the strain-response $\varepsilon(t)$ under a random stress-impact $\sigma(t)$.

$$a_0 \cdot \sigma + \sum_{i=1}^4 a_i \frac{d^i \sigma}{dt^i} = b_0 \cdot \varepsilon + \sum_{i=1}^4 b_i \frac{d^i \varepsilon}{dt^i} \quad (1)$$

a_i and b_i are functions that depend on both the dashpot viscosities (η_i) and all spring stiffness (E_1) and (E_0). The time dependency of the viscosities and stiffness are herein described by form functions. Further details concerning the definition of a_i and b_i , are given elsewhere, e.g. (Hermerschmidt, 2016).

2.1 Numerical Solution

For inhomogeneous differential equations with time-dependent coefficients an analytical solution is only possible until order 2. For problems of higher order, it is necessary to solve such equations in a numerical way. In general, it is common to use RUNGE-KUTTA formulations as solving algorithms. For stiff problems, there exist some special routines, like the Runge-Kutta based ROSENBROCK-WANNER-method as included in some mathematical suites, like MATLAB.

2.2 Incremental Solution

Although there exist some open-source implementations written in FORTRAN by one of the developers of the Rosenbrock-Wanner-method (Hairer and Wanner, 1996), an implementation in or porting that algorithm to arbitrary programming languages is not trivial.

A reasonable solution which also helps to save further computation-time, is to shift the obvious problem as first approximation to a incremental/stepwise-solution, treating the equation as initial-value-problem. Therefore it has to be assumed that:

- the time-steps in the restraint analysis are so small that a change of the material-parameters a_i, b_i within a single step is negligible,
- the stress that acts on the model is applied stepwise and remains constant during a single time-step and
- the resulting error caused by the simplification shall remain small for practical issues, even though the simplification seems to be doubtful from a mathematical perspective.

These assumptions enable to derive eq. (2) as a simplified version of eq. (1). It holds for a single time-step:

$$a_0 \cdot \sigma = b_0 \cdot \varepsilon + \sum_{i=1}^4 b_i \frac{d^i \varepsilon}{dt^i} \quad (2)$$

Without any change of stress within a single step, all derivatives of σ vanish. The initial conditions as well as the transitional conditions remain the same as for the original problem, see (Hermerschmidt, 2016). Finally, the simplified equation eq. (2) can be solved for ε by a separation into a homogeneous and a particular part, where $A \cdot t + B$ suffices as approach for the particular part. The total solution for a single time-step yields to eq. (3)

$$\varepsilon(t) = \sum_{i=1}^4 C_i \cdot e^{\lambda_i t} + \frac{a_0}{b_0} \sigma_k, \quad (3)$$

where λ_i are the roots of the characteristic polynomial and σ_k denotes the stress-increment that acts within the considered time-step $t_{k+1} - t_k$. The constants C_i can be derived by solving eq. (3) as initial value-problem with appropriate transitional conditions. For further details see (Heinrich *et al.*, 2015).

The amount of the state-variables that have to be stored for every element directly refers to the order of the differential equation: An equation of order n needs n state-variables in storage: ε as well as its 1 ... $(n-1)$ -derivative.

3. CALIBRATION

The material parameters a_i, b_i in eq. (2) consist of 9 model-parameters that partly influence each other. These parameters describe mainly the development of the time-dependent model properties of spring stiffness and dashpot viscosities. Further information can be found in (Hermerschmidt, 2016) where one can find also values for them which were derived from comprehensive experiments with Temperature-Stress-Testing-Machines and represent the viscoelasticity under tension for young concrete.

For the purpose of simulating holistic stress histories consisting of compressive stresses as well as tensile stresses, the present contribution aims at a calibration against the creep curves given in (Eurocode 2, 2012) with consideration of a modified creep under tension according to the proposal of (Schlicke, 2014). In detail, a Trust-Region method from the optimization toolbox of the MATLAB-suite was applied to determine the model parameters for a best possible fit to the reference curves. Fig. 4 gives the results for creep under compressive stressing, while Fig. 5 shows the results for creep under tensile stressing.

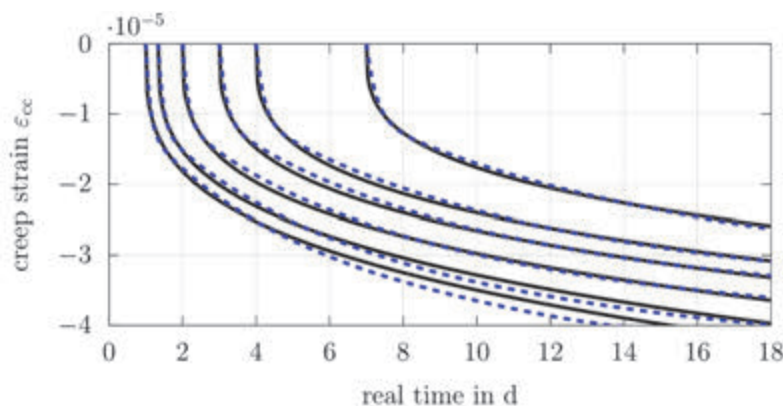


Fig. 4: Result of best possible fit to given creep curves under compressive stresses

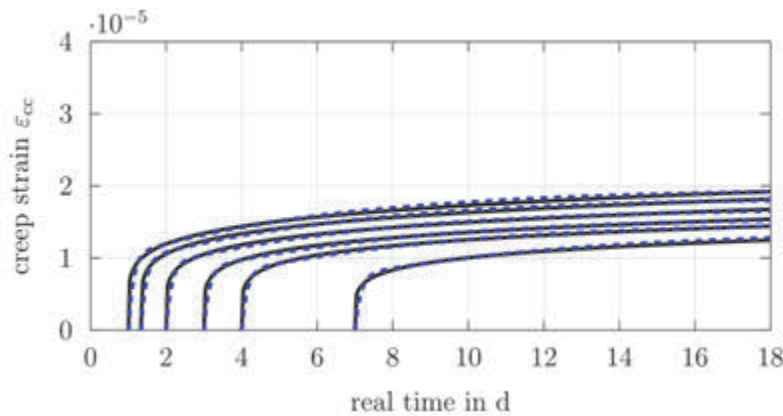


Fig. 5: Result of best possible fit to given creep curves under tensile stresses

The black solid lines show the “objective” creep curves and the blue dashed curves show the creep behaviour after fitting the model to the objective curves. The optimization has taken all 6 objective creep-curves into account.

4. IMPLEMENTATION IN A FINITE ELEMENT MODEL

For the simulation of restraint stress history of hardening concrete the presented rheological body was implemented in a volumetric FE-model. In the present case, the commercial FE-framework SOFiSTiK was used which consists of several modules that allow thermomechanical simulations. After generating a 3D element mesh with the module SOFiMSHA, the development of temperature is calculated in the module HYDRA on basis of hydration heat release in each element according to the equivalent aging as well as thermal boundary conditions on the outer surfaces of the member. Following, the module ASE calculates the corresponding stresses to the determined thermal strains and additional impacts due to shrinkage as well as self weight activation. In the present solution with the commercial FE-framework SOFiSTiK, the viscoelastic stress determination consists of two steps. Firstly, these stresses were calculated with the assumption of linear-elastic behaviour. Secondly, viscoelastic effects were included on basis of the linear-elastic results. This inclusion was finally achieved by the implementation of a user defined material model, see (Sofistik, 2016).

The whole procedure is based on the principle of deformation compatibility whereby viscoelastic strain increments were explicitly considered in each element and time step. In accordance with the simplified approach in (Schlicke, 2014), the implementation was based on the local axis of each element (x, y, z) depending on the actual stress-state in the considered direction. Of course, an implementation on principal axis is possible and will be pursued in future. However, it should be noted that there is no significant difference between implementation on principal axes and implementation on local element axes in case of restraint analysis with 3D-volume-elements. The reason is the very low shear stressing so that local stresses and principal stresses do not differ significantly. Thus, the determined viscoelastic strains fit to the total stress state of the element.

5. APPLICATION AND VALIDATION

The presented FE-model was used to simulate one of the restraining frame experiments presented in (Turner *et al.*, 2017). The applied thermomechanical material model for aging, heat release, shrinkage and evolution of stiffness was taken from (Schlicke, 2014). The concrete properties applied in this study refer to a concrete of the strength-class C 35/45 and comply with the ones given in (Schlicke, 2014). Fig. 6 shows the experimental set-up and the calculation model used.

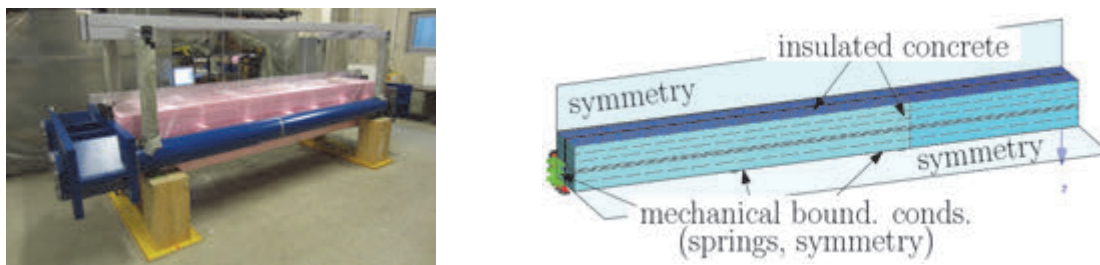


Fig. 6: Experimental set-up and calculation model of the restraining frame experiment

Fig. 7 compares the measurement with results of different simulations: The solid black line shows the stress measurement and the blue dashed line shows the calculation result for the presented model with distinction between different viscoelastic behaviour under compressive stresses and under tensile stresses (two parameter sets).

For sensitivity analyses, Fig. 7 shows also the results of a simulation without distinction between different viscoelastic behaviour under compression and under tension (only one parameter set; red dotted line, where only parameters for compressive creep were used) and the results without consideration of viscoelastic behaviour at all (solid grey line).

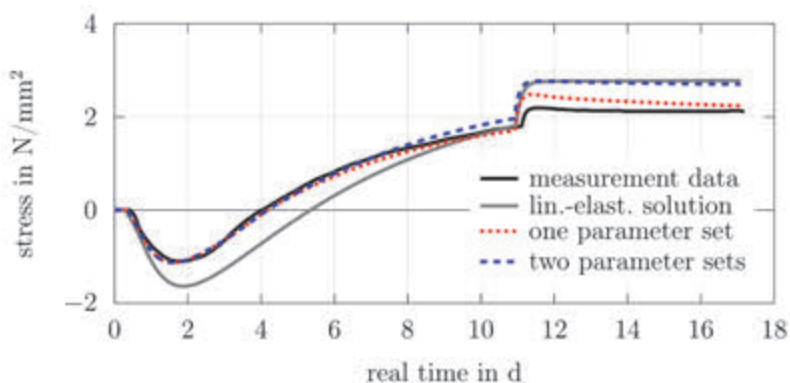


Fig. 7: Comparison of measurement data and results of the FE simulations

In order to confirm the applicability of the aforementioned assumptions for the application of the incremental solution Fig. 8 compares the results of the FE simulation using the incremental solution (blue dashed line) with a MATLAB calculation in which the differential equation is solved numerically (magenta dash-dotted line).

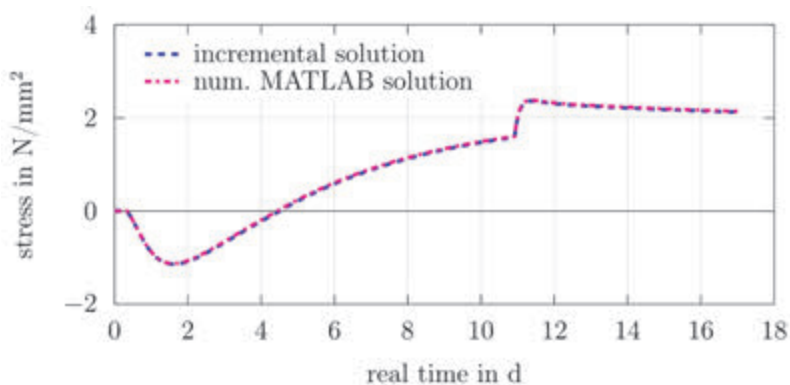


Fig. 8: Influence of the incremental solution

6. CONCLUSIONS

The modelling of viscoelastic strains in hardening concrete over the course of time on basis of rheological bodies can provide an efficient solution, however, the calibration of these rheological bodies as well as their application is not trivial. This contribution presents the calibration of a rheological body in form of a generalized Maxwell-model and its implementation in a time step based Finite element simulation. In detail, the model was calibrated against the creep curves given in (Eurocode 2, 2012) with consideration of a modified creep under tension according to the proposal of (Schlicke, 2014). This model was then implemented in a Finite element solution and applied for the simulation of experimental studies with restraining frames of (Turner *et al.*, 2017), whereby a satisfying agreement between experiments and simulation could be achieved.

Besides, the comparison between the measurements of restraining frame experiments and the results of their simulation indicated that the distinction between tensile and compressive creep leads to a better agreement. This refers mainly to the behaviour after temperature equalization (here: $t > 11$ d). In detail, the computational results with one parameter set indicate an ongoing relaxation after temperature equalization, which was never observed in the experiments.

Next to this, the comparison between the results of the FE simulation using the incremental solution with the results of a MATLAB calculation in which the differential equation is solved numerically (Fig. 8) confirms the conclusion of (Heinrich *et al.*, 2015), that the accuracy of the incremental solution is suitable.

Altogether, the presented model is seen as a suitable model for comprehensive simulations of the stress development in large structures. Compared to the aforementioned conventional model with stress recording, the simulation time can be reduced by the presented model in a multiple.

7. REFERENCES

- Eurocode (2012), “Eurocode 2: Design of concrete structures – Part 1: General rules and rules for buildings”, Österreichisches Normungsinstitut, Wien, Austria.
- Hairer, E. and Wanner, G. (1996), “Solving Ordinary Differential Equations II. Stiff and Differential-Algebraic Problems”, Springer Series in Computational Mathematics 14, Springer-Verlag 1991, Second Edition, Berlin, Germany.
- Heinrich, P. J., Schlicke, D. and Tue, N. V. (2015), “Serviceability and Stability of Unreinforced Mass Concrete Structures – EC 2 Compatible Design Concept Derived from Comprehensive FE-Studies on Real Structural Behaviour”, Proceedings of CONCREEP 10, pp. 1299-1307, <https://doi.org/10.1061/9780784479346.154>
- Hermerschmidt, W. (2016), “Modelle zur Beschreibung der thermomechanischen Materialeigenschaften jungen Betons”, PhD thesis, Braunschweig University of Technology, Germany.
- Knoppik, A. (2017), “COST TU1404 WG2 Benchmark program – Stage 1. Macro-modelling of concrete and concrete structures at early age”, (in preparation)
- Schlicke, D. (2014), “Mindestbewehrung für zwangbeanspruchten Beton”, 2. Aufl., PhD thesis, Graz University of Technology, Austria, doi:10.3217/978-3-85125-473-0
- Schlicke, D., Tue, N. V. (2013), “Consideration of Viscoelasticity in Time Step FEM-Based Restraint Analyses of Hardening Concrete”. Journal of Modern Physics.
- Sofistik (2016), “AQUA – Materials and Cross Sections”, SOFiSTiK-Manual Version 16.03, Oberschleissheim, Germany.
- Turner, K., Schlicke D. and Tue, N. V. (2017), “Systematic Investigations with Restraining Frames for Reinforced Concrete”, 2nd Int. RILEM/COST Conf. on Early Age Cracking and Serviceability in Cement-based Materials and Structures (EAC-2), Brussels, Belgium.

OPTIMISATION OF TBM TUNNEL IN THE SHANGHAI METRO EXTENSION USING MACRO SYNTHETIC FIBRE

Károly Péter Juhász¹, Péter Schaul², Lóránt Nagy²

¹ *Budapest University of Technology and Economics, Department of Mechanics, Materials & Structures*

Műegyetem rakpart 1-3, Budapest, Hungary

² *JKP Static Ltd.*

Reitter Ferenc 73, Budapest, Hungary

SUMMARY

Shanghai metro extension is one of the most enormous TBM tunnel investigation nowadays in Republic of China. Because of the size of the investment several research connected to the project. The Customers tried to use the most economic concrete reinforcement, and joint element between the rings. The Tongji University made a real scale test about the full precast concrete tunnel ring. The test was verified with numerical models. After the clarification of the material parameters, finite element analysis was done to optimize the steel bar reinforcement in the ring, and replace it with synthetic fibres. To find the optimum joint formation different models were carried out. The effect of the different bolt types (curved or straight) was significant, just like the use of fibres. With the optimum solution the structure will be more ductile than with the original formation.

1. INTRODUCTION

The authors were engaged to optimize a traditional rebar cage reinforced concrete segmental lining by means of Finite Element Analysis (FEA) using macro synthetic fibres for the Shanghai metro extension. The aim of this study was to reduce or entirely replace the original steel reinforcement of the segmental lining, in order to make the precast production process faster and more economic.

A one-to-one full scale model of an assembled tunnel ring using the original reinforcement cages was tested at Tongji University in Shanghai, July 2013. The ring was tested to differing load levels where load and displacement were measured until failure (Liu et al, 2016). The author's first step was to calculate the real displacement characteristics of the original reinforced concrete ring, then calculate the numerically modelled version, so as to compare them. The numerical modelling undertaken has shown good correlation with the full scale physical test results. Optimization of the lining reinforcement was achieved through the addition of fibres, resulting in a substantial reduction (~50-70 %) of the steel rebar cages (Juhasz et al, 2014). After the analysis the weak points of the tunnel and the type of failure could be visualised easily. For this type of tunnel and its loading, the mechanism of failure was at the segment joints where the connecting bolts burst out from the concrete. The authors investigated the bolted segment joints and the influence of the macro synthetic fibre on its performance (Juhasz, Nagy and Schaul, 2016).

The numerical calculations were performed by Atena Finite Element software (Cervenka, 2013), with the help of the Modified Fracture Energy Method (Juhasz, 2013). In this paper the design process and the steps of the finite element analysis will be presented.

2. ORIGINAL DESIGN AND LABORATORY TEST

2.1 Geometry and reinforcement

This typical Shanghai metro tunnel example has an inner diameter of 5500 mm, an outer diameter of 6200 mm and a wall thickness of 350 mm. One ring is made from six segments. The key and the invert segment have a different geometry and reinforcement whilst the lateral ones are identical. The invert segment has an angle of 84 degrees, the key 16 degrees, and the four sides 65 degrees.

The longitudinal length of one segment is 1200 mm. The segments were connected with 400 mm long and 30 mm diameter straight bolts at two points, so the six segments were connected at 12 points. The longitudinal bolts are similar to the circumferential. Only one ring was checked in the laboratory test so the longitudinal connections were not included in the test. The segments were hoisted at two points whereas the key segment was hoisted at a single point only. Geometry and loading configuration can be seen in Fig. 1.

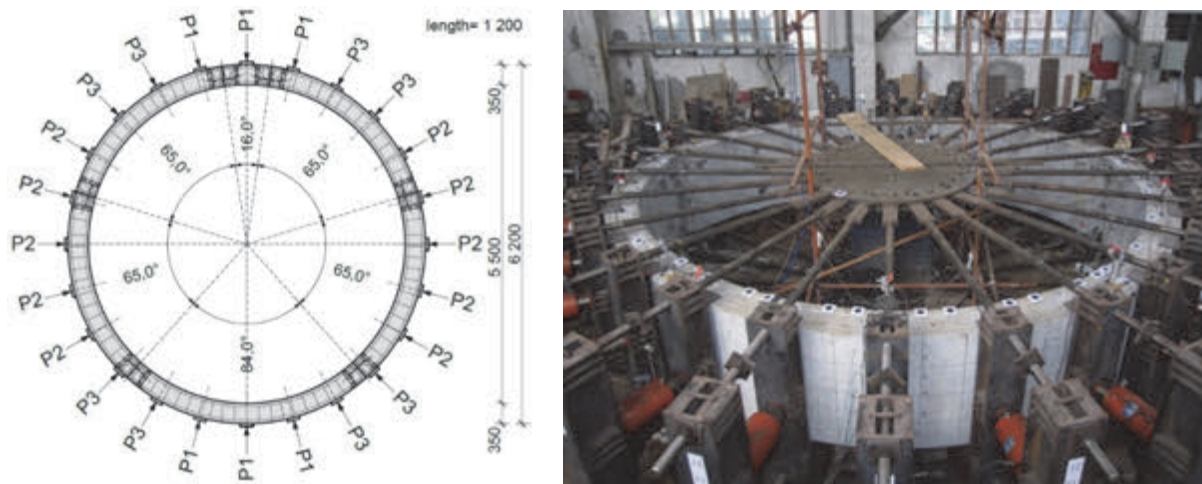


Fig. 1: Geometry, loading configuration and the real scale test

The aspect ratio of the segments, which is the developed length over the lining thickness, computes to 12.2 for the invert segment and 9.5 for the regular lateral ones. Given that a segment aspect ratio not exceeding 10 generally provides a safe opportunity for a fibre only solution, the lateral segments present no problem (Winterberg, 2012). However, the invert segment's aspect ratio is over this threshold, so it was decided to use combined steel and synthetic fibre reinforcement for the numerical studies.

The steel reinforcement, as per the original design, altogether amounts to a total of 559 kg per ring. This yields an average reinforcement ratio of 72 kg per cubic meter of concrete for the invert and side segments. This is not a very high degree of reinforcement, however, the other driver in using FRC for segmental linings is the enormous gain in productivity, giving this technology more and more momentum in countries with already high or still soaring labour costs, such as China. Replacing the complex rebar cages of a segment cuts out the time required for cutting and bending, fixing or welding, placing and checking of the position of the cage.

2.2 Materials

The general tests to characterize the materials were carried out after the full scale laboratory test. The mean concrete compressive strength was determined to be 50 MPa cubic, the strain

at this stress was 1.8 ‰ (0.0018). A concrete class C40/50 according to the European design standard was used, Eurocode 2 (2004), for the finite element analysis. The grade of the steel bar reinforcement was HRB335 with a yield strength of 335 MPa, using ribbed bars.

2.3 Full scale laboratory test

Tongji University in Shanghai has carried out a full scale test in their laboratory loading a full segmental ring and measuring the load and the referring displacements. The ring was loaded at 24 points, with hydraulic jacks located every 15 degrees. The load was distributed on the ring by means of transverse beams onto the segments as a line load. This closely spaced, distributed load modelled the loading from the soil under permanent condition. The load configuration and the one to one laboratory test setup can be seen in Fig. 1.

During loading the 24 loading jacks applied varying levels of load. At the invert and at the crown a load P_1 was acting at three points respectively. At the benches the load P_2 was applied as a function of P_1 and at the walls a load P_3 as a function of P_1 and P_2 . Because of the different loads the structure not only experienced different central thrust force, but has undergone eccentricity as well, modelling the real conditions of the tunnel. The loading phase had two stages. In the first stage the functions of the loads were the following:

$$P_2 = 0.65P_1 \text{ and } P_3 = \frac{P_1 + P_2}{2} = 0.825P_1$$

Load P_1 was increased until P_2 reached its design value which was 292.5 kN. In the second stage the load P_2 was unchanged, where load P_3 had the following function:

$$P_3 = \frac{P_1 + P_2}{2}$$

and P_1 was increased until its design value of 455 kN. With these functions it was able to model the loading changes as a function of the tunnel depth below surface.

The displacement was measured at 14 points of the ring. The most important positions herein were the 0, 180, and the 90, 270 degrees positions, which are measuring the horizontal and vertical displacements. From these results a load-displacement diagram was generated, showing load P_1 over the displacements at the different angles, which can be seen in Fig. 2.

3. FINITE ELEMENT ANALYSIS OF THE TUNNEL

3.1 Material tests for input of the FEA

To produce the most realistic calculation, material tests were carried out with different dosages of macro synthetic fibres, using the original concrete mix design at Tongji University. Four point beam tests were carried out on 450 mm span and the load was applied in the third points. The beam was loaded until 4 mm central displacement and the load-displacement diagram was recorded. The material tests for FRC were done with 6 and 10 kg/m³ dosage of macro synthetic fibre.

3.2 Material models

The concrete was modelled with an advanced material model, using the combined fracture surface criteria (Cervenka, 2008). This material model can handle the different behaviour of

the concrete in tension and in compression and also capable to calculate the non-linear behaviour after cracking.

The fibre reinforced concrete was modelled with the Modified Fracture Energy Method (Juhasz, 2013). The main idea is to use the concrete fracture energy (G_f) as an initial value and then increase it with an additional fracture energy (G_{ff}) from the post-crack FRC performance. The performance of the fibre was determined with inverse analysis from the existing beam tests. This method is recommended also by the ITAtech Activity Group (2015). The concrete has a stress-strain diagram according to Eurocode 2 (2004). The crack width was calculated from the stress-crack width diagram, determined by means of inverse analysis, with the help of the characteristic length, which is a function of the size of the element and the angle of the crack within the element. This method is the only one that could realistically represent the cracks in the quasi-brittle material. This is the main advantage of this advanced material model.

Steel rebars and bolts were modelled as discrete link elements with a uniaxial ideal elastic-plastic stress-strain material model. The rebars link element was connected to every single concrete brick element which was crossed. The bolts had no connection with the concrete brick elements, however, at both ends they were held by the nuts on the concrete surface, which were only able to undergo tension.

The connection surface of two adjacent segments was connected with an interface material, which could hold compression only through friction on the surface. With this special interface material the connections of the segments were modelled, which could be open or closed for bending, where tension would be held by the connection bolts.

3.3 Numerical model of the tunnel

After defining the accurate material model the geometry was defined. Firstly, the concrete and reinforcement and then the loads and supports must be defined. The tunnel is symmetric at the horizontal and the vertical axis, so only a quarter of the full ring geometry is sufficient to model the structure with symmetrical support conditions on the symmetrical plane. This also helps to define the boundary conditions and makes the calculation faster. Finally, the monitoring points need to be defined, where the load and resulting displacements were to be measured. The loads were positioned at exactly the same locations and with the same values as in the full scale laboratory test.

4. RESULTS OF THE FINITE ELEMENT ANALYSIS

4.1 Result of the original RC solution

After running the FEA the results were checked. Most important was the load-displacement diagram, which was compared to the full scale laboratory result. It can be seen in Fig. 2 that the result of the laboratory test and the result of the FEA are similar in both characteristic and values and show the same maximum load capacity.

The maximum compressive stress of the concrete was 35.9 MPa, while the maximum crack width just before complete failure was 5.0 mm. The steel bars were grouped according to the stress-levels experienced and selection was based on the ones that could be said to be not providing any input and which could be reduced or completely omitted as a first step.

According to the computed stress levels, the remaining steel bars could be reduced in diameter in accordance with the computed stress value. Full animation could be done and the entire loading process could be observed from the formation of the crack until total failure. In this way the weak points of the tunnel and the type of failure could be visualised easily. For this type of tunnel and its loading, the mechanism of failure was at the segment joints where the connecting bolts burst out from the concrete, see Fig. 2.

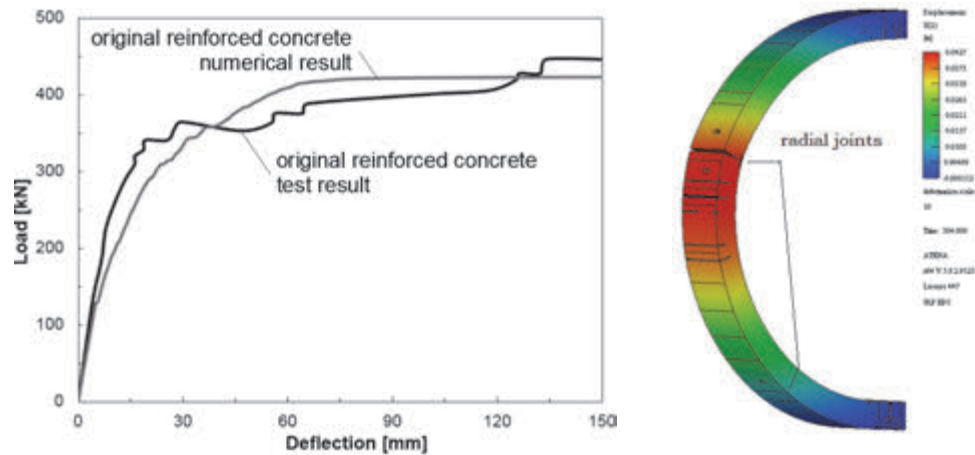


Fig. 2: Results of the laboratory test and FEA

4.2 Optimizing the segmental lining with synthetic fibre reinforcement

After the successful modelling of the original RC ring, the optimization could be started, recalculating with reduced steel bars and added fibre. Firstly, the lowest stress-level steel bars were omitted and replaced with a moderate dosage of fibre. Then, with increasing fibre dosage, more and more steel bars were omitted. These calculation processes were laborious as adding fibre also changes the occurring deformations, thereby changing the arising eccentricity, and eventually, can change the failure mode, too. However, the ruling failure mode always was radial joint bursting at the bolt pockets. After these calculations were made three viable solutions were proposed, which can be taken from Tab. 1.

Tab. 1: Reinforcement optimization with using synthetic fibres

	original solution	solution 1	solution 2	solution 3
added fibre (kg/m ³)	-	6	7	10
max. crack width (mm)	5.0	2.3	2.1	1.9
used reinforcement in one full ring	559 kg steel	344.3 kg steel (-39.8%) +46.3 kg fibre	282.4 kg steel (-49.5%) +54.0 kg fibre	140.4 kg steel (-75.0%) +77.2 kg fibre

Adding fibre in conjunction with steel bar reduction improved control of both crack width and crack propagation. The crack width of the original RC solution was 5.0 mm before total failure, where in solution one this was reduced to only 2.3 mm with less visible cracks. This is a reduction of crack widths of more than 50 %, which provides a substantial gain of durability.

From the calculated solutions, number two seemed to be the most viable. However, the FEA is valid only for this given situation, where for other conditions more parameters would need to be checked. The characteristic failure mode occurred at the radial joints (connection bolts and their surrounding area) so review and redesigning of this part could lead to a more optimized solution. The final recommendation is 7 kg/m^3 macro synthetic fibre in conjunction with 50 % steel rebar reduction. This solution is planned to be verified by physical laboratory testing in the near future.

5. INVESTIGATION OF THE BOLTS

5.1 Finite element model of the joints

The three main types of connectors used in tunnel segments are: curved bolts, straight bolts and dowels. The advantages and disadvantages of these connectors are studied in the publication of Delus, Jeanroy and Klug (2010). In this article the mechanics of the curved and straight bolt connection was investigated by advanced FEA. The research has two main parts: (A) modelling only the joints to determine the moment capacity; and (B) modelling the whole tunnel with the same joints to determine the loadbearing capacity of the tunnel. All joints are modelled with plain concrete (PC), fibre reinforced concrete (FRC), traditional reinforced concrete (RC) and hybrid solution (HYB: traditional steel bar reinforcement with fibre reinforcement). The reinforcement was the same like in the full round models.

The material model for the concrete elements was the same like in the previous chapter. The material model for the steel bolts is a uniaxial ideal elastic-plastic stress-strain material. Straight bolts were modelled with a 1D link element that had no connection with the concrete brick elements, however, at both ends they were held by the nuts on the concrete surface, which were only able to undergo tension. Curved bolts needed to be modelled as a 3D element with a connection surface at all side. The adjacent surfaces were linked by connection elements. These connection elements can only hold compression through friction on the surface. The bolts' tensile strength is 500 MPa, the elastic modulus is 200 GPa.

The joints were modelled like a 3 point loaded beam, supported at the two edges and loaded in the centre. This geometry layout can be tested in reality, too. The load and the central point deflection was monitored during the analysis.

The whole tunnel model and the loadings were adopted from the previous FEA of the Shanghai Metro Extension tunnel (Juhasz et al. 2014). Geometry and loading configuration of the joints can be seen in Fig. 3.

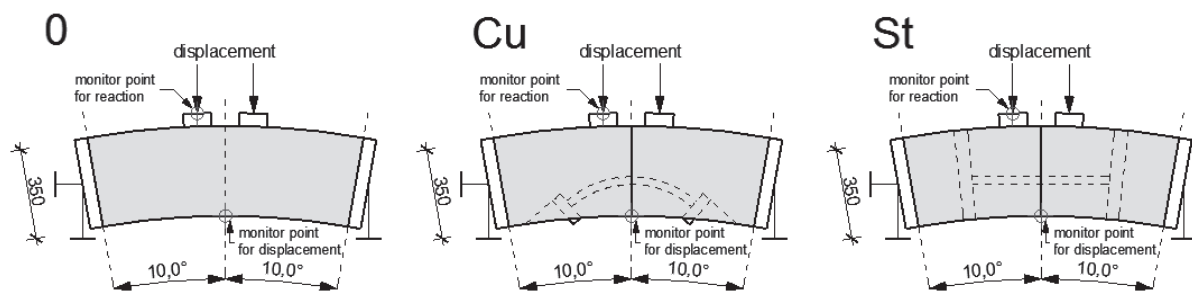


Fig. 3: Geometry and loading configuration of the joints

5.2 Results of the Finite Element Analysis's joint and tunnel model

In the joint models with plain concrete the stiffness and load bearing capacity of the connection with straight bolts was slightly higher, but the ductility (which is determined as the area under the load-displacement curve) was greater for the curved bolts. By adding fibre, the sequence has changed: the joint with curved bolts had the higher load bearing capacity and showed remarkably increased ductility. At this modelling phase, the added fibre has a bigger effect on the joint with curved bolts, although in general, the capacity and the ductility of both connection types has increased (Fig. 4a). The added fibre significantly changed the crack propagation, which could be the reason for the increase of the load bearing capacity.

Joints with traditional reinforcement showed a smaller difference, but the tendency is the same: by adding fibre reinforcement both the load bearing capacity and the ductility has increased (Fig. 4b).

Without traditional reinforcement the tunnel lining will fail between the joints, because the joints are stronger than the middle section of a lining (segment). By changing the stiffness of the joint (straight to curved bolt) the failure point will also change, but the load bearing capacity is almost the same (Fig. 4c). The tunnel lining with curved bolts has some post crack load bearing capacity, while with straight bolts the load immediately drops. By adding fibre the load bearing capacity and ductility is greatly increased to almost the same level for both connection types. Generally, with added fibre the crack localization could be eliminated.

Adding fibre to the reinforced concrete will also increase the load bearing capacity of the tunnel (Fig. 4d). It is noteworthy that the highest load bearing capacity was reached with straight bolts and hybrid solution, but this was not reflected in the joint tests where the capacity of the curved bolts was slightly higher. Hence, the capacity of the joints is not the only factor that will affect the global capacity of the tunnel ring.

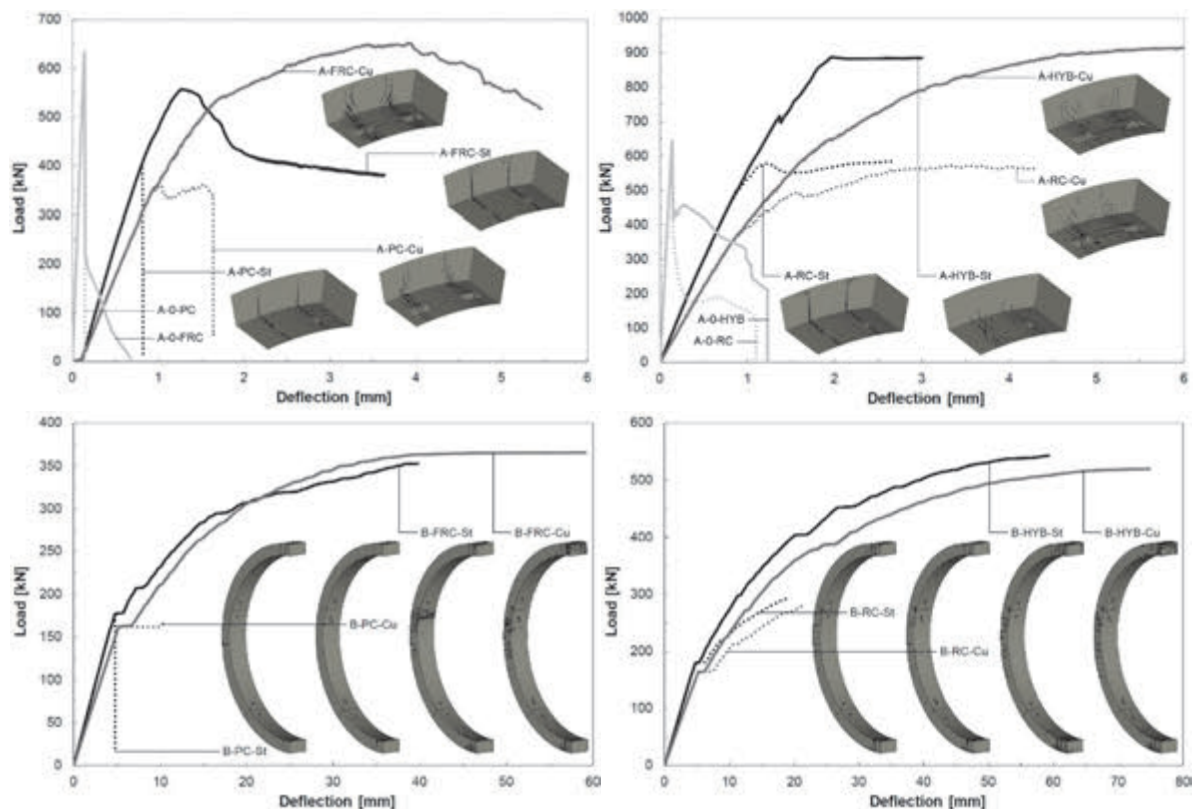


Fig. 4: Results of the joint and tunnel models with different type of joint and reinforcement

6. CONCLUSION

A full scale TBM segmental tunnel ring was modelled with an advanced material model in FEA. By using the modified fracture energy method an accurate material model can be used for FRC. A typical Shanghai Metro extension TBM tunnel segmental ring was tested to full scale at the Tongji University, Shanghai, and the load-displacements results were compared with the FEA. The similarity was deemed appropriate, so the model has been justified. Low-stressed steel bars within the section were reduced and macro synthetic fibre was added to the structure. By using macro synthetic fibre reinforcement the volume of steel bars could be reduced. This, in return, leads to significant cost savings in both material and labour, as well as a reduction of the production cycle times.

Three different joint types were modelled in FEA to investigate the effect of them to the capacity of the tunnel. The present numerical research showed that there is no influence of the fibre to the stiffness of the joints. Straight bolts provide a higher stiffness of the joints than curved bolts, but less ductility. The load bearing capacity and crack propagation are significantly improved by adding macro-synthetic fibres for both plain and conventionally reinforced concrete, and for both straight and curved bolts. With advanced design of bolted joints it is possible to increase the load bearing capacity of the entire tunnel, even if the moment capacity of the joint does not reach the moment capacity of the lining (semi-rigid joint).

7. ACKNOWLEDGEMENT

The research was supported by the FibreLab, co-founded by the Nemz_15-1-2016-0026 Programme and the European Union Horizon 2020 Framework.

8. REFERENCES

- Bi X, Liu X and Wang X, (2016), "Experimental investigation on the ultimate bearing capacity of continuous-jointed segmental tunnel linings", China Civil Engineering Journal.
- Cervenka J. and Papanikolaou V.K. (2008), "Three dimensional combined fracture-plastic material model for concrete", International Journal of Plasticity (24): 2192-2220
- Delus C., Jeanroy B. and Klug D.R. (2010), "International Practices for Connecting One Pass Precast Segmental Tunnel Linings", North American Tunneling Conference 2010, Society for Mining, Metallurgy, and Exploration, 140-146
- EUROCODE EN 1992, (2004), "European Code for design of concrete structures", European Committee for Standardization (CEN). Available from: <http://eurocodes.jrc.ec.europa.eu/> (European Committee for Standardization)
- ITAtch Activity Group Support (2015), "ITAtch Design Guidance For Precast Fibre Reinforced Concrete Segments" ITAtch Report n7, draft
- Juhász K.P. (2013), "Modified fracture energy method for fibre reinforced concrete", in Fibre Concrete 2013: Technology, Design, Application (ed. Kohoutkova A, et al) pp. 89-90
- Juhász K., Nagy L. and Winterberg R. (2015), "Full-round numerical analysis of traditional steel bar and macro synthetic fibre reinforced concrete segments for the Shanghai Metro Extension", SEE Tunnel: Promoting Tunneling in SEE Region, ITA WTC 2015 Congress and 41st General Assembly, Lacroma Valamar Congress Center, Dubrovnik, Croatia
- Juhász K.P., Nagy L., Schaul P. (2016), "Influence of macro synthetic fibre on the performance of bolted segment joints", 6th International Symposium on Tunnels and Underground Structures in SEE 2016, Split, Croatia
- Winterberg, R. (2012), "Segmental Tunnel Linings with Fibre Reinforced Concrete", SPET Journal No. 35, Society of Professional Engineers Thailand, Bangkok

SHEAR DESIGN OPPORTUNITIES FOR SYNTHETIC REINFORCED CONCRETE BEAMS

Péter Schaul, György L. Balázs

Budapest University of Technology and Economics, Department of Construction Materials and Technologies

Műgyetem rakpart 1-3, Budapest, Hungary

SUMMARY

Synthetic reinforcements in concrete structures are becoming more widely used because of their most important advantage to be resistant against electrolytic corrosion. The fibre reinforced polymer (FRP) bars can increase the capacity of beams as main reinforcement and as stirrups. Macro synthetic fibres can increase the ductility of the elements and the shear capacity of the concrete structures as well. For design with FRP and synthetic fibre reinforcement concrete structures some guidelines exist but there is no standard available for them. In the literature several articles can be found which modify the formulas for steel bars and for steel fibres to be able to use for synthetic as well. Because one of the most dangerous failure mode in concrete structures is the shear failure, it is important to determine the shear resistance properly. In this article shear design opportunities will be presented for synthetic reinforced concrete beams.

1. INTRODUCTION

The shear and the punching shear failure is one of the most dangerous failure modes in all structural elements especially in reinforced concrete slabs and beams. The shear phenomena is complex, contains many different component (Balázs, 2010). During shear failure of the reinforced concrete beams an inclined crack is appearing on the side of the concrete beam, and the beam starts to separate along the crack. The mechanism can proceed very quickly. Because the premission of this failure mode is very important part of the design, the reinforced concrete standards (ACI, JSCE, Eurocode) have a different section for the shear design. These standards usually calculate the shear capacity of the concrete and the steel reinforcement with separate terms.

These standards specify the stirrups as they are made of steel and the formulas are only valid for steel as well. However, the synthetic reinforcements, such as fibre reinforced polymer (FRP) rebars and synthetic fibre reinforcement in concrete may become alternative non-metallic reinforcement for concrete structures. The FRP bars are made from longitudinal fibres, usually glass, carbon and basalt, and from a thermoset or a thermoplastic resin. The fibres carry the load and the resin protects the fibres and transfers the loads to the fibres. Usually these bars have an orthotropic behaviour because of the manufacture. The process of the manufacture called pultrusion. The bars can be used as main reinforcement and as stirrups also, but with using thermoset resin the bars cannot be bent after the manufacture procedure. With thermoplastic resin the bars can be formed after the pultrusion as well with applying heat to the bar, however, the strength of the bar will be lower. Significant field for using FRP bars are the MRI rooms in hospitals, tramlines, where no magnetic material can be used. Also

an alternative reinforcement can be the FRP bars in concrete roads and bridges where the electrolytic corrosion can be significant.

Synthetic macro polymer fibres became a well-used material in concrete structures at the second part of the 20th century. Similar to the steel fibres, this reinforcement must be added into the concrete until it will be equally mixed. The average length of the fibres is from 40 mm up to 60 mm and their material is usually polymer (olefin, polypropylene etc.). The fibres can increase the residual flexural strength of the concrete. In the literature a considerable amount of publication can be found about how the synthetic fibres can increase the shear capacity of the concrete elements (Li et al., 1992; Juhász and Schaul, 2015). The main area of using synthetic fibres are the precast industry, the industrial floors, the tunnels (shotcrete or segmental) and the tramlines- concrete railways.

Both of these synthetic reinforcements can increase the reinforced concrete elements' shear capacity, however there is no standard for the calculation method. In this article the formulas and recommendations will be presented which can help in the shear design of synthetic reinforced concrete beams.

2. SHEAR IN CONCRETE STRUCTURES

The shear stresses are special tension stresses which always perpendicular to the direction of the principal compressive stress trajectories. These trajectories in a simply supported beam can be seen in Fig. 1. The crack pattern in a beam where only main reinforcements are follows the trajectory lines.

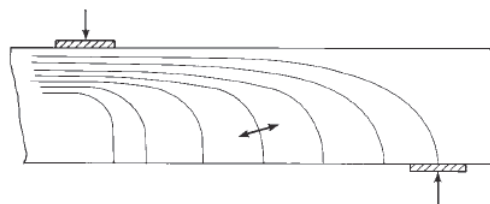


Fig. 1: Principal compressive stress trajectories in a simple supported beam (Wight and Macgregor, 2012)

In a reinforced concrete beam the shear resistance comes from a contribution of several different effects.

2.1 Effect of the un-cracked compressed concrete zone

In reinforced concrete beams the depth of the compressive zone highly determines the shear resistance of the element. This part of the beam is un-cracked, therefore, a part of the vertical forces can be transferred here.

2.2 Aggregate interlock

In the tensile zone, shear forces transfer across a crack by mechanical interlock, when the shear displacement is parallel to the direction of the crack (Fig. 2). Considerable amount of scientific research tried to determine the contribution of the aggregate interlock to the full shear resistance. Some researchers questioned the existence of the effect (Völgyi et al. 2016) and some of them determined the contribution can be even 50% (Taylor, 1970). The vast

majority of the articles locate the contribution between 33 and 50% but with increasing the crack width this value can be reduce as well (Walraven, 1981).

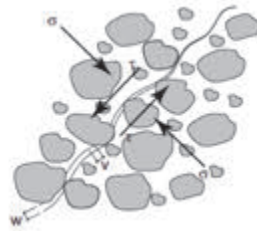


Fig. 2: Mechanism of aggregate interlock (*fib* Bulletin 40, 2007)

2.3 Dowel action

The dowel action is a combination of the tensile resistance of the concrete near to the flexural reinforcement and the bending and transverse shear resistance of the main reinforcement. According to the literature this shear component has the smallest contribution in the full shear resistance (Kotsovos, 1999).

2.4 Shear reinforcement

Shear links (stirrups), bent main reinforcement and fibre reinforcement can also take a contribution of a shear resistance of reinforced concrete beams. The bars bridge the two parts of the crack and can transfer the shear forces between the upper and the downer part of the crack. The most efficient bars are perpendicular to the crack. The fibre reinforcement can also increase the shear resistance by bridging the cracks. These small fibres with a randomly distribution can be effective independently of the place of the shear crack.

Determination of the shear resistance requires a lot of attention, the contribution of the different effects can change in beams with different geometry, main or shear reinforcements. The current standards try to simplify the shear mechanism, and summarize the different effect in a simple formula, which can be used for every reinforced concrete beam. One of the oldest explanations for the behaviour of reinforced concrete beams is the truss analogy. It says that the behaviour of a simply supported concrete beams is similar to a truss: the tension is carried by the flange members and the shear is carried out by the inclined compressed concrete trusses and by the shear reinforcement. This analogy is the basis of the formulas in many standards, they calculate the shear resistance for the concrete and for the shear reinforcement as well. Some standards define the angle of the concrete truss in a specific value (Eurocode) and some of them give the opportunity of the determination to the designer. However, in a reinforced concrete beam these two effects can exist parallel, the codes allow to use only one of them (the shear resistance of concrete or that of the reinforcement).

3. SHEAR DESIGN OF FRP REINFORCED CONCRETE BEAMS

The shear behaviour of the FRP reinforced concrete beams are similar to the traditional steel bar reinforced beams, because the mechanism is the same, just the material parameters are different. However, this different material parameters and material behaviours can change the contribution to some of the shear components. The material behaviour of FRP bars can be considered as perfectly linear-elastic: the stress-strain relationship is linear up to the failure there is no plastic part of the diagram. This means that the failure can occur without any preliminary sign, which make the proper design necessary. The elastic modulus of these bars

is from 50 MPa (glass) to 220 MPa (carbon). From the shear components the effect of the compressive concrete zone changes most significantly. In FRP reinforced concrete (FRP RC) beams the area of the compression zone after cracking is smaller than the traditional RC structures because of the low elastic modulus. However, in case of traditional RC structures the depth of the neutral axis decreases significantly after the yield of the steel bars. This phenomenon is not happening in case of FRP bars because of the material behaviour, the depth of the neutral axis is continuously increasing after the first crack (Fig. 3).

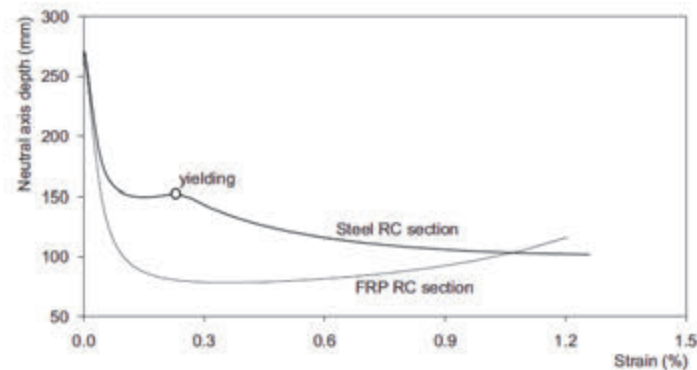


Fig. 3: Depth of the neutral axis in terms of the longitudinal reinforcements' strain (*fib* Bulletin 40, 2007)

Because of the low elastic modulus of polymers the cracks are larger in case of concrete beams with FRP bars than RC structures in the same load level, the effect of the aggregate interlock is smaller. Also because of the FRP bars have a really low transversal stiffness, the dowel action is negligible (Kanakubo and Shindo, 1997). The effect of the shear reinforcement depends on the tensile strength of the material which is usually the yield strength of the steel bars. In case of FRP the maximal elongation and the bond between the bar and the concrete is more significant because of the linear- elastic material behaviour. Because of this usually the standards use the strain limit for FRP bars: the strains in the bars must be under a defined value.

The codes and the guidelines contain separate chapters for shear design of FRP bar reinforced concrete structures. These formulas are usually the modification of the formulas for traditional RC structures, with taking into consideration the mentioned phenomenon.

3.1 ACI 440.1R (American Concrete Institute 440 Committee, 2015)

The formulas in the ACI recommendation are modifications for the shear formulas for RC structures according to the ACI 2005, but with using the maximum strain limit. The formula for concrete's shear resistance contains the effect of the FRP bars in the part of the calculating the depth of the compressive zone. The formula for concrete shear resistance with FRP main reinforcement is the following:

$$V_{cf} = 0.4\sqrt{f'_c}b_w c$$

where $c = k \cdot d$ for rectangular cross section

$$k = \sqrt{2\rho_f n_f + (\rho_f n_f)^2} - \rho_f n_f$$

$$\text{where } \rho_f = \frac{A_f}{b_w d}$$

A_f is the area of the FRP reinforcement.

In the presented equations b_w is the width of the cross section, d is the effective depth, and n_f is the ratio of the elastic modulus of the FRP and the concrete.

The contribution of the FRP stirrups is similar to the steel ones, but defining the tensile strength of the FRP bar as $0.004 E_f$. The code defines also the minimum reinforcement ratio for FRP stirrups as $0.35/0.004 E_f$.

3.2 Design approach of Guadagnini et al. (2003) (Modification of EN 1992-1)

This recommendation based on the Eurocode 2 (European Committee for Standards, 2004) shear formula for calculating the shear resistance of the concrete with taking into consideration the ratio of the elastic modulus of the FRP and the steel bars.

$$V_{cf} = 0.12 \left(1 + \sqrt{\frac{200}{d}}\right) \left(100 \cdot \frac{A_f}{b_w d} \cdot \frac{E_f}{E_s} \cdot \phi_s \cdot f_{ck}\right)^{1/3} b_w d$$

where E_f is the elastic modulus of the FRP, E_s is the elastic modulus of the steel bars, f_{ck} is the characteristic value of the concrete's compressive strength.

The formula for FRP stirrups uses the strain limit as well, it defined the maximum strain as 0.45%. The minimum reinforcement ratio for FRP stirrups can be calculated according Guadagnini et al. (2003) as:

$$0.08 \sqrt{f'_c} \cdot \frac{1}{0.0045 \cdot E_f}$$

4. SHEAR DESIGN OF SYNTHETIC FIBRE REINFORCED CONCRETE BEAMS

The fibre reinforcement is a well-used material for shear strengthening, several recent studies show promising results with using steel fibre reinforcement (SFRC) as shear reinforcement (Kovács and Juhász, 2013). The added fibres increase the fracture energy of the concrete which makes the structure more ductile, and raise the residual flexural strength of the material. Because it was mentioned that the shear crack is a special type of the tensile cracks, the randomly distributed fibres can bridge the crack, and can transfer loads between the two parts. Also the fibre reinforcement decreases the crack width which helps to the aggregate interlock to be more efficient. The *fib* MC 2010 (*fib*, 2013) the RILEM (Dupont and Vandewalle, 2003) recommendation and many literature gives design formulas for steel fibre reinforcement as shear reinforcement, but there is no guideline for synthetic fibre reinforced concrete structures. However in the literature several recent articles show (Li et al., 1992; Juhász and Schaul, 2015), that synthetic fibre reinforcement (SYFRC) can used as shear reinforcement as well. According to Yazdanbakhsh et al. (2015) the *fib* and the RILEM formulas can lead to proper results with SYNFRFC as well, and with these the synthetic fibre reinforced concrete shear resistance can be calculated.

4.1 *fib* MC2010 (*fib*, 2013)

The Model Code 2010 (*fib*, 2013) defines the fibre reinforced concrete beam with longitudinal reinforcement by adding the effect of the fibre reinforcement to the concrete's shear resistance:

$$V_{frc} = 0.18 \left(1 + \sqrt{\frac{200}{d}}\right) \left(100 \cdot \frac{A_f}{b_w d} \cdot \left(1 + 7.5 \frac{f_{Ftuk}}{f_{ctk}}\right) \cdot f_{ck}\right)^{1/3} b_w d$$

where f_{ctk} is the characteristic value of the concrete's tensile strength.

$$f_{Ftu}(w_u) = f_{Fts} - 0.5 \cdot f_{R3} + 0.2f_{R1} \quad (1)$$

In Eq. 1 the $w_u=1.5\text{mm}$ and the $f_{Fts}=0.45f_{R1}$. The f_{R1} and f_{R3} values are the residual tensile stress values at Crack Mouth Opening Distance (CMOD) stage 0.5 mm and 2.5 mm respectively. These values can measure from three point bending beam tests according to RILTEM TC 162 (2003).

4.2 RILEM

The formula (Dupont and Vandewalle, 2003) was developed at the beginning of the 21st century to present a simple tool with a huge amount of safety for SFRC structures. During the years the formula modified, but the original one gives better correlation for synthetic fibre reinforced concrete beams.

The shear resistance of a SYFRC beam can be calculated by summarize the shear capacity of the concrete and the added shear resistance by the fibres.

$$V_c = 0.15 \cdot \sqrt[3]{3\left(\frac{d}{a}\right) \cdot k(100 \cdot \rho \cdot f'_c)^{1/3}}$$

$$V_{SYF} = \frac{1600 - d}{1000} \cdot 0.5 \frac{d}{a} f_{e,3}$$

$$V_{frc} = V_c + V_{SYF}$$

where a is the shear span, ρ is the reinforcement ratio, $f_{e,3}$ is the equivalent flexural strength.

5. SHEAR DESIGN OF SYNTHETIC FIBRE REINFORCED CONCRETE BEAMS WITH FRP BARS

The combination of using FRP bars as longitudinal reinforcement and synthetic fibre reinforcement as shear reinforcement can be an alternative solution for traditional reinforced concrete where the conditions require the non-corrosivity of the reinforcement. In the standards, guidelines or codes there is no design formula for these structures. However, according to the mentioned literature the shear resistance of a synthetic fibre reinforced concrete beam with longitudinal FRP reinforcement and without stirrups can be estimate as follows:

$$V_{frc,f} = 0.12(1 + \sqrt{\frac{200}{d}})(100 \cdot \frac{A_f}{b_w d} \cdot \frac{E_f}{E_s} \cdot \phi_s \cdot (1 + 7.5 \frac{f_{Ftu}(k)}{f_{ctk}}) \cdot f_{ctk})^{1/3} b_w d \quad (2)$$

However, this equation must be verified by laboratory tests, it can be a good opportunity to predict analytically the shear resistance of a non- corrosive reinforced concrete beam. The formula takes into consideration the ratio of the FRP and steel material, and the additional shear capacity from synthetic fibre reinforced concrete as well. The basis of Eq. 2 is the shear resistance formula for FRP reinforced concrete beams according to Guadagnini at all and the fib MC2010 shear resistance formula for steel fibre reinforced concrete beams.

6. NUMERICAL MODELLING OF THE SYNTHETIC REINFORCED CONCRETE BEAMS

Another possible way to calculate the concrete beams with synthetic reinforcement is the advanced Finite Element Modelling. Because the effect of the reinforcements mostly prevail after the cracking of the concrete, it is necessary to choose software which can handle the non-linear behaviour of the concrete, and the different behaviour in tension and in compression. For example the Finite Element Software called ATENA meets with these requirements. It uses the combined fracture surface model to handle the difference in compression and in tension, and uses the Crack Band Method to model the cracking of the concrete (Cervenka and Papanikolaou, 2008).

If the software can follow the plain concrete's behaviour well, there are several methods to model FRP bars. The worldwide used is to model the bars as 1D link element. In this case it is possible to define the shape (hooked end, etc.) and the position of the bars. With defining the bond-slip law, which models the connection between the bar and the concrete, proper results can be obtained for shear capacity of the concrete beams (Juhász and Schaul, 2015). Another way is to model the FRP bar with its exact cross section (ribs surface etc.) with 3D elements. In this case the connection between the concrete and the bar must be a 2D interface material. The parameters for both of the contact materials can be obtained from pull out tests.

One of the widely used methods the Modified Fracture Energy Method is a proper opportunity to model fibre reinforcement in concrete beams. The main idea of the model is to use the concrete fracture energy (G_f) as an initial value and then increase it with an additional fracture energy (G_{ff}) from the post-crack FRC performance. The performance of the fibre can be determined with inverse analysis from the three point bending beam tests. This method is recommended also by the ITAtech Activity Group (2015). Another way is to model the fibres discretely into the concrete (Schaul and Balázs 2016). With this method the random distribution of the fibres, and the effect of the formworks (wall effect) can be modelled as well. Also with generating different random distributions virtual beam test series can be performed.

7. CONCLUSIONS

The shear failure of reinforced concrete beams is one of the most complex failure modes, where inclined cracks disconnect the upper and the lower part of the beam. The shear resistance of reinforced concrete beams depends on several different effects such as effect of the compressed concrete zone, the aggregate interlock, the dowel effect and the effect of the shear reinforcement. The contribution of these effects depends on many parameters, such as beam geometry, reinforcement ratio, type of shear reinforcement, and also has an impact on each other.

Standards, codes and guidelines specify the shear resistance for steel reinforced concrete beams and steel fibre reinforced concrete beams as well. For non-corrosive materials, such as FRP bars or synthetic fibre reinforced concrete elements the literature recommends formulas to calculate the shear resistance. These formulas are basically the modification of the shear capacity equations for traditional steel reinforced concrete.

With combining the different formulas for FRP reinforced concrete beams and for SYFRC beams the shear capacity of the synthetic fibre reinforced concrete beam with longitudinal FRP reinforcement can be estimated according to Eq (2). The formula summarizes the effect of

the FRP bars to the concrete's shear resistance, and the additional shear capacity of synthetic fibre reinforcement.

Structures with FRP bars and with synthetic fibre reinforcement are more and more frequent in modern constructions, the development of a proper analytical model for shear resistance became necessary.

With defining a proper material model and choosing an advance finite element software which can model the concrete's complex behaviour well, it is also possible to calculate the concrete beams shear capacity with FRP main reinforcement and with synthetic fibres as shear reinforcement.

With this overview and our future work we intend to contribute in the development of a proper and precise analytical model for shear capacity of concrete beams with non-metallic reinforcement.

8. REFERENCES

- ACI (2015): ACI 440.1R-15: Guide for the Design and Construction of Concrete Reinforced with FRP Bars
- Balázs, G. L. (2010), "A historical review of shear", in *fib Bulletin 57 "Shear and punching shear in RC and FRC elements"*, ISBN 978-2-88394-097-0, pp. 1-10
- Cervenka J. and Papanikolaou V.K. (2008): "Three dimensional combined fracture-plastic material model for concrete", *International Journal of Plasticity* (24): 2192-2220
- European Committee for Standards: (2004) "Eurocode 1992-3: Design of Concrete Structures – Part 3" 6.2. Shear
- Dupont D. and Vandewalle L. (2003), "Shear capacity of concrete beams containing longitudinal reinforcement and steel fibers" in *ACI Special Publ. 216* pp. 79–94.
- fib* (2013): "fib Model Code for Concrete Structures 2010", Ernst & Sohn Wiley, ISBN 978-3-433-03061-5
- fib* Task Group 9.3. (2007) "fib Bulletin 40 – FRP reinforcement in RC structures", Sprint-Digital-Druck, ISBN 978-2-88394-080-2
- Guadagnini, M., Pilakoutas, K. and Waldron, P. (2003), "Shear Performance of FRP Reinforced Concrete Beams", *Journal of Reinforced Plastics and Composites*, 22(15), pp. 1389-1408.
- ITAtch Activity Group Support (2015): "ITAtch Design Guidance For Precast Fibre Reinforced Concrete Segments" ITAtch Report n7, draft
- Juhász, K.P, Schaul, P. (2015), "Shear behaviour of synthetic fibre reinforced concrete beams reinforced with FRP rebars" *Proceedings of 11th CCC Congress, Hainburg*, pp.42-46.
- Kanakubo, T., and Shindo, M. (1997), "Shear Behaviour of Fiber-Mesh Reinforced Plates", *Third International Symposium on Non-Metallic (FRP) Reinforcement for Concrete Structures, Sapporo, Japan*, pp. 317-324.
- Kotsovos, M. D., and Pavlovic, M. N. (1999), "Ultimate Limit State Design of Concrete Structures -A New Approach", Thomas Telford, Ltd., London, UK.
- Kovács G. and Juhász K.P. (2014), "Synthetic and steel fibres in prestressed, precast long span beams", in: *Proceedings of CCC 2014, Czech Republic*
- Li V.C, Ward R, Hamza A.M. (1992), "Steel and synthetic fibers as shear reinforcement" *ACI Material Journal* 89 pp. 499–508.
- Rilem TC. 162-TDF (2003), "Test and design methods for steel fibre reinforced concrete, σ - ε design method" (ed.: Chairlady L. Vandewalle). *Mater Structures* 36 pp. 560–567.

- Schaul P. and Balázs L.Gy. (2016), "Shear behaviour of concrete beams reinforced with FRP bars" *Concrete Structures* 17. pp. 37-40.
- Taylor, H. P. J. (1970), "Investigation of the Forces Carried Across Cracks in Reinforced Concrete Beams in Shear by Interlock of Aggregate", 42.447, *Cement and Concrete Association*, London, UK.
- Vecchio, F.J. and Collins, M.P. (1986), "The Modified Compression-Field Theory for Reinforced Concrete Elements Subjected to Shear" *ACI Journal*, Title no.83-22.
- Völgyi, I. and Windisch, A., (2016): "Contribution of aggregate interlock to the shear resistance of RC beams", in press
- Wight, J.K., and Macgregor, J.G. (2012), "Reinforced concrete : mechanics and design - 6th edition", ISBN-13: 978-0-13-217652-1
- Walraven, J. C. (1981), "Fundamental Analysis of Aggregate Interlock, *Journal of the Structural Division*", *Proceedings of the American Society of Civil Engineering* 107 (No. ST11), pp. 2245-2269.
- Yazdanbakhsh, A., Altoubat, S. and Rieder K.A. (2015), "Analytical study on shear strength of macro synthetic fiber reinforced concrete beams" *Engineer Structures* 100, pp. 622-632.

VALIDATION OF THE FIB 2010 AND RILEM B4 MODELS FOR PREDICTING CREEP IN CONCRETE

George C. Fanourakis
University of Johannesburg
Department of Civil Engineering Technology
PO Box 17011
Doornfontein
2028
South Africa
georgef@uj.ac.za

SUMMARY

Creep strain, a requirement of the concrete design process, is a complex phenomenon that has proven difficult to model. Although laboratory tests may be undertaken to determine the creep, these are generally expensive and not a practical option. Hence, empirical code-type prediction models are used to predict creep strain.

This paper considers the accuracy of both the relatively new international fib Model Code 2010 (MC 2010) and RILEM Model B4, when compared with the actual strains measured on a range of concretes under laboratory-controlled conditions. Both models investigated underestimated the creep strain. In addition, the MC 2010 (2012) model, which yielded an overall coefficient of variation (ω_{all}) of 50,4 %, was found to be more accurate than the RILEM B4 (with a (ω_{all}) of 102,3 %).

1. INTRODUCTION

Creep of concrete is a complex phenomenon that has proven difficult to model. Nevertheless, for many reinforced and prestressed concrete applications, a reasonably accurate prediction of the magnitude and rate of creep strain is an important requirement of the design process. Although laboratory tests may be undertaken to determine the deformation properties of materials, these are time consuming, often expensive and generally not a practical option. In addition, this is not often an option at the design stage of a project when decisions about the actual concrete to be used have not yet been taken.

Hence, empirical based design code type models are often used for the estimation of creep deformation, by considering one or more intrinsic and/or extrinsic variables such as concrete stiffness and age at first loading as input.

This paper assesses the accuracy of two such models, the fib Model Code 2010 (2012) and the RILEM Model B4 (2015), when compared with the actual strains measured on a range of South African concretes which were subjected to a compressive strength related uniform load, under laboratory controlled conditions (relative humidity and temperature), for a period of approximately six months. These concretes included two strength grades (w/c's of 0,56 and 0,4) and three aggregate types (quartzite, granite and andesite).

The accuracy of the fib Model Code 2010 (MC 2010) and RILEM B4 (2015) Models was compared to the accuracy of other models, which were assessed (using the same concrete mixtures) during previous investigations.

In the abovementioned assessments, the predicted and measured creep results were presented in the form of specific creep (C_c), which is the creep strain per unit stress, as defined by Equations 1 and 2.

$$C_c = \frac{\varepsilon_c(t)}{\sigma} \quad (1)$$

Which can also be expressed as:

$$C_c = \frac{\varphi(t)}{E} \quad (2)$$

Where: $\varphi(t)$ is the creep coefficient at time t .
 E is the elastic modulus of the concrete.

2. MODELS INVESTIGATED

The two models evaluated in this investigation were the fib Model Code 2010 (MC 2010) and RILEM B4 Model (2015).

The Comité Euro-International Du Béton - Federation Internationale De La Précontrainte (CEB-FIP) Model Code (2010), fib Model Code 2010 (MC 2010), superseded the CEB-FIP (1990) model, which was in turn superseded by the CEB Model Code 90-99 which accounted for particular characteristics pertaining to high strength concretes.

The RILEM Model B3 (1995) was superseded by the RILEM Model B4 (2015), which accounts for additional parameters including the cementitious material type, admixtures and aggregate type (Wendner et al., 2013). The RILEM B3 AND B4 Models are relatively complex in comparison to the creep prediction models of international design codes.

3. EXPERIMENTAL DETAILS

3.1 Materials

CEM I 42,5 cement, from the Dudfield factory of Alpha Cement (now AfriSam), was used for all the tests carried out in this investigation. Quartzite (Q) from the Ferro quarry in Pretoria, granite (G) from the Jukskei quarry in Midrand and andesite (A) from the Eikenhof quarry in Johannesburg were used as both the coarse and fine aggregates for the concrete. The stone was 19 mm nominal size and the fine aggregate was crusher sand.

3.2 Preparation of prisms

For each of the concretes, six prisms were prepared, measuring 100 x 100 x 200 mm and cast with the 200 mm dimension vertical. After de-moulding, these prisms were continuously water cured up to an age of 28 days. After curing, three of the six prisms of each mix were used for creep tests and the remaining three were used for shrinkage measurements.

3.3 Elastic Modulus measurements

The creep test prisms were stacked into creep loading frames and subjected to elastic strain measurements, within 10 minutes of application of the loads, which were used to determine the secant moduli of the concretes.

3.4 Creep and Shrinkage measurements

The creep tests commenced immediately after the elastic modulus measurements were taken. These tests entailed subjecting the prisms in each frame to an applied load of approximately 25 % of the 28-day compressive strength, for the 168-day period, in a room controlled at 22 ± 3 °C and RH of 65 ± 5 %.

The shrinkage (companion) prisms were placed on a rack in the same room as the creep samples and, in order to ensure a drying surface area equivalent to the creep samples, the two 100 mm square ends were dipped in warm wax to prevent drying from these surfaces.

Creep and shrinkage measurements were recorded daily for the first week, thereafter, weekly for the remainder of that month and then monthly until the culmination of the approximately six-month total loading period. The strain of each group of prisms, that is the three creep prisms or the three companion shrinkage prisms of a particular mix, was taken as the average of the strains of the prisms in that group.

The results of shrinkage measurements were subtracted from the total time-dependant strain of the loaded specimens to determine the total creep strain.

3.5 Mix details

Details of the mixes used are given in Tab. 1.

Tab. 1: Details of the mixes and laboratory test results (after Fanourakis, 2011)

Aggregate Type	Quartzite		Granite		Andesite	
	Q1	Q2	G1	G2	A1	A2
Mix Number						
Water (l/m ³)	195	195	195	195	195	195
CEM I 42,5N (kg/m ³)	348	488	348	488	348	488
19 mm Stone (kg/m ³)	1015	1015	965	965	1135	1135
Crusher Sand (kg/m ³)	810	695	880	765	860	732
w/c Ratio	0.56	0.4	0.56	0.4	0.56	0.4
a/c Ratio	5.24	3.50	5.30	3.55	5.73	3.83
Slump (mm)	90	50	115	70	95	55
Cube Compressive Strength (MPa)	37	65	38	65	48	74
Cylinder Compressive Strength (MPa) ^a	30	53.5	30.7	53.5	38	59
Characteristic Cube Strength (MPa)	30	50	30	50	30	50
Characteristic Cylinder Strength (MPa) ^a	25	40	25	40	25	40
Concrete Density (kg/m ³)	2371	2410	2385	2432	2596	2585
Average Elastic Modulus of included Aggregate (GPa)	73		70		89	

^a Inferred from cube strength using the conversions from EC 2 (2004)

4. RESULTS AND DISCUSSION

4.1 Specific Creep with Time

Figs. 1 to 3 show the comparisons between the measured results for the six mixes (Q1, Q2, G1, G2, A1 and A2) and the corresponding strains predicted by the MC 2010 (2012) and RILEM B4 (2015) Models.

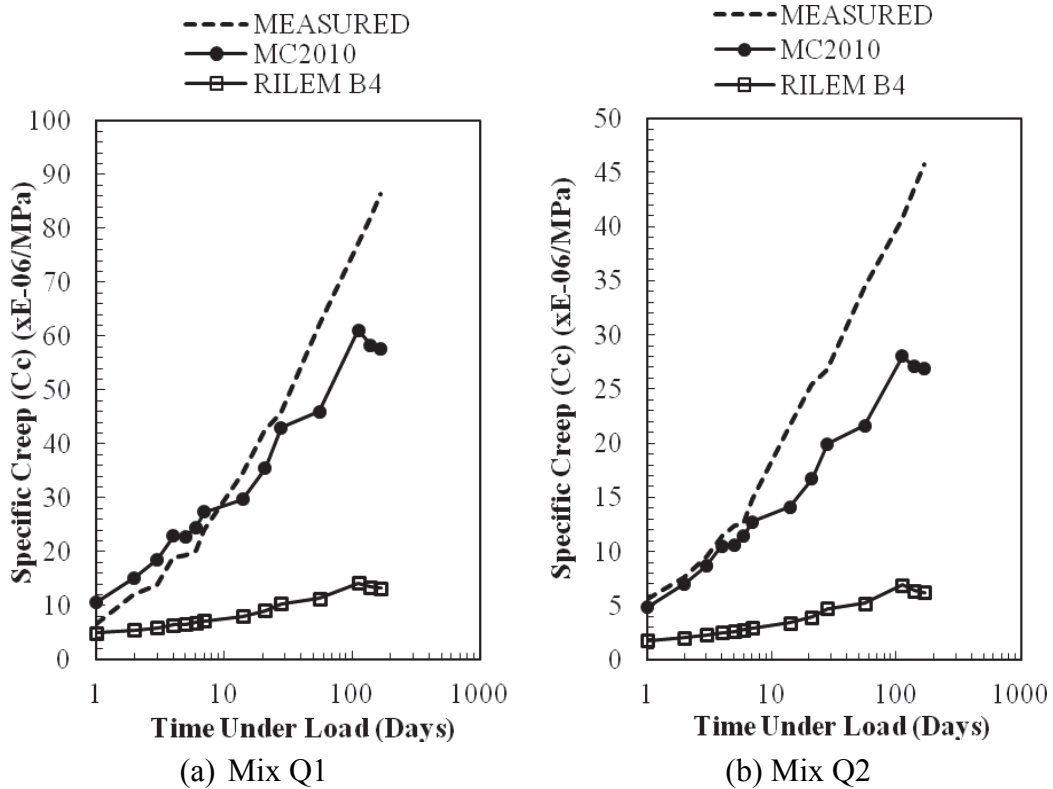


Fig. 1: Measured and predicted specific creep for quartzite concretes

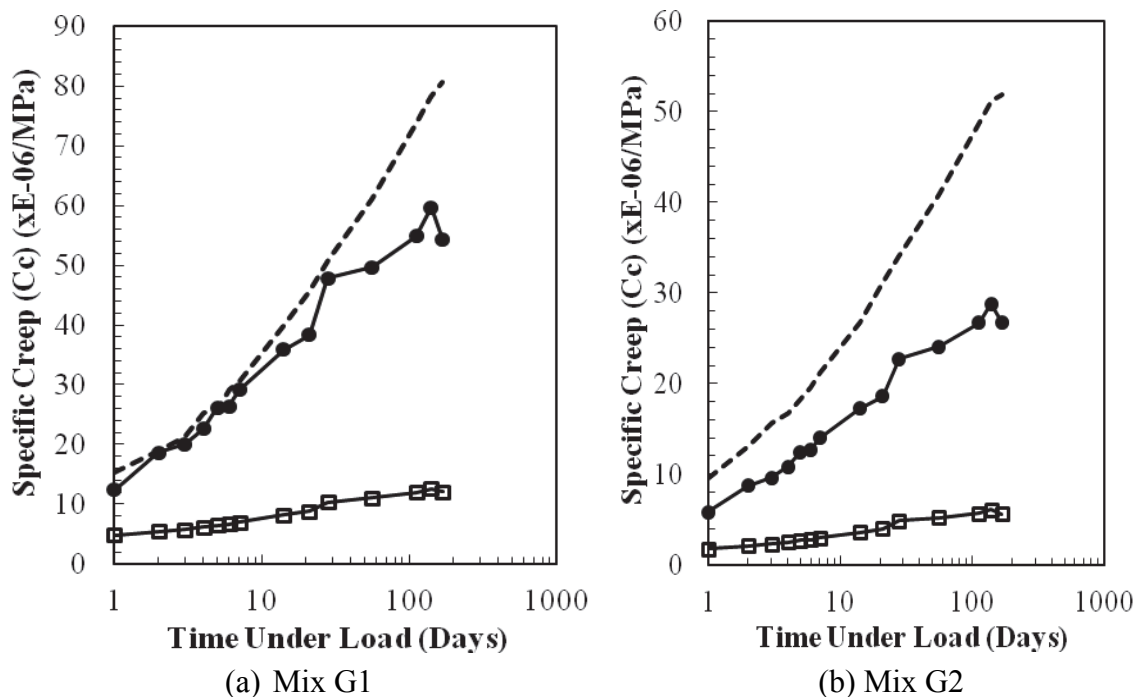


Fig. 2: Measured and predicted specific creep for granite concretes

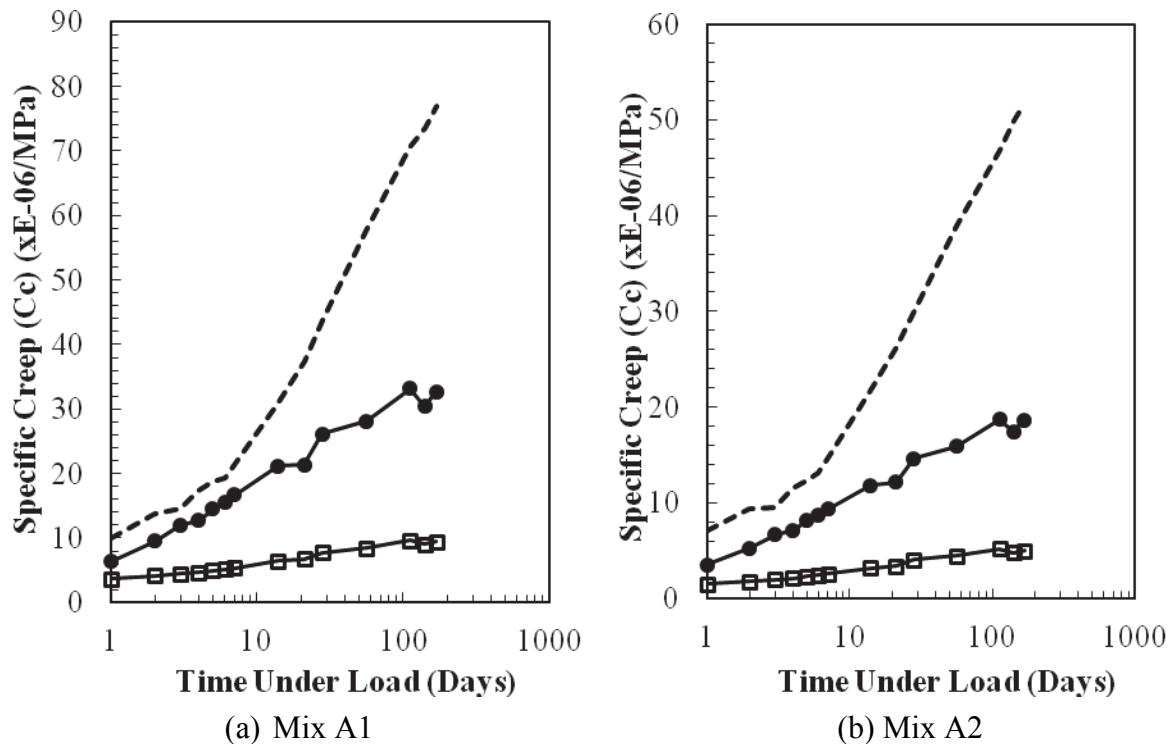


Fig. 3: Measured and predicted specific creep for andesite concretes

From Figs. 1 to 3, the following is evident regarding the prediction models.

- Both the MC 2010 (2012) and RILEM Model B4 (2015) models under-predicted the creep strain for all six of the concrete mixes.
- The MC 2010 (2012) Model was more accurate than the RILEM Model B4 (2015), in the case of all six mixes.
- In the case of each aggregate type, for both models, the mix with the lower w/c (0,4) yielded lower creep magnitudes than the mix with the higher w/c (0,56).
- In the case of the andesite concretes (A1 and A2), the rate of creep predicted by the MC 2010 (2012) model did not increase after approximately one week of loading to replicate the trend observed in the case of the measured creep strains.
- In the case of all the mixes, the rate of creep predicted by the RILEM Model B4 (2015) did not increase after approximately one week of loading to replicate the trend observed in the case of the measured creep strains.

When considering the effect of the aggregate type on the measured specific creep, the following was evident.

- For each aggregate type, the mix with the lower w/c ratio (stiffer mix) yielded relatively lower specific total creep values.
- No correlation was found to exist between the specific total creep strains and the stiffness of the included aggregate.

Detailed information regarding the effect of these aggregates on creep strain is given in Fanourakis and Ballim (2006a).

4.2 Accuracy of the Models Assessed

In order to provide a statistical basis for comparing the results of creep prediction methods, Bazant and Panula (1979) define a coefficient of variation of errors (ω_j) for single data sets as well for a number of data sets compared against the same prediction model (ω_{all}). The more accurate the prediction, the lower the value of ω_j . The calculated values of ω_j and ω_{all} for the different models assessed are shown in Tab. 2.

Tab. 2: Coefficients of variation for specific creep of the MC 2010 and B4 Models

Prediction Method	Coefficients of Variation (ω_j)						ω_{all}
	Mix Q1	Mix Q2	Mix G1	Mix G2	Mix A1	Mix A2	
Fib Model Code 2010 (2012)	32.6	42.0	26.3	48.8	63.6	72.7	50.4
RILEM Model B4 (2015)	102.1	101.9	95.9	101.4	105.0	109.0	102.3

From Tab. 2, it is evident that the RILEM Model B4 (2015) was the least accurate of the two models assessed with a ω_{all} of 102.3 %.

4.3 Comparison with the Accuracy of other Models

The Coefficients of variation of other code-type models that were assessed during previous investigations by Fanourakis (1998), Fanourakis and Ballim (2006b) and Fanourakis (2011) are included in Tab. 3.

A comparison of the results in Tab. 3 with those of other investigations is included in Fanourakis and Ballim (2003).

When comparing the accuracy of the MC 2010 (2012) and RILEM B4 (2015) Models, assessed in this paper, with other the accuracy of other models, it is evident that the MC 2010 (2012) was less accurate than its predecessor CEB - FIP (1990), which was only applicable to normal strength concretes. Furthermore, for the mixes used, the RILEM B4 (2015), which was the most complex of all the models considered, was the least accurate of the seventeen models validated in all the investigations, including the model it superseded (Model B3).

In addition, Wendner et al., (2015) found the relative accuracy of laboratory test total creep, of six models considered, to increase in the order GL (2000), ACI 209 (1992), MC 2010 (2012), RILEM Model B3 (1995), CEB – FIP (1999) and RILEM Model B4. The results of the two models investigated in this paper and those of previous investigations (shown in Tab. 3) agree with the relative order of accuracy of Wendner (2015), except in the case of the RILEM Model B4 which was found to be the least (and not most) accurate of the six models.

Tab. 3: Coefficients of variation for specific creep for various models

Prediction Method	Coefficients of Variation (ω_j)						ω_{all}
	Mix Q1	Mix Q2	Mix G1	Mix G2	Mix A1	Mix A2	
BS 8110 (1985)	29	27.4	26.5	8.6	26.9	15.5	23.6
SABS 0100 (1992)	20.1	41.4	26.5	8.6	47.9	26.5	31.3
SABS 0100 (1992) modified	45.2	17.3	49.5	31.9	34.4	15.2	34.7
ACI 209 (1992)	52.6	36.3	45.7	45.1	60.8	58.4	50.5
AS 3600 (1988)	12.5	n/a	13.4	n/a	47.2	n/a	29.2
AS3600 (2001)	67.4	16.6	51.1	13.2	25.5	25.8	38.6
AS3600 (2009)	103.0	84.2	85.8	42.6	68.6	43.9	74.7
GL (2000)	24.4	56.6	7.9	21.7	21.1	36.5	31.9
GL (2004)	26.5	62.0	9.7	26.0	22.9	41.1	35.4
GZ (1993)	58.4	46.8	46.3	37.4	55.7	49.8	49.5
CEB - FIP (1970)	18.1	31.3	15.0	12.3	13.9	9.9	18.1
CEB - FIP (1978)	66.0	148.6	53.9	95.1	65.6	112.8	96.1
CEB - FIP (1990)	32.7	19.8	27.7	31.2	39.6	38.3	32.2
EC 2 (2004)	28.0	26.5	20.8	38.3	35.3	45.5	33.4
RILEM Model B3 (1995)	45.6	29.3	33.0	21.9	45.3	32.6	35.6

5. CONCLUSIONS

- Both the MC 2010 (2012) and RILEM Model B4 (2015) models under-predict the creep strain for all six of the concrete mixes.
- The MC 2010 (2012) Model was more accurate than the RILEM Model B4 (2015), in the case of all six mixes.
- Both the MC 2010 (2012) and RILEM B4 (2015) Models were less accurate than the models that their predecessor CEB-FIP (1990) Model and RILEM Model B3, respectively.
- The RILEM Model B4 (2015), which yielded a ω_{all} of 103,2 %, was the most complex yet least accurate of all seventeen models validated by the author to-date.

6. REFERENCES

American Concrete Institute (ACI) (1992), "Prediction of Creep, Shrinkage and Temperature Effects in Concrete Structures", ACI Committee 209, Subcommittee II Report ACI 209R-92, Detroit, March, pp. 1- 12.

- AS 3600 (1988), "Concrete Structures - AS 3600-1988", Standards Association of Australia, North Sydney, pp. 8-14, 32-34.
- AS 3600 (2001), "Concrete structures - AS 3600- 2001", Standards Association of Australia, Sydney.
- AS 3600 (2009), "Concrete structures - AS 3600- 2009", Standards Association of Australia, Sydney.
- Bazant, Z. P. and Panula, L. (1979), "Practical Prediction of Time Dependent Deformations of Concrete", Parts I-VI, Materials and Structures, Vol. 12, pp. 169-183.
- BS 8110 (1985), "Structural Use of Concrete, Part 2, Code of Practice for Design and Construction", London, British Standards Institution.
- BS EN 1992-1-1 (2004), "Eurocode 2: Design of concrete structures, Part 1-1: General-Common Rules for Buildings and Civil Engineering Structures", London: British Standards Institution (BSI).
- CEB-FIP (1970), Comité Euro-International du Béton - Federation Internationale De La Precontrainte, "International Recommendations for the Design and Construction of Concrete Structures", Principles and Recommendations, FIP Sixth Congress, Prague, pp. 27-28.
- CEB-FIP (1978), Comité Euro-International du Béton - Federation Internationale De La Precontrainte, "International System of Unified Standard Codes of Practice for Structures", Volume II - CEB-FIP Model Code for Concrete Structures, 3rd ed. Lausanne, pp. 56, 331-344.
- CEB-FIP (1990), Comité Euro-International du Béton, CEB-FIP Model Code 1990, First Draft, Lausanne, Mar., pp. 2-3, 2-28 to 2-40 (Information Bulletin No. 195).
- CEB-FIP (2012), "CEB-FIP Model Code 2010 (2012) Final Draft", Federation Internationale Du Béton", Bulletins 65 & 66, Lausanne, pp. 125-155.
- Fanourakis, G.C. and Ballim, Y. (2003), "Predicting Creep Deformation of Concrete: A Comparison of Results from Different Investigations", Proceedings of The 11th FIG International Symposium on Deformation Measurements, Santorini, Greece, 25-28 May, pp.591-598.
- Fanourakis G.C. and Ballim, Y. (2006a), "The Influence of Aggregate Stiffness on the Creep of Concrete", Concrete Beton, No 112, April 2006, pp. 5-12.
- Fanourakis, G. C. and Ballim, Y. (2006b), "An Assessment of the Accuracy of Nine Design Models for Predicting Creep in Concrete", Journal of the South African Institution of Civil Engineering, Vol. 48, No. 4, pp. 2-8.
- Fanourakis, G. C. (2011), "Validation of International Concrete Creep Prediction Models by Application to South African Concretes", Journal of the South African Institution of Civil Engineering, Vol. 53, No. 2, pp. 23-30.
- Fanourakis, G.C. (1998), "The Influence of Aggregate Stiffness on the Measured and Predicted Creep Behaviour of Concrete", MSc (Eng) dissertation, University of the Witwatersrand, Johannesburg.
- Gardner, N. J. (2004), "Comparison of Prediction Provisions for Drying Shrinkage and Creep of Normal Strength Concretes", Canadian Journal for Civil Engineering, Vol. 31, No. 5, pp. 767-775.
- Gardner, N. J. and Lockman, M. J. (2001), "Design Provisions for Drying Shrinkage and Creep of Normal Strength Concrete", ACI Materials Journal, Vol .98, No. 2, pp. 159-167.
- Gardner, N. J. and Zhao, J. W. (1993), "Creep and Shrinkage Revisited", ACI Materials Journal, Vol. 90, No. 3, pp. 236-246.
- SABS 0100 (1992), "Code of Practice for the Structural Use of Concrete. Part 1: Design", South African Bureau of Standards.
- RILEM Model B3 (1995), "Creep and Shrinkage Model for Analysis and Design of Concrete Structures - Model B3", draft RILEM Recommendation, prepared by Bazant, Z. P. and

- Baweja, S., *Materials and Structures*, Vol. 28, pp. 357-365, 415-430, 488-495, with Errata in Vol. 29 (1996) pp. 126.
- RILEM Model B4 (2015), “Model B4 for Creep, Drying Shrinkage and Autogenous Shrinkage of Normal and High Strength Concretes with Multi- Decade Applicability”, Draft Recommendation: TC-242-MDC Multi-Decade Creep and Shrinkage of Concrete: Material Model and Structural Analysis (2015), prepared by Bazant, Z. P., *Materials and Structures*, Vol. 48, pp. 753-770.
- SABS 0100 (1992), “Code of Practice for the Structural Use of Concrete, Part 1 : Design”, Pretoria: South African Bureau of Standards.
- Wendner, R., Hubler, M. H. and Bazant, Z. P. (2013), “The B4 Model for Multi-Decade Creep and Shrinkage Prediction”, *Proceedings of the Ninth International Conference on Creep, Shrinkage and Durability Mechanics (CONCREEP-9)*, pp. 429-436.
- Wendner, R., Hubler, M. H. and Bazant, Z. P. (2015), “Statistical Justification of Model B4 for Multi-Decade Concrete Creep Using Laboratory and Bridge Databases and Comparisons to Other Models”, *Materials and Structures*, Vol. 48, pp. 815-833.

VISUAL PROGRAMMING AND BIM TECHNOLOGY IN PARAMETRIC CONCRETE BRIDGE SUPERSTRUCTURE DESIGN

Marek Jasiński, Tomasz Płaszczuk, Marek Salamak
Silesian University of Technology
Akademia Street 5, 44-100, Gliwice, Poland

SUMMARY

The paper describes the BIM technology and visual programming applied to standard, concrete, road bridge, superstructure design. The Building Information Modelling is a modern tool used to collect structure data, including its physical (e.g. concrete strength) and functional properties. The database might be represented in geometrical way as a 3D model. Visual programming is a graphical version of prevalent textual programming. Its concept bases on operational components and relations between them. Resultant of the code can be a bridge solid exported to common BIM software. Typical two-girder cross-sections of concrete road bridges are enough simple to describe them using mathematical formulas. The paper presents implementation of the visual programming methods in creation of parametric concrete bridge models. The code of solution and parametric cross-sections were described.

1. COMPUTER AIDED DESIGN

The character of the design process in civil engineering has been evolving over the last twenty years. The mainstream of the changes was based on computerization and informatization of tools and operations, including dissemination of software for numerical analysis, introducing digital archives of documentation and computer methods to create it. One of the most important aspects of such evolution was replacing the classic drawing boards with more and more popular CAD software (Eng. Computer Aided Design). Parts of an object were transferred from paper to the digital workspace by replacing hand-drawn lines and characters with vector graphics. It allowed designers to increase the accuracy of the created documentation and improve editorial operations. Even though, philosophy of work in CAD systems does not significantly differ from previous methods. Despite the introduction of new computer tools, interpretation of the documentation and its subsequent purpose still depend on the engineer's approach. A paper representation of the structure, as well as its CAD version, is a flat assembly of primal elements with no engineering meaning. As separate objects, isolated from adjacent instances, they do not carry any information about the modelled construction. The problem still occurs even after introducing three-dimensional CAD.

Further use of such documentation entails the need of running additional tools and sources. Because of lack of interoperability between software, given information is split, duplicated and introduced repeatedly at different steps of a design procedure. Transferring data between them significantly impedes the coordination of the process, especially in the case of document revision management, completing and archiving parts of the same project, as well as no compatibility between types of engineering software. An example of such the poorly coordinated process can be the manual creation of a numerical model basing on conceptual drawings and CAD drafts. In the next step, more detailed documentation is created, including cost estimates and schedules. The process does not provide error check and clash detection. In

conceptual design, optimization of the design approach can be disturbed as the time it takes between the decision and observation of its effects is long enough so the analysis of the given solution stops in a few steps and the optimal variant can be finally omitted.

The CAD concept, by definition, is limited to the design stage of the building process. It does not lead directly to a real improvement in other stages, e.g. construction, maintenance and operation. Paradoxically, while advantages of the CAD systems remain in the design stage, some of the mentioned drawbacks can have an impact on the entire building process. Lack of clash detection and limited perception in 2D modelling can lead to errors that stay hidden in the design stage, appear during construction and generate additional costs or delays. Therefore the construction industry requires another approach that brings opportunities to use undoubted information at every stage of the building process, its adequate coordination, interoperability, as well as easy reviewing, modifying and updating effects of changes in the process.

2. BIM TECHNOLOGY

Described limitations in dataflow lead to lower productivity in the construction industry. Between 1964 and 2003, the American Bureau of Labor Statistics was monitoring changes in values of productivity indices in the key sectors of the economy (Gilbert, 2012). The productivity index was defined as the value of the contract referred to workhours of hourly workers involved in the process. Fig. 1. shows a variation of such the indicator over forty years in the United States, differentiating construction and non-construction sectors, excluding farm industry.

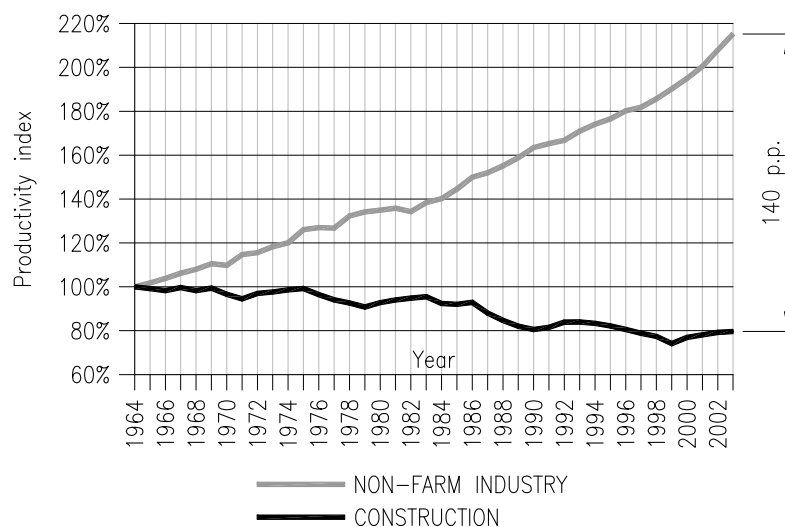


Fig. 1: Construction and non-farm labour productivity indices (1964-2003) (Gilbert, 2012)

Despite the introduction of CAD techniques into general design practice in the early '90s, the productivity index in the construction industry has not changed or even declined slightly. In the same time, other industry sectors have grown markedly what was caused mostly by automation of production lines and the digitalization of control or supervisory processes. Moreover, solid 3D modelling was a long time standard in several mechanical industries – at the beginning basing on physical prototypes of elements – later on producing, computing and analyzing their numerical forms.

A similar approach in the construction industry is included in BIM technology, expanded usually as Building Information Modelling. Its main idea assumes a three-dimensional model

of a building as a kind of database complemented with a different kind of information regarding the whole project and its parts. While in CAD systems, construction elements are defined by lines, arcs and solids with their parameters, e.g. coordinates of begin and end points, directional vectors, lengths, areas, volumes, colours and line types, BIM environment introduces elementary objects in form of parametric blocks of special function in the building, such as a beam, a column, a wall or a floor. As parts of the model they contain various information, not only about placement and dimensional values but also about the material, costs, staging and several parameters corresponding to their construction role. An essential part of such the characteristic database is also hosting feature of selected objects against secondary elements and ability to manage their mutual relations. This kind of information can be then used by another type of engineering software, e.g. to generate flat drawings, computational models, cost estimates, schedules or quantity lists. BIM environment can be also a multi-faceted platform for cooperation between individuals involved in the construction process. It is possible by local models being sent and merged into one central model with additional features available in modelling tools like clash detection and communication utilities.

An essential foundation of the BIM technology is its interoperability, not only in the 3D modelling environment but also out of the modelling software. The exchange of information usually bases on a two-way communication – on the one side, given data can be sent from modelling tool to external software. In the opposite direction, model receives data that was prepared or computed in the external environment. In cases where modelling process is tedious and labourious, it is justified to implement set of tools to define and edit geometry of the model. Most popular BIM modelling software is designed primarily for the creation of residential or industrial buildings as cubature objects and solids based on a regular grid and layouts of mutually perpendicular views. Such the forms usually do not consist of complex curvatures and masses, as opposite to bridges, including concrete bridges. It applies to brave bridge concepts as well as to typical road viaducts. Their form is often based on gradelines and their vertical and horizontal alignment defined by sloped lines, arcs and transition curves as well as their combinations. Any deviation from the perpendicularity, or the regularity in general, can be an obstacle to the modelling process, especially when simplified geometry may limit adequacy and usability of the model.

An exemplary method of modifying boundary conditions, input data and forcing its impact on the behavior of the 3D model as well as managing its usage in the whole construction process is the implementation of programmable algorithms. The convenient way to create them is to use visual programming languages as a more intuitive concept in comparison to classic textual languages. Modelling based on the visual programming provides a wide range of capabilities regarding parametrization of buildings and their parts, implementation of iterative analytical methods and quick access to basic object characteristics used in the design.

3. PARAMETRIC SUPERSTRUCTURE OF A TYPICAL CONCRETE BRIDGE

One of most popular bridge constructions in Poland is a prestressed concrete beam road bridge, in cross-section consisting of two girders and a deck across the top of them (named here as WD bridge). Less popular variation of such the construction can have three or more girders. A large number of bridges of this type are built along expressways and motorways or along passageways crossing over them. In the second case, they are usually designed as two-span concrete bridges supported by massive abutments and one middle support located in a greenbelt.

An attempt to create a geometrical model of a typical road bridge in a BIM environment can be preceded by a manual definition of a parameterized component of a cross-section type (Fig. 2.). The cross-section can be then assigned to a specified reference curve drawn in the 3D space, e.g. as a road gradeline. In the case of a transition curve being part of the horizontal plan of the gradeline, it is important to ensure the possibility to vary chosen parameters along the curve, especially with regard to transverse slopes of the deck that tend to change linearly at the distance between start and end points of the transition curve. In the given example of the parametrized cross-section, two sets of cross-sectional parameters can be imposed at the beginning and at the end of a chosen gradeline segment where the variation occurs.

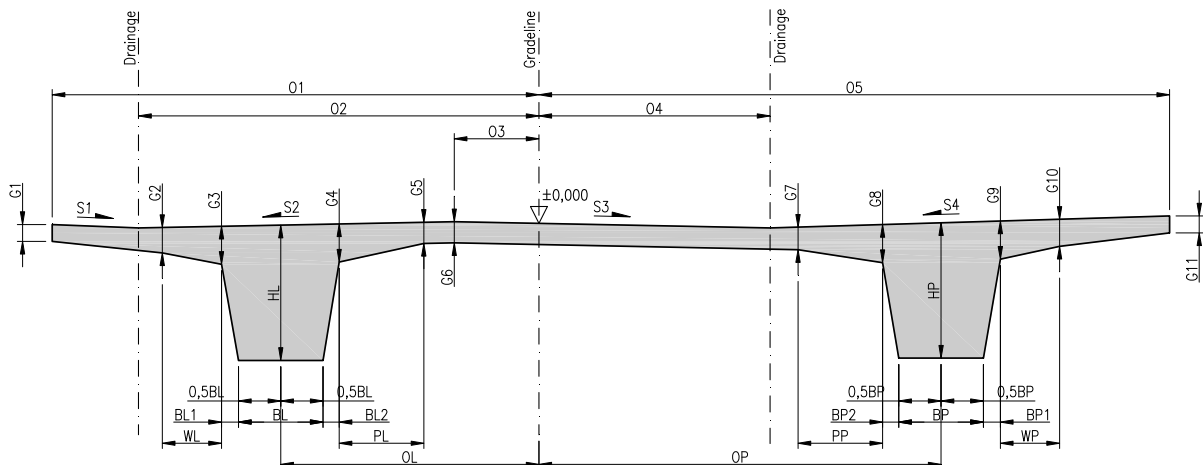


Fig. 2: Exemplary set of cross-sectional parameters of WD bridge

The presented cross-section can be controlled by 35 independent parameters, including 34 numerical parameters (dimensions) and one parameter of the Boolean type. The next 44 parameters are inaccessible for a user and are calculated automatically by the software, basing on specified values of dimensions shown in the Fig. 2. The shape of the section is controlled by 79 parameters in total. A given combination of dimensions that are provided by the user allows for visualization of most of the design approaches for this type of road bridges. Exemplary parameter values are lengths of the cantilevers, the height of the girders, the thickness of the slab and transversal slopes. It is possible to resign from the bilinear underside surface of the cantilevers or the slab, from the symmetry of the section or from the transverse camber of the deck by adjusting chosen values of the parameters to bring selected edge to required position. Introduced formulas should ensure computing all positive, negative and zero values with no errors.

Set of parameters, apart from cross-sectional dimensions and its slopes are i.a. span lengths, contain more general values as skew angles of supports related to the bridge axis, information about foundations, equipment, materials, quantities or staging. In the BIM environment, creating a geometrical model of a building is the basic task in the BIM process. Another kind of data is assembled simultaneously during modelling or is resultant of analysis performed on the geometrically introduced information. Each change of a single parameter leads to the automatic correction of all parts of the project that are related to modified part of the model. Such ability can be useful in conception design or during optimization. Proper information management can be performed in the modelling environment but due to limitations of the graphical user interface, it may be arduous for irregular forms. In particular cases, access to several operations carried on the model is straightened or even impossible. One of most

explicit examples is introducing of iterative loops with optimization algorithms that seek to find an optimal volume or concrete consumption ratio, that cannot be used by default in the modelling tools without access to the API functions and procedures (Eng. Application Programming Interface). Ability to carry out this and other complex operations and analysis can be achieved using graphical programming languages, e.g. Dynamo, together with modelling tools.

4. VISUAL PROGRAMMING LANGUAGES

Visual programming languages (VPL) are languages which have at least two dimensions defining their substance. Examples of such a dimension are the spatial position of code element (x, y coordinates) or multidimensionality of its elements (2D graphs) (Webster, 2002). Visual Programming Environment (VPE) is a tool used to generate textual programming languages (TPL) from diagrams. It is not classified as a complete visual programming language but rather as the solution in the middle. Separate topics are program visualisation (PV) systems used to show program code execution and graphical user interface (GUI) creators used to describe programs frontend. Visual programming languages can be recognized by its spatial, multidimensional objects with defined relations.

Programming paradigms are extended descriptions of programming language taxonomies (classifications). They apply both to their textual and visual versions. They define the way in which language code is organised and executed – its style. Code organisation is described with grammar and syntax. Code execution is described with execution model. Execution model describes the order of language instructions evaluation. The main difference exists between control flow and data flow. In first flow – instruction position and type determines program execution sequence. This solution is typical in textual languages. In second flow – data position and type determines program execution sequence. Due to its nature, mostly used in visual languages.

Basic programming paradigms for both textual and visual languages are:

- Imperative – earliest, computer native, used in low-level assembler languages. Flow is controlled strictly and its sequence is clearly visible. Commands operate on certain data. Statements are used to change the state of machine – there are global variables in use. Subroutines and “goto” instructions are characteristic for this paradigm.
- Procedural/Structural – used in high-level textual programming languages (e.g. Pascal, C, C++). Control flow is defined with conditions (e.g. “if”) and loops (e.g. “for”, “while”). It is a higher abstraction of imperative languages.
- Functional – used in mathematical lambda languages (e.g. LISP). Control flow is executed through function calls (e.g. $\cos(\cos(x))$). Changes of machine global state are avoided – there are no variables in use. Complex function calls and recursion (function self-calling) are characteristic for this paradigm.
- Declarative – used in modern query languages (e.g. SQL). Flow is controlled with commands but their sequence is not visible. Commands show the only logic of computation, not control flow of program – in opposition to imperative programming.
- Object oriented – used in high-level textual programming languages (e.g. C++, C#, Java). Control flow is based on communication between objects with the use of procedural/structural programming. Objects consist of data and methods (functions). The main difference between earlier paradigms lies in code organisation rather than control flow. It is a further abstraction of previous languages.

- Dataflow – used in parallel numerical calculations (e.g. LabVIEW). Unlike in other paradigms – flow sequence is specified by execution of data on certain commands. Machine state is easily visible while previously it was hidden.
- Multi-paradigm – most of the modern high-level programming languages are oriented at least at two programming paradigms. A different approach is necessary for solving different problems.

Additional, specific paradigms were proposed for visual programming languages. First proposal (Myers, 1986) was very limited and not useful to properly distinct visual languages. Second is a basis of visual languages classification in ACM publications (Burnett, Baker, 1994). Taxonomy was based on published papers analysis. Following paradigms were developed: parallel, parametric, dataflow, spreadsheets, functional, imperative, logic, multi-paradigm, object, programming by demonstration and rule-based. Most significant (Webster, 2002) paradigms in visual programming languages are:

- Imperative programming by demonstration – used in graphical data analysis software. The user defines program behaviour with use of its GUI and introduced examples. Filtering protein data can be such example.
- Spreadsheet-based programming – popular office spreadsheet programs are based on visual programming. Language is presented graphically as a data and functions contained in spreadsheet cells.
- Dataflow programming – identical with the textual paradigm. The only difference is a graphical representation of the code.

5. VPL EXAMPLES

Engineering sciences are a specific area of visual programming languages (VPL) application. Spatial issues with a high degree of complexity are easier modelled graphically. First, visual programming environments (VPE) were used to prepare graphical user interfaces (GUI) for traditional, textual languages. Next, textual languages were made from visual programming environments diagrams. Based on previous experiences, standalone visual programming languages were created. At first applied only in narrow areas, later they gained recognition in more general domains of electronics, bioinformatics and construction industry. Most popular in the construction industry are:

- LabVIEW G – used for data acquisition and analysis (DAQ). Developed since 1986 by National Instruments, US. Based on dataflow paradigm, supports imperative, procedural/structural and functional programming at various levels. Created as an easy language for engineers and scientists. Due to its longevity, it delivers a big amount of ready solutions and good quality libraries. LabVIEW compiler and IDE are proprietary products, thus limiting usage of language.
- Grasshopper 3D – used for parametric architectural modelling. Developed since 2007 by R. McNeel & Assoc. Based on dataflow paradigm and functional programming. Provides easy to learn an alternative to scripting languages. Integrated with Rhinoceros modelling software. Proprietary license limits language development.
- Dynamo – used for construction modelling. Developed since 2014, lately acquired by Autodesk. Integrated with Autodesk Revit is Grasshopper alternative for construction.

6. DYNAMO VPL

Dynamo is both visual programming language (VPL) and integrated development environment (IDE). The user interface consists of two workspaces, displaying program visual code (VPL) and program graphical output preview (PV). Language interpretation mechanism allows for quick adjustments and live preview of output. IDE workflow is based on managing connections between program nodes. Nodes consist of input and output ports and are objects themselves (see object-oriented paradigm). Connections between nodes are made with wires, which are used to control data flow in the program (Fig. 3).

Dynamo supports functional and dataflow programming paradigms. Visual language originates from Scheme textual language – dialect of functional LISP. Flow sequence is controlled with data, executed by instructions in nodes. Data is passed between the nodes at multiply flow paths (parallel calculations). In each executed path – only one node is active. Lack of support for procedural/structural programming is characteristic for this language. Iterations have to be obtained with use of recursion. Directly there is no support for the object-oriented paradigm. However, imperative, functional and object-oriented paradigms are supported indirectly by embedded textual Design script and Python language. The extension is possible with the use of special purpose nodes. Dynamo language is still in ongoing development and missing useful solutions – such as procedural/structural paradigm programming.

7. DYNAMO VPL IN CONCRETE BRIDGE EXAMPLE

An example of Dynamo VPL in parametric concrete bridge modelling is a cross-section of typical WD bridge used in Poland (Fig. 3).

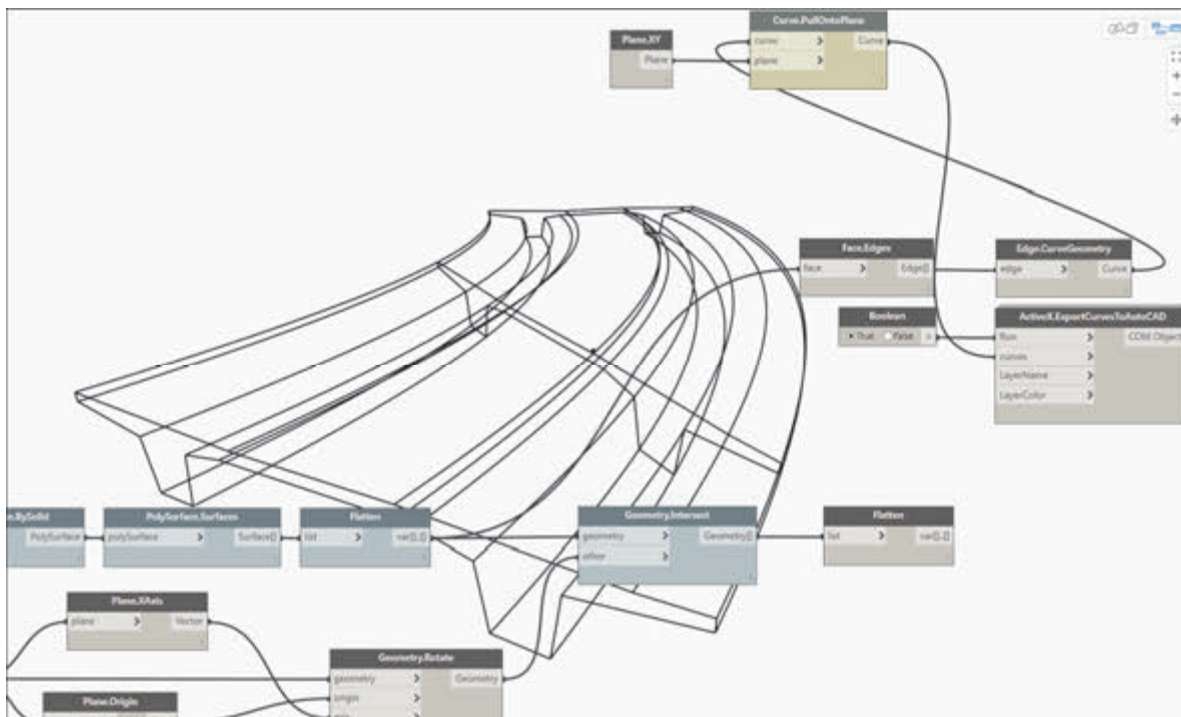


Fig. 3: VPL application in WD bridge

WD bridge characterized by simple geometry was chosen as an example – to explore its parametric design possibilities with the use of BIM and visual programming language Dynamo. Most of WD objects are designed nowadays with the use of CAD software. Their

omnipresence on highway road system forces hundreds of similar projects to be made yearly. Various approaches were made to parametrize them in CAD systems, none of them has been widely adopted. This is partly because most of the designs were made in 2D. BIM technology introduces 3D modelling thus providing new possibilities of parametrization with possibility to export parameterized geometry to flat drawings, including export to CAD systems.

Geometry construction was based on arc curve made as a fillet between two lines placed in Dynamo 3D workspace. Lines were defined, each with two geometrical points, tangent to the beginning and the end of the arc. Arc radius was provided as a parameter. Additionally, curve trimming function was applied to limit the length of the bridge. Revit parametric, structural framing, the family type described in the previous paragraph was used to create beam along the curve, creating bridge geometry. As a next step geometry was prepared for further analysis in AutoCAD software. Bridge solid is extracted and converted to the polysurface (set of surfaces). Polysurface is then further broken into the list of separate surfaces. Surfaces edges are detected and converted to curves, then projected to plane and exported to AutoCAD. Further studies will conclude relations between exported cross-section geometry.

8. CONCLUSIONS

The necessity of CAD systems development towards BIM technology is a result of low construction sector performance compared to the rest of industrial complex. BIM technology is based on construction 3D model, which contains information about its physical properties. Geometry is defined with intelligent objects such as – beam, wall, column etc. instead of simple lines. Information provided this way describes reality better than one provided with CAD technology. It allows for better interoperability and data analysis.

Complex relations in BIM model can be replaced with simple visual programming languages. One of them is Dynamo language, capable for simple and advanced geometry modelling, as shown in WD bridge example. It allows for simpler and faster bridge superstructure prototyping thus lowering costs of design. At the same time it allows to improve final quality of project. Authors are currently working on other types of visual programming applications in concrete bridges.

9. REFERENCES

- Burnett M. M. and Baker M. J. (1994), “A Classification System for Visual Programming Languages”, *J. Vis. Lang. Comput.* No. 3, 1994, pp. 287–300.
- Gilbert S. W. (2012), “Characterization of the U.S. Construction Labor Supply”, National Institute of Standards and Technology, U.S. Department of Commerce. Special Publication No. 1135, December 2012.
- Myers B. A. (1986), “Visual Programming, Programming by Example, and Program Visualization: A Taxonomy”, *Proc. SIGCHI Conf. Hum. Factors Comput. Syst.*, ACM, 1986, pp. 59–66.
- Webster J. G. (2002), “Wiley Encyclopedia of Electrical and Electronics Engineering”, *Biomed. Instrum. Technol.* No. 5, 2002, p. 355.

EVALUATION OF THE CREEP COEFFICIENTS OF THE FIB 2010 AND RILEM B4 CONCRETE CREEP PREDICTION MODELS

George C. Fanourakis
University of Johannesburg
Department of Civil Engineering Technology
PO Box 17011
Doornfontein
2028
South Africa
georgef@uj.ac.za

SUMMARY

Creep of concrete is an important design consideration. National design codes therefore provide empirical based models for the estimation of creep deformation. Such models generally estimate a creep coefficient (ϕ) and an elastic modulus (E) of the concrete, both of which are used to predict the creep strain at any age. This paper assesses the accuracy of the creep coefficients (ϕ) predicted by the relatively new international *fib* Model Code 2010 (MC 2010) and RILEM Model B4 using a laboratory test programme. The measured creep coefficient (ϕ) values were statistically compared to those predicted by the models considered. The MC 2010 (2012) Model, which yielded an overall coefficient of variation (ω_{all}) of 44.9 %, was found to be more accurate than the RILEM Model B4 (with a (ω_{all}) of 103.3 %). Both the models validated were found to yield less accurate creep coefficients than their respective predecessor models.

1. INTRODUCTION

Creep magnitude is an important design consideration for the durability, long-term serviceability and the load carrying capacity of structures.

The magnitude of creep can be determined by laboratory testing or estimated by means of empirical based models of various complexities. In general, the more deformation sensitive the structure, the more justifiable the cost and time of laboratory testing or complexity of the estimation method employed. In cases where only a rough estimate of the creep is required, design code-type models are ideal for predicting the creep

With the exception of the RILEM Model B3 (1995), creep models express creep strain in terms of the creep coefficient, (ϕ), where:

$$\varepsilon_c(t, \tau) = \phi(t) \varepsilon_{e,\tau} \quad (1)$$

In Equation 1, $\varepsilon_c(t, \tau)$ is the creep strain at any concrete age t for a concrete loaded at age τ , where $t > \tau$ and $\varepsilon_{e,\tau}$ is the elastic strain of the concrete at age τ . The creep coefficient (ϕ) is empirically determined by considering one or more intrinsic and/or extrinsic variables such as concrete stiffness and age at first loading. The elastic modulus used to estimate the elastic strain is estimated using an empirical equation prescribed by that method.

The RILEM Model B3 (1995) and RILEM Model B4 (2015) are, by comparison, more complex than the design code models and take a more fundamental materials approach to creep prediction. In the case of these models, an elastic modulus is estimated, which is used in the calculation of the compliance function for additional creep due to drying and may be used to calculate the creep coefficient ($\phi_{(t)}$) from the relevant compliance function equations (by dividing ϵ_c by ϵ_e).

Previous work by Fanourakis (1998), Fanourakis and Ballim (2006), Fanourakis (2011) and Fanourakis (2016) collectively assessed the accuracy of fifteen code-type creep prediction models when applied to South African concretes.

Fanourakis (2011) investigated the correlation between the predicted specific creep (C_c) and the estimated elastic (E) and established that most accurate creep prediction model, the CEB-FIP (1970), (for the C_c) was the least accurate in estimating elastic modulus (E). Furthermore, the models that yielded the most accurate estimation of elastic modulus (E) (SANS 10100, 2000 and AS 3600, 2009) did not yield the most accurate estimation of specific creep (C_c).

Subsequently, Fanourakis (2016) established that a highly significant ($P = 0.001$ %) correlation ($r = 0.901$) exists between the creep coefficient (ϕ) and specific creep (C_c) predicted by the fourteen models considered.

This paper assesses the accuracy of the creep coefficients estimated by the relatively new *fib* Model Code 2010 (2012) and the RILEM Model B4 (2015), when compared with the actual creep coefficients measured on a range of South African concretes under laboratory controlled conditions, for a period of approximately six months. These concretes included two strength grades (w/c 's of 0.56 and 0.4) and three aggregate types (quartzite, granite and andesite).

The accuracy of the *fib* Model Code 2010 (MC 2010) and RILEM B4 (2015) Models was compared to the accuracy of their predecessor models.

2. MODELS INVESTIGATED

The two relatively new models evaluated in this investigation were the *fib* Model Code 2010 (MC 2010) and RILEM B4 Model (2015).

The Comité Euro-International Du Béton - Federation Internationale De La Précontrainte (CEB-FIP) Model Code (2010), *fib* Model Code 2010 (MC 2010), superseded the CEB-FIP (1990) model, which was in turn superseded by the CEB Model Code 90-99 which accounted for particular characteristics pertaining to high strength concretes.

The RILEM Model B3 (1995) was superseded by the RILEM Model B4 (2015), which accounts for additional parameters including the cementitious material type, admixtures and aggregate type (Wendner et al., 2013).

3. EXPERIMENTAL DETAILS

3.1 Materials

CEM I 42,5 cement, from the Dudfield factory of Alpha Cement (now AfriSam), was used for all the tests carried out in this investigation. Quartzite (Q) from the Ferro quarry in Pretoria,

granite (G) from the Jukskei quarry in Midrand and andesite (A) from the Eikenhof quarry in Johannesburg were used as both the coarse and fine aggregates for the concrete. The stone was 19 mm nominal size and the fine aggregate was crusher sand.

3.2 Preparation of prisms

For each of the concretes, six prisms were prepared, measuring 100 x 100 x 200 mm and cast with the 200 mm dimension vertical. After de-moulding, these prisms were continuously water cured up to an age of 28 days. After curing, three of the six prisms of each mix were used for creep tests and the remaining three were used for shrinkage measurements.

3.3 Elastic Modulus measurements

The creep test prisms were stacked into creep loading frames and subjected to elastic strain measurements, within 10 minutes of application of the loads, which were used to determine the secant moduli of the concretes.

3.4 Creep and shrinkage measurements

The creep tests commenced immediately after the elastic modulus measurements were taken. These tests entailed subjecting the prisms in each frame to an applied load of approximately 25 % of the 28-day compressive strength, for the 168 day period, in a room controlled at 22 ± 3 °C and RH of 65 ± 5 %.

The shrinkage (companion) prisms were placed on a rack in the same room as the creep samples and, in order to ensure a drying surface area equivalent to the creep samples, the two 100 mm square ends were dipped in warm wax to prevent drying from these surfaces.

Creep and shrinkage measurements were recorded daily for the first week, thereafter, weekly for the remainder of that month and then monthly until the culmination of the approximately six-month total loading period. The strain of each group of prisms, that is the three creep prisms or the three companion shrinkage prisms of a particular mix, was taken as the average of the strains of the prisms in that group.

The results of shrinkage measurements were subtracted from the total time-dependant strain of the loaded specimens to determine the total creep strain.

3.5 Mix details

Details of the mixes used are given in Tab. 1.

Tab. 1: Details of the mixes and laboratory test results (after Fanourakis, 2011)

Aggregate Type	Quartzite		Granite		Andesite	
	Q1	Q2	G1	G2	A1	A2
Mix Number						
Water (l/m ³)	195	195	195	195	195	195
CEM I 42,5N (kg/m ³)	348	488	348	488	348	488
19 mm Stone (kg/m ³)	1015	1015	965	965	1135	1135
Crusher Sand (kg/m ³)	810	695	880	765	860	732
w/c Ratio	0.56	0.4	0.56	0.4	0.56	0.4
a/c Ratio	5.24	3.50	5.30	3.55	5.73	3.83
Slump (mm)	90	50	115	70	95	55
Cube Compressive Strength (MPa)	37	65	38	65	48	74

Cylinder Compressive Strength (MPa) ^a	30	53.5	30.7	53.5	38	59
Characteristic Cube Strength (MPa)	30	50	30	50	30	50
Characteristic Cylinder Strength (MPa) ^a	25	40	25	40	25	40
Concrete Density (kg/m ³)	2371	2410	2385	2432	2596	2585
Average Elastic Modulus of included Aggregate (GPa)	73		70		89	
^a Inferred from cube strength using the conversions from EC 2 (2004)						

4. RESULTS AND DISCUSSION

4.1 Predicted versus actual ϕ values

Figs. 1 to 3 show the relationships between the predicted ϕ and actual ϕ for the six mixes (Q1, Q2, G1, G2, A1 and A2), pertaining to the MC 2010 (2012) and RILEM B4 (2015) Models. The “ $r = 1$ ” line (predicted equals actual) is included in each figure to display the relative accuracy of the predicted values.

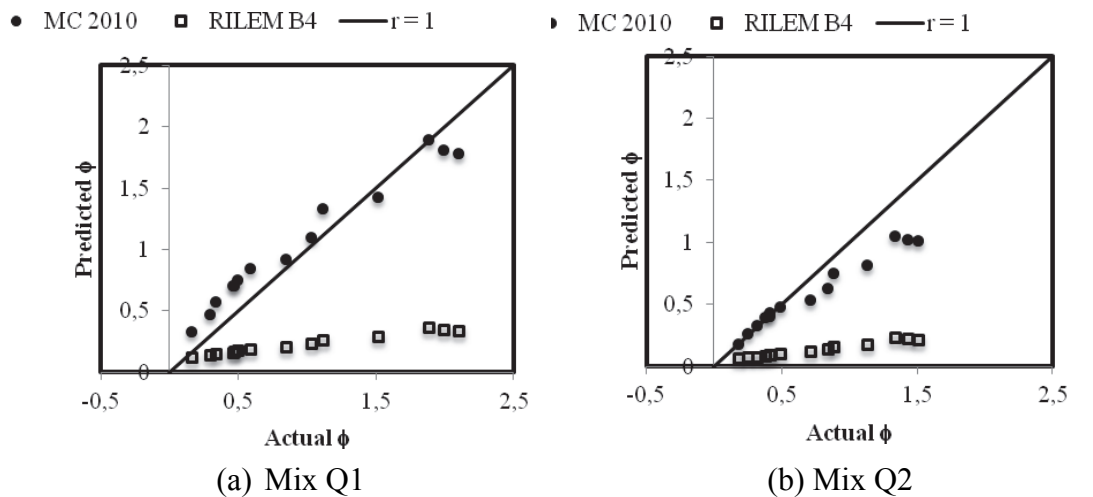


Fig. 1: Predicted versus actual creep coefficients (ϕ) for quartzite concretes

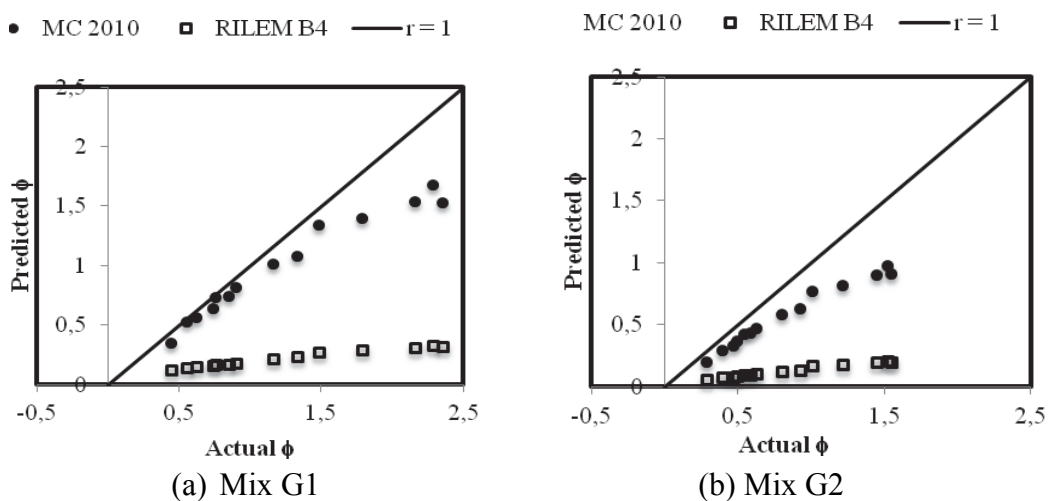


Fig. 2: Predicted versus actual creep coefficients (ϕ) for granite concretes

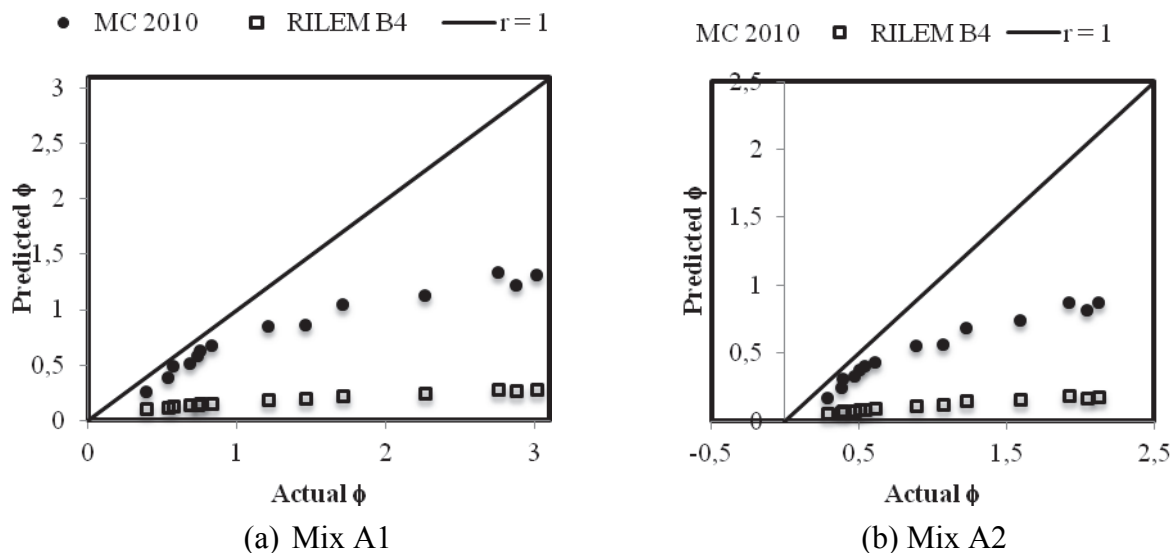


Fig. 3: Predicted versus actual creep coefficients (ϕ) for andesite concretes

From Figs. 1 to 3, the following is evident.

- Both the models considered general under-predicted the creep coefficients (ϕ).
- The MC 2010 (2012) Model predicted the ϕ values more accurately than the RILEM Model B4 (2015) Model, in the case of all six mixes.
- The variation in predicted ϕ values, with time, in the case of the RILEM Model B4 (2015) was relatively low (low rate of creep).
- The MC 2010 (2012) Model was the least accurate in the case of the andesite concretes (mixes A1 and A2), where the accuracy of the predicted ϕ values decreased after 7 days, indicating a decrease in the rate of creep.
- The trend lines pertaining to the MC 2010 (2010) model and RILEM B4 (2015) Models yielded pooled correlation coefficients (r) of 0.983 (0.967 to 0.987) and 0.988 (0.984 to 0.989), respectively.
- All the correlations established were highly significant, being at the $P = 7.1E-06$ % and $P = 1.4E-07$ % levels, in the case of the MC 2010 (2010) Model and RILEM B4 (2015) Models, respectively.

4.2 Accuracy of the models assessed

In order to provide a statistical basis for comparing the results of creep prediction methods, Bazant and Panula (1979) define a coefficient of variation of errors (ω_j) for single data sets as well for a number of data sets compared against the same prediction model (ω_{all}). The more accurate the prediction, the lower the value of ω_j . The calculated values of ω_j and ω_{all} for the different models assessed are shown in Tab. 2.

Tab. 2: Coefficients of variation for ϕ of the MC 2010 and B4 Models

Prediction Method	Coefficients of Variation (ω_j)						ω_{all}
	Mix Q1	Mix Q2	Mix G1	Mix G2	Mix A1	Mix A2	
<i>fib</i> Model Code 2010 (2012)	22.1	31.5	29.4	39.7	61.9	66.0	44.9
RILEM Model B4 (2015)	100.7	100.9	98.0	99.1	109.7	110.6	103.3

From Tab. 2, it is evident that the RILEM Model B4 (2015) was the least accurate of the two models assessed with a ω_{all} of 103.3 %. Both models yielded (slightly) more accurate predictions in the case of the low strength mixes.

4.3 Comparison with predecessor models

When comparing the accuracy of creep coefficient (ϕ) predictions, the CEB-FIP (1990) was more accurate than the succeeding MC 2010 (2012), yielding a ω_{all} of 27.7 %. Similarly, the RILEM Model B3 (1995) was more accurate than the succeeding RILEM B4 (2015) model, yielding a ω_{all} of 40.8 % (Fanourakis, 2016). Furthermore, for the mixes used, the RILEM B4 (2015), which is the most complex of all the models validated by the author, was the least accurate of the seventeen models considered in all the investigations.

5. CONCLUSIONS

- Both the models considered general under-predicted the creep coefficients (ϕ).
- The MC 2010 (2012) model predicted the ϕ values more accurately than the RILEM Model B4 (2015) model, in the case of all six mixes.
- The trend lines pertaining to the MC 2010 (2012) and RILEM B4 (2015) Models yielded pooled correlation coefficients (r) of 0.983 (0.967 to 0.987) and 0.988 (0.984 to 0.989), respectively.
- Both the MC 2010 (2012) and RILEM Model B4 (2015) models were less accurate than the models that their predecessor CEB-FIP (1990) Model and RILEM Model B3, respectively.
- The RILEM Model B4 (2015), which yielded a ω_{all} of 103.3 %, was the most complex yet least accurate of all seventeen models validated by the author to-date.

6. REFERENCES

- AS 3600 (2009), "Concrete structures - AS 3600- 2009", Standards Association of Australia, Sydney.
- Bazant, Z. P. and Panula, L. (1979), "Practical Prediction of Time Dependent Deformations of Concrete", Parts I-VI, Materials and Structures, Vol. 12, pp. 169-183.
- CEB-FIP (1970), Comité Euro-International du Béton - Federation Internationale De La Precontrainte, "International Recommendations for the Design and Construction of Concrete Structures", Principles and Recommendations, FIP Sixth Congress, Prague, pp. 27-28.
- CEB-FIP (1990), Comité Euro-International du Béton, CEB-FIP Model Code 1990, First Draft, Lausanne, Mar., pp. 2-3, 2-28 to 2-40 (Information Bulletin No. 195).
- CEB-FIP (2012), "CEB-FIP Model Code 2010 (2012) Final Draft", Federation Internationale Du Béton", Bulletins 65 & 66, Lausanne, pp. 125-155.
- Fanourakis, G. C. and Ballim, Y. (2006), "An Assessment of the Accuracy of Nine Design Models for Predicting Creep in Concrete", Journal of the South African Institution of Civil Engineering, Vol. 48, No. 4, pp. 2-8.
- Fanourakis, G.C. (2016), "Evaluation of the Creep Coefficients of International Concrete Creep Prediction Models", *fib* (CEB-FIP) Symposium 2016, Performance-Based Approaches for Concrete Structures, Cape Town, South Africa, 21 to 23 November 2016.
- Fanourakis, G. C. (2011), "Validation of International Concrete Creep Prediction Models by Application to South African Concretes", Journal of the South African Institution of Civil Engineering, Vol. 53, No. 2, pp. 23-30.

- Fanourakis, G.C. (1998), "The Influence of Aggregate Stiffness on the Measured and Predicted Creep Behaviour of Concrete", MSc (Eng) dissertation, University of the Witwatersrand, Johannesburg.
- RILEM Model B3 (1995), "Creep and Shrinkage Model for Analysis and Design of Concrete Structures - Model B3", draft RILEM Recommendation, prepared by Bazant, Z. P. and Baweja, S., *Materials and Structures*, Vol. 28, pp. 357-365, 415-430, 488-495, with Errata in Vol. 29 (1996) pp. 126.
- RILEM Model B4 (2015), "Model B4 for Creep, Drying Shrinkage and Autogenous Shrinkage of Normal and High Strength Concretes with Multi- Decade Applicability", Draft Recommendation: TC-242-MDC Multi-Decade Creep and Shrinkage of Concrete: Material Model and Structural Analysis (2015), prepared by Bazant, Z. P., *Materials and Structures*, Vol. 48, pp. 753-770.
- SANS 10100 (2000), *The Structural Use of Concrete, Part 1: Design*. South African Bureau of Standards.
- Wendner, R., Hubler, M. H. and Bazant, Z. P. (2013), "The B4 Model for Multi-Decade Creep and Shrinkage Prediction", *Proceedings of the Ninth International Conference on Creep, Shrinkage and Durability Mechanics (CONCREEP-9)*, pp. 429-436.

DEFORMATION OF THE GROUND CAUSED BY MINING EXPLOITATION AND INTERNAL FORCES IN FREELY SUPPORTED BRIDGE

Andrzej Śliwka

Faculty of Civil Engineering, Silesian University of Technology

Akademia 5, 44-100 Gliwice, Poland

SUMMARY

Bridges in the mining area are influenced by ground. Deformations in objects statically indeterminate cause additional internal forces. Due to the scale of those impacts and the uncertainty about the actual magnitude of area deformation, the aim is to minimize the impact of deformable ground through the use of statically determinate systems, and ensuring the freedom of movements of bridge elements. Nevertheless, due to the fact that they are three-dimensional objects and the need for proper connection access roads it cannot completely eliminate these influences. The paper presents the forms of ground deformation influence on internal forces caused by mining exploitation in the freely supported bridge, treated at the typical design beyond the mining areas as a statically determinate, supported by the results of many years of observation of the object located in the IV category of mining damage area.

1. INTRODUCTION

Rock mass deformation observed at the surface area is caused by mining. The observed results are ground depression, horizontal movement, changes in slope, ground deformations and curvature. Values of deformation parameters determine the category of mining area. Those categories are 0-V, where slope value T for category V exceeds 15mm/m, deformation absolute value ϵ is higher than 9 mm/m, and absolute value of curvature radius R is smaller than 4 km (Tab. 1) (Kwiatkiewicz J., 2002; Collective work, 1980). Civil structures in mining areas, including bridges, are often exposed to very intensive effects of mining exploitation. Although those effects are predicted, they are often underestimated due to changes in planned exploitation of deposits, impact of other or previous mining activities, and unpredicted behaviour of rock masses. There is a tendency not to restrain structure deformation and to provide free movement between spans and supports caused by significance variability of such impacts and their values. For that purpose, statically determinate structures are used – spans are freely supported on one fixed bearing and one-direction sliding (guide) bearing placed on the second support, opposite to the fixed bearing. Displacement between supports and spans and required expansion gaps are determined on the basis of kinematic analysis (Collective work, 1980; Ledwoń J.A., 1983; Rosikoń A., 1979; Collective work, 1998; Śliwka J. et al., 2005; Wytoczne ..., 1977; Śliwka J., 2000; Śliwka J., 1994), which regards individual elements of the structure as rigid bodies.

It was assumed that by completing kinematic analysis and ensuring proper movement of bearings and expansion gaps, we could eliminate the mining impact of ground deformation on internal forces inside the load-carrying structure. However, in practice we cannot eradicate every effect of ground deformation. Moreover, generated forces may be often powerful and cannot be neglected while analysing the structure. Those are mainly connected with:

- necessary connection of the structure with access roads and related embankment impact on the structure;
- mining front diagonal to the axis of a structure or a diagonal structure.

This paper presents such effects using the example of structures observed in the mining damage area of category IV.

Tab. 1: Categories of mining area regarding continuous ground deformation

Category	Inclination T mm/m	Radius of curvature R km	Horizontal deformation ϵ mm/m
0	$T \leq 0,5$	$40 \leq R $	$ \epsilon \leq 0,3$
I	$0,5 < T \leq 2,5$	$20 \leq R < 40$	$0,3 < \epsilon \leq 1,5$
II	$2,5 < T \leq 5$	$12 \leq R < 20$	$1,5 < \epsilon \leq 3$
III	$5 < T \leq 10$	$6 \leq R < 12$	$3 < \epsilon \leq 6$
IV	$10 < T \leq 15$	$4 \leq R < 6$	$6 < \epsilon \leq 9$
V	$15 < T$	$ R < 4$	$9 < \epsilon $

2. EFFECT OF EMBANKMENT

When the load-carrying structure is connected with the embankment (bridge head) by means of expansion joints, no additional effects resulting in strong internal forces in the structure can be observed (Fig. 1) (Reports ..., 2002-2017).

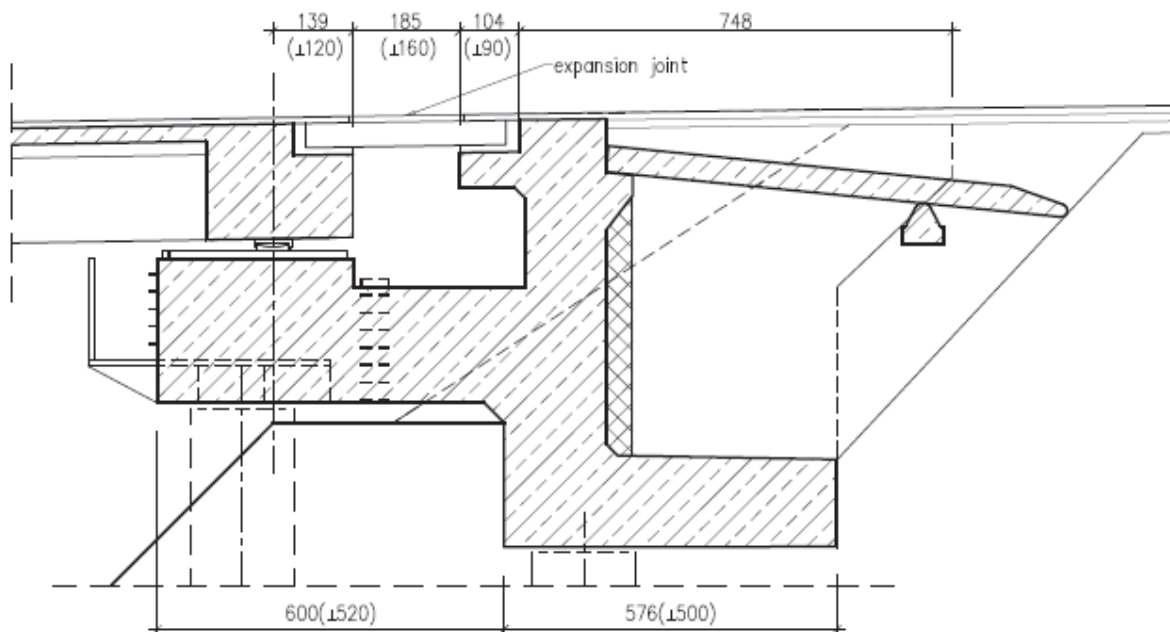


Fig. 1: Exemplary solutions for connecting the structure with embankment by means of expansion joints

It is a good solution as it does not affect the generation of extra internal forces in the load-carrying structure. Moreover, it eliminates some uncertainty about pressure distribution towards the load-carrying structure. If expansions joints are not contaminated or seized, no additional impact on the load-carrying structure is observed. Proper design of expansion joints is crucial to provide horizontal movement in two directions and vertical movement.

Considerable costs are regarded as the drawback of that solution. They are driven up by possible movement in three directions and within a large distance – often up to more than twenty centimetres, particularly in case of structures located in the mining area of damage category IV and V.

Costs can be reduced by using another solution - expansion joints are replaced with an approach slab. Fig. 2 illustrates the approach slab (Fig. 3).

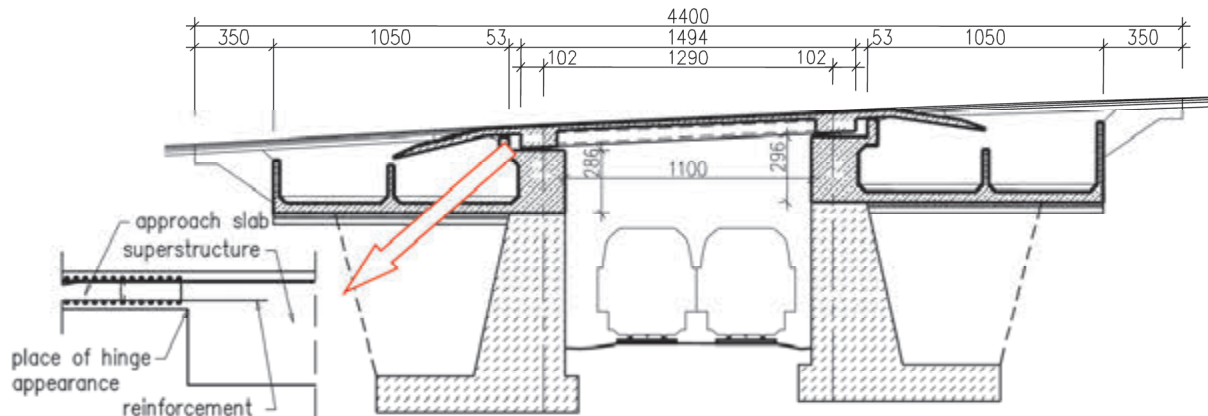


Fig. 2: Exemplary solutions for connecting the structure with embankment by means of an approach slab



Fig. 3: Connecting the structure with embankment by means of an approach slab

The approach slab connects the structure with the embankment. Displacement will be made on the length of the approach slab. The approach slab together with the pavement construction will act as a kind of expansion joint. Using that solution, we can expect some damage in the transition zone. However, costs of periodical repair can be lower than the price of expansion joints. Movement consists in slab pushing and pulling from the embankment and its rotation. A slip layer and sharp slab end (Fig. 4) minimise those forces. Slip layer reducing friction is made by laying two layers of tar paper or film covered with grease over and above the transition plate and placing them on a certain length in the embankment. Due to this the forces can be neglected during the structure analysis, as well. The slab fixing to the ground is the additional result. The expected span rotations on bearings may result in the momentum of slab

fixation to the load-carrying structure. If the hidden or designed joint is assumed to be used in the place of fixing, the effect is eliminated and its impact on the load-carrying structure can be neglected.

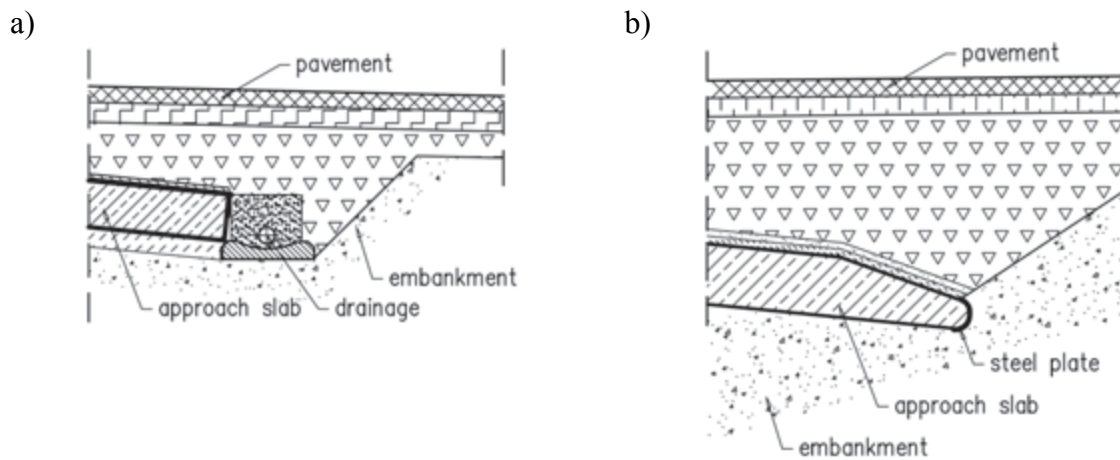


Fig. 4: Typical approach slab end (a) and sharp slab end (b) in mining damage areas

Massive bridge heads are usually used in such a solution (Fig. 2, Fig. 3). However, their cost is also high. The load-carrying structure with cantilevers can be used to reduce further costs while taking into account local conditions (Fig. 5, Fig. 6) (Reports ..., 2002-2017). The structure is connected with the embankment by means of an approach slab. As previously, surface damage can be also expected in the transition zone.

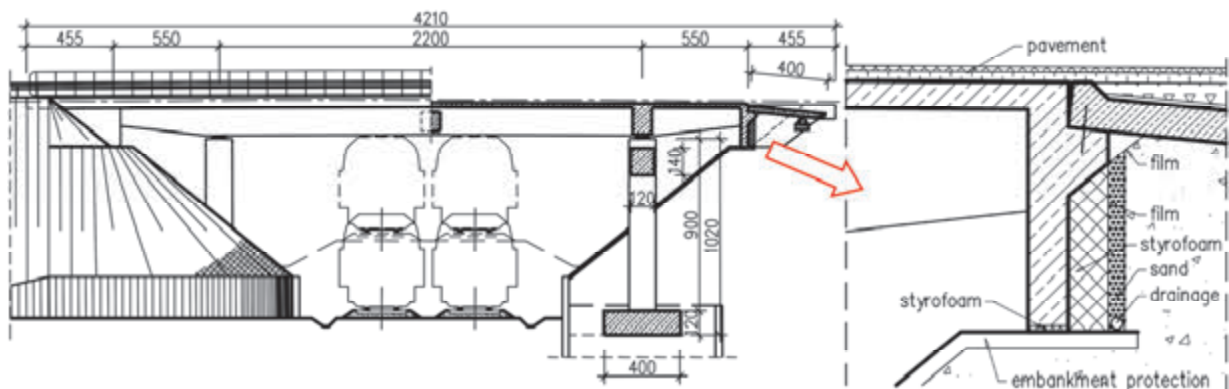


Fig. 5: Exemplary solution of the load-carrying structure with cantilevers

This solution requires embankment constraint consisting in using a marginal cross beam with suspended wings. Considerable ground pressure is expected as the result of soil creeping. Pressure is also influenced by temperature changes, but they are negligibly small compared to soil creeping due to the impact of mining exploitation. The expected elongation caused by the increase in temperature in the case presented in Fig. 4 is about 1 cm, while the expected elongation due to mining influences is about 30 cm. To reduce those forces, layers of compressible material are used (Fig. 5). However, that material can be subjected to compression if mining area is exploited many times in the structure vicinity (or causes the same deformations or not all the effects are retreated). Consequently, much greater pressure is exerted on cross beams, and thus on the load-carrying structure. Pressure distribution can be diversified and difficult to determine. So, the load-carrying structure may require regular relief. This is done by replacing the compressed material.



Fig. 6: Exemplary solution of the load-carrying structure with cantilevers

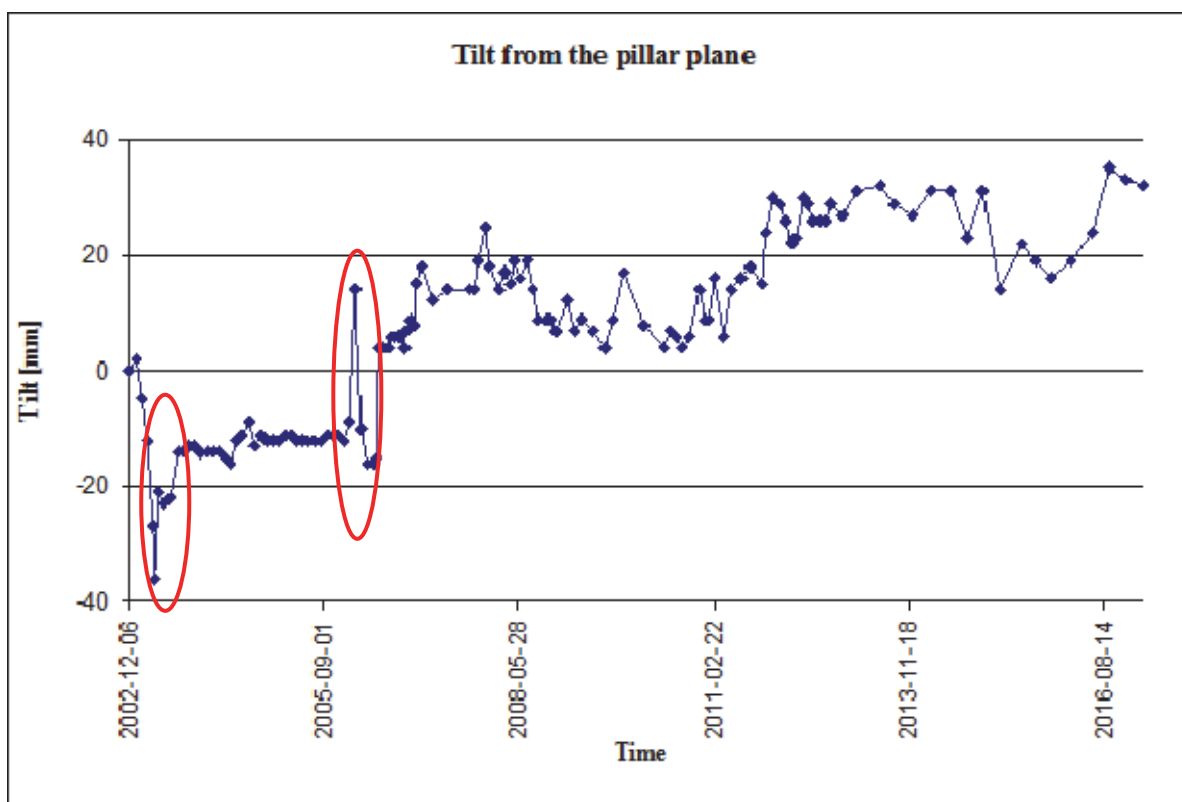


Fig. 7: The diagram of column tilt from the pillar plane caused by vertical force of the ground pressure caused by mining impact. The observed rapid straightening of the column is related to the fixed bearing chamfer

Asymmetrical location of the fixed bearing can produce an additional effect. The load-carrying structure is subjected to non-sustainable pressure, which is then transmitted to the support through the bearing. Consequently, strong forces can be applied on the support. If they are not taken into account, the observed result can be damage or fixed bearing chamfer

(Fig. 7, Fig. 8). The column tilt shown in Fig. 7 was determined geodetic by measuring the coordinates of two points fixed at the column height. This measurement can also be done in a simple manner using the plumb-line (Fig. 9).



Fig. 8: Stabilisation of displacement direction of chamfered fixed bearing

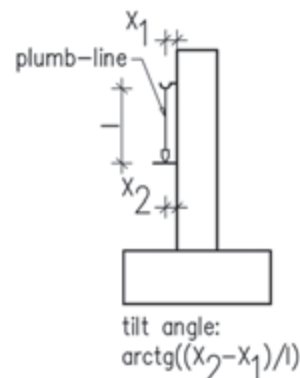


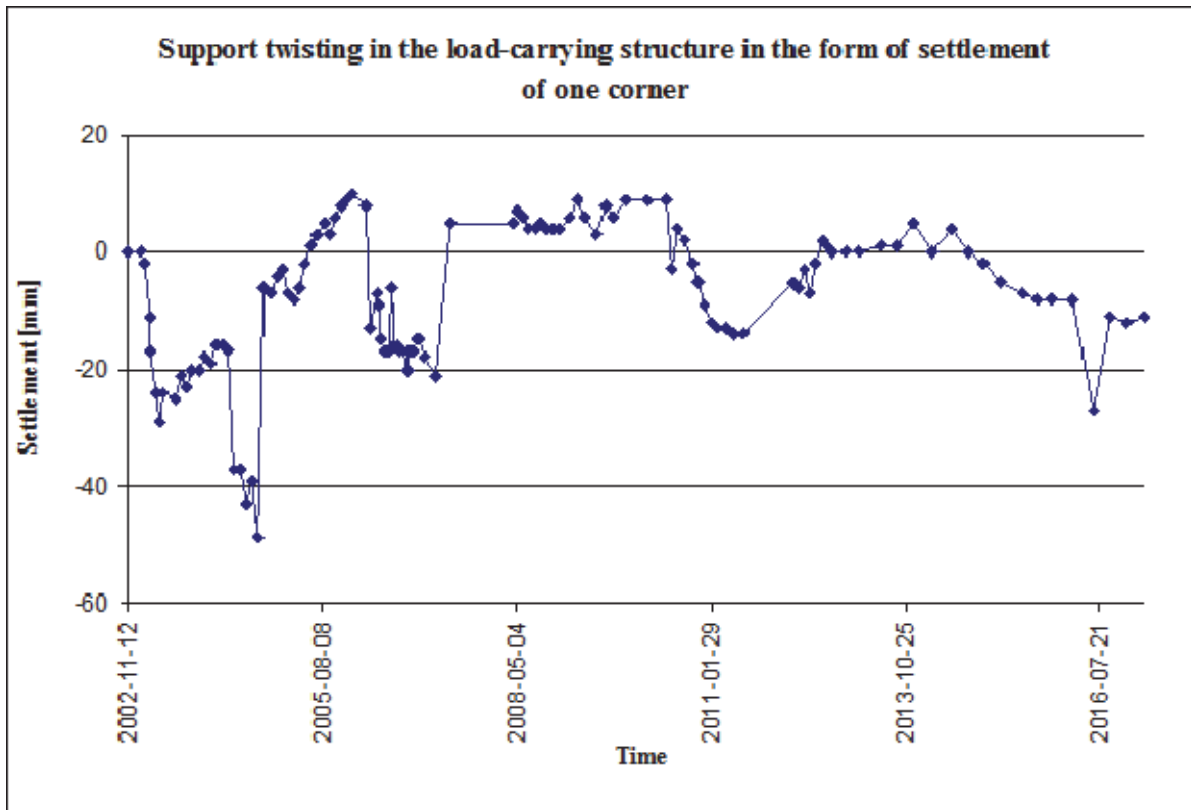
Fig. 9: Scheme of measurement of the tilt of the support by means of plumb-line

3. THE STRUCTURE SLANT AND EXPLOITATION FRONT DIAGONAL TO THE STRUCTURE AXIS

If the supports are diagonal, and the mining front is not perpendicular to their axis, or if the mining front is neither parallel nor perpendicular to the structure axis due to non-uniform settlement of supports, their twisting in the vertical plane is observed (Fig. 10). Twisting was defined as the difference in settlement at the measuring points: (Point 1 – Point 2) – (Point 4 – Point 3).

The ground curvature cause the non-uniform settlement of the supports - their displacement within the plane is observed. However, displacement is not the same for all the supports due to diagonal type or location of the mining front. Thus, twisting of the supports occurs, which influences the whole load-carrying structure generating considerable internal forces. The more rigid the load-carrying structure is, the stronger internal forces are generated. Such an interaction can be described as settlement of one corner of the load-carrying structure.

a)



b)

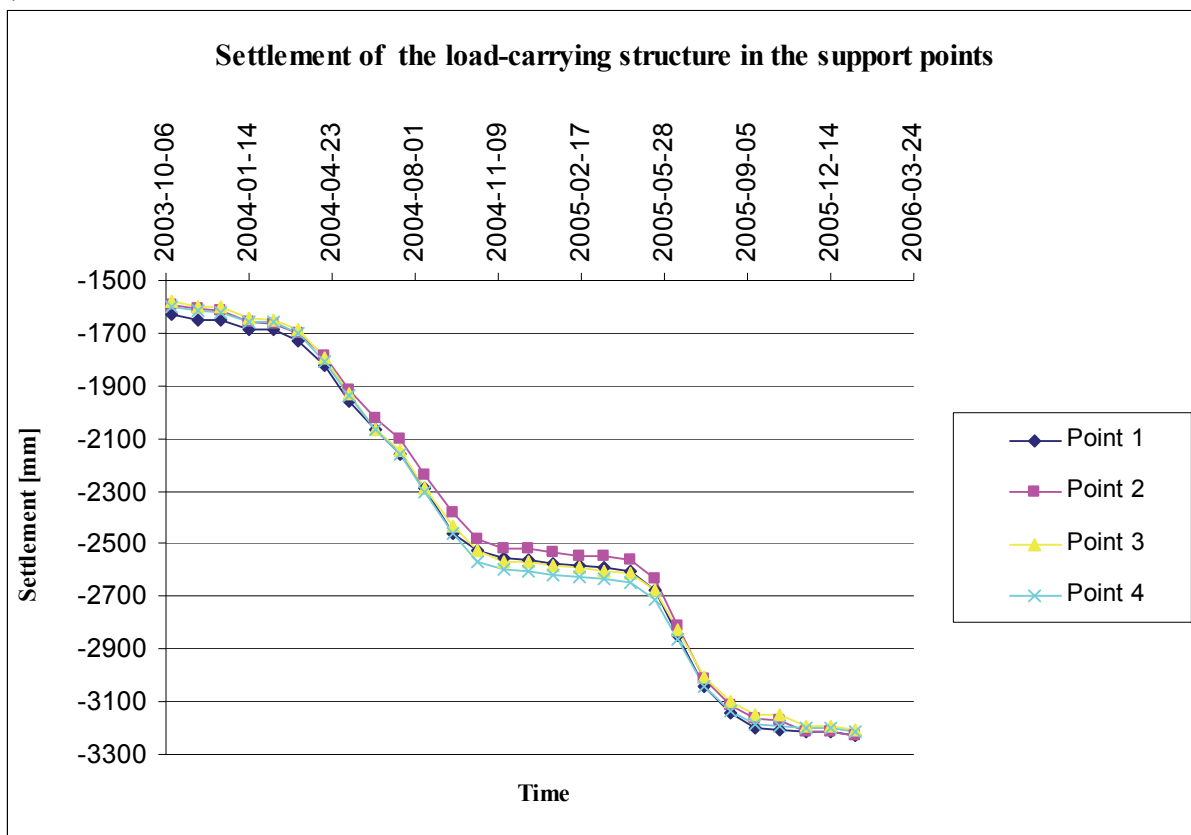


Fig. 10: Diagram illustrating the effect of support twisting in the load-carrying structure in the form of settlement of one corner of such a structure: support twisting (a), settlement in support points in chosen period (b)

4. CONCLUSIONS

Designing structures in the area of mining damage requires solutions for eliminating their impact on the internal forces, mainly those in the load-carrying structure. Therefore, it is common to use the free-supported load-carrying structure and to provide the unrestrained movement by using the suitable bearing scheme. Unfortunately, all the effects cannot be eliminated due to the spatial dimension of bridge structures and necessary connection with the access roads. Those effects are often neglected during the structure analysis; however, the generated internal forces should be taken into account. This paper presents only basic effects on free-supported structures. They were observed for the structures located in the mining area classified as category IV. Such effects should be considered every time. Moreover, we should always analyse whether solutions for the particular structure are not connected with other interactions.

5. REFERENCES

- Collective work (1980) "Ochrona powierzchni przed szkodami górnictwami". Wydawnictwo „Śląsk”, Katowice
- Collective work (1998) "Ochrona obiektów budowlanych na terenach górnictwami". GIG, Katowice
- Kwiatkiewicz J. (2002) "Obiekty budowlane na terenach górnictwami". GIG, Katowice
- Ledwoń J.A. (1983) "Budownictwo na terenach górnictwami". Arkady, Warszawa
- "Ocena wpływów eksploatacji dokonanej i projektowanej wraz z określeniem przyczyn zaistniałego zagrożenia utraty stabilności wiaduktu I najazdów w ciągu drogi DW 933 w aspekcie ich bezpiecznego użytkowania do 2010 r." (2007) Promost-Wisła, Wisła
- Reports from bridges monitoring (2002-2017)
- Rosikoń A. (1979) Budownictwo komunikacyjne na terenach objętych szkodami górnictwami
- Śliwka J. (1994) "Analysis of kinematics and loads for bridge structures in mining areas". International Land Reclamation and Mine Drainage Conference and Third International Conference on the Abatement of Acidic Drainage. Proceedings of a conference held in Pittsburgh, April 24 - 29. Bureau of Mines. Vol. 4 of 4: Abandoned mine lands and tropical issues, ss. 419.
- Śliwka J. (2000) "Nośność mostowych i oporowych konstrukcji uszkodzonych przemieszczeniami podłoża". Zeszyty Naukowe Politechniki Śląskiej, Wydawnictwo Politechniki Śląskiej, Gliwice
- Śliwka J., Śliwka A. (2005) "Monitoring obiektów mostowych na szkodach górnictwami". X Konferencja Naukowo-Techniczna Ochrona powierzchni na terenach górnictwami w subregionie zachodnim województwa śląskiego, NOT SITG Oddział Rybnik, Rybnik
- "Wytyczne techniczno-budowlane projektowania i wykonania obiektów na terenach eksploatacji górnictwami" (1977). Ministerstwo Komunikacji, Wydawnictwo Katalogów i Cenników, Warszawa

COMPARISON OF SHEAR STRENGTH ASSESSMENT ACCORDING TO EUROCODE 2 AND MODEL CODE 2010 DESIGN PROCEDURES

Damian Szczech¹, Monika Kaszubska¹ Renata Kotynia²

¹ PhD student, Lodz University of Technology, Poland

² Associate Professor, Lodz University of Technology, Poland

SUMMARY

Shear issue in the support regions of reinforced concrete (RC) beams is a complex problem still intensively investigated all over the world. It results from the combination of the shear force and the bending moment in the support region of RC beams. The paper presents the comparison of two design approaches proposed for the shear strength according to Eurocode 2 and the Model Code 2010. The results from the comparative analysis were used to evaluate the shear strength resistance and stirrups spacing, which varies in relation to the adopted design standard and the level of approximation. The increase in the level of approximation caused an increase in the accuracy of calculations in Model Code 2010 and stirrups spacing. The most similar results for the shear strength and the spacing stirrups according to Eurocode 2 were obtained for second level of approximation in MC 2010.

1. INTRODUCTION

Shear is one of the complex problem governing the capacity of reinforced concrete (RC) members due to combination of shear force and bending moment. There is not yet an international consensus on shear design provisions, because the knowledge on shear failure mechanism seems to be incomplete in the engineering community. Existing design code provisions for shear are based on empirical relationships for members without shear reinforcement and on the truss model (Mörsch, 1929), or a combination of truss and empirical models, for members with shear reinforcement.

Generally, the shear strength of RC members is affected by the following shear mechanisms: un-cracked concrete compressive zone, friction forces (named aggregate interlock action) developing along the length of a diagonal shear crack, the shear dowel action of longitudinal reinforcement and the shear strength provided by the transverse reinforcement (if it exists). The empirical methods proposed for design approach based mainly on formulas derived from the regression analysis of variable experimental test results. The commonly used Eurocode 2 (EC-2) (Eurocode 2, 2008) design procedure for shear is based on empirical relationships for members without shear reinforcement and it is based on the truss model for RC members with shear reinforcement. The shear slenderness ratio a_v/d (where, a_v is a distance between the edge of the support and the edge of the loading plate) is considered in EC-2 by the reduction factor of $a_v/(2d)$ to reduce the shear force V_{Ed} .

The Model Code 2010 (MC 2010) (Model Code 2010, 2012) shear design approach is based on Simplified Modified Compression Field Theory (SMCFT) (Bentz et al., 2006) for members without shear reinforcement and it is based on a general stress field approach for members with shear reinforcement. The models are especially suitable for the design of

discontinuity regions (D-regions) at supports or transverse applied forces. Alternatively, a cross-sectional design procedure may be applied.

The main difference between EC-2 and Model Code 2010 is taking into account the contribution of concrete to the shear strength of members with stirrups. The MC2010 includes the new approach, namely the “level of approximation” (LoA). The design model should be more or less complex depending on the level of detail needed at the time of calculation (assessment or detailed design) and the level of importance of the structural element (Muttoni & Fernández, 2012). In MC 2010 there are three levels of approximation for members without stirrups and four levels of approximation for members with transversal reinforcement. In the case of the last levels (III and IV, respectively for elements without and with stirrups) shear strength is obtained by numerical modelling. Single physical model is adopted for all levels (except for the one mentioned above) and lower level is derived from the higher level by certain simplification and assumptions. The outlines the background to the fib Model Code 2010 shear rules and two design examples (for deck slab and prestressed concrete bridge girder) could find also in (Sirgist et al., 2013).

MC 2010 similar to EC-2 considers sections placed closer to the support than the distance d should be designed for the same shear force as at the control section provided that the member is directly supported. Unless more refined modelling techniques are used to consider loads taken directly to a support through strut or arch action according to the following rules:

- the contribution of point loads applied within a distance of $d < a_v \leq 2d$ from the face of the support to the design shear force V_{Ed} is reduced by the factor $\beta = a_v/(2d)$.
- in the case of point loads applied as close as $a_v \leq d$ from the face of the support, the design shear force V_{Ed} shall be calculated with $\beta = 0.5$ as if the load is applied at $a_v = d$.

The paper presents the design case of the shear strength calculations performed for the RC beam according to both codes (EC-2 and MC 2010) with a discussion of the calculated results.

2. DESIGN EXAMPLE

A double span T-section RC beam with the axial span of 7 m analysed in the example is shown in Fig.1. The characteristic permanent and service loads are $g=15$ kN/m ($\gamma_g=1.35$; $g_d=20.25$ kN/m) $q=28$ kN/m ($\gamma_q=1.5$; $q_d=42$ kN/m), respectively with the corresponding load factors and the factored loads in brackets. The bending moment and the shear force diagrams shown in Fig. 2 are calculated based on the structural analysis, with a minimum value of $M_{Ed,B}$ over the support of 381.28 kNm and the maximum value of $M_{Ed,A}$ in the mid-span (214.47 kNm). The required negative (top) and positive (bottom) flexural reinforcement are $A_{st} = 34.34$ cm² (7 Ø 25) and $A_{sb} = 14.72$ cm² (3Ø25), respectively. Two control sections for the shear analysis placed at a distance of 445 cm from the edge of the extreme support (1-1) and the mid-support (2-2) are considered.

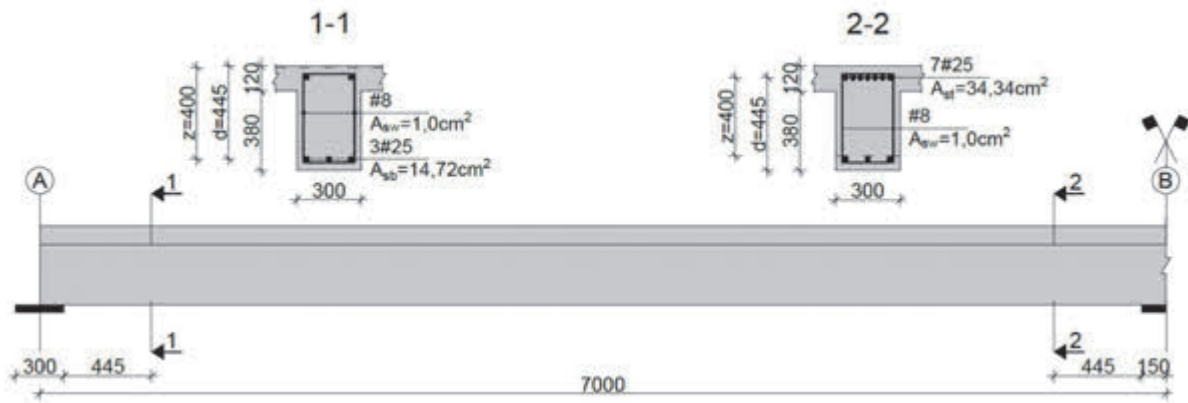


Fig. 1: Details of the example beam

The following parameters are adopted for the calculated analysis:

- thickness of concrete cover 35mm,
- concrete class C20/25, $f_{ck} = 20$ MPa ($\gamma_c = 1.5$),
- effective flexural depth in sections 1-1 and 2-2; $d = 445$ mm,
- steel bottom and top flexural reinforcement of 25 mm diameter,
- steel transverse reinforcement of 8 mm diameter, $\alpha = 90^\circ$,
- steel yielding strength and elasticity modulus: $f_{yk} = 500$ MPa, $E_s = 200$ GPa ($\gamma_s = 1.15$),
- support width 30 cm.

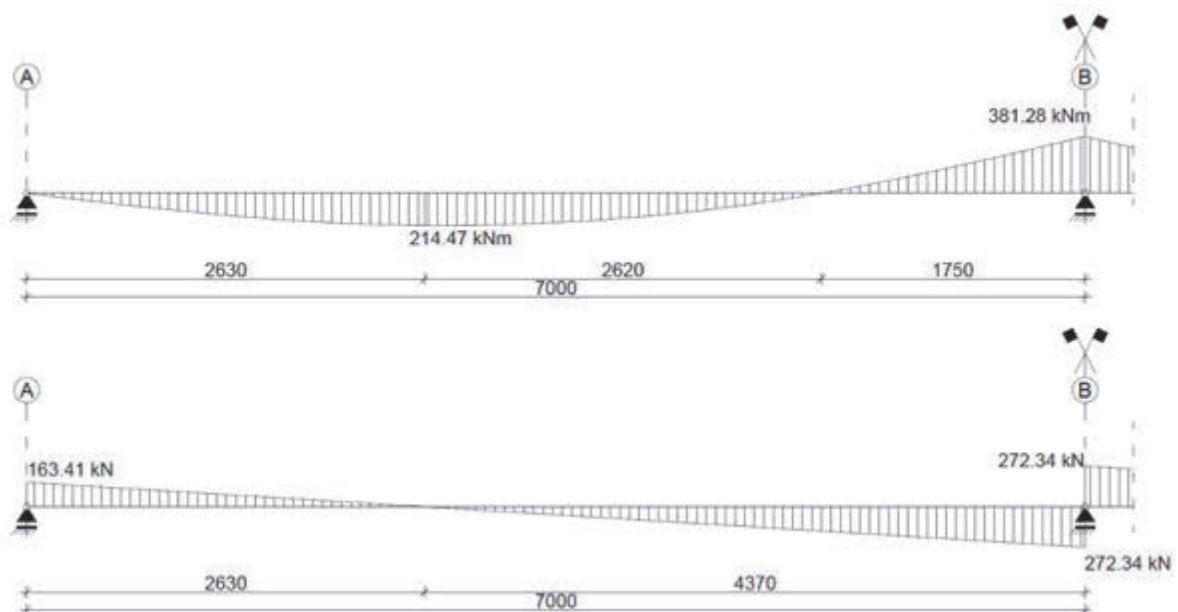


Fig. 2: Bending moment and the shear force diagrams

3. CALCULATIONS ACCORDING TO MODEL CODE 2010

The Model Code 2010 shear design approach is based on Simplified Modified Compression Field Theory (SMCFT) and for members with the shear reinforcement on a general stress field approach. The shear resistance V_{Rd} is determined from equation:

$$V_{Rd} = V_{Rd,s} + V_{Rd,c} \geq V_{Ed}$$

where, $V_{Rd,s}$ and $V_{Rd,c}$ are the stirrups and concrete contribution to the shear resistance at the control section.

The shear resistance is determined for the control sections using three levels of approximation (LoA). The inclination of the truss chord is assumed as the lowest as possible for each LoA. The value $\sqrt{f_{ck}}$ is limited to a maximum of 8 MPa for members with higher concrete strength due to smoother crack faces where cracks pass through the aggregate particles. The minimum transverse reinforcement ratio should be $\rho_w \geq 0.08\sqrt{f_{ck}}/f_{yk} = 0.00072$, and the maximum stirrup spacing is $s_w \leq 33.3$ cm (based on $s_{w,min} \leq 0.75d = 33.3$ cm or 50 cm).

The bending moment and the shear force in the control section 1-1 according to the structural analysis, equal of $M_{Ed}=86.84$ kNm and $V_{Ed}=126.06$ kN, respectively. The results of calculated analysis in the control sections 1-1 and 2-2 are summarized in Table 1.

3.1 First level of approximation

The longitudinal concrete strain ε_x at mid-depth of z (where, $z = 0.9d = 400.5$ mm) is not directly needed in LoA I, but should be $\varepsilon_x \leq 0.0001$. In the control section 1-1 this condition is satisfied, Eq.(1).

$$\varepsilon_x = \frac{\frac{M_{Ed}}{z} + V_{Ed} + N_{Ed} \left(\frac{1}{2} \pm \frac{\Delta e}{z} \right)}{2E_s A_s} = \frac{86.64}{0.438} + 126.06 + 0}{2 \cdot 200 \cdot 14.72 \cdot 10^2} = 0.00058 \quad (1)$$

In LoA I the shear strength is assumed as: $V_{Rd} = V_{Rd,s} \leq V_{Rd,max}$ and $V_{Rd} \geq V_{Rd,c}$. This lower limit, the shear strength of the same element without stirrups, is calculated according to the simplified formulas:

$$k_v(I) = \frac{180}{1000 + 1.25z} = \frac{180}{1000 + 1.25 \cdot 438} = 0.12 \quad (2)$$

$$V_{Rd,c} = k_v(I) \frac{\sqrt{f_{ck}}}{\gamma_c} z b_w = 0.12 \cdot \frac{\sqrt{20}}{1.5} 438 \cdot 300 \cdot 10^{-3} = 42.94 \text{ kN} \quad (3)$$

The compressive stress field inclination is limited to $\theta_{min} \leq \theta \leq 45^\circ$, where for reinforced concrete members $\theta_{min} = 30^\circ$. The minimum inclination of the compressive stress field is chosen $\theta = 30^\circ$.

The strength reduction factor $k_c = k_e \eta_{fc}$ includes the strain effect k_e and the brittleness factor η_{fc} :

$$\eta_{fc} = \min \left\{ \begin{array}{l} \left(\frac{30}{f_{ck}} \right)^{1/3} = \left(\frac{30}{20} \right)^{1/3} = 1.14 \\ 1 \end{array} \right. = 1 \quad (4)$$

The strain effect factor k_e can be established as a fixed value of 0.55, so the strength reduction factor k_c is equal to 0.55. The upper limit of shear strength is due to the crushing of concrete:

$$V_{Rd,max} = k_c \frac{f_{ck}}{\gamma_c} b_w z \sin \theta \cos \theta = 0.55 \cdot \frac{20}{1.5} \cdot 300 \cdot 438 \cdot \sin 30^\circ \cdot \cos 30^\circ \cdot 10^{-3} = 381.10 \text{ kN} \quad (5)$$

The required spacing of stirrups is obtained from the equation for the shear resistance provided by stirrups assuming that $V_{Rd,s} = V_{Ed}$:

$$s_w = \frac{A_{sw}}{V_{Ed}} z f_{ywd} \cot \theta = \frac{1 \cdot 10^2}{126.06} 438 \cdot 435 \cdot \cot 30^\circ \cdot 10^{-4} = 24.0 \text{ cm} \quad (6)$$

Finally, the two stirrup legs of 8 mm diameter at 24 cm spacing are adopted.

3.2 Second level of approximation

In LoA II, the shear strength is assumed to be the same as for LoA I: $V_{Rd,c} \leq V_{Rd} = V_{Rd,s} \leq V_{Rd,max}$. The minimum inclination of stress field in this level is equal to:

$$\theta_{\min} = 20^\circ + 10000 \varepsilon_x = 20^\circ + 10000 \cdot 0.00058 = 25.8^\circ \quad (7)$$

Principal tensile strength ε_1 is defined by a Mohr's circle of strain, where the adequate approximation of the negative concrete strain is taken as the concrete peak strain $\varepsilon_{c0} = 0.002$:

$$\varepsilon_1 = \varepsilon_x (\varepsilon_x + 0.002) \cot^2 \theta = 0.0005 \cdot (0.0005 + 0.002) \cdot \cot^2 25.8^\circ = 0.01161 \quad (8)$$

The factor of strain effect is calculated according to:

$$k_\varepsilon = \min \left\{ \frac{1}{1.2 + 55 \varepsilon_1} = \frac{1}{1.2 + 55 \cdot 0.01175} = 0.54, \frac{1}{0.65} = 0.54 \right\} \quad (9)$$

$$k_c = k_\varepsilon \eta_{fc} = 0.54 \cdot 1 = 0.54 \quad (10)$$

$$V_{Rd,max} = k_c \frac{f_{ck}}{\gamma_c} b_w z \sin \theta \cos \theta = 0.54 \cdot \frac{20}{1.5} \cdot 300 \cdot 438 \cdot \sin 25.8^\circ \cdot \cos 25.8^\circ \cdot 10^{-3} = 341.34 \text{ kN} \quad (11)$$

The lower limit of shear strength is calculated according to LoA II for members without stirrups. In this case, the factor $k_v(II)$ includes the „strain effect” (ε_x), the „size effect” (z) and the influence of the maximum size of aggregate (d_g) specified as 16 mm:

$$k_{dg} = \max \left\{ \frac{32}{16 + d_g} = \frac{32}{16 + 16} = 1, \frac{32}{0.75} = 42.67 \right\} = 1 \quad (12)$$

$$k_v(II) = \frac{0.4}{1 + 1500 \varepsilon_x} \frac{1300}{1000 + k_{dg} z} = \frac{0.4}{1 + 1500 \cdot 0.00058} \frac{1300}{1000 + 1 \cdot 438} = 0.20 \quad (13)$$

$$V_{Rd,c} = k_v(II) \frac{\sqrt{f_{ck}}}{\gamma_c} z b_w = 0.20 \cdot \frac{\sqrt{20}}{1.5} 438 \cdot 300 \cdot 10^{-3} = 70.91 \text{ kN} \quad (14)$$

The required spacing of stirrups is:

$$s_w = \frac{A_{sw}}{V_{Ed}} z f_{ywd} \cot \theta = \frac{1 \cdot 10^2}{126.06} 438 \cdot 435 \cdot \cot 25.8^\circ \cdot 10^{-4} = 28.6 \text{ cm} \quad (15)$$

Finally, the two stirrup legs of 8 mm diameter at 28 cm spacing are adopted.

3.3 Third level of approximation

The minimum inclination of stress field in this case is the same as for the level of approximation II. The shear capacity in LoA III is the sum of the resistances attributed to the concrete and stirrups, if $V_{Rd} < V_{Rd,max}(\theta_{min})$. With respect to the previous calculations $V_{Rd,max}(\theta_{min}) = 341.34 \text{ kN}$ and $V_{Ed} = V_{Rd} = 126.06 < V_{Rd,max}(\theta_{min}) = 369.08 \text{ kN}$. The condition is satisfied, hence shear capacity is equal to:

$$V_{Rd} = V_{Rd,s} + V_{Rd,c} \quad (16)$$

The shear strength attributed to concrete:

$$k_v(III) = \max \left\{ \frac{0.4}{1+1500\varepsilon_x} \left(1 - \frac{V_{Ed}}{V_{Rd,max}(\theta_{min})} \right), 0 \right\} = \frac{0.4}{1+1500 \cdot 0.00055} \left(1 - \frac{126.06}{369.08} \right) = 0.14 = 0.14 \quad (17)$$

$$V_{Rd,c} = k_v(III) \frac{\sqrt{f_{ck}}}{\gamma_c} z b_w = 0.14 \cdot \frac{\sqrt{20}}{1.5} 438 \cdot 300 \cdot 10^{-3} = 48.16 \text{ kN} \quad (18)$$

The required spacing of stirrups taking into account the shear force transferred by concrete is:

$$s_w = \frac{A_{sw}}{V_{Ed} - V_{Rd,c}} z f_{ywd} \cot \theta = \frac{1 \cdot 10^2}{126.06 - 56.67} 438 \cdot 435 \cdot \cot 25.8^\circ \cdot 10^{-4} = 46.4 \quad (19)$$

Finally, the two stirrups leg of 8 mm diameter at 33 cm spacing are adopted.

4. CALCULATIONS ACCORDING TO EUROCODE 2

As in the case of MC 2010, the control section according to Eurocode 2 is placed at a distance $d = 445 \text{ cm}$ from the edge of the support (595 cm from the axis support), the minimum transverse reinforcement ratio should be $\rho_w \geq 0.08 \sqrt{f_{ck}} / f_{yk} = 0.00072$, and the effective shear depth z is defined as $z = 0.9d = 400.5 \text{ mm}$. There is a small difference in the determination of the maximum stirrups spacing (minimum value from $0.75d = 33.3 \text{ cm}$ and 60 cm), but finally the same value is received (33.3 cm). The control section 1-1 is presented in the paper, where according to the structural analysis the bending moment and the shear force are equal to $M_{Ed} = 86.84 \text{ kNm}$ and $V_{Ed} = 126.06 \text{ kN}$, respectively. The results for control section 2-2 are summarized in Table 1.

The compressive stress field inclination is limited to $1 \leq \cot \theta \leq 2.5$ ($21.8^\circ \leq \theta \leq 45^\circ$). The factor which takes into account the stress state in compressed truss is equal to $\alpha_{cw}=1,0$ (for non-prestressed members), and the reduction factor for cracking concrete is:

$$v_1 = 0.6 \cdot \left(1 - \frac{f_{ck}}{250}\right) = 0.6 \cdot \left(1 - \frac{20}{250}\right) = 0.55 \quad (20)$$

$$V_{Rd,max} = \frac{\alpha_{cw} b_w z v_1 f_{cd}}{\cot \theta + \tan \theta} = \frac{1 \cdot 300 \cdot 438 \cdot 0.55 \cdot \frac{20}{1.5} \cdot 10^{-3}}{\cot 21.8^\circ + \tan 21.8^\circ} = 326.33 \text{ kN} \quad (21)$$

At the beginning, the shear strength member is determined. The beam is not prestressed, so $\sigma_{cp}=0$.

$$C_{Rd,c} = \frac{0.18}{\gamma_c} = \frac{0.18}{1.5} = 0.12 \quad (22)$$

$$k = \min \left\{ \begin{array}{l} 1 + \sqrt{\frac{200}{d}} = 1 + \sqrt{\frac{200}{445}} = 1.67 \\ 2 \end{array} \right. = 1.67 \quad (23)$$

$$v_{min} = 0.35 \cdot \sqrt{k^3 \cdot f_{ck}} = 0.35 \cdot \sqrt{1.67^3 \cdot 20} = 0.34 \text{ MPa} \quad (24)$$

$$\rho_l = \min \left\{ \begin{array}{l} \frac{A_{s1}}{b_w d} = \frac{14.72 \cdot 10^2}{300 \cdot 455} = 0.011 \\ 0.02 \end{array} \right. = 0.011 \quad (25)$$

$$V_{Rd,c} = (C_{Rd,c} k \cdot \sqrt[3]{100 \rho_l f_{ck}} + k_1 \sigma_{cp}) b_w d = (0.12 \cdot 1.67 \cdot \sqrt[3]{100 \cdot 0.011 \cdot 20}) \cdot 300 \cdot 445 = 75.00 \text{ kN} \quad (26)$$

The shear capacity of a member without stirrups should not to be taken as less than:

$$V_{Rd,c,min} = (v_{min} + k_1 \sigma_{cp}) b_w d = (0.34 + 0.15 \cdot 0) \cdot 300 \cdot 445 \cdot 10^{-3} = 45.08 \text{ kN} \quad (27)$$

The shear force in section 1-1 is bigger than the shear strength transferred by concrete, $V_{Ed}=126.06 \text{ kN} > V_{Rd,c}=75.00 \text{ kN}$, so the transverse reinforcement is required. The required spacing of stirrups is obtained through the transformation of the equation for the shear resistance provided by stirrups and assumed that $V_{Rd,s} = V_{Ed}$:

$$s_w = \frac{A_{sw}}{V_{Ed}} z f_{ywd} \cot \theta = \frac{1 \cdot 10^2}{126.06} 438 \cdot 435 \cdot \cot 21.8^\circ \cdot 10^{-4} = 34.7 \text{ cm} \quad (28)$$

Finally, the two stirrup legs of 8 mm diameter at 33 cm spacing are adopted.

5. CONCLUSIONS

The results of the calculations performed according to the design provisions according to Model Code 2010 and Eurocode 2 are summarized in Tab. 1.

Tab. 1: Comparison of calculated parameters

Parameters	Model Code 2010						PN-EN 1992-1-1:2008	
	Control section 1-1			Control section 2-2			Control section	
	I	II	III	I	II	III	1-1	2-2
$C_{Rd,c}$ [-]	-						0.12	
k [-]	-						1.67	
v_l [-]	-						0.55	
v_{min} [-]	-						0.34	
ε_x [-]	0.00058			0,00059			-	
ε_l [-]	-	0,01161		-	0,01158		-	
η_{fc} [-]	1						-	
k_e [-]	0.55	0.54		0.55	0.55		-	
k_c [-]	0.55	0.54		0.55	0.55		-	
k_v [-]	0.12	0,20	0.14	0.18	0,20	0.056	-	
θ_{min} [°]	30	25.8		30	25.9		21.8	
θ [°]	30	25.8		30	25.9		21.8	
$\cot\theta_{min}$ [°]	1.73	2.07		1.73	2.06		2.5	
$V_{Rd,max}$ [kN]	381.10	341.34		381.10	342.05		326.33	326.33
$V_{Rd,min}$ [kN]	-						45.08	
$V_{Rd,c}$ [kN]	42.94	70.91	48.16	42.94	70.62	23.81	75.00	99.48
s_w [cm]	24.0	28.6	46.4	12.9	15.3	17.1	34.7	18.6
Assumed s_w [cm]	24	28	33	12	15	17	33	18
$V_{Rd,s}$ [kN]	126.13	128.96	109.42	252.26	240.17	211.92	132.41	242.75
V_{Rd} [kN]	126.13	128.96	157.58	252.26	240.17	235.72	132.41	242.75
V_{Ed} [kN]	126.06			234.99			126.06	234.99
$s_{w,max}$ [cm]	33.3						33.3	

The increase in the level of approximation caused an increase in the accuracy of calculations in MC 2010 and stirrups spacing. The increase in the shear capacity between the level of approximation I and II is about 2% for the control section 1-1, while for the control section 2-2 the decrease in the shear strength of about 4% is obtained. The main reason of the difference in the shear strength is θ_{min} and the variable stirrups spacing. θ_{min} is assumed 30° and 25.8° for LoA I and LoA II, respectively at the control section 1-1 and 30° and 25.8° for LoA I and LoA II, respectively at the control section 2-2. The stirrups spacing between LoA I and LoA II increased from 24 cm to 28 cm and from 12 cm to 15 cm for the control sections 1-1 and 2-2, respectively. In the control section 1-1, when the shear concrete strength is considered in LoA III, the total shear strength increased in 25%.

The shear strength in LoA III for the control section 1-1 is 22% higher than the that for LoA II, but the stirrups spacing increased by 18% due to the limit spacing. In the case of the control section 2-2, the discrepancies between the respective levels of approximation are lower. The shear capacity in this section decreased in LoA III by 2% relative to LoA II, and the spacing of stirrups increased by 13%. The minimum angle of inclination of the compression chord θ_{min} with the increase in the accuracy of calculations is reduced. The adoption of this angle resulted in a decrease in the maximum load capacity of the compression chord and an increase in the shear strength provided by the stirrups.

When passing from the first level of estimation to the second one, the cross-section capacity provided by the same member without stirrups also increased. On the other hand, in the third level of approximation, where the shear strength of the concrete is taken into account in the total shear capacity, the part provided by the concrete is significantly reduced in comparison with the shear concrete strength $V_{Rd,c}$ for the second level of approximation. This approach is

compatible with the assumption presented in the paper (Reineck, 2009), where it is pointed out that the load bearing capacity of the shear concrete in the RC member without transverse reinforcement is not equal to the bearing capacity of the concrete in the transverse reinforcement.

The minimum inclination of the concrete compression chord in accordance with the EC-2 is similar to that obtained for the levels of approximation II and III in MC 2010. The spacing of stirrups in both sections obtained according to EC 2 is closest to the spacing obtained for LoA II in MC 2010. The significantly higher (by 56% and 318% for control section 1-1 and 2-2, respectively) shear strength of the RC member without stirrups $V_{Rd,c}$ is obtained in accordance to Eurocode 2 than in accordance to MC 2010 in LoA III. Furthermore, in the EC-2, in contrast to Model Code 2010, the concrete shear capacity is higher for section 2-2 due to higher reinforcement ratio, while according to Model Code 2010 the concrete contribution to the shear strength decreases due to deformation of the cross section.

6. REFERENCES

- Bentz, E. C., Vecchio, F. J., Collins, M. P.: The Simplified MCFT for Calculating the Shear Strength of Reinforced Concrete Elements. ACI Structural Journal, vol. 103, No. 4, 2006, pp. 614–624.
- Model Code 2010, Final draft, fib Bulletin 65, 2012
- Mörsch E., Der Eisenbetonbau, seine Theorie und Anwendung. Bd 1, Verlag K. Wittwer, Stuttgart 1929
- Muttoni, A., Fernández Ruiz, M.: Levels-of-Approximation Approach in Codes of Practice, Structural Engineering International, vol. 22, No. 2, 2012, pp. 190–194.
- EN 1992-1-1:2008. Eurocode 2: Design of Concrete Structures. Part 1-1: General Rules and Rules for Buildings.
- Reineck, K.-H., Review of basic assumptions for the shear design. Paper SP 265-17 in: Thomas T.C. Hsu Symposium, Part 3, Five decades of progress in shear. ACI SP 265, 2009
- Sigrist V. et al. Background to the fib Model Code 2010 shear provisions – part I: beams and slabs. Technical Paper, Structural Concrete 14 (2013), No.3.

MODELLING THE BEHAVIOUR OF CONCRETE ADDITIVES VIA DISCRETE ELEMENT NUMERICAL SIMULATION

*Miklós Gálos, Ákos Orosz, János P. Rádics, Kornél Tamás
Budapest University of Technology and Economics
Műegyetem rkp. 3., H-1111 Budapest, Hungary*

SUMMARY

The nature of the additives is based on their physical and geometrical properties, which are described with the geological parameters. The gravel and crushed stone aggregates have a big variety of geological and geometrical parameters. The concrete additives, as an aggregate are classified based upon their geophysical nature and the properties gained during their processing. While the aggregate which is made of gravels (natural rocks) usually contains grains with rounded edges, the manufactured aggregate involves grains manufactured by crushing solid rocks (manufactured rocks) which have sharp, angular, polyhedron-like shape. The nature of an aggregate with predefined gradation is highly dependent on the grain shape. Using discrete element method, the gravels can be modelled with clumps, which are particles made up by spheres. The manufactured rocks can be simulated with polyhedral elements.

1. INTRODUCTION

Concerning the design of different concrete, the qualification of concrete and the quality of the product certification, the properties of the used additives, as traditionally, are usually the materials that make up the quality of the concrete. Our attention is usually limited to cement rating, cement delivery, water-cement factor, and the role of various additives. We accept that the raw materials for making the concrete, as they are generally mineral-based, having the right strength and strength properties, ensure the conformity of the finished product. Usually, we do not think that sandy gravel, gravel products, and crushed stone rocks produced from aggregate rocks show great variations in both their rocks and strength, weather resistance and geometric properties. Concretes made using sandy gravel, pebbles, or crushed stone as a product have a high degree of bearing on the material properties of the additives used.

In the technological process of concrete making, the interaction between the additive and its constituent parts can be evaluated by the phases of preparation. The behaviour of the aggregates forming the additive can be treated separately in the first phase of the concrete preparation during mixing and application and can be evaluated separately when the material structure connections have been formed between the granules of the additive in the solidified concrete.

During the transportation, mixing and application process, the granules graze and impact with each other. Their response to these loads is based on to their material and geometry. The changes in the characteristics of the additive can be described by the changing of the aggregate properties: gradation and shape or flakiness index. The aforementioned behaviour can be modelled using computer simulation techniques. The discrete element method (DEM) is suitable for the task, as it has the ability to virtually track the behaviour of individual particles in the aggregate. This simulation requires the proper material model.

2. THE DISCRETE ELEMENT METHOD

According to the definition of Cundall and Hart (1992), a numerical technique is called discrete element method or distinct element method, when it contains discrete particles (elements) with independent and finite motional and rotational degrees of freedom, the model can track them, and interactions can raise or extinguish between these elements. The definition does not mention it, but this approach is mainly used in 2D and 3D mechanical simulations. The most applied version of the DEM is called the time step method. It is based on the principles of dynamics: Newton's and Euler's laws of motion, and solves them with numerical integration (Bagi, 2007). The length of time between two successive iterations is the time step. Such a model have the capability to simulate the dynamic behaviour of bulk materials, which makes the DEM suitable for modelling rock aggregates.

Alongside with Newton's and Euler's laws, the behaviour of a discrete element model is determined by its material model, which consists the definition of the elements and interactions (constitutional model), and the values of the parameters. The element's material can be ideally rigid or deformable. Also it has a big variety in shapes. The most common is the sphere, but other more complex geometries exist. The interactions can be divided into two groups: contact (e.g. normal force, friction) and remote (e.g. viscous) forces. The definition of the material model represents the element-level (micromechanical) behaviour, which results the aggregate-level (macromechanical), measurable nature. There is large number of DEM material models for different applications and every material has its own set of parameters. Many of them are implemented in software products.

In this research on modelling different concrete additives, the focus was on the shape of the particles. The simplest solution is the usage of spheres. They also has an advantage in computational speed. However, they cannot model the interlocking effect between the grains, therefore, more complex geometries were examined. Possible solutions – besides many other opportunities – are clumps (particles made up from spheres with rigid connection between them) and polyhedra. The clean aggregates are cohesionless, so there is no need in the interaction law to include remote forces, only the modelling of normal and shear forces during contact is essential. The applied program is the Yade discrete element software (Šmilauer et al., 2015).

3. MODELING THE BEHAVIOR OF GRAVEL BASED MATERIALS.

In the grain-based aggregate of sandy gravel and gravel products, which are produced by underwater excavation, the particle of the forming grains is rounded as a result of sedimentary rock formation process. Fig. 1 shows a characteristic gravel additive.



Fig. 1: 16/32 mm grain size gravel subassembly

3.1 Modelling the shape of natural rocks

The smooth surface, round edges and corners of the natural rocks make them suitable to be modelled with clumps. Two kind of shapes were created: 16/32 mm equant (Fig. 2,a) and 16/32 mm elongated (Fig. 2,b) grains. When measured with shape index gauge, the elongated rocks are technically classified as flat. Each clump contains 3 spheres.

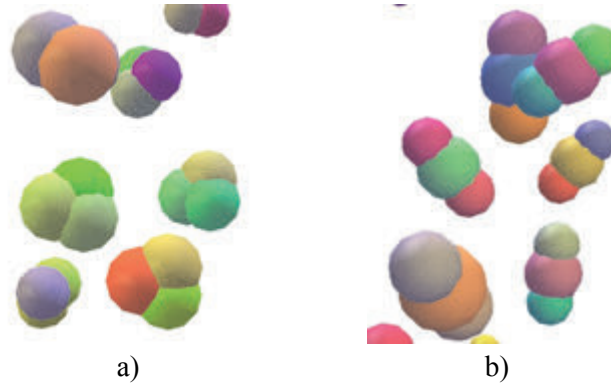


Fig. 2: a) Clump representation of 16/32 mm equant and b) flat grains

3.2 Interaction law of clump material model

The arising contact forces between the elements are computed via the classical Cundall and Strack (1979) constitutional law. This model was originally created for individual spheres, but it also can be applied to clumps. In this simplification, the particles are ideally rigid, the forces came from the overlapping of elements. The normal force (F_n [N]) has a linear elastic behaviour. Its magnitude is proportional to the length of overlapping (u_n [m]) by a material parameter called normal stiffness (k_n [N/m]) (Eq. 1), and it acts between the centroid of the spheres. The shear force (F_s [N]), which is perpendicular to the normal force and represents the friction, is proportional to the mutual movements and rotations of spheres (u_s [m]) by the shear stiffness (k_s [N/m]), where the changes in normal direction are neglected (Eq. 2). The maximum value of the shear force (F_s^{\max} [N]) is regulated by the Coulomb friction law (Eq. 3), where φ [rad] is the internal friction angle.

$$F_n = k_n u_n \quad (1)$$

$$F_s = k_s u_s \quad (2)$$

$$F_s^{\max} = F_n \tan(\varphi) \quad (3)$$

The normal and shear stiffness's are computed from the radii (R_a , R_b) and the given material parameters (E_a , E_b elastic moduli and, ν_a , ν_b Poisson coefficients) of spheres a and b (Šmilauer et al., 2015). The method is represented by Eq. 4 and 5. The used material parameters are shown on Tab. 1.

$$k_n = \frac{2E_a R_a E_b R_b}{E_a R_a + E_b R_b} \quad (4)$$

$$k_s = \frac{2E_a R_a \nu_a E_b R_b \nu_b}{E_a R_a \nu_a + E_b R_b \nu_b} \quad (5)$$

Tab. 1: Material parameters of clumps

	El. mod. [N/m ²]	Poisson coeff. [-]	Friction ang. [rad]	Density [kg/m ³]
Gravel	$2 \cdot 10^{12}$	0.001	0.6	2600
Steel	$2 \cdot 10^{14}$	0.001	0.4	7800

4. MODELING THE BEHAVIOR OF CRUSHED STONE ADDITIVES WITH POLYHEDRON ELEMENTS

The crushed stone aggregates, yielded by blasting explosives and processed in mills are composed of sharp, rough grains. Fig. 2 shows a characteristic crushed stone aggregate in which the grains, forming the aggregate, bear the characteristics of their formation process.



Fig. 3: 22/32 mm grain size crushed stone subassembly

4.1 Modelling the geometry of crushed rocks

The manufactured rocks have rough, but flat surfaces and sharp edges and corners. Therefore, it seems a good approximation to model them with polyhedra. The grain geometries are randomly generated using Voronoi method (Asahina and Bolander, 2011) with the desired sieve size and aspect ratio (length:width:height). Two types of aggregates were created: 16/32 mm equant (2:2:1) (Fig. 4,a) and 16/32 mm flat (4:2:1) (Fig. 4,b).

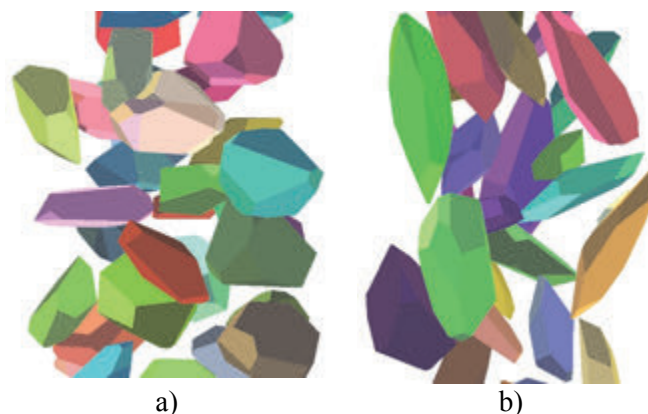


Fig. 4: Modelling the shape of 16/32 mm a) equant and b) flat manufactured rocks with polyhedra

4.2 Constitutional law of polyhedral model

The chosen interaction law (Eliš, 2014) is fairly similar to the one that was used for modelling natural rocks, as it only differs in the computation method of normal force. The magnitude of the normal force is linearly proportional to the overlapping volume of polyhedra (V_l [m^3]) by a factor called normal volumetric stiffness (k_{nv} [N/m^3]) (Eq. 6) and its direction is perpendicular to the plane fitted on the intersection curve using least-square method.

$$F_n = V_l k_{nv} \quad (6)$$

Instead of elastic moduli and poisson coefficients, the normal volumetric stiffness (K_{nvi}) and shear stiffness (K_{si}) need to be given for each material (i). The combined stiffness's of different (a and b) materials are computed via Eq. 7 and 8. The parameters are represented on Tab. 2.

$$k_{nv} = \frac{K_{nva} K_{nvb}}{K_{na} + K_{nb}} \quad (7)$$

$$k_s = \frac{K_{sa} K_{sb}}{K_{sa} + K_{sb}} \quad (8)$$

Tab. 2: Material parameters of polyhedra

	Norm. vol. stiff. [N/m^3]	Shear stiff. [N/m]	Friction ang. [rad]	Density [kg/m^3]
Gravel	$2 \cdot 10^{12}$	$2 \cdot 10^8$	0.6	2600
Steel	$2 \cdot 10^{14}$	$2 \cdot 10^9$	0.4	7800

5. UNIAXIAL COMPACTON TEST

The validation of the material models are performed by comparing measurement and simulation data of a unidirectional press (oedometric) test. For that, the device of so called Hummel test (former Hungarian standard MSZ 18287/3) was utilized. Before the measurement-simulation comparison, also the results of compaction tests with different element shapes were performed and examined.

5.1 Measurements

In the measurement process with Hummel device, the aggregate is packed in a steel cylinder with 170 mm diameter and 150 mm height. Then a steel loading plate compresses the aggregate with constant velocity. The normal force on the plate and its displacement is measured. When the normal force reaches the desired maximum value, unloading begins.

5.2 Discrete element model

The simulation geometry corresponds to the dimensions of the Hummel device. The cylinder builds up from triangular facets, the loading plate is modelled with wall type element in case of clumps, and with a special shaped polyhedron in case of polyhedral particles.

The creation process of the model starts with the random generation of elements. Then they are compacted with so called gravitational deposition to create a dense pack.

After the gravitational deposition the spare elements above the determined height are deleted, the top plate is applied at the highest point of the aggregate, and the compaction starts. Upon reaching the maximum force, the unloading begins. When the normal force reaches approximately zero, the simulation stops. The Fig. 5 shows different types of aggregates before compaction.

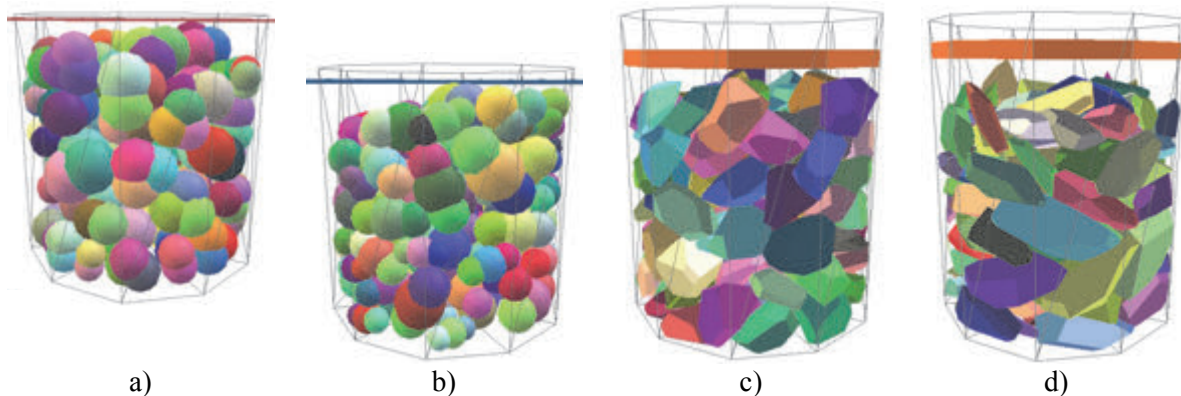


Fig. 5: The DEM model of the compaction test before loading with 16/32 mm a) equant and b) flat clumps, and c) equant and d) flat polyhedra

6. RESULTS

6.1 Simulation data

The Fig. 6 shows the results of 4 simulations: compaction test of equant and flat clumps (Fig. 6,a) and polyhedra (Fig. 6,b). Each of them had 150 mm mean aggregate height before compression and the maximum force was 600 kN.

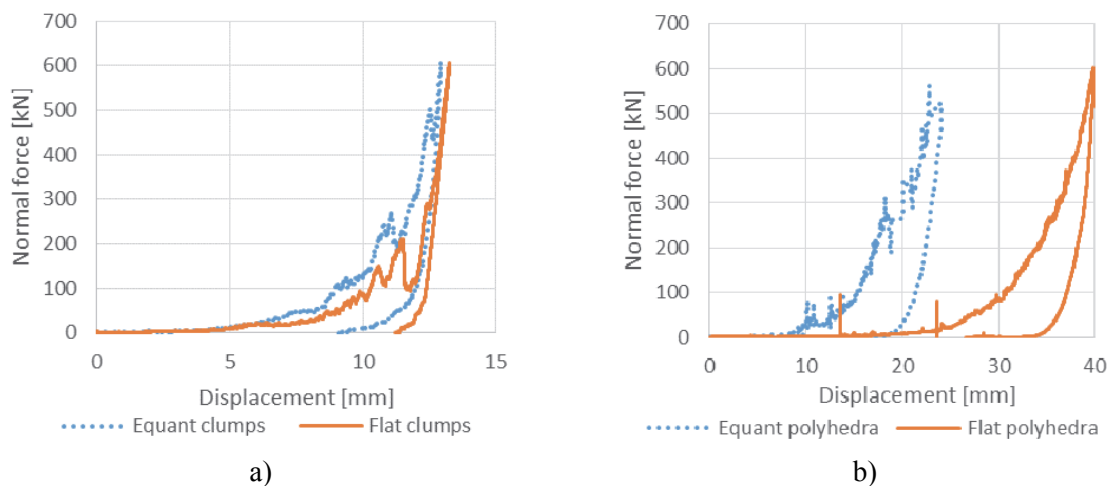


Fig. 6: The force-displacement curves of the compaction simulations with a) clump and b) polyhedral elements

Despite, the micromechanical laws are simple and linear, the whole aggregate have nonlinear characteristics under compaction in all cases, which is specific to DEM and is a significant advantage. The results of the simulations fulfils the theoretical expectations. The nonlinear behaviour comes from the interlocking effect of grains.

The aggregates that are containing flat particles, as well as the manufactured rocks compared to natural rocks, have bigger displacement, because of their higher porosity at the beginning and better compaction ratio.

6.2 Measurement-simulation comparison

The Fig. 7 shows the measurement and simulation data of a compression test performed on 88 mm tall natural rock aggregate containing 60 % equant and 40 % flat grains. The maximum normal force was 600 kN. Other measurements and simulations were performed with manufactured rocks. 111 mm high equant aggregate, and 94,5 mm high flat aggregate were tested. The maximum normal force was 60 kN in both cases. The curves of the simulation results were translated in the negative displacement direction to be comparable to the measurements. It is essential, as the virtual aggregates have rough surface (Fig. 5) unlike in the measurements, where the weight of the top part of the device resulted a pre loading and smoothing effect. This behaviour will be involved in the simulation model in the further research.

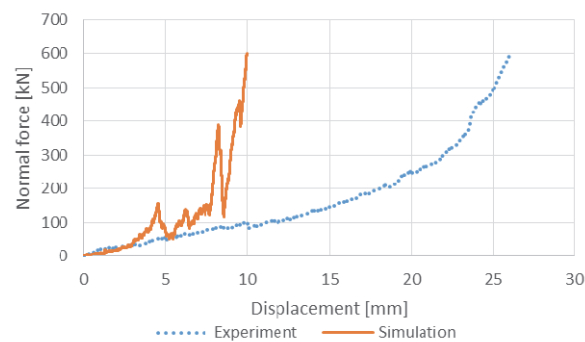


Fig. 7: Comparison of the normal force-displacement curve of the oedometric test of natural rocks and its simulation

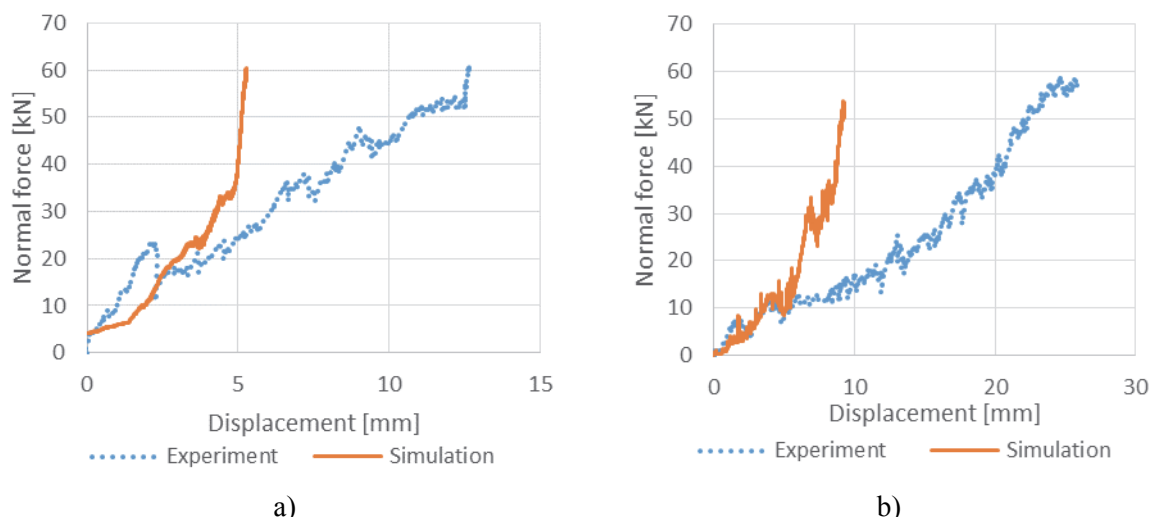


Fig. 8: The normal force-displacement responses of compaction tests and their simulations with a) equant and b) flat manufactured rocks

The simulations agrees the measurements with a good approximation in the low-force region. As the stress grows, the load-displacement curve of the simulations becomes steeper than the measurements⁷. Its reason is that the crushing behaviour was not involved in the virtual model.

7. CONCLUSIONS

The behaviour of the aggregate products, such as concrete additives, is depends on the structural and geometrical properties of the individual grains forming the whole aggregate. These products are treated as a nonlinear behaviour continuum in the three-phase model of materials. The discrete element method creates the possibility of evaluating the effect of the size distribution of the aggregate and shape properties of grains on the behaviour of the whole aggregate using only linear micromechanical material models.

The following conclusions were made in this paper on the discrete element modelling of concrete additives:

- the used clump material model simulates the behaviour of the natural rocks in the non-crush load region with good approximation
- the used polyhedral material model simulates the behaviour of the manufactured rocks in the non-crush load region with good approximation
- at higher loads, the modelling of crushing is needed
- the surface of the aggregate has to be smoothed in the model in order to avoid posterior translation of force-displacement curve.

8. ACKNOWLEDGEMENTS

We are thankful for the fellow workers of the laboratory of Department of Construction Materials and Technologies, BME: Gyula Emszt, department engineer and Bálint Pálinkás technician for their aid in performing the measurements.

9. REFERENCES

- Asahina, D. and J.E. Bolander, (2011), "Voronoi-based discretizations for fracture analysis of particulate materials", *Powder Technology*, Vol. 213, pp. 92–99.
- Bagi, K. (2007), "A diszkrét elemek módszere", BME Department of Structural Mechanics, Budapest, 5-12.
- Cundall, P.A. and Strack, O.D.L. (1979), "A discrete numerical model for granular assemblies", *Géotechnique* Vol. 29, No. 1, pp. 47–65.
- Cundall, P.A. and Hart, D.H. (1992), "Numerical modelling of discontinua", *Journal of Engineering Computations*, Vol. 9, No. 2, pp. 101-113.
- Eliáš, J. (2014), "Simulation of railway ballast using crushable polyhedral particles", *Powder Technology*, Vol. 264, September 2014, pp. 458–465.
- Šmilauer V. et al. (2015), "Yade Documentation 2nd ed.", The Yade Project, DOI 10.5281/zenodo.34073 (<http://yade-dem.org/doc/>).

COMPARISON OF DIFFERENT CALCULATION METHODS AND MODELS FOR MIXED CORE-FRAME STRUCTURAL SYSTEM

Slaven Katalinić¹, Anđelko Vlašić²

¹ *ULTRA STUDIO Ltd.*

Pantovčak 27, 10000 Zagreb, Croatia

² *Faculty of Civil Engineering, University of Zagreb,*

Kačićeva 26, 10000 Zagreb, Croatia

SUMMARY

Paper presents different calculation methods for lateral load analysis of mixed reinforced concrete core and frame structural systems in tall buildings. Presented calculation methods include approximate analytical methods, based on closed-form solution of differential equations, and numerical finite element models. Example tall building comprises of peripheral rigid frames and partially closed inner core with uni-symmetric arrangement in plan and constant properties along the height. Deflection and rotation results obtained by the analysis are plotted comparatively. Conclusion is derived from results and accuracy analysis.

1. INTRODUCTION

Lateral rigidity system for reinforced concrete tall buildings may comprise of centrally positioned core and peripheral rigid frames, providing resistance to wind and earthquake forces. Under horizontal loads, rigid frames and core assume different deflection shapes. Frames deflect in shear mode, having maximal slope near the base of the building, whereas core bends in flexural mode, having maximal slope at the top of the building. Core and frames are interconnected at floor levels by reinforced concrete slabs, substituted in structural analysis model by rigid diaphragms, assuming in plane rigid body behaviour. Compatibility of horizontal deflections is causing different types of bents to interact through the connecting slabs. Interaction forces between different bents occur along the height of the structure, increasing stiffness and decreasing overall horizontal deflections. Therefore, joint behaviour of two bents is favourable, but interaction forces between them are making the calculation procedure rather complex.

Applicable calculation methods may be broadly categorised into two main groups: analytical methods, which have closed-form solution, and numerical methods. A significant amount of research has been done on approximate analytical methods suited for rapid hand calculation in preliminary phase of building analysis. Some of these methods, based on continuum models, were developed by (Heidebrecht and Stafford Smith, 1973; Rutenberg and Heidebrecht, 1975; Stafford Smith, Kuster and Hoenderkamp, 1984; Hoenderkamp and Stafford Smith, 1988; Coull and Wahab, 1993; Hoenderkamp, 1995; Zalka 2009; Zalka 2010). Analytical methods presented herein (Heidebrecht and Stafford Smith, 1973; Rutenberg and Heidebrecht, 1975; Stafford Smith et al., 1984; Hoenderkamp, 1995) are used for estimating deflections and rotations of an exemplary structure. These methods are compared to more comprehensive finite element models based on wide column analogy and shell element models. The purpose of the paper is to investigate applicability of individual method for calculation of mixed core frame structure by comparing deflection characteristics and providing accuracy analysis.

2. ANALYTICAL METHODS

Analytical methods proposed in (Heidebrecht and Stafford Smith, 1973) and (Stafford Smith et al., 1984) are developed for symmetric multi-bent structures, which may be uniform or non-uniform along the height, with properties change occurring at discrete locations along the height of the structure. Methods proposed in (Rutenberg and Heidebrecht, 1975) and (Hoenderkamp, 1995) serve as an extension to the previous methods, providing solution to general asymmetric multi-bent structures, which may comprise of combination of shear walls, coupled walls, rigid frames and braced frames. Presented methods provide closed-form solution of governing differential equations in the form of polynomials.

2.1 Mathematical models

Presented methods are based on continuum models. In (Heidebrecht and Stafford Smith, 1973) and (Rutenberg and Heidebrecht, 1975) bents with different deflection characteristics are represented accordingly with flexural and shear cantilevers. Both cantilevers are linked horizontally by axially rigid continuum, therefore having same horizontal deflections along the height. To maintain the compatibility, distributed interaction force along the height and concentrated interaction force on top are introduced in the model.

Methods developed in (Stafford Smith et al., 1984) and (Hoenderkamp, 1995) are based on coupled-wall theory, exploiting ability of coupled shear walls to deflect in three characteristic ways. In extreme cases it may assume flexural shape of overall bending due to axial deformation of vertical members of the bent, pure flexural shape due to flexural bending of flexural members and shear shape due to racking shear. Therefore, it is beneficiary to treat different bents as coupled shear walls, interconnected by an equivalent continuous medium substituting discretely positioned connecting beams. Equivalent coupled shear walls are lumped together, forming shear-flexural cantilever. Depending on equivalent medium stiffness properties, shear-flexural cantilever may assume deflection profile which is, in case of multi-bent structure, a superposition of three distinctive deflection shapes.

2.2 Solving governing differential equations

In the case of analytical methods for non-twisting structures, governing differential equations are given by

$$\frac{d^4 y}{dx^4} - \alpha^2 \frac{d^2 y}{dx^2} = \frac{w(x)}{EI} \quad (1)$$

for flexural and shear cantilevers (Heidebrecht and Stafford Smith, 1973), and for coupled-wall cantilever (Stafford Smith et al., 1984) by

$$\frac{d^4 y}{dx^4} - (k\alpha)^2 \frac{d^2 y}{dx^2} = \frac{w}{EI} \left[1 - (kx)^2 \frac{(k^2 - 1)}{k^2} \cdot \frac{x^2}{2} \right] \quad (2)$$

in which $\alpha^2 = (GA)/(EI)$, $k^2 = 1 + I_v/(Ac_i^2)$ and $w(x)$ is lateral load intensity. Eq. 1 and Eq. 2 can be solved directly from corresponding boundary conditions. Solutions to Eq. 1 and Eq. 2

are presented in (Heidebrecht and Stafford Smith, 1973) and (Stafford Smith et al., 1984) respectively.

Methods developed for non-symmetrical structures (Rutenberg and Heidebrecht, 1975; Hoenderkamp, 1995) take into account torsional behaviour of structure according to the bending analogy principle. Governing differential equations for general asymmetric case are coupled. Simplification is achieved by assuming the centroid of flexural bents as referent point for coordinate system and by writing the equations in matrix form. Therefore, governing equation for flexural-shear cantilevers (Rutenberg and Heidebrecht, 1975) may be expressed in matrix form

$$\begin{Bmatrix} Y \\ r\theta \end{Bmatrix}^{IV} - \begin{bmatrix} \alpha^2 & \frac{a}{r}\alpha^2 \\ \frac{a}{r}\alpha^2 & \beta^2 \end{bmatrix} \begin{Bmatrix} Y \\ r\theta \end{Bmatrix}^{II} = \frac{w}{EI} \begin{Bmatrix} 1 \\ e/r \end{Bmatrix} \quad (3)$$

in which $\alpha^2 = (GA_y)/(EI_y)$, $\beta^2 = (GA_y)/(EI_\omega)$ and $r^2 = (EI_\omega)/(EI_y)$, and for coupled-wall cantilever (Stafford Smith et al., 1984) by

$$\begin{Bmatrix} \frac{d^4 y}{dx^4} \\ r \frac{d^4 y}{dx^4} \end{Bmatrix} - \begin{bmatrix} (k\alpha)^2 & \frac{a}{r}(k\alpha)^2 \\ \frac{a}{r}(k\alpha)^2 & (k\alpha^2)_\theta \end{bmatrix} \begin{Bmatrix} \frac{d^2 y}{dx^2} \\ r \frac{d^2 y}{dx^2} \end{Bmatrix} = \frac{q - M\beta^2}{EI_y} \begin{Bmatrix} 1 \\ e/r \end{Bmatrix} \quad (4)$$

in which $\alpha^2 = GA_y/EI_y$, $k^2 = 1 + (EI_i)/(EAc_i^2)$ and $\beta^2 = (GA_y)/(EAc_i^2)$. Process of uncoupling Eq. 3 and Eq. 4 is analogous to the modal superposition method in dynamic analysis. Thereby, the problem is reduced to eigenvalue problem of set of uncoupled equations. The process requires determining the eigenvalues and eigenvectors for the homogeneous form of Eq. 3 and Eq. 4. Further, obtained matrix of eigenvectors is used in transforming the geometric coordinates to the generalised coordinates. This yields uncoupled equations in generalized displacement coordinates with modal participation factors. Solutions to these equations are deflection functions of normalised structure. Deflection and rotation equations for real structure are obtained by transferring deflections back to geometric coordinate system. Solutions to Eq. 3 and Eq. 4 are given in (Rutenberg and Heidebrecht, 1975) and (Hoenderkamp, 1995) respectively.

3. EXAMPLE

3.1 General description and structural properties

Calculation example will be given for a characteristic structure, often present in tall buildings. The floor plan of the 20 storey building structure is shown in Fig. 1. Lateral rigidity system of the structure consists of peripheral concrete rigid frames and inner concrete core having one axis of symmetry (z axis) in plan. Subjected to horizontal loading in z direction building exhibits non-twisting behaviour, while horizontally loaded in y direction the structure exhibits both lateral deflection in y direction and rotation about vertical x axis. The storey height is 3 m. Horizontal loading of 50 kN/m is uniformly distributed along the height and acting at the centre of the building in both directions exclusively. The modulus of elasticity of 3.3×10^6 kN/m² is

taken for concrete C30/37. Multi-bay rigid frames are comprised of columns 35x35 cm and beams 35x60 cm. Core walls have thickness of 30 cm. On one side the core is partially closed by lintel beams having 30x60 cm cross section. Stiffness properties are shown in Tab. 1 in which EI is flexural rigidity, GA racking shear rigidity, EAc_i^2 flexural rigidity due to axial deformation of columns, EI_w is warping torsion rigidity and GJ is St. Venant's torsion rigidity.

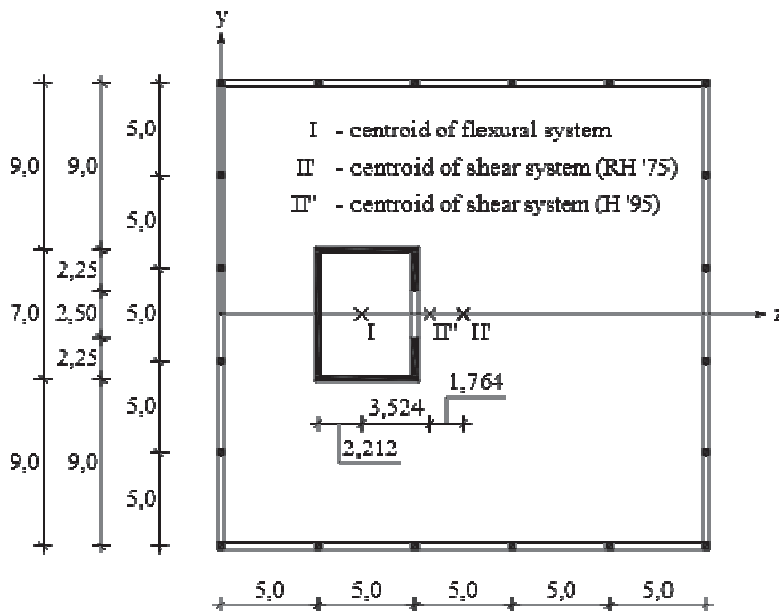


Fig. 1: Floor plan. All dimensions are given in meters

Tab. 1: Stiffness properties of individual bents

	EI_i (kNm ²)	GA_i (kN)	EAc_i^2 (kNm ²)	EI_w (kNm ⁴)	GJ_x (kNm ²)
Frame 1 to 4	2,476E+05	2,363E+05	1,769E+09	-	-
Core in z dir.	9,029E+08	4,726E-05	3,537E-01	1,798E+10	1,616E+08
Core in y dir.	1,770E+09	4,726E-05	3,537E-01		

3.2 Analytical methods

The structure is analysed in two directions separately, applying different analytical methods for every direction. In z direction methods for symmetrical structure are applied (Heidebrecht and Stafford Smith, 1973 and Stafford Smith et al., 1984). Corresponding calculation parameters are given in Tab. 2 in which $\alpha^2 = GA/EI$, $k^2 = 1+I/\sum(Ac^2)$ and H is total height of the structure.

Tab. 2: Calculation parameters in z direction

α^2 (m ⁻²)	αH (-)	k^2 (-)
5,229E-04	1,3721	1,2554

In y direction methods for asymmetrical structure are used (Rutenberg and Heidebrecht, 1975 and Hoenderkamp, 1995). Corresponding calculation parameters are presented in Tab. 3a (in which p_1^2, p_1^2 are eigenvalues, $\gamma = (\alpha^2 - p_1^2)/((a/r) \alpha^2)$, c_1 and c_2 are participation factors.) and Tab. 3b (in which $(k\alpha)_u^2$ and $(k\alpha)_v^2$ are eigenvalues, $f = ((k\alpha)^2 - (k\alpha)_u^2)/((a/r) \alpha^2)$, p_u and p_v are participation factors).

Tab. 3a: Calculation parameters in y direction (Rutenberg and Heidebrecht, 1975)

α^2 (m ⁻²)	β^2 (m ⁻²)	r^2 (m ²)		
2,670E-04	1,777E-04	10,25		
p_1^2 (m ⁻²)	p_2^2 (m ⁻²)	γ (-)	c_1 (-)	c_2 (-)
2,56E-04	1,78E-02	0,0252	0,9581	1,6760

Tab. 3b: Calculation parameters in y direction (Hoenderkamp, 1995)

$(k\alpha)^2$ (m ⁻²)	$(k\alpha)_\Theta^2$ (m ⁻²)	r^2 (m ²)		
4,006E-04	1,778E-04	10,25		
$(k\alpha)_u^2$ (m ⁻²)	$(k\alpha)_v^2$ (m ⁻²)	f (-)	p_u (-)	p_v (-)
3,894E-04	1,779E-02	0,025	0,958	1,676

3.3 Numerical models

Three dimensional numerical models were developed in finite element analysis software (SAP2000), using beam and shell finite elements for modelling different structural members. Beam elements are one dimensional finite elements having six degrees of freedom in each node. Shell finite element is two dimensional four node finite element which can be used for modelling membrane and plate (out-of-plane) bending behaviour. Shell finite elements based on thin plate behaviour are used in the models, neglecting transverse shear deformation. Material, geometric and loading assumptions are same as for analytical methods. Concrete slabs were not modelled. In-plane rigid behaviour at floor levels was modelled by rigid diaphragm constraint, constraining deflections and rotations in horizontal plane. While rigid frames were always modelled using beam elements, core was modelled in 3 different ways combining beam and shell finite elements.

- Wide column analogy model comprises entirely of beam finite elements. Individual core walls were substituted with vertical beam elements of corresponding cross-sectional characteristics. Torsional stiffness GJ of the core is distributed evenly between vertical beam elements. At floor levels flexural rigid arms were added around the core perimeter. Main function of rigid arms is to preserve cross-sectional shape under bending and twisting, and to offset nodes for connecting lintel beams across an opening in the core (MacLeod, 1990).
- In shell+beam model core walls are modelled using shell finite elements, while connecting beams are modelled by beam finite elements. Rigidly connecting beam to shell element causes compatibility problems which can be solved by introducing flexural rigid dummy beam elements. Indirectly connecting beam and shell element through dummy element, which spans across two finite elements, allows transfer of bending moments between these two elements.
- In pure shell model entire core (walls as well as girders) is modelled using shell finite elements, with added openings.

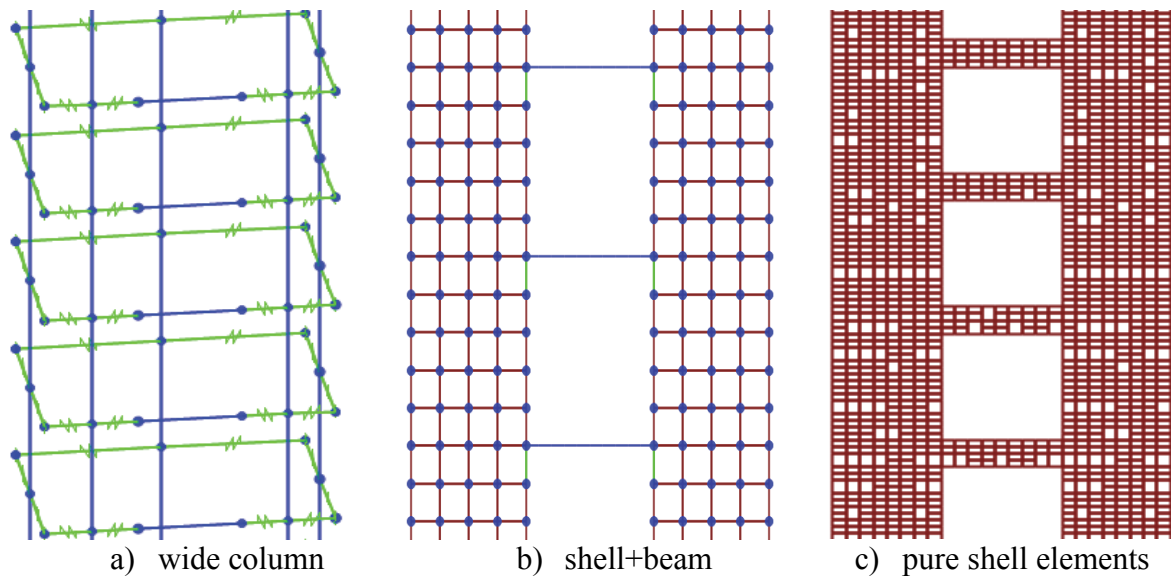


Fig. 2: Different numerical models: a. wide column, b. shell+beam, c. pure shell elements

4. RESULTS

Deflections in both directions and rotation about vertical axis are calculated in shear centre of example structure. Deflection and rotation profiles are given in Fig. 3.

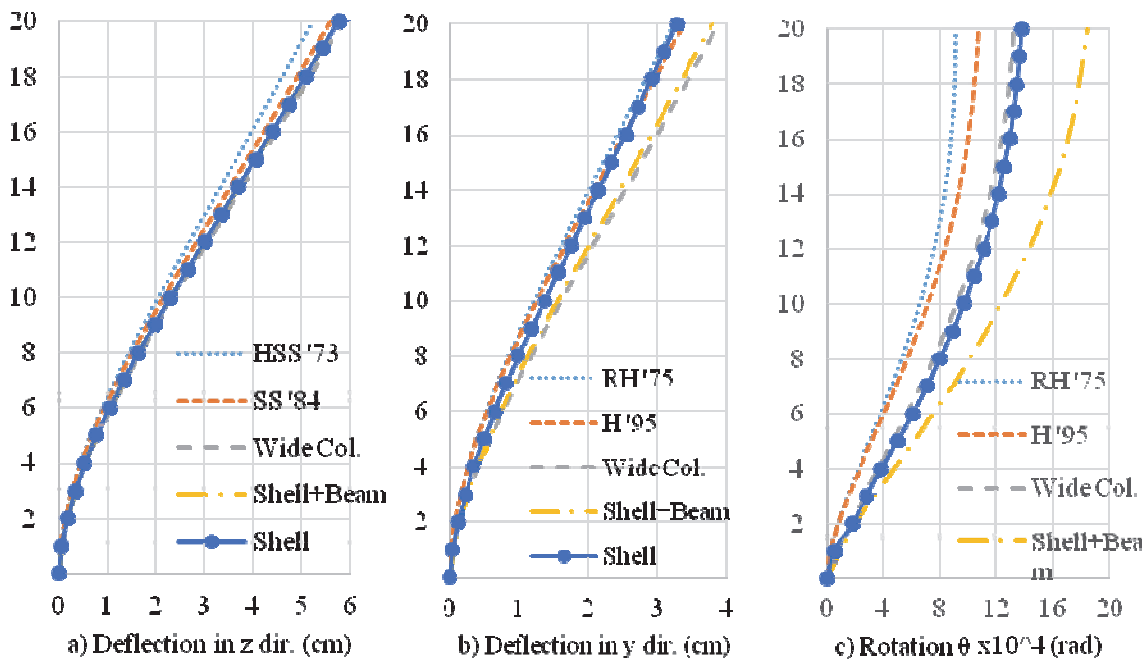


Fig. 3: Deflection and rotation of shear centre of example structure

5. ACCURACY

Values of deflections and rotation, obtained by calculation methods presented in the paper, are compared with shell model which is taken as referent. Deviations from referent values are shown in Fig. 4. Positive values are bigger than the referent.

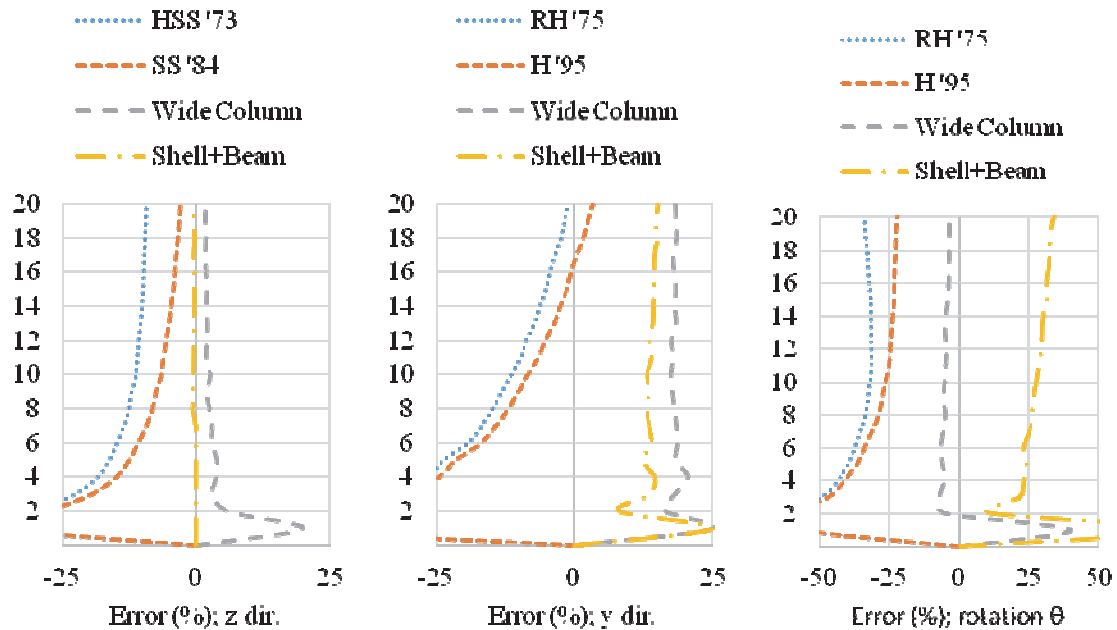


Fig. 4: Deviation of deflection and rotation values along the height.

6. CONCLUSION

A simplified analytical methods suited for rapid hand calculation are presented in the paper and compared to more comprehensive numerical models. Deflection and rotation results are obtained for example reinforced concrete structure, comprised of peripheral rigid frames and inner core with uni-symmetric layout in plan. Results are plotted, showing difference in deflection and rotation values along the height of the structure. Considering shell elements model as most comprehensive, it was taken as referent, assuming it will closely represent the behaviour of the structure.

Analysis in z direction (axis of symmetry) gives values of lateral deflection that show maximal difference of -9,4% for HSS '73, while other calculation methods show difference less than $\pm 3\%$. Deflection results in y direction show difference of less than $\pm 3\%$ for analytical methods. Wide column and shell+beam models exhibit deviation from referent value of +18,3% and +15,2% respectively. Value of rotation around x axis show deviation ranging from -33,8% to +34,1%. Shapes of deflection curves are similar for all calculation methods.

Since analytical methods presented herein provide exact solution only for combination of identical frames and single shear walls, results obtained for mixed core frame structure may differ significantly. Furthermore, methods HSS '73 and RH '75 assume axially rigid columns, neglecting contribution of axial column deformation to overall bending and twisting, therefore giving smaller values of deflection and rotation than other calculation methods.

Wide column model exhibits larger deflections than referent model. The cause to such behaviour is overestimated shear flexibility (Kwan, 1992). Distribution of shear along discrete edge nodes causes additional parasitic moments. Also, incompatibility between lintel beam and wall elements leads to overestimated flexibility. Because of relatively flexible wall-beam connections in shell+beam model, lateral deflection and rotation may be significant.

Assumptions used in calculations are within elastic theory, neglecting second order effects. Another assumption, considering rigid diaphragm behaviour, is valid for cases in which inter storey slabs lack large openings and re-entrant corners. Analytical methods applied to mixed core frame structure provide approximate solution, therefore having limited applicability. The main advantage of using analytical methods over numerical is simplicity which makes them suitable for preliminary rapid calculation. Numerical methods have much wider applicability, making them suitable for more detailed analysis.

7. LIST OF NOTATIONS

a	centroid of shear system;
A	cross-sectional area;
Ac^2	axial stiffness;
c	distance from neutral axis of column to centroid;
e	lateral load eccentricity;
E	modulus of elasticity;
EI	flexural rigidity;
EI_{ω}	warping torsion rigidity;
GA	racking shear rigidity;
GJ	torsional shear rigidity;
h	storey height;
H	total height of the structure;
I	moment of inertia;
I_{ω}	warping constant;
J	torsional constant;
M	bending moment;
q	general horizontal load;
w	lateral load.

8. REFERENCES

- Heidebrecht, A. C. and Stafford Smith, B. (1973), "Approximate analysis of tall wall-frame structures", Journal of the Structural Division, Vol. 99, No. 2, February 1973, pp. 199-221.
- Hoenderkamp, J. C. D. (1995), "Approximate deflection analysis of non-symmetric high-rise structures", Proceedings of the 5th World Congress on Habitat and the High-Rise Tradition and Innovation, 14-19 May 1995, Amsterdam, The Netherlands, pp. 1185-1209.
- Kwan, A. K. H. (1992), "Reformulation of the frame method", Proc. Instn Civ. Engrs Structs & Bldgs, Vol. 94, No. 1, February 1992, pp. 103-116.
- MacLeod, I. A. "Analytical modelling of structural systems", Ellis Horwood Limited, 1990.
- Rutenberg, A. and Heidebrecht, A.C. (1975), "Approximate analysis of asymmetric wall-frame structures", Build. Sci., Vol. 10, 1975, pp. 27-35.
- Stafford Smith, B., Kuster, M. and Hoenderkamp, J. C. D. (1984), "Generalized method for estimating drift in high-rise structures", Journal of Structural Engineering, Vol. 110, No. 7, July 1984, pp. 1549-1562.

INTEGRATED LIFECYCLE ANALYSIS OF A CONCRETE BRIDGE

*Mateusz Żarski, Tomasz Płaszczyk, Marek Salamak
Silesian University of Technology, Gliwice, Poland*

SUMMARY

The paper describes the need for developing certain computational methods for calculating the total amounts of costs and environmentally harmful emissions in the lifecycle of a bridge. Those are especially needed because of the increasing popularity of the “design, build, operate, maintain” building contracts, the concept of sustainable development and legal requirements in some countries. The following parts of the paper contain information regarding current knowledge covering the conducting of analyses contained in global literature, including various calculation and methodology approaches, the practice of application of technology for concrete bridges and lastly, conclusions and constructive criticism towards suggested methodology. It also describes issues concerning the weighting system of each of the analysis elements and draws attention to the need of maintaining particular caution while performing them.

1. THE BASIS OF ANALYSIS

With the continuous pursuance of the idea of sustainable growth (Fig. 1) in vast majority of industries in developed countries (USA, Canada, Sweden), comes the need of developing certain computing tools which would allow to monitor the current state of technology and provide information that indicates aspects needed to be improved in future. Such tools currently in use in mentioned countries include Lifecycle methods and analyses that integrate each product’s economic, environmental and social aspects.

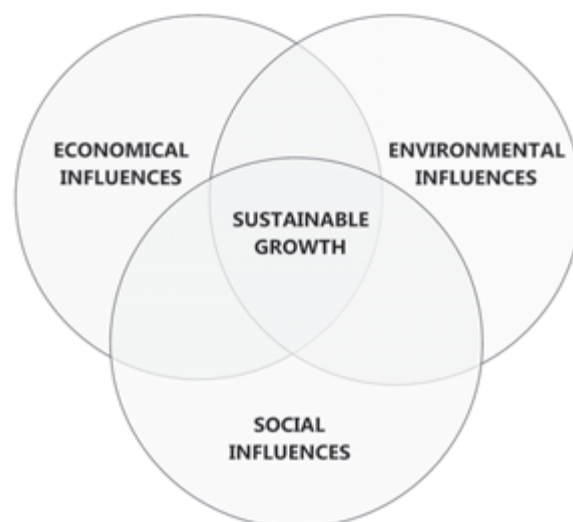


Fig. 1: The three basic components of sustainable growth ideology

It didn't take long for such tools to reach out from the manufacturing industry to infrastructure industry, where presently in some countries (including Poland), they are being incorporated into legal regulations covering public tenders, but are not in full use yet.

The principles of sustainable development are implemented not only by the country's legal requirements but also by increasing popularity of the 'design-build-operate-maintain' system, which slowly takes up the place of the basic warranty system. With the possibility of usage of the mentioned system, state's contracting entities are more than willing to release themselves from the necessity of carrying out repairs and maintaining the object. At the same time, in order to maximize profits, private companies are turning to use Lifecycle methods, setting the whole public procurement system in motion towards the idea of sustainable development.

Although the given analysis can refer to any type of object, from this point on, it will refer only to prestressed concrete bridges.

2. BASIC ASSUMPTIONS AND METHODOLOGY OF THE ANALYSIS

Before dividing the integrated analysis into its individual components, the fundamentals of calculations from an engineering standpoint has to be explained. As an integrated analysis of the life cycle of a building is meant an advanced analysis of the given object as a whole (superstructure, supports, access roads) throughout its life cycle. The life cycle of an object is defined as a set of all processes from the first conceptual works to the demolition and disposal or sale of material residues. This cycle is depicted in Fig 2.

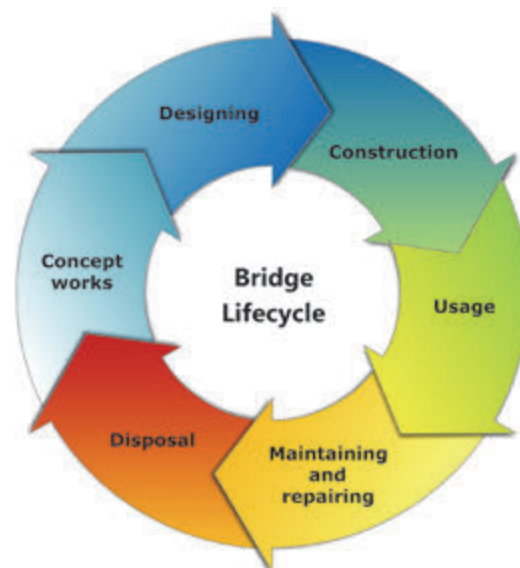


Fig. 2: The life cycle of bridge structures

As mentioned above, the main goal of carrying out this type of analysis is to follow a sustainable development strategy, which aims to work out a compromise between the economic, environmental and social aspect of the structure so as to achieve the greatest possible benefits in each of them. The following paragraphs will describe the components of integrated analysis in an order consistent with the historical chronology of its development. They will take into account each of component's significance and their methodology of calculations.

2.1 Economic analysis – LCC

The idea of carrying out such calculations is based on the basic economic dependence of long-term public procurement objects - their initial costs often represent only a fraction of the actual expenditure incurred during the use of an object. For this reason, it is not unreasonable

to carry out calculations that can improve the management of the funds used to service the bridge's structure during the several decades of its life cycle.

At present, in most countries involved in LCC (Life Cycle Cost) development, the legal status of conducting the analysis for the purpose of selecting the best variant in a public tender is regulated to a similar degree to that in Poland, that is, they may be performed at the request of the tender organizer, however they do not stand as strict requirement. Despite this, it is strongly promoted in USA (Walls J., Smith M.R., 1998), frequent EU directives (2014/24/EU and 2014/25/EU), and its use in the Member States most involved in it (Scandinavia) exceeds 30% of investments in which the procedure is considered significant.

2.1.1 Methodology of LCC

The first and also the key problem in conducting economic calculations within LCC is the division of object's costs. Miscellaneous works created in parallel around the world refer differently to the division of LCC analysis into its components (Green A., 2009). This is important not only due to the sharing of life cycle costs among individual participants (eg, social costs or costs incurred by a single user) but also because of the possibility of conducting different analyses within the LCC (eg BCR analysis). The difference between various divisions can be crucial in the final economic evaluation of an object, so it is important to compare the analyses with the same preliminary assumptions (Sundquist H., Karoumi R., 2016). The current trend in the breakdown of the LCC analysis into components is to divide the participants of the life cycle of the bridge into individual units, which include the investment agency, single user and the public. However, in most cases, for the sake of simplicity of calculation and for the obvious dominance of the expenses incurred by the agency, in the analysis, the costs taken into account usually apply only to the investment agency.

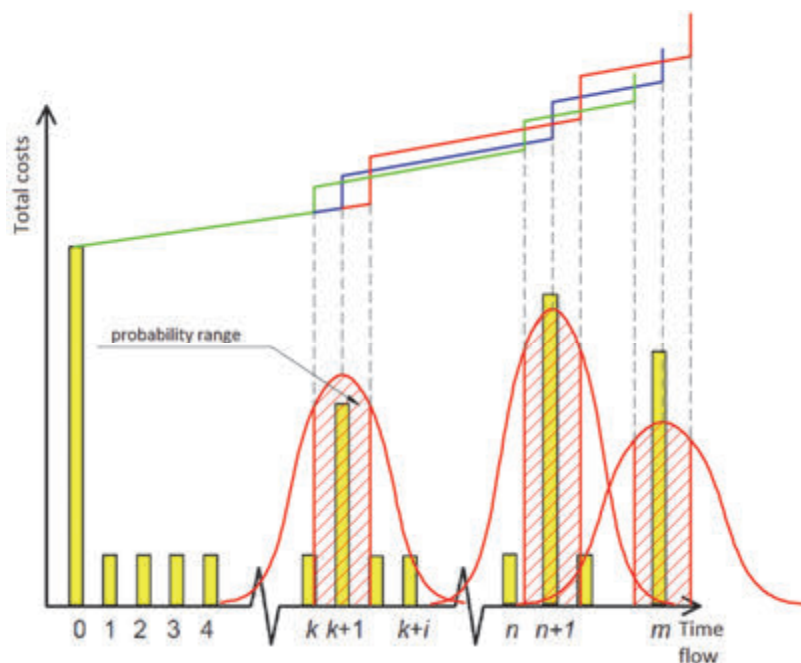


Fig. 3: Money flow in object's life cycle

Currently preferred computational methods for conducting the analysis are most often based on probabilistic analysis, which takes into account the uncertainty of the cost, time of its occurrence in object's life cycle, and the frequency of its occurrence. Favored in the early

days of technology, the deterministic approach (although still used to a limited extent), is in many cases now considered to be inferior to probabilistic analyses in both the accuracy and quantity of parameters (Lounis Z., Daigle L., 2008). The probabilistic approach has a direct bearing on the fact that instead of a single analysis result, as a result of the calculations, a certain spectrum of results with a certain probability is obtained.

The mentioned results are directly correlated with the life cycle of the object whose exemplary appearance, together with the cumulative chart of the cost of the object and the probability distributions for all of the occurrences of events generating them, are presented in Fig. 3. Events depicted in successive bars in the graph are: its annual maintenance costs, single repair, rehabilitation of the whole facility and its disposal.

In order to use the results of the calculations in an integrated analysis, a functional unit which would take into account differences in the parameters of the object must be considered, as a direct comparison of the construction of different scales, construction material or carrier would be unreasonable. In recent works published in Scandinavia (Dequidt T., 2012), it is recommended to convert the analysis result with the use a functional unit (FU) derived from formula (1):

$$FU = \frac{1}{A_d \cdot l_s} \quad (1)$$

This particular unit, used later on in sample calculations takes into account bridge's deck area (A_d) and the whole object's expected lifespan (l_s), which still can differ from originally expected one (Koris K., Bodi I., 2010).

2.2 Environmental analysis – LCA

From the historical point of view, the origins of environmental analyses are directly related to the period of the Great Depression of the late 1960's and early 1970's. Initially, it was focusing mainly on the use of materials in industrial production. Currently, these are standardized calculation methods described in ISO 14040.

As like LCC analyses, they are based on calculations performed on object's life cycle, but in that case, the cycle is a bit more elaborate, because instead of monitoring cash flows, it focuses on monitoring material emissions and energy demand from the moment the raw material is collected until its disposal.

Still, as with LCC analyses, environmental analyses currently are not required by law in any country. Due to their shorter history, in addition to the description in the ISO standards, no legal requirements are being used, and their status in many countries is not different from the Polish one. Information on their applicability is usually included only in the tendering procedures.

2.2.1 Methodology of LCA

The LCA (Life Cycle Analysis) methodology is divided into three basic components, but it should be noted that the whole process is iterative and its fragmentary results are to be under constant interpretation.

The first component is the process of defining the purpose and scope of the study, including the categories of assessment taken into account. This is important because even a slight change in input can seriously affect the results of the analysis. In practice, for analyses performed for public purposes, the purpose is usually to determine the total greenhouse gas emissions measured in kilogramme CO₂ equivalents and possibly, the release of other harmful substances or energy demand, followed by a comparative analysis. As the scope of the study is chosen, the time period and space on which the facility will operate will be chosen in accordance with the assumptions provided by the procuring entity (Hammervold J., Reenaas M., 2009).

The second element of the LCA is an analysis of the data set. The main task is to determine the LCA's component processes for the object. In order to obtain the most accurate results of the analysis, the whole life cycle of the object is divided into a set of unit processes, depicted in Fig. 4, but because of their abundance and the overall small amount of emissions data related to particular processes, it is very difficult. Instead, it is common to estimate emission data using data of materials of similar parameters, but the accuracy of such an approach is, unfortunately highly debatable.

The last part of the method is the LCIA (Life Cycle Impact Assessment). It is a rating of the data from the previous analysis in the scope of preset criteria. Such data, derived from the two preceding stages of analysis, is called 'eco-profile' and is interpreted by the different categories of impact. The categories of impact assessment are different between the LCA studies. Likewise, the problem of weighing the elements of analysis remains also unresolved. In general terms, however, this part concludes the analysis of the environmental impact of construction, being the starting point for conducting integrated analyses, analogically to the LCC.

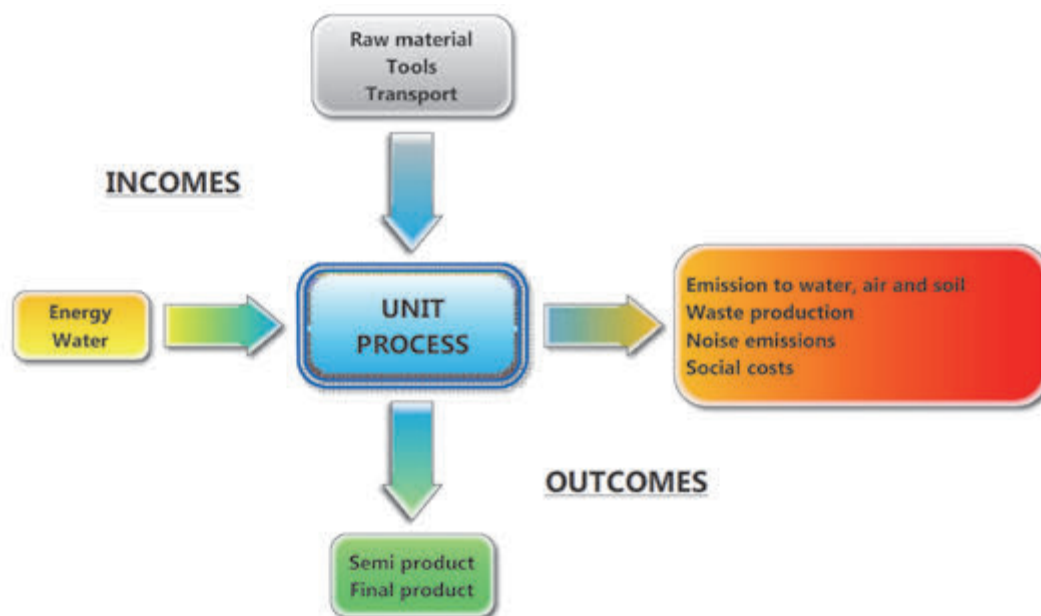


Fig. 4: Unit process

2.3 Social analysis – S-LCA

Chronologically this is the youngest part of the integrated analysis and therefore also the least developed. It derives from the idea created in 1996, proposing to supplement the LCA analysis for the social part, but work on its implementation did not begin before 2000's. The discussion on overall shape, variables and technology indicators lasted from 2003 to 2006 and

has resulted in the development of early methodologies and basic parameters such as employment rates, salaries, and positive and negative health impacts.

The current status of analysis in the world is characterized by the smallest formalization among mentioned technologies (Sala S. Vasta A., 2015). Because of the lack of formal methodology and low actual social demand for it, the S-LCA (Social-Life Cycle Analysis) remains in slow development and hence the timing of its possible implementation as a valid tool for assessing the effectiveness of a product, won't likely occur in the present decade (Norris C.B., Traverso M., 2013). Furthermore, bridges do not meet S-LCA requirements due to nature of their origination. The bridge, as a public investment, is intended to meet certain positive social criteria such as access to infrastructure, transport facilitating or economic activation of the region. For this reason, the social assessment may be subject, for example, to the social needs of an object or the form of an investment, as it is a public utility, permanently inscribed in the landscape. However, these criteria do not require complex calculation methodologies, and therefore can be conducted by surveys in areas close to the planned investment.

3. EXAMPLE OF INTEGRATED ANALYSIS

For the purpose of the paper, an integrated analysis was carried out for three prestressed concrete bridges located in Poland, differing in scale and bearing systems. For the sake of the analysis clarity, only bridge's superstructure was taken into account, assuming the same substructures in all of bridges.

The first one is a dual carriageway viaduct with a carrier system in the form of beams of varying height. The second is a much smaller, the most common form of the bridge which is a single-lane structure in a two-beam prestressed concrete system. The third one is similar to the previous but with a slab carrier system. Their overall looks including their scale are depicted in Fig. 5.



Fig. 5: Analyzed bridges

3.1 Separate analysis

Each of the integrated analysis components analyses was performed according to the calculation assumptions made by the American Prestressed Concrete Association for prestressed concrete structures (Bonstedt H., 2004). The life cycle of the facilities was assumed to be 100 years long, and the cost of construction and repairs was referred to the official cost estimate made by the contractor. Calculations were done with the help of a computational program written for the purpose. For all variables treated as probabilistic, the probability range of 5-95% was assumed. For the individual parts of the analysis, the assumed range of weights was: 1 to 3 for economic analysis and 0 to 1 for environmental. The results of separate analysis of Bridge-01 are depicted in Fig. 6.

3.2 Analyses combined

The previously calculated data of the end life costs and emissions were contained in 3D charts, taking into account the functional unit, the range of weights of the individual analyzes and the assumed probabilities. The diagram describing Bridge-01 is shown in Fig. 7. It is important to notice, that the preferred variant of the bridge in the analysis is the one with lower outcome results.

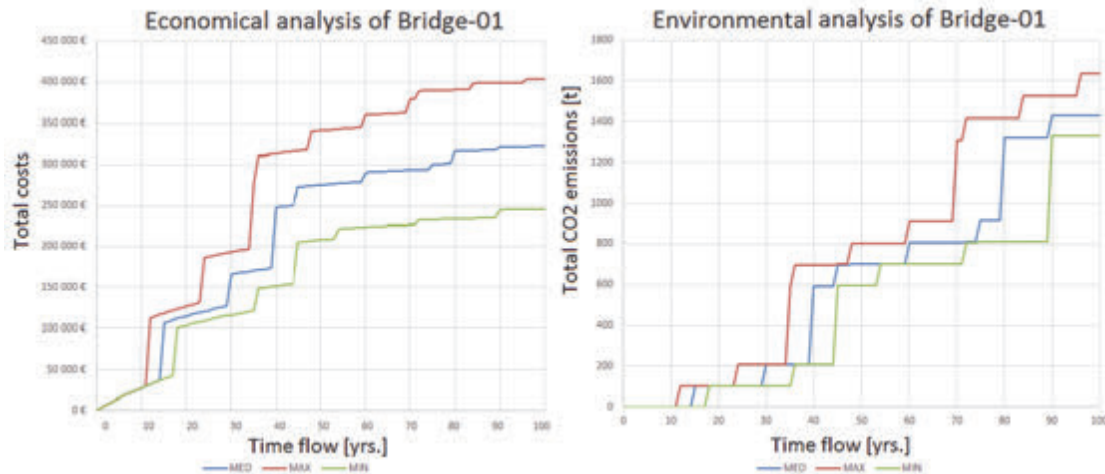


Fig. 6: Results of through-life flows of separate analysis for Bridge-01

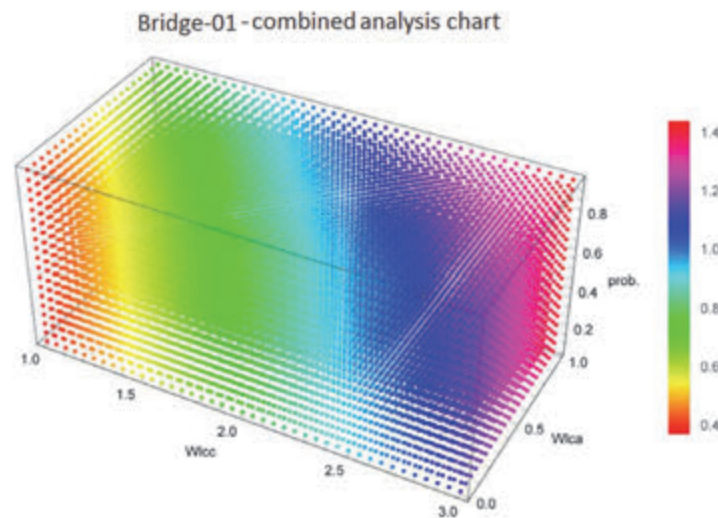


Fig. 7: Integrated analysis chart for Bridge-01

Fig. 7 depicts a full spectrum of analysis's results for every given set of data (weights of analysis's element and probability) in specified ranges. However, in order to obtain a single, coherent result, the above-mentioned data was calculated using a given functional unit and then, using the formulas (2) and (3), the final score and sustainability coefficients for each object were calculated. The results of those calculations are shown in Tab. 1.

$$S_i = \iiint_V \left(\frac{LCC_i(p)}{\sum_{i=1}^n LCC_i} \cdot w_{lcc} + \frac{LCA_i(p)}{\sum_{i=1}^n LCA_i} \cdot w_{lca} \right) dw_{lca} dw_{lcc} dp, \quad (2)$$

where V is a 3-dimensional space defined:

$$V \in \langle w_{lcc,min}, w_{lcc,max}; w_{lca,min}, w_{lca,max}; p_{min}, p_{max} \rangle,$$

$$R_i = \left(1 - \frac{\int_{w_{lcc,min}}^{w_{lcc,max}} \int_{p_{min}}^{p_{max}} f(LCC_i(p)) dp dw_{lcc}}{\int_{w_{lca,min}}^{w_{lca,max}} \int_{p_{min}}^{p_{max}} f(LCA_i(p)) dp dw_{lca}} \right), \quad (3)$$

Tab. 1: Results of the analysis

Object	Score obtained [-]	Sustainability coefficient [-]
Bridge-01	1,621	1,454
Bridge-02	1,520	0,990
Bridge-03	1,360	0,621

4. CONCLUSIONS

As can be seen in Tab. 3, mostly due to the high weights of economic analysis, the winner of integrated calculations proved to be the simplest and cheapest of considered bridges – Bridge-03. However, it should be noted, that with this newly developed methodology, any number of an arbitrary factor selected by the agency, without the limitation in a number of dimensions used, may be included in the calculation, potentially giving significantly different results.

In conclusion, life cycle analyses have the potential to be a useful engineering tool for assessing the benefits and potential risks associated with building an object. However, particular attention should be paid to the collected data describing considered criteria of analysis and their weight values used in the evaluation of their validity. It is of great importance since as in the example presented above, the weighting system has a crucial impact on the outcome of the analysis.

It is also important for them to define a specific, standardized methodology for their implementation and to continually update their calculation methods in line with the development of the civil industry.

5. REFERENCES

- Bonstedt H. (2004), “Life Cycle Cost Analysis for Bridges In Search of Better Investment and Engineering Decisions”, Prestressed Concrete Association of Pennsylvania.
- Dequidt T. (2012), “Life Cycle Assessment of a Norwegian Bridge”, Norwegian University of Science and Technology.
- Green A. (2009), “Introducing the new standards for Life Cycle Costing in Construction”, Stockholm Conference 27 November.
- Hammervold J., Reenaas M. (2009), “Environmental Effects – Life Cycle Assessment of Bridges”, Methodology Overview, ETSI Bridge Life Cycle Optimisation.
- Koris K., Bodi I. (2010), “A probabilistic approach for the service life estimation of precast concrete girders”, 2nd International Symposium on Service Life Design for Infrastructures, Bagnoux: RILEM Publications, pp. 331-338.
- Lounis Z., Daigle L. (2008), “Reliability-based decision support tool for life cycle design and management of highway bridge decks”, NRC Publications Archive.
- Norris C.B., Traverso M. (2013), “Methodological sheets for subcategories in social life cycle assessment”, United Nations Environment Programme.

- Sala S. Vasta A. (2015), "Social Life Cycle Assessment: State of the art and challenges for supporting product policies", JRC Technical Reports.
- Sundquist H., Karoumi R. (2016), "Life Cycle Cost Methodology and LCC Tools", ETSI Bridge Life Cycle Optimisation.
- Walls J., Smith M.R. (1998), FHWA-SA-98-061.
- ISO 14040:2006 - Environmental management - Life cycle assessment - Principles and framework.
- Federal Highway Administration: P3 Defined,
www.fhwa.dot.gov/ipd/p3/defined/design_build_operate.aspx (access 2017).

FIBRE REINFORCED CONCRETE CONSTITUTIVE LAWS FOR NUMERICAL SIMULATION

Tereza Sajdlová¹, Radomír Pukl¹, Károly Péter Juhász², Lóránt Nagy², Péter Schaul²

¹ Červenka Consulting

Na Hřebenkách 55, Prague, Czech Republic

² JKP Static Ltd.

Reitter Ferenc Street 73, Budapest, Hungary

SUMMARY

Determination of appropriate material parameters for the fibre reinforced concrete material model in design and assessment of structures is an important task, which is necessary for realistic modelling of FRC structures. Various recommendations and definitions are specified by specialized groups as RILEM, *fib* or ACI. These recommendations deal with test results of beam submitted to three or four point bending load with or without notch. Authors compared these documents and applied the determined parameters in numerical simulations. As the achieved results were not very satisfactory, a new solution for definition of the FRC parameters should be found. Presented solutions involve inverse analysis of results and method proposed by Juhász (Juhász, 2013). This methodology applies so-called modified fracture energy: the fracture energy of concrete is extended by energy contribution related to fibres.

1. INTRODUCTION

There are many guidelines to model and design fibre reinforced concrete, such as RILEM TC162-TDF (Vandewalle et al., 2003), *fib* Model Code 2010 (*fib* Model Code, 2010), ÖVBB Richtlinie Faserbeton (Richtlinie Faserbeton, 2008), ACI 544.8R-16 (ACI 544.8R-16, 2016), CNR DT (CNR-DT 204/2006, 2007). All of these guidelines are based on a three or four point bending tests. Obtained test results as load-displacement or load-CMOD diagrams are converted to the parameters that can be used as a material model. RILEM and *fib* Model Code 2010 use residual strengths and define "stress-crack width" or "stress-strain" diagrams that can be applied as material laws. ACI describes an indirect method to obtain the stress-strain response.

In finite element model the stress-strain diagram can be used if the characteristic length and the direction of the principal stress is known. In this case, the stress-strain can be converted to stress-crack width and the crack localization can be handled. For this purpose, the crack band size method can be used (Bazant, 1984).

These stress-strain models based on guidelines can be applied if the Bernoulli-Navier hypothesis is valid (and as a consequence there is a linear elastic stress distribution in the cross section). However, in reality, the stress distribution will be different due to the notch that is usually in the middle of the specimen for three point bending test or due to the cracks in the material that are formed during the test.

In this case, it is necessary to obtain material laws for finite element analysis by different method. As was shown in previous papers (Pukl et al., 2013), (Sajdllová & Pukl, 2014) material parameters can be determined by inverse analysis of results from basic tests as three of four point bending. Another method was proposed by Juhász (Juhász, 2013) and it works with fracture energy of material composed of concrete matrix and fibres. It is reasonable to model the FRC with "stress-crack width", instead of "stress-strain" diagram. The shape of the softening curve after post crack can depend on the type of the fibre and the dosage, but most of the time it can be simplified as a constant value after crack (so called residual strength). The area under the "stress-crack width" diagram is the fracture energy. This fracture energy could be divided into 2 parts: fracture energy of the concrete matrix G_F and added fracture energy of fibres G_{FF} , see Fig. 1. These two methods are discussed in this paper and compared with material laws obtained by guidelines.

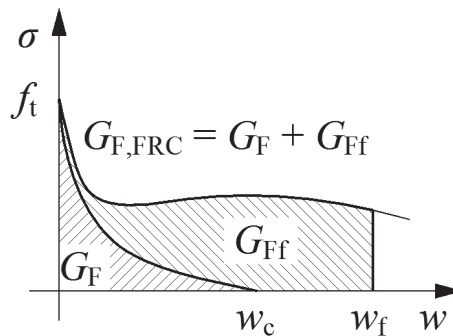


Fig. 1: Fracture energy of the concrete and added fracture energy by the fibres

2. FINITE ELEMENT ANALYSIS

Behaviour of FRC material is analysed in program ATENA (Cervenka et al., 2016) for non-linear analysis of concrete structures. ATENA is capable of a realistic simulation of concrete behaviour in the entire loading range with ductile as well as brittle failure modes as shown for instance in (Cervenka, 2002). It is based on the finite element method and non-linear material models for concrete, reinforcement and their interaction. The tensile behaviour of concrete is described by smeared cracks, crack band and fracture energy and the compressive behaviour of concrete by a plasticity model with hardening and softening. The constitutive model is described in detail in (Cervenka & Papanikolaou, 2008). Nonlinear solution is performed incrementally with equilibrium iterations in each load step.

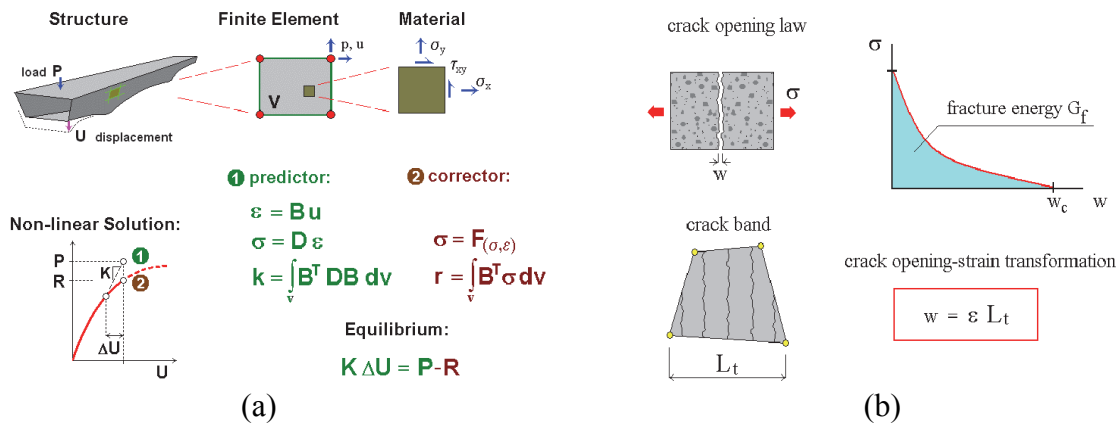


Fig. 2: (a) Scheme of the nonlinear finite element method, (b) smeared crack model for tensile behaviour of concrete

2.1 FRC Material Models

The tensile response of FRC differs from normal concrete not only in the values like tensile strength and especially fracture energy, but also in the shape of tensile softening branch. The original exponential function valid for normal concrete can be used as a first approach, but preferably would be to use more realistic form of the tensile constitutive law. Therefore, special material models at macroscopic level are needed for modelling of fibre reinforced concrete.

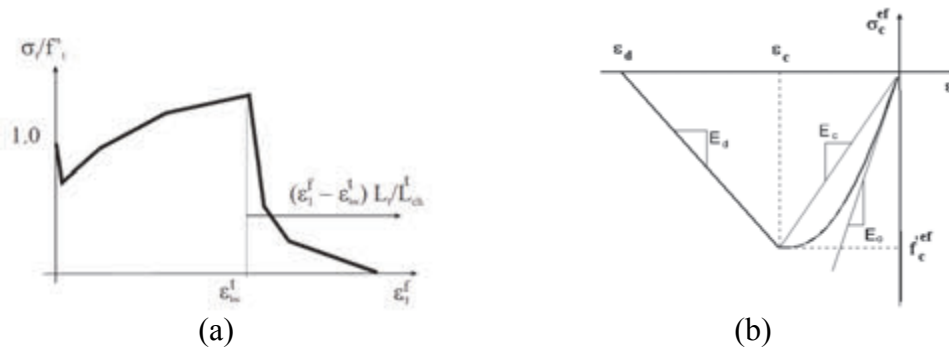


Fig. 3: (a) User defined tensile behaviour, (b) compressive stress-strain law

The most sophisticated and most general model of FRC material represents an extension to the fracture-plastic constitutive law (Cervenka & Papanikolaou, 2008) called 3D NLC2 User model. It describes the tensile behaviour according to the material response measured in tests point-wise in terms of the stress-strain relationship. The first part of the diagram is the usual stress-strain constitutive law. After exceeding the localization strain ε_{loc} the material law assumed for the characteristic crack band width L_{ch} is adjusted to the actual crack band width L_t . The characteristic crack band width (characteristic length) is the size (length) for which the defined material law is valid. The same procedure (with eventually different characteristic length) is used for the compression part of the material law. Compressive stress-strain law of mentioned material models is described in Fig. 3. The softening law in compression is linearly descending and the end point of the softening curve is defined by plastic displacement w_d (corresponding to ε_d in Fig. 3b). By increasing material parameter w_d the contribution of the fibres to the compressive behaviour of concrete is considered. Another important compressive parameter for FRC modelling is reduction of compressive strength due to cracks which says how the strength is reduced while the material is subjected to lateral tension.

3. EXPERIMENTAL PROGRAM

Experimental program focused on application of synthetic fibres called BarChip48 in concrete C25/30 is chosen for the presented study. Different dosages of fibres were tested as is shown in load-displacement diagrams in Fig. 4b. Six tests were provided for each dosage, the plotted curves represent mean values. Geometry of the specimen and test setup corresponds to EN 14651 (EN 14651, 2005). Beams were tested under three point bending condition. The cross section is 150x150 mm and span is 500 mm. The central part of the beam is weakened by notch 25 mm long, see Fig. 4a.

Result for fibre dosage 2 kg/m³ was chosen for numerical analysis presented in this paper.

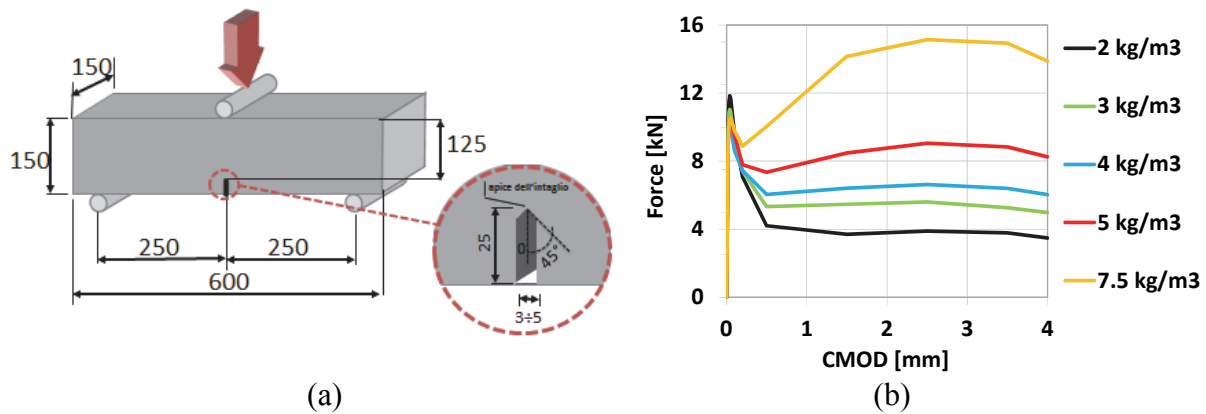


Fig. 4: (a) Geometry of tested specimen, (b) comparison of LD diagrams for different fibre dosages

4. MATERIAL LAW FOR FIBRE REINFORCED CONCRETE

4.1 Recommendations from guidelines

As a representative document, RILEM TC162-TDF is chosen for determination of the material law. Experimental programme described in previous chapter involves the same test procedure and specimen geometry that is described in RILEM. Flexural tensile strengths $f_{R,i}$ are determined Based on Bernoulli-Navier hypothesis by expression:

$$f_{R,i} = \frac{3F_{R,i}L}{2bh_{sp}^2} \quad (1)$$

where b is width of the specimen,
 h_{sp} is distance between tip of the notch and top of cross section,
 L is span of the specimen,
 $F_{R,i}$ is load recorded at $CMOD_i$.

Maximal flexural strength $f_{fcm,fl}$ and residual flexural strengths for crack mouth opening displacement $CMOD$ 0.5 mm ($f_{R,1}$) and 3.5 mm ($f_{R,4}$) are used for the determination of material law, see Fig. 5 left. Stress-strain diagram defined by RILEM is trilinear, for the numerical model part after the peak is important. Final diagram utilized in the numerical analysis contains bilinear softening as is shown in Fig. 5 right.

The finite element model for bending test is made for a plane stress simplification, with low order quadrilateral elements with 2x2 integration scheme, with the square elements shape and size of 5 mm, i.e. 30 elements through the height (25 elements above notch), see Fig. 6a. The loading is applied by force on the top loading plate. $CMOD$ is calculated as difference between horizontal displacement of the right and left bottom part of the notch. Characteristic length for tensile stress-strain diagram is equal to the element size, i.e. 5 mm.

Comparison of the load-displacement diagram from test and numerical simulation is shown in Fig. 6b. Model can correctly describe behavior on the tail of the diagram but there are differences after the crack localization. Model according to RILEM underestimate the flexural strength of the material.

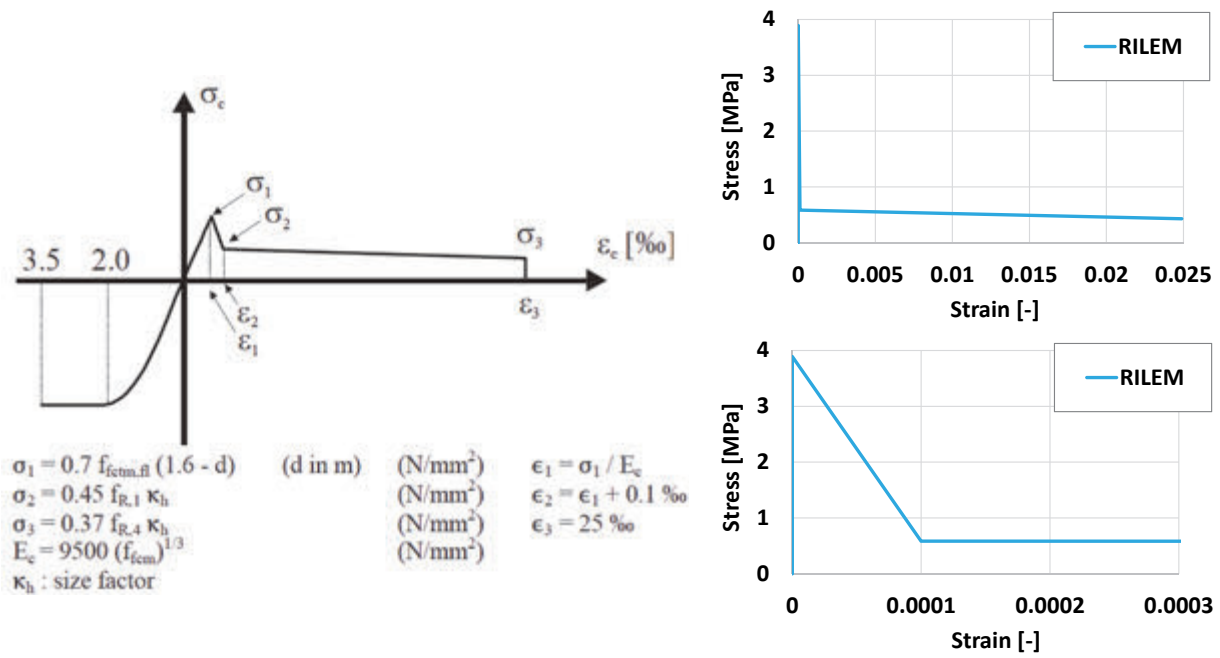


Fig. 5: (left) Stress-strain diagram according to RILEM TC162-TDF (Vandewalle et al., 2003), (right top) diagram for material with fibre dosage 2 kg/m³, (right bottom) detail of the diagram until strain 0.0003

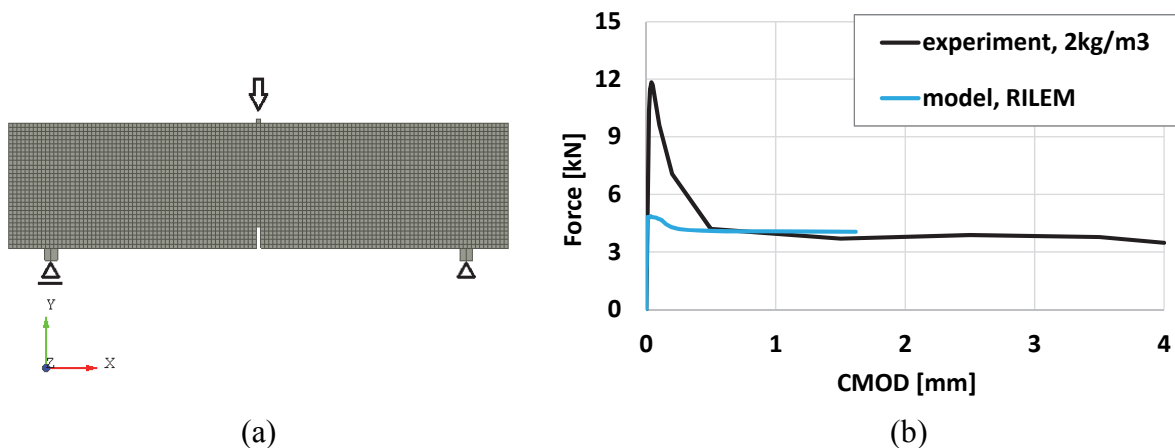


Fig. 6: (a) FEM model of three point bending test, (b) comparison of experimental result for fibre dosage 2 kg/m³ and model with RILEM material law (characteristic length 5 mm)

4.2 Inverse analysis

Another way how to obtain FRC material law for nonlinear finite element analysis is inverse analysis of experimental results which consists of two main steps. The first one is the estimation of material law based on mixture, contents and type of fibres, etc. or guidelines recommendations. The second step is modification of initial law by inverse analysis of material tests, mainly four-point bending test until the required accuracy of results is achieved.

In this case, RILEM material law was utilized as an initial function and by several simulations it was modified to the optimal material law for investigated FRC that is shown in Fig. 7a. It is obvious that material law is described in more detail compared to the RILEM and it leads to more accurate behaviour during bending test, see Fig. 7b.

Advantage of this approach is that it can be used for any experimental result and specimen geometry and it is possible to describe material very precisely. As a disadvantage, more than one numerical simulation are necessary for satisfactory result. For example, presented result was found by performing three analyses.

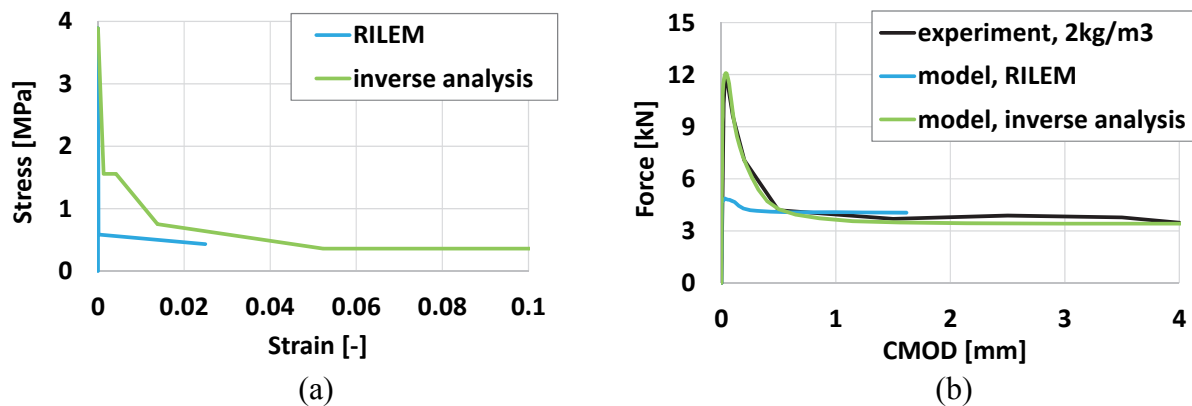


Fig. 7: (a) Stress-strain from inverse analysis in comparison with RILEM, (b) comparison of experimental result for fibre dosage 2 kg/m³ and model with RILEM material law and law obtained by inverse analysis

4.3 Modified fracture energy method

The third method was proposed by Juhász (Juhász, 2013) and it utilizes the fracture energy of the FRC.

A thin band with micro-cracks will appear due to the tensile stress in the concrete – which is called the crack process zone. By increasing the stress the concrete reaches its tensile strength when the micro cracks are touching each other. After this point the tensile capacity of the concrete will decrease, the cracks will bypass or cross the aggregates and then the entire section will be crossed by the crack. The area under the "tensile stress – crack width" diagram is the fracture energy.

The fracture energy of the concrete is influenced by a number of factors which are clearly not related to the concrete's strength class. Most of the existing design methods neglect the fracture energy of the concrete and do not pay much attention to the tensile strength. However, when designing FRC structures these parameters cannot be ignored.

The main goal in this method is to separate the fracture energy of the concrete (G_F) and added fracture energy by the fibres (G_{Ff}). According to previous research (Juhász, 2015), the added fracture energy depends on the fibre type, dosage and cement mortar (cement, water and sand). By knowing these values the added fracture energy could be defined and used as a parameter partly independent from the concrete. In this research, concrete with the same cement mortar but with different aggregate type and size was made. In the case of normal aggregate (type A, B and C) the added fracture energy (G_{Ff}) was mostly unchanged.

Application of this method in the numerical modelling to compare result with methods mentioned in the previous chapters will be provided during the further research.

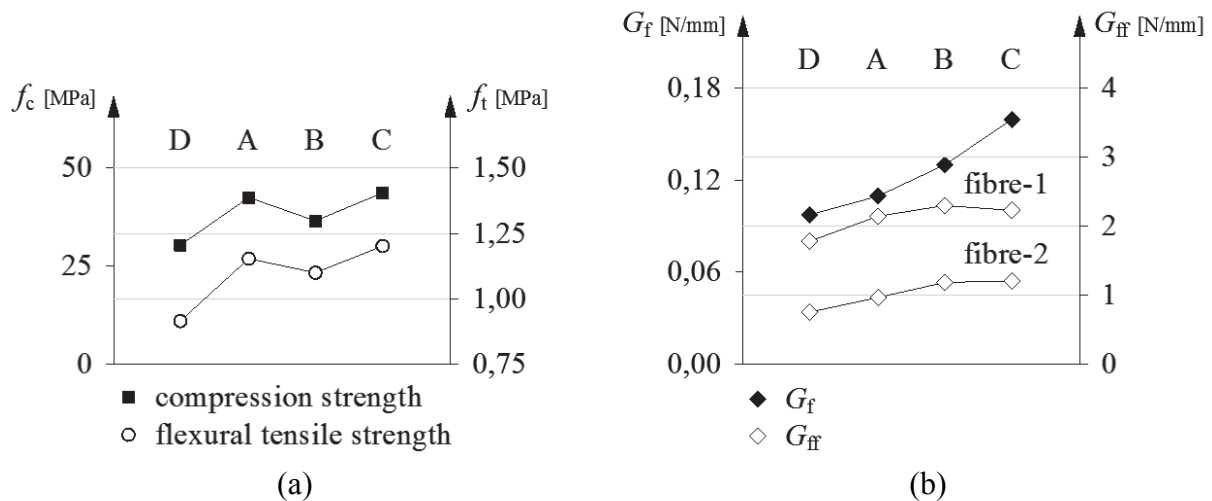


Fig. 8: (a) Compression strength and flexural tensile strength of concrete A, B, C and D, (b) fracture energy of the concrete A, B, C, D and added fracture energy of fibre-1 and fibre-2

5. CONCLUDING REMARKS

A study utilizing different methodologies for determining FRC material parameters and consequent numerical analyses were performed. As the recommendations from guidelines for the FRC tensile material law are not sufficient for numerical simulations, it is necessary to find another options. The first one is inverse analysis of results that is general and can be applied to any experiment. However, this procedure can be time-consuming because it requires several simulations. The next goal is to create tool for automatic inverse analysis of FRC material parameters in software ATENA. Another option is modified fracture energy method proposed by Juhász (Juhász, 2013). Knowing or estimating the added fracture energy could be a useful parameter to the FRC model, however it depends on the concrete mortar. Further research is required to determine the degree of impact of the cement grout alteration on the added fracture energy and also to find relation with the dosage of the fibres. The advantage of the model is that the fibre reinforced concrete can be described by one parameter.

6. ACKNOWLEDGEMENTS

The presented results are based on the research performed within Eurostars project E!10316 "Virtual Lab for Fibre Reinforced Concrete Design by Simulation Prototyping". Authors gratefully acknowledge this support.

7. REFERENCES

- ACI 544.8R-16 (2016), "Report on Indirect Method to Obtain Stress-Strain Response of Fiber-Reinforced Concrete (FRC)", ACI Committee 544, 2016.
- Bazant, Z.P., Oh, B. H. (1984), "Crack Band Theory for Fracture of Concrete", Materials and Structures, Vol. 16, 1984, pp. 155-177.
- Cervenka, J., Jendele, L., Cervenka, V. (2016), "ATENA Program documentation", Cervenka Consulting, www.cervenka.cz.
- Cervenka, J., Papanikolaou, V.K. (2008), "Three dimensional combined fracture-plastic material model for concrete", Int. J. Plast., 24:2192–220, doi:10.1016/j.ijplas.2008.01.004.

- Cervenka, V. (2002), "Simulating a response", Concrete Engineering International, Vol. 4, No. 4, 2002, pp. 45-49.
- CNR-DT 204/2006 (2007), "Guide for the design and construction of fibre reinforced concrete structures", CNR – Advisory Committee on Technical Recommendations for Construction, Rome, 2007.
- EN 14651 (2005), "Test method for metallic fibered concrete - Measuring the flexural tensile strength (limit of proportionality (LOP), residual)", European Committee for Standardization, 2005.
- fib* Model Code for Concrete Structures 2010 (2010), Wilhelm Ernst & Sohn, Berlin, Germany, 2013, ISBN 978-3-433-03061-5.
- Juhász, K. P. (2013), "Modified fracture energy method for fibre reinforced concrete", Fibre Concrete 2013, Prague, Czech Republic, pp. 89-90, ISBN 978-80-01-05238-9.
- Juhász, K. P. (2015), "Szintetikus szálerősítésű betonok hozzáadott törési energiája az adalékanyag függvényében", Építés – Építészettudomány, 43 (3-4), 2015, pp. 315-327, ISSN 0013-9661.
- Pukl, R., Sajdlová, T., Lehký, D., Novák, D. (2013), "Multi-level optimization of input parameters for modeling of fibre reinforced concrete", *fib* Symposium 2013, Tel Aviv, Israel, 2013, pp. 135-138.
- Richtlinie Faserbeton (2008), Österreichische Bautechnik Vereinigung (ÖVB), Wien, 2008.
- Sajdlová, T., Pukl, R. (2014), "Optimization of input parameters for material model of fibre reinforced concrete and application on the numerical simulation of tunnel lining", ACI-*fib* International Workshop FRC, Montreal, Canada, 2014.
- Vandewalle, L. et al. (2003), "RILEM TC162-TDF: 'Test and Design Methods for Steel Fibre Reinforced Concrete: bending test' (final recommendation)", Materials and Structures. Vol. 36, 2003, pp. 560-567.

NUMERICAL MODELLING OF A PRECAST FIBRE REINFORCED CONCRETE TRACK SLAB

Károly Péter Juhász¹, Péter Schaul¹, John Hammond²

¹ *JKP Static Ltd.*

Reitter Ferenc str. 73, Budapest, Hungary

² *Precast Advanced Track Ltd.*

King Street, Knutsford, United Kingdom

SUMMARY

In this article a macro synthetic fibre reinforced precast concrete trackslab's design process will be presented. The analysis was done with using an advanced finite element software called ATENA (Cervenka et al 2013). Beside the static loads, the precast slab was also checked for dynamic and fatigue loads. The structure was verify for early ages, for de-moulding, rotating, lifting and for transport as well. With the analysis a necessary fibre dosage was determined. After the design AECOM prepared a real scale test for two full slab. During the test the displacements were measured on different places with using Geophones. Finite element model of the test was made with all the details of the real scale test. The results from the tests and from the finite element models were close to each other in every checked case.

1. INTRODUCTION

PreCast Advanced Track's (PCAT) unique 100 per cent macro synthetic BarChip fibre reinforced precast concrete slab structure is set to revolutionise the construction and repair of the world's railways (Hammond, 2016). The system was developed by the PreCast Advanced Track Company, and the JKP Static ltd was charged with the finite element modelling of the structure. During the design process AECOM and Mott MacDonald were also involved as a consultant company. To different geometries were checked, one for off- streets and the other is for streets, which means the traffic can cross the slab as well. To see the exact behaviour of the full structure, one and a half slab was modelled with the connection cables. The analysis was done with different soil parameters, to see the effect of the unequal subgrade as well. The slab was checked for different loads and load cases, to find the worst effect during the lifetime. Beside the static loads, the structure was also checked for dynamic and fatigue loads. The structure was verify for early ages, for de-moulding, rotating, lifting and for transport as well. The analysis was done with using an advanced finite element software specialized for concrete structures, called ATENA (Cervenka et al 2013). The software uses the combined fracture surface model (Cervenka and Papanikolaou, 2008) to model the different behaviour of the concrete in compression and in tension. The fibre reinforced concrete material was modelled with the Modified Fracture Energy Method (Juhász, 2013). With the analysis a necessary fibre dosage was determined. After the design AECOM prepared a real scale test for two full slab. The slabs were placed to a concrete pool filled with compacted sand. The test was made with using a Rail Trackform Stiffness Tester (RTST) (Govan et al, 2015). During the test the displacements were measured on different places with using Geophones. Finite element model of the test was made with all the details of the real scale test. The results from the tests and from the finite element models were close to each other in every checked case.

In this article the design process and the steps of the finite element analysis will be presented.

2. THE PCAT SYSTEM

PCAT is a new concept in railway construction which can challenge the traditional engineering method of supporting railway tracks on ballast. Whilst ballasted tracks have some advantages, they also have significant drawbacks that can be overcome by adopting slab track systems. PCAT's innovative lightweight slab structure represents a world first for precast track slabs as it is manufactured entirely from BarChip 48 macro synthetic fibre reinforced concrete, without steel reinforcement being required. This ensures that if the concrete cracks there is no steel to corrode, providing a long life structure, as fibres continue right to the edge of the structure this enhances durability and resistance to accidental damage. It also reduces maintenance, material costs and the fibre reinforcement is safer to handle than steel during manufacture. The PCAT slab design is based on a channel beam upper profile which provides a high modulus slab structure, this maximises the slab strength and minimises the stiffness needed for the track foundation. This allows PCAT tracks to be constructed quicker than conventional track. It also means PCAT is particularly suitable for adoption where poor or variable ground support and flooding conditions exist.

The PCAT distinctive deep edge beam is designed to be formed higher than the adjacent rail without conflicting with the train underside gauge. This has the potential to reduce rail and wheel contact noise by obstructing the sideways bypass of noise. The high strength of the edge beam is likely to be adequate to prevent a derailed train from coming off the PCAT slab track structure and thus increase track safety. The upper slab profile collects surface water and conveys this to drainage outlets via the transverse and longitudinal ducting system accommodated within the slab. This disperses water away from the track foundation and increases the resilience of the track, preventing damage to the associated earthwork structures. The ducts can accommodate track cables and services in a secure environment which prevents theft and damage.

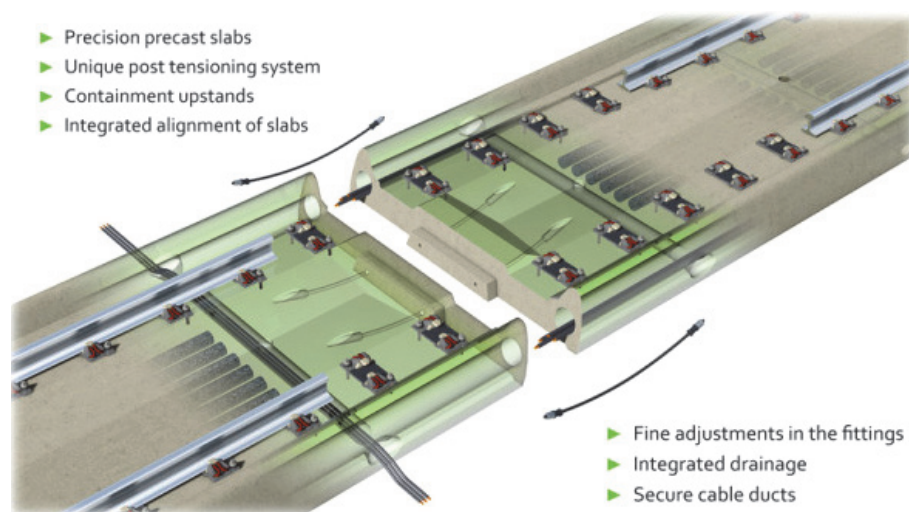


Fig. 1: The PCAT system

The slabs connecting to each other with a dry male –female joint (came from the geometry) and with curved connection cables as well. This is designed to permit a rapid laying and joining process to form the monolithic structure. Curved steel connectors between adjacent

units are easily inserted and tensioned from the slab surface as erection proceeds. This allows rapid installation to take place from the occupied track to provide the monolithic structure, even in tunnels with restricted space. Uniquely, if needed, PCAT slabs can be simply decoupled, levels adjusted or slabs removed and replaced without affecting the track structure. Two type of slabs was developed to serve all the needs. One is the mentioned standard slab (off-street slab) with the side beams, which is highly optimised and can easily installed. The other one is a more robust structure, but with a straight upper surface and with hidden rails (on-street slab). This type of the slab can be used in streets as well, thanks to the sunk rails the traffic can easily cross the slab. The full length of both geometry was 5000 mm, the minimum thickness of the off-street slab was 150 mm and the thickness under the rails in case of on-street slab was 200 mm. The slabs were designed for 120 year lifetime.

3. STRUCTURAL DESIGN – NUMERICAL MODELLING

3.1 Finite element model of the structure

The numerical modelling of the PCAT slabs were done in a Finite Element Software called ATENA. This software specialized for concrete structures, with an advanced material model, presented in the next chapter. To determine the necessary fibre dosage both of the slab geometry were modelled. The finite element models of the structures can be seen in Fig. 2.

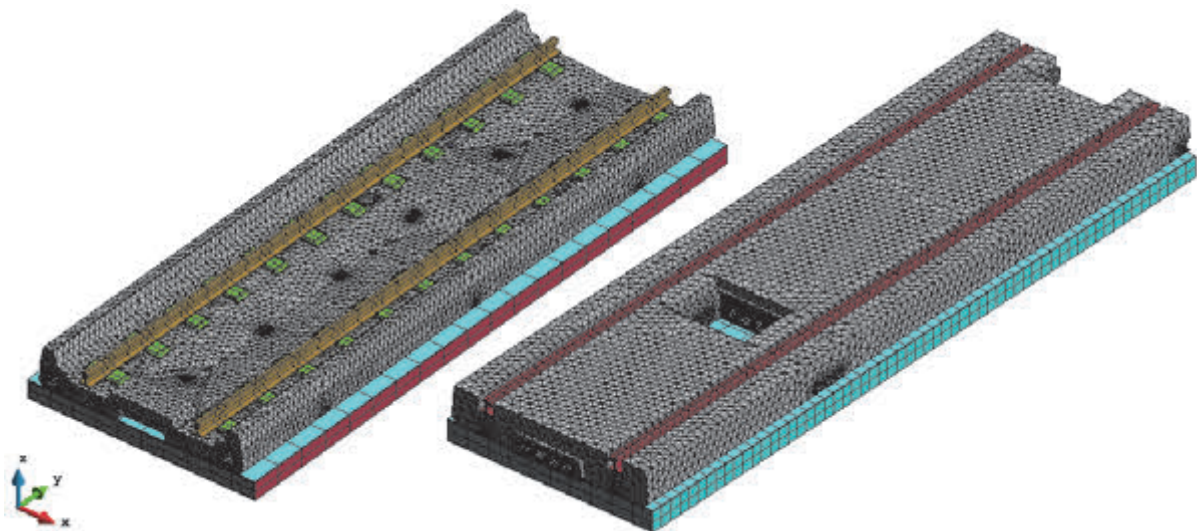


Fig. 2: Numerical models of the precast slabs

To ensure the connection between the model and the real structure's behaviour, all the details were modelled including the connection ducts, the injection holes, the rail slippers and the rails with their exact geometry. In the models one and a half slab was modelled to be able to investigate the behaviour of the joints. For the connecting surface an interface material was determined, which could bear only compression stresses. It occurs that the slabs during the loading process could open along the connection surface, and the ducts bear the tension stresses. Under the slabs a bedding layer and a HBM (Hydraulically Bound Mixture) layer was modelled. For the subgrade non-linear springs were used. To investigate the effect of the soil parameters all the models were checked for a higher (350 MPa) and a lower (175 MPa) HBM layer as well.

In the model various material models were used for the different structural elements. For the concrete slab and advanced concrete material was used (see the details in the next chapter).

For modelling the subbase and the subgrade linear elastic materials were used with different elastic modulus. The same material model was used for slippers as well. For the steel elements, such as rails and connection cables a Von Mises material model was used which can handle the yield of the steel elements. Two different interface elements were used, one to model the friction between the concrete slab and the steel duct, and one to model the transfer of the compression forces between the two slabs. The parameters were determined in both case to be as close to the real behaviour as possible.

For the slab a structured tetrahedral mesh were generated, with 3.0 cm side length. This value was reduced close to the longitudinal and transvers holes, injection holes and pits. For subgrade, rails, slippers and ducts brick elements were used to speed up the running time of the model.

3.2 Material model of concrete and FRC

The concrete was modelled using an advanced material model, which means using combined failure surfaces. With this material model the different behaviour (elastic-plastic or brittle, compressive and tensile strength, fracture energy) of concrete in tension and compression can be modelled. There are many such models available in the literature, the most commonly used are: Von-Mises and Rankine; Drucker- Prager and Rankine; and Menétrey-William and Rankine (Rankine cube is at the tension side). However, it is important to note that these models only define the peak strength of the material, not the post-cracking response. Numerous other models can be used to approximate the post-cracking capacity of FRC. The model presented in the ITAtech guideline (ITAtech Activity Group Support, 2015) was used here.

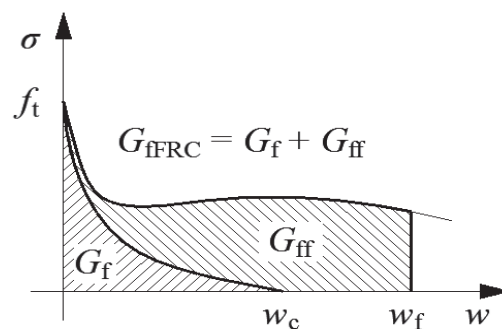


Fig. 3: Fracture energy of the FRC

When stresses exceed the tensile strength of the concrete it will crack. There will be residual stress at the crack surface that depends on the crack width opening distance. This stress is associated with an energy, called fracture energy (G_f). This energy is influenced by the aggregate type (round or crushed), size, and its bond to cement mortar. Fibres increase this fracture energy (G_{ff}), thereby making the concrete a more ductile material. This approach is called the modified fracture energy method (Juhasz, 2013). The most important criterion for the selection of the FRC material model is to be able to model this increased fracture energy (G_{ffrc}) and select a value that is appropriate to the FRC used for a design (see Fig. 3). For our models the additional fracture energy was modelled with a constant residual strength, f_{idu} , as can be seen in Fig. 4.

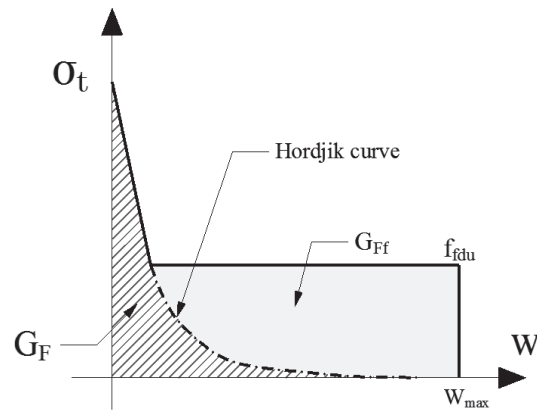


Fig. 4: Used tensile function for numerical calculation

The concrete was modelled as a three dimensional (3D) brick element with a material model consisting of a combined fracture-plastic failure surface (Cervenka and Papanikolaou, 2008). Tension is handled herein by a fracture model, based on the classical orthotropic smeared crack formulation and the crack band approach. It employs the Rankine cube failure criterion, and it can be used as a rotated or a fixed crack model. The plasticity model for concrete in compression uses the William-Menétrey failure surface (Menétrey and William, 1995). Changing aggregate interlock is taken into account by a reduction of the shear modulus with growing strain, along the crack plane, according to the law derived by Kolmar (1986).

The concrete has a stress-strain diagram according to Eurocode 2 (Eurocode, 2004). The crack width was calculated from the stress-crack width diagram, determined by means of inverse analysis, with the help of the characteristic length, which is a function of the size of the element and the angle of the crack within the element. This method is the only one that could realistically represent the cracks in the quasi-brittle material. This is the main advantage of this advanced material model.

3.3 Design and load cases

To check all the possible effect on the slabs, different loading scenarios were carried out in the finite element software. During the lifecycle various effect will occur to the trackslab. Because the slab is pre-casted the first effect comes from the demoulding of the element. In this case a time dependent material model was used, which mean the material parameters changed during the analysis follow the hardening of the concrete. With this analysis the optimum demoulding time can estimate as well. To demoulding a lifting and a tearing force was added to the early age concrete slab. After this, but also in early ages, a rotation effect was occurred: the demoulding was made upside down, but the racking of the slabs were in the other direction. In this two load case also the lifting and rotating elements were checked. The next situation was the storing load case. In this case the weight of three elements were added to the slab, simulating the effect of the racking.

The highlighted design target was to check the ultimate and the serviceability limit states under the train load. The geometry of the trains were added. To examine the worst loading case, and to model the passage of the train, seven different loading scenarios were carried out in different positions. In Ultimate Limit State (ULS) the principal stresses, in Serviceability limit State (SLS) the crack widths and the vertical displacements were checked. During the calculation the unequal rail loading was also take into consideration.

To be able to calculate the effect of the cyclic loading fatigue analysis was done also for all the loading positions. The number of the cycles were calculated back from the estimated lifetime of the structure and the average daily traffic. The finite element software calculate two additional fatigue strain for the maximal fracturing strain (Pryl et al. 2010), one handle the tensile strength reduction during the cyclic load (according to the Wöhler curve), and the other takes into consideration the crack opening effect during the cyclic load.

4. RESULTS

The structure complies with all the design requirements both in ULS and in SLS. In ULS the target was that the structure bear the loads with safety factors and with design material parameter values without the failure of the structure. In SLS the aim was that the crack widths should be less than the value according to Eurocode 2 (0.2 mm). Both design case met with the requirements in every loading position and design situation.

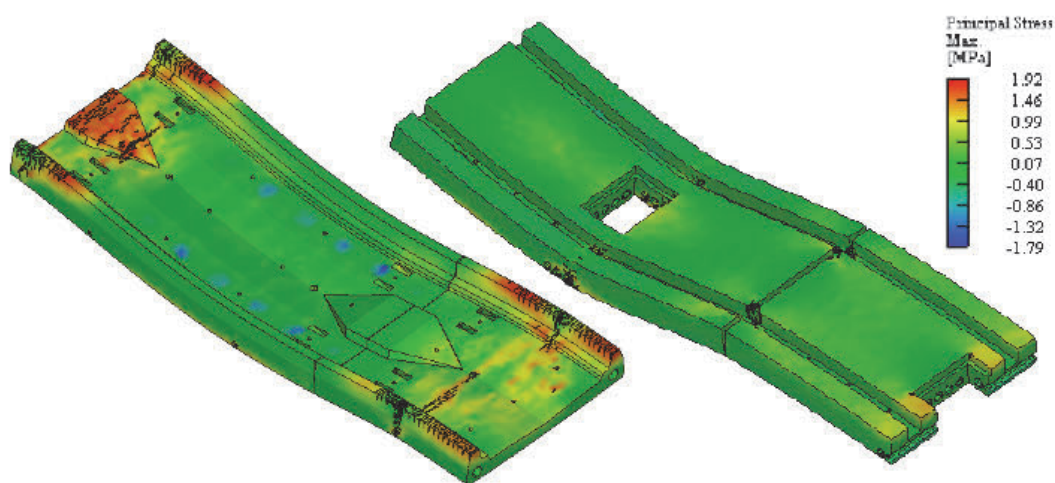


Fig. 5: Principal stresses and cracks in deformed Atena model

The slabs deformation was realistic, it followed the expectation under the different loads. The connection between the two slabs worked well. It also can be seen that the structure is highly optimized, in ULS several crack appeared in the surface of the structure, but without failure, and in SLS almost no visible crack appeared on the structure.

5. REAL SCALE TEST WITH RTST

At the AECOM Pavement Test Facility in Nottingham was installed the PCAT slab within their test pit to measure the deflection of the slab along the structure using an applied load at different series of locations. The position of the load was replicated the arrangement used in the FEM simulation. The PCAT off-street slab has been designed for 12 tonne axle loads. For the testing it was proposed after the first suit of loading at 8 tonne the load was increased in 4 tonne increments up to 24 tonne, subject to slab performance during the testing.

The loading of the slab was carried out using the Rail Trackform Stiffness Tester (RTST) (Fig. 6) which has been developed by AECOM to replicate the loading requirements of high-speed or heavy-haul lines through the use of an increased range of pulse-loading conditions. The weight is fully enclosed within the machine, which greatly reduces operator risk. The RTST apparatus is mounted on a transport frame that can moved along on rubber-caterpillar tracks whilst off track and then switch to rail wheels. On ballasted track geophones measure

the deflection response of the ballast, sub-ballast, formation and subgrade enabling the assessment of layer stiffness. During testing of the PCAT slab an array of 9 geophones were positioned above the concrete slab surface to record the deflection in microns.



Fig. 6: The RTST testing (AECOM PCAT Test report)

6. VERIFICATION

To ensure the numerical model's property, a finite element analysis was made about the RTST test. The model contained the whole test setup: the concrete pit, the compacted soil, and the two slab with the mentioned detail as well. The soil parameters in the finite element model were chosen according to the used values in the laboratory test. The effect of the RTST was added to the slab with using a steel plate which corresponds to the loading beam's foot. The materials and the material models were the same like in the previous analysis. The measured value in the finite element model was the vertical deflection. It was measured in 9 different points, where in the test the geophones were. The position of the loading plate in the finite element model followed the RTST machines position in the test.

The results in every loading case were close to each other. The finite element analysis followed well the reality, the differences between the measured deflections in the model and in the test was less than 0.1 mm. Only one loading scenario was where the difference was higher, where the load was over the female joint. This was in contribution with the AECOM report which determine a very poor subgrade stiffness in this area. The results of the test and the FEA can be seen in Fig. 7.

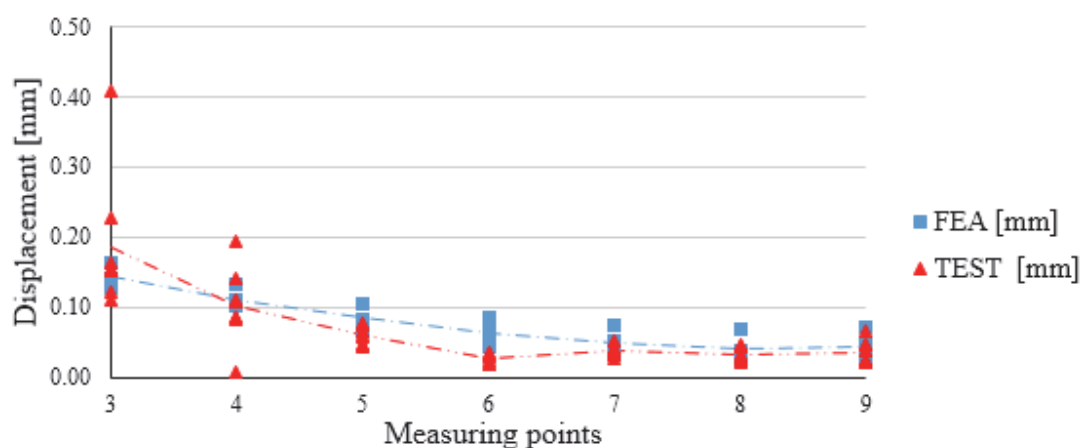


Fig. 7: Results of RTST and FEA

7. CONCLUSION

A new, highly optimized only macro synthetic fibre reinforced concrete trackslab was developed by the PreCast Advanced Track Ltd. The slab because its precast nature can be easily installed, and the reparation can be also quick. To determine the optimum fibre dosage finite element analyses were done, with a concrete specific finite element software, ATENA. The results showed that the structure can bear the load in every ULS design case, and the crack widths in SLS are always under the limit according to the Eurocode. The analysis showed also, that the structure will work well after the 120 year lifecycle. To verify the finite element model a real scale test was carried out by AECOM. The test represent the real behaviour of the slab under train load. A finite element model was made to represent the test. In both examination the vertical displacements of the slab were measured. The results were close to each other in every design cases, and also the finite element analysis was capable to show where the soil stiffness was inappropriate.

Further researches will carried out in the future, where a mock up line will build by using the PCAT system.

8. ACKNOWLEDGEMENT

The research was supported by the FibreLab, co-founded by the Nemz_15-1-2016-0026 Programme and the European Union Horizon 2020 Framework.

9. REFERENCES

- Cervenka, J. and Papanikolaou, V.K. (2008), "Three dimensional combined fracture-plastic material model for concrete" *International Journal of Plasticity* (24): 2192-2220
- Cervenka, V., Jendele, L., Cervenka, J. (2013), "ATENA Program Documentation: Part 1 Theory" Cervenka Consulting s.r.o., Prague, 318 p.
- EUROCODE EN 1992. (2004), "European Code for design of concrete structures", European Committee for Standardization
- Govan C., Sharpe P., Brough M. (2015), "The Rail Trackform Stiffness Tester – Development and early trials to assess stiffness characterisation of novel trackforms". *Railway Engineering*, Edinburgh
- Kolmar, W. (1986), "Beschreibung der Kraftuebertragung über Risse in nichtlinearen Finite-Element-Berechnungen von Stahlbetontragwerken", Dissertation, T.H. Darmstadt.
- Hammond J. (2016), "Construction and reinforcement" in *Railing Professional* October 2016 Issue pp. 162-163.
- ITAtch Activity Group Support (2015), "ITAtch Design Guidance For Precast Fibre Reinforced Concrete Segments" ITAtch Report n7, draft
- Juhász, K.P. (2013), "Modified fracture energy method for fibre reinforced concrete", in: *Proceedings of Fibre Concrete 2013: Technology, Design, Application*. Prague, Czech Republic 2013, pp. 89-90.
- Menétrey, P., William K.J. (1995), "Triaxial Failure Criterion for Concrete and Its Generalization", *ACI Structural Journal* 92(3). pp 311-318.
- Pryl D., Cervenka J., Pukl R. (2010), "Material model for finite element modelling of fatigue crack growth in concrete" *Procedia Engineering* 2 pp. 203–212

COMPARISON OF DIFFERENT MODELS ON DIFFERENT CAST-IN-SITU RC JOINTS

Zsolt Roszevák, István Haris

Budapest University of Technology and Economics, Department of Structural Engineering

1111 Budapest, Műegyetem rkp. 3-9. Hungary

zsolt.roszevak@gmail.com; haris.istvan@epito.bme.hu

SUMMARY

The paper presents numerical analysis of different types of cast-in-situ reinforced concrete structural joints using a non-linear, three-dimensional, FEM software specifically developed for the modelling of reinforced concrete structures. The best-used, typical reinforced concrete joints were built up by a variety of formation of the reinforcements and by modelling the constructional gaps. During the numerical analysis, exclusively the vertical loads were examined. A comparison study was made between the simplified, and of course the most common used FE modelling procedures (theoretical boundary conditions of the static model) in practice and the real (bending-rotation) behaviour of the joints according to the numerical results. The modelling procedure used in this article was performed on a previous experimental study (Haris, Roszevák, 2017), which was supported and verified by lab tests. We revised the widely applied typical static models used by the practice and their results.

1. INTRODUCTION

Nowadays there are more and more reinforced concrete structure research projects to better understand connections between different structural elements. In most cases, shear walls are used to prevent the stability of buildings, therefore it is very important to have an exact knowledge of how shear walls react to different types of loads (vertical and lateral loads as well as their interactions). Recently, many investigations have been conducted on cast-in-situ and precast reinforced concrete shear walls.

The majority of research works found in professional literature show that shear wall (lateral) load tests are only performed in plane. There is a very limited amount of investigations published in the professional literature on the connection between cast-in-situ shear walls and slabs, due to the fact that these elements are always tested separately. To get a better understanding of wall-slab connections it is necessary to test and analyse them together. If this connection was modelled, it would be possible to examine different types of loads, for example vertical loads on the slab together with lateral loads on the shear wall. Furthermore, tests on lateral quasi-static and cyclic loads could be done.

It is very important not only to examine the loads on the structure but also to put emphasis on building a numerical model. Different results can be achieved with various numerical models, which contain a lot of derelictions and simplifications in many cases. These settings greatly influence the behaviour of the structure and the results.

2. PROBLEM STATEMENT

In the studies available, researchers investigate only loads in plane to the shear wall, even though shear walls get lateral loads out of plane only in few cases. Shear wall structures connect in almost every case with other structural elements (slabs, beams, etc.), which greatly affects the distribution of stresses in the walls. So, investigations should involve shear walls with the slabs connected. This enables an analysis of vertical and lateral loads on the slabs connected to the walls and the installation of lateral loads out of plane of the shear walls. These numerical analyses and aleatory experiments make it possible to examine the behaviour of complex RC joints in circumstances most corresponding to realistic construction and load layout.

Based on professional experience, practicing engineers produce the shear wall-slab connection by using simple connections in numerical models. This setting is not a default, as if it was the reinforcement properly formed for the simple connection. In many cases it can be seen that the numerical models were made using simple connections, but the reinforcement is designed so that the connection can convey moment. It can be a wrongly designed connection because the structural connection was not calculated for the generated moment.

3. LITERATURE REVIEW

From the 1970s T. Pauly investigated the resistance of RC shear walls from lateral wind and earthquake loads. Pauly and many researchers recognized that shear walls offer considerable lateral stiffness and they can protect buildings from non-structural damage. They realized that there is a need to know more about the behaviour of shear wall structures. In the 1980s many experiments and analyses were performed on shear walls and the types of research studies showed rapid development. In 1980 T. Pauly and R. L. Williams examined energy dissipation in shear walls and they also provided a detailed description of capacity design procedures. With the development of finite element methods and softwares from the 1990s, several numerical analyses were made to investigate the behaviour of cast-in-situ RC shear wall structures against lateral loads. With the appearance of precast reinforced concrete elements, a new research area has opened up.

Recently, tests and analyses of precast shear walls were performed by Sorensen et al. They investigated a construction-friendly shear connection for the assembly of precast reinforced concrete shear wall elements. This experiment presents a new solution for the connection of precast shear wall elements, which makes construction faster and easier and also improves structural performance compared to the conventional solution. This new design differs in the way the U-bar loops are oriented, it allows a construction-friendly installation (lowering of the precast panels) with no need to clash rebars and without pre-bending and post straightening U-bars. Thanks to this new design it is also possible to use U-bars with a larger diameter. They replaced the lace bar with a so called double T-headed rebar, aiming to enable the transfer of tension between the overlapping U-bars and also to achieve an increased anchorage of the short lacer reinforcement. Due to the new design, it was possible to obtain higher load-carrying capacities. In addition, they also presented upper bond rigid plastic models for the prediction of the critical failure mode and the load-carrying capacity of the new connection design. A simple tool is used for the models to optimize the geometry of keyed joint interfaces to enhance the ductile behaviour of the connection.

Another research by Lu et al. discussed an innovative joint connection beam for precast concrete shear wall structures. Because of construction convenience, safety, high quality, and

low pollution, a precast shear wall structure is outstanding for green buildings. These shear walls are connected by multiple joints. These joint connecting beams connect the vertical reinforcement in precast concrete shear walls. With this solution it is possible to save steel and to ensure convenient operation. Comparisons between cast-in-situ walls and precast walls with joint connecting beams showed that the joint connecting beam effectively transfers the load of precast walls. The experiment focused on failure modes, hysteretic curve, skeleton curve, bearing capacity, ductility, and energy dissipation capacity. Finite element models were also produced by using ABAQUS for simulations; the simulation results agreed with the experimental results. They specified that the larger height of the joint connecting beam can slow stiffness degradation in squat walls. The way joint connecting beams can transfer the load of precast walls is unclear yet, so more investigations are to be performed.

4. NUMERICAL MODELS

The numerical analysis contained a total of 4+4+1 tests. During the program the most common shear wall-slab connections (see Fig. 1) were investigated, as listed below:

- Type A: Shear wall-slab joint with “L” connection,
- Type B: Shear wall-slab joint with “T” connection,
- Type C: Shear wall-slab joint with rotated “T” connection,
- Type D: Shear wall -slab joint with “positive” connection.

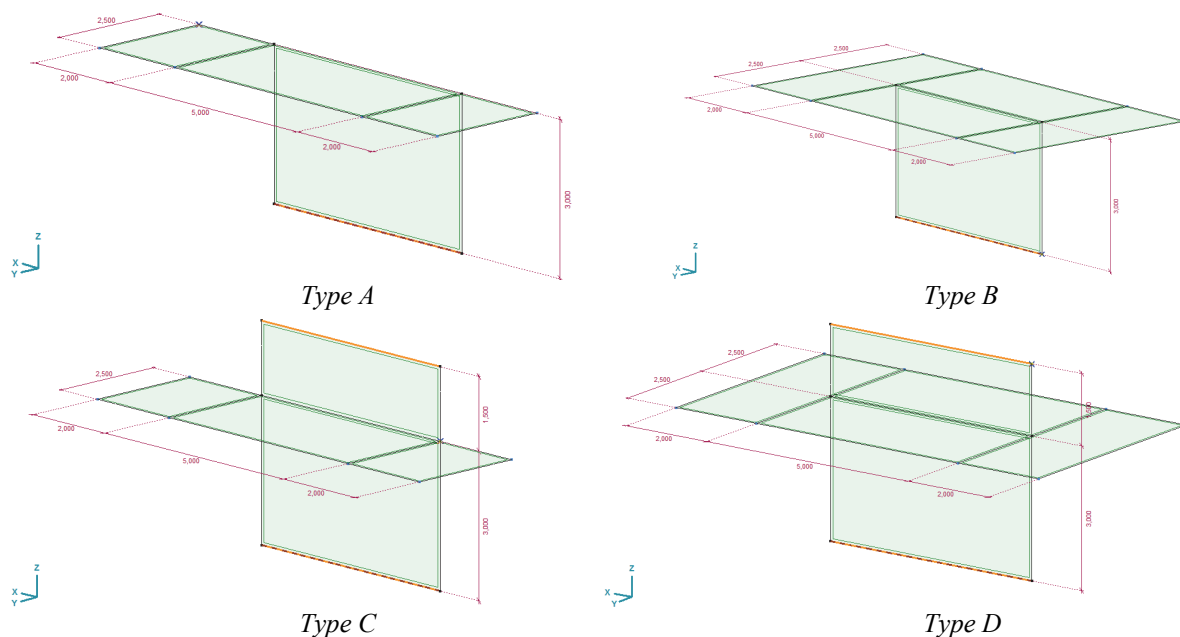


Fig. 1: Types and geometry of joints

It was considered important to use a program used by engineers in daily design. So, during the numerical analysis, a linear two-dimensional (AxisVM13) finite element software was used. To achieve more complex results, a non-linear three-dimensional (ATENA 3D) finite element software was also used, specifically developed for the modelling of reinforced concrete structures. The first four + four analyses were completed by Axis VM 13 for all types of joints. The remaining program was analysed by ATENA 3D for Type D only.

4.1 2D analysis

The general geometry was the same in each case, the thickness of the slab was 20 cm and that of the wall was 25 cm. The applied concrete was marked as C25/30. In every case the wall and the slab were modelled with symmetry. On the slab the vertical loads were placed, and on the top of the wall the vertical load from higher levels was also placed. A nominal horizontal load was used in the plane of the slab. Four models were made using a rigid wall-slab connection, and four models were made using a simply connected wall-slab connection.

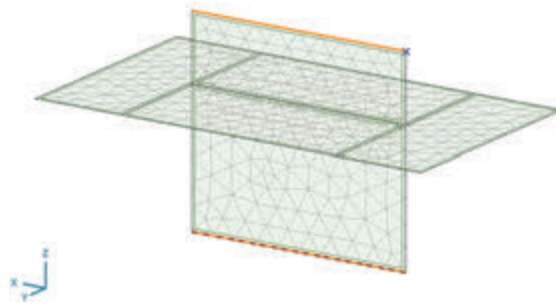


Fig. 2: Finite element mesh

The basic mesh size of the models was 50 cm. The shell elements were modelled as 6-node, planar, isoparametric finite elements (Axis VM Manual, 2017). Taking Type D as an example, the finite element mesh is shown in Fig. 2. Axis VM was used to perform linear calculations without material and geometric non-linearity.

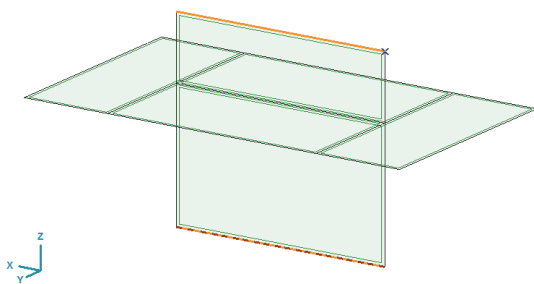


Figure 3. Rigid wall-slab connection

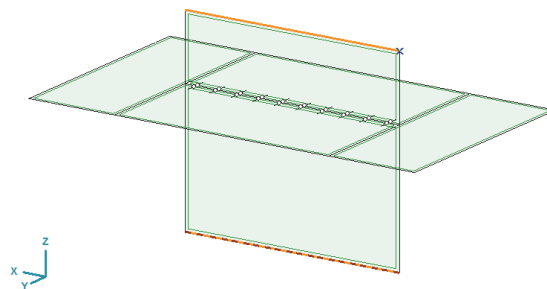


Figure 4. Simple wall-slab connection

The numerical analysis involved models with both rigid wall-slab connection and with simple connection, see Figures 3 and 4. To observe the differences of stresses and moments, in this paper only the vertical loads are put on the slab and on the top of the wall. Lateral loads will be investigated later. The load layout is shown in Fig. 5.

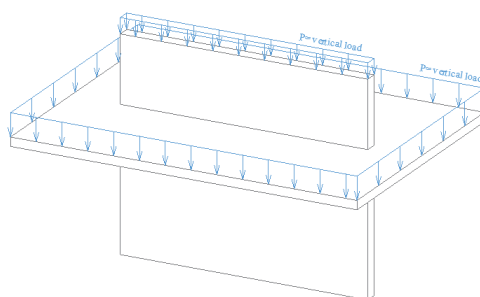


Fig. 5: Loads on the model

4.2 3D analysis

A finite element model was constructed using the program ATENA 3D to simulate the behaviour of the shear wall-slab connection. The concrete was modelled with so called “C25/30 mean values” (Cervenka et al. 2014) as a 20-node quadratic brick element and the reinforcement was modelled with the real stress-displacement characteristic of the S500B (Cervenka et al. 2014) rebar. In the wall and the slab, a reinforcement with $\text{Ø}12/200/200$ mm was used. The concrete and the rebars were modelled with the real geometry and formation, see Fig. 6.

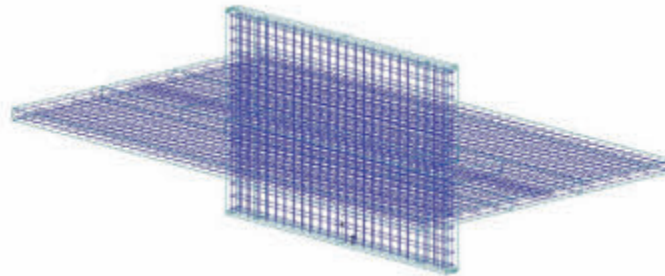


Fig. 6: Geometry and reinforcement

The bond-slip relationship between the concrete and the steel bars was realized according to the CEB-FIB model code 1990 (Cervenka et al. 2014). The basic mesh size of the model was 20 cm, but on the two ends of the wall and on the slab surrounding the end of the wall the mesh size was reduced to 5 cm (Haris, Roszevák, 2017), see Fig. 7. The model was subjected to quasi-static vertical loads on the slab and on the top of the wall, see Fig. 8.

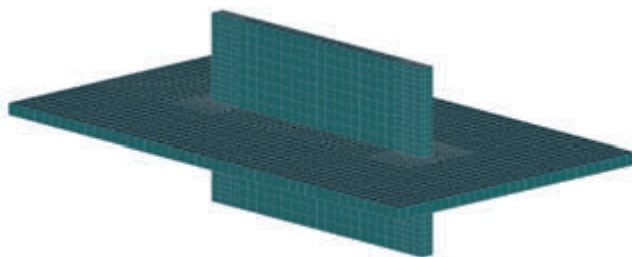


Fig. 7: FE mesh

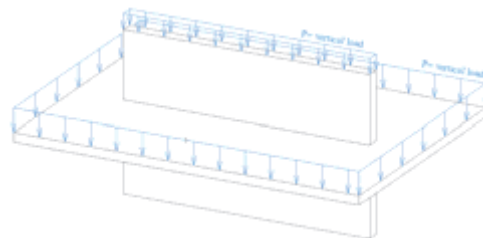


Fig. 8: Vertical loads on the model

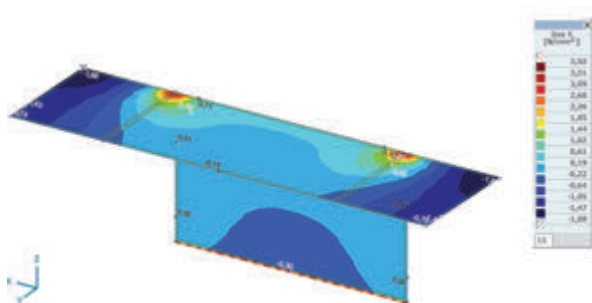
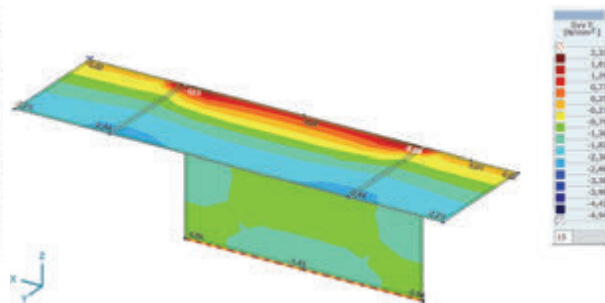
The Newton-Raphson algorithm was used for numerical simulation. To solve the problem, the well-known Cholesky decomposition was used.

5. NUMERICAL RESULTS

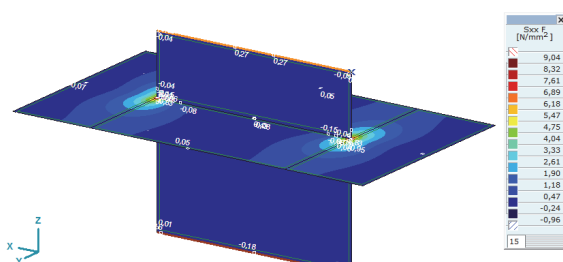
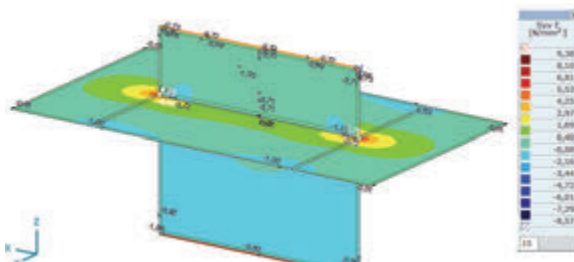
In this chapter, the results of the numerical models are presented. First of all, the 2D models and second, the 3D models will be described. In this paper, only the stresses and the moments of the various numerical models were investigated.

5.1 2D analysis

The first numerical analyses were performed with the rigid wall-slab connection. Results are presented on the easiest structural formation Type A and on the most complicated structural formation Type D. Figures 9 and 10 show the σ_x and σ_y stresses on the model by using vertical loads.

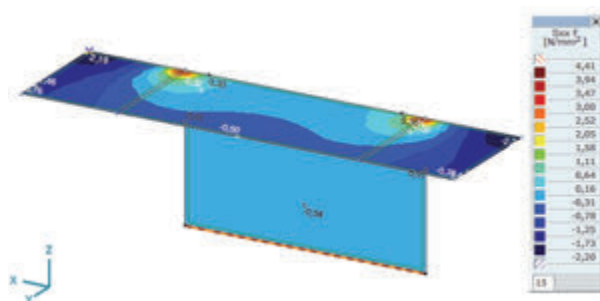
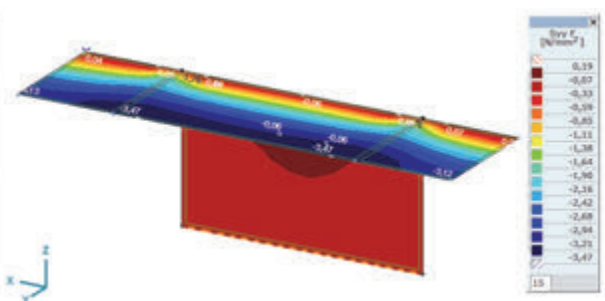
Fig. 9: Type A, Stress σ_x Fig. 10: Type A, Stress σ_y

In Fig. 10, significant stress ($\sigma_y = 1.23 \text{ N/mm}^2$) is observable on the wall-slab connection, as expected. For Type D, moment illustrations are also produced, see Figures 11 and 12.

Fig. 11: Type D, Stress σ_x Fig. 12: Type D, Stress σ_y

It can be observed in the stress figures at Type A and Type D that the stress σ_x (Type A: $\sigma_x = 0.37 \text{ N/mm}^2$, Type D: $\sigma_x = 0.40 \text{ N/mm}^2$) is almost zero in the middle of the slab in the middle of the connection. In Type D at the edges of the wall, a stress peak is generated in the slab ($\sigma_x = 6.85 \text{ N/mm}^2$). In the direction “Y”, the stress σ_y is significant and almost consistent ($\sigma_y = 1.57 \text{ N/mm}^2$) in the middle of the slab, but at the edges of the wall there is also a stress peak ($\sigma_y = 9.38 \text{ N/mm}^2$) in the slab.

The second numerical analysis investigated the simply connected wall-slab models. The following section presents the stress figures of the models. It shows the results for both Type A and Type D. Figures 13 and 14 show the stress σ_x and σ_y in Type A. In the middle of the connection, the stress σ_x is almost zero ($\sigma_x = 0.11 \text{ N/mm}^2$) in the slab and it can be seen, as in the previous cases, that there is a stress peak ($\sigma_x = 4.41 \text{ N/mm}^2$) at the edges of the wall in the slab. The stress σ_y is almost zero ($\sigma_y = 0.04\text{-}0.07 \text{ N/mm}^2$) in the slab along the full length of the connection.

Fig. 13: Type A, Stress σ_x Fig. 14: Type A, Stress σ_y

As expected, similar results are obtained for Type D as for Type A. In the directions ‘X’ and ‘Y’ in the middle of the connection, the magnitude of the stresses σ_x and σ_y is almost zero ($\sigma_x = 0.04\text{-}0.06 \text{ N/mm}^2$, $\sigma_y = 0.03\text{-}0.08 \text{ N/mm}^2$) in the slab. But in each direction at the edges

of the wall a forceful stress peak ($\sigma_x = 1095 \text{ N/mm}^2$, $\sigma_y = 1801 \text{ N/mm}^2$) appears in the slab. The moment figures are shown in Figures 15 and 16.

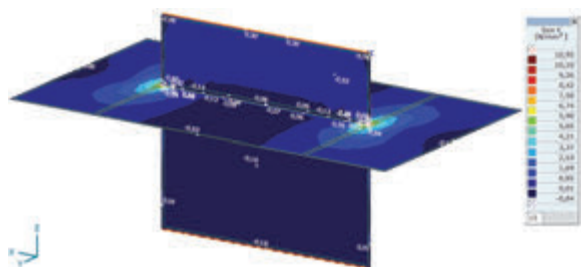


Fig. 15: Type D, Stress σ_x

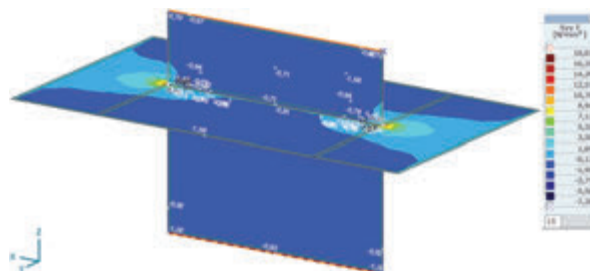


Fig. 16: Type D, Stress σ_y

5.2 3D analysis

The 3D non-linear numerical analysis was performed by using ATENA 3D. The following section presents the stress figures because the program cannot produce moment figures. Figures 17 and 18 show the stresses σ_x and σ_y .

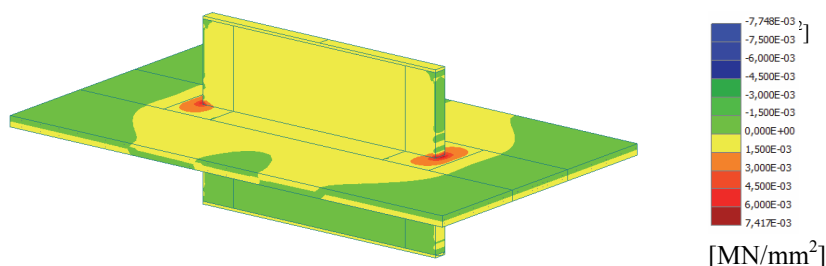


Fig. 17: Stress σ_x from 3D analysis

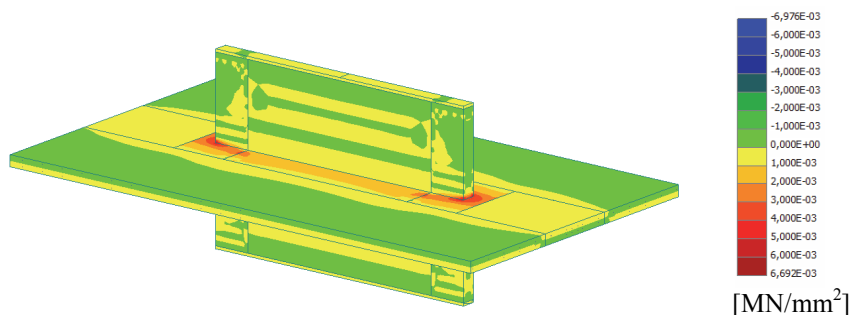


Fig. 18: Stress σ_y from 3D analysis

Fig. 17 shows the stress σ_x , where the stress in the middle of the connection is almost consistent ($\sigma_x = 1.50 \text{ N/mm}^2$) in the slab. At the edges of the wall a significant stress peak appears in the slab and also in the wall ($\sigma_x = 748 \text{ N/mm}^2$). The stress σ_y indicates a stress figure similar to the stress σ_x , but in the middle of the connection a significant stress ($\sigma_y = 2.00 \text{ N/mm}^2$) is generated in the slab. At the edges of the wall a stress peak ($\sigma_y = 6.92 \text{ N/mm}^2$) also appears, expanding both to the slab and the wall. To illustrate the stresses in the 3D structure, sections were made in the directions “X” and “Y” along the symmetry axis. Fig. 19 shows the stress σ_x , where the tensioned and the compressed zone of the section can be clearly seen. The stresses in the lower and the upper side of the wall are consistent ($\sigma_x = 1.50 \text{ N/mm}^2$), but at the edges of the wall there is a stress peak ($\sigma_{x,tens} = 7.41 \text{ N/mm}^2$, $\sigma_{x,comp} = 7.75 \text{ N/mm}^2$) in the slab and also in the wall.

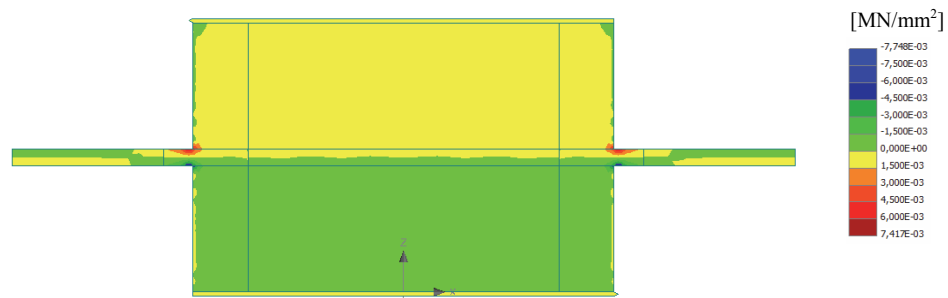
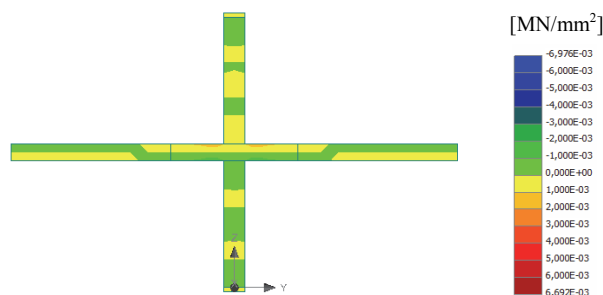
Fig. 19: Section "X-Z", Stress σ_x

Fig. 20 shows the section "Y-Z", where the stress σ_y is presented. In this figure, the tensioned and the compressed concrete zones can also be observed, clearly showing the significant stress surrounding the connection ($\sigma_{y,tens} = 2.00 \text{ N/mm}^2$, $\sigma_{y,comp} = 1.00 \text{ N/mm}^2$) at the upper and lower side of the slab.

Fig. 20: Section "Y-Z", Stress σ_y

6. COMPARISON OF THE RESULTS

At Type A, the 2D linear numerical results are different in case of the rigid and the simple wall-slab connection. In the middle of the slab it can be observed that the stresses σ_x are almost equal (rigid: $\sigma_x = 0.37 \text{ N/mm}^2$, simple: $\sigma_x = 0.11 \text{ N/mm}^2$). In the direction 'X' there is a slight difference at the edge of the wall in the slab between the stresses (rigid: $\sigma_x = 3.92 \text{ N/mm}^2$, simple: $\sigma_x = 441 \text{ N/mm}^2$). In the direction 'Y' a larger difference can be seen between the stresses (rigid: $\sigma_y = 2.37 \text{ N/mm}^2$, simple: $\sigma_y = 0.06 \text{ N/mm}^2$) at the edge of the wall in the slab. The same stresses show a minor difference in the middle of the slab (rigid: $\sigma_y = 0.87 \text{ N/mm}^2$, simple: $\sigma_y = 0.04\text{-}0.07 \text{ N/mm}^2$).

At Type D, the 2D linear numerical results are also different for the rigid and the simple wall-slab connection. The stresses σ_y show huge differences in the middle of the slab (rigid: $\sigma_y = 1.57 \text{ N/mm}^2$, simple: $\sigma_y = 0.03\text{-}0.08 \text{ N/mm}^2$). In the middle of the slab it can be observed that the stresses σ_x are almost equal (rigid: $\sigma_x = 0.40 \text{ N/mm}^2$, simple: $\sigma_x = 0.04\text{-}0.06 \text{ N/mm}^2$). In the direction 'Y' there is a bigger difference between the stresses (rigid: $\sigma_y = 9.38 \text{ N/mm}^2$, simple: $\sigma_y = 1801 \text{ N/mm}^2$) at the edge of the wall in the slab. In the direction 'X' also a massive difference can be seen between the stresses (rigid: $\sigma_x = 6.85 \text{ N/mm}^2$, simple: $\sigma_x = 10.95 \text{ N/mm}^2$) at the edge of the wall in the slab. It can be identified that in the middle of the wall stress differences are not too large. But at the edges of the wall a huge stress increase can be observed at the simply connected models.

The numerical results of Type D are also different between the 2D and 3D analyses. The simply connected 2D and 3D numerical results are completely different. The stresses σ_y show huge differences in the middle of the slab (3D: $\sigma_y = 2.00 \text{ N/mm}^2$, simple:

$\sigma_y = 0.03-0.08 \text{ N/mm}^2$). In the middle of the slab it can be seen that the stresses σ_x differ from each other (3D: $\sigma_x = 1.50 \text{ N/mm}^2$, simple: $\sigma_x = 0.04-0.06 \text{ N/mm}^2$). In the direction 'Y' a larger difference is indicated between the stresses (3D: $\sigma_y = 6.92 \text{ N/mm}^2$, simple: $\sigma_y = 18.01 \text{ N/mm}^2$) at the edge of the wall in the slab. In the direction 'X' there is also a massive difference between the stresses (3D: $\sigma_x = 7.41 \text{ N/mm}^2$, simple: $\sigma_x = 10.95 \text{ N/mm}^2$) at the edge of the wall in the slab. The simply connected 2D and 3D numerical results are completely different. In the rigidly connected 2D and 3D numerical results, a similarity can be observed considering the stresses. The stresses σ_y show a slight difference in the middle of the slab (3D: $\sigma_y = 2.00 \text{ N/mm}^2$, rigid: $\sigma_y = 1.57 \text{ N/mm}^2$). In the middle of the slab it can be seen that the stresses σ_x differ more (3D: $\sigma_x = 1.50 \text{ N/mm}^2$, rigid: $\sigma_x = 0.40 \text{ N/mm}^2$). In the direction 'Y' also a minor difference is shown between the stresses (3D: $\sigma_y = 6.92 \text{ N/mm}^2$, rigid: $\sigma_y = 9.38 \text{ N/mm}^2$) at the edge of the wall in the slab. In the direction 'X', there is also a small difference between the stresses (3D: $\sigma_x = 7.41 \text{ N/mm}^2$, rigid: $\sigma_x = 6.85 \text{ N/mm}^2$) at the edge of the wall in the slab. Based on the numerical calculations it can be established that the simply connected wall-slab models conduct huge stress peaks at the edges of the wall in the slab. The 3D numerical analysis where the real attributes of the materials are defined, the results are between the simple 2D model and the rigid 2D model. Specifically, the result matches better with the rigid 2D model, but the rigid 2D model can yield slightly higher stress values. This does not mean that a mistake was made during the design. When that 2D rigid model is used, no design is possible at the expense of safety.

7. CONCLUSIONS

In this paper, analyses were performed for shear wall-slab connections using different types of numerical modelling techniques. The analyses investigated shear wall-slab connections subject to vertical loads. A four-four numerical model was calculated with a 2D linear finite element software. A numerical model was also created by a 3D non-linear finite element program. In the 2D linear analyses four models were made with rigid wall-slab connections, and four models were also made where the wall-slab connection was simply connected. In the 3D non-linear analysis, the real properties of the materials. The concrete was modelled with a "C25/30 mean values" concrete material model and the reinforcement was modelled with a real stress-displacement characteristic. Between concrete and steel bars a bond-slip relationship was realized. It was established that at the rigid and the simply connected wall-slab connections huge differences are produced in terms of the stresses. This was expected because the two models are fundamentally different. It was also identified that with the available results of 3D non-linear analysis are between the results yielded by the 2D rigid and the 2D simply connected models. However, the results of the 2D rigid model are closer to the results of the 3D non-linear model. 3D non-linear analysis can probably reach better and more accurate results, but it may not be worthwhile to generate a complex 3D model. So, no huge mistake can be made by using the 2D rigid model in daily design.

8. FURTHER RESEARCH

This paper discussed a numerical analysis of shear wall-slab connections with vertical loads. A 2D linear analysis was used, which can be used by engineers in their everyday design work. In order to better understand the behaviour of the connection a 3D non-linear calculation was also made, which can be used for generating much more specific models. Further research studies will involve the creation of models with a variety of reinforcement formations. Investigations will focus on the behaviour of shear wall-slab connections against lateral loads in plane and also out of plane. In this phase of the research only quasi-static vertical loads

were analysed, but in further investigations we calculations will be made with cyclic lateral (with quasi-static vertical) loads to identify the behaviour of the connection and to specify cyclic degradation as well as the effect of the formation of the reinforcement on the connection.

9. REFERENCES

- T. Pauly: Some aspects of shear wall design, *Bulletin of N.Z. Society for Earthquake Engineering*, Vol. 5 No. 3, September 1972, pp. 89-105,
- Oesterle, R. G.; Fiorato, A. E.; Johal, L. S.; Carpenter, J. E.; Russel, H. G.; and Corley, W. G, Earthquake Resistant Structural Walls – Tests of Isolated Walls, Report to National Science Foundation, Portland Cement Association, Skokie, Nov. 1976, 44 pp. (Appendix A, 38 pp.; Appendix B, 233 pp.)
- T. Pauly, R.L. Williams: The Analysis and design of and the evaluation of design actions for reinforced concrete ductile shear wall structures, *Bulletin of N. Z. National Society for Earthquake Engineering*, Vol. 13 No. 1, June 1980, pp. 108-143,
- Oesterle, R. B.; Fiorato, A. E.; and Corley, W.G., Reinforcement Details for Earthquake-Resistant Structural Walls, *Concrete International*, Vol. 2 No. 12, 1980, pp. 55-66,
- Vincenzo Colotti, Shear Behaviour of RC Structural Walls, *Journal of Structural Engineering*, Vol. 119, Issue 3, March 1993,
- Wallace, J. W., New Methodology for Seismic Design of RC Shear Walls, *Journal of Structural Engineering*, Vol. 120, Issue 3, March 1994,
- Xilin Lu, Xiaohan Wu, Study on a new shear wall system with shaking table test and finite element analysis, *John Wiley and Sons*, Earthquake Engineering and Structural Dynamics, Vol. 29, Issue 10, 2000, pp. 1425-1566,
- Nicolae Ile, and J. M. Reynouard, Nonlinear Analysis of Reinforced Concrete Shear Wall Under Earthquake Loading, *Journal of Earthquake Engineering*, Vol. 04, Issue 02, April, 2000,
- Pedro A. Hidalgo, Christian A. Ledezma, and Rodrigo M. Jordan (2002) Seismic Behavior of Squat Reinforced Concrete Shear Walls. *Earthquake Spectra*: May 2002, Vol. 18, No. 2, pp. 287-308.
- Z. W. Miao, X. Z. Lu, J. J. Jiang, L. P. Ye, Nonlinear FE Model for RC Shear Walls Based on Multi-layer Shell Element and Microplane Constitutive Model, *Computational Methods in Engineering and Science EPMESC X*, Aug. 21-23, 2006, *Sanya Hainan, China*, Tsinghua University Press & Springer-Verlag,
- fib* Model Code for Concrete Structures, (2010), *Wilhelm Ernst & Sohn, Verlag für Architektur und technische Wissenschaften GmbH & Co. KG.*, Berlin, 2010,
- V Cervenka., L. Jendele, J. Cervenka (2014), „ATENA Program Documentation Part 1, Theory” *Cervenka Consulting s.r.o.*, 19. September 2014,
- Zs. Roszevák (2015), „Numerical and experimental analysis of prefabricated reinforced concrete beams”, *TDK thesis*, Budapest, 2015, *in Hungarian*,
- Francisco J. Molina, Pierre Pegon, and Perre Labbé, Stiffness-Displacement Correlation from the RC Shear Wall Tests of the SAFE Program: Derivation of a Capacity Line Model, *Advances in Materials Science and Engineering*, Volume 2016 (2016), Article ID 5750672, 21 pages
- Hamze Zarei Chargoat, Seyed Shaker Hashemi, Mohammad Vaghefi, Cyclic Analysis of RC Shear Walls, Considering Bar-Concrete Interaction, *Journal of Seismology and Earthquake Engineering*, Vol. 18, No. 2 (2016),
- Zs. Roszevák (2016), „Analysis of behaviour of reinforced concrete structure with different numerical modelling techniques”, *MSc. diploma thesis*, Budapest, 2016, *in Hungarian*,

- Xilin Lu, Lu Wang, Dung Wang, Huanjun Jiang. An innovative joint connecting beam for precast concrete shear wall structures. *Structural Concrete*. 17 (2016) No. 6:972–986. <https://doi.org/10.1002/suco.201500193>,
- Sorensen JH, Hoang LC, Olesen JF, Fischer G. Test and analysis of a new ductile shear connection design for RC shear walls. *Structural Concrete*. 2017;18:189–204. <https://doi.org/10.1002/suco.201600056>,
- R. Aghayari, M. Ashrafy and M. Tahamouli Roudsari, Estimation the base shear and fundamental period of low-rise reinforced concrete coupled shear wall structures, *Asian Journal of Civil Engineering* (BHRC) Vol. 18, No. 4(2017), pp. 547-566,
- P.P. Debnath and S. Choudhury, Nonlinear analysis if shear wall in unified performance based seismic design of buildings, *Asian Journal of Civil Engineering* (BHRC) Vol. 18, No. 4(2017), pp. 633-642,
- I. Haris, Zs. Roszevák, (2017), „Numerical and experimental analysis of prefabricated reinforced concrete beams” *Concrete Structures: Hungarian Group of FIB: Annual technical journal XIX*: (1) pp. 2-11. (2017), in *Hungarian*,
- Axis VM user manual v13r3 8. edition, 2017, 1991-2016 inter-CAD Kft, in *Hungarian*.

STATIC AND DYNAMIC RESPONSE OF DAMAGED PRESTRESSED RC BEAMS FLEXURAL STRENGTHENED WITH CFRP

Tomislav Brozović¹, Tomislav Kišiček², Ana Mandić Ivanković²

¹ Institute IGH, Department for Materials and Structures, Structural Testing Laboratory

² University of Zagreb, Faculty of Civil Engineering, Department for Structures and Bridges
tomislav.brozovic@igh.hr

SUMMARY

This paper presents experimental results of static and dynamic response of damaged RC beams strengthened with CFRP strips and sheets. Three prestressed RC beams with T cross section were tested. Beams were subjected to monotonic loading with increasing load steps with four-point bending setup in order to generate different damage levels in specimens. CFRP strengthening was applied on the specimens after they were damaged by loading to 50% of their flexural capacity. Modal tests were carried out after each loading-unloading cycle. Beams were excited by the impact hammer. Frequency response functions were processed using Dewesoft software to obtain natural frequencies, and corresponding damping ratios and mode shapes.

1. INTRODUCTION

Exposure to aggressive environment and consequential degradation process of the material is the main reason for rapid deterioration and durability issue of concrete bridges. Insufficient serviceability maintenance leads to deterioration, especially in case of bridge decks with poor details design, lack of waterproofing and thin concrete layer. Except durability aspects, bridge superstructures on main highways are everyday under exposure of heavy traffic. Also, new European standards for seismic and wind actions are much more rigorous than the older national standards that was mandatory for columns and frames design of an existing old bridges. All above may be a reason to repair deteriorated and damaged bridges in terms of bridge rehabilitation and strengthening. In the last decade externally bonded FRP strips and sheets have been the most commonly used techniques for strengthening RC structures and bridges. Fact that FRP does not corrode, and its good mechanical performance, made this material very popular to use.

Prior to design and application of FRP strengthening measures, it is of major interest for designers to evaluate condition of deteriorated and damaged bridge structures. One of the most popular non-destructive techniques to evaluate structural health is modal testing. In this work Experimental Modal Analysis (EMA) is used as a technique to evaluate beam stiffness loss due to damage and also effectiveness of FRP strengthening in terms of stiffness recovery. It is a very common technique, based on fact that changes in local stiffness influence on global dynamic parameters (frequencies, mode shapes and modal damping). Generally, bridge dynamic testing can be performed either to confirm theoretical values of modal parameters for a new bridges or to evaluate condition of an existing bridges (Vibration Based Structural Health Monitoring). Contribution to modal testing of a large structures and bridges was development of the Operational Modal Analysis accompanied with improvements on testing devices (acceleration transducers, acquisition systems, etc.). In combination with static load

testing (performed with loaded trucks), modal testing on real bridges can be expensive. Also, results from modal tests are very susceptible on boundary conditions and temperature. Instead of testing a real bridge superstructure, numerous laboratory tests have been carried out using smaller beam specimens.

In the past decade a several laboratory tests were carried out with goal to evaluate effectiveness of FRP flexural strengthening on RC beams by modal testing (Capozucca, 2014, Bonfiglioli and Pascale, 2006, Baghie, Esfahani and Moslem, 2009, Li, Samali and Smith, 2007). On the same topic some theoretical researches were performed as well (Massenzio, Jacquelin and Ovigne, 2005, Hamad, Owen and Hussein, 2014, Musial 2012). In most of the experiments, testing specimens were non-prestressed RC beams, usually with rectangular cross section, simply supported during static part of testing, and hanged during modal test (to avoid influence of rigid supports on modal results).

One similar experimental research (that is in a scope of research project of assessing FRP application on concrete bridge strengthening) is presented in this paper. Regarding the lack of research activities on prestressed beam specimens, and considering that lots of RC bridge superstructures were built with prestressed girders, it was decided to perform laboratory testing in order to investigate, besides a non-prestressed, also the prestressed beams. The aim of this research was to evaluate beam stiffness loss due to damage and also effectiveness of FRP strengthening in terms of stiffness recovery by modal test.

2. EXPERIMENTAL RESEARCH

2.1 Outline of the experiment

Static and dynamic modal tests were carried out on a total of three specimens. One of the specimens was the referent one and non-strengthened, while the others were strengthened with CFRP strip or sheet (Tab. 2).

Specimens were built in a precast concrete factory with concrete class of C40/50. Steel grade of the re-bars was B500B. For adhesion prestressing 0.5” strands were used with steel grade Y1860S7 (Tab. 1).

Tab. 1: Cross section properties

Beam type	Cross section dimensions	Tension reinf.	Shear reinf.	Prestressing	
	[cm]			Strand	Force
Prestressed	$b_w/b_{eff}/h/h_f=15/30/35/12$	2Ø10	Ø8/10 cm	1 × 0.5”	75 kN

Beams were submitted to monotonic loading with increasing load steps with symmetric four-point bending setup, and with shear span of 1.0 m. CFRP strengthening was applied on the beam specimens after they were damaged by loading to 50% of their flexural capacity (Fig. 1). Modal tests were carried out after each loading-unloading cycle. To avoid influence of a rigid supports on the modal results specimens were hanged (Fig. 2). An impact excitation was used to induce free vibrations. Dynamic response was registered with one accelerometer located at the midspan (multi input – single output method). Frequency response functions (FRF) were processed using Dewesoft software to obtain natural frequencies, and corresponding damping ratios and mode shapes (Figs. 4 and 5).

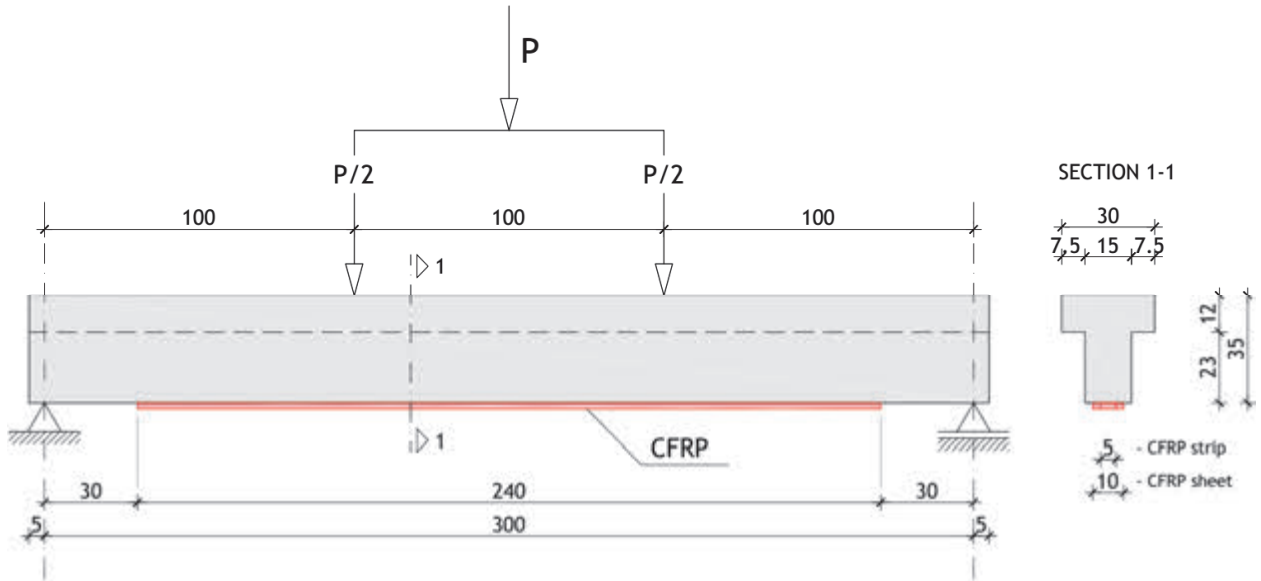


Fig. 1: Four point bending test scheme

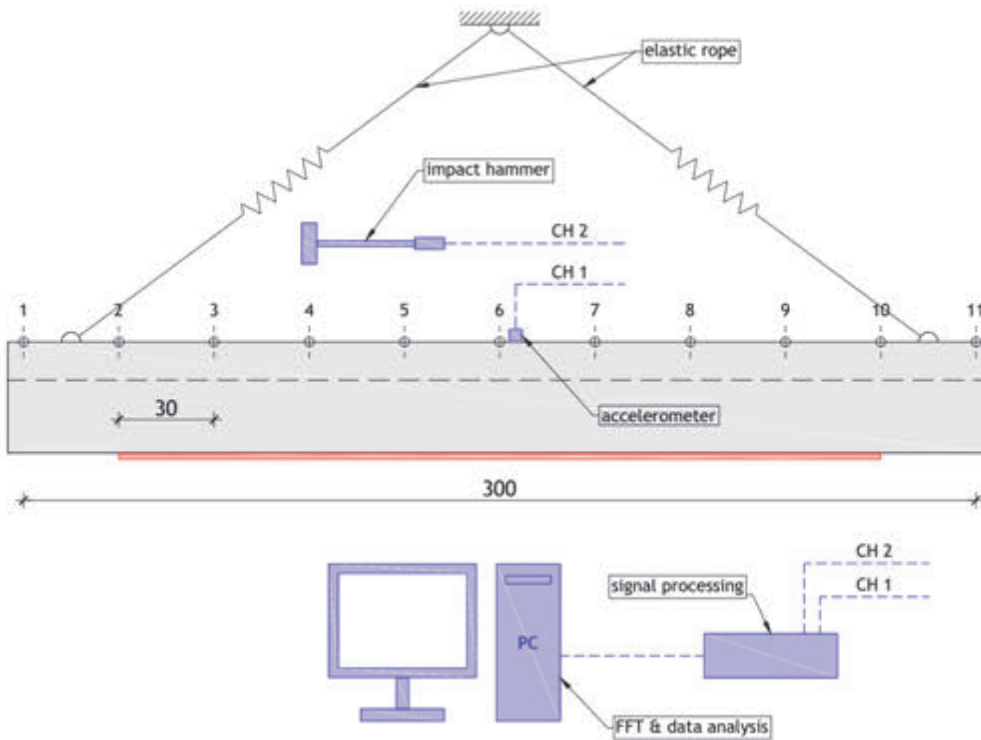
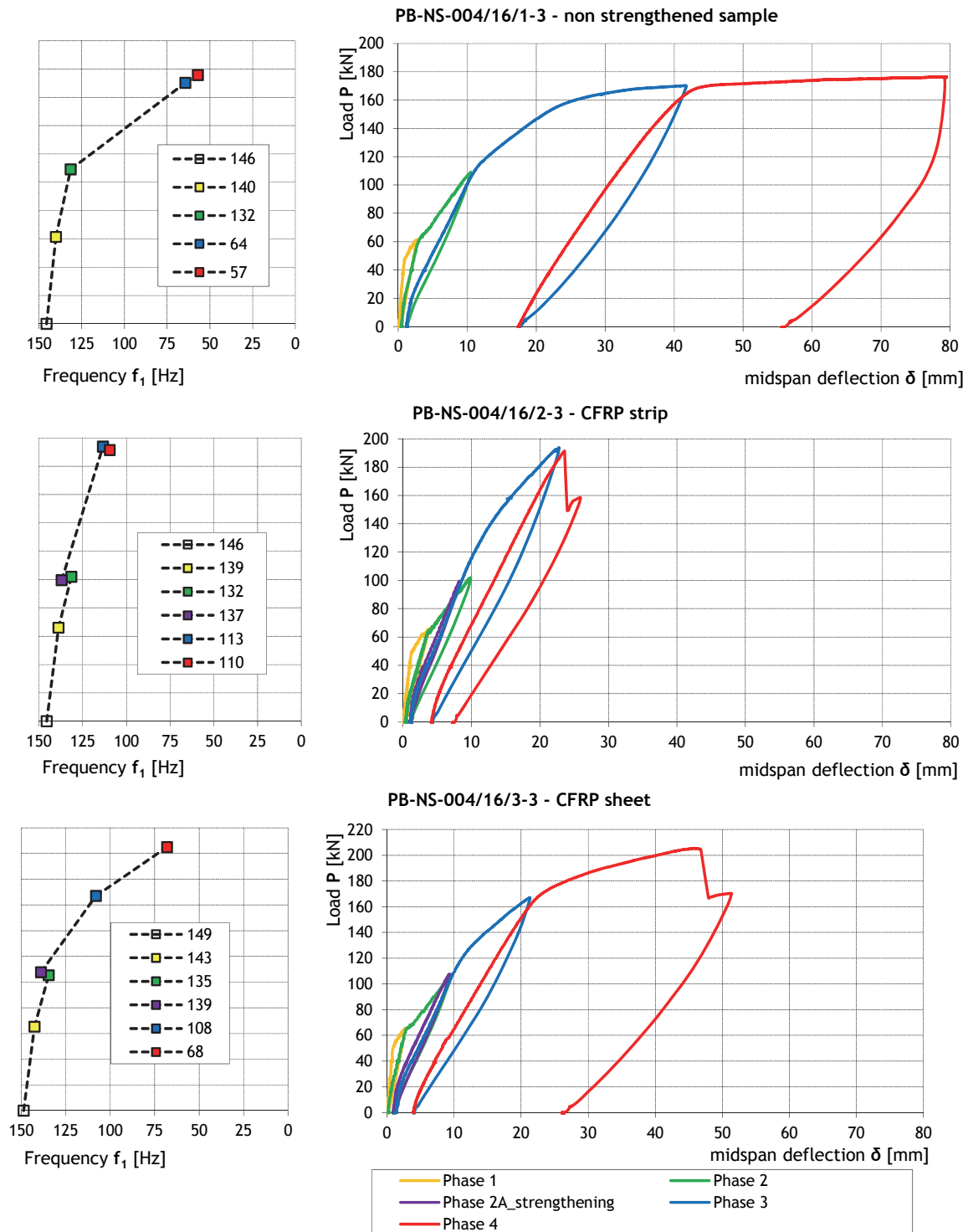


Fig. 2: Modal test scheme

2.2 Results and discussion

Basic results from the static and dynamic modal tests are presented at the Fig. 3 in forms of $P-\delta$ and $P-f$ relations. Comparing the diagrams, it is evident that modal testing in terms of frequency decrease analysis enables to evaluate and predict extreme beam loading that caused local beam stiffness loss (cracking of concrete in tension and yielding stress stage in reinforcement).


 Fig. 3: P- δ and P-f relation for RC prestressed beams

Tab. 2: Results from the static four point bending test

Specimen	Type of strengthening	Failure mode	P_u	P_u/P_{ref}	δ_u	δ_u/δ_{ref}
			[kN]		[mm]	
PB-NS-004/16/1-3	-	SY/CC	175.8	-	79.2	-
PB-NS-004/16/2-3	CFRP strip	BL	191.4	1.09	23.6	0.30
PB-NS-004/16/3-3	CFRP sheet	BL	204.9	1.17	46.7	0.59

SY/CC – Steel yielding followed by concrete crushing; BL – bond loss

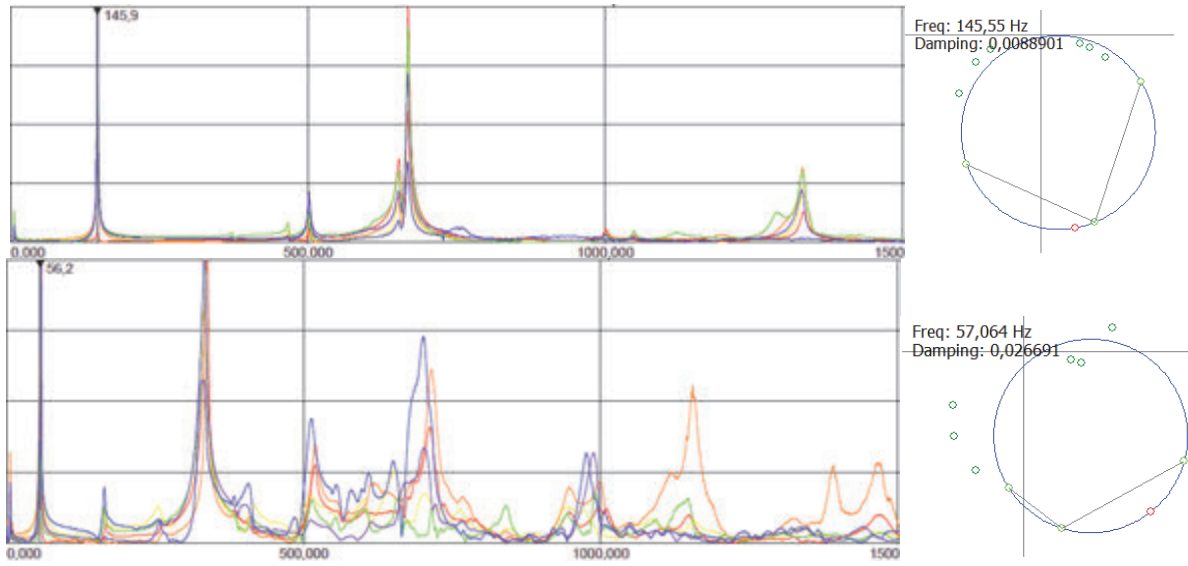


Fig. 4: Comparison of the magnitude spectra of the FRF functions and modal circles in virgin and failure step mode for the non-strengthened specimen

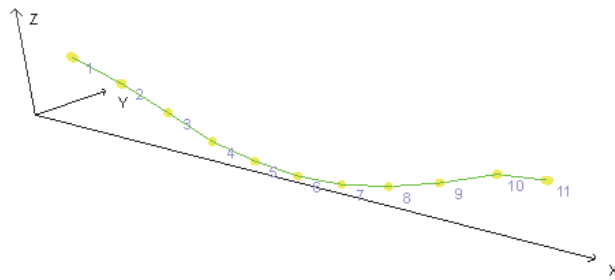


Fig. 5: First bending mode shape

From the P- δ diagram of the specimen that was strengthened with CFRP strip (PB-NS-004/16/2-3), deficiency of ductility can be noticed. Bond failure mode in terms of peeling-off in an anchorage zone occurs on both strengthened specimens (Fig. 6). Specimen that was strengthened with CFRP sheet had a bigger value of ductility coefficient than the one strengthened with CFRP strip.

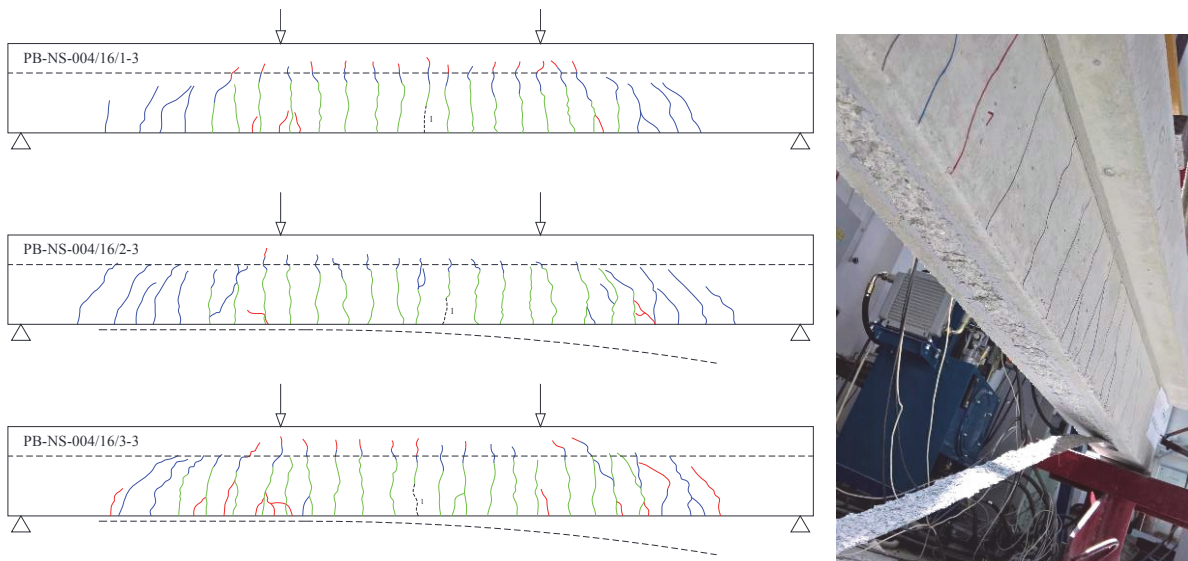


Fig. 6: Cracking pattern and failure mode caused by loss of composite action

3. CONCLUSIONS

In this paper experimental results of the static and dynamic tests carried out on a damaged prestressed RC beams flexural strengthened with CFRP are presented.

Static load test confirmed that flexural strengthening increase load bearing capacity and flexural stiffness of the prestressed beams but also decrease ductility behavior. Numerous tests have shown that bond failure modes are dominant and it is very hard to reach full tension strength of the FRP and ULS with full composite action. Therefore, the bond failure modes are well investigated and propositions for anchor length design and other calculations were proposed in a standards and technical reports issued by the *fib*, ACI and other national committees. Nevertheless, it is obvious that in force transfer between composite and concrete in most of the cases bond failure occur due to shear concrete failure and de-bonding in concrete near the surface. So extra effort has to be made to increase the capability of the bond shear force transfer, either with shear connectors or possibly with upgrading the concrete by adding an additional layer of fiber reinforced mortar on a beam surface before applying a FRP strengthening system. These issues will be investigated further.

Dynamic modal test presented in this paper, confirmed previous investigations that with precise measurements it is possible to determine and evaluate decrease of stiffness due to damage caused by static loading and also evaluate effectiveness of the FRP flexural strengthening on the stiffness recovery. Modal analysis is a popular and useful non-destructive method for damage detection and structural health monitoring of the bridges and other structures. In the future research activities this method should be proved also on a real case study to evaluate the effectiveness of FRP flexural strengthening on a real bridge superstructure.

4. REFERENCES

- Baghie, N., Esfahani, M. R. and Moslem, K. (2009), "Studies on damage and FRP strengthening of reinforced concrete beams by vibration monitoring", *Engineering Structures*, Vol. 31, pp. 875-893
- Bonfiglioli, B. and Pascale, G. (2006), "Dynamic assessment of reinforced concrete beams repaired with externally bonded FRP sheets", *Mechanics of Composite Materials*, Vol 42, No. 1, pp. 1-12
- Capozucca, R. (2013), "A reflection on the application of vibration tests for the assessment of cracking in PRC/RC beams", *Engineering structures*, Vol. 48, pp. 508-518
- Hamad, W. I., Owen, J. S. and Hussein, M. F. M. (2014), "Modelling the degradation of vibration characteristics of reinforced concrete beams due to flexural damage", *Structural Control and Health Monitoring*, 2014
- Massenzio, M., Jacquelin, E. and Ovigne, P. A. (2005), "Natural frequency evaluation of a cracked RC beam with or without composite strengthening for a damage assessment", *Materials and Structures*, Vol. 38, December 2005, pp. 865-873
- Musial, M., Kaminski, M. and Ubysz, A., (2009), "Free vibration frequencies of the cracked reinforced beams – methods of calculation", 18th International Conference on the Applied Computer Science and Mathematics in Architecture and Civil Engineering, Weimar, Germany, 07-09 July 2009
- Li, J., Samali, B. and Smith, S. T. (2005), "Stiffness estimation and damage detection of fiber reinforced polymer strengthened reinforced concrete beams using a vibration-based method", 4th Australasian Congress on Applied Mechanics

STRUCTURAL CONSEQUENCES OF FIRE ON CONCRETE STRUCTURES - REVIEW ARTICLE

Naser Alimrani, György L. Balázs

Department of Construction Materials and Technologies

Budapest University of Technology and Economics

H-1521 Budapest

SUMMARY

Concrete structures are frequently exposed to fire. Present paper intends to give an overview of possible consequences of fire on concrete structures in order to be able to further develop aspects of material characteristics and structural design. Fire assessment and design must include thermal analysis as well as considerations on material and structural characteristics. Assessment of load bearing and heat exposure is required together with an analysis of structural response and an appropriate choice of structural system and components, including joints and supports. As one of the most serious structural consequences of fire, explosive spalling of concrete cover is likely to occur when rate of heating during fire increases causing serious consequences to structure and people.

1. INTRODUCTION

1.1 Fire action

Fire in buildings occurs with unwelcome frequency. In spite of intensive efforts, it has not been possible to reduce the consequences of the fire substantially. Fire protection is achieved through a range of measures, including planning of evacuation routes and protection against smoke or toxic gases, as well as the fire design of load-bearing members (*fib*, 2010). The increasing internal temperature causes a fall-off in the elastic modulus and the yield strength of the steel reinforcement. The effects of temperature on the steel properties become noticeable at 200 °C; they are significant at 400 °C and very serious at 600 °C (*fib*, 2010). The compressive strength and stiffness reductions are severe; the load-bearing capacity of individual members can fall to the level of the sustained loads, which are acting, so local collapse can occur. Large deflections take place prior to collapse owing to the loss of elastic stiffness in both the steel and concrete. At an even earlier stage, structural damage will commence with spalling of cover concrete at edges and corners due to temperature gradients (See more details on spalling in Section 4.2.). If the structure is prone to progressive collapse, the loss of one member due to the effects of fire can trigger an overall collapse (*fib*, 2010).

1.2 Heating of the structure

The most direct effect of a fire on a structure is the temperature increase in a first phase, and then a progressive decrease as the fire reduces until extinction (*fib*, 2008). During the heating phase (During cooling phase also) heat is introduced in (or evacuated from) the structure by a combination of:

- convection from the surrounding gas,
- radiation from the surrounding gas if it is opaque, fire resource or compartment (*fib*, 2008).

1.3 Factors affecting failure

It has very often been pretended that temperature is not uniform in concrete elements whereas it is more or less uniform in steel elements because of the significant difference in thermal conductivity: approximately 45 W/(m·K) for steel and 2 W/(m·K) for concrete (*fib*, 2008). The thermal conductivity of concrete depends on the conductivities of its constituents. The major factors are the moisture content, the type of aggregate and the mix proportions (Schneider, 1988).

The level of temperature differences observed in a section depends on several factors, the most important ones being (*fib*, 2008):

- The increase rate of the fire. The faster the elevation of temperature is, the higher the temperature differences are.
- The severity of the fire, in terms of duration and maximum temperatures. A short fire will obviously not allow sufficient energy to be introduced in the section.
- The shape of the section. In fact, the thermal massivity considered, as the ratio between the exposed surface and the volume to be heated, is a good indication of the level of temperature differences. A thin column will have lower than a massive one.

2. THERMAL PROPERTIES

Fire assessment and design calculations must include thermal analysis as it is required for simplified and complex calculations. It is also required for analysis of separating or load-bearing function. A key to the success of thermal analysis is the appropriate choice and use of the thermal properties (*fib*, 2007). Nevertheless, design practically for thermal expansion only requires rough estimates of how the structure will expand and deform under fire, although it may be necessary to consider also the cooling down period (*fib*, 2010).

2.1 Thermal expansion of concrete

The thermal expansion of concrete can be expressed as a function of temperature. Siliceous concrete has values of about $10 \times 10^{-6} \theta_c$ for concrete temperatures (θ_c) between 20 and 200 °C and of about $12 \times 10^{-6} \theta_c$ for θ_c over 200 °C (Fig. 1). For the simple assessment of normal reinforced concrete in fire in case of $\theta_c \approx 600$ °C, we may take (*fib*, 2010):

$$\frac{\Delta l}{l} = 14 \times 10^{-6} \theta_c \quad (1)$$

For concrete made with lightweight aggregates

$$\frac{\Delta l}{l} = 14 \times 10^{-6} \theta_c \quad (2)$$

2.2 Thermal expansion of steel

Average thermal expansion for ferrite steel over a temperature (θ_s) range of 100 to 650 °C is shown in Fig. 2. The coefficient of expansion for steel also does not vary linearly with temperature, but increases as temperature increases (Abrams, 1977). For the simple assessment of normal steel, average values of thermal expansion are about $12 \times 10^{-6} \theta_s$ (*fib*, 2010).

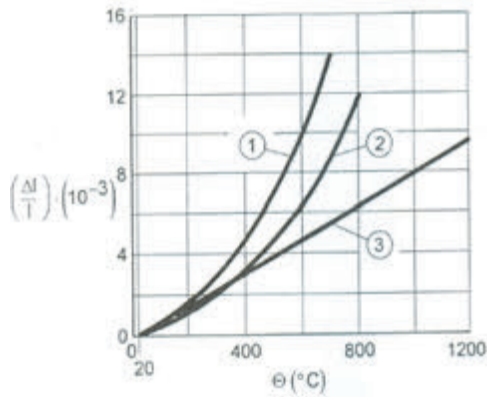


Fig. 1: Thermal elongation of concrete
(1): Silicious aggregate, (2) Calcareous aggregate, (3) Lightweight aggregate

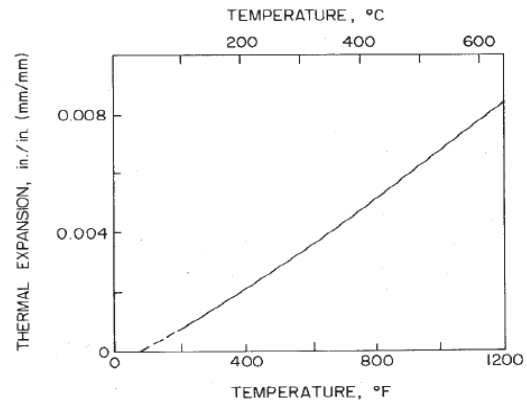


Fig. 2: Thermal expansion of ferrite steels

2.3 Load induced thermal strains

Load induced Thermal Strain (LITS) is obtained from the difference in strain between the thermal strain of an unloaded concrete specimen and the strain measured under constant load applied prior to heating and maintained constant during heating (Fig. 3; *fib*, 2007).

During initial phase of heating an expansion occurs in aggregate while cement paste experiences shrinkage. Results are shown in Fig. 4. It would seem that thermal incompatibility between the aggregate and cement paste could cause damage to concrete, however it does not happen. During the virgin heating the concrete's components move mutually, shrinking cement paste accommodate to aggregate expansion and consequently concrete under compression. Therefore shortening could appear against elongation in loaded structural elements (Chudzik et al., 2017). Aforementioned phenomenon defined as a transient thermal creep (TTC) was probably the first reported by Johansen and Best in 1962 and after that was confirmed by other scientists (Khoury et al., 1985). TTC is normally by far the largest component of LITS (*fib*, 2007). It occurs in concrete during first heating to a given temperature, but not during cooling or re-heating to the same temperature under load.

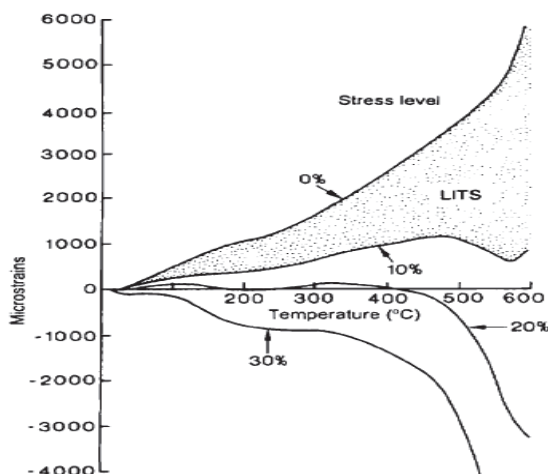


Fig. 3: LITS for the BI-Basalt concrete during heating at 1°C/minute, determined as the difference between the thermal strains under 0%, 10% 20% and 30% load

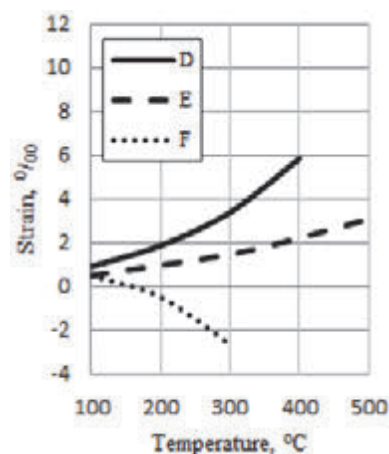


Fig. 4: Experimental results obtained during heating: D-gravel concrete, E-basalt concrete, F-cement paste (Chudzik et al., 2017).

Expansion joints

As a rough guide, the minimum width (e) of an expansion joint for fire should be $e = 40$ mm, at 30 m spacing. The joint filling material should have sufficient durability and must be non-combustible; the sealing material may be combustible (Fig. 5; *fib*, 2010).

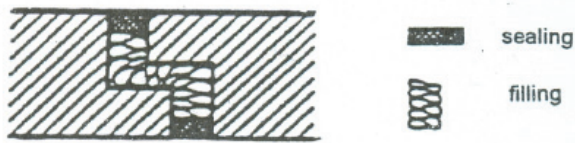


Fig. 5: Example of expansion joint (*fib*, 2010)

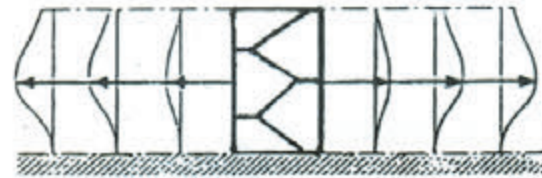


Fig. 6: Effect of central stairwell on surrounding columns (no expansion joint) (*fib*, 2010)

Further issues regarding expansion joints include the following example. Considering the columns supporting the slab in the case of the central constraint provided by the staircase, severe displacement at the column heads is likely to occur, as in Fig. 6 with horizontal forced acting on the columns. Expansion joints would be needed to protect the columns. It should be noted that expansion joints in separating walls and slabs need special detailing (*fib*, 2010).

3. STRUCTURAL FIRE DESIGN

3.1 Fire severity

The severity of a fire in a structure is dependent on many factors. However, building authorities assume for design purposes that a structure will be subjected to the worst case fire, and indeed this approach is supported by the conventional wisdom of fire brigade experience, which is that any kind of combustible material will eventually burn (*fib*, 2010). The severity of a fire depends on three main factors:

- available fuel,
- ventilation, i.e. air supply available to promote its growth,
- the characteristics of the compartment where the fire commences (*fib*, 2010).

Current building controls in most countries express the standard of safety for a building in terms of the fire requirements for individual elements. The intention is to ensure that the building structure does not collapse and that the separating elements are maintained during fire. Fire resistance requirements are expressed for specified periods ranging from 30 to 240 minutes (*fib*, 2010). According to the limit states philosophy a strength limit state is reached when a member can no longer carry its design load when combined with any additional thermally-induced loading.

3.2 Structural response

Building regulations in most countries provide for a minimum fire-protection strategy. Additional standards contain design aids for fire in the form of tables for minimum dimensions and minimum concrete cover of beams, slabs, columns, tension members. New standards such as the Eurocodes allow for additional computational methods to predict the development of fire in buildings and the response of the structure to the fire (*fib*, 2010).

In the design of a concrete structure for fire, an assessment of the loads and heat exposure is required, together with an analysis of structural response and an appropriate choice of structural system and components, including joints and supports.

The fire response of reinforced concrete (RC) members is influenced by the characteristics of constituent materials, namely, concrete and reinforcing steel. These include (a) thermal properties, (b) mechanical properties, (c) deformation properties, and (d) material specific characteristics such as spalling in concrete (Kodur, 2014). All these properties vary as a function of temperature and depend on the composition and characteristics of concrete as well as those of the reinforcing steel (Kodur and Harmathy, 2008).

3.3 Fire resistance

The fire resistance of a whole concrete structure would not necessarily be that ascribed to its individual elements. It could be better or worse. Better fire behaviour could arise from such factors as robustness, adequate continuity of reinforcement, reduced level of loading, load sharing mechanisms and the availability of alternative paths for load support. Continuity of reinforcement in design allows the redistribution of forces and moments to gradually take place towards the parts of the structure not exposed to the fire (*fib*, 2007). Worse fire resistance could arise from loads introduced by the thermal deformations, acting also on unexposed parts of the structure. For instance, columns can shear off as a result of the thermal expansion of a fire exposed floor, (Fig. 7). These thermal loads can cause deteriorations in concrete structures, such as cracks, leading to a reduced load-bearing capacity thus, premature failure could occur. It is, therefore, necessary to pay particular attention to detailing of reinforcement and building layout (*fib*, 2007).

4. DAMAGE CAUSED BY FIRE EXPOSURE

Reparability means the ability of a structure or a part thereof, to be restored to an agreed level of safety, in practical use comparable to that before the fire occurred. Its judgment in most cases will be influenced by economic considerations, but under specific circumstances, high financial expenses for the repair may be unjustifiable (CEB, 1991). Judgment of reparability should start with the attempt to obtain an overall image of the event, the fire (*fib*, 2010).

A visit to the place of the fire should be undertaken by an expert in fire design as soon as it seems possible without endangering any persons. Not only the specific damages of the affected structural members, such as deformations, cracks, spalling and disintegration of concrete, etc., but the overall condition of the structure and the building should be carefully recorded (*fib*, 2010). The damage is generally material and structural damage with different ratios. This paper is covering the structural damage only.

4.1 Structural damage

The bond between concrete and reinforcement may be affected by the heating process. The residual bond strength does not only depend on the temperature reached and on the exposure time, but in addition on the condition of the steel surface. The pre-stress which possibly decreases during a fire, can partly be regained during the cooling down period. Fig. 8 shows, results derived from tests with high tensile pre-stressing wires of 9 mm diameter.

Cracks occur in any reinforced or pre-stressed concrete element when exposed to a heating, extinguishing and cooling down process. There are several reasons causing this phenomenon, such as (*fib*, 2010):

- deformation due to mechanical influences and the thermal conditions,
- the temperature gradient in the cross section,
- different temperature rise at the change of the size and shape of a cross section,
- different thermal elongation of cement matrix-aggregates, or concrete-reinforcing steel
- restraints of the re-contraction during the cooling-down process,
- sudden cooling-down by a fire extinguishing hose stream.



Fig. 7: Example of a shear failure in an unexposed concrete column due to the thermal expansion of the fire exposed floor connected to it (Beitel and Iwankiw, 2002)

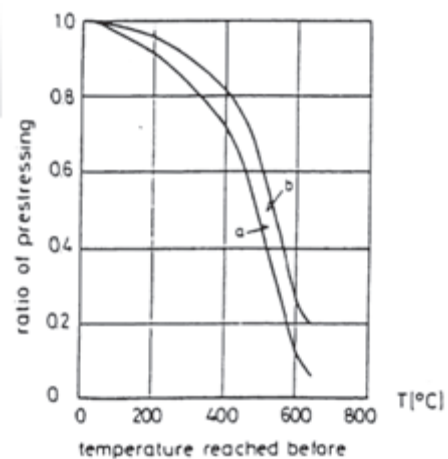


Fig. 8: Decrease of pre-stressing force under elevated temperature (a) and after cooling down (b) (CEB, 1991)

4.2 Spalling

Spalling is the violent or non-violent breaking off of layers or pieces of concrete from the surface of a structural element when it is exposed to high and rapidly rising temperatures as experienced in fire (Khoury, 2006). The rates of heating of the concrete surface in building fires are typically 20-30 °C and in tunnel fires can arise by about 250 °C/minute. Spalling could be grouped into six categories (*fib*, 2007):

- aggregate spalling,
- explosive spalling,
- surface spalling,
- sloughing off spalling,
- corner spalling and
- post cooling spalling.

Among these categories, which have no clear dividing line between some of them, explosive spalling is considered to be the most serious form of spalling in a fire situation. It could result in explosive removal of a concrete layer up to 25-100 mm thick (*fib*, 2007). Spalling of concrete cover may have two reasons: (1) internal vapour pressure (mainly for conventional concretes) and (2) overloading of concrete compressed zones (mainly for high strength

concretes) (Balazs and Lubloy, 2009). The spalling mechanism of concrete cover can be seen in Fig. 9.

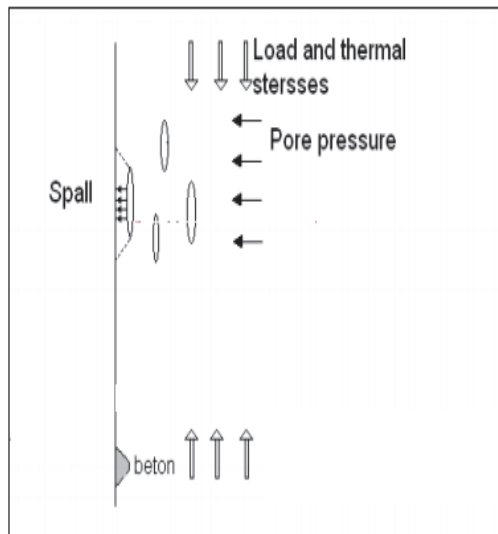


Fig. 9: Mechanism of spalling (Høj, 2005)

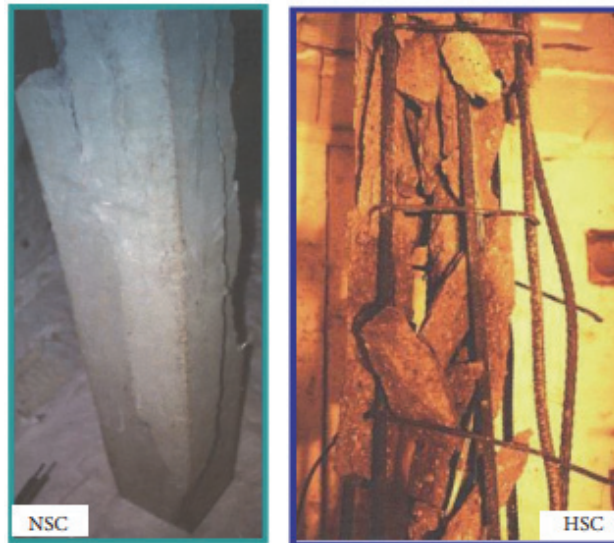


Fig. 10: Relative spalling in NSC and HSC columns under fire conditions (Kodur, 2014)

For example, thermal stress spalling would not develop in a concrete that has zero thermal expansion as experienced with some lightweight aggregate concretes. This allows the determination of the influence of pore pressure spalling. However, it should be noted that lightweight aggregate is highly porous and the additional moisture in the pores would promote pore pressure spalling (Khoury, 2008). For more details, see: "Explosive spalling of concrete in fire", PhD research by Eike Wolfram Heinrich Klingsch (2014).

Although spalling might occur in all concretes, high strength concrete (HSC) is believed to be more susceptible to spalling than normal-strength concrete (NSC) (See Fig 10), because of its low permeability and low water-cement ratio (Noumowe et al, 2009). The high water vapor pressure, generated due to a rapid rise in temperature, cannot escape due to high density (and low permeability) of HSC, and this pressure build-up often reaches the saturation vapor pressure (Deideriches et al, 1995). Balazs and Lubloy (2012) suggested that thin and short steel fibers contribute to the residual compressive strength after high-temperature loading (Balazs and Lubloy, 2012).

Factors influencing explosive spalling (fib, 2010)

Permeability: It is an important factor because it affects the rate of vapour release. Concrete of higher quality generally possess higher density and a finer pore structure and therefore offers higher resistance to moisture flow.

Age of concrete: The majority of reports suggest that the probability of spalling reduces with age, although this may be due to the low moisture level in older concretes.

Strength of concrete: Ironically, poor quality concrete is superior to good concrete in spalling. High strength concrete with low permeability and good durability is in fact a low performance concrete at high temperature.

Type of aggregate: It can be generally concluded that the likelihood of thermal stress explosive spalling is less for concrete containing a low thermal expansion aggregate

Cracking: Internal cracking has a dual effect upon explosive spalling. While micro cracks facilitate the escape of moisture, they also provide sites for crack propagation.

There are also other affecting factors such as: reinforcement, cover to reinforcement, steel fibres and polypropylene fibres.

Preventing explosive spalling

Khoury (2008) proposes that "In terms of prevention, the correct approach would be to address the mechanisms when it comes to the design of the concrete, or alternatively use a thermal barrier which could be significantly more expensive but which would also provide benefits in preventing the deterioration of mechanical properties owing the lower temperatures of exposure to the substrate concrete". He stated two suggestions, thermal barriers and concrete mix design in order to prevent or even to decrease spalling (Khoury, 2008).

5. CONCLUSIONS

Concrete structures are frequently exposed to fire. Structures exposed to fire are generally experiencing increasing of elevated heat from ignition to distinction of fire. Fire assessment and design calculations must include thermal analysis since constituents of concretes including reinforcement behave in different ways when exposed to fire. During heating concrete also experiences thermal strain, shrinkage, as well as load induced thermal strain (LITS). LITS comprises several components such as irrecoverable transient thermal creep.

Fire response of concrete structural members is dependent on the thermal, mechanical, and deformation properties of concrete which vary significantly with temperature and depends on the composition and characteristics of concrete batch mix as well as heating rate and other environmental conditions. Damage of the structure includes damage of material and reduction of structural properties. There are two mechanisms of explosive spalling, thermal stress spalling and pore pressure spalling. Rapid heating during fire could induce explosive spalling with serious consequences to structure and people.

Present paper intended to give an overview of possible consequences of fire on concrete structures in order to be able to further develop aspects of material characteristics and structural design.

6. ACKNOWLEDGEMENTS

Authors acknowledge the support by the Hungarian Research Grant NVKP_16-1-0019 "Development of concrete products with improved resistance to chemical corrosion, fire or freeze-thaw".

7. REFERENCES

- Abrams, M. S. (1977), "Performance of Concrete Structures Exposed to Fire", Research and Development Bulletin RD060, Portland Cement Association.
- Balazs, G. L. Lubloy E. (2009) "Concrete in fire", Műszaki Szemle, folyóirat, Kolozsvár, Románia. Vol. 47, pp 3-10, ISSN 1454-0746

- Balazs, G. L. Lubloy, E. (2012), "Post-heating strength of fiber-reinforced concretes", Fire Safety Journal, Vol 49. pp 100-106, Elsevier
- Beitel, J. Iwankiw, N. (2002), "Analysis of Needs and Existing Capabilities for Full-Scale Fire Resistance Testing", NIST report GCR 02-843, Gaithersburg, USA.
- CEB (1991), "Fire design of concrete structures", Bulletin 208. Comité Euro-International du Béton, Lausanne, Switzerland.
- Chudzik, P. Kowalski, R. Abramowicz, M. (2017), "Strains of concrete in RC structures subjected to fire". International Conference on Analytical Models and New Concepts in Concrete and Masonry Structures AMCM'2017. Elsevier Ltd.
- Diederichs, U. Jumppanen, U. Schneider, U. (1995) "High temperature properties and spalling behaviour of high strength concrete," in Proceedings of the 4th Weimar Workshop on High Performance Concrete, HAB, Weimar, Germany.
- fib* (2007), "Fire design of concrete structures, materials, structures and modelling", *fib* Bulletin 38, International Federation for Structural Concrete
- fib* (2008), "Fire design of concrete structures, materials, structural behaviour and assessment", *fib* Bulletin 46, International Federation for Structural Concrete
- fib* (2010), "Structural Concrete – Textbook on behaviour, design and performance", *fib* Bulletin 54, International Federation for Structural Concrete
- Høj, N. P. (2005) "Keep concrete attractive - Fire design of concrete structures", Proceedings of fib symposium on Keep concrete attractive, edited by Gy. L. Balázs, A. Borosnyói, 23-25 May 2005 Budapest, pp.1097-1105
- Khoury, G. A. (2006), "Strain of concrete during two thermal cycles. Part 1 : strain over two cycles, during first heating and at subsequent constant temperature". Magazine of Concrete Research, 58, No. 6, August, 367-385
- Khoury, G. A. (2008), "Fire and concrete. Encontro Nacional Betão Estrutural". BE2008 – Guimarães – 5, 6, 7 de Novembro.
- Khoury, G. A. Grainger, B. N. Sullivan, P. J. E. (1985), "Transient thermal strain of concrete: literature review, conditions within specimen and behaviour of individual constituents". Magazine of Concrete Research. Vol. 37, No. 132, pp. 131-144.
- Klingsch, E. W. H. (2014) "Explosive spalling of concrete in fire", PhD Research. Institute of Structural Engineering (IBK), ETH ZURICH. Gifhorn, Germany.
- Kodur, V. R. (2014), "Properties of Concrete at Elevated Temperatures", Civil Engineering Volume Hindawi Publishing Corporation ISRN, Article ID 468510, 15 p.
- Kodur, V. R. Harmathy, T. Z. (2008) "Properties of building materials," in SFPE Handbook of Fire Protection Engineering, P. J. DiNenno, Ed., National Fire Protection Association, Quincy, Mass, USA
- Noumowe, A. N. Siddique, R. Debicki, G. (2009) "Permeability of high-performance concrete subjected to elevated temperature (600 °C)," Construction and Building Materials, vol. 23, no. 5, pp. 1855–1861, 2009
- Schneider, U. (1988), "Concrete at high temperatures—a general review," Fire Safety Journal, vol. 13, no. 1.

AUTHOR'S INDEX

Abed, Mohammed	179	Hawryszków, Paweł	427
Al-Basha, Ahmed J.	135	Heinrich, Peter Joachim	542
Alimrani, Naser	665	Hlavička, Viktor	246
Alupoai, Dragoș	459	Hofer, Bernhard K.	467
Andrzej, Śliwka	590	Horváth, Aliz	368
Apostolidi, E.	284	Huber, Helmut	346
Arnuga, Iztok	23	Huss, Michael	263
Bačuvčík, Michal	143	Ille, Mario	501
Bai, Jianfeng	163	Ivanković, Ana Mandić	659
Balázs, György L.	78, 327, 557, 665	Jasiński, Marek	575
Bambuchová, Markéta	150	Jaskulski, Roman	111
Bergmeister, K.	284	Jaśniok, Tomasz	127
Bílek, Vlastimil	150	Joseph, Miquel	70, 187
Biliszczuk, Jan	427	Juhász, Károly Péter	549, 632, 640
Bleiziffer, Jelena	509	Kadrić, Reuf	379
Bober, Waldemar	487	Kaszubska, Monika	598
Bódi, István	388	Katalinić, Slaven	615
Boehme, Luc	70, 187	Kausay, Tibor	102
Boita, Emanuela	277	Keršner, Zbyněk	481
Boneczková, Sabina	150	Kišiček, Tomislav	659
Boros, Vazul	255	Kleiser, Michael	346
Bosiljkov, Violeta Bokan	86	Klepo, Ivan	48
Brozović, Tomislav	659	Klikowicz, Piotr	396
Bruwer, Cronje	292, 306	Kolísko, Jiří	31, 94, 354
Červenka, Jan	525	Kollegger, Johann	435
Červenka, Vladimír	525	Köllö, Gavril	459
Čítek, David	94	Kopp, Michaela	533
Coufal, Robert	31	Koris, Kálmán	388
Csíki, Béla	15	Kosec, Tadeja	86
Czoboly, Olivér	78	Kőszeghy, Károly	15
Dan, Daniel	277	Kotynia, Renata	598
Daněk, Petr	481	Krawczyk, Łukasz	404
Domagała, Katarzyna	211	Kremnitzer, P.	248
Durovsky, Gábor	449	Kromoser, Benjamin	435
Džajić, Igor	501	Krykowski, Tomasz	127
El Mir, Abdulkader	233	Krzakała, J.	202
Enache, Sergiu	459	Kubissa, Wojciech	111
Fanourakis, George C.	566, 583	Łaziński, P.	40, 202
Floruț, Sorin Codruț	277	Legat, Andraž	86
Frantík, Petr	481	Li, Hongyuan	163
Freytag, Bernhard	410	Li, Jiabin	70, 163, 187
Fritsch, Michael	23	Lindlbauer, Wolfgang	346
Gajdošová, Katarína	143, 313	Lublóy, Éva	240, 246
Galic, Josip	48	Ludvig, Péter	195
Gálos, Miklós	607	Machelski, Czesław	410
Geng, Yongwang	163	Martin, Boháč	171
Gołdyn, Michał	404	Martina, Drdlová	171
Gyurkó, Zoltán	179	Massaer, Jeroen	70
Halvoník, Jaroslav	143, 313	Mészöly, Tamás	62
Hammond, John	640	Metes, Elena	459
Han, Daguang	163	Milić, Ivana	509
Haris, István	648	Milost, Egon	86
Haus, Andreas	219	Morlin, Bálint	298

Nabil, Abdelmelek	240	Śliwka, Andrzej	118, 590
Nagrodzka-Godycka, Krystyna	443	Słomka-Słupik, Barbara	225
Nagy, János	368	Smolana, Mateusz	396
Nagy, Lóránt	549, 632	Sólyom, Sándor	327
Nagy-György, Tamás	277	Sonnenschein, Róbert	313
Nehme, Salem G.	233	Sparowitz, Lutz	410
Nemes, Rita	179	Stoian, Valeriu	277
Newton, Craig M.	135	Strauss, A.	284
Nguyen, Viet Tue	263	Sýkora, Miroslav	354
Noppe, Dylan	70	Szczech, Damian	598
Novák, Balthasar	255	Szijártó, Anna	179, 327
Novák, Drahomír	525	Tamás, Kornél	607
Olipitz, Michael	337	Teichgraeber, Marco	427
Oppeneder, Johannes	410	Teiter, Zoltán	493
Orosz, Ákos	607	Tej, Petr	94
Orosz, Árpád	368	Terzić, Vedad	379
Oslaković, Irina Stipanović	86	Thék, Eörs Henrik	449
Paulík, Peter	143, 313	Tichý, Jan	475
Péity, Ágnes	233	Todea, Viorel Constantin	277
Perczel, Zoltán	15	Tóth, Mária Erdélyiné	298
Petzek, Edward	459	Tue, Nguyen Viet	263, 542
Piątek, Bartosz	319	Urban, Tadeusz	404
Pisarek, Bartosz	410	Vacek, Vítězslav	354
Płaszczyk, Tomasz	575, 623	Vančík, Vladimír	354
Pluzsik, Anikó	298	Vašátko, Radek	31
Pluzsik, Tamás	298	Vill, Markus	62
Pukl, Radomír	525, 632	Vítek, Jan L.	31
Pytlík, David	150	Vlašić, Anđelko	615
Rádics, János P.	607	Weier, Herbert	362
Randl, Norbert	62, 467	Weldon, Brad D.	135
Rauch, C.	284	Wiater, Agnieszka	270
Recha, Faustyn	127	Windisch, Andor	517
René, Čechmánek	171	Winkler, P.	284
Répáczki, Imre	368	Wiśniowska, Marta	443
Rocha, Vanessa V.	195	Yang, Yupeng	155, 163
Roszevák, Zsolt	648	Ying, Chunli	163
Rydval, Milan	94	Zábrádi, Ernő	368
Sajdlová, Tereza	525, 632	Żarski, Mateusz	623
Šajna, Aljoša	86	Zofia, Szweda	118
Salachna, Artur	40	Zybura, Adam	225
Salamak, Marek	40, 396, 575, 623		
Schaul, Péter	557, 632, 640, 649		
Schedler, Robert	23		
Schembera, B.	284		
Schlicke, Dirk	542		
Schneider, Martin	467		
Sedlmajer, Martin	481		
Sekulić, Dalibor	501		
Ševčík, Stanislav	475		
Sierens, Zeger	70, 187		
Simon, Tamás K.	102		
Simon, Tamás	111		
Šimonová, Hana	481		
Siwowski, Tomasz	319		
Slánský, Bohuslav	475		